Geophysical and GIS applications to exploration for Proterozoic sediment-hosted Zn-Pb mineralisation, northern Australia

by

Mark Leslie
Mark L. Duffett B.Sc. (Hons)

Submitted in fulfilment of the requirements for the degree of

Doctor of Philosophy Earth Sciences

University of Tasmania

March, 2000

Declaration of originality:

This thesis contains no material that has been accepted for a degree or diploma by the University of Tasmania or any other institution, except by way of background information and as duly acknowledged in the thesis. To the best of my knowledge and belief it contains no material previously published or written by another person except where due acknowledgement is made in the text of the thesis.

Mark Duffett

Statement of authority of access:

This thesis may be made available for loan and limited copying in accordance with the *Copyright Act 1968*.

Abstract

Geophysical and geographic information systems (GIS) methods have been applied to investigate the regional three-dimensional geological setting and geophysical signature of sediment-hosted Zn-Pb mineralisation in the Proterozoic Carpentaria Zinc Belt of northern Australia. The study focused on the setting of two particular Zn-Pb deposits, HYC in the McArthur Basin and Lady Loretta in the Mount Isa Basin.

A GIS incorporating geophysical interpretations, geological and geochemical data was designed and implemented for a region in the McArthur Basin encompassing the giant HYC Zn-Pb-Ag deposit. The GIS incorporates geological attributes that encode depth information implicit in the stratigraphic column. This data structure, in conjunction with topological attributes, allows queries based on the stratigraphic relationships of spatial elements.

The GIS was used to identify and analyse constraints on base metal metallogeny and to gain insights into the 3-D evolution of the McArthur Basin. Mass balance calculations derived from lithogeochemical data, together with volumes calculated from geophysical and stratigraphic data, indicate that an unrealistic proportion of the carbonate-dominated McArthur Group would have been required to source sufficient base metal to form the HYC mineralised system. At least a major portion of the metals contained in HYC are inferred to have originated deeper in the basin. Automatic identification of the location and magnitude of unconformities on geological maps was used to suggest the location and size of active sub-basins at the time of the formation of HYC mineralisation. HYC's situation at the northeastern edge of one of these sub-basins is consistent with topographic and bounding growth fault control on the palaeohydrogeological regime that focused mineralising fluids in the vicinity of the deposit.

Petrophysical measurements from the Mount Isa Basin indicate that the only highly magnetic units are the Eastern Creek and Kamarga Volcanics. All other units, including Fiery Creek Volcanics basalts, are at most weakly magnetic. Densities of Proterozoic sedimentary units are largely a function of the relative proportion of carbonate and siliciclastic material. The same, albeit weaker relationship was observed with respect to sonic velocity and resistivity, though acoustic impedance contrasts between basin units remain significant.

Pb-Zn ore at Lady Loretta has a high density contrast with the highly pyritic layers enclosing it, which in turn are significantly denser than the host dolomitic siltstone. The Lady Loretta ore is also much more chargeable than any of its host units, but there is little resistivity contrast between the ore and host carbonaceous siltstones. Gravity and IP methods are indicated as most likely to distinguish base metal mineralisation from other conductive bodies in this region.

Airborne magnetic and radiometric data flown over the Lady Loretta region were processed and interpreted to identify areas of anomalous response with respect to the 'normal' signatures of individual basin units. Integration of magnetic, radiometric and lithogeochemical data from the Eastern Creek Volcanics has enabled geophysical identification of alteration phases. Magnetite destruction, Fe

depletion and possibly K depletion, consistent with chlorite + albite-type alteration, are associated with subdued magnetic signals adjacent to Zn-Pb (Lady Loretta) and Cu (Lady Annie) mineralisation. Anomalously high levels of K and quiet magnetic responses are apparent adjacent to the Mammoth Cu deposits. Variable K, Th and U signals from McNamara Group sequences are interpreted to indicate the location and nature of syn-depositional basin structures and sediment source regions, including evidence of anomalous sub-basin development represented by the Lady Loretta host sequence.

The structure and volume of basin units in the Lady Loretta area were inferred from geophysical modelling. Basin structures in this region have been overprinted to varying degrees by the Isan Orogeny. In lower strain areas, there is a WNW trend in pre-Isan Orogeny structures. The area north of the Redie Creek and Leopard Faults appears to have been persistently uplifted from Myally Subgroup through to early McNamara Group time, with a depocentre to the south during this period. The Lady Loretta deposit is situated on the north-western margin of this former depocentre, immediately adjacent to the uplifted area to the north. The proximity to mineralising fluid conduits in the form of bounding or former growth faults was probably a major factor in the formation of the Lady Loretta mineralisation.

GIS and geophysics can be used at all scales in exploration for Zn-Pb mineralisation. Analysis of regional geophysics, geology and geochemistry in a GIS can identify provinces and regions containing the requisite source lithologies, basin architecture and trap rocks to generate major Zn-Pb deposits. More detailed analysis of geophysical data can distinguish areas where 'base metal-depleting' alteration may have originated mineralising fluids from potentially rich source rocks such as the Eastern Creek Volcanics. Geophysical analysis can also help to locate structures capable of focusing mineralising fluids in favourable areas and, with gravity and IP methods, directly detect Lady Loretta-style deposits.

Acknowledgements

I wish to thank my supervisors, Michael Roach, David Leaman, Peter McGoldrick, Ross Large and Peter Gunn, each of whom freely contributed their wisdom on demand. Michael Roach and David Leaman in particular are gratefully acknowledged for their prompt and helpful reviews.

This work was financially supported by an Australian Geological Survey Organisation Postgraduate Research Award. As well as this, I would also like to thank AGSO for the assistance provided by its personnel. All of the many with whom I dealt were without exception extremely helpful and obliging. While they are too numerous to list here, I would especially like to acknowledge fruitful discussions with Lesley Wyborn, Deb Scott, Chris Tarlowski and Jim Leven.

Fellow postgraduate students and staff at the Centre for Ore Deposit Research (CODES SRC) and School of Earth Sciences, University of Tasmania, especially members of the sediment-hosted base metal research team, are thanked for the many illuminating insights which they shared during discussions. In particular, David Rawlings, Peter Winefield, John Dunster, David Cooke, Stu Bull, Richard Keele, Peter Rice, David Selley, Bruce Anderson, Jamie Rogers and Lachlan Heasman contributed from their respective expertise on numerous occasions. My Ph.D. student colleagues are also thanked for helping keep body as well as mind exercised.

The project received support from numerous outside public and private organisations. The Northern Territory Department of Mines and Energy greatly facilitated acquisition of geological and mineral deposit data for Bauhinia Downs. Mining Project Investors, Normandy Exploration, North Exploration and WMC are thanked for their sponsorship of the original GIS compilation. Fieldwork at Lady Loretta was generously supported financially and logistically by the former owners, Pancontinental Mining; Mel Jones and Geoff Webber were instrumental in this. This support was continued by the current owners, Buka Minerals NL. Staff at the Aberfoyle Resources (now Western Metals) office in Townsville, in particular Tony Hespe, obligingly permitted access to their drillcore. Keith Jones at Ashton Mining, Bernie Stockill at the Queensland Department of Minerals and Energy and CRA's (now Rio Tinto) exploration office in Mount Isa are all gratefully acknowledged for their sharing of geophysical data. Bob Richardson of Mineral Resources Tasmania assisted with geophysical data processing.

Colleagues at the Northern Territory University are thanked for their understanding.

I would like to acknowledge the continuing love and support of my family, especially my grandfather. I hope the wait has not been too long.

Most of all I will be forever grateful to my wife, Catherine, who unhesitatingly sacrificed a great deal so that this thesis would see the light of day. It is dedicated to her, with love.

Table of Contents

List of Figures

List of Tables

1. Introduction

1.1 Introduction

The stratiform Zn-Pb deposits occurring in the Palaeoproterozoic and earliest Mesoproterozoic sedimentary sequences of northern Australia ('Carpentaria Zinc Belt'; Sweet et al., 1993; McGoldrick and Large, 1998b) represent one of the largest accumulations of base metals known in Earth's crust. Examples include the supergiant deposits of Mount Isa, Century and McArthur River (HYC). Natural sedimentary basin processes operating to concentrate base metals in quantities up to 200 million tonnes at several orders of magnitude over average crustal concentration must have required a special combination of geological circumstances, encompassing a large volume of rock, in order to produce such deposits.

Such geological circumstances must have incorporated (following Wyborn et al., 1995b):

a source for the metals

a solvent (probably basinal brines) to carry them

aquifers (permeable strata or fracture systems) to provide a conduit and focusing mechanism for the metal-bearing fluid

and suitable host rock, probably reduced carbonaceous fine-grained sediments, to sequester the metals from the basin brine into the sedimentary sequence in ore-level concentrations (upwards of 10% by weight).

Model-based prediction of where other large Zn-Pb orebodies might occur is thus a four-dimensional problem requiring knowledge not only of structures governing where metal-bearing fluids might have been focused to intersect a stratum of reducing sediment, but also when the special conjunction of factors existed to permit this to occur. All this must be evaluated within the context of a sedimentary basin - a dynamic, continually evolving, three-dimensional system. A primary issue in predicting deposit location is hence to reconstruct basin geometry as it was when the mineralisation event(s) occurred over 1600 million years ago; not as it is now, several deformation events and erosion episodes later. Approaches to resolution of this problem are the main focus of this thesis.

Geophysical and GIS-based approaches are adopted in pursuit of several aims. The first of these is to investigate and demonstrate how GIS can be used in exploration for stratiform sediment-hosted Zn-Pb deposits. A second primary goal is to characterise the physical properties of Carpentaria Zinc Belt base metal ore deposits, and to compare these with the properties of stratigraphic units in the host basin sequences. The third aim is to use gravity, magnetic and radiometric data interpretation to characterise the three-dimensional architecture of a region encompassing significant Zn-Pb mineralisation. A secondary aspect of this objective is to investigate the extent to which these geophysical data can be used to identify alteration related to mineralisation.

1.2 Scope of research

This study is mainly aimed at the stratiform sediment-hosted base metal deposit type, described in section 2.8, in which most of the Zn and Pb endowment of northern Australia is manifest. Stratiform sediment-hosted base metal deposits are arguably better known as 'sedex' (short for 'sedimentary-exhalative') deposits. This title has quite specific genetic implications, and the former name, abbreviated to SSHBM, is preferred here.

Research directions were largely dictated by the opportunities available to the project. Research eventually coalesced around two main objectives. The first of these was an examination of the utility of GIS in exploration for and metallogeny of SSHBM deposits. This arose from the availability of a wide range of geoscientific data sourced and generated by a long-running interdisciplinary project on north Australian Proterozoic SSHBM metallogeny at the Centre for Ore Deposit Research, University of Tasmania (McGoldrick and Large, 1998b). The most detailed and thematically extensive data were available for the region corresponding to the Bauhinia Downs 1:250,000 map sheet in the northeastern Northern Territory, in particular the district surrounding the HYC deposit (Fig. 1.1). This area became the focus of the GIS study.

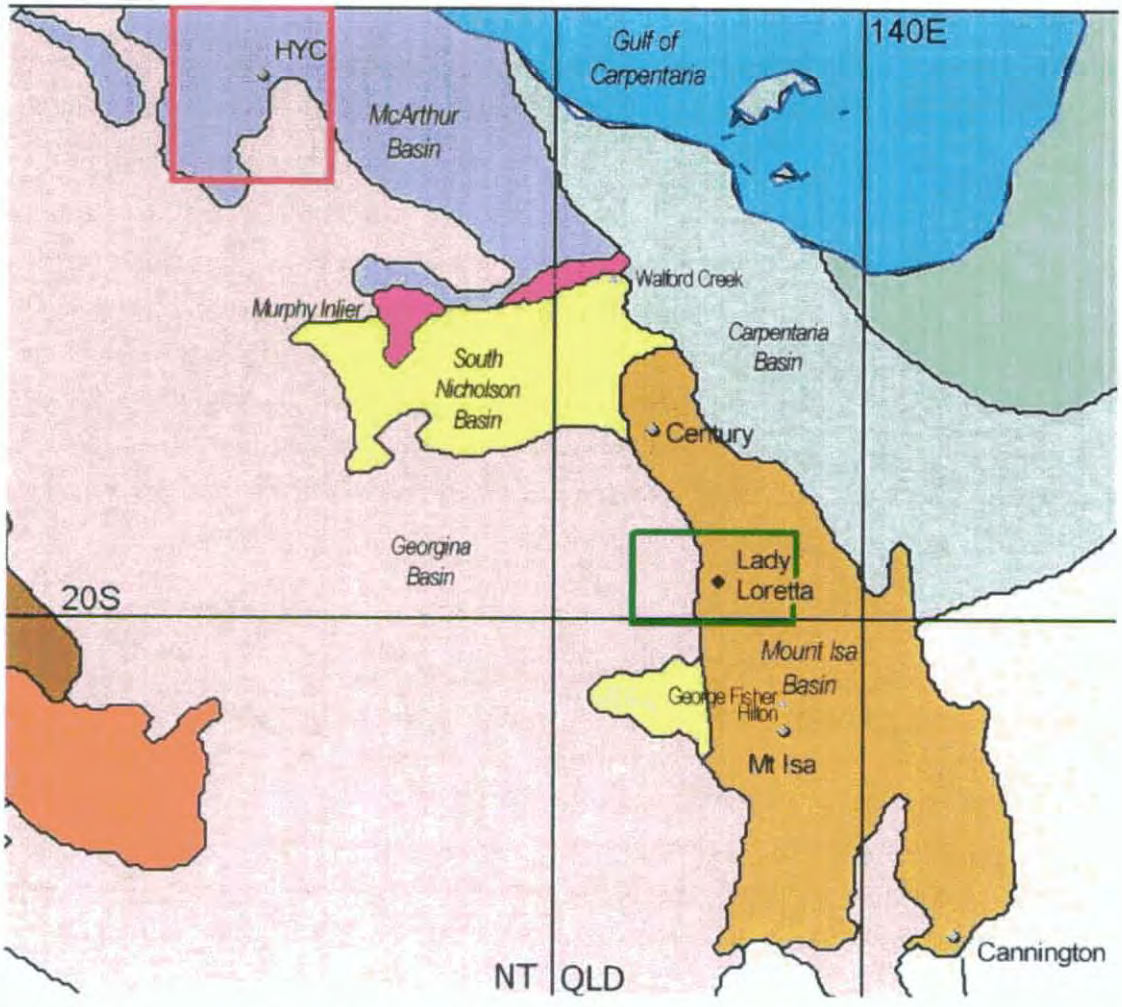

Figure 1.1 Carpentaria Zinc Belt. Bauhinia Downs GIS study area outlined in red, Paradise Valley study area outlined in green

The second objective was to examine the three-dimensional basin setting and geophysical signature of a SSHBM deposit in detail. Access and logistical support were made available by the then owners of the Lady Loretta deposit in Paradise Valley, northwest Queensland (Fig. 1.1). This provided the opportunity to examine a SSHBM deposit of moderate size and grade which had not undergone any significant extraction, yet had a large geological database resulting from decades of exploration, including many tens of kilometres of diamond drilling. High resolution airborne magnetic and radiometric data were also available for the surrounding area, which was hence chosen for an integrated geophysical study. The lack of adequate petrophysical data for the region required that considerable effort be devoted to rectifying this. The Lady Loretta mineralisation as well as a wide range of lithologies from the regional host basin stratigraphy were sampled for petrophysical determinations. The physical properties of other SSHBM deposits in northern Australia were also examined for comparison. Results from this petrophysical phase of the study were used in the subsequent qualitative and quantitative geophysical interpretation of the Paradise Valley region, centred on Lady Loretta. Interpretation focused on the identification of alteration assemblages, as well as on basin architecture and structure.

1.2 Study areas

1.2.1 Bauhinia Downs GIS

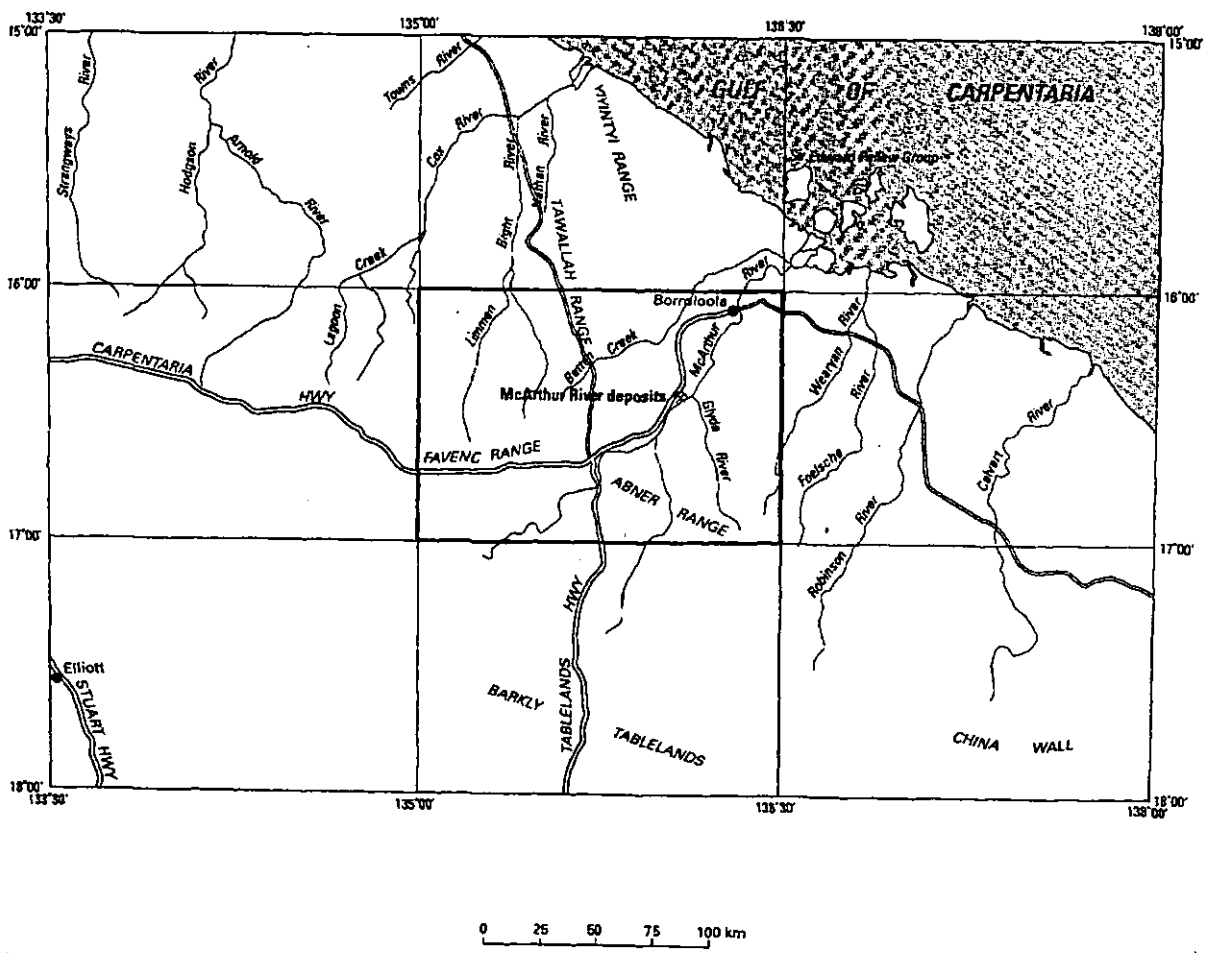

Figure 1.2 Location of Bauhinia Downs study area, after Pietsch et al. (1991)

The boundaries of the Bauhinia Downs 1:250,000 map sheet are defined by latitudes 16° and 17° south, and longitudes 135° and 136°30′ east. The township of Borroloola is situated in the northeastern corner of the area, at the head of the navigable portion of the McArthur River, which flows northeastwards through the centre of the study area. Bauhinia Downs is accessible via sealed road from the west and south on the Carpentaria and Tablelands Highways. The HYC Zn-Pb-Ag deposit, currently being worked by Mount Isa Mines Ltd., is located on the northern bank of the McArthur River in eastern central Bauhinia Downs. A sealed road also proceeds from the mine to barge loading facilities on the Gulf of Carpentaria coast at Bing Bong, north of Borroloola.

1.2.2 Paradise Valley Region

'Paradise Valley Region' in this thesis refers to the area of the Mammoth Mines 1:100,000 special geological map (Hutton and Wilson, 1985), as well as the area adjoining the western edge of this map, up to the road connecting the Burketown-Camooweal Road with the Barkly Highway (Figure 1.3). This region is bounded by latitudes 19°30′ and 20° south, and longitudes 138°50′ and 139°30′ east. It is named after Paradise Creek, which flows through the centre of the area.

The main access to Paradise Valley is by unsealed roads that lead north from the Barkly Highway (Figure 1.3). One of these, McNamara's Highway, proceeds via the Lady Loretta and Lady Annie mines en route to the disused OP and Jack McNamara mines to the north, as well as connecting with Thorntonia homestead near the north-western corner of the study area. The other, a made gravel road, passes through the eastern portion of Paradise Valley, leading to the Mammoth and Mount Oxide copper mines. The township at Mammoth is the only permanent human habitation in the region apart from pastoral homesteads at Barr Creek, Koolamara and Thorntonia. Maintenance personnel periodically occupy the mining camp at Lady Loretta, which was used as a base during field work for this study.

Access of moderate quality is provided to the remainder of Paradise Valley by a number of other tracks in various states of disrepair, though this has been improved in some areas by recent mineral exploration activity.

Most of Paradise Valley lies at an elevation of around 300 metres above sea level, with relief varying up to 100 metres above and below this height. This relief is superimposed on a very gentle slope down to the north and north-west, such that the general level of the country near the Mount Kelly copper prospect approaches 400 m, compared to less than 200 m in Gunpowder Creek gorge in the north-north-west near Mount Oxide. The south-western quadrant of the study area lies astride the divide between two continental drainage systems, the northern-flowing systems ultimately debouching into the Gulf of Carpentaria, and the other southwards into Lake Eyre via the Georgina River.

The area has a semi-arid climate, receiving most of an average ~500 mm annual rainfall during a short wet season between November and April. For much of the rest of the year, very high evaporation rates and warm to very hot temperatures prevail, though with large diurnal variations.

This climate supports extensive spinifex (*Triodia* spp.) and snappy gum (*Eucalyptus brevifolia*) in the large areas of good Proterozoic outcrop, but this vegetation rarely attains sufficient density to block

access on foot to most areas. Lancewood (*Acacia shirleyi*) is notably dominant in areas of red lateritic and other soils. Woodland tends to be scarcer in the flatter country developed on Cambrian and Mesozoic sediments to the west.

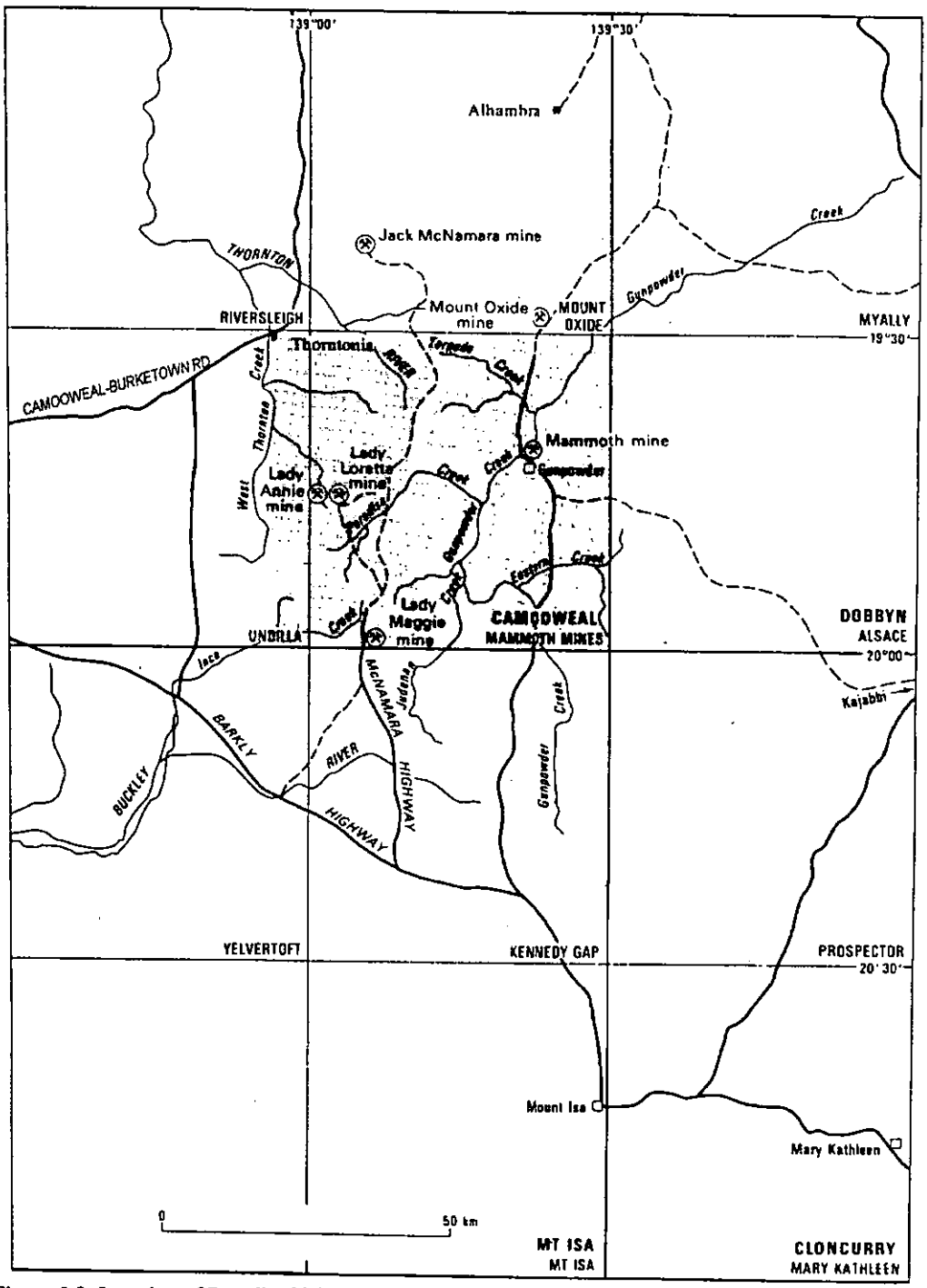

Figure I.3 Location of Paradise Valley study area, modified after Hutton and Wilson (1985)

The Lady Loretta and Lady Annie deposits are situated within the drainage basin-divide zone where de Keyser (1958) observed lateritic weathering to be best developed. Pre-mid-Mesozoic, early to mid-Tertiary and late Tertiary-Quaternary peneplain erosional surfaces have been recognised in the Mount Isa Basin by Twidale (1964), and it is likely that all three are present in the Lady Loretta area. Additionally, the numerous thin Cambrian outliers throughout the region imply at least subaqueous if not subaerial exposure of the Proterozoic rocks during this period also. These superimposed erosion episodes have

resulted in depths of weathering exceeding 100 m in the Lady Loretta district, deepest oxidation usually being associated with faults. An extreme example of this phenomenon is the 'Mount Lorrie Deep Weathering Trough', defined by drilling as a zone of deep oxidation extending below 320 m depth (Lewis, 1975).

1.3 Thesis organisation

Characteristics of SSHBM deposits in the study region and their regional geological setting are recounted in chapter 2. Compositional, palaeocurrent and sediment provenance aspects of the Proterozoic stratigraphy are emphasised in this review.

Details of the construction of a GIS in conjunction with a relational geodatabase for Bauhinia Downs are given in chapter 3. The rationales for adoption of the data structures utilised are discussed.

A primary aim of analysis of the Bauhinia Downs GIS was the extraction of information pertaining to the three-dimensional evolution of the McArthur Basin over time, from the 2-D and 2.5-D datasets available. Techniques developed to satisfy this aim, and their results, are reported in chapter 4. These techniques are essentially based on incorporation of stratigraphic thickness data with surface geological mapping. Their integration with geophysical interpretations is used to infer basin architecture present around the time of HYC mineralisation. Constraints on metallogenic models for HYC in the context of the McArthur Basin are also evaluated using the GIS.

Chapters 5 and 6 are devoted to a laboratory-based study of the petrophysics of the Carpentaria Zinc Belt, centred on the Lady Loretta deposit. Density, porosity, magnetic susceptibility, sonic velocity, galvanic resistivity, chargeability and gamma ray emission were measured. Chapter 5 is concerned with the bulk physical properties of regional stratigraphic units. Most formations, in particular those immediately preceding and including the Lady Loretta mineralisation were extensively sampled from drillcore. After integration with data previously reported in the literature, the petrophysical results are discussed in terms of their implications for interpretation of regional geophysical surveys, in particular potential field data. Relationships between geochemical composition and physical properties are also evaluated through comparison with geochemical data derived from a subset of the petrophysically-measured samples.

Physical properties of Carpentaria Zinc Belt SSHBM ore bodies and their host rocks are examined in chapter 6. Density, magnetic susceptibility, sonic velocity, resistivity and chargeability results from numerous samples obtained from drillcore at Lady Loretta are compared with similar data from other Carpentaria Zinc Belt SSHBM deposits. Most of the latter were obtained from the literature, supplemented by some extra determinations on additional samples available to the project from HYC, Hilton and Mount Isa. Rocks from geochemical haloes as well as apparently barren host material adjacent to the deposits were also measured. Their contrast in physical properties with those of ore samples is used to suggest geophysical methods most likely to aid detection of base metal mineralisation.

Qualitative interpretations resulting from the integration of digital geological data with airborne magnetic and radiometric data flown over Paradise Valley are reported in chapter 7. Each stratigraphic unit

examined is characterised in terms of its apparent magnetic and radiometric signature. Following this, unit-specific stretches of the geophysical data are performed in order to maximise contrast within the units, with anomalous compositions and structures consequently emphasised. In some cases these are interpreted in terms of alteration, which may denote the generation or passage of base metal-mineralised fluids. Most radiometric features in sedimentary units are interpreted in terms of sediment provenance and basin analysis.

Chapter 8 reports results from quantitative analysis of gravity and airborne magnetic data, the former being mainly surveyed by the author. A series of interlocking 2-D forward models constructed in an array across the Paradise Valley study area is presented. These are discussed with particular reference to major structural features revealed in the models. Structural surface and thickness maps generated from the 2-D modelling are used to interpret the basin history of the Paradise Valley region. The possible role of identified syn-depositional structures in generating and localising base metal mineralisation at Lady Loretta is discussed.

Key results from all chapters are summarised in chapter 9. These are used to synthesise an integrated approach to base metal exploration in the Carpentaria Zinc Belt using GIS and geophysics. A model suggesting how base metal bearing fluids might have been generated, forced to migrate and localised at Lady Loretta is presented.

1.4 Data management and presentation

All GIS data was edited, analysed and stored using Arc/Info software produced by Environmental Systems Research Institute of Redlands, California, USA. Geophysical image analysis and profile extraction was performed using Earth Resources Mapping's ER Mapper software.

All spatial data are referenced to the 1966 Australian Geodetic Datum. Maps presented are in the Universal Transverse Mercator projection, unless stated otherwise. The Bauhinia Downs GIS is in UTM zone 53, while Paradise Valley is in UTM zone 54.

2. Regional Geology and Mineralisation

2.1 Introduction

This chapter describes the geological framework of the Carpentaria Zinc Belt, with particular reference to those areas studied in detail in this thesis. Emphasis is given to the bulk compositional characteristics of units, especially those directly affecting their physical properties. This is coupled with sedimentological and other observations most pertinent to the structural evolution of the McArthur and Mount Isa Basins. These are reviewed within the regional stratigraphic framework currently established in the literature for each basin, supplemented where possible by radiometric dating results.

Salient characteristics of base metal mineralisation in the region are briefly summarised, with emphasis given to Zn-Pb deposits generally and the Lady Loretta deposit in particular. Some further details of Carpentaria Zinc Belt orebodies are given in chapter 6.

2.2 Geology of the Carpentaria Zinc Belt

The geology of the Carpentaria Zinc Belt (Sweet et al., 1993) is essentially that of the Mount Isa Basin (McConachie et al., 1993) and southern McArthur Basin, a belt of Palaeo- to Mesoproterozoic rocks over 1000 kilometres long and several hundred kilometres wide (Fig. 1.1). Metamorphic grades vary regionally from essentially unmetamorphosed in the McArthur Basin to granulite facies in the southeastern Mount Isa Basin. The Murphy Inlier separating the Mount Isa Basin from the McArthur Basin contains metamorphic basement to the subsequent basin sequences, as does the southeastern portion of the Mount Isa Basin. The Carpentaria Zinc Belt is surrounded by Phanerozoic basins which are filled with sediments from most periods of this eon, but which generally have either Cambrian or Cretaceous sediments exposed at the surface today. Typical of these is the Georgina Basin to the southwest, which contains sediments ranging from late Precambrian to Devonian in age. Remnants of Cretaceous sedimentation are scattered across much of the area.

The entire region has experienced weathering for much of the Tertiary Period (Twidale, 1964). Usually lateritic, this weathering is regionally best developed in the vicinity of the watershed boundary between the Gulf Fall (Stewart, 1954) and Lake Eyre interior drainage systems (de Keyser, 1958). Outcrops of weathering-resistant Proterozoic rocks presently comprise the vast majority of positive topographic features, rising above plains of Quaternary alluvium and black soil veneering Phanerozoic sediments and recessive Proterozoic units. Though relief in any given locality rarely exceeds 150 metres, the total elevation range over the whole region is from sea level on the Gulf of Carpentaria coast to a maximum of 550 m in the southern Mount Isa Basin.

2.3 McArthur Basin

The McArthur Basin extends northwest from the Murphy Inlier along the western coast of the Gulf of Carpentaria into eastern Arnhem Land. Only the area of the Bauhinia Downs 1:250,000 map sheet was examined in detail in this thesis (Fig. 1.1). The discussion of McArthur Basin stratigraphy below thus focuses on units present in this district. Units of the sequence including and preceding HYC mineralisation (Fig. 2.1) are examined in most detail, as these will have the greatest bearing on metallogenic hypotheses for the deposit. This section of the McArthur Basin is best exposed in central portion of the Bauhinia Downs study area (Fig. 2.2), in the area known as the Batten Fault Zone or Batten Trough. Other tectonic elements of this part of the McArthur Basin are the largely flat-lying Wearyan Shelf extending west of the Emu Fault to the Murphy Inlier, and the gently folded Bauhinia Shelf east of the Tawallah Fault.

2.3.1 Stratigraphy

2.3.1.1 Scrutton Volcanics

The oldest unit exposed in the study area, the Scrutton Volcanics, are dated at 1857±30 Ma (Pietsch et al., 1991). They are correlated with the Cliffdale Volcanics in Murphy Inlier and the Leichhardt Volcanics in the Mount Isa Basin (see below). These units are all related to the Barramundi Orogeny continent-wide deformation and felsic magmatism (Etheridge et al., 1987). The Scrutton Volcanics were probably erupted immediately following the most intense Barramundi Orogeny tectonism (Rawlings, 1994). They consist of thick pyroclastic sheets of K-rich dacitic and rhyodacitic composition, with minor felsic and mafic lavas.

2.3.1.2 Tawallah Group

The Tawallah Group represents the Redbank package (Rawlings, 1999), and as such is believed to have a depositional age range of 1815-1710 Ma. It is composed of sandstones with bimodal igneous intrusions and lavas, lutite, conglomerate and dolostone. Three cycles of sedimentation and igneous activity have been recognised within the Tawallah Group (Rogers, 1996), which may represent several superimposed basin phases (Rawlings, 1999).

The Yiyintyi Sandstone and Sly Creek Sandstone at and near the base of the Tawallah Group represent at least 3.5 km of siliciclastic material, out of a total Tawallah Group maximum stratigraphic thickness of a little over 5 km (Pietsch et al., 1991). Other predominantly sandstone units higher in the Tawallah Group are the Wununmantyala Sandstone and Warramana Sandstone, which together represent an additional sandstone thickness of up to 640 m. Depositional environments for the Tawallah Group sandstone units are mainly braided river and braidplain to nearshore settings (Rogers, 1996).

The Yiyintyi/Sly Creek Sandstone sequence is interrupted by the Seigal Volcanics, a major episode of mafic flood volcanism. Thicknesses up to 1600 m (Rawlings, 1999) imply correspondingly large volumes of extruded mafic material. The later Settlement Creek Volcanics and Gold Creek Volcanics,

which are largely dolerite sills intruding the Wollogorang Formation, represent a later phase of mafic magmatism of lesser volume than the Seigal Volcanics, with total thickness not exceeding 300 m. All three mafic igneous units have sub-alkaline tholeiitic compositions, with REE relationships consistent with an intraplate tectonic setting (Rogers, 1996).

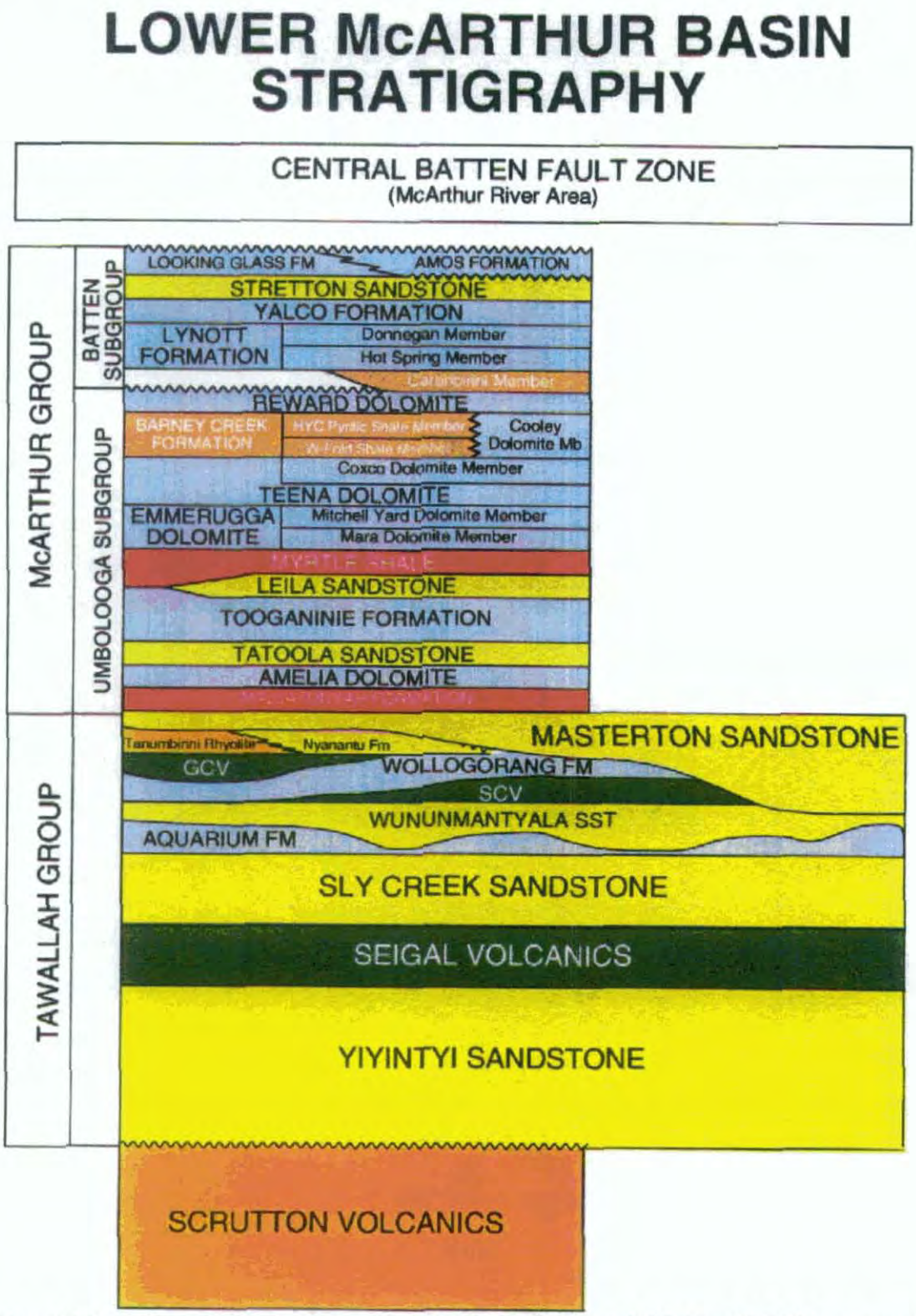

Figure 2.1 Lower McArthur Basin stratigraphy, modified after Pietsch et al. (1991) and S. Bull (pers. comm., 1998). Units are colour-coded according to dominant composition, with felsic volcanics orange, sandstones yellow, mafic igneous units green, dolostones light blue, oxidised shales and siltstones red and reduced carbonaceous shales and siltstones brown

The Aquarium Formation and Wollogorang Formation are mainly dolomitic with some interbedded sandstone. The Wollogorang Formation also contains bituminous nodules and disseminated sulphides in mudstones (Pietsch et al., 1991). Both were deposited in shallow subaqueous environments (Rogers, 1996) and have fairly constant thickness across the study area (100-200m; Pietsch et al., 1991).

At the top of the Tawallah Group, the Tanumbirini Rhyolite dated at 1713±7 Ma (Page and Sweet, 1998) comprises localised rhyolite domes with associated subaerial lava flows. These were erupted amongst a braided river depositional environment (represented by sandstones of the Nyanantu Formation, which is not preserved in the study area). The Tanumbirini Rhyolite is the only example of felsic magmatism in Tawallah Group. Outcropping examples are thin (< 100 m) but represent part of an extensive predominantly felsic magmatic episode in the McArthur Basin (Fagan Phase; Rawlings, 1994).

2.3.1.3 McArthur Group - Umbolooga Subgroup

The carbonate-dominated McArthur Group approximates to the Glyde package (Rawlings, 1999) and is correlated with the Fickling, McNamara and Mount Isa Groups of the Mount Isa Basin. The Umbolooga Subgroup comprises approximately the lower two-thirds of the McArthur Group in thickness terms.

While sandstones are relatively minor constituents of the Umbolooga Subgroup, they are most common in its lower portion. The Masterton Sandstone at the base of the Umbolooga Subgroup is a fine to medium grained quartzarenite. It was unconformably deposited on the Tawallah Group, incising as deep as the Wununmantyala Sandstone (Fig. 2.1). Highly variable thickness across the region from 50 to 600 m, and the common appearance of conglomerate at the base, are interpreted to indicate a high relief palaeosurface prior to Masterton Sandstone deposition (Pietsch et al., 1991). This deposition was mainly in alluvial fan and braided river environments, with beach and intertidal facies becoming more prevalent towards the top of the formation (Jackson et al., 1987). The Tatoola Sandstone, the other main sandstone unit in Umbolooga Subgroup, was deposited in a deeper, subtidal but storm-affected environment, changing up sequence to intertidal with intermittent emergence (Jackson et al., 1987). The Tatoola Sandstone's thickness is regionally variable from <20 m to 350 m. The uppermost sandstone unit in Umbolooga Subgroup, the Leila Sandstone, is volumetrically insignificant (<30 m thick), but is an important marker bed (Pietsch et al., 1991). Both the Tatoola Sandstone and Leila Sandstone have a significant dolomitic component, and gradational conformable contacts with the predominantly dolomitic units enclosing them.

The Mallapunyah Formation overlying the Masterton Sandstone also has a dolomitic component, but is mainly composed of oxidised shale and siltstone. It commonly contains pseudomorphed evaporite minerals, which together with botryoidal quartz ('cauliflower chert') nodules after anhydrite and desiccation cracks constitute evidence for predominant continental and coastal sabkha deposition (Jackson et al., 1987). The Mallapunyah Formation ranges in thickness from 100 to 400 m (Pietsch et al., 1991). The only other oxidised shale and siltstone unit in McArthur Group is the thin (40-60 m) Myrtle Shale overlying the Leila Sandstone. It also is interpreted as an evaporitic redbed unit with a possible aeolian component, deposited in a lacustrine and/or low-gradient alluvial plain setting (Jackson et al., 1987).

Dolostone, usually fine grained, is the most prevalent lithology in Umbolooga Subgroup. Evaporite mineral pseudomorphs are common in most dolomitic Umbolooga Subgroup units, which together with other sedimentological evidence such as desiccation cracks and stromatolites have been used to suggest marginal marine sabkha and saline lacustrine depositional environments. The first significant appearance of dolostone in the Umbolooga Subgroup, the Amelia Dolomite above the Mallapunyah Formation, is mainly dololutite ranging from 50 to 180 m thickness (Pietsch et al., 1991). The 200 m-thick Tooganinie Formation above the intervening Tatoola Sandstone is of similar composition to the Amelia Dolomite, with dolomitic shale and siltstone interbeds. Above the Myrtle Shale, the Emmerugga Dolomite and Teena Dolomite represent the thickest dolostone development in Umbolooga Subgroup, up to 700 m thick. The comparatively thin Teena Dolomite (~70 m) is distinguished by intercalated siliciclastics, with its Coxco Dolomite Member at the top containing distinctive acicular radiating crystal casts ('coxco needles'). The Emmerugga Dolomite has abundant stromatolites near its base, but towards the top is massive with few internal features. At the top of the Umbolooga Subgroup, the Reward Dolomite has a large thickness range (30-350 m), similar to the underlying Barney Creek Formation with which it has a gradational contact. The Reward Dolomite contains pseudomorphs after pyrite as well as sulphate minerals (Pietsch et al., 1991).

The Barney Creek Formation is a dolomitic, carbonaceous and pyritic shale and siltstone. As such, it is the only reduced unit in Umbolooga Subgroup. The Barney Creek Formation hosts the HYC mineralisation. Its thickness is highly variable, from 10 to 900 m (Pietsch et al., 1991). A SHRIMP zircon age derived from tuffaceous beds in the Barney Creek Formation is 1639±2 Ma (Page and Sweet, 1998).

2.3.1.4 McArthur Group - Batten Subgroup

The Batten Subgroup is generally still more dolomitic than the Umbolooga Subgroup. Although its boundary with the Umbolooga Subgroup is defined by a local regolithic unconformity surface developed at the top of Reward Dolomite, the Reward Dolomite contact with the Caranbirini Member at the base of the Batten Subgroup may be conformable when the latter is present. The age of the Batten Subgroup is well constrained by SHRIMP zircon ages of 1625±2 Ma for the Stretton Sandstone and 1614±4 Ma for the Amos Formation (Jackson et al., in press quoted in Rawlings, 1999).

The Lynott Formation at the base of Batten Subgroup essentially consists of dolomitic siltstone. The Caranbirini Member at its base additionally contains carbonaceous pyritic shale, similar to the Barney Creek Formation. Also similar to Barney Creek Formation is the Caranbirini Member's highly variable stratigraphic thickness (0-300 m; Pietsch et al., 1991) and interpreted sub-wavebase euxinic depositional environment (Rawlings, 1999). The Caranbirini Member is a significant contributor to overall Lynott Formation thickness variability (50-600 m). Overlying the Lynott Formation, the Yalco Formation has similarly variable thickness (<50-250 m) of mainly stromatolitic dolostone. The sequence from the top of the Caranbirini Member to the top of the Yalco Formation is interpreted to have been deposited in mainly intertidal to supratidal and sabkha environments. The laterally equivalent Amos Formation and Looking Glass Formation at the top of Batten Subgroup are both mainly composed of dolostone, not known to

exceed 90 m thickness. A depositional date of 1614±4 Ma has been obtained for the Amos Formation (Jackson et al., in press; quoted in Rawlings, 1999).

The Stretton Sandstone is the only significant siliciclastic unit in the Batten Subgroup. Its thickness is highly variable, ranging up to 270 m. The presence of glauconite in the Stretton Sandstone is interpreted to indicate deposition in a shallow marine environment.

2.3.1.5 Nathan Group

The Nathan Group generally overlies the McArthur Group unconformably, although radiometric dates of 1613±4 and 1609±3 Ma (cf. Amos Formation, above) and a paraconformable relationship observed near the base of the Nathan Group in the southern portion of the study area led Rawlings (1999) to group this part of the Nathan Group with the McArthur Group in his basin-wide Glyde package. Elsewhere, basal polymict conglomerate and pebbly lithic (chert) sandstone in the Smythe Sandstone mark the base of the Nathan Group. The remainder of the Nathan Group mainly consists of dolostone contained in the Balbirini Dolomite (up to 1500 m thick) and Dungaminnie Formation (up to 240 m thick), though there are beds of fine sandstone and siltstone in the lower portion of the latter. Thickness variations in Nathan Group are mostly due to post-depositional erosion. A date of 1589±3 Ma from the middle of the Balbirini Dolomite is held to best represent the age of the main part of the Nathan Group (Rawlings, 1999).

2.3.1.6 Roper Group

The Roper Group is almost entirely siliciclastic, being mainly composed of quartz sandstone with micaceous siltstone (Plumb et al., 1990). Its base is marked by a regional unconformity developed on the Nathan and McArthur Groups. The Roper Group thickens from east to west across the Bauhinia Downs study area, from less than 1 km up to 5 km, marking a substantial shift in depocentre from the earlier McArthur Basin sequences (Plumb and Wellman, 1987). It consists of nine formations deposited in a series of five upward-coarsening cycles (Jackson et al., 1988), and characterises the basin-spanning Wilton package of Rawlings (1999). Numerous dolerite and gabbro dykes and sills intrude the Roper Group, but there is no evidence that these are volumetrically significant in the study area. One of these, dated at ~1280 Ma (K-Ar), provides a minimum age constraint on the Roper Group (McDougall et al., 1965). A diagenetic illite Rb-Sr age of 1429±31 Ma from near the top of the Roper Group (Kralik, 1982) pushes its likely depositional age further back towards 1500 Ma.

2.3.1.7 Phanerozoic

Cambrian sandstones (Bukalara Sandstone) and limestones (Top Springs Limestone) of the Georgina Basin blanket portions of the study area. These are generally only a veneer not exceeding 100 m thickness, but the Bukalara Sandstone is up to 300 m thick in the Abner Range, in the south of the McArthur Basin study area.

Isolated outliers of Cretaceous conglomerate, sandstone, siltstone and mudstone, usually less than 20 m thick (Pietsch et al., 1991) are scattered across much of the southern McArthur Basin. Cainozoic

sediments also overlie much of the McArthur Basin study region, concealing large areas of Proterozoic section in the subsurface.

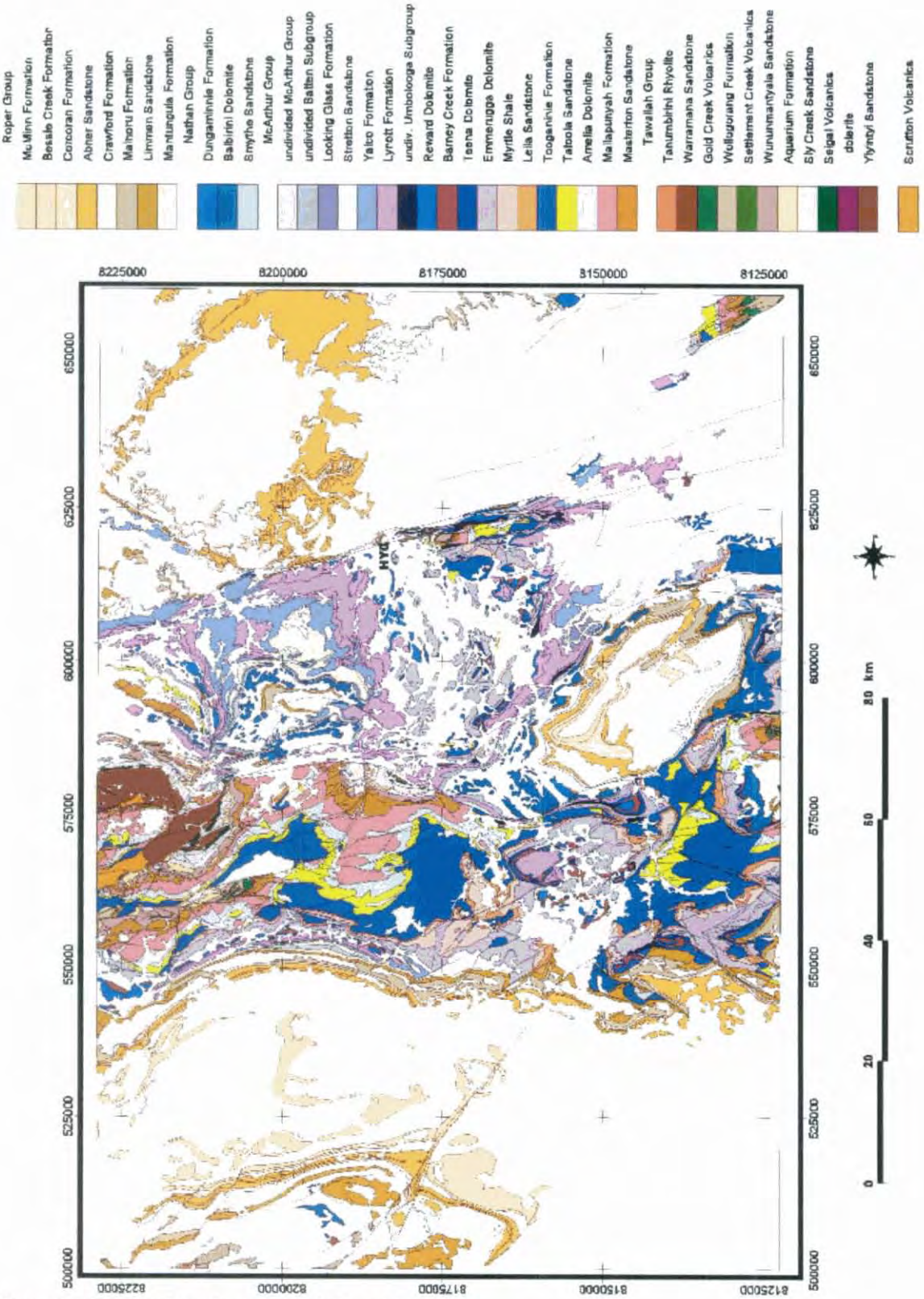

Figure 2.2 Proterozoic geology, Bauhinia Downs study area

2.3.2 Structure and tectonic evolution

The McArthur Basin is widely recognised to have been subjected to several episodes of structural development and stress regimes, both compressional and extensional (Plumb, 1987; Etheridge and Wall, 1994; Rogers, 1996; Leaman, 1998). An intracratonic rift-sag geodynamic framework has generally been assumed, with most dispute concerned with extension controls, magnitude, direction and timing in this context. The following short synthesis of McArthur Basin tectonic evolution draws mainly on common or complementary components of the proposed models.

Basement to McArthur Basin was deformed, metamorphosed and subjected to significant felsic magmatism prior to ~1850 Ma, during the Barramundi Orogeny. The resulting structural framework is generally accepted to have controlled subsequent structural development (Rawlings, 1999). Various fundamental basement influences have been identified, with northeast, north-northwest and northwest trends being the most common (Etheridge et al., 1987; Etheridge and Wall, 1994; Scott et al., 1997; Leaman, 1998). These have been repeatedly reactivated during the evolution of the McArthur Basin by a succession of extension, thermal subsidence and compression regimes.

North-south extension during Tawallah Group deposition was interrupted by east-west compressional event in mid-Tawallah Group time (Bull and Rogers, 1996). This was followed by a period of thermal subsidence (Etheridge and Wall, 1994) during which the McArthur Group was deposited. Extension causing block faulting was apparently superimposed on regional subsidence at the commencement of Barney Creek Formation deposition, resulting in north-northwest to south-southeast and east-west trending half-graben west of the Emu Fault (Neudert and McGeough, 1996), which may have been active as a transfer fault at this time. The McArthur Basin experienced inversion soon after due to a northwest-southeast compressional event (Rogers, 1996), possibly simultaneous with HYC mineralisation which occurs towards the top of the Barney Creek Formation (Hinman et al., 1994; Hinman, 1996). N-S trending depocentres redeveloped subsequently according to Neudert and McGeough (1996), creating accommodation space for subsequent sedimentation up to and including the Caranbirini Member. Relatively quiescent thermal subsidence then appears to have been the main influence on basin development, at least until Roper Group deposition. The final major structural event in the McArthur Basin was northeast-southwest-directed shortening which affected all Proterozoic units including the Roper Group (Rogers, 1996). Apparent reactivations of N-S trending faults affecting Cambrian units may be related to far-field effects of Australian Phanerozoic tectonic events such as the Alice Springs Orogeny.

In spite of a long structural history, McArthur Basin strata are generally only gently folded with shallow dips. Some exceptions exist near faults where bedding often steepens to 20-40°, and occasionally up to 70° (Pietsch et al., 1991). While little is known of fault attitudes at depth, most are considered to be very steep, although some reverse faults with dips as shallow as 60° have been recorded (Plumb et al., 1990).

2.4 *Mount Isa Basin*

2.4.1 Development of continental crust

The present crustal substrate of the Mount Isa Basin was probably created no later than the latest Archaean/earliest Palaeoproterozoic (McCulloch, 1987). The main lines of evidence for this arise from U/Pb dates derived from inherited zircons (2.7 - 2.2 Ga; Page, 1988; Connors and Page, 1995) and Sm-Nd depleted mantle model ages of 2290-2130 Ma which McCulloch (1987) interpreted as representing a period of primary crustal formation. The oldest preserved outcropping rocks in the Mount Isa Basin are however probably much younger than this. A sequence of sediments, volcanics and intrusives was emplaced in the period 2.0-1.9 Ga (Page and Williams, 1988), probably in a basin developed on a primordial continental crust substrate, before experiencing regional metamorphism and deformation in the 1880-1850 Ma Barramundi Orogeny (Etheridge et al., 1987). These rocks comprise basement to the subsequent Mount Isa Basin cover sequences.

2.4.2 Tectono-stratigraphic elements

The Mount Isa Basin has been divided lithostratigraphically and structurally into several sequences/provinces by a number of authors over a period of decades. Tectonic elements were first defined by Carter et al. (1961), and have been refined by Plumb (1979) and Blake (1987). Other schemes have been proposed, notably by McConachie et al. (1993) and Dunnet (1976). Blake (1987) defined a gross stratigraphic framework for the Proterozoic volcano-sedimentary packages which was applied across the entire Mount Isa Basin, dividing them into four major sequences ('basement' plus three 'cover sequences'). The cover sequences are major stratigraphic packages with preserved thicknesses up to several kilometres, interrupted by regional unconformities. This scheme, as refined by absolute age dating, has attained widespread usage amongst workers in the region. It is summarised in section 2.4.2.1, and details of individual formations constituting the cover sequences in the study area are given in section 2.5.

2.4.2.1 Stratigraphic elements

The first of the cover sequences consists largely of felsic volcanics, which have been dated by various radioisotope studies (e.g. Page, 1988) at between 1870 and 1850 Ma. Neither basement nor cover sequence 1 outcrop in the Mount Isa Basin study area, but they are supposed to underlie it (Derrick, 1982). The felsic volcanics have been related by Wyborn (1988) to a continent-wide episode of felsic magmatism associated with the waning stages of the Barramundi Orogeny. Examples of probable correlatives are the Cliffdale Volcanics of the Murphy Inlier and the Scrutton Volcanics in the McArthur Basin.

Bimodal volcanic and sedimentary rocks deposited between ~1790 to 1760 or possibly 1720 Ma (Blake and Stewart, 1992b) constitute cover sequence 2. Cover sequence 3 differs from it in having a proportionally lesser volume of bimodal volcanics, and generally finer siliciclastic rocks. Carbonates are

also much more prevalent in cover sequence 3 than in the older packages. This sedimentary phase was thought to be temporally confined in a relatively narrow range around ~1680–1670 Ma (Blake et al., 1990), but recent work (Page and Sweet, 1998; Carr et al., 1996) has demonstrated that cover sequence 3 sedimentation spans at least the interval from 1710 to 1590 Ma. A fourth Proterozoic episode of basin development probably accompanied or slightly postdated the main phase of the Isan Orogeny, resulting in extensive deposition of siliciclastic sediments (South Nicholson Group). These may once have covered much of the Mount Isa Basin, but today are only preserved in some northern and western parts of it.

2.4.2.2 Tectonic elements

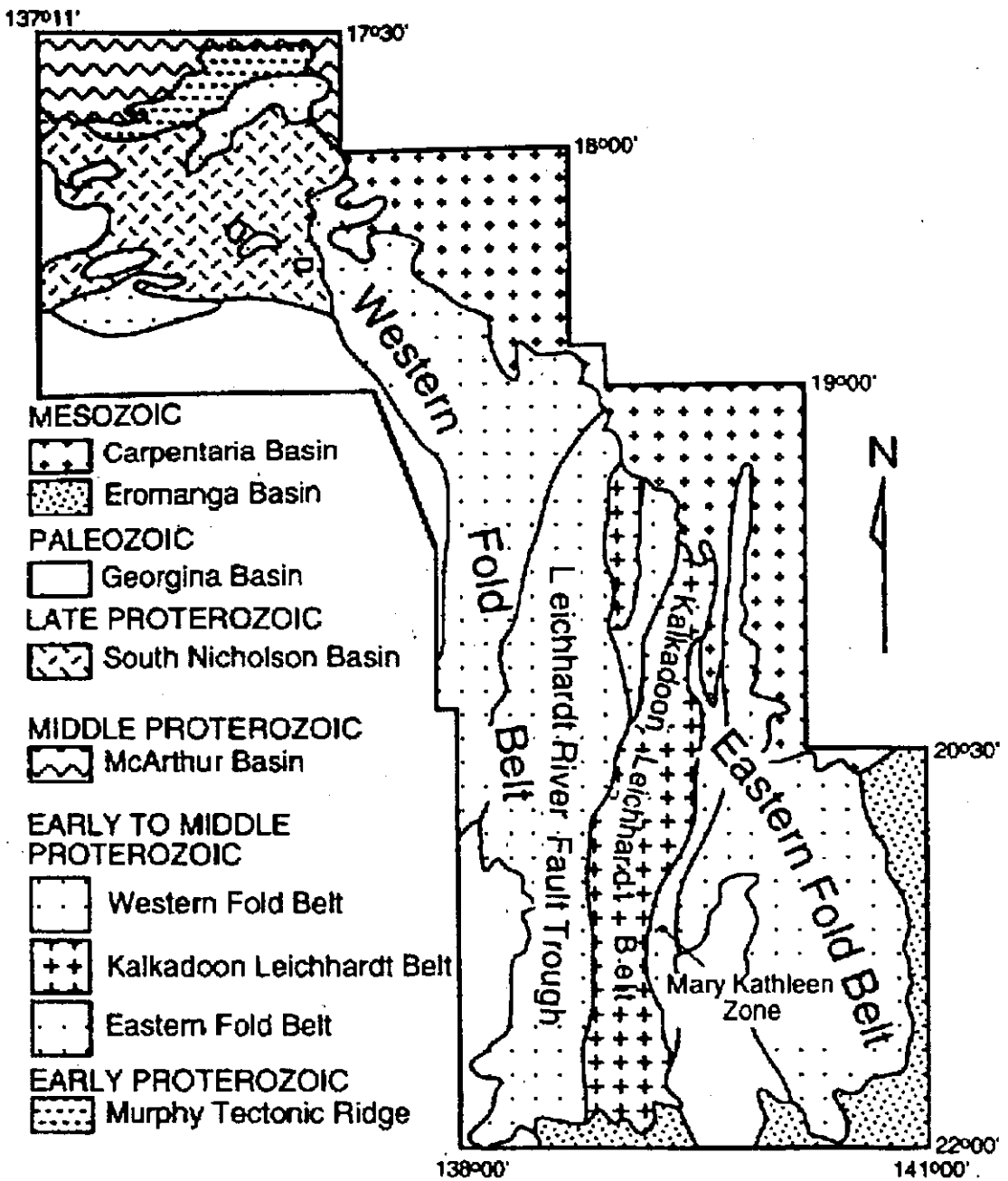

Figure 2.3 Tectonic subdivisions of the Mount Isa 'Inlier' after Blake (1987) and O'Dea et al. (1997a)

Carter et al. (1961) developed a structural subdivision for the Mount Isa Basin (also known as the Mount Isa Inlier; Blake, 1987) which has remained in widespread use with little substantial modification until recently. They recognised western and eastern 'geosynclinal' basins, separated by a central 'tectonic welt'. Each of these terranes is bounded by major faults or changes in structural style. As defined by Blake (1987) and Blake et al. (1990), the three major structural provinces are meridional belts known as (from east to west) the Eastern Fold Belt, Kalkadoon-Leichhardt Belt and Western Fold Belt. The Western Fold Belt has been itself subdivided into the Leichhardt River Fault Trough (LRFT) and, west of the LRFT, Lawn Hill Platform (Fig. 2.3).

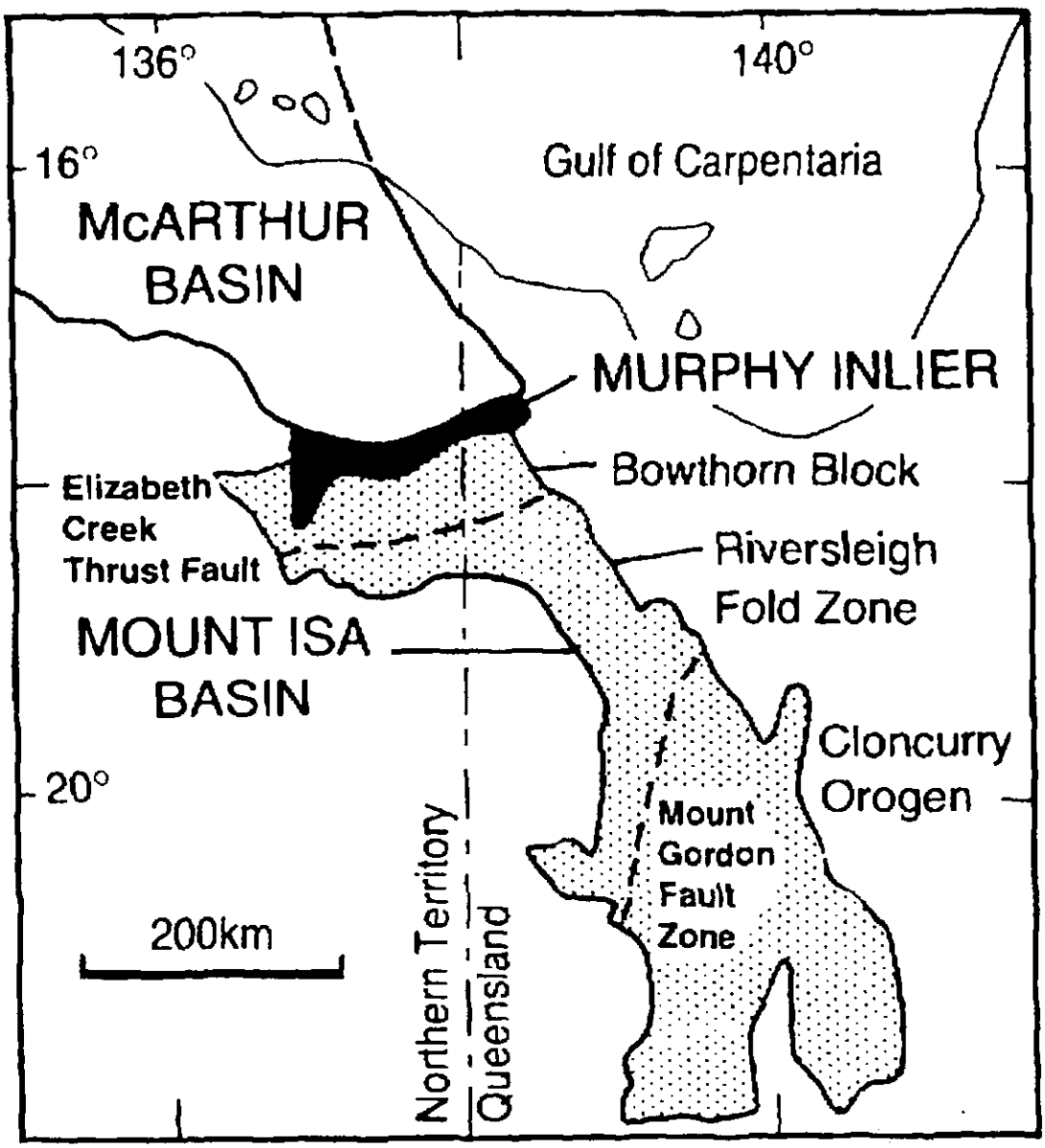

Figure 2.4 Structural elements of the Mount Isa Basin, after McConachie et al. (1993)

This thesis retains much of this conventional nomenclature, but also utilises the terms 'Riversleigh Fold Zone' and 'Bowthorn Block' which McConachie et al. (1993) defined to denote areas of discrete structural styles in the framework of their interpretation of the Mount Isa Basin as a deformed foreland basin (Fig. 2.4). The Riversleigh Fold Zone and Bowthorn Block together are equivalent to the Lawn Hill

Platform. This thesis is mainly concerned with the Leichhardt River Fault Trough and Riversleigh Fold Zone.

2.5 Western Mount Isa Basin Stratigraphy

There are several regions encompassing the western Mount Isa Basin with their own stratigraphic schemes, but they are considered essentially equivalent at most levels (Blake, 1987). Only units represented in the Paradise Valley study area are described here. The oldest and youngest portions of the Mount Isa Basin sequence, while not outcropping in the study area, are additionally included for completeness.

2.5.1 Pre-Barramundi Orogeny basement

Basement outcrops are seldom exposed in the Western Fold Belt, being confined to the far south, west (Yaringa Metamorphics, west of Mount Isa) and far north and north-west (Murphy Metamorphics, in the Murphy Inlier and Carrara Range). They are composed of deformed pelitic, felsic, chlorite-sericite and pyritic carbonaceous schist, gneiss and minor migmatite and amphibolite, and were metamorphosed into this state during the Barramundi Orogeny between 1890 and 1870 Ma (Page and Williams, 1988). Protoliths to this assemblage were thought to be turbidites, felsic volcanics and granite by Blake et al (1990).

2.5.2 Cover sequence 1

Representative units of cover sequence 1 do not outcrop within the Western Fold Belt, however they are thought to be present at depth (Derrick, 1982). The nearest exposed equivalents are the predominantly felsic Leichhardt Volcanics within the Kalkadoon-Leichhardt Belt, which comprise the bulk of cover sequence 1. These were erupted from 1870 to 1850 Ma - in the latter stages of the Barramundi Orogeny - and consist of subaerial felsic ignimbrites with some rhyolite and dacite lavas. The Kalkadoon Batholith and Ewen Batholiths intruded the Leichhardt Volcanics, and are at least partly co-magmatic with them (Wyborn and Page, 1983); having similar chemistry and radiometric dates (around 1860-1840 Ma). Granodiorite and monzogranite are the most common lithologies in the Kalkadoon-Ewen Batholiths and their correlates throughout the Mount Isa and McArthur Basins (Wyborn, 1988). 'Small amounts' of magnetite were noted in lower greenschist and upper amphibolite grade Kalkadoon and Ewen Batholith samples by Wyborn and Page (1983).

2.5.3 Bottletree Formation

The Bottletree Formation is included in cover sequence 2, but is not exposed in the study area. It consists of bimodal volcanics and clastic sediments, which lie unconformably on the Kalkadoon Granite and basement rocks. The felsic component of the Bottletree Formation volcanics has been dated at around 1790 Ma (Page, 1983). Eriksson et al. (1992) included the Bottletree Formation with the lowermost Haslingden Group in the first of two rift-sag cycles that they defined within cover sequence 2.

2.5.4 Haslingden Group

The Haslingden Group is the main constituent of cover sequence 2 in the Western Fold Belt, and outcrops of this unit dominate the Leichhardt River Fault Trough in particular. Its thickness ranges from 6000 to over 18000 m (Derrick et al., 1976). West of the study area the Haslingden Group is observed to overlie felsic volcanics of the Bottletree Formation (also classified as part of cover sequence 2) which have been dated at 1790 Ma (Page, 1983). A minimum age constraint of 1740 Ma for the Haslingden Group may be inferred by correlation of the overlying Quilalar Formation with the Corella Formation (Page, 1983).

2.5.4.1 Leander Quartzite

The Leander Quartzite at the base of the Haslingden Group is the oldest unit exposed in Paradise Valley, within the Leichhardt River Fault Trough in the western part of the region. It is only observed in the core of anticlinal structures, associated with significant vertical displacement on bounding faults. The most common rock type observed in outcrop is medium-grained orthoquartzite, though feldspathic quartzite, sandstone and, rarely, mafic volcanics are also present. The Leander Quartzite is correlated with the Mount Guide Quartzite in exposures of Haslingden Group to the south (Carter et al., 1961), which has been interpreted as being deposited in a clastic shoreline depositional environment (Simpson and Eriksson, 1991). The thickness of the Leander Quartzite exceeds 1000 m, and may be considerably greater. It is overlain, apparently conformably, by the Eastern Creek Volcanics.

2.5.4.2 Eastern Creek Volcanics

The Eastern Creek Volcanics are an extremely thick accumulation of tholeiitic basalts with relatively minor intercalated siliciclastic beds. The unit outcrops extensively in the southeastern corner of the study area; in the Leichhardt River Fault Trough and in tightly folded elongate slivers associated with the Mount Gordon Fault Zone. It is also exposed in the core of the Fiery Creek Dome north of the study area. A regional total-rock Pb-Pb age of 1710±50 Ma was determined by Gulson et al. (1983), consistent with a minimum age of 1740-1730 Ma derived from the Burstall Granite, which intrudes the Eastern Creek Volcanics (Page, 1983).

The oldest of the three members which constitute the Eastern Creek Volcanics, the Cromwell Metabasalt Member, is about 2500 m thick in the Paradise Valley study area (Hutton and Wilson, 1985), but is known to be over 5000 m thick to the south (Derrick et al, 1976). Most basalt flows are from 20 to 50 m thick, being well defined by amygdaloidal bases and tops, and massive, coarse to medium-grained fining-upward middle sections. The metabasalts are mainly composed of plagioclase with chlorite, actinolite and minor quartz, sphene and opaques. Sediments intercalated with the basalt flows towards the top of the Cromwell Metabasalt (Paroo Beds of Robinson, 1968) consist of dolomitic siltstones, sandstones and quartzites.

The Lena Quartzite Member is a substantial (up to over 300 m thickness) sequence of fine-grained feldspathic quartzite and orthoquartzite, denoting a hiatus in volcanism within the Eastern Creek Volcanics. It generally thins from north to south-south-west within the study area. Palaeocurrents from

the south-east are indicated by cross-bedding in south-eastern Paradise Valley (Hutton and Wilson, 1985) but to the north range from north-west to north-east (Hutton and Wilson, 1984).

At the top of the Eastern Creek Volcanics, the Pickwick Metabasalt Member is composed similarly to the Cromwell Metabasalt, exceptions being the greater abundance of relict primary clinopyroxene, opaques and apatite in the Pickwick Metabasalt. The metabasalt is mostly fine-grained and aphyric (Hutton and Wilson, 1984). Its thickness varies between 200 and 500 metres in Paradise Valley.

Alteration is nearly ubiquitous in the Eastern Creek Volcanics, although the majority of it appears to have been isochemical (Wilson et al., 1985). While primary basaltic textures are commonly preserved in the most common alteration type, original calcic plagioclase has invariably been pseudomorphed by albite, and the primary ferromagnesian minerals have been replaced by chlorite and actinolite. These comparatively little-altered samples have chemical compositions similar to continental tholeiites (Hutton and Wilson, 1985).

The Kamarga Volcanics exposed in the Kamarga Dome approximately 100 km north of the study area are possible equivalents of the Eastern Creek Volcanics.

2.5.4.3 Myally Subgroup

The Myally Subgroup represents a return to siliciclastic sedimentation following the massively voluminous mafic volcanism of the Eastern Creek Volcanics, though some of this mafic magmatism persists into the lower Myally Subgroup in the form of dolerite sills and minor basalt flows. It comprises a series of four formations, all of which are in conformable relationship with each other.

The Alsace Quartzite conformably overlies the Pickwick Metabasalt, and is composed of fine- to medium grained, slightly feldspathic and clayey sandstone, with subordinate thick-bedded medium- to coarse-grained orthoquartzite. Palaeocurrents from the north and northwest are indicated by cross-bedding (Hutton and Wilson, 1985). The unit is 50-300 m thick.

The Bortala Formation reaches a thickness of up to 500 m within the north-eastern portion of the Paradise Valley study area, but is generally 100-200 m thick. It comprises fine-grained feldspathic sandstone, quartzite, ferruginous dolomitic sandstone and silicified siltstone. The majority of cross-beds indicate south-west to southerly-derived palaeocurrents, but most ripple marks record currents from the north-east (Hutton and Wilson, 1984).

Conformably overlying the Bortala Formation is the Whitworth Quartzite, which consists of coarse to medium-grained quartzite interbedded with medium to fine-grained feldspathic sandstone, as well as ferruginous, locally dolomitic, clayey sandstone. An amygdaloidal metabasalt layer 40 m thick has been recognised within the Whitworth Quartzite near Mammoth Cu deposit (Scott and Taylor, 1982). Palaeocurrents generally range in direction between easterly and northerly sources, with a subordinate component from the south and south-west (Hutton and Wilson, 1984 and 1985). Exceptions have been noted in westerly exposures, where a westerly source component is apparent (Hutton and Wilson, 1984). The formation is around 1000 m thick, but thins to approximately 200 m in south-eastern Paradise Valley.

The uppermost unit of the Myally Subgroup is the Lochness Formation, comprising dolomitic feldspathic sandstone, dolomitic siltstone and clayey ferruginous sandstone, accompanied by other minor siliciclastic and dolomitic components. Palaeocurrents range from the north and south are indicated by cross-bedding, with a westerly component becoming dominant in outcrops to the north (Hutton and Wilson, 1984). The Lochness Formation appears to be the most compositionally immature of the Myally Subgroup formations, with up to 30% lithic fragments in some sandstone samples (Hutton and Wilson, 1984), in contrast to the Alsace Quartzite at the base. The Lochness Formation is usually about 400 m thick (Hutton and Wilson, 1985).

Depositional environments of the Myally Subgroup may be generally characterised in the range between fluvial and nearshore marine settings, with shallow lacustrine facies incorporating periodic subaerial emergence common. The presence of significant amounts of ferruginous minerals, particularly haematite and limonite towards the top of the Lochness Formation, have been attributed to deposition in an arid climate (Hutton and Wilson, 1985) or to palaeosol preservation (Derrick et al., 1976).

The sequence from the base of the Haslingden Group up to and including most of the Myally Subgroup has been widely interpreted as being deposited in a rift setting (Derrick, 1982; 'Leichhardt Rift', O'Dea et al., 1997b). The remainder of cover sequence 2, being the mixed quartz-carbonate Quilalar Formation (see below) and possibly the upper Myally Subgroup, has been commensurately ascribed to the 'sag' phase of the rift-sag geodynamic model, for example by O'Dea et al. (1997a).

2.5.4.4 Quilalar Formation

Though not formally defined as part of the Haslingden Group, the Quilalar Formation is concordant with the Myally Subgroup, and conformably overlies the Lochness Formation, but is only present in the northeastern corner of Paradise Valley. Two sub-units are distinguishable; the lower, composed mainly of siliciclastics (orthoquartzite and feldspathic sandstone), was probably deposited in tidal channels and lagoons (Hutton and Wilson, 1985) on a platform marginal to a N-S trending trough within an intracratonic basin (Jackson et al., 1990). A deep ocean basin to the north and/or south of the intracratonic basin was also postulated by Jackson et al. (1990). The upper sub-unit contains a greater proportion of carbonates, with dolomitic siltstone and mudstone, stromatolitic dolomite and tuff. These were deposited in lagoonal or shallow marine shelf environments, with a N-S shoreline trend (Derrick et al., 1980). Geodynamically, Quilalar Formation deposition is ascribed to the second sag phase of cover sequence 2, following rift-related volcanism and sedimentation (Jackson et al., 1990).

The Quilalar Formation is over 1000 m thick in eastern Paradise Valley (Hutton and Wilson, 1984), but is apparently absent to the southwest. Based on correlations with the Corella Formation (Derrick et al., 1980) in the Cloncurry Orogen, the Quilalar Formation is probably from 1730 to 1740 m.y. old (Page, 1983).

2.5.5 Cover Sequence 3 - Bigie Formation and Fiery Creek Volcanics

Development of cover sequence 3 commenced with renewed coarse clastic sedimentation (Bigie Formation) accompanied by bimodal volcanism of the Fiery Creek Volcanics. The Weberra Granite (~1700 Ma) in the north of the study region appears comagmatic with the Fiery Creek Volcanics (Wyborn et al., 1988), which have been dated radiometrically at 1709±3 Ma (Page and Sweet, 1998). This datum firmly constrains the onset of cover sequence 3 basin development, which has been interpreted as a renewed phase of rifting (Bigie Rift) by Betts et al (1996). The Fiery Creek Volcanics are correlated with the Tanumbirini Rhyolite in the McArthur Basin (Pietsch et al., 1994).

The Bigie Formation was deposited unconformably on a surface which truncates the underlying Myally Subgroup and Quilalar Formation sediments, locally at high angles (Bigie Unconformity of O'Dea et al., 1997a). It comprises highly ferruginous, poorly sorted feldspathic and lithic sandstone, quartzite, dolomitic sandstone and conglomerate. Where present, the thickness of the Bigie Formation varies markedly over distances as short as 2 km (0-800 m near Mount Oxide mine; Hutton and Wilson, 1984) but is generally less than 200 m thick. Palaeocurrents indicated by cross-bedding and ripple marks are generally from the west and northwest, with minor components from the southeast and northeast. These features probably developed in a fluvial environment (Hutton et al., 1981).

The Fiery Creek Volcanics, as originally defined by Hutton et al. (1981) conformably overlie the Bigie Formation, but based on work in the Fiery Creek Dome area in the north of the study area, McPherson (1994) considered these units equivalent. Where the Bigie Formation facies is absent, the Fiery Creek Volcanics unconformably overlies Myally Subgroup or Quilalar Formation. Bimodally composed, with both felsic and mafic lavas and associated ferruginous feldspathic sandstones and conglomerates, the Fiery Creek Volcanics occur only in isolated patches in southern Paradise Valley, but outcrop more extensively to the north. The mafic volcanics are much more widespread than the felsic volcanic rocks, which are largely restricted to the vicinity of rhyolite domes in the north of the study area. Most outcrops of this unit display intense potassic and haematitic alteration. The igneous units of the Fiery Creek Volcanics may be up to 250 m thick.

2.5.6 Surprise Creek Formation

The Surprise Creek Formation was deposited with angular unconformity (Surprise Creek Unconformity of O'Dea et al., 1997a) on older units, but the magnitude of this angle varies from high to sub-parallel within the study area. The implied depositional hiatus is broken only south of the study region by the Carters Bore Rhyolite, a felsic porphyry dated at 1678 Ma (Page, 1978) which is probably largely intrusive, and comagmatic with a phase of the voluminous Sybella Batholith which outcrops extensively south of the study area, west of Mount Isa. The Surprise Creek Formation generally thins westward (Derrick et al., 1980).

The Surprise Creek Formation has been informally divided into two sub-units, designated by Hutton and Wilson (1985) as P_ra and P_rd. P_ra is the coarser of the two, comprising medium to coarse-grained feldspathic sandstone and conglomerate, although a fine-grained feldspathic sandstone and siltstone sub-

unit is distinguishable adjacent to the Mount Gordon Fault Zone (P_ra_2, Figure 2.5). The coarse siliciclastic units contain lithic clasts similar to the underlying Fiery Creek Volcanics and Bigie Formation. Palaeocurrents from the west and northwest have been observed in this sub-unit, which may vary in thickness from 230 m in the west up to 1000 m in the northeast of the study area (Hutton and Wilson, 1984). This is at variance with unimodal current directions from the south and southwest recorded by Derrick et al. (1980) west of the study area. As with the Bigie Formation beneath the basal unconformity, P_ra was deposited in a fluvial environment (Hutton and Wilson, 1985) consistent with derivation from significantly uplifted regions (Derrick et al., 1980).

The subsequent, finer-grained sub-unit, P_rd, consists mainly of fine-grained micaceous siltstones, interbedded with fine-grained feldspathic sandstones. This grain size decrease relative to the lower Surprise Creek Formation may be the result of a marine transgression. When present, P_rd may be up to 500 m thick. In Paradise Valley P_rd appears to have been extensively eroded, with the McNamara Group deposited disconformably on massive basal sandstone (that is, P_ra) of the Surprise Creek Formation (Derrick et al., 1980).

2.5.7 McNamara Group

Siliciclastic sediments were deposited at the base of the McNamara Group, compositionally similar to the underlying Surprise Creek Formation and generally fining upwards. These subsequently gave way to carbonate deposition, the carbonate mainly in the form of dolomite, accompanied by silts and shales. Evidence of extensive biological activity during this period was preserved in the form of stromatolites, as well as widespread carbonaceous shales. Some spatial variation in basin fill composition is apparent in the correlative Mount Isa Group to the south of the study region, wherein silts and shales are predominant over dolomite. Geodynamically, the McNamara/Mount Isa Group has been interpreted as representing the sag phase of basin fill following the rifting initiated at the base of the Bigie Formation (O'Dea et al., 1997a). Rare tuffs within the McNamara Group sedimentary sequence may represent distal volcanism, and zircons contained within them are the source of all the recently acquired absolute age constraints on McNamara Group deposition (Table 2.1). The granitic Sybella Batholith west of Mount Isa and south of the study area is a possible source of at least some of the tuff-depositing volcanism; major phases of it were emplaced between 1664 and 1650 Ma (Connors and Lister, 1995).

Higher in the McNamara Group, carbonate sedimentation diminished in favour of siltstone and sandstone, with carbonaceous shales continuing to comprise a significant portion. Large volumes of turbidites were also deposited at this time. This upper section of the McNamara Group has been best preserved in the northern half of the Western Fold Belt, and together with the lower McNamara Group is correlated with the Fickling Group abutting the southern edge of the Murphy Inlier. Recent radiometric age determinations of supposed tuffs in the McNamara Group (Page, 1997) have demonstrated that McNamara Group deposition continued at least until ~ 1590 Ma. In all, the post-Haslingden Group sequence totals over ten kilometres of sedimentary section, though this is unlikely to have been deposited in any one location. The greatest thicknesses of McNamara Group sediments have been observed in the central Western Fold Belt.

The following sections, predominantly derived from Hutton and Sweet (1985), detail the lithological and sedimentological characteristics of the McNamara Group in the Paradise Valley district. Each formation is considered in stratigraphic order, from oldest to youngest. Reference is made throughout to sequence stratigraphic units defined during recent studies in the Riversleigh Fold Belt and Bowthorn Block by Jackson et al. (1996) and Southgate et al. (1997). A summary of this information is presented in Table 2.1. All references to unit thickness in this section are based on observations from the Paradise Valley study area, unless stated otherwise.

2.5.7.1 Torpedo Creek Quartzite

Medium-grained orthoquartzites, arkosic sandstones and conglomerates of the Torpedo Creek Quartzite initiated the McNamara Group sedimentary phase. They were deposited as a transgressive sand sheet (Jackson et al., 1996) with mild angular unconformity on an erosive surface which cuts across older units including the Surprise Creek Formation down as far as the Whitworth Quartzite in southern Paradise Valley (cf. O'Dea et al., 1997a). These and all other earlier authors are contradicted by Betts et al. (1996) who consider the Torpedo Creek Quartzite an upper member of the Surprise Creek Formation. Palaeocurrents from a south to southeasterly direction have been interpreted from cross bedding, though ripple marks indicate north and northeasterly sources. These structures were formed in high-energy (ranging from alluvial to sub-tidal) environments (Hutton and Wilson, 1985; Jackson et al., 1996). Though 120 m thick in its type section, and absent from the stratigraphic column in some areas, the Torpedo Creek Quartzite attains a thickness of 420 m northwest and west of Gunpowder (Hutton and Wilson, 1985).

2.5.7.2 Gunpowder Creek Formation

The Gunpowder Creek Formation, mainly composed of siltstone and shale with minor sandstone, dolomite and quartzite, conformably overlies the Torpedo Creek Quartzite, though it unconformably overlies the Surprise Creek Formation and Myally Subgroup where the Torpedo Creek Quartzite is absent. The most common facies in the Paradise Valley region is a red and green micaceous siltstone near the base of the formation which is often hundreds of metres thick. The general siliciclastic nature of the lower Gunpowder Creek Formation has been interpreted as a continuation of the Torpedo Creek Quartzite transgression (sequence A of Jackson et al., 1996). Dolomitic and carbonaceous shale become more prevalent near the top of the formation (Hutton et al., 1981; lower sequence B of Jackson et al., 1996), and this facies varies in thickness from near absence up to around one hundred metres. In all, the Gunpowder Creek Formation is up to 1000 m thick.

Group	*Formation/ Subgroup*	*Lithology*	*Thickness (m)*	*Palaeo-environment*	*Palaeo-currents*	*Age (Ma)*	*Sequence*	*Equivalents*
Cainozoic		colluvium, sand, silt, gravel				1		
Mesozoic		conglomerate, sandstone, siltst	0-60	fluvial, shallow marine		100		Gilbert River Fm
Georgina Basin	Cambrian	lmst, slst, phosphorite, sdst	0-330			515		Bukalara Sdst, Top Springs Lmst
South Nicholson#			1400-6900		E, W	1510±120@		Roper Group
McNamara	upper					1636-1589β		Batten Subgroup
McNamara	Riversleigh Siltstone	siltst., car. slst., qtzt., sdst., dlst.		lagoon, shallow marine				Lynott Fm.
McNamara	Shady Bore Quartzite	qtzite, sandstone, slst., dlst.	250	marine shoreline				
McNamara	Lady Loretta	dolostone, dmt. slst., car. py. shle	650-1800	intertidal→supra-tidal flats		1647#		Barney Ck. Fm., Teena Dolomite
McNamara	Esperanza	chert, siltstone, sandstone, dlst.	80-350	subtidal→supra-tidal flats		1657#	D, E	Myrtle Shale
McNamara	Paradise Creek	dolostone, silty dlst., dmt. slst.	250-1900	shallow-water shelf, subtidal		1653β 1659#	B, C	Tooganinie Fm-Amelia Dolomite
McNamara	Gunpowder Creek	siltstone, shale, sandst., dlst.	20-1000	semi-emergent shallow marine		?1694#	A, B	Mallapunyah Fm. Moondarra Siltst.
	Sybella Batholith	alkali feld. grt. granodiorite		syn-rift, sag		1671#, 1660$, 1655$		Carters Bore Rhyolite
	Carters Bore Rhyolite	rhyolite qz feld porph.	250	syn-rift		1678&,β		Sybella Batholith
McNamara	Torpedo Ck Quartzite	quartzite, sdst., conglomerate	120-420	marine shoreline proximal alluvial	S, SE, N, NE	?1694#	A	Masterton Sandst. Warrina Pk Qtzite
	Surprise Creek	mic. slst., f.g. sdst., feld. sdst.	230->1000	offshore lagoonal fluvial	W, NW; S, SW			Masterton Sandst.
	Weberra Granite	granite				1698%		Fiery Creek Volcanics
	SURPRISE		CREEK		UNCONF.	O'Dea et al.		1997a
	Fiery Creek Volcs + Bigie	rhyolite, basalt, red sdst., congl.	0->250	subaerial fluvial	W, NW, SE, NE	1709#		Tanumbirini Rhy. (1713±6)
	BIGIE				UNCONF.	O'Dea et al.		1997a
	Quilalar	qtzite, feld. sdst. dolomitic siltstone	800	lagoonal, tidal channel	—			Wollogorang Fm Corella Fm
Haslingden	Myally Subgroup	quartzite, feldsp. sandstone, congl.	750 - 2200	arid tidal/lagoonal, fluvial, lacustrine	N & S, SE↔NE S, SW, NW			mid-Tawallah Gp
Haslingden	Eastern Creek Volcanics	metabasalt, quartzite	1000 - 3300	continental, sub-aerial, rift	SE, NW↔NE	>1730α		Seigal Volcanics Magna Lynn Metb.
Haslingden	Leander Quartzite	orthoquartzite, feldspathic qtzite	> 1000	clastic shoreline	—			Yiyintyi Sdst Mt Guide Qtzite
	Yeldham Granite	granite				1820%		Big Toby Micro-granite
	Leichhardt Volcanics	porphyritic dacite, rhyodacite	> 4000			1867α, 1865&, 1852α		Scrutton (1851) Cliffdale Volcs. Kalkadoon Grt

Table 2.1 Summary stratigraphic, sedimentological and correlation table ordered by age, western Mount Isa Basin. 'Upper' McNamara Group comprises Lawn Hill Formation plus Termite Range Formation. Symbols denoting radiometric age sources as follows: @ Compston and Arriens, 1968; & Page, 1978; α Page, 1983; % Wyborn et al., 1988; $ Connors and Page, 1995; # Page, 1997; β Page and Sweet, 1998

Lateral facies variations within the Gunpowder Creek Formation are most apparent in the vicinity of the Mount Gordon Fault Zone; the formation generally becoming sandier in this area. Conglomerate beds within a fine sandstone and siltstone sequence, along with thinning of the formation to as little as 20 m thick, may be evidence of syndepositional tectonic activity. In the Fiery Creek Dome area, stratigraphic wedges of Gunpowder Creek Formation were identified in the hanging wall of syn-depositional faults by Betts et al. (1996). In the remainder of Paradise Valley however, the dominant signature is that of a

marine transgression (Hutton and Wilson, 1985), culminating in a maximum flooding surface at the top of the formation (Jackson et al., 1996), with pyrite being developed at this horizon in westerly outcrops.

2.5.7.3 Paradise Creek Formation

Carbonates are the dominant lithology in the Paradise Creek Formation, with subordinate argillaceous and arenitic components. Most of the carbonate is in the form of dolomite. The Mount Oxide Chert Member, a laminated chert up to 10 m thick, defines the base of the formation. This horizon was identified as marking the onset of a renewed 'sag' phase of basin development by Betts et al. (1996). An additional four facies above the chert have been defined in the type section (Hutton et al., 1981), and most of these are recognisable throughout the study region. The lowermost is composed of silty dolostone and siltstone with chert and limestone beds. This grades upwards into a stromatolitic dolostone facies, which incorporates abundant breccia and intraclast grainstones between the stromatolites.

A stromatolitic chert several metres thick denotes the base of another stromatolitic dolostone facies, characterised by gypsum and anhydrite (cauliflower chert) pseudomorphs. The stromatolitic chert is interpreted as a sequence boundary by Jackson et al. (1996). The upper stromatolitic dolostone facies (apparently equivalent to sequence C of Jackson et al., 1996) is not distinguishable in all areas.

The Paradise Creek Formation varies in thickness from 250 m in the vicinity of the Mount Gordon Fault Zone to 1900 m in central Paradise Valley. Most sections are near the midpoint between these extremes, though thicknesses up to 1400 m persist in the western part of the study region (Hutton et al., 1981). The formation generally has characteristics compatible with deposition on a periodically emergent, shallow-water shelf. In contrast to underlying units, no evidence for contemporaneous fault activity is observed (Betts et al., 1996). Tidal channels in the west compared with subtidal facies to the east may indicate a landmass to the west, beneath what is now the Undilla Basin (Hutton and Sweet, 1982). A detrital zircon grain in the Paradise Creek Formation has apparently been sourced from a Barramundi age (1880 Ma) terrane (Page and Sweet, 1998). A depositional age of 1653±7 Ma for the formation is provided by other zircons obtained from a tuff bed near the base (Page and Sweet, 1998).

2.5.7.4 Esperanza Formation

The Esperanza Formation outcrops as a sequence of stromatolitic chert beds interbedded with dolostone, dolomitic siltstone, siltstone and sandstone. Varying levels of relief on the stromatolites suggest depositional environments ranging from supratidal to several metres below tidal influence (Hutton and Wilson, 1985). The silicification giving rise to the chert is not necessarily present throughout the region. The Esperanza Formation ranges from 80 to 350 m in thickness, and lies conformably between the Paradise Creek Formation (below) and Lady Loretta Formation (above). Though thin in comparison to formations above and below it, the Esperanza Formation encompasses two major depositional sequences (D and E) according to Jackson et al. (1996).

2.5.7.5 Lady Loretta Formation

As defined by Hutton et al (1981), the Lady Loretta Formation consists of dolostone, dolomitic siltstone and carbonaceous, often pyritic shale. More recently, Dunster (1997) has noted a regional compositional variation from south (more argillaceous) to north (carbonate-dominated). Other minor lithological components include sandstone, quartzite, chert, barite and tuff. The Lady Loretta Formation has been subdivided into a number of sub-units in the vicinity of the Lady Loretta deposit, but these have not proved traceable regionally (Dunster, 1997). In Paradise Valley the Lady Loretta Formation is from 600 m up to 2500 m thick (Dunster, 1997; Dunster and McConachie, 1998).

2.5.7.6 Shady Bore Quartzite

Conformably overlying the Lady Loretta Formation, the Shady Bore Quartzite is only present in western Paradise Valley. It is composed of orthoquartzite, sandstone, mudflake conglomerate, siltstone and dolostone, which were deposited on a high-energy marine shoreline (Hutton and Sweet, 1982). Where measurable, the Shady Bore Quartzite is around 250 m thick in the study region.

2.5.7.7 Riversleigh Siltstone

This is the uppermost unit of the McNamara Group observed in Paradise Valley. It outcrops as massive brown and grey siltstone, micaceous siltstone, orthoquartzite, sandstone, dolostone and dolomitic siltstone. These facies are consistent with deposition in the vicinity of a marine coastline, varying from low energy lagoons to high energy shoreline environments. The Riversleigh Siltstone is generally preserved only near the western edge of the outcropping Mount Isa Basin in the study area.

2.5.8 South Nicholson Group and equivalents

Unconformably overlying large parts of the McNamara Group north of the study area (Bowthorn Block and northern Riversleigh Fold Zone) are several thousand metres of siliciclastic sediments - the South Nicholson Group, comprising the Constance Sandstone, Mullera Formation and Mittiebah Sandstone. The Constance Sandstone contains minor siltstone, while the Mullera Formation is dominantly composed of micaceous siltstone, shale and fine-grained sandstone. The basin in which the South Nicholson Group was deposited appears to have been entirely intracontinental, with sediments sourced from both east and west (Carter et al., 1961). South Nicholson Group deposition is early Mesoproterozoic in age, but took place after the Isan Orogeny, and dips within it generally do not exceed 30°.

Probable equivalents of the South Nicholson Group with shallow (5-10°) dip to the west have been intersected beneath Undilla Basin Cambrian sediments (see below) in the wildcat petroleum exploration well Morstone 1 west of the Paradise Valley study area (Stewart and Hoyling, 1963). Though Stewart and Hoyling (1963) interpreted the siliciclastic sediments beneath the unconformity at the base of the Cambrian as possible equivalents of what is now known as the lower McNamara Group, the total absence of carbonate in these pre-Cambrian sands and silts strongly mitigates against this possibility. Later authors such as Tucker et al. (1979) and Shergold and Druce (1980) have tentatively linked the

Precambrian sediments intersected by drillholes in this region with the South Nicholson Group and the 300 m - thick Pilpah Sandstone outcropping to the south, an interpretation with which the author concurs.

2.5.9 Cambrian

Middle Cambrian sediments of the Undilla Basin, a sub-basin of the Georgina Basin, form a thin veneer over Palaeoproterozoic rocks extending from the west of the Paradise Valley region. They gradually thicken west towards the centre of the basin, concomitant with a general change in composition from mixed siliciclastic/carbonate through limestone to dolostone (de Keyser and Cook, 1972). Carbonates tend to be more prevalent in subsurface samples than in equivalent outcrops, due to silicification associated with weathering (Smith, 1972).

At the base of the Cambrian section is the Mount Hendry Formation, a sandstone and conglomerate unit only a few metres thick. It grades up into limestones and dolostones of the fossiliferous Thorntonia Limestone, which is up to 18 m thick in drillholes near the eastern margin of the Undilla Basin (Howard and Cooney, 1976) but is over 100 m thick in Morstone 1 (Stewart and Hoyling, 1963) and may attain thicknesses up to 180 m elsewhere in the district (Shergold and Druce, 1980).

The Beetle Creek Formation conformably overlies the earlier Cambrian units, and is composed of phosphatic cherts and siltstones as well as phosphorite. It is up to 22 m thick in the Lady Annie Outlier (Shergold and Druce, 1980). The Beetle Creek Formation is overlain by the Inca Formation, the youngest Cambrian unit preserved in the Lady Annie Outlier, comprising siltstone, shale and chert. It is contemporaneous with the Currant Bush Limestone observed further west in the Undilla Basin and in Morstone 1, where it is overlain by V-Creek Limestone, Mail Change Limestone and Split Rock Sandstone. The combined thickness of these four units exceeds 200 m; 116 m of Currant Bush Limestone, 99 m of V-Creek Limestone, 4.5 m of Mail Change Limestone and 10 m of Split Rock Sandstone being intersected in Morstone 1 (Stewart and Hoyling, 1963). The Mail Change Limestone both conformably underlies and grades laterally into the 10 - 20 m thick Split Rock Sandstone (Smith, 1972). Still further west in the Undilla Basin, these units (Thorntonia Limestone to Split Rock Sandstone inclusive) interfinger with the Age Creek Formation and Camooweal Dolomite (de Keyser and Cook, 1972; Smith, 1972; Shergold and Druce, 1980).

Tholeiitic basalts of probable lower Cambrian age, several tens of metres thick, are exposed on the northern margin of the Georgina Basin, north-west of the study area (Peaker Piker Volcanics of Smith and Roberts, 1963; Colless Volcanics of Carter et al., 1961). A gradational contact has been recorded between the Thorntonia Limestone and Colless Volcanics (Shergold and Druce, 1980). These have been nominated as eastern extensions of the Antrim Plateau flood basalt province by Bultitude (1976). No mafic volcanics have been observed within the Cambrian sequence in the Undilla Basin; it is possible they occur at depth, but their absence in the equivalent stratigraphic position in Morstone No. 1 (Stewart and Hoyling, 1963) mitigates against this.

2.5.10 Mesozoic

Conglomerates, sandstones, quartzites and siltstones correlated with Jurassic to Cretaceous strata in the Carpentaria Basin form a patchy cover over older rocks in western and northern Paradise Valley. These outliers often occur as mesas rising up to 30 m above the surrounding terrain. The greatest thickness of Mesozoic sediments known in Paradise Valley is in the central northern part of the study area, where over 50 m of coarse siliciclastics with minor mudstone interbeds are present beneath a Tertiary weathering surface (Clarke, 1992).

2.5.11 Cainozoic

Erosional processes were active in the southern Paradise Valley region during the Cainozoic, but limestones (including the Riversleigh fossil site) and siliciclastics were deposited in the central northern parts of the study area. Products of these processes include widespread deep laterite development, particularly in the central part of the region (Hutton and Wilson, 1985), soils and colluvium. The latter is mainly composed of sand, silt and gravel, which are also the constituents of Quaternary deposits associated with watercourses.

2.6 Western Mount Isa Basin Intrusives

A number of granitoid plutons of A-type affinity intruded in anorogenic settings during Mount Isa Basin development (Wyborn et al., 1987). They are distinguishable from Barramundi-age (1880-1840 Ma) igneous units by relatively high K, U and Th, and higher Fe^{3+}/Fe^{2+} ratios (Wyborn et al., 1988). Some representatives of these suites occur near or conceivably beneath the study area, and these are detailed below.

2.6.1 Yeldham Granite

The Yeldham Granite outcrops in the core of the Kamarga Dome less than 100 km north of the study area. It is unconformably overlain by the Kamarga Volcanics (Jones, 1986). Radiometric dates indicating intrusion between 1820 and 1800 Ma have been derived for the Yeldham Granite (Wyborn et al., 1988), which may suggest correlation with younger phases of 'transitional' (from the 1880-1840 Ma Barramundi felsic magmatism) igneous units elsewhere in the region (Ewen Granite, Nicholson Granite Complex). As such the Yeldham Granite is a component of basement to Haslingden Group (cover sequence 2) and later basin sedimentation phases.

The Yeldham Granite has been described from outcrop as a medium-grained muscovite granite (Hutton and Sweet, 1980), while samples cored in GSQ Lawn Hill 3 are still more potassic (alkali granite and alkali syenite). On the basis of these, Hutton (1983) concluded that the Yeldham Granite is an altered I-type. Hutton (1983) also noted the presence of minor magnetite in the Yeldham Granite drillcore.

2.6.2 Big Toby Batholith

Consisting mainly of two plutons in the extreme south-west of the Riversleigh Fold Zone, the Big Toby Batholith is a S-type granitic body dated at 1804±15 Ma (U-Pb) by Wyborn et al. (1988). The northern pluton is microcrystalline and heterogeneous, with compositions ranging from tonalite to monzogranite; granodiorite being most common. It is low in K_2O and U compared to other post-1820 Ma rocks of the region (Wyborn et al., 1988).

2.6.3 Weberra Granite

The Weberra Granite outcrops over an area of about 25 km^2 about 30 km north of the Paradise Valley study area, where it has produced a narrow metamorphic aureole in older rocks (Quilalar Formation and Myally Subgroup; Hutton and Wilson, 1984). It is mainly composed of medium to coarse-grained syenogranite to alkali feldspar granite, with the proportion of mafic minerals including biotite and chlorite increasing towards the margin. Wyborn et al. (1988) classified the Weberra Granite as a fractionated I-type, which crystallised at around 1698±21 Ma, providing a lower limit on the age of cover sequence 2 deposition. The Weberra Granite may be comagmatic with the Fiery Creek Volcanics on grounds of geochemical similarity and spatial and geophysical association (Wyborn et al., 1988; Appendix 7).

Both the Weberra Granite and Fiery Creek Volcanics have very high (around 12%) levels of K_2O, while associated country rocks do not, implying that primary levels were also high (Wyborn et al., 1988). The presence of iron as haematite is reflected by high Fe_2O_3/FeO ratios.

2.6.4 Sybella Batholith

The Sybella Batholith does not outcrop in the study area; its exposures being restricted to the Riversleigh Fold Zone south of the Barkly Highway. Phases of the Sybella Batholith are likely to have been contemporaneous with McNamara Group deposition, and the possibility that equivalent granitoid intrusions extend beneath the study area also cannot be discounted. The Sybella Batholith consists mainly of granodiorite and alkali feldspar granite, within which up to five phases are petrographically and geochemically distinguishable (Wyborn et al., 1988). More felsic compositions (a β-quartz-bearing phase and a microgranite) tend to dominate within the northern half of the batholith outcrop, although the microgranite is thought to have a distinct petrogenesis from the balance of the Sybella Batholith. As with the near-coeval Weberra Granite, the main and β-quartz phases of the Sybella Batholith have been classified as fractionated I-types (Wyborn et al., 1988).

Emplacement ages from 1670 to 1650 Ma were determined by Connors and Page (1995) for both the main and β-quartz phases of the batholith, compatible with earlier determinations of 1671±8 Ma and 1668±24 Ma by Page and Bell (1986) for the same suites. Connors and Page (1995) also determined similar ages (1655±4 and 1660±5 Ma) using $^{207}Pb/^{206}Pb$ dating for a third phase of the Sybella Batholith, the Queen Elizabeth pluton west of Mount Isa, discounting the 1610 U-Pb age obtained by Page and Bell (1986). These data suggest probable equivalence of Sybella Batholith plutons with the Carters Bore Rhyolite, as well as putative tuffs in the McNamara Group. Southgate et al. (1997), based on a date of

1694 Ma for the lower Gunpowder Creek Formation and sequence stratigraphic interpretations, have suggested a major depositional break within the Gunpowder Creek Formation occupied by Sybella Batholith emplacement and Carters Bore Rhyolite. This is partly controverted by Hill et al. (1975) who observed pebbles of β-quartz phase Sybella Batholith within the basal conglomerate of the McNamara Group (Torpedo Creek Quartzite).

The Sybella Batholith is metamorphosed to greenschist facies in its north and north-western portions, but is of amphibolite grade elsewhere (Wyborn et al., 1988).

2.6.5 Dykes

Multiple dyke generations of various relative ages are present in the study area. Most are of mafic composition, with the exception of rhyolite, porphyry, trachyte and granophyre dykes associated with the Weberra Granite and Fiery Creek Volcanics (Carter et al., 1961; Hutton and Wilson, 1984). Dolerite dykes in and around the Weberra Granite contain around 8% iron oxides (Hutton and Wilson, 1984).

Mafic dykes are abundant in the Leichhardt Volcanics and Kalkadoon Granite (Blake, 1980), but most of the mafic dykes in the study area are confined within the Haslingden Group, and many may have been feeders to the Eastern Creek Volcanics and thin metabasalt layers in the Myally Subgroup. Two mafic dyke types were recognised in the Eastern Creek Volcanics by Robinson (1968): voluminous coarse-grained gabbros, and finer-grained dolerites that appear very similar to the intruded basalts. The gabbro dykes are generally meridionally oriented, with some examples over 1 km wide and 15 km long intruding the Eastern Creek Volcanics, while the dolerites are much shorter and narrower (< 30 m). Rafts of basalt within the coarse-grained gabbro dykes and localised deformation on the dyke margins imply that they postdate eruption of the basalt sequence. They may be equivalent to extensive medium grained dolerite sills that occupy some levels within the Myally Subgroup (Fig. 2.5). Some of these, particularly near the Mammoth copper mine (Fig. 2.5), have suffered extreme potassic alteration, which was attributed by Hutton and Wilson (1985) to circulation of hypersaline fluids through these rocks soon after their emplacement.

Post-Isan Orogeny mafic dykes are also known in the LRFT and RFZ; these tend to be oriented between north and northeast, and may correlate with the 1116 Ma Lakeview Dolerite (Blake and Stewart, 1992b).

2.7 Structure

The nature of the Mount Isa Basin tectonic elements introduced in section 2.4.2.2 as manifested in the Paradise Valley study area are here described in detail. Structural disposition and deformation styles are discussed initially, followed by a review of the competing structural models proposed to account for the observed structures.

2.7.1 Leichhardt River Fault Trough (Cloncurry Orogen)

The area east of the Mount Gordon Fault Zone indicated as 'Leichhardt River Fault Trough' on Figure 2.4 is part of the Cloncurry Orogen (McConachie et al., 1993). This terrane may have been initiated at the beginning of Haslingden Group deposition as the Leichhardt Rift (O'Dea et al., 1997a). The Leichhardt River Fault Trough (Derrick, 1982) is dominated in outcrop by cover sequence 2 sediments and volcanics of the Haslingden Group, which are structurally repeated by movement on east-west fault structures. It is separated from putative basement (Ewen Granite, Leichhardt Volcanics) outcropping in the Kalkadoon-Leichhardt Belt to the east by the Quilalar Fault Zone (Blake and Stewart, 1992a), and from the Lawn Hill Platform/Riversleigh Fold Zone to the west and north-west by the Mount Gordon Fault Zone. The structure of the Leichhardt River Fault Trough in the study area is grossly that of a broad north-plunging anticline, with Myally Subgroup and younger units exposed on the flanks and to the north, while rocks as old as Leander Quartzite outcrop in the cores, particularly to the south.

2.7.2 Mount Gordon Fault Zone

The Mount Gordon Fault Zone separates the Cloncurry Orogen from the Riversleigh Fold Zone to the west. The Mount Gordon Fault itself is a dextral strike-slip fault whose total displacement may be up to 10 km (Hutton and Sweet, 1985). The Mount Gordon Fault Zone contains many other NNE-striking faults in a belt that ranges from 1 km to 7 km wide in the study area. Many of these are bedding-parallel, and thus their displacement also is difficult to determine.

2.7.3 Riversleigh Fold Zone

West of the Mount Gordon Fault Zone, both the exposed structural level and structural style change markedly. Dolomites, dolomitic siltstones and shales of the McNamara Group are the dominant exposed lithology, overlying siliciclastics and minor bimodal volcanics (Surprise Creek Formation, Bigie Formation, Fiery Creek Volcanics) which in turn lie unconformably on the Haslingden Group and Quilalar Formation. The Quilalar Formation only appears in the northern half of the region.

The dominant structural style is one of basin-and-dome folding with wavelengths up to many kilometres, though Keele (pers. comm.) believes the structuring to be somewhat more brittle. The gross sense of regional plunge is reversed to that of the Leichhardt Rift, with older units generally becoming more prevalent northwards. An overall N-S tectonic grain was imposed on the region during E-W shortening (D2) (of the Isa Orogeny). In the Paradise Valley region (Fig. 2.5), this E-W (Isan Orogeny) deformation appears to be accentuated in a north-trending high strain zone 'bounded by the Russell Creek and Western Border Faults, here called the Russell Creek Strain Zone (Keele, pers. comm.).

2.7.4 Structural history

The Mount Isa Basin has experienced a complex series of deformations, incorporating high and low angle faulting, and folding (Bell, 1983). Most of this deformation (in terms of strain) occurred during a tectonic episode known as the Isan Orogeny (Blake et al., 1990), which postdated McNamara Group

sedimentation and was responsible for the regional metamorphism, which developed up to amphibolite facies. The regional compression and metamorphism of the Isan Orogeny took place between 1520 and 1620 Ma (Blake and Stewart, 1992a) but the precise timing and nature of many of the structural movements is controversial (cf. Bell 1983, 1991, 1993; Lister, 1993; Connors and Page, 1995; O'Dea et al. 1997a).

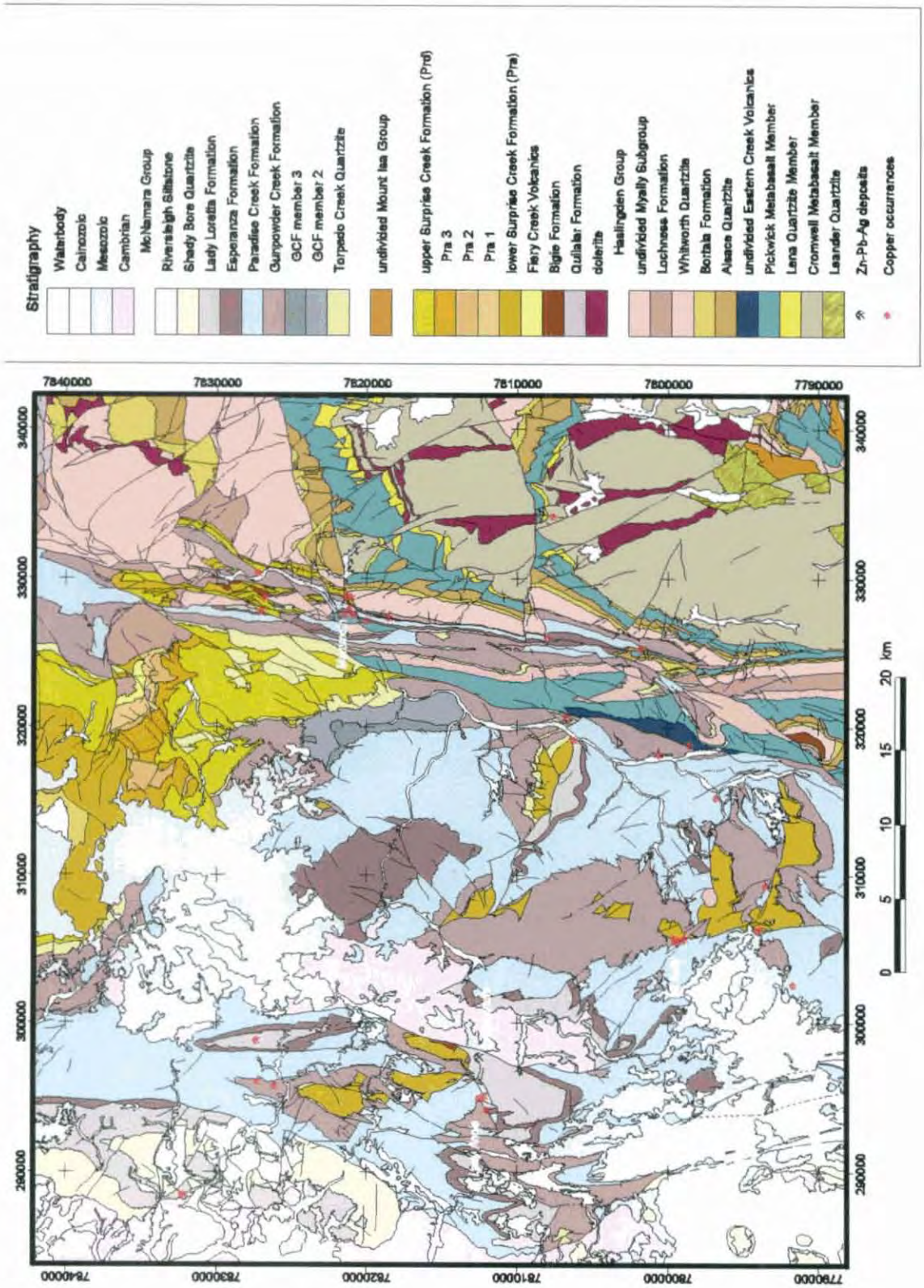

Figure 2.5 Paradise Valley geology, modified after Hutton and Wilson (1985)

Most workers agree that the major N-S trending folds observed were the result of a regional E-W compressional event, and that this event resulted in a system of conjugate strike-slip faults striking NE and NW (Opik et al., 1973); but there is little consensus on the nature of almost all other major structures observed. Significant displacements on major regional strike-slip faults have also been recorded younger than 1550 Ma, postdating the main phase of the Isan Orogeny. Many north-trending segments of these younger fault arrays are transpressional (Blake et al., 1990).

Much conflict between structural models may be characterised as being between 'syn-depositional deformation' and 'post-depositional deformation'.

2.7.4.1 Basin evolution

A number of different models have been advanced to explain the disposition of Mount Isa Basin units in terms of basin evolution, as well as in the context of the Isan Orogeny. Many authors have recognised the need to invoke structures developed during various phases of basin evolution prior to the Isan Orogeny in order to account for observed relationships.

Most tectonic settings proposed for Mount Isa Basin evolution are variations on an extensional theme, from intracontinental rifting (Derrick, 1982; O'Dea et al., 1997a) to continental margin (Wilson, 1978; Plumb et al., 1980; Dunster and McConachie, 1998). Carter et al. (1961) were the among the first to suggest normal fault activity generating accommodation space during Mount Isa Basin development, with their identification of what would today be called growth faults in the Eastern Creek Volcanics. Extension in a north-northeast-south-southeast direction leading to formation of a west-northwest trending graben ('Paradise Graben') during Mount Isa Basin development was recognised by Dunnet (1976).

Blake (1987, 1990), Blake and Stewart (1992b) and Eriksson et al. (1992) proposed two rift-sag cycles within cover sequence 2. Their first cycle rift components are the Bottletree Formation and lower Mount Guide Quartzite (Leander Quartzite correlate), with thermal subsidence represented by the upper Mount Guide Quartzite. This first rift-sag cycle is interpreted as being restricted to the Leichhardt River Fault Trough. The second rift-sag cycle extended further east, from the LRFT across the Kalkadoon-Leichhardt Belt to the Pilgrim Fault, according to Eriksson et al. (1992). It is represented by the Eastern Creek Volcanics and Myally Subgroup, being the rift phase, while the Quilalar Formation is interpreted as sag-phase sedimentation. Further rifting followed by thermal subsidence was postulated by Blake and Stewart (1992b) to account for cover sequence 3 and subsequent deposition in the Mount Isa Basin; an extensional event which they also related to emplacement of the Weberra Granite at 1700 Ma and the Sybella Batholith at 1660 Ma. Blake et al. (1990) did not favour the continental margin model because of lack of evidence for subduction.

A slightly different interpretation of the same successions was made by O'Dea et al. (1997a and b) and Betts et al. (1996, 1999). They retain a model of superimposed intracontinental rifting episodes, albeit more complex than that of Blake (1987). Their east-west extensional Leichhardt Rift was filled with Bottletree Formation and Haslingden Group up to and including the Cromwell Metabasalt, followed by

north-south extension resulting in development of E-W oriented south-tapering basins accommodating the Pickwick Metabasalt and Myally Subgroup ('Myally Rift Event'). A subsequent sag phase during which the Quilalar Formation was deposited was followed by episodic NW-SE extension commencing at Bigie Formation/Fiery Creek Volcanics time ('Mount Isa Rift Event'), which continued at least into the lower Gunpowder Creek Formation (Betts et al., 1999), with thermal subsidence thereafter. Most evidence presented for the Mount Isa Rift Event is from the region around the Fiery Creek Dome to the north of the Paradise Valley study area.

Wyborn et al. (1988) applied the crustal detachment - asymmetric continental extension model of Lister et al. (1986) in order to explain the volume and disposition of felsic igneous units in relation to coeval basin development. Examples of this phenomenon include intrusion of the Yeldham Granite remote from coeval felsic igneous units such as the Bottletree and Argylla Formations, intrusion of Wonga Batholith plutons apparently both adjacent to and coeval with up to 10 km of Haslingden Group deposition in the Leichhardt River Fault Trough, and intrusion of Weberra Granite and Sybella Batholith plutons both adjacent and immediately prior, possibly even contemporaneous with, lower McNamara Group accommodation space development.

2.7.4.2 Isan Orogeny

The Isan Orogeny is here defined as the related series of deformations that culminated in peak regional metamorphism of Mount Isa Basin sediments. Terminology introduced by Bell (1983) to describe Isan Orogeny deformation has become generally accepted by most workers. D_1 refers to an episode of north-south compression resulting in major N-S directed thrusting and E-W oriented folding, dated by Page and Bell (1986) at approximately 1620-1610 Ma, though this date has been discounted by Connors and Page (1995). Bell (1983) interpreted east-west thrust faults in the Leichhardt River Fault Trough as manifestations of D_1 thrust duplexes, as did van Dijk (1991) in Paradise Valley. This interpretation envisages the E-W to ESE-WNW trending rift-bounding faults of other workers (Dunnet, 1976; O'Dea et al., 1997b) as north- and south-dipping thrusts (van Dijk, 1991) over which displacements of up to hundreds of kilometres have occurred (Bell, 1983).

Regional metamorphism peaked during D_2, when the north-south trending, generally open, upright folds that dominate much of the central and southern Mount Isa Basin formed in response to a phase of east-west compression. The age of this event (both prograde metamorphism and D_2 deformation) was estimated at 1532±7 Ma by Connors and Page (1995). This orogenic episode may also have been responsible for the west-block-up north-trending high-angle reverse faults (for example the Western Border Fault; van Dijk, 1991) which Plumb et al. (1980) noted as major structures west of the Kalkadoon-Leichhardt Belt. These may correspond to the west-dipping thrusts apparent west of the Pilgrim Fault on the Mount Isa seismic transect (MacCready et al., 1997).

A younger age limit to the Isan Orogeny is given by intrusion of the post-tectonic Williams and Naraku Batholiths into the Eastern Fold Belt at around 1500 Ma, as well as pooled Mount Isa and McArthur Basin Rb-Sr data which indicate cessation of regional metamorphism by 1480 Ma (Page, 1978; Page, 1981), which provides a younger age limit on D_3 (below).

2.7.4.3 D_3 and later strike-slip faulting

Many major faults (usually N to NNE-trending) in the Mount Isa Basin describe transcurrent displacements of many kilometres, truncating Isan Orogeny D_2 folds. At least some of these may be due to a waning stage of the Isan Orogeny associated with a steeply dipping NNW-SSE striking foliation (D_3 of Page and Bell, 1986) but many have also experienced multiple reactivation and movement during the Phanerozoic, possibly resulting from far-field effects of distant events such as the early Carboniferous Alice Springs Orogeny (Spikings et al., 1996). Faults of this age tend to have north-westerly trends, often reactivating Precambrian structures (Smith, 1972). Faults active post-Cambrian were noted throughout the Mount Isa Basin by Carter et al. (1961). A number of examples of Phanerozoic movement on faults are present in the Lady Loretta region, including the Western Border Fault (see Fig. 8.1) and the West Thornton Fault, a north-west to west-trending structure about 20 km west of Lady Loretta which was clearly active during Cambrian sedimentation (de Keyser and Cook, 1972). Post-depositional faulting, often west-trending, has also occurred along exposed Proterozoic/middle Cambrian contacts (Howard and Cooney, 1976), particularly on the northern margin of the Undilla Basin. Mild tectonic events of late Mesozoic and Cainozoic age have also been noted in northwest Queensland (Smith, 1972).

2.7.4.4 Later uplift

The presence of numerous epi-continental Cambrian, Mesozoic and Cainozoic outliers in the Riversleigh Fold Zone, particularly in the Lady Loretta area, implies that the rocks now exposed in this region have experienced a number of episodes involving uplift to near-exposure followed by sedimentation and minor subsidence. Evidence of very slow uplift and unroofing through the latter half of the Phanerozoic has been obtained by apatite fission track dating (Page, 1978; Spikings et al., 1996) suggesting that rocks currently exposed in the Mount Isa Basin have been cooler than 100° to 120°C since the late Palaeozoic, preceded by an uplift episode contemporaneous with the Alice Springs Orogeny.

2.7 Metamorphism

2.7.1 Barramundi Orogeny

The Barramundi Orogeny is the first regional metamorphic event recorded in the Proterozoic of northern Australia, affecting rocks now considered basement to the Mount Isa Basin. This was a generally low-P high-T event (andalusite-sillimanite facies; Etheridge et al., 1987). Peak metamorphism during the Barramundi Orogeny has been dated at 1890±10 Ma (Page, 1990).

2.7.2 Isan Orogeny

Isan Orogeny metamorphism affected all rocks up to and including the McNamara Group. A pronounced metamorphic gradient is present across the Mount Isa Basin, commensurate with changes in deformation intensity, from upper amphibolite facies in the south and east (Cloncurry Orogen) to lower greenschist, possibly as low as prehnite-pumpellyite facies at the basin's northern edge (Bowthorn Block). Based on

studies west of Mount Isa, Connors (1992; quoted in Connors and Page, 1995) proposed the intrusion of mafic sill complexes into the middle crust to account for this low-P, high-T metamorphic event, the effects of which have been noted throughout the Mount Isa Basin.

2.8 Mineralisation

The Carpentaria Zinc Belt's large Zn-Pb endowment is mainly contained in stratiform sediment-hosted base metal (SSHBM) deposits. The definition of stratiform sediment-hosted base metal deposits is essentially encapsulated in their name, which describes the mode of occurrence of these deposits without genetic connotations. 'Base metal' largely refers to zinc and lead, however it should be noted that most deposits of this type also contain economically significant silver grades. Copper is also often (though not necessarily) observed in economic amounts in association with SSHBM deposits, but sediment-hosted copper deposits are excluded from the definition of SSHBM as they generally fall under their own distinct classification. The qualifier 'stratiform' distinguishes SSHBM deposits from Mississippi Valley-type or MVT lead-zinc mineralisation, which while stratabound in geometry, is generally discordant with individual sedimentary layers.

In addition to the Zn-Pb deposits examined in this thesis, known significant resources of other commodities in the region are also reviewed briefly below.

2.8.1 Zn-Pb Mineralisation

Several SSHBM deposits with significant base metal tonnage occur in the Carpentaria Zinc Belt (Fig. 1.1). Their features are summarised in Table 2.2 in order of increasing metamorphic grade, which in geographic terms describes a trend from north-west to south-east. Pb-Zn deposits in the Cloncurry Orogen such as Dugald River, Cannington and Pegmont have been considered beyond the scope of this project, both geographically and in terms of ore deposit models, the latter two belonging more to the Broken Hill type of Pb-Zn deposit (though these may also have a syn-sedimentary origin).

SSHBM deposits are characterised by single or multiple lenses of laminated or massive sphalerite and galena, which are usually accompanied by large amounts of pyrite, Century being a major exception. Each lens is of the order of several tens of metres thick (McGoldrick and Large, 1998a). The Carpentaria Zinc Belt examples are hosted within carbonaceous shales and siltstones, but these host sequences are interpreted to have been deposited in a range of settings from shallow (< 10 m) evaporitic lagoons (Lady Loretta; Dunster, 1996) to deep (sub-photic zone), extensive (> 20 km) water bodies (HYC; Oehler and Logan, 1977; Large et al., 1996).

All SSHBM deposits discovered in the Carpentaria Zinc Belt thus far have been situated on or near major regional faults, but these have not necessarily been active during deposition of the ore host sequence. Notwithstanding this, these faults have regularly been invoked in genetic models as conduits for mineralising hydrothermal fluid flow (e.g. McGoldrick and Large, 1998a; Fig. 2.6).

Name	*Size*	*Mineralisation*	*Host*	*Age (Ma)*	*Metamorphism /deformation*	*Zoning*	*Halos*	*References*
HYC	227Mt @ 9.2% Zn, 4.1% Pb. Current project 104 Mt @ 14.1% Zn, 6.1% Pb & ~60 g/t Ag. 8 ore lenses in ~70 m strat.	stratiform, f.g. py sp gn minor ccp apy	Barney Ck Fm; HYC Pyritic Shale Mbr. Pyr car dmt slst, c.g. sed bx. interbeds, minor tuff, up to 7% TOC	1640±7	essentially unmetamorphosed; slight basin inversion faulting but no penetrative deformation	small v. Cu-rich zone in N; general (Cu-) Pb - Zn	py; Tl regionally; Fe, Mn in carbonates	Logan et al. 1990, 1993 & references therein, Crick 1992
Walford Creek	several ore (Cu, Zn, Pb) grade intercepts of a few m.; covers 6 x 1.5 km area, 3 stacked lenses	stratiform py lenses; sp & gn as matrix in pyr beds	(Fickling Gp) Mt Les Siltstone. Dmt shle regionally; car dmt pyr shle & interdigitating talus bx locally	1640±7	sub-greenschist, relatively flat-lying, but bounded by Fish River Fault (major regional structure)		py	Rohrlach et al 1996, Page et al 1994, Webb & Rohrlach 1992, Page et al. 1994
Century	118 Mt @ 10.2% Zn, 1.5% Pb, 36 g/t Ag. 40 m thick mineralised sequence	stratiform sp py gn ± ccp, assoc. with organic matter & authigenic silica	(upr McNamara Gp) Lawn Hill Fm; mbr Pmh4. Car shle & barren sid slst interbeds, minor tuff	1595±6	sub-greenschist open folding; OB faulted into 2 zones, other faulted contacts	highest Zn grades transgress mineralised sequence from SE to NW	py envelope; sd in slst	Waltho et al. 1993, Page et al. 1994, Broadbent et al 1996
Lady Loretta	8.3 Mt @ 18.4% Zn, 8.5% Pb, 125 g/t Ag. Single lens ~50 m thick recognisable over several km²	stratiform py sp gn tth brt, tr. hem	Lady Loretta Fm. Car pyr dmt sd slst & shle	1647±4	lower greenschist open - tight syncline (probable D2) locally, more open folding regionally	Pb-Zn core to Zn-Ba on NE edge of mineralisation	py, sd, Mn, Tl	Hancock & Purvis, 1990 & references therein, McGoldrick et al. 1996
George Fisher	108 Mt @ 11.5% Zn, 5.4% Pb, 93 g/t Ag in 11 stacked ore lenses	As for Mt Isa	As for Mt Isa	As for Mt Isa	As for Mt Isa	not known	py	MIM 1995 Annual Report
Hilton	120 Mt @ 10.2% Zn, 5.5% Pb, 100 g/t Ag in 7 stacked ore lenses	As for Mt Isa	As for Mt Isa	As for Mt Isa	As for Mt Isa	upper OBs most Cu-rich; (Cu-) Pb - Zn up-dip	sd slst	Valenta 1994, Mathias et al. 1973, Forrestal 1990
Mount Isa	150 Mt @ 7% Zn, 6% Pb, 150 g/t Ag (est. pre-production reserve) 30 stacked en echelon ore lenses in ~1000 m	stratiform py sp gn tth ± po	(Mount Isa Gp) Urquhart Shale. Car (gr) pyr dmt slst; 'tuff'	1652±7	greenschist ore lenses dip steeply W deformations D1 - D3	(Cu-) Pb - Zn	py, Tl; ?Fe, Mn enrichment in carb	Forrestal, 1990 & references therein

Table 2.2 Summary of Carpentaria Zinc Belt Zn-Pb deposits examined in this study, modified after McGoldrick and Large (1998). brt = barite, car = carbonaceous, ccp = chalcopyrite, hem = haematite, gn = galena, po = pyrrhotite, py = pyrite, sd = siderite, tth = tetrahedrite, TOC = total organic carbon

The timing of base metal mineralisation with respect to its host sediments has been the subject of controversy for many decades, particularly at Mount Isa, the longest-known example. Reinterpretation of Mount Isa as a syngenetic-exhalative deposit from the initial hydrothermal replacement hypothesis was precipitated by discovery of the similar yet almost unmetamorphosed HYC deposit (Myers et al., 1996). With some variations involving early diagenetic replacement (e.g Hinman, 1996 for HYC; McGoldrick et al., 1996 for Lady Loretta), essentially syn-depositional mineralisation has remained the consensus model for most Carpentaria Zinc Belt SSHBM deposits including Mount Isa. The opposing 'syntectonic' model proposes that the Mount Isa Zn-Pb ore is cogenetic with the Cu mineralised system, and that other Carpentaria Zinc Belt deposits may also be syntectonic (Perkins, 1995; Laing et al., 1990; Myers et al., 1996). The genetic model most recently proposed for Century is in some ways intermediate between the syngenetic and syntectonic models, with ore minerals forming in the deep subsurface, associated with a hydrocarbon accumulation, during late diagenesis at the onset of basin inversion (Broadbent et al., 1996).

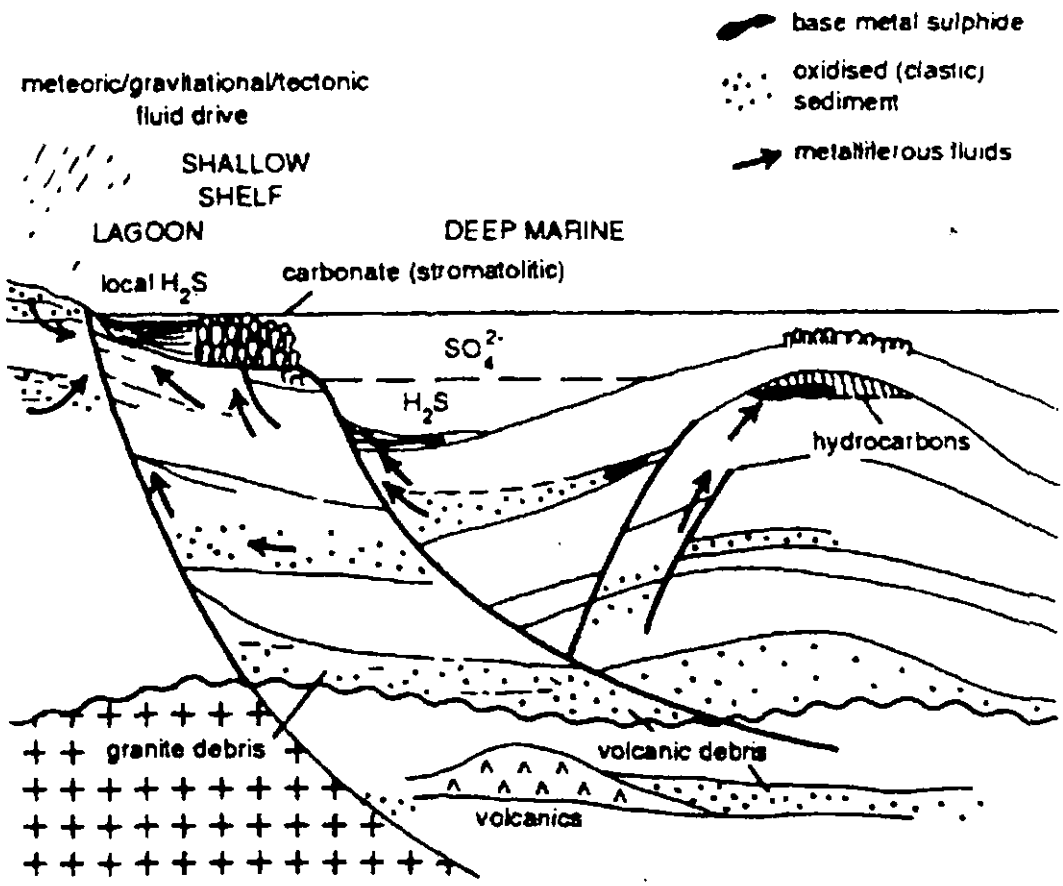

Figure 2.6 Schematic metallogenic scenarios for Proterozoic SSHBM deposits, after McGoldrick and Large (1998a)

2.8.1.1 Lady Loretta

The Lady Loretta deposit is situated 115 km NNW of Mount Isa, and is hosted within carbonaceous and dolomitic shales and siltstones of the Lady Loretta Formation. Currently defined ore reserves consist of 8.3 million tonnes averaging 8.5% Pb, 18.4% Zn and 125 g/tonne Ag (Hancock and Purvis, 1990). It was discovered in 1969 following indications from soil geochemical surveys in the vicinity of the Lady Annie Cu mine 2 km to the west (Alcock and Lee, 1974). More details of the Lady Loretta orebody and its geological context are given in the chapter on the physical properties of the deposit and its surroundings (chapter 6).

As discussed above, the timing of the Lady Loretta ores has been considered by most authors to be syngenetic to very early diagenetic. Highly variable Pb isotope ages of 1600-1540 Ma obtained by Sun et al. (1994) are at variance with this interpretation, given the U-Pb zircon age of 1647 Ma derived by Page (1997) from putative tuffs within the ore host sedimentary sequence. This and other, sedimentological lines of reasoning led Dunster (1997) to propose an epigenetic age for the mineralisation, though Sun et al. (1994) also pointed out the possibility of incomplete homogenisation of Pb from multiple sources. More detailed information on Lady Loretta and its setting within carbonaceous and dolomitic shales of the Lady Loretta Formation (middle McNamara Group) may be found in McGoldrick et al. (1996) and Dunster (1996, 1997).

2.8.2 Cu mineralisation

Copper occurrences are much more common regionally than Pb-Zn-Ag prospects, however few have proved economic. The Mammoth deposit is currently being worked by Western Metals Ltd. Other notable copper deposits in the Paradise Valley region include Mount Oxide (Hutton and Sweet, 1982), Mount Kelly (Bampton et al., 1977) and Lady Annie, near Lady Loretta (Lewis, 1975).

2.8.2.1 Mammoth

The Mammoth stratabound orebodies at Gunpowder are the largest known in the western Mount Isa Basin after Mount Isa itself. Resources in the total mineralised system (recently renamed Mount Gordon) were recently revised upwards to 15Mt at ~5% Cu (http://www.mining-investor.com/Releases/west%2045.htm). Mammoth Cu is hosted by the Whitworth Quartzite of the Myally Subgroup, and is thought to have been sourced from the Eastern Creek Volcanics via fluids that migrated up the Mammoth Extended and associated faults (Scott and Taylor, 1982).

2.8.2.2 Mount Oxide

The Mount Oxide deposit is one of the best-developed examples of secondary mineralisation in the Mount Isa Basin (Carter et al., 1961). Ore minerals included malachite and azurite near the surface, but mineralisation was mainly in the form of chalcocite below about 30 m depth. It appears structurally controlled, being hosted by a north-east trending zone of tectonic breccia, but is contained within folded graphitic shales of the Gunpowder Creek Formation. Over 22,000 tons of copper have been produced from ore grades ranging from 2.5% up to ~20% Cu (Brooks, 1990).

2.8.2.3 Lady Annie

Lady Annie and the associated Flying Pig orebody lie only 1.5 km west of the Lady Loretta Pb-Zn-Ag deposit, but working of copper at Lady Annie predates the discovery of Lady Loretta by almost 50 years (Lewis, 1975). The orebodies are disseminated replacement deposits hosted by brecciated Paradise Creek Formation carbonaceous shale in the hanging wall of an east-trending fault (Brooks, 1956). Ore minerals include cuprite, malachite and tenorite. Indicated and inferred reserves of 48,000 tons at 9% Cu have been published (Brooks, 1956), but recent work by the current lease-holders (Buka Minerals NL) is likely to have increased this figure.

2.8.2.5 Other Cu occurrences

Many other minor occurrences of secondary Cu mineralisation are present in the study area. Copper minerals occur disseminated within the host rock (usually sheared and or brecciated McNamara Group dolomitic shales), on fracture and bedding planes, and in fine veins. All these are invariably associated with faults and shears (de Keyser, 1958). Examples include Mount Kelly, Lady Agnes, Busy Bee, Mt. Maggie, Mt. Clarke and McLeod Hill. Further details of these and other prospects in Paradise Valley may be found in de Keyser (1958), Guy (1975), Bampton et al. (1977) and van Dijk (1991).

2.8.3 Other commodities

2.8.3.1 Phosphate

A significant proportion of Australia's phosphate reserves occurs within the Cambrian sediments of the Lady Loretta district. The Lady Annie and associated Lady Jane phosphate deposits extend through much of the Cambrian outliers east of Lady Loretta. The phosphate beds average 4-6 m thickness, ranging up to 22 m. Reserves of 250 Mt at 18% cut-off P_2O_5 grade have been proved at Lady Annie and Lady Jane (de Keyser and Cook, 1972), which has been worked sporadically since discovery in 1967. The D-Tree deposit 16 kilometres west of Lady Loretta occupies over 38 km^2 of the Cambrian Beetle Creek Formation, associated with a siltstone-chert facies (de Keyser and Cook, 1972). A reserve of 250 Mt at 18.6% P_2O_5 has been calculated for this deposit, which has not yet been worked.

2.8.3.2 Uranium

Most uranium occurrences within the western Mount Isa Basin are hosted within the Eastern Creek Volcanics (Carter et al., 1961). All U mineralisation in the ECV is developed in altered carbonate lenses within the basalts (de Keyser, 1958). While U mineralisation is widely distributed in the region, no economic accumulations have yet been identified.

2.9 Summary

SSHBM mineralisation in the Carpentaria Zinc Belt occurs within extensive dolomitic and subordinate fine grained siliciclastic sequences in the McArthur and Mount Isa Basins, which are up to several kilometres thick. The reduced carbonaceous and usually pyritic siltstones and shales that directly host base metal mineralisation are unusual but not uncommon in this context. The dolomitic accumulations were preceded by several previous episodes of basin evolution over a period approaching 250 million years, which created large volumes of accommodation space by fault-controlled rifting or other brittle extension processes, and thermal subsidence. These were filled by a wide range of lithologies, including basalt from a major episode of continental flood volcanism, several thick sandstone-dominated sequences, and felsic igneous material. A significant portion of the latter was intruded periodically throughout evolution of the western Mount Isa Basin, ceasing around the time of Mount Isa and Lady Loretta Zn-Pb mineralisation. All this took place on a substrate of widespread felsic magmatic material that was emplaced immediately following the Barramundi Orogeny.

3. McArthur Basin Metallogenic GIS Design

3.0 Introduction

The McArthur Basin GIS compilation incorporated a range of geoscientific data in the Arc/Info GIS software, in order to enable metallogenic analysis and modelling. The geoscientific data are from three main sources: geological surface mapping (Pietsch et al., 1991; Plumb, 1988; Blake, 1987), structure contours and isochores interpreted from geophysical data (Leaman 1992, 1993a, 1993c, 1993e, 1994b, 1998), and lithogeochemistry from several separate studies (Brown et al., 1969; Corbett et al.; 1975; Large, 1979; Plumb et al., 1992; Rogers, 1996). These comprise a variety of point, line, polygon and gridded datasets. These were divided into four modules; geology, geophysics, geochemistry and miscellaneous datasets including cultural features. The proprietary nature of the geophysical and geochemical databases necessitated some form of processing or interpretation constituting significant enhancement or degradation before incorporation into the GIS. References to 'geophysical' and 'geochemical' datasets in this chapter generally refer to derived coverages rather than to raw data.

Metallogenic analysis in the GIS had three aims:

investigation of the geological setting of mineral deposits, particularly stratiform sediment-hosted Zn-Pb deposits,

identification of metallogenic constraints on the formation of the HYC deposit, and

incorporating results from 1) and 2), indicate criteria that might be used to identify districts and locations capable of hosting HYC-type deposits elsewhere in the Carpentaria Zinc Belt.

This chapter details the design and construction of a GIS for the accomplishment of these aims, incorporating data from the McArthur Basin. Results and implications of the metallogenic analysis are described in Chapter 4.

3.1 Data Model - Arc/Info

Arc/Info is a GIS software package produced by the Environmental Systems Research Institute Inc. of Redlands, California, USA. It employs a geo-relational model where vector-based spatial data is linked to attribute information stored in a relational database (INFO). The three basic geographic information types in Arc/Info are points, lines (arcs) and polygons. These are linked to point attribute tables (PATs), arc attribute tables (AATs) and polygon attribute tables (PATs) respectively, in INFO. INFO's support of relational data structures greatly improves attribute data storage, retrieval and analysis efficiency.

Arc/Info also supports a number of other geographic data models. Those that have been utilised in this project include the TIN (Triangulated Irregular Network) and GRID modules. Their primary use has been for 2.5D visualisation of structural data.

One of the primary reasons for choosing Arc/Info as a platform for the GIS was its ability to support a wide range of analytical and display tools for raster datasets, as well as and coupled with its powerful vector data analysis functions. Another was the already widespread utilisation of Arc/Info by other GIS users, facilitating potential data exchanges. The availability of sufficient computing power, ready access to a licence and software-specific expertise within the School of Earth Sciences at the University of Tasmania were also significant factors.

All geographic data in the McArthur Basin GIS was transformed to the Universal Transverse Mercator projection, and referenced to the Australian Map Grid, Zone 53.

3.2 Datasets

3.2.1 Geology

The primary geological data sources were the 1:250,000 scale Bauhinia Downs geological map and explanatory notes (Pietsch et al., 1991), and the 1:1,000,000 McArthur Basin geological map (Plumb, 1988). These have been supplemented by additional compilation and synthesis from the literature, references to which appear in the relevant portions of this chapter.

3.2.1.1 Initial editing procedures

The Bauhinia Downs map was scanned from the original Mylar film separates by the Australian Geological Survey Organisation (AGSO) using Intergraph equipment (C. Malouf, pers. comm.) and thus retains a high degree of spatial accuracy, consistent with the standards suggested by AGSO (Hazell and Wyborn, 1995; http://www.agso.gov.au/information/data_dictionary.html). The vectorising software attempted to differentiate line symbols based on their width. Unfortunately this process was only partially successful; inadequacies of the scanning software and the nature of the original geological map being chiefly responsible.

The failure to adequately separate line symbols presented the most serious difficulty. Arcs representing geological boundaries, faults, dip/strike symbols, joints, lineaments and the map frame were distributed amongst seven layers with effectiveness only moderately better than random. Additionally, a large number of spurious micro-arcs were created in each raw coverage by the scanning and vectorising process. The first step in the editing process was to separate each line type from the 'noise' arcs and into its own coverage. Geologically meaningful arcs were manually assigned a numeric attribute (LINECODE) in the AAT (Arc Attribute Table). Geological arc types and their corresponding linecodes are listed in Table 3.1.

Individual coverages for each line category were then produced by reselecting based on LINECODE. All further line editing was performed on the separated coverages. No distinction was made between non-fault geological boundaries and their inferred or concealed equivalents, as it was judged that this would introduce unnecessary complexity to the editing process for little gain in useful geological information.

Line Type	LINECODE
Joint	10
Dip/strike	20
Lineament	30
Geological boundary	40
Frame	50
Fault	100
Fault (inferred)	110

Table 3.1 Linecodes assigned to scanned geological linework in order to facilitate their editing and separation.

3.2.1.2 Arc coverages

Most of the strictly arc-type coverages required little further editing. The *joints* coverage was left virtually as it was scanned, with little arc editing and no attribute data. Mapped joint lines are confined mainly to the Abner (Mesoproterozoic) and Bukalara (Cambrian) Sandstones. No further editing work on joints was justified, as they are ambiguous in terms of structural interpretation (Davis, 1984) and, especially in the case of the Cambrian sandstones, of little probable relevance to Proterozoic base metal mineralisation.

The *bedding* coverage is composed of strike lines derived directly from scanned dip/strike symbols. Airphoto-interpreted bedding trends with qualitative or no dip information were also incorporated in this layer. Its attribute table contains dip angles (in the DIP item, measured in degrees) and dip directions (N, S, E or W; in the DIR item) for each strike line representing a dip/strike measurement, thus wholly defining the dip plane.

The *lineaments* layer consists of a limited number of arcs, up to several kilometres in length (check), with no attribute data. They only appear on a small percentage of the Bauhinia Downs map sheet area, mainly in narrow strips within the southern portion. The patchy nature of the lineament mapping severely restricts its usefulness for regional metallogenic studies.

Fold axes were not included in the original scanning but were manually digitised from a laminated copy of the Bauhinia Downs 1:250,000 map sheet (Pietsch et al., 1991). Fold axes are defined as anticlines or synclines according to a numeric item in its attribute table, with the arbitrarily assigned integers 50, 55, 60 and 65 denoting synclines, inferred synclines, anticlines and inferred anticlines respectively. Plunge direction on the fold axes is designated by arc directionality as defined during digitising. Another item, PLUNGE, in the *folds* attribute table contains the value 0 if no plunge exists or has been measured, and 1 otherwise.

Faults mapped on Bauhinia Downs have been copied from the primary geology layer (discussed below) and split into two sub-layers, each layer containing different attribute data. The first layer (*faults*) has a two-fold subdivision only, with the item 'LINECODE' in the corresponding arc attribute table identifying the fault as either observed (LINECODE = 100) or approximate and/or inferred (LINECODE = 110). *1stfaults*, the second faults layer, attempts to define the major regional faults as they are observed to outcrop in Bauhinia Downs. Whether a fault is in the category of a 'major regional fault' has been

decided on somewhat subjective criteria, including identifiable presence in more regional geological compilations by previous authors, primarily Plumb (1988) and tectonic sketches in Pietsch et al. (1991). In translating gross structures from 1;1,000,000 or smaller scale, the author (assisted by J. Rogers, pers. comm.), has been generous in selection of some mapped 1:250,000 scale faults as first-order structures, resulting in their appearance as 'fault zones' rather than discrete arcs in some places. This can be justified by inspection of the McArthur Basin study area map (Figure 2.2), whereby it is clear that many of the individual faults in a given fault zone accommodate significant displacement, rather than any one fault. The fault zones may be flower structures with individual faults merging into a single 'stem' fault at depth. The gross basin architecture as interpreted from gravity and magnetics (Leaman, 1998; see section 3.2.3) can also be used to argue that any one of many faults in a 'fault zone' or 'structural corridor' may be tapping deep basin fluid reservoirs, and thus should be included as major structures for metallogenic studies. Presently the *1stfaults* layer relates to only one item of attribute data in a related data table, that being the name of the fault. There is obvious scope for addition of further attribute data to this table, for example 'fault type' where this could be classified as strike-slip, normal, reverse or combinations of these, but a sufficiently detailed structural assessment of the region was not available.

A *culture* layer was included in order to provide additional geographic context to the geologic data. The line component of *culture* has a two-fold classification into highways and unsealed roads or tracks.

3.2.1.3 Polygon coverages

A major obstacle in constructing topologic polygons from the scanned geological map was the number of boundaries with approximate or inferred status, which were represented as dashed instead of continuous. This was a particular problem in the case of faults, where many dashes were so nearly as short as their width, and the distance between them so great, that automatic scanning and editing procedures had no possibility of correctly interpolating a continuous line. Many obviously incorrect or, more seriously, misleading arcs resulted. Careful, intensive manual editing procedures and extensive head-up digitising were hence required to reconstruct continuous fault arcs from their erroneously scanned antecedents.

Fortunately, dash separations in many of the non-fault geological boundaries were sufficiently small such that the dashes could be automatically joined by judicious employment of the GENERALIZE (a command designed to eliminate excess vertices from lines) in Arc/Info's editing module, ArcEdit. The majority of these arcs, however, also had to be joined manually or redigitised.

A clean, topologically correct geological map data layer (*primgeol*) was finally produced after all arc intersection errors had been displayed and resolved. Automated spatial data cleaning routines such as Arc/Info's CLEAN command were not employed at any stage. These can impart slight shifts to the original data, creating extraneous 'sliver' polygons at acutely converging arcs (Wyborn et al., 1995a) as well as the inherent loss of spatial accuracy. Apart from correction of minor errors discovered during polygon attributing, no further editing of arcs was performed. Faults were extracted into their own layer (*faults*) where this was convenient, by selecting on the LINECODE item, only at the end of the polygon attributing process. This procedure ensured exact congruence between the faults layer containing many polygon-bounding faults, and the primary geology polygons. Any further editing of fault data

subsequently found to be necessary was performed on *primgeol* and the fault layer then re-created from the primary geology data, in order to maintain consistency.

3.2.1.3.1 Geological attribute data

The attribute structure for the digital geology polygons largely follows the scheme described by McClenaghan et al. (1994). This was in preference to adopting data structures developed by AGSO (Ryburn et al., 1993; http://www.agso.gov.au/minerals/lookup_table.html), which are more geared to the needs of a national corporate database than a project-specific compilation. Some data storage efficiency has been sacrificed in order to maximise the ease of performing queries in Arc/Info. This is manifest in many cases by duplication of some fields in many of the attribute tables. Wherever possible, attribute codes have been taken from existing AGSO authority tables.

Each stratigraphic unit present in the study area has been assigned a unique four digit integer ID (CODE) based on its relative stratigraphic position. This number is the primary key linking the geology polygons to all their related attribute tables. Although stratigraphic relationships are specifically encoded in the polygon attribute scheme, the numbering system is also hierarchical with ID codes incremented according to their stratigraphic status, e.g. individual formations are given ID codes in increments of 10, while sub-groups increment in multiples of 100. Exceptions occur in the case of presumed stratigraphic equivalents in different regions, for example McArthur Group (3000) and McNamara Group (3100/3200). Maintenance of this relationship greatly assists automatic legend production with map units appearing in their stratigraphic order, and facilitates polygon selection according to relative stratigraphic age where this is not adequately defined by radiometric dating. For example, queries such as 'select all Umbolooga Subgroup units older than the Teena Dolomite' are possible using the stratigraphically-ordered hierarchical coding system, a set which could not be calculated directly from radiometric age constraints.

Stratigraphic information is encoded in the table STRAT.DAT. There is a many-to-one correspondence between the *primgeol* polygon attribute table (PAT) and this table, with the field CODE being common to both tables. A typical extract from STRAT.DAT is given as Table 3.2.

A full listing of the STRAT.DAT table is given in Appendix 9. Some blank or invariant fields (REGION, SPGRP, EPOCH, DIV, DESC) have been omitted from the extract shown in Table 3.2. The important features of each field are described below.

SYMBOL refers to the shorthand symbol for the unit on published maps.

MINAGE and MAXAGE give absolute age constraints on each unit (in m.y.) derived from published radiometric dating (Page and Sweet, 1998; Page, 1988; Kralik, 1982).

STRMIN and STRMAX are the minimum and maximum measured true thicknesses of the formation (in metres). Note that these dimensions are indicative only, being based on a limited number of measured sections and photo-interpretation both within and outside the mapped region. A STRMIN equal to zero thus means that the unit is observed to lens out, but a STRMIN greater than zero does not necessarily imply that the unit occurs throughout the basin.

STRAT.DAT

CODE	SYMBOL	LOCAL	GRP	SBGRP	FRM	MBR	ERA	PERIOD	MIN AGE	MAX AGE	STR MIN	STR MAX
3600	P_m		4029	7403	0	0	PP	ST	1600	1719	2000	3300
3610	P_mx		4029	7403	2202	0	PP	ST	1600	1647	30	350
3620	P_mq		4029	7403	344	0	PP	ST	1633	1647	10	900
3630	P_mp		4029	7403	2418	0	PP	ST	1633	1719	15	130
3632	P_mpc		4029	7403	2418	3534	PP	ST	1633	1719	15	70
3640	P_me		4029	7403	3629	0	PP	ST	1633	1719		620
3642	P_mei		4029	7403	3629	4075	PP	ST	1633	1719		
3644	P_mea		4029	7403	3629	4007	PP	ST	1633	1719		
3650	P_mf		4029	7403	1914	0	PP	ST	1633	1719	40	60
3660	P_mi		4029	7403	1502	0	PP	ST	1633	1719	0	30
3670	P_mt		4029	7403	2483	0	PP	ST	1633	1719		200
3680	P_md		4029	7403	8343	0	PP	ST	1633	1719	80	350
3681	P_md	TP	4029	7403	8343	0	PP	ST	1633	1719	80	150
3690	P_ma		4029	7403	241	0	PP	ST	1633	1719	50	150
3691	P_ma	SB	4029	7403	241	0	PP	ST	1633	1719	150	180
3710	P_ml		4029	7403	95	0	PP	ST	1633	1719	100	450
3711	P_ml	MD	4029	7403	95	0	PP	ST	1633	1719	200	220
3712	P_ml	TR	4029	7403	95	0	PP	ST	1633	1719	200	220
3713	P_ml	MH	4029	7403	95	0	PP	ST	1633	1719	100	110
3714	P_ml	FI	4029	7403	95	0	PP	ST	1633	1719	250	300
3715	P_ml	WB	4029	7403	95	0	PP	ST	1633	1719	300	450

Table 3.2 Extract from the stratigraphic data table STRAT.DAT

The REGION field (not shown in Table 3.2) describes the affiliation of each stratigraphic unit to continent-scale geological provinces, and uses codes defined by the AGSO GEOPROVS authority table (Ryburn et al., 1993; http://www.agso.gov.au/minerals/lookup_table.html). In the case of Table 3.2, every record shown has REGION = 52 (for the McArthur Basin). The coarse REGION classification is subdivided by the LOCAL field, which uses two-letter codes to denote geographic or descriptive geologic localities (e.g. 'TR' = 'Tawallah Range', 'FI' = 'Foelsche Inlier'). The use of sub-province names with genetic connotations like 'Batten Trough' or 'Wearyan Shelf' has been avoided wherever possible. Stratigraphic formations that vary systematically in thickness and/or composition between localities across the region have been given their own unique CODE in order to retain this spatial variability. An example of a stratigraphic unit with multiple CODEs in Table 3.2 is the Mallapunyah Formation (P_ml) which has codes ranging from 3710 to 3715 depending on locality, and correspondingly varying thickness attributes.

The stratigraphic position of a rock unit is defined by five fields: SPGRP, GRP, SBGRP, FRM and MBR, which specify the level of the unit within the regional stratigraphic scheme. Each record in the stratigraphic table also has its place in higher levels in the stratigraphic hierarchy explicitly encoded in the relevant fields, thus a unit defined as a formation (i.e. FRM is non-null) will also have non-null entries in SBGRP, GRP and SPGRP wherever this is applicable. Numeric codes in these fields are derived from the AGSO authority table for stratigraphic names, STRATLEX (http://www.agso.gov.au/information/structure/isd/database/stratname2.html), which defines five digit codes for all ratified Australian stratigraphic units.

ERA, PERIOD, EPOCH and DIV define a unit's stratigraphic age according to the recently ratified international system for the Proterozoic (Plumb, 1991). These fields employ two-letter codes according to authority tables defined by the author. The STRAT.DAT extract (Table 3.2) indicates all units to be of the Palaeoproterozoic era ('PP') and the Statherian period (ST). The uncertainty and paucity of absolute radiometric dates, as well as the possibility of groups straddling critical time divisions necessitated definition of composite codes for some units, e.g. 'EC' for Ectasian-Calymmian. EPOCH and DIV are not used by any of the Proterozoic units, but are included as a contingency against the possible development of a more detailed local relative time scale based on magnetostratigraphy or stromatolite and microfossil biostratigraphy.

MINAGE and MAXAGE define the absolute age constraints for all units based on radiometric dating. Age estimates are conservative in that they employ the upper (older) bound in the case of MAXAGE, and the lower (younger) bound in the case of MINAGE, rather than using the mean or best estimate of a formation's age. Hence, Umbolooga Subgroup units below the Barney Creek Formation (dated from tuffs at 1640±7 Ma) have a minimum age of 1633 Ma rather than 1640, while the Reward Dolomite (above the Barney Creek Formation) has a maximum age of 1647 Ma. Most radiometric ages used are those quoted in Pietsch et al. (1991), subsequently updated with ages reported by Page (1997) and Page and Sweet (1998). In the absence of radiometric dating, limits have been assigned IUGS minimum and/or maximum ages based on stratigraphic relationships and generally accepted correlations. Thus, the McArthur Group has a MINAGE of 1600 Ma in spite of the absence of any reasonable absolute age constraint above the Barney Creek Formation.

Lithological information is encoded in the table LITH.DAT (Table 3.3), which has a many-to-many correspondence with *primgeol*'s PAT, linked by the unique geological map unit ID CODE. Each record in LITH.DAT represents a unique lithology present within the rock unit defined by CODE. A one-to-many relationship thus exists between the stratigraphic (STRAT.DAT) and lithological (LITH.DAT) attribute tables through the CODE item. Selection of a given stratigraphic unit, for example the Wollogorang Formation (CODE = 4040) will retrieve all lithological attribute records with the corresponding CODE. This relationship also works in reverse; thus selection of all lithologies containing pyrite (MIN = 'PY') will retrieve all stratigraphic units satisfying this criteria, even though not all lithologies for those CODES actually contain pyrite.

Lithological attributes are constructed hierarchically after McClenaghan et al. (1994), in order to facilitate queries on as many levels as possible. Encoded levels of lithological classification range from detailed (for example sedimentary structures in TEXT) to very basic (igneous/sedimentary/metamorphic categorisations in CLASS). These and other attribute fields in LITH.DAT are discussed more fully below. While this scheme makes the overall attribute database somewhat larger than is strictly necessary, this slight disadvantage is far outweighed by gains in the simplicity of queries. A request to select all sedimentary rocks, for example, might otherwise have to be constructed by the selection of all possible sedimentary lithologies, with all the extra effort and possibility of error or omission that such a query would entail.

LITH.DAT

CODE	CLASS	TYPE	COMP	GEN	ENV	LITH	PROP	TEXT	MIN	WEATH
4040	S	CHEM	CARB	N	lc fl	DLST	20	F TN SUL BTM	PY	rc
4040	S	CHEM	CARB	N	lc fl	DLST	5	F STRO SUL BTM	PY	rc
4040	S	EPC	CARB	N	lc fl	BX	1	C DMT		rc
4040	S	EPC		N	lc fl	SHLE	15	EVPT PS		rc
4040	S	EPC		N	lc	SHLE	15	ORG SUL DMT	PY	rc
4040	S	EPC		S		SDST	15	FER DMT XB		rc
4040	S	EPC	QZ	S		ARNT	20	WH		rc
4040	S	EPC		S		CNGL	5	PB		rc
4040	S	CHEM	CARB	P	lg em	DLST	5	XL		rc
4050	I	EXV	MAF	V	sa	BLT	30	RE BR GY F M		rc
4050	I	EXV	FLS	V	sa	RHY	10	AB BA		rc
4050	S	EPC		N	lc lg	SHLE	15	HFL		rc
4050	S	CHEM	CARB	N	lc lg	DLST	10	F SLY HFL		rc
4050	S	EPC		N	lc lg	SDST	5	FER		rc
4050	S	EPC	CARB	N	lc lg	BX	5	DMT		rc
4050	I	ITV	MAF	I		DLT	25	HK MTS		rc

Table 3.3 Extract from lithological data table LITH.DAT

All entries appearing as capitals in the extract from LITH.DAT (Table 3.3) with the exception of the item GEN relate to codes in AGSO authority tables (mainly LITHNAMES; M. Duggan, pers. comm.), adapted to the structure of this GIS. Lower case codes denote those defined by the author for data categories not adequately covered by AGSO tables available at the time of compilation. All abbreviations and authority tables used are documented in Appendix 7.

The fundamental classification of lithologies involves one compositional and two genetic orders of categorisation. The items CLASS and TYPE are together roughly equivalent to the ROCK_TYPE codes described in AGSO's field notebook guide (Blewett, 1993). CLASS is a single-character text field containing the simplest genetic lithological divisions (Igneous, Metamorphic, Sedimentary, Unconsolidated), which are in turn subdivided by the TYPE item (three- or four-character codes), essentially on a more detailed genetic basis. Virtually all sedimentary rocks in the McArthur Basin classify as being of epiclastic (EPC) or chemical (CHEM) origin. Mixtures of the two are handled using qualifiers; thus a silty dolomite is categorised as being of CHEM type, but will contain SLY (for silty) in the TEXT field.

COMP describes the dominant composition of the lithology. Minor constituents or mixed compositions are encoded using the TEXT qualifiers, though following AGSO's usage some exceptions have been made, e.g. QF for 'quartzo-feldspathic' as well as QZ (quartzose) and FEL (feldspathic).

Depositional environments interpreted for each lithology are encoded in two items - GEN, for 'genesis', and ENV for 'palaeo-environment', the latter being a subdivision of the former. GEN is a single-character field encoding a coarse subdivision; with most sedimentary lithologies in the McArthur Basin interpreted as either shallow marine (S) or non-marine (N). For the case where the genesis of a single lithology is ambiguous interpreted or grades from one category to the other, the code B for 'both shallow marine and/or non marine' has been defined. ENV defines the depositional environment of the lithology more specifically in the form of two-character codes, with up to three environments allowed for any one

lithology. Examples from Table 3.3 include 'lc' for 'lacustrine', 'lg' for 'lagoonal' being the saline equivalent of lacustrine; 'em' for 'emergent' and 'sa' for 'subaerial'. These codes for ENV are from AGSO's palaeo-environment authority tables developed for characterisation of petroleum basins (J. Bradshaw, pers. comm.).

The LITH field explicitly characterises the lithology in terms of codes from the AGSO LITHNAMES authority table (M. Duggan, pers. comm.; http://www.agso.gov.au/information/structure/isd/database/lookups.html). A convention of four-character codes for sedimentary lithologies and three-character codes for igneous and metamorphic lithologies is generally followed. Most defined lithologies are taken directly from Pietsch et al (1991), supplemented by Jackson et al (1987) who used a basic grainsize terminology for the classification of carbonates, such as dololutite and dolarenite. These terms are not supported by LITHNAMES, and have been adapted for this GIS by use of the relevant qualifiers on the general rock name DLST (for dolostone); thus a dololutite is coded in LITH as DLST, with F (for 'fine-grained') in the TEXT field.

The PROP item, for 'proportion', is an integer field giving an indication of the volumetric proportion of the particular lithology, expressed as a percentage of the total stratigraphic unit. These have been estimated from text descriptions, as well as published measured stratigraphic sections in Pietsch et al (1991) and Jackson et al. (1987). As such, they are strictly a qualitative indication only, particularly because of the likelihood of lateral variations within stratigraphic units away from measured sections.

The TEXT field contains qualifiers that enable a full description of a given lithology by modifying or augmenting the coarser classifications of the other fields. Up to 30 characters may be entered, separated by spaces. The qualifiers may be of any type, indicating compositional, grainsize, internal structural, sorting and other features. These range from basic descriptors like P or W for 'poorly-sorted' and 'well-sorted', through to more exotic designations like SUL for 'sulphidic' or LTX for 'low-angle trough cross bedding'.

Unusual or diagnostic minerals appear in the MIN ('mineralogy') field. There may be some overlap between this field and TEXT, thus PY (pyrite) may appear in MIN in addition to PYR (pyritic) or SUL (sulphidic) in TEXT. MIN entries for many lithologies may actually refer to pseudomorphs of the given mineral (usually GP for 'gypsum' or HL for 'halite'), but these have been retained for their diagnostic value.

3.2.1.4 Point coverages

The most important point coverage in the McArthur Basin GIS is the mineral occurrence database. Initially this was constructed from data for 58 mines, prospects and other mineral occurrences tabulated in the Bauhinia Downs explanatory notes (Pietsch et al., 1991). These were subsequently superseded and augmented by data extracted from the Northern Territory Geological Survey (NTGS) database (B. Roberts, pers. comm.). The new NTGS data covers a large portion of the northeastern NT south of the Gulf of Carpentaria, including the GIS study area. Minor corrections were made to some database entries after validation against geological mapping (using point-in-polygon overlay) and literature sources

(mainly Ahmad et al., 1989; Walker et al., 1983; Williams, 1978a; Walker et al., 1977) wherever available.

Attribute data for the deposits is contained in several items in MINOCC.PAT (Table 3.4). Many of these consist of codes relating to authority tables, some of which have been defined by the author, but most are based on AGSO authority tables.

MINDEP -ID	NAME	MAJ COM	MIN COM	OPS	SHAPE	HOST	HOST LITH	ORE MIN1	ORE MIN2	SEC MIN1	GRAIN SIZE	STYLE
25	Biondi	Pb		P	SB	3610	188	GN				
26	Emu Plains	Pb Zn	Ag	P	SF	3620	195	SP	PY GN CCP		VF	LA
27	Barney Creek	Pb	Ag	O	SF	3642	216	GN		CER	C	MV
28	Barneys	Pb	Ag	O	SF	3630	202	GN		CER	C	DI MV
29	HYC	Zn Pb Ag	Cu	OM	SF	3620	195	SP GN	PY CCP	HMM	VF	LA BE
30	Cooley II	Cu	Pb Zn	D	SB	3640	212	CCP	BN GN SP PY		C	BR
31	Cooley I	Zn Pb	Cu	D	SB	3640	212	GN	SP	CER	C	BR MV
32	Cooley III	Pb Zn	Cu	D	SB	3640	212	GN SP			C	BR
33	Ridge I	Pb Zn	Cu	D	SB	3620	198	GN SP	PY TTH		C	BR
34	Ridge II	Pb Zn	Cu	D	SB	3620	198	GN	SP PY TTH		C	BR
35	Buffalo Lagoon	Pb		O	SB	3642	216	GN	PY	CER	C	DI
36		Ba		O	VN	4050	366	BRT			VC	
37	Mitchell Yard	Zn Pb		P	SF	3620	195	SP	GN PY		F	DI
38	Myrtle Basin	Pb Zn	Ag Cu	P	SF	3620	195	SP	GN		M F	MV
39	Cooks	Zn Pb		D	SB	3610	191	GN SP	PY MCS CCP	CER	C	BR MV NO
40	Cox	Zn Pb		D	SB	3610	191	SP GN	PY MCS CCP	CER	C	BR MV NO

Table 3.4 Extract from mineral deposit database (MINOCC.PAT)

NAME is a text field of up to 30 characters containing the name of the occurrence. Mineral commodities present in the occurrence have been split into major and minor classifications (MAJCOM and MINCOM) depending on the relative proportion of metals present, with metals being represented by their chemical symbol. For example, the HYC deposit has MAJCOMs Zn, Pb and Ag, and MINCOM Cu. OPS gives the operating status of each occurrence, employing codes used by AGSO in their mineral deposit database (Ewers and Ryburn, 1993). OPS tends to be loosely related to the size of the mineral occurrence, with 'O' for 'occurrence' grading up through 'P' ('prospect') and 'D' ('deposit') to 'OM' or 'operating mine', of which HYC is the only example in the study area. There are insufficient grade/tonnage data for the vast majority of mineral occurrences in the region to justify including these parameters in dedicated fields.

The morphology of each deposit is encoded in SHAPE following the categorisation of Pietsch et al. (1991), with two-letter codes from an AGSO authority table identifying the mineralisation as stratabound (SB), irregular (IR), vein (VN) or stratiform (SF). Host stratigraphic units and lithologies are described by links to the stratigraphic and lithology data tables (Tables 3.2 and 3.3) through corresponding integer codes in the HOST and HOSTLITH fields. Similar links to the lithological data table through three other

fields (SUBHOSTLITH, WALLROCK and SUBWALLROCK; not shown in Table 3.4) describe subordinate and adjacent 'wallrock' lithologies. Major ore minerals are given in OREMIN1, with other economically significant minerals in OREMIN2. Major and minor secondary minerals associated with mineralisation appear in SECMIN1 and SECMIN2 respectively. All fields describing mineralogical data are populated by three-letter codes from the relevant AGSO authority table (AGSOMINERALS). GRAINSIZE and STYLE (describing geometric habit, for example DI = disseminated, BR = brecciated, LA = laminated) both refer to the mineralisation itself, and not necessarily the host rock. AGSO authority tables have also been used in these fields.

3.2.2 Geochemistry

Lithogeochemical data in the McArthur Basin is largely confined to the Bauhinia Downs 1:250,000 map sheet area, with many hundreds of samples from four major studies: Brown et al. (1969); Corbett et al. (1975); Large (1979) and ROCKCHEM (Plumb et al., 1992). Supplementary data was derived from the NTGS (Pietsch et al., 1991), AGSO (L. Wyborn, pers. comm.), Davidson (1998); Rogers (1996) and Large and McGoldrick (1993). The resultant database provides reasonable coverage of the regional stratigraphy. The total dataset has however been somewhat biased in favour of certain lithologies by the particular aims of individual lithogeochemical studies.

In spite of the good coverage of units younger than Roper Group, because the vast majority of samples have been obtained from a limited number of drillholes (most in or near the HYC deposit), short measured sections and easily accessible areas, the overall geographic distribution of data points is highly clustered. The problem is most acute in the (common) case of data from drillholes, where a number of samples, often from different formations, have the same spatial coordinate. This makes it impractical if not impossible to assess spatial patterns in the geochemical data using the methodology adopted for the AGSO Mount Isa metallogenic GIS (Jagodzinski et al., 1993), whereby the mean geochemical element or ratio level derived from sampling within a given rock unit polygon was normalised against the globally averaged value for all samples of the unit. As well, as discussed in section 3.0, the proprietary nature of some datasets made it necessary to degrade or simplify them in some way before publication or presentation to the commercial clients who sponsored this GIS compilation.

The compromise solution adopted was to extract separate sets of summary statistics from each of the input datasets, to be used as the primary data source in the GIS. Mean, median, minimum and maximum values were calculated using Microsoft Excel macros for each element analysed, from every geological map unit sampled, in each dataset. Calculations were performed separately on each dataset as well as on a compilation of all data in order to preserve possible discrepancies between datasets resulting from differences in sampling bias and analytical technique. The resulting statistics for each dataset were assembled as tables related on the CODE item in geochemical attribute tables, an example of which is given as Table 3.5. The geochemical data are thus classified on the stratigraphic subdivision defined by the 1:250,000 scale mapping of Pietsch et al. (1991). This necessitated some consolidation of Corbett et al.'s (1975) samples from members of the Barney Creek Formation into a single unit. Sample statistics from the same geological unit (CODE) but having different originators may be specified and compared using the SOURCE item.

An unfortunate consequence of the use of summary statistics is the loss of spatial information. Sample location layers have been retained, but linked on SOURCE only; that is, disconnected from the raw geochemical data. The derived summary statistics dataset remains a useful means of mapping compositional variations between stratigraphic units, as well as defining both extreme and background geochemical levels for most pre-Roper Group formations and members.

Analysed elements have been separated into three tables based on the AGSO ROCKCHEM database structure (Plumb et al., 1992). MAJORS.DAT contains concentrations for a standard set of major elements, converted to oxide and expressed as a percentage. The form of expression of Fe levels (FEO, FE2O3, FE2O3TOT) could not be standardised across datasets, due to the ambiguous or incomplete expression of Fe concentrations in many datasets. Comparison of data from different SOURCEs is hence limited. Organic carbon (CORG), CO2, S, H2OPLUS and H2OMIN are included in MAJORS.DAT, but have not been analysed in all the original geochemical datasets. A comprehensive listing of MAJORS.DAT is given in Appendix 9. Also included in MAJORS.DAT are LOI (loss on ignition), REST and TOTAL fields.

Table 3.5 was generated by selecting SOURCE = 'all', which is the character code for summary statistics calculated from the compilation of all original data. COUNT gives the number of samples in a given unit, by a given originator, on which the summary statistics are based.

CODE	COUNT	SIO2 mean	SIO2 med	SIO2 min	SIO2 max	AL2O3 mean	AL2O3 med	AL2O3 min	AL2O3 max
3310	1	77.67	77.67	77.67	77.67	10.95	10.95	10.95	10.95
3315	10	58.80	59.05	27.60	83.30	2.48	2.12	0.54	6.40
3320	6	76.07	80	43	91	7.96	7.95	3.58	11.8
3330	79	48.35	48.2	6.95	85.2	3.91	2.64	0.36	15.2
3340	12	63.17	61.65	50.7	79.9	8.29	8.65	2.88	13.5
3342	24	50.14	50.55	17.7	78.5	5.81	5.2	0.44	11.7
3344	197	52.95	53.6	10.8	93.1	5.72	5.6	0.17	13.4
3346	129	58.66	58.4	18	80.7	7.17	7.1	2.02	14.7
3610	53	25.27	22.77	0.66	84.33	2.76	2.16	0.1	13.91
3620	99	38.85	39.7	6.8	82.5	7.14	6.95	0.04	15.8
3630	20	21.81	14.655	1.82	73.4	2.82	1.265	0.4	14.79
3632	32	13.30	8.185	3.66	70.95	2.82	1.32	0.64	15.3
3642	31	3.60	1.54	0.25	26.91	0.42	0.31	0	2.06
3644	111	18.74	6.86	0.15	95.83	0.95	0.39	0	11.4
3650	8	40.66	47.105	10.85	53.13	6.92	7.99	0.14	11.18
3660	5	26.06	26.82	14.56	36.5	2.42	1.57	0.69	6.58
3670	31	31.18	23.44	4.33	84.66	3.02	1.19	0.27	12.43
3680	9	68.93	80.2	9.54	98.08	6.43	4.86	0.6	14.87
3690	48	26.70	20.89	1.45	65.57	2.77	1.23	0.21	15.57
3710	25	59.11	60.47	27.76	88.65	4.70	5.19	0.2	9.54
3720	1	90.76	90.76	90.76	90.76	4.79	4.79	4.79	4.79

Table 3.5 MAJORS.DAT extract.

Data summarising the concentration of rarer geochemical elements in two other tables, structured similarly to Table 3.5 (see Appendix 7). The TRACES.DAT table gives the concentration of trace elements (mainly transition metals) expressed in parts per million. The PPB.DAT table stores the concentration of trace elements expressed in parts per billion. With few exceptions, most datasets have only analysed for Au, Ag and Pt in the ppb range.

3.2.3 Geophysics

As stated above, the 'geophysical' datasets would perhaps more accurately be called 'geophysically-derived' coverages. However, as shall be demonstrated, it is far more useful in terms of geological import and metallogenic analysis to bring the tools of GIS to bear on structures and surfaces interpreted from the geophysical data, rather than on the data itself.

The geophysical component of the McArthur Basin GIS is composed of interpretations by Leaman (1998 and associated references) from gravity, magnetic and seismic data of the most volumetrically significant units in the basin. An account of the interpretation methodology is given in Leaman (1997a), Leaman (1996) and Leaman (1994a).

The geophysical layers were constructed by digitising interpretive contour plots produced by Leaman for various McArthur Basin sub-regions (D. Leaman, pers. comm.), and compiling them for the entire basin; an area stretching from the Urapunga Fault Zone in the north-west to the Riversleigh Fold Zone in the south-east and including the main Bauhinia Downs study area. The source data used in the GIS is thus somewhat more detailed than that appearing in Leaman (1998). Each contoured surface (either structure contours or isochores) defined by Leaman's work has been built as a Triangulated Irregular Network (TIN), then transformed into a lattice using quintic interpolation. Every cell in the resulting grid thus has a value representing either depth-to-interface or unit thickness, measured in metres. Zero or small negative values arising from gridding artefacts were converted to NODATA values.

This gridding process enables 3-D visualisation and surface analysis of the structure contours or isochores defined by the potential field interpretation. Resampled contours have been generated for all surfaces to permit visual relation of the lattices to their cell values, thus every grid coverage has an arc (contour) equivalent. These grids can then be overlain by any of the other datasets contained in the GIS, for the purpose of elucidating relationships between deep, fundamental basin structures and the observed surface geology and mineral occurrence distribution. Examples are shown in Duffett and Leaman (1997).

The original interpretation was of coarse resolution; the isochores and structure contours being at spacings ranging from 100 metres to 5 kilometres vertically, with an uncertainty of similar magnitude in horizontal location. This is partly due to the sparseness of the original potential field data (gravity generally 11km spacing, aeromagnetic flight lines generally 1500m apart), and partly due to the primary objectives of the interpretation, which were to convey the style and shape and gross volume of basin forms rather than to provide precise estimates of their three-dimensional location (Leaman, 1993b).

Consequently, there is a danger of over-enlarging and over-interpreting this material. However, there are a number of advantages to this method of presenting geophysically-derived information. All the tools commonly used to enhance visualisation of primary geophysical data can be applied to lattices that carry much more 'value-added' geological information than the raw gravity and magnetic data. Grid analysis can also be used to generate derived surfaces, for example a grid of 'total volcanics' produced by addition of two other grids representing interpreted thickness of separate components of the volcanic pile. The grids may additionally be used a starting point for gross basin analysis by backstripping (through subtraction of grids). One limitation is the 2.5D nature of Arc/Info's grid analysis tools, in that for each

surface, only one z can be defined for any given x,y coordinate. This appears not to be a serious drawback as far as the McArthur Basin is concerned, with little evidence of extensive intense folding or overthrusting extant.

Five structural surfaces have been constructed covering the entire southern McArthur Basin region. From the lowest (generally) unit upwards, these are: depth to basement granite, depth to base of the felsics (a pre-Tawallah Group igneous accumulation of uncertain affinity, possibly containing a significant mafic component; see Leaman, 1998 and Leaman, 1996), thickness of the felsic volcanics, base of the mafic volcanics, and thickness of the mafic volcanics. Complementing the basement granite structural surface, an additional polygon coverage (*grancomp*) was constructed to represent plutons within it interpreted to have different composition (physical properties) and, possibly, different age.

Other surfaces have been produced which are restricted to the main Bauhinia Downs GIS study area, and represent units higher in the basin stratigraphy than the major igneous accumulations described above. These include grids of thickness and depth-to-top (structure contours) of the upper Tawallah Group mafic volcanics (Leaman 1992, 1993a), also the thickness of more massive (in terms of density) McArthur Group carbonate-dominated units. These lattices are confined almost entirely to the 'Batten Trough' region occupying much of the Bauhinia Downs study area east of the Tawallah Fault.

3.2.4 Culture

A drillhole database (*drilhole*) was compiled as part of a general suite of coverages incorporating cultural information for the Bauhinia Downs study region. The data was obtained principally by S. Bull (pers. comm.) from inspection of NTGS records, and Mount Isa Mines Pty. Ltd. data (P. Winefield, pers. comm.). Attributes including name, total depth, and drillhole type are incorporated in the attribute table associated with points representing drill collar locations. While digital capture of geological drill log information was impractical for this project, the total depth attribute was observed to be a useful proxy for mapping the depth extent of strata (in particular pyritic carbonaceous Barney Creek Formation) considered prospective by explorers.

The other cultural point coverage, *culture*, consists of a two-fold classification on the CULTURE-ID item of settlements into towns and station homesteads. Settlement names are the only attribute included.

Vehicular access routes (*roads* coverage) and watercourses (*streams*) were also digitised from the regional 1:500,000 map (Plumb, 1988) in order to provide additional geographic context to the geological features. *Roads* is subdivided into highways (attributed with their name) and tracks.

4. GIS Analysis for Base Metal Metallogeny

4.0 Introduction

This study aimed to evaluate the utility of GIS in exploration for Zn-Pb deposits in the Carpentaria Zinc Belt. This Proterozoic terrane extending from northwest Queensland to the western Gulf of Carpentaria is known to contain base metal mineralisation of global significance (chapter 2; Fig. 2.1). Much of this endowment is contained in the supergiant stratiform sediment-hosted deposits of Mount Isa, Century and McArthur River (HYC). Model-based prediction of where other such Zn-Pb orebodies might occur is a four-dimensional problem requiring knowledge not only of structures governing *where* metal-bearing fluids might have been focused to intersect a volume of reducing sediment, but also *when* the special conjunction of factors existed to permit this to occur. A major problem in accounting for and predicting deposit location is hence to reconstruct 3-D sedimentary basin architecture as it was when the mineralisation event(s) occurred; not as it is now, several deformation events and erosion episodes later.

This chapter presents a number of GIS-based approaches to the problem of reconstruction of McArthur Basin architecture. The region containing the HYC deposit, the central-southern Batten Fault Zone of the McArthur Basin, was chosen for evaluation. The McArthur Basin comprises the northern portion of the Carpentaria Zinc Belt (Fig. 2.1).

It was soon recognised that approaches involving empirical spatial correlation of base metal deposit occurrences with various geological factors (e.g. Bonham-Carter, 1990) were unlikely to be fruitful. A primary reason for this is the small number of significant known orebodies available to 'train' or develop a set of decision rules for such an approach. Another problem is the lack of extensive outcrop in many areas of the Carpentaria Zinc Belt. This is exacerbated by the recessive nature of many of the prospective stratigraphic units, such that prospective host rocks and mineralisation-controlling structures are obscured. This situation is in direct contrast to precious metal provinces in Canada and Western Australia, where GIS has been successfully applied to prospectivity mapping using statistical methods (Wright and Bonham-Carter, 1992; Knox-Robinson et al., 1992). In these areas, economic concentrations of the commodity sought occur in a large number of structurally controlled deposits in well-exposed or easily-geophysically-mappable terrain. Economic stratiform sediment-hosted base metal mineralisation, on the other hand, is typically concentrated in a few major deposits, whose spatial controls are unclear. A theoretical, essentially model-driven approach has hence been adopted for this study.

The geographic controls on metallogeny may be assessed in terms of metal sources, brine sources and reservoirs, mineralising fluid migration pathways and mechanisms, mineralisation traps, and fluid outflow alteration systems. Significant economic mineralisation will only be created through the optimal conjunction of these systems in four dimensions. Base metal metallogeny in particular is critically dependent on controls operating in the depth (z) dimension. Of the controls outlined above, metal sources, mineralising fluid migration pathways and mineralisation traps are most amenable to analysis given the

available data. The other systems are either too poorly constrained by the available data, or demand sophisticated fluid modelling techniques beyond the scope of this thesis.

In the rare cases where GIS approaches to stratabound base metal prospectivity mapping have been attempted, such as in Jagodzinski et al. (1993), the spatial controls utilised (major regional faults and reducing 'trap' units) have presumably been identified on both empirical and theoretical grounds. Prospectivity maps based on such regional spatial criteria successfully encompass most known base metal occurrences, but are a rather blunt instrument in that the identified prospective area remains quite large in comparison to the extent of the deposits sought, and the size of the metallogenic province.

Conventional regional geological data and data models are inadequate to address the metallogenic problems outlined above. The main aims of this chapter are to redress this; firstly by presenting results from new techniques developed to extract and visualise information pertinent to four-dimensional base metal metallogeny from standard regional geological data, secondly by combining this with interpretations of regional geophysical data, and thirdly by demonstrating how operations on surfaces representing geophysically-interpreted basin architecture can be used to place constraints on metallogenic models. The rationale of the metallogenic constraint analysis was to ascertain minimum constraints on the volume of rock required to source sufficient quantities of base metals to form a deposit such as HYC, and accordingly to use the GIS to visualise the extents of basins and concentration factors required. Volumetric parameters of basin components derived from geophysics were coupled with a compilation of summary lithogeochemical data defining the elemental composition of the basin units.

The common theme in all these approaches is the extraction of the maximum three-dimensional information from the available data, in order to define the geometry of the host basin. The derived products are used to make inferences concerning the 'palaeo-geometry' of the basin, which will have been a first-order control on the localisation of Zn-Pb mineralisation.

The datasets used and their structure have been described in chapter 3. A summary of the key lower portion of McArthur Basin stratigraphy referred to is given in Fig. 2.1. Geophysical issues in the interpretation of 3-D structure in the McArthur Basin are discussed in Leaman (1996; 1998).

4.1 Geological attribute-based basin visualisation

An initial 3-D picture of the basin, relying solely on surface geological data and measured stratigraphic thicknesses, was developed by generation of coverages comprising 'predicted' structure contour values for any given stratigraphic unit.

The method (Fig. 4.1) is based on a stratigraphic attribute table (STRAT.DAT) keyed to the geological map coverage. Representative stratigraphic thicknesses were derived for each unit by calculating the mean of all values measured (mainly sourced from Pietsch et al., 1991) in the study region. In many cases, this was simply the midpoint between the quoted minimum and maximum stratigraphic thicknesses. The results were entered into the field STRMED, with some additional records and stratigraphic codes created to handle gross regional changes in measured thickness in some units. A

datum surface was defined at the top of the Proterozoic McArthur Basin sequence, i.e. the top of the Roper Group, and the STRMED value converted to a number (ZMEAN) representing the stratigraphic distance, in metres, from this datum surface. ZMEAN for any given unit *i* is essentially given by the total thickness of overlying units plus half the thickness of the unit *i*, multiplied by −1 to express elevation with respect to the datum at the top of the Roper Group; or, algebraically:

$$ZMEAN = -1 * \left(\sum_{1}^{i-1} STRMED_i + STRMED_i / 2 \right).$$

These values represent elevation with respect to this datum surface and thus are negative, decreasing with stratigraphic age. Each Proterozoic geology polygon was thus attributed (via the link to STRAT.DAT) with a value representing the elevation of the outcropping unit within the basin stratigraphic sequence. These values range from -133 in the case of the McMinn Formation at the top of the Roper Group, down to -12560 for the Yiyintyi Sandstone at the base of the Tawallah Group.

The geological data were thus used to directly infer present basin geometry, by making the simplifying assumption of 'layer-cake' stratigraphy (Fig. 4.1). The resulting maps (e.g. Fig. 4.2) provide a quantitative visualisation of basin structure not obvious on casual inspection of the standard geological map, and particularly emphasise the magnitude of vertical displacement across faults. The Tawallah Fault is especially prominent in these terms (Fig. 4.2), as is the Abner Fault which is evidently a continuation of the Tawallah Fault on the western edge of the Abner Range, albeit at a higher level in the stratigraphy (cooler colours in Fig. 4.2). The Emu Fault is of rather enigmatic character with little apparent displacement across its northern and southern ends in Fig. 4.2, but major deformation in the vicinity of the fault within 25 km of the HYC deposit. The structurally anomalous character of the Tawallah Group inlier adjacent to the Emu Fault (Masterton Horst) is especially striking. The predominantly strike-slip character of the Mallapunyah Fault is clearly apparent. A feature with quite striking apparent vertical displacement is the fault splaying northeastwards from the Emu Fault from around 8200000N. A major reason for this is the absence of the Nathan Group, as well as faulting. The magnitude of regional folds is also prominently displayed, the N-S-trending Broadmere Syncline and the Abner Range, both of which have upper Roper Group in their cores, being examples. More subtle but nonetheless potentially significant is the intra-McArthur Group uplift in the region southwest of HYC (see also Fig. 4.2), which appears to have an E-W trending aspect. The gross structure implied is similar to an anticlinal box fold with a wavelength around 15 km. In dimensions it appears similar to the uplift represented by the Batten Range on the adjacent western side of the Tawallah Fault, and may have a common origin.

Unit	STRMED (thickness in m)	ZMEAN (av. elevation w.r.t. datum)	Implied basement depth ($zmean_{unit} - zmean_{basement}$)
Roper Group	2120	-1060	10890
Nathan Group	1600	-2920	9030
Batten Subgroup	580	-4010	7940
Umbolooga Subgroup	2650	-5625	6325
Tawallah Group	5000	-9450	2500
basement (base Tawallah)		-11950	0

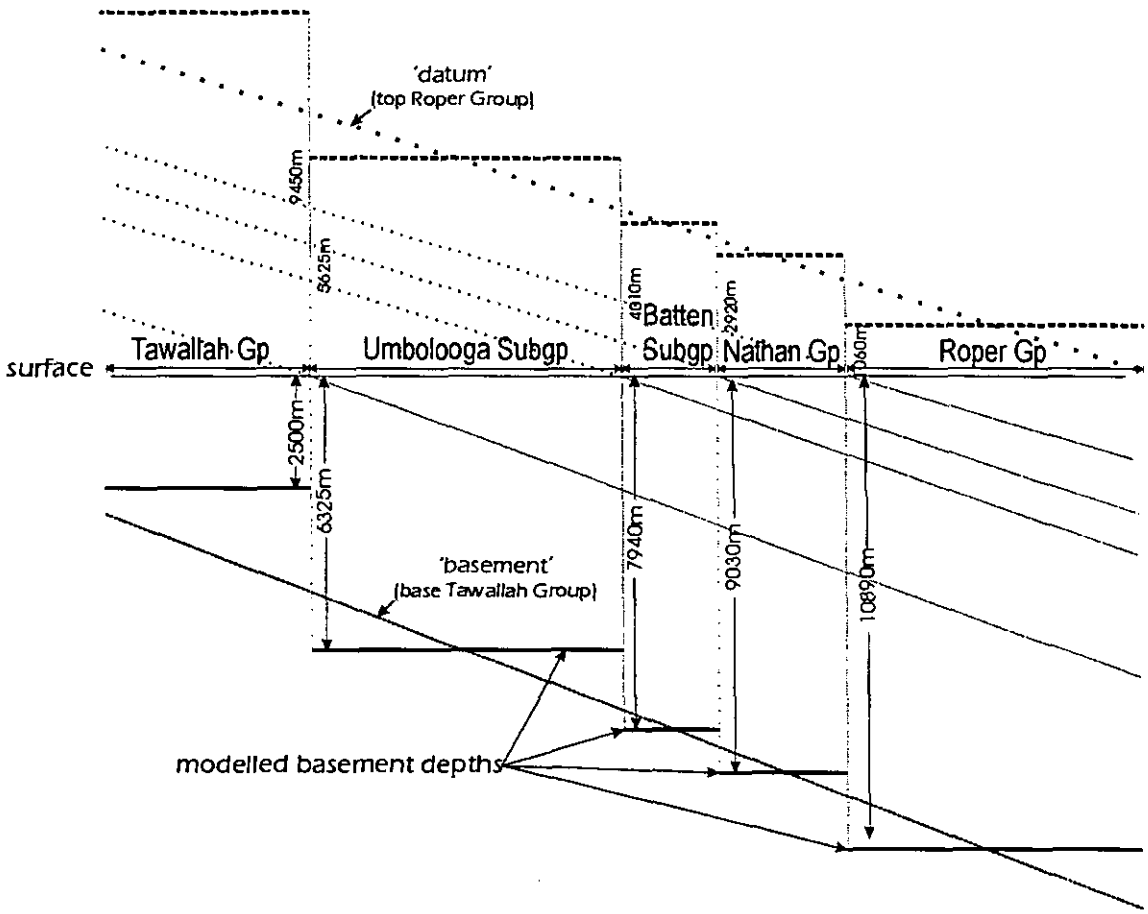

Figure 4.1 Schematic diagram using a simplified example to demonstrate how basement (or any other basin stratigraphic horizon) depth may be modelled using thickness attributes in a GIS

Fig. 4.2 and other maps such as Fig. 4.3 made possible by the stratigraphic thickness data structure described (which might be termed *stratigraphic topology*) effectively make explicit the knowledge of depth extent implied by the stratigraphic column. The depth of an underlying unit or contact may be predicted from surface geology and the attribute table; for example the base of the McArthur Group (base Masterton Sandstone), from which McArthur Group thickness in Fig. 4.3 was derived. This enables 'actual' three-dimensional basin architecture inferred from geophysical data to be analysed in terms of its anomalous character with respect to surface geology (see below; Fig. 4.9).

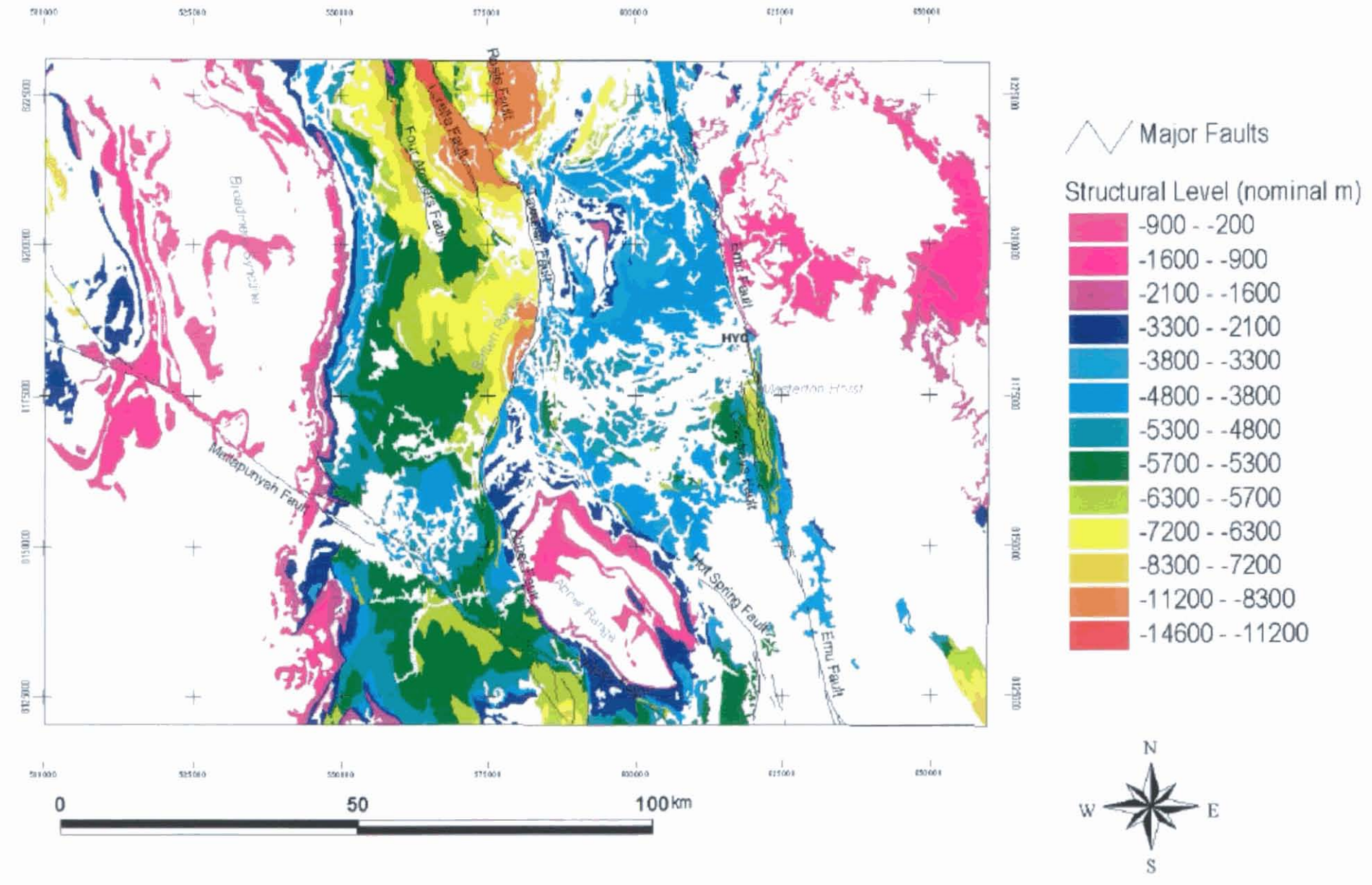

Figure 4.2 Structural level exposure map. Warm colours indicate structurally uplifted areas. See text for details

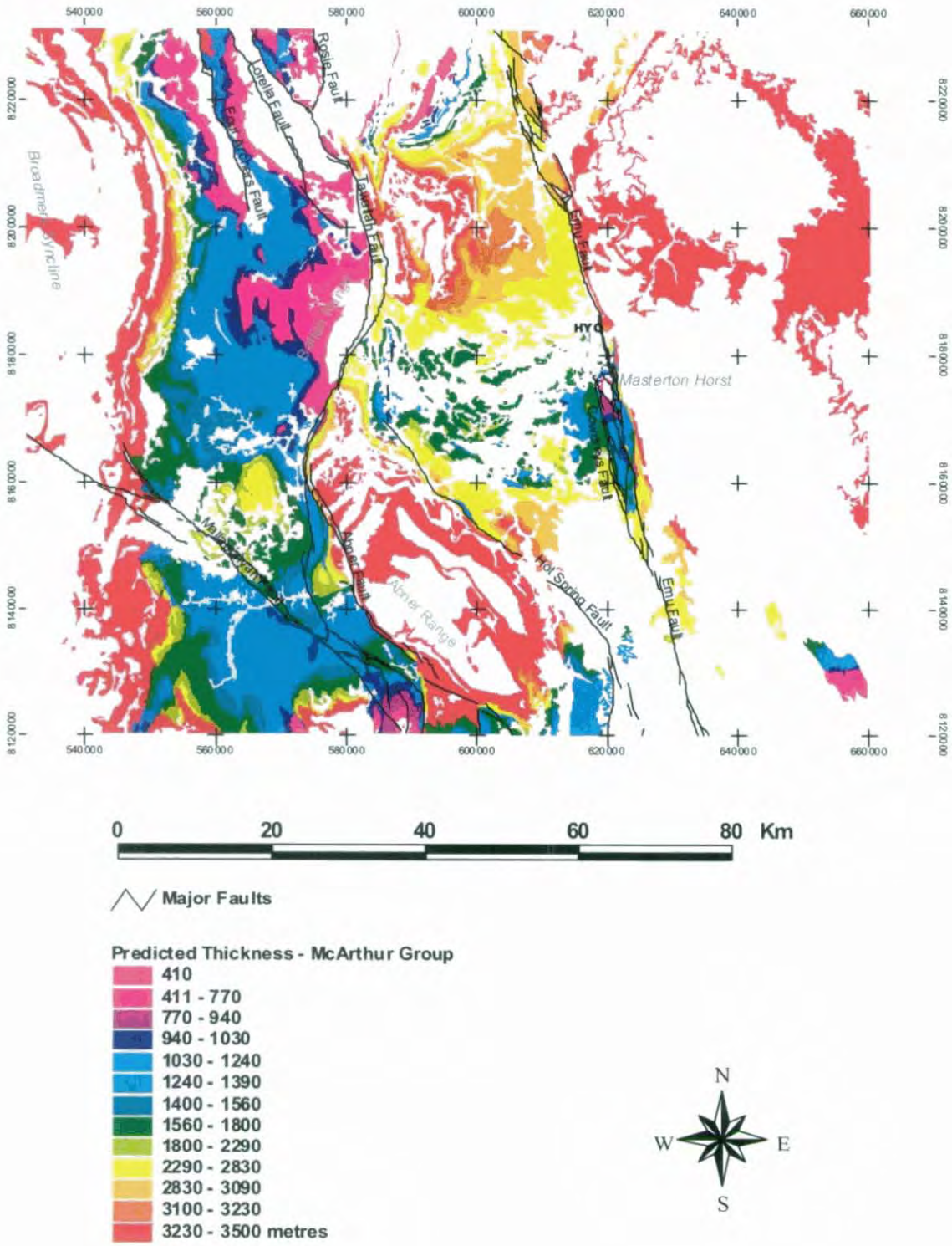

Figure 4.3 McArthur Group thickness, inferred from outcrop geology and stratigraphic thickness attributes

There are some obvious limitations to this approach. The same stratigraphic level is applied to the entire extent of each geology polygon, with no distinction between areas of the polygon near upper or lower stratigraphic contacts (Fig. 4.1). This results in mis-estimation of the depth of underlying units by up to ½*a* tan *?* where *a* is the apparent thickness of the surface unit and *?* is dip, in the worst-case situations at the upper and lower contacts of the exposed unit. The relative magnitude of this error diminishes with

increasing stratigraphic distance between the surface unit and the horizon of interest, and is largely negligible where the mapped stratigraphic resolution is sufficiently high.

Depth of underlying units is additionally underestimated by a factor of 1 / cos ?, being the difference between the true stratigraphic thicknesses modelled and vertical thickness. However, dips exceeding 25° (equating to a thickness underestimation of ~10%) are comparatively rare in the region of the McArthur Basin studied, being generally restricted to zones adjacent to major faults. These geometric errors are not considered unduly significant in the semi-quantitative context of subsequent analysis and interpretation.

Another drawback is that stratigraphic levels cannot be derived for areas obscured by thin Cainozoic cover, limiting the extent to which comparisons can be made with interpretations of underlying broad structure.

All of these objections could be addressed to some extent in further work by attaching the stratigraphic level attribute to bounding arcs as well as to polygons, incorporation of dip and strike data, and use of airborne EM or other geophysical data to infer Proterozoic geology beneath thin cover. The former two refinements might be implemented by interpolation of geology polygons and arcs, incorporating dip and strike information, to a grid data structure. Conversion to raster is a step required in any case to enable direct comparison and analysis with respect to the geophysically derived structural surfaces.

4.2 Automatic unconformity detection

Intra-basinal unconformities denote areas that have been elevated with respect to the contemporaneous basin, resulting in erosion or lack of deposition. As such, their spatial and stratigraphic distribution effectively maps both the location and timing of intra-basinal uplifts and, by omission, possible sub-basin locations.

A technique for automatic extraction of unconformities from detailed geological maps was developed utilising the topological data structure of Arc/Info and two attribute fields added to the stratigraphic look-up table STRAT.DAT. For each record (representing a stratigraphic unit) in the look-up table, these fields (UNDER and OVER) contain the unique code for the stratigraphic unit which would, in a complete basin sequence, conformably underlie and overlie the unit described by the record (Table 4.1).

These stratigraphic polygon attributes were attached to their bounding arcs by hard links based on internal arc record numbers identifying the polygons on the left and right side of the arcs (LPOLY# and RPOLY#). Following queries to eliminate faults and arcs representing nonconformable Proterozoic/Phanerozoic contacts, the stratigraphic unit on the left side of each non-fault arc bounding a Proterozoic geological polygon was identified using the LPOLY# item. The polygons on the right side of the selected arcs were then queried through the RPOLY# item. If the result did not match the 'expected' geologic entity code corresponding to the units conformably above or below the unit originally identified on the left side of the polygon, the arc was identified as an unconformity, and tagged as such in the arc attribute table. The UNDER and OVER attributes were utilised to designate the unconformity as one of four types: intra-group (where both the underlying and overlying units belong to the same stratigraphic

group), 'expected' inter-group (where an unconformity is present by definition, but both the topmost underlying formation/member and the basal overlying formation/member of the respective groups are present), inter-group 1 (where one or more of either the topmost underlying or basal overlying units is missing at the unconformity surface), and inter-group 2 (where an entire group is absent).

CODE	UNIT	UNDER	OVER
3610	Reward Dolomite	3620	3346
3620	Barney Creek Formation	3632	3610
3630	Teena Dolomite	3640	3632
3632	Coxco Dolomite Member	3630	3620
3640	Emmerugga Dolomite	3650	3630
3642	Mitchell Yard Dolomite Member	3644	3630
3644	Mara Dolomite Member	3650	3642
3650	Myrtle Shale	3660	3644
3660	Leila Sandstone	3670	3650
3670	Tooganinie Formation	3680	3660

Table 4.1 Extract from appended stratigraphic data table. The CODE field contains the identification number unique to each stratigraphic unit in the study area, to which the 'stratigraphic topological' attributes UNDER and OVER also refer.

This method was extended to calculate the 'magnitude' of the unconformity, by reference to the stratigraphic thickness attributes described above. Using the absolute stratigraphic level described by ZMEAN, the total measured thicknesses (obviously measured elsewhere in the basin) of 'missing' units (stratigraphically between the polygons on either side of the arc) were used to determine the amount of missing sedimentary section, in metres. This figure was also calculated to the arc attribute table. The link via the left- and right- polygon codes to the stratigraphic attribute table also identifies the stratigraphic time interval represented by the unconformity.

The resulting arc attribute data were extracted into unconformity attribute tables for further analysis (Figs. 4.5-4.7). These tables relate the standard GIS line attributes, such as length, through a unique ID and the stratigraphic attribute table, to the unconformity attributes of type, stratigraphic position (defined by both underlying and overlying unit) and thickness of missing sediment.

The unconformity maps which can be generated as a result of this process (e.g. Fig. 4.4) indicate areas of uplift or low subsidence during basin development, where stratigraphic units are absent due to erosion, lack of deposition, or both. The unconformity magnitude can be interpreted as indicating the magnitude and persistence of these locally elevated regions within the basin, which can act as focusing structures or drivers of basinal fluid flow. Importantly, the unconformities mapped can be queried on the basis of the relative age of their overlying or underlying units, so that the distribution of unconformities within certain intervals may be examined.

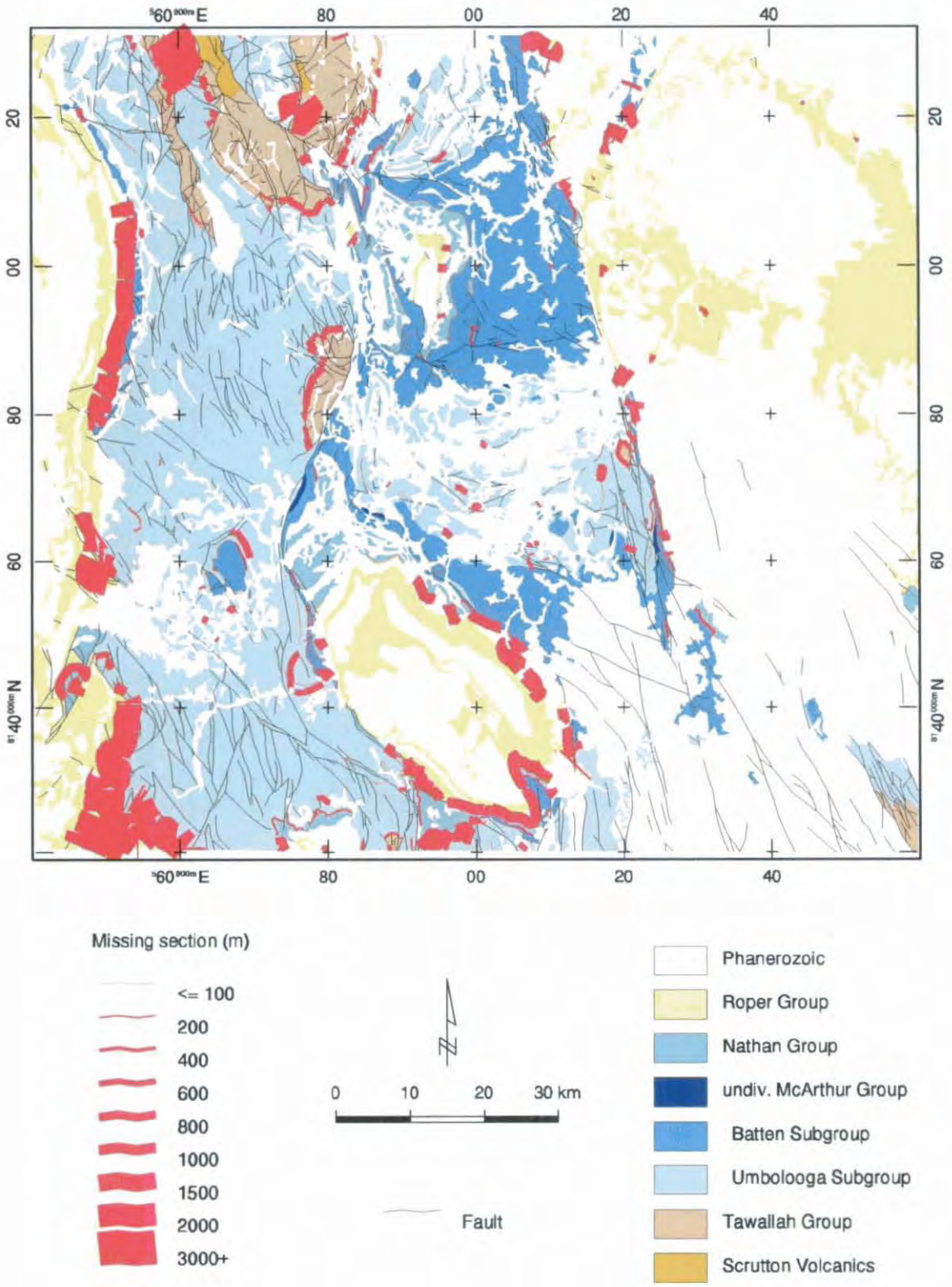

Figure 4.4 McArthur Basin unconformity map, showing amount of missing section

The most prominent unconformities (where the greatest thicknesses of a notional complete section are absent) invariably comprise contacts between stratigraphic entities at the group level (Figure 4.5). The frequent absence of the Tanumbirini Rhyolite, Warramana Sandstone and Gold Creek Volcanics from the top of the Tawallah Group accounts for the identification of several hundred metres of missing section at the Tawallah/McArthur Group contact in many areas. This observation is consistent with deposition of

the upper Tawallah Group in a syn-rift setting. The largest absence of section is observed in the section dipping west and north away from the Tawallah Group inlier in the Batten Range. This supports the proposition based on palaeocurrent and structural data (Bull and Rogers, 1996) that the Batten Range region was elevated during latter Tawallah Group time. Generally, there are a few hundred metres of section missing at all top-Tawallah Group contacts west of the Emu Fault, including the Masterton Horst near HYC and Mallapunyah Dome. Notable exceptions are a small section (~ 12 km long) around 562000E 8212000N (near several base metal prospects including Great Scott and Johnstons) and the Foelsche Inlier area, where no or minor hiatuses are identified. These may denote late Tawallah Group time sub-basins or otherwise relatively depressed areas enabling preservation of a near-complete Tawallah Group sequence.

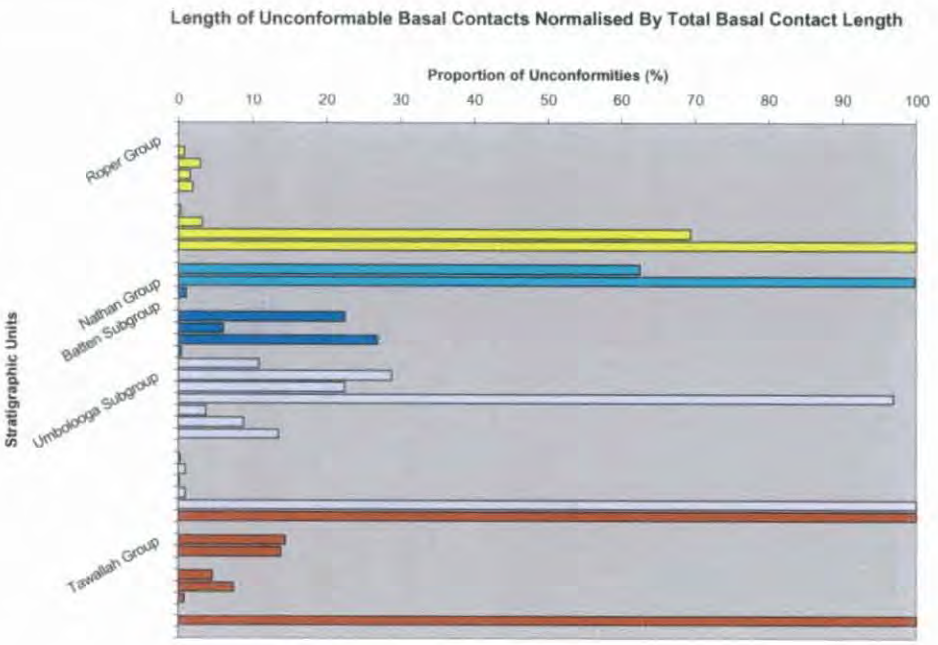

Figure 4.5 Distribution of unconformable surfaces in the stratigraphic column, based on the unconformity attribute data generated within the GIS. Each bar in the chart corresponds to the lower contact of an individual stratigraphic unit (formation or member), and the length of each bar indicates the proportion of these contacts that are unconformable surfaces. The location of an unconformity within the column is defined by the overlying unit.

There are a number of intra-Umbolooga Subgroup unconformities detected, suggesting a reasonable level of structural activity during this phase of basin development. Many of these unconformities (probably disconformities) occur within a strip oriented ENE, extending from the Mallapunyah Fault near 560000E 8160000N to the Emu Fault immediately south of HYC. Many 'unconformities' are associated with the absence of either the Teena Dolomite or its subordinate Coxco Dolomite Member. As these units are differentiated substantially on the basis of diagenetic features, interpretations of these contacts as unconformities in the classic sense must be treated with caution. Other unconformities identified in Fig. 4.6 appear more genuine, and may be mapping a zone of irregular, discontinuous uplifts in the vicinity of the ENE-oriented strip referred to above, active in middle to later Umbolooga Subgroup time. This phase of activity seems to have been more persistent west of the Tawallah Fault, where there are a number of points at which a small amount of section (usually either the Barney Creek Formation or Reward Dolomite) is missing. East of the Tawallah Fault, little erosion appears to have taken place near the

Umbolooga/Batten Subgroup boundary, though some unconformities may be obscured by the generally more extensive Cainozoic cover in this region.

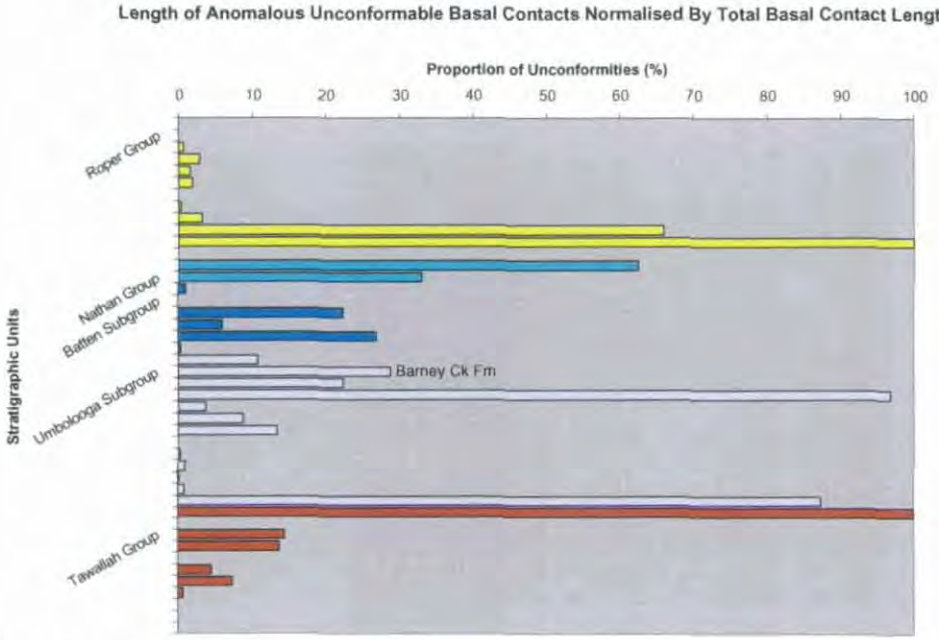

Figure 4.6 Distribution of unconformable surfaces in the stratigraphic column, constructed as in Figure 4.5 but with 'expected' unconformities between complete sections of stratigraphic groups removed. The bar denoting the base of the Barney Creek Formation, host unit of the HYC deposit, is labelled for reference.

The anomalous intra-basinal structural activity characterising the upper Umbolooga Subgroup appears to have waned during Batten Subgroup time, with few unconformities detected.

The Nathan Group marks a substantial shift in regional deposition patterns, which largely accounts for the substantial unconformity defined at its base (the Nathan Group actually rests directly on the Tawallah Group in the Tanumbirini Inlier in the west of the study area, with the entire McArthur Group missing). Instability in sedimentation patterns appears to have persisted well into Nathan Group time however (Figs. 4.6 and 4.7), and it may be that significant topographically driven fluid flow took place at this time also.

The most significant intra-Proterozoic tectonic event recorded by the automatic unconformity detection method took place in the interval between the Nathan Group and the time recorded by the base of the Roper Group. Queries of the stratigraphic attribute table indicate that the basal units of the Roper Group (Limmen Sandstone and Mantungula Formation) incise as deep as the Tatoola Sandstone, well down in the McArthur Group. The magnitude of sediment removed at this interval may be seen in Fig. 4.7. Fig. 4.7 indicates that this sediment removal took place mostly on the western side of the Batten Fault Zone, and reached a maximum in the southwestern corner of the study area.

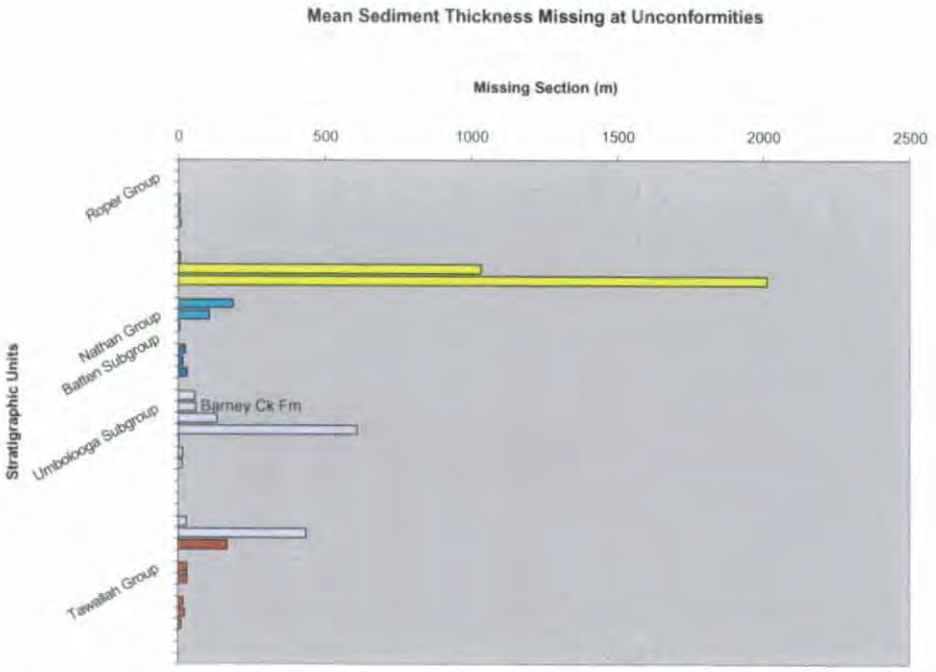

***Figure 4.7** Volume of sediment absence/removal through time, as indicated by the average thickness of section missing at the base of McArthur Basin units. The mean value was calculated for each stratigraphic unit by $\Sigma L_i M_i / C$ where C is the total length of all basal contacts of the stratigraphic unit, L is the contact length in metres (derived from the unconformity subset of the arc attribute table), and M is the thickness in metres of missing section (derived from the stratigraphic attribute table), for each mapped unconformable contact i. The bar denoting the base of the Barney Creek Formation, host unit of the HYC deposit, is labelled for reference.*

4.3 Metallogenic Constraints Analysis

The amount of metal required to form an HYC-sized deposit was taken as the total economically significant tonnage of metal contained in the HYC deposit, reported by Logan et al. (1990) as 227 Mt at 9.2% Zn, 4.1% Pb and 41 g/t Ag. This equates to approximately 21 Mt Zn, 9.3 Mt Pb and 9300 t Ag. These tonnages were then multiplied by average concentrations of the corresponding element in major basin units derived from the summary geochemical data to arrive at a figure for the total volume of average rock required to source the metals concentrated in an HYC-sized ore deposit.

Basin volumes contained are represented by grids denoting thickness of major basin components - 'isopach surfaces'. These surfaces can be viewed as representations of the accommodation space created in the basin during deposition of the unit being considered, assuming negligible subsequent uplift and removal of section. This assumption is violated in the more highly deformed portions of the McArthur Basin, particularly in areas where lower stratigraphic levels have been exposed. These relatively small inliers excepted, the bulk of units older than the Batten Subgroup remain preserved in the basin, at least west of the Tawallah Fault. An approach for restoring the missing section in uplifted areas, in order to arrive at an improved reconstruction of palaeo-accommodation space, is presented below.

This approach to constraining the metallogenic origin of base metals in the McArthur Basin is obviously subject to considerable uncertainty. The economic reserves quoted for the HYC deposit are only a minimum estimate of the total base metal tonnage in the mineralised system, as they do not take into account mineralised but uneconomic rock or metal present in various 'satellite' deposits in the district,

such as the Ridge and Cooley deposits. Estimates of the original bulk geochemical composition of basin packages based on contemporary samples may have been affected by post-depositional addition or removal of base metals, possibly by the very event(s) that resulted in the formation of large ore deposits. Recognising this possibility, base metal concentrations in equivalent modern lithologies have been sought and presented if available.

There is also some scope for refinement of Leaman's (1998) 2-D potential field models used to construct the 2.5-D basin architecture presented. Trade-offs between bodies of different physical properties may be employed to vary the volumes of various model components, though the scope for this is limited by the constraints of outcrop, an interlocking 2-D profile array and the need to produce geologically realistic geometries. However, it is contended, following Leaman (1996), that the relative volumes and overall shapes of basin sequences are unlikely to be significantly changed by further fine model adjustment.

Given these potential sources of error, the metallogenic constraint analysis is at best semi-quantitative. An error of up to 25% in terms of unit thickness can be anticipated at a given location. Despite this inaccuracy, however, the exercise is considered justified as a starting point to evaluate the plausibility of metallogenic models.

4.3.1 McArthur Group carbonate package

This grouping corresponds to that portion of the McArthur Group predominantly composed of carbonate (dolostone); the high density of which enables its interpretation as a distinct geophysical unit. An estimation of the combined bulk base metal concentration in this unit was made utilising the geochemical data summarised and compiled in an INFO table related through the unique stratigraphic unit identifier to the geological map attributes (principally the lithological attribute table). This relationship was used to extract data only from McArthur Group units predominantly composed of carbonate. Data for concentrations of Zn, Pb and Ag were then unloaded into a spreadsheet, where weighted mean elemental concentrations were derived using the following formula:

n x thickness-weighted mean = $\Sigma n_i T_i C_i / \Sigma n_i T_i$

where n = number of analyses from each unit, T = median thickness of unit, C = elemental concentration in unit, in ppm and i represents each individual stratigraphic formation or member.

Results of this extraction and weighted mean calculation are presented in Table 4.2.

The 'weighted mean of medians' in bold italics (5 ppm Zn, 4 ppm Pb, 0.6 ppm Ag) has been taken as best representing the bulk composition of the McArthur Group carbonate packages, since means have generally been skewed upwards by outlying very high values in what are invariably highly asymmetric frequency distributions. Assuming a carbonate density of 2.78 t/m^3 (the same as that used for the geophysical interpretation), this implies required carbonate volumes of 1.5×10^{12} m^3 for Zn, 7.7×10^{11} m^3 for Pb and 5.7×10^9 m^3 for Ag.

unit	strmed (m)	Zn med	Zn mean	Zn max	Pb med	Pb mean	Pb max	Ag med	Ag mean	Ag max	n
Amos Fm	90	1	1	1	2	2	3	0	0	0	2
Looking Glass Fm	50	6	6	6	5	5	5	0	0	0	1
Yalco Fm	150	8	12	106	5	9	70	0	0	0	80
Reward Dolomite	190	5	24	360	8	15	200	2	2	3	67
Teena Dolomite	73	4	43	527	7	22	214	1	1	3	34
Coxco Dolomite Mbr	43	12	18	180	2	4	19	2	2	3	39
Mitchell Yard Dolomite Mbr	150	4	13	142	3	7	36	1	1	3	35
Mara Dolomite Mbr	160	6	11	126	3	5	43	1	1	3	123
Tooganinie Fm	200	5	21	656	6	11	67	0	0	1	53
Amelia Dolomite	165	1	7	80	1	6	30	0	0	0	47
median		*5*	*13*	*134*	*4*	*7*	*40*	*0.5*	*0.5*	*2*	
mean		*5*	*16*	*218*	*4*	*9*	*69*	*0.6*	*0.7*	*1.6*	
n x thick weighted mean		*5*	*15*	*242*	*4*	*9*	*79*	*0.6*	*0.7*	*1.8*	
volume implied (m^3)		*1.5×10^{12}*	*4.9×10^{11}*	*3.1×10^{10}*	*7.7×10^{11}*	*3.8×10^{11}*	*4.3×10^{10}*	*5.7×10^{9}*	*4.6×10^{9}*	*1.9×10^{9}*	

Table 4.2 Summary base metal geochemical data for McArthur Group carbonate-dominated stratigraphic units. 'strmed' is a representative stratigraphic thickness of the units listed, in metres. All element concentrations are in ppm. n is the number of analyses from each unit. 'Volume implied' is the volume of rock required (in this case carbonate) to contain equivalent base metals to the HYC deposit at the concentrations given. Maximum levels measured in each unit are included as an indication of the magnitude of the positive skewness of the frequency distributions. They also provide a conservative upper limit on palaeo-bulk base metal concentrations. Refer to text for details of the weighted mean calculation.

This calculation was repeated using data from all carbonate package units (defined as all units from the Amelia Dolomite to the top of the McArthur Group inclusive) older than the Barney Creek Formation, including interbedded siliciclastic units, on the grounds that these could potentially have participated in any regionally pervasive fluid flow system giving rise to base metal mineralisation. The resulting weighted mean values are however very similar to those calculated for carbonate units only, in spite of the siliciclastics' generally higher base metal tenor, as their relatively low total thickness and number of samples gives them low weight in calculations.

The most obvious flaw in the approach detailed above is the possibility that base metals have been depleted from their original depositional or early diagenetic levels by the very processes which may have resulted in the formation of major orebodies, or by more recent weathering in the case of outcrop samples. A comparison based on base metal concentrations in modern carbonates is thus warranted. The implied volume given in Table 4.3 above was recalculated using a value of 100 ppm Zn in carbonate (from Taylor and McLennan, 1985). The resulting implied volume of carbonate required to contain sufficient Zn to form HYC assuming complete depletion and 100% efficient transport is 7.6×10^{10} m^3. This figure represents a conservative estimate of the lower bound on the volume of McArthur Group carbonate rock required as a metal source.

unit	strmed	Zn med	Zn mean	Zn max	Pb med	Pb mean	Pb max	Ag med	Ag mean	Ag max	n
Teena Dolomite	73	4	43	527	7	22	214	1	1	3	34
Coxco Dolomite Mbr	43	12	18	180	2	4	19	2	2	3	39
Mitchell Yard Dolomite Mbr	150	4	13	142	3	7	36	1	1	3	35
Mara Dolomite Mbr	160	6	11	126	3	5	43	1	1	3	123
Myrtle Shale	50	14	18	34	6	8	28	1	1	2	10
Leila Sandstone	15	10	10	14	15	13	19	1	1	2	5
Tooganinie Fm	200	5	21	656	6	11	67	0	0	1	53
Tatoola Sandstone	215	1	7	43	11	16	76	0	0	0	9
Amelia Dolomite	165	1	7	80	1	6	30	0	0	0	47
median		*5*	*13*	*126*	*6*	*8*	*36*	*1*	*1*	*2*	
mean		*6*	*16*	*200*	*6*	*10*	*59*	*0.7*	*0.8*	*1.9*	
thickness weighted mean		***4***	***15***	***227***	***5***	***10***	***61***	***0.3***	***0.5***	***1.5***	
n x thick weighted mean		*5*	*14*	*250*	*4*	*8*	*54*	*0.6*	*0.6*	*2.0*	
implied volume (m^3)		*1.6E+12*	*5.2E+11*	*3.0E+10*	*8.7E+11*	*4.2E+11*	*6.2E+10*	*5.3E+09*	*5.3E+09*	*1.7E+09*	

Table 4.3 Summary base metal geochemical data for the McArthur Group carbonate package predating the Barney Creek Formation. A weighted mean based only on formation thickness is presented as an indicator of bulk concentration with sampling bias minimised. Refer to Table 4.2 for an explanation of column and row headings.

A visual representation of the calculated volumes of McArthur Group carbonate package required to source HYC is presented as Fig. 4.8. This depiction effectively treats the McArthur carbonate isopach surface as a basin by multiplying grid values denoting thickness by –1. The basin is then 'filled' to the level required to contain the requisite amount of the base metal element in question, and it is this level which is represented in Fig. 4.8 and subsequent figures.

Clearly, from Fig. 4.8, an inordinately high proportion of the McArthur Group sediments would have been required to provide enough metal to source the HYC deposit, assuming reasonable base metal chemical extraction efficiency and fluid concentration mechanisms. Additional contributions to the base metal budget must be sought from deeper in the McArthur Basin sequence.

Other candidate base metal source packages deeper in the basin, geophysically distinguishable by their density and/or magnetic property contrasts, were assessed. Most are both intrinsically richer in base metals (felsic volcanics such as the Scrutton Volcanics or sandstone-dominated siliciclastic packages equated with the Yiyintyi Sandstone, to name two examples) and much more voluminous than the McArthur Group. Consequently, only a relatively small fraction of these deeper packages needs to be tapped in order to source base metals in HYC-level quantities. This is demonstrated below with the example of one of the deeper packages (section 4.3.2).

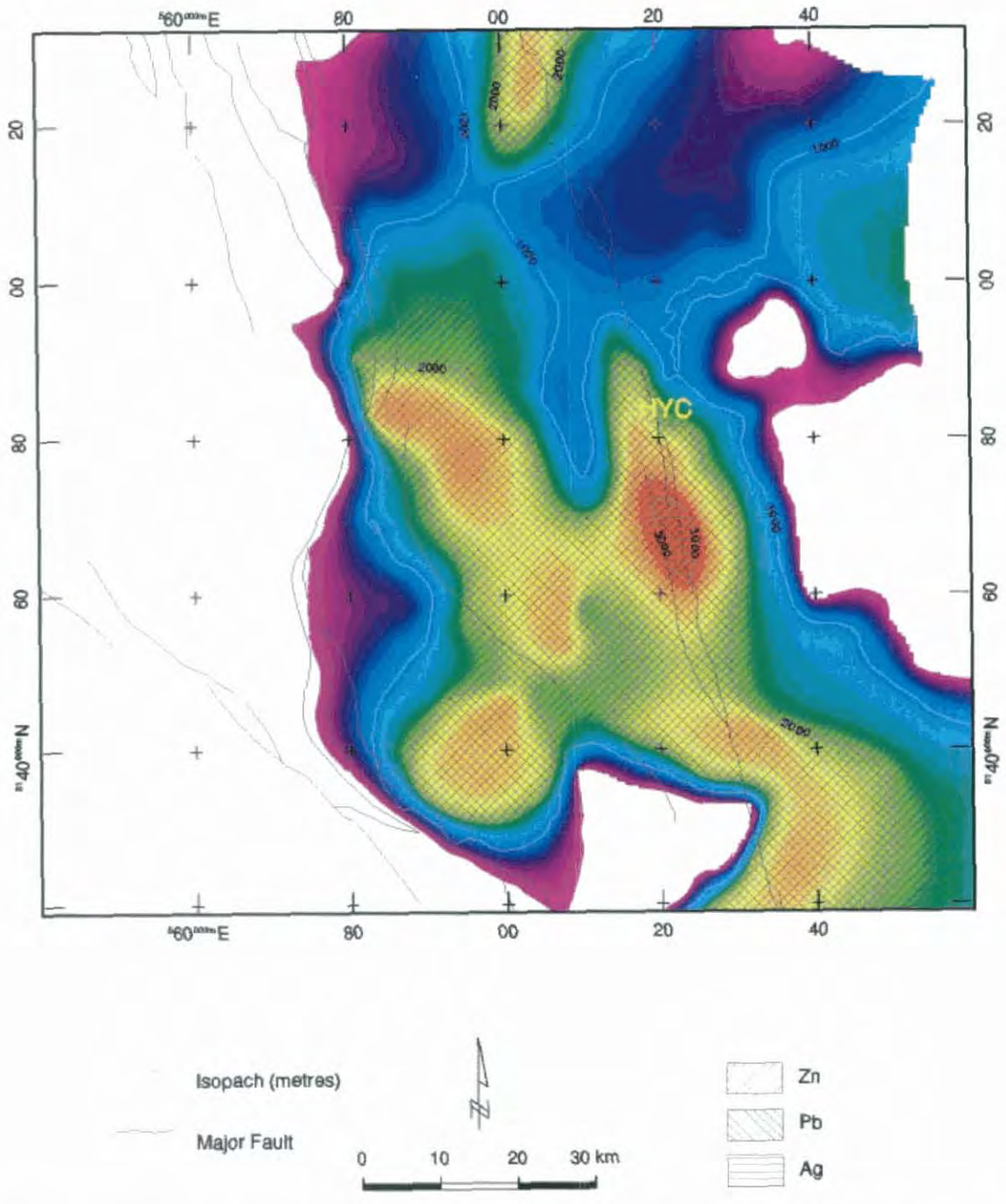

Figure 4.8 Metallogenic potential of upper McArthur Group, showing McArthur Group carbonate package volume required to source HYC, assuming current lithogeochemical base metal concentrations (5 ppm Zn, 4 ppm Pb, 0.6 ppm Ag; Table 4.3). Grid is AMG, Zone 53

4.3.2 Basal mafic volcanic package

This designation comprises the highly magnetic 'mafic volcanic' unit of Leaman (1998). Its outcropping stratigraphic equivalents are uncertain, but probably encompass the Seigal Volcanics and possibly the Scrutton Volcanics. The package is believed to have affinities with the Eastern Creek Volcanics of the Mount Isa Basin, which are known to be several kilometres thick.

unit	Zn med	Zn mean	Zn max	Pb med	Pb mean	Pb max	n
Seigal Volcanics	87	97	200	7	56	495	12
dolerite	126	126	138	15	16	21	3
mean	*107*	*112*	*169*	*11*	*36*	*258*	
n weighted mean	*95*	*103*	*188*	*9*	*48*	*400*	15
required volume	*7.8E+10*	*7.2E+10*	*3.9E+10*	*3.8E+11*	*6.8E+10*	*8.2E+09*	

Table 4.4 Summary base metal geochemical data for the basal mafic volcanic package (possibly equivalent to the Seigal Volcanics)

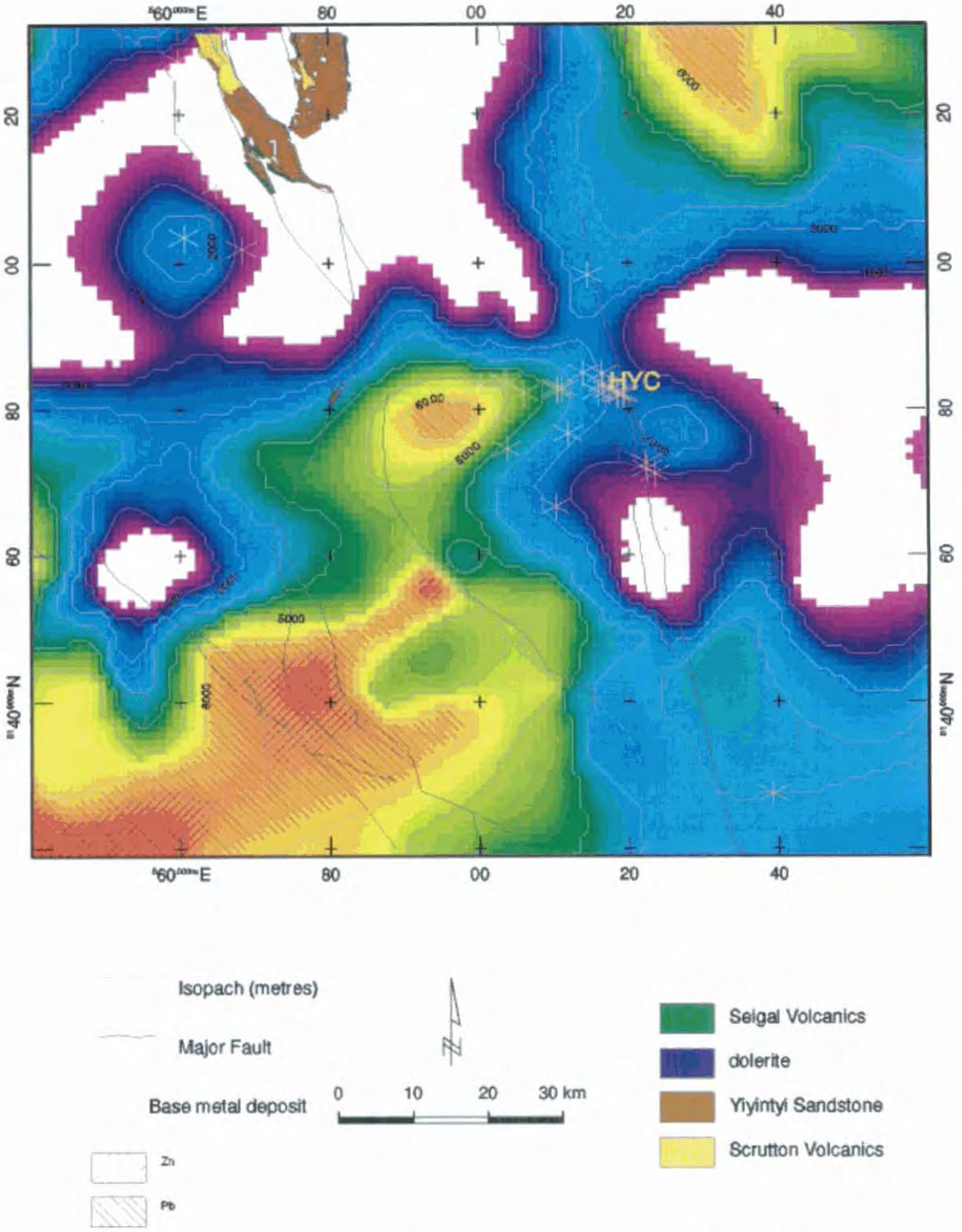

Figure 4.9 Metallogenic potential of basal mafic volcanic pile (possibly equivalent to the Seigal Volcanics), showing volume required to source HYC, assuming current lithogeochemical base metal concentrations (95 ppm Zn, 9 ppm Pb; Table 4.4). Grid is AMG, Zone 53

The mafic volcanics are a richer source of base metals than the carbonates of the McArthur Group (Table 4.4). This, coupled with the greater interpreted volume of the mafic volcanics (more extensive and up to several times thicker than the McArthur Group carbonates) means that a much lower proportion of the total rock volume is required to source an HYC-sized deposit (Fig. 4.9). A major E-W structure is apparent in Fig. 4.9; possibly a major basin-bounding fault which could have focused deep basin fluid flow in the vicinity of the HYC deposit.

4.4 Basin Reconstruction

Knowledge of the basin shape contemporaneous with mineralisation is critical for understanding of the palaeohydrogeological factors resulting in the focusing of mineralising fluids. Significant portions of the sediment originally filling the basin have subsequently been lost through deformation, uplift and erosion. This section presents a rapid, easily implemented procedure for inferring palaeo-basin structure. It builds on the method described above for estimating the depth to any basin unit, given the outcrop of a unit higher in the stratigraphy. The resulting map (exemplified by Fig. 4.2) representing the stratigraphic depth dimension keyed to geological map polygons is used as a baseline for comparison with the geophysically interpreted 2.5-D representation of present basin volume. Areas where the interpreted depth to the base of the McArthur Group carbonate package (depicted as the raster surface in Fig. 4.8) is in excess of that predicted from outcrop geology are inferred to have been sub-basins, since the preserved basin sediment fill is anomalously thick. Conversely, regions where an anomalously thin volume of basin fill is preserved with reference to the stratigraphic elevation of outcropping units are interpreted to have been relatively elevated within the basin during deposition.

The technique relies on the assumption that basin strata dip only shallowly in the area considered. This is violated to a degree in some parts of the McArthur Basin, where dips steepen up to 70° near faults (see discussion in section 4.1), but these zones are not considered sufficiently extensive to invalidate the method as applied at 1:250,000 scale.

The McArthur Group carbonate portion of the basin fill (essentially comprising the entire group excepting the mainly siliciclastic Mallapunyah Formation and Masterton Sandstone at the base; hereafter referred to as the upper McArthur Group) is examined in this instance. The amount of section between the surface and the base of the upper McArthur Group is calculated for each McArthur Group polygon younger than the Mallapunyah Formation from the difference between its related ZMEAN stratigraphic depth attribute, and the ZMEAN corresponding to the base of the upper McArthur Group units (basal Amelia Dolomite). The resulting new stratigraphic attribute ('predicted upper McArthur Group thickness') describes in terms of thickness the amount of implied upper McArthur Group sediment between the outcropping unit and the base of the upper McArthur Group carbonate-dominated package.

A 100m grid cell raster was created from the geology polygons and the predicted upper McArthur Group thickness attribute. This enabled comparison of upper McArthur Group thickness predicted from surface geology with the geophysically interpreted present upper McArthur Group carbonate volume (Fig. 4.8). It was assumed for this exercise that a full section of upper McArthur Group was present beneath the younger Proterozoic Nathan and Roper Groups, thus a nominal maximum predicted upper McArthur

Group thickness value of 2650m was assigned to these areas. Phanerozoic and pre-upper McArthur Group units (Mallapunyah Formation and older) were initially designated as null values.

Predicted upper McArthur Group thickness values were subsequently interpolated in areas of Phanerozoic cover using a three-stage procedure. The initial grid was first converted into a lattice of points attributed with the predicted upper McArthur Group thickness value. A TIN was then created from these points, incorporating all faults as barrier lines. Finally this TIN was linearly interpolated back to a lattice, and areas of pre-upper McArthur Group outcrop covered by the interpolation masked out.

The resulting grid was subtracted from the grid representing present McArthur Group carbonate thickness as interpreted by Leaman (1998), and the residual map of anomalous upper McArthur Group carbonate package thickness is shown in Fig. 4.10.

A number of interesting features are present in Fig. 4.10. The area adjacent to the Emu Fault from the Masterton Horst southwards shows the greatest anomalous thickness, but a significant portion of this is probably due to structural repetition and unusually steep dips in this complexly deformed zone. Of more significance is the overall anomalously thick area extending southwest from HYC across most of the region as far as the Tawallah Fault, forming a rough quadrilateral slightly elongated in an E-W direction. This feature is interpreted as a sub-basin (hereafter called the Hot Spring-Emu sub-basin) present in upper McArthur Group time, i.e. broadly contemporaneous with formation of the HYC deposit.

The boundaries of this sub-basin, probably defined by faults, were potentially conduits for mineralising fluids. It is notable that most of the mineral deposits in the region are localised in the vicinity of these boundaries, which are distinguished by a comparatively rapid transition from anomalously thick to anomalously thin areas. The most prominent of these bounding zones extends westwards from just north of HYC, though it is embayed around 608000E. This embayment is part of a low north-south trending ridge, which partially bisects the Hot Spring-Emu sub-basin. It also is spatially associated with stratiform Zn-Pb mineralisation. The two basin cells on the western and eastern sides of the ridge are bounded on their far sides by the Hot Spring and Emu Faults respectively. Either may have acted as a reservoir for base metal-bearing fluids, prior to their release upwards along bounding faults or other discontinuities at the cell edges, accounting for the localisation of stratiform Zn-Pb mineralisation in suitable trap rocks in these areas.

Other sub-basins are identified in Fig. 4.10, though they do not appear as voluminous as the Hot Spring-Emu sub-basin. One is at the northern edge of the study area in the Sawtooth Range, where an anomalous thickness of upper McArthur Group is inferred to have existed. No Zn-Pb mineralisation has yet been identified in this area, though suitable reducing trap rocks (Barney Creek Formation, Caranbirini Member) are present.

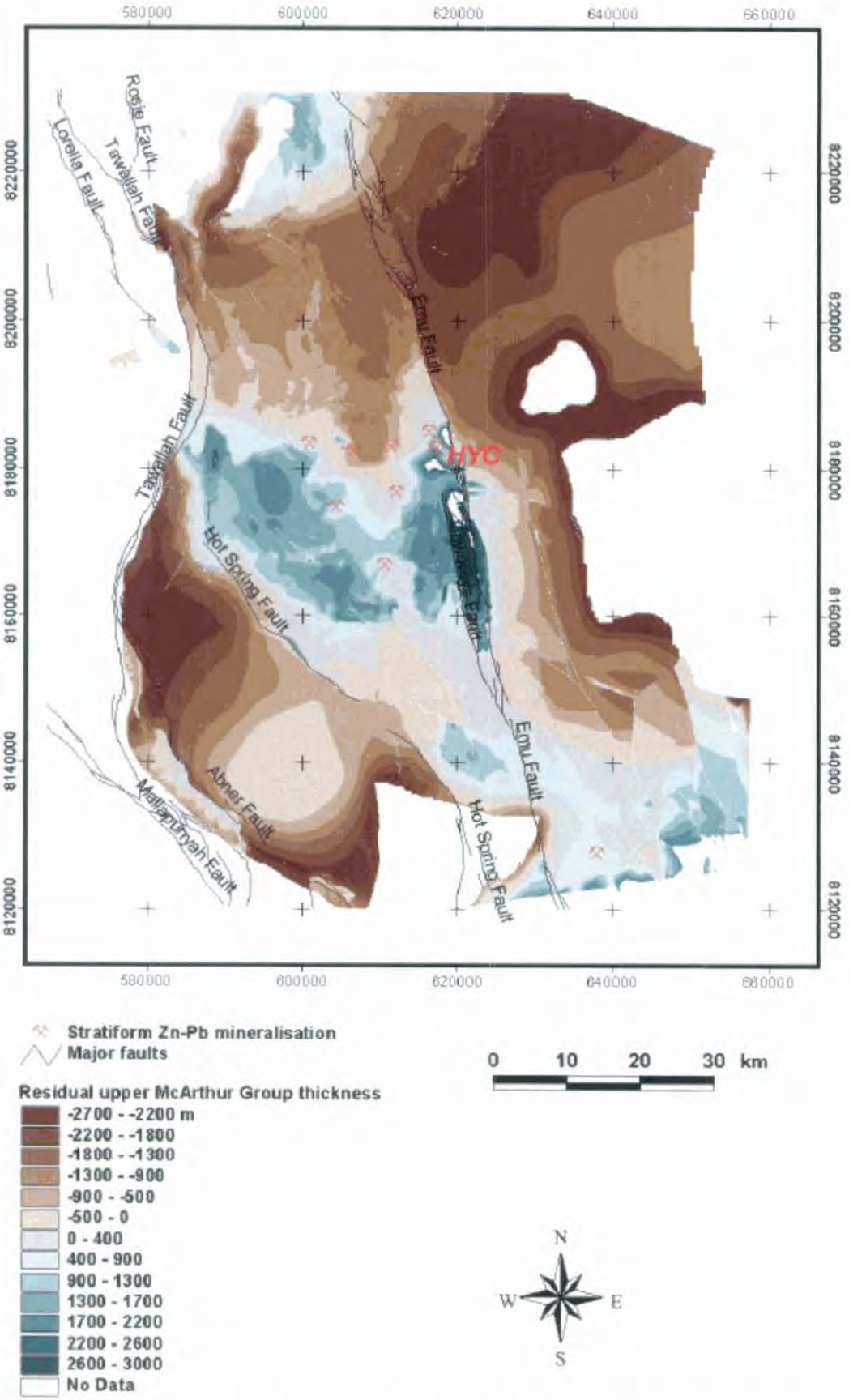

Figure 4.10 Residual upper McArthur Group thickness, calculated by subtracting presumed current thickness of upper McArthur Group units implied by outcrop geology from the interpreted preserved thickness of McArthur Group. Negative values (brown shades) thus denote areas where there is less upper McArthur Group preserved than would be expected in a 'normal' sedimentary section, and are interpreted as areas which were elevated during upper McArthur Group deposition. The reverse applies to areas of positive residual values, which are interpreted as palaeo-sub-basins. Grid is AMG Zone 53

The area between the Foelsche Inlier and Hot Spring Fault in the south-eastern corner contain only slightly anomalous patches of upper McArthur Group, which are considered either too small or too diffuse to have concentrated large amounts of mineralising fluids. Only one stratiform base metal prospect is known in this region (Mountain Home), and it does not contain significant Zn-Pb grades. Some of the more intensely anomalous features at the extreme south-eastern edge of the map in Fig. 4.9 are interpolative edge artefacts arising from the lack of outcrop geological control in this area, which is largely covered by Cambrian sandstone of the Georgina Basin (Bukalara Sandstone).

4.5 Summary

Field measurements of stratigraphic unit thickness contained in published literature have been used to establish a stratigraphic data structure, keyed to conventional geological map polygons, which effectively makes explicit the 3-D information implicit in geological maps. This has been used to create maps that facilitate easy visualisation of outcropping basin structures and deformation.

Utilisation of the 'stratigraphic topological' information contained in the attribute data structure enabled automated identification of unconformity surfaces in the geological map, which provide insights into the magnitude and location of intra-basinal deformation events in space and time. Pre-Roper Group uplift increasing in magnitude to the south is highlighted, as are instances of missing section within the Umbolooga Subgroup west and south of HYC.

Geophysical interpretations of basin architecture derived from regional potential field data after Leaman (1998) have been used to assess the volumes and shape of major basin sequences. These have been combined with lithogeochemical data to quantitatively assess these packages in terms of their potential to act as sources or reservoirs of base metals to the HYC deposit. An inordinately high proportion of the carbonate-dominated McArthur Group is required to source sufficient base metals to form the HYC deposit, assuming reasonable original base metal contents and extraction efficiencies. Additional or alternative contributions to the base metal budget were probably extracted from deeper, more voluminous and fertile basin units. The extent to which this occurred is critical to the likelihood of further deposits comparable in size to HYC being discovered in the McArthur Basin.

The 3-D-enhanced geological data have been combined with the geophysical interpretations of basin architecture to derive residual structural surfaces and isopach maps which attempt to restore to the present basin volume those portions of the stratigraphic column which have been lost through erosion at any given location. These can be interpreted in terms of basin shape at the time of deposition. The HYC deposit is located at the northeastern corner of the largest sub-basin identified, the Hot Spring-Emu sub-basin, which is composed of two elongated cells on either side of a shallow central ridge. Stratiform Zn-Pb mineralisation is spatially associated with the edges or shoulders of the sub-basin cells. Other palaeo-sub-basins are present, but these are not as voluminous and are not spatially associated with currently known significant Zn-Pb occurrences.

5. Regional Petrophysics

5.1 Introduction

A comprehensive suite of physical property measurements have been made on a sizeable set of samples from the Paradise Valley district and adjacent areas. The primary motivation for this work was the requirement to constrain interpretations of gravity, magnetic and radiometric data sets detailed elsewhere in this thesis. A particular interest was to determine if individual formations within the lower McNamara Group could be distinguished geophysically, and thus provide an avenue to more finely characterise the three-dimensional architecture of the Paradise Valley area.

A second objective was characterisation of the effect of weathering on the physical properties of McNamara Group rocks. This was an imperative dictated by the variability and extreme depth (> 100 m) of weathering defined by drilling in and around the Lady Loretta and Lady Annie deposits.

A third objective was to derive information on McNamara Group sedimentary provenance and basin history in general from gamma-ray spectrometric measurements. The possibility of augmenting the spatial detail of gamma-ray logging performed by the NABRE research group at AGSO (Southgate et al., 1996) was also recognised.

5.1.1 Sampling

Samples for the study were obtained from three main sources. The first suite (numbered between 1000 and 2000 in Appendix 3) was obtained from surface samples within a few kilometres of the Lady Loretta and Lady Annie prospects. At least three specimens were obtained from each significant lithology represented in every outcropping formation, supplemented with samples from drillcore also obtained in the Lady Loretta-Lady Annie area, making a total of just under one hundred samples. The majority of the drillcore sub-set are from the Lady Loretta Formation, with the remainder being samples of a metabasalt intersected in drilling (drillhole Q68) a few kilometres north of Lady Annie.

The second suite (numbered in the range 2000-2999 in Appendix 3) was acquired from a series of cores drilled by Aberfoyle Resources Ltd. north, north-west and north-east of Lady Loretta in the Paradise Valley region. As well as sampling a disparate range of McNamara Group stratigraphy, the Aberfoyle data set also has the valuable attribute of being distant (kilometres) from any known significant base metal mineralisation. However, some sampling bias is likely to be present, as the drillcore is a product of an exploration program focused on the assessment of black shales and other highly conductive rocks as possible hosts for mineralisation.

A third set of samples (identified by their Geology Dept. catalogue number in Appendix 3) was retrieved from the rock store of the Geology Department at the University of Tasmania. These were collected by other Lady Loretta researchers (principally P. McGoldrick and J. Dunster), mostly since 1993. The majority are from the Lady Loretta ore body and its host sequence. Many of the samples originating with

McGoldrick were collected for a geochemical study of sedimentary alteration, with sulphides avoided if possible (McGoldrick, 1993b). The geochemical data from this dataset were presented by McGoldrick (1994b), and are employed here in a comparative analysis of geochemical and petrophysical parameters. Stratigraphic units from the Constance Sandstone to the Eastern Creek Volcanics inclusively are also represented in the Geology Department collection, and were utilised in this study.

This chapter considers the bulk physical properties of stratigraphic units, and their implications for regional geophysical interpretations. As such, it deals only with the essentially non-mineralised samples from the consolidated data set. Samples from within and immediately adjacent to Lady Loretta and other mineralised systems are considered in the following chapter (6).

5.2 Previous work

Though a number of desultory petrophysical measurements in the Mount Isa Inlier have been made by workers whose investigations have been more regional in scope (Neumann, 1964; Gibb, 1967; Shirley, 1976), the first major physical property study in the region was that by Hone et al. (1987). This dataset is reasonably comprehensive in that it contains representatives from nearly all significant stratigraphic units in the Mount Isa Inlier, but tends to be biased towards highly metamorphosed units of the Eastern Succession, particularly the Corella Formation. The comparative lack of samples from the Western Succession is particularly marked in the case of the McNamara Group. The Hone et al. (1987) dataset also contains a large proportion of samples obtained from outcrop, and thus bulk property estimations based on simple arithmetic means from these data alone, especially density, are likely to be too low.

Most samples measured by Hone et al. (1987) were also the subject of geochemical analyses on pre-Haslingden Group meta-igneous rocks reported by Wyborn and Page (1983), Wilson (1983), Wyborn et al. (1987), Wyborn (1988) and Wyborn et al. (1988). These datasets have not yet been examined in conjunction, to the best of the author's knowledge. The original geochemical data were extracted from AGSO's ROCKCHEM database and related to the petrophysical data using sample ID numbers listed in Hone et al. (1987). Relationships identified between geophysical and geochemical properties of the pre-Haslingden Group basement suite are discussed in section 5.4.1.1.

The only significant study of magnetic remanence in terms of implications for geophysical interpretation is that of Clark (1980). This work was mainly devoted to the Eastern Creek Volcanics, with a significant portion of the samples examined being obtained from within the Paradise Valley study area south of Gunpowder. While Koenigsberger ratios determined were quite high (Q often >> 1), normal and reversed remanence polarities were equally common and ubiquitous, with magnetisation directions changing over scales of tens of metres. Clark (1980) concluded that for the purposes of geophysical interpretation the magnetisation of the Eastern Creek Volcanics may be considered to be due to induction alone, with remanent magnetisation responsible for the high frequency magnetic anomalies observed over outcropping ECV (see chapter 7).

A large petrophysical dataset has been accumulated over many years in the vicinity of the Mount Isa Mine by the operators, Mount Isa Mines Limited. These data are summarised in Fallon and Busuttil

(1992) and Young (1984). While they describe the orebody and its immediate surrounds well, extrapolations of individual formations' bulk properties from the mine environment to regional scales may be misleading, as pointed out by Leaman (1991a).

All previously published data from discrete samples have been combined with data generated by the author in subsequent analysis. These are tabulated in Appendix 3, and summarised in Table 5.12.

5.3 Methods

5.3.1 Mass properties

Density determinations were made using Archimedes' Principle. Samples were first oven-dried at a temperature of 90°C for at least 24 hours, then weighed with an electronic balance (precision 0.1 g) in air. Following at least a week's immersion in Hobart tap water at room temperatures and pressures, samples were weighed in water using a wire basket. Excess water on the surface of the sample was then removed with a towel before a second weighing on the electronic balance. Bulk dry density, bulk wet density and an estimate of porosity were calculated (after Emerson, 1990) from these measurements.

5.3.2 Magnetic

Magnetic susceptibility was measured with an Exploranium KT-5 hand-held susceptibility meter. No corrections were made for sample geometry, and the highest value from several measurements in varying sample-meter configurations was recorded as best indicating the bulk susceptibility. In most drillcore samples, the optimal configuration for measurements (on the flat surface of half-core splits or on the flattened ends of whole core) was attainable. For some samples of low mass (< 100 grams) or small-diameter drillcore samples, the measurements probably underestimate bulk susceptibility by up to 50%.

5.3.3 Sonic velocity

A PUNDIT (Portable Ultrasonic Non-Destructive Digital Indicating Tester) apparatus employing longitudinal acoustic pulses with a frequency of 54 kHz was used to determine the transit time of sound waves through samples. All measurements were performed on water-saturated samples following electrical property determination (see section 5.3.4 below). Prior to measurement, flat surfaces as close to parallel as possible were prepared on opposite ends of each sample using a rock saw and fine orbital grinder. Both transmitter and receiver transducers were smeared with medical ultrasound gel in order to maximise effective contact between the sensors and the water-saturated sample. The sensors were then applied to the surfaces with hand pressure only, in as close as practicable to a direct transmission configuration, and the lowest sustainable travel time noted. Velocity calculations were made following measurement of sample length with a ruler. The accuracy of transit time measurements is quoted as ±1% in the PUNDIT manual, but uncertainties in determining path length are generally in the order of 1-3%, and may range as high as 5% for awkwardly-shaped specimens. The uncertainty in derived sonic velocities is thus in the range of a few tens of metres per second.

5.3.4 Electrical

Resistivity and IP measurements were performed using the ABEM RIPS-3 four-electrode apparatus. Samples were immersed in Hobart mains water at room temperature and pressure for at least one week prior to measurement. Immediately prior to measurement, surface moisture was removed; first with a towel, then by rapid drying using a heat gun. Electrical property determinations were invariably made through the longest axis of each sample, except in cases where samples were tested for anisotropy. Geometric parameters of samples (length and cross-sectional area) were estimated with the aid of a ruler and approximation to simple geometries; a procedure which should prove reasonably accurate with drillcore samples, but may be less so in the case of some irregular specimens obtained from outcrops.

IP properties were calculated following procedures outlined in the RIPS-3 manual, which return the parameters V_{IP} and V_P. The IP% figure listed in all the experimental results herein is obtained by (V_{IP} / V_P) * 100, where V_{IP} is the secondary voltage across the sample measured at a constant time interval determined by the apparatus (1.2 sec) after cut-off of the primary voltage V_P. IP% is thus dimensionless.

5.3.5 Radiometrics

Spectrometric gamma-ray measurements were made using an EDA portable gamma-ray spectrometer. This instrument records five channels of gamma-ray energies, corresponding to total count (two channels), potassium, uranium and thorium. To minimise noise from background radiation, the device was shielded with a 'lead castle' constructed from several sheets of ~1.5 mm thick soldering lead, as well as a number of iron slabs. These measures attenuated background radiation levels by approximately 70 to 75%. Following the suggestion of Emerson (pers. comm.), only samples whose dry weight exceeded 300 g were measured, in order to obtain reasonable signal/noise ratios. This limit was lowered to 150 g in cases where this could be justified by the geometry of drillcore (i.e. length exceeding that of the detector crystal by a considerable amount in spite of low overall mass of sample) and the rarity of the lithology or formation sampled. Instances of application of the lower weight limit are highlighted within the relevant appendices.

Readings were taken for a period of 120 seconds per channel, with the higher-energy total count channel (tc2) being omitted. A determination of background levels in each channel was also made based on up to one hour of readings, made over a period of several weeks. The averaged background level was subtracted from sample readings, which are reported in units of counts per minute.

5.4 Results - Regional Stratigraphy

5.4.1 Pre-Haslingden Group basement

SUMMARY

Groups	*Count*	*Sum*	*Average*	*Variance*
Ewen Granite	1	2.69	2.69	#DIV/0!
Bottletree Fm	1	2.65	2.65	#DIV/0!
Argylla Fm	11	29.59	2.69	0.00798
Tewinga Gp	12	31.9	2.658333	0.004815
Yeldham Granite	11	29.55195	2.686541	0.003954
Leichhardt Volcanics	7	18.52	2.645714	0.000529
Kalkadoon Granodiorite	21	56.2	2.67619	0.002775
Big Toby Granite	5	13.39	2.678	0.00242

ANOVA

Source of Variation	*SS*	*df*	*MS*	*F*
Between Groups	0.014102	7	0.002015	0.510633
Within Groups	0.240658	61	0.003945	
Total	0.25476	68		

Table 5.1 Pre-Haslingden Group density ANOVA

Table 5.1 above demonstrates that density measurements on pre-Haslingden Group basement rocks are statistically indistinguishable, thus can be treated as one unit as far as gravity interpretation is concerned. Histograms of the density measurements (Figs. 5.1, 5.2) arguably show a small sub-population centred around 2.74 t/m^3 composed of a range of lithologies identified by Hone et al. (1987) as alkali-feldspar syenites, alkali-feldspar granites, agglomerate and amphibolite. The main population at around 2.66 t/m^3 is mainly composed of true granites/rhyolites, metasediments (phyllites and schists) and gneisses of uncertain origin, however this assemblage is not unique to any sub-set of pre-Haslingden Group stratigraphic units, that is, this sub-variation is not mappable. These variations will thus be integrated at the scale of regional interpretations. Spatially, there is a suggestion that lighter lithologies predominate in the Leichhardt Volcanics and Kalkadoon Granodiorite north of 7750000 N, but sampling is insufficient to draw definite conclusions.

The pre-Haslingden Group units are variably magnetic up to reasonably high values (Fig. 5.3), but this variation is not systematic, with the possible exception of the Kalkadoon Granodiorite which appears to be of uniformly low magnetic susceptibility. There is no strong lithological control on magnetic properties, although Tewinga Group samples identified as gneisses by Hone et al. (1987) are all non-magnetic. There appear to be two populations present - one characterised by strong correlation between density and (low) magnetic susceptibility, and the other by scattered, moderately high magnetic susceptibility and little correlation with density. These are interpreted in geological terms as corresponding to ilmenite-series and magnetite-series felsic igneous assemblages, respectively. The felsic

igneous rocks in this suite are generally I-type (Wyborn et al., 1987) but magnetic samples are in a distinct minority, emphasising that I-type rocks are not necessarily magnetic.

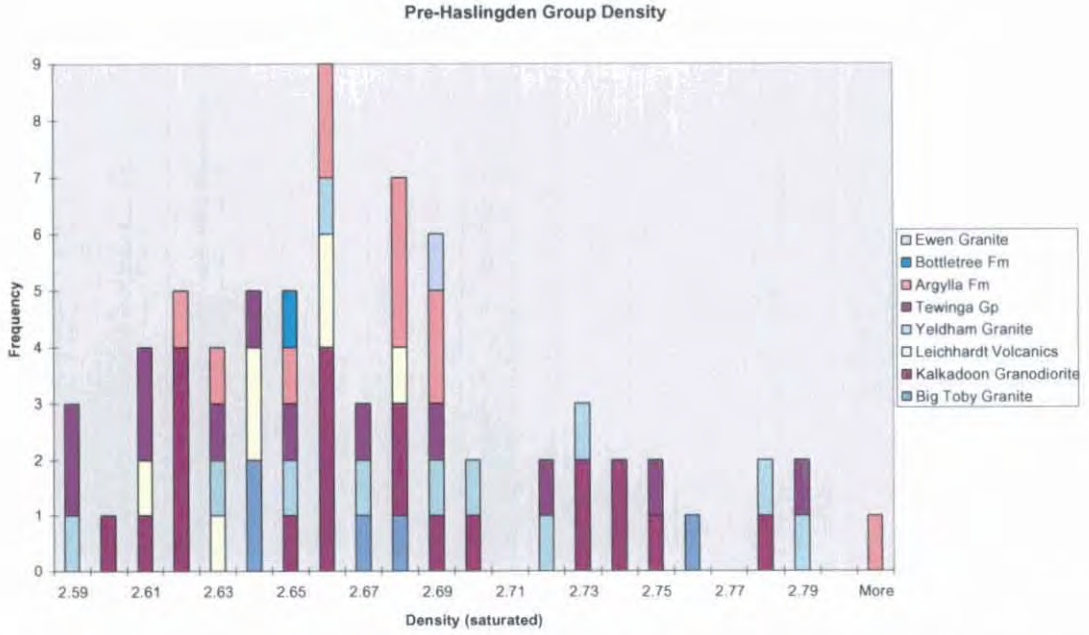

Figure 5.1 Frequency histogram of Pre-Haslingden Group unit density measurements, classified by mapped unit

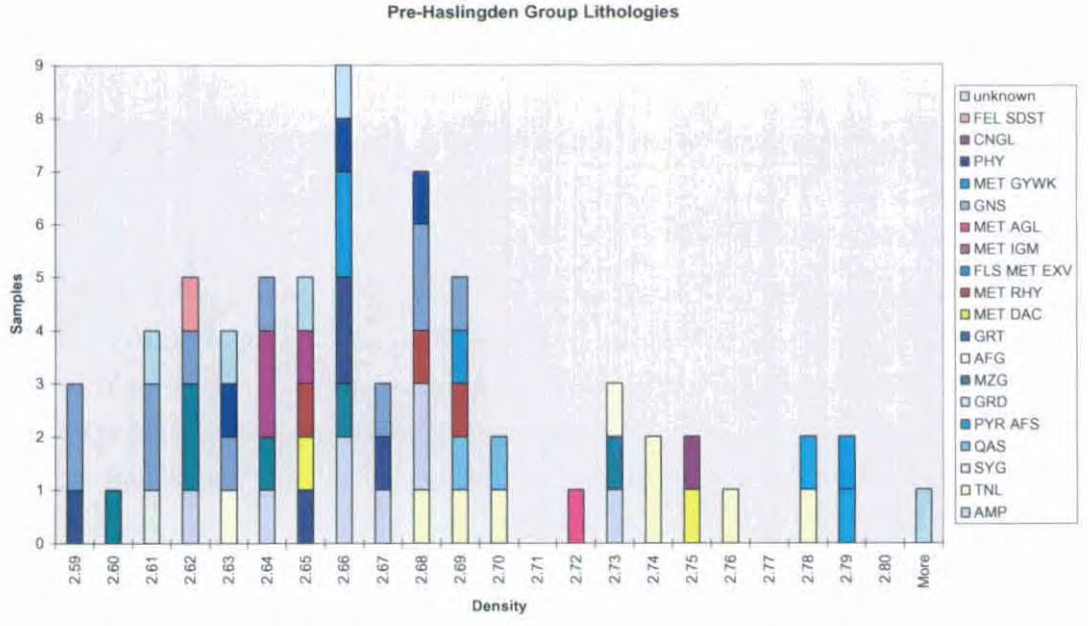

Figure 5.2 Frequency histogram of Pre-Haslingden Group unit density measurements, classified by lithology. All lithological abbreviations used in this and subsequent figures are from the standard AGSO authority table, reproduced in Appendix 7 as LITH.AUT.

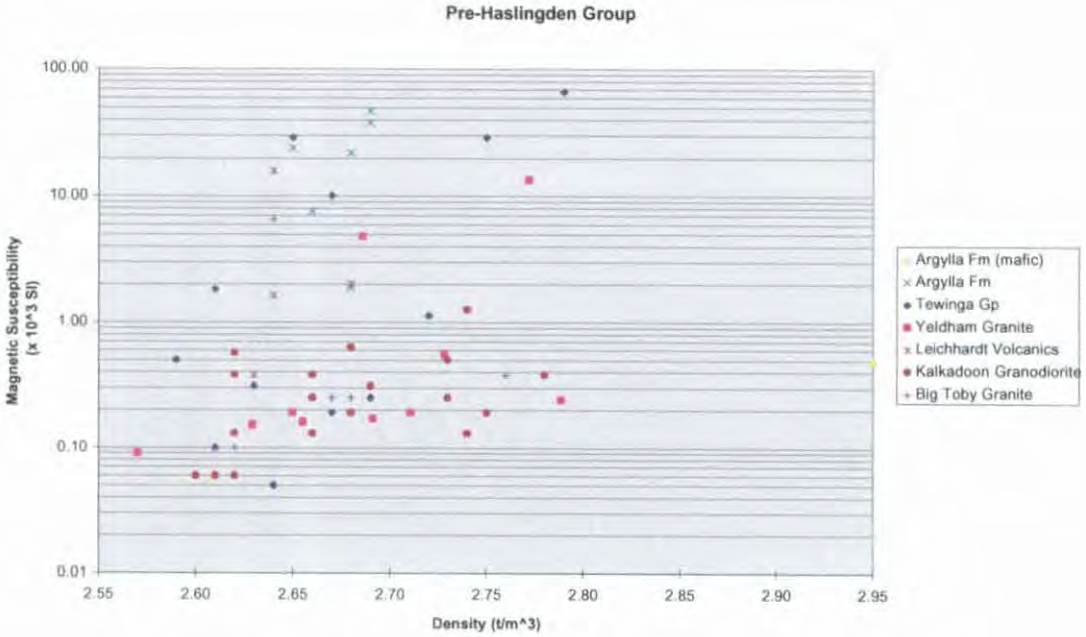

Figure 5.3 Pre-Haslingden Group density and magnetic susceptibility

	Porosity	*Density*	*Mag susc*	*log MS*	*Velocity*	*Resistivity*	*log R*	*IP%*
Porosity	1							
Density	-0.44978	1						
Mag susc	-0.05786	-0.01923	1					
log MS	-0.16353	0.239238	0.464993	1				
Velocity	-0.7805	0.461353	0.162533	0.378536	1			
Resistivity	-0.32579	0.067584	0.105346	0.403274	0.569685	1		
log R	-0.73716	0.351172	0.118673	0.34906	0.951528	0.745451	1	
IP%	0.13157	0.062257	-0.21108	-0.01223	-0.40969	0.250015	-0.25049	1

Table 5.2 Pre-Haslingden Group igneous basement (whole population) petrophysical correlation coefficients. In this and subsequent tables log means log $_{10}$

There are only moderate correlations between density and velocity, and between density and log resistivity (Table 5.2). Only weak correlation is apparent between density and log magnetic susceptibility. The negative correlation between porosity and density has an obvious direct cause. Porosity may also be at least partly responsible for the positive correlation between velocity and resistivity. Also notable is the lack of correlation between density and magnetic susceptibility in this whole-population data.

The pre-Haslingden Group was divided in two in order to separate the effects of paramagnetic and ferrimagnetic minerals. A threshold value of 1.0×10^{-3} SI was chosen, being the maximum susceptibility generally attained by paramagnetic minerals and non-magnetite-bearing lithologies (Clark, 1997). Positive correlation between density and magnetic susceptibility is much more apparent in Table 5.3 than in Table 5.2. This demonstrates the effect of concentrations of dense, paramagnetic (Puranen, 1989 quoted in Clark, 1997) mafic minerals such as ilmenite, biotite and hornblende, which tend to increase in inverse proportion to the light mineral quartz.

	Porosity	Density	Mag susc	log MS	Velocity	Resistivity	log R	IP%
Porosity	1							
Density	-0.50492	1						
Mag susc	-0.14813	0.421465	1					
log MS	-0.12198	0.460651	0.767211	1				
Velocity	-0.78321	0.480882	0.537311	0.586864	1			
Resistivity	-0.43811	0.093184	0.143584	0.173029	0.687919	1		
log R	-0.7815	0.395685	0.326387	0.357636	0.971207	0.756682	1	
IP%	0.170077	0.196891	0.051587	0.082783	-0.63432	-0.37975	-0.62687	1

Table 5.3 Pre-Haslingden Group igneous basement (magnetic susceptibility < 1.0 x 10^{-3} SI) petrophysical correlation coefficients

	Porosity	Density	Mag susc	log MS
Porosity	1			
Density	0.121906	1		
Mag susc	-0.15939	-0.09988	1	
log MS	0.080817	0.053457	0.714985	1

Table 5.4 Pre-Haslingden Group igneous basement (magnetic susceptibility > 1.0 x 10^{3} SI) petrophysical correlation coefficients

A lack of correlation between density and magnetic susceptibility is apparent in Table 5.4, demonstrating the ability of low concentrations of ferromagnetic minerals to greatly affect magnetic properties without significantly influencing density.

	Porosity	Density (t/m^3)	Mag susc (x 10^{-3} SI)	Velocity (m/s)	Resistivity (Ωm)	IP%
Mean	0.012	2.670	64	5474	54961	2.33
S.E.	0.003	0.008	58	127	27246	0.34
Median	0.006	2.66	0.38	5565	23151	2.15
Mode	0	2.66	0.25	#N/A	#N/A	#N/A
S.D.	0.021	0.067	459	359	81738	1.01
S.V.	0.000	0.004	210263	128713	6681044406	1.02
Kurtosis	35.75	4.79	62.88	0.29	3.79	0.44
Skew	5.37	0.74	7.93	-1.14	2.01	0.95
Min.	0	2.450	0.001	4810	312	1.13
Max.	0.158	2.95	3644	5840	246326	4.29
Count	65	69	63	8	9	9
C.L.(95%)	0.005	0.016	113	249	53401	0.660

Table 5.5 Summary statistics of pre-Haslingden Group rock properties. S.E. = standard error, S.D. = standard deviation, S.V. = sample variance, C.L. = confidence level.

Combining the two sub-populations discussed above (Table 5.5), the pre-Haslingden Group felsic igneous units have a mean density of 2.67 t/m^3. This figure is likely to closely approximate the integrated bulk properties of these units, though these may vary regionally between the means of the low-density, quartz-rich granitoid and high-density, more feldspathic and granodioritic subpopulations (2.65 t/m ^{3} and 2.76 t/m^3). Characterising the bulk magnetic properties is more problematic due to the extreme range of data values, and limited sampling. A true'bulk value is likely to lie between extremes defined by the mean

(64 x 10^{-3} SI) and median (0.38 x 10^{-3} SI), and is probably well towards the lower end of this range. This assertion is supported by the geometric mean of the magnetic susceptibility data, which is 0.80 x 10^{-3} SI. The arithmetic mean is skewed upwards by one extremely magnetic sample of over 3600 x 10^{-3} SI. When this sample is excluded, the arithmetic mean magnetic susceptibility falls to 4.5 x 10^{-3} SI.

The felsic igneous rocks have moderately high velocities for surface samples, at around 5500 m/s. They have high resistivity and low porosity, and are non-polarisable.

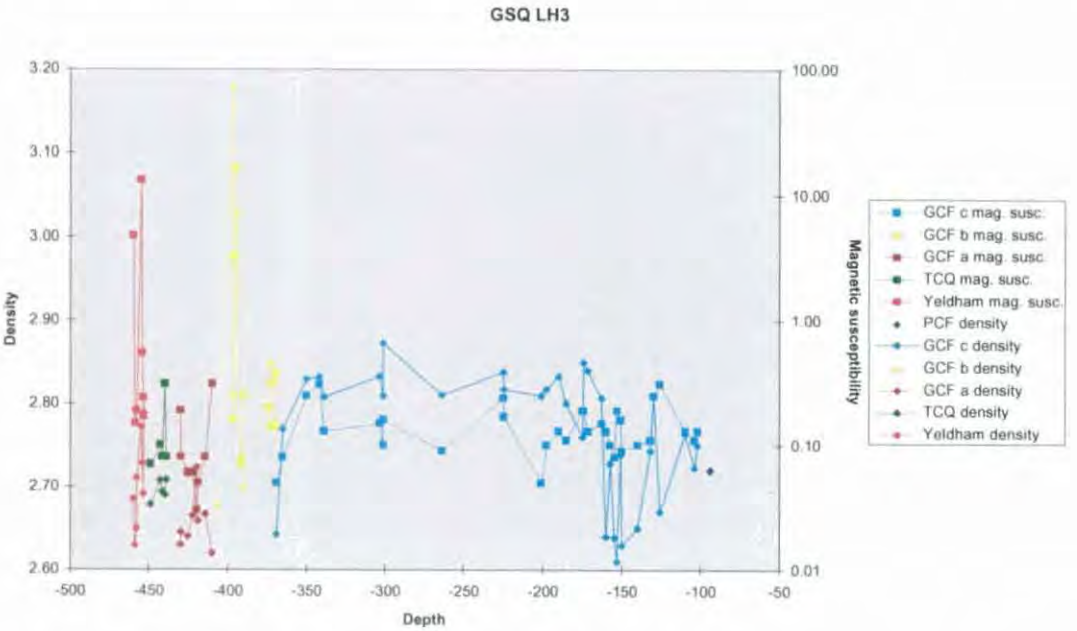

Figure 5.4 Drillhole GSQ Lawn Hill 3 density and magnetic susceptibility. Data from Hone et al. (1987) and this study. PCF = Paradise Creek Formation, GCF = Gunpowder Creek Formation, TCQ = Torpedo Creek Quartzite. Depth is expressed in metres of elevation with respect to the surface.

A plot of density and magnetic susceptibility of Yeldham Granite intersected in the drillhole GSQ Lawn Hill 3 (Fig. 5.4) demonstrates the variability in these properties over distances of metres or less, underscoring the necessity of extensive sampling to adequately characterise these basement units. In this case, the possibility exists that these samples have been biased in some way by their proximity to the nonconformity surface, for example by sub-exposure to a palaeo-erosion surface prior to Torpedo Creek Quartzite deposition, or by subsequent alteration associated with fluid flow concentrated along the unconformity.

5.4.2 Lower Haslingden Group siliciclastics (Leander Quartzite and equivalents)

Included in this grouping are the Leander Quartzite, Mount Guide Quartzite and May Downs Gneiss. No new data were acquired from these units in the course of this study, and those listed in Appendix 3 are entirely based on the compilation of Young (1984). Nothing more meaningful than a mean density can be calculated for this unit (2.644±0.011 t/m^3), given the scarcity of data. These units are virtually non-magnetic.

5.4.3 Eastern Creek Volcanics

There are significant variations in physical properties within this stratigraphic unit. A histogram of density for all samples in the unit (Fig. 5.5) is somewhat skewed to the left (skewness = -1.14), but samples in this lower tail of the distribution are all either altered, extremely weathered (Kamarga Volcanics outcrop samples), or are of the subordinate siliciclastic strata (Lena Quartzite) intercalated with the ECV metabasalts. If these samples are excluded, the remaining relatively fresh unaltered metabasalts approach a normal distribution about a mean of 2.91 ±0.02 t/m^3.

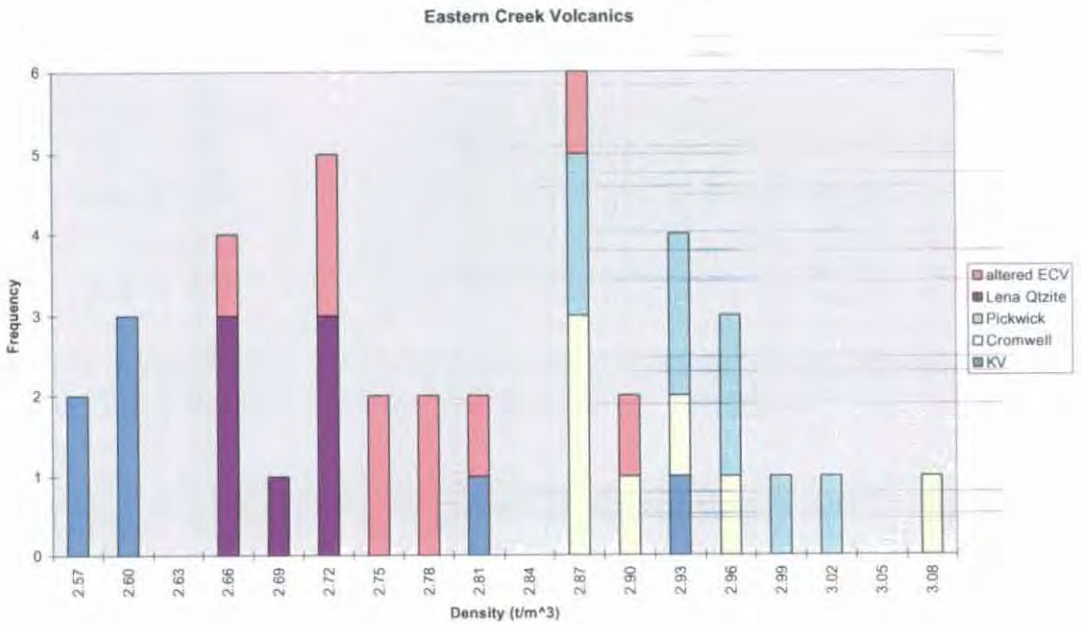

Figure 5.5 Eastern Creek Volcanics and correlative Kamarga Volcanics (KV) density histogram

A plot of magnetic susceptibility against density for the Eastern Creek Volcanics and correlates (Fig. 5.6) shows several distinct populations. Fresh, unaltered Eastern Creek Volcanics samples are generally both highly magnetic and dense, with the obvious exception of the Lena Quartzite which has a signature typical of metamorphosed coarse siliciclastics. The two metabasalt members (Cromwell and Pickwick) both have similar properties to undifferentiated fresh Eastern Creek Volcanics. Differences in density and magnetic properties of the two members are statistically insignificant at the 95% confidence level (but see also chapters 7 and 8).

The Kamarga Volcanics are considered equivalent to the Eastern Creek Volcanics. Most samples from Kamarga Volcanics outcrop were heavily weathered; the single relatively fresh sample plotting close to the main ECV field is considered most likely to represent the bulk properties of the Kamarga Volcanics.

Samples classified as 'altered' Eastern Creek Volcanics have been obtained from 'greenstone basement' at Mount Isa (Young, 1984; Leaman, 1991b; this study) and from similar rocks intercepted in drillcore (Q68, P69, P72) in the vicinity of Lady Loretta. These samples thus have a clear spatial association with base metal mineralisation. The physical properties of these samples are quite variable, but magnetic

susceptibility and density appear significantly reduced from the main body of Eastern Creek Volcanics data.

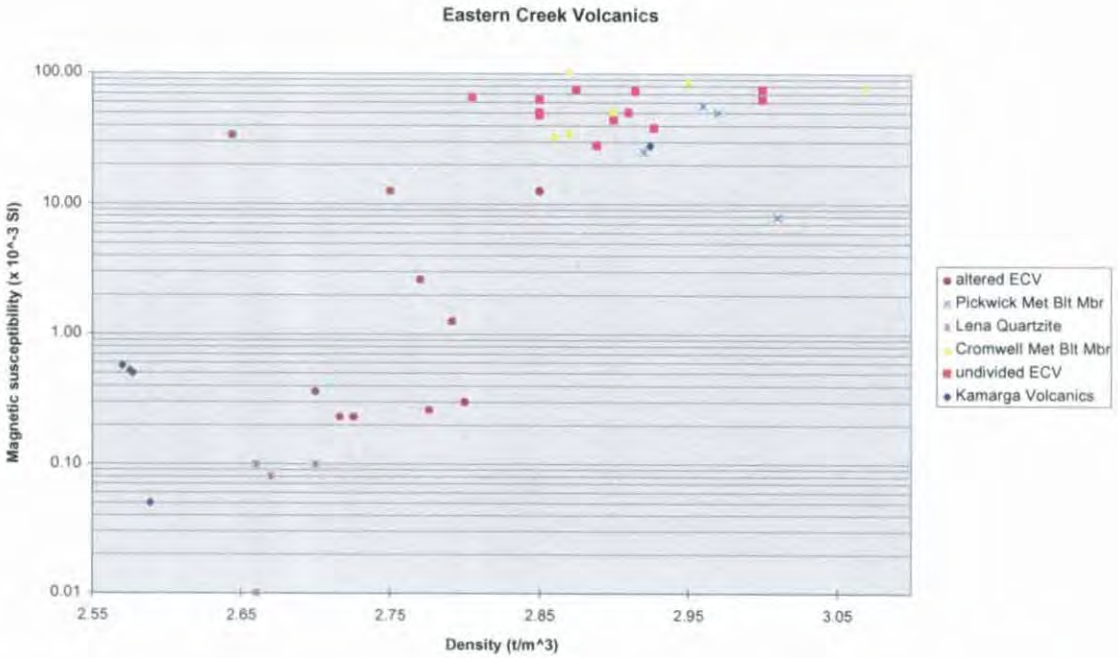

Figure 5.6 Density vs. magnetic susceptibility, Eastern Creek Volcanics and correlative Kamarga Volcanics

5.4.4 Myally Subgroup and Cover Sequence 3 Sediments

It was hypothesised at the outset of this study that the predominantly siliciclastic formations comprising the bulk of the section between the top of the Eastern Creek Volcanics and the onset of carbonate sedimentation in the McNamara Group would be geophysically indistinguishable, due to their compositional similarity. A histogram of density values obtained from these units (Fig. 5.7) is presented in support of this contention.

The negative skew of the frequency distribution (the category '<=2.54' in Fig. 5.7 includes densities ranging as low as 2.12 t/m^3) is ascribed to weathering effects on these samples, which are predominantly from outcrop. If the unreasonably low (<=2.54 t/m^3) samples are excluded, the distribution of the remainder (while not normal) appears to have a meaningful central tendency. No one formation (with the possible exception of the Bigie Formation, from which there are only three relevant samples) appears to occupy any preferred portion of the distribution. This statement is supported by results of an analysis of variance test, which shows no significant difference between the stratigraphic units at the 5% significance level (Table 5.6).

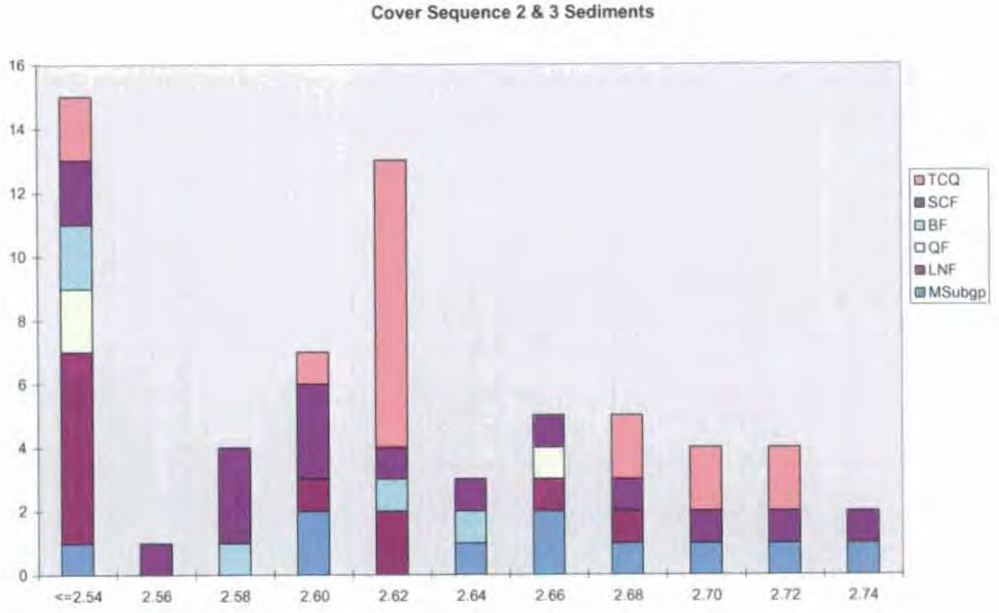

Figure 5.7 Density values derived from the sequence from Myally Subgroup to Torpedo Creek Quartzite, excluding the Fiery Creek Volcanics. MSubgp = Myally Subgroup, LNF = Lochness Formation, QF = Quilalar Formation, BF = Bigie Formation, SCF = Surprise Creek Formation, TCQ = Torpedo Creek Quartzite

SUMMARY

Groups	*Count*	*Sum*	*Average*	*Variance*
Torpedo Ck Qtzite	16	42.22435	2.639022	0.001837
Surprise Ck Fm	14	36.77797	2.626998	0.003535
Bigie Formation	3	7.816966	2.605655	0.001455
Quilalar Formation	1	2.65	2.65	#DIV/0!
Lochness Formation	5	13.11695	2.623391	0.001114
Myally Subgroup	9	23.965	2.662778	0.002207

ANOVA

Source of Variation	*SS*	*df*	*MS*	*F*	*P-value*	*F crit*
Between Groups	0.011476	5	0.002295	0.978313	0.442223	2.437694
Within Groups	0.098536	42	0.002346			
Total	0.110013	47				

Table 5.6 Analysis of variance, Myally Subgroup and pre-Gunpowder Creek Formation sediment densities

The characterisation of the bulk properties of the Myally Subgroup-Torpedo Creek Quartzite sequence sedimentary units (listed in Table 3.8) is somewhat uncertain due to the scarcity of drillcore and underground samples,. The mean density of non-outcrop samples is 2.67±0.02 t/m^3 (median 2.68 t/m^3), which may be compared with a mean of 2.64±0.01 t/m^3 from all samples above the 2.54 t/m^3 threshold. The former value might be accepted as representative of the Myally Subgroup to Torpedo Creek Quartzite (TCQ) clastic packages, except that the drillhole samples (Torpedo Creek Quartzite from GSQ Lawn Hill 3, Fig. 5.4) are extremely proximal to their sediment sources (Kamarga Volcanics and Yeldham Granite). The TCQ here thus has an unusually high proportion of lithic and feldspar grains in comparison to the formation regionally. Significant levels of sulphides (mainly pyrite) are also present in TCQ intersected

in GSQ Lawn Hill 3, possibly associated with the nearby epigenetic Kamarga base metal deposit (Jones, 1986). Both factors mentioned will contribute to increased local density. A regionally representative bulk value for these units probably lies in the range 2.64-2.67 t/m^3. Regional spatial variations in this value are likely given variations in cementation, metamorphic grade and proportions of fine-grained siliciclastics and minor dolostone in the Myally Subgroup and Surprise Creek Formation.

Magnetic susceptibility is very low, at around 0.01 SI x 10^{-3}. Velocities are moderately high at around 5400 m/s, even in samples obtained from outcrop, which were generally highly silicified. In unsilicified samples, weathering effects are quite pronounced, with velocities reduced to around 4000 m/s and resistivities decreased by up to several orders of magnitude, into the 100-10000 Ωm range. Chargeability is low, as expected.

Based on limited measurements on hand specimens, the Lochness Formation (Myally Subgroup), Surprise Creek Formation (SCF) and Torpedo Creek Quartzite may be discriminated using radiometrics (see also chapter 7). Lochness Formation samples have very high total count rates; four or more times those observed from similarly sized SCF and TCQ samples. The SCF, while of generally low total count in the area sampled (inliers north of Lady Loretta), is significantly more radioactive than the TCQ according to a t-test at the 95% confidence level.

In Table 5.7 cover sequence 2 and cover sequence 3 siliciclastics show slight positive correlation between density and IP%, which may be partly though not completely explained by the presence of pyrite in Torpedo Creek Quartzite samples. A lack of correlation between density and velocity is notable in this suite, as this is usually present to some degree in sedimentary lithologies (Woollard, 1962). This may indicate a compositional (that is, non-porosity) control on density. The apparent lack of relationship between electrical and radiometric properties is also somewhat surprising, as resistivity and radioactivity levels are both often interpreted as indicating the proportion of fine-grained material in siliciclastic sequences (Telford et al., 1990).

	Porosity	*SG sat*	*Susc.*	*Velocity*	*Resistivity*	*log R*	*IP%*	*TC1*	*K*	*U*	*Th*	*K/Th*	*K/U*	*Th/U*	*K/TC*
Porosity	1.00														
SG sat	-0.34	1.00													
Susc.	0.24	0.12	1.00												
Velocity	-0.03	-0.20	-0.01	1.00											
Resistivity	-0.35	0.20	-0.20	0.16	1.00										
log R	-0.72	-0.17	-0.34	0.40	0.69	1.00									
IP%	-0.06	0.68	-0.03	-0.43	-0.14	-0.44	1.00								
TC1	0.55	0.41	0.39	0.22	-0.15	-0.58	-0.22	1.00							
K	0.42	0.53	0.26	0.30	-0.07	-0.44	-0.17	0.92	1.00						
U	0.46	0.13	0.28	0.07	-0.21	-0.42	-0.12	0.44	0.33	1.00					
Th	0.10	0.13	-0.07	0.12	0.22	0.08	-0.36	0.18	0.32	0.04	1.00				
K/Th	-0.07	0.47	-0.02	0.32	-0.01	-0.16	0.21	0.24	0.26	0.02	-0.49	1.00			
K/U	-0.05	0.28	0.17	0.09	0.10	-0.06	-0.05	0.47	0.50	-0.49	-0.03	0.30	1.00		
Th/U	-0.14	-0.23	-0.07	-0.15	0.12	0.29	-0.14	-0.16	-0.15	-0.54	0.35	-0.72	0.32	1.00	
K/TC	0.32	0.58	0.29	0.33	0.11	-0.21	-0.08	0.80	0.91	0.24	0.31	0.18	0.55	0.00	1.00
TC1/m	0.08	0.73	0.14	0.28	0.45	0.12	-0.14	0.54	0.54	0.37	-0.01	0.37	0.10	-0.32	0.57

Table 5.7 Correlation coefficients between petrophysical parameters, cover sequence 2 & cover sequence 3 siliciclastics (SG > 2.54 t/m^3)

5.4.5 Fiery Creek Volcanics, Weberra Granite, Sybella Granite

These igneous units were emplaced between 1710 Ma and 1650 Ma, spanning the period of basin evolution from the Bigie Formation to the lower McNamara Group. Unfortunately, no sub-surface samples of these units were available, and the dataset consists entirely of outcrop samples. The effects of weathering on this restricted sample set are clearly apparent in the density histogram (Fig 5.8) in the form of a severe negative skew. Consequently it is difficult to determine the significance of the distinct difference between the Sybella Granite and the other felsic igneous units, as these outcrops are almost 200 km apart and thus may have experienced different weathering regimes. Notwithstanding this, after excluding obviously weathered samples ($\rho < 2.58$ t/m^3) it appears likely that the Weberra Granite and felsic Fiery Creek Volcanics are of lower bulk density than the Sybella Granite, implying a generally more felsic composition. A true bulk density value for the Fiery Creek Volcanics basalts probably lies in the range between 2.94 t/m^3 (mean of samples >= 2.75 t/m^3) and the value of the porosity vs. density regression line at the lowest measured porosity value (2.99 t/m^3; Fig. 5.9). Similarly, densities between 2.60 t/m^3 and 2.64 t/m^3 are indicated for fresh Fiery Creek Volcanics sedimentary and felsic igneous rocks.

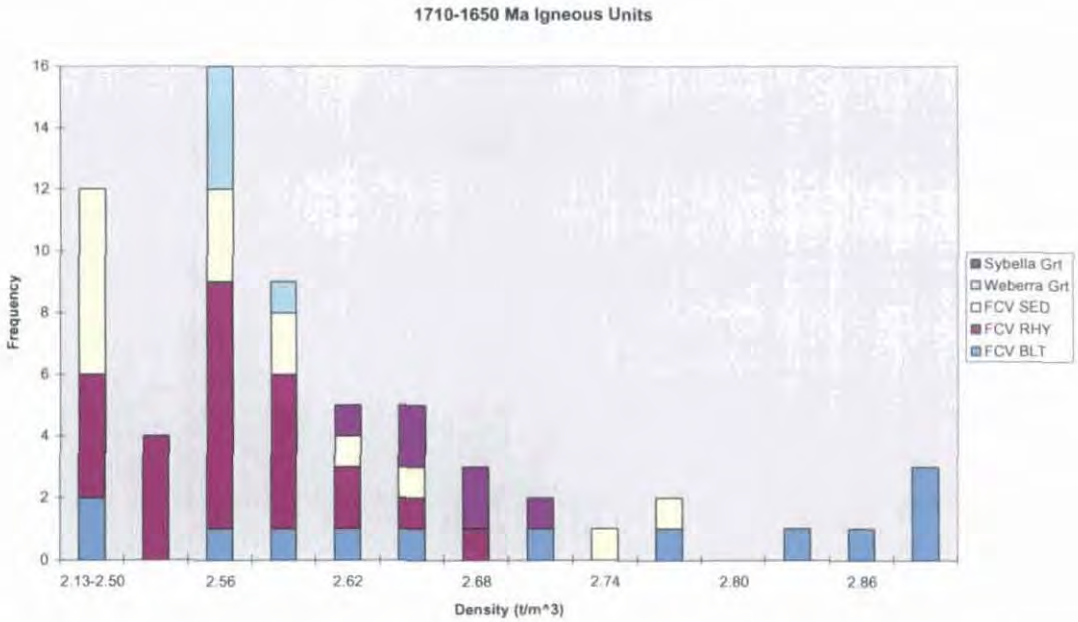

Figure 5.8 Density of Fiery Creek Volcanics (FCV), Weberra Granite and Sybella Granite

Neither the Weberra Granite nor any components of the Fiery Creek Volcanics are magnetic (Fig. 5.10). The slightly elevated magnetic susceptibility of some Fiery Creek Volcanics basalt samples is interpreted as being due simply to higher concentrations of paramagnetic iron as haematite or ilmenite (cf. Puranen, 1989 quoted in Clark, 1997), rather than any difference in iron mineralogy. The magnetic susceptibility of the one Sybella Granite sample measured in this study (16.2 SI x 10^3) is unexpectedly high, given that the Sybella Granite has not hitherto been considered a significant magnetic unit (Derrick, 1992), although it is an I-type granite (Wyborn et al., 1992). Unfortunately the affinity of this sample, retrieved from the Geology Department archive, is slightly uncertain given its lack of location data.

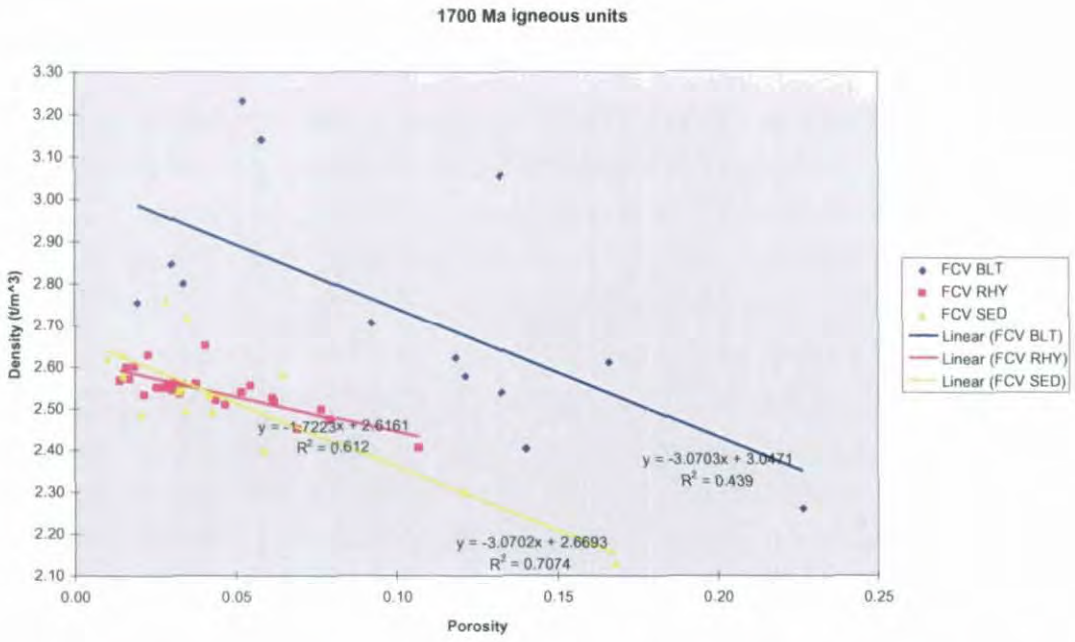

Figure 5.9 Relationship between density and porosity in samples from Fiery Creek Volcanics outcrops. Linear regression has been used to extrapolate possible bulk density for unweathered (therefore presumably low-porosity) equivalents (see text)

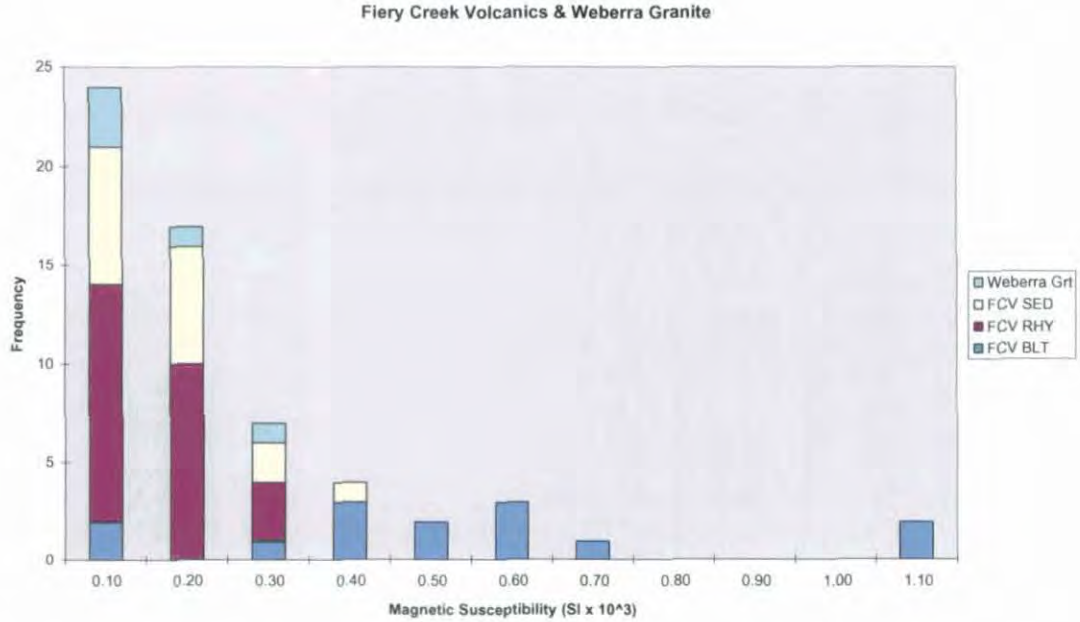

Figure 5.10 Magnetic susceptibilities, Fiery Creek Volcanics and Weberra Granite

Velocity measurements of the Fiery Creek Volcanics basalts (Fig. 5.11) are depressed due to the high porosity of many of the samples. A true bulk velocity value is probably closer to the regression line-derived low porosity value (0.01; 5060 m/s) than the mean value (4670 m/s). Similarly, weathering appears to exert strong control on the resistivity values measured on the Fiery Creek Volcanics basalts, which are only moderately high.

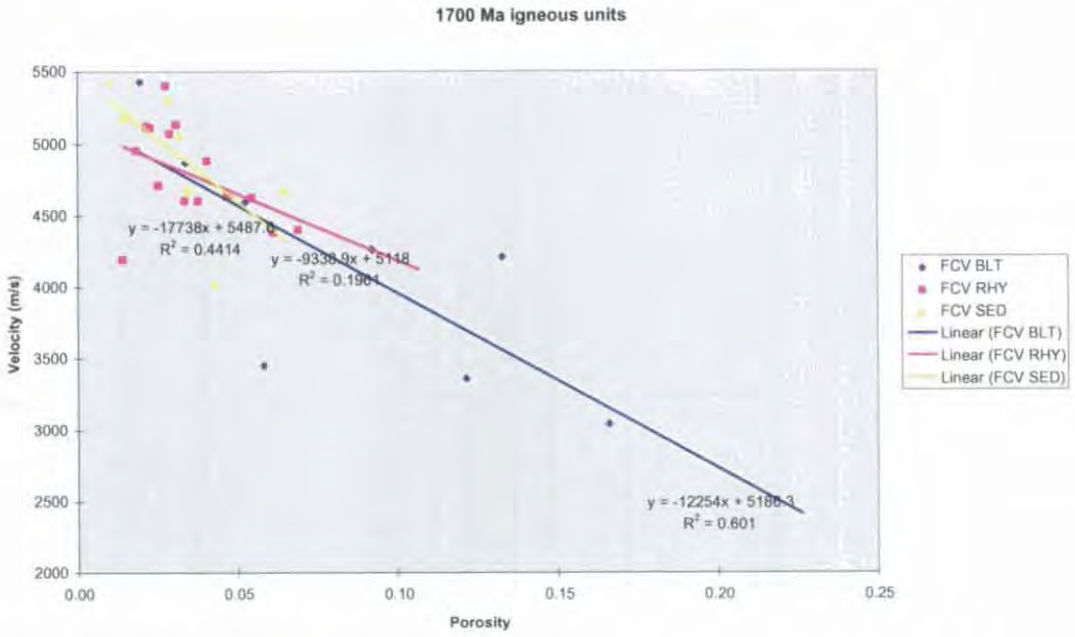

Figure 5.11 Velocities and porosities, Fiery Creek Volcanics

5.4.6 Gunpowder Creek Formation

A histogram of density measurements of drillcore samples of the Gunpowder Creek Formation (Fig 5.12) presents a symmetric distribution centred on 2.73 t/m^3. This is somewhat higher than expected given descriptions of the Gunpowder Creek Formation (GCF) as predominantly siliciclastic in most areas (Hutton et al., 1981; Hutton and Wilson, 1985; McConachie et al., 1996; Sami et al., 1997). Significant concentrations of dolomite in the sediments, not readily apparent in outcrop, may be responsible for the higher than expected density. Sample bias may also be exerting a control in this respect, as most drillholes sampled have been targeted on conductive horizons near the top of the formation and have therefore not intersected the coarser siliciclastic sequences documented from lower sections of the stratigraphy.

The sample sources in Fig 5.12a are arranged in order from north to south, with the four sample suites at the bottom (informal members Plug 1-3 and Misc2) representing outcrop samples mainly from the vicinity of Lady Loretta. The effects of weathering are clearly apparent; the densities of outcrop samples are almost exclusively below 2.50 t/m^3. Less obvious in Fig. 3.15a and Fig. 5.13a is a negative trend in density and resistivity from north to south, probably in response to an increasing proportion of siliciclastics. There are only moderate correlations (correlation coefficients in the range 0.3-0.4) between density, velocity and resistivity.

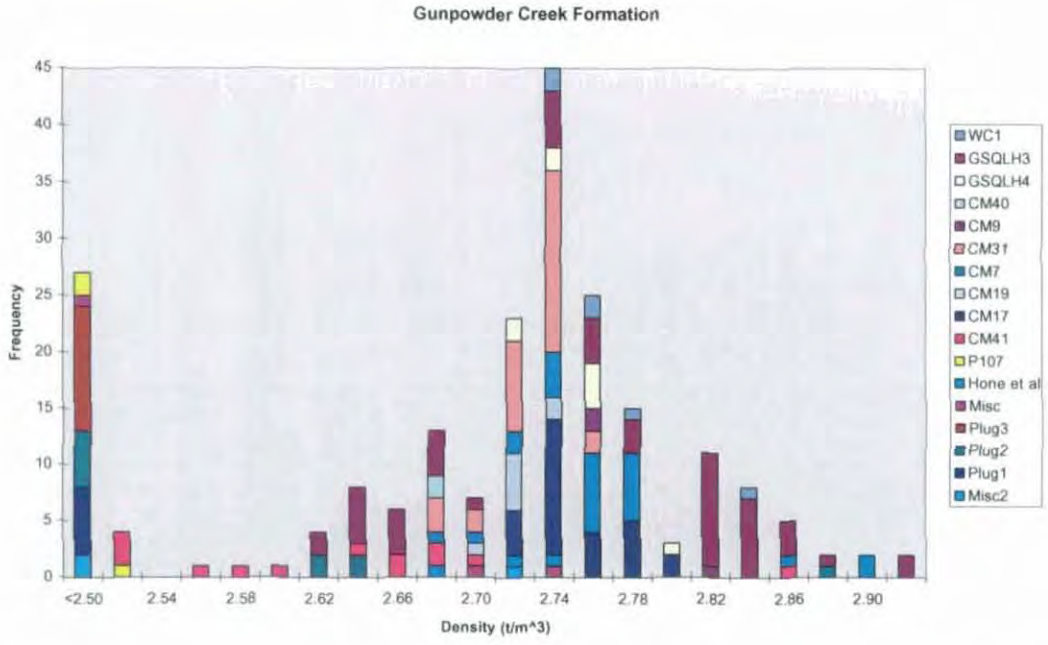

Figure 5.12a Density measurements, Gunpowder Creek Formation. Sources listed in the legend on the right mostly refer to drillholes, while others are from outcrop (see text; Appendix 3)

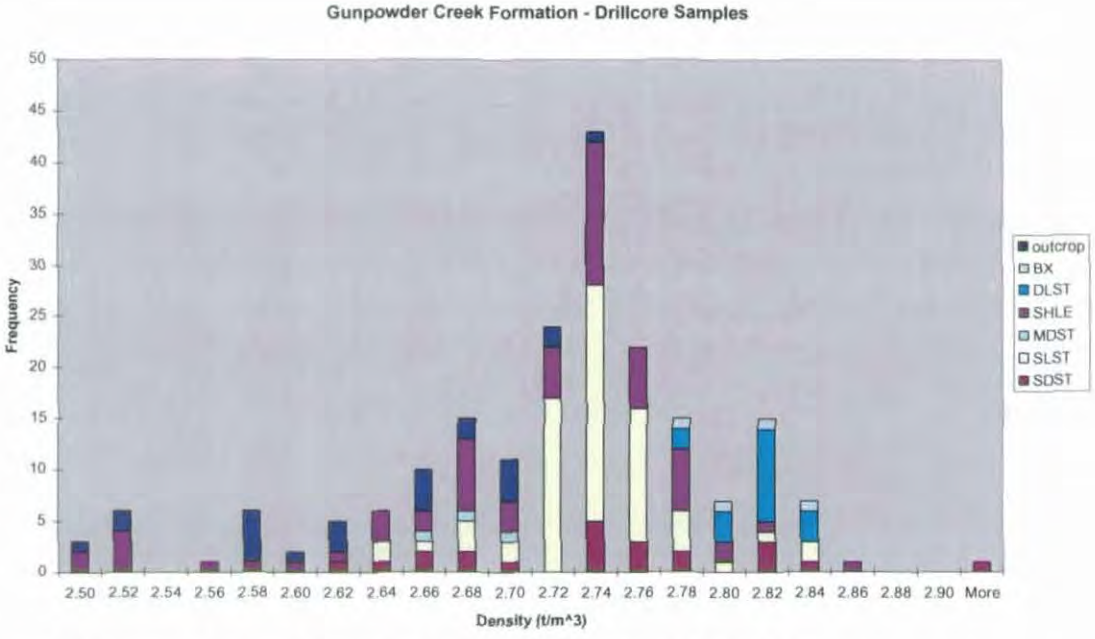

Figure 5.12b Gunpowder Creek Formation density measurements, coded by lithology

Further general insight into the physical properties of typical lithologies in the GCF (and other Proterozoic formations in the region) may be gleaned from Figs. 5.12b and 5.13b. The clear (and expected) tendency is for dolostones and dolomitic breccias to have densities in excess of 2.74 t/m^3, while siliciclastics tend to be lower. Variations in the proportion of these two basic types (in the form of, for example, dolomitic siltstone or sandy dolarenite) give rise to the overlap observed. An obvious implication is that the first-order control on the bulk density of formations in mixed carbonate-siliciclastic sequences such as the lower McNamara Group will be the relative proportion of the lithological types depicted in Fig. 5.12b. These lithological controls are also manifest in Fig. 5.13b, where a positive

correlation between density and resistivity maps the relative proportion of dolostone and siliciclastics in the drillcore samples observed. The regional variation in bulk density suggested in Figs. 5.12a and 5.13a is thus interpreted to result from primary spatial compositional variability, rather than other factors such as differences in metamorphic grade. Apart from substantially lowering density, weathering tends to homogenise conductivity properties at moderate levels (500-4000 Ωm; Fig. 5.13b).

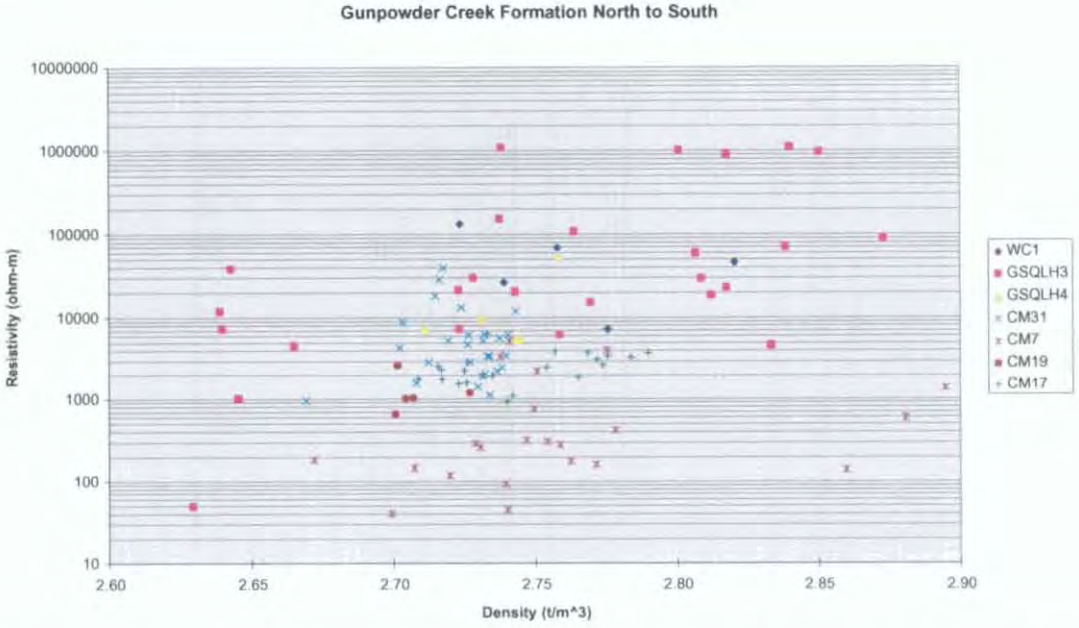

Figure 5.13a Gunpowder Creek Formation density and resistivity, classified by sample source. Drillholes listed in legend in geographic order from north to south

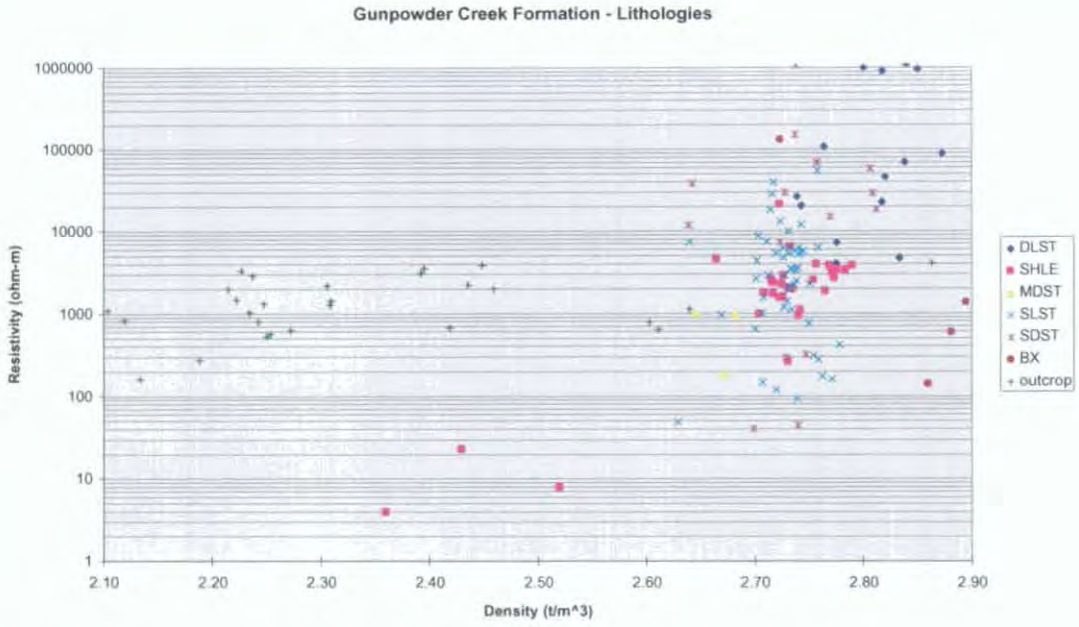

Figure 5.13b Gunpowder Creek Formation density and resistivity, classed by lithology

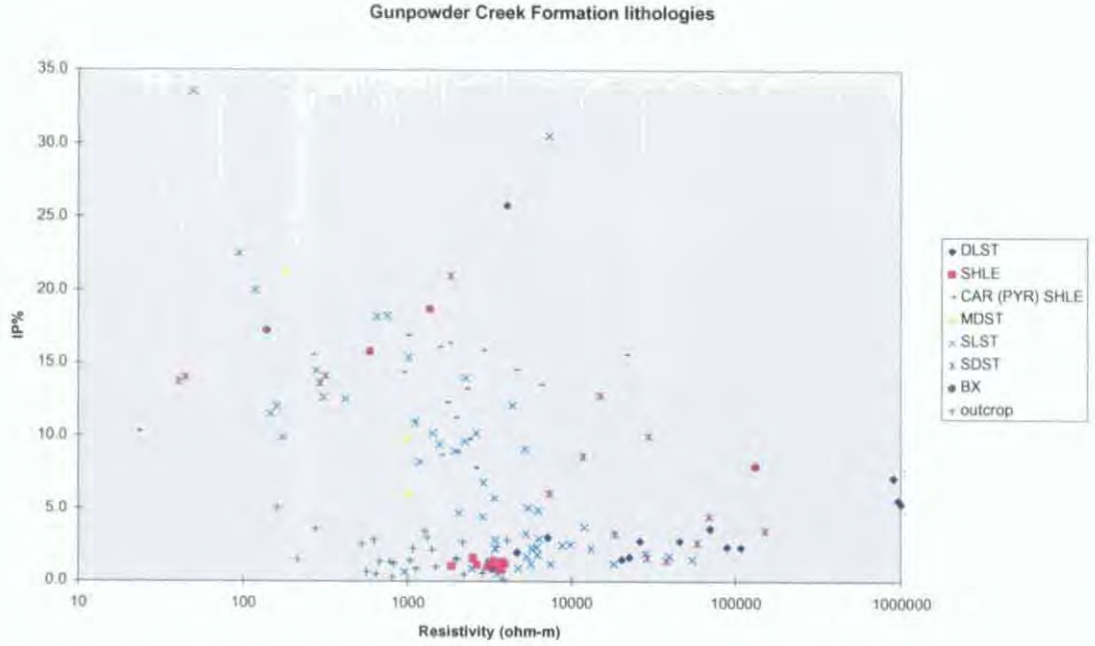

Figure 5.13c Gunpowder Creek Formation resistivity and chargeability, classed by lithology

Highly dolomitic lithologies are dense, resistive and have high velocities, while fine-grained siliciclastic rocks have lower resistivity and density. Elevated densities in the latter are probably due to concentrations of pyrite. The coarser siliciclastic rocks (silts and sands) have similar densities to their fine-grained counterparts, but their resistivity, while highly variable, is generally higher. Sandstones have the highest velocities of the siliciclastic samples followed by siltstones, mudstones and shales respectively.

Fig. 5.13c demonstrates that many unmineralised GCF samples have moderately high chargeability. Shales in particular exhibit a distinct bimodality in IP properties. Carbonaceous material (possibly bearing microscopic pyrite) was noted in most samples comprising the higher IP% population; also noteworthy is that many of these samples are quite resistive.

Velocities in the GCF are predictably dependent on lithology (Fig. 5.14). High acoustic impedance contrasts are indicated for compositional changes. The notably high velocity of sandstones in relation to other siliciclastics in Fig. 5.14 is ascribed to the highly cemented (silicified), non-porous nature of these rocks. Outcrop velocities are up to several thousand metres per second lower than their unweathered equivalents.

Gamma ray spectrometer measurements on the GCF show similar levels of radioactivity to older sedimentary units, and ratios of various channels do not vary significantly from older units. Outcrop samples have significantly higher total count than those from drillholes, but K/Th/U ratios are statistically indistinguishable between the two datasets. The reason for the apparent enrichment of radioelements by weathering is not known, but may be due to dissolution and removal of carbonate constituents. The difference in proportion of siliciclastics between samples from the north and south of the study area is again apparent in total count measurements, with levels measured in drillholes GSQLH3 and GSQLH4 much lower than those in the south (CM series). Negative correlations between total count and density

and between velocity and resistivity (see for example Fig. 5.15) are consistent with proportions of K-bearing siliciclastic grains being the controlling factor.

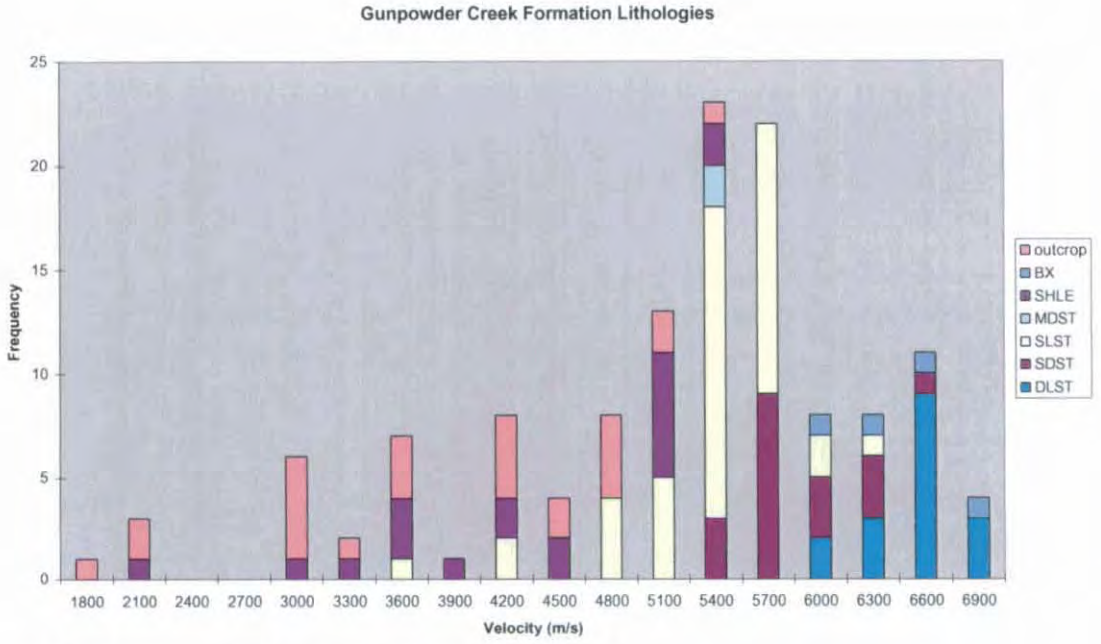

Figure 5.14 Gunpowder Creek Formation velocity, classed by lithology

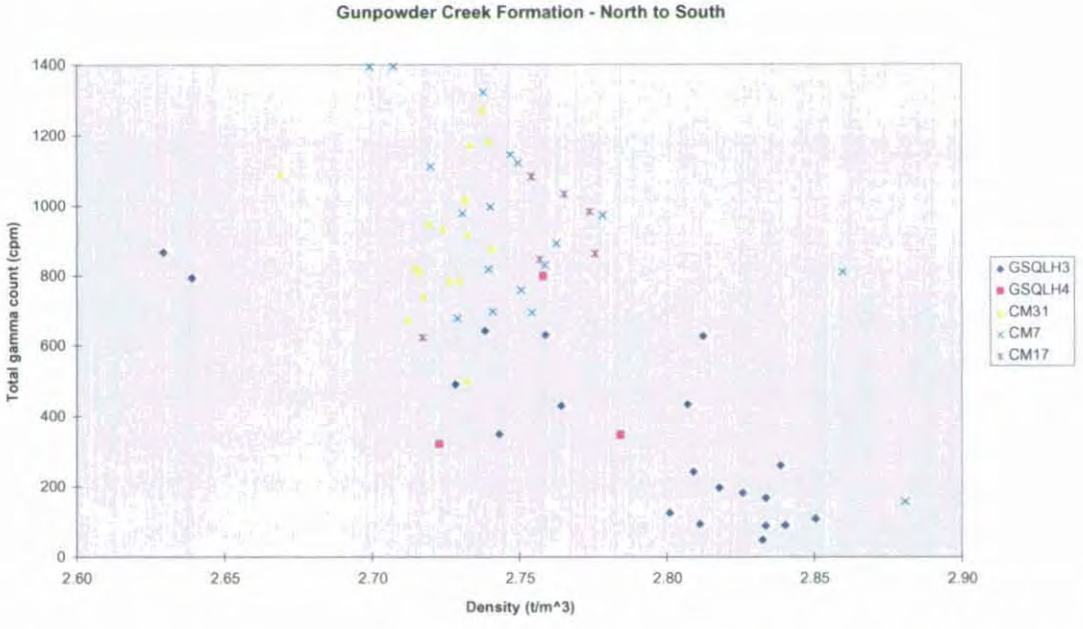

Figure 5.15 Density and gamma ray count, Gunpowder Creek Formation. Drillcore sources in key arranged from north (top) to south (bottom)

5.4.7 Paradise Creek Formation

There is a distinct dichotomy in the Paradise Creek Formation (PCF) between carbonate-dominant and siliciclastic-dominant samples. The relative proportions of rock types in the sample set are considered to be reasonably representative of those in the formation regionally. The most common lithology, dolostone, shows a normal distribution centred around 2.81 t/m^3 (Fig. 5.16), while the siltstones and shales have less well developed central tendency in their density histograms. This is likely due to varying proportions of dolomite 'contamination' in the fine siliciclastics and, particularly in the shales, pyrite and carbonaceous material. Based on averages of density measurements, shales and siltstones are likely to have density contrasts of around -0.10 t/m^3 with dolostones in the PCF. Figs. 5.16 and 5.17 clearly imply that at least the cement matrix and some of the clastic component in the 'arenites' is in fact dolomite.

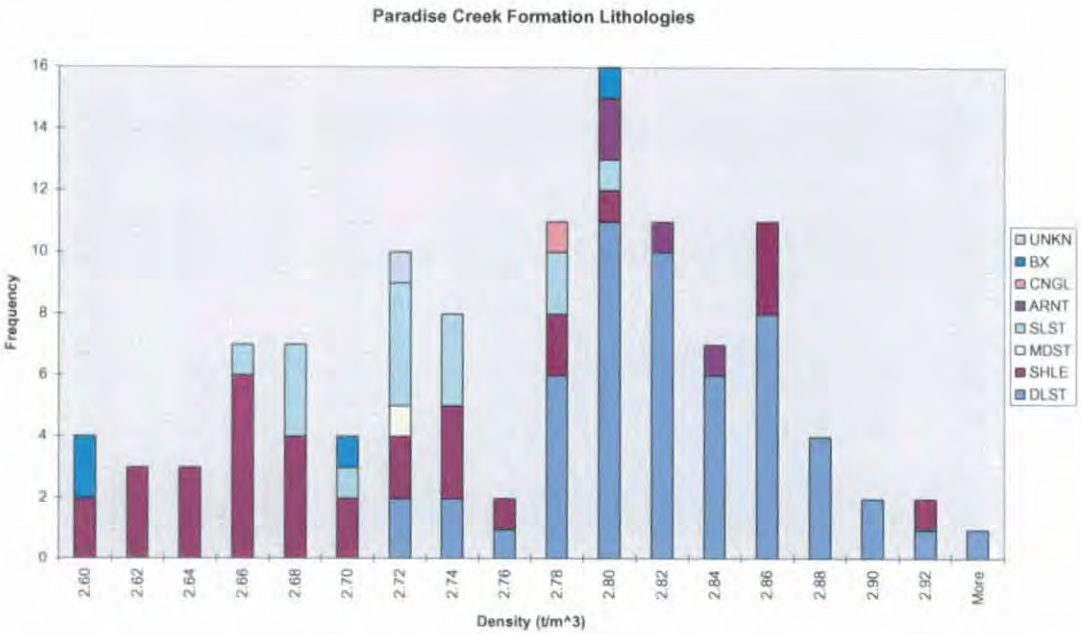

Figure 5.16 Paradise Creek Formation density measurements

Magnetic susceptibility of all samples is uniformly negligible, the one exception being a ferruginous ooid sample from near Kamarga Dome (7.85 x 10^{-3} SI). One possible cause is authigenic magnetite formed by reaction of haematite in the presence of hydrocarbons (Machel and Burton, 1991). Unfortunately this specimen, collected for teaching purposes, could not be subjected to further testing, so the source of this magnetisation remains unknown. A frequency histogram of velocities of PCF lithologies (Fig 5.17) appears similar to the equivalent histogram of densities, with dolostones comprising a distinct normally distributed population centred (mean 6200 m/s) significantly above the more scattered velocity measurements made on shale and siltstone samples (mean 4470 and 4950 m/s respectively). Velocities in the PCF are generally greater than in the Gunpowder Creek Formation mainly due to the increased proportion of carbonate minerals.

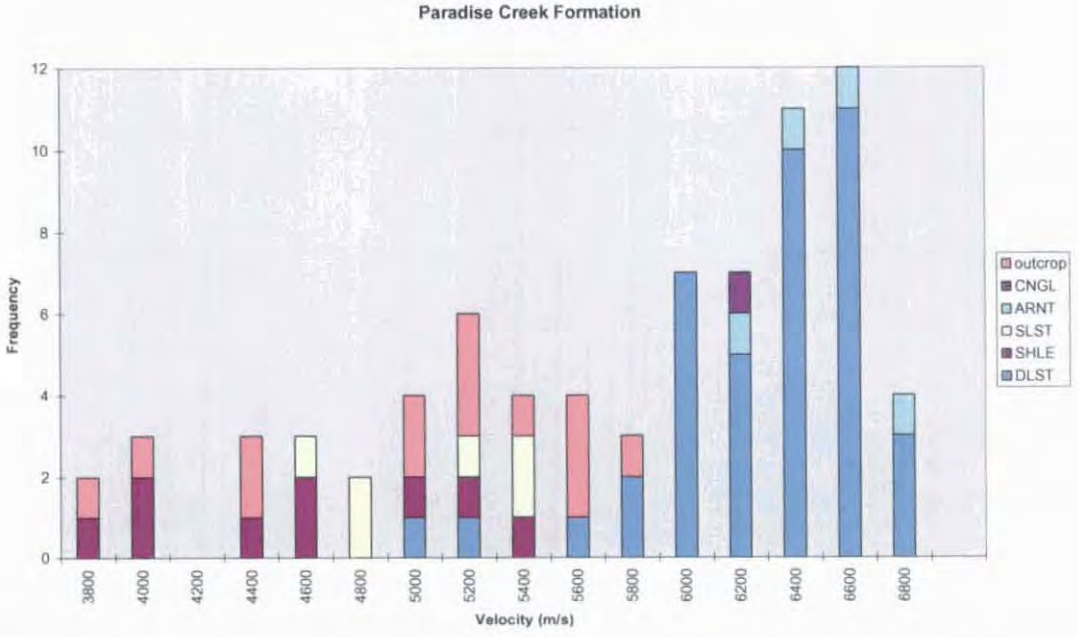

Figure 5.17 Paradise Creek Formation velocities

There is a distinct bimodality to the distribution of resistivity measurements (Fig. 5.18) with dolostones, while ranging widely, often being orders of magnitude more resistive than siliciclastics. Many dolostone samples had resistivities too high to be measured with the apparatus used (shown as > 7.0'in Fig. 5.18 and resistivity = 10000000 Ωm in Fig. 5.19). The dolostone/shale-siltstone dichotomy is illustrated even more clearly by Fig. 5.19, with a high resistivity-high density field defined by dolostones and a low resistivity-low density field defined by shales and siltstones. These two fields overlap because of dolomite 'contamination'in siltstones and vice-versa. The outlying high density/low resistivity shale sample contains a significant amount of pyrite.

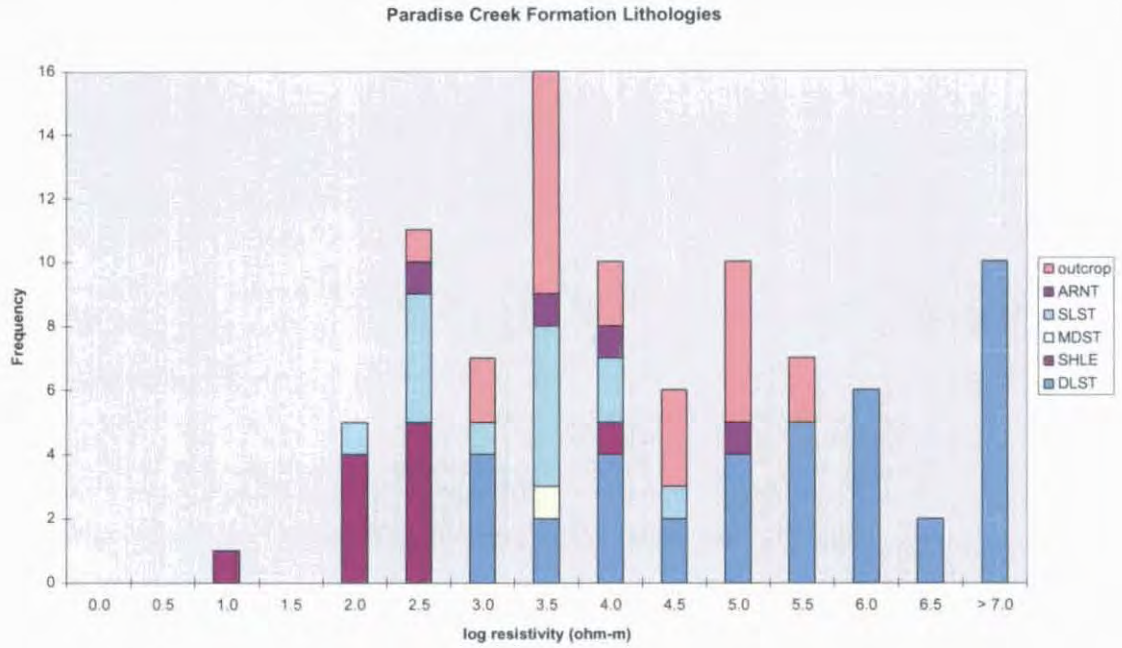

Figure 5.18 Resistivity measurements, Paradise Creek Formation

The contrast in physical properties between carbonates and siliciclastics in the PCF is reflected in Table 5.8, with positive correlations between density, velocity and (log) resistivity; and negative correlation between these parameters and total gamma ray count. A positive correlation (R=0.80) between IP% and total count (Table 5.8; Fig. 5.21) is related to the chargeable nature of many of the fine-grained siliciclastic samples.

	SG dry	*Porosity*	*SG sat*	*Susc.*	*log MS*	*Velocity*	*Resistivity*	*log R*	*IP%*	*TC1*	*K/Th*	*K/U*	*Th/U*	*K/TC*
SG dry	1.00													
Porosity	-0.42	1.00												
SG sat	1.00	-0.37	1.00											
Susc.	-0.05	0.08	-0.23	1.00										
log MS	-0.06	-0.02	-0.08	0.72	1.00									
Velocity	0.80	-0.67	0.79	0.02	-0.01	1.00								
Resistivity	0.31	-0.40	0.29	-0.14	-0.13	0.32	1.00							
log R	0.68	-0.68	0.65	-0.22	-0.23	0.65	0.64	1.00						
IP%	-0.45	0.46	-0.43	0.11	0.14	-0.53	-0.26	-0.73	1.00					
TC1	-0.66	0.55	-0.64	0.06	0.07	-0.79	-0.35	-0.84	0.80	1.00				
K/Th	-0.13	0.18	-0.12	-0.11	-0.15	0.07	-0.25	-0.21	0.14	0.19	1.00			
K/U	-0.17	0.11	-0.17	-0.17	-0.15	0.01	-0.19	-0.01	-0.19	-0.02	0.42	1.00		
Th/U	0.04	-0.12	0.03	-0.15	-0.12	0.01	0.09	0.29	-0.36	-0.34	-0.62	0.33	1.00	
K/TC	-0.18	-0.09	-0.20	-0.17	-0.13	-0.02	0.10	0.08	-0.31	0.03	0.08	0.64	0.25	1.00
TC1/m	-0.80	0.59	-0.79	0.09	0.10	-0.95	-0.18	-0.66	0.61	0.84	-0.10	-0.11	-0.10	0.07

Table 5.8 Correlation coefficients between petrophysical parameters, Paradise Creek Formation drillcore

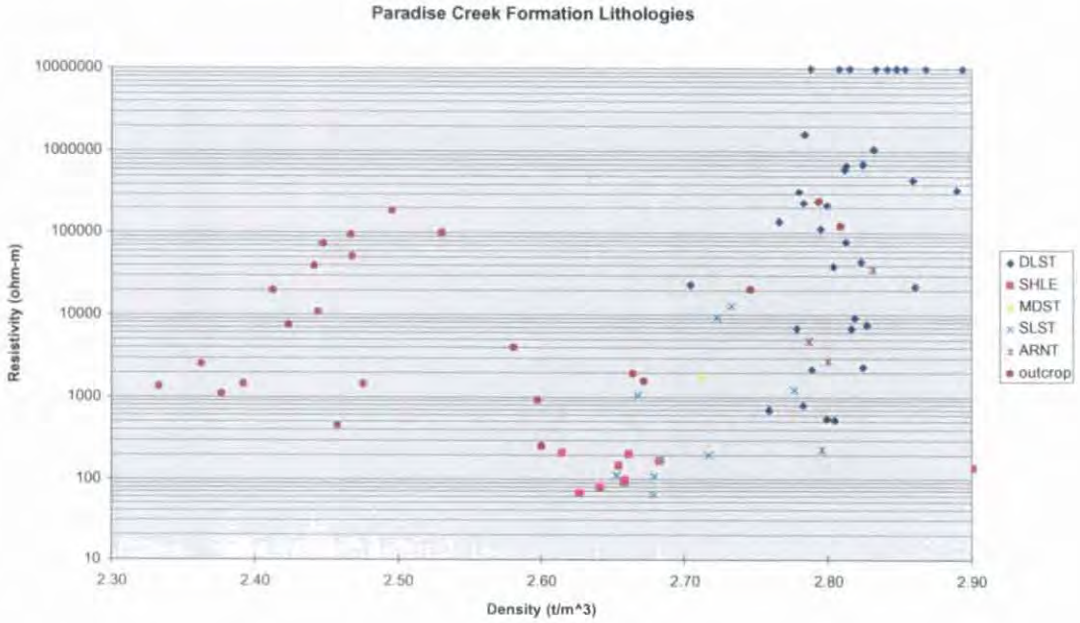

Figure 5.19 Density and resistivity relationships, Paradise Creek Formation

Similarly, in Fig. 5.20, the two samples with both very high density and high chargeability contain quantities of sulphides. High chargeability is also associated with low-density carbonaceous shales that do not contain visible sulphides. Chargeabilities of dolostone samples are variable, but are generally moderate to low.

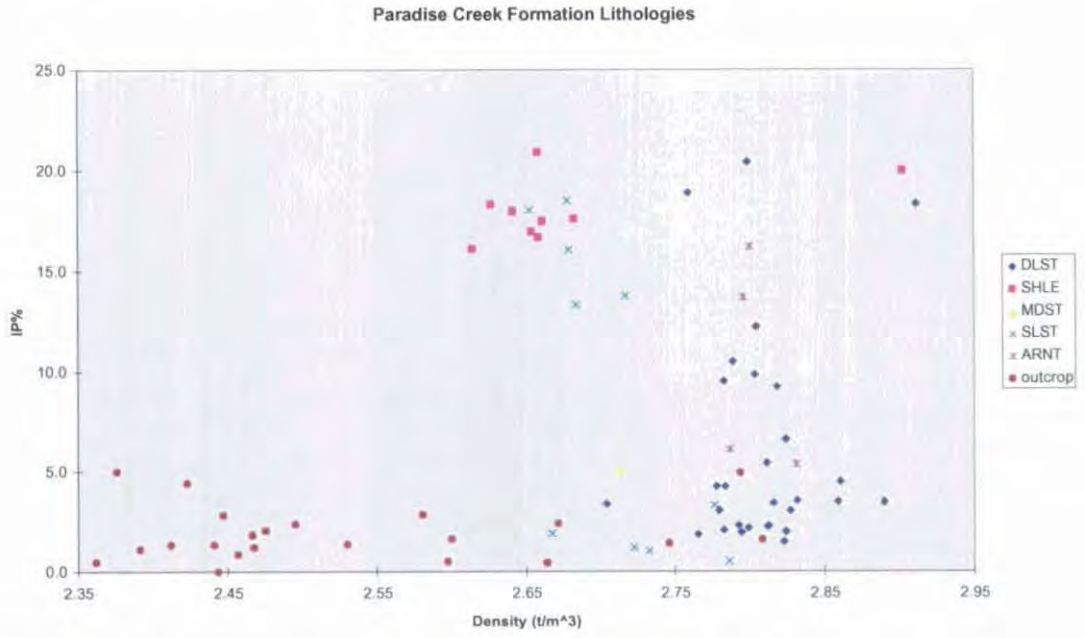

Figure 5.20 Density and chargeability relationships, Paradise Creek Formation

The distinct differences in the properties of PCF lithologies make the mean formation values given in Table 5.12 somewhat less meaningful, at least in the case of properties relevant to methods sensitive to rapid spatial variations (velocity, resistivity, chargeability). The reliability of putative representative bulk values will depend strongly on the relative proportion of carbonates and siliciclastics in any given location. Generally, velocities are higher in the PCF than in the GCF, essentially due to the prevalence of carbonates in the former. In the light of this, it is surprising that consolidated mean values for electrical properties of the Paradise Creek Formation are within error of those of the Gunpowder Creek Formation.

Gamma ray total counts are lower in weathered and outcropping Paradise Creek Formation samples than in equivalent Gunpowder Creek Formation specimens. This is possibly due to silicified outcrop samples being over-represented in the dataset because of their greater resistance to weathering than unsilicified samples. That fine silts and muds are responsible for the higher IP responses observed in the Paradise Creek Formation is strongly suggested by Fig. 5.21, where the strong positive correlation between shales and siltstones, high gamma ray counts (almost certainly sourced from K) and chargeability is readily observed.

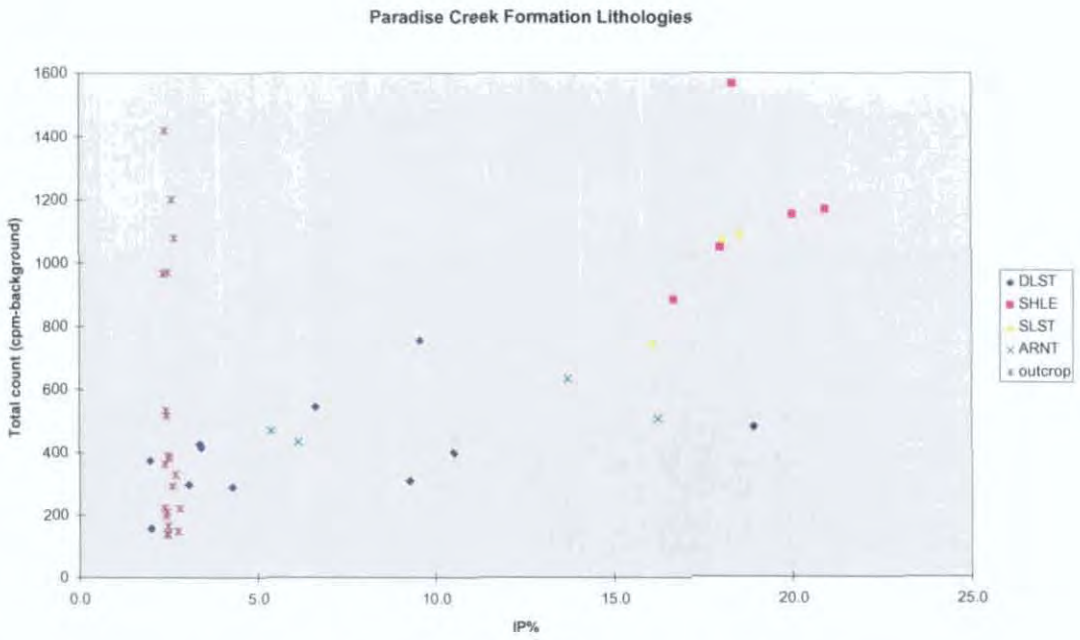

Figure 5.21 Relationship between IP and gamma ray response, Paradise Creek Formation

5.4.8 Esperanza Formation

Dolomite is less common in the Esperanza Formation (EF) than in the PCF, and consequently its physical properties approach those of typical McNamara Group shales and siltstones. The histogram of density measurements (Fig. 5.22) shows a normal distribution centred on 2.68 t/m^3 consisting mainly of shales and siltstones. There is a small outlier of dolostones at densities exceeding 2.84 t/m^3. Velocities are also lower overall than in the PCF, again reflecting a lower proportion of dolomitic sediments, although both dolostone and shale end-members are present (Fig. 5.23). Even the most dolomitic samples from the EF do not attain the highest densities observed in the PCF.

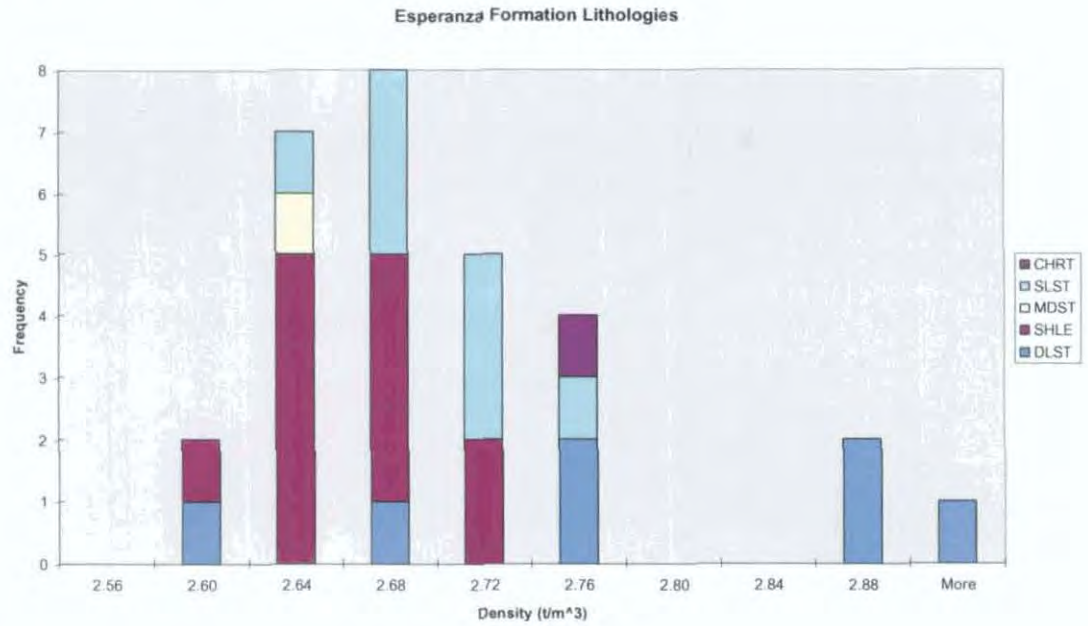

Figure 5.22 Esperanza Formation densities

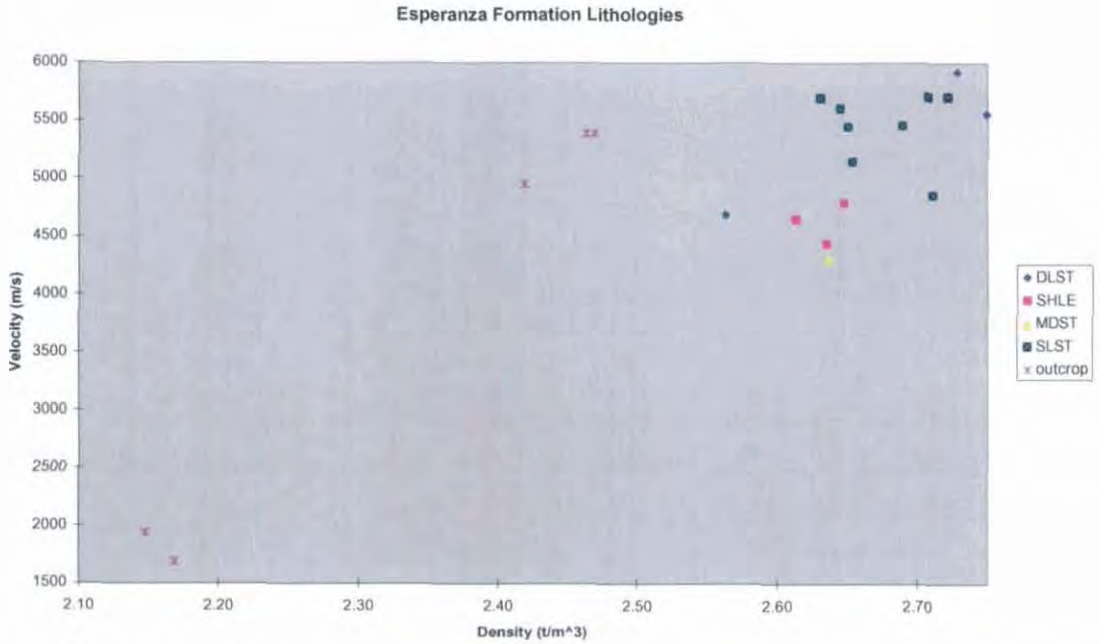

Figure 5.23 Velocity and density, Esperanza Formation

There is the usual correlation between fine-grained siliciclastic content and electrical properties, with shales being associated with higher chargeabilities, lower resistivities and higher radioactivity (Figs. 5.23, 5.24). The depressive effects of weathering on density and velocity are clearly visible in the samples obtained from outcrop, although velocity does not appear to have been greatly affected in the outcrop samples (cherts) plotting in the 2.4-2.5 t/m ^{3} density range (Fig. 5.23). In bulk terms, the Esperanza Formation's electrical properties are similar to those of older McNamara Group units, while gamma ray signatures measured are similar to those of the Paradise Creek Formation (Fig. 5.24).

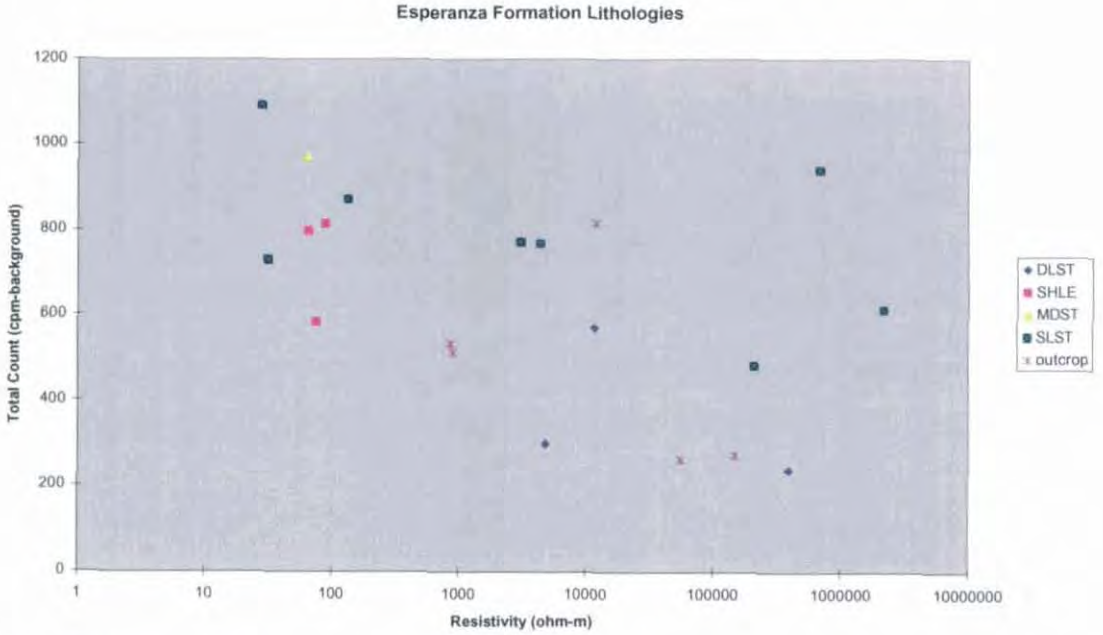

Figure 5.24 Resistivity and gamma ray response, Esperanza Formation

5.4.9 Lady Loretta Formation

Samples from those portions of the Lady Loretta mine stratigraphy most distant from the orebody (the Upper Clastic and Lower Carbonate units of Dunster, 1997) have been included in the regional compilation classed by source (figures suffixed 'a'), and appear indistinguishable from other regional samples. Samples from the Cyclic Unit'overlying the Lady Loretta ore sequence (Dunster, 1997) were additionally included in figures investigating lithological properties (suffixed 'b'), and some of these contain minor quantities of sulphides.

The histogram of density values measured from non-mineralised Lady Loretta Formation (LLF) displays a distinct bimodality (Fig. 5.25a). No general regional trend is apparent, though major differences across short distances (< 1 km) may be observed by comparison of measurements obtained from drillholes CM2 and CM35 (Fig. 5.26a). At 2.78 ±0.02 t/m^3, the mean density of the Lady Loretta Formation is statistically indistinguishable from that of the Paradise Creek Formation, and their median values are also similar (2.79 and 2.78 t/m^3 respectively).

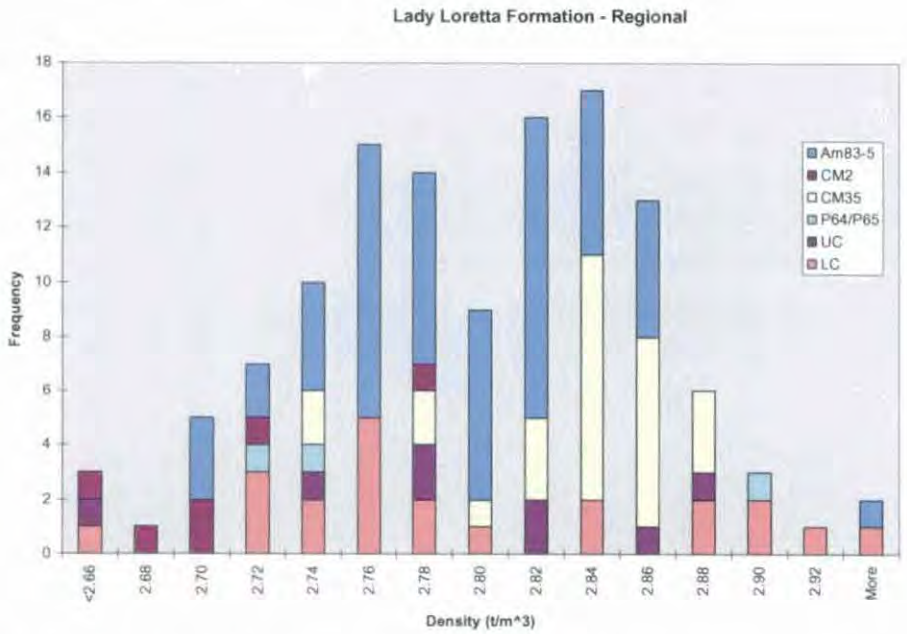

Figure 5.25a Lady Loretta Formation density measurements, classed by source drillhole

The histogram of density for regional samples classed by lithology (Fig. 5.25b) shows the usual dichotomy between dolomite-dominated and siliciclastic-dominated lithologies, though this is not as pronounced as in the Paradise Creek Formation. The presence of sulphides regionally in the formation as well as in the orebody may be responsible for this blurring of the usual distinct difference in density, as well as for the marginally denser character of the Lady Loretta Formation compared to the Paradise Creek Formation. Sulphides (usually pyrite) and other ferruginous minerals have been noted in many samples exhibiting the more extreme density properties, both high and low. The latter is attributed to high sulphide reactivity resulting in excessive porosity, and the former to the intrinsically dense nature of unoxidised sulphides and other ferroan minerals.

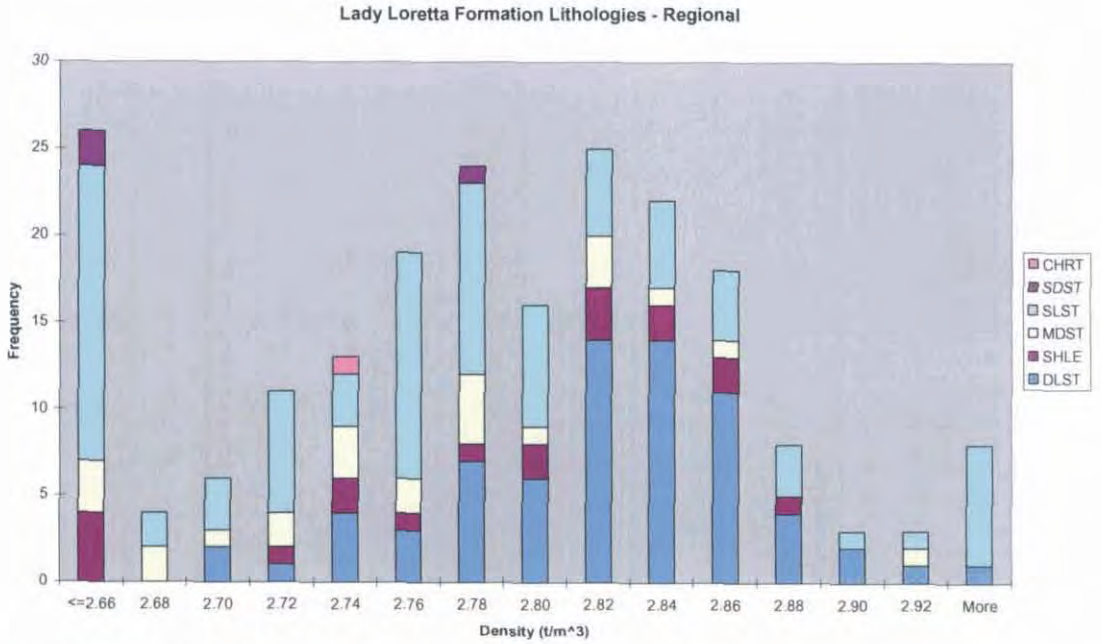

Figure 5.25b Lady Loretta Formation density measurements classed by lithology (includes outcrop samples)

Magnetic susceptibilities are very low regionally. Little correlation is present between density and magnetic susceptibility in drillhole samples (Fig. 5.26a). There does however appear to be a slight correlation between density and magnetic susceptibility in the case of fine-grained siliciclastics (siltstones, mudstones and shales; Fig. 5.26b). No correlation is apparent in highly dolomitic samples, which invariably have very low magnetic susceptibility.

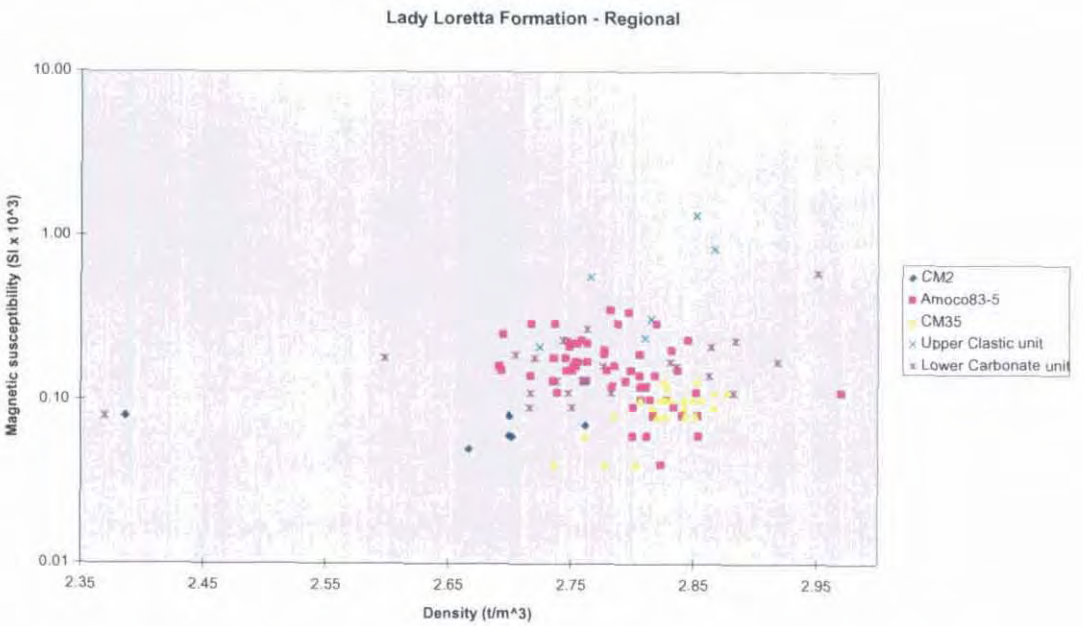

Figure 5.26a Lady Loretta Formation density and magnetic susceptibility classed by drillhole source

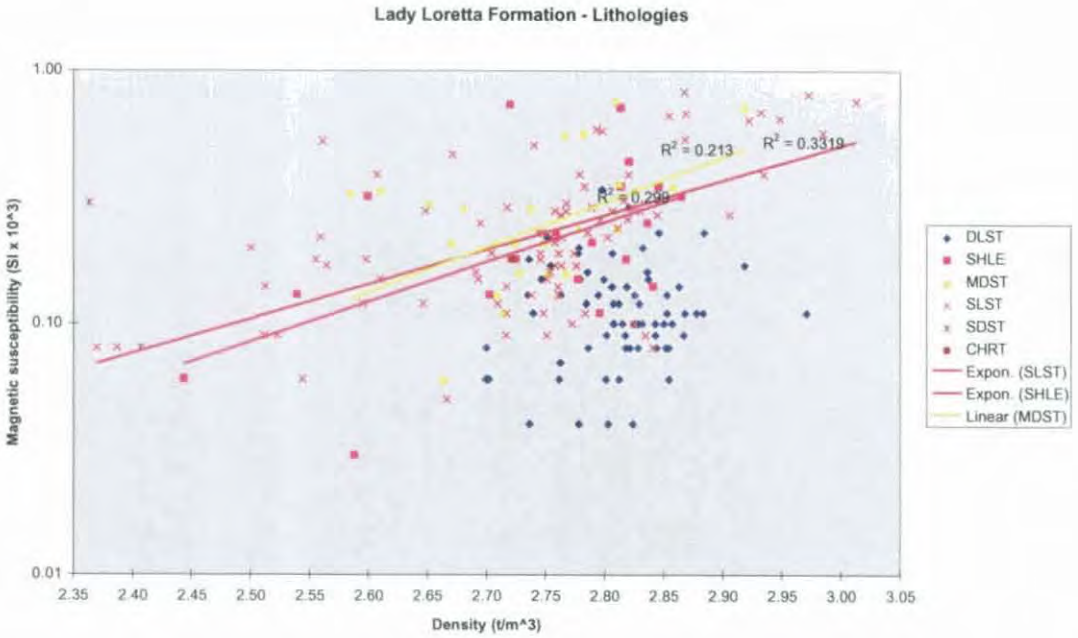

Figure 5.26b Lady Loretta Formation density and magnetic susceptibility, classed by lithology (note scale change from Fig. 5.26a)

The correlation between density and velocity is much stronger (R = 0.85; Fig. 5.27a), particularly in drillholes with a high proportion of dolomite (Fig. 5.27b). Associated with this is a clear negative correlation between velocity and porosity. Velocities in the Lady Loretta Formation regionally are high, ranging up to 6810 m/s, with most centred around 5700 m/s. Included in this range are a dolomitic population with velocities centred on 6000 m/s, and a fine-grained siliciclastic (mainly siltstone) population with velocities mainly less than 5500 m/s (Fig. 5.27b).

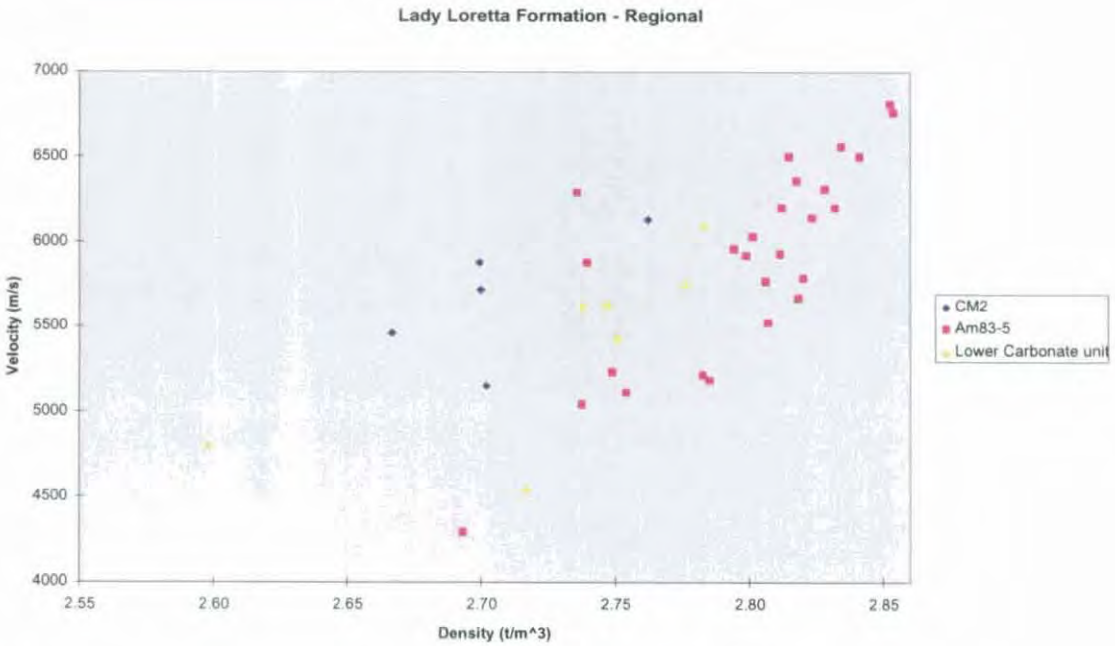

Figure 5.27a Lady Loretta Formation densities and velocities, classed by drillhole source

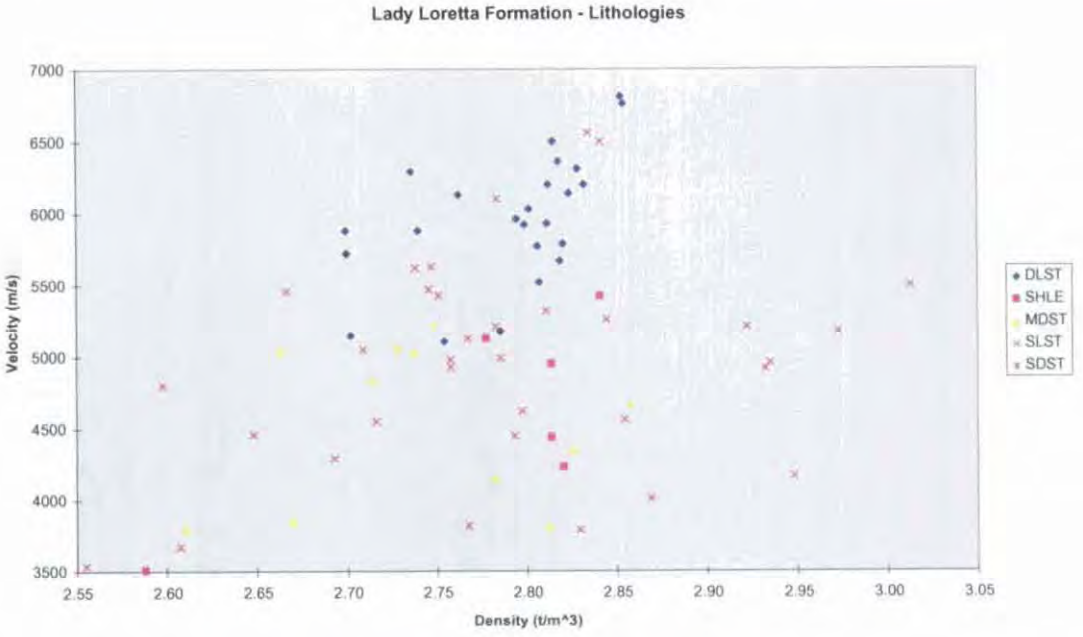

Figure 5.27b Lady Loretta Formation densities and velocities, classed by lithology

Electrical properties of the Lady Loretta Formation regionally are fairly typical for the McNamara Group. Resistivity data are distributed over an extremely wide range, from 100 to well over 100000 Ωm (Fig. 5.28a), with an overall geometric mean of 4160 Ωm. Dolomitic samples range upwards in resistivity from 1000 Ωm, though there is considerable overlap between this field and that of the siliciclastic samples (Fig. 5.28b). A very weak positive correlation ($R^2 = 0.09$) is arguably present between density and resistivity in the dolomitic samples only (Fig. 5.28b). The purest (non-dolomitic) siliciclastic samples are least resistive, generally less than 1000 Ωm. The wide spread in densities at this resistivity level is due to the presence of sulphides; positive variations where sulphide minerals have remained intact, and negative where they have oxidised (both pre- and post-drilling) to form significant secondary porosity.

The Lady Loretta Formation is generally of low chargeability, with the majority of regional samples measured having IP% less than 5 (Fig. 5.29a). Siltstones are generally slightly more polarisable than dolostones. Most of the more chargeable samples plotted in Fig. 5.29b are from within a few hundred metres of the Lady Loretta orebody (Cyclic Unit as well as Lower Carbonate and Upper Clastic unit samples which are also plotted in Fig. 5.29a). This may be due to minerals associated with the halo to the mineralisation (documented in Large and McGoldrick, 1998) as well as to the pyrite common in this section of the stratigraphy. This relationship is explored further in chapter 6.

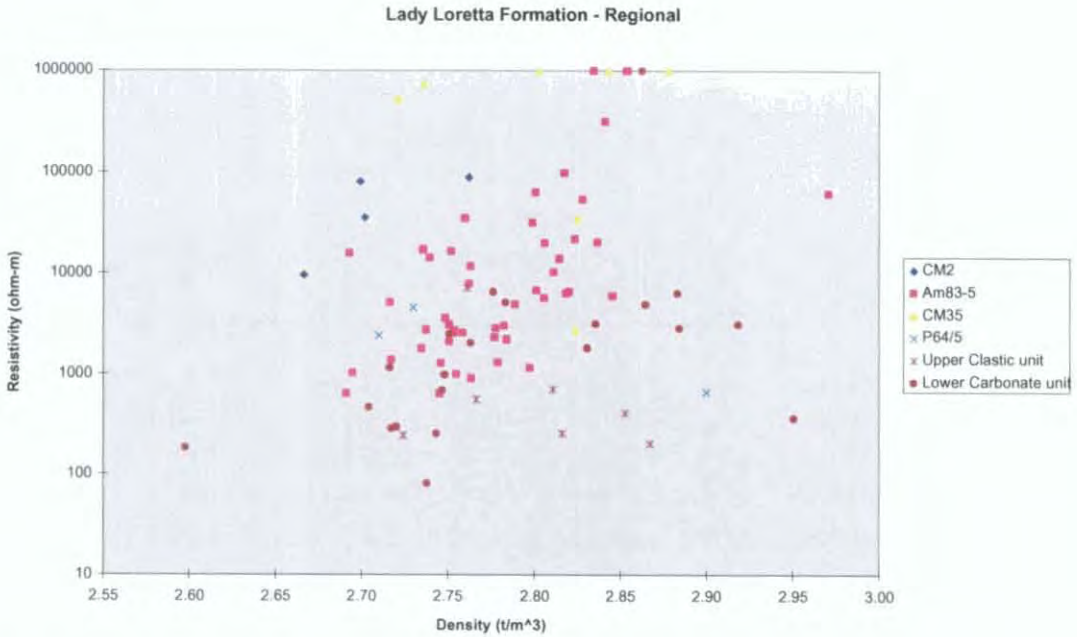

Figure 5.28a Densities and resistivities classified by drillhole source, Lady Loretta Formation

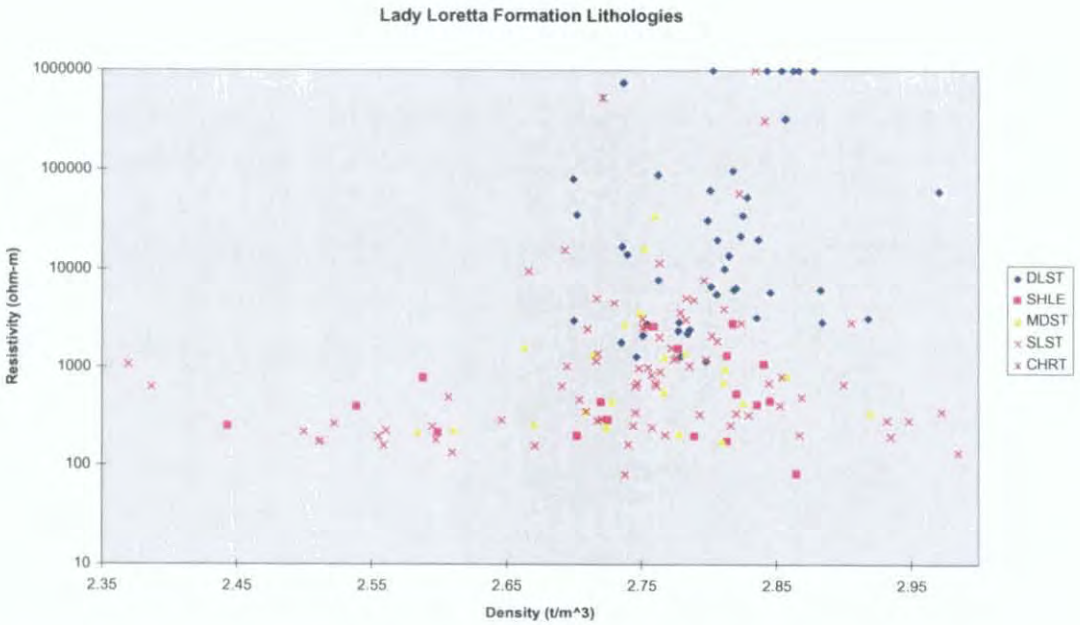

Figure 5.28b Densities and resistivities classified by lithology, Lady Loretta Formation

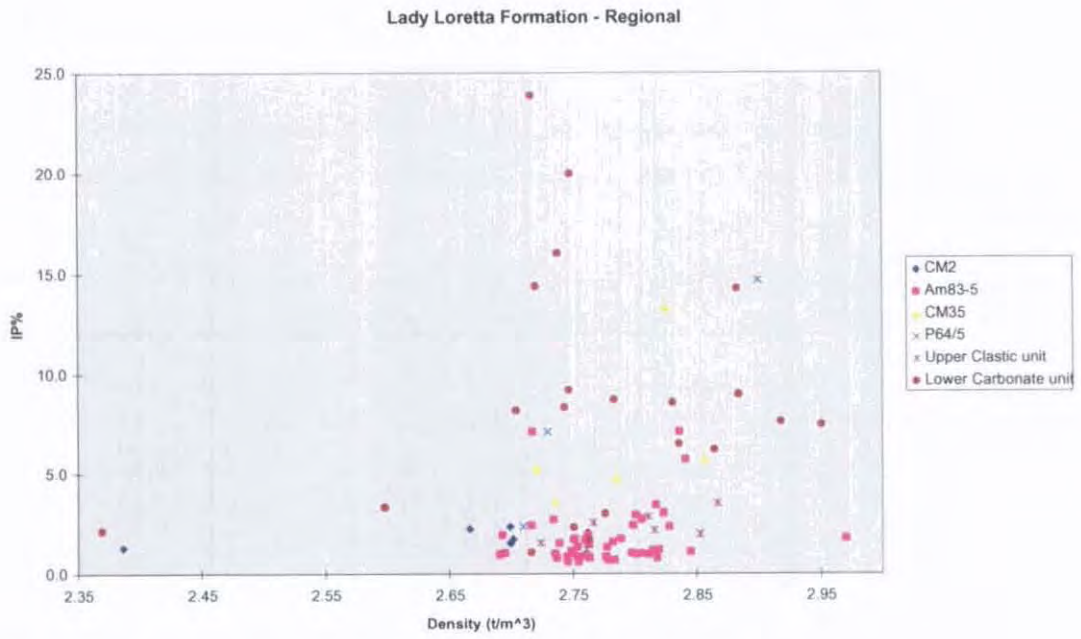

Figure 5.29a Density and chargeability classed by source, Lady Loretta Formation

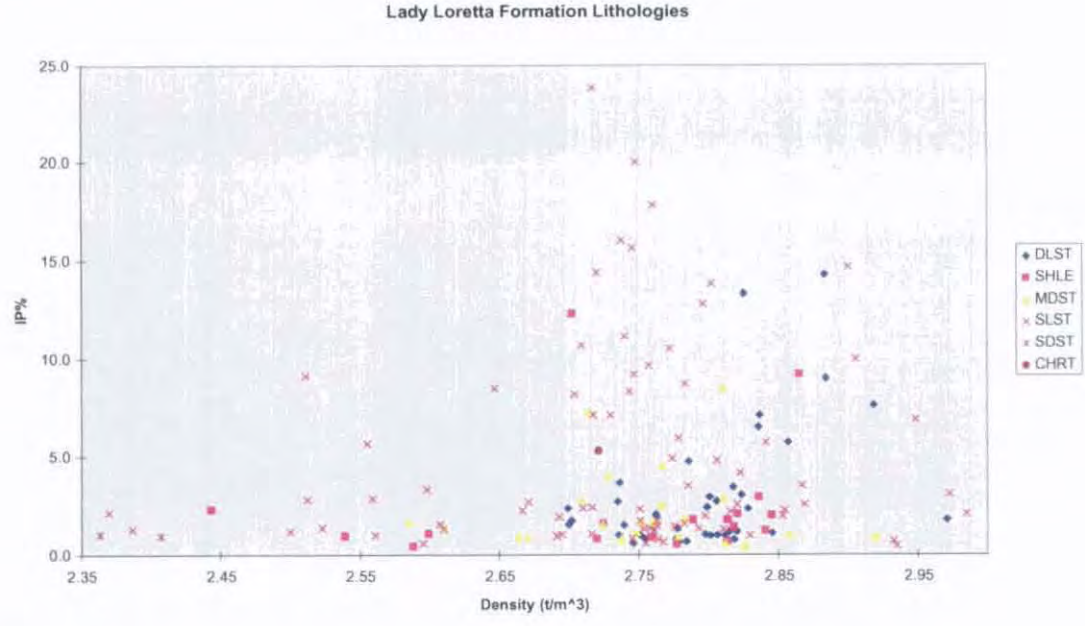

Figure 5.29b Density and chargeability classed by lithology, Lady Loretta Formation

5.4.10 Shady Bore Quartzite

No drillcore samples of the Shady Bore Quartzite were available for this study. Property determinations were made on a few (four) outcrop samples, but these are subject to weathering effects similar to those documented for units discussed above (mainly porosity creation and density and resistivity reduction). The values measured are thus typical of outcropping sandstones in the region, most of which are strongly affected by weathering (cf. section 5.4.4, Fig. 5.7). Densities are centred around 2.37 t/m^3, with very low magnetic susceptibilities, moderate to low velocities, very high resistivities and low chargeabilities.

There is a notably low level of gamma radiation emanating from the Shady Bore Quartzite samples, particularly in the potassium channel; a somewhat surprising result given that over half the samples measured consisted of mud clast conglomerate. For interpretation purposes, the Shady Bore Quartzite is considered to have bulk properties commensurate with formations of similar composition and metamorphic grade (Torpedo Creek Quartzite, Surprise Creek Formation, Myally Subgroup; see section 5.4.4).

	SG dry (t/m^3)	Porosity	SG sat (t/m^3)	Mag susc ($SI \times 10^3$)	Velocity (m/s)	Resistivity (Ωm)	IP%	TC (cpm)
Mean	2.35	0.02	2.37	0.02	4,953	133,639	2.60	168.5
Standard Error	0.023	0.003	0.020	0.002	85	40,218	0.223	39
Median	2.35	0.02	2.37	0.02	4,985	156,123	2.43	161
Standard Deviation	0.045	0.006	0.041	0.005	170	80,435	0.446	79
Sample Variance	0.002	0.000	0.002	0.000	29,025	6.5×10^9	0.199	6182
Kurtosis	-2.355	-0.171	-1.801	4.000	-2.45	0.00	2.529	-3.2
Skewness	0.328	0.227	0.136	2.000	-0.61	-1.10	1.633	0.326
Range	0.10	0.01	0.09	0.01	360	173422	0.96	170
Minimum	2.30	0.02	2.33	0.02	4740	24444	2.29	91
Maximum	2.40	0.03	2.42	0.03	5100	197867	3.25	261
Count	4	4	4	4	4	4	4	4
CL(95%)	0.044	0.005	0.040	0.005	167	78825	0.437	77.054

Table 5.9 Summary statistics, Shady Bore Quartzite petrophysical data

5.4.11 Riversleigh Siltstone

Carbonates are much rarer in the Riversleigh Siltstone than in the lower McNamara Group (Lady Loretta Formation and older), and this is reflected in the Riversleigh Siltstone's physical properties. Density values are spread over a smaller range due to the reduced lithology diversity, centred on a typical value for siliciclastics of 2.67 t/m^3 (Fig. 5.30).

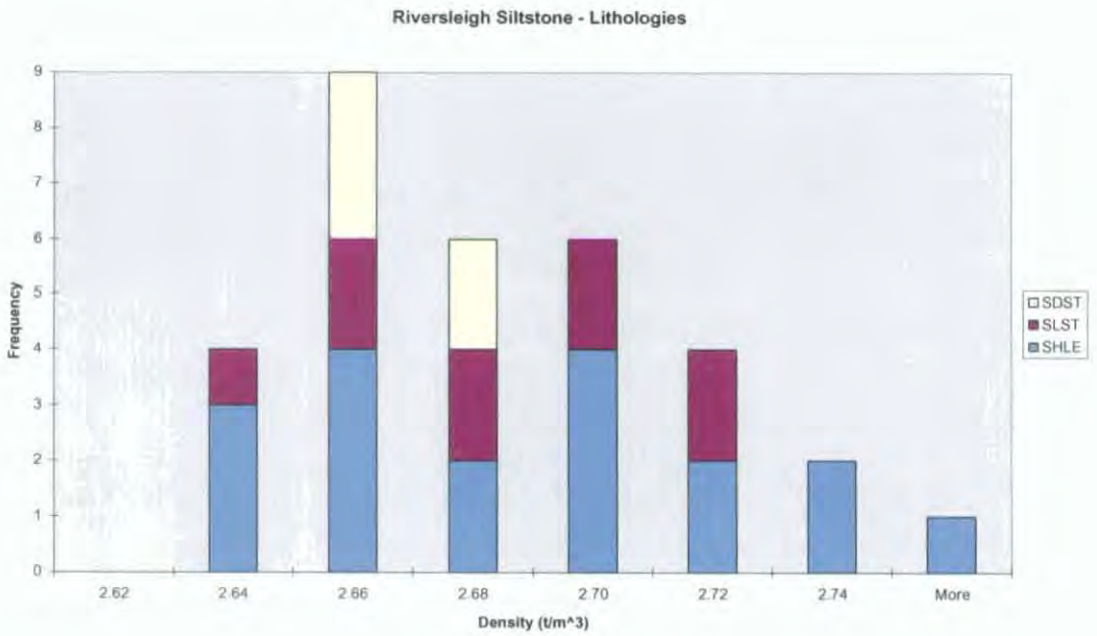

Figure 5.30 Density measurements classed by lithology, Riversleigh Siltstone

Magnetic susceptibilities are very low, in keeping with other McNamara Group siliciclastics. Several outliers obscure a weak positive correlation between density and magnetic susceptibility (Fig. 5.31). No such correlation is apparent in Fig. 5.32, where most velocities measured plot within a narrow band between 5400 and 5800 m/s. Two outliers with velocities less than 4800 m/s are anomalous, and indicate the median is the best estimate of the bulk velocity of the Riversleigh Siltstone, at a moderately high 5570 m/s.

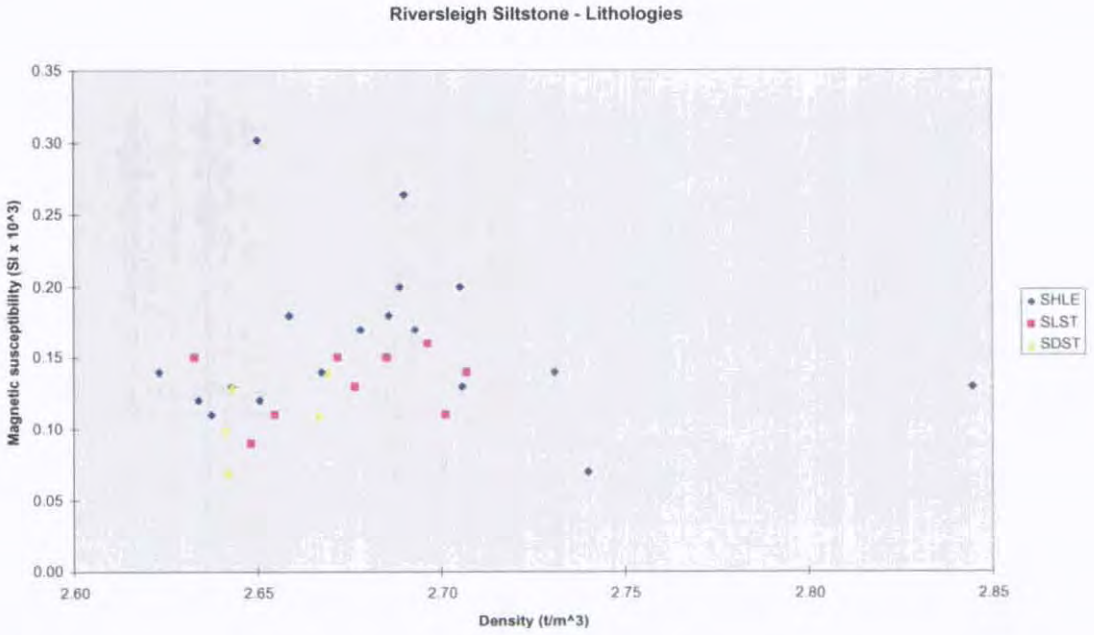

Figure 5.31 Density and magnetic susceptibility classed by lithology, Riversleigh Siltstone

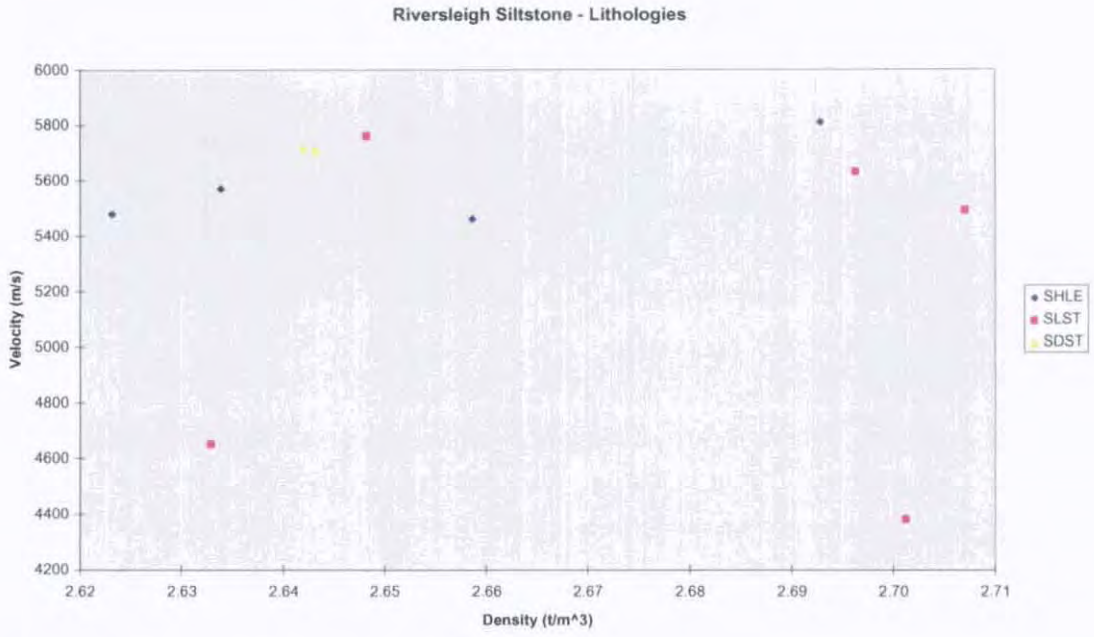

Figure 5.32 Density and velocity classed by lithology, Riversleigh Siltstone

Fig. 5.33 depicts a bimodal element in the distribution of Riversleigh Siltstone resistivities, with populations separated by over an order of magnitude in the case of each lithology (shale, siltstone,

sandstone). The reasons for this are probably not solely compositional. Many of the low-resistivity samples contain visible pyrite and carbonaceous material, but so too do some of the higher-resistivity population. Rather, the main control on resistivity appears to be porosity, as seen in Fig. 5.34. Porosity is likely to be an increasingly important control of other physical properties as metamorphic grade decreases, with concomitant decreases in density and velocity. Most Riversleigh Siltstone samples come from a drillhole over 100 km to the NNW of Lady Loretta (Amoco 83-1; see below), where metamorphic grade is slightly less than in the Lady Loretta district.

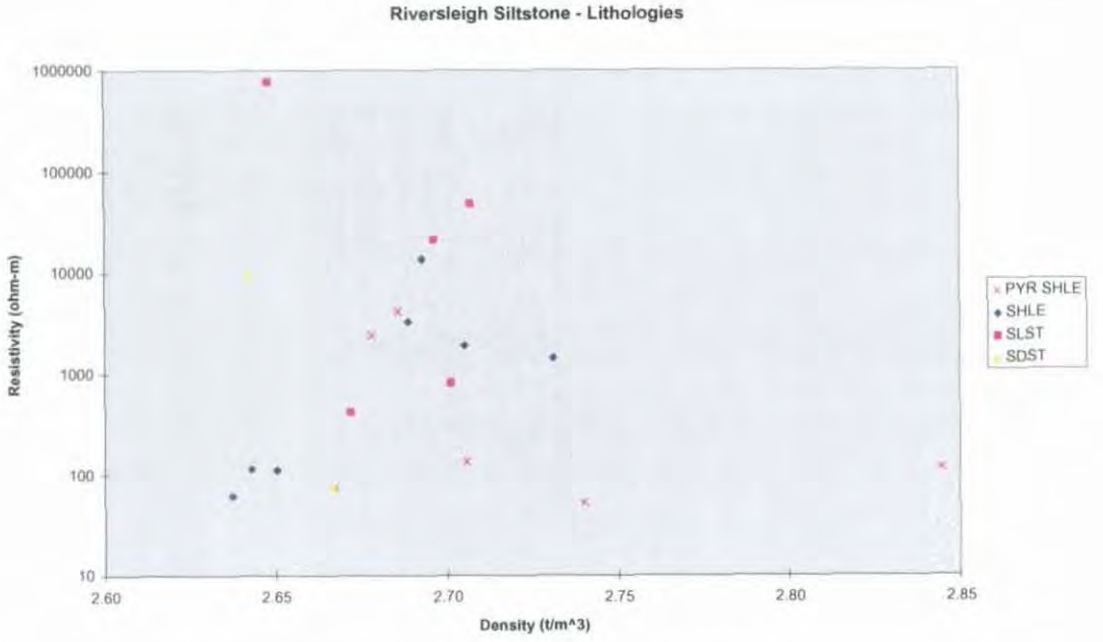

Figure 5.33 Density and resistivity classed by lithology, Riversleigh Siltstone

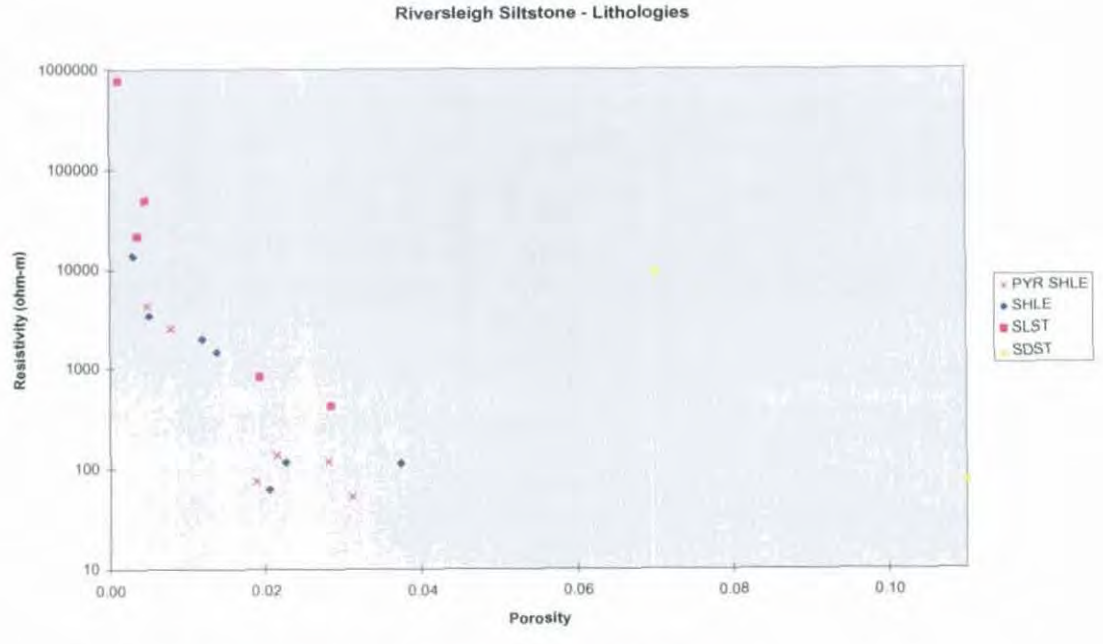

Figure 5.34 Porosity and resistivity classed by lithology, Riversleigh Siltstone

Chargeabilities are moderate though variable in the Riversleigh Siltstone (Fig. 5.35). The most polarisable samples (IP% > 8) are generally carbonaceous shales containing visible traces of pyrite. Carbonaceous material is interpreted to be responsible for the negative correlation between density and chargeability observed in much of the Riversleigh Siltstone sample population. Porosity, the other major parameter potentially affecting density, appears to have no correlation with IP effect (Fig. 5.36). Pyrite is clearly responsible for departures from the 'normal' density/IP% trend.

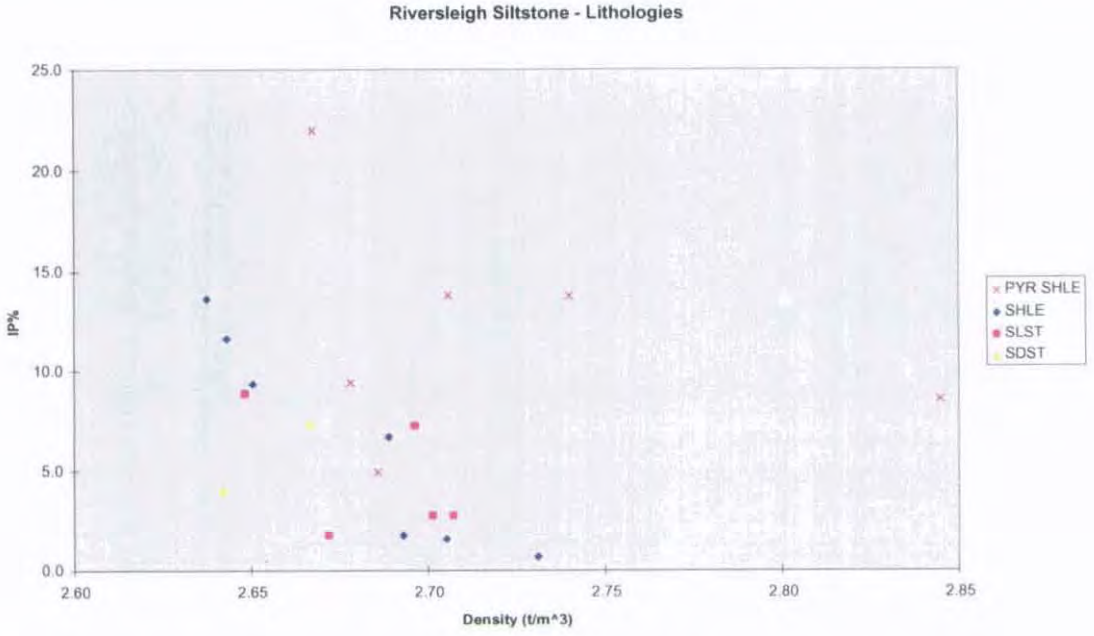

Figure 5.35 Density and chargeability classed by lithology, Riversleigh Siltstone

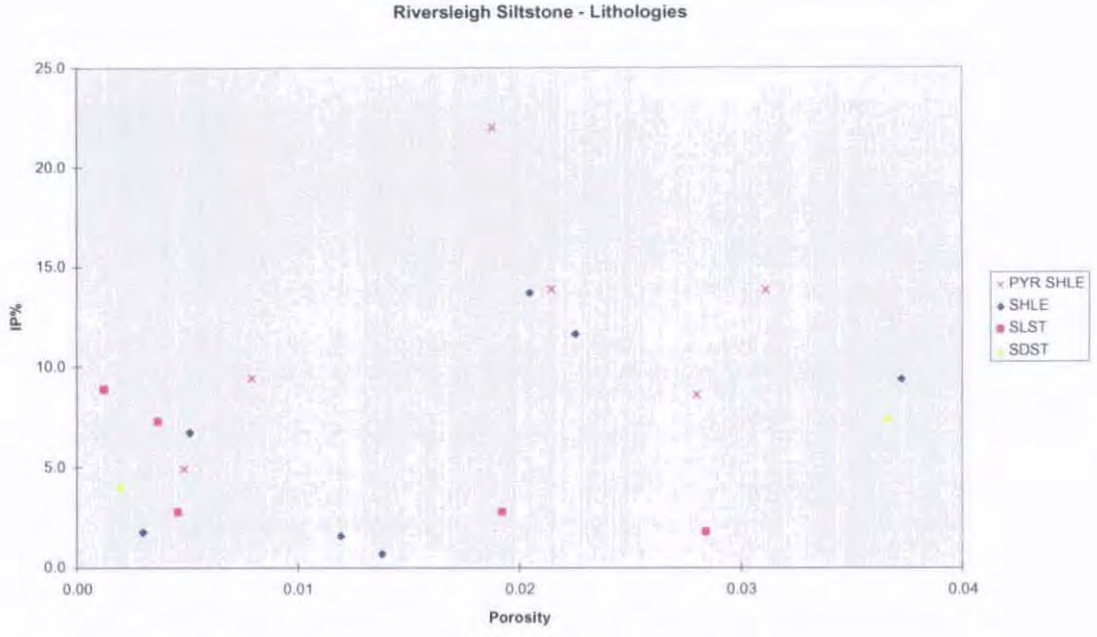

Figure 5.36 Porosity and chargeability classed by lithology, Riversleigh Siltstone

Most Riversleigh Siltstone samples are from the stratigraphic drillhole Amoco 83-1. This subset may be used to gain insight into the nature of intraformational physical property variations in the upper

McNamara Group (Figs. 5.37-42). Inferences are obviously limited by the highly aliased nature of the data, which is only a small fraction of the information obtainable from downhole logging, but unfortunately no such data were available to this project.

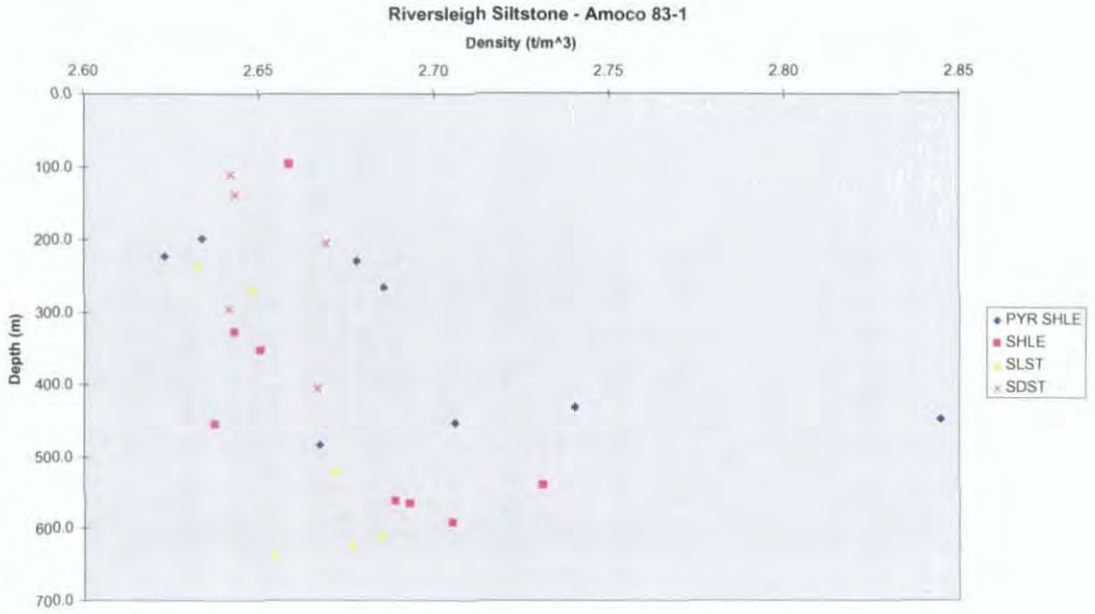

Figure 5.37 Densities measured on samples from Amoco 83-1, classed by lithology

Apart from isolated anomalous densities caused by concentrations of pyrite, there is a distinct trend of increasing density with depth. Two possible causes are indicated; increasing concentration of dolomite (but still low, since no significant amounts were apparent in hand specimen), or decreasing porosity.

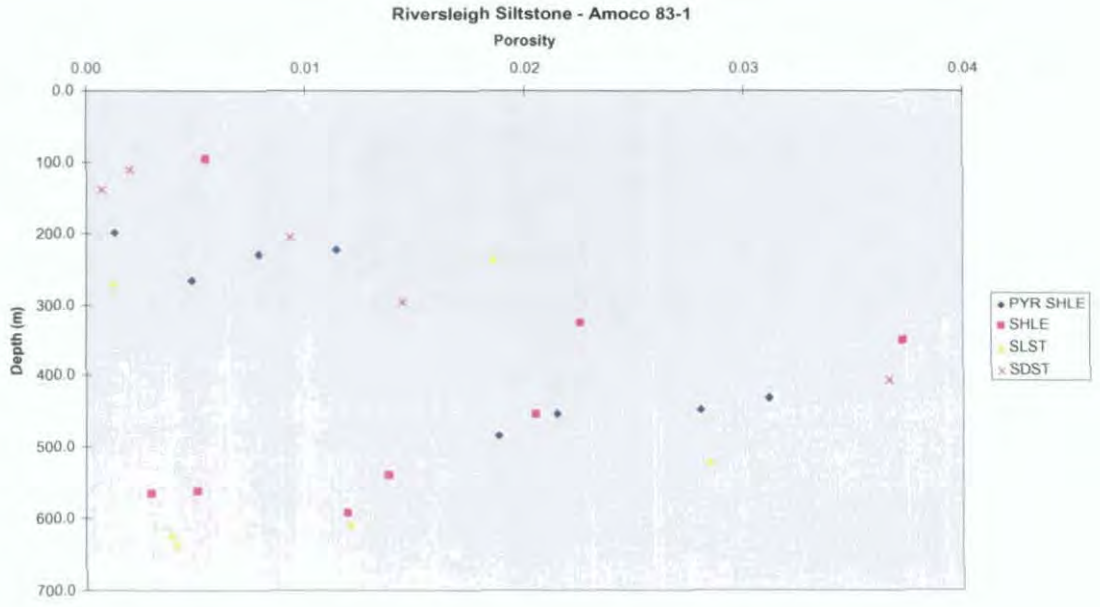

Figure 5.38 Porosities measured on samples from Amoco 83-1, classed by lithology

The 'porosity control' model is only partially supported by the data shown in Fig. 5.38. The expected porosity decrease with depth is only observed below around 400 m depth, while this trend is reversed

above 400 m. This could be interpreted as analogous to an overpressured zone in a modern sedimentary basin, and it is conceivable that an earliest Mesoproterozoic equivalent is represented here. Whatever the controls on porosity, compositional factors, possibly an increased sandy component or a decrease in dolomite content, must be responsible for the decrease in density with depth above 400 m in Amoco 83-1. Fe content as indicated by magnetic susceptibility measurements (maximum 2.6 wt% Fe, following the equation of Puranen, 1989 quoted in Clark, 1997) does not appear to be a significant control on density. Fig. 5.39 illustrates that variations and absolute values of magnetic susceptibility are minimal in Amoco 83-1, and correlation with density is vague at best (correlation coefficient 0.13; cf. Fig. 5.32).

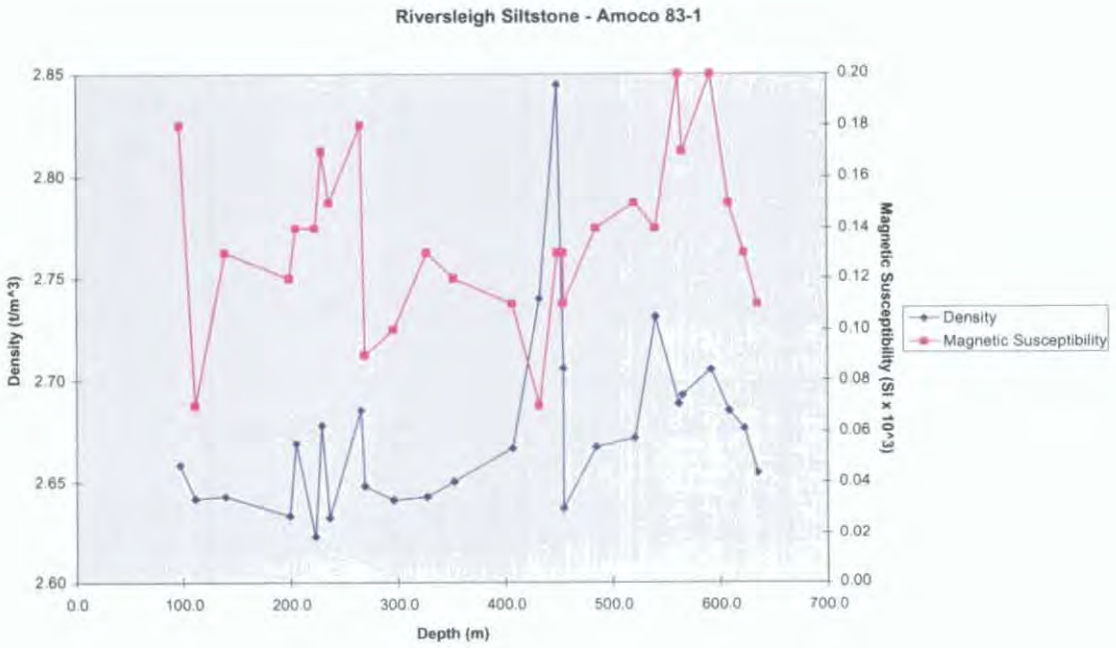

Figure 5.39 Density and magnetic susceptibility, Amoco 83-1. Note low range of magnetic susceptibility scale

With few exceptions, porosity exerts a strong control on resistivity (Fig. 5.40). This is likely to be accentuated where pore fluids are more saline than the water used in this laboratory study. The influence of porosity appears to be at least as important an influence on resistivity as rock compositional factors such as the presence of pyrite and/or shale (cf. Fig. 5.34). The presence of a coherent 200m-thick low-resistivity layer in Amoco 83-1 strongly controlled by porosity (pyrite was noted in half of the samples defining this layer) has important implications for interpretation of electrical and electromagnetic survey data in this region.

Most velocities measured on Amoco 83-1 samples are in the band 5500-5800 m/s (Fig. 5.41). There is a strong negative correlation between porosity and velocity (correlation coefficient -0.91) and a weaker positive correlation between density and velocity (0.42), but this is based on relatively few determinations.

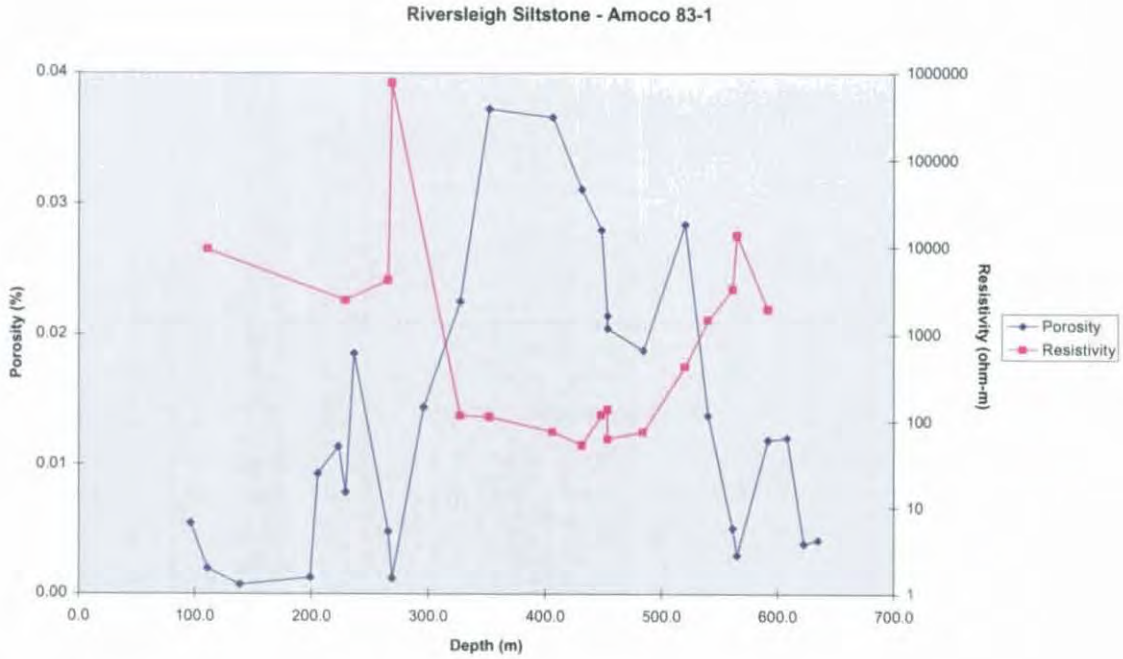

Figure 5.40 Porosity and resistivity, Amoco 83-1

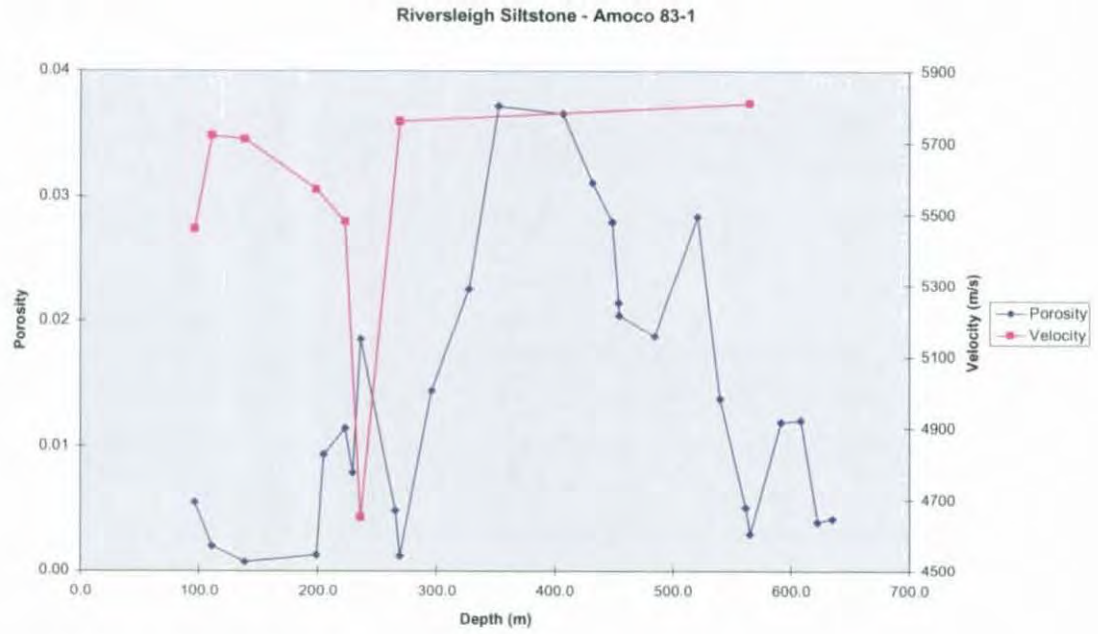

Figure 5.41 Porosity and velocity, Amoco 83-1

Chargeability appears to track pyrite concentration and, to a lesser extent, carbonaceous shales more strongly than the other geophysical properties measured. Pyrite has been noted in some of the coarser-grained samples in Amoco 83-1 above the richest pyrite concentration between 430 m and 480 m depth, while none has been observed below this level (Fig. 5.42).

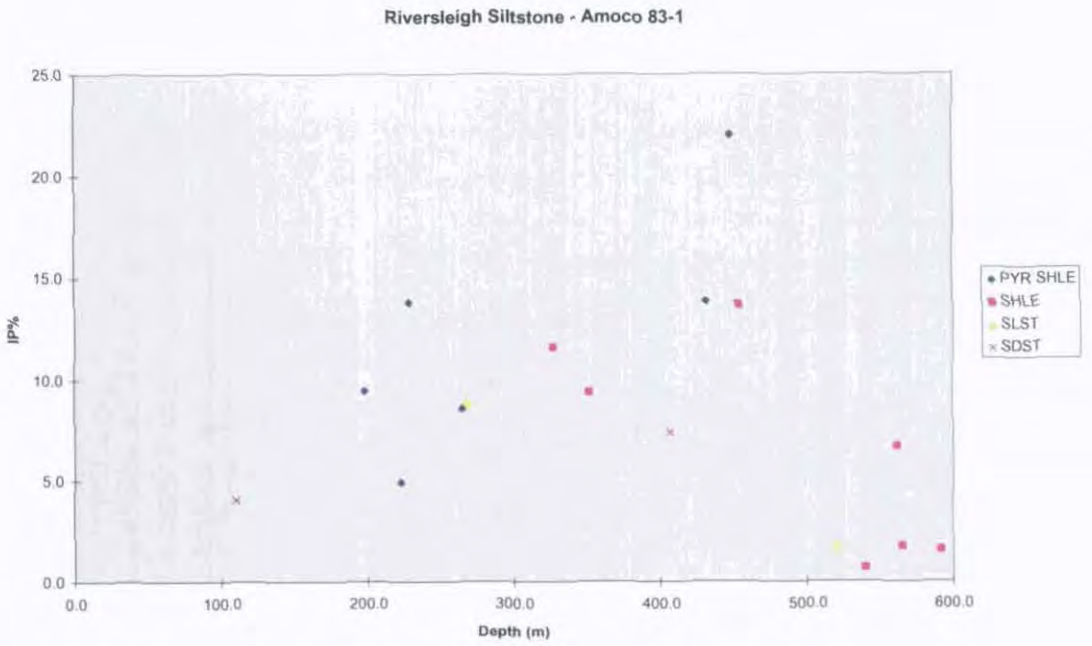

Figure 5.42 Chargeability measurements classed by lithology, Amoco 83-1

5.4.12 South Nicholson Group

South Nicholson Group samples obtained for this study were from two drillholes, Amoco 83-3 north-west of Lady Loretta and Morstone 1, which penetrated South Nicholson Group correlates beneath the Undilla Basin Cambrian sequence. The latter are supplemented by density and resistivity measurements reported by Stewart and Hoyling (1963). All are from the Constance Sandstone except an interval of a little over 100 metres at the top of the Precambrian sequence in Morstone 1 which may possibly be Mullera Formation.

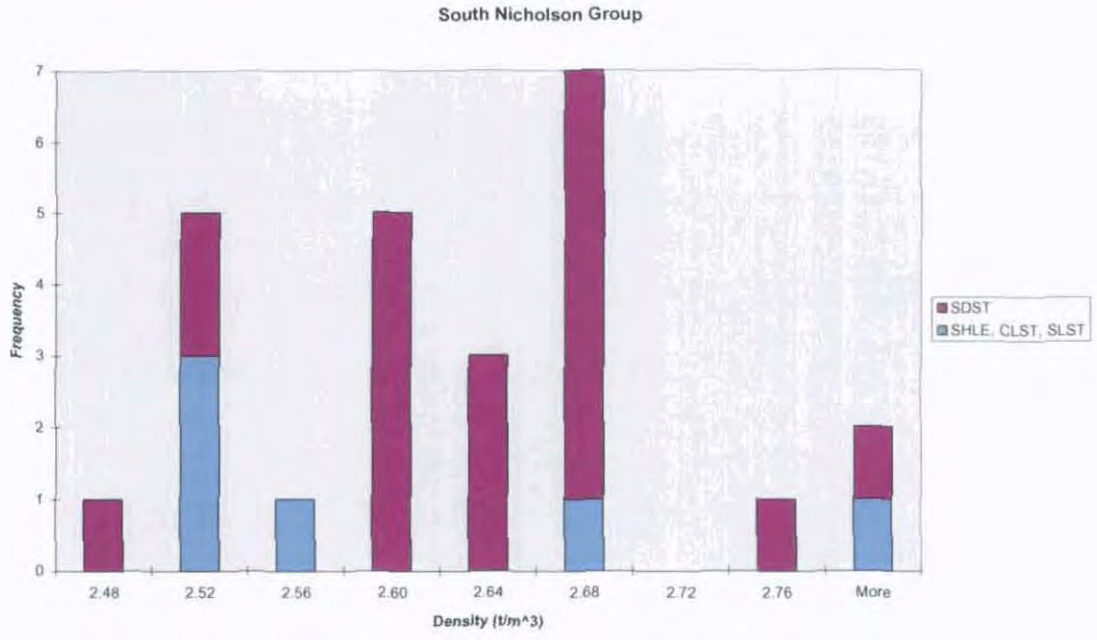

Figure 5.43 Density measurements classed by lithology, South Nicholson Group

Densities of South Nicholson Group drillcore samples are quite variable. Though the distribution is irregular (Fig. 5.43), this may be due to insufficient sampling. The effects of anomalous compositions (highly ferruginous claystone) and porosity variability are particularly acute in this dataset, being responsible for both the low- and high-density outliers. Either the mean (2.61 ±0.04 t/m^3) or median (2.60 t/m^3) values are considered reasonable estimates of the bulk properties of this unit.

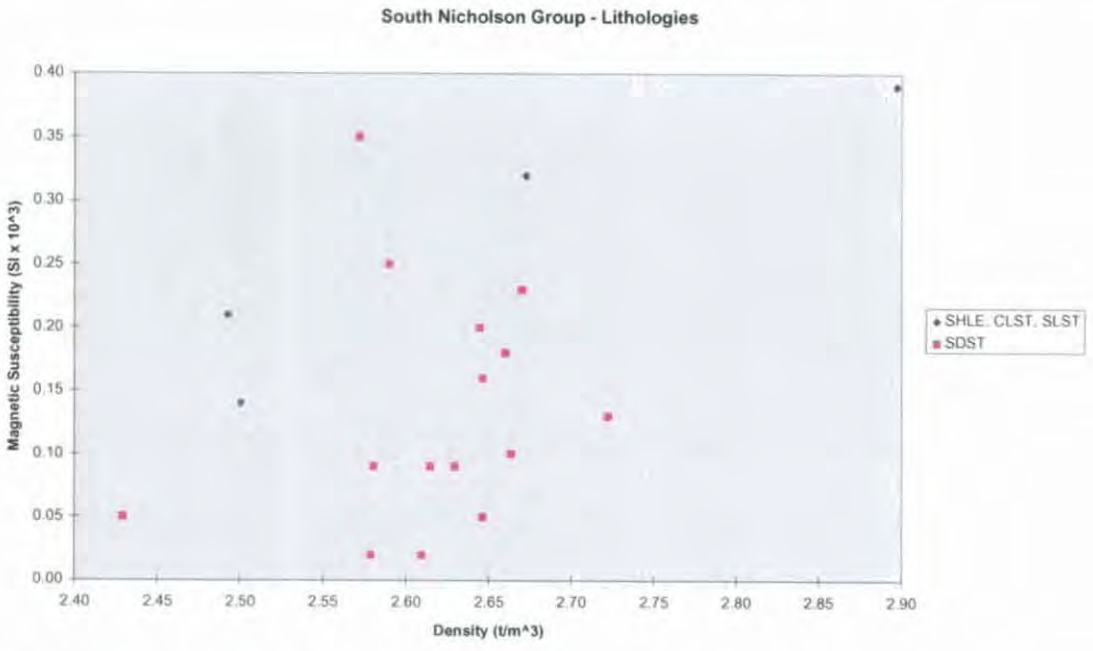

Figure 5.44 Density and magnetic susceptibility classed by lithology, South Nicholson Group

Magnetic susceptibilities are low (mean 0.16±0.05; median 0.15 SI x 10^3), even in samples sufficiently ferruginous as to strongly affect their density (samples with density > 2.7 in Fig. 5.44). It is hence inferred that the ferruginous material is composed of paramagnetic minerals (probably haematite and siderite; see also Carter et al., 1961), and that ferromagnetic minerals are not present in more than trace amounts. Porosities are substantially higher than in McNamara Group and older units, but in spite of the strong negative correlation between velocity and porosity, velocities are still reasonably high; generally over 5000 m/s (Fig. 5.45).

Porosity again appears to exert the most significant control on resistivity (Fig. 5.46), with a distinct negative correlation (R = -0.5) and generally moderate resistivity values; similar in range to those measured in the McNamara Group with the exception that extremely high values were not observed. Resistivity is positively correlated with velocity (Fig. 5.47); high values of both being associated with silicified sandstones. Chargeabilities are very low and are weakly correlated with density in Amoco 83-3 (Fig. 5.48).

Gamma ray measurements of South Nicholson Group, with the exception of slightly lower K/Th ratios, do not appear greatly different from the carbonate-dominated McNamara Group samples.

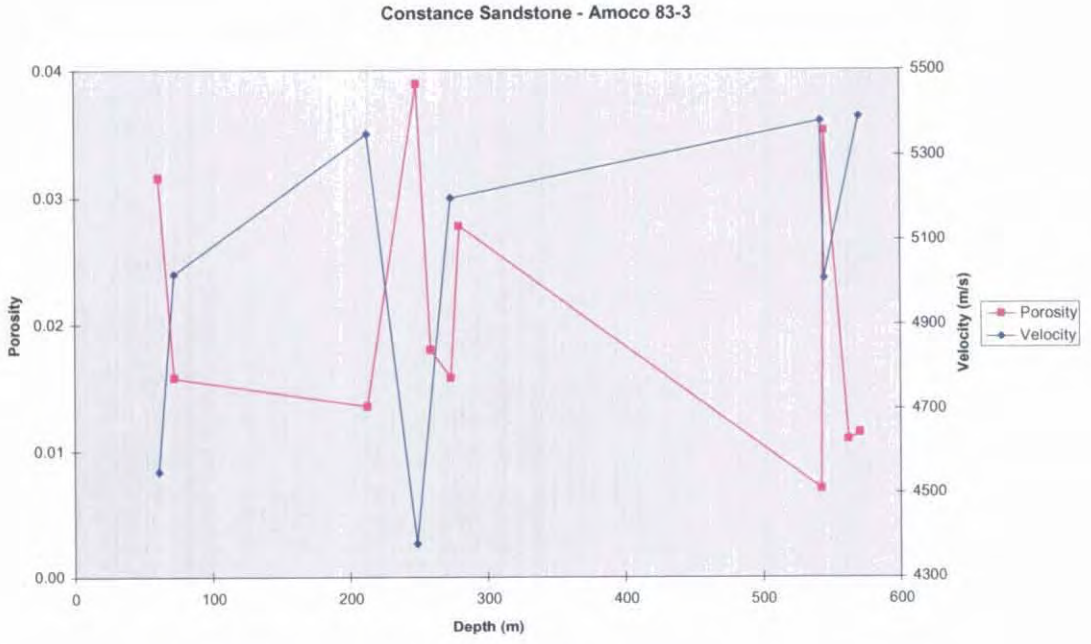

Figure 5.45 Porosity and velocity, Amoco 83-3 (Constance Sandstone)

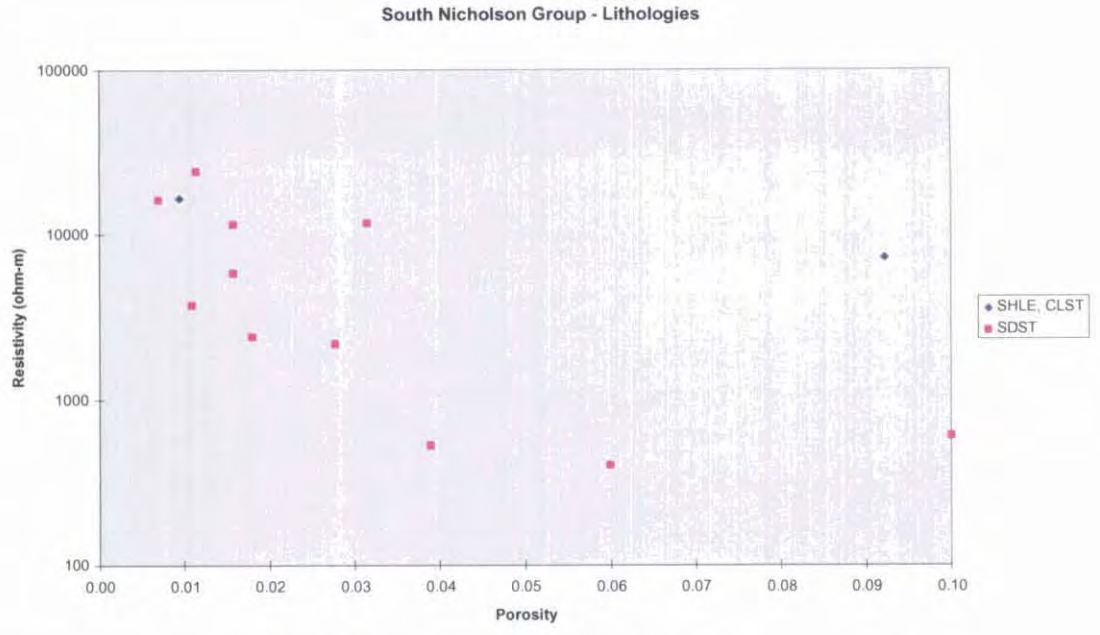

Figure 5.46 Porosity and resistivity classed by lithology, South Nicholson Group

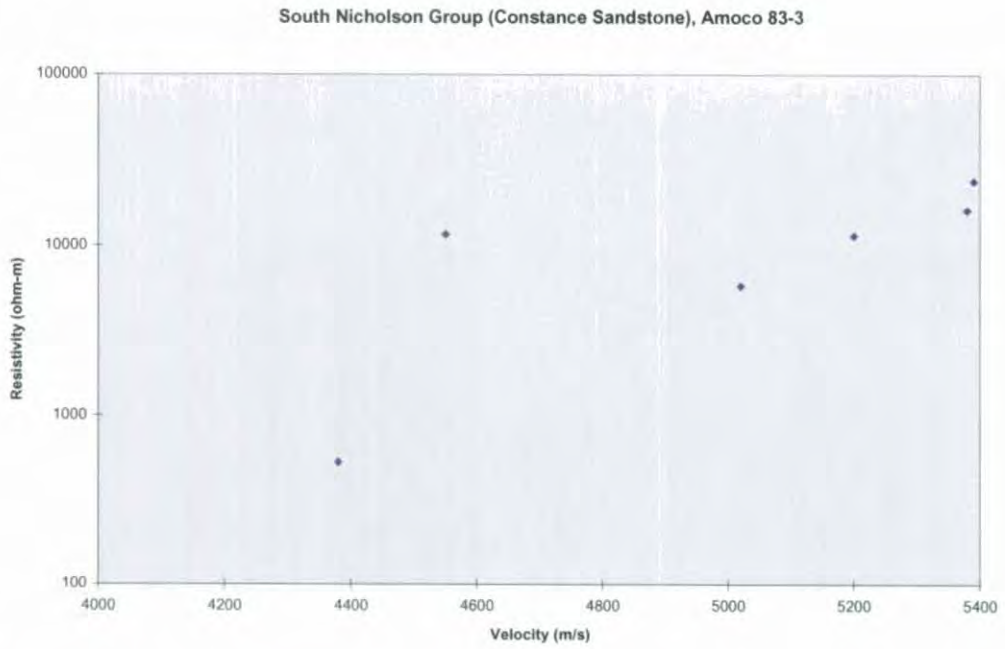

Figure 5.47 Velocity and resistivity, South Nicholson Group sandstones

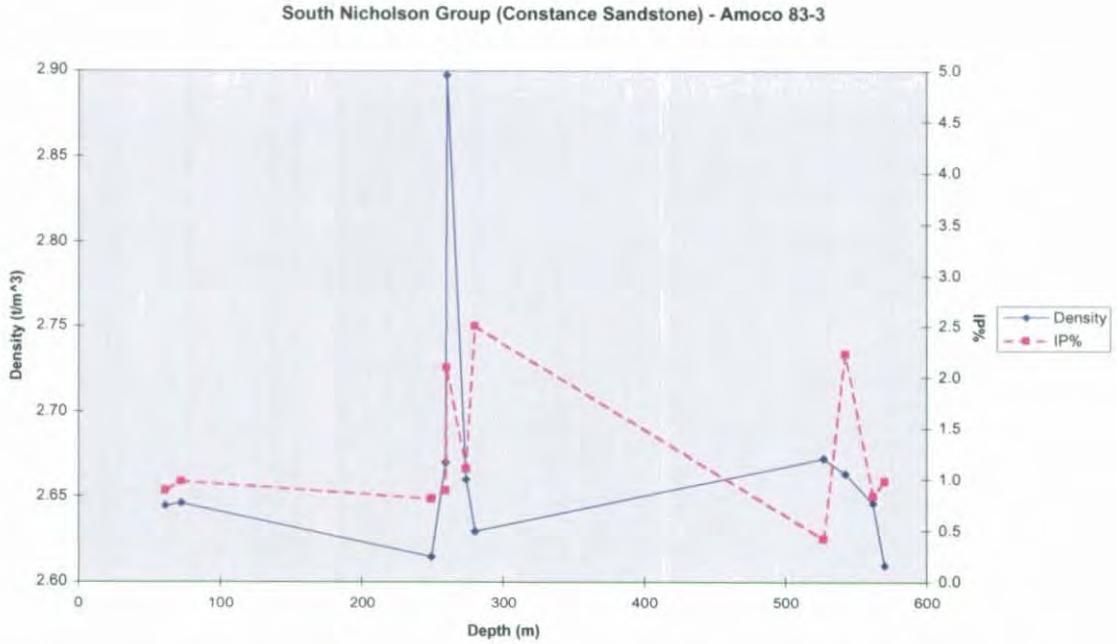

Figure 5.48 Density and chargeability, Amoco 83-3 (Constance Sandstone). Note very low IP% levels

5.4.13 Cambrian sediments

Aside from a few values determined in other studies (Harrison, 1980; Neumann, 1964; Gibb, 1967) all Cambrian petrophysical data presented are from samples of Thorntonia Limestone, Currant Bush Limestone and V Creek Limestone intersected in Morstone 1. These include density and resistivity determinations recorded in the Morstone 1 well completion report (Stewart and Hoyling, 1963) as well as measurements by the author. The prevalence of carbonate over siliciclastics in the Cambrian section of this drillhole is typical of the Undilla Basin. It is responsible for properties that are fairly similar to those

of the McNamara Group in spite of the great difference in age and metamorphic grade, with mean density 2.65±0.11 t/m^3 and very low magnetic susceptibility. Variability can be attributed to generally higher porosity, ranging up to 0.08 with a mean of 0.04, though massive crystalline limestones of very low porosity are not uncommon in outcrop. High porosity is probably responsible for the low resistivities observed (ranging from 5 to 2000 Ωm, with a geometric mean of 130 Ωm).

Vuggy and cavernous porosity noted in the Cambrian Georgina Basin carbonates by Smith (1972) may result in these units having a somewhat lower bulk density than indicated by petrophysical measurements. Equivalents of the Colless Volcanics Cambrian basalts near the northern margin of the Georgina Basin appear to be moderately magnetic, being associated with low-amplitude short-wavelength anomalies (Wells et al., 1966). De Keyser and Cook (1972) noted Georgina Basin phosphorites as having a high specific gravity, presumably relative to other Cambrian sediments.

5.4.14 Mesozoic sediments

Densities of 1.75, 2.20, 2.34, 2.10 and 2.50 t/m^3 have been given by Neumann (1964), Gibb (1967), Tucker et al. (1979), Harrison (1980) and Leaman (1994b), respectively for Mesozoic sandstones in the region. The values of Gibb (1967), Tucker et al. (1979) and Harrison (1980) are considered the most reasonable bulk values, as they are based on both borehole samples and gravity modelling. Mesozoic sediments only occur as a highly weathered thin veneer of sandstone in the Paradise Valley study area, however. These may be characterised by densities towards the lower end of the confidence interval listed in Table 5.12, closer to the 1.75 t/m^3 reported for outcrop samples by Neumann (1964).

5.5 Geochemistry and petrophysics

5.5.1 Pre-Haslingden Group basement

Table 5.10 indicates very strong geochemical controls on the density of pre-Haslingden Group felsic rocks. As expected, there is negative correlation between density and SiO_2; a relationship, which holds across all felsic lithologies (Figs. 5.49, 5.50), and positive correlation between density and elements associated with mafic minerals (MgO, Al_2O_3, Fe_2O_3, TiO_2, CaO; Fig. 5.51). There is also a strong negative correlation between density and K_2O, presumably due to the low density character of felsic minerals. The strength of these correlations was somewhat surprising, given that elemental and not mineralogical parameters were compared with density. The positive correlations of density with MnO, P_2O_5 and H_2O^+ are presumably due mainly to an association with mafic minerals.

	Porosity	SG sat	Susc	NRM	Q
SIO2	0.003	-0.892	-0.055	0.010	0.032
TIO2	-0.111	0.913	0.042	-0.009	-0.050
AL2O3	0.075	0.734	0.110	0.032	0.031
FE2O3TOT	-0.074	0.922	0.051	-0.055	-0.088
FE2O3	-0.343	0.764	0.152	0.020	0.007
FEO	0.115	0.892	-0.022	-0.096	-0.138
MNO	0.101	0.830	0.131	-0.310	-0.355
MGO	-0.011	0.916	-0.059	-0.064	-0.104
CAO	0.079	0.842	-0.021	-0.031	-0.029
NA2O	-0.401	-0.146	0.291	-0.007	-0.049
K2O	0.018	-0.819	0.080	0.204	0.211
P2O5	-0.157	0.757	0.009	-0.052	-0.107
H2OPLUS	0.158	0.782	-0.115	0.061	0.039
H2OMIN	-0.330	0.361	0.186	-0.165	-0.208
CO2	-0.014	0.301	-0.048	-0.065	-0.015
TOTAL	0.042	0.006	0.252	0.161	0.061

Table 5.10 Pre-Haslingden Group physical and chemical property correlation coefficients. Fe $_2O_3$TOT calculated from Fe_2O_3 and FeO. Petrophysical data including natural remanent magnetism (NRM) and Koenigsberger ratio (Q) from Hone et al. (1987); geochemical data from AGSO's ROCKCHEM database

The strong negative correlation between density and felsic minerals, and positive correlation between density and mafic minerals, demonstrates at least in principle that felsic lithologies may be mapped with reasonable confidence and precision using gravity controlled by petrophysical observations.

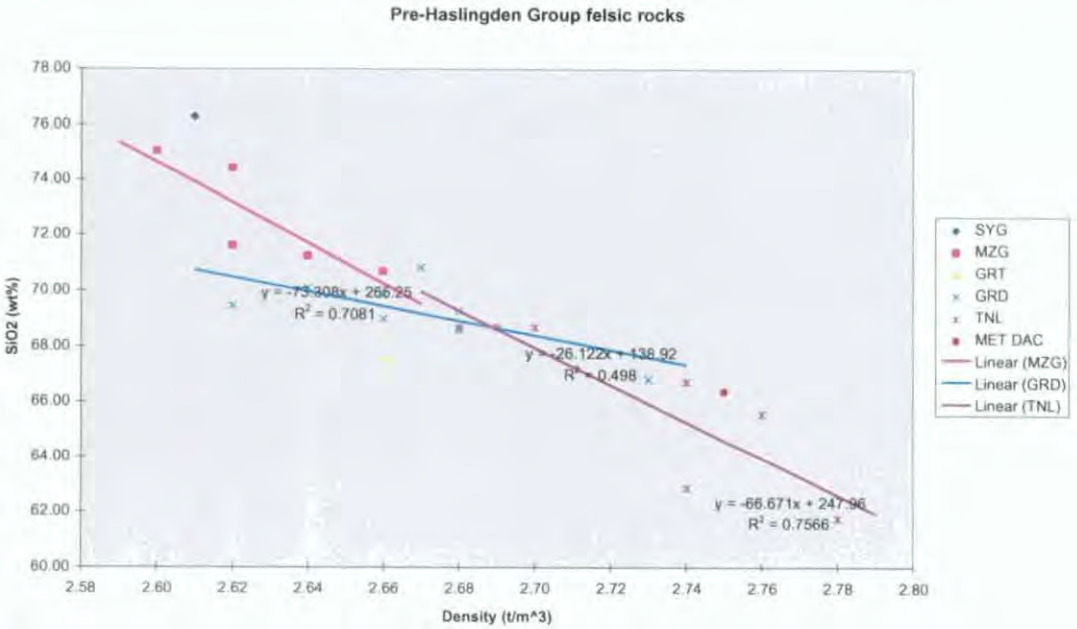

Figure 5.49 Relationship between SiO_2 content and density for pre-Haslingden Group felsic rocks, with linear regression calculated for common rock types

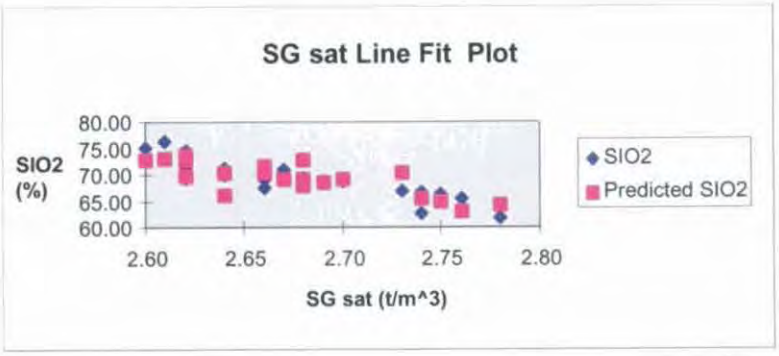

Figure 5.50 Comparison of actual vs predicted SiO_2 values derived from least squares regression for pre-Haslingden felsic rock samples

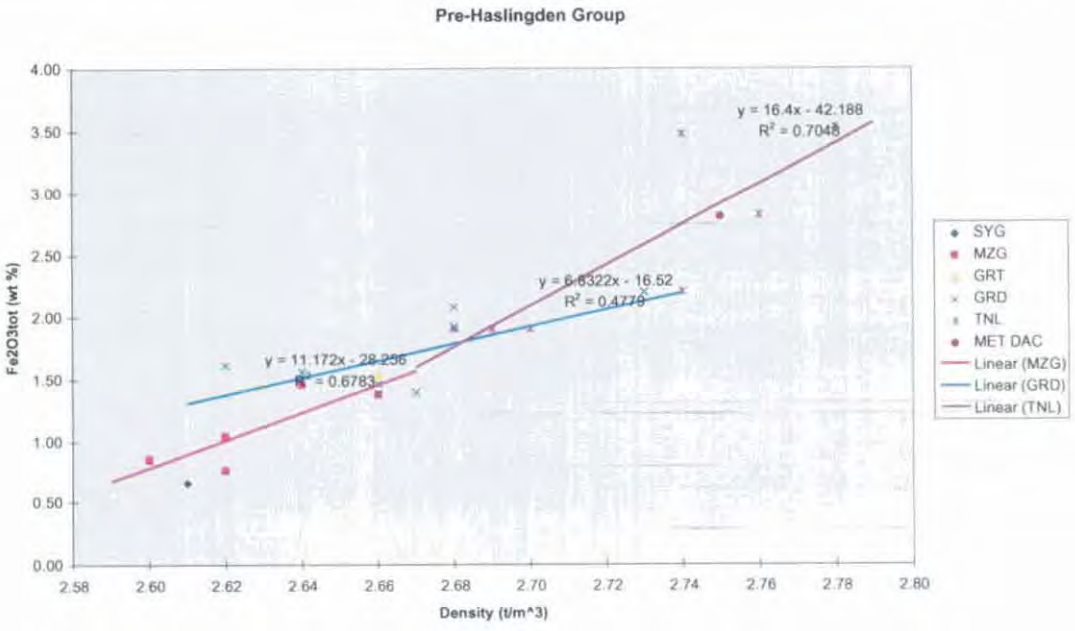

Figure 5.51 Relationship between density and Fe content for pre-Haslingden Group felsic rocks (mainly Kalkadoon Granodiorite)

There is very little correlation between magnetic properties and any element concentration. This is a surprising result in the case of Fe, since it was thought that at least the low range of magnetic susceptibilities might be linearly related to paramagnetic effects of haematite and ilmenite concentrations (Puranen, 1989 quoted in Clark, 1997). Nor is there any clear correlation between magnetic properties and Fe oxidation state. Presumably, any such relationships are obscured by the disproportionate effects of small concentrations of magnetite on magnetic susceptibility.

Trace element concentrations obviously have no direct discernible effect on bulk physical properties (gamma ray signatures excepted). It is however interesting to compare the concentration of base metals in these potential mineralisation source rocks with their physical properties.

There is moderate correlation between density and Zn abundance, but little or no correlation between density and Pb, and density and Cu (Fig. 5.52). Presumably, this denotes an association between Zn and more mafic minerals, in what is predominantly a felsic suite. Pb displays no such preference, while Cu is generally low.

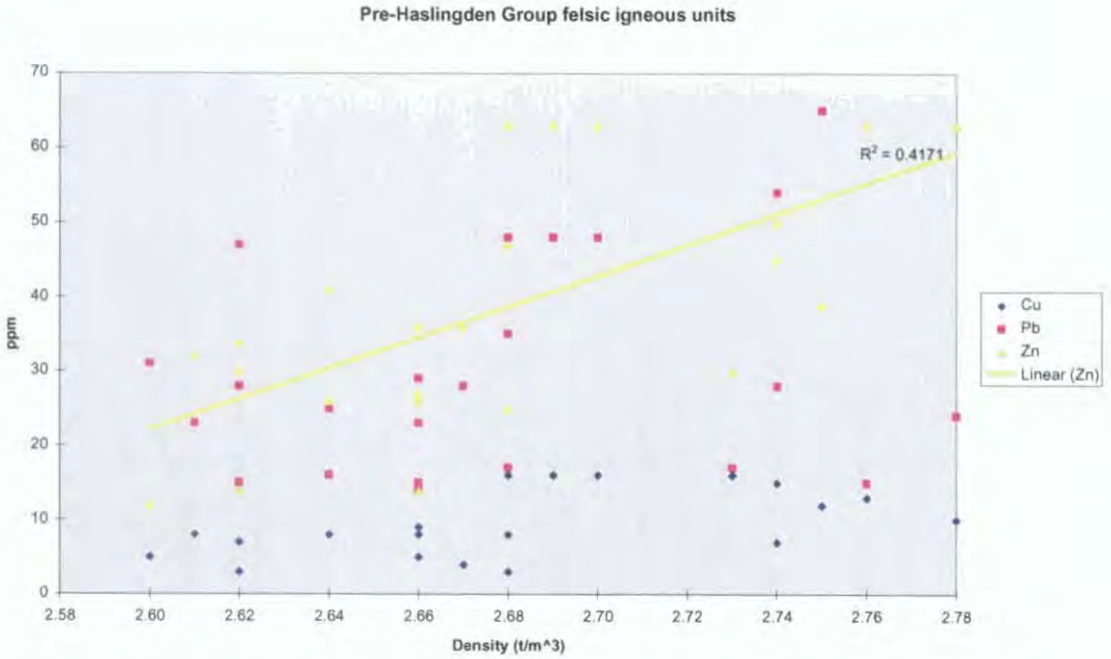

Figure 5.52 Pre-Haslingden Group density and base metal concentration

5.5.2 Eastern Creek Volcanics

	Porosity	SG sat	Susc	NRM	Q
SIO2	-0.724	0.081	-0.474	0.860	0.893
TIO2	0.099	-0.073	0.833	-0.582	-0.656
M+A+F	0.910	-0.469	0.089	-0.298	-0.362
AL2O3	0.215	0.141	-0.893	0.276	0.353
FE2O3TOT	0.074	-0.275	0.933	-0.413	-0.515
Fe2+/Fe3+	-0.422	0.597	-0.823	0.342	0.476
FE2O3	0.193	-0.455	0.922	-0.391	-0.511
FEO	-0.292	0.342	0.621	-0.325	-0.338
MNO	-0.026	-0.495	0.691	-0.271	-0.312
MGO	0.585	-0.142	-0.628	0.130	0.164
CAO	-0.041	0.783	-0.849	0.045	0.148
NA2O	-0.125	-0.574	0.306	0.088	0.091
K2O	-0.824	0.658	-0.430	0.255	0.351
P2O5	0.121	-0.033	0.775	-0.649	-0.720
H2OPLUS	0.839	-0.609	0.249	-0.357	-0.443
H2OMIN	0.055	-0.016	0.685	0.033	-0.009
CO2	0.361	-0.794	0.792	-0.255	-0.352
TOTAL	-0.089	-0.817	0.503	0.625	0.509

Table 5.11 Eastern Creek Volcanics physical and chemical properties correlation coefficients. Fe $_2O_3$TOT calculated from Fe_2O_3 and FeO. Petrophysical data from Hone et al. (1987); geochemical data from AGSO's ROCKCHEM database. M+A+F is the sum of MgO, Al $_2O_3$ and Fe_2O_3TOT

Relationships between petrophysical and geochemical parameters in the ECV metabasalts are less clear than in the pre-Haslingden Group felsics, and understanding is hampered by the fact that there are only six samples with both geochemical and physical property analyses. There are few significant correlations between density and elemental concentrations (density and CaO being among the exceptions; Table 5.11). The lack of correlation between density and SiO_2 is a particularly notable contrast to the pre-Haslingden

Group felsics. A strong positive correlation between SiO_2 and NRM is equally interesting, and may be caused by any number of geological processes affecting grain size and magnetic mineral microstructure (Clark, 1997).

In contrast to the felsic igneous units, there is strong positive correlation between magnetic susceptibility and Fe concentration (Fig. 5.53). Other mafic elements (MgO, CaO) are negatively correlated with magnetic susceptibility. According to the relation of Puranen (1989) quoted in Clark (1997), the susceptibilities observed correspond to a magnetite content of ~0.2-3%. In combination with Fig. 5.53, the implied concentration of non-magnetic Fe minerals ranges between six and nine per cent, with up to 50% of the $Fe_2O_{3\,tot}$ content in excess of 6% contained in magnetite. Increased oxidation state is also associated with increased magnetic susceptibility (Table 5.11). Magnetic properties of the ECV are thus controlled by both the concentration and mineralogy of Fe.

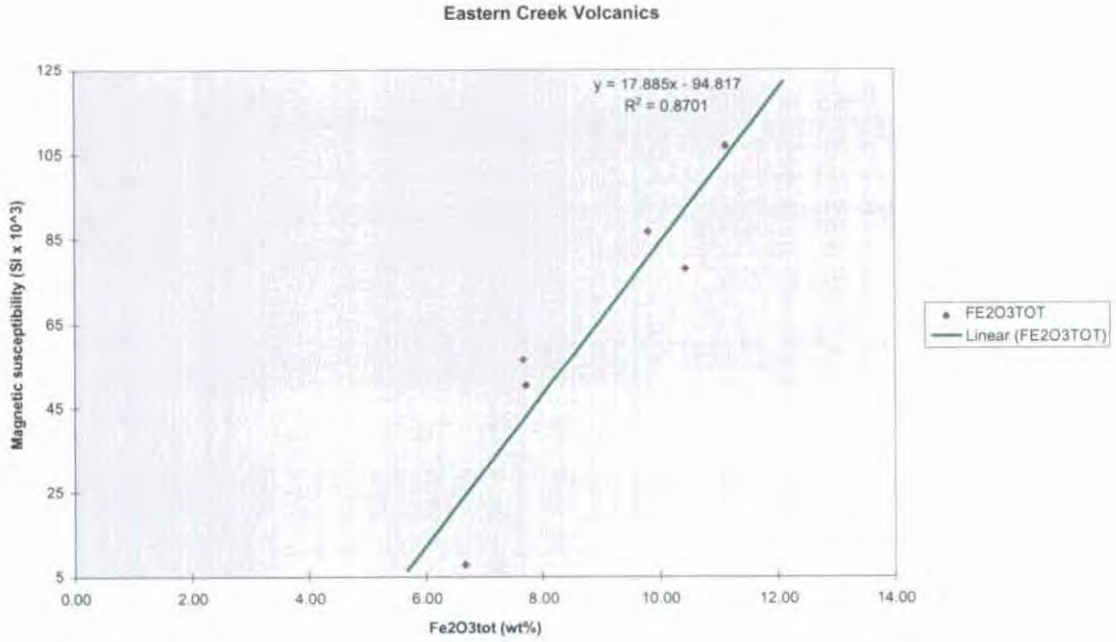

Figure 5.53 Eastern Creek Volcanics Fe content and magnetic susceptibility

5.5.3 McNamara Group

Many of the unmineralised McNamara Group samples analysed in this study were previously used in a geochemical study by McGoldrick (1994b), from which the data used in this section was taken.

SiO_2 concentration exerts an extremely strong control on the density of unmineralised McNamara Group rocks (Table 5.11, Fig. 5.54). The relationship is very nearly linear, with just a slight suggestion of a levelling off above 2.80 t/m^3 in samples where SiO_2 is a relatively minor component.

	SiO_2	TiO_2	Al_2O_3	Fe_2O_3	MnO	Fe +Mn	MgO	sedex Al	Al3	CaO	Mg +Ca	Na_2O	K_2O	P_2O_5	Loss	S
SG dry	-0.96	-0.67	-0.84	-0.59	0.10	-0.59	0.97	-0.93	-0.78	0.96	0.97	-0.73	-0.56	-0.51	0.94	-0.51
Porosity	0.52	0.68	0.71	0.82	-0.14	0.82	-0.59	0.64	0.74	-0.64	-0.62	0.20	0.44	0.68	-0.56	0.70
SG sat	-0.96	-0.64	-0.82	-0.54	0.09	-0.53	0.97	-0.92	-0.75	0.95	0.96	-0.76	-0.54	-0.46	0.95	-0.46
Susc.	0.53	0.54	0.63	0.68	0.15	0.69	-0.54	0.54	0.71	-0.57	-0.56	0.20	0.39	0.27	-0.57	0.03
Velocity	-0.62	-0.88	-0.89	-0.75	0.19	-0.73	0.66	-0.42	-0.57	0.73	0.70	0.06	-0.88	-0.78	0.72	-0.51
Resistivity	-0.63	-0.61	-0.63	-0.39	0.07	-0.38	0.63	-0.47	-0.45	0.64	0.64	-0.27	-0.59	-0.44	0.65	-0.16
log r	-0.80	-0.72	-0.85	-0.75	-0.04	-0.75	0.85	-0.86	-0.83	0.86	0.86	-0.46	-0.51	-0.57	0.81	-0.49
IP%	0.34	0.01	0.26	0.26	0.38	0.27	-0.38	0.51	0.43	-0.34	-0.36	0.53	-0.15	0.10	-0.29	0.29

Table 5.11 Correlation coefficients, McNamara Group geochemical and petrophysical data

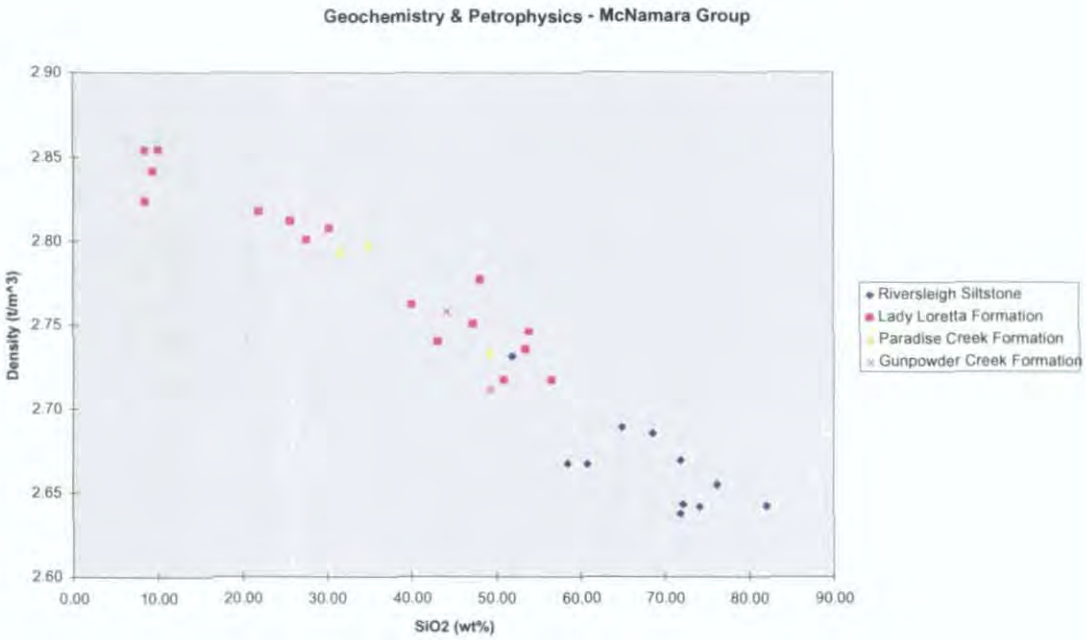

Figure 5.54 Relationship between SiO_2 concentration and density, McNamara Group

MgO and CaO are very strongly correlated with a near-constant ratio, consistent with these elements mainly being present in the form of dolomite (McGoldrick, 1994b). Their combined concentration is presented in Figure 5.55 as an indicator of dolostone content. The distribution observed is virtually a mirror image of that seen in Fig. 5.54, right down to the slight flattening at high density values. This is interpreted as indicating that densities in unmineralised McNamara Group are for most practical purposes entirely controlled by the proportions of siliciclastic sediment and carbonate.

It is noteworthy that porosity is more strongly correlated with Fe_2O_3 than with any other geochemical constituent (Table 5.11, Fig. 5.56). The reasons for this relationship are unclear, given that the samples presented are all from drillcore in apparently good condition. Possibly, a proportion of the Fe is present as sulphides, and this has resulted in greater susceptibility to chemical reactions involving loss of volume. This may have occurred in situ or at some stage after drilling. The positive correlation between porosity and S, while not as strong as that between porosity and Fe_2O_3 (Table 5.11), tends to support this hypothesis.

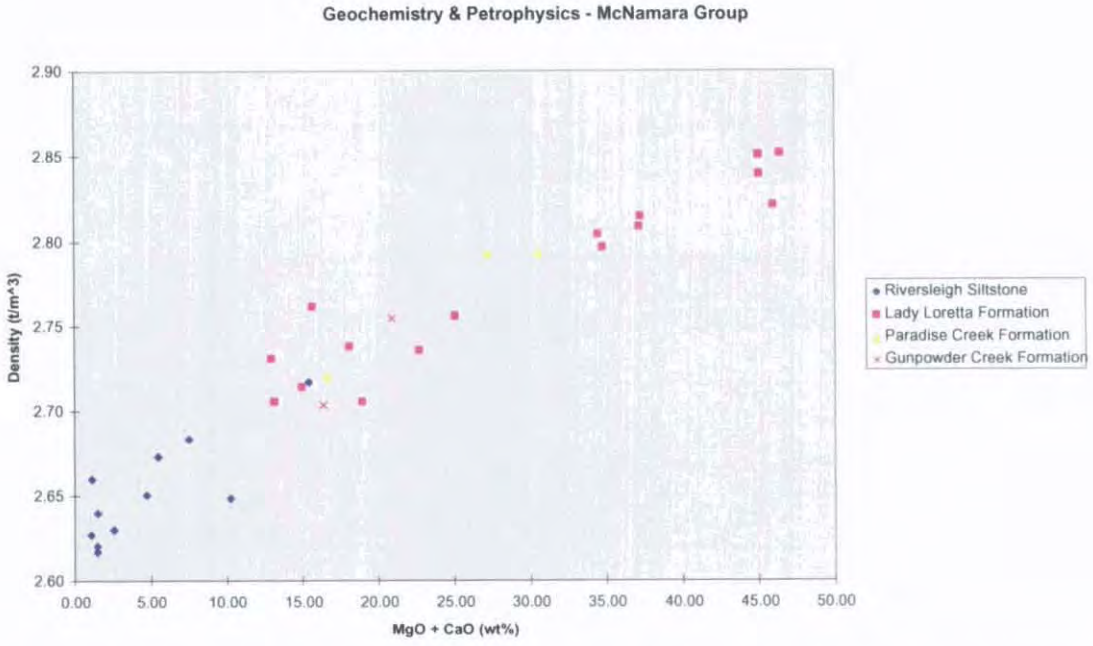

Figure 5.55 Relationship between direct geochemical indications of dolomite content (MgO + CaO) and density, McNamara Group

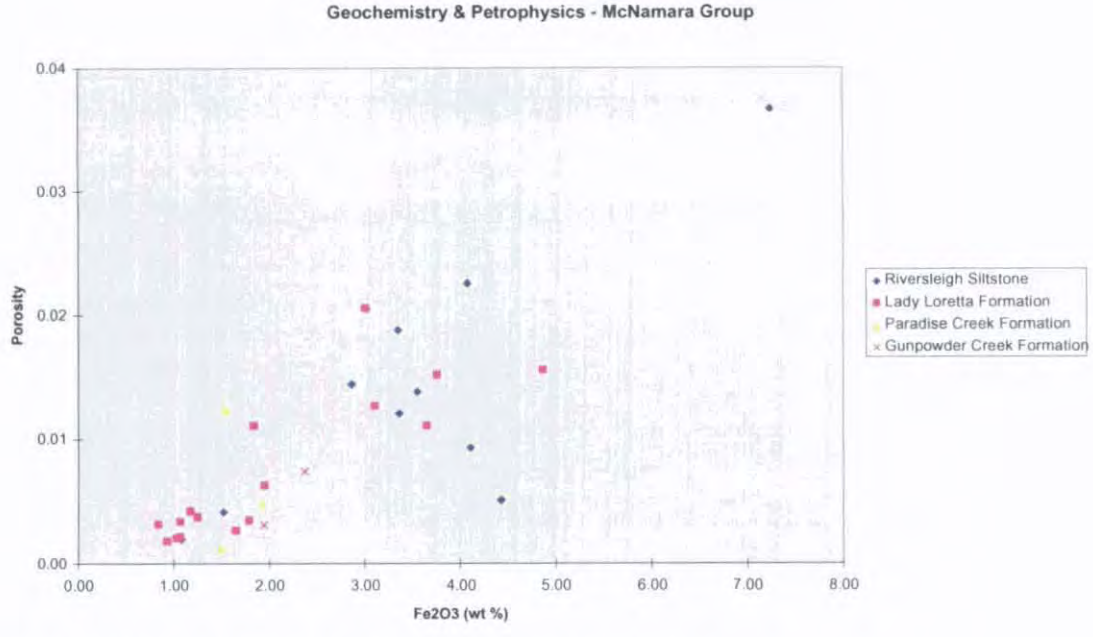

Figure 5.56 Relationship between Fe_2O_3 and porosity, McNamara Group

The positive correlation (R = 0.68) between Fe_2O_3 and magnetic susceptibility (Fig. 5.57) has a more self-evident cause. It is perhaps surprising that the relationship is as strong as it is given the virtual absence of ferromagnetic (as defined by Clark, 1997) minerals in the McNamara Group, and non-standardised sample masses and geometries. This reinforces the potential for magnetic susceptibility to be used as a guide to the concentration of paramagnetic as well as ferromagnetic minerals, even at quite low levels (Puranen, 1989; quoted in Clark, 1997). Some manganese minerals (psilomelane, rhodochrosite) are paramagnetic to a similar degree of susceptibility to more common weakly ferromagnetic or paramagnetic

Fe minerals such as haematite, ilmenite, goethite and siderite (Bleil and Petersen, 1982; quoted in Clark, 1997). In this regard, it is interesting to also compare the sum of Fe_2O_3 and MnO with measured magnetic susceptibility. Though MnO concentrations are over an order of magnitude less than those of Fe_2O_3, the correlation is marginally better (R = 0.69; Table 5.11) than with Fe_2O_3 alone, possibly reflecting a contribution to magnetic susceptibility from Mn minerals.

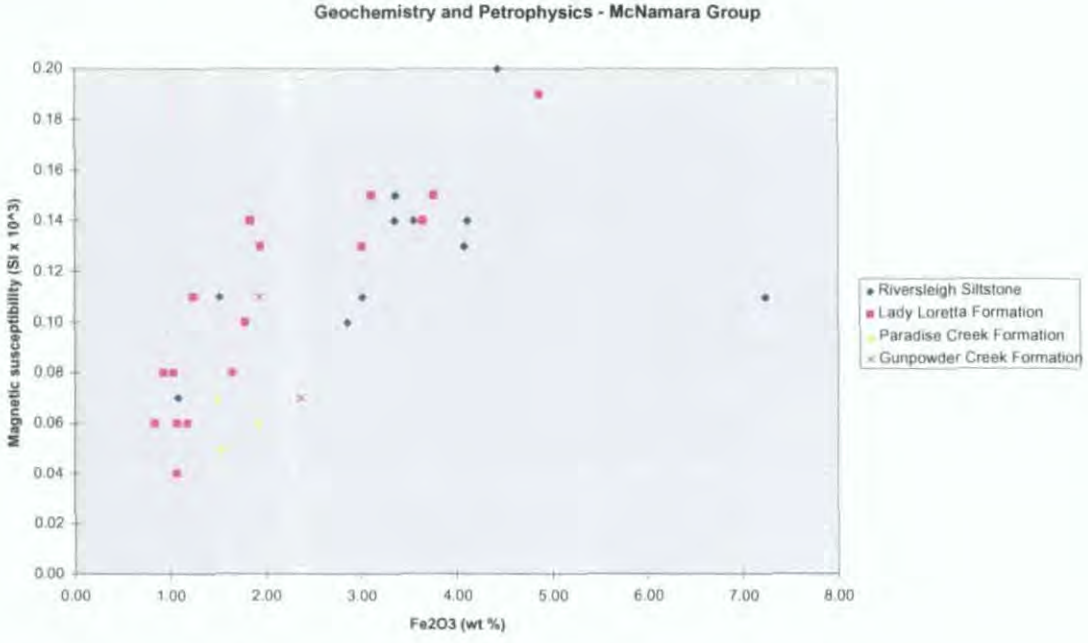

Figure 5.57 Relationship between Fe_2O_3 and magnetic susceptibility, McNamara Group

Magnetic susceptibility is moderately negatively correlated with MgO and CaO, and moderately positively correlated with SiO_2, TiO_2 and Al_2O_3 (Table 5.11). This suggests that the magnetic minerals tend to be associated with siliciclastics rather than dolostones. It is unlikely that pyrrhotite or rarer iron sulphides such as smythite or greigite carry a significant proportion of the observed magnetic susceptibility, since there is no correlation with S (Table 5.11).

Large and McGoldrick (1997) reported the development of a number of geochemical alteration indices designed to operate as indicators of the proximity of stratiform Zn-Pb-Ag ore. Two of these, the SEDEX AI and 'AI_3', have FeO and MnO as their positive (numerator) indicator parameters (SEDEX AI = ((FeO + 10MnO) x 100) / (FeO + 10MnO + MgO)). Since Fe- and Mn-bearing minerals feature prominently in compilations of paramagnetic minerals such as that of Clark (1997), the relationship between these geochemical indices and magnetic susceptibility was investigated. It was hoped that this could lead to the possibility of using magnetic susceptibility meters in the field as a rapid reconnaissance indicator for SEDEX AI and AI_3, consequently reducing the necessity for extensive and expensive geochemical sampling in exploration. It should be noted that the samples used in this portion of the study were originally selected by Large and McGoldrick (1997) from core drilled distal to mineralisation, in order to provide background calibration for their AI_3 and other alteration indices. It thus contains generally low, 'background' AI_3 values.

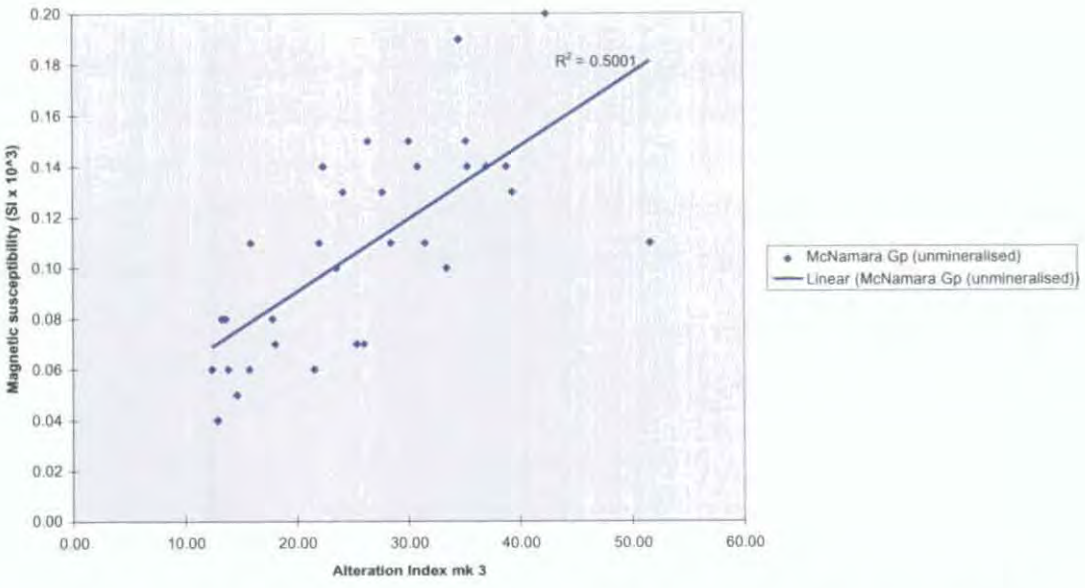

Figure 5.58 Relationship between AI_3 and magnetic susceptibility, McNamara Group. $AI_3 = 100 * (FeO + 10MnO) / (FeO + 10MnO + MgO + Al_2O_3)$

Fig. 5.58 demonstrates that there is a moderate but definite positive correlation (R = 0.71) between AI_3 and magnetic susceptibility (k). The significance of this correlation was tested statistically with a t-test:

Null hypothesis H_0: $\rho = 0$ (no correlation between k and AI_3)

H_1: $\rho \neq 0$

$t = r\sqrt{((n - 2)/(1 - r^2))}$ where r = 0.71

n = 32 (number of samples)

so t = 5.5 with 30 degrees of freedom. At $\alpha = 0.05$, $t_{crit} = 1.70$, so reject null hypothesis (no correlation), i.e. there is a significant correlation between magnetic susceptibility and AI_3 in this unmineralised McNamara Group dataset.

The correlation coefficient between k and AI_3 is slightly greater than between k and Fe_2O_3 alone (Table 5.11), suggesting a possible contribution from Mn as well as Fe to magnetic susceptibility. In order to evaluate the nature of Mn contribution to k (if any), the difference in correlation coefficients was tested, and found not to be statistically significant (F-Test Two-Sample for Variances, $\alpha = 0.05$).

If the high-AI_3 outlier is removed, the correlation between k and AI_3 ($k\backslash AI_3$), and between k and Fe_2O_3 ($k\backslash Fe_2O_3$), improves further (to R values of 0.79 and 0.84 respectively), with the correlation now slightly better for $k\backslash Fe_2O_3$ than for $k\backslash AI_3$. Again, though, an F-Test Two-Sample for Variances test gave the result that the difference is not significant at the 95% confidence level. The question of whether magnetic susceptibility is simply related to Fe concentration, or is also capable of resolving effects from additional elements related to prospective alteration such as Mn, remains open.

These preliminary results are sufficiently encouraging to suggest that follow-up studies using more precise magnetic susceptibility measuring equipment may be warranted. Much of the scatter from the trendline shown in Fig. 5.58 may be due to non-standardised sample size and geometry for magnetic susceptibility measurements, though some variability is undoubtedly inherent. Instruments specifically configured for measurement of drillcore magnetic susceptibility are now available which enable standardised, rapid, high frequency sampling of drillcore. Further work utilising such devices may result in clarification of the magnetic susceptibility /AI_3 relationship to a level where MS measurements may be used as a direct, real-time indication of the prospectivity of strata in the field.

Results from testing the hypothesised correlation between magnetic susceptibility and AI_3 in a mineralised environment are presented in the following chapter.

As expected, velocity is positively correlated with dolostones (represented by MgO and CaO), and is negatively correlated with SiO_2, Al_2O_3 and K_2O, presumably associated with siliciclastic sediments (Table 5.11). Of the latter, however, the strongest control on measured velocities is by concentration of elements comprising clay minerals and other fine fractions (Al_2O_3 and K_2O; Table 5.11, Fig. 5.59). It would thus seem that the presence of clays and silts (possibly also associated with carbonaceous material) exerts a stronger negative influence on sonic velocity than do coarser, more quartz-rich sediments.

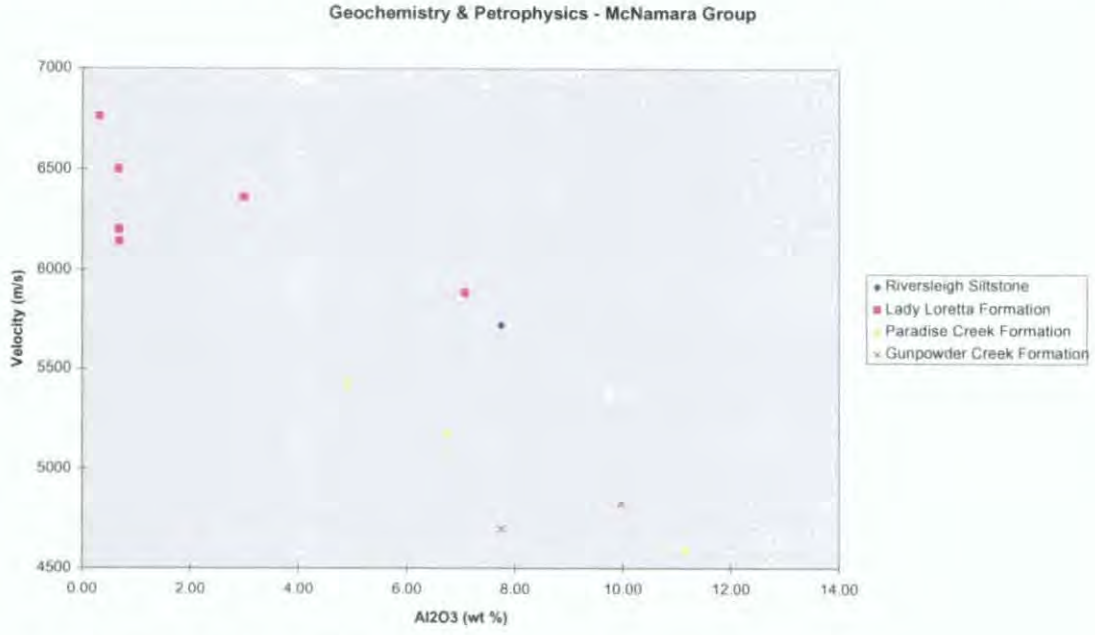

Figure 5.59 Relationship between Al_2O_3 and sonic velocity, McNamara Group

Compositional controls on resistivity as indicated by geochemistry are similar to those on density and velocity. Maintaining the assumption of MgO + CaO as a proxy indicator, dolomite concentration is demonstrated to be positively correlated with resistivity (Fig. 5.60). Notable excursions from the general trend, for example in the Riversleigh Siltstone, are primarily caused by the presence of sandstone (above the trend) and pyritic black shale (below). Siliciclastics generally tend to decrease resistivity, as there is a negative correlation between SiO_2 and resistivity (Table 5.11).

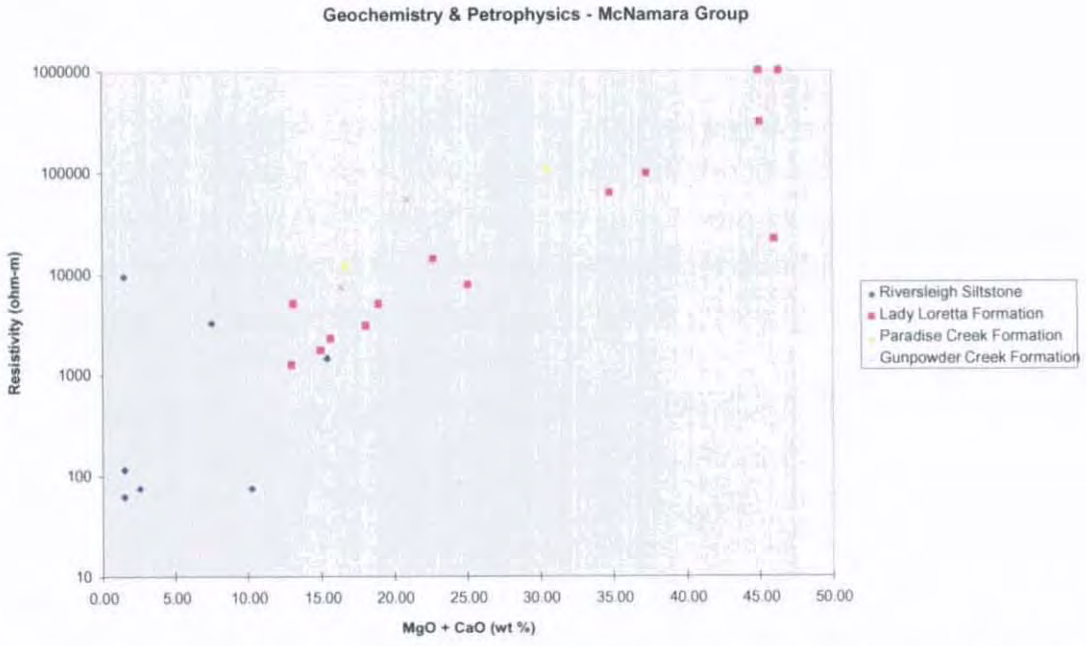

Figure 5.60 Relationship between dolomite concentration (indicated by MgO + CaO) and resistivity, McNamara Group

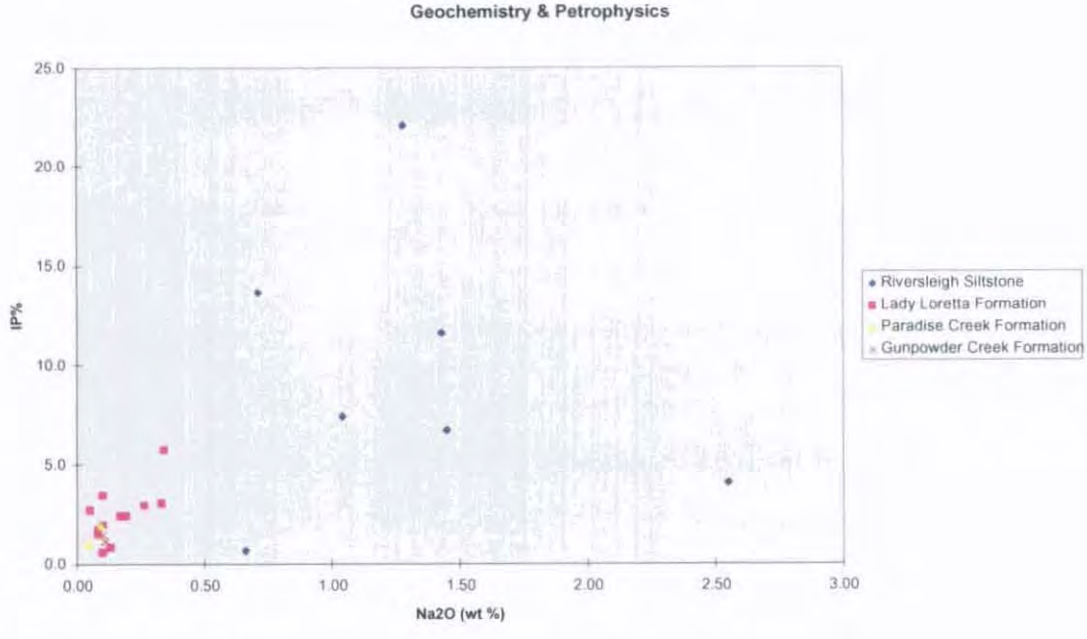

Figure 5.61 Relationship between Na_2O and chargeability, McNamara Group

There do not appear to be any strong compositional controls on IP properties. The strongest correlation with IP% occurs in the case of Na_2O (R = 0.53; Table 5.11; Fig. 5.61). Some control by clay minerals and or grain size on chargeability properties may be indicated, though militating against this hypothesis is the lack of any strong correlation of IP% with either Al_2O_3 or K_2O.

Surprisingly, correlation between S concentration and IP% is poor (R = 0.29; Fig. 5.60). It had been thought that S would be present largely as pyrite, which would then be reflected in bulk chargeability. The S levels in much of the dataset (< 0.5 %) may be too low to have an appreciable effect on bulk IP

properties. In this regard, the two outliers present in Fig. 5.62 are worthy of comment. The high-IP sample actually contains visible pyrite, so the analytical result of 0.22% S is puzzling, and probably results from sample heterogeneity. Large and McGoldrick (1997) specifically avoided visible sulphides as far as possible in their geochemical sampling, and the sulphide-bearing sample measured for the petrophysical study represents the sample remnant rejected by Large and McGoldrick (1997), so the portion of the original sample consumed in geochemical analysis may well have been significantly lower in S. The high-S outlier is similarly enigmatic, as in hand specimen it is a silty coarse-grained sandstone. A possible explanation for this anomaly is the presence of microscopic pyrite. This is supported by high levels of Fe also measured in this sample, and IP% levels which, while not approaching the levels of the high-IP outlier (~22%), are still within the highest quartile of the sample set.

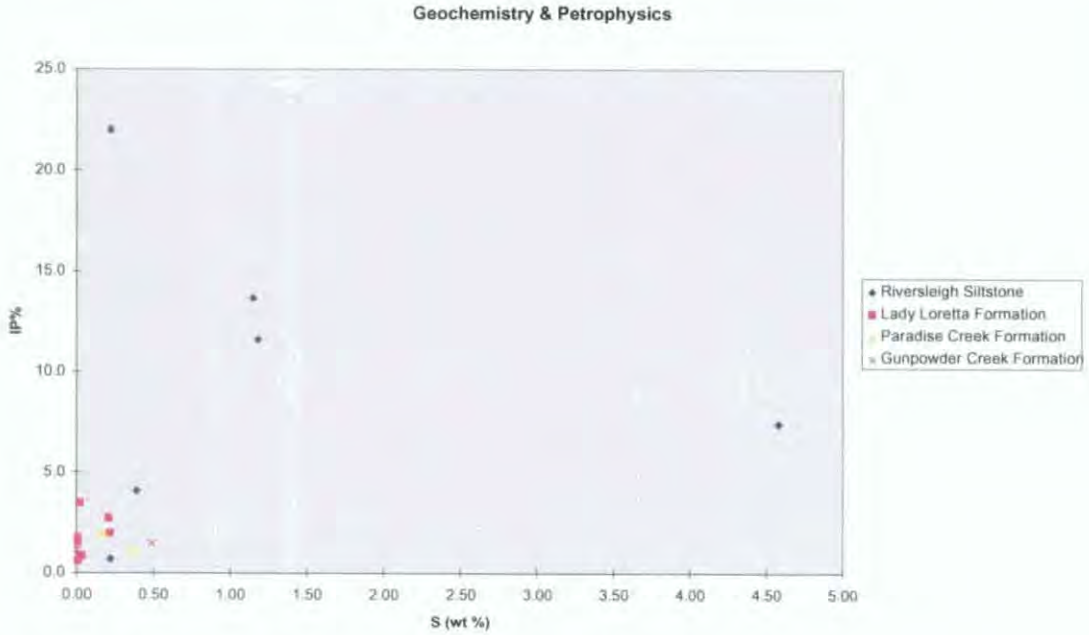

Figure 5.62 Relationship between S and chargeability, McNamara Group

5.6 Summary and implications for regional geophysical interpretation

Table 5.12, summarising data compiled from the literature and this study, should form the basis for all geophysical interpretation in this region. Some stratigraphically adjacent units have been grouped together based on their geophysical indistinguishability, as detailed in this chapter. Where samples of specific units have not been available, qualitative inferences have been made from remotely sensed geophysical data and observations contained in the literature.

Unit	Density (t/m^3)	MS (SI x 10^3)	Velocity (m/s)	Resistivity (Ωm)	IP%	TC (cpm)	K/Th	K/U	U/Th
Mesozoic	2.18±0.25								
Cambrian	2.66±0.11	0.05±0.04		var (250-2000)					
SNG drillcore	2.61±0.04	0.16±0.05	5110±270	mod (2200-3100)	1.3±0.4	880±270	5.9±1.8	2.7±0.4	0.48±0.12
RS drillcore	2.67±0.02	0.14±0.02	5570±280	mod/low (1100)	7.6±2.4	1080±720	7.1±3.9	3.8±2.1	0.53±0.01
SBQ outcrop	2.37±0.04	0.02	4950±170	high (103000-156000)	2.6±0.4	170±80	4.6±0.9	2.2±0.4	0.49±0.10
LLF drillcore (regional)	2.78±0.02	0.16±0.03	5610±260	mod/high (3100-110000)	4.4±1.3	880±220	7.9±1.1	3.4±0.5	0.46±0.09
EF outcrop	2.24-2.33	0.06±0.05	3870±1660	high (9400-43000)	2.5±0.7	480±200	6.4±1.9	3.1±0.5	0.51±0.09
EF drillcore	2.67±0.03	0.13±0.04	5450±270	mod/high (2700-200000)	9.7±3.3	700±120	7.5±1.5	3.6±0.4	0.55±0.12
PCF outcrop	2.33-2.52	0.07 (0.04, 0.28)	4680±200	high (5700-140000)	2.3±0.6	570±200	6.0±0.5	3.0±0.3	0.51±0.04
PCF drillcore	2.77±0.03	0.10±0.01	5850±200	mod/high (2200-110000)	10.1±2.5	640±150	9.4±2.0	3.5±0.6	0.44±0.09
GCF outcrop	2.36±0.07	0.11±0.05	4010±420	1200	1.8±0.4	1100±250	6.2±0.7	3.1±0.2	0.51±0.05
GCF drillcore	2.73±0.01	0.33±0.20	5420±170	mod/high (3500-55000)	8.3±1.3	730±90	7.1±0.6	3.1±0.2	0.49±0.05
Sybella Granite	2.66±0.02	16.2		high (15000)	2.5	1171	11.6	3.2	0.28
Weberra Granite	2.56±0.02	0.10							
FCV seds	2.61±0.06	0.14±0.05	4910±360	very high (61000+)	2.8±1.2	930±350	7.1±2.9	3.4±0.5	0.56±0.18
FCV rhyolite	2.56±0.02	0.11±0.02	4990±170	high (4800-6900)	1.3±0.5	1050±340	8.9±2.1	3.9±0.5	0.51±0.15
FCV basalt	2.96±0.08	0.50±0.15	4980±570	moderate (1800-2900)	low (2.5±0.8)	660±230	10.0±3.7	4.0±0.7	0.46±0.10
TCQ, SCF, BF, QF, MS	2.64-2.67	0.09±0.02	5410±120	extreme (700000)	low (4.1±1.7)	variable	6.1±1.1	2.9±0.3	0.54±0.09
altered ECV	2.76±0.03	0.93 (0.63, 2.9)	4800±400	high (4000-5700)	low (2.0±0.3)	low (190)	7.3±1.3	3.2±0.4	0.47±0.02
ECV sil'clastics	2.68±0.02	0.07±0.04							
ECV metabasalt	2.91±0.02	54±8	6000±600	high (12600-26000)	mod. (9.0)	400	5.0±0.5	2.8	0.56
lower HG qtzites	2.64±0.01	0.10							
Pre-Haslingden felsics	2.67 (2.65, 2.76)	0.8 (0.4, 65)	5500	high (15500-55000)	low (2.3±0.7)	high (950)	high (21)	4.6	0.24
Pre-HG SG<=2.7	2.65±0.01	0.77 (0.31, 80)							
Pre-HG SG>2.7	2.76±0.03	0.90 (0.50, 7.6)							

Table 5.12 Physical properties, western Mount Isa Basin; compiled and summarised from this study and various published and unpublished data (see text). All values except for the Mesozoic and lowest 7 units (ECV and older) are derived mainly from data obtained for this study. SNG = South Nicholson Group, RS = Riversleigh Siltstone, SBQ = Shady Bore Quartzite, LLF = Lady Loretta Formation, EF = Esperanza Formation, PCF = Paradise Creek Formation, GCF = Gunpowder Creek Formation, FCV = Fiery Creek Volcanics, TCQ = Torpedo Creek Quartzite, SCF = Surprise Creek Formation, BF = Bigie Formation, QF = Quilalar Formation, MS = Myally Subgroup, ECV = Eastern Creek Volcanics, HG = Haslingden Group. For units where the distribution of values is significantly different from normal, the geometric mean is listed, with alternative indicators of central tendency (median, arithmetic mean) in brackets

The 'pre-Haslingden Group felsics' grouping represents all units dominated by felsic igneous and metasedimentary rocks with primary age 1790 Ma or older, including cover sequence 1, Barramundi Orogeny and older, basement rocks. Density measurements from all units of this grouping (Big Toby Granite, Kalkadoon Granodiorite, Leichhardt Volcanics, Yeldham Granite, Tewinga Group, Argylla Formation, Bottletree Formation, Ewen Granite) fall into two distinct density populations, but these are

not simply related to mappable units. Possible exceptions to this generalisation include the Leichhardt Volcanics which tend to be restricted to the higher density population, but sampling has not been adequate to resolve these issues with confidence. All that can be safely concluded is that bulk regional density of the pre-Haslingden Group felsic units lies in the range 2.65-2.76 t/m^3. There is scope for refinement during interpretation in local areas well constrained by geological and other geophysical data. The density of the pre-Haslingden felsics is very strongly controlled by their chemical composition, such that their SiO_2 content may be confidently estimated to within a few per cent from their density, and vice versa. A complementary, strong positive correlation between density and mafic elements ($Fe_2O_{3\ tot}$, MgO, CaO) is also present. This provides clear scope for extension of the relationships between geophysics and geochemistry established by Goncharov et al. (1997) in the Mount Isa region.

Magnetic susceptibility varies over several orders of magnitude in the pre-Haslingden felsics, with the bulk effect likely to be one of slight to moderate magnetic susceptibility. No simple relationship could be discerned between geochemical abundances and magnetic susceptibility in these rocks, unlike density.

Velocities are typical of felsic lithologies in the upper crust, at around 5500 m/s. Resistivities measured are extremely high, and not likely to be representative of bulk rock response due to the effects of broader scale discontinuities and associated permeability. Chargeability is low. Of the pre-Haslingden felsic suite, only the K-feldspar-rich Yeldham Granite was sampled for gamma ray spectrometry, and the count rates recorded were high.

Density recorded from the lower Haslingden siliciclastics is slightly lower than in the underlying rocks, though this is based on very limited sampling. Lower density would in any case be expected from the mainly quartzites and sandstones of which this grouping (represented by the Leander Quartzite in the study region) is comprised. The lower Haslingden siliciclastics are non-magnetic.

The metabasaltic Eastern Creek Volcanics are in many ways the dominant geophysical unit in the region. They are consistently magnetic, at levels well above those observed from any other volumetrically significant unit (in excess of 50 x 10^{-3} SI). Densities observed are similarly high (around 2.91 t/m^3), while the few velocities measured (around 6000 m/s) are generally higher than observed in the pre-Haslingden felsics which are of similar or slightly higher metamorphic grade. Resistivities, while still high, appear slightly lower than in the pre-Haslingden felsics.

Probable altered correlatives of the Eastern Creek Volcanics sampled from deep drilling in the vicinity of Lady Loretta and in the Mount Isa Mine ('greenstone basement') have physical properties quite distinct from their unaltered counterparts. Their density has been reduced to the moderate level of 2.76 t/m^3, and destruction of their magnetic minerals appears to have been near complete, with measured susceptibilities of little more than 1.0 x 10^{-3} SI. Velocities and resistivities are also significantly lower than in unaltered Eastern Creek Volcanics. This together with geochemical evidence is consistent with the interpretation of pervasive alteration by fluids capable of dissolving and removing base metals from the basalt. There is also some suggestion that total gamma ray count has been reduced in the altered metabasalt, while the ratio of K to other radioelements may have been increased.

The stratigraphic interval spanning the Myally Subgroup, Quilalar Formation, Bigie Formation, Surprise Creek Formation and Torpedo Creek Formation includes a number of unconformities and represents several tens of millions of years, but unfortunately is largely petrophysically homogenous. These sedimentary units have densities in a fairly narrow range between 2.64 and 2.67 t/m^3, and are non-magnetic. Only seismic reflection profiling is likely to resolve structures within this sequence on a regional scale. Pervasive silicification completely filling pore space in many outcrop samples has resulted in measured sonic velocities being rather high for exposed specimens, at around 5400 m/s. Resistivities are extremely high, while chargeability is low.

The Fiery Creek Volcanics, which occur within the Myally Subgroup-Torpedo Creek Quartzite sequence, contains rhyolites and basalts that might be expected to be geophysically prominent. Unfortunately its patchy extent and thickness (rarely much in excess of 100 m), as well as the apparent absence of magnetite from the basalt, mitigates against its geophysical detectability. The basalt is dense (similar to the Eastern Creek Volcanics), and slightly magnetic (around 1.0 x 10^{-3} SI, probably from haematite), but the lack of volume precludes it from detection in all but near-surface mapping applications so far as potential field methods are concerned. Seismic reflection should however reveal the basaltic sequence as a strong reflector, having a high acoustic impedance contrast with the enclosing sediments and rhyolites. The rhyolites' density and magnetic susceptibility are both very low. Potassic alteration is widespread in the Fiery Creek Volcanics, and this is reflected in elevated gamma ray counts from hand specimens, particularly of the rhyolites.

The Weberra Granite is directly related to the Fiery Creek Volcanics rhyolite, and its density and magnetic susceptibility are essentially identical to those of the FCV rhyolites. The very low density value (2.56 t/m^3) may be a slight underestimate due to the lack of drillcore sampling - 'outcrop' is synonymous with 'weathered' in this region. The Weberra Granite may be a correlate of at least one intrusion episode in the multi-phase Sybella Granite, but unfortunately the latter has not been sampled sufficiently to characterise it. A magnetic susceptibility of 16.2 x 10^{-3} SI recorded from one sample of the Sybella Granite, not hitherto regarded as a significantly magnetic body, is intriguing, but unfortunately its origin is not adequately documented to be followed up.

While the Gunpowder Creek Formation has been intensively sampled in drillcore, the mean density figure obtained (2.73 t/m^3) is somewhat higher than might have been expected from its description in extant literature as a predominantly siliciclastic unit. The uppermost, most dolomitic portion of the unit is probably over-represented in the sample set used due to the targeting of exploration drillcore on conductive black shales near the top of the formation. A regional bulk density value for the formation may need to be adjusted slightly downwards from 2.73 t/m^3, based on gravity observations. Resistivities are highly variable, though again the range given in Table 5.12 may be biased upwards by the over-representation of dolomitic lithologies. There is marked contrast between the generally moderate to high resistivities measured and the values obtained from several carbonaceous pyritic shale samples, which can be up to five orders of magnitude more conductive. This observation supports the field data of Anderson et al. (1993) and Rivera and Challis (1972) who both observed extremely conductive horizons near the top of the Gunpowder Creek Formation, and attributed them to black shales. Velocities in the Gunpowder Creek Formation are indistinguishable from those measured in older sedimentary units

(~5400 m/s). Chargeability is also highly variable in the Gunpowder Creek Formation, but elevated values tend to be associated with fine-grained siliciclastics including but not restricted to carbonaceous pyritic shales. Gunpowder Creek Formation samples from outcrop are more representative of regional lithological variation than the drillcore used, but weathering has had severe effects on rock properties, well beyond the range due to compositional variation in fresh samples. Outcrop sample densities are around 0.4 t/m^3 lower than in drillcore samples, while resistivity, chargeability and velocity are all also significantly reduced. Gamma ray counts observed from Gunpowder Creek Formation hand specimens are generally high, and the unit is essentially non-magnetic.

Samples from the mainly dolomitic Paradise Creek Formation have a mean density typical for this composition, 2.77 t/m^3. This figure makes it the densest volumetrically significant unit to accumulate in the Mount Isa Basin since the Eastern Creek Volcanics (the Fiery Creek Volcanics basalts are too thin and patchy). Mean velocities are similarly high at almost 6000 m/s, with velocities measured in many of the dolostone samples comfortably exceeding this value. The presence of shaly beds amongst the more common dolostones makes for a very wide range of resistivities from rather low to extremely high levels; hence it is not very meaningful to assign an overall bulk resistivity value to the unit. Many of the shale samples and even some of the dolostones have unusually high chargeability. Of these samples, most contain a significant proportion of carbonaceous material and occasionally visible pyrite. Overall gamma ray counts in the Paradise Creek Formation are little more than half those from the Gunpowder Creek Formation. However total counts observed from Paradise Creek Formation shales are just as high as from similar lithologies in the Gunpowder Creek Formation, and overall K/Th ratios are significantly higher in the Paradise Creek Formation. The Paradise Creek Formation is non-magnetic. Outcrop samples of the Paradise Creek Formation are greatly depressed in density and velocity compared to their drillhole counterparts, but resistivity is if anything higher. Observed gamma ray counts were roughly the same, though K/Th ratios were lower in the weathered samples. Chargeability of outcrop hand specimens measured was uniformly low.

The cherts and shales of the Esperanza Formation are markedly less dense than both the underlying and overlying units, but the small thickness of the unit means that its presence may not be significant for many regional potential field applications, at least where the strata are only shallowly dipping. Again, the mixture of lithologies present makes for a very wide range of observed resistivities, with shales low and cherts high. Interpretation of the Esperanza Formation as a strongly conductive unit (Anderson et al., 1993) may imply that the resistive (in both the weathering and electrical sense) cherts which are a distinguishing feature in outcrop are not representative of the Esperanza Formation at depth. Velocities are typical of Palaeoproterozoic sediments in this region at ~5500 m/s. As in the Paradise Creek Formation, carbonaceous shales, often but not necessarily carrying visible pyrite, are usually highly chargeable while cherts and dolostones mostly are not.

The bulk composition of the Lady Loretta Formation is essentially similar to the Paradise Creek Formation, and this similarity extends in most respects to their physical properties. The mean IP% values recorded from the Lady Loretta Formation are the lowest of all McNamara Group units sampled in drillcore. This unexpected result may be attributable to the large number of siltstones (as distinct from shales) present in the sample set used. This factor may also be responsible for mean measured velocities

being lower (though not significantly so) than in the Paradise Creek Formation. Otherwise properties are as would be expected from a mixed dolomitic/fine siliciclastic sequence, with high (for sediments) density and velocity, and resistivity highly variable in response to the relative proportion of silt and dolomite.

With the Shady Bore Quartzite the McNamara Group demonstrates a marked change in character, as dolostones become much less common. Unfortunately no drillcore of the Shady Bore Quartzite was obtainable, but from similar lithologies sampled elsewhere in the sequence, low density (~2.60 - 2.65 t/m^3), non-magnetic, resistive, non-chargeable, moderately low velocity, low gamma-ray-count bulk properties may be inferred. Measurements made on outcrop samples do not contradict these inferences.

The preponderance of siltstones and black shales within the Riversleigh Siltstone results in a rather low bulk density compared to other McNamara Group formations (2.67 t/m^3 mean value). Density may be elevated above this base mean value in proportion to pyrite concentration. The Riversleigh Siltstone as with all other McNamara Group units is practically non-magnetic, indicating the continued absence of pyrrhotite though pyrite is frequently visible. Velocity is typical for fine-grained McNamara Group siliciclastics in this region, at around 5500 m/s. Resistivities are still quite variable in spite of the near-absence of dolostone and sandstone, and the reason for the high resistivity of some siltstones and shales is not clear, but may be accentuated by the fresh water used in laboratory determinations. Porosity is an important control on electrical properties, in addition to compositional factors. However, the Riversleigh Siltstone is usually noticeably more conductive than older McNamara Group units. Moderately high chargeabilities are not uncommon, particularly in carbonaceous shale samples, many of which are pyritic. Total gamma ray counts are high.

Some general observations may be made on the physical properties of common rock types in the McNamara Group. In the majority of cases the petrophysics of a given rock volume can be predicted from its position on the compositional continuum between the two end-members of pure shale or siltstone and pure dolostone (and vice-versa). The ideal shale end-member has low density (~2.65 t/m^3), low velocity (~5400 m/s), low resistivity and high total gamma ray count. Coarser-grained siliciclastics i.e. sandstones (relatively uncommon from the lower Gunpowder Creek Formation upwards) are similar with the exception of slightly lower density and velocity, and lower radioactivity. The reverse is true of the ideal pure dolostone, which has high density (~2.85 t/m^3), high velocity (~6500 m/s), extremely high resistivity and low total gamma ray count. In the absence of other factors such as porosity and sulphide concentration whose effects are reasonably predictable in any case, the composition of a rock may be inferred with some confidence once these physical properties are determined. The converse, deriving petrophysical properties from compositional data, is also applicable. Controls on IP properties are much less clear cut. While there is a clear correlation between high IP% values and carbonaceous pyritic shales, the relationship is far from simple. No sulphides are visible in many of the high IP% samples, nor even is carbonaceous material in some cases. Also, some carbonaceous pyritic shales were not particularly chargeable, though in many of these the visible pyrite was both rare and coarse.

The South Nicholson Group is separated from the McNamara Group by at least several tens of millions of years, the Isan Orogeny and a regional angular unconformity, and its metamorphic grade is

correspondingly lower. This has undoubtedly been a primary factor in the preservation of porosity at levels much higher than is generally the case in the McNamara Group, which in turn exerts marked effects on the South Nicholson Group's bulk physical properties. The prevalence of sandstones and micaceous siltstones is also a fundamental reason for the South Nicholson Group's low density (~2.62 t/m^3) and velocity (~5100 m/s). Resistivities are moderate, with the effects of highly resistive sand grains balanced against those arising from the relatively high proportion of pore space. Chargeabilities are invariably low, probably mainly due to the lack of carbonaceous and or pyritic shale. Though there is some sedimentological evidence for the South Nicholson Group being proximally sourced, no detrital magnetite appears to have been preserved, and even in the highly ferruginous samples, magnetic susceptibilities are very low.

The Cambrian sediments of the Georgina Basin contain large amounts of massive limestone in this region, and this is mainly responsible for the Cambrian sediments actually being significantly denser than the South Nicholson Group underlying it, which is 1000 million years older. The purest limestones have densities approaching the dolostones of the McNamara Group, but bulk density of the Undilla Basin sequence as a whole is diluted to ~2.65 t/m^3 by the siltstones, shales and cherts also in the sequence. This combination of rock types has predictable effects on resistivity properties, which range from fairly low to moderate levels. No Cambrian samples measured had significant magnetic susceptibility, but unfortunately no samples of the Colless Volcanics basalt known to outcrop to the northwest of the study area were obtainable.

The density value obtained from the literature for the Mesozoic sandstone of the region is extremely low (~2.1 t/m^3), but is unlikely to be significant in most regional geophysical models due to its very low thickness in the study area (< 50 m).

6. Base Metal Mineralisation Petrophysics

6.1 Introduction

Physical property measurements were made on a large set of samples from the vicinity of the Lady Loretta prospect and the Lady Loretta orebody itself. The main objective of this work was the detailed characterisation of the response of the Lady Loretta orebody to geophysical methods, and its physical property contrast with its immediate geological environment. Spatial and stratigraphic variation in physical properties within the Lady Loretta mineralised system were intensively examined.

The physical properties of other Carpentaria Zinc Belt deposits, and their respective host rocks, were also investigated. Most of these were sourced from the literature, with some additional determinations made on samples obtained from HYC, Hilton and Mount Isa by the author. Inferences made from geophysical survey results have also been incorporated as a source of data on ore deposit petrophysics. The results from Lady Loretta are compared with those obtained from the other SSHBM deposits in the Carpentaria Zinc Belt.

6.1.1 Sampling

Samples for this mineralisation-centred phase of the petrophysical study were obtained from some of the same sources as the regional study (outlined in section 5.1.1). Most are from drillcore extracted from the Lady Loretta mineralised system. Samples collected from Lady Loretta drillcore by the author are numbered between 1000 and 2000 in Appendix 3. The bulk of the Lady Loretta samples were collected by several workers (P. McGoldrick, M. Aheimer and J. Dunster) within the last eight years, and retrieved from the rock store of the Geology Department at the University of Tasmania. These are identified by their original catalogue numbers in Appendix 3. As stated in section 5.1.1, some of the samples originating with McGoldrick were collected for a geochemical study of sedimentary alteration, with sulphides avoided if possible (Large and McGoldrick, 1998). This bias is largely counterbalanced by collection of pyritic samples for a subsequent S isotope study by McGoldrick, and the study by Aheimer (1994) which focused on the ore.

The HYC, Hilton and Mount Isa orebodies are represented by a few samples in the Geology Department collection, and these also were retrieved and measured. Some additional samples of the HYC mineralisation were obtained from orebodies 2 and 4 during an underground visit by the author. For comparison, these were supplemented by samples obtained from barren core drilled over 20 km from HYC.

6.2 Methods

All methods used in physical property determinations have been documented in section 5.3.

6.3 Previous work

Petrophysical data obtained from SSHBM mineralisation in the Carpentaria Zinc Belt have mainly been reported in studies on single mines. These are reviewed within sub-sections devoted to each deposit in section 6.4. Data generated by the author have been combined with all previously published data from discrete samples before subsequent review and analysis. All these data are tabulated in Appendix 3, and summarised in Table 6.10.

Physical properties of stratiform sediment-hosted ores were briefly outlined within a more general summary of zinc deposit geophysics by Bishop and Emerson (1993,1999). They point out that zinc orebodies are likely to present a difficult geophysical target, as sphalerite is resistive, non-magnetic and relatively light in comparison to other sulphides. Direct ore detectability is thus largely dependent on the nature and proportion of associated sulphide minerals. The most common of these in most stratiform sediment-hosted orebodies are galena and iron sulphides (usually pyrite and/or pyrrhotite). Fortunately, these minerals manifest a large contrast in density, conductivity and chargeability (and magnetic susceptibility in the case of monoclinic pyrrhotite) to most likely host sediments (Bishop and Emerson, 1999).

6.4 Results

6.4.1 HYC

The geophysical signature of the HYC orebody has been the subject of articles by Shalley and Harvey (1992) and Hishida et al. (1993). The general case history recounted by Shalley and Harvey (1992) demonstrates the efficacy of induced polarisation, resistivity, gravity and modern airborne EM (GEOTEM and QUESTEM systems) in delineating anomalous responses associated with mineralisation. IP values of over 30 mV/V appear associated with areas of strong lateral contrast at the western edge of the orebody (where the ore strata steepen towards the surface), but are more subdued (10-13 mV/V) over the centre of the deposit, where the shallowly-dipping ore is over 300 m deep. Apparent resistivities as low as 25 Ωm are observed closely associated with the IP anomalies. High IP values and low resistivities are also present both in the hanging wall to the orebody and in correlative strata to the south, though the electrical response is not quite as pronounced as over the western edge of the deposit. The anomalous response in these latter areas has been attributed via drilling to pyritic shales. Direct measurements on drillcore (Fig. 5 of Shalley and Harvey, 1992) show generally low resistivities (in the range 100-250 Ωm) in all but the footwall to the orebody, which has resistivities well in excess of 1000 Ωm and IP less than 5 mV/V. The orebody and pyritic carbonaceous shales in the hanging wall have similar electrical properties, with measured resistivities ~80 Ωm and IP 10-15 mV/V. Shalley and Harvey (1992) noted that IP peaks (up to 25 mV/V) correspond to resistivity highs in the drillcore measurements. These results are somewhat at odds with the field measurements, since the IP and resistivity responses of mineralisation do not appear particularly different from those of other hanging wall lithologies. Possibly the correlation of pronounced IP and resistivity anomalies with known near-surface mineralisation is not solely a response unique to mineralisation, but may also be a function of the geometry of the high-

contrast contact between the base of the HYC Pyritic Shale Member (where the HYC orebody is positioned) and the much more resistive, less chargeable and more dolomitic rocks in the footwall. Time-domain airborne EM systems have revealed anomalies whose highest apparent conductivity peaks are coincident with the centre of the ore deposit, but the relative contribution of base metal mineralisation and overlying pyritic shale to these effects is difficult to establish.

Extensive density measurements on drill core, surface and underground rock samples from the HYC deposit and environs were reported by Shalley and Harvey (1992). They give indicative ranges of 2.4-2.7 t/m^3 for clastic units, 2.7-2.9 t/m^3 for dolomitic units and 3.2-3.3 t/m^3 for ore zone samples. Though the gravity field in the area of HYC is dominated by a steep gradient caused by the contrast between the dolomitic McArthur Group and sandstones of the Roper Group across the Emu Fault, a superimposed gravity high is apparent associated with the mineralised zone. This is easily accounted for using the properties quoted for ore, though as reported by Shalley and Harvey (1992) such features may also be caused by accumulations of highly pyritic sediments, as turned out to be the case for a gravity anomaly of similar appearance north of the orebody.

Geophysically distinguishing base metal sulphides from pyrite thus appears equally difficult with electrical as with gravity methods in the HYC environment, with good understanding of local geology being particularly important for gravity to be used as a direct ore-finding method.

Physical property determinations made for this study are generally in accord with those of Shalley and Harvey (1992), but differ somewhat in detail. Petrophysical measurements were performed on samples acquired from the No. 2 and No. 4 orebodies at HYC by the author. A summary of these results is included in Table 6.10. The mean value of 3.39 ± 0.05 t/m^3 (saturated) is comparable with the figure of 3.3 t/m^3 (dry) for all mineable ore generally utilised by McArthur Mine personnel (verbal communication), and is slightly higher than the figure given by Shalley and Harvey (1992). Magnetic susceptibilities are very low. The ore is only moderately conductive at around 500 Ωm but is highly polarisable, with IP% values consistently between 10 and 20. Radiometric observations were made of a few HYC ore samples, but no signatures distinct from those of unmineralised dolomitic sediment were noted.

For comparison purposes, a number of density measurements were made on barren core from holes drilled about 25 km away from HYC (Myrtle 4 and Myrtle 5). These are presented in Figures 6.1 and 6.2. The contrast between units, even between different members of the same formation, is very striking. Clearly, relative proportions of shale and carbonate exert a primary control on bulk density, with second order effects arising from pyrite content of the shaly units. Myrtle 4 was targeted on a pronounced 1.5 mGal anomaly (Bomman, 1982), whose cause is clearly indicated as a consequence of the high contrast between shallow, dense Teena and Emmerugga Dolomite and an attenuated shale-dominant sequence.

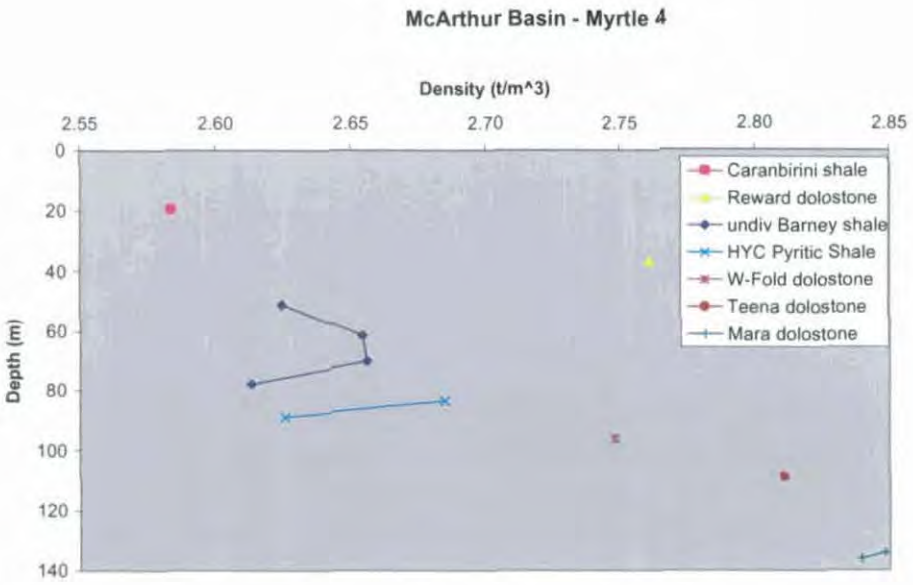

Figure 6.1 Density measurements classed by stratigraphic unit, Myrtle 4

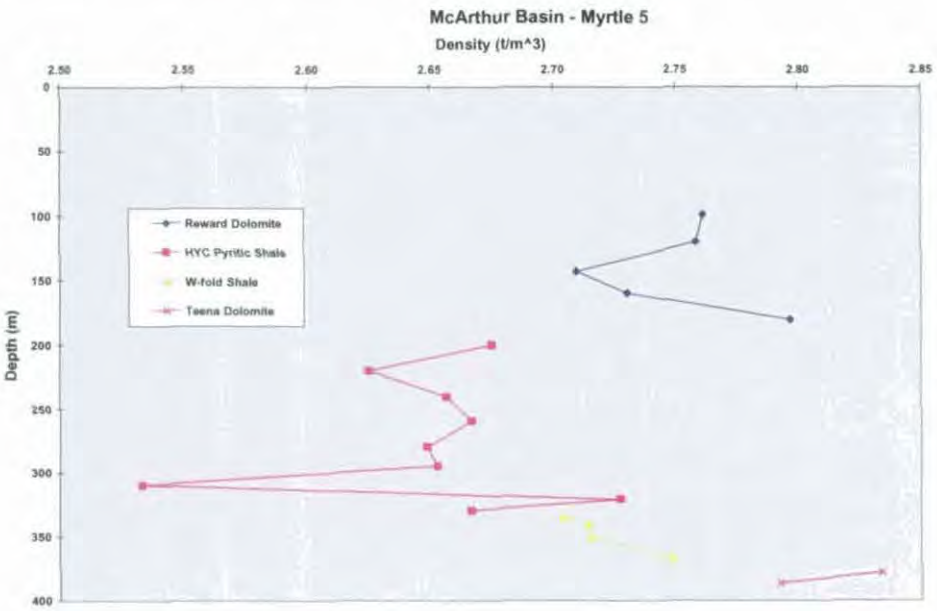

Figure 6.2 Density measurements classed by stratigraphic unit, Myrtle 5

6.4.2 Walford Creek

Walford Creek is a sub-economic base metal prospect, but is included in this chapter as a demonstration of the properties of a significant sulphide deposit in the study region consisting mainly of pyrite, with little base metal mineralisation. The main sulphide accumulation at Walford Creek consists of three stacked lenses of stratiform massive pyrite; the uppermost (known as No. 1) being the largest and most regionally extensive with a strike length of six kilometres. The deposit is bound by the regional-scale Fish River Fault separating the host Mount Les Siltstone from older units to the north, and extends over 1500 m south from the fault. The sulphide lenses are up to 30 m thick, and lie under very thin Phanerozoic cover at depths ranging from within a few metres of the surface to over 350 m. The

subordinate base metal mineralisation is confined to a smaller areal extent than that of the pyrite lenses. It is present as both stratiform and a later discordant sphalerite, galena and chalcopyrite overprint associated with dolomite talus breccias proximal to the Fish River Fault.

The main source of data on Walford Creek is a paper by Webb and Rohrlach (1992). They report the use of ground-based TEM as the primary geophysical exploration tool, which was successful in mapping the distribution of the No. 1 pyrite lens. An interesting feature of the Walford Creek environment noted by Webb and Rohrlach (1992) is the apparently poorly conducting nature of the highly carbonaceous shales hosting the sulphide bodies. Presumably this is because the carbonaceous shales lack either graphite or sufficient pyrite, though a depth-conductivity pseudosection presented by Webb and Rohrlach (1992) depicts background resistivities of 100 Ωm - still relatively low in the context of core samples measured for this study. Webb and Rohrlach (1992) considered airborne TEM systems to be subject to a conductor detection limit of 150 m depth in the generally resistive environment of Walford Creek, though conductivity anomalies associated with the No. 1 lens were interpreted at depths exceeding 300 m using coincident-loop ground TEM.

A large density contrast between host carbonaceous dolomitic shale and the pyrite lenses is demonstrated by semi-regional gravity data compiled and presented in Webb and Rohrlach (1992). An anomaly of around 0.6 mGal over the pyrite bodies is clearly apparent despite the proximity of a steep gradient attributable to the Fish River Fault.

6.4.3 Century

The zinc-rich Century deposit (118 Mt at 10.2% Zn, 1.5% Pb and 36 g/t Ag; Waltho et al., 1993) discovered in 1990 has already been the subject of significant geophysical work. Thomas et al. (1992) presented results from a range of geophysical techniques applied in the exploration of the deposit and its environs. They detected little or no distinguishing signal from the ore deposit using gravity, magnetics or TEM, but clearly anomalous responses to resistivity and induced polarisation methods. However, while Thomas et al. (1992) state that the mineralisation has a "definitive" resistivity response, much of the anomalous resistivity is probably due to conductive lithologies including pyritic black shales in the hangingwall and footwall, and their contrast with overlying resistive Cambrian limestones. Ore zone resistivity is variable (100-300 Om) but generally slightly higher than that of the enclosing Mesoproterozoic strata (60-80 Om; Thomas et al., 1992; Table 6.10). Seismic surveying was also attempted but adjudged unsuccessful in defining detailed orebody or host rock structure, due to insufficient ore/host velocity contrast and the uneven nature of the high velocity Cambrian limestone unconformably overlying much of the Mesoproterozoic surface in the Century area (Thomas et al., 1992).

Importantly, Thomas et al. (1992) also reported extensive use of downhole geophysical logging in characterising the petrophysics of the Century deposit and its host rock. These results appear in Table 6.10 below. Natural gamma levels measured in the ore zone were lower than in the host Proterozoic sediments. Also notable are the properties which Thomas et al. (1992) give for Cambrian limestones: density 2.8 t/m^3, high porosity (from neutron logging), resistivity in excess of 1000 Ωm and very low

total gamma ray counts. These are similar in many respects to the properties observed from correlative units in Morstone 1 several tens of kilometres to the south.

Inversions of DC resistivity and IP phase data performed by Oldenburg et al. (1998) show contrasting responses to the ore deposit from these two methods. The ambiguity of the resistivity response is emphasised by the lack of correlation between mineralisation and the recovered 2-D resistivity model, with the main conductivity contrast being between unmineralised Mesoproterozoic host siltstones and shales (particularly at both ancient and contemporary weathering surfaces) and unconformably overlying Cambrian limestones. The recovered resistivity model is supported by borehole petrophysical measurements given by Oldenburg et al. (1998), which almost certainly are taken from the work reported by Thomas et al. (1992; Table 6.10), though Oldenburg et al. (1998) do not mention the earlier paper. IP phase values derived from Oldenburg et al.'s (1998) inversion are also given in the relevant column in Table 6.10.

IP data show themselves to be an effective ore detector in this environment, capable of resolving structures displacing the ore strata after inversion (Oldenburg et al., 1998). The contrast between ore and hanging wall properties is particularly marked, but strongly polarisable rock in the inverted IP model of Oldenburg et al. (1998) extends well below the limits of the orebody defined by drilling. This is ascribed by Oldenburg et al. (1998) (supported by unspecified downhole IP and petrophysical data) to the footwall sediments being weakly chargeable, as well as to an artefact of the inversion process.

The Century orebody is notable for its lack of pyrite in relation to other stratiform ore deposits in the Proterozoic of northern Australia. This along with a high proportion of sphalerite probably accounts for the resistive nature of the ore in comparison to its host sediments. That ore minerals are responsible for the highly anomalous IP response of the orebody is also self-evident. The reason for the slight to moderate chargeability of the footwall sediments is less apparent; however it is pertinent that many unmineralised McNamara Group samples, particularly shales, may also be characterised as moderately chargeable (sections 5.4.6-5.4.11 inclusive), especially when carbonaceous material is present as has been noted in this portion of the Lawn Hill Formation (Waltho et al., 1993).

6.4.4 Hilton & George Fisher

While the Hilton and George Fisher (formerly known as Hilton North) Pb-Zn-Ag deposits are major base metal accumulations in their own right (see section 2.8), little has been published on their geophysical signatures, probably because much interest has been diverted to their giant sibling metal accumulation 18 km south - the Mount Isa Mine. Another possible reason for the comparative lack of geophysical attention to the Hilton deposits is their similarity in many respects to the Mount Isa Pb-Zn-Ag deposit (Myers et al., 1996), so that conclusions on geophysical signatures drawn from Mount Isa can be applied with some confidence to Hilton and George Fisher. Apart from size, the major difference between Hilton/George Fisher and Mount Isa is that no Cu accumulation in anything approaching Mount Isa-like proportions has been identified to date.

Hilton was the subject of some of the earliest geophysical work in the Mount Isa region, but the methods applied (Turam EM, SP and vertical force magnetics) do not appear to have met with much success in defining the ore signature (Shalley, 1997). Technological improvements in these methods since that time (1950s) may well justify re-examination of these methods as ore-finders in this environment, since minerals sensitive to these methods (monoclinic pyrrhotite, pyrite) are present in significant quantities associated with the sphalerite-galena ore.

The one physical parameter of the Hilton deposit well defined in extant literature is density. Young (1984) gives a figure of 3.03 t/m^3 (standard deviation 0.43) derived from almost 2400 samples of the Hilton ore zone; a value with which Leaman and Mutton (1993) concurred in their Bouguer gravity modelling of the ore deposit and its environs. A mean of 3.52±0.32 t/m^3 for Hilton ore samples has been calculated from determinations by the author on 6 samples from the Geology Department archive, as well as 2 others listed by Hone et al. (1987). It would appear likely that unusually sulphide-rich portions of the orebody are represented in the latter two data sets, and the 3.03 t/m^3 estimate is preferred as best characterising the bulk density of the Hilton ore body.

The magnetic character of pyrrhotite-rich samples from Hilton implies that the sulphide accumulation here should theoretically be detectable with magnetic methods, assuming the dominating effect of the Eastern Creek Volcanics against which the Hilton ore host sequence (Urquhart Shale) is faulted can be removed.

Moderately high galvanic resistivities (median 1100 Ωm, mean 4700 Ωm) measured on samples of Hilton ore from the Geology Department archive are extremely surprising, being several orders of magnitude greater than resistivities measured on Mount Isa ore (see section 6.4.5) and should probably be treated with some scepticism. The values observed are more akin to what would be expected from unmineralised host rock (Urquhart Shale). Possible explanations are that inadequate electrical coupling was made with the samples, which were large (around 0.5 kg) and irregularly shaped. They may also have developed a resistive oxidised or grimy rind after a long period of storage in the Geology Department. Measurement scale effects may also be important, with layers of highly resistive material such as carbonate and siltstone interrupting sulphide continuity in the hand specimens tested. The very low salinity of water used in these petrophysical experiments is unlikely to be a factor, since the Hilton samples all have very low porosity (< 0.01).

6.4.5 Mount Isa

Though Mount Isa Pb-Zn ore was discovered in 1923, the first widely circulated publication of petrophysical data from Mount Isa ore did not appear until 1984, when Young published tables of density and magnetic susceptibility data supporting gravity and magnetic forward models of the Mount Isa district. This paper was undoubtedly preceded by many unpublished or otherwise restricted internal company reports, whose data are summarised in tables 1 and 2 of Young (1984). Even this paper omits much detail to do with the Pb-Zn ore itself, not giving any value for ore density. Density values from several Pb-Zn ore samples are tabulated in Hone et al. (1987), and a high value for ore density is implied by Leaman (1991a and b), but the first summary of Pb-Zn ore density from Mount Isa Mines (MIM)

Ltd.'s considerable petrophysical database did not appear until the publication of Fallon and Busuttil (1992), who give a value of 3.48 t/m3 based on over a thousand samples.

The host Urquhart Shale sequence contains significant quantities of pyrite and pyrrhotite in the vicinity of the base metal orebodies, and must be considered as a separate geophysical entity from the host sediment distant from mineralisation. Young's (1984) rather ambiguous Table 1 indicates its density as 2.90±0.01 t/m^3, as does Leaman (1991b) though the latter figure may be sourced from the same data as Young (1984). Leaman (1991a) gives a range of 2.85-3.10 t/m^3 for the Urquhart Shale in the mine area, while Fallon and Busuttil (1992) state 3.30 t/m^3 for 123 'pyritic shale' Urquhart Shale samples and 3.06 t/m^3 for 'disseminated sulphide' Urquhart Shale (8089 samples). Since all these summary figures are in all probability based on the same petrophysical database (MIM's), it may be concluded that the different means given arise from differences in lithologic and stratigraphic classifications adopted by each author. The means given may conceal some systematic variation within the measured values, such as variation with distance along strike from the orebodies or some other parameter. The figure of 2.90 t/m^3 appears to best characterise the bulk properties of the Urquhart Shale in the vicinity of Pb-Zn mineralisation as it or a figure within 0.02 t/m^3 of it has been utilised in modelling of the ore environment by many of the above authors (see for example Leaman's (1991b) Figure 5 and Fallon and Busuttil's (1992) Figure 3).

'Normal' Urquhart Shale densities relevant to rock volumes outside the sulphide-mineralised system at Mount Isa were first reported by Leaman (1991a), who gave a range of 2.75-2.77 t/m^3. These values were supported by Fallon and Busuttil (1992) with a mean of 2.77 t/m^3 for unmineralised Urquhart Shale, albeit based on an unknown number of samples.

Magnetic properties of the Mount Isa Pb-Zn orebodies have also only been publicly detailed relatively recently. Young (1984) stated only that 'the lead-zinc orebodies...have moderate susceptibility - generally less than 0.001 emu (12.5×10^{-3} SI)'. This level of susceptibility was also measured in pyrrhotite/pyrite-rich Urquhart Shale. That the entire mineralised system at Mount Isa has a bulk magnetic susceptibility of the order of 12.5×10^{-3} SI was supported by the modelling of Leaman (1991b). Again, differences in the definition of what constitutes a 'mineralised' or 'sulphidic' sample probably accounts for the discrepancy between this value and the mean of 6.12×10^{-3} SI given by Fallon and Busuttil (1992) for 5699 samples of 'disseminated sulphide' Urquhart Shale. A component of remanent magnetism in the same direction as Earth's present magnetic field may also account for some differences between measured susceptibilities and bulk properties implied in modelling. Ordinarily the magnetic signature resulting from the susceptibilities observed would be easily discernible in contrast to the remainder of the Mount Isa Group, but the proximity of the Eastern Creek Volcanics against which the ore host sequence is faulted obscures the magnetic signal resulting from mineralisation. The Mount Isa Cu orebody is essentially non-magnetic (Young, 1984), probably because only minor amounts of pyrrhotite are directly associated with it (Fallon and Busuttil, 1992). Similarly, unmineralised (non-sulphidic) Urquhart Shale was treated as negligibly magnetic by Young (1994) and Leaman (1991a and b); with an arithmetic mean of 0.20×10^{-3} SI given by Fallon and Busuttil (1992) for 35 samples of unmineralised Urquhart Shale.

Some electrical properties are given by Fallon and Busuttil (1992), but the most comprehensive summary of properties to date for the Mount Isa district appears in Jackson et al. (1996), and relevant values from this paper appear in Table 6.10. These resistivity values are generally very low in comparison to those obtained in this study for similar lithologies. Possible reasons for the systematic difference in absolute values include scale of measurement, the use of inductive rather than galvanic resistivity determination methods, or the utilisation of more saline pore fluid. Unfortunately, apart from a statement that measurements were collected "from drillhole logging and core measurements", no details of property determination methodology are given by Jackson et al. (1996).

The very low resistivity of Mount Isa Pb-Zn ore (<0.01 Ωm) is particularly notable in comparison with resistivities measured on ore samples from Hilton (Table 6.10), implying that the sphalerite component does not present significant impedance to current flow. Also notable in this context is that the metamorphically remobilised Dugald River Pb-Zn ore in the Eastern Fold Belt of the Mount Isa Basin is similarly conductive (~0.003 Ωm; Macnae and Mutton, 1996), while graphitic shale hosting this orebody has similar properties to that at Mount Isa (~1 Ωm). It may be that increasing metamorphic grade and recrystallisation tends to decrease the resistivity of stratiform sediment-hosted base metal orebodies. Otherwise the relative resistivities of units present in the Mount Isa ore environment are generally as expected, with Eastern Creek Volcanics the most resistive (>10000 Ωm) followed by background Mount Isa Group units (9-1500 Ωm) and carbonaceous Mount Isa Group (0.05-50 Ωm).

6.4.6 Lady Loretta

The Lady Loretta Formation has been locally subdivided into a number of informal members encompassing several hundred metres of section intersected by drilling above and below the Lady Loretta ore sequence (Hancock and Purvis, 1990; Fig. 6.3). A slightly simplified version of this scheme is referred to extensively in this section, and is briefly reviewed here. A representative cross section of the Lady Loretta deposit is shown in Fig. 6.2.

The lowest informal member recognised, more than 150 m below the ore sequence, is the Lower Siltstone (LS) unit, which is characterised by silts, shales and intercalated dolostones with occasional pyrite lenses. It grades up into the Lower Carbonate (LC) unit, which is composed of generally more dolomitic and coarser material than the LS, and also contains minor interbeds of fine laminate pyrite. Siderite becomes the dominant carbonate mineral towards the top of the LC, which is up to ~170 m thick.

The Pyritic Unit (PU) overlying the sideritic LC is composed of up to 90% pyrite, the balance being mainly pyritic and sideritic shale and sand. The Ore Horizon (OH) immediately overlying the PU is generally even more sulphidic, the major compositional difference being the presence of high concentrations of finely banded massive sphalerite and galena. The OH encompasses all ore-grade material at Lady Loretta. A barite-chert-sphalerite (galena poor) facies occurs within the OH, mainly in the northeast section of the deposit. Both the PU and OH range up to 50 m thick (usually 25-30 m). An apparently unmineralised sediment facies (Ore Sediments or OS) also occurs within the OH, generally towards the top. The OH and OS together have been termed the Ore Sequence (Dunster, 1997; Fig. 6.4).

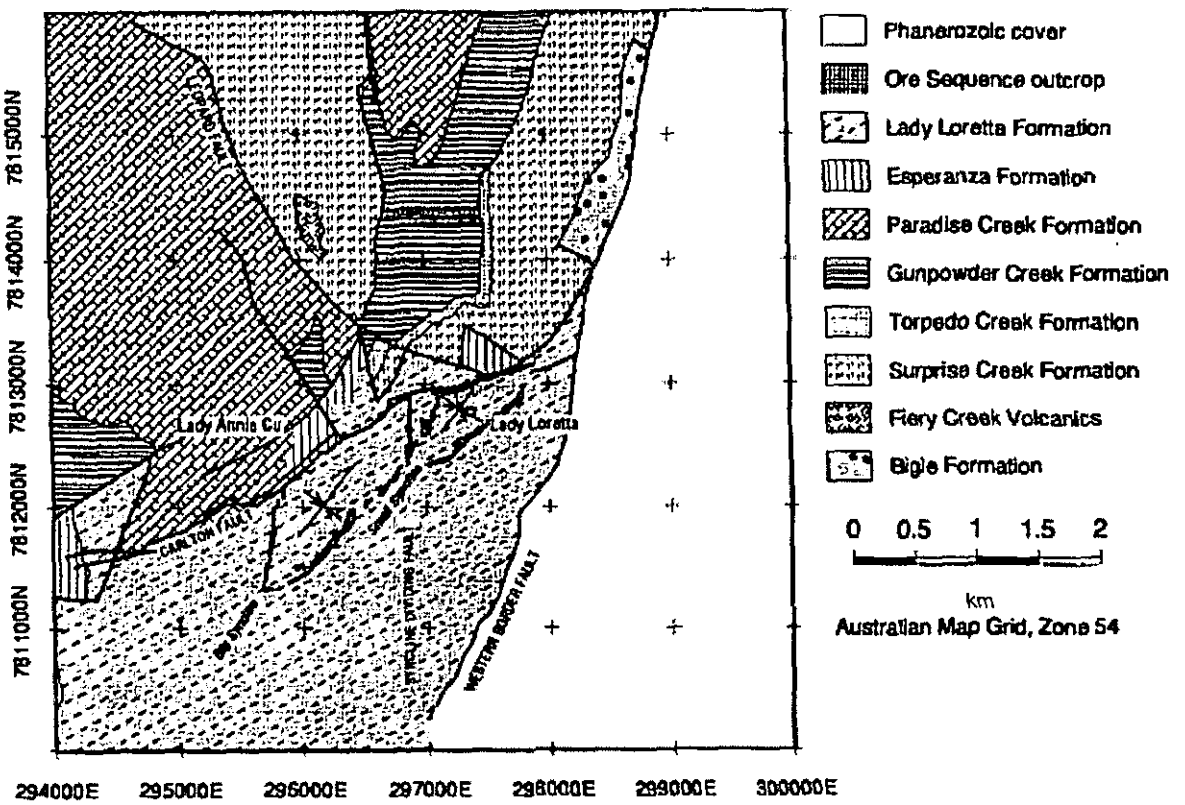

Figure 6.3 Lady Loretta geology, modified after Hutton and Wilson (1985) and unpublished company mapping. "Ore Sequence" refers to the consolidated Ore Horizon and Ore Sediments (see text)

The mineralisation is overlain by more than 220 m of rhythmically layered pyritic siltstone, dolomitic fine-grained sandstone and minor carbonaceous shale. At the base of this sequence is a single very thick (2–15 m, generally 4 m) siltstone/shale depositional cycle known as the Massive Unit (MU). The remainder is designated the Cyclic Unit (CU). The uppermost informal member is the Upper Clastic (UC) unit, a sequence of mainly carbonaceous shale with fine micaceous sandstone and siltstone towards the top. Up to 240 m thick, it is strongly affected by deep surface weathering and has only been intersected by drilling in the Big Syncline (Fig. 6.3).

Most samples obtained for the Lady Loretta petrophysical study were referenced by the original collectors to the stratigraphic scheme described above. Although this stratigraphy has since been revised and superseded (Dunster, 1997), the former designations have been retained for convenience.

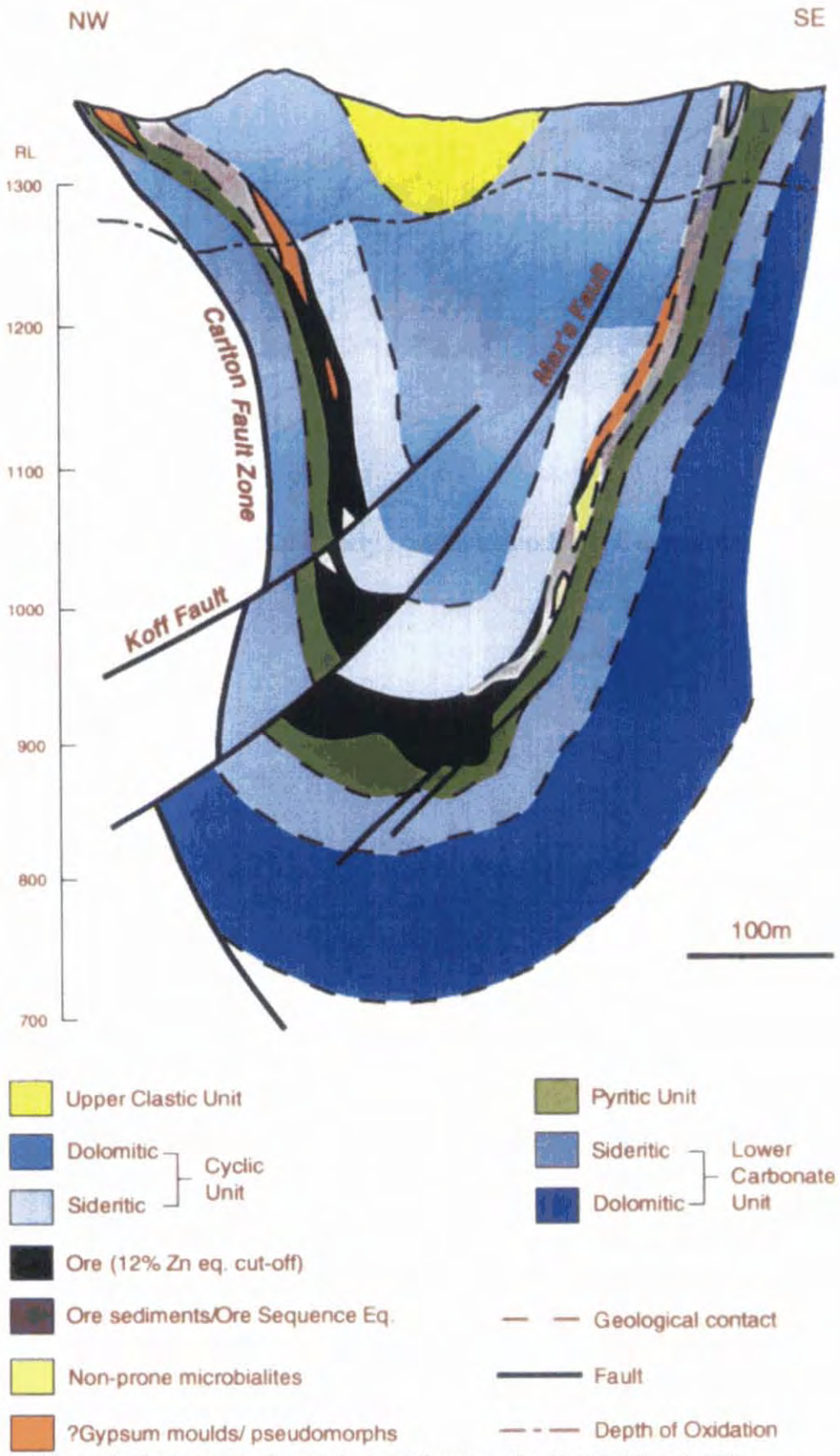

Figure 6.4 A typical cross section through the Small Syncline, after McGoldrick et al., 1997

A series of projected long sections was created to facilitate the visualisation of spatial variations in physical properties within the Lady Loretta deposit, in particular the petrophysical manifestation of the geochemical halo known to envelop it (Large and McGoldrick, 1998). The position of each sample

defined by its downhole depth had been plotted on mine cross section maps showing the drillholes, and the along-hole distance to the nearest significant ore intersection recorded (P. McGoldrick, pers. comm.). This distance was corrected to true'distance-to-ore using the angle of drillhole intersection with the OH, with the base of the OH defined as the vertical datum (being generally a sharper contact than the top). Samples from below the base of the OH were thus assigned negative elevation values in metres. The horizontal coordinate is the Lady Loretta mine grid northing, also in metres. For reference, Fig. 6.4 represents mine section 2300N, which is positioned in the exact centre of the Small Syncline 'syncline' map symbol in Fig. 6.3, and perpendicular to it. The long sections thus purport to represent an unfolded long section of the orebody, with samples projected onto a vertical plane perpendicular to the unfolded strata.

Petrophysical values obtained from each sample were interpolated to a grid using an inverse-distance-weighting algorithm with weight factor of 2 (weight falls off with square of distance). A 400 m (horizontal) x 100 m (vertical) window was employed in order to account for the stratiform geometry of the mineralised system. Sample densities are quite high within a few hundred metres of the OH in the Small Syncline, but fall away with vertical distance away from the orebody, and to some extent to the southwest in the Big Syncline (on the left-hand-side of all long-section diagrams). This has resulted in a number of gridding artefacts in these areas. The area of no data in the centre of long-section diagrams showing both Big Syncline and Small Syncline data (suffixed 'a'in figure numbering) manifests the effect of the Syncline Dividing Fault (Fig. 6.3).

6.4.6.1 Density

Results from density measurements on samples from the Lady Loretta orebody, its halo and host stratigraphy are presented in Figure 6.5. The distribution is clearly bimodal, with the higher peak almost entirely composed of ore of various grades. The sampling bias towards sediments in the ore horizon (McGoldrick, 1993b) has resulted in a downward skew to the frequency distribution of ore horizon samples. Figure 6.5 also suggests that porosity creation is a factor in the observed downward skew of density, probably as a result of reactive pyrite (see below). The median (3.90 t/m^3) probably better represents the bulk density of the in situ ore horizon than the mean. The median is also more in accord with the average for ore of 4.0 t/m^3 obtained by Rivera and Challis (1972) from 24 samples exceeding 10% combined Zn/Pb.

The Pyritic Unit'(PU) at Lady Loretta is somewhat surprisingly not well represented in the higher density peak. This result should be viewed with a little caution because of the poor condition of many of the Lady Loretta pyritic samples, caused by extreme oxidation after exposure to air, with resultant density reduction. Pyrite degradation may also be responsible for the 'Ore Sediment'unit's fairly low density with respect to other sedimentary samples more distant from ore, in which pyrite is rarer and possibly less reactive.

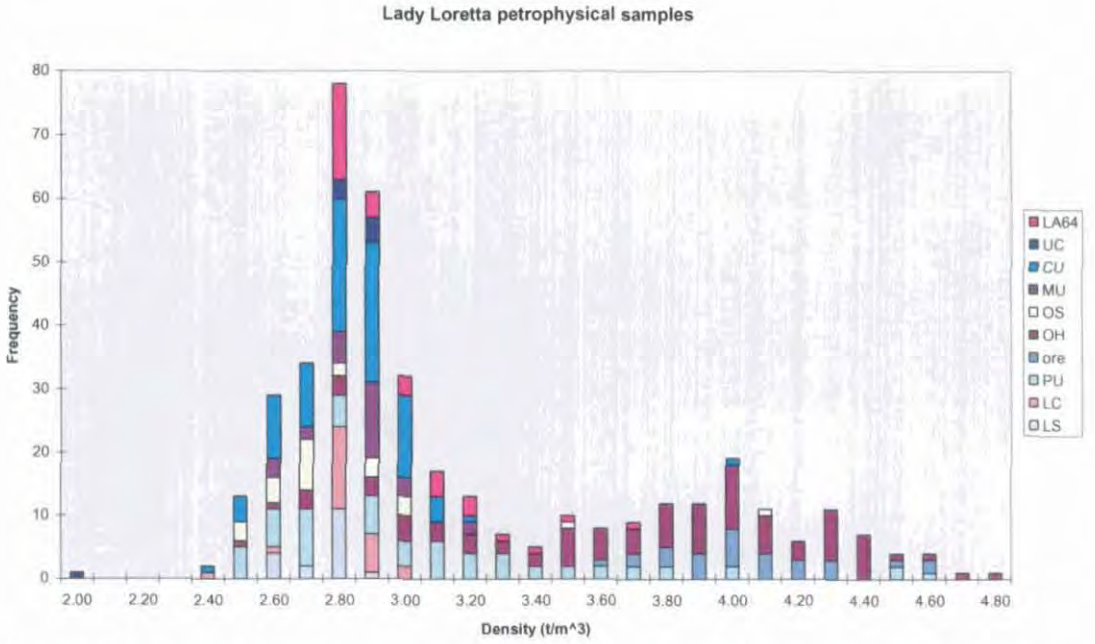

Figure 6.5 Lady Loretta density measurements, classed by mine stratigraphy. 'Ore' refers mainly to material sampled by Aheimer (1994), supplemented with some high-grade material sampled by the author. 'LA64' is a drillhole a few kilometres northeast of Lady Loretta collared in the Cambrian cover east of the Western Border Fault (see text)

Other host units in the mine stratigraphy define the lower peak in the density frequency distribution, centred around 2.80 t/m^3 (Fig. 6.5) and comprising the majority of the sample set. The 'Lower Carbonate' unit, which has dolomite and siderite as dominant constituents, is seen to occupy the higher portions of this non-ore density distribution, with higher densities than the other, more siliciclastic (turbiditic) host units.

Those samples classed as 'LA64' in Fig. 6.5 are from a drillhole of this name into correlates of the Lady Loretta host sequence on the eastern side of the Western Border Fault, west of the deposit. These densities were determined by Emerson (1995) on carbonaceous and/or pyritic shale, which was selectively sampled, other lithologies present being ignored. They are presented in Fig. 6.5 alongside data from Lady Loretta itself to illustrate the density contrast between carbonaceous shale, highly pyritic yet base-metal-poor rock, and Zn-Pb ore.

Generally, as borne out in Figs. 6.6a and 6.6b, the density contrast between the ore and its host rock is seen to be both large and distinct, with host rock largely confined below 3.10 t/m^3 (most are of substantially lower density than this), and ore samples centred around 3.90 t/m^3. Specimens occupying the range between these values are usually the OH or PU samples with an unusually high proportion of sediment referred to above. Anomalously high densities observed apparently stratigraphically well below the OH are probably due to a structural repetition of the PU, which is also visible in the grids depicting many of the other petrophysical parameters.

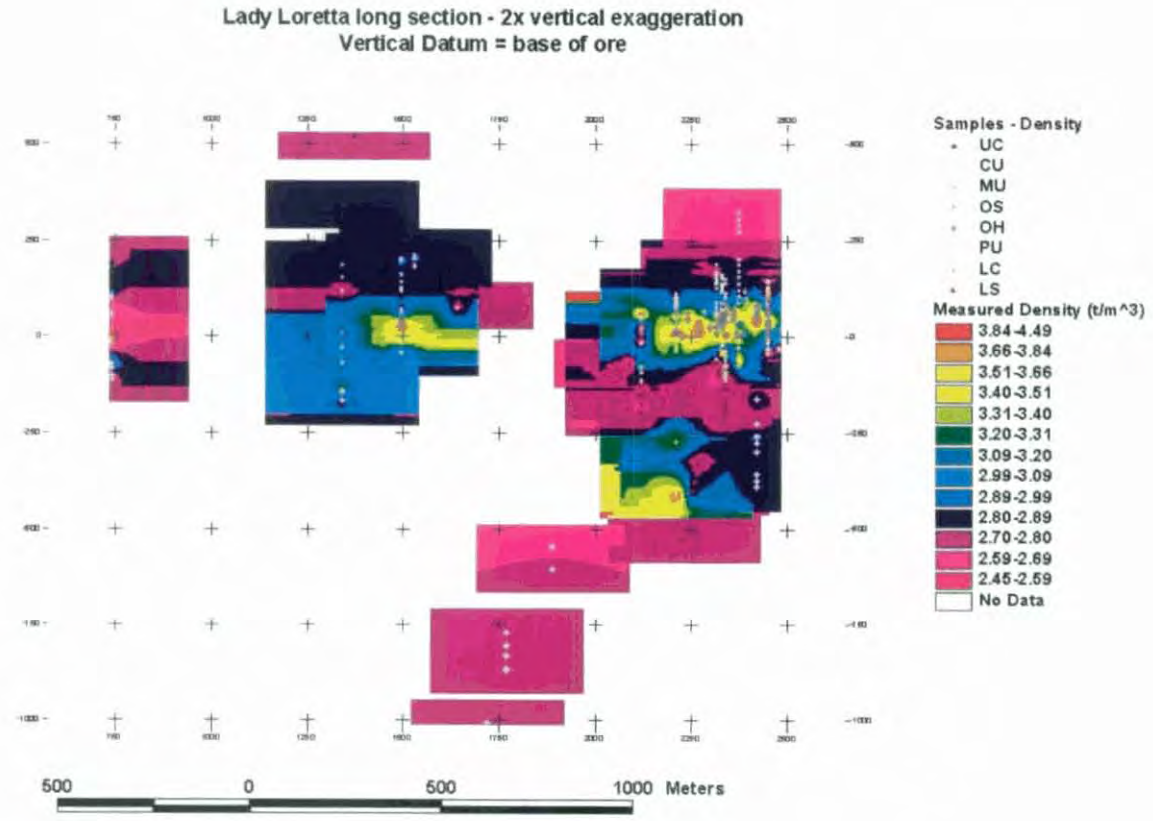

Figure 6.6a Density measurements projected onto Lady Loretta long section and gridded. The same gridding parameters were used in all the following long-section grids (see text)

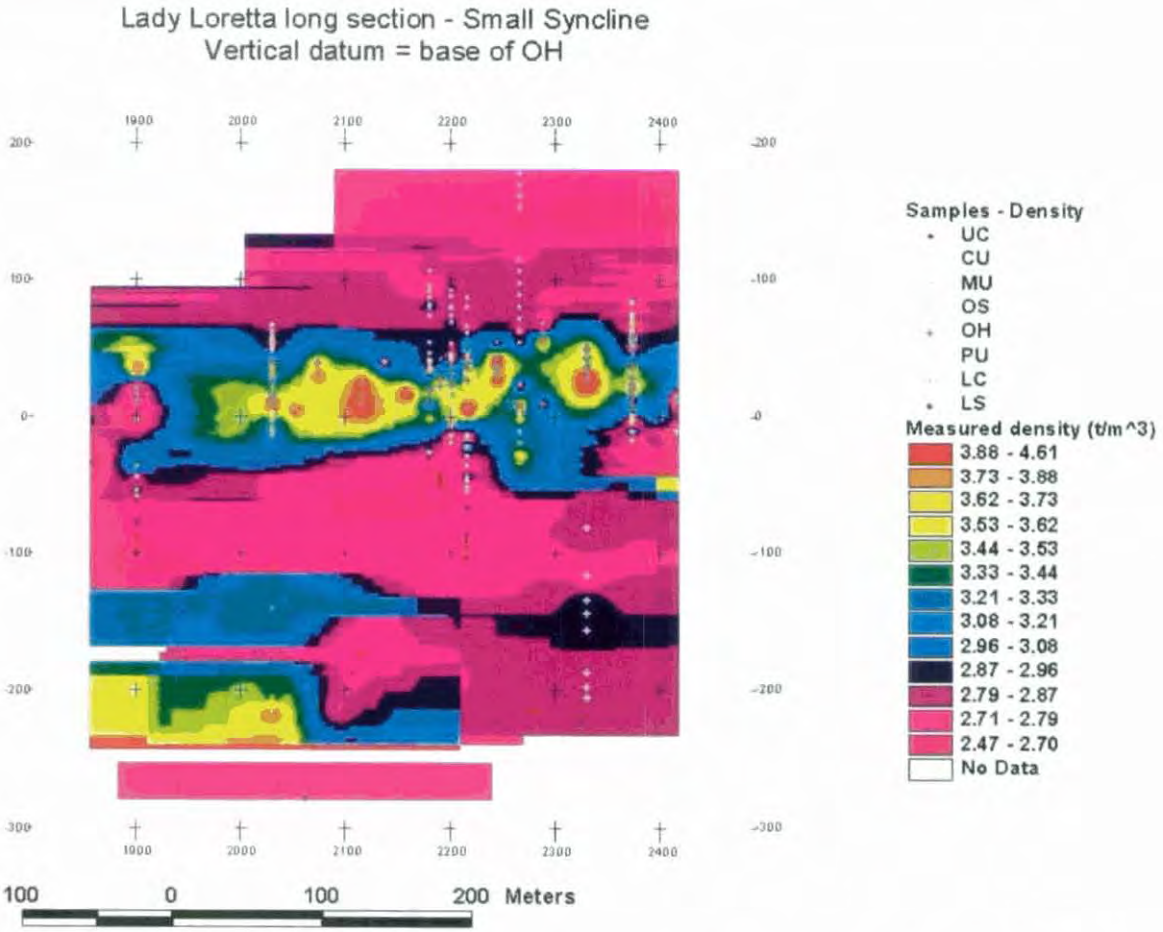

Figure 6.6b Density measurements projected onto Lady Loretta long section and gridded (Small Syncline only)

6.4.6.2 Porosity

Porosity was observed to exert a strong control on the density of host rock samples, but is a less important control on the density of highly sulphidic specimens (Fig. 6.7). The measured values are likely to be overestimates of true in situ values, as the extreme reactivity and consequent oxidation and loss of pyrite in many specimens has created spurious extra porosity. This effect is particularly prevalent in the host units closest to the ore, where pyrite is most prevalent. Interestingly, the more massive pyrite in the Pyritic Unit itself does not appear to be as reactive, and its porosity is consequently lower.

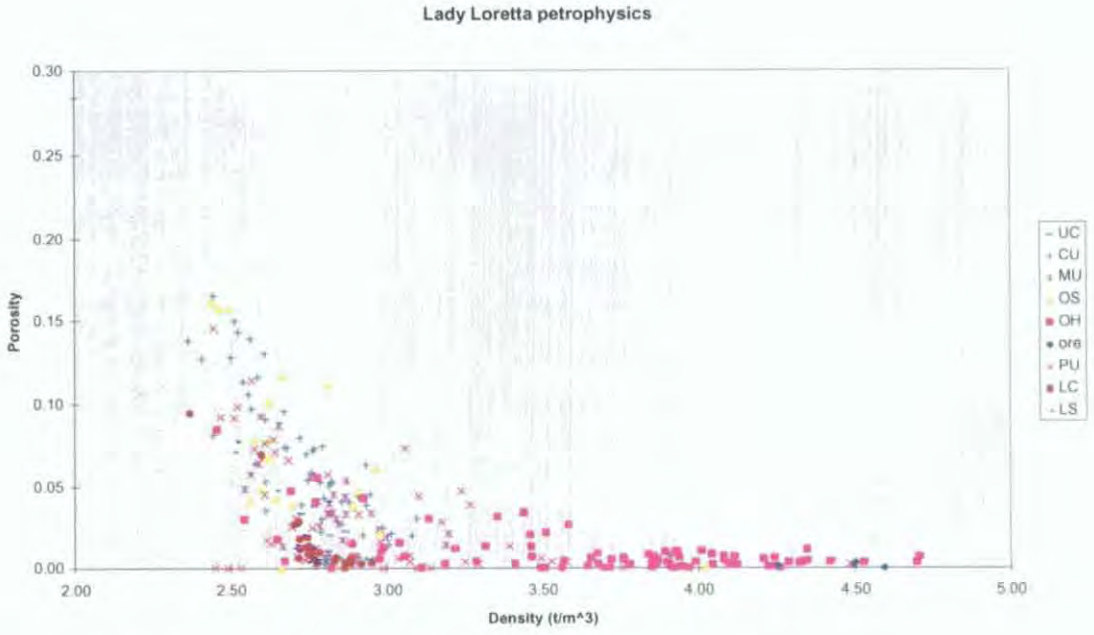

Figure 6.7 Density and porosity measurements, Lady Loretta

6.4.6.3 Magnetic susceptibility

Magnetic susceptibilities at Lady Loretta are confined to low levels (Figs. 6.8-6.10), and by reference to standard diagrams such as Figure 4 of Clark and Emerson (1991) it may be concluded that ferrimagnetic minerals (monoclinic pyrrhotite, magnetite) cannot be present in more than trace amounts. Such magnetic susceptibility levels that are present may be ascribed (in the environs of Lady Loretta) to any or all of: rare iron sulphide species (monoclinic pyrrhotite, smythite, greigite), weakly ferromagnetic minerals such as haematite and paramagnetic minerals; principally siderite with possibly a minor contribution from manganese-bearing ferromagnetic and paramagnetic minerals such as jacobsite, rhodochrosite and psilomelane. Pyrite is virtually non-magnetic (Table 1 of Clark, 1997).

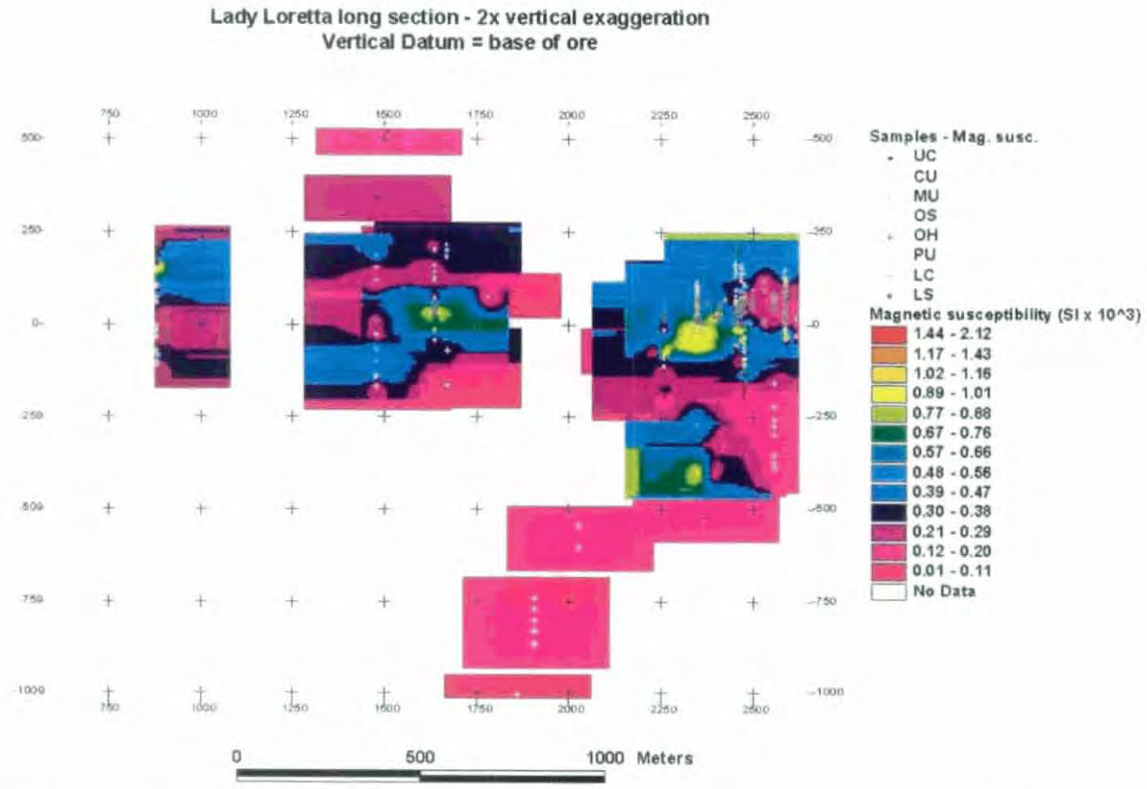

Figure 6.8a Magnetic susceptibility measurements projected onto Lady Loretta long section and gridded

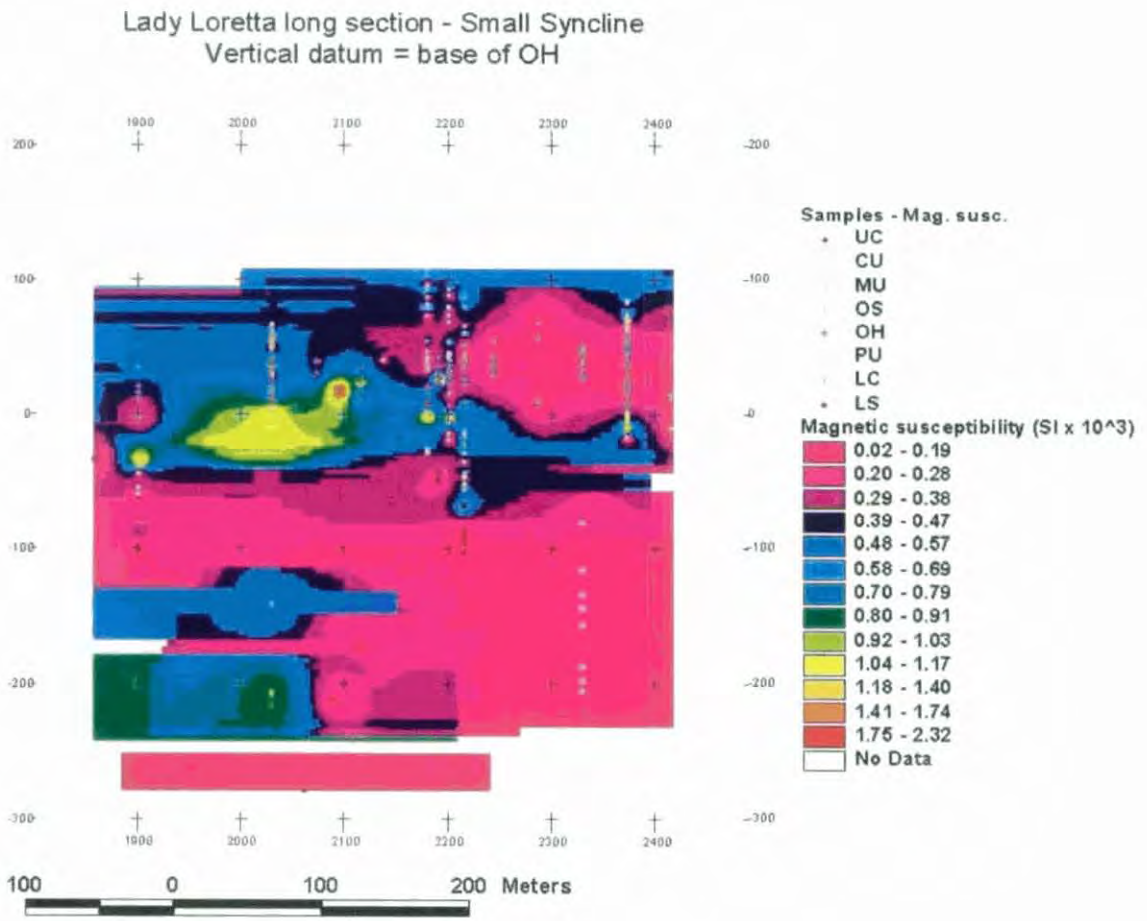

Figure 6.8b Magnetic susceptibility measurements projected onto Lady Loretta long section and gridded (Small Syncline only)

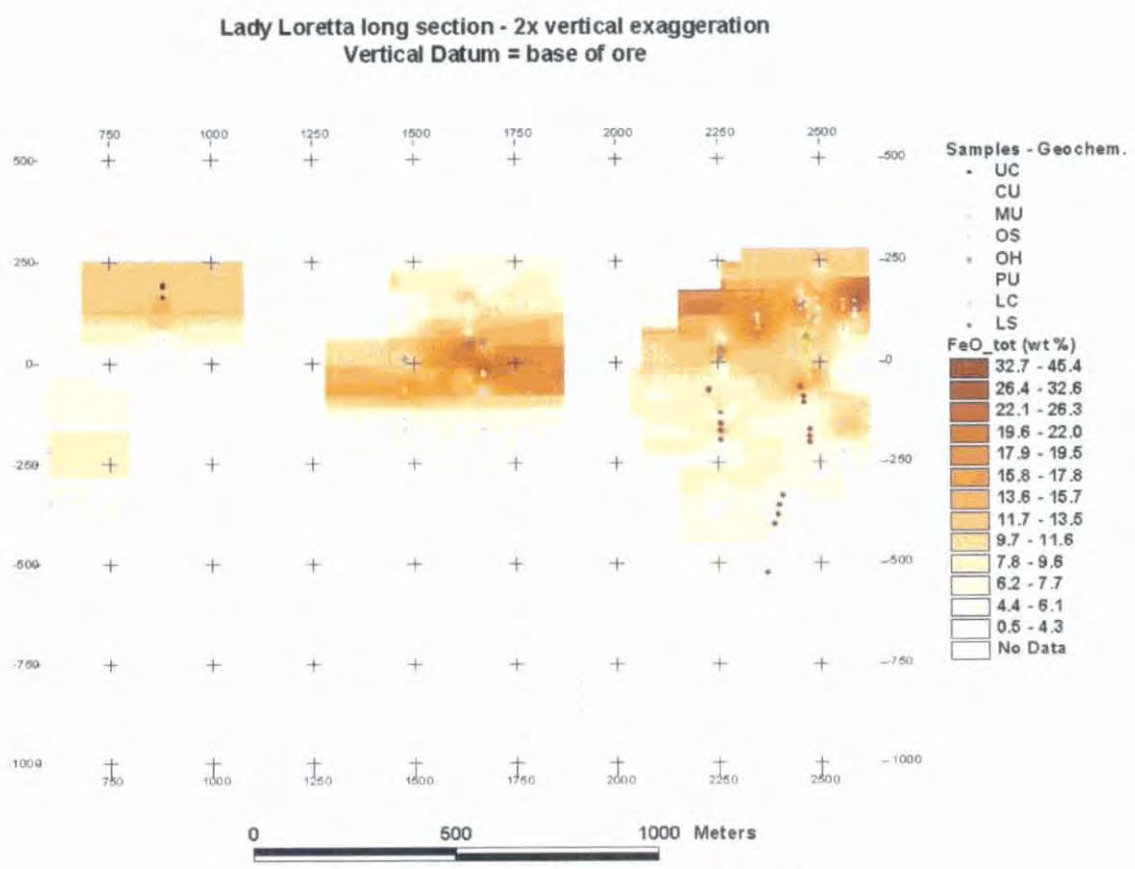

Figure 6.9a FeO_{tot} measurements projected onto Lady Loretta long section and gridded

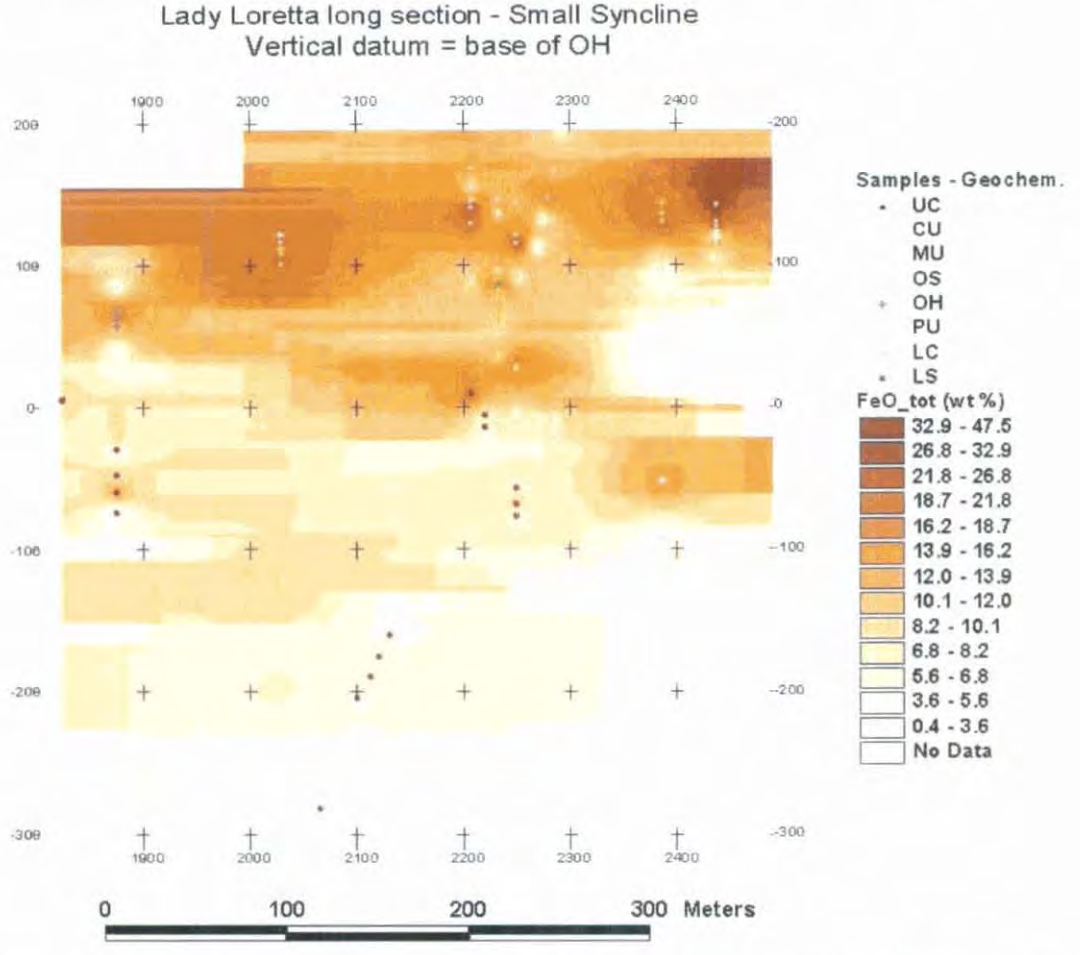

Figure 6.9b FeO_{tot} measurements projected onto Lady Loretta long section and gridded (Small Syncline only)

Accordingly, the fact that magnetic susceptibility in Lady Loretta base metal ore is highly variable, but ranges between 0 and 2.50 x 10^{-3} SI, is interpreted in terms of variation in non-pyrite Fe-bearing mineral concentration, following Puranen (1989, quoted in Clark 1997). An exception to this general relationship is observed within the orebody itself, where the presence of high concentrations of diamagnetic ore minerals and the occurrence of iron almost exclusively as pyrite both result in subdued magnetic susceptibility, particularly in the barite-sphalerite facies at the north-eastern end of the mine. More broadly, magnetic susceptibility levels observed are slightly higher than those measured in the Lady Loretta Formation regionally (see chapter 5), reflecting the anomalous concentration of Fe around the mine. This also explains why the Pyritic Unit is the most magnetic of all the units in the local mine stratigraphy (Fig. 6.10, 3.65), though it must be emphasised that pyrite itself was avoided in sampling, as discussed earlier. Other units usually remain at low levels of magnetic susceptibility (< 0.35 x 10^{-3} SI), with excursion to higher levels (most frequently observed in the 'Cyclic' and 'Massive' units) invariably due to the presence of relatively rare Fe-bearing (usually siderite) patches. Overall, there is a clear halo of higher magnetic susceptibility associated with the mineralised system (Figs. 6.8-6.9).

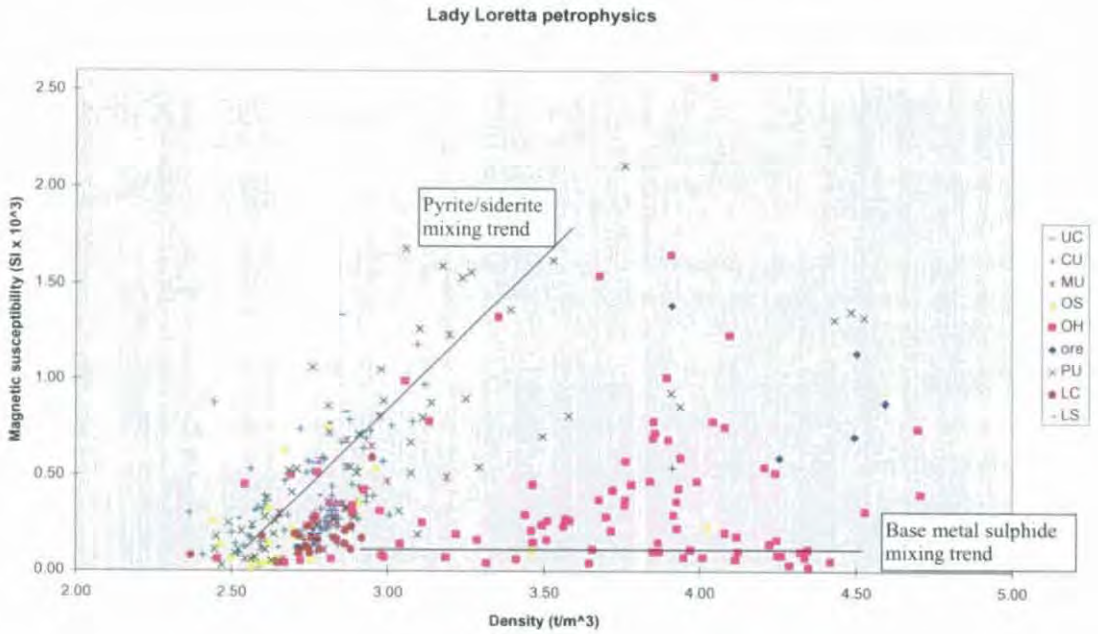

Figure 6.10 Density and magnetic susceptibility measurements, Lady Loretta

6.4.6.4 Velocity

Few contrasts between local stratigraphic units are apparent from raw velocity measurements, the exceptions generally being carbonates, which tend to have higher velocities than the norm, or base metal rich specimens, which are inclined to be of lower velocity. Contrasts between the various units are most apparent in density-velocity space (Fig 6.12), in which differently composed units are seen to have distinctly different density-velocity relationships. These differences are particularly marked in the case of sulphide-bearing units. Base metal sulphidic samples overall have slight negative correlation between density and velocity, in alignment with the trend connecting pure sphalerite (4.0 t/m ^{3}, 5100 m/s) and pure galena (7.5 t/m^3, 3100 m/s) shown in Emerson and Yang (1997), albeit with some contaminating influences from gangue material such as barite, quartz and sedimentary material, and minor porosity.

Figs. 6.11a and 6.11b both demonstrate the negative effect which sulphide minerals have on velocity, as velocities are broadly depressed in the vicinity of the ore body.

Acoustic impedances were calculated for all samples from which velocity measurements were obtained, and these are presented in Figure 6.13. Those units containing ore-grade base metal samples (ore, OH) clearly have a significant positive impedance contrast with their host sedimentary units, far exceeding the magnitude of the (expected) impedance contrast between carbonate- and siliciclastic-dominated groupings, such as the Lower Carbonate and Lower Siltstone. Assuming reasonable exploration depths and seismic wave parameters for this geological environment (5000 m/s velocity, 100 Hz dominant frequency), stratiform bodies greater than 12.5 m thick should be resolvable, according to the Rayleigh limit. It is therefore concluded that Lady Loretta-style mineralisation of economic size and burial depth should be relatively easily detected by reflection seismic methods in the Carpentaria Zinc Belt.

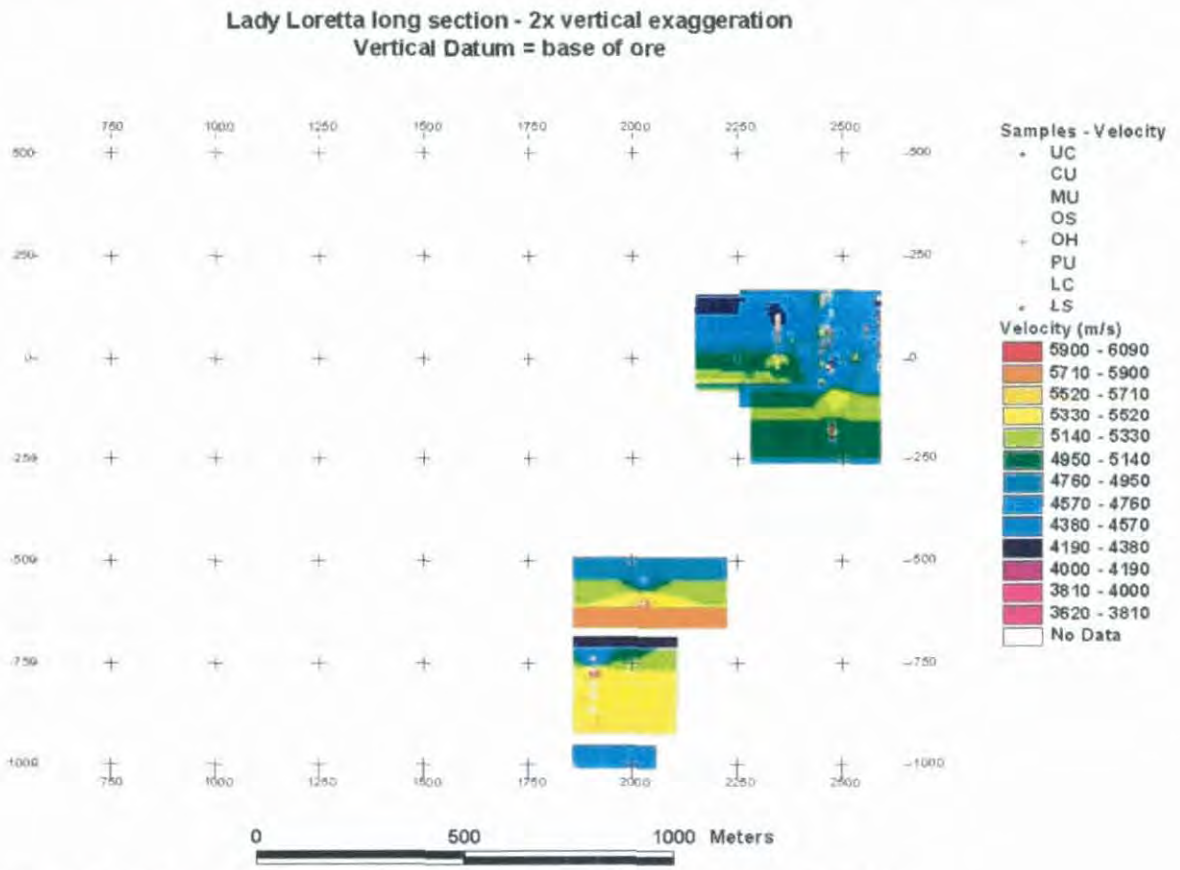

Figure 6.11a Velocity measurements projected onto Lady Loretta long section and gridded

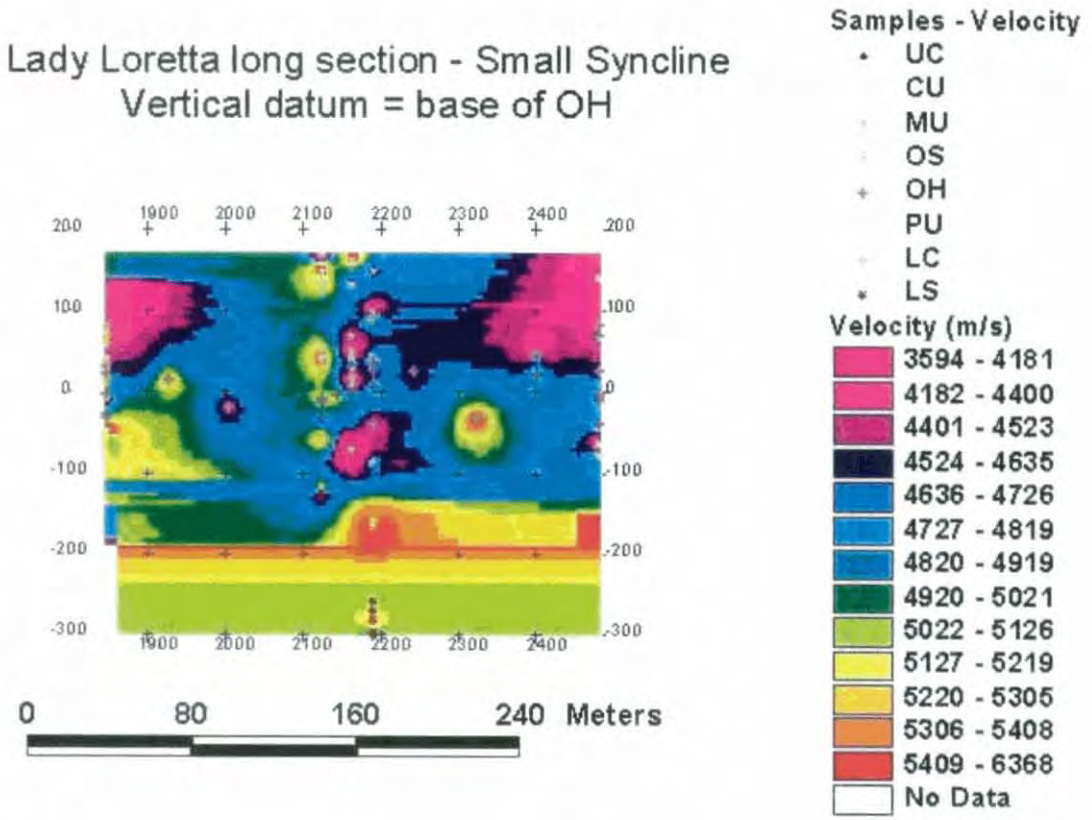

Figure 6.11b Velocity measurements projected onto Lady Loretta long section and gridded (Small Syncline only)

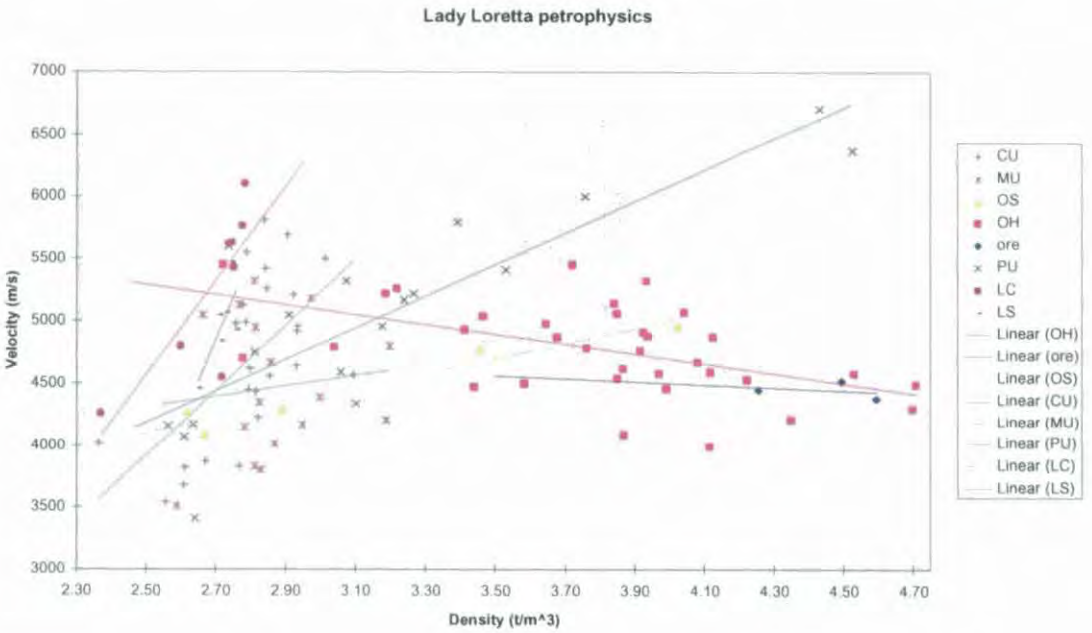

Figure 6.12 Density and velocity measurements with calculated lines of best fit, Lady Loretta

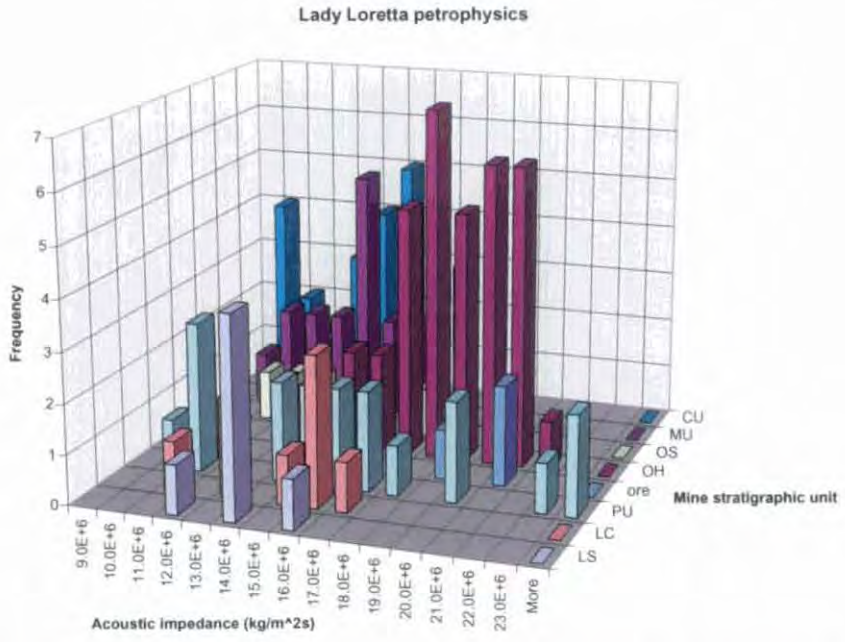

Figure 6.13 Acoustic impedance calculated from density and velocity measurements, Lady Loretta

6.4.6.5 Resistivity

Resistivities spanning over five orders of magnitude have been measured on Lady Loretta samples, even within individual local stratigraphic units such as the Ore Horizon and Pyritic Unit (Figs. 6.14-6.15). The bulk of host rock resistivities tend to lie in the middle of this range (Fig. 6.15), and it is particularly notable that resistivities of the highest grade ore samples (blue in Fig. 6.15) are essentially the same as those of the host siliciclastics. Resistivities in carbonate-dominant samples are up to tenfold greater than in unmineralised sediments where dolomite is uncommon or absent. Overall, geometric means and medians of the sulphidic units (~240-420 Ωm) are only very slightly lower than those of the host units (~450-550 Ωm), a difference which is dwarfed by the variance and total overlapping range observed in both groupings (Figs. 6.14a-6.14b). Even the lowest resistivities observed, in samples rich in pyrite and/or galena, do not have as great a contrast with the siliciclastic host units as values given in standard texts such as Telford et al. (1990) would suggest. This would suggest the presence of fractures or insulating minerals such as sphalerite interrupting current flow even in quite massive sulphides, or conductive materials (possibly graphite and trace sulphides) in the host rock, or both. Further investigation of this issue is warranted, but beyond the scope of this study. It may be concluded that positive direct detection of a Lady Loretta ore signature relying solely on resistivity techniques is likely to be difficult.

Resistivity is quite variable laterally as well as across local mine stratigraphy (Figs. 6.14a, 6.14b). Lateral variability in resistivity is particularly apparent between the barite-sphalerite facies at the north-eastern end of the ore body and the more galena- and pyrite-rich (barite absent) portions to the south-east.

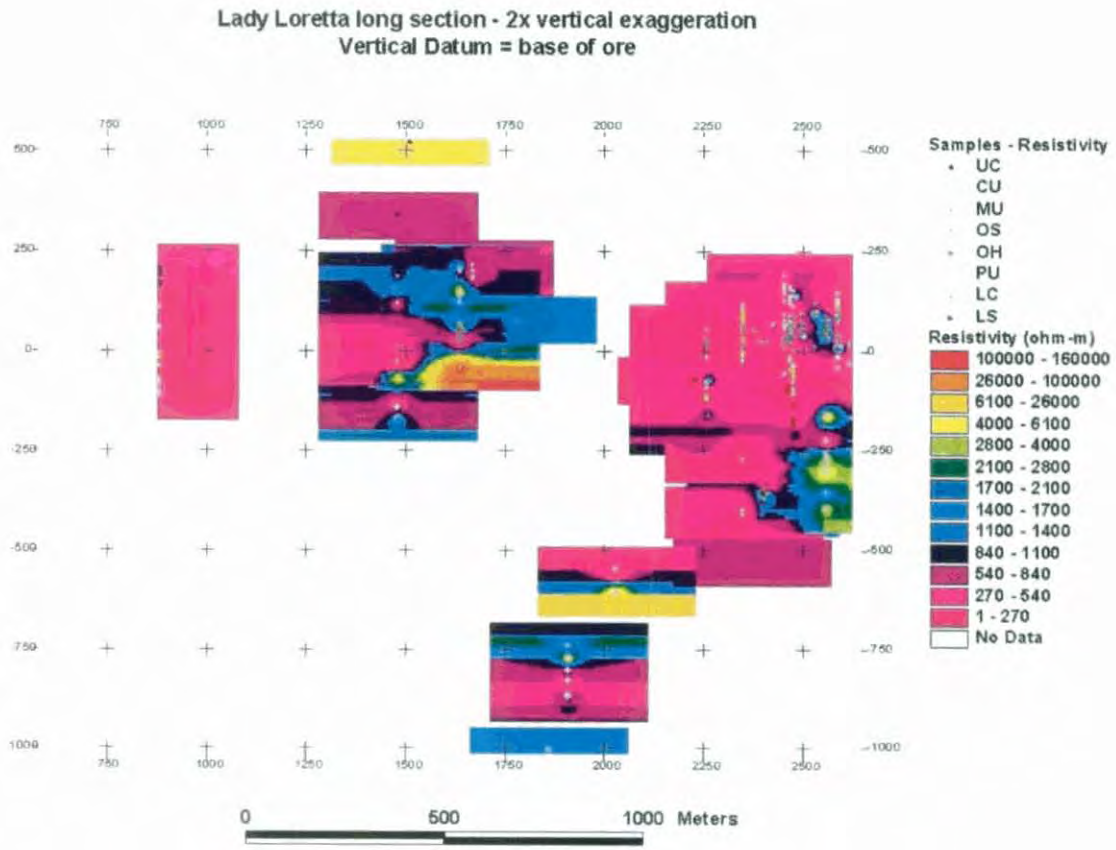

Figure 6.14a Resistivity measurements projected onto Lady Loretta long section and gridded

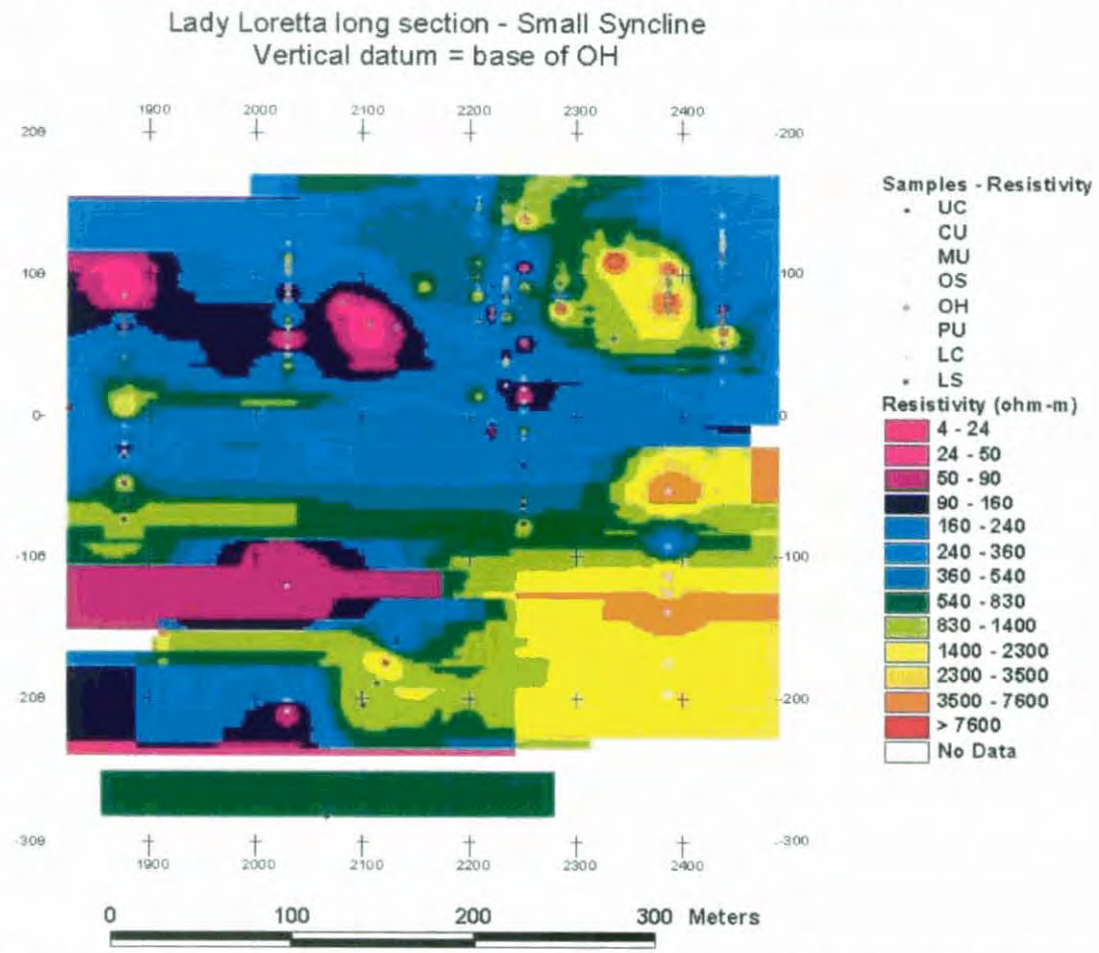

Figure 6.14b Resistivity measurements projected onto Lady Loretta long section and gridded (Small Syncline only)

Crossplots with respect to density give much insight into the various controls on resistivity properties (Fig. 6.15). The very wide range observed in the sulphide-bearing units is seen to be the result of a number of competing influences from different compositional components of the Lady Loretta mineralised system. Of the unmineralised host units, it may be seen that the higher resistivities (> 1000 Ωm) tend to be associated with higher densities, as would be expected in dolostones. Samples consisting mainly of siltstone and shale are largely responsible for the host rock resistivities observed between 100 and 1000 Ωm, with the spread in densities between 2.25 and 2.90 t/m^3 apparent in this field probably controlled by porosity. A stronger negative correlation between density and resistivity within this field is thus likely to become apparent in the case of more saline pore fluid.

In the mineralised system, the presence of pyrite and galena tends to drive resistivities lower, accompanied by strongly elevated density. A rise in resistivity up to almost 2000 Ωm as 4.0 t/m^3 is approached is interpreted as mapping increased sphalerite concentration. Very high resistivities observed in the Ore Horizon are almost invariably observed in samples consisting mainly of barite and sphalerite. Dilution of barite by pyrite and galena results in elevated density and greatly reduced resistivity, while the presence of sediment in the barite-rich samples has marked effects on density and depresses resistivity by around an order of magnitude. The high resistivity/low density samples from the Pyritic Unit and Ore Horizon are highly cherty or otherwise silicified.

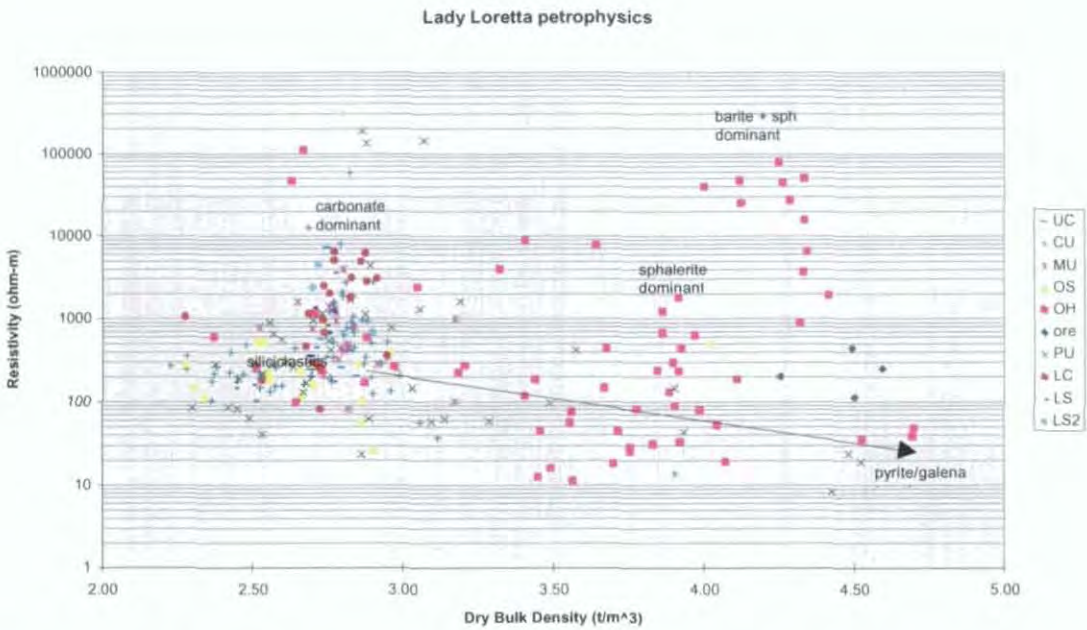

Figure 6.15 Density and resistivity measurements with interpreted mineral end-member influences, Lady Loretta

A plot of resistivity against magnetic susceptibility (Fig. 6.16) is instructive for its insight into iron geochemistry at Lady Loretta. The weakness of the negative correlation between magnetic susceptibility and resistivity (R = -0.26; Table 6.1) is consistent with pyrite being the dominant Fe phase at Lady Loretta, but the existence of the correlation suggests that other iron sulphides may be exerting some control on magnetic susceptibility through much of the mineralised system.

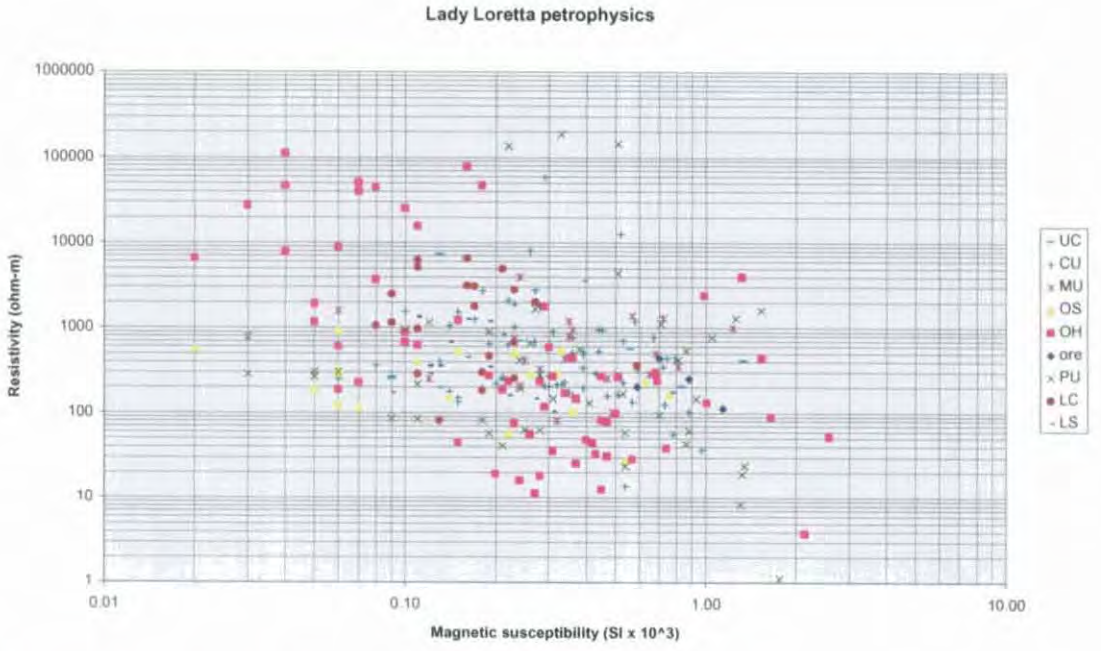

Figure 6.16 Magnetic susceptibility and resistivity measurements, Lady Loretta

6.4.6.6 Chargeability

Most highly chargeable Lady Loretta samples are from within the OH, but this association is far from uniform (Fig. 6.17). A significant number of high (>10 IP%) IP% values are also observed outside the OH, particularly in the footwall. There are also significant lateral chargeability variations within the local Lady Loretta stratigraphic units, especially the OH. Some of the highest IP% values were measured on OH samples in the Big Syncline (southwest/left of 2000E in Fig. 6.17a), where base metal mineralisation is much reduced in comparison to the Small Syncline. Conversely, chargeabilities are subdued in substantial sections of the Small Syncline, particularly towards the northeastern end (right of 2320E in Fig. 6.17b) where the OH assemblage mainly comprises barite and sphalerite.

Figures 6.18-6.20 depicting IP properties against density, magnetic susceptibility and resistivity respectively confirm that, as expected, sulphide-bearing units tend to be more chargeable than the more barren rocks of the Lady Loretta halo. This grouping is far from clear-cut, however, as a significant minority of host rock unit samples overlap with the range (> 10 IP%) occupied by many ore horizon and pyritic unit samples.

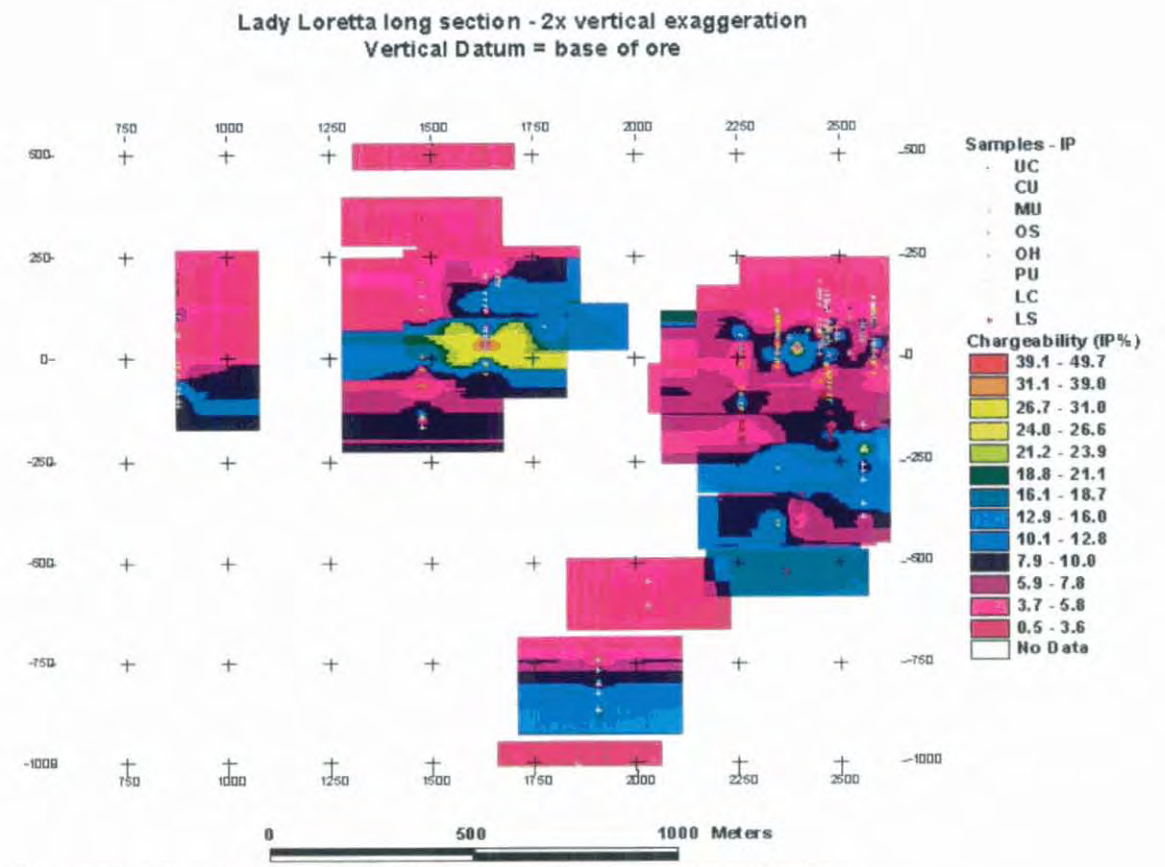

Figure 6.17a IP measurements projected onto Lady Loretta long section and gridded

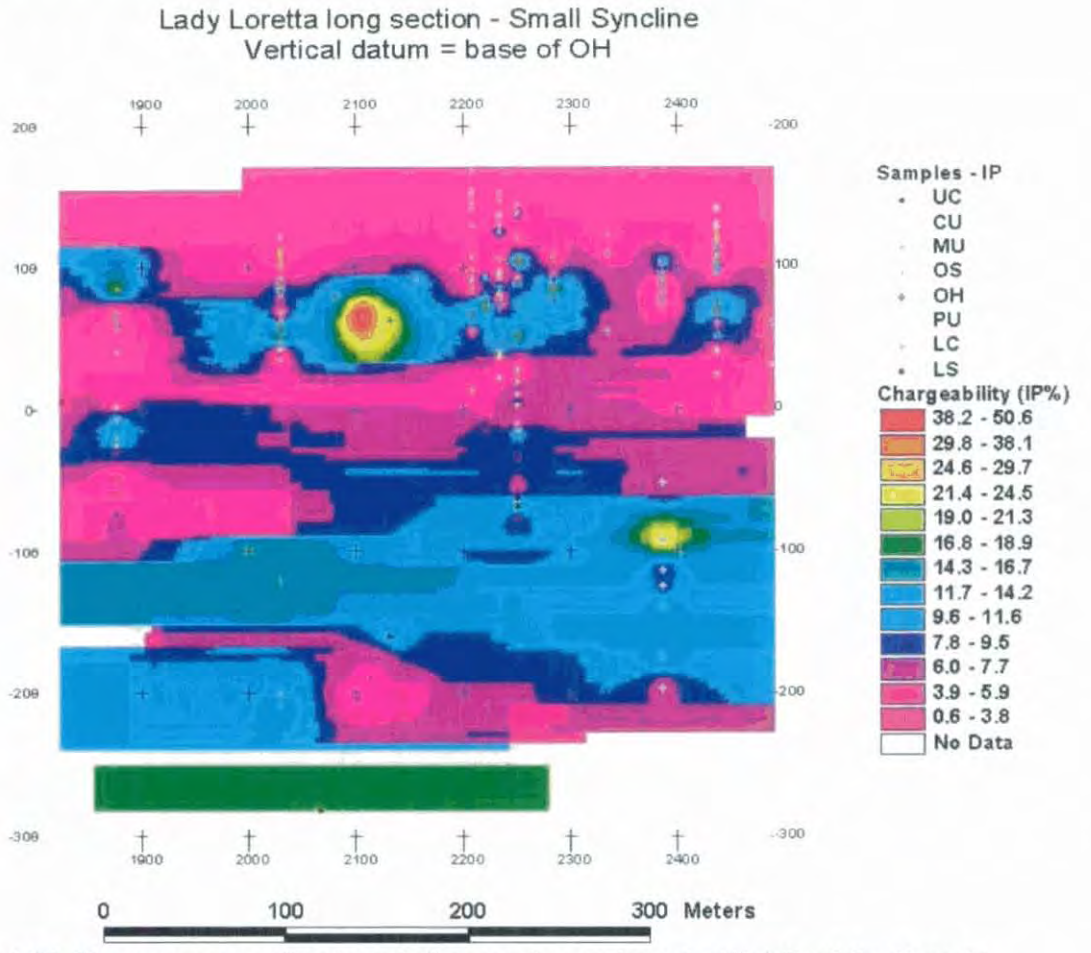

Figure 6.17b IP measurements projected onto Lady Loretta long section and gridded (Small Syncline only)

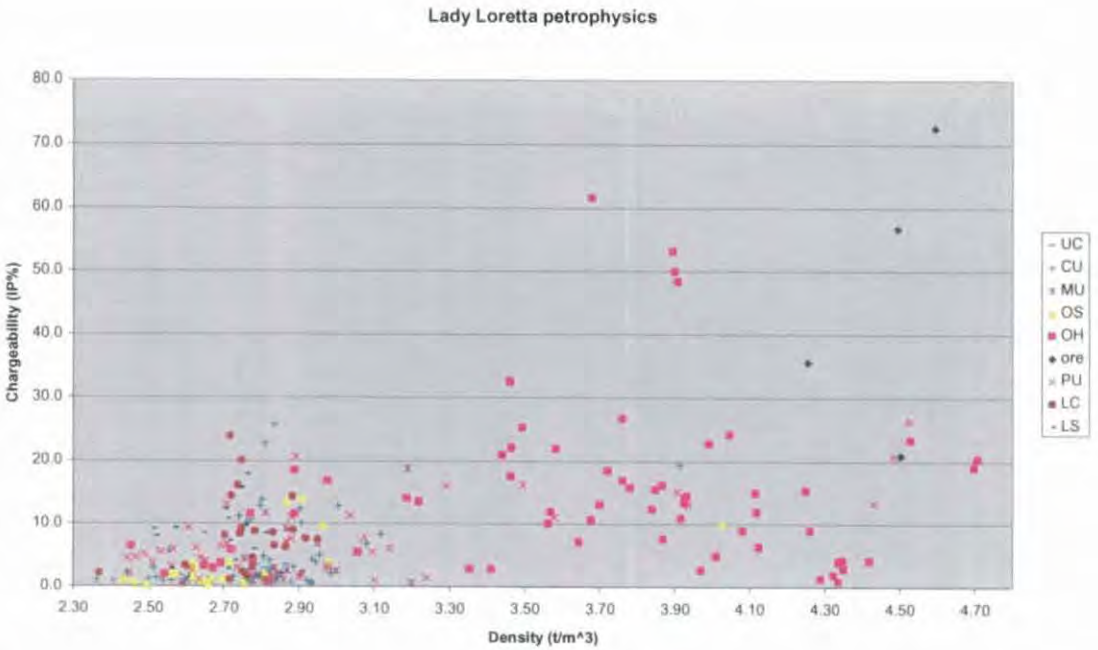

Figure 6.18 Density and IP measurements, Lady Loretta

Most of the OH samples with anomalously low chargeability (<5 IP%) consist largely of barite, though some of these also contain some sphalerite. Chargeabilities exceeding 15 IP% are more typical of the OH though, strongly associated with the presence of galena, pyrite and sphalerite. In a similar vein, low IP% samples nominally from the PU are in fact siltstones, while samples with more typical PU composition (i.e. highly pyritic) have higher chargeabilities, of the order of 10 IP% and higher. Bulk in situ chargeabilities of the PU unit may well be higher, as many of the less chargeable non-siltstone PU samples are those which have clearly suffered the post-extraction oxidisation discussed in section 6.4.6.1 (which is why these low IP% PU samples have correspondingly lower density).

High chargeabilities are not unknown in the nominally sedimentary host units (LS, LC, OS, MU, CU, UC) but where present are usually in samples containing visible percentage levels of pyrite. As may be seen in the corresponding sample density, this sulphide concentration may not necessarily be high, and in fact a few highly chargeable samples contain no visible sulphides, but are merely siltstones and shales, often with carbonaceous material. No carbonaceous material was noted in samples with chargeabilities less than 5 IP%.

One of the influences on IP properties may be seen in Fig. 6.19, where a mild positive correlation between magnetic susceptibility and IP% is interpreted as denoting the influence of trace paramagnetic and possibly ferromagnetic Fe sulphides in what are generally ore- or pyrite-rich samples. A separate field of uniformly low chargeability is interpreted as representing samples in which magnetic susceptibility is controlled entirely by non-polarisable Fe- and possibly Mn-bearing minerals, mainly siderite and haematite. The presence of base metals appears to have a cumulative effect with pyrite on IP properties, resulting in quite good separation between ore/OH and PU samples in Fig. 6.19.

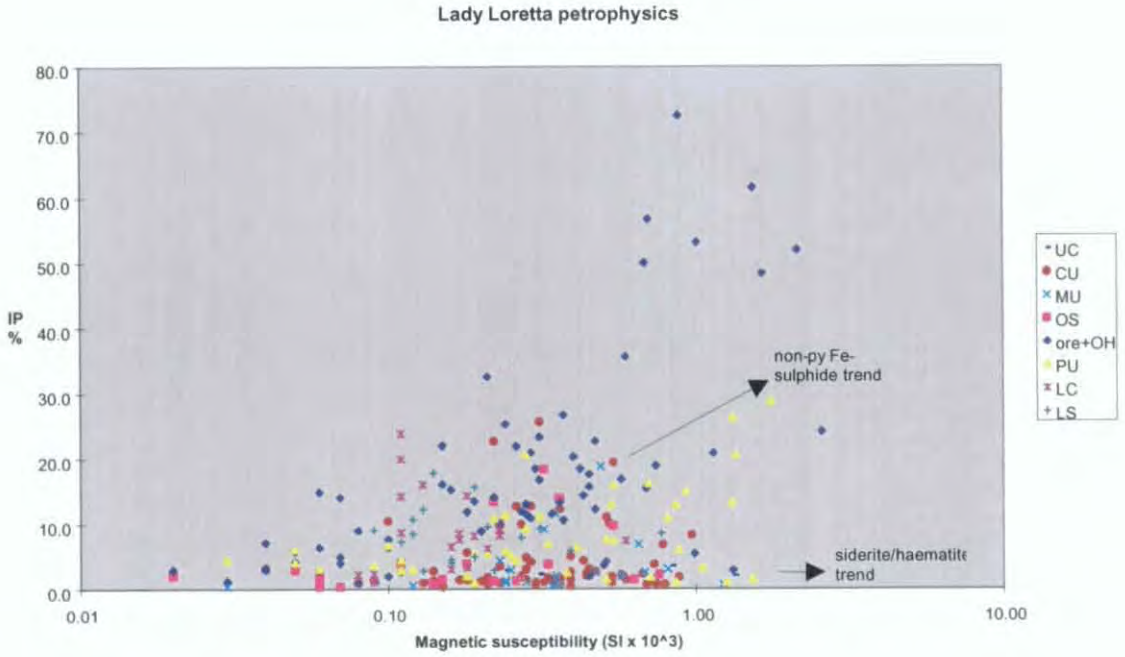

Figure 6.19 Magnetic susceptibility and IP measurements, Lady Loretta

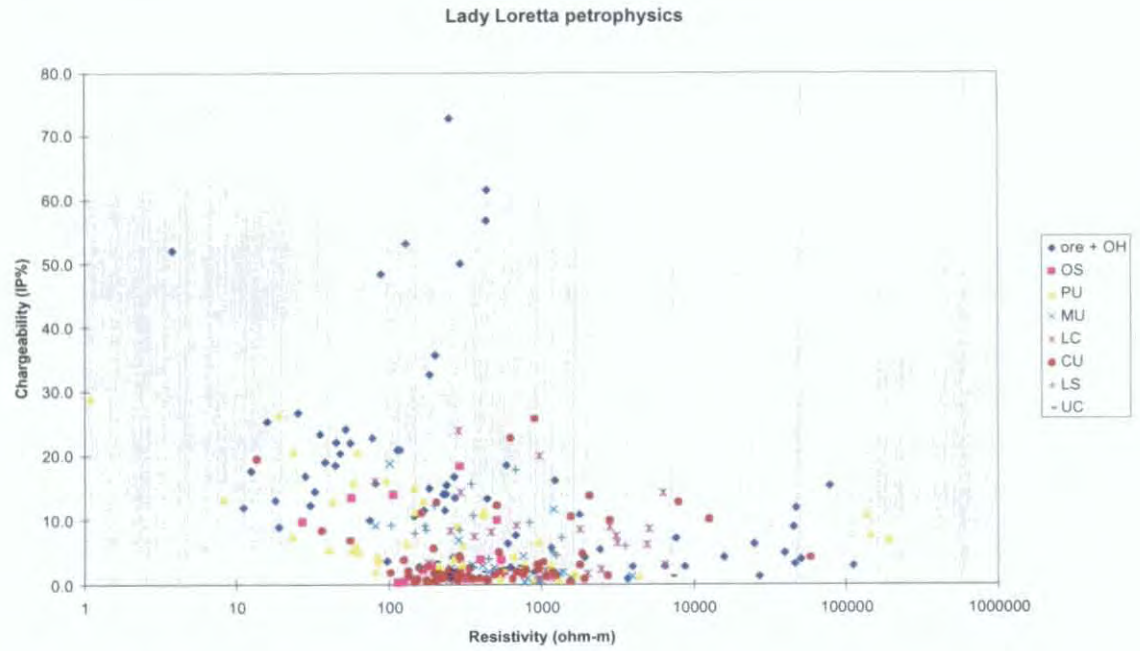

Figure 6.20 Electrical property measurements, Lady Loretta

Galvanic electrical properties of the Lady Loretta sample set are presented in Fig. 6.20. The main feature of note is the correlation between resistivity and IP%: reasonable in PU samples, but fairly weak to non-existent in the other units.

6.4.6.7 Physical property summary, mine stratigraphic units

	Porosity	*SG sat*	*Susc.*	*Velocity*	*Resistivity*
SG sat	-0.57	1.00			
Susc.	-0.02	0.16	1.00		
Velocity	0.03	-0.54	0.02	1.00	
Resistivity	-0.13	-0.01	-0.26	-0.04	1.00
IP%	-0.21	0.27	0.58	-0.24	-0.26

Table 6.1 Property correlation coefficients, Lady Loretta ore

Table 6.1 reflects to some extent the influence of sulphide minerals on the physical properties of rocks in the Lady Loretta mine environment. This influence is most marked in the case of density and velocity, and to a lesser degree in the weak correlation between density and chargeability. As discussed above, the correlation between susceptibility and chargeability is mostly attributed to pyrite.

The following tables (Tables 6.1-6.9) and diagrams (Figs. 6.21-6.25) statistically summarise the data presented above in terms of the local stratigraphic units, in order that conclusions may be drawn regarding their bulk properties.

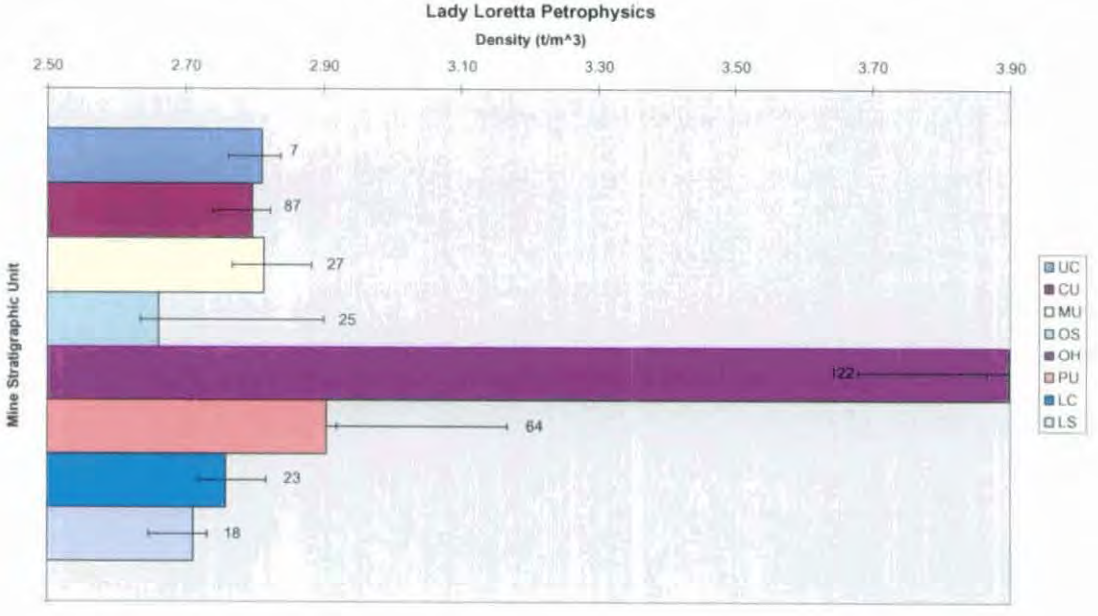

Figure 6.21 Density of Lady Loretta mine units. Coloured boxes denote median values; whiskers indicate confidence intervals (95% level) about the mean. Number of samples shown next to bar

Base metal ore at Lady Loretta clearly manifests a strong positive density contrast with the surrounding rock, not excluding that of the pyritic unit (Fig. 6.21; Tables 6.2-6.9). The median density value of the PU is only slightly elevated above the other host units, in which sulphide is less common.

There is some support in Fig. 6.21 for Dunster's (1997) redefinition and simplification of the local mine stratigraphy as consisting only of the ore sequence, contained wholly within a pyritic unit, with two predominantly clastic units ('Cyclic Unit'and 'Upper Clastic Unit'above the pyritic unit and a carbonate unit below it.

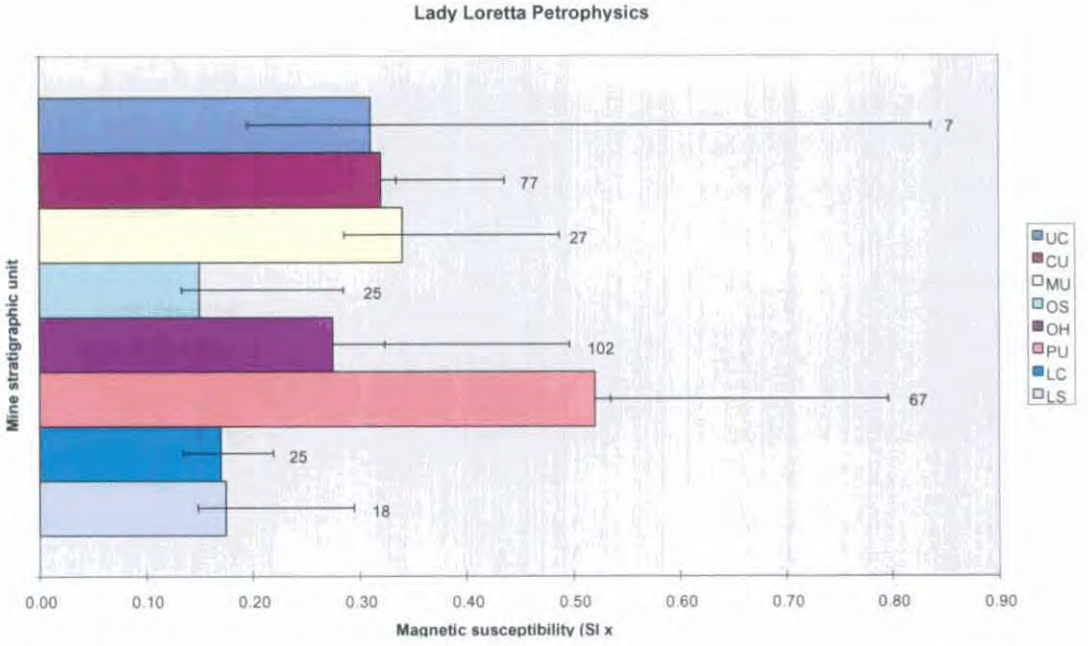

Figure 6.22 Magnetic susceptibility of Lady Loretta mine units. Coloured boxes denote median values; whiskers indicate confidence intervals (95% level) about the mean. Number of samples shown next to bar

The pyritic unit is the only clearly distinguishable one in the vicinity of Lady Loretta on the basis of magnetic susceptibility (Fig. 6.22; Tables 6.2-6.9). There is a suggestion that units above the ore body tend to be more magnetic than those below. At these very low levels, none of these contrasts in magnetic properties between the individual units are likely to be significant in an exploration sense except possibly to downhole, drillcore and detailed ground surveys. Taken as a whole, the general ore body environment may theoretically be detectable to high resolution, low level airborne surveys, but in practice would be extremely difficult to distinguish from geological and other noise. The logarithmic nature of the distribution is indicated by the consistent skewing of the confidence intervals upwards from the medians.

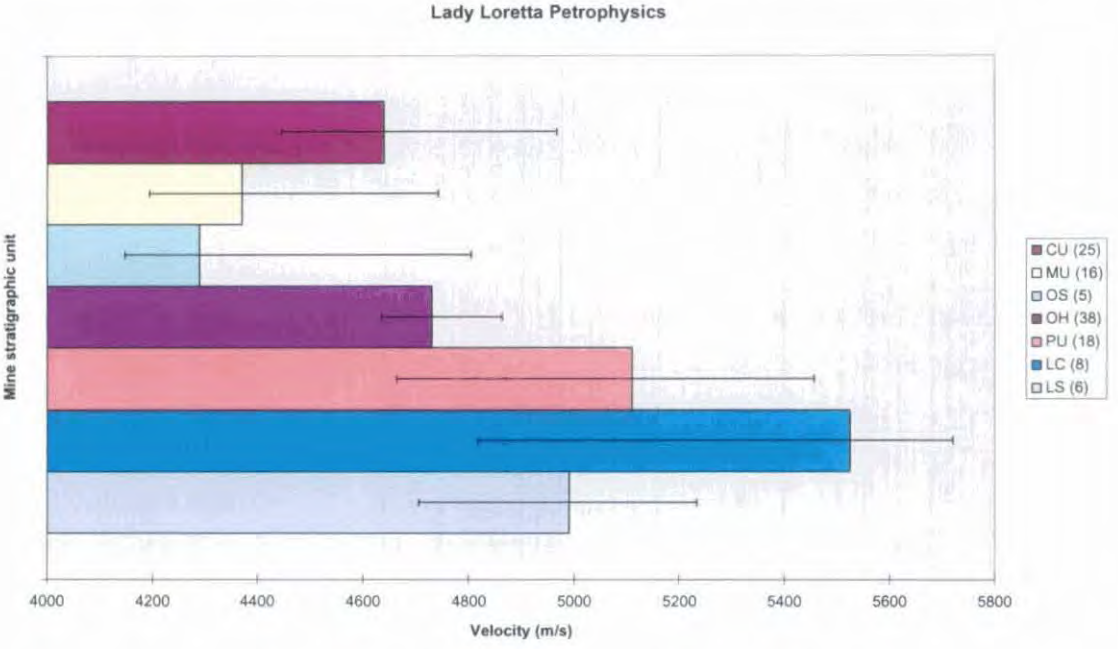

Figure 6.23 Velocity of Lady Loretta mine units. Coloured boxes denote median values; whiskers indicate confidence intervals (95% level) about the mean. Number of samples in brackets in legend

Velocities are clearly depressed in the vicinity of the orebody at Lady Loretta (Fig. 6.23). The presence of carbonaceous material in the Upper Carbonaceous unit also appears to have caused lower velocities in this unit, in comparison to the more typical Lady Loretta Formation values observed in the lower carbonate and siltstone units. The latter also serve to demonstrate the general velocity contrast between carbonate-dominated (higher) and siltstone-dominated (lower) samples.

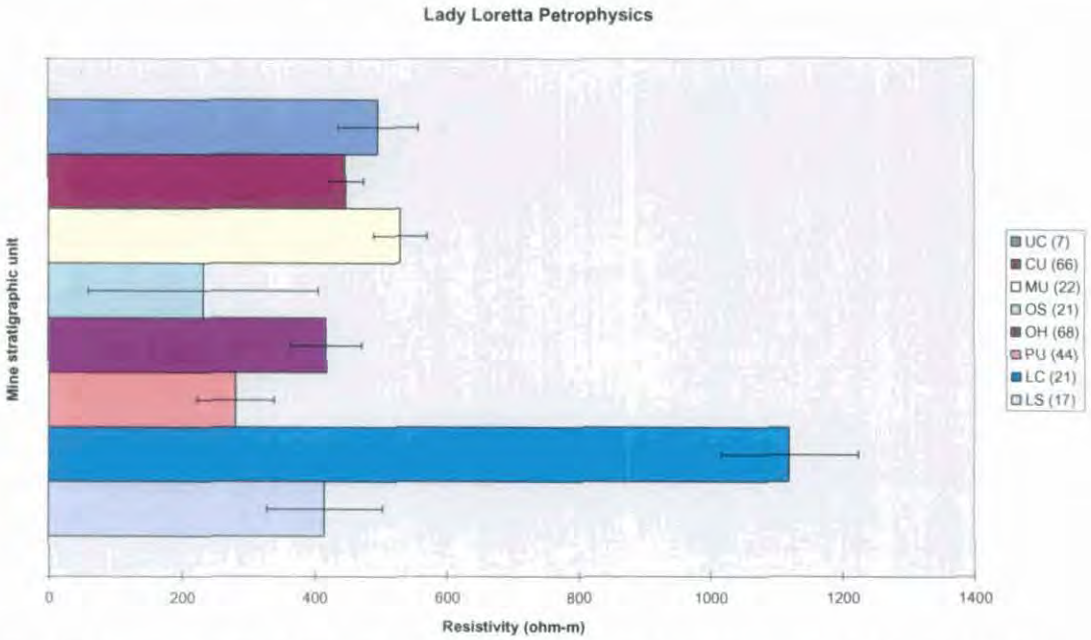

Figure 6.24 Resistivity of Lady Loretta mine units. Coloured boxes denote geometric mean values; whiskers indicate confidence range (95% level). Number of samples in brackets in legend

Fig. 6.24 summarises the effects of various sulphide resistivity properties in the Lady Loretta mine environment. Pyrite has depressed resistivities immediately adjacent to the orebody, though sphalerite in the ore body itself results in it actually being rather more resistive than in the most proximal 'halo' units (ore sediments and pyritic unit). Resistivities are generally slightly lower than in the Lady Loretta Formation regionally, with the exception of the lower carbonate unit. These properties, observed from drillcore samples, are broadly consistent with the results of field surveys carried out over the ore body, including the airborne EM survey reported in Anderson et al. (1993) and older surveys detailed in numerous unpublished reports held on-site at Lady Loretta. Conductivity anomalies are observed in the location of the Small Syncline in these studies, but these are far from the most conductive features observed in the Lady Loretta Formation and other McNamara Group units.

The Lady Loretta Zn-Pb mineralisation is clearly highly chargeable, with OH IP% values clearly higher than in any other unit (Fig. 6.25; Tables 6.2-6.9). Footwall units are significantly more chargeable than those in the hanging wall. The apparent equivalence of the 'Lower Carbonate' and 'Lower Siltstone' units with the 'Pyritic Unit' in terms of IP properties is unexpected, given the generally higher sulphide concentrations known to be present in the latter. This may be due in part to the sampling bias against sulphides noted previously, though bedded pyrite concentrations well in excess of 50% are present in the LC as well as the PU (Carr, 1984). The moderately high IP response of the LS may be contributed to by the more disseminated manifestation of pyrite at this level, in contrast to the bedded massive sulphides observed higher in the local stratigraphy.

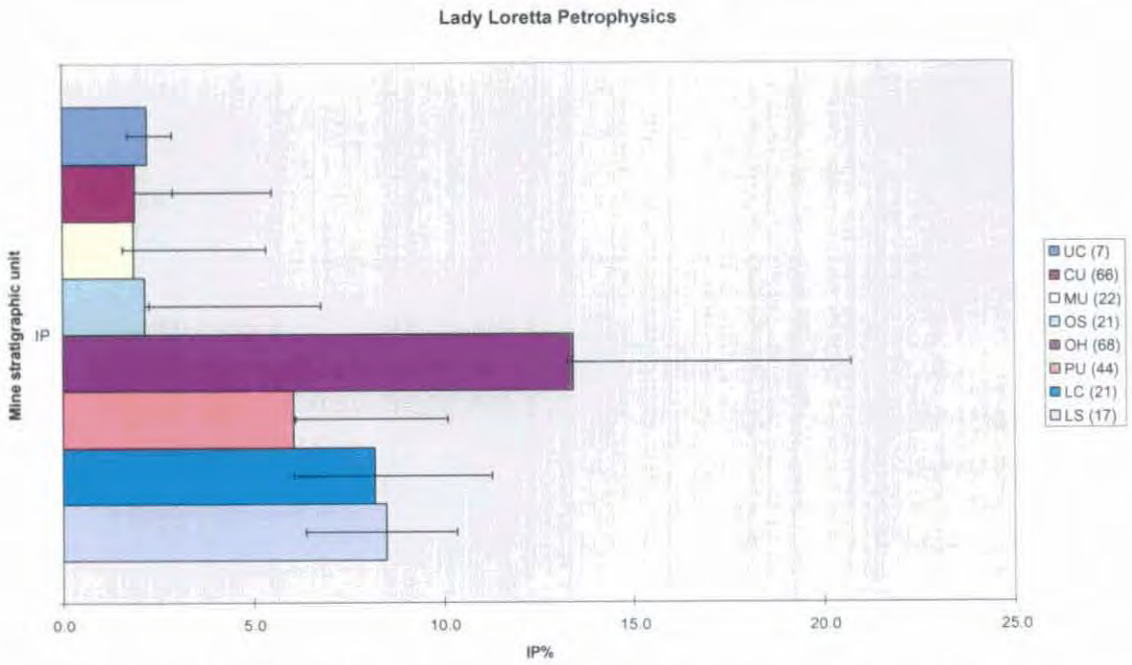

Figure 6.25 Chargeability of Lady Loretta mine units. Coloured boxes denote median values; whiskers indicate confidence intervals (95% level) about the arithmetic mean. Number of samples in brackets in legend

	SG dry	*Porosity*	*SG sat*	*Susc.*	*Velocity*	*Resistivity*	*IP%*	*TC1*	*K/Th*	*K/U*	*Th/U*
Mean	3.76	0.009	3.77	0.41	4749	7865	17.0	32	6.2	2.5	0.4
Std. Err.	0.05	0.001	0.05	0.04	58	2423	1.9	5	0.4	0.3	0.1
Median	3.88	0.005	3.90	0.28	4730	245	13.4	37	5.8	2.2	0.4
Std. Dev.	0.54	0.014	0.53	0.44	359	19980	15.7	13	0.90	0.62	0.13
Minimum	2.37	0.000	2.46	0.02	3980	3.8	0.9	7	5.6	2	0.3
Maximum	4.70	0.084	4.71	2.57	5450	111724	72.6	41	7.8	3.4	0.6
Count	121	93	122	102	38	68	68	6	5	5	5
Conf. Level (95%)	0.10	0.003	0.09	0.09	114	4749	3.7	10	0.8	0.5	0.1

Table 6.2 Statistical summary of petrophysical data, Lady Loretta ore/OH

	SG dry	*Porosity*	*SG sat*	*Susc.*	*Velocity*	*Resistivity*	*IP%*
Mean	2.71	0.06	2.77	0.21	4476	306	4.5
Std Err	0.07	0.01	0.07	0.04	167	48	1.2
Median	2.60	0.05	2.66	0.15	4290	287	2.1
Std Dev	0.37	0.05	0.34	0.19	374	218	5.3
Sample Var	0.13	0.00	0.11	0.04	140130	47690	27.8
Kurtosis	6.69	-0.32	7.80	2.06	-2.21	2.21	1.2
Skewness	2.28	0.76	2.56	1.55	0.51	1.31	1.5
Minimum	2.28	0.00	2.44	0.02	4080	27	0.4
Maximum	4.02	0.16	4.03	0.76	4960	943	18.4
Count	25	24	25	25	5	21	21
Conf Level (95%)	0.14	0.02	0.13	0.08	328	93	2.3

Table 6.3 Statistical summary of petrophysical measurements, Lady Loretta Ore Sediments'(OS)

A small number of gamma ray spectrometric measurements were made on drillcore samples from the OH, MU and LC (Tables 6.2, 6.5, 6.6). These indicate that the presence of base metal minerals substantially reduces count rates observed from hand specimens, but this is not obviously reflected in airborne radiometric data from Lady Loretta (see section 7.4.10).

	SG dry	Porosity	SG sat	Susc.	Velocity	Resistivity	IP%	TC1	K/Th	K/U	Th/U
Mean	3.02	0.028	3.04	0.67	5060	11126	8.1	407	6.62	4.50	0.75
Std Err	0.07	0.005	0.06	0.07	202	6073	1.0	323	1.07	1.29	0.31
Median	2.89	0.013	2.90	0.52	5110	240	6.0	160	6.19	4.19	0.50
Std Dev	0.52	0.035	0.51	0.54	857	40287	6.8	646	2.14	2.57	0.61
Kurtosis	0.98	1.43	1.17	-0.07	-0.29	12.68	1.66	3.02	0.39	-2.06	3.55
Skewness	1.11	1.42	1.19	0.91	0.08	3.70	1.39	1.74	0.97	0.48	1.87
Minimum	2.30	0.000	2.45	0.03	3410	1.1	1.0	-45	4.60	1.94	0.35
Maximum	4.52	0.146	4.53	2.11	6710	189192	29.0	1353	9.50	7.67	1.67
Count	64	57	64	67	18	44	44	4	4	4	4
Conf Level (95%)	0.13	0.009	0.12	0.13	396	11904	2.0	633	2.09	2.52	0.60

Table 6.4 Statistical summary of petrophysical measurements, Lady Loretta Pyritic Unit'(PU)

	SG dry	Porosity	SG sat	Susc.	Velocity	Resistivity	IP%	TC1	K/Th	K/U	Th/U
Mean	2.79	0.036	2.82	0.39	4469	789	3.5	843	6.0	3.6	0.6
Std Err	0.03	0.004	0.03	0.05	140	177	1.0				
Median	2.79	0.034	2.81	0.34	4370	472	1.9	843	6.0	3.6	0.6
Std Dev	0.16	0.021	0.15	0.27	558	829	4.5				
Kurtosis	1.15	1.31	1.33	2.54	-1.19	9.94	5.94				
Skewness	0.43	1.11	0.62	1.31	-0.01	2.81	2.39				
Minimum	2.49	0.007	2.54	0.03	3510	82	0.4	843	6.0	3.6	0.6
Maximum	3.18	0.093	3.20	1.23	5320	3938	18.8	843	6.0	3.6	0.6
Count	27	27	27	27	16	22	22	1	1	1	1
Conf Level (95%)	0.06	0.008	0.06	0.10	274	346	1.9				

Table 6.5 Statistical summary of petrophysical measurements, Lady Loretta Massive Unit'

	SG dry	Porosity	SG sat	Susc.	Velocity	Resistivity	IP%	TC1	K/Th	K/U	Th/U
Mean	2.75	0.016	2.77	0.18	5269	2088	8.7	1128	8.3	3.4	0.4
Std Err	0.03	0.005	0.02	0.02	230	449	1.3	117	0.8	0.4	0.1
Median	2.75	0.009	2.76	0.17	5525	1147	8.2	1047	8.2	2.9	0.4
Std Dev	0.14	0.022	0.12	0.11	651	2060	6.1	332	2.4	1.1	0.2
Kurtosis	5.61	7.37	4.94	8.70	-1.24	-0.10	0.72	-1.21	0.01	-0.83	-0.80
Skewness	-1.85	2.70	-1.59	2.37	-0.49	1.02	1.00	0.37	-0.16	0.83	-0.44
Minimum	2.28	0.000	2.37	0.01	4260	82	1.1	708	4.3	2.1	0.2
Maximum	2.95	0.094	2.95	0.59	6100	6486	23.9	1640	11.8	5.0	0.6
Count	23	23	23	25	8	21	21	8	8	8	8
Conf Level (95%)	0.06	0.009	0.05	0.04	451	881	2.6	230	1.6	0.7	0.1

Table 6.6 Statistical summary of petrophysical measurements, Lady Loretta Lower Carbonate Unit'

	SG dry	Porosity	SG sat	Susc.	Velocity	Resistivity	IP%
Mean	2.74	0.049	2.78	0.39	4706	1778	4.2
Std Err	0.02	0.005	0.02	0.03	133	901	0.7
Median	2.77	0.041	2.80	0.32	4640	344	1.9
Std Dev	0.23	0.045	0.20	0.23	667	7320	5.4
Kurtosis	7.06	-0.23	11.35	1.14	-1.02	57.73	5.25
Skewness	1.08	0.85	1.90	1.09	-0.15	7.43	2.29
Minimum	2.23	0.000	2.36	0.06	3540	14	0.4
Maximum	3.90	0.165	3.91	1.18	5810	58489	25.7
Count	87	74	87	77	25	66	66
Conf Level (95%)	0.05	0.010	0.04	0.05	261	1766	1.3

Table 6.7 Statistical summary of petrophysical measurements, Lady Loretta 'Cyclic Unit'

	SG dry	Porosity	SG sat	Susc.	Velocity	Resistivity	IP%
Mean	2.66	0.032	2.69	0.22	4970	683	8.4
Std Err	0.03	0.007	0.02	0.04	135	206	1.0
Median	2.70	0.018	2.71	0.18	4990	355	8.5
Std Dev	0.12	0.029	0.09	0.16	330	848	4.2
Kurtosis	-0.78	-0.97	-0.51	8.68	1.44	8.51	0.44
Skewness	-0.85	0.73	-0.84	2.70	-0.07	2.71	0.77
Minimum	2.44	0.003	2.51	0.09	4460	103	2.8
Maximum	2.77	0.088	2.81	0.77	5470	3558	17.8
Count	18	18	18	18	6	17	17
Conf Level (95%)	0.05	0.013	0.04	0.07	264	403	2.0

Table 6.8 Statistical summary of petrophysical measurements, Lady Loretta 'Lower Siltstone Unit'

	SG dry	Porosity	SG sat	Susc.	Resistivity	IP%
Mean	2.78	0.024	2.80	0.52	1368	2.3
Std Err	0.02	0.004	0.02	0.16	974	0.3
Median	2.80	0.023	2.81	0.31	410	2.2
Std Dev	0.06	0.010	0.05	0.43	2578	0.8
Kurtosis	-1.04	-1.22	-1.18	1.08	6.89	-0.44
Skewness	-0.42	0.08	-0.12	1.31	2.62	0.32
Minimum	2.69	0.011	2.72	0.13	203	1.3
Maximum	2.84	0.038	2.87	1.33	7200	3.5
Count	7	7	7	7	7	7
Conf Level (95%)	0.04	0.008	0.04	0.32	1910	0.6

Table 6.9 Statistical summary of petrophysical measurements, Lady Loretta 'Upper Clastic Unit'

6.5 Summary

Direct comparisons of bulk ore physical properties are difficult because the definition of 'ore' is dependent on economic factors. Notwithstanding this, some general observations and contrasts may be drawn.

All SSHBM deposits examined have a positive density contrast with their immediate host rocks, but the magnitude of this is variable (Table 6.10). Lady Loretta ore has the highest density in absolute terms, as well as the greatest contrast with its host. Even the 'Pyritic Unit' component of the Lady Loretta host stratigraphy is significantly less dense than the Zn-Pb ore material. The Century mineralisation has the poorest density contrast with non-sulphidic host rocks, though at Hilton there is evidently little contrast between the base metal mineralisation and strongly pyritic components of the host Urquhart Shale. The relatively low density of the Century orebody is presumably due to the lack of associated pyrite and unusually low galena content in comparison to other SSHBM deposits.

Only the Hilton and Mount Isa ore systems are significantly magnetic (Table 6.10). This is presumably due to their higher metamorphic grade (greenschist facies) in comparison to that of the other SSHBM deposits studied (sub-greenschist or lower), with concomitant creation of monoclinic pyrrhotite from precursor Fe sulphides. The much lower but still distinctly elevated magnetic susceptibility of the Lady Loretta mineralised system may also be partly due to trace monoclinic pyrrhotite or other rare ferromagnetic Fe sulphide minerals. However, paramagnetic Fe- and Mn-carbonate minerals, principally siderite, also appear to contribute to the higher magnetic susceptibilities associated with the Lady Loretta ore environment, in particular the 'Pyritic Unit'.

All the SSHBM ores examined are highly chargeable, with mean IP% values exceeding 15. While this generally presents a significant contrast to barren host units, the chargeability of host rocks adjacent to mineralisation can approach similar values.

The resistivity of SSHBM deposits appears to decrease with increasing metamorphic grade. The virtually unmetamorphosed HYC ore is distinctly more resistive than its mainly pyritic carbonaceous shale host. The Century orebody, while of a slightly higher metamorphic grade than HYC, is a similarly poor conductor in comparison to its host rock, which may be related to a comparative lack of galena as well as associated pyrite. The Lady Loretta mineralised system is generally slightly more conductive than the host Lady Loretta Formation regionally. However, large quantities of pyrite and carbonaceous shale in the rocks enveloping the Lady Loretta ore sequence as well as within it mean that there is little conductivity contrast directly associated with the ore. Strata immediately adjacent to it are actually slightly more conductive than the ore itself. Only highly dolomitic portions of the host stratigraphy are significant more resistive than base metal mineralisation.

Sonic velocities of Lady Loretta ore samples are generally not greatly different from those of their host rocks, though higher velocities are observed in more carbonate-rich parts of the local host sequence. Impedance contrast calculations indicate that Lady Loretta-style mineralisation should be detectable with seismic reflection methods in most circumstances relevant to base metal exploration.

Gamma ray emissions from strata hosting base metal mineralisation appear subdued in comparison to those from adjacent host rocks. This is presumably due to the attenuating effect of massive sulphides, particularly galena, as well the obvious low concentration of clay, silt and organic material implied by high sulphide concentrations. Consequently, outcropping equivalents of mineralised strata may not necessarily manifest as areas of anomalously low count rate in airborne radiometric surveys, as sulphides are likely to be preferentially removed by weathering.

Deposit	Density (sat; t/m^3)	Porosity	MS (x 10^{-3} SI)	Velocity (m/s)	Resistivity (Ωm)	IP%	TC (cpm)	K/Th	K/U	U/Th
HYC orebody	3.39±0.05	0.019± 0.007	0.12		430-470	15.2±1.8	440±210	6.0±2.1	3.8± 0.9	0.66± 0.20
HYC host	2.65±0.11	0.023± 0.006	0.03		low (120-200)					
Walford Ck pyrite	high		very low		low (5-10 - apparent)					
Walford Ck host	low		very low		mod-low (~100 - apparent)					
Century orebody	2.95±0.05	low (~700 neut. API)	very low		100-300	high (15-20 mrad)	variably low (100 API)			
Century host (slst & shle)	2.7	mod (1200 neut. API)	very low		75-80	mod-low (3-15 mrad)	mod-high (125-180 API)			
Century host (sdst)	2.6	high (1600 neut. API)	very low		60-80	mod-low (3-15 mrad)	high (160 API)			
Lady Loretta ore	3.90±0.09	0.005± 0.003	0.41± 0.09	4750± 110	250-420	17.0±3.7	32±10	6.2±0.8	2.5± 0.5	0.4± 0.1
Lady Loretta pyritic unit	3.04±0.12	0.028± 0.009	0.67± 0.13	5060± 400	240-280	8.1±2.0	160-410	6.6±2.1	4.5± 2.5	0.75± 0.60
Lady Loretta host seds.	2.77±0.03	0.040± 0.007	0.34± 0.04	4710± 180	450-550	5.2±2.7	1100±210	8.1±1.5	3.4± 0.7	0.45± 0.10
Hilton ore	3.03±0.02	0.004± 0.002	6.4±2.4	5820± 320	1100-4700	19.7±6.2				
Mt Isa/Hilton host (pyritic)	2.90		6.1-12.5		0.01-1.0					
Mt Isa ore	3.48	0.001	~12		0.001-0.01					
Mt Isa host (non-pyritic)	2.76±0.01		0.20		0.2-50					

Table 6.10 Compilation of petrophysical data for stratiform Pb-Zn deposits in the Proterozoic of northern Australia. Direct measurements are given where available, otherwise estimations from interpretation of field data have been used. MS = magnetic susceptibility, TC = total count, cpm = counts per minute

7. Airborne Geophysical Image Processing and Interpretation

7.1 Introduction

Airborne magnetic and gamma-ray radiometric data are now in common use as aids to geological mapping and mineral exploration in many areas, including the Mount Isa Basin. However, there are some particular (but far from unique) factors to consider in the Paradise Valley study area. There are no units with significant magnetic susceptibility stratigraphically higher than the Eastern Creek Volcanics in the southern Mount Isa Basin; the only possible exceptions being dolerite dykes and sills and rare metabasalts in the lower Myally Subgroup (see chapter 5). Consequently there is a lack of high-frequency magnetic information to assist in structural mapping through most of the region, giving rise to the need to extract information in the z-dimension (detailed in chapter 8). In addition, good quality 1:100,000 geological maps already exist for the study area, and the airborne geophysical data does not contribute significantly to redefinition of the distribution of major rock units.

These considerations contributed to the approaches taken in this study, which were firstly to map facies variations, alteration systems and other 'anomalous compositions' in outcrop or subcrop within the mapped geological units, and secondly to extract as much three-dimensional information from the geophysical data as practical (see chapter 8). The former approach is detailed in this chapter.

7.2 Data

Airborne geophysical data have been acquired by several surveys in the Paradise Valley region. One of these, flown by Geoterrex for Ashton Mining in 1987 (Queensland Dept. of Mines and Energy open file report CR18153B; Keith Jones, written communication 1995), is now in the public domain. This survey is the source of airborne magnetic (Fig. 7.1) and four-channel (potassium-uranium-thorium + total count) radiometric data (Figs. 7.2 and 7.3) displayed in this thesis. Flight lines were oriented north-south, with a nominal spacing of 250 m and terrain clearance 80 m. The data presented in the images have been gridded to a 50 m by 50 m grid cell size by Ashton Mining, after the IGRF was removed and 5000nT added to the magnetic data. This data was then reduced to the pole (RTP) using ER Mapper software, and the RTP version of the data is displayed in all figures in this chapter unless stated otherwise.

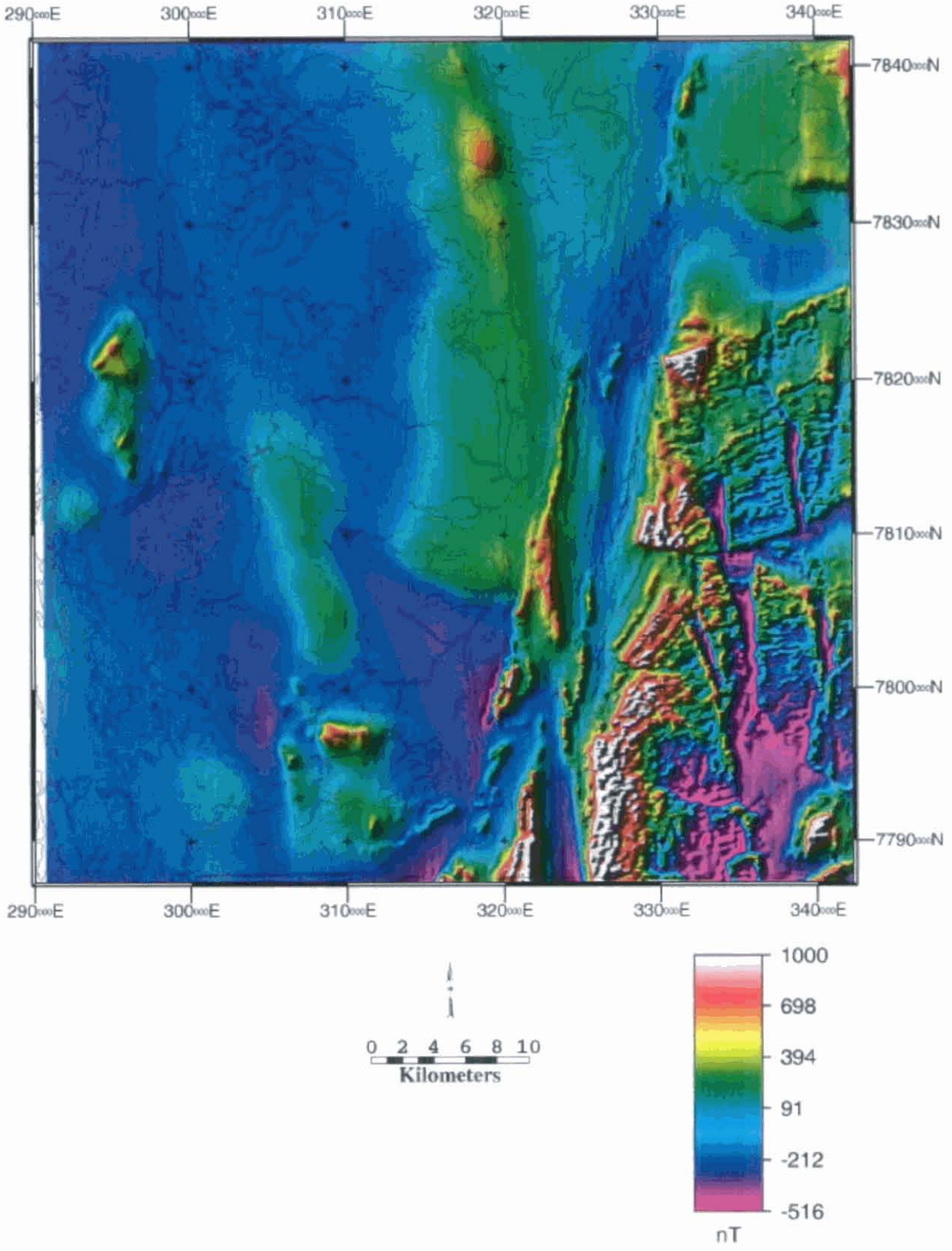

Figure 7.1 Paradise Valley region total magnetic intensity (TMI) image. All magnetic data in this chapter is reduced-to-pole and displayed with an intensity layer simulating NW illumination unless stated otherwise. Geology outline overlay in black modified after Hutton and Wilson (1985) and Fig. 2.5. Grid in this and all subsequent figures is the Australian Map Grid (Australian Geodetic Datum 1966), Zone 54

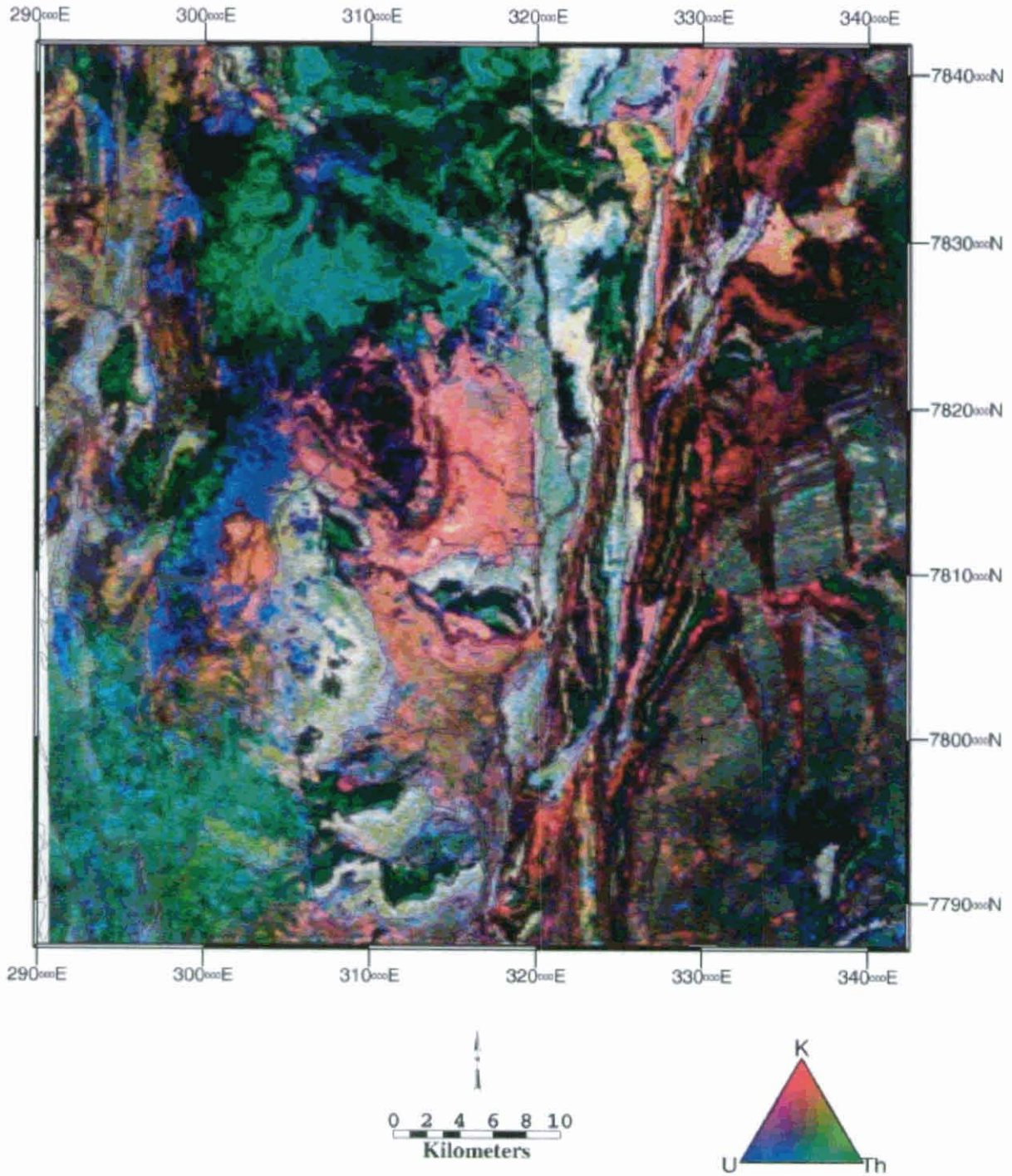

Figure 7.2 Paradise Valley radiometric data with linear histogram transform

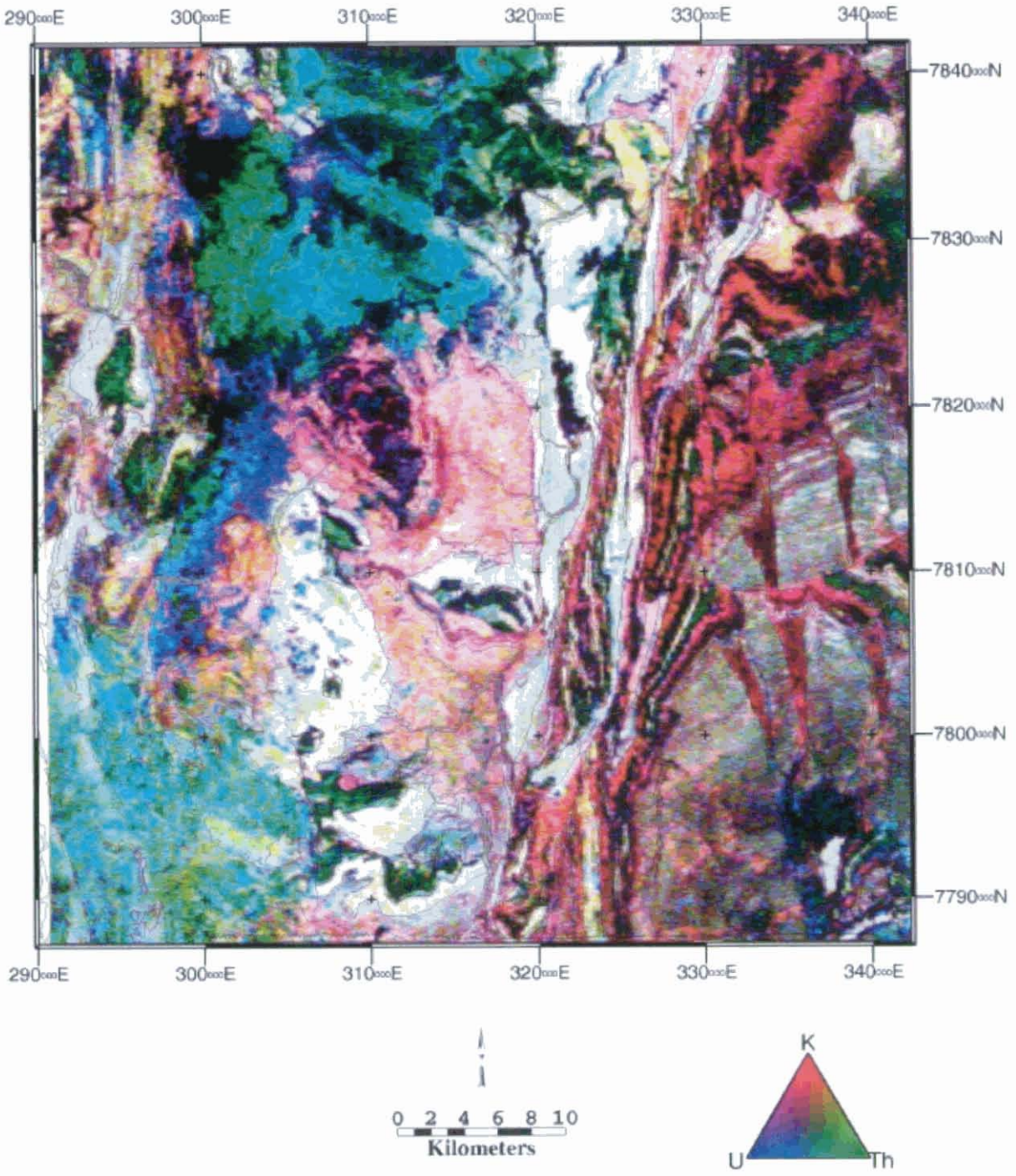

Figure 7.3 Paradise Valley radiometric data with histogram-equalised transform

Histograms of the K, Th and U-channel radiometric data taken as a whole (Fig. 7.4) are positively skewed, with peaks around a few tens of counts-per-second (cps), and tails extending up through the hundred cps range (several hundred, in the case of K). There are suggestions of a number of sub-populations with different means and variances in the histograms, particularly that of the K channel.

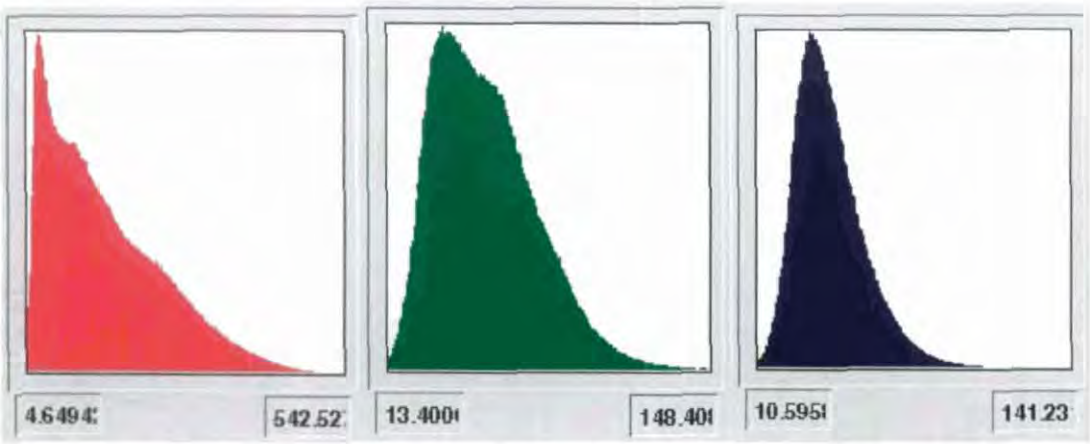

Figure 7.4 Histograms of K- (red), Th- (green) and U- (blue) channel radiometric data. Count per second levels at the lower and upper ends of the distribution shown on the x-axes

Scattergrams of Th v K, Th v U and K v U (Fig. 7.5) exhibit few distinct classes in these data spaces. Two and possibly three ratio classes may be distinguished in the Th v K scattergram (Fig. 7.5), the most distinct of which, with a very high Th:K ratio, probably corresponds to Cainozoic sediments and weathering surfaces (areas of saturated green in Fig. 7.3; see also section 7.12). Data in the Th vs U scattergram is strongly clustered into a single elliptical field (Th:U slightly less than 1), with sparsely populated high and low Th:U fields which is probably due mainly to noise spikes. Inspection of a Th:U pseudocolour image confirms this hypothesis, there being no geographically coherent occurrences of high or low Th:U levels. The K v U scattergram may be interpreted similarly.

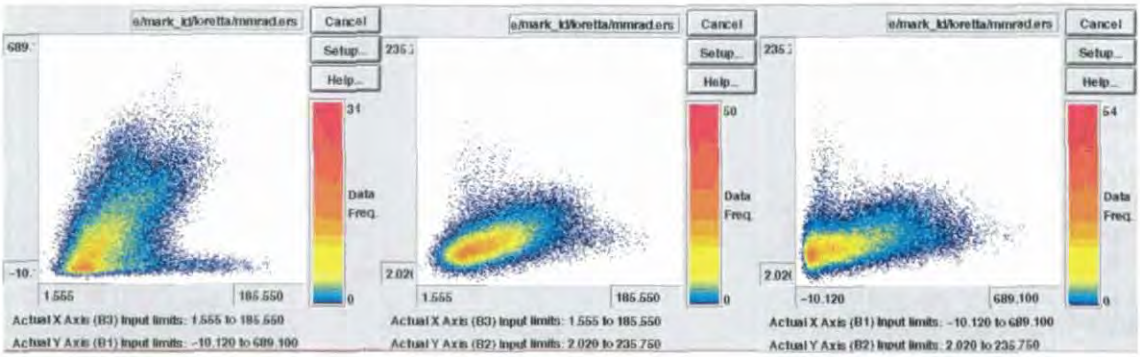

Figure 7.5 Scattergrams of radiometric data. B1 = K channel cps, B2 = U channel cps, B3 = Th channel cps

7.3 Method

An integration of structural information from the magnetic data with chemo-stratigraphic information from the radiometric data was attempted. The magnetic data was included as a fourth band in addition to the K, Th and U channels of radiometric data, and an unsupervised ISODATA classification algorithm applied to the integrated dataset. Successful convergence of the algorithm was only achieved when an unusably high number of classes was allowed (> 220), many of which had little contiguity. The lack of a useful result from the unsupervised classification may be attributable to high levels of correlation between radiometric bands, noise inherent in the radiometric data (particularly the uranium channel) and geometric effects in the magnetic data. The unsupervised classification would be improved by filtering and principal components analysis of the radiometric data in order to reduce noise and correlation between

bands, and conversion of the magnetic data to apparent magnetic susceptibility. This was beyond the scope of this study.

An approach integrating GIS with the geophysical image processing and interpretation was adopted, utilising the good geological data available for the study area (Hutton and Wilson, 1985). Each geological unit investigated was selected in the GIS and used as a mask for subsequent image processing and enhancement. This had the effect of limiting the range of the geophysical data to that observed in the geological unit of interest. Areas of anomalous structures or radioelement concentration in the context of the unit were thus highlighted following histogram-stretch enhancements. These 'unit-specific stretches' were interpreted in terms of basin architecture and structure, sedimentology and alteration systems.

7.4 Interpretation

The radiometric data are generally presumed to reflect bedrock composition, although the signal is modified by a number of factors resulting from regolith processes. Weathering tends to result in K depletion (Dickson and Scott, 1997), but this will not unduly affect the interpretation as long as all units studied are affected similarly or in predictably systematic fashion. While shales tend to be more susceptible to relative K depletion than arenites (Dickson and Scott, 1997), these lithologies may still be easily distinguished by their contrast in overall count rates (high and low respectively). The presence of transported material will tend to mask the signal of bedrock-derived radioelements, but there is little evidence that such processes (colluvial and aeolian transport, soil movement, clay eluviation) have operated in the region except in well-defined Cainozoic deposits. There is sufficient relief in most areas of Proterozoic outcrop to minimise the possibility of a significant buildup of an aeolian Th- and U-bearing fine dust component in soils, but not so much relief as to indicate extensive soil movement. Neither is there sufficient topographic relief to greatly influence the signal through source/detector geometry changes. Some possible exceptions are indicated within section 7.4. Overall, the congruence of most observed radiometric signatures with mapped geological features and strike directions increases confidence to the assumption of a direct relationship between radiometric signal and exposed Proterozoic rock composition in most of the study area.

7.4.1 Leander Quartzite

Both RTP (reduced-to-pole) magnetics and radiometrics are low over the Leander Quartzite, with all radiometric channel values falling within the lowest quartile of the total dataset. The apparent difference in magnetic base level from west (low) to east (high) probably arises from a magnetic unit still deeper in the section (Bottletree Formation or other pre-Haslingden Group felsic and mafic igneous units are likely candidates), or possibly residual geometric effects from the adjacent Eastern Creek Volcanics. Overall negative magnetic field strength values tend to confirm the latter as being the primary control in this area (Fig. 7.6).

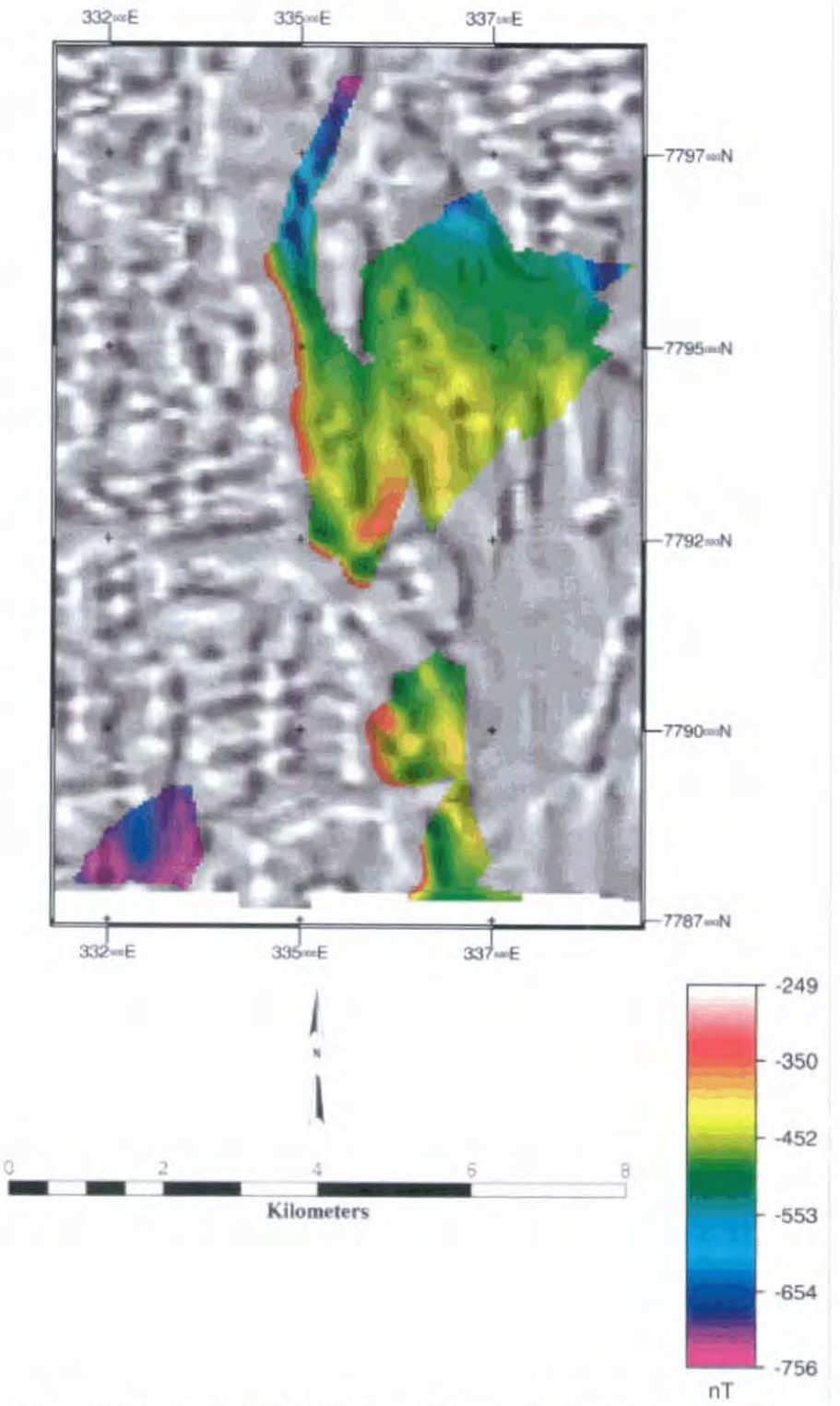

Figure 7.6 Leander Quartzite RTP total magnetic intensity. Coloured area corresponds to Leander Quartzite outcrop or subcrop. Intensity layer is TMI continued downward 25 m with automatic gain control and illuminated from the northeast. This area represents the total extent of Leander Quartzite in the study region

Another possibility is that the eastern domain Leander Quartzite has been thrust over Eastern Creek Volcanics. There is a long-wavelength increase in magnetic values towards the southern fault contact of the most extensive Leander Quartzite outcrop, indicating a possible deep magnetic source. Additionally the presence of a N-S oriented truncation at 336100E 7793500N, and another linear high at 335700E 7792750N in a NW orientation, suggest magnetic sources at shallow depths beneath the Leander

Quartzite. Increased dyke density within the area bounded by these two features is another possible cause; this would need to be investigated through field observations.

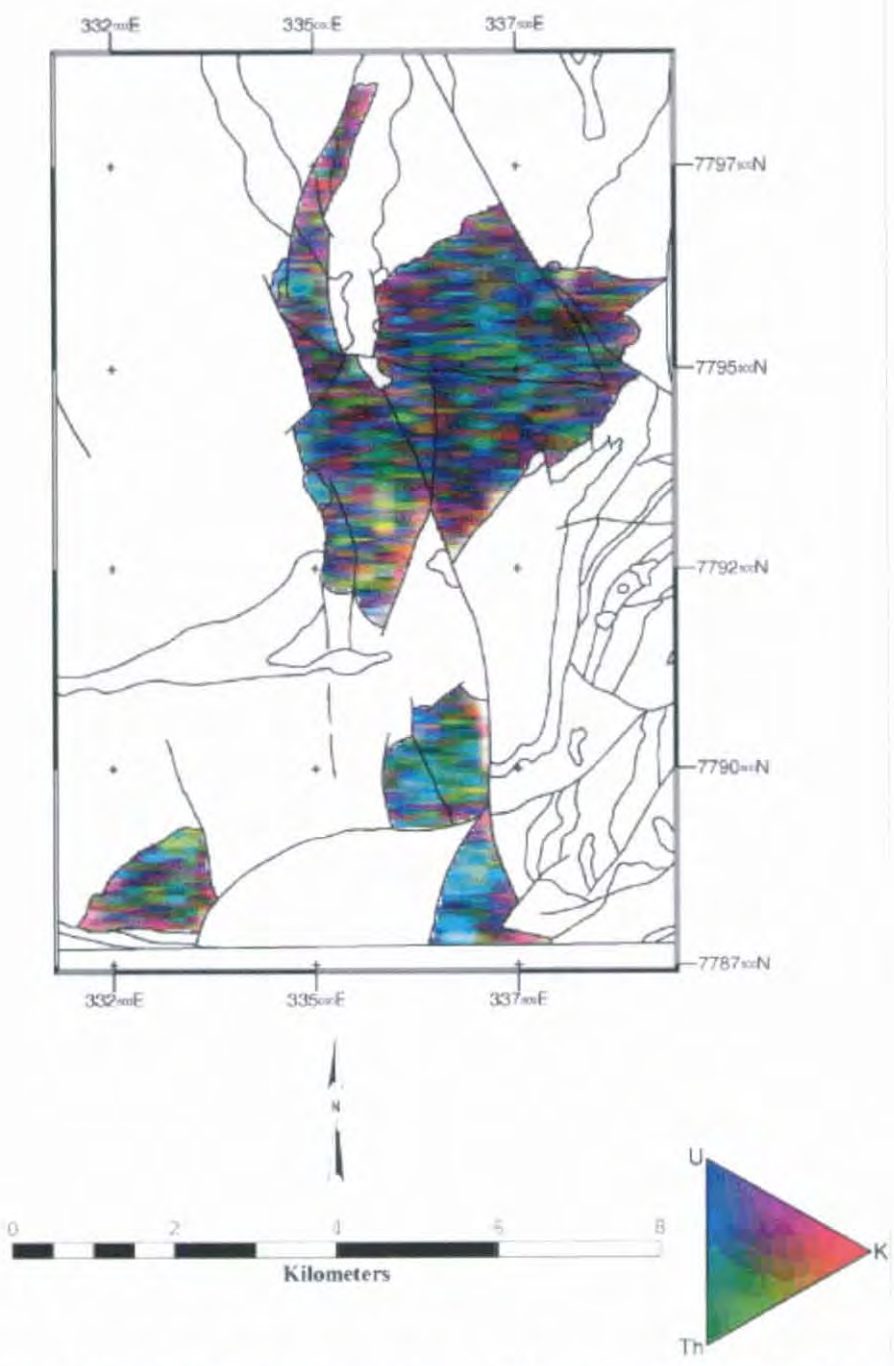

Figure 7.7 Leander Quartzite radiometric image. Geology outline overlay in this and subsequent figures modified after Hutton and Wilson (1985)

Downward continuation of the magnetic field by 25 metres coupled with automatic gain control filtering reveals structural trends to the NNW, parallel to dolerite dykes mapped in the region; and NE, concordant with bedding (Fig. 7.6). Most of the mapped dykes appear to be associated with high TMI linear features, but some correspond to magnetic lows, implying both magnetisation in a direction broadly reverse to that of the Earth's present field, and high Koenigsberger ratios. This may imply at least two generations of dyke intrusion, or slightly different Curie temperature cooling ages and coercivities arising from factors such as different cooling histories or grain size.

Radiometric data acquired over the Leander Quartzite (Fig. 7.7) show no apparent geological character, having a speckled appearance which is indicative of a high signal/noise ratio and generally low count rates for this unit. Ratios of radiometric bands do not appear to convey additional geological information, which is also the case for all other units investigated.

7.4.2 Eastern Creek Volcanics

There is little change of magnetic character in the vicinity of Leander Quartzite/Cromwell Metabasalt Member conformable contacts (Fig. 7.1), a surprising observation given the generally highly magnetic nature of the Cromwell Metabasalt (see below, also chapter 5). Reasons for this may be effective thinning of the Eastern Creek Volcanics (ECV) towards the Leander Quartzite (LQ) contact; or magnetite-destructive alteration at the base of the Cromwell Metabasalt Member. The lack of high frequency character in the ECV near (~1 km) the stratigraphic contacts would suggest the latter. In this case, any magnetite-destructive alteration is likely to have taken place before these units were faulted into their present position, given the apparent stratigraphic control.

The magnetic data suggest that the Phanerozoic cover units obscuring the LQ/ECV contact in fact largely overlie the ECV, consistent with the generally recessive nature of this unit in comparison to the LQ.

Magnetic effects from the dykes mentioned in section 7.4.1 appear to penetrate a short distance (less than a kilometre) into the ECV, and it appears likely that they have acted as feeders to the Cromwell Metabasalt.

Increases in TMI with stratigraphic level through the Cromwell Metabasalt (Figs. 7.8 and 7.9) are consistent with the north-plunging anticlinal overall geometry of the ECV in the study area, but there may be a petrophysical component additionally controlling this variation. A slight but distinct increase in radiometric counts in the direction of stratigraphic younging in the Cromwell Metabasalt supports the notion that the change in magnetic field strength may be partly controlled by compositional variations. The radiometric data are discussed further below.

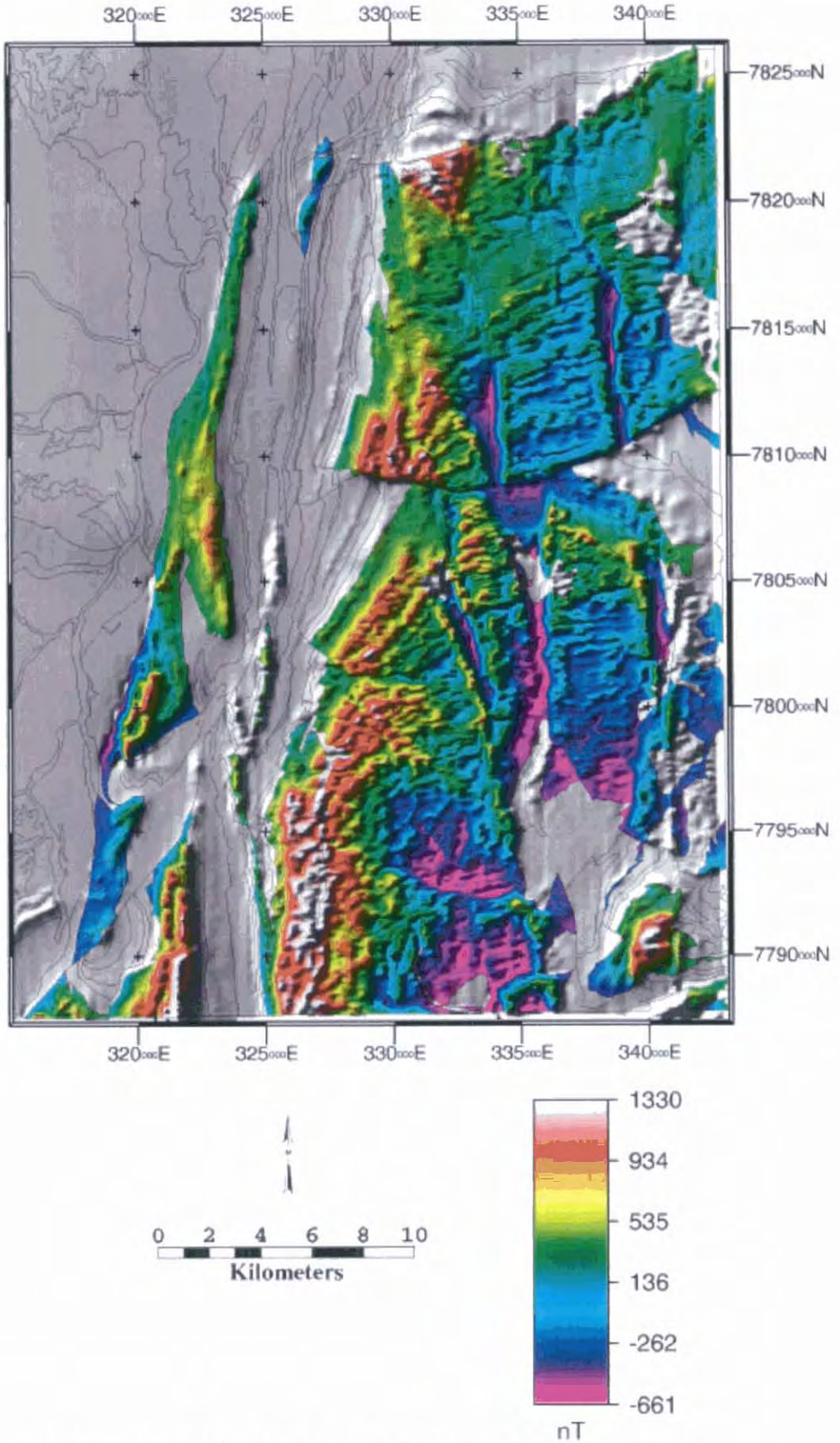

Figure 7.8 Eastern Creek Volcanics total magnetic intensity (RTP), linear transform

The magnetic response from the Pickwick Metabasalt suggests that it is less magnetic than the Cromwell Metabasalt (Fig. 7.8). The clearest example of this is in the fault-bounded block of Cromwell Metabasalt

flooring the upstream end of Waggaboonya Lake 3 km east of Mammoth (332000E 7821000N), which is marked by a magnetic high of almost 1000 nT amplitude above levels recorded over the surrounding Pickwick Metabasalt. From the extension of this anomaly beneath lower Myally Subgroup sediments, it may be inferred that the Mammoth Extended Fault is a north-dipping normal fault in this area. Elsewhere in the limbs of the major anticlinal structure encompassing the Eastern Creek Volcanics, the Pickwick Metabasalt manifests as a horizon of distinctly lower TMI than the Cromwell Metabasalt immediately underlying the intervening non-magnetic Lena Quartzite.

The magnetic signature of tightly folded Pickwick Metabasalt outcrops in the Mount Gordon Fault Zone and in the extreme south-eastern corner of the study area are more enigmatic. The very high TMI values recorded in some of these areas, for example around 321500E 7789000N, suggest anomalously high concentrations of magnetite in comparison to the majority of Pickwick Metabasalt outcrops in the study area. A curious association of signatures occurs in the westernmost outcrop of ECV, in the Mount Gordon Fault Zone between 320000E 7802000N and 325000E 7821000N. A highly magnetic bed with coincident potassium-dominant radiometric signature is consistent with Pickwick Metabasalt seen elsewhere, and is mapped as such by Hutton and Wilson (1985), but the all-channel radiometric high/magnetic low signature encasing it is unlike any other observed in the Eastern Creek Volcanics in the study region.

Trends concordant with bedding are evident in the magnetic data from both volcanic members, implying differences in magnetic properties across strike, possibly between (meta-)basalt flows as well as intercalated sediments.

There are also significant differences between the radiometric signatures of the Cromwell and Pickwick Metabasalt Members. The bluish-green colours of the Cromwell Metabasalt in Figs. 7.10 and 7.11 denote higher concentrations of Th and U than in the Pickwick Metabasalt, whose generally reddish or dark colour reflects relatively high potassium and overall low radioelement concentration, respectively. An anomaly in the Cromwell Metabasalt's radiometric signature occurs a little over a kilometre east-south-east of the Mammoth Cu mineralisation (most apparent in Fig. 7.10), where the typical Th-dominant response is less prominent but a whitish colour indicates moderate to high levels of all radioelements. The K channel shows around 180 cps in this area (~331500E 7821000N), compared to 120 cps typically elsewhere. The Cromwell Metabasalt appears to have been progressively enriched in radioelements as the magmatic system evolved, manifest as an increase from dark through bluish-green shades to near-white with successive stratigraphic horizons. The origin of discordant reddish (K-rich) patches in the Cromwell Metabasalt is uncertain, but may relate to alteration systems or thin Cainozoic veneers and soil development.

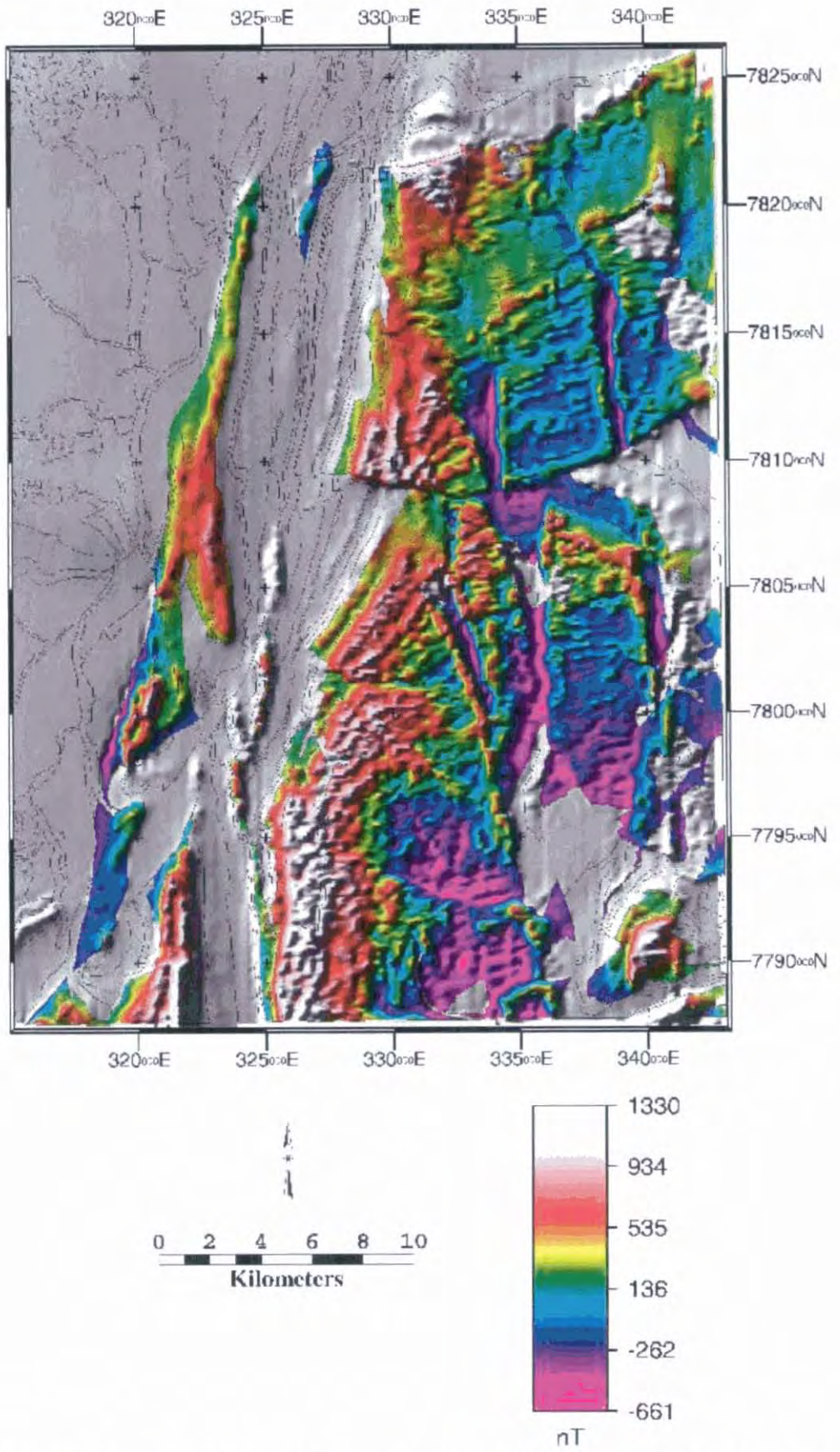

Figure 7.9 Eastern Creek Volcanics total magnetic intensity (RTP), histogram-equalised transform

For the most part, sedimentary interbeds within the Eastern Creek Volcanics, including the Lena Quartzite Member, appear to have very low radioelement concentrations. A notable exception is the

quartzite' sub-member of the Cromwell Metabasalt (Phc $_q$), which is high in all channels (for example at 335600E 7816800N).

The Pickwick Metabasalt exhibits discrete variations in radiometric signature across the study area. Within most of the main anticlinal body of the Leichhardt River Fault Trough, the Pickwick Metabasalt appears red with various levels of saturation. The implied potassium concentration is comparable to or even higher than that observed in the uppermost Cromwell Metabasalt. Very little signal is present in the thorium and uranium channels in the Pickwick Metabasalt. A trend of decreasing K concentration from west to east is superimposed on this general picture around the northing of the Mammoth Cu deposit (~7820000N-7825000N), such that around 337000E and 340000E there is little or no radiometric signal.

Elsewhere the Pickwick Metabasalt radiometric signature is both different and highly variable, particularly within the Mount Gordon Fault Zone. The sinuous strip of red in the Mount Gordon Fault Zone between 320000E 7802000N and 325000E 7821000N whose magnetic signature was discussed above is typical of the main Pickwick Metabasalt radiometric signature, but it is encased by outcrop with apparently very high overall radioelement levels, also mapped as Pickwick Metabasalt. This radiometric signature is similar to that observed from undifferentiated Eastern Creek Volcanics mapped around 320000E 7800000N, but the latter differs in having a variably high magnetic signature, while the former is low. A further example of this highly radioactive/non-magnetic Pickwick Metabasalt association occurs at 320000E 7789000N, where it is separated by faults from reddish white (still highly radioactive, but with slightly lower levels of thorium and uranium), extremely magnetic 'Pickwick Metabasalt' immediately to the east.

Both the radiometric and magnetic signatures of this latter 'Pickwick Metabasalt' outcrop appear similar to that of the Cromwell Metabasalt a few kilometres further east. The radiometric and magnetic signatures arising from the inner portion of the 'Pickwick Metabasalt' outlier in the south-eastern corner of the study area (around 340000E 7790000N) are also similar to those typical of the Cromwell Metabasalt, and it may be that these are in fact outcrops of Cromwell rather than Pickwick Metabasalt as mapped by Hutton and Wilson (1985).

The outcrop area of dolerite dykes intruding the Eastern Creek Volcanics appears to have been exaggerated by the mapping of Hutton and Wilson (1985), particularly in the block south of the Investigator Fault. Both magnetic and radiometric images of the Eastern Creek Volcanics (Figs. 7.10 and 7.11) show the extremely subdued magnetic and radiometric signatures of the dolerite dykes to be less extensive than the boundaries indicated by the outlined geology polygons would suggest.

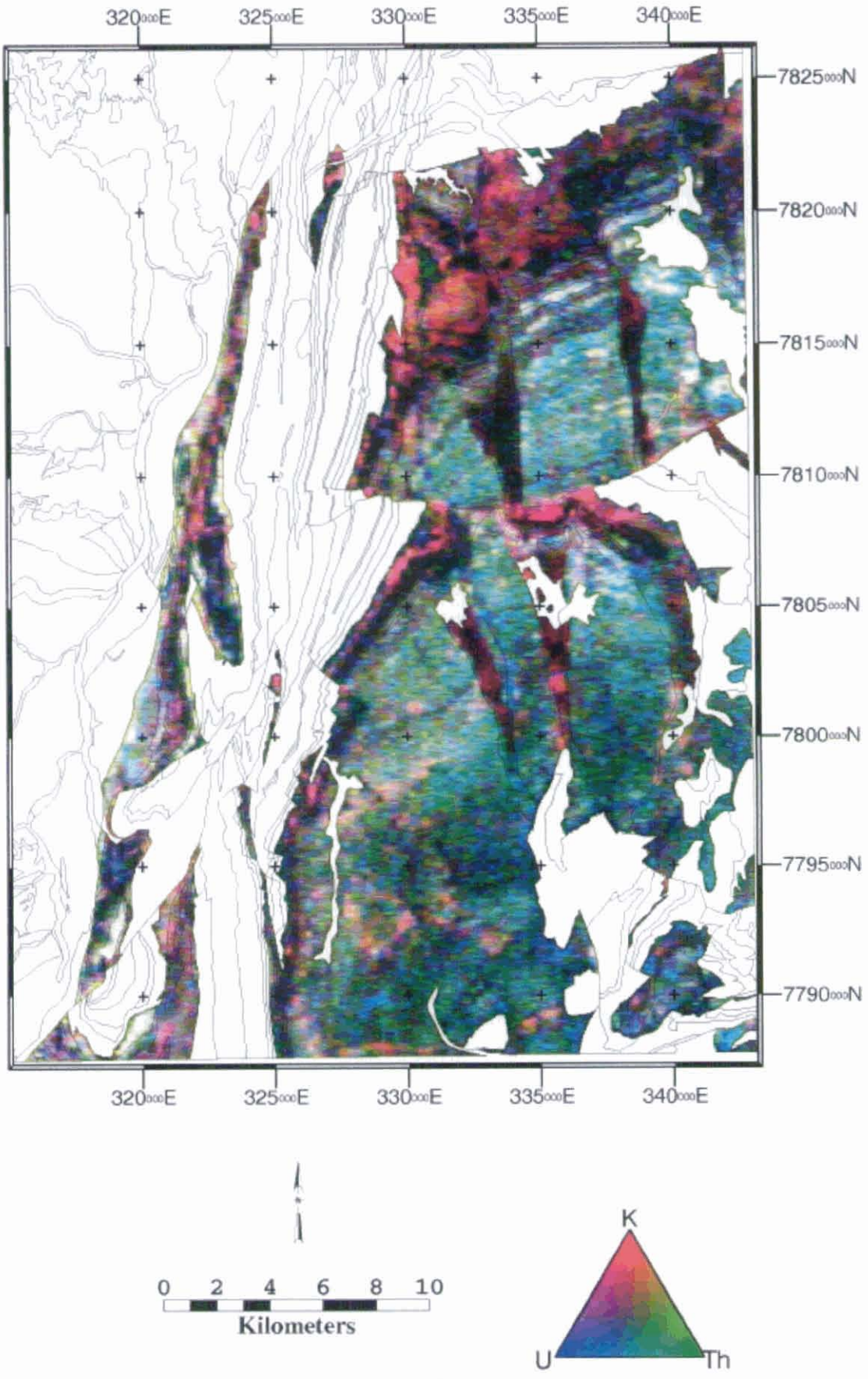

Figure 7.10 Eastern Creek Volcanics radiometric image, linear transform

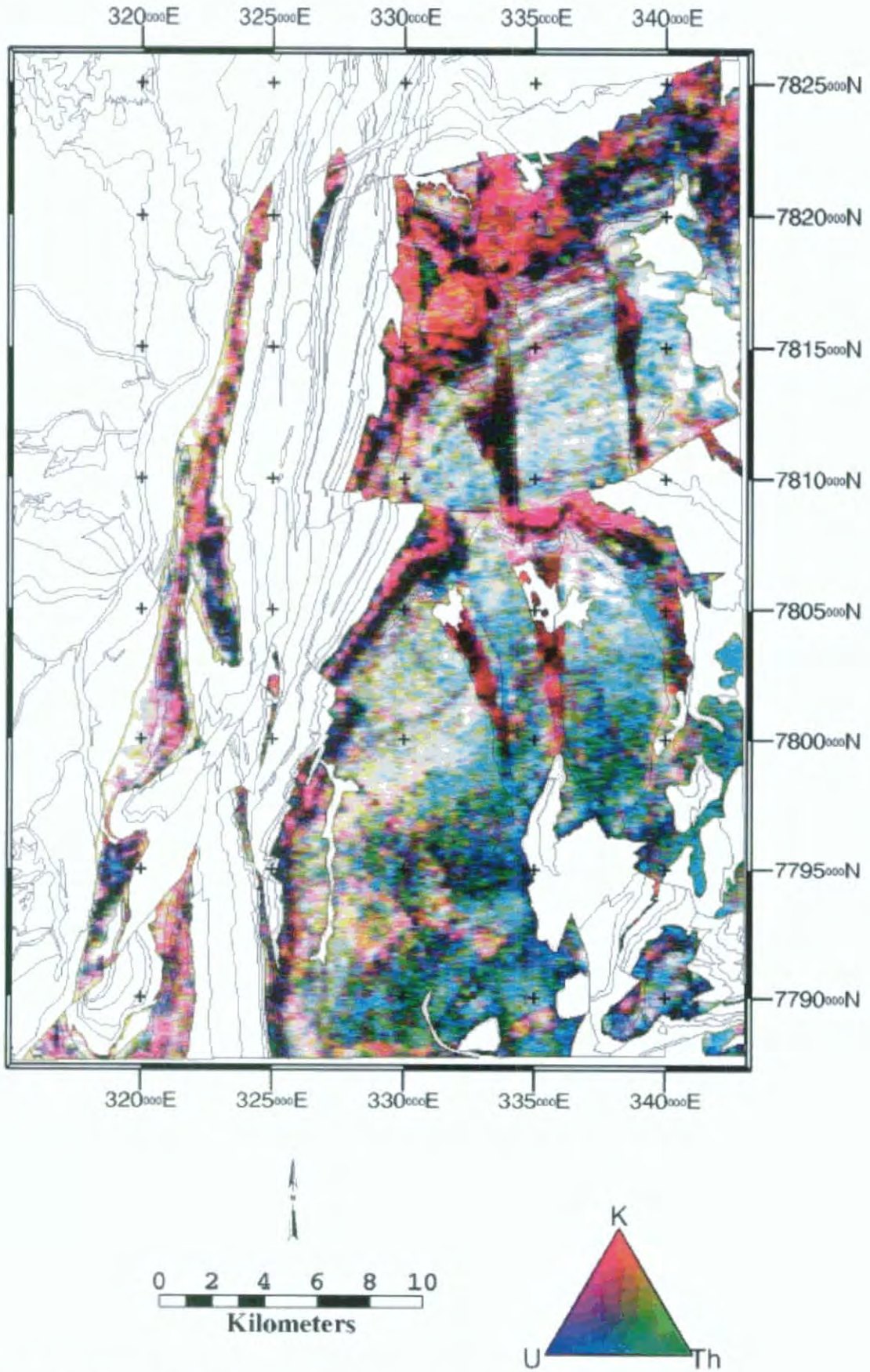

Figure 7.11 Eastern Creek Volcanics radiometric image, histogram-equalised transform

Neither the magnetic nor the radiometric data furnish much support for Hutton and Wilson's (1985) conclusion from geochemical similarities that the wide N-S trending dolerite dykes were comagmatic

with the Eastern Creek Volcanics. Based on their similar geophysical signatures (non-magnetic, very low radiometric signal) it is more likely that these dykes are comagmatic with sills in the overlying Myally Subgroup. This statement does not apply to dolerite sills intruding tuffs at the top of the Cromwell Metabasalt, which from their geophysical resemblance (slightly magnetic, similar K signal) may very well be comagmatic with the Pickwick Metabasalt.

7.4.2.1 Relationships to geochemistry and petrology

The magnetic and radiometric signatures of the Eastern Creek Volcanics may be calibrated by geochemical and petrological studies of the Eastern Creek Volcanics and associated mafic intrusives in the study area by Scott and Taylor (1982), Ellis and Wyborn (1984), Wilson et al. (1985) and Wyborn (1987). Many of these authors identified alteration systems in the Eastern Creek Volcanics that they related to copper mineralisation in the region, in particular the Mount Isa and Mammoth deposits. Geochemical species most affected by alteration identified by Wilson et al. (1985) included Cu, Zn, K and the oxidation state of Fe. This reinforces the prospect that alteration assemblages in the Eastern Creek Volcanics firstly may be important to base metal metallogeny, and secondly may be mappable with airborne geophysics.

Eastern Creek Volcanics geochemical data used by Wilson et al. (1985) and Wyborn (1987) were sourced from AGSO's ROCKCHEM database, and are presented in Figs. 7.12-7.19. Strike is generally E-W in the areas sampled (locations shown in Fig. 7.12), with northward younging direction caused by regional plunge. Northing can thus be used as a proxy for stratigraphic position in Figs. 7.13-7.19, with the sequence being interrupted and repeated by the Investigator Fault around 7809000N.

7.4.2.1.1 Metabasalt member signatures

The geophysical signatures discussed above imply differences in K, Th, U and Fe geochemistry across the stratigraphic components of the Eastern Creek Volcanics. These trends are discernible but have not been emphasised in previous geochemical studies, which have instead concentrated on alteration systems as the major controls on metabasalt geochemistry. Such observations as have been made of stratigraphically systematic geochemical differences within the ECV are summarised in Table 7.1, together with the concomitant observed geophysical response.

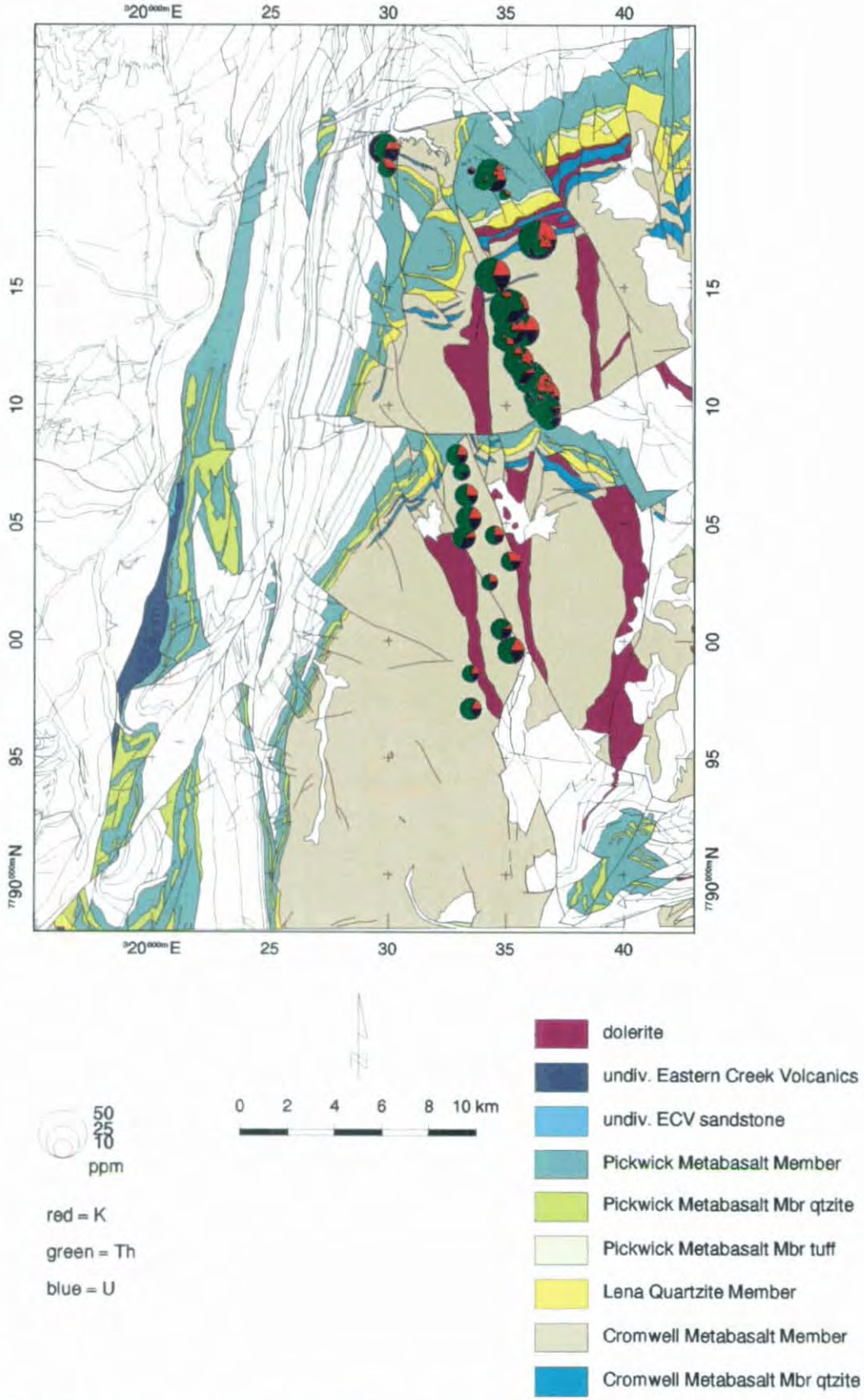

Figure 7.12 Eastern Creek Volcanics outcrop geology and radioelement concentration derived from geochemical analyses in the AGSO ROCKCHEM database. Size of circles indicating sample location is proportional to total radioelement concentration. K is ^{40}K concentration derived by converting K_2O values from ROCKCHEM to ppm equivalent and multiplying by the natural $^{40}K/^{39}K$ ratio (0.012%; Telford et al., 1990)

Geochemical observation	Author(s)	Geophysical response
mid-upper Phc Fe-enriched	S & T (1982)	mid-upper Cromwell highly magnetic
basal Phc high in Fe_{tot}, also high in K_2O, Th(?)	W, D & P (1985)	Not apparent - lower Phc not highly magnetic, low in K and Th. Arguably W,D&P (1985)'s observation is not even supported by the geochemical data (Figs. 7.14-16; also W,D&P 1985, their Fig 4)
$Th_{Phc} > Th_{Php}$ (ratio ~2:1) $U_{Phc} > U_{Php}$ (ratio ~4:1)	W, D & P (1985); their Table 1	Strongly supported - very little Th signal in Php. U similar

Table 7.1. Stratigraphic differences in Eastern Creek Volcanics geochemistry - geophysically and metallogenically important elements. Phc = Cromwell Metabasalt Member, Php = Pickwick Metabasalt Member. S & T (1982) = Scott and Taylor, 1982; W, D & P (1985) = Wilson et al., 1985

Scott and Taylor (1982) noted that the middle to upper portion of the Cromwell Metabasalt appeared to be enriched in Fe, consistent with the highly magnetic nature of this portion of the Eastern Creek Volcanics. Wilson et al. (1985) did examine the issue of geochemical differences between the metabasalt components of the Eastern Creek Volcanics, with statistical analyses performed separately on both metabasalt members, but few differences in element concentration are apparent in their data presentation. They recognised the basal quarter of the Cromwell Metabasalt Member (CMM) as marked by high levels of total Fe, K_2O, Cu, Zn and, less certainly, Th; while the overlying sequence had a "very consistent" composition. The Pickwick Metabasalt Member (PMM) was regarded as being less fractionated than the upper CMM by Wilson et al. (1985), with only half as much Th. In both datasets, the highest levels of K_2O and Th were invariably recorded in the siltstones and tuffs intercalated with the metabasalt flows. No systematic geochemical differences between metabasalt members of the Eastern Creek Volcanics were mentioned by Wyborn (1987).

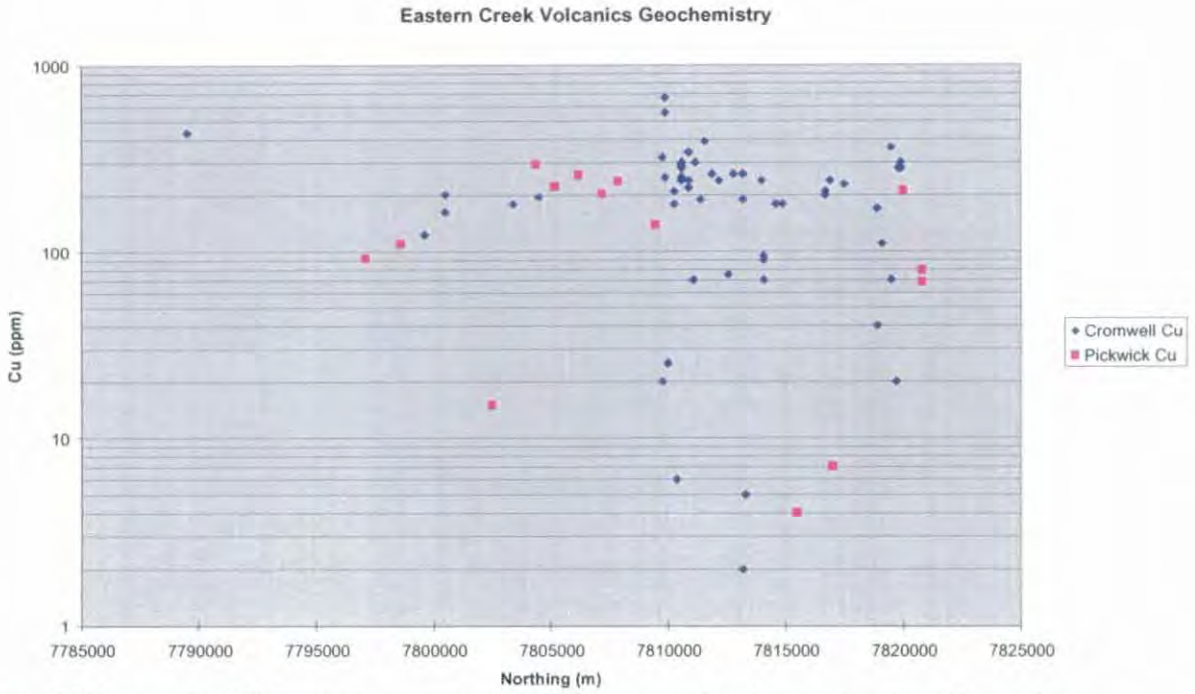

Figure 7.13 Eastern Creek Volcanics Cu concentration in relation to stratigraphic position, classed by member

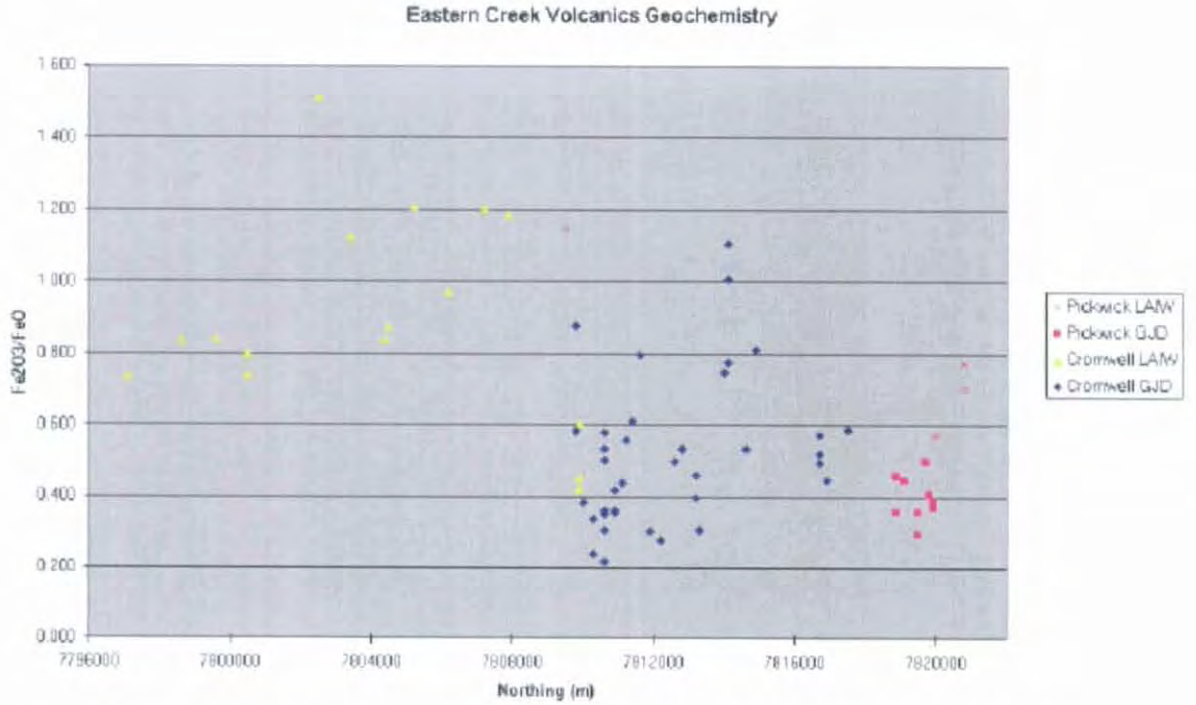

Figure 7.14 Eastern Creek Volcanics Fe_2O_3/FeO ratio classed by stratigraphic unit and originator (LAIW = Lesley Wyborn, GJD = Geoff Derrick)

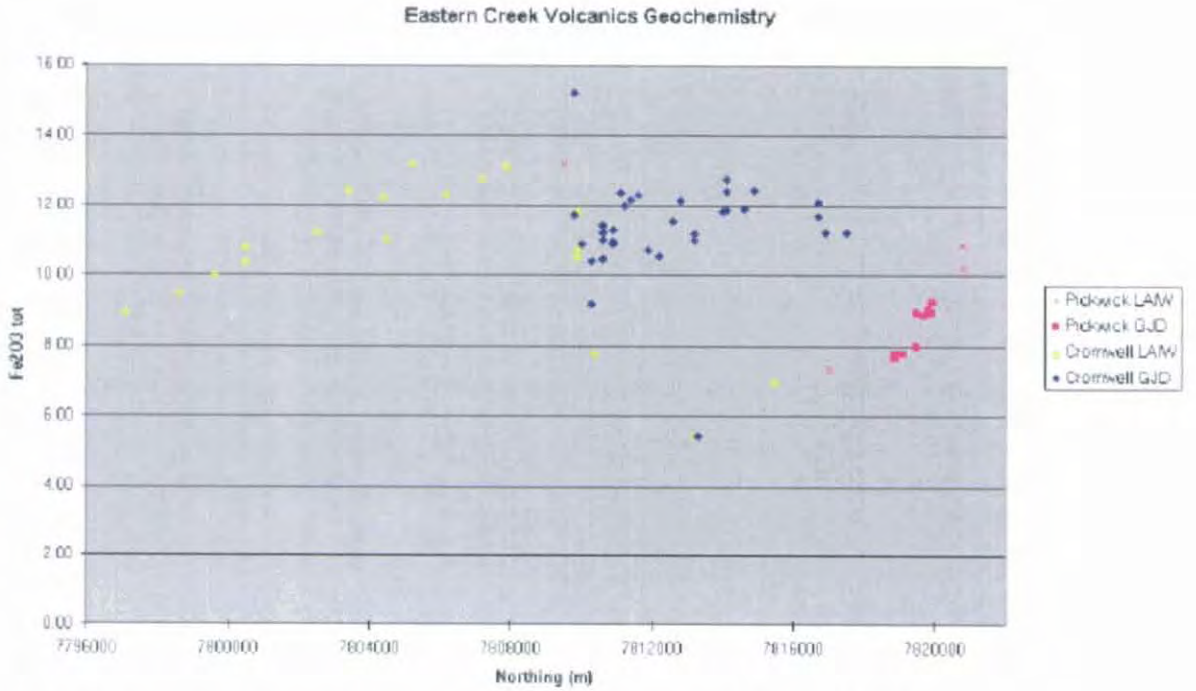

Figure 7.15 Eastern Creek Volcanics Fe concentration classed by stratigraphic unit and originator

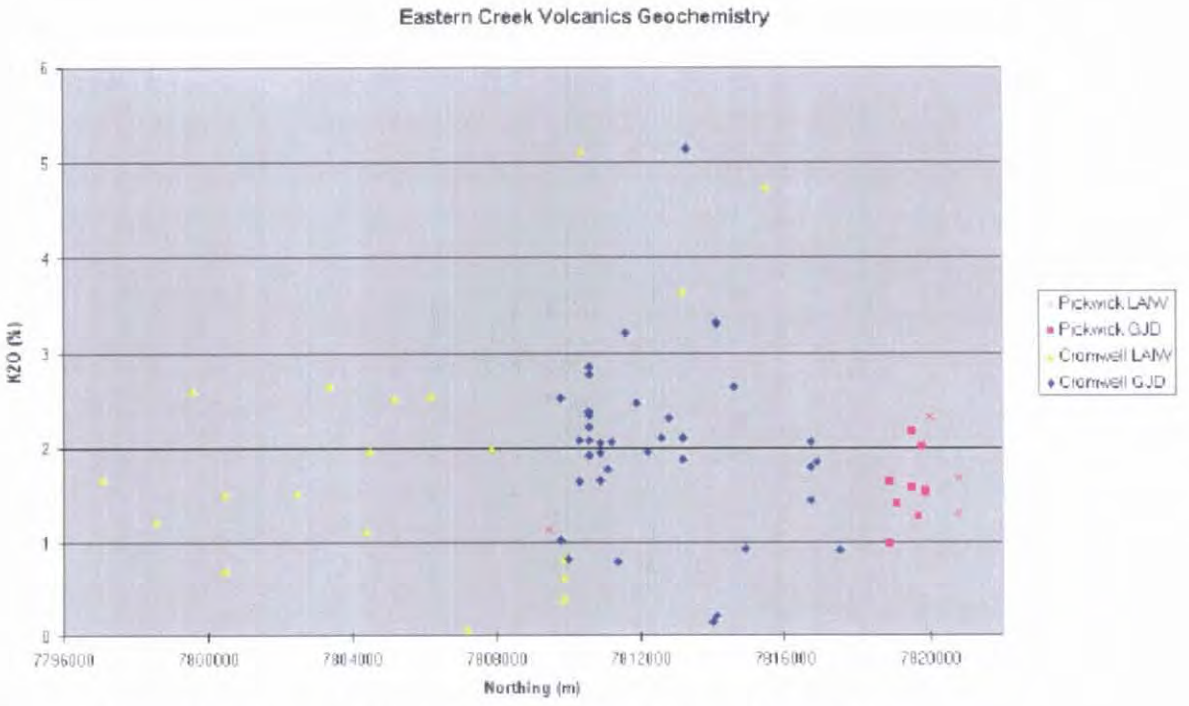

Figure 7.16 Eastern Creek Volcanics K_2O concentration classed by stratigraphic unit and originator

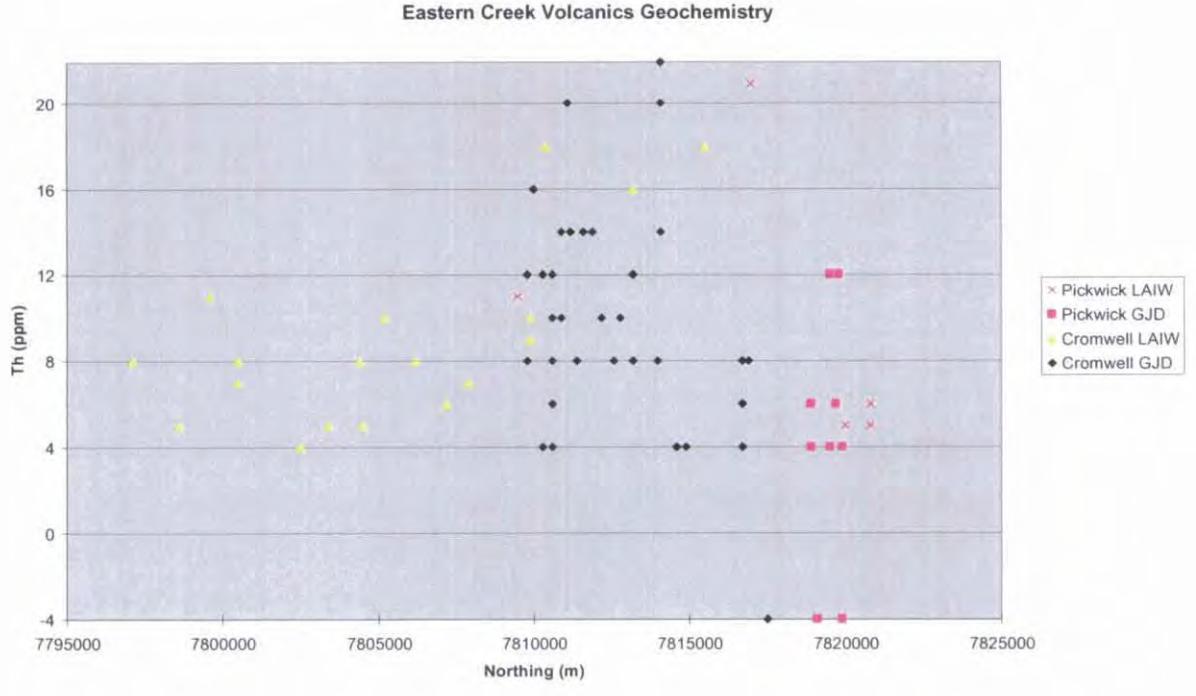

Figure 7.17 Eastern Creek Volcanics Th concentration classed by stratigraphic unit and originator

There are major differences across the Investigator Fault, across which the Eastern Creek Volcanics stratigraphy is repeated. Fe in the Cromwell Metabasalt appears significantly more oxidised in the upper portion of the member south of the Investigator Fault, with Fe_2O_3/FeO ratios around double those observed north of the fault in a lower section of the stratigraphy (Fig. 7.14). It is possible that this may be caused by different alteration systems, but a stratigraphic control is indicated by upward trends in the Fe_2O_3/FeO ratio within the CMM on both sides of the fault. A similar (upward-increasing) trend is

exhibited within the PMM, but the Fe_2O_3/FeO ratio appears to be 'reset' to levels similar to the basal Cromwell Metabasalt at the base of the Pickwick Metabasalt around 7819000N. Total Fe content (Fig. 7.15) expresses similar patterns, though there is less difference in absolute terms across the Investigator Fault than in the plot of Fe_2O_3/FeO ratio. Stratigraphic controls, possibly reflecting evolution of the source magma reservoir with time, are again indicated. A prominent feature of Fig. 7.15 is the much lower concentration of Fe in the Pickwick Metabasalt, which may at least partly explain why the Pickwick Metabasalt appears less magnetic than the Cromwell Metabasalt. The Pickwick Metabasalt immediately south of the Investigator Fault defies this generalisation, but unfortunately is only represented by one sample, which is one of several anomalous Fe_{tot} analyses from near the Investigator Fault.

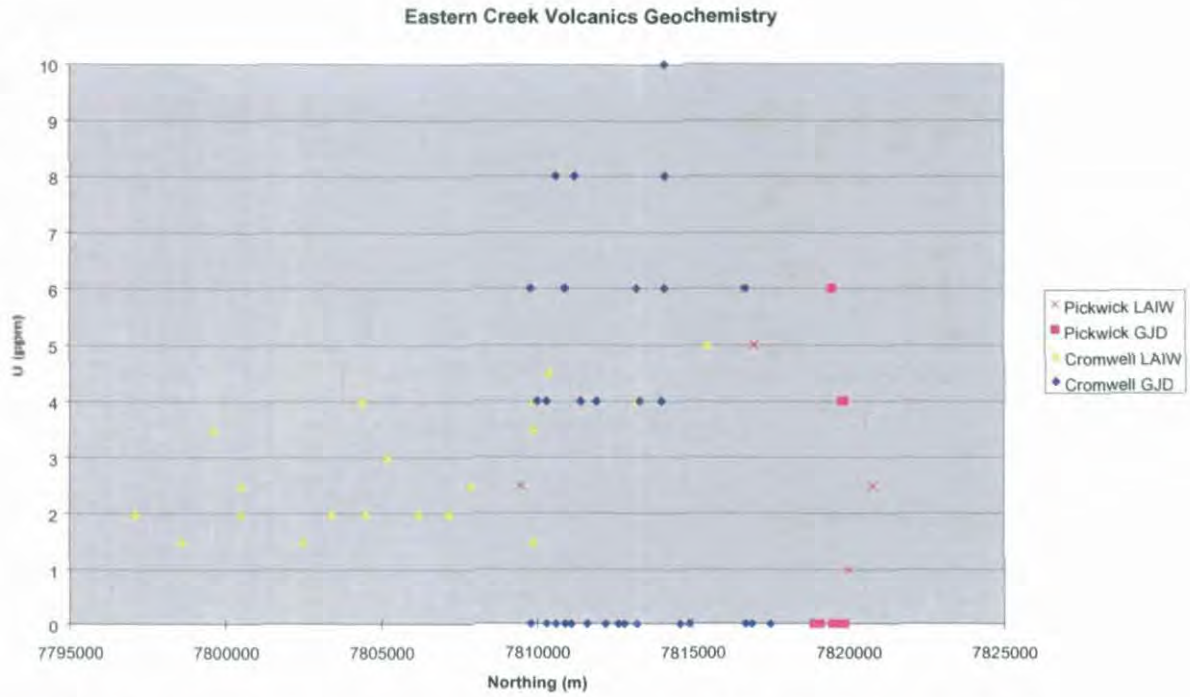

Figure 7.18 Eastern Creek Volcanics U concentration classed by stratigraphic unit and originator. Samples shown with 0 ppm were below the 4 ppm detection limit nominated for GJD-originated data in ROCKCHEM

K levels appear slightly lower in the Pickwick Metabasalt than in the Cromwell Metabasalt (Fig. 7.16). Although a one-tailed t-test finds no significant difference in means at the 90% confidence level, the difference in medians is 0.42 weight %. The highest levels observed in the radiometric data for the PMM implies that K is higher in this unit, at least in the weathered profile, in apparent contradiction to the geochemical data. Differences between the Th and U content of the CMM and PMM, while unclear in the geochemical data (Figs. 7.17 and 7.18), are obvious in the radiometric data (Figs. 7.10 and 7.11).

Of some concern for attempts to draw conclusions from the two combined geochemical datasets (Figs. 7.17 and 7.18) is a systematic difference between the Th and U data from Wilson et al. (1985) and Wyborn (1987) across the same stratigraphic section of Eastern Creek Volcanics between 7810000N and 7821000N. Wilson et al. (1985)'s analyses are significantly higher, though this may possibly be due to differences in sampling strategy rather than analytical error. Notwithstanding this, the geochemical data show Th and U to be higher in the Cromwell Metabasalt north of the Investigator Fault than that to the south. The radiometric data are more equivocal on this point.

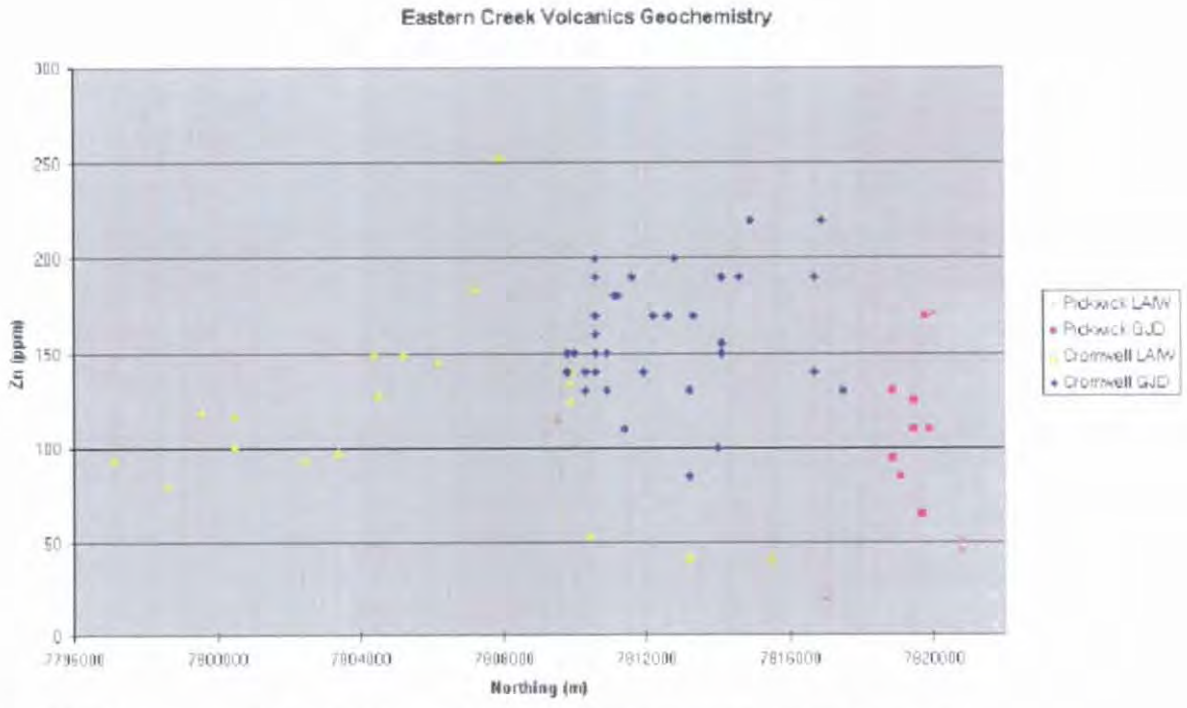

Figure 7.19 Eastern Creek Volcanics Zn concentration classed by stratigraphic unit and originator

7.4.2.1.2 Alteration assemblages

Cu depletion was accompanied by K-enrichment (up to fivefold) and moderate Fe-depletion in data obtained from a drillcore intersection of the Pickwick Metabasalt near the Mammoth Cu mine by Scott and Taylor (1982). Coupled with the fact that the main Fe-bearing mineral noted in the alteration near Mammoth was haematite, the expected signature of metabasalt having sourced Cu-bearing fluids would be a region of near-neutral TMI in IGRF-residual terms. Such a response is observed over the Pickwick Metabasalt at Mammoth. Though this magnetic signature in this area is distorted by geometric effects associated with the nearby steeply dipping metabasalt/sediment contact, a depression in apparent magnetic susceptibility is clearly apparent in a fault-bounded strip over a kilometre wide extending south for several kilometres from the Mammoth Extended Fault at 330000E. This zone is marked by the subdued nature of the ubiquitous high frequency magnetic anomalies in this district.

K-channel levels over the Pickwick Metabasalt closest to Mammoth are among the highest observed in this unit regionally. Within the area of low magnetic susceptibility near Mammoth, high K levels are confined north of 7820000N. The northern third of the Pickwick Metabasalt slice at 327000E immediately east of Mammoth is also very high in K. Th likewise appears anomalously high in this area and in the main body of Pickwick Metabasalt south and west of Waggaboonya Lake. Unfortunately, neither Th nor U were examined by Scott and Taylor (1982).

Variance in major and trace element concentration was taken as an indicator of alteration intensity by Wilson et al. (1985). On this criterion, the Cromwell Metabasalt north of the Investigator Fault would appear to be the 'most altered', particularly in Fig. 7.15. Other than some stratigraphically controlled variations, no anomalous signals are apparent in the corresponding area of the radiometric image.

Samples with $CO_2 > 0.20\%$ were identified with alteration by Wilson et al. (1985), and high CO_2 levels were identified with magnetite creation in this context by Wyborn (pers. comm., 1996); thus the altered rock described by Wilson et al. (1985) in their Gunpowder section (between the Investigator Fault at 336700E 7809800N and 333500E 7819900N) should be highly magnetic. This section of the ECV generally appears to have moderate to high susceptibility, but the CO_2-rich assemblage is not localised to any particular area within the study region (Wilson et al., 1985), and in detail the association between altered samples (as defined by the $CO_2 > 0.20\%$ criterion) and local magnetic highs is not strong. It may be concluded there are additional controls on magnetite creation in the ECV as well as CO_2 concentration. Other characteristics of samples identified as altered by Wilson et al. (1985, their Table 1) include slightly increased Fe_2O_3/FeO ratios (from 0.42 to 0.68), depleted K_2O (1.97 to 1.65) and slightly decreased Th and U (10 to 8 and 4 to 3, respectively). This style of alteration would therefore be expected to produce slightly subdued magnetic and radiometric signatures. Unfortunately, it is difficult to explicitly identify and spatially locate the samples assigned to the various alteration types of Wilson et al. (1985) from their paper.

Wyborn (1987) recognised four alteration assemblages, and established paragenetic relationships between them. Their characteristics are listed in Tables 7.2 and 7.3 below.

Alteration type after Wyborn (1987)	**Radiogenic & magnetic minerals**	**Other features** (Wyborn, 1987)	**Expected geophysical signature**
albite + actinolite	minor sphene, K-feldspar, biotite; magnetite	high magnetic susceptibility; possibly assoc. with Zn-Pb mineralisation at Mt. Isa	high K, mod. Th & U in sphene; magnetic
epidote ± sphene	sphene, minor biotite, K-feldspar	end-member non-magnetic; assoc. with major faults & fractures near Gunpowder	mod.-high K, high Th & U; non-magnetic
calcite + magnetite	minor biotite, K-feldspar	rare near Gunpowder	mod.-low K, low Th & U; magnetic
chlorite + albite	sphene, minor biotite	mainly occurs in subsurface at Mt. Isa Mine	very low K, mod. Th & U; non-magnetic

Table 7.2 Geophysically important features of Eastern Creek Volcanics alteration assemblages defined by Wyborn (1987)

The albite + actinolite alteration type probably corresponds to the albite-rich Eastern Creek assemblage identified by Scott and Taylor (1982). Its end-member composition may be represented by the K-metasomatised, Cu-depleted Pickwick Metabasalt from a drillhole immediately ENE of Mammoth described by Scott and Taylor (1982) and discussed above. However, these correlations are uncertain as Wyborn (1987) unfortunately did not refer to Scott and Taylor's (1982) work in her paper. A noteworthy feature of geochemical data representing albite (Na-rich) alteration (Table 2 of Scott and Taylor, 1982) is a very high level (6.60%) of CO_2 (probably as calcite). Wyborn (pers. comm., 1996) suggested that CO_2 is an important accessory to magnetite formation. This is in accord with Wyborn's (1987) description of the albite + actinolite assemblage as being highly magnetic. Albite + actinolite alteration constitutes 70% of samples collected in traverses south-east of Gunpowder and north of the Investigator Fault (Fig.7.12) according to Wyborn (1987).

The epidote + sphene and calcite + magnetite alteration types are compositionally quite similar apart from increased CO_2 and the presence of magnetite in the latter (Wyborn, 1987). Both types are spatially associated with relatively intense deformation and faulting, with alteration intensity greatest adjacent to

faults (Wyborn, pers. comm.). Samples identified by Wyborn (pers. comm.) as belonging to the epidote + sphene alteration assemblage do in fact come from locations within magnetically quiet areas observed around 335000E 7818000N and 334800E 7814500N. Calcite + magnetite alteration is rare in the study area (Wyborn, 1987), but there is an association between high CaO samples and magnetic highs, in particular the high at 333000E 7807000N. .

Chlorite + albite, the final alteration type described by Wyborn (1987), is mainly known from the subsurface at Mount Isa Mine, and has not previously been identified at all in the study area. As seen in Table 7.3, K is strongly depleted in this assemblage, as is Fe_2O_3, resulting in low Fe_2O_3/FeO ratios and low total Fe. This Fe loss, coupled with Wyborn's (1987) observation that chlorite + albite alteration apparently formed by destruction of the calcite + magnetite assemblage, leads to the expectation that magnetic susceptibility of chlorite + albite altered metabasalt will be low, while low levels of K have obvious implications for its radiometric signature. This is in accord with the geophysical interpretation of a large volume of low-susceptibility ECV beneath the Mount Isa mine (Leaman, 1991a).

The summary of geochemical data in Table 7.3 shows significant variations in K_2O between several of the alteration assemblages, with consequent implications for their radiometric signature. Based on this data, albite + actinolite alteration should result in elevated counts in the K channel, while epidote + sphene and calcite + magnetite alteration will have more subdued K response. Chlorite + albite alteration, directly associated by Wyborn (1987) with the Mount Isa Cu mineralisation, is predicted to result in very low K-channel counts. Unfortunately Wyborn (1987) did not present Th and U analyses; and no confident inferences on magnetite concentration can be made from the geochemical data alone.

Analysis of Eastern Creek Volcanics geochemical data does not show any strong correlation between geophysically important elements (Fe, K, Th, U) and base metal concentrations, apart from a correlation coefficient of 0.99 between Pb and U.

Type	**albite + actinolite**		**epidote + sphene**		**calcite + magnetite**		**chlorite + albite**		**P69 chloritic metabasalt**
samples	31		19		34		48		1
	x	*SD*	*x*	*SD*	*x*	*SD*	*x*	*SD*	
Fe_2O_3	4.28	1.32	6.19	2.58	5.04	2.53	0.58	0.48	1.73
FeO	10.06	1.53	7.72	1.85	8.90	1.61	8.65	4.01	6.61
Tot. Fe	14.91	1.90	14.29	2.49	14.43	2.54	9.11	2.97	8.17
K_2O	1.93	0.61	1.08	0.81	1.04	0.84	0.48	0.52	1.35
Pb	17	12	34	13	45	47	<50		35
Cu	220	91	102	68	162	152	8	18	5
Zn	140	47	153	55	147	49	78	28	55

Table 7.3. Summary geochemical data for base metals and geophysically significant elements in Eastern Creek Volcanics alteration assemblages, after Wyborn (1987) and Wilson (1982, quoted in Hutton and Wilson, 1985).

7.4.2.2 Implications for base metal metallogeny

While alteration may be ubiquitous in the Eastern Creek Volcanics (Wilson et al., 1985), it is clear that stratigraphic differences are an important, and perhaps the dominant control on geochemistry so far as geophysically measurable parameters are concerned. The Cromwell Metabasalt contains higher levels of

Fe_2O_3, Fe_{tot}, Th, U, Pb, Zn and Cu than the Pickwick Metabasalt, and the general geochemical homogeneity along strike implied by the geophysical data implies a strong primary compositional control on the geochemical data observed. Alteration systems in the Eastern Creek Volcanics must be viewed in this context.

At least two and possibly three alteration types have been associated with the passage of base metal mineralised fluids passing through or sourced from the Eastern Creek Volcanics. These, derived from reviews of geochemical analyses reported in Scott and Taylor (1982), Hutton and Wilson (1985), Wilson et al. (1985) and Wyborn (1987) are summarised in Table 7.4. Mammoth Cu mineralisation is associated with extreme K enrichment of the Pickwick Metabasalt in the subsurface nearby (Scott and Taylor, 1982). While K-enrichment is not prominent in proximal outcropping equivalents observed geophysically, it is likely that this would be the case if the extreme K_2O levels measured in drillcore (up to 11%) extended to nearby outcropping Pickwick Metabasalt. K_2O concentrations approaching 4% in Pickwick Metabasalt outcropping 1 km east of Mammoth do manifest as highs in the K channel. A 'Mammoth-type' Eastern Creek Volcanics geophysical alteration signature should include high K levels coupled with low apparent magnetic susceptibility. Th levels may also be slightly elevated in Mammoth-type alteration, based on inspection of the airborne radiometric data. Other areas where this alteration may be present in the study area include the Pickwick Metabasalt overlying the lens of Php_q (Pickwick Metabasalt Member quartzite) around 332500E 7816000N, and extending ESE from where the Pickwick Metabasalt is truncated by the Investigator Fault at 337000E 7809600N. Structural environments favourable for Mammoth-style Cu mineralisation associated with the latter alteration system may exist within the Myally Subgroup adjacent to the Investigator Fault.

Alteration type	Geophysical effect	Geochemical cause
Mammoth Cu	K high, mag low	K metasomatism (microcline, mica), Fe depletion & possibly magnetite destruction
Pb-Zn (P69)	mag low, K ~low, U low?	Fe depletion, chlorite + albite alteration?
Mount Isa Cu (chlorite + albite)	K low, mag low	K loss, magnetite destruction & overall Fe depletion

Table 7.4. Geophysical signatures of metallogenically significant Eastern Creek Volcanics alteration

No author has examined the alteration systems of the Eastern Creek Volcanics in terms of Pb-Zn metallogeny in detail. Wyborn (1987) mentioned that the albite + actinolite alteration may have been related to the Mount Isa Pb-Zn orebodies, but only on the basis of its relatively early timing. In this regard, it is notable that of the four alteration types defined by Wyborn (1987), chlorite + albite has by far the lowest average Zn concentration (Table 7.3). In this context it is interesting that of all the alteration types shown in Table 7.3, chloritic metabasalt sampled from drillhole P69 less than 2 km NW of the Lady Loretta Pb-Zn deposit is most chemically similar to the average composition of the chlorite + albite assemblage. They share very low Fe_2O_3/FeO ratios, low total Fe, low MnO, very high MgO, very low CaO, very low Cu and low Zn (Table 7.3). K_2O at 1.35% in P69 is also slightly lower than in unaltered Eastern Creek Volcanics regionally.

Mitigating against a genetic relationship between the chlorite + albite alteration and Pb-Zn mineralisation at Mount Isa is its late timing (late Isan Orogeny; syn-Cu mineralisation according to Wyborn, 1987). This assumes hypotheses of early diagenetic timing for Pb-Zn mineralisation are correct. Additionally, Wyborn (1987) ascribed chlorite + albite alteration to low pH reduced fluids, whereas Cooke et al. (1998) have suggested that fluids carrying base metals to stratiform sediment-hosted base metal mineralised sites in the north Australian Proterozoic are oxidised and near-neutral.

The spatial association of chlorite + albite-like alteration in P69 with a sizeable Pb-Zn deposit (Lady Loretta), coupled with a clear depletion in Zn (Table 7.3), provides some support for the association of chlorite + albite alteration with Pb-Zn mineralisation. Unfortunately (though possibly not coincidentally; see McGoldrick and Keays, 1990), at Lady Loretta as at Mount Isa, the relationship is clouded by the presence of a significant Cu deposit (Lady Annie) nearby.

Wyborn (1987) has concluded that formation of the chlorite + albite alteration was probably genetically related to the formation of the Mount Isa Cu ore bodies. Based on the geochemical data presented, the chlorite + albite assemblage is expected to be low both in K-channel radiometric signature and apparent magnetic susceptibility. Such signatures are not uncommon in the Pickwick Metabasalt, particularly north and east of 336000E 7820000N, in the southern two-thirds of the small outcrop west of Mammoth, and through much of the N- to NNE-striking uppermost Eastern Creek Volcanics extending north from 325000E 7787000N. Additional possibilities include the area around 319000E 7795000N and around the rim of the inlier in the southeastern corner of the study area, though here the metabasalt signatures are obscured by intercalated quartzite. Any of these regions may possibly have sourced Mount Isa-style Cu mineralising fluids, but of the examples mentioned only the latter two are proximal to potentially suitable (similar to Urquhart Shale) trap rocks, in the form of the Paradise Creek Formation and Moondarra Siltstone respectively. Similar alteration may be present in the Cromwell Metabasalt, but it is difficult to identify due to the relatively low levels of K in the member regionally. One possibly prospective example is at 365000E 7792500N, where Cromwell Metabasalt with the chlorite + albite alteration signature (K low, reduced magnetic response) is faulted against the Moondarra Siltstone.

The only sample of (probable) Eastern Creek Volcanics in the study area with a chlorite + albite-like alteration signature is the sample from drillhole P69 near Lady Loretta referred to above. Its very low Cu concentration compared to the Eastern Creek Volcanics regionally (Table 7.3) constitutes *prima facie* evidence that the rocks intersected have sourced Cu-bearing fluids. Direct physical measurements on the P69 metabasalt (chapters 5 and 6, Appendix 3) demonstrate the low magnetic susceptibility predicted for the chlorite + albite alteration. The magnetic high immediately north of Lady Loretta (see section 7.4.5) is subdued in comparison to what might have been expected given that Eastern Creek Volcanics correlates are known from drilling to occur close to the surface (<600 m), but the fact that a magnetic high exists at all is an indication that the altered volume may be limited (see also interpretation of line 170 in chapter 8).

Other alteration assemblages worthy of mention in terms of metallogeny are the epidote + sphene and calcite + magnetite alteration related by Wyborn (1987) to small U deposits hosted within the Eastern Creek Volcanics. A number of these occur in the undivided Eastern Creek Volcanics outcropping within

the Mount Gordon Fault Zone, part of which (including the area hosting the mineralisation) possesses an unusual radiometric signature (very high in all channels) and highly variable apparent magnetic susceptibility (best illustrated around 320000E 7800000N). These signatures are consistent with the presence of both epidote + sphene and calcite + magnetite alteration (sphene being an important carrier of Th and U).

7.4.3 Myally Subgroup

The Myally Subgroup is shown by the near complete absence of high frequency character in the highlighted areas of Fig. 7.20 to be uniformly non-magnetic, the sole exception being a basalt flow in the Whitworth Quartzite ('40 m metabasalt' of Scott and Taylor, 1982) where it strikes south from the Mammoth Cu deposit (329000E 7821000N). Variations in the pseudocolour rendering of the magnetic field in Fig. 7.20 are related almost entirely to the geometry of the underlying Eastern Creek Volcanics. Fig. 7.20 hence generally maps the preserved thickness of Myally Subgroup, so that outcrops of the Alsace Quartzite (lowermost unit of the Myally Subgroup) tend to be marked by magnetic highs, and those of the Lochness Formation (uppermost Myally Subgroup) are associated with magnetic lows. Some interesting exceptions to this general rule occur at 332000E 7838000N in the Mount Gordon Fault Zone and 309000E 7797000N, where magnetic highs occur over the Whitworth Quartzite, which is relatively high in the Myally Subgroup. In both these cases, it appears likely that major fault displacements have introduced elements of the Eastern Creek Volcanics into juxtaposition with upper units of the Myally Subgroup. In the case of the magnetic high at 309000E 7797000N, a shallowly-dipping fault has apparently transported younger rocks over the Eastern Creek Volcanics, which may only be a few hundred metres below the surface at this location. As well as this, it may also be that the Myally Subgroup is much thinner west of the Mount Gordon Fault Zone, which would also at least partly account for the Eastern Creek Volcanics being at very shallow depths beneath the Myally Subgroup inlier at 309000E 7797000N.

Also notable in Fig. 7.20 is the virtually non-magnetic character of the post-Myally Subgroup intrusive dolerites. The N-S trending dykes in the Eastern Creek Volcanics appear to have similar properties, though these are obscured by geometric effects arising from the enclosing metabasalt. The only magnetic character arising from dolerites intruding the Myally Subgroup appears to be a small edge effect on the (stratigraphic) upper edge of the dolerite sill centred on 338200E 7834500N. This signature appears to continue concordant with bedding along or near the upper surface of a recessive sub-unit of the Whitworth Quartzite (Phw_s) mapped as 'feldspathic sandstone' (Hutton and Wilson, 1985). This unit may incorporate a continuation of the dolerite sill, or its highly weathered equivalent.

Figs. 7.21 and 7.22 show the Myally Subgroup formations to be quite distinct in their radiometric signatures, with this treatment (unit-specific stretch) of the data throwing them into sharp contrast, in spite of their broadly similar composition (predominantly feldspathic sandstone). The signature of the Alsace Quartzite is dominated by the Th-channel response, which is interpreted as being caused by palaeoplacer concentrations of heavy minerals including sphene and possibly allanite sourced from the underlying Eastern Creek Volcanics. Any feldspathic component in the sandstone is likely to be mainly composed of plagioclase rather than K-feldspar, since K appears virtually absent. This signature appears fairly uniform

through all outcrops of Alsace Quartzite in the study area. The radiometric signature suggests that the Alsace Quartzite comprises the base of the undivided Myally Subgroup within the Mount Gordon Fault Zone between 322000E and 324000E, but if present, it can only be very thin.

The Bortala Formation's near-white colour with greenish blue overtones in Fig. 7.21 is interpreted as representing a greater concentration of mica and clay minerals than in the Alsace Quartzite. The slight predominance of U and Th over K is ascribed to high concentrations of heavy minerals in the sandstones. There appears to be little regional variation in the radiometric signature of the Bortala Formation.

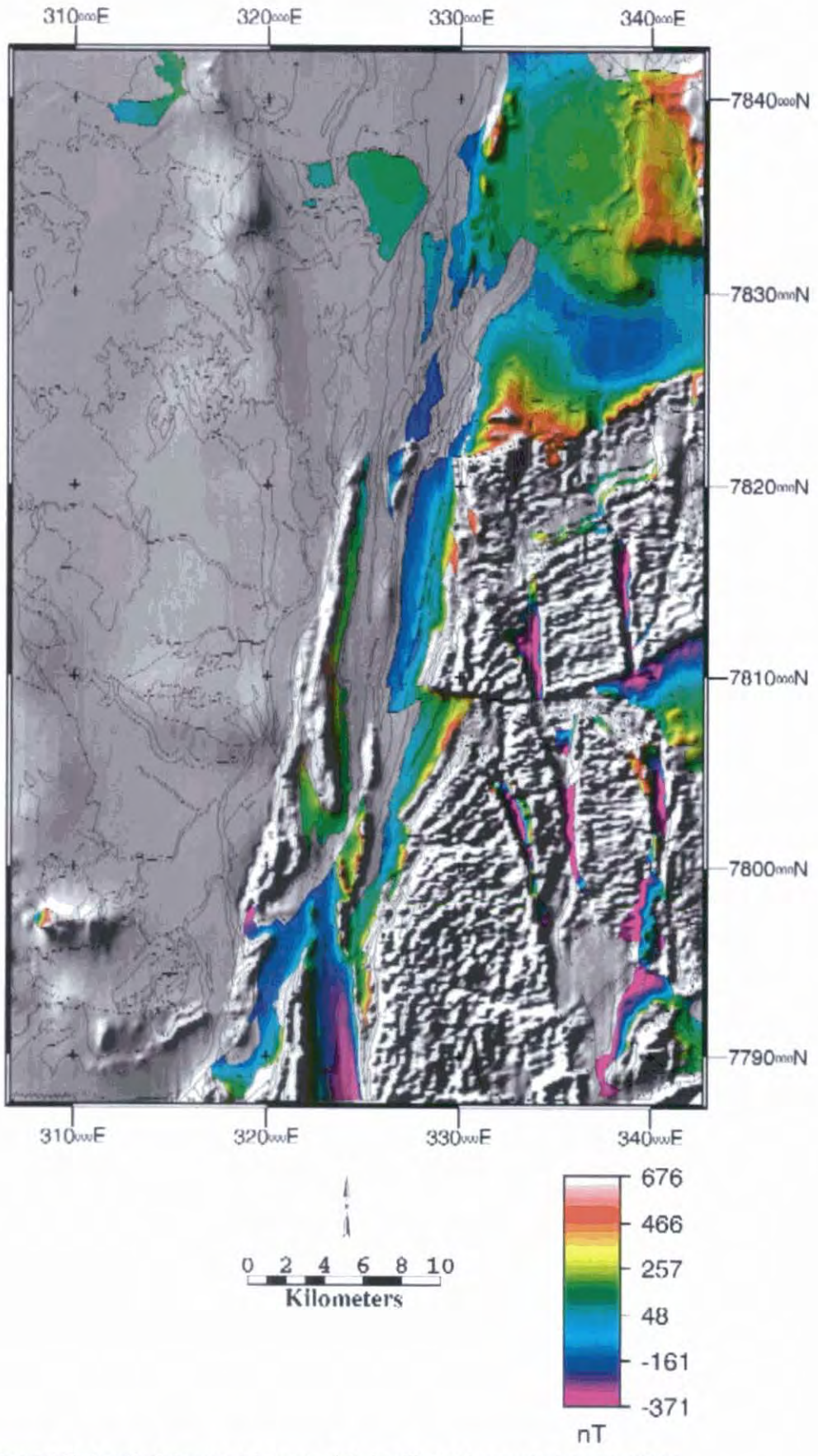

Figure 7.20 Myally Subgroup + intrusive dolerite sills, total magnetic intensity (RTP)

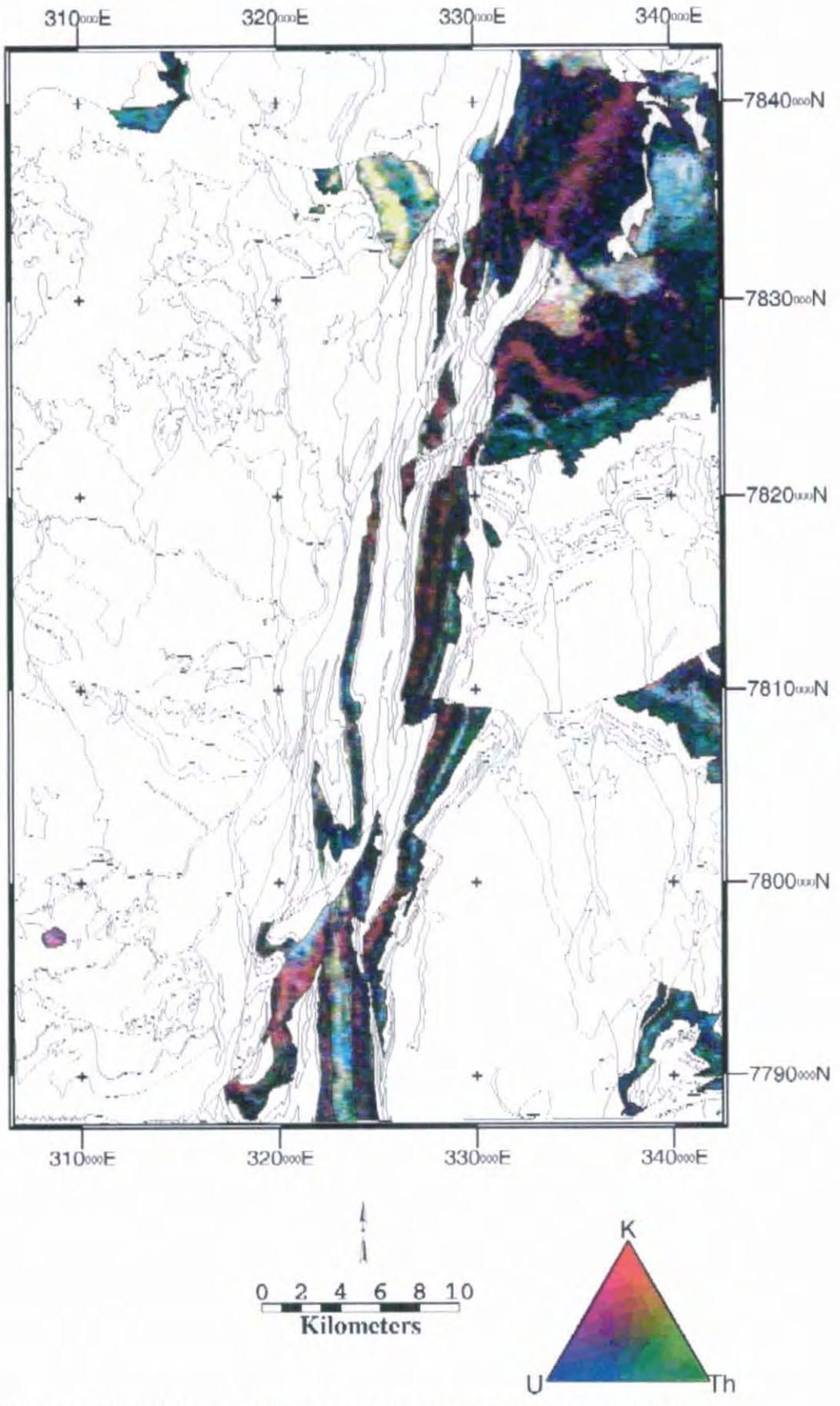

Figure 7.21 Myally Subgroup + intrusive dolerite sills radiometric image, linear transform

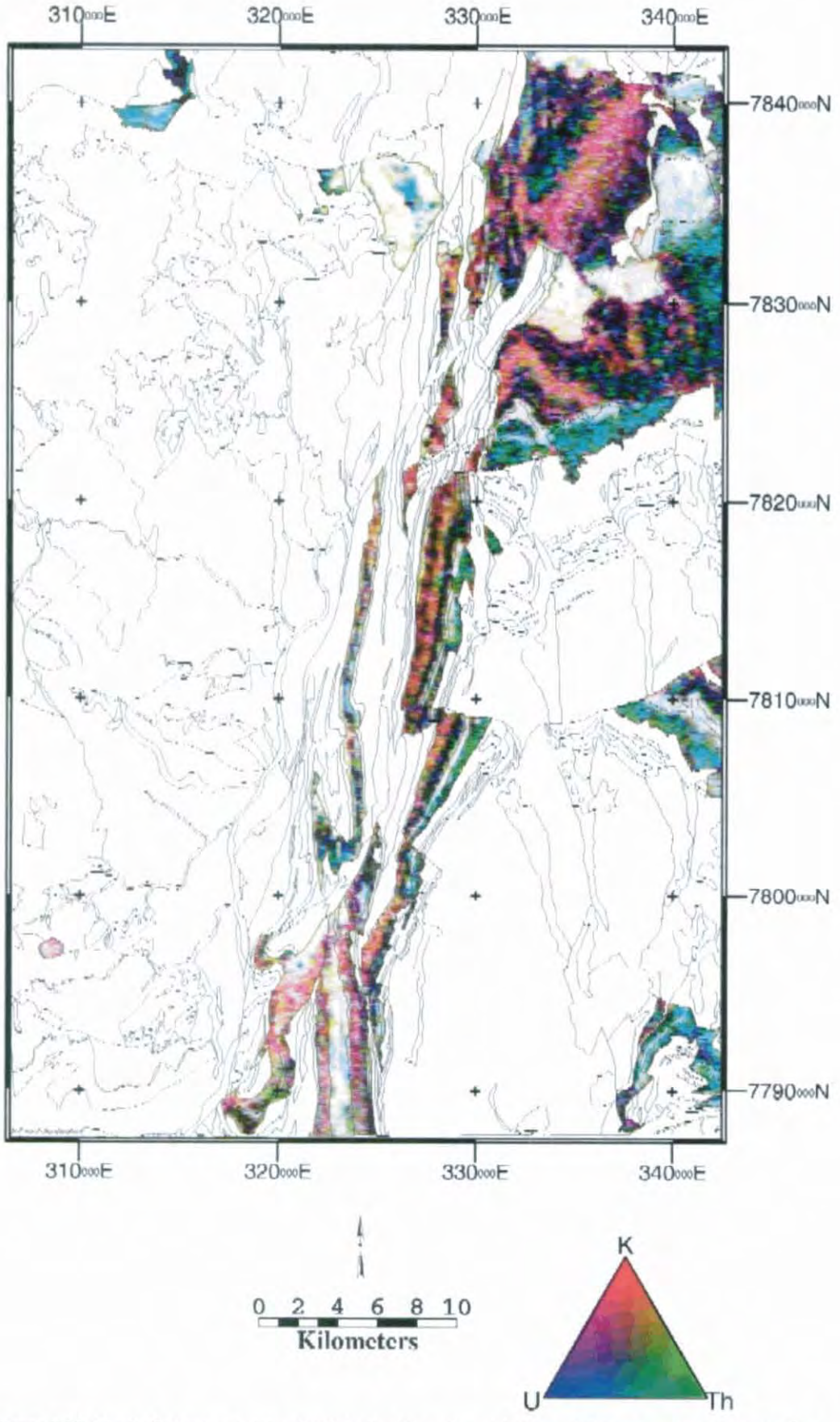

Figure 7.22 Myally Subgroup + intrusive dolerite sills radiometric image, histogram-equalised transform

The Whitworth Quartzite is the least radiogenic of Myally Subgroup units, but a potassium-rich layer probably representing a concentration of interbedded siltstone, poorly sorted muddy sandstone and/or K-

feldspar-rich sandstone, not mapped by Hutton and Wilson (1985), is persistent throughout the formation regionally. This hitherto-unrecognised informal member appears red with purple and yellow patches in Figs. 7.21 and 7.22, and attains a thickness of at least several hundred metres in the northern part of the study area. The gradational nature of the increase in K is best seen by comparing the width of the K-rich layer in Figs. 7.21 and 7.22 (linear and histogram-equalised treatments). K (and hence the silt/clay component) reaches a maximum towards the top of the layer, which may represent a first-order maximum flooding surface. This horizon's distinctive radiometric signature is identifiable on both limbs of the tight syncline in the southern part of the study area at 323000E, and in other areas mapped as undivided Myally Subgroup. This provides support to Hutton and Wilson's (1985) conjecture that the lower portion of the Myally Subgroup is absent and generally thinner west of the Leichhardt River Fault Trough, as a thinned Whitworth Quartzite directly overlies the Pickwick Metabasalt. The inlier of undivided Myally Subgroup at 309000E 7797000N also has a signature typical of the silty/clayey informal member of the Whitworth Quartzite. The lower Myally Subgroup may however be present in the core of an anticline at 321000E 7796500N, wherein occurs a radiometric signature typical of the Bortala Formation.

The Lochness Formation is one of the more radiogenic Myally Subgroup units, and has similar radiometric characteristics to the Bortala Formation. This is in keeping with its lithology (Hutton and Wilson, 1985) which is notably lacking in quartzite compared to the Whitworth and Alsace Quartzites. However, its radiometric signature does vary regionally, with outcrops east of the Mount Gordon Fault Zone appearing distinctly more reddish (higher in K), particularly in Fig. 7.21, possibly resulting from sediments in the palaeo-depocentre containing a higher percentage of mica and clay minerals. The SW- to S-dipping area of Lochness Formation around 326000E 7836000N contains a bed with high Th and total gamma counts. This may indicate a sequence of heavy mineral-bearing, ferruginous or low-K clayey sandstone in the middle of the formation.

7.4.4 Bigie Formation/Fiery Creek Volcanics

Small magnetic responses are associated with thicker, more extensive outcrops of the Fiery Creek Volcanics north of the study area (Betts et al., 1994), but scant evidence for even this slight level of magnetic susceptibility can be found in the Paradise Valley study area (Fig. 7.23). An isolated magnetic high occurs at the southern end of the fault-bounded block of Bigie Formation immediately to the north of Lady Loretta (298200E 7814100N). This may denote preservation of a small amount of slightly magnetic Fiery Creek Volcanics basalt down-dip of the Bigie Formation exposure in a palaeo-half-graben adjacent to what is now the Western Border Fault. Otherwise there is little indication that Fe in the Fiery Creek Volcanics exists except as a constituent of non-magnetic silicate minerals and haematite. The lack of any magnetic anomaly associated with the most extensive Fiery Creek Volcanics outcrop (around 323000E 7835000N) is important evidence in support of this conclusion. This interpretation is supported by low magnetic susceptibility measurements ($< 1.2 \times 10^{-3}$ SI) observed by the author on the basalt outcrop coincident with the magnetic high at 296000E 7814300N. The preferred interpretation for this and other magnetic anomalies north and west of Lady Loretta is that they arise from Eastern Creek Volcanics lying at shallow depths beneath thinned Surprise Creek Formation and extremely attenuated, possibly even absent Myally Subgroup.

The Bigie Formation and the Fiery Creek Volcanics appear to be generally low in all radiometric channels (Figs. 7.2, 7.24). This is surprising given the level of potassic alteration reported elsewhere (Hutton and Wilson, 1984). Only one outcrop of Fiery Creek Volcanics is of sufficient extent in this area to have its radiometric signature mapped reliably given the 50x50 m grid cell size, and here all channels are low, with the exception of a local U- and K-enriched patch on the eastern side (324000E 7835000N). The massive rhyolite mapped 1 km SSE of the McLeod Hill Cu prospect (307000E 7793000N), where a sample containing 7.56% K has been recorded (Pfc_r; Hutton and Wilson, 1985) marks the only other possible occurrence of this very high K Fiery Creek Volcanics signature in the study area.

Spatial variation is more extreme in the Bigie Formation, ranging from high count rates in the northern Mount Gordon Fault Zone (though due to the small, narrow nature of the outcrops, there is contamination by overlapping signals from the adjacent proximal units) to extremely low in the outcrop north of Lady Loretta abutting the Western Border Fault. The signature of the only major outcrop of Bigie Formation in the study area, adjacent to the southern Mount Gordon Fault at 319000E, is reminiscent of the Alsace Quartzite at the base of the Myally Subgroup, and may indicate a similar lithology and tectonic environment, i.e. heavy mineral-rich clastics symptomatic of the onset of a new cycle of rifting.

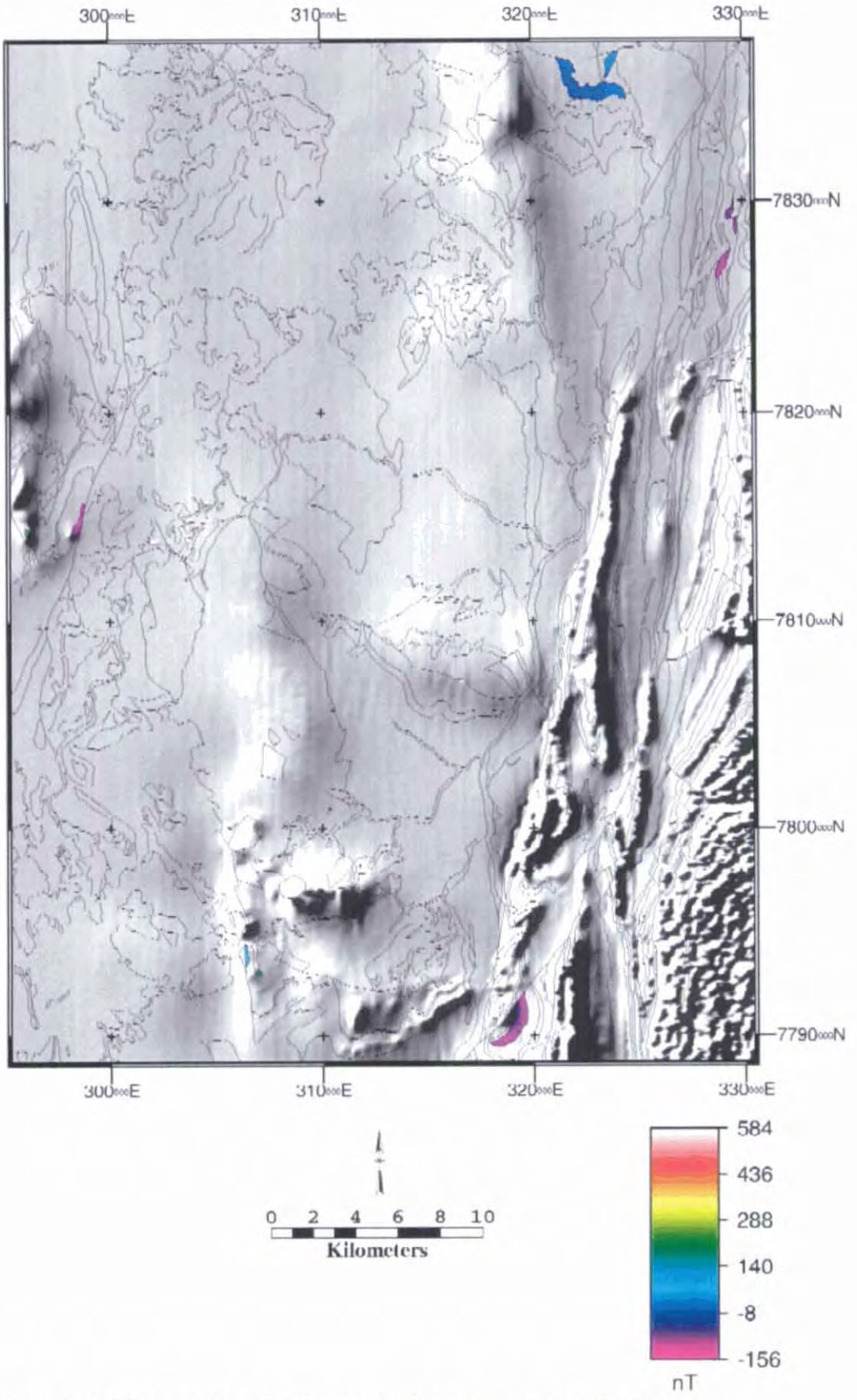

Figure 7.23 Bigie Formation + Fiery Creek Volcanics total magnetic intensity (RTP)

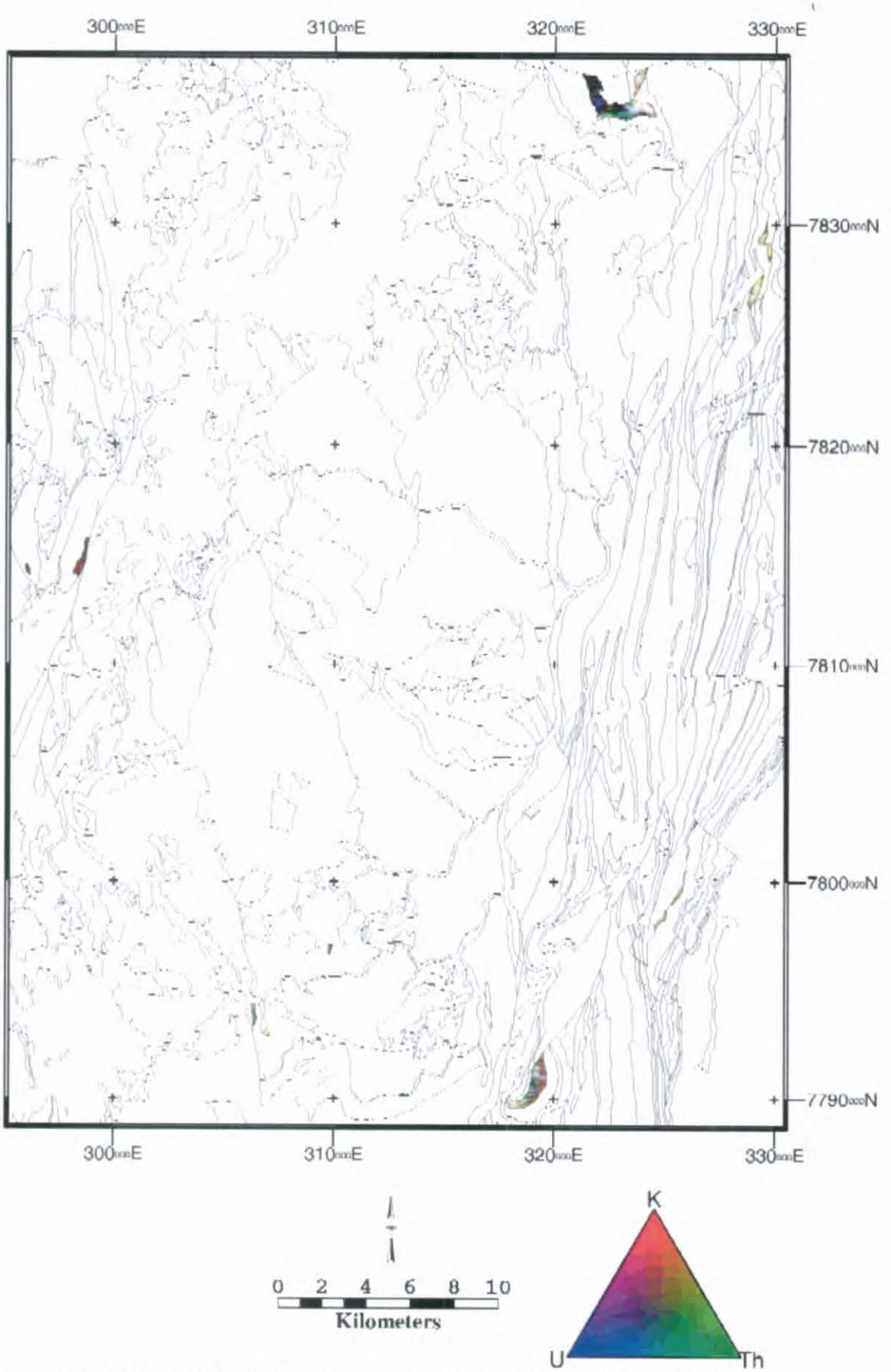

Figure 7.24 Bigie Formation + Fiery Creek Volcanics radiometric image, histogram-equalised transform

7.4.5 Surprise Creek Formation

There is no suggestion that the Surprise Creek Formation (SCF) itself is magnetic (contrary to Anderson et al., 1993), but there are a number of prominent magnetic features within its outcrop area (Fig. 7.25), attributed to ECV at depth. Thinning or absence of the Myally Subgroup is indicated in these areas, but whether lack of deposition or faulting is responsible is not immediately apparent. A linearly extensive NNW-trending anomaly centred at 319000E 7835000N is broadly associated with a regional anticline. While this feature represents elevated Eastern Creek Volcanics in the subsurface, its breadth indicates that the ECV remain at some depth in this area. The culmination of this TMI high at 319000E 7835000N is particularly anomalous in that overlying it is the informal mid-SCF member Pra $_3$, rather than one of the lower members which might have been expected to accompany such an anomaly if the entire basin fill had only undergone simple competent folding. Any faulting involved is likely to be at a low angle, since no fault has been mapped at the location of the steeper eastern edge of the magnetic anomaly. A concealed thrust may be responsible. An alternative hypothesis is that this feature was an elevated fault scarp in pre-SCF (but post-Eastern Creek Volcanics) time.

Such concepts may be invoked for the magnetic features NNW of Lady Loretta, where NNE trends in the magnetic anomalies can be directly related to similarly oriented faults bounding the eastern edge of the SCF blocks. The magnetic data imply that these faults continue through (or at least beneath) the SCF, contrary to indications from mapping (Hutton and Wilson, 1985). This may also constitute evidence either for movement on faults displacing the Eastern Creek Volcanics prior to SCF deposition, or for very low angle thrusts formed during the E-W shortening phase of the Isan Orogeny.

Also notable in Fig. 7.25 is that the three largest known mineral deposits in the study area (Lady Loretta, Mammoth, Mount Kelly) are adjacent to regions of low TMI relative to other areas where SCF is exposed. Apparent changes in the magnetic properties of subsurface Eastern Creek Volcanics (i.e. magnetite-destructive, epidote ± sphene or chlorite + albite alteration) are especially evident in the generally N-dipping blocks of SCF SE and E of Mount Kelly (306000E 7799000N), and immediately west of the Western Border Fault at Lady Loretta (298000E 7814000N). This anomalously low SCF magnetic field signature is also present in an area (315000E 7792000N) not currently known to contain base metal mineralisation, but which may be prospective where it is faulted against potential host rocks in the lower McNamara Group. In the Mount Kelly region the boundaries of the anomalously low TMI areas appear to constitute (possibly subsurface) extensions to faults which have only been recognised in field mapping where they have cut marker units such as the Torpedo Creek Quartzite.

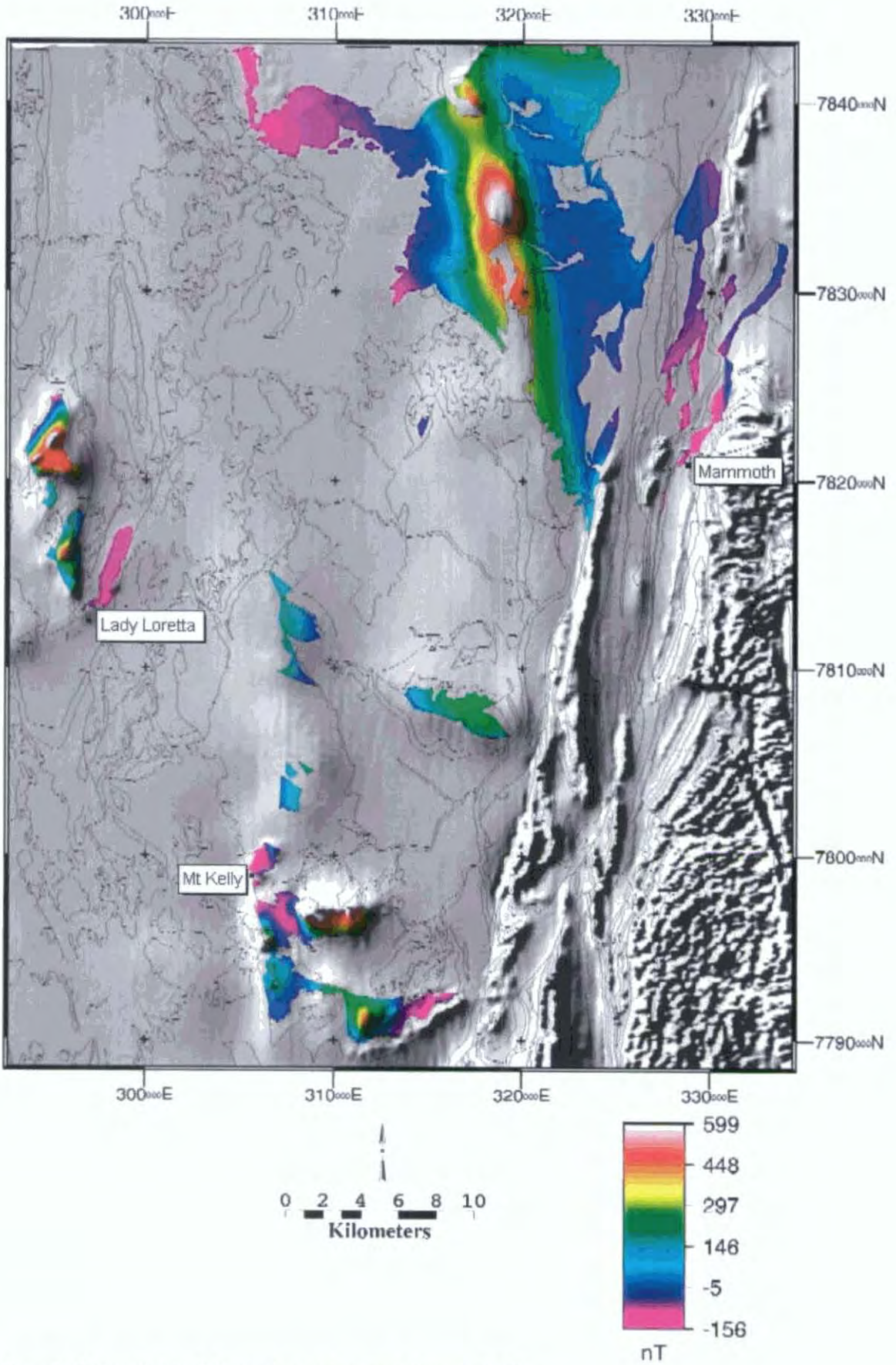

Figure 7.25 Surprise Creek Formation total magnetic intensity (RTP)

There is a strong radiometric contrast between the lower and upper members of the Surprise Creek Formation (Figs. 7.26 and 7.27). Across most of the region, only the lower, arenaceous unit (coded Pra

by Hutton and Wilson, 1985) has been preserved/deposited, and outcrops of it generally display low radiometric response, with the green shades indicating a predominance of thorium. In some of these areas, there are indications that this thorium concentration is stratigraphically controlled, in particular by the informal sandstone member Pra_2, which according to Hutton and Wilson (1985) is feldspathic, clayey and micaceous. All these characteristics will tend to enhance radioelement concentration; in addition, the relatively high concentration of thorium may imply the presence of heavy minerals. A corollary of this correlation is that stratigraphically concordant thorium highs in undivided Pra may represent unmapped equivalents of Pra_2. Examples occur in the vicinity of 308200E 7812500N, and at the very top of the preserved SCF east of Mount Kelly and Mount McLeod (e.g. 311000E 7796000N and 313000E 7790500N). The correlation of these horizons with Pra_2 implies that the overlying McNamara Group has incised progressively more deeply in to the SCF southwards from the area of maximum preservation north of 7830000N.

An anomalous response in the context of the lower SCF occurs at the eastern end of the Redie Creek Fault (319000E 7806500N) where K rather than Th is predominant. This possibly reflects increased feldspathic, micaceous or heavy mineral detrital components sourced from the east, or an unmapped equivalent of the upper SCF (see below). A third possibility for this area is an alteration system associated with Cu mineralisation at the nearby Big Bend prospect, which is hosted within the Lady Loretta Formation on the other side of the Redie Creek Fault.

The upper unit of the SCF (Prd of Hutton and Wilson, 1985) is strikingly high in all channels, consequent from its much more argillaceous composition than the lower unit. The radiometric signal tends to diminish in outcrops to the west due to increasing masking effects from Phanerozoic weathering and cover, or dilution by a mature, quartzose sedimentary source. Though this unit was not subdivided by Hutton and Wilson (1985), the radiometric data clearly indicate some systematic stratigraphic variations within it. The lower portion of the unit in the northern part of the study area is characterised mainly by Th and K signal (yellowish green in Fig. 7.26), changing to a more U-dominated response (bluish) higher up. The implied Th loss/U gain over time may be due to a loss of heavy mineral detrital input and commensurate increase in a dolomitic component, while relatively steady deposition of clay minerals and micaceous silts continued. The K (red) component in the lower portion of Prd appears progressively more pronounced south from 7834000N, where there is also a noticeably heterogenous aspect to the lower Prd'signature, which indicates significant lateral variability in sedimentation at this stratigraphic level. The reasons for this are not apparent, though structural factors are obviously important; the high K'Prd is confined to a syncline south of 7823000N by a fault. There are indications of a transitional contact between the SCF and the overlying, low-count Torpedo Creek Quartzite in this area.

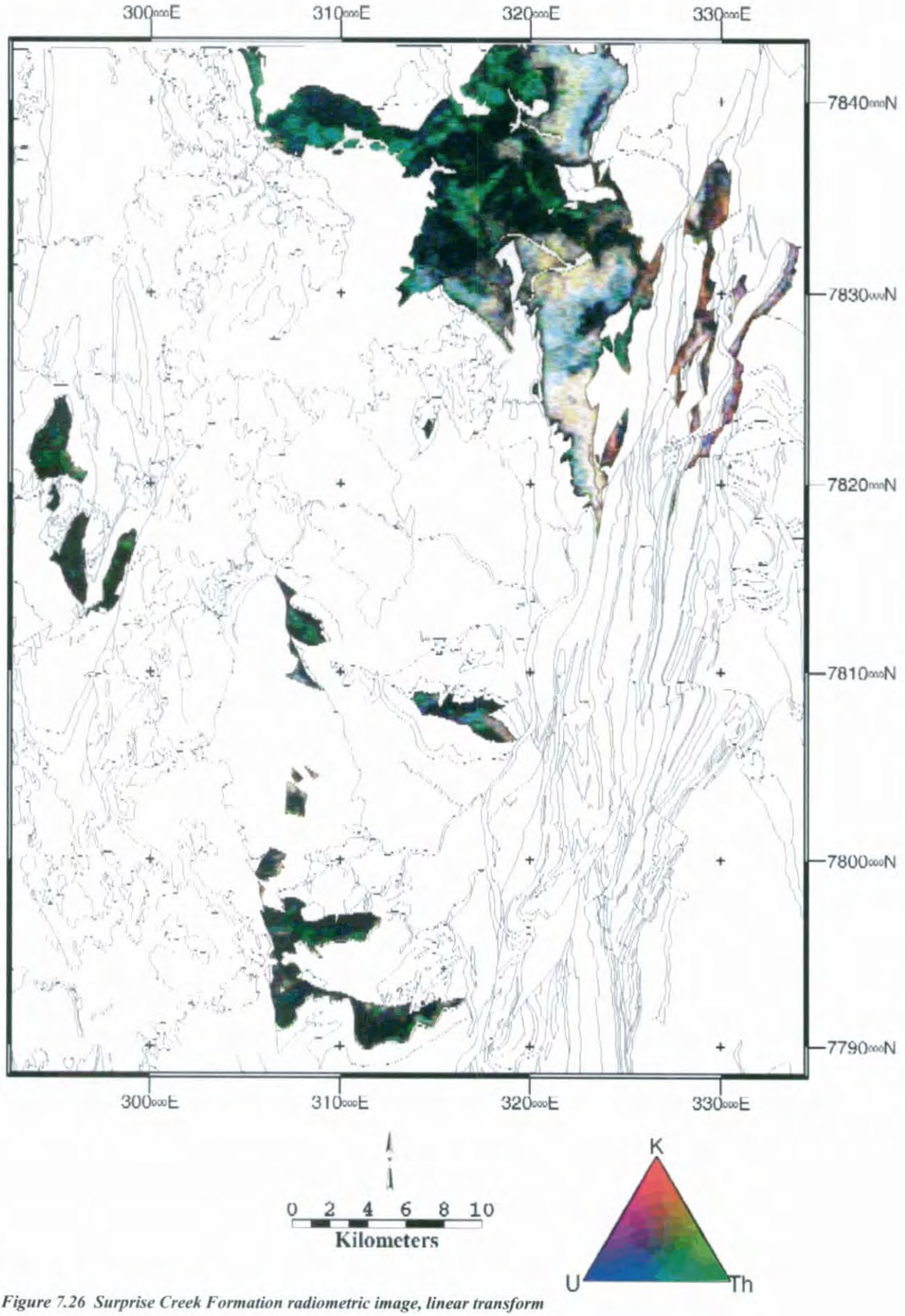

Figure 7.26 Surprise Creek Formation radiometric image, linear transform

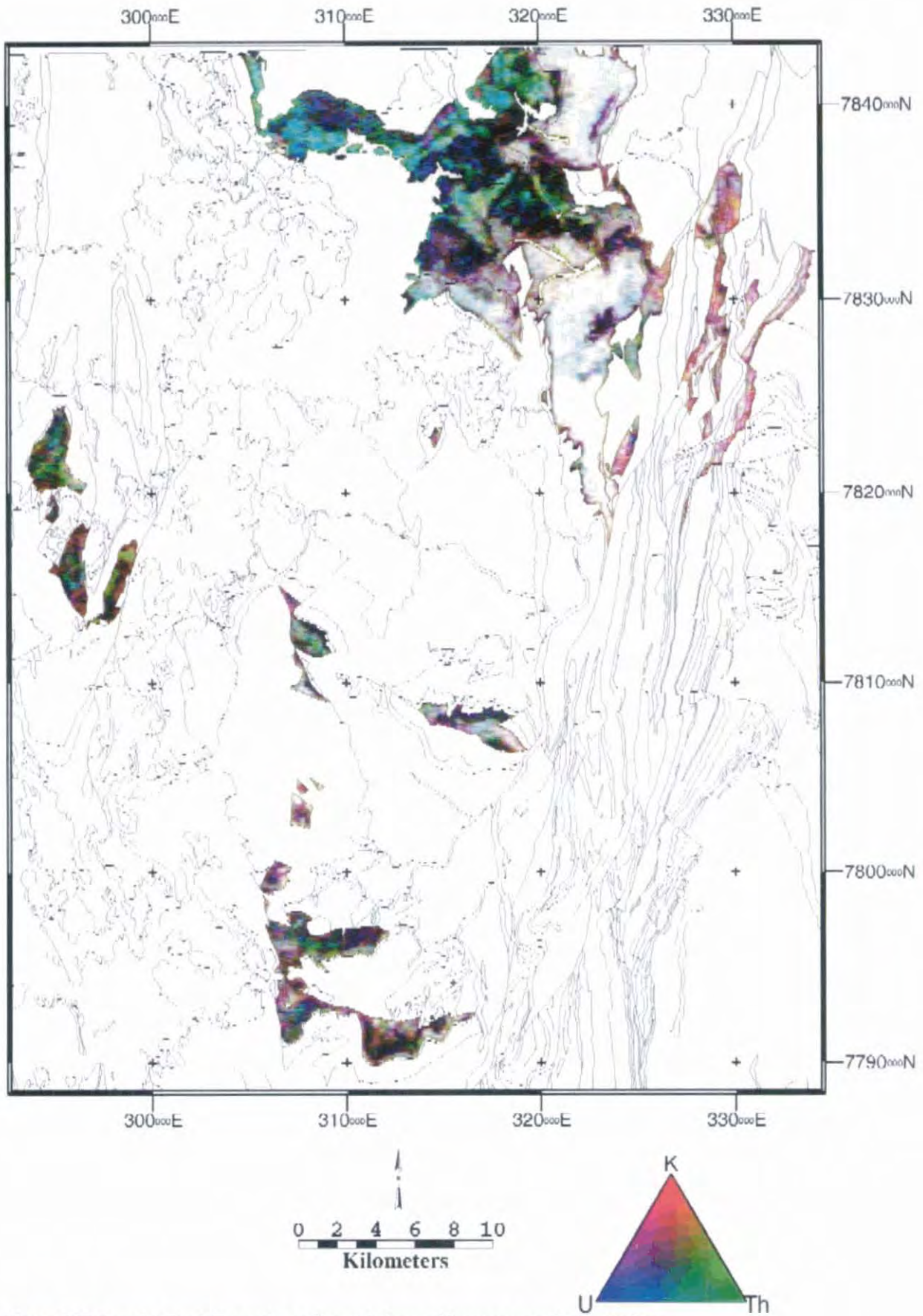

Figure 7.27 Surprise Creek Formation radiometric image, histogram-equalised transform

The discussion above mainly refers to the Surprise Creek Formation west of the Mount Gordon Fault Zone. Within the fault zone itself and the Leichhardt River Fault Trough, the character of the SCF

radiometric signal changes markedly from that of the flatter-lying strata to the west. While Pra retains a low-count response indicating mature quartz sandstone composition, Prds appearance in Fig. 7.26 is red to purple in colour but less intense than in equivalent outcrops to the west, implying lower levels of Th and U, and to a lesser extent K. No variation in this signature is obviously visible in the vicinity of the Mammoth Cu deposit. Taken together with an apparent thinning, the SCF in this area is interpreted as consisting mainly of feldspathic sandstone deposited in a region of less accommodation space than the more clay- and silt-rich part of the sub-basin to the west. However, the clay-rich, high-count SCF signature is not observed anywhere west of 314000E, which may define a western limit to the sub-basin apparently present during Surprise Creek Formation time.

7.4.6 Torpedo Creek Quartzite

The Torpedo Creek Quartzite at the base of the McNamara Group is often too thin (less than 100 metres) to be delineated by airborne radiometrics, especially where it directly overlies the compositionally similar arenaceous unit of the Surprise Creek Formation. Only where the argillaceous Surprise Creek Formation has been preserved beneath relatively flat-lying Torpedo Creek Quartzite can the Torpedo Creek Quartzite be clearly distinguished as a dark (low count), arenaceous unit (Fig. 7.3). The Torpedo Creek Quartzite signature can be discerned more easily when depicted with the Gunpowder Creek Formation (Figs. 7.28 and 7.29) with which it has a high radiometric contrast. This presentation clearly demonstrates the near absence of radioelements in the Torpedo Creek Quartzite (exemplified around 314800E 7809100N and 324500E 7828400N), as would be expected from a clean quartzite.

7.4.7 Gunpowder Creek Formation

The Gunpowder Creek Formation is one of the most radioactive of all outcropping units in this region, equalled only by the upper argillaceous/micaceous member of the Surprise Creek Formation. At least four members of the Gunpowder Creek Formation are discernible from the radiometric images (Figs. 7.29 and 7.30). A thin, patchy basal member of low readings in all channels, albeit relatively Th-rich, is transitional from the underlying Torpedo Creek Quartzite. It soon gives way to high-count micaceous siltstones, sandstones and carbonaceous shales (e.g. 310000E 7795000N, 308700E 7805000N, 315000E 7810000N). This response diminishes slightly near the middle of the formation (e.g. 312000E 7794500N, 307600E 7808700N, 321000E 7815000N), possibly resulting from an increase in proportion of carbonates, before increasing again at the top of the formation (e.g. 310000E 7790000N, 310800E 7804000N, 319800E 7820000N). The latter signature, which is often K-dominated, is interpreted to correspond to carbonaceous shales known to occur at the top of the Gunpowder Creek Formation (Hutton and Wilson, 1985).

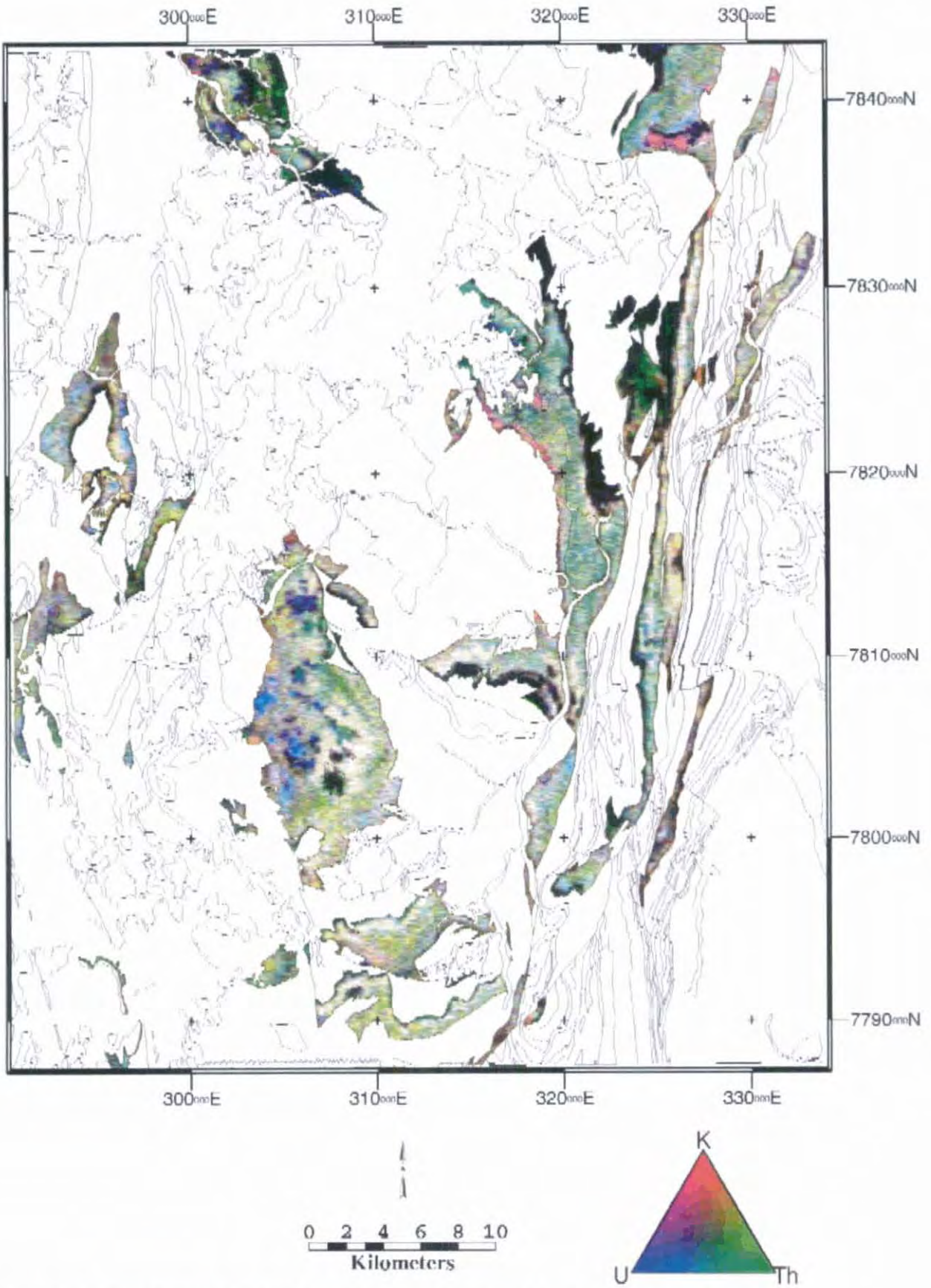

Figure 7.28 Torpedo Creek Quartzite + Gunpowder Creek Formation radiometric image, linear transform

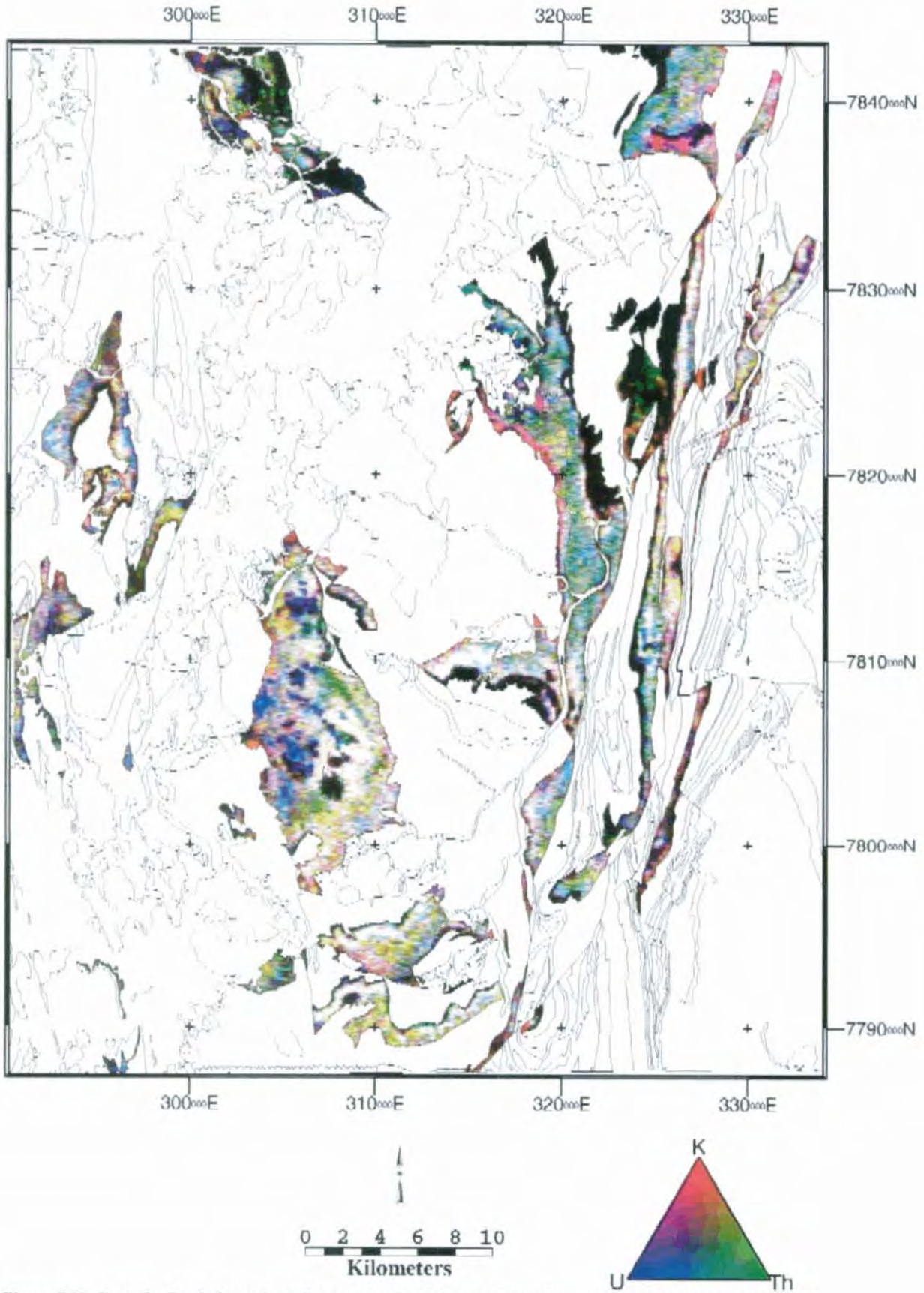

Figure 7.29 Torpedo Creek Quartzite + Gunpowder Creek Formation radiometric image, histogram-equalised transform

Regional variability in the Gunpowder Creek Formation's radiometric signature is considerable. The high-count layer near the base is not present everywhere, but is best developed in the fault-repeated south-dipping blocks east of Mount McLeod (around 310000E 7795000N) where they diminish in intensity

eastwards, in patches north of the Redie Creek Fault (315000E 7810000N), on the eastern limb of the anticline NNW of Lady Loretta (296000E 7822000N), in the core of the very open, broad anticline centred around 308000E 7805000N, and in the east-dipping strata west of the Mount Gordon Fault Zone extending several kilometres north and south from 7829000N.

A bluish-green'overlying layer indicating high relative Th and U count rates is generally representative of the informal member designated Pmw_2 by Hutton and Wilson (1985), exemplified by the area around 321000E 7815000N. Given that this unit is distinguished by micaceous (and therefore presumably K-rich) siltstones and sandstones, it is not clear why its radiometric signature should be dominated by Th and not K. It may be that this unit contains a high proportion of Th- and U-bearing phosphates and oxides as well as mica, all of which may have been sourced from an older S-type granitic terrain, or even tuffs associated with the contemporaneous emplacement of the Sybella Granite. Alternatively, anomalous Th and U may be associated with the ferruginous sandstone recorded in the Gunpowder Creek Formation (Hutton and Wilson, 1985). Slightly higher levels of K are apparent in irregular patches north of the mapped facies boundary separating Pmw_2 from undivided Gunpowder Creek Formation (319000E 7824000N), but otherwise this area could also be assigned to Pmw_2. Pmw_2 is also interpreted to be present through much of the Gunpowder Creek Formation outcrop surrounding 326000E 7840000N and in other areas within the Mount Gordon Fault Zone, but it generally thins westwards to the point of complete absence west of the Western Border Fault.

A yellowish (higher K) facies, probably indicating a higher proportion of shale, overlies the green Th-dominant Pmw_2-type signature in many areas, particularly in the central corridor of the study area between the Mount Gordon and Western Border Faults. This signature becomes confused on the western limb of the broad, open dome structure centred several kilometres north of Mount Kelly (305000E 7807000N), where blue (U-rich) patches probably indicate residual Cambrian phosphates. The K-rich facies may be represented a few kilometres west of Lady Loretta and in the central and northern parts of the Mount Gordon Fault Zone. K levels (and, presumably, proportions of shale in the sequence) continue to increase towards the top of the Gunpowder Creek Formation in the eastern half of the study area, but this is generally not true of outcrops to the west. A maximum flooding surface is indicated, but may be confined to a small meridional area centred north of the Redie Creek Fault and close to what is now the Mount Gordon Fault Zone, where the carbonaceous shale-rich informal member Pmw_3 was mapped by Hutton and Wilson (1985). In some areas radioelement concentrations actually appear to decrease as the contact with the Paradise Creek Formation is approached. Both the increasing and decreasing trends in K concentration are frequently continued into the overlying Paradise Creek Formation in their respective areas.

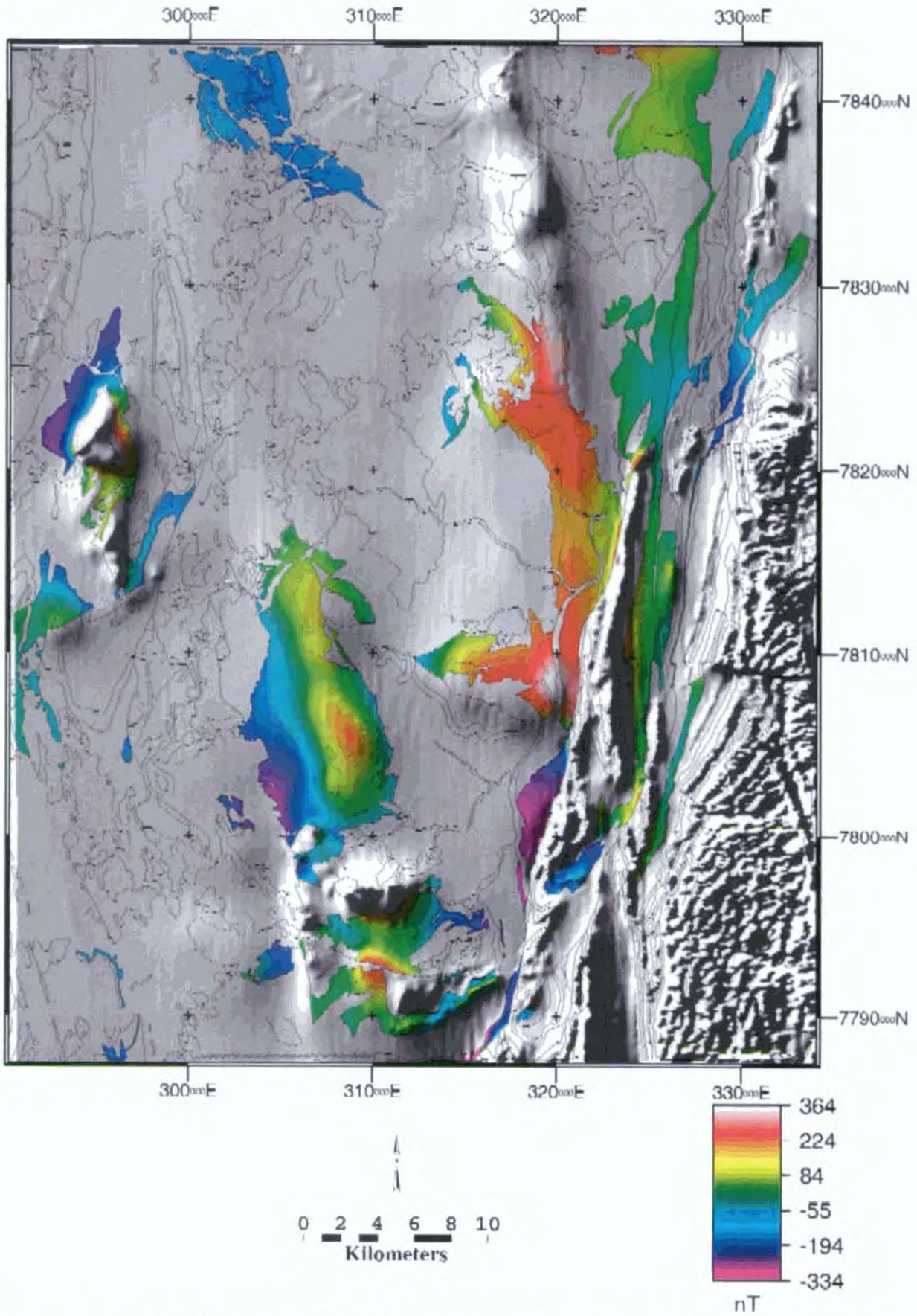

Figure 7.30 Torpedo Creek Quartzite + Gunpowder Creek Formation total magnetic intensity (RTP)

Atypical Gunpowder Creek Formation signatures are present in much of the area north and west of Lady Loretta (298000E 7812500N), where the radiometric signal is subdued but U is relatively prominent, and

in the north-western and south-eastern corners of the study area where large areas of low count rate in a generally thinner sequence may indicate mature sandstone deposition in relatively elevated areas. Outcrops of the lower Gunpowder Creek Formation in the fault-bounded blocks north of Lady Loretta appear less radioactive than their counterparts west of Lady Loretta and elsewhere. This may result from a higher proportion of coarser siliciclastic sediments, possibly reflecting proximity to syn-sedimentary faults. Alternatively, the subdued responses may be due to lack of continuity and areal extent of the lower GCF outcrops immediately north of the Carlton Fault.

The strongest magnetic field in the Gunpowder Creek Formation (Fig. 7.30) is associated with the region of the possible maximum flooding surface inferred from the radiometric data. This may indicate that the Myally Subgroup is greatly thinned or largely absent in much of the region west of the Mount Gordon Fault Zone, as suggested above. Peaks in TMI in this area are attributed to faulting of Eastern Creek Volcanics into higher levels. In the case of the southern anomaly near the intersection of the Redie Creek and Mount Gordon Faults (320000E 7806500N) this is supported by recognition of thrust repetition of the Torpedo Creek Quartzite in this area (McConachie et al., 1996). Substantial thicknesses of Myally Subgroup or other non-magnetic sediment may be preserved south of the Redie Creek Fault and west of the Mount Gordon Fault Zone, as indicated by the low TMI values over the Gunpowder Creek Formation in this area.

7.4.8 Paradise Creek Formation

The dichotomy in magnetic field signatures north and south of the Redie Creek Fault over the Gunpowder Creek Formation is even more pronounced in the Paradise Creek Formation (Fig. 7.31), and is consistent with the sedimentary section from the Gunpowder Creek Formation to Myally Subgroup inclusive being considerably thicker south of the Redie Creek Fault than to the north. Higher TMI north of the Redie Creek Fault may also be contributed to by thickening of the Eastern Creek Volcanics at depth. South-dipping tilt blocks bounded by north-dipping normal faults are indicated east of Mount Kelly. This is best demonstrated by the magnetic high extending north from the E-W fault centred at 310000E 7797000N separating the Paradise Creek Formation from the Surprise Creek Formation/Fiery Creek Volcanics/?Whitworth Quartzite sequence, where there is clearly only a small thickness of sediments overlying a significant volume of Eastern Creek Volcanics. Localised magnetic lows in this central southern portion of the study area are related to those interpreted as possible magnetite-depleted alteration systems within the Eastern Creek Volcanics in section 7.5.

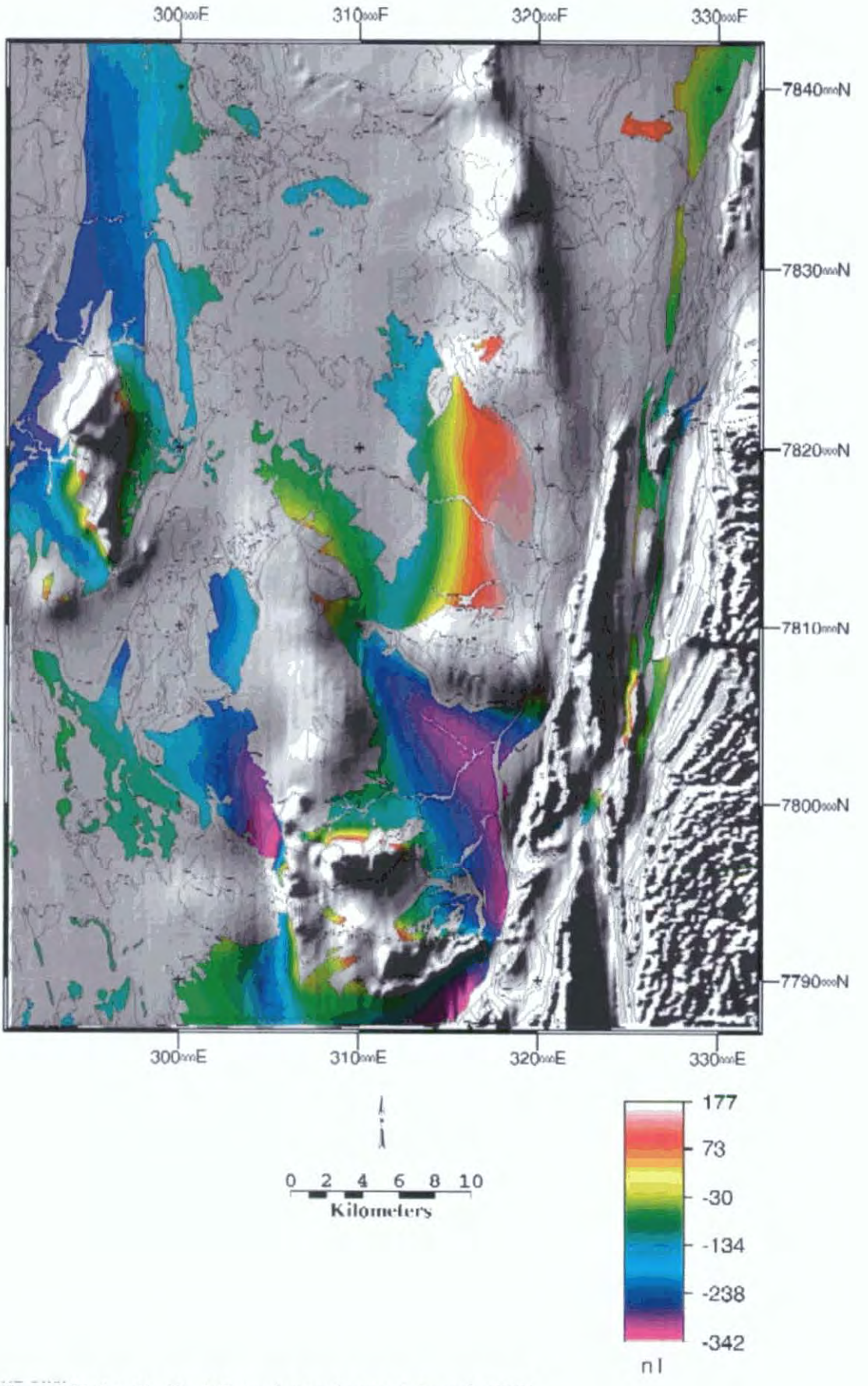

Figure 7.31 Paradise Creek Formation total magnetic intensity (RTP)

Radiometric signatures in the Paradise Creek Formation (Figs. 7.32 and 7.33) vary considerably both across and along strike. Potassium dominates the radiometric signature of a large portion of the Paradise

Creek Formation, although its influence diminishes considerably to the south and west. This K-dominance is surprising given that most authors have described carbonate (usually dolomite) rather than fine siliciclastics as being the main constituent of the Paradise Creek Formation. The blue and green hues observed adjacent to the Russell Creek Fault in the north-western quadrant of the study area are more typical of what might have been expected based on lithological descriptions of the Paradise Creek Formation.

A number of factors could be responsible for the variability in K relative to other radioelements, including changes in the proportion of tuffaceous input to sedimentation (Page, 1981), and reductions in total siliciclastic input, with a corresponding increase in dolomite content. Heterogeneity of radiometric signature is most clearly demonstrated north and south of the Redie Creek Fault, where a low-K bed at the top of the formation (GR 313000E 7815000N) has no counterpart below the Esperanza Formation south of the fault (GR 317000E 7804000N). This bed overlies a high count rate layer which reaches its greatest intensity between Paradise Creek and the Redie Creek Fault, but is also traceable to the north and west. This unit may also be represented in the Mount Gordon Fault Zone; but again has no apparent equivalent south of 7807000N. A common feature through much of the K-poor (and presumably dolostone-rich) portion of the Paradise Creek Formation in the south and west of the study area is a U-rich layer at its base. This unit is in the same position but is thicker than the Mount Oxide Chert Member. The significance of this layer is not clear, but may possibly be associated with concentrations of carbonaceous material or phosphatic minerals. Overall, the radiometric data may be interpreted as indicating a siliciclastic- and possibly tuff-rich portion of the depositional basin in the centre of the study area, with fine detritus possibly being received from what is now the Leichhardt River Fault Trough (Mount Gordon Arch'of Derrick, 1982; possibly an inversion of the Leichhardt Rift of O'Dea et al., 1997a). This was accompanied by contemporaneous carbonate deposition on a platform west of the Western Border Fault and Mount Kelly. The low count rate layer near the contact with the Esperanza Formation in the centre of the area is interpreted as arising from chert layers localised in this region at this stratigraphic level (Hutton and Wilson, 1985).

In the areas where no clear layered structure can be defined from the radiometric signature, such as the south-eastern corner of the study area, it is possible that much of the radiometric signal (particularly in the U and Th channels) has been derived from transported colluvium, soil or residual Cambrian cover. This possibility is reinforced by the fact that the predominant U and Th signals observed in these areas are very similar to those mapped as Cainozoic cover. The low count rate patches in the far north-western corner of the study area are also notable in this regard, as they are associated with extensive outcrops (usually 10-20 m high mesas) of Mesozoic sandstone.

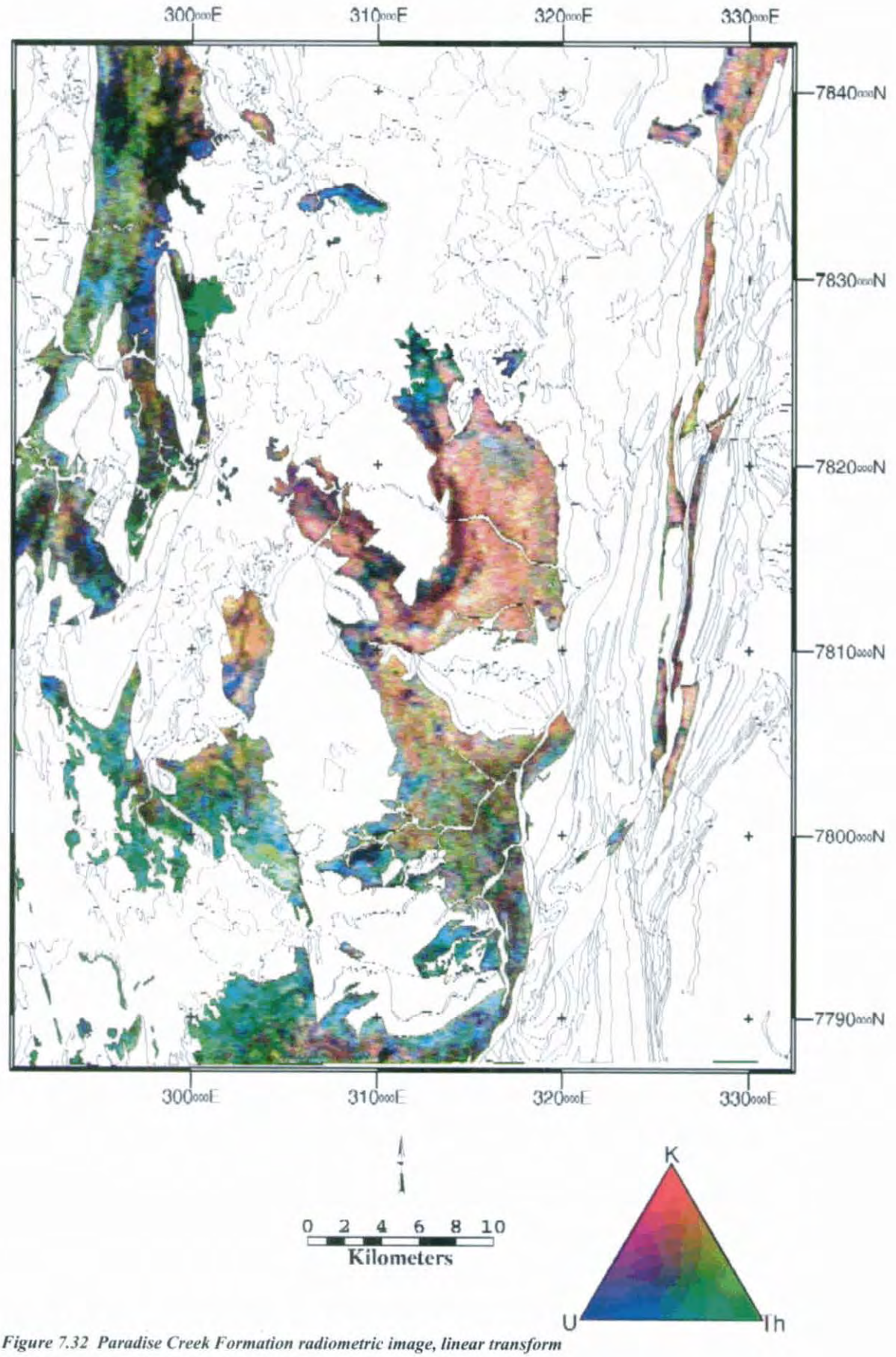

Figure 7.32 Paradise Creek Formation radiometric image, linear transform

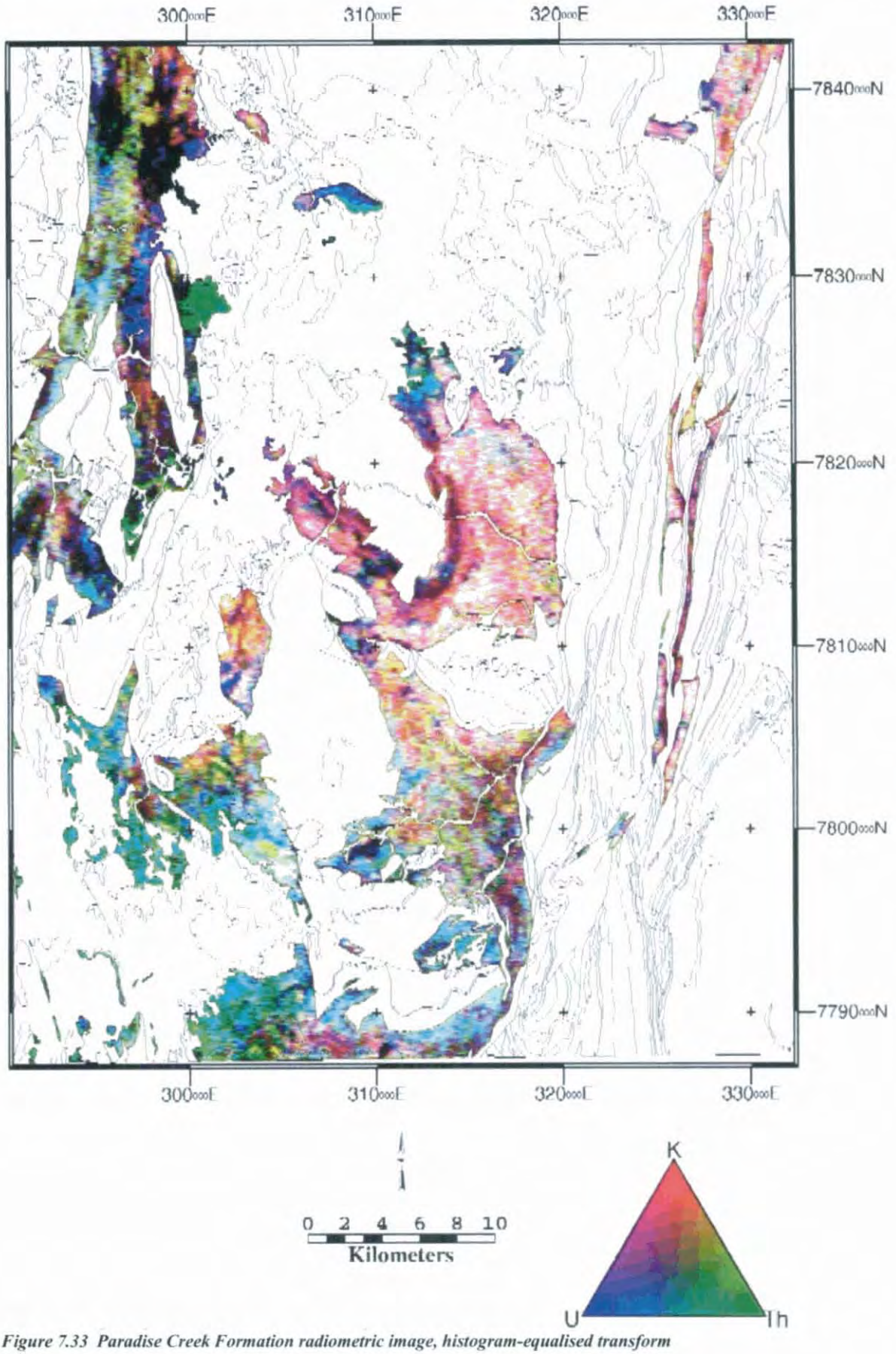

Figure 7.33 Paradise Creek Formation radiometric image, histogram-equalised transform

The signature of the Paradise Creek Formation in the Lady Annie/Lady Loretta area is atypical of the formation regionally, being quite subdued radiometrically. This pattern is similar to variations observed

in the Gunpowder Creek Formation in the same area, and may indicate locally sandier composition or attenuation of the formation radiometric signal due to the effects of deep prolonged weathering (Lewis, 1975). The former hypothesis is supported by geological observations by the author and unpublished exploration reports stored at Lady Loretta, and also by Hutton and Sweet (1982) who inferred a possible landmass to the west during Paradise Creek Formation deposition. Virtually the only exception to the reduced Paradise Creek Formation radiometric signature is a small strip about 4 km NW of Lady Annie (292500E 7816500N) which appears similar to the K-rich facies observed in the centre of the study area.

7.4.9 Esperanza Formation

Few anomalous regions are apparent in the generally low magnetic field over the Esperanza Formation (Fig. 7.34). A notable exception is the small zone of high TMI north of the fault at 7797000N, which has been discussed in the section on the Paradise Creek Formation. Another is the high a few kilometres west of Lady Annie (293000E 7811000N) where north-dipping Eastern Creek Volcanics at depth may be separated from overlying Esperanza Formation by a south-dipping fault. This structural configuration is the mirror image of that envisaged to explain the anomaly associated with the fault at 7797000N. Sub-basins may be indicated by the magnetic lows south of the Redie Creek Fault and east of the Western Border Fault east of Lady Loretta, though geometric effects arising from the Redie Creek Fault itself are also present in the former case.

The Esperanza Formation's low thickness (as little as the equivalent of five grid cells in the many moderately steeply dipping areas) makes its radiometric signature (Figs. 7.35 and 7.36) difficult to characterise. A potassium-rich horizon marks its base where it is thickest (> 350 m; Hutton and Wilson, 1985) in the centre of the study area on either side of Paradise Creek. This probably corresponds to the maximum flooding surface identified from gamma ray logging by Southgate et al. (1996). It is similar in signature to much of the underlying Paradise Creek Formation. However, this distinctive layer is obscured in areas where bedding is steeply inclined, thus restricting outcrop area. The remainder of the Esperanza Formation is generally low in all channels, consistent with its major lithology noted in outcrop being stromatolitic chert beds. Thin silty bands of high K similar to but not as prominent as the basal layer only become apparent where shallow dips enable apparent bed thicknesses to exceed the sample spacing. An exception to this generally low radioelement signature is the thin band of Esperanza Formation immediately south of the Redie Creek Fault, where the basal K-rich horizon may be thicker.

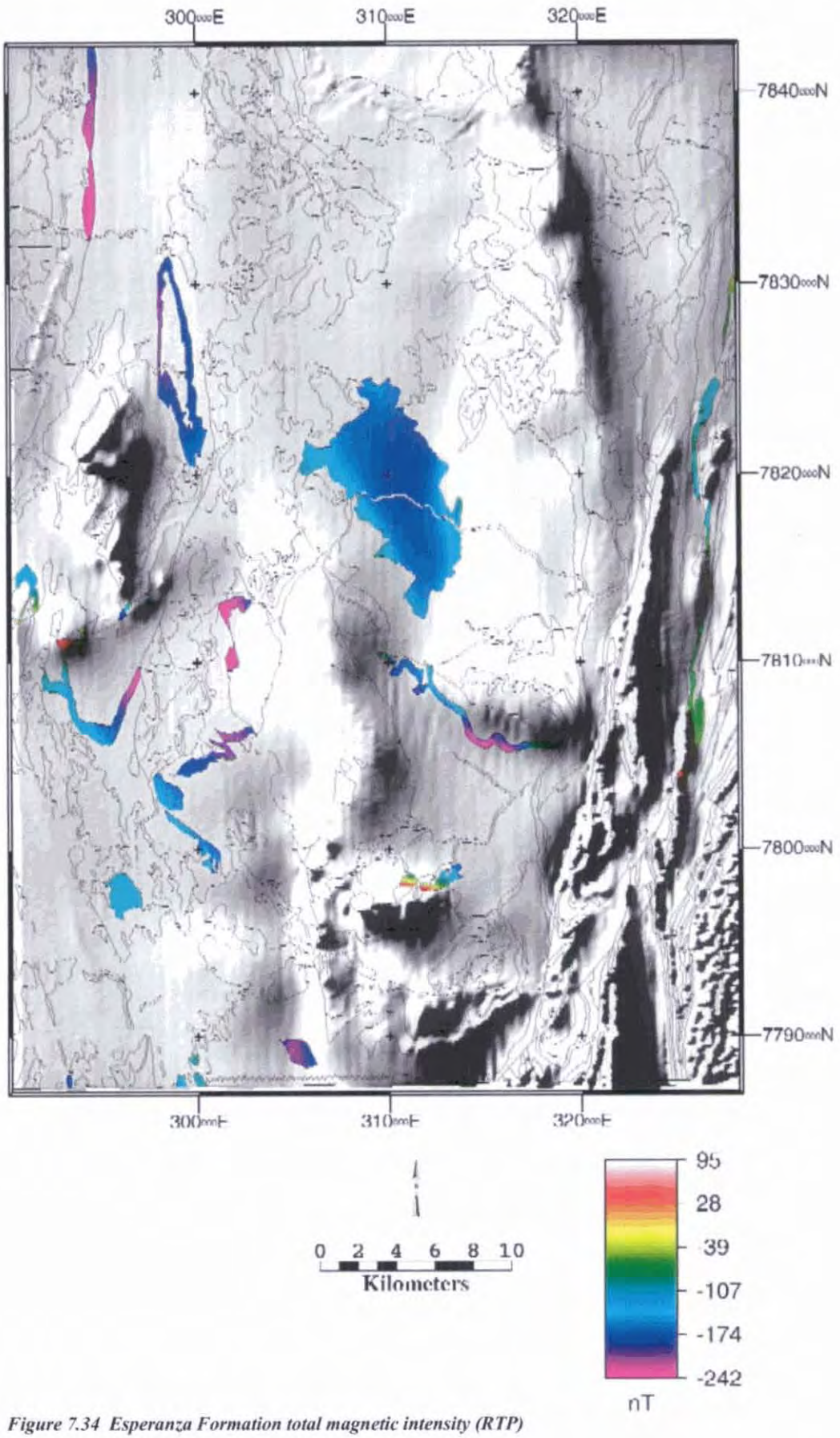

Figure 7.34 Esperanza Formation total magnetic intensity (RTP)

Regional variation in the Esperanza Formation is somewhat masked by Phanerozoic sediments and colluvium, particularly towards the southwest. For this reason outcrops appearing particularly high in U

and to a lesser extent Th must be treated with caution. Within the remaining areas, where outcrop signatures may be interpreted with reasonable confidence, spatial variations are quite pronounced. The high count rate K-rich layer at the base of the Esperanza Formation appears fairly ubiquitous, but is subdued in many areas. Relative proportions of K and Th also appear to fluctuate along strike within the basal layer. In contrast, the large low count rate area around Paradise Creek in the centre of Figs. 7.34 and 7.35 presumably resulting from shallowly dipping cherts is only replicated in one fairly small region centred on a pair of faulted synclines at the south-eastern extremity of Esperanza Formation outcrop south of the Investigator Cu prospect (326000E 7806000N). Hence it may be that the proportion of chert in the Esperanza Formation regionally is not as large as implied in much of the literature (Hutton et al., 1981; Hutton and Wilson, 1985), with the central region of shallowly dipping rocks being an exception rather than the rule.

Implications of these radiometric facies variations for palaeo-basin geometry are not entirely clear. Basin subsidence was maximised in the vicinity of Paradise Creek north of the Redie Creek Fault (based on measured thicknesses given in Hutton and Wilson, 1985), but this portion of the basin was completely starved of clastic sediments for much of Esperanza Formation time, with only occasional incursions of K-bearing muds. Silt and shale sedimentation was more prevalent south of the Redie Creek Fault, along with minor dolostone which is interpreted as being responsible for the less K-rich zones observed, at least in those areas where the radiometric signal is inferred to result mainly from Proterozoic sources. This north-south dichotomy is reversed east of the Mount Gordon Fault. Th presents a strong component of the Esperanza Formation's radiometric signature west of the Western Border Fault from the greater Lady Loretta Syncline northwards, and the signal in this region is generally more subdued than in the silt-rich outcrops to the east. A relatively high percentage of carbonate may be indicated, but the possibility of contamination and masking by Phanerozoic material is considered particularly acute given this region's proximity to a number of outliers of Cambrian, Mesozoic and Cainozoic sediment.

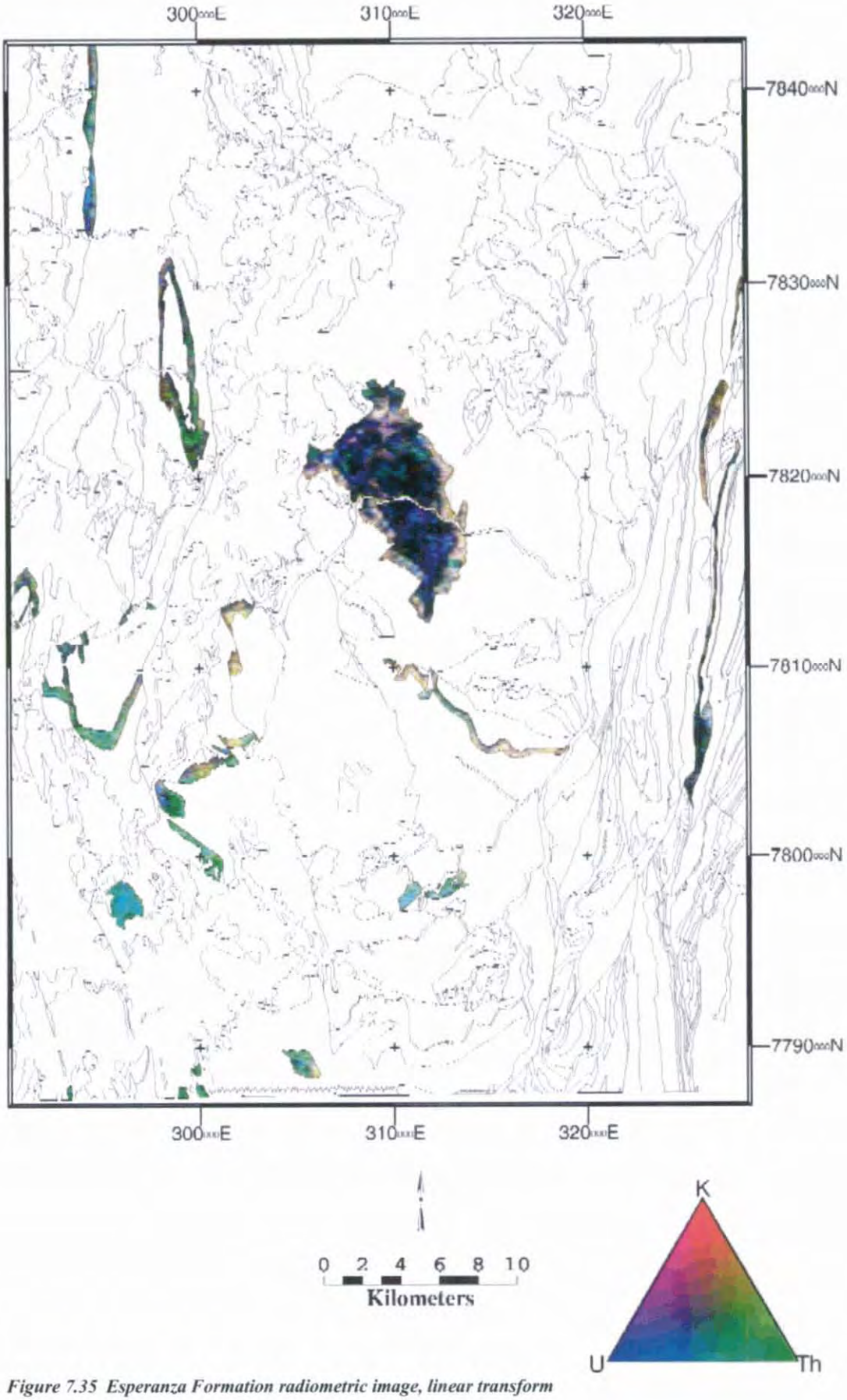

Figure 7.35 Esperanza Formation radiometric image, linear transform

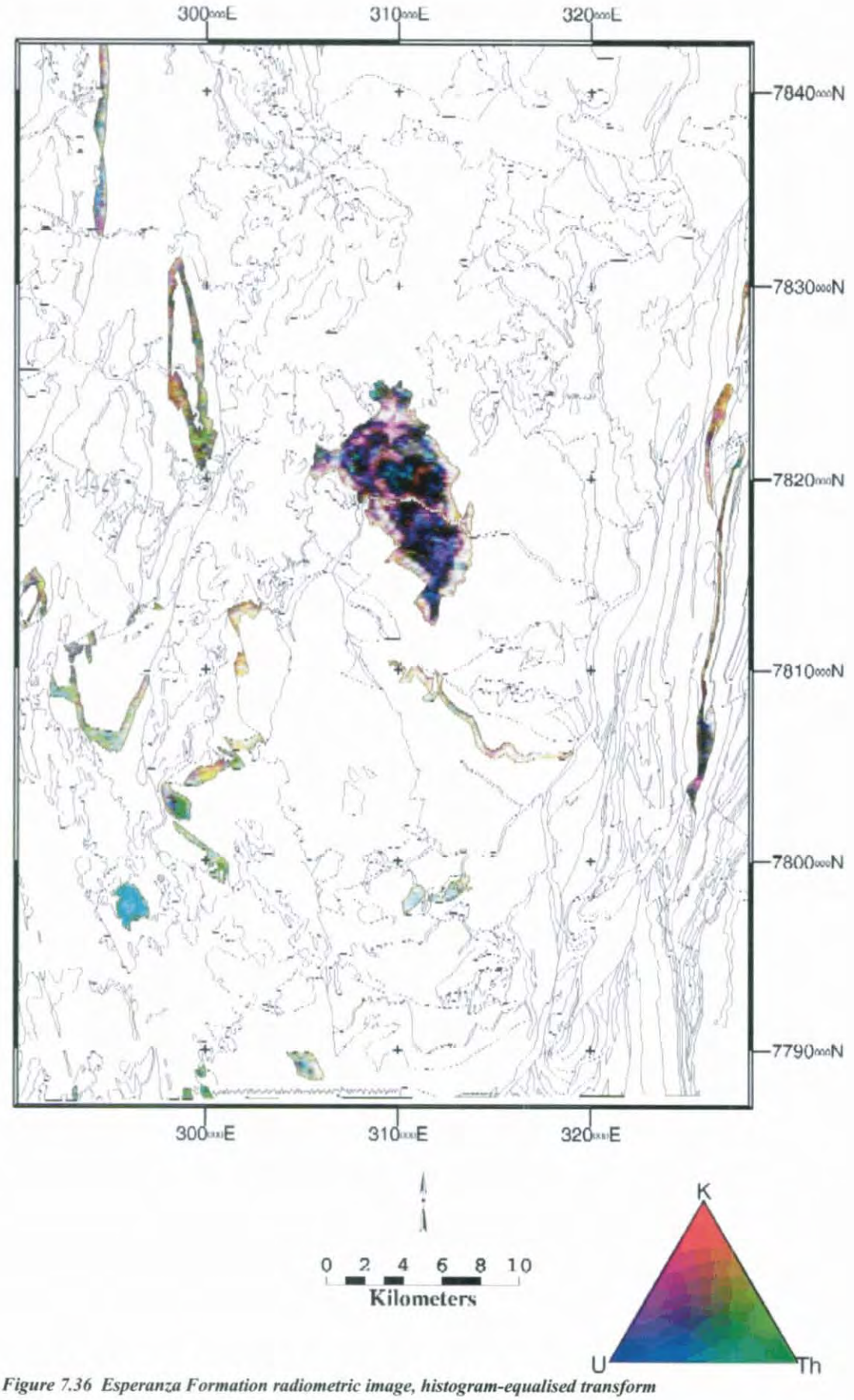

Figure 7.36 Esperanza Formation radiometric image, histogram-equalised transform

7.4.10 Lady Loretta Formation

The magnetic field intensity over the Lady Loretta Formation is generally low (Fig. 7.37), as might be expected given that thousands of metres of stratigraphy separate the Lady Loretta Formation from the magnetic sources of the Eastern Creek Volcanics. One area in which this stratigraphy may be anomalously thick is in the magnetic low centred beneath the outlying Cambrian Lady Annie phosphate deposits east of Lady Loretta, adjacent to the Western Border Fault (298500E 7813000N). As discussed in section 7.4.2.1.2 and chapters 6 and 8, this magnetic low may also arise from depression of the Eastern Creek Volcanics'magnetic susceptibility in this region. This explanation for the magnetic low beneath and to the east of the Lady Loretta deposit entails magnetite-destructive alteration of ECV by hydrothermal fluids, similar to that mapped on a wider scale in the footwall of the Mount Isa Mine by Leaman (1991a). The 'alteration'model for the low is supported by relatively very low magnetic susceptibilities ($0.25x10^{-3}$ SI) measured on greenstones drilled from over 500 m depth 1.5 km north of Lady Annie. The spatial association of the magnetic low with the Lady Annie Cu deposit on its western edge as well as the Lady Loretta Zn-Pb deposit near its centre is suggestive that magnetite-destructive alteration may be significant for both Cu and Zn-Pb metallogeny.

There is no direct ore response in the aeromagnetic data over Lady Loretta itself, consistent with the virtual absence of magnetite or pyrrhotite from the ore sequence and associated sulphides.

Other than the area affected by geometric distortions arising from a major discontinuity at depth associated with the Redie Creek Fault, only one area in the Lady Loretta Formation appears to have unusually high TMI. This is the anomaly a few kilometres west of Lady Loretta, which is also apparent in the adjacent Esperanza, Paradise Creek, and Gunpowder Creek Formations, all of which the Lady Loretta Formation is faulted against in this structurally complex zone. Clearly, a block of Eastern Creek Volcanics has been introduced into higher stratigraphic levels in this region, but the structural nature of this emplacement is not clear.

The Lady Loretta Formation marks a return to the generally higher-count, more potassic signatures of the Paradise Creek Formation, though the Lady Loretta Formation is the most heterogeneous of all McNamara Group units (Figs. 7.38 and 7.39). A distinct absence of radioelements at the base possibly denotes the onset of a new depositional cycle marked by fine sandstone noted in the greater Lady Loretta Syncline (295000E 7807000N) by Hutton and Wilson (1985), as well as the basal ferruginous cherty breccia noted by many authors and summarised by Dunster (1997).

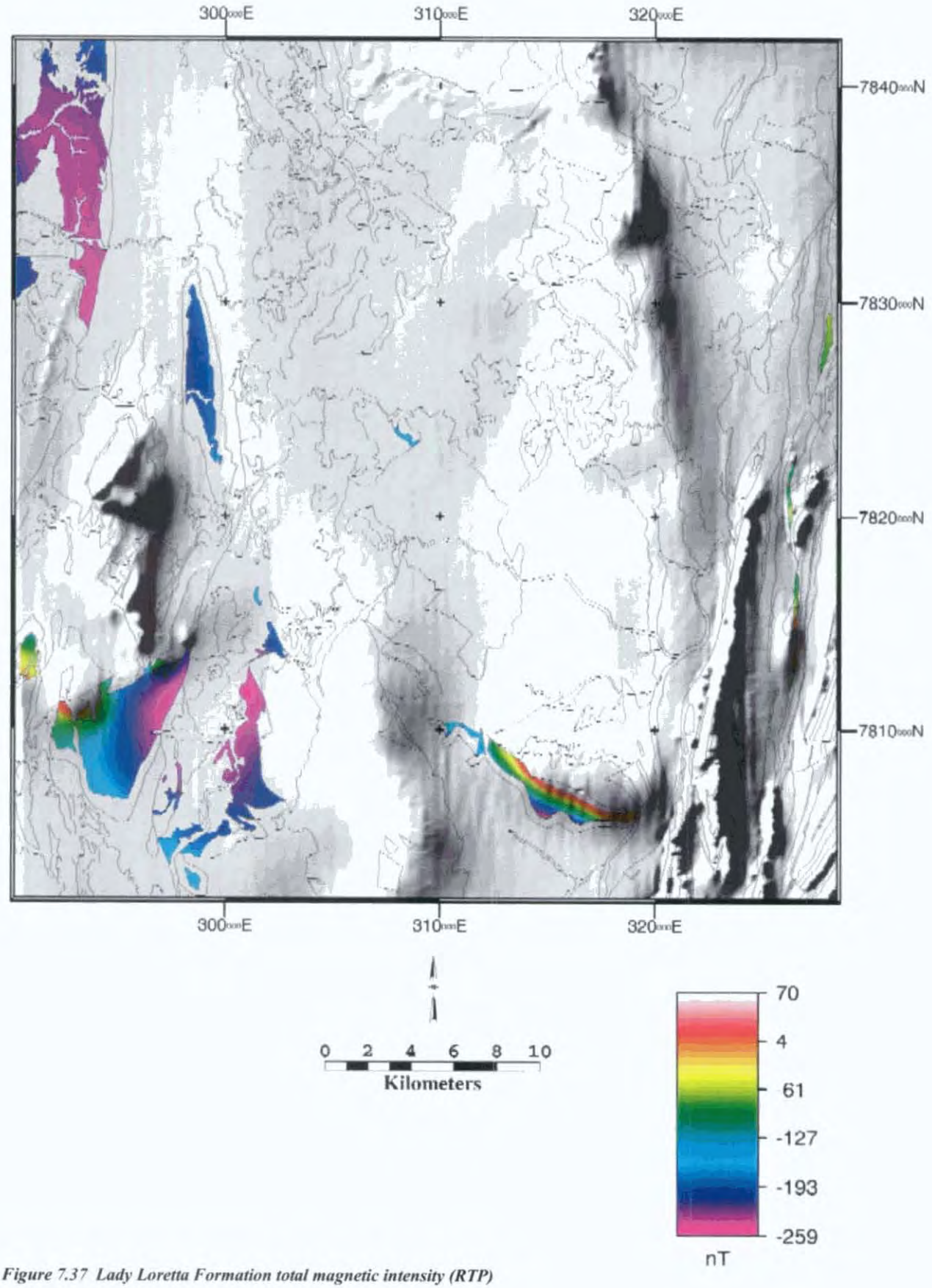

Figure 7.37 Lady Loretta Formation total magnetic intensity (RTP)

Resumption of shale and siltstone-dominant sedimentation with associated dolostone deposition can be seen regionally in the K-rich bands overlying the basal unit, but this facies is either obscured or absent in the Dayview or Debut Syncline north of Lady Loretta (GR 299000E 7826000N). Similar low count rate

areas in the Lady Loretta Formation are observed in the core of a south-plunging syncline west of Lady Loretta (291000E 7814000N), a few kilometres south-west of Lady Annie (292500E 7810000N), in the location of the Lady Annie phosphate processing plant (302200E 7814000N), and in the north-western corner of the study area (where scattered Mesozoic sandstone mesa outliers may be responsible). A common factor in all these locations is the proximity of Cambrian outliers, which may lend these dark areas their slight bluish tinge from uranium associated with the Cambrian phosphatic sediments.

The Lady Loretta Formation's radiometric signature in the north-western corner of the study area is largely interpretable on the basis of Hutton and Wilson (1985) who observed that the Lady Loretta Formation may be divided into a lower dolomite-rich and an upper clastic-rich unit in this region. The radiometric detection of generally low count layers with patchy Th and U signals overlain by brighter K- and Th-rich facies is entirely consistent with lower dolostones and cherts giving way to a more shale and silt rich sequence in this area. In this scenario the Lady Loretta Formation in the Dayview Syncline is assessed as being entirely composed of the lower dolomitic unit, possibly overlying the basal low count rate sandstone or cherty breccia layer noted above.

Considerable regional sedimentary diachroneity is implied. The entire sequence observed in the north-western corner discussed above (650-1000 m thick according to Hutton and Wilson, 1985) is confined to the lower half of the thicker (1800 m) Lady Loretta Syncline, and also correlates to the Lady Loretta Formation facies association preserved south of the Redie Creek Fault. This makes the sedimentary sequence containing the Lady Loretta mineralisation unique in the Paradise Valley study area. Whether this is the result of an anomalous 'extra' episode of sub-basin development in the Lady Loretta district, or extensive removal of the Lady Loretta Formation by the overlying Shady Bore Quartzite to the north-west is beyond the scope of this study. The former hypothesis may be indicated by the presence of a darker horizon at the top of the formation in the north-west, interpreted as due to increasing prevalence of sandstone marking a transitional contact with the Shady Bore Quartzite, as described by Dunster (1997).

No distinct signature related to the Lady Loretta mineralisation itself is manifest except for slightly subdued counts in all channels in the vicinity of the Small and Big Synclines, probably influenced by high local topographic relief as well as geology. The host stratigraphy of the Lady Loretta deposit (297200E 7812600N) does however appear quite distinct from the rest of the Lady Loretta Formation, with Th and to a lesser extent U prominent to an extent not observed elsewhere. This signature is consistent with the presence of dolomitic shales rich in carbonaceous material (with which U is frequently associated). Also notable is a high count rate layer in the footwall strata, which is most prominently developed in the nose of the Big Syncline (296000E 7811000N).

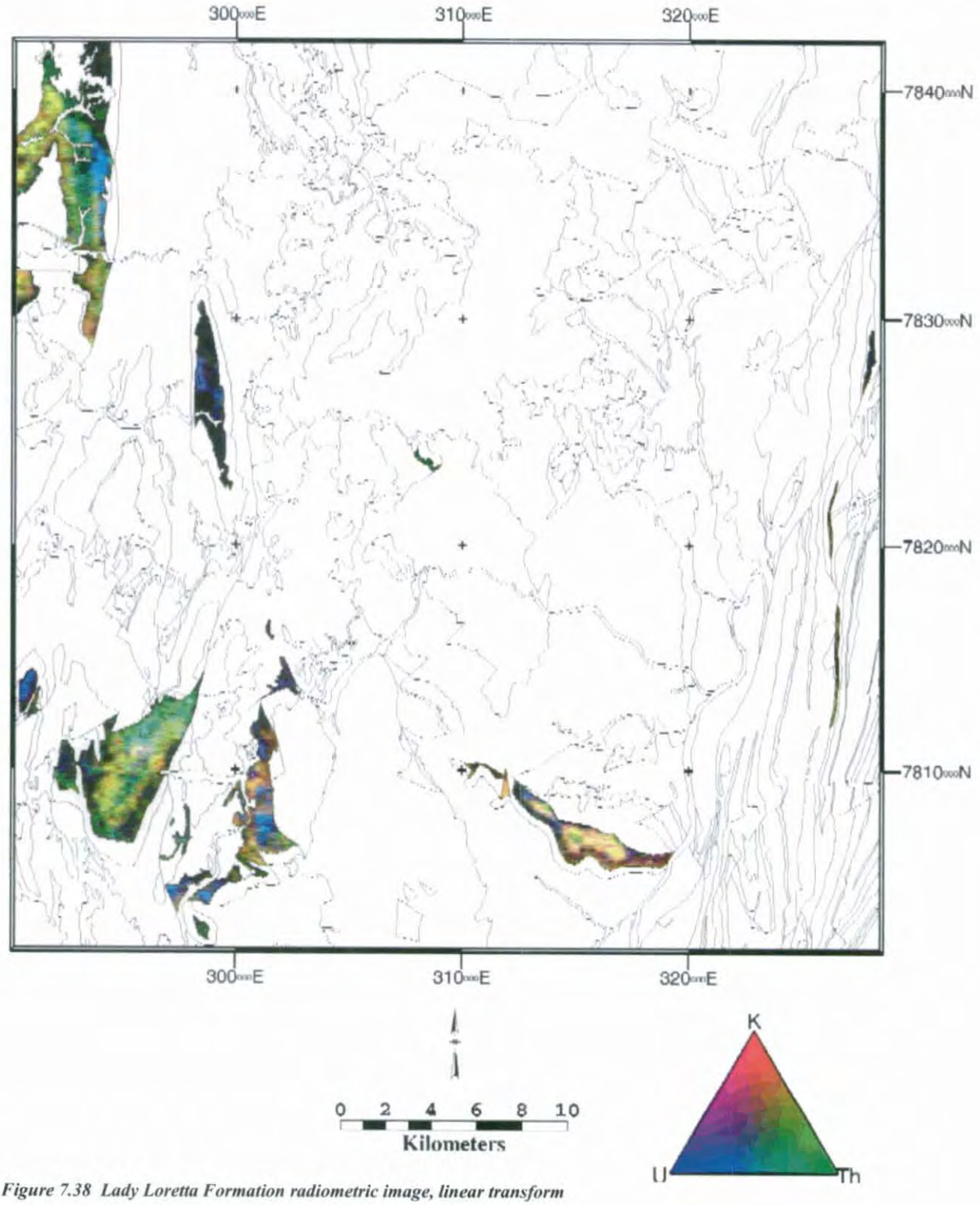

Figure 7.38 Lady Loretta Formation radiometric image, linear transform

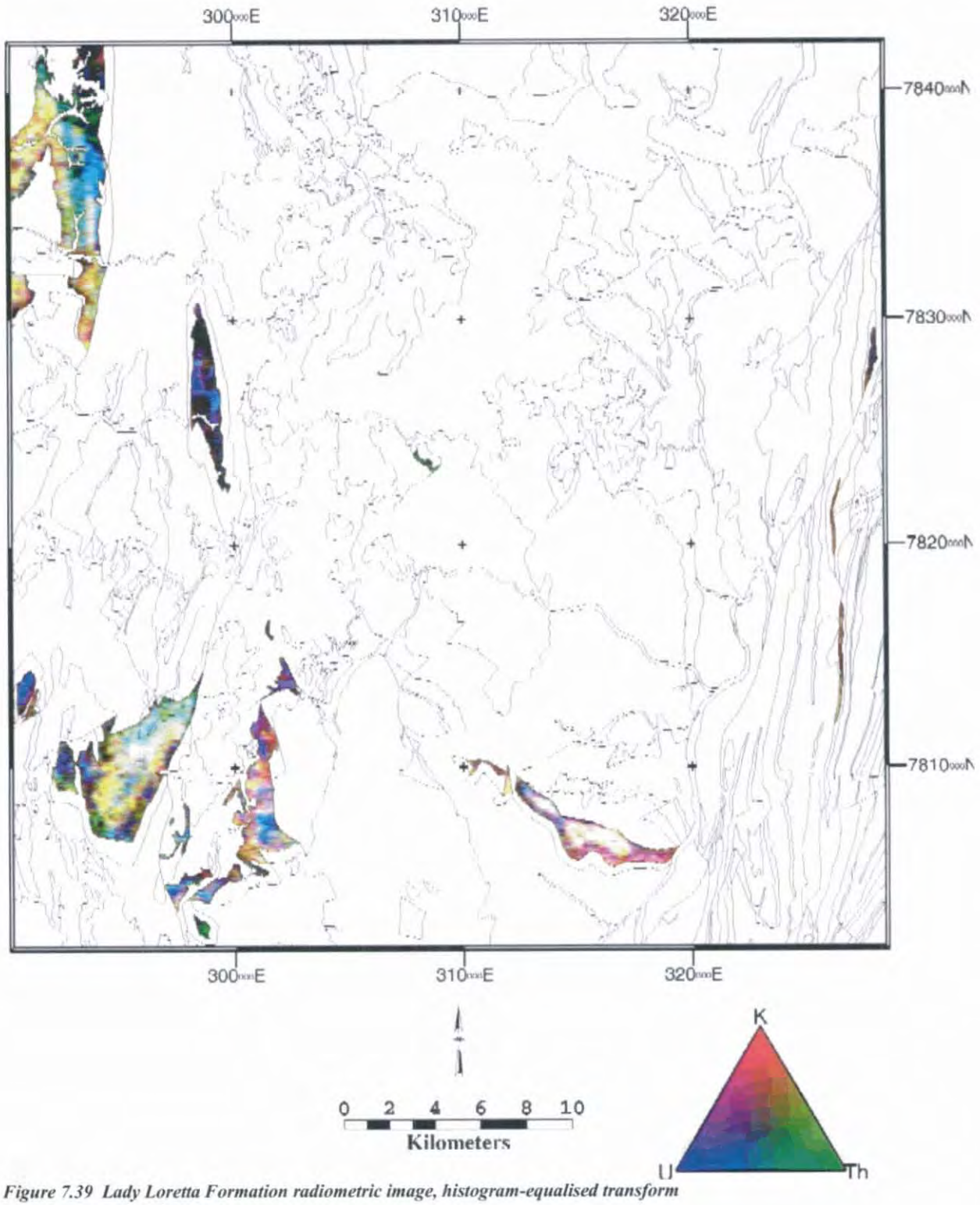

Figure 7.39 Lady Loretta Formation radiometric image, histogram-equalised transform

7.4.11 Upper McNamara Group

A short exposition of the radiometric signature of the remainder of the McNamara Group is given for completeness, and to provide a comparison with the older elements of the sequence. The Shady Bore Quartzite is characterised by low count rates in all channels (Figs. 7.3 and 7.4), as expected from its quartzite-dominated composition. Occasional Th patches may be reflecting concentrations of heavy minerals in the quartzite, but these have little continuity along strike. A transitional contact between the

Lady Loretta Formation and the Shady Bore Quartzite is apparent in the extreme north-western corner of the study area, and in fact this boundary between the two formations could on this evidence easily be placed a few hundred metres further west.

The Riversleigh Siltstone is confined to a fairly small region in the north-west of the study area, west of the Russell Creek Fault, but is still sufficiently extensive for its radiometric signature to be readily defined. It is marked by high count rates, but not to the same degree as the Gunpowder Creek and Surprise Creek Formations. Two radiometric facies are distinguishable, one prevalent to the north and the other to the south. The northern type is slightly more K-rich (reddish) than its southern counterpart, and is probably composed mainly of the micaceous siltstone recorded by Hutton and Wilson (1985). The more yellowish tinge of the southern signature type indicates a higher concentration of Th, which may be borne by carbonaceous shales interbedded with siltstones. This signature appears very similar to that of the Paradise Creek Formation on the other (eastern) side of the Russell Creek Fault, so the possibility of the Th being contained in dolostones or tuffs within the Riversleigh Siltstone sequence cannot be discounted.

7.4.12 Phanerozoic

Patches of high U-channel count within Phanerozoic cover east of Lady Loretta relate to uranium associated with major Cambrian accumulations of phosphate. These are the Lady Annie Phosphate deposits (not to be confused with the nearby Lady Annie Cu deposit west of Lady Loretta), from which some extraction has taken place intermittently over the last few decades. Many other Cambrian outliers also appear anomalous in U, presumably associated with phosphatic minerals, while others have low count rates in all channels.

Mesozoic outliers show a pronounced dichotomy. The most common radiometric signature is of high levels of Th and very little else. The origin of this Th is not clear, but may be palaeoplacer heavy minerals. Exceptions occur in the south-east of the study area, where a yellowish tinge from a K component in some outcrops (Fig 7.4) presumably denotes a silty matrix. Many other outliers, particularly towards the north-western corner of the study area, have low count rates in all channels and are probably composed of relatively clean sandstones.

Th is also present in much of the area mapped as Tertiary deep-weathering profiles (Tpf), with very high concentrations observed around the margins of the Tertiary weathering surface developed on Mesozoic rocks known as The Desert (approximately 305000E to 315000E and 7825000N to the northern edge of the study area), associated with a zone of elevated U signal. Elsewhere this unit (Tpf) is quite low in radioelements, with K and U almost completely absent. Cainozoic iron-cemented gravels mapped as Czg are extremely low in all radioelements. These were described as late Cainozoic fan or outwash deposits by Hutton and Wilson (1985).

The extensive Cainozoic covering soils and colluvium in the south-eastern region of the study area are commonly characterised by moderate to high levels of Th. The cautionary implications of this for

interpretation of Proterozoic signatures have been noted above. Patches of higher K and U are associated with reworking of older weathering profiles surrounding inliers of Proterozoic bedrock.

7.5 Summary

The 'unit-specific stretch' image processing technique applied to radiometric images effectively emphasises radioelement compositional variations within basin components. Application to magnetic units such as the Eastern Creek Volcanics enables additional information on magnetic susceptibility variability to be derived from magnetic data, while unit-specific stretches of magnetic data from non-magnetic units is useful in highlighting anomalous sub-surface structures. Both stratigraphically-controlled and lateral (along strike) changes have been identified. These can be used to interpret aspects of basin evolution and distinguish various alteration systems.

Several alteration systems affecting the Eastern Creek Volcanics are distinguishable from the magnetic and radiometric data. These can be related to various alteration assemblages defined by previous geochemical studies of the Eastern Creek Volcanics. The rock volumes affected by the alteration may constitute source, transport or outflow zones in mineral system terms (Wyborn et al., 1995b). Anomalously high K and subdued magnetic susceptibility, possibly associated with epidote ± sphene alteration, are observed in the Eastern Creek Volcanics adjacent to the Mammoth Cu deposits. Magnetic susceptibility reduction and K-depletion associated with chlorite + albite alteration of the Eastern Creek Volcanics enable this assemblage to be mapped using airborne geophysics. Geochemical data and spatial association with ore deposits implicate chlorite + albite alteration as a possible source of both Cu and Zn-Pb mineralisation.

All McNamara Group formations with the possible exception of the Gunpowder Creek Formation exhibit a distinct increase in K and Th from west to east, approaching the Mount Gordon Fault. This may reflect increasing immaturity, tuffaceous input to sedimentation or proximity to a mixed felsic/mafic sediment source. These and other regional intraformational radiometric variations detailed above appear likely to arise from sources other than eustatic sea level changes. Possible pitfalls in attempts to construct a regional sequence stratigraphic framework based on gamma logs from a small number of locations (for example Southgate et al., 1996) may be indicated, in that gamma ray peaks and cycles present in some areas appear likely from the remotely-sensed data to be subdued or completely absent in others. This problem may however represent an opportunity, in that remotely-sensed radiometric data may be used to track at least the low frequency variations in gamma-ray signature across the entire outcrop area of the basin, thus assisting in correlation between detailed logging sites and possibly defining areas of anomalous sub-basin development.

8. Quantitative gravity and magnetic interpretation

8.0 Introduction

This chapter presents quantitative analyses of gravity and magnetic data from the Paradise Valley area described in chapters 1 and 2. This portion of the study sought to define Mount Isa Basin subsurface structures, in particular those which may have sourced and focused base metal-bearing fluids similar to those responsible for the formation of the Lady Loretta Zn-Pb deposit. Basin sequences are examined in as much stratigraphic detail as possible within the density and magnetic susceptibility contrasts and constraints identified in chapter 5. Each McNamara Group unit up to and including the Lady Loretta Formation is assessed. The Torpedo Creek Quartzite has been grouped with the Surprise Creek Formation, Bigie Formation and Myally Subgroup on the basis of similar composition (predominantly sandstones and quartzites, with some siltstones).

8.0.1 Geology

The Palaeoproterozoic Mount Isa Basin sequences outcrop over a substantial proportion of the Paradise Valley area (Figure 8.1), thus enforcing stringent controls on the geometry of geophysical models. Siliciclastic sediments and voluminous mafic volcanics of the Haslingden Group (cover sequence 2 of Blake, 1987 and O'Dea et al., 1997) dominate the area east of the Mount Gordon Fault Zone. The oldest exposed unit is the Leander Quartzite, though older rocks (Ewen Granite, Leichhardt Volcanics) outcrop just beyond the eastern edge of the area. The Haslingden Group sequence generally youngs northwards; a trend which is interrupted and repeated by a series of E-W striking faults.

West of the Mount Gordon Fault Zone, both the exposed structural level and structural style change markedly. Dolomites, dolomitic siltstones and shales of the McNamara Group are the main exposed lithology, overlying siliciclastics and minor bimodal volcanics (Surprise Creek Formation, Bigie Formation, Fiery Creek Volcanics) which in turn lie unconformably on the Haslingden Group and Quilalar Formation. The Quilalar Formation, a mixed carbonate/siliciclastic sequence correlated with the sag or thermal subsidence phase of Blake's cover sequence 2 (1987), is only apparent in the northern half of the region.

The dominant structural style is one of basin-and-dome folding with wavelengths of many kilometres. The gross sense of regional plunge is reversed when compared to the Leichhardt Rift, with older units generally more prevalent northwards. An overall N-S tectonic grain was imposed on the region during E-W shortening (D2) of the Isan Orogeny. Isan Orogeny deformation appears to be accentuated in a north-trending zone of higher strain bounded by the Russell Creek and Western Border Faults in the western portion of the region (Keele et al., 1996).

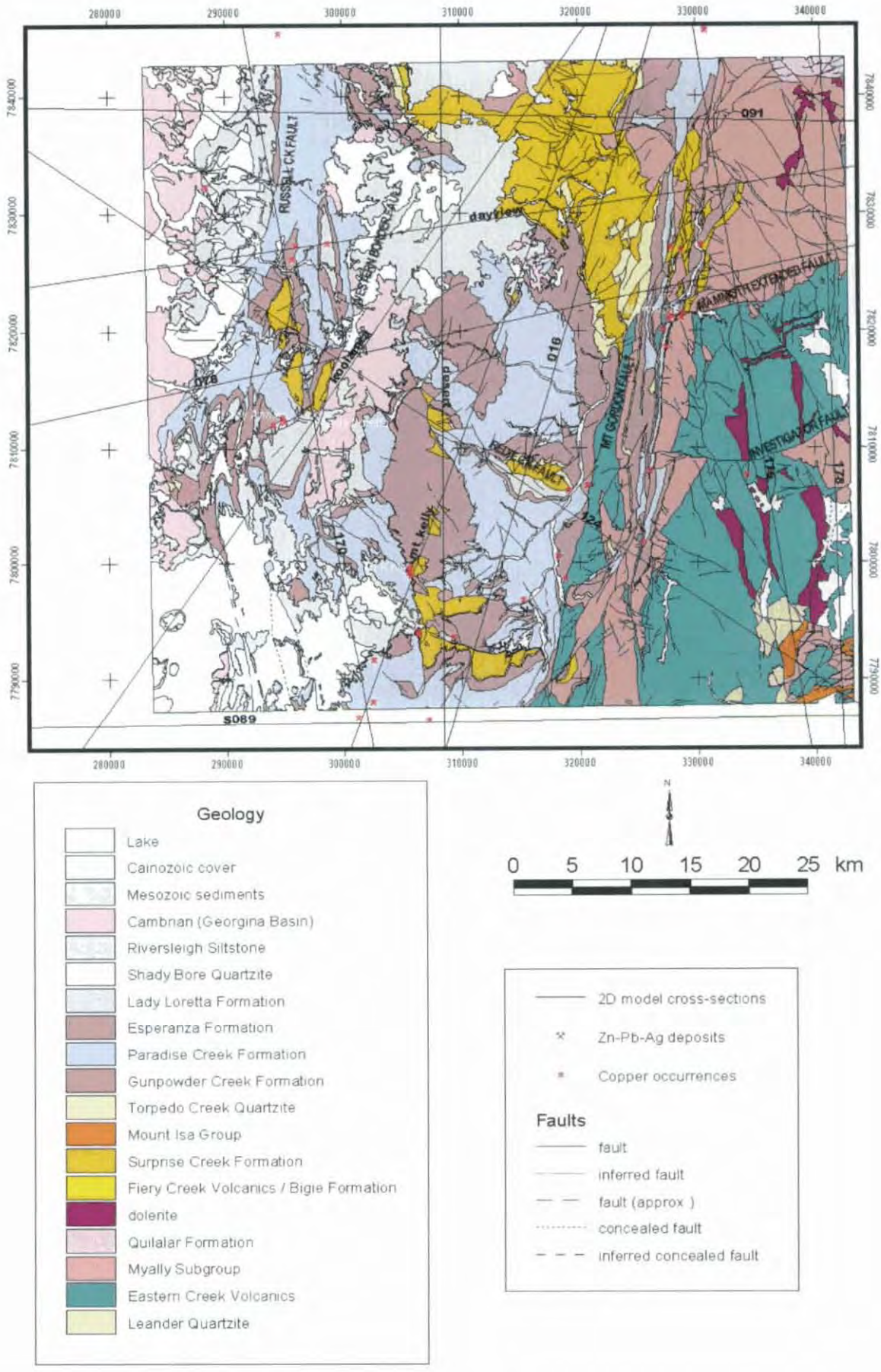

Figure 8.1 Paradise Valley geology, mineral deposits and 2-D profiles (labelled straight black lines). Geology after Hutton and Sweet, 1985

8.0.2 Mineralisation

Locations of base metal mineralisation are shown in Fig. 8.1. The only notable stratiform sediment-hosted Pb-Zn deposit amongst these is the Lady Loretta Pb-Zn-Ag orebody (see chapters 2 and 6; Hancock and Purvis (1990), McGoldrick et al. (1996) and Dunster (1996)).

Other base metal mineralisation consists mainly of copper occurrences; the largest of these being the stratabound Mammoth orebodies. Mammoth Cu is hosted by the Whitworth Quartzite of the Myally Subgroup, and is thought to have been sourced from the Eastern Creek Volcanics via fluids that migrated up the Mammoth Extended and associated faults (Scott and Taylor, 1982). It is currently being mined by Western Metals Ltd. Other notable copper deposits in the Paradise Valley area include Mount Oxide (Hutton and Sweet, 1982), Mount Kelly (Bampton et al., 1977) and Lady Annie, near Lady Loretta (Lewis, 1975).

8.1 Geophysical data

8.1.1 Gravity

Gravity data were acquired at two scales, the first at approximately 250 m spacing in a 6 x 5 km area centred on the Lady Loretta deposit, and the second at 1 km spacing on vehicular tracks within 30 km of Lady Loretta (Fig. 8.2, Appendix 2). These were observed over two field seasons in 1993 and 1994. A base station established by Western Mining Corporation personnel at Lady Loretta (M. Webb, pers. comm.; Appendix 1) was utilised as the primary base for all subsequent gravity work.

Height control for the higher resolution survey was mainly from spot heights on detailed topographic maps derived from controlled photogrammetry, as well as numerous surveyed trigonometric points and drill collars, with independent control from a pair of microbarometers. Stations were observed on a semi-regular basis depending on the availability of elevational and positional control, with a nominal spacing of 250 m. Height accuracy for the local survey is estimated at better than ±1.5 m, while many stations will be of substantially better accuracy than this. Overall accuracy in Bouguer anomaly is estimated at about ±0.25 mGal.

Elevation determinations for the semi-regional survey were derived from loop traverses with three microbarometers, utilising the methods of Leaman (1984) and absolute height controls from state permanent marks, bench marks and spot heights wherever practicable. However, absolute elevation controls are much scarcer than in the vicinity of Lady Annie and Lady Loretta, and hence height accuracy is poorer (±2 m). Horizontal positions were determined with the aid of a hand-held Magellan GPS unit, but are also less precise than in the area of detailed mapping covered by the Lady Annie-Lady Loretta prospect-scale survey (±80 m). The resulting uncertainty in absolute Bouguer gravity values for this survey is estimated not to exceed 0.5 mGal.

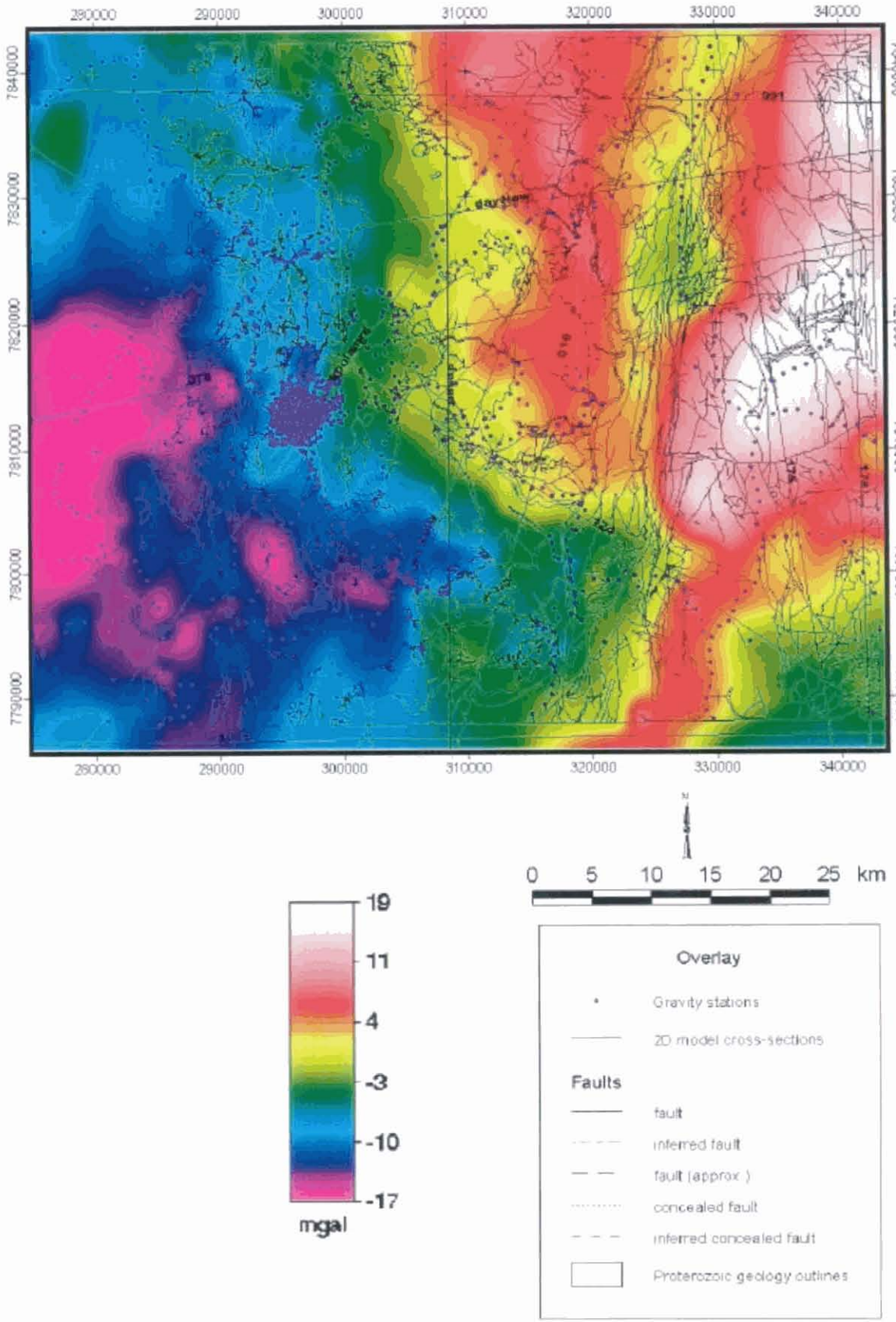

Figure 8.2 Paradise Valley gridded Bouguer anomaly data and gravity station locations with geology outline overlay modified after Hutton and Wilson (1985)

All prospect-scale gravity data were fully terrain-corrected out to a radius of 21 km, as well as the semi-regional traverse data wherever the terrain effect was judged likely to exceed 0.05 milligals. These data have been merged with regional Geological Survey of Queensland 1 km spaced traverse data (B. Stockill, pers. comm.) and Australian Geological Survey Organisation 11 km spaced reconnaissance data as well as a limited number of stations acquired by mineral exploration companies (C. Stegman, Rio Tinto Exploration, pers. comm.; R. Myers, Western Mining Corporation, pers. comm.). All externally sourced data were thoroughly checked, and stations apparently in error (identified by Bouguer anomaly values well outside the range defined by nearby stations) removed.

Bouguer anomaly values were gridded to a cell size of 200 m using minimum-curvature spline interpolation. Data for 2D modelling was extracted by automatically sampling 299 points (the maximum allowed by the modelling software) from the grid at equal distances along the line of the modelled profiles. This equates to a sub-sampling interval of approximately 350 to 650 metres, depending on the length of the profile. 'Observed gravity' data points in the profiles presented (section 8.6.1) represent these sub-sampled points, and are not actual gravity stations. This represents an oversampling of the gravity data in some profile sections that pass through areas of sparse gravity stations. Such instances, where trends apparent in the 'observed' data are largely the result of interpolation and are not well controlled by gravity station data, are noted in section 8.6.1. Conversely, the interpolated gravity data are somewhat aliased in profile sections within the area of dense data coverage around Lady Loretta.

8.1.2 Magnetics

The principal source for airborne magnetic data (Fig. 8.3) displayed in this paper is a survey flown by Geoterrex for Ashton Mining in 1987 (Queensland Dept. of Mines and Energy open file report CR18153B; Keith Jones, written communication 1995), described in chapter 7. Data from this survey was upward continued to a height of 150 m in order to match with AGSO regional data (see below).

The Ashton data were merged with aeromagnetic data from four separate AGSO surveys on 1:250,000 map sheets that join at the south-eastern corner of the study area (Camooweal, Dobbyn, Cloncurry and Mount Isa). These were flown at a nominal terrain clearance of 150 m. The rectangular hole' in the south-western corner of the magnetic map (Fig. 8.3) denotes missing data on a number of flight lines from the Camooweal survey as received from AGSO. Both the Dobbyn and Cloncurry surveys (east and south-east of Camooweal, respectively) have an east-west line direction and a line spacing of 1500 m; the older Camooweal and Mount Isa surveys have east-west flight lines approximately 3000 m (2 miles) apart.

All data were gridded to a 50 m by 50 m cell size, then merged using ECS' AGP software. The AGSO survey flown most recently (Dobbyn; 1985) was used as the datum for the grid joining algorithm. The resulting unified aeromagnetic map shows residual data (IGRF removed), with a dc shift of 5000 nT added. For 2D modelling purposes, the magnetic data grid was subsampled using the same method as for the gravity data (see above, section 8.1.1).

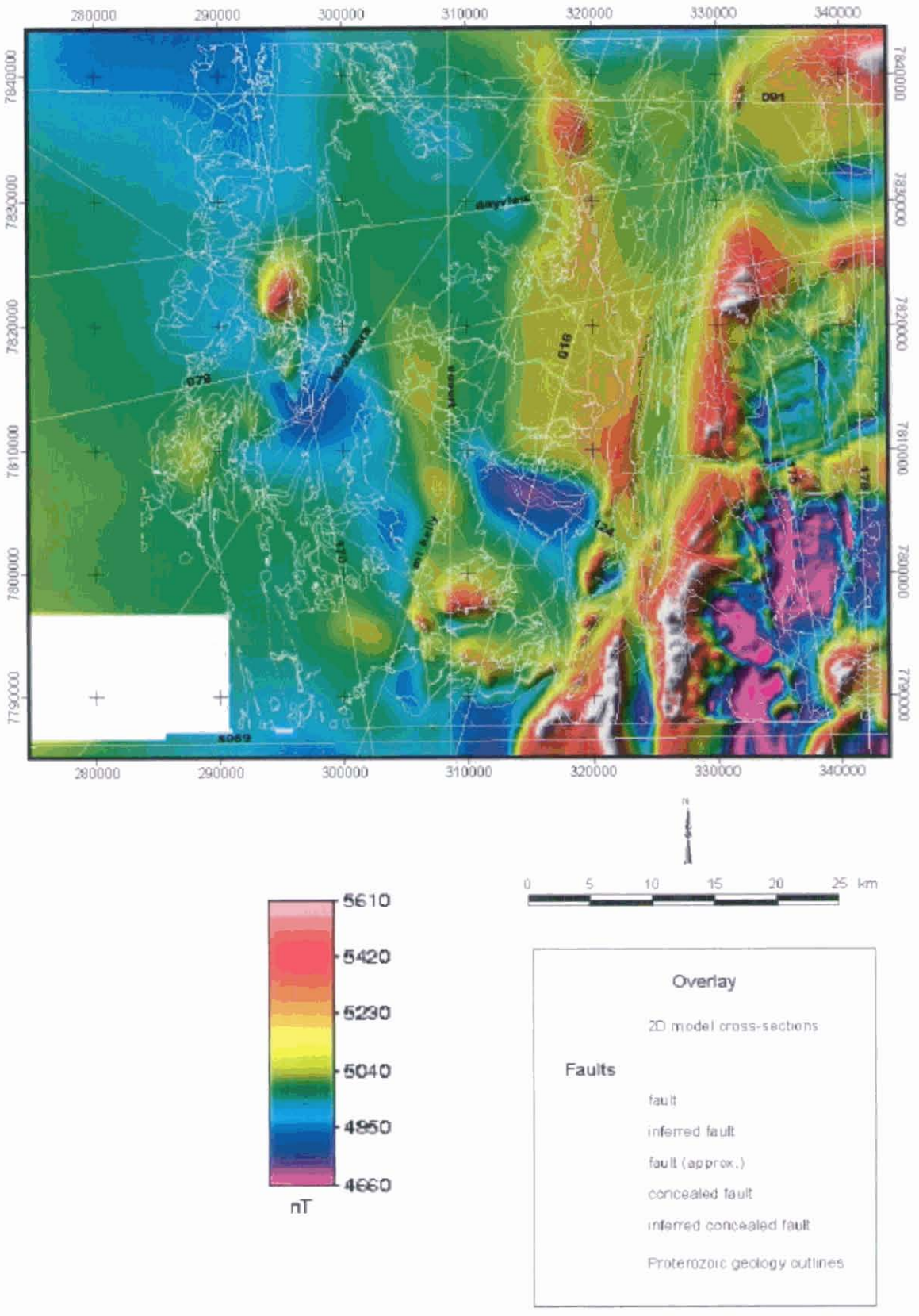

Figure 8.3 Paradise Valley gridded magnetic data with 2D profiles and geology outlines overlaid in light grey

8.2 Potential field description

Both gravity and magnetic data are dominated by NNW to NNE oriented features, though sub E-W trends are also apparent. Among the most prominent features in the combined gravity (Fig 8.2) and magnetic (Fig. 8.3) data are coincident gravity and magnetic highs associated with the Eastern Creek Volcanics either in outcrop or at shallow depths in the Cloncurry Orogen (east of the Mount Gordon Fault Zone). High frequency trends within the volcanics define the position and orientation of intercalated siliciclastic sedimentary layers. N-S trending dolerite dykes, clearly less magnetic than the volcanics that they intrude, are visible as prominent magnetic lows.

Over most of the study area the gravity field slopes decreases gradually to the west, with an abrupt negative gradient and low Bouguer values (< -30 mGal) approximately 30-35 kilometres west of Paradise Valley. Magnetic data only trace this apparent major gravimetric boundary in a limited fashion, with a high amplitude, long wavelength magnetic anomaly partly coincident with the gravity low. Far-field effects of these features extend into the study area.

To the north, a NE-SW oriented coincident gravity and magnetic low is clearly associated with the Weberra Granite. Emplacement of the granite beneath the Fiery Creek Dome and further to the south-west, terminating near the extreme north-western corner of the Paradise Valley study area, is implied. The geophysical data tend to confirm that the Weberra Granite and Fiery Creek Volcanics may be comagmatic, as suggested by Wyborn et al. (1988), as there is an obvious spatial association of the gravity and magnetic low with the most extensive and voluminous occurrences of Fiery Creek Volcanics. The absence of any similarly obvious granitoid-related geophysical features in Paradise Valley may explain the comparative thinness or absence of Fiery Creek Volcanics in much of the study area.

8.3 Previous work

Some interpretation of AGSO regional geophysical data has been undertaken previously in the region of Paradise Valley, but this has generally been only semi-quantitative at most. Wellman (1992a,b) has subdivided the Mount Isa Basin region (Mount Isa Geophysical Domain) into a number of zones based on qualitative assessments of gravity and magnetics. He fixed the western boundary of the Mount Isa Domain' *east* of outcropping Mount Isa Basin rocks based on truncation of structures in the data, though a discrepancy between indications from gravity and magnetic data was noted in the Camooweal region. Wellman suggested that the 'geophysical boundary' might be gradational in this area. He also observed the Mount Isa region to be a relative high on continental Bouguer and free-air gravity maps, and ascribed this to the Mount Isa Domain' crust being of relatively high density.

Control of the regional gravity field by relief on the Moho has been postulated by a number of authors. Crustal thinning from 40 km to 38 km coincident with outcrop and subsurface extensions of the Cloncurry Orogen was interpreted principally from regional gravity by Shirley (1979). However, this work did not adequately define crustal thickness on the western margin of the Mount Isa Basin. Variations in crustal thickness ranging from 33 to over 35 km were invoked to account for regional Bouguer gravity gradients by Tucker et al. (1979) in their regional gravity and magnetic study of the

Georgina Basin, though the possibility of gross lateral density changes in the crust contributing to the regional gravity gradient was also canvassed.

A combined sedimentary accumulation of up to 13 km including 5000 m of 'Adelaidean' sediments (possibly intended to refer to equivalents of the South Nicholson Group) and 8000 m of 'Carpentarian Lawn Hill Formation' was modelled to fit the large gravity low west of the study area by Tucker et al. (1979). Marked basement shallowing eastwards over a distance of a few tens of kilometres from 13 km depth to less than 200 metres beneath subcrop of Mount Isa Basin rocks was thereby inferred. This basement was suggested to be composed of rocks with affinities to the Hatches Creek Group and Warramunga Group of the Tennant Creek Inlier. The boundary between these units ('Aljawarra Craton') and the 'Mount Isa Orogen' was placed 20 km east of the wildcat hydrocarbon exploration drillhole Morstone No.1 (~239000E 7834000N), hence about 15 km beyond the western edge of the Paradise Valley study area, by Tucker et al. (1979).

Seismic refraction data provide some information on upper crustal geology in the region. Finlayson (1987) quoted a Moho depth of between 51 and 54 km for the region between Tennant Creek and Mount Isa. Low velocity zones (5.9-6.25 km/s) were attributed to 'Leichhardt Metamorphics with interspersed granites', and interpreted to persist to depths of at least 15 km (Finlayson, 1982). Lower velocities persist to greater (middle-lower crustal; 25-35 km) depths at Mount Isa compared to other Proterozoic cratonic areas in northern Australia (Fig. 8.4). Finlayson (1987) noted unusually thick high-velocity layers in the lower crust beneath fold belt provinces such as the Cloncurry Orogen/Riversleigh Fold Zone compared to surrounding intracratonic basins. Such features are likely to be a significant control on regional gravity gradients.

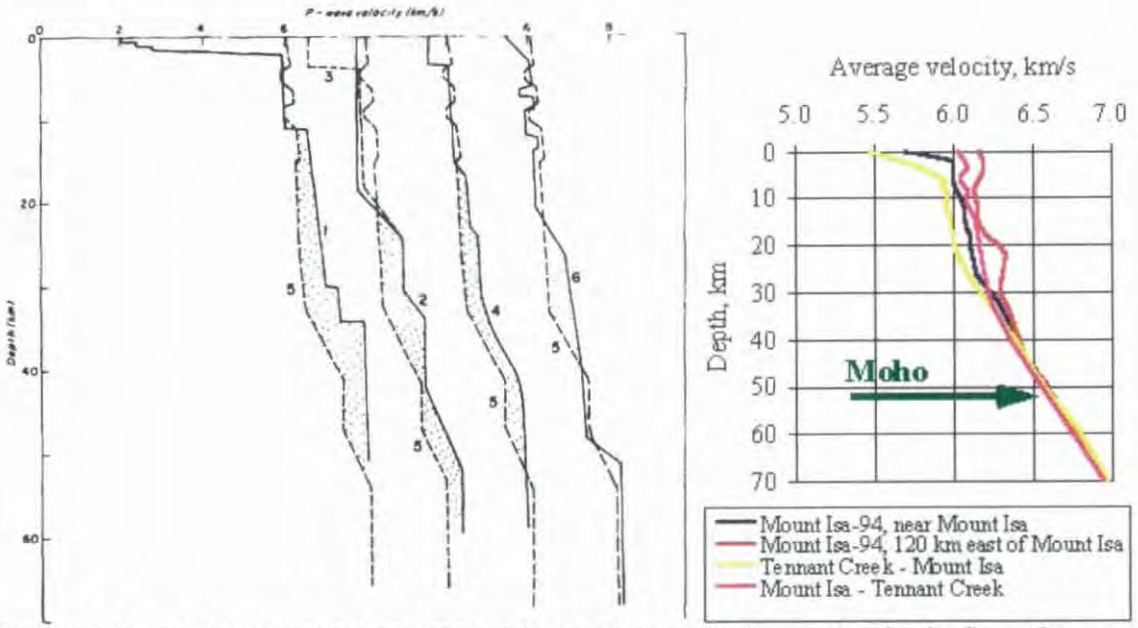

Figure 8.4 P wave average velocity-depth functions from north Australian Proterozoic refraction lines, after Finlayson (1982; left) and Goncharov et al. (1997; right). Key to locality of models at left: 1=West Arafura Sea, 2,3=west McArthur Basin, 4=east McArthur Basin, 5=Mount Isa, 6=Tennant Creek

Crustal seismic velocity models for the southern portion of the Mount Isa Basin have been refined in the course of AGSO's seismic reflection/refraction traverse across the Riversleigh Fold Zone and Cloncurry Orogen (Goncharov et al., 1996). Crustal thickness was assessed at 50-55 km, though this was at the base

of a transitional layer up to 15 km thick (Goleby et al., 1996). Velocities west of Mount Isa are seen to be generally relatively lower at upper to lower-mid crustal depths in comparison to the central Cloncurry Orogen (Figs. 8.4, 8.5). The improved seismic refraction model, still essentially consistent with the velocity model of Finlayson (1982), can be used as evidence for gross crustal density changes and arguably crustal thickness changes (Fig. 8.5).

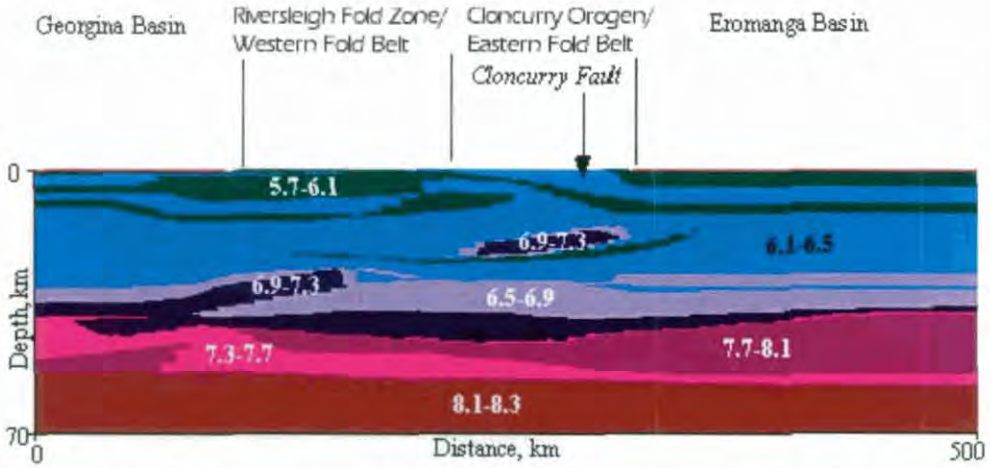

Figure 8.5 Modelled seismic velocity (km/s) distribution along the Australian Geodynamic Cooperative Research Centre's Mount Isa seismic transect, which is positioned approximately 100 km south of Paradise Valley in a west-east orientation. Modified after Goncharov et al. (1996) and http://www.agcrc.csiro.au/projects/1019AO/

A seismic reflection survey (Robertson, 1963) conducted in the Undilla region near Morstone No. 1 was only partially successful, obtaining reflections from a maximum depth of 3000 m. This provides partial support for Tucker et al.'s (1979) hypothesis of a massive sedimentary accumulation below this part of the Georgina Basin.

Leaman (1998) modelled much of the Carpentaria Zinc Belt region extending north from the study area to the western Gulf of Carpentaria, using similar methods to those adopted in this study. Many features of this interpretation were related by Leaman (1998) to elements of the sequence exposed in the western Mount Isa Basin. Among these features were extensive voluminous basalts with properties similar to those of the Eastern Creek Volcanics, and deeper, similarly extensive, moderately magnetic (up to 40×10^{-3} SI) and moderately dense (>2.77 t/m^3) sources ascribed to massive felsic volcanics with a small proportion of mafic volcanics. The latter were tentatively related to the Cliffdale Volcanics of the Murphy Inlier and the Leichhardt Volcanics. The igneous bodies were deposited in a complex network of rift cells (Leaman, 1998).

The discrepancy between seismically-derived crustal thickness values (50-55 km) and those derived from gravity (33-40 km) probably arises from differences in definition of the Moho and density contrast uncertainties, which can in turn be traced to the transitional nature of the crust-mantle boundary in this region. Gravity methods suggest a depth corresponding to the top of the transitional layer as the base of the crust, while seismic methods place the boundary beneath the transitional layer. Whatever the definition, lateral density variations at all levels within and at the base of the crust defined by previous regional gravity and seismic studies are likely to form a significant component of regional gravity gradients. Contrasts in magnetic properties are also likely to accompany the lateral density and velocity changes identified in previous geophysical work, subject to the Curie temperature depth. Heat flow

measurements in this part of Australia (Cull, 1991) are normal for continental crust at ~70 mW/m^2, implying attainment of the Curie temperature for magnetite (~575°C) at a depth of around 20 km. The probability of crustal-scale sources contributing very long wavelength components to the observed gravity and magnetic fields in the Paradise Valley area must therefore be recognised.

8.4 Rock properties and other constraints

The physical properties of the units modelled in Paradise Valley have been discussed in chapter 5. Table 5.12 has been used as the basis for interpretation. While the Lady Loretta Formation and the Paradise Creek Formation are virtually indistinguishable in terms of density and magnetic susceptibility, constraints derived from outcrop geology enable them to be modelled separately. The relatively thin Esperanza Formation was only included in models where it was sufficiently thick or close to the surface to exert a discernible influence on the gravity field; otherwise it was incorporated in the Lady Loretta Formation. The Gunpowder Creek Formation was generally modelled with a density intermediate between the Paradise Creek Formation and the underlying sandy units. However, in some areas where its upper, more dolomitic and silty section (highly over-represented in the petrophysical data set) was demonstrably missing or highly attenuated this unit was assigned a lower density befitting a sandier composition.

The Torpedo Creek Quartzite, Surprise Creek Formation, Fiery Creek Volcanics, Bigie Formation and Myally Subgroup are indistinguishable in terms of gravity and magnetics at the scale modelled (see chapter 5). Nevertheless, for reasons of stratigraphic clarity the Surprise Creek Formation (incorporating the Torpedo Creek Quartzite, Bigie Formation and Fiery Creek Volcanics if present) and the Myally Subgroup were retained as separate entities in most models. Older Haslingden Group units (Eastern Creek Volcanics, Leander Quartzite) have been assigned the bulk properties shown for them in Table 5.12, with some exceptions, which are detailed in the text below.

In some profiles there is evidence for magnetic bodies beneath the Leander Quartzite. Where these have been included, they have been given properties consistent with those measured from the Argylla Formation, Bottletree Formation or units with similar composition (generally felsic igneous) outcropping east of the study area. These, designated 'pre-Haslingden felsics' in Table 5.12, have been assigned intermediate magnetic susceptibilities and moderately low densities (less than 2.70 t/m^3), which are estimated bulk averages of what in reality are highly heterogeneous units (cf. Leaman, 1998).

These rock properties, along with surface and stratigraphic geological constraints on modelling and previous geophysical work, form the foundation for interpretation. The only other notable geological data available is from the borehole Morstone No.1, drilled about 60 km west-northwest of Lady Loretta to test the hydrocarbon potential of the northeastern Georgina Basin. It intersected little more than 300 m of Cambrian Georgina Basin sediments, but then continued through another several hundred metres of alternating sandstones and siltstones, which are tentatively correlated with the Constance Sandstone or Mullera Formation of the Mesoproterozoic South Nicholson Group.

8.5 Modelling methods

Forward modelling methods were applied to interpretation. The software used, MODEL2D developed by Michael Roach (U. Tas.), utilises standard 2D polygonal algorithms (Talwani et al., 1959; Talwani and Heirtzler, 1964). The interpretation was designed and carried out using the methods of Leaman (1994). Twelve cross sectional models incorporating geological information with corresponding gravity and magnetic data were constructed across the Paradise Valley study area (Fig. 8.1). All extend at least 25 km beyond the area of interest shown in Fig. 8.1 in order to minimise edge effects, but only those parts of the models within the study area are depicted in section 8.6.1 below. The 2-D profiles have been positioned and oriented in order to sample as many geophysical and geological features across strike as possible, in areas of reasonable data coverage. Due to the complex and intense deformation in this region compared to areas further north in the Bowthorn Block and north of the Murphy Inlier, 3-D (off line) effects have been unavoidable in many areas, particularly on the western and eastern edges of the study area, and near the Mount Gordon Fault Zone and Lady Loretta.

Earth's magnetic field parameters used were: Total strength 50500 nT, inclination -50°, declination 6°, estimated from charts of the Australian Geomagnetic Reference Field published by AGSO for the 1990.0 epoch. All models interlock consistently at their intersection points. Reference properties employed in modelling are 2.74 t/m^3 and 0.0 SI, representative of non-magnetic metamorphic basement, following the standard used by Leaman (1996, 1998) elsewhere in the Carpentaria Zinc Belt. The models have a depth extent of 15 km, but to maximise clarity of stratigraphic detail in the depth dimension only the upper 7 km is shown, except where there are features of interest in the 7-15 km depth range.

8.6 Interpretation

A base level of 5000 nT was used in all modelling, being the dc shift added to the original data after IGRF removal. In order to account for a very long wavelength gradient in the magnetic field across the region (possibly caused by the presence of mafic material at upper mid-crustal levels beneath the Leichhardt Rift; see Gunn, 1983; Goncharov et al., 1996), magnetic base level was shifted upwards by 50 nT in north-south oriented profiles on the eastern edge of the study area, and 50 nT downwards in N-S profiles on the western edge.

A granitic basement with density contrast -0.05 t/m^3 and nil magnetic susceptibility contrast, consistent with basement granitoids outcropping elsewhere in the Mount Isa Basin (chapter 5; Hone et al., 1987) has been modelled at the base of all profiles (15 km depth). This layer's thickness varies from zero up to around 4 km, generally decreasing westwards from the eastern edge of the study area. Relief on the upper surface of this granitoid basement is very low, and a component of the long wavelength variations in the gravity field modelled by it may actually be due to gross lateral variations in crustal properties (density, thickness) discussed above in section 8.3.

The extensive magnetic low on the western side of the study area is apparently a geometric effect associated with a very large (high amplitude, long wavelength) magnetic high still further west. It is associated with a major N-S trending gravity low, which has a steep gradient on its eastern flank. These

features were modelled in western extensions to E-W oriented models of the study area in order to minimise edge effects. Siliciclastics of the South Nicholson Group account for a portion of the gravity low, but the gross features of the combined magnetic high/gravity low are best explained by a body of density ~2.69 t/m^3 and magnetic susceptibility 30 x 10^{-3} SI, extending to as much as 15 km depth. Alternatives involving low density South Nicholson Group sandstones overlying a magnetic basaltic basement similar to the Eastern Creek Volcanics were examined, but found unable to concurrently account for both the gravity and magnetic fields. Physical properties of the hypothesised body are consistent with a limited set of lithologies, among them felsic to intermediate/andesitic volcanics and I-type granitoids, and their metamorphic equivalents (Clark and Emerson, 1991). The Cliffdale Volcanics, Bottletree Formation and Argylla Formation, all mainly consisting of metamorphosed felsic volcanics, are hence possible candidate units to account for this body, but its shape as modelled (15 km depth, rounded top) is suggestive of a granitoid intrusion. While I-type granites are prevalent over S-types in the Mount Isa Basin (Wyborn et al., 1987), the majority, including the nearest outcropping examples (Weberra Granite, Yeldham Granite, Sybella Granite) are not particularly magnetic. The body may actually be part of an entirely separate terrane. Whatever the nature and origin of the body, its exact geometry and composition are not critical to accounting for the long wavelength component of the gravity and magnetic fields affecting the study area. Further investigation of the nature of the speculated boundary between the Mount Isa Basin and the adjoining terrane is beyond the scope of this thesis.

8.6.1 2D models

The profiles have informal working titles based either on their orientation (in degrees from true north) or localities which they were designed to investigate. These designations have no particular significance other than as a mechanism to link the profiles presented (Figs. 8.6-8.17) to their position in plan view shown in Fig. 8.1.

Observed gravity and magnetic data points extracted from gridded data as described in section 8.1 are shown on all models as open squares (gravity) and triangles (magnetic), connected by dotted line segments. Bouguer gravity and magnetic anomalies calculated from the modelled bodies are shown as lighter and darker solid lines, respectively.

Unit	Abbreviation	Density (t/m^3)	k ($\times 10^{-3}$ SI)
Mesozoic	M	2.18	0
Cambrian	C	2.66	0.05
South Nicholson Group	Ps	2.61	0.15
Riversleigh Siltstone	Pmr	2.67	0.15
Shady Bore Quartzite	Pms	2.62	0.02
Lady Loretta Formation	Pml	2.78	0.15
Esperanza Formation	Pmz	2.67	0.15
Paradise Creek Formation	Pmx	2.77	0.10
Gunpowder Creek Formation	Pmw	2.72	0.30
undifferentiated Torpedo Creek Quartzite, Surprise Creek Formation, Fiery Creek Volcanics, Bigie Formation	Pr	2.64-2.67	0.10
Fiery Creek Volcanics	Pfv	2.8	0.50
undifferentiated Torpedo Creek Quartzite-Myally Subgroup inclusive	Pr-hm	2.64-2.67	0.10
Myally Subgroup	Phm	2.64-2.67	0.10
Eastern Creek Volcanics	Phe	2.91	55
Leander Quartzite	Phq	2.64	0.10
'pre-Haslingden Group felsics'	Pht	2.65-2.76	0.4-65

Table 8.1 Basin unit abbreviations used in models (Figs. 8.6-8.17) with representative physical properties based on Table 5.12

The profiles in approximately west-east orientation tend to be dominated by structures attributed to the main east-west compressional phase of the Isan Orogeny. In profile S089 (Fig. 8.6), Isan Orogeny folds increase in intensity from west to east. The Mount Gordon Fault separating the Riversleigh Fold Zone from the Leichhardt Rift at 149000 m dips moderately steeply to the west. A similar interpretation was made by Goleby et al. (1997) from a regional east-west seismic traverse tens of kilometres to the south.

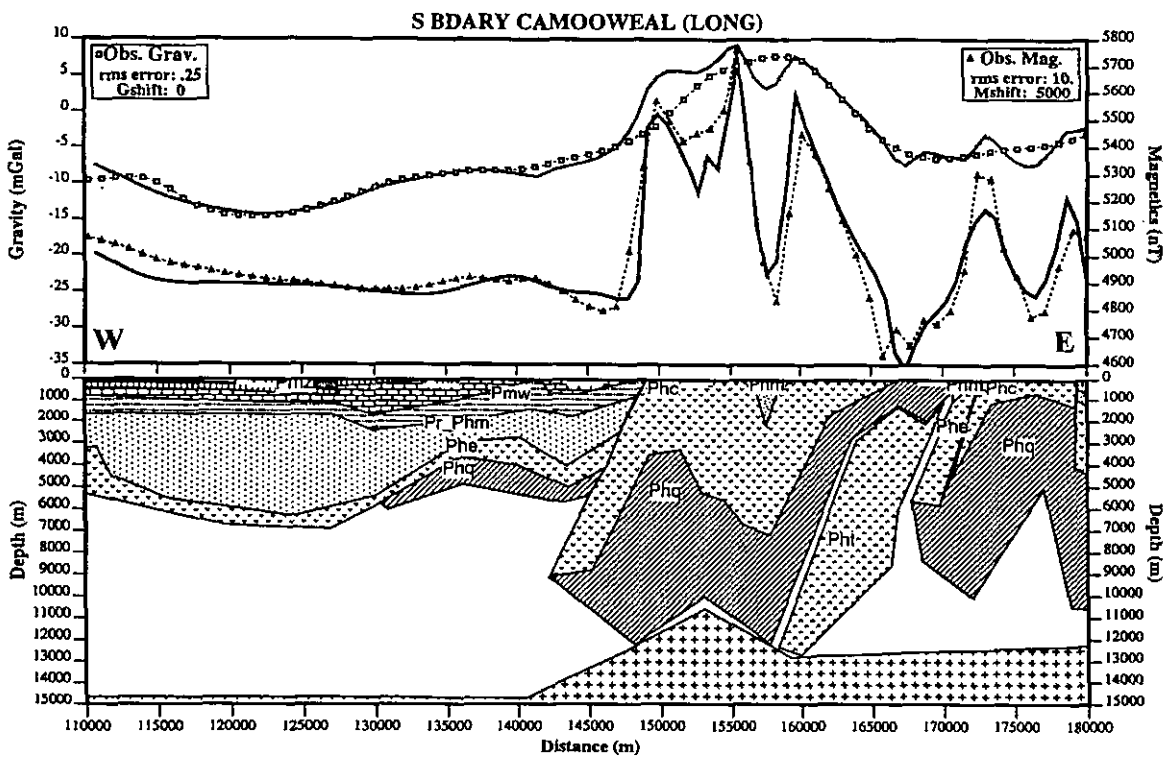

Figure 8.6 Profile 'S089'

S089 was extended over 100 km past the eastern edge of the study area, beyond the eastern limit of outcropping rocks of the Cloncurry Orogen, in order to characterise the geophysical response of units postulated to comprise 'basement' to much of the Mount Isa Basin, particularly 'pre-Haslingden felsics' mentioned in chapter 5. This confirmed the highly variable signatures of these units, especially their magnetic properties. Outcropping Bottletree Formation, Argylla Formation and Leichhardt Volcanics, representative of the 'pre-Haslingden felsics' suite, appeared highly magnetic in some sections and virtually non-magnetic in others. Both these units consist mainly of varying proportions of felsic and mafic igneous lithologies, implying similar variability in density. The pre-Haslingden felsics are represented on profile S089 by a moderately dense, slightly magnetic body (2.80 t/m^3 0.001 SI) beneath the Leander Quartzite around 165000 m. This body (labelled Pht) was inserted mainly to satisfy the requirements of the gravity data.

The inlier of Surprise Creek Formation crossed by profile 078 (Fig. 8.7) at 131000 m contains a core of Eastern Creek Volcanics extending to within 1500 m of the surface. This inlier appears to have been faulted into place along steeply west-dipping faults, similar in orientation to the Western Border Fault (136000 m on profile 078) as suggested by van Dijk (1991), who interpreted the Western Border Fault as a thrust soling out at a depth of several kilometres. Also noteworthy is the extreme attenuation of the Myally Subgroup-Torpedo Creek Quartzite sequence (Pr-Phm) in the middle of profile 078 (Fig. 8.7).

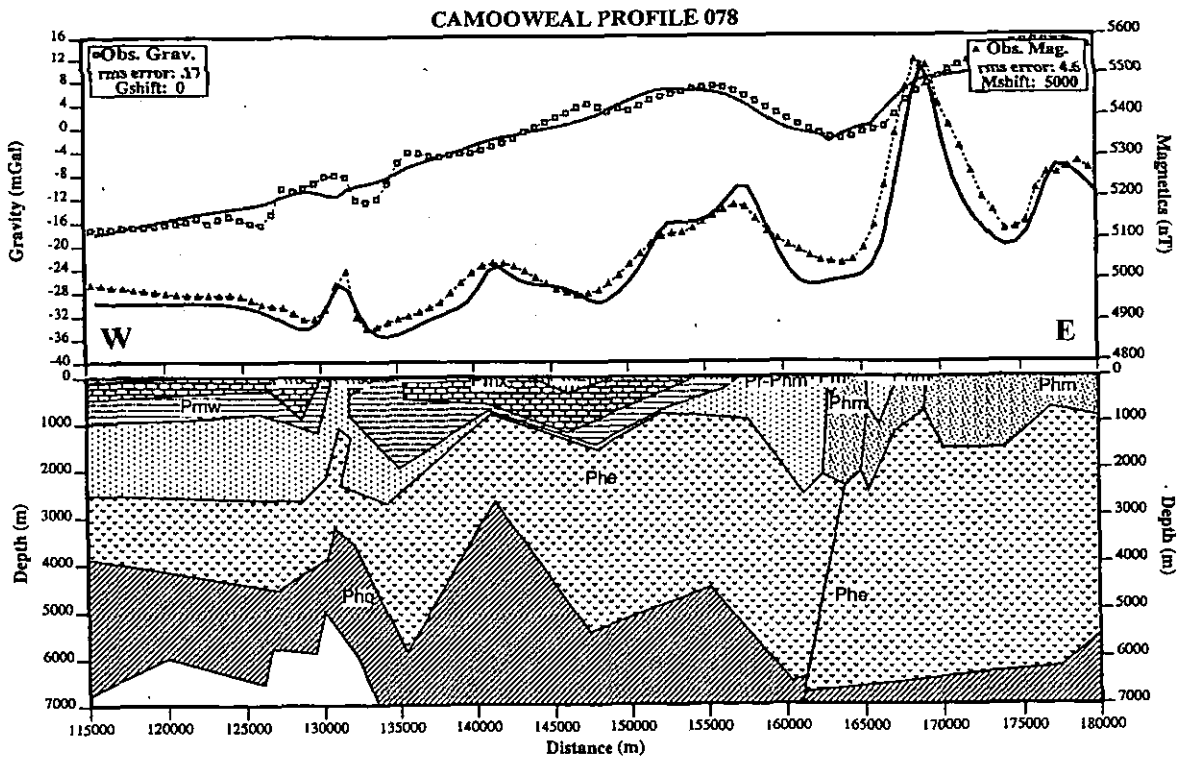

Figure 8.7 Profile '078'

The 'dayview' profile was positioned to sample the Dayview Syncline (also known as the Debut Syncline) which is centred around 39000 m in Fig. 8.8. This profile also samples the Russell Creek Fault, which is here interpreted as a near-vertical fault with over 2 km of apparent vertical displacement. The misfit between the observed and calculated magnetic data in the vicinity of the Mount Gordon Fault at

69000 m is ascribed to off-line geometric effects caused by large volumes of Eastern Creek Volcanics outcropping a few kilometres south of the line at this point.

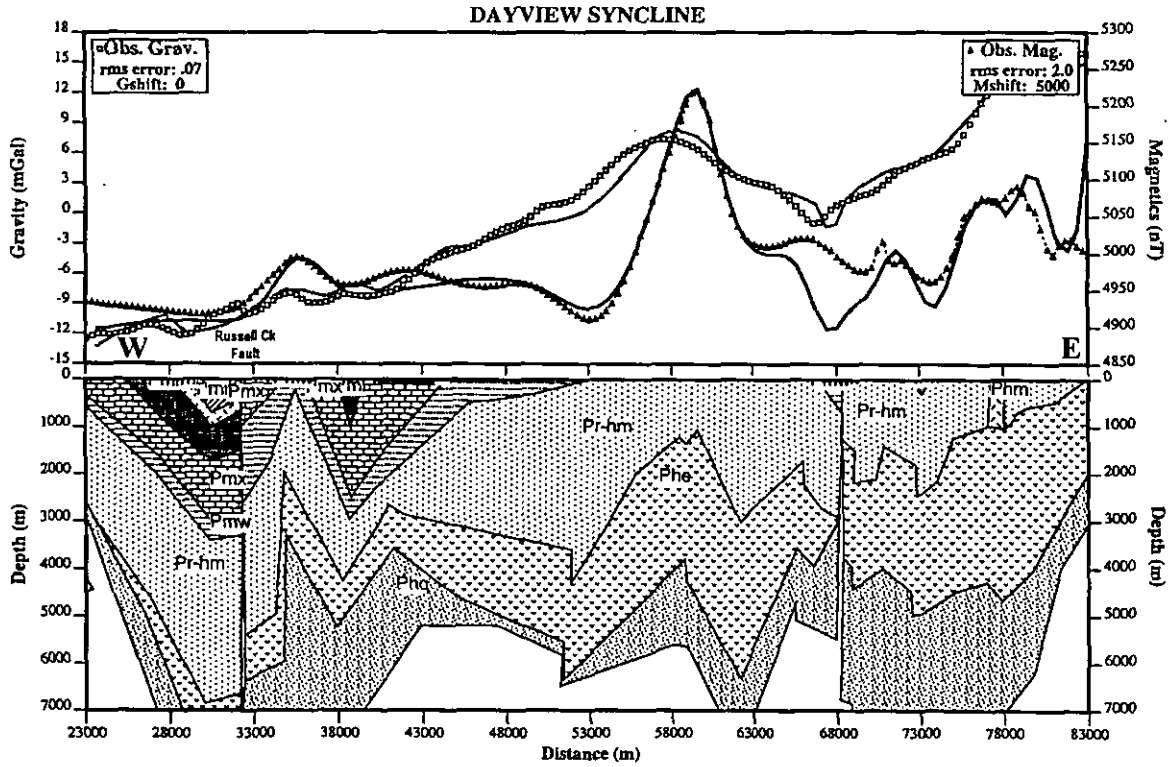

Figure 8.8 Profile 'dayview'

Westwards attenuation of the lower Mount Isa Basin sequence above undifferentiated basement is clearly illustrated in profile 091 (Figure 8.9). A major structure, possibly a steep reverse fault based on the magnetic data, apparently occurs around 150000 m, though there are few indications of significant displacement within the Surprise Creek Formation outcropping at this point. The Mount Gordon Fault at ~164000 m retains the steep westerly dip observed further south.

Profile 178 (Figure 8.10), running approximately north-south on the eastern edge of the study area, was positioned in order to sample as many features of the Leichhardt Rift (O'Dea et al., 1997b) as possible. Northward-tilting blocks separated by faults 10-20 km apart (Mount Oxide, Gunpowder, Investigator, Eastern Creek and Crystal Creek blocks of O'Dea et al., 1997b) are seen to be responsible for repetition of the Haslingden Group section several times within the Leichhardt Rift. Significant thickness variations are apparent between a number of the tilt blocks, with the Eastern Creek Volcanics (ECV) generally increasing in thickness from south (~2.5 km) to north (> 5 km). Both these values refer to complete sections. There does not appear to be a consistent structural style governing the faults separating the tilted blocks. The Mammoth Extended and Investigator Faults at ~97000 m and ~111000 m respectively are tentatively interpreted as currently being moderately steeply north-dipping reverse faults. This interpretation is inconsistent with the development of the northward-tilting blocks as extensional half-graben, as in O'Dea et al.'s (1997b) description of the 'Myally Rift event', but does conform more closely to interpretations of these structures as north-dipping thrusts (van Dijk, 1991; Bell, 1983).

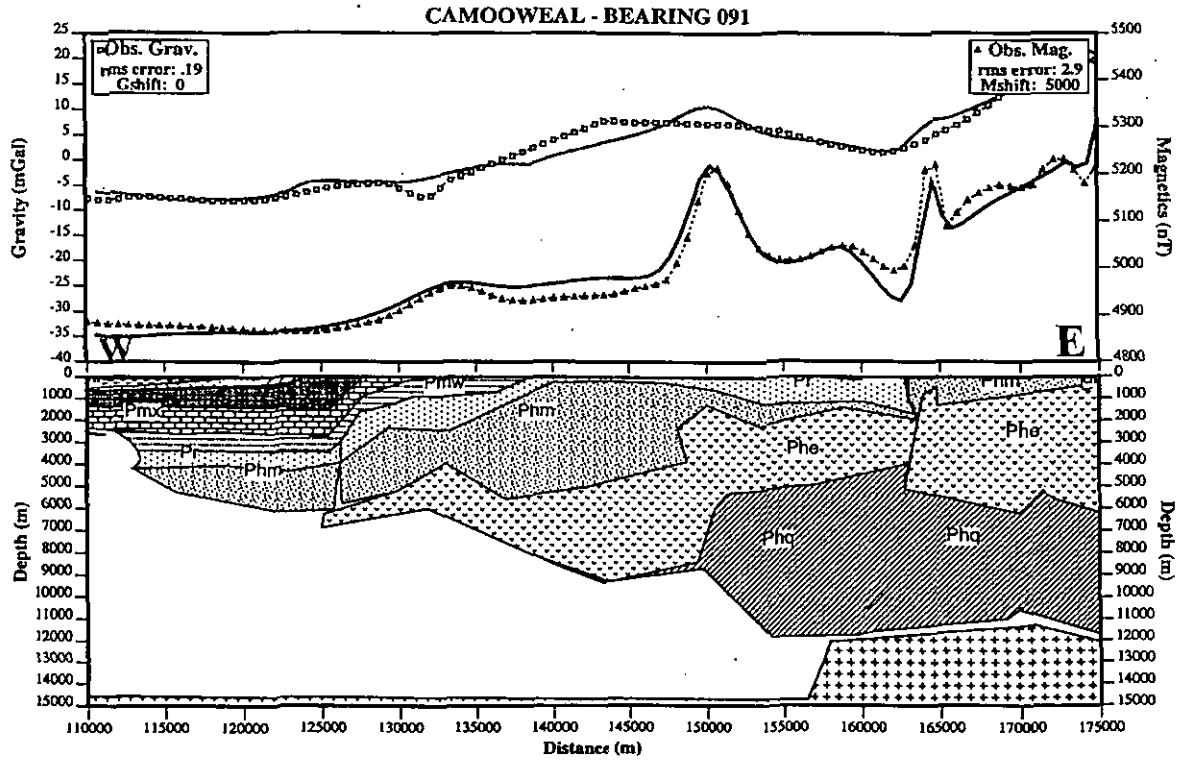

Figure 8.9 Profile '091'

There is a caveat on this aspect of the interpretation. As the ECV are the only significant magnetic unit in each model, fault dip information can only be extracted where faults comprise bounding surfaces of the ECV. Accordingly, the orientation of boundaries separating model bodies with the same properties is arbitrary, except where these boundaries are collinear with significant offsets in the upper or lower bounding surfaces. The disposition of faults affecting the Eastern Creek Volcanics is also subject to considerable uncertainty because of the ubiquitous alteration discussed in chapter 7. The fluids responsible for this alteration are most likely to have been concentrated in and near major faults, as has clearly occurred in the form of magnetite-destructive alteration along faults as described in chapter 7 (see Fig. 7.9; Wyborn, 1987). Magnetite creation as a result of albite + actinolite or calcite + magnetite alteration is also a potential source of variability in ECV magnetic properties (see section 7.2.1.2; Fig. 7.9; Wyborn, 1987). If these alteration systems affect the bulk properties of volumetrically significant ECV rock masses adjacent to fault planes, estimations of fault dip will be strongly affected, and possibly invalidated. This may be occurring north of the Investigator Fault (~110000 m, Fig. 8.10), where a better fit was obtained by removing a small section of ECV at the surface north of the fault - effectively assigning zero magnetic susceptibility and a neutral density of 2.74 t/m^3 to this volume. These properties are consistent with chlorite + albite and epidote ± sphene alteration, or simply deep, intense weathering.

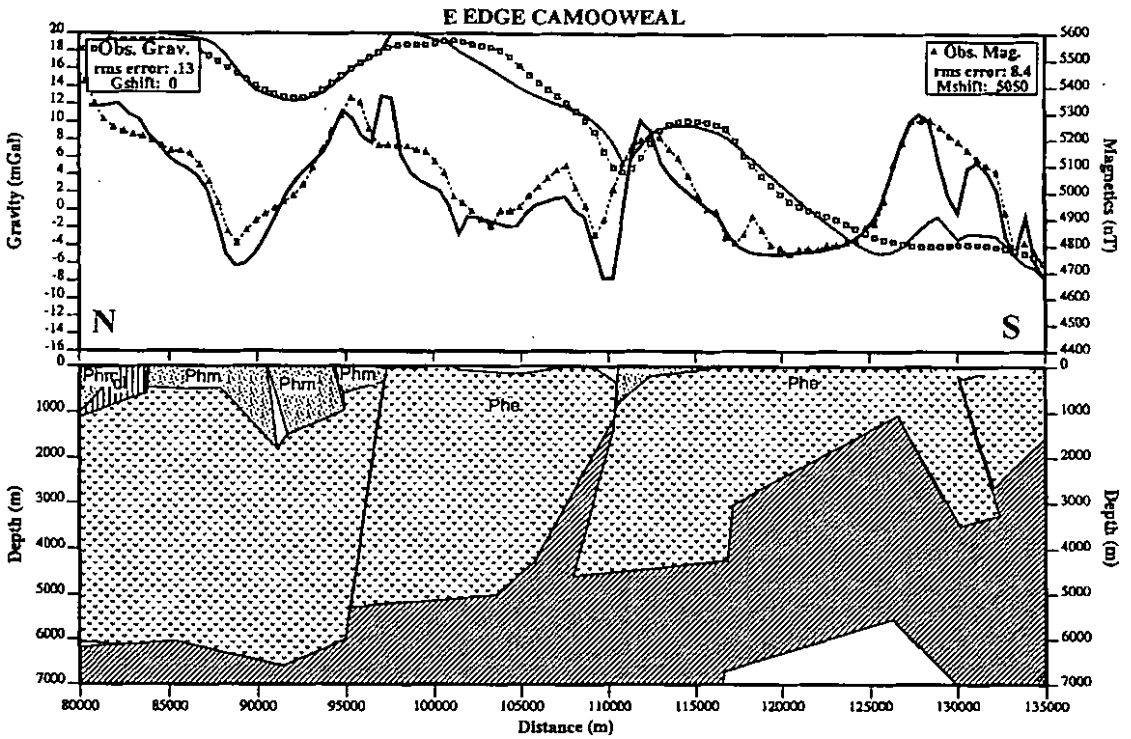

Figure 8.10 Profile '178'

Extensional structures are better preserved in the line to the west (Profile 175, Figure 8.11) north of the Mammoth Extended Fault (~102000 m). This configuration is consistent with north-south extension resulting in E-W oriented structures which controlled deposition of the sequence ranging from the Pickwick Metabasalt to the Whitworth Quartzite in the Myally Subgroup, as proposed by O'Dea and Lister (1995) and O'Dea et al. (1997b). Compressional structures are more prevalent at the southern end of the line, where the Leander Quartzite is interpreted to be thrust over younger strata including the Mount Isa Group (lower McNamara Group equivalents) and Myally Subgroup.

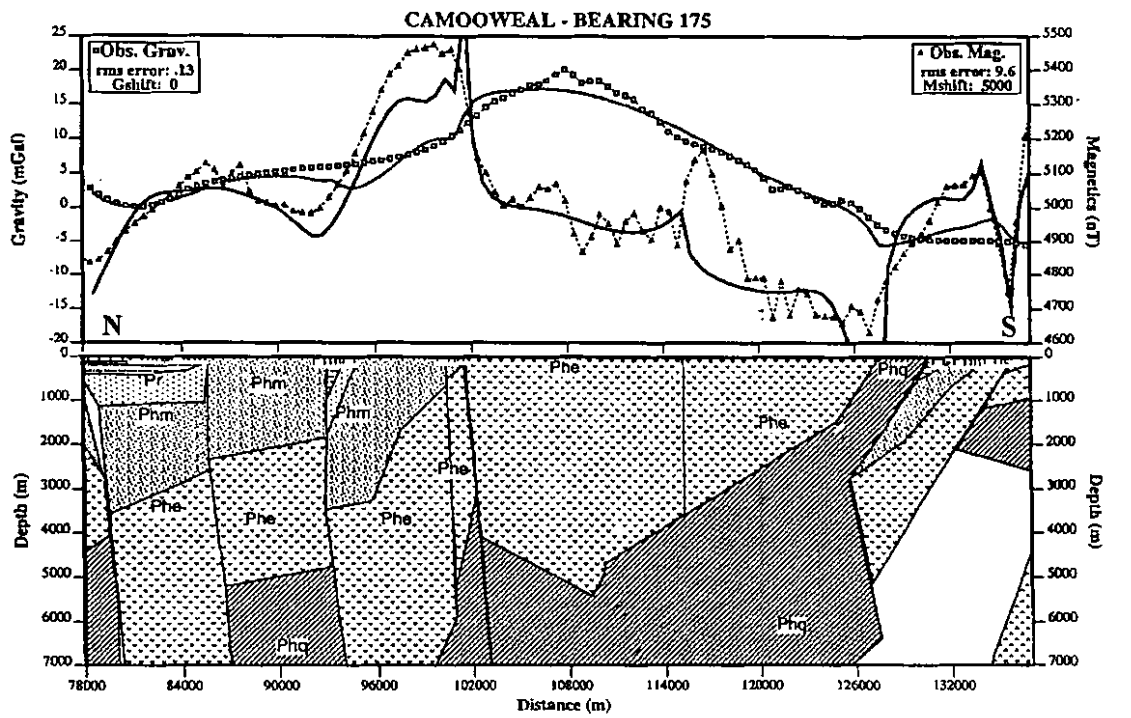

Figure 8.11 Profile '175'

It is impractical to exactly model the higher frequency magnetic signal observed in line 175 over outcropping ECV. This character may be due to combinations of a number of factors such as weathering depth, primary lithological variation, magnetite-affecting alteration and remanence variation. The sharp magnetic high at 116000 m mainly coincides with Pickwick Metabasalt outcrop, and may be caused by increased magnetite created during stratigraphically-controlled alteration of this unit, as discussed in chapter 7. This uncertainty in local magnetic properties means that the orientation of the Investigator Fault at ~115000 m is ambiguous.

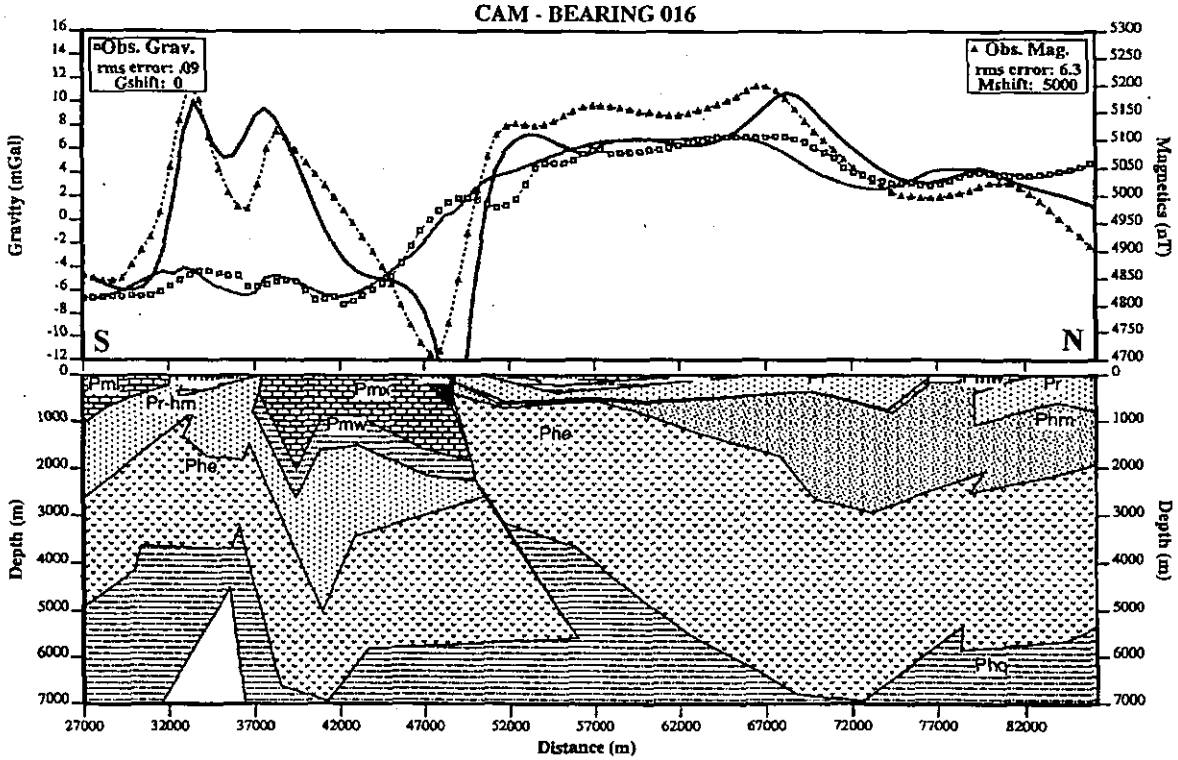

Figure 8.12 Profile '016'

The Redie Creek Fault crossed by Profile 016 (Figure 8.12) at 50000 m is modelled as a north-dipping thrust fault. This structure may represent the southern boundary of an inverted half-graben active during ECV or earlier time, but the possibility that this fault may have had a different orientation or sense of displacement at other stages during its history cannot be discounted. Additional uncertainty is introduced by the violation of 2-D assumptions introduced by the N-S trending folds formed during the Isan Orogeny. The much thicker Myally Subgroup - Paradise Creek Formation sequence to the south of the Redie Creek Fault suggests a depocentre in this area during this period. The modelling indicates that mapped faults bounding Surprise Creek Formation inliers towards the southern end of the profile are south-dipping thrusts.

The Redie Creek Fault is interpreted to be near-vertical on the mt_kelly profile (51000 m in Fig. 8.13), west of profile 016. South-dipping faults are again observed towards the southern end of the profile, but here they appear to have a normal sense of displacement. There are indications of reverse faulting affecting the Eastern Creek Volcanics at depth towards the northern end of the mt_kelly model (Fig. 8.13), but the relationship between these inferred structures and faults within the Myally Subgroup-Gunpowder Creek Formation sequence exposed in this area is not clear.

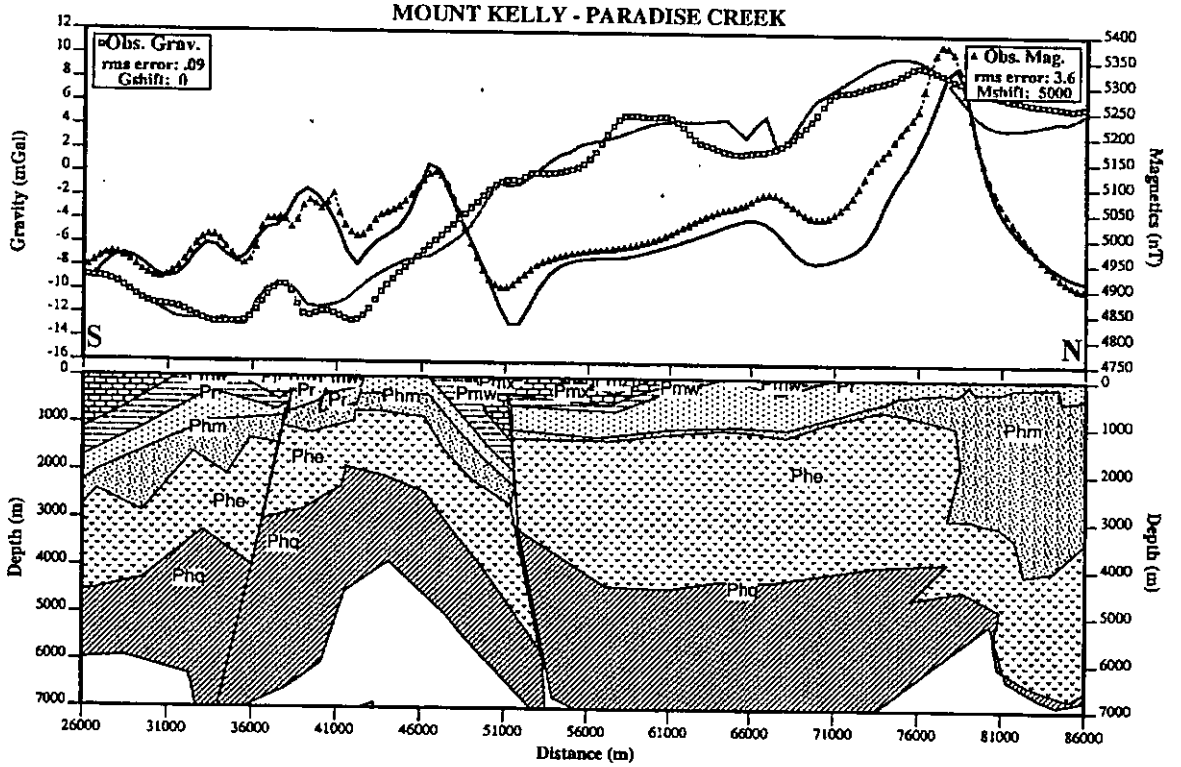

Figure 8.13 Profile 'mt_kelly'

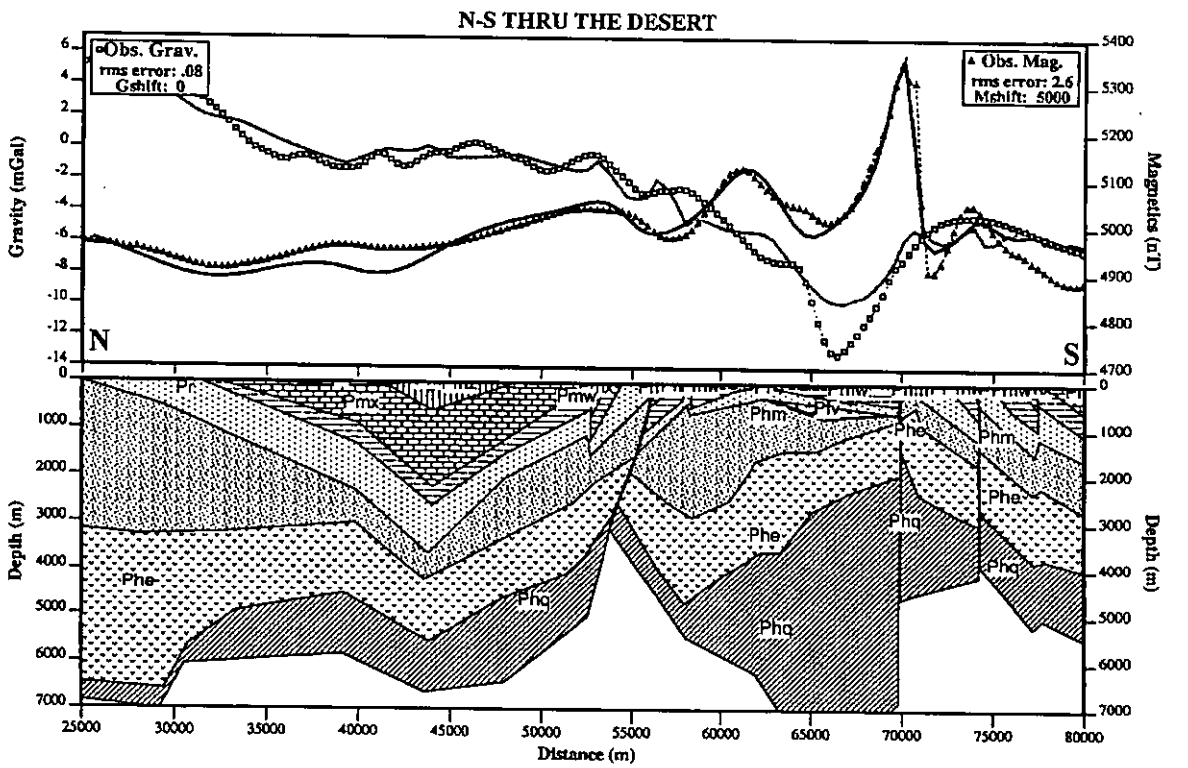

Figure 8.14 Profile 'desert'

Still further west, the Redie Creek Fault at 56000 m on the 'desert' profile (Fig. 8.14) appears to have a southerly dip. This model was positioned to traverse the extensive area covered by Tertiary duricrust and Mesozoic sediments known locally as The Desert, centred around 40000 m in Fig. 8.14. This area is interpreted to be underlain by shallowly dipping Paradise Creek Formation. The line almost coincides with an anticlinal axis towards its southern end, which caused some difficulty in fitting the gravity data. The problem is apparently most acute around 67000 m, but the sharp 'observed' gravity low interpolated

in this area (corresponding to 308400E 7801500N, Fig. 8.2) is poorly controlled by gravity station data, and may be spurious. Better definition of the gravity field in this region may result in a reduction in thickness of the wedge of Leander Quartzite currently modelled north of 70000 m (Fig. 8.14).

The 'koolamra' profile (Figure 8.15) was designed to investigate areas blanketed extensively by Phanerozoic sediments. These are interpreted to cover flat-lying Shady Bore Quartzite (around 35000 m) and Paradise Creek Formation (70000-85000 m). A southern extension of the Russell Creek Fault (*sensu* van Dijk, 1991) is crossed at 43000 m where Gunpowder Creek Formation is faulted against Shady Bore Quartzite, with over 2 km of apparent vertical displacement. As the ECV are interpreted to be very thin in this area, the fault having no associated magnetic signature, it is difficult to glean information on its dip. The line also crosses the Western Border Fault but does so obliquely, so little confidence can be attached to the steep south-westerly dip shown in Fig. 8.15. The magnetic signal in this area (51000-61000 m; around 298000E 7813000N, Fig. 8.3) is strongly affected by geometric effects arising from the upfaulted mass of Eastern Creek Volcanics less than a kilometre off-line to the north-west, on the north-western side of the Western Border and Carlton Faults.

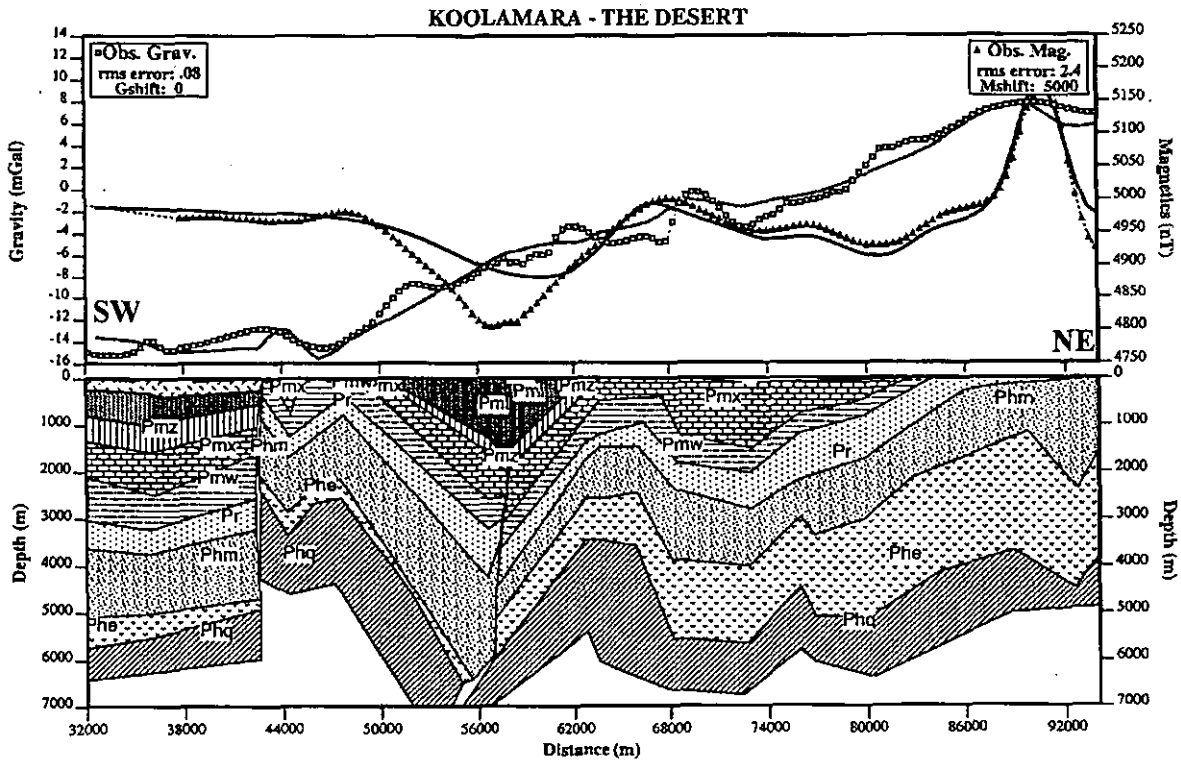

Figure 8.15 Profile 'koolamra'

The host sequence for the Lady Loretta Pb-Zn-Ag deposit is sampled by profile 170 (Figure 8.16). The deposit itself is located on and just to the east of the line at 113000 m. Immediately north of the deposit, the Carlton Fault dips south. This interpretation is informed by drilling in the vicinity of Lady Loretta and Lady Annie documented in unpublished data stored at the mine site. The hypothesis that the arcuate Leopard-Carlton Fault system is a north- and northeast-dipping spoon-like fault thrusting units at least as old as Bigie Formation over younger McNamara Group sediments (van Dijk, 1991) is not supported by this interpretation of the potential field data or by local drilling data. Other faults dissecting the inliers north of Lady Loretta apparently dip steeply southwards. Structures north of and including the Russell Creek Fault at 93000 m are crossed obliquely by this profile, which in conjunction with extremely thinned

ECV means that little can safely be concluded regarding their orientation. The Surprise Creek Formation-Myally Subgroup sequence (Pr-Phm) is extremely attenuated in the fault block north of Lady Loretta, to the point that the Myally Subgroup, several kilometres thick elsewhere, is virtually absent. South of the Carlton Fault, this sequence is up to 2 km thick.

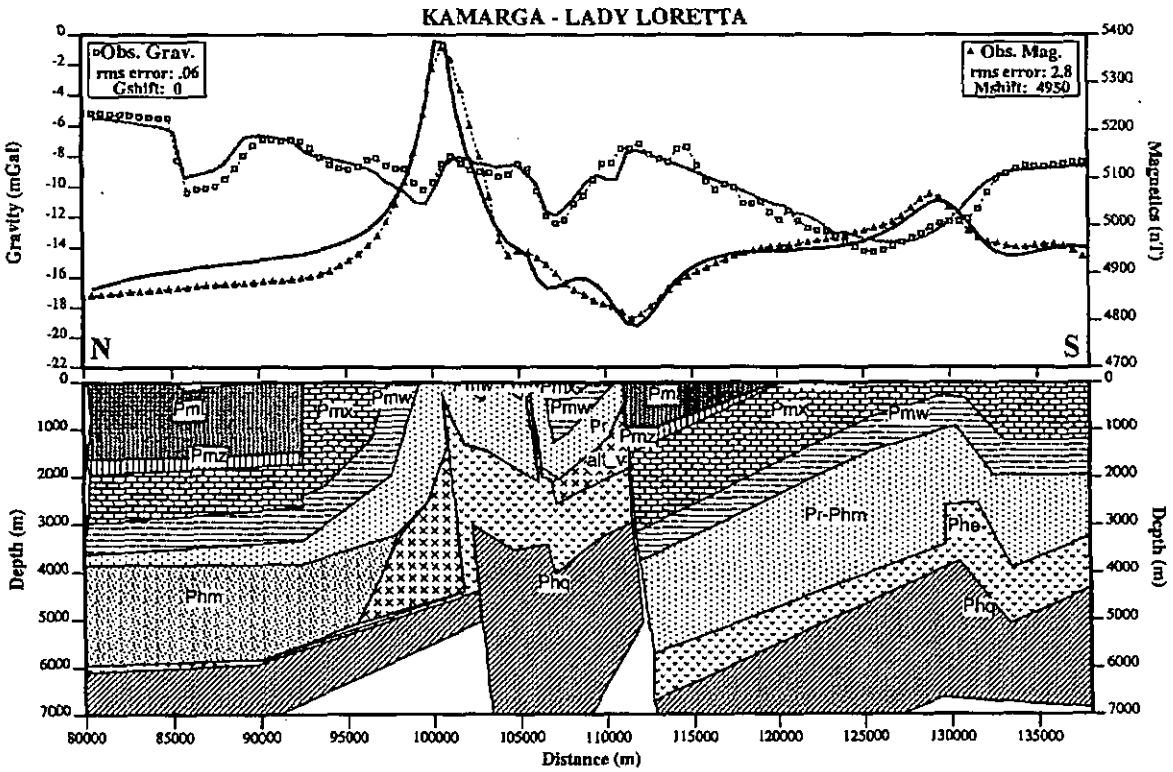

Figure 8.16 Profile 170

An important feature of the profile 170 model is the volume of altered volcanics (labelled 'alt_v' in Fig. 8.16) within the upfaulted ECV north of Lady Loretta. The altered volcanics have been assigned depressed density and magnetic susceptibility properties (2.76 t/m^3, 1 x 10^{-3} SI; cf. 'normal ECV 2.91t/m^3 and > 50 x 10^{-3} SI) consistent with those measured on the chloritic metabasalt intersected at around 500 m depth in the Q68 drillhole, which is located less than 2 km west of the 111000 m point on the profile. Apart from the indications from drilling, models containing altered volcanics most easily satisfy the requirements of the gravity and magnetic data in this area. As discussed in chapter 5, this alteration is thought to be of the chlorite + albite type, and may have sourced Zn-Pb and Cu-mineralising fluids.

The disposition of the Eastern Creek Volcanics in profile 124 (Fig. 8.17) indicates that the Russell Creek Fault at 153000 m is a steeply WNW-dipping normal fault, but the magnetic signature observed is mainly due to the effects of the faulted anticline a few kilometres to the south-east. The fault cutting this anticline may also be related to the Russell Creek Fault system. Vertical faults including the Western Border Fault around 161000 and 164000 m have decreasing apparent vertical displacement with depth, indicating lateral wrenching as the major component of movement on these structures. The Mount Gordon Fault which is exposed near 185000 m is again interpreted to be west-dipping, but the structure is obscured by bedding being near-parallel to the fault as a result of major synclines and anticlines west and east of the fault, respectively. It appears likely that both wrenching and thrusting have occurred to varying degrees in the complexly faulted zone up 7 km southeastwards from the main Mount Gordon

Fault. Further southeast along the profile the macro-structure is that of a relatively simple anticline, though this is again truncated by a major fault at 206000 m where Mount Isa Group has been faulted against Leander Quartzite, possibly by approximately S-directed thrusting as discussed above in relation to profiles 175 and 178 which also traverse this area.

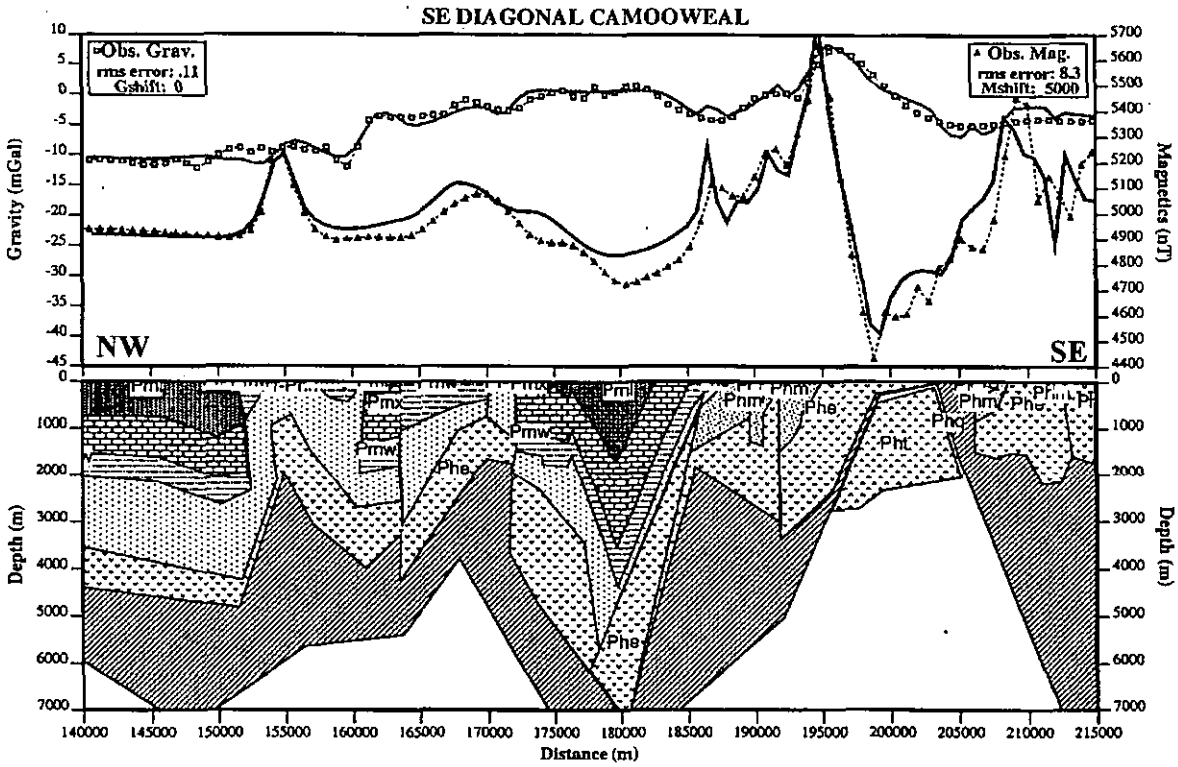

Figure 8.17 Profile 124

8.6.2 2.5-D structural surfaces

2.5-D structural surfaces (equivalent to structure contours) which together describe a 3-D model for the Paradise Valley region were constructed from the 2-D models. Picks of the upper and lower contacts of modelled basin units (Lady Loretta Formation, Paradise Creek Formation, Gunpowder Creek Formation, Torpedo Creek Quartzite-Myally Subgroup inclusive, Eastern Creek Volcanics, Leander Quartzite) were taken from the 2-D model cross-sections, transferred onto a plan view map of the study area and digitised into a GIS. These were interpolated into a 2.5-D surface using the ANUDEM algorithm (Hutchinson, 1989). This procedure incorporated additional elevation constraints from geological map data in the GIS, with all outcrops equivalent to or older than the unit modelled assigned a depth of zero. This ensures that all interpolated structural surfaces intersect the topographic surface in the correct location, so that, for example, the surface describing the base of the Paradise Creek Formation reaches zero depth (i.e. is exposed) at the contact between the Paradise Creek Formation and the underlying Gunpowder Creek Formation. Topographic relief in the study area is not significant on the scale of this modelling.

Grids describing the thickness of modelled units (equivalent to isopachs) were obtained by raster subtraction of each modelled unit's lower structural surface from its upper one. The thickness maps derived are interpreted to indicate the volume and shape of the accommodation space developed during deposition of the modelled unit, subject to limitations inherent in the method used to derive thickness.

The thicknesses shown in the models will be less than true pre-orogenic stratigraphic thicknesses where a portion of the unit has been removed by erosion, and will be exaggerated in areas of steep dip. Notwithstanding these restrictions, useful indications of syn-deposition basin structure may still be extracted.

8.6.2.1 Leander Quartzite

Pre-Leander Quartzite basement is inferred to occur within 1000 metres of the surface in the core of the Leichhardt River Fault Trough regional anticline in the south-eastern corner of the study area (Fig. 8.18). Evidence for the N-S-trending Leichhardt Rift hypothesised by O'Dea et al. (1997a; similar to the Leichhardt River Fault Trough of Derrick, 1982) is seen in the much thicker Leander Quartzite deposits in the eastern third of the area (Fig. 8.19), though it should be noted that a proportion of the apparent thickening observed on the western flanks of this structure is due to steeper dips in the vicinity of the Mount Gordon Fault zone. The western boundary of the Leichhardt River Fault Trough/Leichhardt Rift has hitherto been difficult to define (Sweet, 1983; O'Dea et al., 1997b), but based on Figs. 8.19 and 8.21 it should be placed between 310000E and 315000E, several kilometres west of the Mount Gordon Fault. Leander Quartzite west of the former Leichhardt Rift is generally much thinner or absent. Some of the Leander Quartzite sequence apparently missing around 7795000N and 7830000N within the Leichhardt Rift may have been removed by erosion before further deposition, possibly on rift shoulders associated with the Myally Rift event of O'Dea et al. (1997b; see below).

8.6.2.2 Leander Quartzite / Eastern Creek Volcanics contact

Fig. 8.20 shows a structure map for the base of the Eastern Creek Volcanics, which provides a clear indication of the nature and magnitude of deformation in the region. The ambiguity of this surface inherent in the magnetic modelling is reduced by the requirements of the gravity data, which enforce strong constraints on the thickness of the Eastern Creek Volcanics. Long wavelength magnetic effects also provide useful indications of the form of the basal ECV at the scale of this modelling.

Greatest uplift of the basal Eastern Creek Volcanics has occurred in the south-eastern corner of the study area (Fig. 8.20), while north-side-down displacement on the Investigator (~7810000N) and Mammoth Extended (7823000N) Faults is indicated.

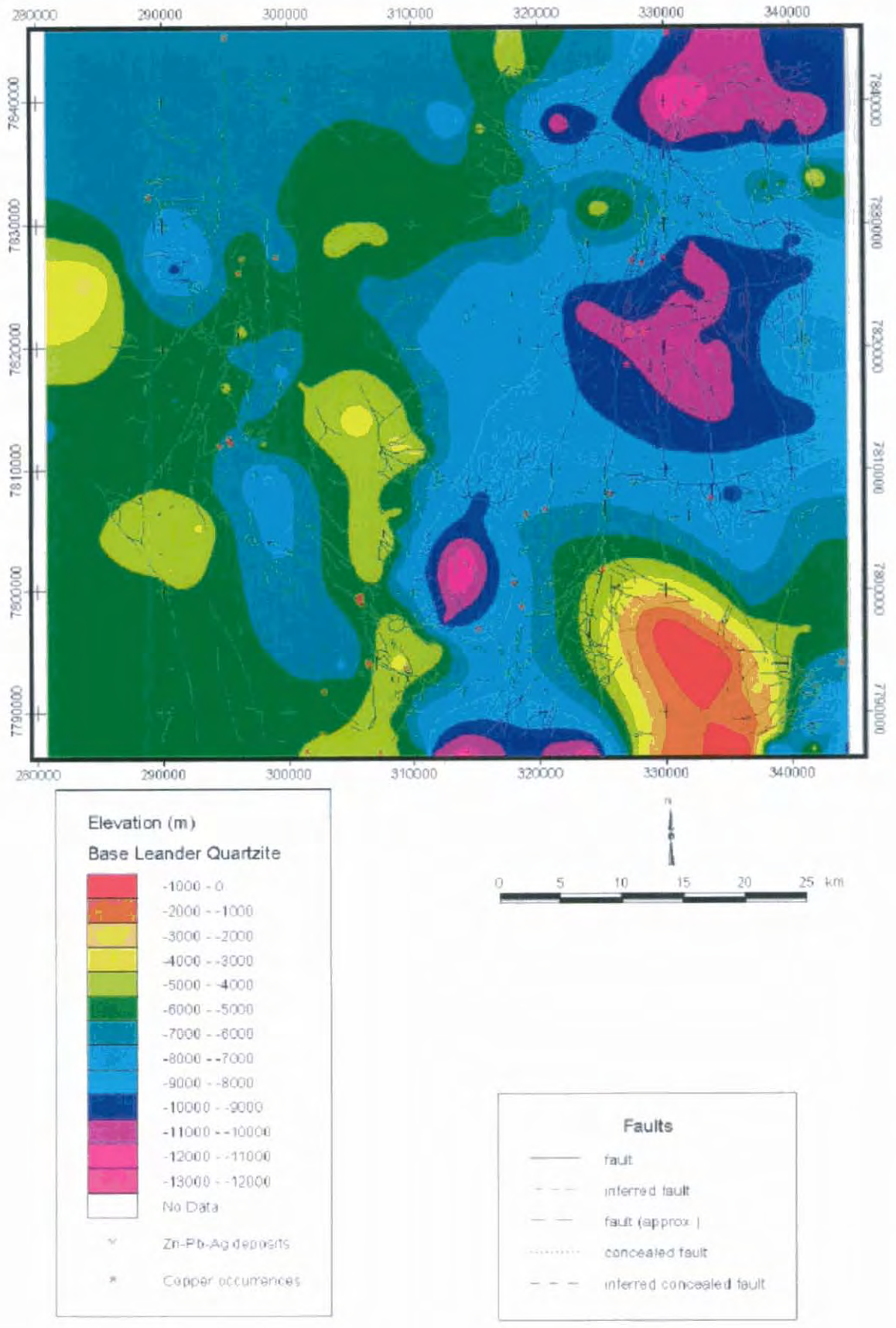

Figure 8.18 Leander Quartzite base

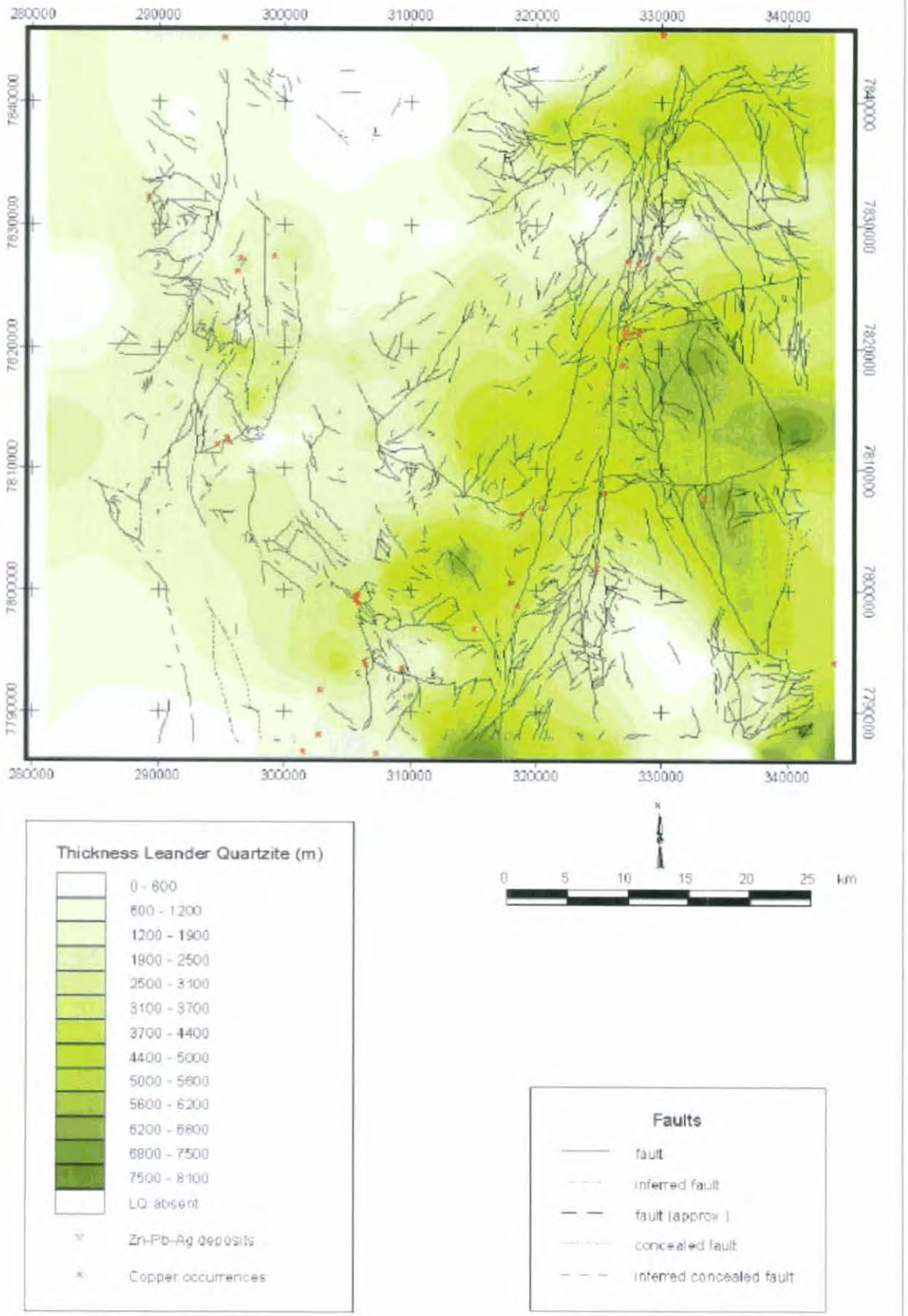

Figure 8.19 Leander Quartzite thickness

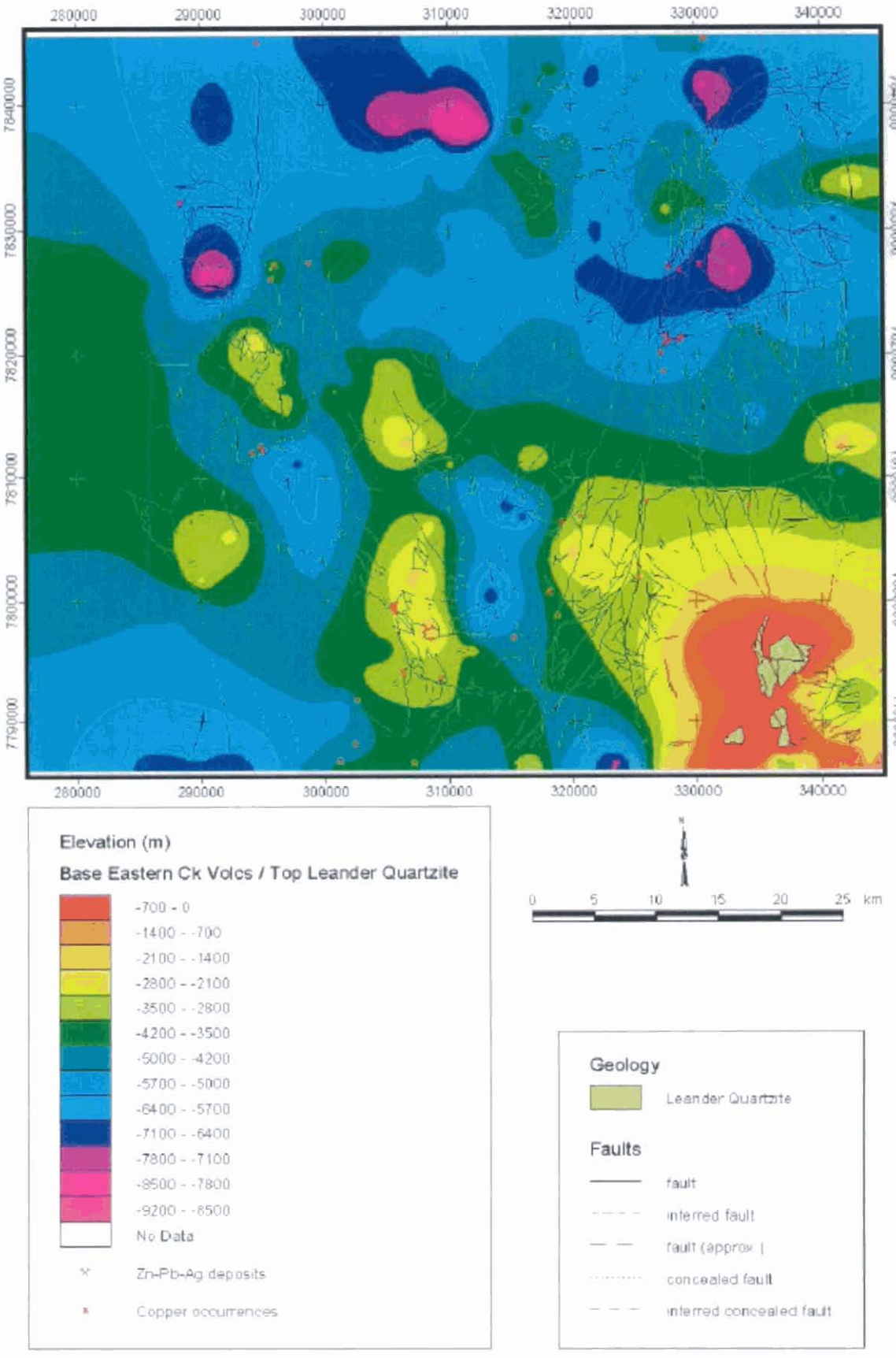

Figure 8.20 Leander Quartzite top / Eastern Creek Volcanics base

8.6.2.3 Eastern Creek Volcanics thickness

Further evidence for the existence and location of the Leichhardt Rift can be seen in Fig. 8.21, as the isopach pattern of the Eastern Creek Volcanics is similar to that of the Leander Quartzite with the largest volumes contained in a N-S-trending strip in the eastern third of the area, in particular just east of the Mammoth Cu deposit. There are also suggestions of WNW-trending depocentres extending away from the Leichhardt Rift, in particular north of Lady Loretta. These may be structures arising from the Myally Rift event, which O'Dea et al. (1997b) defined as an episode of N-S directed extension resulting in E-W striking half-grabens. The Myally Rift event spanned the stratigraphic interval from the Pickwick Metabasalt to the Whitworth Quartzite, so accumulations of Eastern Creek Volcanics in the WNW-trending structures may mostly consist of Pickwick Metabasalt. The ECV have been largely removed by erosion in the south-eastern corner of the study area.

8.6.2.4 Eastern Creek Volcanics / Myally Subgroup contact

Overall, the gravity and magnetic field interpretation is most sensitive to the contrast between the Eastern Creek Volcanics and the overlying Myally Subgroup, so Fig. 8.22 provides the best representation of present-day regional structure. The N-S grain imparted by the main E-W compression phase of the Isan Orogeny is the most prominent feature, but there are also other trends of more uncertain tectonic affinity. The NE-trending break extending between 290000E 7820000N and 320000E 78450000N is the most prominent of these, and may be related to the Mount Isa Rift Event as described by Betts et al. (1999).

8.6.2.5 Myally Subgroup – Torpedo Creek Quartzite sequence thickness

It is difficult to separate the effects of syn-depositional structures from subsequent erosion in units younger than the Myally Subgroup, since these units outcrop extensively in the study area, and are therefore eroded to some degree. In spite of, and allowing for this, some syn-depositional structures may still be inferred from Fig. 8.23. The clearest of these is a ~12 km-wide zone extending WNW north of the Redie Creek Fault from the Mount Gordon Fault at 7810000N. In much of this area the Myally Subgroup-Torpedo Creek Quartzite (MS-TCQ) sequence is thinned to the point where the entire Myally Subgroup may be absent in some places, including the zone immediately north of Lady Loretta where apparently thickened areas are due to steeply dipping Surprise Creek and Bigie Formations. The zone north of the Redie Creek Fault is thought have been elevated throughout MS-TCQ time. Conversely, to the south and north of the uplifted zone the MS-TCQ sequence attains thicknesses in excess of 2.5 km in E-W to WNW-ESE oriented sub-basins. The meridional zones of thinned material at ~306000E and ~317000E interrupting the sub-basins may represent transfer fault zones between half-graben, though some of the MS-TCQ sediments have also been removed by erosion in both these areas. The entire MS-TCQ sequence appears to lens out to the west, as the interpreted edge of the Mount Isa Basin is approached.

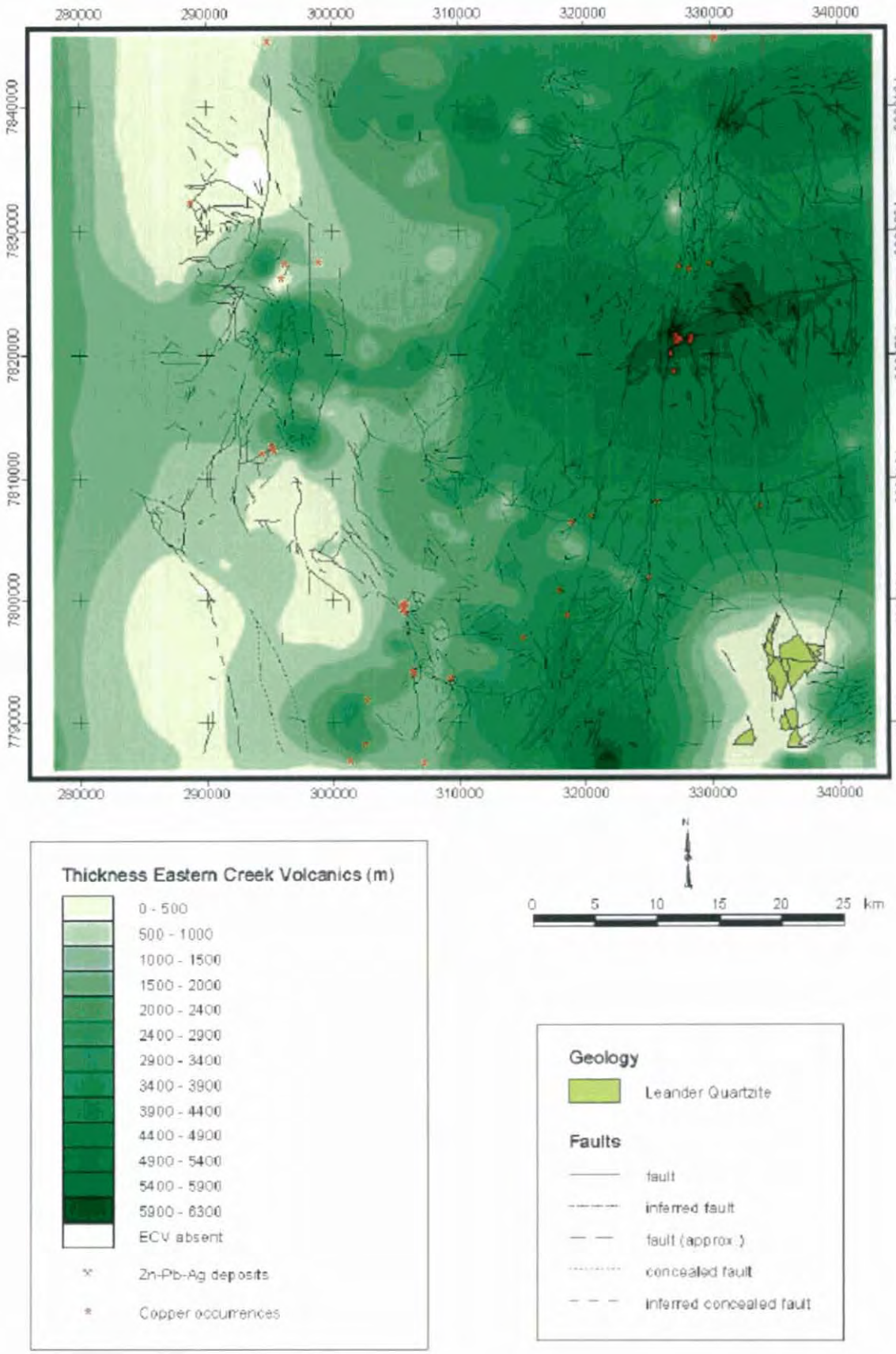

Figure 8.21 Eastern Creek Volcanics thickness

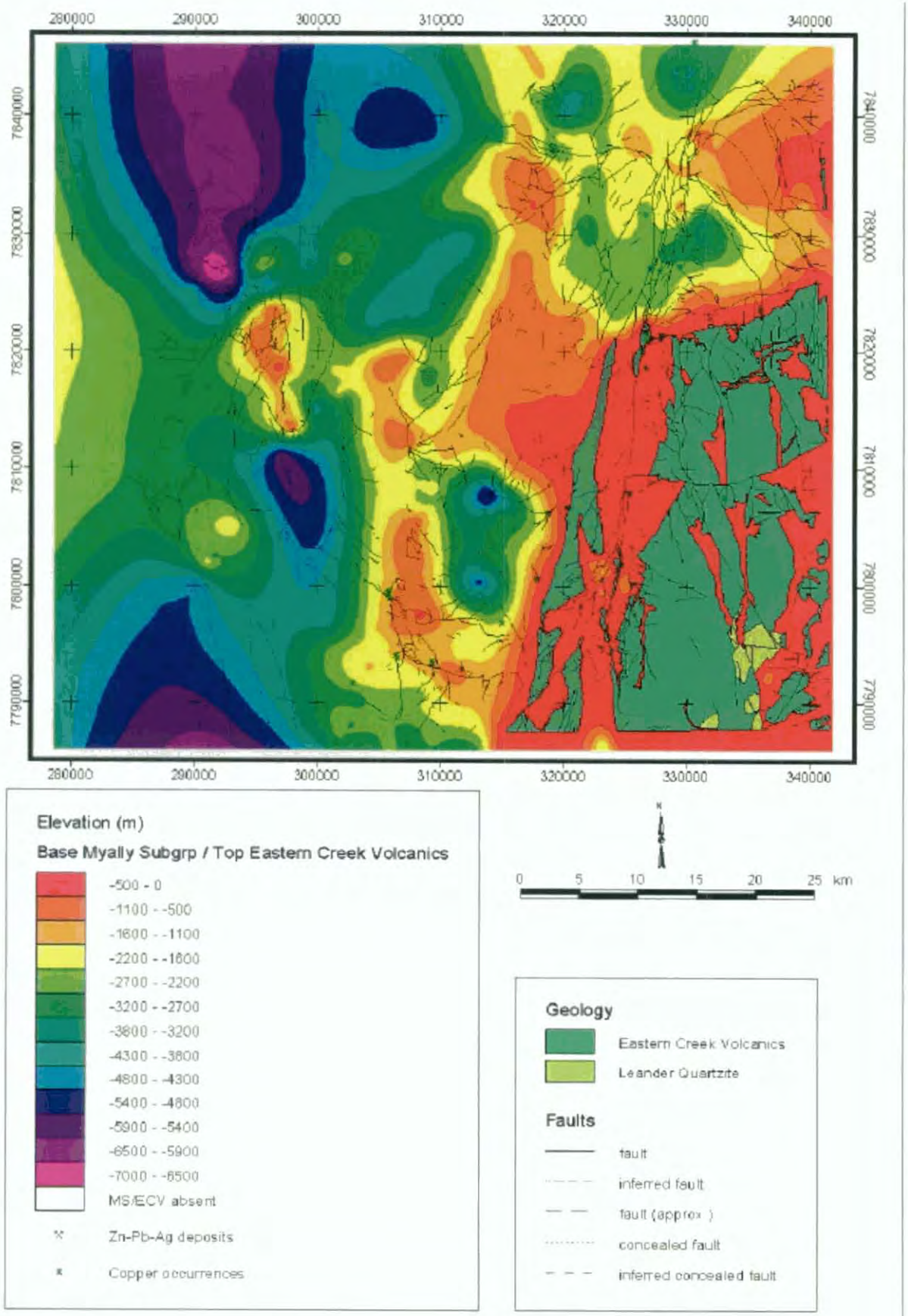

Figure 8.22 Eastern Creek Volcanics top / Myally Subgroup base

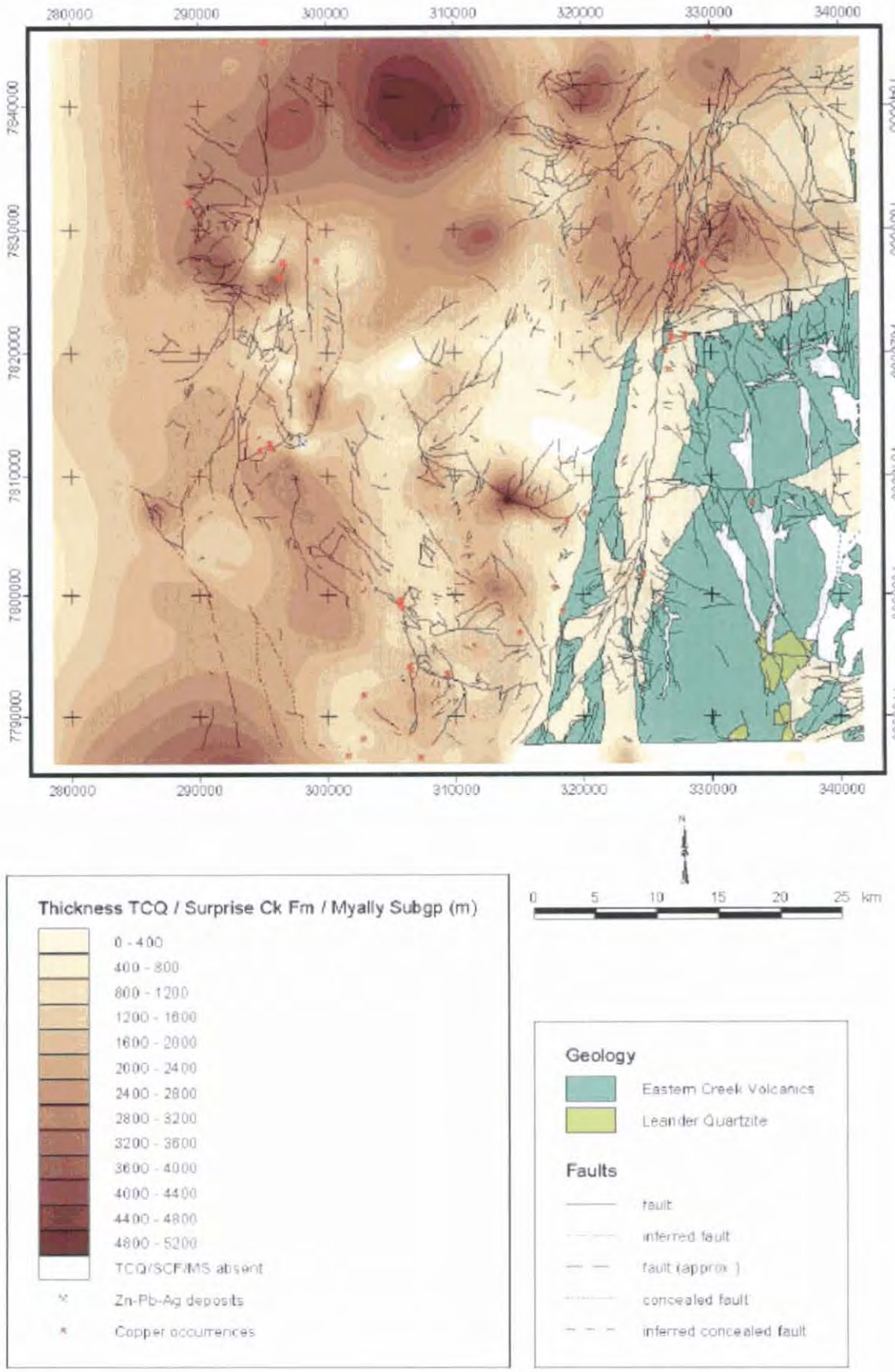

Figure 8.23 Combined Myally Subgroup/Bigie Formation/Fiery Creek Volcanics/Surprise Creek Formation/Torpedo Creek Quartzite thickness

8.6.2.6 Torpedo Creek Quartzite / Gunpowder Creek Formation contact

The depth to the base of the geophysically distinguishable McNamara Group is shown in Fig. 8.24. Relative magnitudes of vertical displacement are evident at this stratigraphic level. The Russell Creek Fault appears to diminish in magnitude southwards from about 291600E 7823000N to near zero by 290200E 7820000N. It may be that the Russell Creek Fault terminates here. The southern extension of the Russell Creek Fault as mapped by van Dijk (1991) and shown in Fig. 8.24 extending SSE from the Torpedo Creek Quartzite inlier at 287000E 7807000N may be a separate fault. It may also be that the Russell Creek Fault is a major wrench structure postdating the main E-W compressional phase of the Isan Orogeny (cf. ODea et al., 1997a) - the relationships shown in Fig. 8.24 are consistent with many kilometres of sinistral movement on the Russell Creek Fault. The Western Border and Carlton Faults attain maximum apparent vertical displacement at the point where they intersect (297600E 7811800N), near Lady Loretta.

8.6.2.7 Gunpowder Creek Formation thickness

Less weight is placed on the interpretation of Gunpowder Creek Formation (GCF) thickness (Fig. 8.25) in terms of basin development than that of older units because of the extent of the area affected by recent removal of material through erosion, the overall thin nature of the unit in comparison to the other basin entities modelled, and fairly low density contrast (0.05 t/m^3 or less) with the underlying MS-TCQ sequence. However, there are some indications that the uplift of the WNW-trending area north of the Redie Creek Fault continued into GCF time. Much of the Paradise Creek Formation and younger units (i.e. where a complete section of GCF is present) outcropping in this area cover only a thin layer of GCF; less than 330 m. Sections up to ~1500 m thick are preserved in equivalent shallowly-dipping areas south of the Redie Creek Fault. The crescent-shaped trench of apparently thickened GCF (around 29700E 7790000N) is mainly an artefact caused by a narrow inlier exposing the Gunpowder Creek Formation/Paradise Creek Formation contact, but may also be partly due to steep dips associated with the nearby faults. An ENE- to NE-trending zone of thicker GCF, in the northwestern corner of Fig. 8.25, is one of the few indications of half-graben caused by a NW-SE extensional event (Mount Isa Rift Event of ODea et al., 1997a) documented by Betts et al. (1999) north of the study area. Other rapid thickness variations seen in Fig. 8.25 may be related to active extensional structures (pull-apart basins, pop-ups) associated with the Mount Isa Rift event.

8.6.2.8 Gunpowder Creek Formation / Paradise Creek Formation contact

Differences in structural elevation from south to north across the Redie Creek Fault are accentuated in Fig. 8.26, where the Paradise Creek Formation/Gunpowder Creek Formation contact is displaced by as much as 2 km. This map serves to emphasise the importance of structures other than the meridional anticlines and synclines caused by the main E-W compression of the Isan Orogeny, though whether these are due to other post-depositional or syn-depositional events is not apparent from Fig. 8.26.

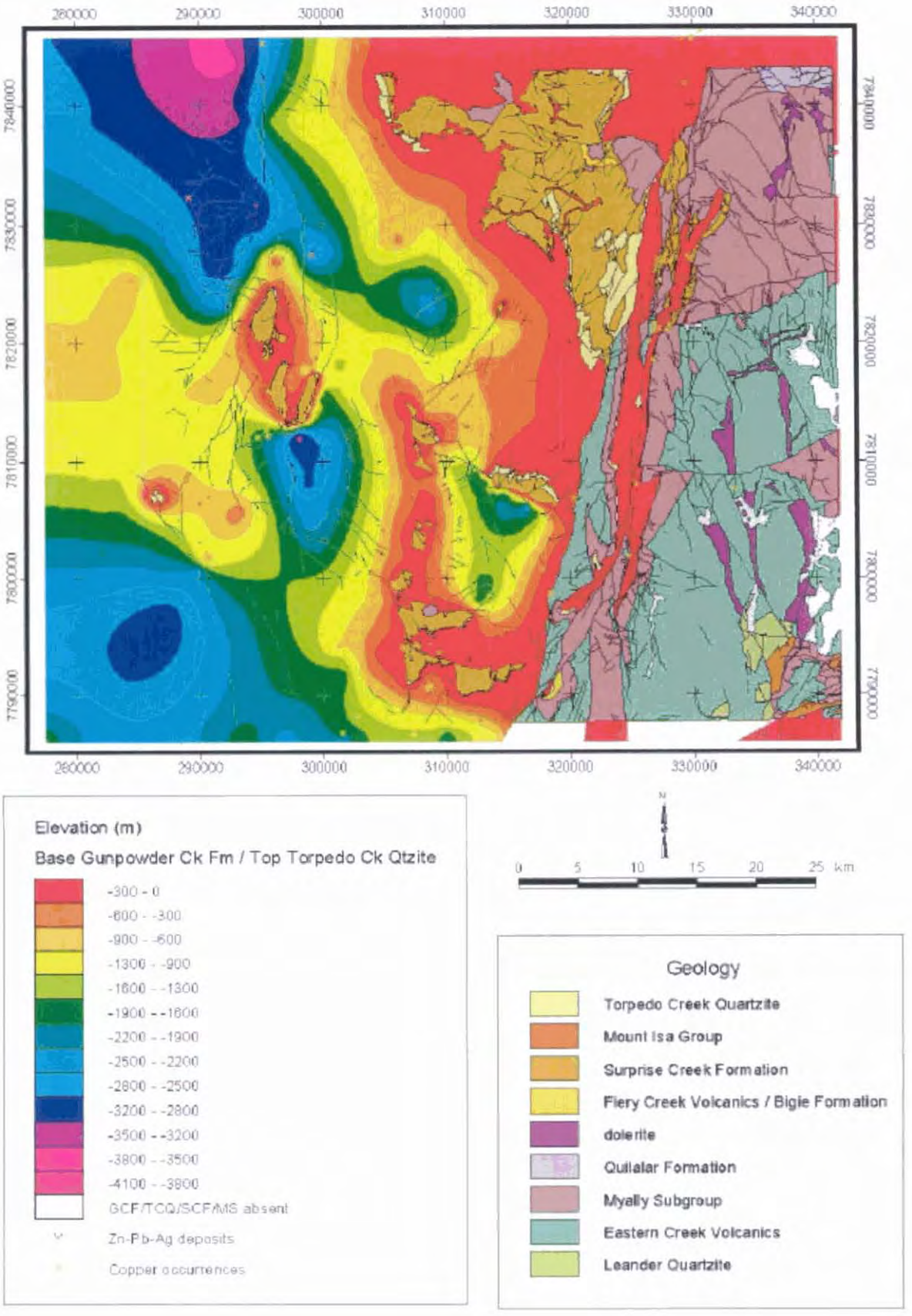

Figure 8.24 Torpedo Creek Quartzite top / Gunpowder Creek Formation base

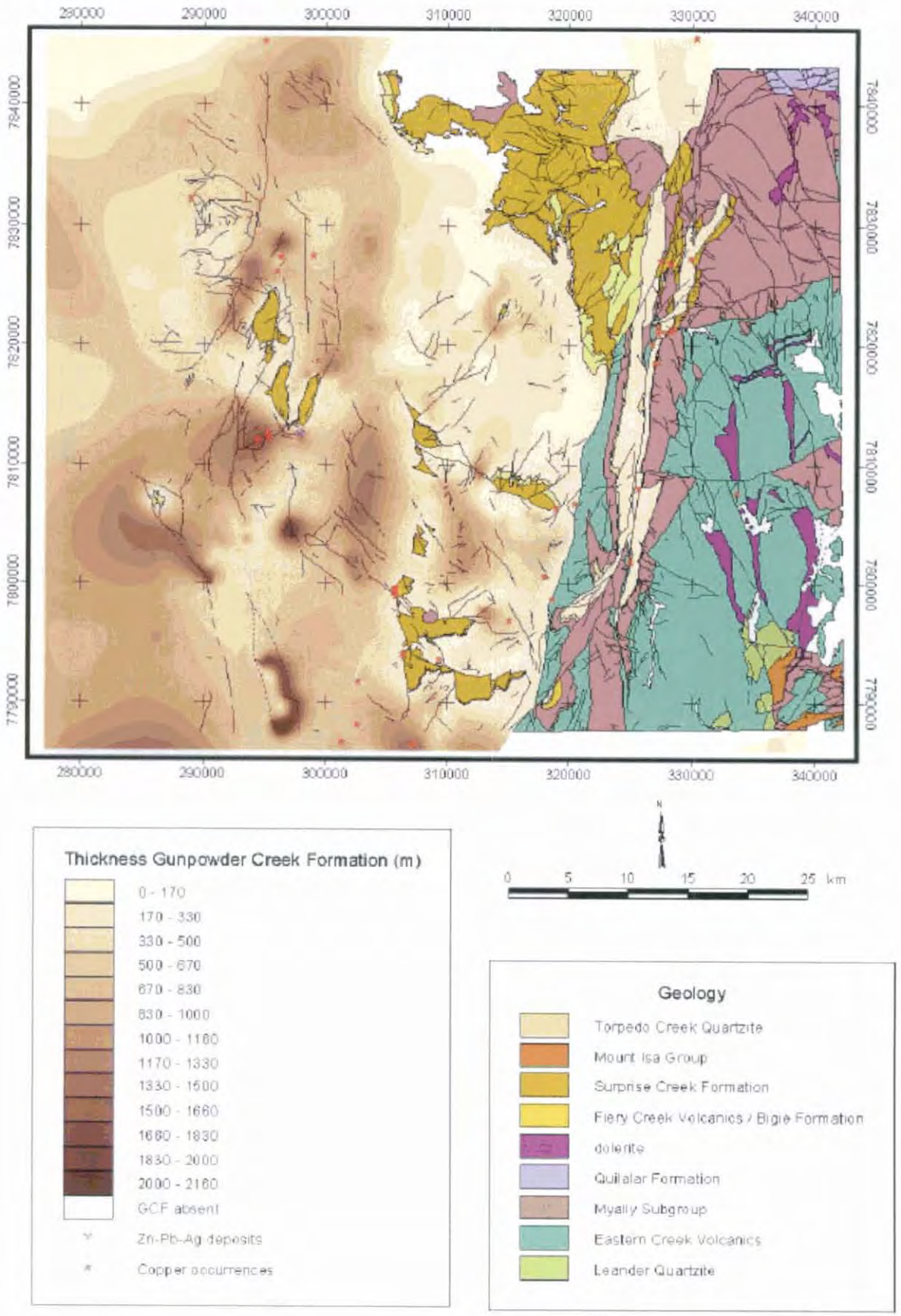

Figure 8.25 Gunpowder Creek Formation thickness

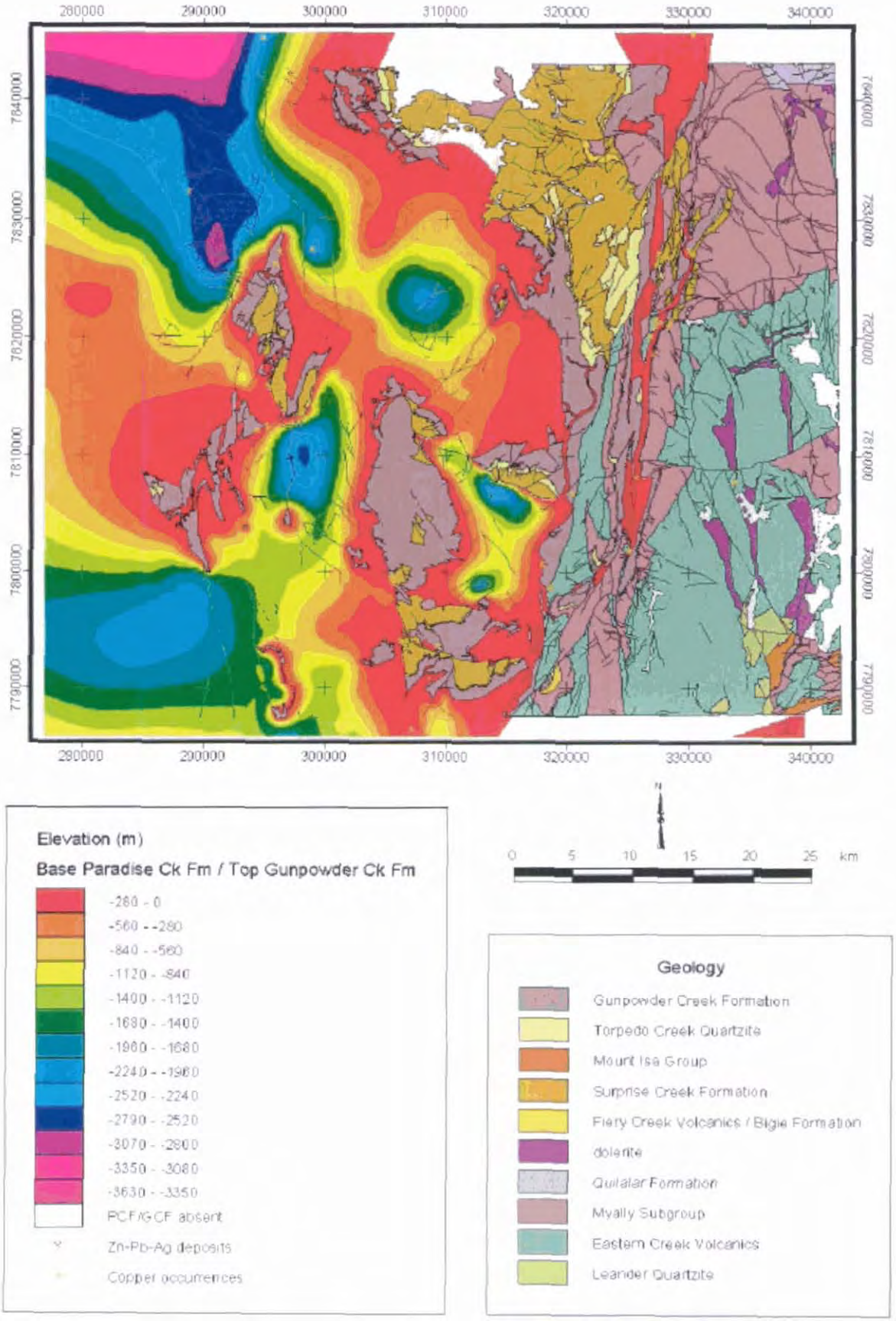

Figure 8.26 Gunpowder Creek Formation top / Paradise Creek Formation base

8.6.2.9 Paradise Creek Formation thickness

The proximity of the western edge of the Mount Isa Basin may be inferred from the thinning of the Paradise Creek Formation (PCF) westward in Fig. 8.27, though there are indications from increased PCF thickness that the basin extends northwestwards from that corner of the study area. The comparative scarcity of complete PCF sections in the central portion of the Paradise Valley region makes it difficult to infer depositional patterns for this period of basin history. It is nonetheless clear that the areas immediately south of Lady Loretta and the Redie Creek Fault remained as substantial depocentres during PCF time. Major sub-basin development in the north-western corner of the region is also inferred to have occurred during PCF time.

The differences in accommodation space created north and south of the Redie Creek Fault noted for older units are less pronounced in the PCF. Over 1000 m of Paradise Creek Formation are interpreted to be present beneath extensive nearly flat-lying Esperanza Formation outcrop just north of the centre of the study area (Fig. 8.27). This reduced differentiation across basin structures is consistent with the PCF being deposited in a period of regional sag following the Mount Isa Rift event (ODea et al., 1997a; 1997b).

8.6.2.10 Paradise Creek Formation top

Fig. 8.28 shows that the Paradise Creek Formation is interpreted to underlie much of the Mesozoic and Cainozoic cover in the central portion of the Paradise Valley between the Western Border and Mount Gordon Faults. A WNW-trending zone of uplift over 15 km wide is inferred beneath Cambrian cover west of Lady Loretta, around 282000E 7817000N.

8.6.2.11 Lady Loretta Formation base

The base of the Lady Loretta Formation (LLF) closely corresponds to the trend defined by the top of the PCF (Fig. 8.29). The magnitude of displacement on the Russell Creek Fault and its putative southern extension (van Dijk, 1991) is again emphasised, while the Western Border Fault appears to have experienced little vertical movement south of Lady Loretta (297500E 7811000N), as evidenced by the continuity of the basal LLF surface across it.

8.6.2.12 Lady Loretta Formation thickness

The thickness of the Lady Loretta Formation (Fig. 8.30) appears to increase from south to north, suggesting a basin deepening in this direction during LLF time. The host sequence of the Lady Loretta Zn-Pb deposit is included in this trend, as the thickness in this area exceeds that in the southwestern corner of the study area, in spite of exposure and consequent sediment removal. The northward-deepening trend is interrupted by the presumed pre-Cambrian uplift and erosion west of Lady Loretta referred to in sub-sections 8.6.2.10 and 8.6.2.11 above.

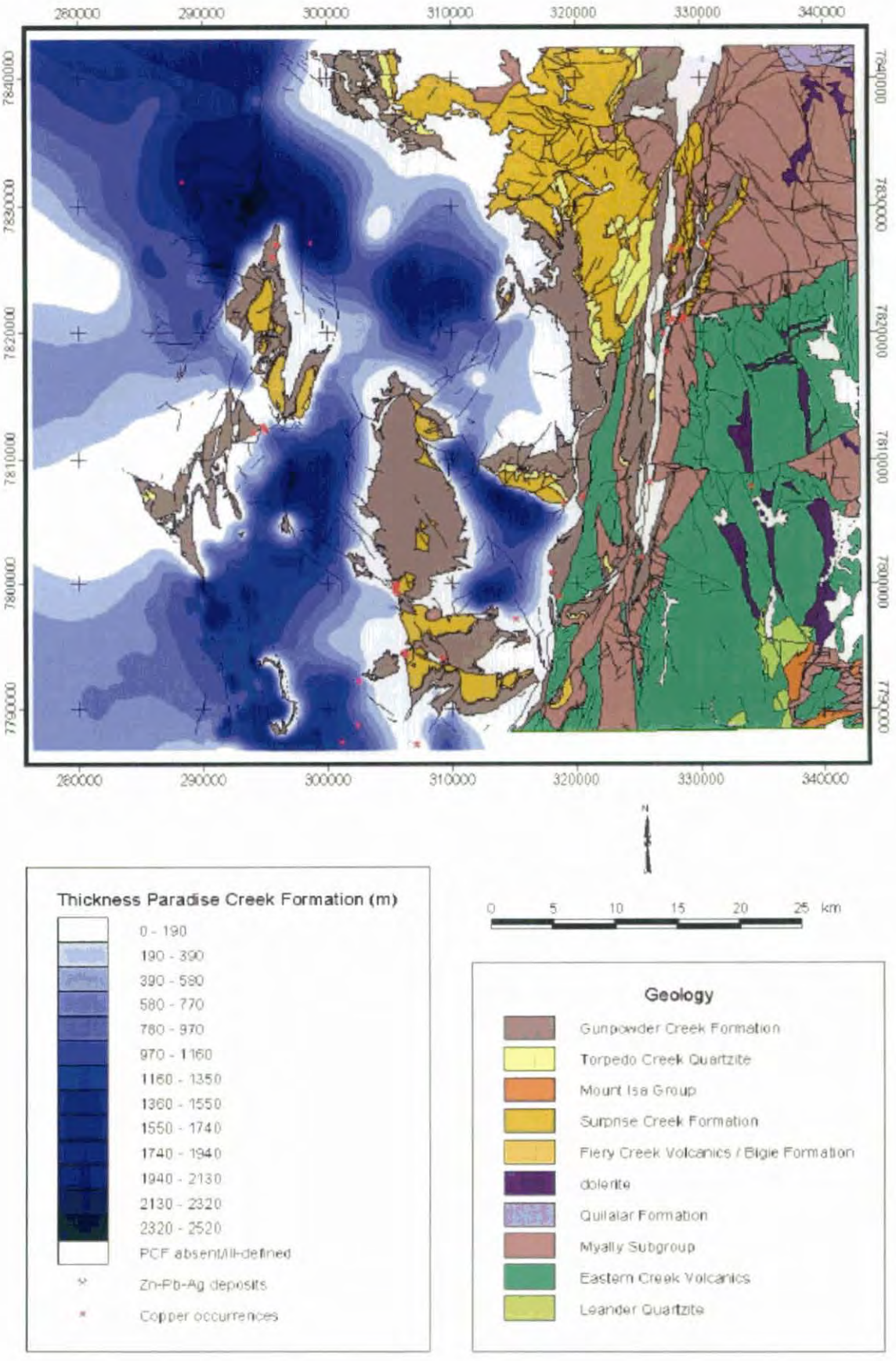

Figure 8.27 Paradise Creek Formation thickness

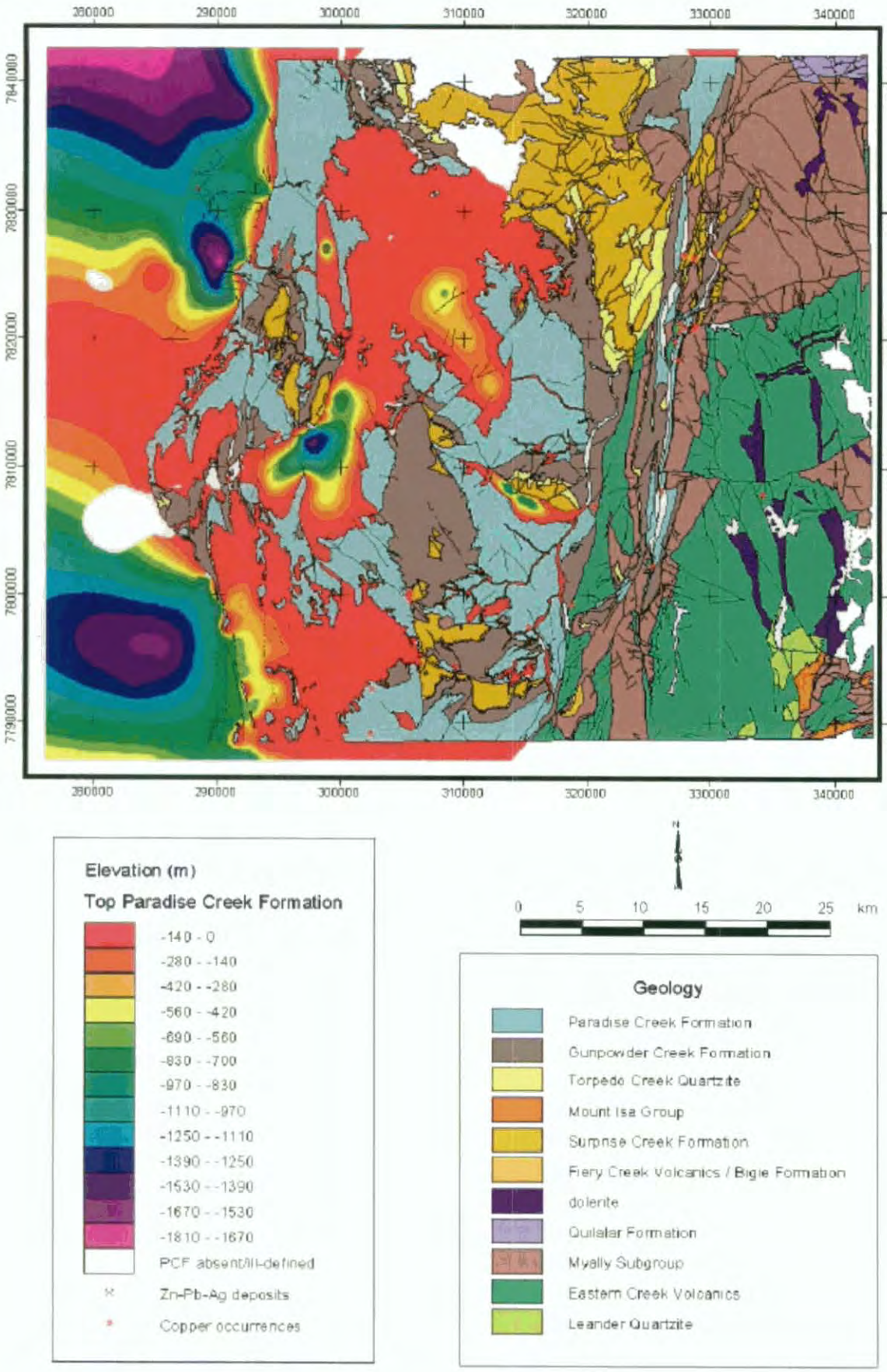

Figure 8.28 Paradise Creek Formation top

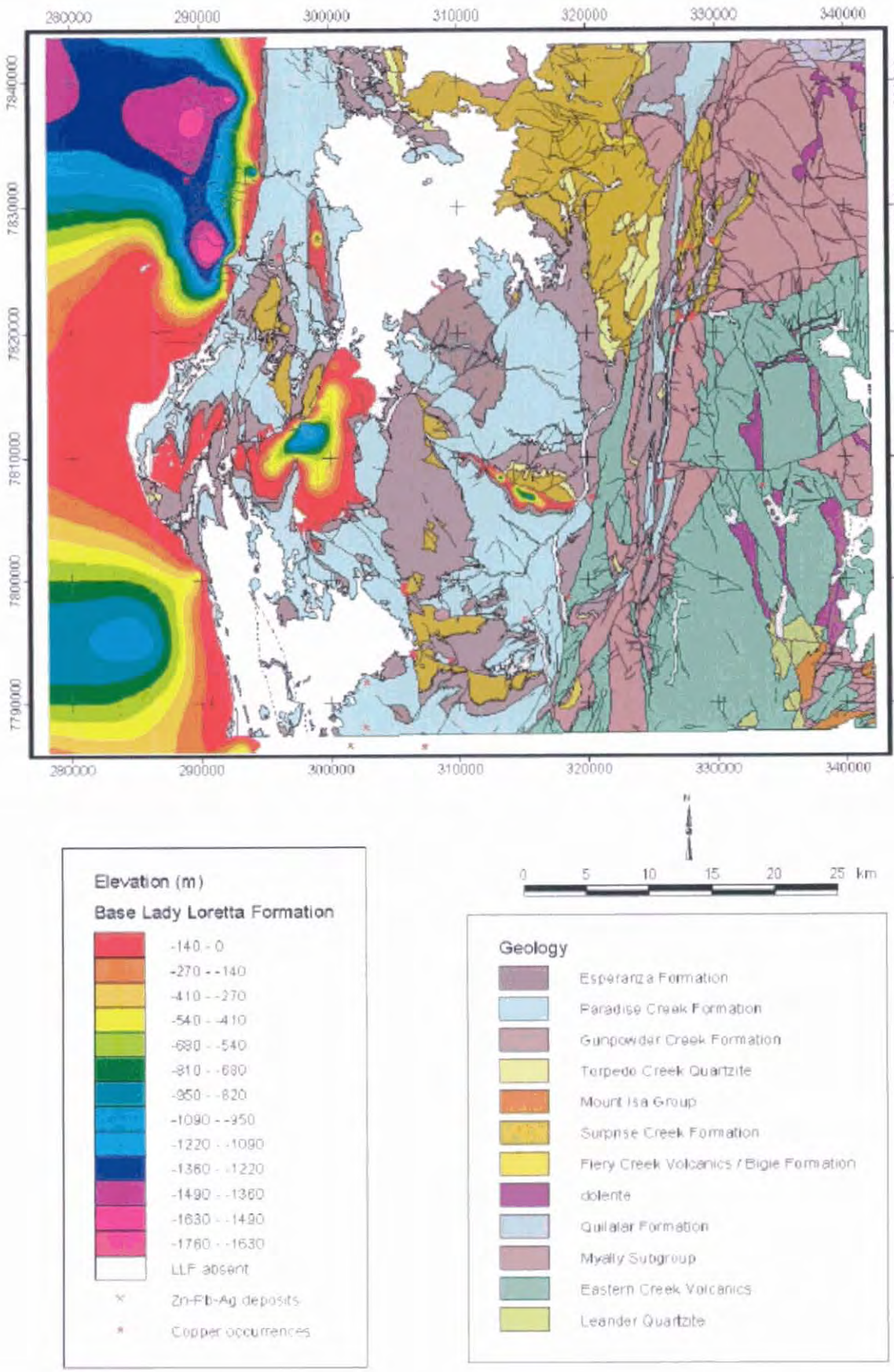

Figure 8.29 Lady Loretta Formation base

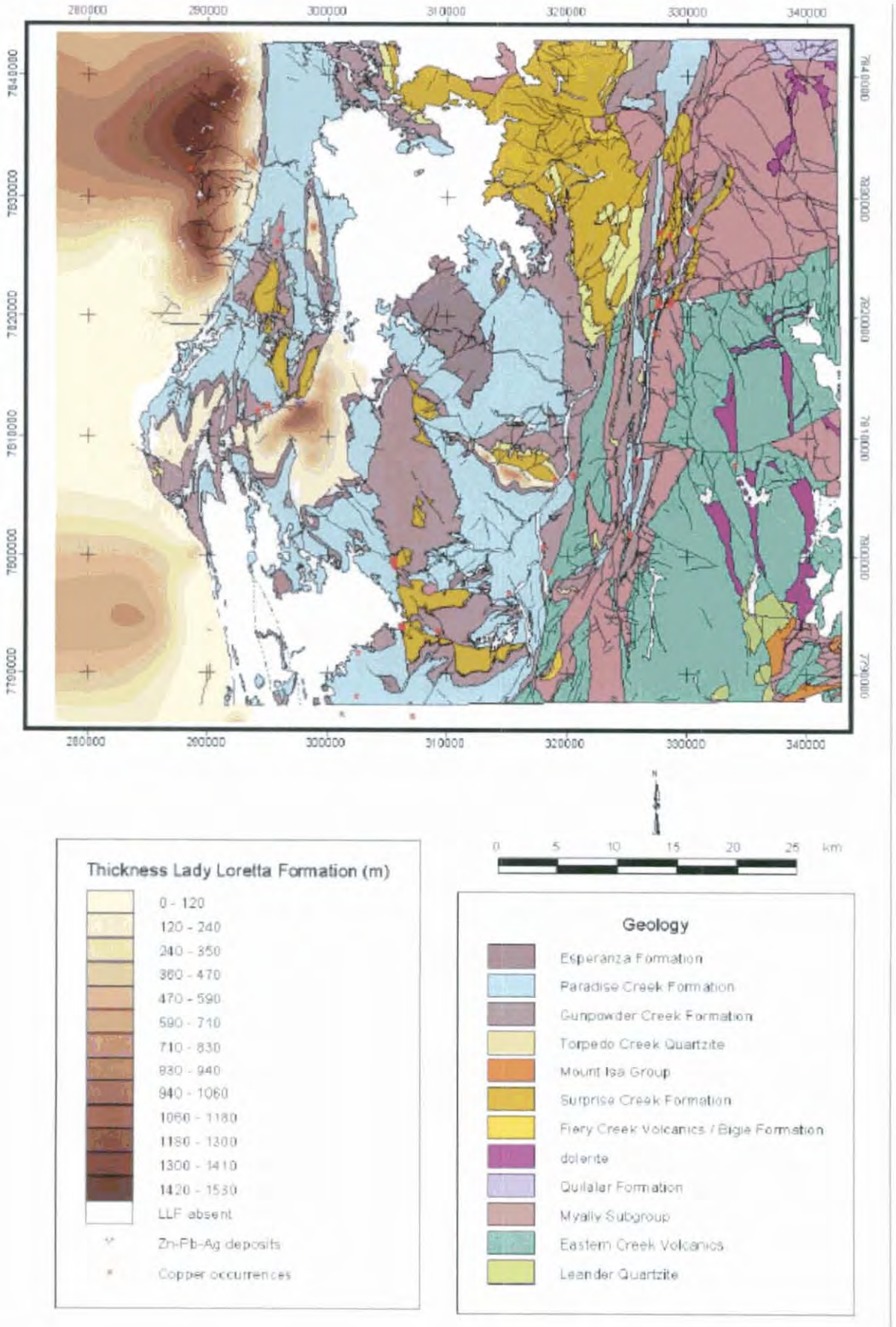

Figure 8.30 Lady Loretta Formation thickness

8.6.2.13 Lady Loretta Formation top

Fig. 8.31 mainly serves to depict the extent of Lady Loretta Formation beneath Phanerozoic cover. It is not thought to range far east of the Western Border Fault (roughly 7 km north and south of Lady Loretta), but does occur extensively beneath Cambrian cover of the Undilla basin to the west. Depths of the upper LLF surface exceeding about 100 m (the maximum likely thickness of Cambrian sediments in the study area) denote areas where the Shady Bore Quartzite and Riversleigh Siltstone overlie the Lady Loretta Formation.

The impression given in Fig. 8.31 and other structural surfaces described above is that the Mount Isa Basin sequence dips gradually from east to west, with exposed lower Haslingden Group stratigraphy in the east giving way to upper McNamara Group disappearing beneath Cambrian cover in the west. This impression is reinforced by the presence of presumed South Nicholson Group equivalents in the Morstone No.1 drillhole 30 km west of the study area.

8.7 Summary

No units older than the Leander Quartzite were modelled explicitly, although they are have been described elsewhere in the Mount Isa Basin (Bottletree Formation, Argylla Formation, Leichhardt Volcanics; Blake, 1987). Large volumes of these or other predominantly felsic units could exist at depth in the Paradise Valley region. In fact it is quite likely that these or similar units, metamorphosed to varying grades, form a substantial proportion of the large volumes of undifferentiated, non-magnetic 'basement' at the reference density of 2.74 t/m ^{3} modelled in many profiles. All that can be said is that at most only a small proportion of these possess the distinctive moderate to high magnetic susceptibility and density which characterise the substantial accumulations of felsic magmatic material hypothesised to occur further north in the Carpentaria Zinc Belt (Leaman, 1996; 1998b).

The unit which most controls both gravity and magnetic response in the forward models in the Eastern Creek Volcanics. Extensive outcrops of the ECV east of the Mount Gordon Fault Zone place tight constraints on interpretation, and generally confirm the petrophysical properties assigned from Table 5.12. A thickness of in excess of 8 km of lower Haslingden Group (Leander Quartzite and Eastern Creek Volcanics combined) has been deposited in much of the meridional Leichhardt Rift (O'Dea et al., 1997a). The western boundary of the Leichhardt Rift may be redefined to around 315000E, west of the Leichhardt River Fault Trough as originally defined by Derrick (1982), as substantial thicknesses of lower Haslingden Group extend west of the Mount Gordon Fault. The Mount Gordon Fault dips steeply west, and as such is generally a normal fault in the Paradise Valley area (cf. Bell, 1991), though the main sense of movement on it may have been lateral for much of its history (Hutton and Wilson, 1985). The Mount Gordon Fault may have acted as an accommodation zone within the Leichhardt Rift, foreshadowing its role as a major wrench fault during the latter stages of the Isan Orogeny. Its activity over a substantial period during basin development is likely to have been a significant control on migration of mineralising fluids which resulted in the numerous base metal accumulations such as the Mammoth and Mount Oxide Cu deposits which occur in close spatial association with the fault zone.

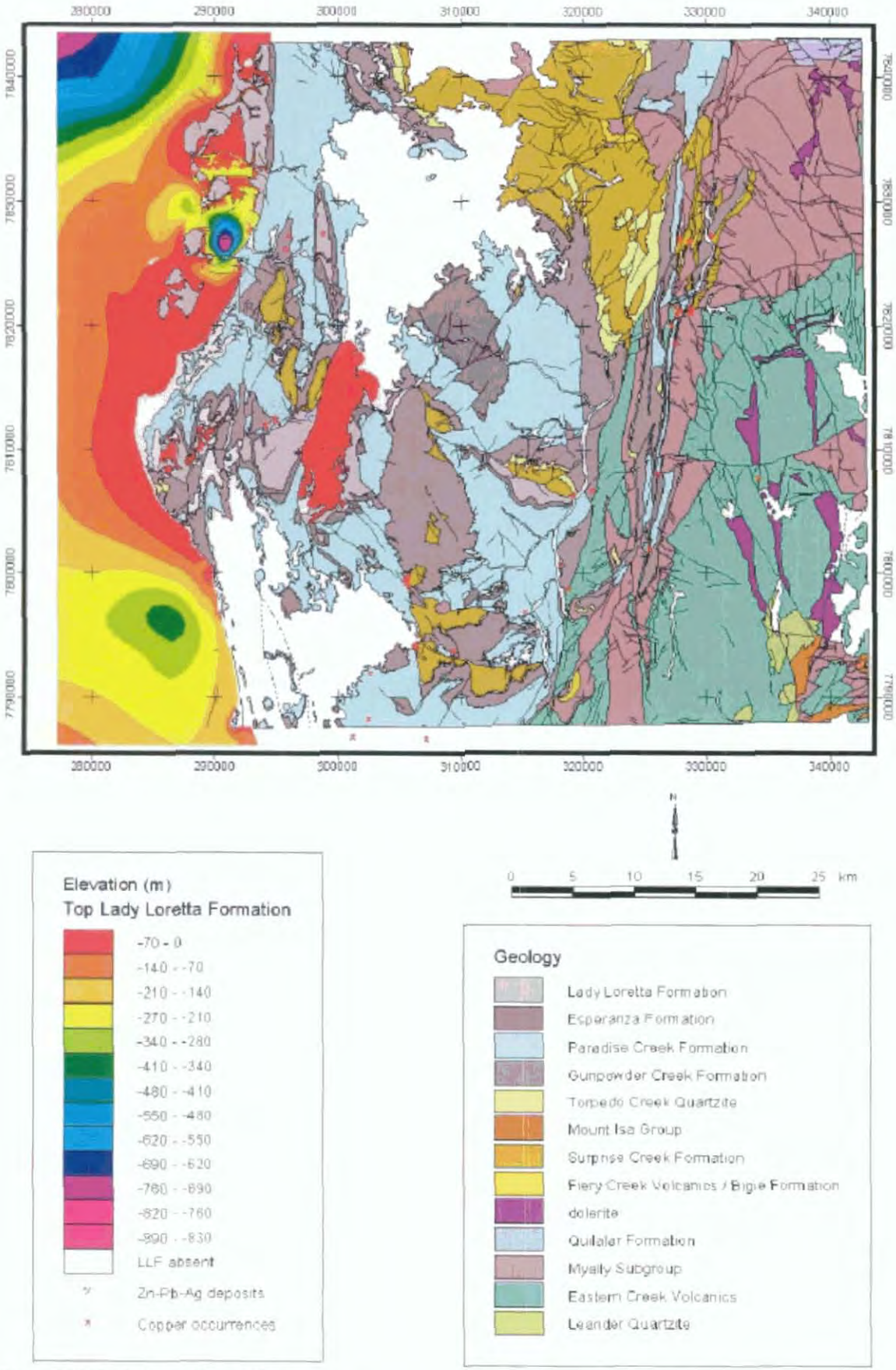

Figure 8.31 Lady Loretta Formation top

Within the Leichhardt Rift, the lower Haslingden Group is affected by a number of E-W-oriented faults. In the northern half of the study area these are south-dipping 'domino' faults separating a series of north-

dipping half-grabens. These may have formed during N-S extension of the Myally Rift event, postulated by O'Dea et al. (1997b) to have been active during deposition of the upper Haslingden Group sequence from the Pickwick Metabasalt to the Whitworth Quartzite. To the south, E-W-oriented faults in the Leichhardt Rift including the Investigator Fault are interpreted to be north-dipping reverse faults or thrusts, though this conclusion is somewhat tentative due to the complicating effects of various magnetite-creating and magnetite-destroying alteration processes concentrated near the faults. The inferred movement on these faults is consistent with the D_1 south-directed thrusting suggested by Bell (1991), but the fault displacements appear to be much less than the hundreds of kilometres hypothesised (Bell, 1991).

Basin structures in the Paradise Valley region have been strongly overprinted by Isan Orogeny deformation, particularly by east-west compression. This has served to obscure earlier structural geometries that may carry information on basin development. However, some areas exhibit less deformation, including the area between the Mount Gordon Fault Zone and Lady Loretta. The most significant structures in this zone are WNW-trending features similar in orientation to the Redie Creek Fault. This is in contrast to sub-N-S to NE-SW trends developed in higher strain zones to the east and west. The WNW structures are considered to have developed concurrently with the basin, and are likely to have influenced sedimentation patterns. The earliest evidence of the influence of WNW structures is seen in the preserved thickness of Eastern Creek Volcanics, which changes abruptly across a line drawn along the Redie Creek Fault WNW through Lady Loretta. The thickness of the volcanic sequence is greater to the north of this line. The relative sense of displacement on this structure appears to have reversed shortly after ECV deposition, as very little of the Myally Subgroup is preserved in a zone over 10 km wide to the north. The effect of this WNW structure is less pronounced in overlying units, but the Bigie Formation, Surprise Creek Formation, Torpedo Creek Quartzite and Gunpowder Creek Formation all appear to be thicker in a zone ~10 km wide south of the fault than in the area immediately to the north. This WNW-trending accumulation approximately corresponds to the eastern portion of the 'Paradise Graben' of Dunnet (1976). The Lady Loretta Zn-Pb deposit is situated near the northwestern edge of this inferred depocentre or sub-basin.

Only the Pickwick Metabasalt-Whitworth Quartzite portion of the basin fill is consistent with the orientation and timing of the Myally Rift Event proposed by O'Dea et al. (1997b). A sub E-W oriented pattern of depocentres alternating with uplifts and connected by N-S oriented transfer fault zones is here interpreted to have persisted from late ECV to as late as early Paradise Creek Formation time. There is little evidence of NW-SE extension resulting in SW-NE oriented structures during Fiery Creek Volcanics/Bigie Formation to Gunpowder Creek Formation time (Mount Isa Rift Event; O'Dea et al., 1997b; Betts et al., 1999), except possibly in the north-western corner of the study area where a larger thickness of Gunpowder Creek Formation is inferred. This does not constitute decisive evidence against the Mount Isa Rift Event having affected the study area, as the largely siliciclastic units deposited during it are difficult to distinguish with gravity and magnetic methods.

The Paradise Creek Formation to Lady Loretta Formation sections of the Mount Isa Basin are interpreted to have been deposited more evenly across the study area than older units. This may be related to a period of regional sag following the earlier rift events. The thickness variations that do exist indicate northward deepening of the Mount Isa Basin during PCF-LLF time.

The Mount Isa Basin does not extend in any substantive fashion far beyond the western edge of the study area, though it may do so to the northwest. The basin may have been overtopped, or subsequent depocentres formed in a foreland basin as the Isan Orogeny progressed. This would account for the presence of South Nicholson Group (which unconformably overlies the McNamara Group elsewhere) equivalents beneath the Cambrian Undilla basin. While the nature of the western boundary of the Mount Isa Basin is beyond the scope of this thesis, westward extensions of some of the E-W models across major negative gravity and positive magnetic anomalies suggested the existence of a major tectonic break between the Mount Isa Basin and an adjoining terrane which may have affinities to the Tennant Creek Inlier or the 'Aljawarra Craton' of Tucker et al. (1979).

There is a clear association between Cu mineralisation and major regional faults. There is also some suggestion of a preferential distribution of Cu occurrences near major early structures that controlled ECV deposition. The Lady Loretta Zn-Pb deposit lies close to a major structure that actively controlled sedimentation during a long period of earlier sub-basin development. It is also proximal to an accumulation of ECV, of which a significant portion has experienced alteration resulting in base metal depletion. These two factors may have important implications for exploration for similar mineralisation in the region.

9. Summary and Conclusions

9.1 Overview

The three-dimensional basin evolution of two regions within the Carpentaria Zinc Belt metallogenic province has been examined using geophysical and GIS methods. A GIS was constructed for a region in the McArthur Basin encompassing the HYC Zn-Pb deposit, incorporating available geophysical interpretations and detailed geological and geochemical data. The GIS was designed for the specific purpose of extracting and visualising 3D spatial and temporal information. Analysis of the GIS data has led to an improved understanding of basin architecture and metallogenic constraints in the region of HYC.

Lady Loretta, a smaller Zn-Pb deposit in the Mount Isa Basin, was the focus of a complementary qualitative and quantitative regional geophysical interpretation. An extensive examination of the petrophysical properties of regional basin units and base metal-bearing mineralised systems was used to provide additional information to help constrain 2D potential field modelling. A 2.5D interpretation of all important basin units in the Lady Loretta area was completed to highlight basin architecture.

9.2 Summary of results

9.2.1 McArthur Basin GIS analysis

A technique was developed for semi-automatic generation of coverages representing 'predicted' structural elevation for any given stratigraphic unit, based purely on outcrop geology and measured stratigraphic thicknesses. The geological data were thus used to generate a baseline prediction for (present) basin geometry, by making the simplifying assumption of 'layer cake' stratigraphy. The resulting maps provide a quantitative visualisation of basin structure not obvious on casual inspection. They particularly emphasise the magnitudes of vertical displacements across faults.

A method for the automatic detection of unconformities in geological maps was developed, which utilised the GIS topological data structure and a look-up table based on the stratigraphic column. This method was extended to calculate the 'magnitude' or thickness of missing sedimentary section represented by each unconformity. The resulting unconformity map clearly indicates areas of uplift or low subsidence during basin development; where stratigraphic units are absent due to erosion or lack of deposition, or both. The unconformity magnitude indicates the extent and persistence of locally elevated regions within the basin, while the relative age of the missing units gives an indication of the time during which these features were present.

Direct indications of 3D structure were obtained by incorporation of geophysical interpretations based on regional gravity and magnetic data. Grid surfaces defining major basin components in 2.5D were created in the GIS from structure contour and isopach maps, which were in turn derived from intensive 2D

potential field forward modelling (Leaman, 1998). These grids show the 3D structure of basin inferred to be capable of sourcing or transporting base metals, and enable inference and visualisation of bounding faults and other possible fluid conduit structures concealed beneath younger rocks. Volumes of major basin components were calculated from the grids and combined with reasonable estimates of the bulk average Zn and Pb concentration in order to assess the likely sources of metals to the HYC deposit. An unreasonably large proportion of the McArthur Group volume would have been required to source sufficient base metal to form HYC. A substantial base metal contribution was probably required from older, richer and/or more voluminous basin units.

A geophysically-derived model for the thickness of the McArthur Group was subtracted from a model of 'predicted McArthur Group thickness' derived purely from outcrop geology to produce a map depicting areas of 'anomalously high' or 'anomalously low' thickness. These zones may be directly interpreted as representing sub-basins and relatively elevated areas present during McArthur Group time. This basin geometry is inferred to have exerted a direct influence on basin fluid flow at the time the HYC ore deposit was formed.

9.2.2 Regional petrophysics

Regional petrophysical data were acquired from a comprehensive suite of samples collected from the Mount Isa Basin in the Paradise Valley area. There are two distinct density populations present in the pre-Haslingden Group, predominantly felsic meta-igneous rocks of the central and western Mount Isa Basin. Density is strongly related to these rocks' position on the felsic-mafic compositional continuum as indicated by corresponding geochemical data. The Eastern Creek Volcanics are generally dense and highly magnetic, but alteration spatially associated with base metal mineralisation has resulted in significant reductions in both density and magnetic susceptibility.

Bulk density, sonic velocity and resistivity of the Proterozoic sedimentary units investigated, particularly the lower McNamara Group, are strongly dependent on the relative proportions of carbonate and siliciclastic material present. Dolostones have high density, velocity and resistivity, while a predominance of siliciclastic material results in low values for these parameters. Porosity also exerts some control on resistivity in McNamara Group rocks, and may be of primary importance in the interpretation of electrical and electromagnetic surveys in areas of both low metamorphic grade and saline groundwater. The reliability of the estimated bulk values derived for each stratigraphic unit is strongly dependent on the assumption that the samples measured are representative of the unit regionally. Systematic compositional variations within formations such the gradational regional change from argillaceous (south) to dolomitic (north) within the Lady Loretta and Gunpowder Creek Formations mean that the bulk property estimations derived should be applied with caution outside the study area. Differences in metamorphic grade are also likely to affect bulk formation physical properties across the region.

The McNamara Group in the Paradise Valley region is compositionally less heterogeneous than the McArthur Group, and this is reflected in a smaller range of petrophysical properties. The physical property distribution in the McNamara Group north of the study area, around Kamarga Dome where at

least the Lady Loretta Formation is more dolomitic than its equivalent to the south, may more closely resemble that sampled in the McArthur Group.

There is a definite positive relationship between magnetic susceptibility and geochemical indices incorporating Fe and Mn, presumably due to weakly ferromagnetic and paramagnetic Fe- and Mn-bearing minerals. Positive correlation between the 'SEDEX alteration index' (Large and McGoldrick, 1998) and magnetic susceptibility indicates magnetic susceptibility logging as a potential tool for rapid reconnaissance detection of alteration spatially associated with stratiform Zn-Pb-Ag deposits in dolomitic sedimentary basins.

9.2.3 Base metal deposit petrophysics

The high grade of the Lady Loretta ore deposit makes it particularly amenable to geophysical detection. Its ore is generally the densest of any of the deposits examined. Lady Loretta ore, particularly the galena-rich portions, also has a high density contrast with the enclosing highly pyritic strata, which are in turn denser than the surrounding sediments. The ore/host density distinction is not as pronounced in other Carpentaria Zinc Belt Zn-Pb deposits as at Lady Loretta, presumably due to their lower grades.

The presence of large quantities of iron sulphides associated with all deposits (Century being a major exception) significantly improves their physical property contrast with their respective host rocks. This is particularly the case at Hilton, George Fisher and Mount Isa, where monoclinic pyrrhotite causes significant magnetic anomalies in conjunction with the ore (e.g. Leaman, 1991a,b). The presence of monoclinic pyrrhotite is apparently the result of higher metamorphic grades than those experienced by the other deposits studied. Pyrite is virtually the only iron sulphide mineral associated with the other Carpentaria Zinc Belt Zn-Pb deposits (HYC, Walford Creek, Lady Loretta). Despite generally low values, magnetic susceptibility may still be used to broadly track non-pyrite Fe concentration in these less-metamorphosed deposits, as was demonstrated at Lady Loretta, even though only weakly ferromagnetic or paramagnetic minerals are present.

Metamorphic grade may also govern the resistivity contrast of Zn-Pb ores with their host sedimentary strata. HYC and Century ores, the least metamorphosed deposits studied, are both more resistive than their respective host rocks, while the opposite is true of Mount Isa, which has experienced the highest metamorphic grades. At Lady Loretta, where metamorphic grade is intermediate within the range defined by HYC and Mount Isa, ore resistivities are little different from those of the enclosing pyritic carbonaceous shales and siltstones. A metamorphic recrystallisation control on the grain size and connectivity of galena, pyrite and other conductive sulphide minerals is indicated.

Carpentaria Zinc Belt Zn-Pb ores are generally more chargeable than their host rocks, even when the host rock is strongly pyritic. The potential for IP to discriminate base metal mineralisation from concentrations of other, more common sulphide minerals makes it a high priority for base metal exploration in the region.

Ore velocities are slightly less than those of their host sediments. In spite of this, the ores' high density imparts a strong positive acoustic impedance contrast with their enveloping sedimentary strata, even if the

host is strongly dolomitic. Seismic reflection methods should therefore be able to detect buried base metal mineralisation in largely flat-lying sequences.

9.2.4 Paradise Valley qualitative geophysical image interpretation

Unit-specific enhancements of airborne magnetic and radiometric data emphasised a number of intra-formational anomalies, which are interpretable in terms of stratigraphic compositional variations, localised alteration and basin sedimentology.

The magnetic data suggest a stratigraphic control on magnetic susceptibilities in the Eastern Creek Volcanics. The Pickwick Metabasalt Member of the Eastern Creek Volcanics is generally slightly less magnetic than the Cromwell Metabasalt Member. The Pickwick Metabasalt also has lower Th- and U-channel radiometric signatures than the Cromwell Metabasalt, but comparable or higher K.

Areas of anomalous magnetic intensity with respect to normal Eastern Creek Volcanics signatures are interpreted as due to alteration either creating or destroying magnetite. Alteration systems are also clearly apparent in the radiometric data. Particularly high levels of K and subdued magnetic signal are observed from the Pickwick Metabasalt closest to the Mammoth Cu deposits. This is interpreted as due to epidote-sphene (Wyborn, 1987) or Mg chlorite-rutile (Heinrich et al., 1995) alteration which may be related to the Cu mineralisation at Mammoth. The magnetic low around Lady Loretta is interpreted to partially result from magnetite-destructive chlorite + albite alteration resulting in depletion of base metals from the Eastern Creek Volcanics at depth (see also Leaman, 1991a).

Magnetic data show that the thickness of the Myally Subgroup varies significantly across the study area. Dolerite sills within the Myally Subgroup are non-magnetic. Hitherto unmapped members within formations of the Myally Subgroup can be identified from their distinctive radiometric signatures, which may be used to improve the stratigraphic resolution of the Myally Subgroup. Most units mapped as 'undivided Myally Subgroup' on the 1:100,000 geological map sheet (Hutton and Wilson, 1985) are interpreted as Whitworth Quartzite from the radiometric data. Radiometrics also indicates the absence of much of the lower Myally Subgroup from the region of the Mount Gordon Fault zone.

The Fiery Creek Volcanics are very weakly to non-magnetic in the study area. Their radiometric signature is very patchy with some areas clearly K-altered, and others radiometrically quiet. Large spatial variation is also observed in the radiometric signature of the Bigie Formation, consistent with deposition in a syn-rift setting.

Magnetic anomalies within the Surprise Creek Formation are mostly interpreted as representing syn-depositional uplifts of Eastern Creek Volcanics-bearing sequences beneath the Surprise Creek Formation, though some of these apparent uplifts may have been emplaced by thrusting associated with the early stages of the Isan Orogeny. Radiometric data may be used to extend mapping of the informal stratigraphic subdivision of the Surprise Creek Formation (Hutton and Wilson, 1985) across the study area. Mappable lateral variations in Surprise Creek Formation radiometric signature are interpreted in terms of variations in provenance and basin setting, with higher radioelement concentrations generally

indicating low-energy depositional environments. The Surprise Creek Formation in the Mount Gordon Fault zone is interpreted to have been deposited proximal to a sediment source to the east.

Lateral variations in radiometric signature are also present in the Gunpowder Creek Formation. A carbonaceous shale-rich facies is inferred at the top of the Gunpowder Creek Formation immediately west of the Mount Gordon Fault zone, which may indicate the onset of quieter, deeper water deposition and generally more subdued basin palaeotopography. A coarser siliciclastic Gunpowder Creek Formation is interpreted north and west of Lady Loretta, consistent with proximity to a local sediment source and/or a (sub)basin-bounding fault.

Magnetic field variations within individual McNamara Group formations can be interpreted in terms of syn-depositional basin structure. Intra-formational differences in composition and inferred basin setting across the Redie Creek Fault persist into the Paradise Creek Formation, though in an opposite sense, with a depocentre interpreted to be located north rather than south of the Redie Creek Fault at this time. Low radiometric signal from the Paradise Creek Formation near Lady Loretta is interpreted to be due to an elevated siliciclastic component in this area, with corresponding implications for proximity to palaeotopography.

A K-rich horizon at the base of the Esperanza Formation may mark a maximum flooding surface. Otherwise the Esperanza Formation is generally low in radiometric signal, presumably due to chert which is a characteristic feature of the Esperanza Formation in outcrop.

A magnetic low within the Lady Loretta Formation in the vicinity of the Lady Loretta Zn-Pb deposit is caused by magnetite-destructive alteration of Eastern Creek Volcanics. At least two sub-units within the LLF may be distinguished from the radiometric data; a lower dolomite-rich member and an upper shale-rich member. The upper shale-rich facies is best developed in the sequence hosting the Lady Loretta deposit, consistent with development of a sub-basin in this region. Elevated levels of Th and U are observed in conjunction with carbonaceous shales which host base metal mineralisation in this area.

9.2.5 Paradise Valley modelling

Pre-Haslingden Group felsic igneous units probably occur at the base of the Mount Isa Basin sequence in the Paradise Valley region, but cannot be quantitatively mapped with confidence due to large, non-systematic variability in physical properties and the influence of the Eastern Creek Volcanics on gravity and magnetic fields.

The main volume of the Eastern Creek Volcanics is preserved within the Leichhardt Rift, but the western boundary of the original Leichhardt Rift is inferred from the distribution of the Eastern Creek Volcanics to lie a few kilometres west of Mount Gordon Fault zone, rather than coincident with the Mount Gordon Fault itself as implied by O'Dea et al. (1997a). The Mount Gordon Fault currently dips west. The gravity and magnetic modelling defines large variations in magnetic and possibly density properties near major faults in the Eastern Creek Volcanics. East-west trending faults in the Leichhardt Rift south of and including the Investigator Fault are interpreted as north-dipping reverse faults or thrusts (cf. Bell, 1983), but may originally have been normal extensional faults, since inverted. Faults north of the Investigator

Fault are south-dipping and separate north-tilted half-grabens, consistent with N-S extension in Eastern Creek Volcanics time. While the Eastern Creek Volcanics is present to some extent through most of the study area, its greatest volume outside the Leichhardt Rift occurs in an inferred WNW-oriented graben north of the Redie Creek Fault, which possibly developed during later Eastern Creek Volcanics (Pickwick Metabasalt) time. The Eastern Creek Volcanics appear not to persist far beyond the western edge of study area.

The thickness of the Myally Subgroup is highly variable. The predominantly siliciclastic Myally Subgroup-Gunpowder Creek Formation sequence is generally attenuated north of the Redie Creek Fault-Lady Loretta trend. This represents a reversal in the sense of displacement across the Redie Creek Fault trend inferred for the Eastern Creek Volcanics. Thickening of the Myally Subgroup-Gunpowder Creek Formation succession south of the Redie Creek Fault, extending WNW to south of Lady Loretta, corresponds to the Paradise Graben of Dunnet (1976), but this depositional centre only appears to have been active during Myally Subgroup-Gunpowder Creek Formation time.

Lady Loretta is situated on the northwestern edge of the Paradise Graben depocentre, albeit within younger, finer, more dolomitic sediments, which is consistent with deposition in an intracontinental sag or passive margin. This palinspastic interpretation is supported by the more even distribution of post-Gunpowder Creek Formation McNamara Group sedimentation, with only subdued variation in palaeobathymetry. Some indication of basin deepening to the north and northwest of the study area during Paradise Creek Formation-Lady Loretta Formation time is one of the few indications of spatial variation in accommodation space development during deposition of the middle to upper McNamara Group.

9.3 Synthesis and Conclusions

The enormous mass of Zn and Pb tonnage contained in many stratiform sediment-hosted deposits in the Proterozoic Carpentaria Zinc Belt of northern Australia requires special conjunctions of geological circumstances for their genesis, arguably to a greater degree than any other base metal deposit style. GIS and geophysics can be used at all exploration scales to identify areas where such conjunctions have occurred. This study has identified a number of ways in which geophysics and GIS can be applied to the identification and mapping of potential mineralising fluid sources, conduits and deposit locations.

Felsic igneous, mafic igneous and feldspathic sedimentary sequences all contain moderate amounts of zinc and lead. Even so, enrichment factors of approximately three orders of magnitude are required to form an ore deposit, and hence correspondingly large volumes of source rocks are required. The distribution of potential base metal source rocks (felsic igneous, mafic igneous and feldspathic sedimentary sequences) can be mapped at depth using gravity and magnetics, and their basin-scale architecture and metallogenic capacity visualised and evaluated using GIS. These methods have been used to demonstrate the presence of sufficient quantities of potential base metal source lithologies to comfortably account for known base metal mineralisation. Source factors alone do not exert strong spatial control on mineralisation, although obviously the chances of producing a significant base metal

deposit are enhanced in the vicinity of large accumulations of source material. Ample metal is available as long as suitable hydrogeological systems operate to tap it.

More stringent requirements are demanded of basin fluid flow systems to source and transport sufficient base metals to form a major deposit. Large, porous and permeable 'percolator' volumes may be needed to both contain and circulate sufficient quantities of fluids and to produce an ore deposit. Sub-basins developed during basin evolution are suitable settings for the deposition of source rocks and the maintenance of long-lived fluid circulation. Gravity and magnetics can be used to help delineate these sub-basins and hence to assist in exploration area selection using a GIS.

The large volume of Eastern Creek Volcanics contained within the Leichhardt Rift and to a lesser extent north of the Redie Creek Fault is a potential base metal source in the Paradise Valley study area. Magnetite destruction, density reduction and K reduction are all associated with epidote + sphene alteration, which may be linked with base metal depletion. Altered Eastern Creek Volcanics that have been depleted in base metals can potentially be detected with magnetics, radiometrics and gravity. Unfortunately radiometric detection of epidote + sphene alteration is limited by the need for surface exposure, hence any mineralisation generated is likely to have been eroded except in special structural circumstances.

Mineralising fluid conduits are the most critical spatial control on the localisation of base metal deposition. Growth faults controlling basin or sub-basin edges are particularly suited to such a role. Mapping of syn-deposition basin geometry is thus critical. Automated unconformity detection and integration of geological data with geophysical interpretation are GIS techniques devised and used in the McArthur Basin to infer anomalous sub-basin development during McArthur Group time, around the period of HYC mineralisation. HYC lies at the confluence of basin-controlling structures at the north-eastern corner of the Hot Spring-Emu sub-basin, where a number of permeable active or former growth faults are likely to have been present.

Gravity and magnetic modelling demonstrates the presence of a sub-basin developed from Myally Subgroup to Gunpowder Creek Formation time in the WNW-trending Paradise Graben. This basin contains a large volume of siliciclastic sediments, and hence a large potential base metal tonnage. This material may comprise at least part of the source of base metals at Lady Loretta, which is situated at the northwestern corner of the sub-basin, above a likely location of growth fault intersection.

An additional or alternative contribution to the Lady Loretta base metal mineralisation may have been derived from epidote + sphene altered Eastern Creek Volcanics in the vicinity, characterised by low magnetic susceptibility and density, which has been both directly sampled and mapped in the subsurface using gravity and magnetics. The presence of Eastern Creek Volcanics with similar physical properties immediately beneath the Mount Isa Zn-Pb deposit (Leaman, 1991a) reinforces the possibility of a genetic association between magnetite destructive Eastern Creek Volcanics alteration and base metal mineralisation.

The final major required factor for localisation of base metal mineralisation is suitably located host lithologies. These lithologies must be reducing in their chemical properties in order to sequester the

metals from the basin brine into the sedimentary sequence in ore-level concentrations. Carbonaceous and/or pyritic fine-grained siliciclastics are generally accepted to be prime candidates (McGoldrick and Large, 1998). These are usually detectable using electrical and EM methods. However, there is not always a significant conductivity contrast with more oxidised sediments. Porosity variations operating in addition to lithological factors may also confound methods relying on resistivity variations to detect suitable ore host strata.

Radiometrics provide an additional avenue for detection of carbonaceous shales in well-exposed dolomitic sequences. Radiometric data indicate that a number of potential host horizons are present in the McNamara Group in addition to the Lady Loretta host sequence. Within these prospective strata, widely dispersed geochemical haloes around stratiform base metal deposits should be mappable with precise magnetic susceptibility measurements, if not with magnetic surveys.

Effective geophysical detection of orebodies depends on contrast with their host units. Petrophysical data indicate that Carpentaria Zinc Belt deposits have variable physical property contrasts with their host units. Some positive density contrast is usually present, with Lady Loretta by far the densest of the Carpentaria Zinc Belt deposits examined. Gravity is effective in detecting the contribution of base metal mineralisation to positive Bouguer anomalies, in addition to that from pyrite at Lady Loretta (Duffett, 1998). Other major deposits have less contrast with pyritic material associated with base metal mineralisation, but the presence of associated pyrite (Century excepted) nonetheless ensures the presence of a positive Bouguer anomaly directly associated with mineralisation.

Ores are consistently more chargeable than their host rock, so IP should also be a primary direct ore detection tool. There is also potential for seismic reflection to detect concealed mineralisation in shallowly-dipping sequences. Sulphide accumulation will only be directly detected with magnetics in regions of moderate to high metamorphic grade where monoclinic pyrrhotite has been produced. Non-IP electrical and EM techniques, while effective in some circumstances, should not be solely relied on for direct ore detection, as there is often little conductivity contrast between ores and host material, and the sign of what contrast there may be is uncertain.

GIS and geophysics, used together, are effective tools in the identification and visualisation of sub-basins in the Proterozoic sequences of the Carpentaria Zinc Belt. The two main stratiform sediment-hosted base metal deposits investigated, Lady Loretta and HYC, are both located on the edge of contemporaneous or immediately antecedent sub-basins. Similar situations should be sought in exploration for further examples of stratiform sediment-hosted base metal ore deposits in the Carpentaria Zinc Belt.

References

Ahmad, M. and Wygralak, A.S., 1989. Calvert Hills, Northern Territory - 1:250 000 Metallogenic Map Series. *Northern Territory Geological Survey Explanatory Notes and Mineral Deposit Data Sheets* SE 53-8.

Aheimer, M.A., 1994. Geology and geochemistry of the Lady Loretta SSH base metal deposit, northwest Queensland. B.Sc. (Hons) thesis, CODES-Geology Department, University of Tasmania (unpublished).

Alcock, P.J. and Lee, M.F., 1974. Aspects of the geology and exploration of the Lady Loretta lead-zinc-silver deposits, North West Queensland. *Australasian Institute of Mining and Metallurgy, Conference Series* 6: 207-215.

Anderson, H.F., Duncan, A.C. and Lynch, S.M., 1993. Geological mapping capabilities of the QUESTEM airborne electromagnetic system for mineral exploration - Mt. Isa Inlier, Queensland. *Exploration Geophysics* 24: 333-340.

Bampton, K.F., Collins, A.R., Glasson, K.R. and Guy, B.B., 1977. Geochemical indications of concealed copper mineralization in an area northwest of Mount Isa, Queensland, Australia. *Journal of Geochemical Exploration* 8: 169-188.

Bell, T.H., 1983. Thrusting and duplex formation at Mount Isa, Queensland, Australia. *Nature* 304: 493-497.

Bell, T.H., 1991. The role of thrusting in the structural development of the Mount Isa mine and its relevance to exploration in the surrounding region. *Economic Geology* 86: 1602-1625.

Bell, T.H., 1993. The role of thrusting in the structural development of the Mount Isa mine and its relevance to exploration in the surrounding region - A reply. *Economic Geology* 88: 479-480.

Betts, P.G., Jones, M. and Valenta, R.K., 1994. Utilisation of aeromagnetic data for structural analysis - the Fiery Creek Dome Region, Mt. Isa Inlier. *7th Australasian Remote Sensing Conference Proceedings* p. 33-38.

Betts, P., Pound, K. and Lister, G., 1996. Episodic rift-sag sequence in cover sequence three, northwestern Mount Isa Inlier. *Geological Society of Australia Abstracts* 41: 32.

Betts, P.G., Lister, G.S. and Pound, K.S., 1999. Architecture of a Palaeoproterozoic rift system: evidence from the Fiery Creek Dome region, Mt Isa terrane. *Australian Journal of Earth Sciences* 46: 533-554.

Bishop, J.R. and Emerson, D.W., 1993. The geophysical properties of zinc deposits. In Mathew, I.G. (ed.), World Zinc '93 Proceedings. *AusIMM Proceedings* 7/93: 151-152.

Bishop, J.R. and Emerson, D.W., 1999. Geophysical properties of zinc-bearing deposits. *Australian Journal of Earth Sciences* 46: 311-328.

Blake, D.H., 1980. The early geological history of the Proterozoic Mount Isa Inlier, northwestern Queensland: an alternative interpretation. *BMR Journal of Australian Geology and Geophysics* 5: 243-256.

Blake, D.H., 1987. Geology of the Mount Isa Inlier and environs, Queensland and the Northern Territory. *BMR Bulletin* 225.

Blake, D.H., Etheridge, M.A., Page, R.W., Stewart, A.J., Williams, P.R. and Wyborn, L.A.I., 1990. Mount Isa Inlier - regional geology and mineralisation. *In* Hughes, F.E. (ed.), Geology of the Mineral Deposits of Australia and Papua New Guinea. AusIMM, Melbourne. p. 915-925.

Blake, D.H. and Stewart, A.J., 1992a. Stratigraphic and tectonic framework, Mount Isa Inlier. *In* Stewart, A.J. and Blake, D.H. (Eds.), Detailed studies of the Mount Isa Inlier. *Bureau of Mineral Resources, Australia, Bulletin* 243: 1-11.

Blake, D.H. and Stewart, A.J., 1992b. The BMR 1983-1990 Mount Isa Project: results, some remaining problems, and bibliography. *In* Stewart, A.J. and Blake, D.H. (Eds.), Detailed studies of the Mount Isa Inlier. *Bureau of Mineral Resources, Australia, Bulletin* 243: 361-374.

Bleil, U. and Petersen, N., 1982. Magnetic properties of natural minerals. In Angenheister, G. (ed.), Physical Properties of Rocks. Landolt-Bornstein numerical data and functional relationships in science and technology, Group V: Geophysics and Space Research 1b: 305-365. Springer-Verlag, Berlin.

Blewett, R., 1993. The AGSO field geological note books - a user's guide. *Australian Geological Survey Organisation Record* 1993/94.

Bonham-Carter, G.F., Agterberg, F.P. and Wright, D.F., 1990. Weights of evidence modelling: a new approach to mapping mineral potential. In Agterberg, F.P. and Bonham-Carter, G.F. (eds.), Statistical Applications in the Earth Sciences. *Geological Survey of Canada Paper* 89-9: 171-183.

Bornman, J.C., 1982. Annual Report on EL 1203 Leila Yard, Northern Territory 7/9/80 – 6/9/81. Shell Company of Australia Ltd. Metals Division. *Northern Territory Dept. of Mines and Energy, Open File Company Report* CR82/20 (unpubl.).

Broadbent, G.C., Myers, R.E. and Wright, J.V., 1996. Geology and origin of shale-hosted Zn-Pb-Ag mineralisation at the Century mine, northwest Queensland. In Baker, T. et al (eds.), MIC '96: The McArthur, Mt Isa, Cloncurry Minerals Province - New Developments in Metallogenic Research, Extended Conference Abstracts. *EGRU Contribution* 55: 24-27.

Brooks, J.H., 1956. Copper mining in the Cloncurry mineral field. *Queensland Government Mining Journal* 57: 891-900.

Brooks, J.H., 1990. Copper deposits in the Cloncurry-Mount Isa district. In Glasson, K.R. and Rattigan, J.H. (eds.), Geological Aspects of the Discovery of some Important Mineral Deposits in Australia. *AusIMM Monograph Series* 17: 107-111.

Brown, M.C., Claxton, C.W. and Plumb, K.A., 1969. The Proterozoic Barney Creek Formation and some associated units of the McArthur Group, N.T.. *BMR Record* 1969/145. 59p.

Bull, S.W. and Rogers, J.R., 1996. Recognition and significance of an early compressional deformation event in the Tawallah Group, McArthur Basin, NT. In Baker, T. et al (eds.), MIC '96: The McArthur, Mt Isa, Cloncurry Minerals Province - New Developments in Metallogenic Research, Extended Conference Abstracts. EGRU Contribution 55: 28-32.

Bultitude, R.J., 1986. Flood basalts of probable early Cambrian age in northern Australia. *In* Johnson, R.W. (ed.), Volcanism in Australasia. Elsevier, Amsterdam. pp. 1-20.

Carr, G.R., 1984. Primary geochemical and mineralogical dispersion in the vicinity of the Lady Loretta Zn-Pb-Ag deposit, NW Queensland. *Journal of Geochemical Exploration* 22: 217-238.

Carr, G.R., Sun, S-s., Page, R.W. and Hinman, M., 1996. Recent developments in the use of lead isotope model ages in Proterozoic terrains. In Baker, T. et al (eds.), MIC '96: The McArthur, Mt Isa, Cloncurry Minerals Province - New Developments in Metallogenic Research, Extended Conference Abstracts. *EGRU Contribution* 55: 33-35.

Carter, E.K., Brooks, J.J. and Walker, K.R., 1961. The Precambrian mineral belt of northwestern Queensland. *BMR Bulletin* 51.

Clark, D.A., 1980. Magnetic properties of rocks from the Mount Isa area. *Restricted Investigation Report* 1149R. CSIRO Division of Mineral Physics.

Clark, D.A., 1997. Magnetic petrophysics and magnetic petrology: aids to geological interpretation of magnetic surveys. *AGSO Journal of Australian Geology and Geophysics* 17: 83-103.

Clark, D.A. and Emerson, D.W., 1991. Notes on rock magnetisation characteristics in applied geophysical studies. *Exploration Geophysics* 22: 547-555.

Clarke, A.M., 1992. Thornton EPM 7245 (The Desert) exploration report, 9/4/91 to 8/4/92. CRA Exploration. *Queensland Dept. of Mines and Energy, Open File Company Report* CR23644 (unpubl.).

Collins, C.D.N., 1983. Crustal structure of the southern McArthur Basin from deep seismic sounding. *BMR Journal of Australian Geology and Geophysics* 8: 19-34.

Compston, W. and Arriens, P.A., 1968. The Precambrian geochronology of Australia. *Canadian Journal of Earth Sciences* 5: 561-583.

Connors, K.A. and Lister, G.S., 1995. Polyphase deformation in the western Mount Isa Inlier, Australia: episodic or continuous deformation? *Journal of Structural Geology* 17: 305-328.

Connors, K.A. and Page, R.W., 1995. Relationships between magmatism, metamorphism and deformation in the western Mount Isa Inlier, Australia. *Precambrian Research* 71: 131-153.

Cooke, D.R., Bull, S.W., Large, R.R. and McGoldrick, P.J., 1998. Oxidised (sulfate-bearing) brines - their importance for formation of Australian Proterozoic Pb-Zn (sedex) deposits. *Geological Society of Australia, Abstracts* 49: 91. 14th Australian Geological Convention, Townsville.

Corbett, J.A., Lambert, I.B. and Scott, K.M., 1975. Results of analyses of rocks from the McArthur Area, Northern Territory. CSIRO Technical Communication 57. CSIRO Minerals Research Laboratories.

Cox, K.G., 1980. A model for flood basalt vulcanism. *Journal of Petrology* 21: 629-650.

Crick, I.H., 1992. Petrological and maturation characteristics of organic matter from the middle Proterozoic McArthur Basin, Australia. *Australian Journal of Earth Sciences* 39: 501-519.

Cull, J.P., 1991. Geothermal gradients in Australia. In Drummond, B. (ed.), The Australian Lithosphere. *Geological Society of Australia Special Publication* 17: 147-156.

Davidson, G.J., 1998. Alkali alteration styles and mechanisms, and their implications for a 'brine factory' source of base metals in the rift-related McArthur Group, Australia. *Australian Journal of Earth Sciences* 45: 33-49.

Davis, G.H., 1984. Structural Geology of Rocks and Regions. John Wiley & Sons, Singapore. 492p.

de Keyser, F., 1958. Geology and mineral deposits in Paradise Creek area, north-western Queensland. *Bureau of Mineral Resources, Geology and Geophysics Record* 1958/100 (unpubl.).

de Keyser, F. and Cook, P.J., 1972. Geology of the Middle Cambrian Phosphorites and Associated Sediments of Northwestern Queensland. *BMR Bulletin* 138.

Derrick, G.M., 1982. A Proterozoic rift zone at Mount Isa, Queensland, and implications for mineralisation. *BMR Journal of Geology and Geophysics* 7: 81-92.

Derrick, G.M., 1992. Brothers in arms: the interaction of geology and geophysics in the Mount Isa Inlier. *Exploration Geophysics* 23: 117-122.

Derrick, G.M., Wilson, I.H. and Hill, R.M., 1976. Revision of stratigraphic nomenclature in the Precambrian of northwestern Queensland. II: Haslingden Group. *Queensland Government Mining Journal* 77: 300-306.

Derrick, G.M., Wilson, I.H. and Sweet, I.P., 1980. The Quilalar and Surprise Creek Formations - new Proterozoic units from the Mount Isa Inlier: their regional sedimentology and application to regional correlation. *BMR Journal of Australian Geology and Geophysics* 5: 215-223.

Dickson, B.L. and Scott, K.M., 1997. Interpretation of aerial gamma-ray surveys – adding the geochemical factors. *AGSO Journal of Australian Geology and Geophysics* 17: 187-200.

Duffett, M.L., 1996. Geophysical environment of the Lady Loretta Pb-Zn deposit. In Baker, T. et al (eds.), MIC '96: The McArthur, Mt Isa, Cloncurry Minerals Province - New Developments in Metallogenic Research, Extended Conference Abstracts. *EGRU Contribution* 55: 45-46.

Duffett, M.L., 1998. Gravity, magnetic and radiometric evidence for the geological setting of the Lady Loretta Pb-Zn-Ag deposit - a qualitative appraisal. *Economic Geology* 93: 1295-1306.

Duffett, M.L. and Leaman, D.E., 1997. McArthur Basin architecture – a new perspective from geophysics and GIS. *Exploration Geophysics* 28: 39-42.

Dunnet, D., 1976. Some aspects of the Panantarctic cratonic margin in Australia. *Philosophical Transactions of the Royal Society* A280: 641-654.

Dunster, J.N., 1996. Sedimentology of the Lady Loretta Formation - a comparison of the regional setting to that of the Lady Loretta orebody. In Baker, T. et al (eds.), MIC '96: The McArthur, Mt Isa, Cloncurry Minerals Province - New Developments in Metallogenic Research, Extended Conference Abstracts. *EGRU Contribution* 55: 47-50.

Dunster, J.N., 1997. The Lady Loretta Formation: Sedimentology and Stratiform Sediment-Hosted Base Metal Mineralisation. Ph.D. thesis, University of Tasmania (unpubl.).

Dunster, J.N. and McConachie, B.A., 1998. Tectono-sedimentary setting of the Lady Loretta Formation: synrift, sag or passive margin? *Australian Journal of Earth Sciences* 45: 89-92.

Ellis, D.J. and Wyborn, L.A.I., 1984. Petrology and geochemistry of Proterozoic dolerites from the Mount Isa Inlier. *BMR Journal of Australian Geology and Geophysics* 9: 19-32.

Emerson, D.W., 1990. Notes on mass properties of rock density, porosity, permeability. *Exploration Geophysics* 21: 209-216.

Emerson, D.W., 1995. Black shale conductivities, McNamara Group, NW Qld.; Petrophysical study for Aberfoyle Resources Ltd. Systems Exploration (NSW) Pty Ltd. (unpubl.). Used with permission from Aberfoyle.

Emerson, D.W. and Yang, Y.P., 1997. Insights from laboratory mass property crossplots. *Preview* 70: 10-14.

Eriksson, K.A., Taylor, S.R. and Korsch, R.J., 1992. Geochemistry of 1.8-1.67Ga mudstones and siltstones from the Mount Isa Inlier, Queensland, Australia; provenance and tectonic implications. *Geochimica et Cosmochimica Acta* 56: 899-909.

Eriksson, K.A., Simpson, E.L. and Jackson, M.J., 1994. Stratigraphical evolution of a Proterozoic syn-rift to post-rift basin: constraints on the nature of lithospheric extension in the Mount Isa Inlier, Australia. In Frostick, L.E. and Steel, R.J. (eds.), Tectonic Controls and Signatures in Sedimentary Successions. Blackwell Scientific, *IAS Special Publication* 20: 203-221.

Etheridge, M.A., Rutland, R.W.R. and Wyborn, L.A.I., 1987. Orogenesis and tectonic process in the early to middle Proterozoic of northern Australia. In Kroner, A. (ed.), Proterozoic Lithospheric Evolution. Geodynamics Series 17: 131-147. American Geophysical Union, Washington D.C..

Etheridge, M. and Wall, V., 1994. Tectonic and structural evolution of the Australian Proterozoic. *12th Australian Geological Convention, Geological Society of Australia, Abstracts* 37: 102-103.

Ewers, G. and Ryburn, R., 1993. User's guide to the OZMIN mineral deposits database. *AGSO Record* 1993/94.

Fallon, G.N. and Busuttil, S., 1992. An appraisal of the geophysical effects of the Mount Isa ore bodies. *Exploration Geophysics* 23: 133-140.

Finlayson, D.M., 1982. Seismic crustal structure of the Proterozoic North Australian Craton between Tennant Creek and Mount Isa. *Journal of Geophysical Research* 87B: 10569-10578.

Finlayson, D.M., 1987. Seismic features of Proterozoic crust in northern Australia and their evolution. In Kroner, A. (ed.), Proterozoic Lithospheric Evolution. Geodynamics Series 17: 99-113. American Geophysical Union, Washington D.C..

Forrestal, P.J., 1990. Mount Isa and Hilton silver-lead-zinc deposits. In Hughes, F.E. (ed.), Geology of the Mineral Deposits of Australia and Papua New Guinea. *AusIMM Monograph* 14: 927-934.

Gibb, R.A., 1967. Western Queensland reconnaissance gravity surveys, 1957-1961. *Bureau of Mineral Resources, Australia, Report* 129.

Goleby, B.R., Drummond, B.J. and MacCready, T., 1996. The Mount Isa geodynamic transect: The deep seismic reflection profile south of Mount Isa and Cloncurry. *AGSO Research Newsletter* 24: 6-8.

Goleby, B.R., Goncharov, A.G., MacCready, T. and Drummond, B.J., 1997. Tectonics of the Mount Isa Inlier from seismic studies. Geodynamics and Ore Deposits Conference abstracts, p. 38-41. Australian Geodynamics Cooperative Research Centre, Ballarat, Victoria.

Goncharov, A.G., Collins, C.D.N., Goleby, B.R., Drummond, B.J. and MacCready, T., 1996. The Mount Isa geodynamic transect: Implications of the seismic refraction model. *AGSO Research Newsletter* 24: 9-10.

Goncharov, A., Sun, S-s and Wyborn, L., 1997. Balanced petrology of the crust in the Mount Isa region. *AGSO Research Newsletter* 26: 13-16.

Grondijs, H.F. and Schouten, C., 1937. A study of the Mt Isa ores. *Economic Geology* 32: 407-450.

Gulson, B.L., Perkins, W.G. and Mizon, K.J., 1983. Lead isotope studies bearing on the genesis of copper ore bodies at Mount Isa, Queensland. *Economic Geology* 78: 1466-1504.

Gunn, P.J., 1983. Recognition of Proterozoic rift systems in the Mount Isa - McArthur Basin area of northern Australia. *Proceedings of the 3rd biennial conference of the Australian Society of Exploration Geophysicists,* Brisbane, 1983. pp. 168-171.

Guy, B.B., 1975. Stratiform copper mineralization in the Proterozoic dolomites of north-western Queensland, Australia. *Economic Geology* 70: 1414-1425.

Hancock, M.C. and Purvis, A.H., 1990. Lady Loretta Ag-Pb-Zn deposit. In *Geology and mineral deposits of Australia and PNG.* AusIMM, Melbourne: 943-948.

Harrison, P.L., 1980. The Toomba Fault and the western margin of the Toko Syncline, Georgina Basin, Queensland and Northern Territory. *BMR Journal of Australian Geology and Geophysics* 5: 201-214.

Hazell, M. and Wyborn, L., 1995. The rigorous steps required in data capture for creating a usable GIS and the need for national data standards. *Proceedings of the 3rd National Conference on the Management of Geoscience Information and Data, 18-20 July 1995.* Australian Mineral Foundation, Adelaide.

Heinrich, C.A., Bain, J.H.C., Mernagh, T.P., Wyborn, L.A.I., Andrew, A.S. and Waring, C.L., 1995. Fluid and mass transfer during metabasalt alteration and copper mineralization at Mount Isa, Australia. *Economic Geology* 90: 705-730.

Hill, R.M., Wilson, I.H. and Derrick, G.M., 1975. Geology of the Mount Isa 1:100,000 Sheet area, northwest Queensland. *Bureau of Mineral Resources, Australia, Record* 1975/175.

Hinman, M., 1996. Constraints, timing and processes of stratiform base metal mineralization at the HYC Ag-Pb-Zn deposit, McArthur River. In Baker, T. et al (eds.), MIC '96: The McArthur, Mt Isa, Cloncurry Minerals Province - New Developments in Metallogenic Research, Extended Conference Abstracts. *EGRU Contribution* 55: 56-59.

Hinman, M., Wall, V., and Heinrich, C., 1994. The interplay between sedimentation, deformation and hydrothermal activity at the McArthur Pb-Zn (-Cu) deposit. *12th Australian Geological Convention, Geological Society of Australia Abstracts* 37: 176-177.

Hishida, H., Tsujimoto, T., Humphries, G. and Linford, G., 1993. MIP test survey over the HYC deposit in McArthur River area, N.T. *Exploration Geophysics* 24: 577-584.

Hone, I.G., Carberry, V.P. and Reith, H.G., 1987. Physical property measurements on rock samples from the Mount Isa Inlier, northwest Queensland. *Bureau of Mineral Resources, Australia, Report* 265. 30pp.

Howard, P.F. and Cooney, A.M., 1976. D Tree phosphate deposit, Georgina Basin, Queensland. In Knight, C.L. (ed.), Economic Geology of Australia and Papua New Guinea. 4. Industrial Minerals and Rocks. *AusIMM Monograph* 8: 265-273.

Hutchinson, M.F., 1989. A new procedure for gridding elevation and stream line data with automatic removal of spurious pits. *Journal of Hydrology* 106: 211-232.

Hutton, L.J., 1983. Stratigraphic drilling report - GSQ Lawn Hill 1-4. *Queensland Government Mining Journal* 84: 228-240.

Hutton, L.J., Cavaney, R.J. and Sweet, I.P., 1981. New and revised stratigraphic units, Lawn Hill Platform, north west Queensland. *Queensland Government Mining Journal* 82: 423-434.

Hutton, L.J. and Sweet, I.P., 1982. Geological evolution, tectonic style and economic potential of the Lawn Hill Platform cover, Northwest Queensland. *BMR Journal of Australian Geology and Geophysics* 7: 125-134

Hutton, L. and Wilson, I.H., 1984. Mount Oxide Region, Queensland - 1:100,000 geological map commentary. BMR, Australia.

Hutton, L. and Wilson, I.H., 1985. Mammoth Mines Region, Queensland - 1:100,000 geological map commentary. BMR, Australia.

Jackson, J.C., Fallon, G.N. and Bishop, J.R., 1996. DHEM at Isa mine. *Exploration Geophysics* 27: 91-104.

Jackson, M.J., Muir, M.D. and Plumb, K.A., 1987. Geology of the southern McArthur Basin, Northern Territory. *BMR Bulletin* 220. 173p.

Jackson, M.J., Sweet, I.P. and Powell, T.G., 1988. Studies on petroleum geology and geochemistry of the middle Proterozoic McArthur Basin, northern Australia I: petroleum potential. *Australian Petroleum Exploration Association Journal* 28: 283-302.

Jackson, M.J., Simpson, E.L. and Eriksson, K.A., 1990. Facies and sequence stratigraphic analysis in an intracratonic, thermal sag basin: the Early Proterozoic Lower Quilalar Formation and Ballara Quartzite, Mount Isa Inlier, Australia. *Sedimentology* 37: 1053-1078.

Jackson, M.J., Southgate, P.N., Krassay, A.A., McConachie, B.A., Wells, A.T. and Scott, D.L., 1996. New techniques/concepts for choosing the right ground for sediment-hosted mineralisation - lower McNamara Group, Lawn Hill Platform. *13th Australian Geological Convention, Geological Society of Australia Abstracts* 41: 216.

Jackson, M.J., Southgate, P.N. and Page, R.W. Gamma-ray logs and SHRIMP dates - essential tools to constrain lithofacies interpretation of Proterozoic depositional systems. In James, N. and Grotzinger, J.P. (eds.), Proterozoic Carbonates. *Society of Economic Paleontologists and Mineralogists Special Publication* (in press).

Jagodzinski, E.A., Wyborn, L.A.I. and Gallagher, R., 1993. Mount Isa Metallogenic Atlas volume 2; Geochemistry. *Australian Geological Survey Organisation, Metallogenic Atlas Series* 1. 49p.

Jones, D., 1986. The Kamarga deposit: stratabound zinc-lead mineralization in the middle Proterozoic McNamara Group, northwest Queensland. *Ph.D. thesis, University of New England* (unpubl.).

Keele, R.A., Bull, S. and Duffett, M., 1996. Possible rifting events in the Paradise Creek high strain zone, Lady Loretta region, Mount Isa. CODES AMIRA/ARC Project P384A Report 2: 9-32.

Knox-Robinson, C.M., Robinson, D.C. and Groves, D.I., 1992. The use of geographical information systems as a gold prospectivity mapping tool, with reference to the Yilgarn Block, Western Australia: Requirements and limitations. In Geological Applications of Geographic Information Systems (GIS). Australian Institute of Geoscientists Bulletin 12: 71-82.

Kralik, M., 1982. Rb-Sr age determinations on Precambrian carbonate rocks of the Carpentarian McArthur Basin, Northern Territory, Australia. *Precambrian Research* 18: 157-170.

Krassay, A.A., 1996. Gamma-ray curves from outcrop and drillcore: techniques, and uses for stratigraphic correlation of Proterozoic sequences in northern Australia. In Baker, T. et al (eds.), MIC '96: The McArthur, Mt Isa, Cloncurry Minerals Province - New Developments in Metallogenic Research, Extended Conference Abstracts. *EGRU Contribution* 55: 60-63.

Laing, W., 1990. Evidence for a replacive origin for the Mount Isa Pb+Zn orebodies in a hydrothermal Cu+Pb+Zn deposit. *Mount Isa Inlier Geology Conference* p.64-66. Monash University.

Large, D.E., 1979. Rock geochemistry study, McArthur Basin Project. Bund. Geowissen. Rohstofe Report. No. 6250/9.

Large, R.R. and McGoldrick, P.J., 1993. Deposit Halos 5: Primary geochemical halos related to Proterozoic sediment hosted Pb-Zn deposits and applications to exploration. CODES AMIRA/ARC Project P384 Report 3: 63-126 (unpubl.).

Large, R. and McGoldrick, P., 1997. Alteration halos associated with stratiform sediment hosted ("sedex") Pb-Zn-Ag deposits; development of an alternative exploration approach. *Geological Society of Australia, Abstracts* 44: 42.

Large, R. R., & McGoldrick, P. J., 1998. Lithogeochemical halos and geochemical vectors to stratiform sediment hosted Zn-Pb-Ag deposits, Part 1. Lady Loretta Deposit, Queensland. *Journal of Geochemical Exploration* 63: 37-56.

Large, R., Bull, S., Cooke, D. and McGoldrick, P., 1996. Review of genetic models at HYC: constraints from new sedimentology, alteration halo studies and fluid chemical modelling. In Baker, T. et al (eds.), MIC '96: The McArthur, Mt Isa, Cloncurry Minerals Province - New Developments in Metallogenic Research, Extended Conference Abstracts. *EGRU Contribution* 55: 72-74.

Leaman, D.E., 1991a. Geophysical constraints on structure and alteration of the Eastern Creek Volcanics, Mt Isa, Queensland. *Australian Journal of Earth Sciences* 38: 457-472.

Leaman, D.E., 1991b. Surface gravity and magnetic responses of mineralization, Mt. Isa, northwest Queensland, Australia. *Geophysics* 56: 542-549.

Leaman, D.E., 1992. Regional geophysics-basin architecture: 1. Batten Trough region. CODES AMIRA/ARC Project P384 Report 1: 1-34 (unpubl.).

Leaman, D.E., 1993a. Regional geophysics-basin architecture: 2. Batten Trough region - update and further analysis. CODES AMIRA/ARC Project P384 Report 2: 1-25 (unpubl.).

Leaman, D.E., 1993b. Issues in interpretation - McArthur Basin: Do volcanic piles really exist? CODES AMIRA/ARC Project P384 Report 2: 27-46 (unpubl.).

Leaman, D.E., 1993c. Regional geophysics-basin architecture: 3. The Wearyan Shelf and Murphy Inlier. CODES AMIRA/ARC Project P384 Report 2: 65-99.

Leaman, D.E., 1993e. Regional geophysics-basin architecture: 4. The Bauhinia Shelf. CODES AMIRA/ARC Project P384 Report 4: 1-15.

Leaman, D.E., 1994a. Criteria for evaluation of potential field interpretations. *First Break* 12: 181-191.

Leaman, D.E., 1994b. Regional geophysics - basin architecture 5. The Lawn Hill Platform. Report 7: 1-35.

Leaman, D.E., 1996. Are thick volcanic piles concealed in north Australian Proterozoic basins? *Exploration Geophysics* 27: 13-20.

Leaman, D.E., 1997a. Application of magnetic methods to deep basin structures. *Exploration Geophysics* 28: 97-105.

Leaman, D.E., 1998. Structure, contents and setting of Pb-Zn mineralisation in the McArthur Basin, northern Australia. *Australian Journal of Earth Sciences* 45: 3-20.

Leaman, D.E. and Mutton, B.K., 1993. Dewatering assessment at Hilton Mine, Queensland - an application of gravity methods. *Exploration Geophysics* 24: 615-622.

Lewis, R.W., 1975. Lady Annie secondary copper deposit. *In* Knight, C.L. (Ed.), Economic geology of Australia and Papua New Guinea; 1, Metals. *Australasian Institute Mining. Metallurgy, Monograph Series* 5: 1023-1033.

Lister, G.S., 1993. The role of thrusting in the structural development of the Mount Isa mine and its relevance to exploration in the surrounding region - A discussion. *Economic Geology* 88: 479.

Lister, G.S., Etheridge, M.A. and Symonds, P.A., 1986. Detachment faulting and the evolution of passive continental margins. *Geology* 14: 246-250.

Logan, R.G., Murray, W.J. and Williams, N., 1990. HYC silver-lead-zinc deposit, McArthur River, Northern Territory. In Hughes, F.E. (ed.), Geology of the Mineral Deposits of Australia and Papua New Guinea, p. 907-911. AusIMM, Melbourne.

Logan, R.G., Leung, K. and Karelse, G.J., 1993. The McArthur River project. In Mathew, I.G. (ed.), World Zinc '93 Proceedings. *AusIMM Publication* 7/93: 27-39.

MacCready, T., Goleby, B.R., Goncharov, A., Lister, G.S. and Drummond, B.J., 1997. An evolutionary framework for the Isan Orogeny. Geodynamics and Ore Deposits Conference abstracts, p. 42-45. Australian Geodynamics Cooperative Research Centre, Ballarat, Victoria.

Machel, H.G. and Burton, E.A., 1991. Chemical and microbial processes causing anomalous magnetization in environments affected by hydrocarbon seepage. *Geophysics* 56: 598-605.

Macnae, J. and Mutton, A., 1996. Can sulphides be discriminated from conductive slates? A case history at Dugald River. *Exploration Geophysics* 27: 119-130.

Mathias, B.V., Clark, G.J., Morris, D. and Russell, R.E., 1973. The Hilton deposit - stratiform silver-lead-zinc mineralisation of the Mount Isa type. *Bureau of Mineral Resources, Australia, Bulletin* 141: 33-58.

McClenaghan, M.P., Roach, M.J. and Bottrill, R.S., 1994. Structure of the GIS databases. *Mineral Resources Tasmania Report* 1994/07 (unpubl.).

McConachie, B.A., Barlow, M.G., Dunster, J.N., Meaney, R.A. and Schaap, A.D., 1993. The Mount Isa Basin - Definition, structure and petroleum geology. *APEA Journal* 33: 237-257.

McConachie, B.A. and Dunster, J.N., 1996. Sequence stratigraphy of the Bowthorn Block in the northern Mount Isa Basin, Australia - implications for the base-metal mineralisation. *Geology* 24: 155-158.

McConachie, B.A., Scott, D.L., Wells, A.T. and Southgate, P.N., 1996. Death of the Gunpowder Creek Formation Intermediate Quartzite (PMW$_Q$) Mammoth Mines 1:100,000 sheet, Mount Isa Basin. *Geological Society of Australia, Abstracts* 41: 281. 13th Australian Geological Convention, Canberra.

McCulloch, M.T., 1987. Sm-Nd isotopic constraints on the evolution of Precambrian crust in the Australian continent. In Kroner, A. (ed.), Proterozoic Lithospheric Evolution. Geodynamics Series Volume 17: 115-130. American Geophysical Union, Washington D.C..

McDougall, I., Dunn, P.R., Compston, W., Webb, A.W., Richards, J.R. and Bofinger, V.M., 1965. Isotopic age determinations on Precambrian rocks of the Carpentaria region, Northern Territory, Australia. *Journal of the Geological Society of Australia* 12: 67-90.

McGoldrick, P.J., 1993b. Deposit Halos 4: Sampling and whole rock analyses for the Lady Loretta deposit. CODES AMIRA/ARC Project P384 Report 3: 31-48 (unpubl.).

McGoldrick, P.J., 1994b. The geochemistry of 'barren' late Palaeoproterozoic sediments from the McNamara Group: background values for the 'SEDEX AI'. AI Mk3' and MnQ$_b$. CODES AMIRA/ARC Project P384 Report 7: 141-148 (unpubl.).

McGoldrick, P.J., and Keays, R.R., 1990. Cogenetic copper-cobalt and lead-zinc-silver mineralization at Mount Isa and the effects of silica dolomite formation. *Mount Isa Inlier Geology Conference Abstracts* p.67-68. Monash University

McGoldrick, P. and Large, R., 1998a. Proterozoic stratiform sediment-hosted Zn-Pb-Ag deposits. *AGSO Journal of Geology & Geophysics* 17(4): 189-196.

McGoldrick, P. and Large, R., 1998b. Geology and mineralisation in the Proterozoic 'Carpentaria Zinc Belt' of northern Australia - Introduction. *Australian Journal of Earth Sciences* 45: 1-2.

McGoldrick, P., Dunster, J., Cooke, D. and Aheimer, M., 1996. New observations from the Lady Loretta Zn-Pb-Ag deposit: towards a new genetic model. In Baker, T. et al. (eds.), MIC '96: The McArthur, Mt Isa, Cloncurry Minerals Province - New Developments in Metallogenic Research, Extended Conference Abstracts. *EGRU Contribution* 55: 81-84.

McGoldrick, P., Dunster, J. and Large, R., 1997. Day 3 – Lady Loretta Formation at Lady Loretta mine; Lady Loretta Formation 'basal' breccia. CODES AMIRA/ARC Project P384A Report 4: 26-35.

McPherson, A.L., 1994. Volcanology and sedimentology of the Palaeoproterozoic Fiery Creek Volcanics and adjacent units, northwest Queensland. B.Sc. (Hons.) thesis, University of Tasmania (unpubl.). 123p.

Myers, R., Ceremuga,C., Clark, D., McSkimming, D., Price, S., Tuesley, M. and Wilkinson, D., 1996. Mount Isa lead-zinc mineralisation: What controversy? In Baker, T. et al. (eds.), MIC '96: The McArthur, Mt Isa, Cloncurry Minerals Province - New Developments in Metallogenic Research, Extended Conference Abstracts. *EGRU Contribution* 55: 85-89.

Neudert, M. and McGeough, M., 1996. A new tectonostratigraphic framework for the deposition of the upper McArthur Group, N.T.. In Baker, T. et al (eds.), MIC '96: The McArthur, Mt Isa, Cloncurry Minerals Province - New Developments in Metallogenic Research, Extended Conference Abstracts. *EGRU Contribution* 55: 90-93.

Neumann, F.J.G., 1964. Normanton to Daly Waters reconnaissance gravity survey, Queensland, N.T. 1959-60. *BMR Record* 1964/131 (unpubl.).

O'Dea, M.G. and Lister, G.S., 1995. The role of ductility contrast and basement architecture in the structural evolution of the Crystal Creek block, Mount Isa Inlier, NW Queensland, Australia. *Journal of Structural Geology* 17: 949-960.

O'Dea, M.G., Lister, G.S., MacCready, T., Betts, P.G., Oliver, N.H.S., Pound, K.S., Huang, W. and Valenta, R.K., 1997a. Geodynamic evolution of the Proterozoic Mount Isa terrain. In Burg, J.P. and Ford, M. (eds.), Orogeny Through Time. *Geological Society Special Publication* 121: 99-122.

O'Dea, M.G., Lister, G.S., Betts, P.G. and Pound, K.S., 1997b. A shortened intraplate rift system in the Proterozoic Mount Isa terrane, NW Queensland, Australia. *Tectonics* 16: 425-441.

Oehler, J.H. and Logan, R.G., 1977. Microfossils, cherts and associated mineralization in the McArthur Deposit, N.T., Australia. *Economic Geology* 72: 1393-1409.

Oldenburg, D.W., Li, Y., Farquharson, C.G., Kowalczyk, P., Aravanis, T., King, A., Zhang, P. and Watts, A., 1998. Applications of geophysical inversions in mineral exploration. *The Leading Edge* 17(4): 461-465.

Opik, A.A., Carter, E.K. and Randal, M.A., 1973. Notes on the first edition Camooweal geological sheet, Queensland, 1961. *BMR Record* 1973/83.

Page, R.W., 1978. Response of U-Pb zircon and Rb-Sr total rock and mineral systems to low grade regional metamorphism in Proterozoic igneous rocks, Mount Isa, Australia. *Journal of the Geological Society of Australia* 25: 141-164.

Page, R.W., 1981. Depositional ages of the stratiform base metal deposits at Mount Isa and McArthur River, Australia, based on U-Pb zircon dating of concordant tuff horizons. *Economic Geology* 76: 648-658.

Page, R.W., 1983. Timing of superposed volcanism in the Proterozoic Mount Isa Inlier, Australia. *Precambrian Research* 21: 223-245.

Page, R.W., 1988. Geochronology of early to middle Proterozoic fold belts in northern Australia: a review. *Precambrian Research* 40/41: 1-19.

Page, R.W., 1990. Developments in U-Pb zircon geochronology in the Mount Isa Inlier. *Mount Isa Inlier Geology Conference Abstracts* p.4-5. Monash University.

Page, R., 1997. Geological constraints provided by U-Pb zircon dating of basin phases in the Lawn Hill and McArthur Basins. NABRE Workshop March 4-5, 1997, Abstracts. *AGSO Record* 1997/12 (unpaginated).

Page, R.W. and Bell, T.H., 1986. Isotopic and structural responses of granite to successive deformation and metamorphism. *Journal of Geology* 94: 365-379.

Page, R.W. and Williams, I.S., 1988. Age of the Barramundi Orogeny in northern Australia by means of ion-microprobe and conventional U-Pb zircon studies. *Precambrian Research* 40/41: 21-36.

Page, R.W. and Sweet, I.P., 1998. Geochronology of basin phases in the western Mount Isa Inlier, and correlation with the McArthur Basin. *Australian Journal of Earth Sciences* 45: 219-232.

Page, R.W., Sun, S. and Carr, G., 1994. Proterozoic sediment-hosted lead-zinc-silver deposits in northern Australia - U-Pb zircon and Pb isotope studies. *Geological Society of Australia Abstracts* 37: 334-335.

Perkins, W.G., 1995. Features of the Mount Isa Cu-Pb-Zn deposit and comparison with Hilton, McArthur River and Mount Novit: Evidence for a late syndeformational replacement origin? In Metallogeny of Proterozoic Basins. *MDRU Short Course Notes* 19. University of British Columbia, Vancouver.

Pietsch, B.A., Rawlings, D.J., Creaser, P.M., Kruse, P.D., Ahmad, M., Ferenczi, P.A. and Findhammer, T.L.R., 1991. 1:250 000 geological map series explanatory notes SE 53-3 Bauhinia Downs. *N.T. Geological Survey.*

Pietsch, B.A., Plumb, K.A., Page, R.W., Haines, P.W., Rawlings, D.J. and Sweet, I.P., 1994. A revised stratigraphic framework for the McArthur Basin, NT. In Hallenstein, C.P. (ed.), 1994 AusIMM Annual Conference Technical Program Proceedings. *AusIMM Publication Series* 5/94: 135-138.

Plumb, K.A., 1979. Structure and tectonic style of the Precambrian shields and platforms of northern Australia. *Tectonophysics* 58: 291-325.

Plumb, K.A., 1987. Proterozoic extension and mineralisation in the McArthur Basin, Northern Territory, Australia. *BMR Record* 1987/51: 72-79.

Plumb, K.A., 1988. Geology of the McArthur Basin 1:1,000,000 map. Bureau of Mineral Resources, Australia.

Plumb, K.A., 1991. New Precambrian time scale. *Episodes* 14: 139-140.

Plumb, K.A. and Wellman, P., 1987. McArthur Basin, Northern Territory: mapping of deep troughs using gravity and magnetic anomalies. *BMR Journal of Australian Geology and Geophysics* 10: 243-252.

Plumb, K.A., Derrick, G.M., and Wilson, I.H., 1980. Precambrian geology of the McArthur River-Mount Isa region, northern Australia. In Henderson, R.A., and Stephenson, P.J. (eds.), The Geology and Geophysics of northeastern Australia. p. 71-83. *Geological Society of Australia, Inc., Queensland Division, Brisbane.*

Plumb, K.A., Ahmad, M. and Wygralak, A.S., 1990. Mid-Proterozoic basins of the North Australian Craton - regional geology and mineralisation. In Hughes, F.E. (Ed.), Geology of the mineral deposits of Australia and Papua New Guinea. Volume 1. *Australasian Institute of Mining and Metallurgy, Monograph* 14: 881-902.

Plumb, K.A., Wyborn, L.A.I. and Ryburn, R.J., 1992. McArthur Basin and Murphy Inlier ROCKCHEM data set documentation. *BMR Record* 1992/37.

Puranen, R., 1989. Susceptibilities, iron and magnetite content of Precambrian rocks in Finland. Geological Survey of Finland, Report of Investigation 90.

Rawlings, D.J., 1993. Mafic peperite from the Gold Creek Volcanics in the Middle Proterozoic McArthur Basin, Northern Territory. *Australian Journal of Earth Sciences* 40(2): 109-114.

Rawlings, D.J., 1994. Characterisation and correlation of volcanism in the McArthur Basin and Transitional Domain, NT. In Hallenstein, C.P. (Ed.), 1994 AusIMM Annual Conference Technical Program Proceedings. *AusIMM Publication Series* 5/94: 157-160.

Rawlings, D.J., 1997. High-level intrusions in the McArthur Basin, NT: Deformation styles in the host stratigraphy and metallogenic implications. *Geological Society of Australia, Abstracts* 44: 59.

Rawlings, D.J., 1999. Stratigraphic resolution of a multiphase intracratonic basin system: the McArthur Basin, northern Australia. *Australian Journal of Earth Sciences* 46: 703-723.

Rivera, R.A. and Challis, A., 1972. Summary and interpretation of geophysical surveys, Lady Annie Project area, Queensland. Placer Prospecting (Australia) Ltd. Report no. 14/72 (unpubl.).

Robertson, C.S., 1963. Undilla Basin seismic survey, Queensland, 1961. *Bureau of Mineral Resources Record* 1963/63.

Robinson, W.B., 1968. Geology of the Eastern Creek Volcanics in the Mount Isa district (with discussion). *Proceedings of the Australasian Institute of Mining and Metallurgy* 226: 89-96.

Rogers, J., 1996. Geology and tectonic setting of the Tawallah Group, southern McArthur Basin, Northern Territory. Ph.D. thesis, University of Tasmania (unpubl.).

Rohrlach, B.D., Fu, M. and Clarke, J.D.A., 1996. Geology and paragenesis of the Walford Creek Zn-Pb-Cu-Ag prospect, northern Mount Isa Basin. In Baker, T. et al (eds.), MIC '96: The McArthur, Mt Isa, Cloncurry Minerals Province - New Developments in Metallogenic Research, Extended Conference Abstracts. *EGRU Contribution* 55: 118-122.

Rollinson, H.R., 1993. Using geochemical data: Evaluation, presentation, interpretation. Longman Scientific, Burnt Mill, Harlow, Essex, England. 352 p.

Ryburn, R., Blewett, R.S., Stuart-Smith, P.G. and Williams, P.R., 1993. User's guide to the NGMA Field Data Base. *Australian Geological Survey Organisation Record* 1993/49.

Sami, T., Southgate, P., James, N. and Jackson, J., 1997. An integrated sequence stratigraphic and sedimentological model for the evolution of the lower McNamara succession. NABRE Workshop March 4-5, 1997, Abstracts. *AGSO Record* 1997/12 (unpaginated).

Sanyoto, P., 1990. Structural setting of the McNamara Group in the Yaringa Creek-Big Toby Creek area, Mt. Isa, Queensland, Australia. *Bulletin of the Geological Research and Development Centre (Republic of Indonesia)*14: 17-28.

Scott, K.M. and Taylor, G.F., 1982. Eastern Creek Volcanics as the source of copper at the Mammoth mine, northwest Queensland. *BMR Journal of Australian Geology and Geophysics 7:* 93-98.

Scott, D., Tarlowski, C., Leven, J. and Martin, S., 1997. Basement studies: Current status of models and dataset integration, part 1. NABRE Workshop March 4-5, 1997, Abstracts. *AGSO Record* 1997/12 (unpaginated).

Shalley, M.J. and Harvey, T.V., 1992. Geophysical responses of the HYC deposit. *Exploration Geophysics* 23: 299-304.

Shalley, M., 1997. Early geophysical exploration at Mount Isa, part I: The beginnings. *Preview* 69: 15-19.

Shergold, J.H. and Druce, E.C., 1980. Upper Proterozoic and lower Palaeozoic rocks of the Georgina Basin. In Henderson, R.A. and Stephenson, P.J. (eds.), The Geology and Geophysics of Northeastern Australia. *Geological Society of Australia, Inc., Queensland Division, Brisbane.* p. 149-174.

Shirley, J.E., 1976. Deep Crustal Structure of North Queensland. Ph.D. thesis, University of Tasmania (unpubl.).

Shirley, J.E., 1979. Crustal structure of north Queensland from gravity anomalies. *BMR Journal of Australian Geology and Geophysics* 4: 309-321.

Simpson, E.L. and Eriksson, K.A., 1991. Depositional facies and controls on parasequence development in siliciclastic tidal deposits from the lower Proterozoic, upper Mount Guide Quartzite, Mount Isa Inlier, Australia. In Smith, D.G., Reinson, G.E., Zaitlin, B.A. and Rahmani, R.A. (eds.), Clastic Tidal Sedimentology. *Memoir of the Canadian Society of Petroleum Geologists* 16: 371-387.

Smith, J.W. and Roberts, H.G., 1963. Mount Drummond, N.T. 1:250,000 geological series explanatory notes, sheet E/53-12. Bureau of Mineral Resources, Geology and Geophysics, Canberra. 17p.

Smith, K.G., 1972. Stratigraphy of the Georgina Basin. *Australian Bureau of Mineral Resources Geology and Geophysics Bulletin* 111.

Smith, W.D., 1969. Penecontemporaneous faulting and its likely significance in relation to Mount Isa ore deposition. *Geological Society of Australia Special Publication* 2: 225-235.

Solomon, M. and Heinrich, C.A., 1992. Are high-heat-producing granites essential to the origin of giant lead-zinc deposits at Mount Isa and McArthur River, Australia? *Exploration and Mining Geology* 1: 85-91.

Southgate, P.N., Bradshaw, B.E., Jackson, M.J., Krassay, A.A., McConachie, B.A., Scott, D.L. and Wells, A.T., 1996. Integrated Proterozoic basin analysis: constructing a regional structural and sequence stratigraphic framework for northern Australia. In Baker, T. et al. (eds.), MIC '96: The McArthur, Mt Isa, Cloncurry Minerals Province - New Developments in Metallogenic Research, Extended Conference Abstracts. *EGRU Contribution* 55: 132-136.

Southgate, P.N., Bradshaw, B.E., Domagala, J., Jackson, M.J., Krassay, A.A., Lindsay, J., McConachie, B.A., Sami, T., Scott, D.L. and Wells, A.T., 1997. Basin fill studies: Overview. NABRE Workshop March 4-5, 1997, Abstracts. *AGSO Record* 1997/12 (unpaginated).

Spikings, R.A., Foster, D.A., Gleadow, A.J.W. and Kohn, B.P., 1996. Phanerozoic tectonic and denudational history of the Mt. Isa Inlier, Qld. *Geological Society of Australia, Abstracts* 41: 414. 13th Australian Geological Convention, Canberra.

Stewart, G.A., 1954. Geomorphology of the Barkly region. In Survey of the Barkly Region, Northern Territory and Queensland, 1947-48. *CSIRO Land Research Series* 3: 113-149.

Stewart, H.W.J. and Hoyling, N., 1963.. Morstone No.1 well completion report, Authority to Prospect 79 P - Queensland. Amalgamated Petroleum Exploration Pty. Ltd. (unpubl.).

Sun, S.-s., Page, R.W. and Carr, G.R., 1994. Lead-isotope-based stratigraphic correlation and ages of Proterozoic sediment-hosted Pb-Zn deposits, the Mount Isa inlier: *AGSO Research Newsletter* 20: 1-2.

Sweet, I.P., 1983. Discussion: A Proterozoic rift zone at Mount Isa, Queensland, and implications for mineralisation. *BMR Journal of Australian Geology and Geophysics* 8: 163-164.

Sweet, I.P., Hutton, L.J. and Leggo, N., 1993. Mount Isa Inlier (Western Fold Belt) - Mount Isa Group, McNamara Group and Fickling Group. In *Carpentaria Zinc Belt Geological Excursion, Gulf Region, Queensland and Northern Territory, The Gulf Classic, Excursion Guide* 1: 1-39. AusIMM, Northwest Queensland and Darwin Branches.

Talwani, M., Worzel, J.L. and Landisman, M., 1959. Rapid gravity computation for two-dimensional bodies with applications to the Mendocino submarine fracture zone. *Journal of Geophysical Research* 64: 49-59.

Talwani, M. and Heirtzler, J.R., 1964. Computation of magnetic anomalies caused by two-dimensional structures of arbitrary shape. In Parks, G.A. (ed.), Computers in the Mineral Industries. School of Earth Sciences, Stanford University. p. 464-480.

Taylor, S.R. and McLennan, S.M., 1985. The Continental Crust: Its Composition and Evolution. Blackwell Scientific Publications.

Telford, W.M., Geldart, L.P. and Sheriff, R.E., 1990. *Applied Geophysics* - 2nd edition. Cambridge University Press. 860pp.

Thomas, G., Stolz, E.M. and Mutton, A.J., 1992. Geophysics of the Century zinc-lead-silver deposit, northwest Queensland. *Exploration Geophysics* 23: 361-366.

Tucker, D.H., Wyatt, B.W., Druce, E.C., Mathur, S.P. and Harrison, P.L., 1979. The upper crustal geology of the Georgina Basin region. *BMR Journal of Australian Geology and Geophysics* 4: 209-226.

Twidale, C.R., 1964. Geomorphology of the Leichhardt-Gilbert area. *CSIRO Land Research Series* 11: 115-124.

Valenta, R., 1994. Syntectonic discordant copper mineralization in the Hilton Mine, Mount Isa. *Economic Geology* 89: 1031-1052.

Van Dijk, P.M., 1991. Regional syndeformational copper mineralization in the western Mount Isa Block, Australia. *Economic Geology* 86: 278-301.

Walker, R.N., Logan, R.G. and Binnekamp, J.G., 1977. Recent geological advances concerning the HYC and associated deposits, McArthur River, N.T. *J. Geology Soc. Aust.* 24: 365-380.

Walker, R.N., Gulson, B. and Smith, J., 1983. The Coxco deposit - a Proterozoic Mississippi Valley-type deposit in the McArthur River district, Northern Territory, Australia. *Economic Geology* 78: 214-249.

Waltho, A.E., Allnutt, S.L. and Radojkovic, A.M., 1993. Geology of the Century zinc deposit, northwest Queensland. In Mathew, I.G. (ed.), World Zinc '93 Proceedings. *AusIMM Publication* 7/93: 111-129.

Webb, M. and Rohrlach, B., 1992. The Walford Creek prospect - an exploration overview. *Exploration Geophysics* 23: 407-412.

Wellman, P., 1992a. Structure of the Mount Isa region inferred from gravity and magnetic anomalies. InStewart, A.J. and Blake, D.H. (Eds.), Detailed studies of the Mount Isa Inlier. *BMR Bulletin* 243: 15-27.

Wellman, P., 1992b. Structure of the Mount Isa region inferred from gravity and magnetic anomalies. *Exploration Geophysics* 23: 417-422.

Wells, R., Milsom, J. and Tipper, D.B., 1966. Georgina Basin aeromagnetic survey Queensland and Northern Territory, 1964. *Bureau of Mineral Resources Record* 1966/142 (unpubl.).

Williams, N., 1978a. Studies of the base metal sulphide deposits at McArthur River, Northern Territory, Australia. I: The Cooley and Ridge deposits. *Economic Geology* 73: 1005-1035.

Wilson, I.H., 1978. Volcanism on a Proterozoic continental margin in northwestern Queensland. *Precambrian Research* 7: 205-235.

Wilson, I.H., 1983. Geochemical discrimination of acid volcanic units in the Mount Isa Region, Queensland. *BMR Journal of Australian Geology and Geophysics* 8: 109-117.

Wilson, I.H., Derrick, G.M. and Perkin, D.J., 1985. Eastern Creek Volcanics; their geochemistry and possible role in copper mineralisation at Mount Isa, Queensland. *BMR Journal of Australian Geology and Geophysics* 9: 319-328.

Won, I.J. and Bevis, M., 1987. Computing the gravitational and magnetic anomalies due to a polygon: Algorithms and Fortran subroutines. *Geophysics* 52: 232-238.

Woollard, G.P., 1962. The relation of gravity anomalies to surface elevation, crustal structure and geology. Research Report 62-9 December 1962. University of Wisconsin Geophysical and Polar Research Center (unpubl.).

Wright, D.F. and Bonham-Carter, G.F., 1992. Two case studies for mapping mineral potential using weights-of-evidence modelling: Gold in Meguma Terrane, Nova Scotia and base metals in Snow Lake area, Manitoba. In Geological Applications of Geographic Information Systems (GIS). Australian Institute of Geoscientists Bulletin 12: 83-84.

Wyborn, L.A.I., 1987. The petrology and geochemistry of alteration assemblages in the Eastern Creek Volcanics as a guide to copper and uranium mobility associated with regional metamorphism and deformation, Mount Isa, Queensland. In Pharaoh, T.C., Beckinsale, R.D. and Rickard, D.T. (eds.), Geochemistry and Mineralization of Proterozoic Volcanic Suites. *Geological Society Special Publication* 33: 425-434.

Wyborn, L.A.I., 1988. Petrology, geochemistry and origin of a major Australian 1880-1840 Ma felsic volcano-plutonic suite: a model for intracontinental felsic magma generation. *Precambrian Research* 40/41: 37-60.

Wyborn, L.A.I. and Page, R.W., 1983. The Proterozoic Kalkadoon and Ewen Batholiths, Mount Isa Inlier, Queensland: source, chemistry, age and metamorphism. *BMR Journal of Australian Geology & Geophysics* 8: 53-69.

Wyborn, L.A.I, Page, R.W., and Parker, A.J., 1987. Geochemical and geochronological signatures in Australian Proterozoic igneous rocks. *In* Pharaoh, T.C., Beckinsale, R.D. and Rickard, D. (Eds.), Geochemistry and Mineralisation of Proterozoic Volcanic Suites. *Geological Society Special Publication* 333: 77-394.

Wyborn, L.A.I., Page, R.W., and McCulloch, M.T., 1988. Petrology, geochronology and isotope geochemistry of the post-1820 Ma granites of the Mount Isa Inlier: mechanisms for the generation of Proterozoic anorogenic granites. *Precambrian Research* 40/41: 509-541.

Wyborn, L.A.I., Wyborn, D., Warren, R.G. and Drummond, B.J., 1992. Proterozoic granite types in Australia: implications for lower crust composition, structure and evolution. *Transactions of the Royal Society of Edinburgh: Earth Sciences* 83: 201-209.

Wyborn, L., Gallagher, R. and Raymond, O., 1995a. Creating mineral province GIS packages - issues, problems, solutions and opportunities. Proceedings of the Second National Forum on GIS in the Geosciences. *AGSO Record* 1995/46: 6-24.

Wyborn, L., Gallagher, R. and Mernagh, T., 1995b. Using GIS for mineral potential evaluation in areas with few known mineral occurrences. Proceedings of the Second National Forum on GIS in the Geosciences. *AGSO Record* 1995/46: 199-211.

Young, M.E., 1984. Gravity and magnetic results from Mount Isa district, Australia. *Transactions of the Institute of Mining and Metallurgy* B93: 78-86.

Appendix 1

Primary gravity base station 93709001 description, Lady Loretta mining camp

Portion of Mammoth Mines 1:100,000 topographic map (Edition 1-AAS, 1974)

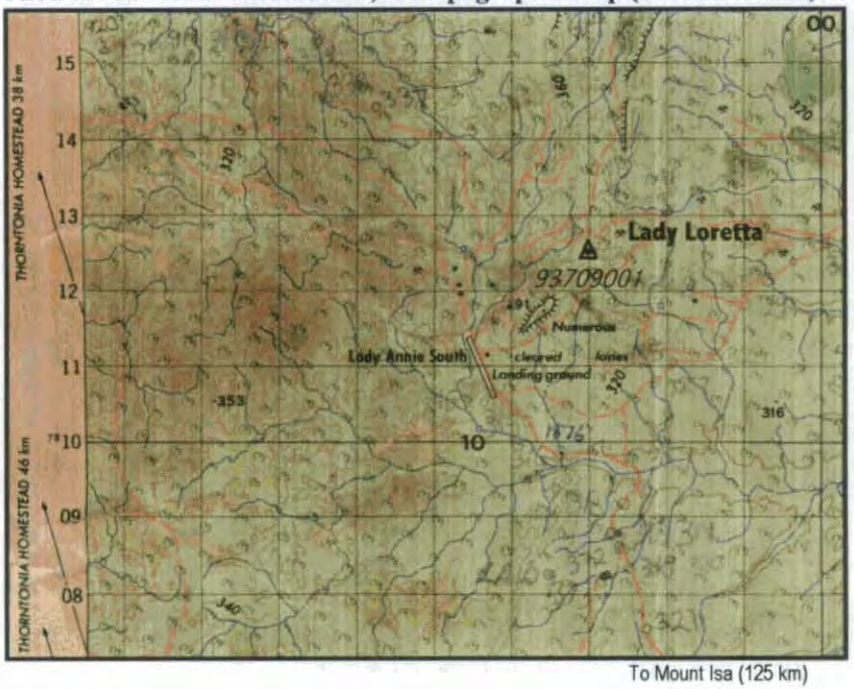

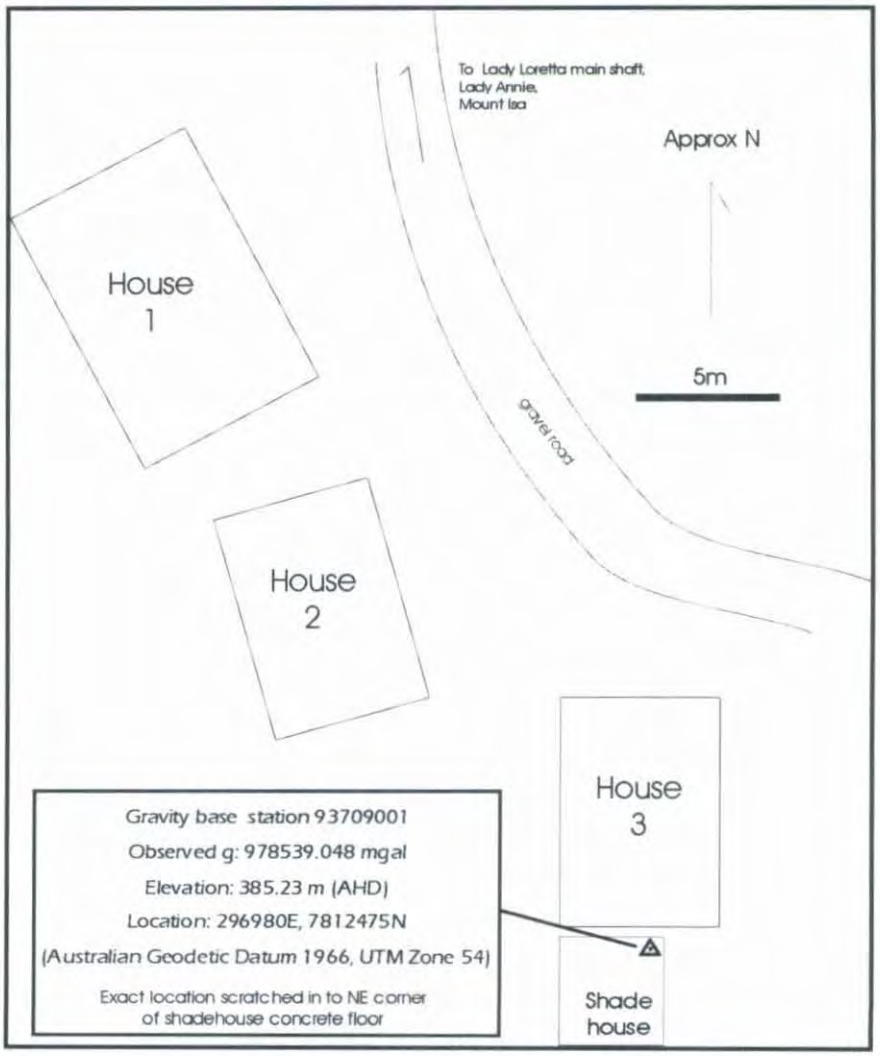

Lady Loretta mining camp schematic map

Appendix 2

Gravity data acquired around Lady Loretta and Paradise Valley 1993 and 1994 field seasons

Column heading abbreviations:

STN_CODE 8-digit unique integer ID comprising concatenation of YR, SVY and STATN

YR 2-digit year

SVY Survey number (70)

STATN 4-digit gravity station field number

ELEV Station elevation in metres above the Australian Height Datum

GOBS Observed gravitational acceleration in milligals

GTHEO Theoretical (GRS67) latitude-corrected gravitational acceleration in milligals

TC Terrain correction in milligals

BOUG Bouguer anomaly value in milligals; Bouguer reduction density 2.67 t/m^3

FLAG Text field usually denoting g-meter model used in station observations. All 1993 stations were observed with a Model G Lacoste & Romberg gravity meter (G-326) hired from Geoterrex; 1994 stations were observed with a Worden gravity meter (W818) hired from the University of Queensland. '93RPT' indicates stations which were observed in both 1993 and 1994; '94RPT' indicates secondary and tertiary base stations in the 1994 survey.

EASTING Zone 54, Universal Transverse Mercator projection on the Australian Geodetic Datum 1966

NORTHING as above

Copies of field notebooks including local terrain descriptions and microbarometric observations at stations are available from the author on request.

STN_CODE	YR	SVY	STATN	ELEV	GOBS	GTHEO	TC	BOUG	FLAG	EASTING	NORTHING
93709001	93	70	9001	385.23	978539.040	978622.948	1.07	-7.00	*LR_G326	296983	7812479
93700486	93	70	486	384.85	978538.570	978623.012	1.04	-7.64	*LR_G326	296993	7812356
93701034	93	70	1034	384.80	978539.860	978622.872	0.82	-6.44	*LR_G326	297013	7812626
93700001	93	70	1	381.60	978539.250	978622.779	0.61	-7.80	*LR_G326	296994	7812806
93700002	93	70	2	378.60	978539.990	978622.707	0.44	-7.75	*LR_G326	297033	7812945
93700003	93	70	3	337.90	978549.320	978622.748	0.25	-6.66	*LR_G326	297367	7812870
93700004	93	70	4	345.20	978548.060	978622.860	0.44	-6.41	*LR_G326	297174	7812652
93700005	93	70	5	345.85	978548.150	978622.867	0.51	-6.13	*LR_G326	297225	7812639
93701037	93	70	1037	376.81	978541.470	978622.909	0.91	-6.35	*LR_G326	297267	7812557
93700006	93	70	6	372.10	978540.860	978622.939	1.12	-7.71	*LR_G326	297348	7812500
93700007	93	70	7	331.00	978550.200	978623.061	0.24	-7.46	*LR_G326	297307	7812265
93700008	93	70	8	386.50	978539.190	978623.008	1.25	-6.48	*LR_G326	297095	7812365
93700009	93	70	9	340.40	978548.500	978622.907	0.24	-7.16	*LR_G326	297527	7812565
93702028	93	70	2028	382.40	978538.320	978623.085	1.53	-7.96	*LR_G326	296760	7812212
93700010	93	70	10	356.10	978544.820	978623.125	0.57	-7.64	*LR_G326	296470	7812132
93701072	93	70	1072	337.92	978548.100	978622.880	0.15	-8.11	*LR_G326	296663	7812607
93700011	93	70	11	344.60	978547.100	978622.963	0.21	-7.82	*LR_G326	296449	7812444
93700012	93	70	12	365.60	978541.940	978622.950	0.98	-8.06	*LR_G326	296712	7812473
93701075	93	70	1075	341.00	978547.750	978622.896	0.39	-7.63	*LR_G326	296746	7812577
93700013	93	70	13	342.80	978547.470	978622.848	0.44	-7.46	*LR_G326	296794	7812670
93701063	93	70	1063	352.40	978545.150	978622.774	0.46	-7.79	*LR_G326	296888	7812814
93700014	93	70	14	343.10	978546.140	978622.742	0.46	-8.60	*LR_G326	296792	7812875
93702030	93	70	2030	376.84	978539.090	978622.718	0.43	-9.02	*LR_G326	296581	7812918
93700015	93	70	15	374.60	978538.780	978622.780	0.52	-9.74	*LR_G326	296483	7812798
93700016	93	70	16	374.60	978539.350	978622.829	0.72	-9.02	*LR_G326	296215	7812701
93700017	93	70	17	354.60	978543.080	978622.679	0.14	-9.66	*LR_G326	296316	7812990
93700018	93	70	18	373.10	978539.280	978622.684	0.81	-9.15	*LR_G326	295923	7812976
93700019	93	70	19	343.10	978546.530	978622.849	0.17	-8.61	*LR_G326	296057	7812660
93700020	93	70	20	351.60	978543.620	978622.957	0.28	-9.84	*LR_G326	295916	7812449
93700021	93	70	21	331.90	978548.880	978623.028	0.07	-8.74	*LR_G326	296048	7812315
93700022	93	70	22	354.60	978544.670	978623.091	0.46	-8.16	*LR_G326	296266	7812195
93700023	93	70	23	331.00	978548.780	978622.906	0.28	-8.69	*LR_G326	296283	7812552
93700024	93	70	24	343.90	978545.710	978622.397	0.33	-8.66	*LR_G326	296575	7813538
93700025	93	70	25	393.60	978534.920	978622.292	0.58	-9.31	*LR_G326	296940	7813743
93700026	93	70	26	366.60	978540.710	978622.271	0.15	-9.24	*LR_G326	297114	7813787
93700027	93	70	27	389.60	978536.370	978622.195	0.55	-8.58	*LR_G326	297309	7813936
93700028	93	70	28	377.10	978538.570	978622.183	0.43	-8.95	*LR_G326	297136	7813956
93700029	93	70	29	383.10	978538.230	978622.146	0.26	-8.24	*LR_G326	296799	7814024
93700030	93	70	30	389.60	978536.370	978622.122	0.58	-8.48	*LR_G326	296549	7814068
93700031	93	70	31	381.10	978538.010	978622.277	0.53	-8.72	*LR_G326	296532	7813768
93700032	93	70	32	346.20	978545.010	978622.271	0.33	-8.78	*LR_G326	296657	7813781
93700033	93	70	33	384.60	978538.140	978622.595	0.52	-8.22	*LR_G326	297077	7813162
93700034	93	70	34	337.60	978548.140	978622.584	0.31	-7.68	*LR_G326	297372	7813185
93700035	93	70	35	383.60	978538.210	978622.392	0.58	-8.09	*LR_G326	297333	7813555
93700036	93	70	36	385.60	978537.650	978622.346	0.42	-8.37	*LR_G326	297359	7813645
93700037	93	70	37	386.10	978537.520	978622.464	0.38	-8.56	*LR_G326	296919	7813412
93700038	93	70	38	366.10	978541.430	978622.435	0.50	-8.44	*LR_G326	296695	7813465
93700039	93	70	39	379.10	978538.000	978622.550	0.87	-9.05	*LR_G326	296488	7813241
93700040	93	70	40	382.60	978537.990	978622.519	0.41	-8.80	*LR_G326	296692	7813304
93702039	93	70	2039	381.64	978538.390	978622.551	0.25	-8.78	*LR_G326	296878	7813244
93700041	93	70	41	319.70	978551.970	978623.194	0.08	-8.21	*LR_G326	297924	7812015
93700042	93	70	42	327.10	978550.260	978623.211	0.11	-8.45	*LR_G326	298218	7811987
93700043	93	70	43	308.60	978554.350	978623.406	0.07	-8.24	*LR_G326	298212	7811610
93700044	93	70	44	309.80	978554.150	978623.351	0.21	-8.01	*LR_G326	297898	7811713
93705045	93	70	5045	310.60	978553.990	978623.323	0.27	-7.92	*LR_G326	297767	7811765
93700048	93	70	48	329.20	978550.030	978623.181	0.13	-8.22	*LR_G326	296953	7812029
93700049	93	70	49	332.20	978549.030	978623.164	0.68	-8.06	*LR_G326	296767	7812060
93702025	93	70	2025	379.81	978538.900	978623.236	1.50	-8.07	*LR_G326	296402	7811917
93700050	93	70	50	384.60	978537.790	978623.303	1.68	-8.12	*LR_G326	296468	7811790
93700051	93	70	51	324.00	978551.210	978623.357	0.25	-8.12	*LR_G326	296647	7811688
93700052	93	70	52	330.10	978550.260	978623.228	0.07	-7.92	*LR_G326	297076	7811941
93700053	93	70	53	325.50	978552.010	978623.278	0.05	-7.14	*LR_G326	297172	7811845
93700054	93	70	54	326.10	978551.350	978623.394	0.05	-7.80	*LR_G326	297143	7811622
93700055	93	70	55	330.10	978550.680	978623.300	0.05	-7.59	*LR_G326	297064	7811801
93700056	93	70	56	325.20	978550.870	978623.458	0.12	-8.45	*LR_G326	296486	7811490

STN_CODE	YR	SVY	STATN	ELEV	GOBS	GTHEO	TC	BOUG	FLAG	EASTING	NORTHING
93700057	93	70	57	315.80	978553.750	978623.457	0.17	-7.37	*LR_G326	296766	7811495
93700058	93	70	58	320.40	978553.150	978623.456	0.06	-7.18	*LR_G326	296976	7811500
93700059	93	70	59	317.50	978554.250	978623.541	0.09	-6.70	*LR_G326	297161	7811339
93700060	93	70	60	321.10	978552.900	978623.563	0.03	-7.42	*LR_G326	297365	7811299
93700061	93	70	61	314.10	978554.150	978623.608	0.14	-7.49	*LR_G326	296965	7811208
93700062	93	70	62	311.80	978554.310	978623.641	0.11	-7.84	*LR_G326	296729	7811140
93700063	93	70	63	322.10	978551.810	978623.589	0.04	-8.33	*LR_G326	296479	7811239
93700065	93	70	65	321.50	978551.130	978623.476	0.31	-8.75	*LR_G326	296282	7811453
93700066	93	70	66	313.30	978552.780	978623.617	0.11	-9.05	*LR_G326	296298	7811182
93700067	93	70	67	319.60	978551.270	978623.567	0.21	-9.17	*LR_G326	296058	7811275
93700068	93	70	68	318.00	978552.230	978623.600	0.07	-8.70	*LR_G326	295747	7811208
93700069	93	70	69	317.50	978553.120	978623.594	0.04	-7.94	*LR_G326	295536	7811217
93700070	93	70	70	321.10	978552.020	978623.450	0.06	-8.16	*LR_G326	295454	7811495
93700071	93	70	71	339.60	978547.660	978623.482	0.50	-8.47	*LR_G326	295702	7811436
93700072	93	70	72	341.60	978546.990	978623.420	0.46	-8.73	*LR_G326	295978	7811559
93700073	93	70	73	327.10	978550.130	978623.183	0.04	-8.62	*LR_G326	295642	7812011
93700074	93	70	74	327.60	978550.070	978623.244	0.05	-8.64	*LR_G326	295574	7811893
93700075	93	70	75	317.80	978552.780	978623.342	0.08	-7.92	*LR_G326	295470	7811703
93700076	93	70	76	336.10	978548.000	978623.350	0.31	-8.88	*LR_G326	295751	7811690
93700077	93	70	77	328.30	978550.870	978623.311	0.23	-7.59	*LR_G326	296039	7811769
93700078	93	70	78	384.10	978537.830	978623.376	1.67	-8.27	*LR_G326	296218	7811645
93700079	93	70	79	326.40	978550.930	978623.220	0.07	-7.97	*LR_G326	296072	7811945
93701147	93	70	1147	333.90	978550.010	978623.232	0.23	-7.26	*LR_G326	296176	7811922
93700080	93	70	80	327.10	978549.700	978622.818	0.04	-8.69	*LR_G326	295490	7812713
93700081	93	70	81	328.00	978548.840	978622.830	0.04	-9.38	*LR_G326	295363	7812688
93700082	93	70	82	327.70	978548.810	978622.827	0.03	-9.48	*LR_G326	295054	7812691
93700083	93	70	83	342.60	978545.930	978622.638	0.13	-9.14	*LR_G326	295065	7813055
93700084	93	70	84	344.60	978544.680	978622.624	0.43	-9.68	*LR_G326	295283	7813085
93700085	93	70	85	330.60	978548.470	978622.747	0.03	-9.17	*LR_G326	295301	7812848
93700086	93	70	86	333.40	978548.550	978622.641	0.10	-8.36	*LR_G326	295533	7813054
93700087	93	70	87	347.10	978544.290	978622.668	0.32	-9.73	*LR_G326	295673	7813004
93702011	93	70	2011	347.89	978544.310	978622.805	0.54	-9.47	*LR_G326	295677	7812741
93700088	93	70	88	342.60	978546.130	978622.967	0.06	-9.34	*LR_G326	294938	7812420
93701011	93	70	1011	360.60	978542.650	978623.092	0.57	-8.89	*LR_G326	294989	7812179
93700089	93	70	89	342.00	978546.980	978623.094	0.42	-8.37	*LR_G326	295366	7812179
93700090	93	70	90	333.60	978548.630	978622.958	0.04	-8.62	*LR_G326	295329	7812441
93700091	93	70	91	326.50	978549.630	978622.906	0.05	-8.95	*LR_G326	295553	7812544
93700092	93	70	92	327.70	978549.240	978622.913	0.08	-9.09	*LR_G326	295726	7812532
93702016	93	70	2016	346.76	978544.620	978623.041	0.51	-9.65	*LR_G326	295713	7812285
93700093	93	70	93	330.60	978548.310	978623.047	0.13	-9.53	*LR_G326	295575	7812273
93700094	93	70	94	333.10	978547.390	978622.212	0.15	-9.10	*LR_G326	295539	7813883
93700095	93	70	95	340.10	978546.000	978622.146	0.20	-9.00	*LR_G326	295656	7814011
93700096	93	70	96	354.10	978542.780	978622.174	0.34	-9.35	*LR_G326	295876	7813960
93700097	93	70	97	381.60	978537.630	978622.238	0.59	-8.90	*LR_G326	296221	7813840
93700098	93	70	98	387.10	978536.790	978622.180	0.44	-8.75	*LR_G326	296357	7813954
93700099	93	70	99	350.60	978543.920	978622.344	0.15	-9.26	*LR_G326	296173	7813634
93700100	93	70	100	339.60	978546.040	978622.278	0.18	-9.21	*LR_G326	295972	7813759
93700101	93	70	101	354.60	978542.820	978622.296	0.35	-9.32	*LR_G326	295624	7813721
93700102	93	70	102	333.00	978547.660	978622.285	0.15	-8.92	*LR_G326	295412	7813739
93700103	93	70	103	348.60	978544.250	978622.405	0.10	-9.43	*LR_G326	296017	7813515
93700104	93	70	104	357.60	978541.780	978622.429	0.30	-9.96	*LR_G326	296162	7813470
93700105	93	70	105	341.00	978545.950	978622.578	0.17	-9.33	*LR_G326	296215	7813184
93700106	93	70	106	348.60	978544.770	978622.593	0.20	-9.00	*LR_G326	295888	7813151
93700107	93	70	107	369.10	978540.040	978622.516	0.46	-9.36	*LR_G326	295782	7813298
93700108	93	70	108	351.60	978543.560	978622.443	0.12	-9.55	*LR_G326	295702	7813439
93700109	93	70	109	351.60	978542.760	978622.427	0.18	-10.27	*LR_G326	295526	7813467
93702009	93	70	2009	352.46	978543.370	978622.563	0.68	-9.13	*LR_G326	295473	7813205
93700110	93	70	110	329.60	978550.490	978623.073	0.07	-7.63	*LR_G326	298052	7812250
93700111	93	70	111	319.00	978552.650	978623.092	0.09	-7.56	*LR_G326	298333	7812218
93700112	93	70	112	322.40	978552.020	978623.008	0.13	-7.39	*LR_G326	298309	7812379
93700113	93	70	113	338.60	978548.660	978622.978	0.20	-7.46	*LR_G326	298099	7812435
93700114	93	70	114	331.30	978550.680	978622.910	0.11	-6.90	*LR_G326	297819	7812562
93700115	93	70	115	324.50	978552.120	978623.089	0.15	-6.94	*LR_G326	297572	7812215
93700116	93	70	116	322.60	978552.660	978623.087	0.10	-6.82	*LR_G326	297839	7812221
93700117	93	70	117	339.10	978548.640	978622.731	0.37	-6.97	*LR_G326	298172	7812911

STN_CODE	YR	SVY	STATN	ELEV	GOBS	GTHEO	TC	BOUG	FLAG	EASTING	NORTHING
93700118	93	70	118	342.10	978547.990	978622.877	0.15	-7.40	*LR_G326	298167	7812629
93700119	93	70	119	335.00	978549.910	978622.820	0.18	-6.79	*LR_G326	297887	7812736
93700120	93	70	120	333.00	978550.620	978622.752	0.10	-6.48	*LR_G326	298039	7812870
93701115	93	70	1115	362.06	978543.990	978622.706	0.46	-6.98	*LR_G326	297673	7812954
93701118	93	70	1118	338.83	978548.670	978622.662	0.52	-6.77	*LR_G326	297597	7813037
93701109	93	70	1109	345.91	978547.780	978622.788	0.43	-6.49	*LR_G326	297501	7812793
93702036	93	70	2036	379.44	978539.440	978622.794	1.19	-7.47	*LR_G326	297663	7812784
93700121	93	70	121	313.10	978553.670	978623.938	0.01	-8.63	*LR_G326	296026	7810560
93700122	93	70	122	312.03	978554.000	978624.048	0.01	-8.62	*LR_G326	296023	7810349
93700123	93	70	123	314.60	978553.420	978624.048	0.01	-8.69	*LR_G326	295898	7810347
93700124	93	70	124	312.60	978554.110	978624.064	0.01	-8.41	*LR_G326	296199	7810319
93700125	93	70	125	307.90	978555.010	978623.958	0.05	-8.29	*LR_G326	296327	7810526
93700126	93	70	126	311.60	978553.460	978623.858	0.02	-9.04	*LR_G326	296017	7810715
93700127	93	70	127	307.10	978554.520	978623.832	0.06	-8.80	*LR_G326	296247	7810768
93700128	93	70	128	309.90	978553.100	978623.696	0.13	-9.46	*LR_G326	296271	7811029
93700129	93	70	129	311.60	978552.850	978623.773	0.03	-9.55	*LR_G326	296106	7810880
93700130	93	70	130	314.60	978553.200	978624.008	0.01	-8.87	*LR_G326	295781	7810423
93702018	93	70	2018	331.20	978549.520	978623.914	0.31	-8.89	*LR_G326	295595	7810601
93700131	93	70	131	318.60	978552.330	978623.791	0.02	-8.73	*LR_G326	295596	7810838
93700132	93	70	132	326.60	978551.090	978623.805	0.14	-8.28	*LR_G326	295483	7810811
93700133	93	70	133	318.10	978552.780	978623.694	0.07	-8.23	*LR_G326	295584	7811026
93700134	93	70	134	320.60	978551.550	978623.717	0.05	-9.01	*LR_G326	295849	7810984
93700135	93	70	135	342.10	978547.590	978622.576	0.64	-7.00	*LR_G326	298344	7813212
93700136	93	70	136	329.66	978551.500	978622.452	0.36	-5.70	*LR_G326	298086	7813448
93700137	93	70	137	337.10	978549.480	978622.401	0.19	-6.37	*LR_G326	298345	7813550
93700138	93	70	138	359.60	978544.130	978622.265	0.32	-7.03	*LR_G326	298281	7813811
93700139	93	70	139	333.70	978549.240	978622.129	1.00	-6.20	*LR_G326	298214	7814072
93700140	93	70	140	362.90	978543.190	978622.141	0.62	-6.89	*LR_G326	298006	7814047
93700141	93	70	141	380.80	978539.780	978622.354	0.32	-7.29	*LR_G326	297811	7813635
93700142	93	70	142	378.10	978540.600	978622.457	0.62	-6.81	*LR_G326	297906	7813437
93700143	93	70	143	332.80	978549.620	978622.553	0.58	-6.84	*LR_G326	297918	7813251
93701137	93	70	1137	334.60	978548.540	978622.622	0.55	-7.67	*LR_G326	297454	7813113
93702038	93	70	2038	380.99	978539.390	978622.477	0.50	-7.59	*LR_G326	297517	7813393
93700144	93	70	144	385.10	978538.720	978622.411	0.38	-7.50	*LR_G326	297585	7813521
93700145	93	70	145	381.60	978539.360	978622.366	0.28	-7.61	*LR_G326	297631	7813609
93700146	93	70	146	378.10	978540.600	978622.361	0.37	-6.96	*LR_G326	297893	7813621
93700147	93	70	147	390.10	978537.290	978622.228	0.34	-7.81	*LR_G326	297655	7813876
93700148	93	70	148	386.60	978537.070	978622.164	0.58	-8.41	*LR_G326	297459	7813997
93700149	93	70	149	378.10	978539.200	978622.282	0.21	-8.44	*LR_G326	297406	7813768
93700150	93	70	150	343.94	978547.340	978622.589	0.35	-7.19	*LR_G326	297778	7813180
93701042	93	70	1042	323.80	978550.390	978623.201	0.06	-9.01	*LR_G326	295333	7811972
93700151	93	70	151	357.10	978543.720	978623.204	0.37	-8.82	*LR_G326	295029	7811964
93700152	93	70	152	327.10	978550.420	978623.331	0.05	-8.47	*LR_G326	295112	7811719
93700153	93	70	153	330.38	978549.750	978623.375	0.05	-8.54	*LR_G326	294922	7811633
93700154	93	70	154	327.60	978550.470	978623.476	0.03	-8.49	*LR_G326	295078	7811439
93700155	93	70	155	326.60	978551.110	978623.543	0.06	-8.08	*LR_G326	295130	7811311
93700156	93	70	156	324.10	978551.430	978623.555	0.03	-8.30	*LR_G326	295262	7811290
93700157	93	70	157	318.60	978552.950	978623.399	0.06	-7.67	*LR_G326	295246	7811590
93700158	93	70	158	321.90	978552.200	978623.306	0.04	-7.70	*LR_G326	295318	7811771
93700159	93	70	159	365.10	978539.960	978622.289	0.62	-9.84	*LR_G326	295274	7813731
93700160	93	70	160	351.60	978541.590	978622.135	1.39	-9.94	*LR_G326	295179	7814027
93700161	93	70	161	359.10	978540.310	978622.202	0.58	-10.62	*LR_G326	294967	7813895
93700162	93	70	162	354.10	978541.750	978622.307	0.28	-10.57	*LR_G326	294916	7813692
93700163	93	70	163	354.60	978542.490	978622.451	0.18	-9.98	*LR_G326	295045	7813415
93700164	93	70	164	348.60	978544.120	978622.527	0.17	-9.61	*LR_G326	295028	7813269
93700165	93	70	165	349.10	978543.740	978622.525	0.23	-9.83	*LR_G326	295190	7813275
93700166	93	70	166	366.60	978540.030	978622.387	0.38	-9.81	*LR_G326	295173	7813540
93700167	93	70	167	320.60	978552.810	978624.066	0.06	-8.09	*LR_G326	296639	7810320
93700168	93	70	168	315.60	978553.980	978623.994	0.05	-7.84	*LR_G326	296749	7810460
93700169	93	70	169	321.10	978552.620	978623.826	0.05	-7.95	*LR_G326	296860	7810786
93700170	93	70	170	306.90	978554.920	978623.704	0.19	-8.18	*LR_G326	296713	7811019
93700171	93	70	171	320.60	978551.700	978623.742	0.07	-8.86	*LR_G326	296377	7810942
93700172	93	70	172	312.60	978554.250	978623.850	0.02	-8.05	*LR_G326	296577	7810736
93700173	93	70	173	312.10	978554.270	978623.911	0.02	-8.18	*LR_G326	296471	7810618
93700174	93	70	174	317.60	978552.770	978624.083	0.03	-8.76	*LR_G326	296859	7810290

STN_CODE	YR	SVY	STATN	ELEV	GOBS	GTHEO	TC	BOUG	FLAG	EASTING	NORTHING
93700175	93	70	175	342.60	978547.350	978623.883	0.43	-8.66	*LR_G326	297156	7810680
93700176	93	70	176	337.10	978548.620	978623.803	0.26	-8.57	*LR_G326	297192	7810834
93702006	93	70	2006	328.69	978550.340	978623.730	0.16	-8.53	*LR_G326	297181	7810974
93700177	93	70	177	322.00	978553.070	978623.729	0.03	-7.24	*LR_G326	297011	7810975
93700178	93	70	178	330.60	978550.000	978623.670	0.11	-8.48	*LR_G326	297418	7811092
93700181	93	70	181	315.10	978553.920	978624.018	0.05	-8.02	*LR_G326	297317	7810421
93700182	93	70	182	313.10	978554.240	978624.075	0.03	-8.17	*LR_G326	297333	7810311
93700183	93	70	183	315.60	978553.430	978623.950	0.16	-8.23	*LR_G326	297582	7810555
93700184	93	70	184	317.10	978552.790	978623.966	0.15	-8.61	*LR_G326	297694	7810525
93700185	93	70	185	314.60	978553.440	978623.696	0.04	-8.29	*LR_G326	298090	7811050
93700186	93	70	186	324.10	978551.490	978623.606	0.08	-8.24	*LR_G326	297638	7811219
93700187	93	70	187	320.60	978552.560	978623.513	0.02	-7.82	*LR_G326	297633	7811397
93700188	93	70	188	322.10	978552.350	978623.425	0.01	-7.66	*LR_G326	297519	7811567
93700189	93	70	189	327.10	978551.280	978623.429	0.12	-7.64	*LR_G326	297679	7811561
93700190	93	70	190	313.30	978554.220	978623.808	0.03	-7.89	*LR_G326	295320	7810803
93700191	93	70	191	315.60	978553.660	978623.792	0.02	-7.99	*LR_G326	295054	7810830
93700192	93	70	192	318.60	978553.520	978623.850	0.02	-7.59	*LR_G326	295139	7810719
93700193	93	70	193	316.60	978553.780	978623.963	0.02	-7.84	*LR_G326	295082	7810501
93700194	93	70	194	317.60	978553.400	978624.071	0.02	-8.13	*LR_G326	295086	7810293
93700195	93	70	195	315.60	978553.380	978624.046	0.02	-8.52	*LR_G326	295341	7810345
93700196	93	70	196	313.10	978554.020	978623.923	0.14	-8.13	*LR_G326	295390	7810583
93700197	93	70	197	303.50	978555.850	978623.089	0.10	-7.40	*LR_G326	299250	7812234
93700200	93	70	200	350.00	978546.350	978622.722	0.47	-7.00	*LR_G326	298428	7812931
93700201	93	70	201	339.00	978548.340	978622.824	0.14	-7.61	*LR_G326	298583	7812737
93700202	93	70	202	334.00	978549.770	978622.916	0.08	-7.32	*LR_G326	298647	7812560
93700203	93	70	203	333.00	978549.580	978623.043	0.10	-7.81	*LR_G326	298635	7812315
93700204	93	70	204	329.00	978550.480	978623.125	0.13	-7.75	*LR_G326	298900	7812160
93700205	93	70	205	337.90	978548.700	978622.710	0.23	-7.26	*LR_G326	298655	7812958
93700206	93	70	206	328.20	978550.500	978622.876	0.05	-7.72	*LR_G326	298949	7812641
93700207	93	70	207	312.03	978555.050	978623.051	0.01	-6.57	*LR_G326	299630	7812310
93700208	93	70	208	310.00	978555.960	978623.056	0.01	-6.06	*LR_G326	299884	7812305
93700209	93	70	209	312.10	978555.300	978623.223	0.02	-6.47	*LR_G326	299838	7811982
93700210	93	70	210	309.00	978555.950	978623.174	0.01	-6.39	*LR_G326	299762	7812076
93700211	93	70	211	321.00	978552.680	978622.732	0.21	-6.65	*LR_G326	299772	7812928
93700212	93	70	212	328.00	978550.970	978622.688	0.05	-7.10	*LR_G326	298770	7813001
93700213	93	70	213	338.00	978548.410	978622.630	0.29	-7.39	*LR_G326	298945	7813115
93700214	93	70	214	318.00	978553.110	978622.613	0.03	-6.88	*LR_G326	299281	7813152
93700215	93	70	215	332.20	978549.940	978622.512	0.44	-6.74	*LR_G326	299360	7813348
93700216	93	70	216	312.00	978554.210	978622.482	0.13	-6.73	*LR_G326	299173	7813402
93700217	93	70	217	318.00	978553.040	978622.509	0.12	-6.75	*LR_G326	298675	7813345
93700218	93	70	218	321.80	978552.310	978622.384	0.08	-6.65	*LR_G326	298724	7813586
93700219	93	70	219	326.60	978550.850	978622.302	0.11	-7.05	*LR_G326	298798	7813746
93700220	93	70	220	320.10	978552.370	978622.349	0.08	-6.89	*LR_G326	298855	7813655
93700221	93	70	221	324.50	978550.990	978622.346	0.09	-7.39	*LR_G326	298999	7813664
93700222	93	70	222	329.00	978550.390	978622.351	0.16	-7.04	*LR_G326	299116	7813654
93700223	93	70	223	329.00	978550.840	978622.231	0.20	-6.43	*LR_G326	299405	7813890
93700224	93	70	224	320.70	978552.360	978622.318	0.29	-6.54	*LR_G326	299640	7813725
93700225	93	70	225	330.70	978550.280	978622.519	0.24	-6.90	*LR_G326	299710	7813338
93700226	93	70	226	328.60	978551.010	978622.284	0.11	-6.48	*LR_G326	299895	7813793
93700227	93	70	227	328.00	978552.350	978622.156	0.05	-5.19	*LR_G326	299963	7814041
93700228	93	70	228	332.00	978550.490	978622.129	0.12	-6.16	*LR_G326	299653	7814090
93700229	93	70	229	313.00	978555.020	978622.126	0.07	-5.42	*LR_G326	299484	7814093
93700230	93	70	230	318.00	978553.350	978622.137	0.05	-6.14	*LR_G326	299110	7814068
93700231	93	70	231	343.00	978547.730	978622.073	0.33	-6.49	*LR_G326	298468	7814183
93700232	93	70	232	350.00	978545.690	978622.001	0.52	-6.89	*LR_G326	298660	7814325
93700233	93	70	233	343.00	978547.070	978621.864	0.45	-6.82	*LR_G326	298756	7814590
93700234	93	70	234	361.00	978544.000	978621.742	0.32	-6.36	*LR_G326	298481	7814822
93700235	93	70	235	349.00	978546.280	978621.712	0.30	-6.43	*LR_G326	298884	7814885
93700236	93	70	236	347.00	978546.100	978621.618	0.19	-7.02	*LR_G326	298854	7815066
93700237	93	70	237	365.00	978542.390	978621.635	0.52	-6.87	*LR_G326	298560	7815030
93700238	93	70	238	343.00	978546.990	978621.401	0.23	-6.66	*LR_G326	298974	7815486
93700239	93	70	239	336.00	978549.200	978621.471	0.07	-6.06	*LR_G326	299125	7815352
93700240	93	70	240	341.00	978547.410	978621.516	0.20	-6.78	*LR_G326	298836	7815263
93700241	93	70	241	339.00	978547.760	978621.435	0.13	-6.81	*LR_G326	298770	7815419
93700242	93	70	242	329.00	978550.320	978621.265	0.14	-6.04	*LR_G326	299025	7815750

STN_CODE	YR	SVY	STATN	ELEV	GOBS	GTHEO	TC	BOUG	FLAG	EASTING	NORTHING
93700243	93	70	243	338.00	978548.260	978621.309	0.22	-6.29	*LR_G326	299172	7815666
93700244	93	70	244	338.50	978548.320	978621.309	0.20	-6.16	*LR_G326	299496	7815670
93700245	93	70	245	316.00	978554.220	978621.152	0.04	-4.69	*LR_G326	299845	7815977
93700246	93	70	246	337.00	978548.750	978621.406	0.21	-6.11	*LR_G326	299790	7815486
93700247	93	70	247	326.00	978551.660	978621.560	0.04	-5.69	*LR_G326	299445	7815185
93700248	93	70	248	337.00	978549.200	978621.532	0.10	-5.89	*LR_G326	299659	7815242
93700249	93	70	249	339.00	978549.130	978621.806	0.17	-5.77	*LR_G326	299851	7814715
93700250	93	70	250	322.00	978553.500	978622.054	0.03	-5.14	*LR_G326	299952	7814237
93700251	93	70	251	318.00	978553.970	978621.938	0.03	-5.34	*LR_G326	299411	7814455
93700252	93	70	252	387.00	978536.860	978622.038	0.36	-8.64	*LR_G326	297495	7814241
93700253	93	70	253	389.00	978537.510	978622.064	0.30	-7.68	*LR_G326	297747	7814193
93700254	93	70	254	383.00	978537.830	978621.895	0.21	-8.46	*LR_G326	297631	7814518
93700255	93	70	255	383.00	978538.900	978621.649	0.27	-7.08	*LR_G326	297975	7814996
93700256	93	70	256	378.00	978540.060	978621.719	0.42	-6.83	*LR_G326	298250	7814865
93700257	93	70	257	387.00	978536.720	978621.623	0.40	-8.32	*LR_G326	297701	7815044
93700258	93	70	258	389.00	978535.980	978621.431	0.43	-8.44	*LR_G326	297863	7815416
93700259	93	70	259	384.00	978537.210	978621.419	0.26	-8.36	*LR_G326	298094	7815441
93700260	93	70	260	386.00	978537.530	978621.465	0.36	-7.59	*LR_G326	298220	7815355
93700261	93	70	261	384.00	978537.970	978621.373	0.39	-7.42	*LR_G326	298394	7815533
93700262	93	70	262	386.00	978536.530	978621.164	0.54	-8.11	*LR_G326	298000	7815933
93700263	93	70	263	363.00	978539.570	978621.191	0.52	-9.64	*LR_G326	297740	7815878
93700264	93	70	264	341.00	978543.330	978621.156	0.07	-10.63	*LR_G326	297410	7815941
93700265	93	70	265	339.00	978542.350	978621.152	0.10	-11.97	*LR_G326	297186	7815946
93700266	93	70	266	347.00	978541.640	978621.351	0.07	-11.33	*LR_G326	297036	7815560
93700267	93	70	267	353.00	978540.760	978621.368	0.13	-10.99	*LR_G326	297267	7815531
93700268	93	70	268	365.00	978539.720	978621.621	0.28	-9.77	*LR_G326	297076	7815040
93700269	93	70	269	363.00	978540.280	978621.678	0.13	-9.81	*LR_G326	296987	7814930
93700270	93	70	270	379.00	978535.470	978621.625	0.61	-10.94	*LR_G326	296915	7815031
93700271	93	70	271	379.00	978536.100	978621.679	0.77	-10.20	*LR_G326	296830	7814925
93700272	93	70	272	361.00	978540.810	978621.695	0.11	-9.71	*LR_G326	296678	7814893
93700273	93	70	273	353.00	978541.780	978621.602	0.28	-10.05	*LR_G326	296615	7815072
93700274	93	70	274	367.00	978539.620	978621.814	0.28	-9.67	*LR_G326	296859	7814665
93700275	93	70	275	370.90	978538.750	978621.872	0.46	-9.65	*LR_G326	296862	7814553
93700276	93	70	276	351.00	978543.410	978621.894	0.11	-9.28	*LR_G326	297103	7814514
93700277	93	70	277	354.00	978543.980	978621.996	0.15	-8.18	*LR_G326	297209	7814319
93700278	93	70	278	377.00	978539.580	978622.042	0.32	-7.93	*LR_G326	297062	7814228
93700279	93	70	279	383.00	978538.280	978621.796	0.29	-7.83	*LR_G326	295969	7814689
93700280	93	70	280	389.00	978537.380	978621.718	0.31	-7.45	*LR_G326	296029	7814840
93700281	93	70	281	389.00	978536.320	978621.663	0.25	-8.52	*LR_G326	296296	7814950
93700282	93	70	282	389.00	978536.470	978621.757	0.35	-8.36	*LR_G326	296388	7814770
93700283	93	70	283	379.20	978538.690	978621.861	0.39	-8.13	*LR_G326	296175	7814567
93700284	93	70	284	375.60	978539.640	978621.941	0.38	-7.98	*LR_G326	296151	7814413
93700285	93	70	285	394.00	978535.180	978622.035	0.50	-8.79	*LR_G326	296497	7814235
93700286	93	70	286	394.00	978535.080	978621.918	0.47	-8.81	*LR_G326	296456	7814460
93700287	93	70	287	394.00	978535.020	978621.492	0.33	-8.58	*LR_G326	296245	7815279
93700288	93	70	288	388.10	978535.350	978621.363	0.40	-9.21	*LR_G326	296440	7815530
93700289	93	70	289	391.00	978534.350	978621.216	0.61	-9.29	*LR_G326	296474	7815814
93700290	93	70	290	381.00	978536.840	978621.267	0.19	-9.24	*LR_G326	296295	7815715
93700291	93	70	291	366.00	978540.510	978621.200	0.17	-8.47	*LR_G326	295822	7815839
93700292	93	70	292	384.00	978536.940	978621.167	0.54	-8.10	*LR_G326	295708	7815900
93700293	93	70	293	388.00	978536.460	978621.330	0.35	-8.14	*LR_G326	295630	7815585
93700294	93	70	294	388.00	978536.590	978621.462	0.29	-8.20	*LR_G326	295717	7815332
93700295	93	70	295	391.00	978536.500	978621.556	0.25	-7.84	*LR_G326	295917	7815152
93700296	93	70	296	387.00	978536.950	978621.940	0.49	-8.32	*LR_G326	295810	7814411
93700297	93	70	297	388.00	978536.740	978621.810	0.46	-8.23	*LR_G326	295694	7814660
93700298	93	70	298	389.00	978536.710	978621.696	0.29	-8.12	*LR_G326	295750	7814880
93700299	93	70	299	378.20	978538.640	978621.526	0.25	-8.19	*LR_G326	295466	7815205
93700300	93	70	300	386.00	978536.570	978621.536	0.60	-8.38	*LR_G326	295332	7815184
93700301	93	70	301	368.00	978539.370	978621.551	0.48	-9.26	*LR_G326	295201	7815154
93700302	93	70	302	351.00	978543.280	978621.877	0.38	-9.12	*LR_G326	295221	7814525
93700303	93	70	303	337.80	978545.920	978621.984	0.28	-9.29	*LR_G326	295522	7814321
93700304	93	70	304	360.00	978541.220	978622.055	0.86	-9.11	*LR_G326	295400	7814184
93700305	93	70	305	326.60	978549.130	978622.121	0.19	-8.51	*LR_G326	295276	7814055
93700306	93	70	306	325.00	978547.820	978622.048	0.11	-10.14	*LR_G326	295055	7814193
93703065	93	70	3065	351.00	978543.270	978621.907	0.31	-9.23	*LR_G326	294990	7814465

STN_CODE	YR	SVY	STATN	ELEV	GOBS	GTHEO	TC	BOUG	FLAG	EASTING	NORTHING
93700307	93	70	307	350.00	978543.660	978621.885	0.41	-8.92	*LR_G326	295020	7814507
93700308	93	70	308	337.00	978546.700	978621.905	0.12	-8.75	*LR_G326	295109	7814470
93700309	93	70	309	327.00	978548.280	978621.793	0.33	-8.81	*LR_G326	295257	7814688
93700310	93	70	310	323.00	978549.410	978621.801	0.36	-8.45	*LR_G326	295050	7814670
93700311	93	70	311	373.90	978537.860	978621.635	0.79	-9.38	*LR_G326	295128	7814990
93700312	93	70	312	368.20	978538.690	978621.545	0.89	-9.48	*LR_G326	295104	7815164
93700313	93	70	313	333.50	978545.950	978621.414	0.20	-9.61	*LR_G326	295003	7815416
93702001	93	70	2001	320.53	978553.080	978623.242	0.06	-7.01	*LR_G326	297593	7811919
93700047	93	70	47	324.10	978552.360	978623.175	0.07	-6.95	*LR_G326	297513	7812047
93700046	93	70	46	329.60	978550.290	978623.370	0.15	-8.05	*LR_G326	297382	7811671
93700045	93	70	45	315.19	978552.880	978623.319	0.10	-8.29	*LR_G326	297872	7811774
93701002	93	70	1002	328.50	978550.760	978623.371	0.15	-7.80	*LR_G326	295802	7811650
93701149	93	70	1149	337.50	978549.240	978623.107	0.15	-7.28	*LR_G326	296367	7812166
93701151	93	70	1151	335.60	978549.070	978623.056	0.10	-7.82	*LR_G326	296454	7812265
93701126	93	70	1126	337.01	978548.630	978623.024	0.20	-7.85	*LR_G326	296591	7812329
93703095	93	70	3095	345.30	978546.670	978622.774	0.28	-7.85	*LR_G326	296824	7812814
93703102	93	70	3102	334.60	978548.990	978622.947	0.10	-7.99	*LR_G326	296366	7812475
93703016	93	70	3016	332.60	978548.460	978622.961	0.26	-8.77	*LR_G326	296034	7812443
93700315	93	70	315	310.00	978554.600	978624.080	0.01	-8.45	*LR_G326	296230	7810290
93700316	93	70	316	301.00	978556.430	978624.316	0.07	-8.56	*LR_G326	296610	7809840
93700317	93	70	317	299.00	978555.880	978624.383	0.03	-9.62	*LR_G326	297480	7809720
93700318	93	70	318	304.00	978554.490	978624.663	0.06	-10.27	*LR_G326	297470	7809180
93700319	93	70	319	309.40	978554.350	978624.865	0.04	-9.57	*LR_G326	297320	7808790
93700320	93	70	320	308.40	978554.350	978625.100	0.07	-9.97	*LR_G326	297550	7808340
93700321	93	70	321	328.00	978550.190	978625.517	0.03	-10.73	*LR_G326	297730	7807540
93700322	93	70	322	311.00	978554.000	978625.857	0.03	-10.61	*LR_G326	298080	7806890
93700323	93	70	323	322.00	978551.620	978626.379	0.03	-11.34	*LR_G326	298400	7805890
93700324	93	70	324	309.00	978554.950	978626.845	0.04	-11.03	*LR_G326	298990	7805000
93700325	93	70	325	317.00	978552.940	978627.412	0.05	-12.02	*LR_G326	299790	7803920
93700326	93	70	326	323.00	978551.820	978627.825	0.04	-12.38	*LR_G326	300130	7803130
93700327	93	70	327	308.00	978555.240	978623.830	0.06	-7.90	*LR_G326	297850	7810790
93700328	93	70	328	307.21	978555.550	978623.780	0.05	-7.71	*LR_G326	298256	7810890
93700329	93	70	329	315.00	978553.930	978623.276	0.03	-7.31	*LR_G326	299000	7811870
93700330	93	70	330	304.00	978557.010	978622.899	0.11	-5.94	*LR_G326	300080	7812610
93700331	93	70	331	304.00	978558.010	978622.719	0.05	-4.82	*LR_G326	300420	7812960
93700332	93	70	332	315.00	978554.930	978622.537	0.04	-5.56	*LR_G326	301290	7813320
93700333	93	70	333	314.00	978556.350	978622.348	0.03	-4.16	*LR_G326	301800	7813690
93700334	93	70	334	300.00	978559.330	978622.359	0.04	-3.93	*LR_G326	302680	7813680
93700335	93	70	335	288.00	978562.390	978622.766	0.04	-3.64	*LR_G326	304080	7812910
93700336	93	70	336	307.00	978557.570	978622.518	0.04	-4.48	*LR_G326	303330	7813380
93700337	93	70	337	325.00	978549.200	978621.920	0.07	-8.67	*LR_G326	294240	7814430
93700338	93	70	338	302.00	978551.240	978621.849	0.11	-11.05	*LR_G326	293590	7814560
93700339	93	70	339	300.00	978550.630	978621.608	0.07	-11.85	*LR_G326	293120	7815020
93700340	93	70	340	294.00	978553.440	978621.382	0.12	-9.95	*LR_G326	292710	7815450
93700341	93	70	341	293.00	978552.250	978620.972	0.13	-10.92	*LR_G326	292510	7816240
93700342	93	70	342	296.00	978552.680	978620.745	0.06	-9.74	*LR_G326	292710	7816680
93700343	93	70	343	287.00	978554.610	978620.632	0.14	-9.39	*LR_G326	292830	7816900
93700344	93	70	344	292.00	978554.070	978620.192	0.15	-8.49	*LR_G326	292870	7817750
93700346	93	70	346	291.00	978552.240	978619.101	0.08	-9.50	*LR_G326	293000	7819860
93700347	93	70	347	286.00	978552.520	978618.955	0.10	-10.04	*LR_G326	292790	7820140
93705203	93	70	5203	311.20	978544.830	978621.612	0.15	-15.37	*LR_G326	289515	7814970
93705204	93	70	5204	280.33	978551.050	978621.441	0.07	-15.14	*LR_G326	286404	7815262
93700348	93	70	348	267.70	978549.640	978620.078	0.02	-17.72	*LR_G326	282720	7817850
93700349	93	70	349	275.10	978548.700	978620.368	0.02	-17.50	*LR_G326	283600	7817300
93700350	93	70	350	271.70	978550.590	978620.733	0.06	-16.60	*LR_G326	283910	7816600
93700351	93	70	351	273.20	978551.020	978621.192	0.05	-16.34	*LR_G326	284470	7815720
93700352	93	70	352	278.10	978551.030	978621.259	0.08	-15.41	*LR_G326	285340	7815600
93700353	93	70	353	280.70	978549.940	978621.661	0.09	-16.38	*LR_G326	287165	7814846
93700354	93	70	354	283.40	978550.270	978622.108	0.25	-15.80	*LR_G326	287618	7813990
93700355	93	70	355	289.80	978549.620	978622.211	0.11	-15.43	*LR_G326	288417	7813801
93700356	93	70	356	300.30	978547.790	978621.821	0.08	-14.84	*LR_G326	289000	7814560
93700357	93	70	357	308.00	978544.660	978621.563	0.07	-16.20	*LR_G326	289780	7815067
93700358	93	70	358	315.50	978542.390	978621.520	0.08	-16.94	*LR_G326	290764	7815162
93700359	93	70	359	317.20	978545.640	978621.553	0.07	-13.40	*LR_G326	291855	7815110
93700360	93	70	360	331.10	978548.510	978623.759	0.07	-10.00	*LR_G326	294293	7810885

STN_CODE	YR	SVY	STATN	ELEV	GOBS	GTHEO	TC	BOUG	FLAG	EASTING	NORTHING
93700361	93	70	361	351.60	978544.220	978623.859	0.47	-9.96	*LR_G326	294274	7810693
93700362	93	70	362	341.60	978546.530	978623.930	0.37	-9.79	*LR_G326	294115	7810554
93700363	93	70	363	335.60	978548.280	978624.013	0.19	-9.48	*LR_G326	294290	7810395
93702041	93	70	2041	333.47	978548.980	978624.059	0.15	-9.29	*LR_G326	294136	7810306
93700364	93	70	364	324.60	978551.300	978624.076	0.02	-8.86	*LR_G326	294366	7810275
93700365	93	70	365	332.60	978548.720	978623.952	0.10	-9.66	*LR_G326	294431	7810515
93702019	93	70	2019	329.60	978549.980	978624.018	0.26	-8.90	*LR_G326	294713	7810391
93700366	93	70	366	321.60	978550.810	978623.851	0.02	-9.71	*LR_G326	294608	7810711
93700367	93	70	367	333.60	978548.530	978623.669	0.12	-9.35	*LR_G326	294092	7811056
93700368	93	70	368	332.60	978547.670	978623.550	0.08	-10.33	*LR_G326	294101	7811285
93700369	93	70	369	340.10	978546.560	978623.499	0.13	-9.86	*LR_G326	294116	7811385
93701041	93	70	1041	320.60	978552.810	978623.582	0.02	-7.64	*LR_G326	294650	7811230
93700370	93	70	370	320.60	978552.590	978623.630	0.01	-7.92	*LR_G326	294863	7811141
93700371	93	70	371	332.60	978549.270	978623.419	0.24	-8.44	*LR_G326	294617	7811545
93700372	93	70	372	316.30	978552.790	978624.938	0.18	-9.71	*LR_G326	297410	7808650
93700374	93	70	374	316.90	978552.150	978625.829	0.05	-11.25	*LR_G326	296820	7806930
93700375	93	70	375	321.70	978550.800	978627.038	0.11	-12.80	*LR_G326	296380	7804600
93700376	93	70	376	346.80	978544.490	978627.544	0.03	-14.76	*LR_G326	294910	7803610
93700377	93	70	377	332.60	978546.500	978628.262	0.02	-16.27	*LR_G326	294900	7802230
93700378	93	70	378	338.10	978544.720	978628.743	0.01	-17.46	*LR_G326	294350	7801300
93700379	93	70	379	338.60	978545.630	978629.177	0.00	-16.89	*LR_G326	293780	7800460
93700381	93	70	381	334.30	978550.330	978630.272	0.01	-14.13	*LR_G326	293010	7798350
93700382	93	70	382	358.90	978546.950	978631.779	0.00	-14.18	*LR_G326	302320	7795570
93700383	93	70	383	348.00	978550.360	978631.671	0.00	-12.81	*LR_G326	300010	7795750
93700384	93	70	384	349.00	978549.980	978631.943	0.01	-13.25	*LR_G326	297450	7795200
93700386	93	70	386	314.20	978548.810	978623.967	0.05	-13.26	*LR_G326	288860	7810420
93700387	93	70	387	306.10	978546.820	978623.361	0.03	-16.26	*LR_G326	289010	7811590
93700388	93	70	388	303.70	978546.240	978622.893	0.10	-16.77	*LR_G326	288810	7812490
93700389	93	70	389	298.00	978558.960	978621.361	0.02	-3.72	*LR_G326	302210	7815600
93700390	93	70	390	303.00	978556.780	978620.977	0.00	-4.55	*LR_G326	302980	7816350
93700391	93	70	391	304.00	978555.850	978620.379	0.00	-4.69	*LR_G326	302600	7817500
93700392	93	70	392	300.00	978556.450	978619.954	0.01	-4.44	*LR_G326	303400	7818330
93700393	93	70	393	293.00	978557.340	978619.354	0.16	-4.18	*LR_G326	304350	7819500
93700394	93	70	394	304.00	978554.540	978618.773	0.04	-4.35	*LR_G326	303090	7820610
93700395	93	70	395	327.00	978549.130	978618.715	0.06	-5.16	*LR_G326	301100	7820700
93706053	93	70	6053	304.77	978548.390	978616.100	0.10	-7.62	*LR_G326	299194	7825740
93706001	93	70	6001	287.53	978548.830	978616.005	0.04	-10.54	*LR_G326	297000	7825900
93706021	93	70	6021	291.16	978549.630	978616.114	0.11	-9.06	*LR_G326	298000	7825700
93706081	93	70	6081	307.26	978549.300	978616.199	0.10	-6.32	*LR_G326	300715	7825566
94700400	94	70	400	341.10	978545.744	978623.169	0.20	-10.08	*UQW818	294050	7812020
94700401	94	70	401	344.60	978545.744	978623.240	0.41	-9.25	*UQW818	294349	7811886
94700402	94	70	402	340.10	978547.177	978623.334	0.14	-9.07	*UQW818	294611	7811708
94700403	94	70	403	327.00	978550.583	978623.372	0.04	-8.38	*UQW818	294752	7811636
94700404	94	70	404	332.60	978547.614	978623.231	0.08	-10.06	*UQW818	294520	7811906
94700405	94	70	405	347.60	978545.192	978623.225	0.13	-9.48	*UQW818	294712	7811920
94700406	94	70	406	348.75	978544.336	978623.098	0.34	-9.77	*UQW818	294297	7812159
94700407	94	70	407	354.60	978542.769	978623.098	0.37	-10.16	*UQW818	294162	7812158
94700408	94	70	408	339.60	978546.060	978622.988	0.06	-10.02	*UQW818	294187	7812370
94700409	94	70	409	345.60	978545.824	978623.030	0.08	-9.09	*UQW818	294536	7812294
94700410	94	70	410	351.60	978544.100	978622.951	0.22	-9.42	*UQW818	294529	7812445
94700411	94	70	411	345.60	978545.733	978622.961	0.04	-9.16	*UQW818	294806	7812429
94700412	94	70	412	357.60	978543.195	978623.086	0.30	-9.20	*UQW818	294738	7812188
94700413	94	70	413	363.03	978539.971	978622.795	1.03	-10.33	*UQW818	294720	7812749
94700414	94	70	414	350.60	978543.955	978622.784	0.31	-9.50	*UQW818	294526	7812768
94700415	94	70	415	337.10	978546.417	978622.638	0.06	-9.80	*UQW818	294506	7813049
94700416	94	70	416	345.10	978544.626	978622.688	0.37	-9.76	*UQW818	294766	7812955
94700417	94	70	417	346.10	978545.427	978622.812	0.08	-9.18	*UQW818	294262	7812710
94700418	94	70	418	347.60	978544.361	978622.753	0.19	-9.78	*UQW818	294100	7812823
94700419	94	70	419	351.60	978543.426	978622.540	0.13	-9.77	*UQW818	294414	7813237
94700420	94	70	420	345.60	978544.483	978622.574	0.04	-10.02	*UQW818	294284	7813169
94700421	94	70	421	350.60	978542.730	978622.542	0.41	-10.39	*UQW818	294102	7813229
94700422	94	70	422	335.60	978546.349	978622.369	0.17	-9.79	*UQW818	294153	7813563
94700423	94	70	423	342.10	978544.786	978622.321	0.34	-9.85	*UQW818	294197	7813657
94700424	94	70	424	355.10	978542.141	978622.421	0.28	-10.10	*UQW818	294342	7813465
94700425	94	70	425	340.10	978546.182	978622.546	0.06	-9.35	*UQW818	294819	7813230

STN_CODE	YR	SVY	STATN	ELEV	GOBS	GTHEO	TC	BOUG	FLAG	EASTING	NORTHING
94700426	94	70	426	357.10	978541.688	978622.465	0.39	-10.09	*UQW818	294818	7813385
94700427	94	70	427	336.00	978545.995	978622.168	0.40	-9.63	*UQW818	294512	7813956
94700428	94	70	428	357.10	978541.515	978622.293	0.28	-10.20	*UQW818	294591	7813715
94700429	94	70	429	334.70	978547.160	978622.307	0.15	-9.11	*UQW818	294752	7813689
94700430	94	70	430	342.80	978544.047	978622.121	0.26	-10.33	*UQW818	294727	7814048
94700431	94	70	431	332.14	978550.294	978622.621	0.33	-6.62	*UQW818	297686	7813118
94700433	94	70	433	321.50	978552.932	978622.513	0.12	-6.17	*UQW818	298349	7813333
94700434	94	70	434	325.60	978551.435	978622.592	0.13	-6.93	*UQW818	298141	7813179
94700435	94	70	435	351.60	978545.934	978622.438	0.75	-6.54	*UQW818	298321	7813479
94705202	94	70	5202	306.28	978551.353	978621.313	0.19	-9.48	*93RPT	292495	7815581
94700500	94	70	500	296.50	978548.753	978622.635	0.00	-15.52	*UQW818	289010	7812990
94700501	94	70	501	309.00	978546.985	978622.962	0.00	-15.15	*UQW818	289625	7812366
94700502	94	70	502	306.60	978548.587	978623.050	0.00	-14.11	*UQW818	289926	7812201
94700503	94	70	503	284.20	978554.190	978619.437	0.00	-9.30	*94RPT	293098	7819213
94700504	94	70	504	296.50	978550.605	978619.024	0.20	-9.85	*UQW818	293999	7820021
94700505	94	70	505	365.10	978537.933	978618.710	0.24	-8.67	*UQW818	294959	7820639
94700506	94	70	506	376.00	978535.156	978618.031	0.34	-8.52	*UQW818	295120	7821955
94700507	94	70	507	284.30	978552.140	978618.477	0.00	-10.37	*UQW818	292585	7821063
94700508	94	70	508	286.10	978551.146	978617.957	0.00	-10.49	*UQW818	292382	7822067
94700509	94	70	509	289.00	978553.010	978619.315	0.00	-9.42	*94RPT	292210	7819438
94700510	94	70	510	291.90	978552.119	978619.446	0.00	-9.87	*94RPT	291358	7819175
94700511	94	70	511	290.90	978551.980	978619.589	0.00	-10.35	*94RPT	290510	7818888
94700512	94	70	512	296.00	978549.606	978619.734	0.00	-11.86	*UQW818	289750	7818600
94700513	94	70	513	277.50	978553.947	978618.168	0.00	-9.60	*94RPT	291542	7821649
94700514	94	70	514	299.60	978549.498	978617.506	0.00	-9.03	*UQW818	292810	7822945
94700515	94	70	515	293.70	978550.545	978617.074	0.00	-8.72	*UQW818	292810	7823780
94700516	94	70	516	282.90	978552.344	978616.558	0.00	-8.53	*94RPT	292890	7824780
94700517	94	70	517	278.60	978552.439	978616.206	0.00	-8.93	*UQW818	292969	7825463
94700518	94	70	518	269.20	978553.511	978615.682	0.00	-9.18	*UQW818	292696	7826477
94700519	94	70	519	267.50	978552.984	978615.203	0.00	-9.56	*UQW818	292511	7827402
94700520	94	70	520	264.00	978553.356	978614.761	0.00	-9.44	*UQW818	292063	7828254
94700521	94	70	521	259.70	978551.314	978612.949	0.00	-10.51	*94RPT	286618	7831707
94700522	94	70	522	259.20	978549.584	978612.806	0.14	-12.06	*UQW818	287178	7831992
94700523	94	70	523	255.50	978551.980	978612.770	0.00	-10.50	*UQW818	287000	7832060
94700524	94	70	524	267.50	978553.157	978615.543	0.00	-9.73	*94RPT	292587	7826744
94700525	94	70	525	282.70	978550.268	978615.534	0.00	-9.62	*94RPT	291595	7826750
94700526	94	70	526	277.90	978550.051	978615.414	0.00	-10.66	*94RPT	290461	7826970
94700527	94	70	527	336.00	978536.471	978615.193	0.58	-12.00	*UQW818	289790	7827390
94709528	94	70	9528	236.10	978557.421	978612.947	0.00	-9.05	*94RPT	284570	7831687
94700529	94	70	529	238.80	978556.781	978611.622	0.00	-7.83	*94RPT	285004	7834268
94700530	94	70	530	248.50	978554.714	978611.552	0.00	-7.92	*94RPT	286291	7834418
94700531	94	70	531	258.60	978553.295	978611.231	0.00	-7.03	*94RPT	287002	7835052
94700532	94	70	532	269.00	978551.124	978611.107	0.00	-7.03	*UQW818	287548	7835299
94700533	94	70	533	243.00	978556.046	978614.982	0.00	-11.10	*94RPT	284457	7827735
94700534	94	70	534	246.00	978555.354	978615.050	0.00	-11.27	*UQW818	284975	7827611
94700535	94	70	535	249.50	978554.359	978617.493	0.00	-14.02	*94RPT	284114	7822866
94705205	94	70	5205	262.18	978550.475	978619.857	0.01	-17.76	*93RPT	282134	7818269
94700536	94	70	536	290.20	978564.722	978623.000	0.00	-1.15	*94RPT	309670	7812519
94700537	94	70	537	354.80	978550.138	978622.940	1.14	-1.82	*94RPT	308920	7812627
94700538	94	70	538	365.00	978547.941	978623.107	0.41	-2.90	*UQW818	308320	7812300
94700539	94	70	539	284.40	978570.587	978625.350	0.00	1.22	*94RPT	313907	7808039
94700540	94	70	540	315.00	978562.464	978624.752	0.60	0.32	*94RPT	312036	7809170
94700541	94	70	541	287.30	978567.767	978624.658	0.28	-0.06	*94RPT	312352	7809354
94709009	94	70	9009	305.80	978557.689	978617.928	0.00	-0.04	*94RPT	307256	7822290
94709542	94	70	9542	271.30	978570.526	978624.170	0.00	-0.24	*94RPT	312550	7810297
94700543	94	70	543	332.00	978561.167	978625.006	0.00	1.51	*UQW818	314726	7808710
94700544	94	70	544	249.10	978576.676	978623.845	0.00	1.87	*94RPT	316954	7810969
94700545	94	70	545	295.00	978570.016	978623.374	0.00	4.71	*UQW818	317204	7811879
94700546	94	70	546	272.30	978568.493	978622.065	0.24	0.27	*94RPT	313492	7814364
94700547	94	70	547	281.80	978569.626	978622.304	0.00	2.79	*94RPT	314206	7813909
94700548	94	70	548	308.00	978563.269	978622.535	0.47	1.83	*UQW818	314781	7813471
94705002	94	70	5002	356.00	978544.801	978630.457	0.00	-15.58	*93RPT	303016	7798111
94700549	94	70	549	284.00	978565.059	978630.147	0.00	-9.18	*UQW818	308235	7798763
94700550	94	70	550	328.40	978553.122	978629.850	0.00	-12.08	*UQW818	305423	7799302
94700551	94	70	551	369.00	978545.225	978629.968	0.00	-12.11	*UQW818	305730	7799079

STN_CODE	YR	SVY	STATN	ELEV	GOBS	GTHEO	TC	BOUG	FLAG	EASTING	NORTHING
94700552	94	70	552	352.80	978549.550	978632.225	0.00	-13.23	*94RPT	295910	7794642
94700553	94	70	553	352.00	978549.913	978632.348	0.00	-13.14	*UQW818	296062	7794408
94700554	94	70	554	240.40	978575.655	978628.126	0.00	-5.15	*UQW818	316576	7802731
94700555	94	70	555	277.20	978571.486	978631.623	0.00	-5.57	*94RPT	317179	7796030
94700556	94	70	556	286.00	978569.652	978631.215	0.00	-5.26	*UQW818	316846	7796808
94700557	94	70	557	252.20	978576.157	978632.179	0.00	-6.38	*94RPT	316686	7794960
94700558	94	70	558	258.80	978572.913	978632.059	0.00	-8.20	*94RPT	316148	7795184
94700559	94	70	559	284.00	978568.433	978631.903	0.00	-7.57	*UQW818	315612	7795476
94700385	94	70	385	309.10	978549.394	978624.662	0.29	-14.13	*93RPT	288150	7809073
94700560	94	70	560	262.80	978550.302	978620.233	0.00	-18.20	*UQW818	281805	7817540
94700561	94	70	561	260.60	978550.856	978620.654	0.00	-18.50	*UQW818	281274	7816720
94700562	94	70	562	262.00	978550.596	978621.109	0.00	-18.94	*UQW818	281105	7815839
94700563	94	70	563	267.50	978549.939	978621.431	0.00	-18.84	*UQW818	280383	7815208
94700564	94	70	564	273.90	978549.558	978621.750	0.00	-18.28	*UQW818	279662	7814583
94700565	94	70	565	287.20	978549.489	978622.849	0.00	-16.83	*UQW818	278386	7812448
94700566	94	70	566	289.70	978548.278	978622.547	0.00	-17.24	*UQW818	279123	7813040
94700567	94	70	567	280.80	978548.555	978622.049	0.00	-18.22	*UQW818	279318	7814002
94700568	94	70	568	277.00	978552.750	978616.081	0.00	-8.60	*94RPT	293622	7825713
94700569	94	70	569	301.60	978545.925	978614.414	0.00	-9.12	*94RPT	296152	7828975
94700570	94	70	570	277.80	978552.024	978616.334	0.00	-9.63	*94RPT	294984	7825239
94700571	94	70	571	300.80	978548.572	978615.637	0.00	-7.85	*94RPT	298456	7826629
94700572	94	70	572	317.10	978544.688	978614.981	0.00	-7.87	*94RPT	298440	7827902
94700573	94	70	573	274.50	978551.617	978612.518	0.00	-6.87	*UQW818	296006	7832654
94700574	94	70	574	301.30	978544.083	978611.515	0.00	-8.12	*UQW818	297873	7834626
94700575	94	70	575	341.60	978546.540	978615.086	0.00	-1.30	*UQW818	307984	7827803
94700576	94	70	576	339.60	978546.764	978612.250	0.00	1.37	*94RPT	309966	7833329
94700577	94	70	577	309.20	978551.790	978611.477	0.00	1.18	*94RPT	307805	7834808
94700578	94	70	578	344.40	978547.889	978612.777	0.00	2.91	*94RPT	311560	7832322
94700579	94	70	579	339.40	978546.548	978613.726	0.00	-0.37	*94RPT	310069	7830463
94700580	94	70	580	345.30	978550.908	978614.819	0.00	4.06	*94RPT	315185	7828396
94700581	94	70	581	313.64	978556.158	978622.345	0.00	-4.45	*94RPT	301619	7813694
94700373	94	70	373	310.70	978553.520	978625.152	0.05	-10.42	*93RPT	297220	7808236
94700582	94	70	582	320.00	978555.276	978631.862	0.00	-13.59	*94RPT	289629	7795263
94700583	94	70	583	315.70	978554.437	978631.712	0.00	-15.13	*94RPT	286386	7795511
94700584	94	70	584	325.90	978553.970	978631.797	0.00	-13.67	*94RPT	285841	7795342
94700585	94	70	585	331.00	978552.309	978631.896	0.00	-14.43	*UQW818	285325	7795147
94700586	94	70	586	334.30	978549.861	978629.123	0.00	-13.46	*94RPT	291135	7800533
94700587	94	70	587	334.00	978548.477	978629.014	0.00	-14.79	*UQW818	292101	7800754
94700588	94	70	588	328.10	978552.110	978631.103	0.00	-14.41	*UQW818	290857	7796733
94700380	94	70	380	328.30	978552.811	978631.623	0.00	-14.19	*93RPT	292100	7795750
94700589	94	70	589	276.10	978553.710	978616.226	0.00	-8.17	*UQW818	294487	7825443
94700590	94	70	590	284.70	978552.127	978616.410	0.00	-8.24	*UQW818	295272	7825095
94700591	94	70	591	283.40	978552.508	978616.481	0.00	-8.19	*UQW818	295969	7824965
94700592	94	70	592	286.70	978554.022	978616.856	0.00	-6.40	*UQW818	296633	7824246
94700593	94	70	593	293.80	978551.652	978617.270	0.00	-7.78	*UQW818	296920	7823449
94700594	94	70	594	298.00	978550.467	978617.751	0.00	-8.62	*UQW818	296926	7822518
94700595	94	70	595	306.00	978548.053	978618.266	0.00	-9.98	*UQW818	297009	7821521
94700596	94	70	596	319.30	978546.643	978618.736	0.00	-9.24	*UQW818	296876	7820612
94700597	94	70	597	317.40	978547.335	978619.158	0.00	-9.34	*UQW818	296458	7819791
94700598	94	70	598	317.00	978548.512	978619.588	0.00	-8.68	*UQW818	296722	7818962
94700599	94	70	599	322.10	978544.282	978620.018	0.00	-12.33	*UQW818	297055	7818136
94700600	94	70	600	297.10	978554.126	978627.388	0.00	-14.78	*UQW818	282224	7803757
94700601	94	70	601	309.50	978550.086	978626.948	0.00	-15.94	*94RPT	281835	7804598
94700602	94	70	602	327.70	978553.650	978631.541	0.00	-13.38	*94RPT	277597	7795730
94700603	94	70	603	327.00	978553.684	978631.886	0.00	-13.83	*UQW818	277529	7795069
94700604	94	70	604	263.00	978552.300	978614.353	0.00	-10.28	*UQW818	272855	7828813
94700605	94	70	605	272.50	978550.337	978614.839	0.00	-10.86	*UQW818	272519	7827865
94700606	94	70	606	265.70	978551.704	978615.153	0.00	-11.15	*UQW818	271800	7827248
94700607	94	70	607	271.80	978550.432	978615.133	0.00	-11.20	*UQW818	270904	7827275
94700608	94	70	608	282.70	978548.840	978615.062	0.00	-10.57	*UQW818	269910	7827400
94700609	94	70	609	281.70	978549.100	978615.038	0.00	-10.49	*UQW818	269338	7827439
94700610	94	70	610	237.63	978553.728	978608.668	0.00	-8.16	*UQW818	278228	7839935
94700611	94	70	611	244.70	978555.786	978613.403	0.00	-9.45	*UQW818	284887	7830806
94700612	94	70	612	239.00	978556.946	978613.891	0.00	-9.90	*UQW818	285078	7829860
94700613	94	70	613	242.40	978556.392	978614.324	0.00	-10.22	*UQW818	284942	7829018

STN_CODE	YR	SVY	STATN	ELEV	GOBS	GTHEO	TC	BOUG	FLAG	EASTING	NORTHING
94700614	94	70	614	343.00	978544.732	978621.361	0.00	-9.11	*UQW818	297509	7815546
94700615	94	70	615	331.40	978543.633	978620.877	0.00	-12.01	*UQW818	297535	7816481
94700616	94	70	616	324.60	978543.746	978620.414	0.00	-12.77	*UQW818	297448	7817374
94700617	94	70	617	281.60	978551.807	978616.385	0.00	-9.15	*UQW818	295879	7825151
94700618	94	70	618	292.90	978548.650	978616.155	0.00	-9.85	*UQW818	296535	7825605
94700619	94	70	619	291.20	978549.446	978616.114	0.00	-9.35	*UQW818	297156	7825691
94700620	94	70	620	291.16	978549.662	978616.262	0.00	-9.29	*UQW818	297758	7825411
94700621	94	70	621	291.60	978549.662	978615.859	0.00	-8.80	*UQW818	295275	7826163
94700622	94	70	622	293.10	978549.671	978615.353	0.00	-7.99	*UQW818	295542	7827146
94700623	94	70	623	292.20	978548.970	978614.947	0.00	-8.46	*UQW818	295985	7827940
94700624	94	70	624	300.00	978546.566	978614.454	0.00	-8.83	*UQW818	295059	7828884
94700625	94	70	625	303.90	978547.197	978615.637	0.00	-8.62	*UQW818	298326	7826628
94700626	94	70	626	304.00	978548.771	978615.917	0.00	-7.30	*UQW818	298858	7826091
94700627	94	70	627	307.00	978546.808	978615.469	0.00	-8.23	*UQW818	298742	7826959
94700628	94	70	628	310.80	978550.008	978616.722	0.00	-5.53	*UQW818	300330	7824549
94700629	94	70	629	320.20	978547.015	978617.077	0.00	-7.03	*UQW818	300357	7823861
94700630	94	70	630	333.74	978543.737	978617.281	0.00	-7.85	*UQW818	300367	7823466
94700631	94	70	631	326.90	978546.176	978617.597	0.00	-7.07	*UQW818	300324	7822854
94700632	94	70	632	321.10	978549.853	978617.867	0.00	-4.81	*UQW818	300940	7822339
94700633	94	70	633	314.80	978551.608	978618.455	0.00	-4.88	*UQW818	300880	7821200
94700634	94	70	634	322.00	978549.394	978618.672	0.00	-5.89	*UQW818	300691	7820779
94700635	94	70	635	326.10	978548.927	978618.894	0.00	-5.77	*UQW818	300922	7820352
94700636	94	70	636	309.09	978550.674	978617.637	0.00	-6.12	*UQW818	301798	7822792
94700637	94	70	637	305.80	978553.157	978618.091	0.00	-4.54	*UQW818	303234	7821930
94700638	94	70	638	305.40	978553.909	978618.557	0.00	-4.53	*UQW818	303241	7821029
94700639	94	70	639	292.20	978558.217	978618.735	0.00	-3.00	*UQW818	304248	7820695
94700640	94	70	640	295.20	978556.850	978619.109	0.00	-4.15	*UQW818	303977	7819970
94700641	94	70	641	338.80	978548.192	978616.741	0.00	-1.86	*UQW818	307819	7824593
94700642	94	70	642	347.70	978545.000	978616.290	0.00	-2.85	*UQW818	307538	7825464
94700643	94	70	643	346.00	978545.458	978615.831	0.00	-2.26	*94RPT	307359	7826351
94700644	94	70	644	342.20	978545.614	978615.353	0.00	-2.38	*UQW818	307630	7827281
94700645	94	70	645	340.40	978546.678	978615.055	0.00	-1.37	*UQW818	308258	7827866
94700646	94	70	646	340.00	978546.739	978614.655	0.00	-0.99	*UQW818	308822	7828648
94700647	94	70	647	345.00	978545.683	978614.268	0.00	-0.67	*UQW818	309416	7829404
94700648	94	70	648	339.70	978546.739	978613.836	0.00	-0.23	*UQW818	309923	7830248
94700649	94	70	649	301.30	978556.331	978618.534	0.00	-2.89	*UQW818	304919	7821092
94700650	94	70	650	305.40	978553.486	978618.359	0.00	-4.76	*UQW818	303934	7821419
94700651	94	70	651	305.60	978553.935	978617.916	0.00	-3.82	*UQW818	303810	7822276
94700652	94	70	652	313.50	978551.678	978617.783	0.00	-4.39	*UQW818	303157	7822525
94700653	94	70	653	297.80	978555.985	978617.804	0.00	-3.20	*UQW818	303803	7822491
94700654	94	70	654	306.80	978557.681	978621.737	0.00	-3.66	*UQW818	301739	7814869
94700655	94	70	655	295.10	978560.354	978622.140	0.00	-3.70	*UQW818	302605	7814102
94700656	94	70	656	284.60	978562.949	978622.119	0.00	-3.15	*UQW818	304508	7814162
94700657	94	70	657	279.00	978564.739	978621.756	0.00	-2.10	*UQW818	305179	7814871
94700658	94	70	658	280.30	978565.388	978621.715	0.00	-1.15	*UQW818	306045	7814959
94700659	94	70	659	292.60	978562.750	978621.588	0.00	-1.24	*UQW818	306924	7815213
94700660	94	70	660	292.50	978563.416	978621.742	0.00	-0.75	*94RPT	307632	7814924
94700661	94	70	661	290.00	978564.436	978621.966	0.00	-0.44	*UQW818	308556	7814502
94700662	94	70	662	292.60	978563.710	978622.342	0.00	-1.03	*UQW818	308795	7813780
94700663	94	70	663	295.50	978564.013	978622.748	0.00	-0.57	*UQW818	309486	7813004
94700664	94	70	664	317.40	978551.980	978625.331	0.01	-10.86	*94RPT	303087	7807959
94700665	94	70	665	337.00	978549.013	978625.463	0.26	-9.85	*UQW818	303471	7807708
94700666	94	70	666	329.80	978551.159	978626.726	0.00	-10.65	*94RPT	302449	7805267
94700667	94	70	667	336.00	978549.308	978626.803	0.00	-11.35	*UQW818	302249	7805117
94700668	94	70	668	332.30	978549.342	978629.209	0.00	-14.45	*UQW818	303578	7800511
94700669	94	70	669	313.90	978550.596	978628.405	0.00	-16.02	*94RPT	281525	7801796
94700670	94	70	670	308.20	978550.631	978626.679	0.00	-15.38	*UQW818	281948	7805118
94700671	94	70	671	306.90	978551.064	978626.446	0.00	-14.97	*UQW818	282378	7805571
94700672	94	70	672	292.80	978555.216	978626.272	0.00	-13.42	*UQW818	283342	7805917
94700673	94	70	673	294.80	978555.060	978626.405	0.00	-13.32	*UQW818	284100	7805670
94700674	94	70	674	324.40	978547.024	978626.724	0.00	-15.84	*UQW818	281055	7805020
94700675	94	70	675	324.90	978546.081	978626.748	0.00	-16.71	*UQW818	280132	7804962
94700676	94	70	676	328.70	978545.060	978626.989	0.00	-17.22	*UQW818	279390	7804490
94700677	94	70	677	334.20	978543.434	978626.867	0.00	-17.65	*UQW818	278394	7804712
94700678	94	70	678	327.00	978544.680	978626.551	0.00	-17.50	*UQW818	277948	7805313

STN_CODE	YR	SVY	STATN	ELEV	GOBS	GTHEO	TC	BOUG	FLAG	EASTING	NORTHING
94700679	94	70	679	333.30	978542.863	978626.379	0.00	-17.91	*UQW818	277056	7805633
94700680	94	70	680	325.70	978543.322	978625.958	0.00	-18.52	*UQW818	276737	7806439
94700681	94	70	681	319.30	978543.503	978625.435	0.00	-19.08	*UQW818	276752	7807446
94700682	94	70	682	306.80	978545.173	978624.971	0.00	-19.41	*UQW818	276997	7808341
94700683	94	70	683	303.30	978545.605	978624.734	0.00	-19.43	*UQW818	277170	7808800
94700684	94	70	684	301.90	978552.776	978627.469	0.00	-15.26	*UQW818	281783	7803597
94700685	94	70	685	312.10	978551.591	978627.934	0.00	-14.91	*UQW818	281849	7802703
94700686	94	70	686	315.30	978551.453	978628.617	0.00	-15.10	*UQW818	282430	7801400
94700687	94	70	687	314.60	978552.785	978628.899	0.00	-14.19	*UQW818	283131	7800866
94700688	94	70	688	263.60	978550.942	978619.465	0.00	-16.63	*UQW818	282817	7819036
94700689	94	70	689	258.40	978552.603	978618.940	0.00	-15.47	*UQW818	282965	7820052
94700690	94	70	690	257.60	978552.776	978618.519	0.00	-15.04	*94RPT	283335	7820872
94700691	94	70	691	253.60	978553.702	978618.030	0.00	-14.41	*UQW818	283748	7821822
94700692	94	70	692	248.50	978554.939	978616.910	0.00	-13.06	*UQW818	284440	7824000
94700693	94	70	693	247.28	978555.492	978616.665	0.00	-12.50	*94RPT	284453	7824474
94700694	94	70	694	249.50	978554.887	978616.155	0.00	-12.16	*UQW818	284493	7825462
94700695	94	70	695	246.20	978555.510	978615.607	0.00	-11.63	*94RPT	284560	7826525
94700696	94	70	696	248.10	978555.008	978615.732	0.00	-11.89	*UQW818	285483	7826294
94700697	94	70	697	252.70	978554.766	978616.002	0.00	-11.49	*UQW818	286282	7825780
94700698	94	70	698	256.20	978555.164	978616.433	0.00	-10.84	*UQW818	286755	7824950
94700699	94	70	699	257.50	978554.593	978616.681	0.00	-11.40	*UQW818	287510	7824480
94700700	94	70	700	258.10	978552.889	978616.884	0.00	-13.19	*UQW818	287810	7824090
94700701	94	70	701	244.70	978556.055	978615.962	0.00	-11.74	*UQW818	283928	7825830
94700702	94	70	702	246.00	978555.103	978616.309	0.00	-12.78	*UQW818	283522	7825153
94700703	94	70	703	315.01	978549.749	978617.513	0.00	-5.75	*UQW818	300949	7823024
94700704	94	70	704	322.00	978543.192	978613.606	0.00	-7.03	*UQW818	298636	7830572
94700705	94	70	705	307.90	978546.133	978613.211	0.00	-6.47	*94RPT	298736	7831339
94700706	94	70	706	288.70	978547.586	978612.999	0.00	-8.58	*UQW818	297710	7831740
94700707	94	70	707	295.40	978547.119	978612.901	0.00	-7.63	*UQW818	296895	7831920
94700708	94	70	708	297.80	978548.944	978612.728	0.00	-5.16	*UQW818	298911	7832279
94700709	94	70	709	297.40	978548.105	978612.468	0.00	-5.82	*94RPT	298993	7832786
94700710	94	70	710	294.10	978548.840	978612.050	0.00	-5.32	*UQW818	298642	7833594
94700711	94	70	711	300.50	978545.398	978611.709	0.00	-7.16	*UQW818	298055	7834250
94700712	94	70	712	307.80	978544.792	978611.547	0.00	-6.16	*UQW818	298333	7834569
94700713	94	70	713	306.70	978544.602	978611.101	0.00	-6.13	*94RPT	298329	7835436
94700714	94	70	714	309.00	978543.858	978610.724	0.00	-6.04	*UQW818	298114	7836167
94700715	94	70	715	300.40	978545.389	978610.626	0.00	-6.10	*94RPT	298845	7836365
94700716	94	70	716	294.10	978545.034	978610.144	0.00	-7.22	*UQW818	298732	7837301
94700717	94	70	717	301.30	978545.804	978610.782	0.00	-5.67	*94RPT	298681	7836059
94700718	94	70	718	320.80	978541.298	978611.182	0.00	-6.73	*UQW818	297859	7835273
94700719	94	70	719	293.00	978544.732	978609.715	0.00	-7.31	*UQW818	298232	7838132
94700720	94	70	720	280.20	978548.676	978610.861	0.00	-7.03	*UQW818	298195	7835901
94700721	94	70	721	275.50	978549.264	978609.290	0.00	-5.79	*94RPT	297623	7838953
94700722	94	70	722	276.40	978549.195	978609.622	0.00	-6.02	*UQW818	297236	7838302
94700723	94	70	723	284.10	978547.906	978610.069	0.00	-6.24	*UQW818	296760	7837425
94700724	94	70	724	296.00	978544.611	978610.495	0.26	-7.36	*UQW818	296289	7836591
94700725	94	70	725	304.50	978539.473	978610.168	0.09	-10.67	*UQW818	295583	7837220
94700726	94	70	726	299.80	978541.142	978610.003	0.44	-9.41	*UQW818	296310	7837550
94700727	94	70	727	277.20	978548.503	978609.051	0.00	-5.98	*UQW818	297716	7839419
94700728	94	70	728	305.90	978541.678	978609.232	0.00	-7.34	*UQW818	299150	7839082
94700729	94	70	729	280.50	978549.835	978609.152	0.00	-4.10	*94RPT	299914	7839246
94700730	94	70	730	310.50	978543.555	978610.504	0.00	-5.83	*UQW818	299759	7836612
94700731	94	70	731	297.20	978547.552	978610.553	0.00	-4.50	*94RPT	300656	7836528
94700732	94	70	732	300.00	978546.332	978610.200	0.00	-4.81	*UQW818	301129	7837220
94700733	94	70	733	291.70	978548.071	978609.941	0.00	-4.45	*UQW818	300937	7837721
94700734	94	70	734	280.20	978551.020	978609.656	0.00	-3.48	*UQW818	301241	7838280
94700735	94	70	735	276.60	978551.185	978609.231	0.00	-3.60	*UQW818	300726	7839102
94700736	94	70	736	307.60	978545.233	978610.347	0.00	-4.56	*UQW818	301586	7836938
94700737	94	70	737	303.20	978547.543	978610.786	0.00	-3.56	*UQW818	301842	7836087
94700738	94	70	738	271.80	978551.392	978608.641	0.00	-3.75	*UQW818	300107	7840245
94700739	94	70	739	264.00	978552.551	978608.102	0.00	-3.58	*UQW818	300741	7841301
94700740	94	70	740	277.20	978549.083	978607.698	0.00	-4.05	*UQW818	300337	7842086
94700741	94	70	741	312.10	978545.337	978611.271	0.00	-4.50	*UQW818	302061	7835147
94700742	94	70	742	320.40	978543.668	978611.744	0.00	-5.01	*UQW818	301944	7834226
94700743	94	70	743	315.90	978543.339	978611.929	0.00	-6.41	*UQW818	301371	7833860

STN_CODE	YR	SVY	STATN	ELEV	GOBS	GTHEO	TC	BOUG	FLAG	EASTING	NORTHING
94700744	94	70	744	321.00	978543.512	978612.196	0.00	-5.49	*UQW818	300538	7833332
94700745	94	70	745	299.30	978548.114	978612.340	0.00	-5.31	*UQW818	299500	7833040
94700746	94	70	746	341.50	978547.482	978613.320	0.00	1.39	*UQW818	310696	7831259
94700747	94	70	747	342.00	978548.114	978612.906	0.00	2.53	*UQW818	311417	7832069
94700748	94	70	748	339.50	978547.958	978612.522	0.00	2.27	*UQW818	310752	7832808
94700749	94	70	749	338.80	978545.977	978612.289	0.00	0.38	*UQW818	309111	7833243
94700750	94	70	750	327.80	978547.604	978612.062	0.00	0.07	*UQW818	308368	7833677
94700751	94	70	751	345.20	978547.085	978614.403	0.00	0.63	*UQW818	310181	7829151
94700752	94	70	752	342.30	978547.854	978614.351	0.00	0.88	*UQW818	311148	7829261
94700753	94	70	753	341.00	978548.477	978614.290	0.00	1.31	*UQW818	312100	7829390
94700754	94	70	754	335.30	978550.674	978614.393	0.00	2.29	*UQW818	313030	7829200
94700755	94	70	755	343.50	978550.458	978614.275	0.00	3.80	*UQW818	313990	7829440
94700756	94	70	756	344.80	978551.730	978614.372	0.00	5.23	*UQW818	314955	7829260
94700757	94	70	757	309.08	978560.613	978614.538	0.00	6.92	*94RPT	316654	7828956
94700758	94	70	758	302.40	978563.424	978615.140	0.00	7.81	*UQW818	318775	7827810
94700759	94	70	759	303.80	978563.528	978615.622	0.00	7.71	*UQW818	318786	7826876
94700760	94	70	760	292.80	978564.843	978623.357	0.00	-0.88	*94RPT	309979	7811835
94700761	94	70	761	294.30	978565.466	978623.707	0.00	-0.31	*94RPT	310419	7811165
94700762	94	70	762	292.90	978566.763	978623.544	0.00	0.88	*UQW818	310735	7811483
94700763	94	70	763	297.20	978566.279	978623.945	0.00	0.84	*UQW818	311264	7810716
94700764	94	70	764	277.00	978567.706	978623.827	0.00	-1.59	*UQW818	311827	7810950
94700765	94	70	765	270.40	978570.595	978623.448	0.00	0.37	*UQW818	311533	7811676
94700766	94	70	766	269.10	978570.491	978623.149	0.00	0.31	*UQW818	311348	7812251
94700767	94	70	767	264.50	978571.123	978623.042	0.00	0.15	*UQW818	312122	7812465
94700768	94	70	768	274.70	978569.315	978622.662	0.00	0.73	*UQW818	312694	7813203
94700769	94	70	769	262.60	978571.132	978621.652	0.00	1.17	*UQW818	314016	7815166
94700770	94	70	770	252.10	978574.972	978621.252	0.00	3.34	*UQW818	314369	7815941
94700771	94	70	771	243.40	978576.616	978620.862	0.00	3.67	*UQW818	314147	7816692
94700772	94	70	772	238.40	978577.654	978620.696	0.00	3.89	*UQW818	313773	7817009
94700773	94	70	773	261.20	978572.602	978623.989	0.00	0.03	*UQW818	313468	7810654
94700774	94	70	774	256.70	978574.773	978623.714	0.00	1.59	*UQW818	314198	7811191
94700775	94	70	775	259.20	978575.405	978623.645	0.00	2.78	*UQW818	315197	7811336
94700776	94	70	776	249.30	978576.365	978623.673	0.00	1.76	*UQW818	316189	7811292
94700777	94	70	777	239.60	978580.456	978623.806	0.00	3.81	*UQW818	317795	7811052
94700778	94	70	778	233.10	978582.048	978623.599	0.00	4.33	*UQW818	318504	7811458
94700779	94	70	779	233.70	978581.780	978623.362	0.00	4.42	*UQW818	319146	7811922
94700780	94	70	780	231.40	978581.166	978623.026	0.00	3.69	*94RPT	319371	7812571
94700781	94	70	781	233.50	978580.050	978622.568	0.00	3.44	*UQW818	319663	7813457
94700782	94	70	782	224.10	978582.973	978622.214	0.00	4.87	*UQW818	320160	7814145
94700783	94	70	783	223.60	978582.229	978621.914	0.00	4.33	*UQW818	319426	7814717
94700784	94	70	784	223.90	978583.120	978621.896	0.00	5.30	*UQW818	318567	7814743
94700785	94	70	785	232.10	978580.759	978621.421	0.00	5.02	*94RPT	319064	7815663
94700786	94	70	786	238.40	978579.634	978621.083	0.00	5.48	*UQW818	318803	7816313
94700787	94	70	787	223.50	978582.697	978622.533	0.00	4.16	*UQW818	320890	7813537
94700788	94	70	788	226.90	978582.385	978622.339	0.00	4.71	*UQW818	320131	7813903
94700789	94	70	789	291.80	978566.331	978624.971	0.05	-1.15	*UQW818	312658	7808755
94700790	94	70	790	287.40	978569.903	978625.281	0.00	1.20	*UQW818	313458	7808167
94700791	94	70	791	272.70	978571.339	978625.742	0.00	-0.72	*UQW818	314476	7807290
94700792	94	70	792	268.70	978573.874	978626.042	0.00	0.72	*UQW818	315135	7806721
94700793	94	70	793	259.50	978576.676	978626.065	0.00	1.69	*94RPT	316029	7806686
94700794	94	70	794	251.00	978578.138	978626.403	0.00	1.14	*UQW818	316774	7806043
94700795	94	70	795	242.70	978578.467	978626.382	0.28	0.14	*UQW818	317630	7806093
94700796	94	70	796	260.50	978575.413	978626.341	0.55	0.90	*UQW818	318418	7806179
94700797	94	70	797	234.70	978581.408	978626.295	0.00	1.31	*94RPT	319317	7806277
94700798	94	70	798	231.00	978582.333	978626.138	0.00	1.67	*UQW818	319783	7806583
94700799	94	70	799	230.80	978582.844	978625.747	0.00	2.53	*UQW818	320126	7807340
94700800	94	70	800	227.60	978583.761	978625.195	0.00	3.37	*UQW818	320235	7808403
94700801	94	70	801	230.80	978581.313	978626.742	0.00	0.00	*UQW818	319152	7805416
94700802	94	70	802	236.10	978578.709	978627.055	0.00	-1.87	*UQW818	319372	7804816
94700803	94	70	803	241.50	978576.789	978627.370	0.00	-3.04	*UQW818	318823	7804206
94700804	94	70	804	241.90	978575.085	978627.878	0.00	-5.18	*UQW818	318391	7803226
94700805	94	70	805	242.80	978575.543	978628.760	0.00	-5.42	*94RPT	318045	7801528
94700806	94	70	806	241.90	978575.085	978628.310	0.00	-5.61	*UQW818	317847	7802389
94700807	94	70	807	245.80	978573.069	978629.147	0.00	-7.69	*94RPT	318149	7800786
94700808	94	70	808	251.70	978574.090	978629.110	0.00	-5.47	*UQW818	317249	7800848

STN_CODE	YR	SVY	STATN	ELEV	GOBS	GTHEO	TC	BOUG	FLAG	EASTING	NORTHING
94700809	94	70	809	269.30	978570.768	978628.740	0.00	-4.96	*UQW818	316822	7801554
94700810	94	70	810	297.50	978564.722	978623.823	0.00	-0.54	*UQW818	309938	7810937
94700811	94	70	811	305.10	978563.874	978624.167	0.00	-0.23	*UQW818	310379	7810279
94700812	94	70	812	316.00	978560.873	978624.170	0.00	-1.09	*UQW818	309435	7810262
94700813	94	70	813	245.20	978575.275	978629.611	0.00	-6.07	*UQW818	318234	7799897
94700814	94	70	814	255.40	978573.303	978630.074	0.00	-6.50	*94RPT	318370	7799011
94700815	94	70	815	252.20	978575.777	978630.540	0.00	-5.12	*UQW818	318516	7798119
94700816	94	70	816	254.70	978575.405	978630.984	0.00	-5.44	*UQW818	318523	7797267
94700817	94	70	817	255.50	978575.457	978631.439	0.00	-5.69	*UQW818	318290	7796394
94700818	94	70	818	258.20	978574.981	978631.920	0.00	-6.11	*UQW818	316570	7795454
94700819	94	70	819	266.50	978574.410	978632.594	0.00	-5.72	*UQW818	316449	7794163
94700820	94	70	820	262.50	978575.128	978633.064	0.00	-6.26	*UQW818	316495	7793264
94700821	94	70	821	264.50	978575.725	978633.581	0.00	-5.79	*UQW818	316654	7792276
94700822	94	70	822	268.60	978576.650	978633.945	0.00	-4.42	*UQW818	316917	7791582
94700823	94	70	823	266.30	978578.242	978634.473	0.00	-3.81	*94RPT	316719	7790571
94700824	94	70	824	256.90	978574.419	978632.740	0.00	-7.75	*UQW818	316888	7793888
94700825	94	70	825	260.80	978575.872	978633.236	0.00	-6.03	*UQW818	316931	7792938
94700826	94	70	826	259.10	978577.645	978633.684	0.00	-5.04	*UQW818	317013	7792082
94700827	94	70	827	265.10	978579.963	978634.850	0.00	-2.70	*UQW818	316612	7789848
94700828	94	70	828	270.50	978579.332	978635.286	0.00	-2.71	*UQW818	316042	7789009
94700829	94	70	829	272.00	978578.692	978635.707	0.00	-3.47	*UQW818	315116	7788195
94700830	94	70	830	249.90	978577.775	978631.715	0.00	-4.75	*UQW818	319048	7795872
94700831	94	70	831	311.00	978560.284	978623.894	0.00	-2.39	*UQW818	308716	7810786
94700832	94	70	832	314.10	978559.411	978623.957	0.00	-2.72	*UQW818	308248	7810661
94700833	94	70	833	315.00	978559.039	978623.563	0.00	-2.52	*UQW818	307715	7811414
94700834	94	70	834	355.70	978547.863	978631.443	0.00	-13.56	*UQW818	301436	7796203
94700835	94	70	835	352.20	978548.884	978631.481	0.00	-13.27	*UQW818	300483	7796120
94700836	94	70	836	345.20	978551.660	978632.009	0.00	-12.40	*UQW818	298395	7795084
94700837	94	70	837	341.70	978551.055	978632.312	0.00	-13.99	*UQW818	294953	7794465
94700838	94	70	838	340.00	978551.470	978632.359	0.00	-13.96	*UQW818	293993	7794363
94700839	94	70	839	330.80	978553.875	978631.998	0.00	-13.01	*UQW818	293366	7795047
94700840	94	70	840	330.70	978553.624	978631.582	0.00	-12.86	*UQW818	292679	7795836
94700841	94	70	841	335.60	978551.262	978631.551	0.00	-14.23	*UQW818	293658	7795907
94700842	94	70	842	331.10	978550.527	978630.555	0.00	-14.85	*UQW818	290991	7797785
94700843	94	70	843	331.40	978551.280	978630.081	0.00	-13.57	*UQW818	291041	7798694
94700844	94	70	844	336.80	978550.363	978629.382	0.00	-12.72	*UQW818	291125	7800035
94700845	94	70	845	339.60	978548.287	978628.551	0.00	-13.41	*UQW818	291103	7801630
94700846	94	70	846	343.20	978546.289	978628.061	0.00	-14.21	*UQW818	291154	7802572
94700847	94	70	847	348.70	978544.429	978627.517	0.00	-14.45	*UQW818	291302	7803619
94700848	94	70	848	347.10	978544.533	978627.213	0.00	-14.35	*UQW818	290710	7804197
94700849	94	70	849	336.20	978547.292	978626.914	0.00	-13.44	*UQW818	289972	7804762
94700850	94	70	850	332.00	978547.015	978626.500	0.00	-14.13	*94RPT	289426	7805552
94700851	94	70	851	329.40	978551.877	978630.688	0.00	-13.97	*UQW818	292461	7797547
94700852	94	70	852	328.00	978547.526	978626.073	0.00	-13.98	*UQW818	289142	7806370
94700853	94	70	853	318.70	978548.538	978625.588	0.00	-14.32	*94RPT	288832	7807299
94700854	94	70	854	318.20	978548.330	978625.267	0.00	-14.30	*UQW818	288379	7807911
94700855	94	70	855	310.30	978550.103	978624.775	0.00	-13.59	*UQW818	288385	7808859
94700856	94	70	856	323.50	978552.422	978631.026	0.00	-14.92	*UQW818	289897	7796869
94700857	94	70	857	319.90	978554.186	978631.465	0.00	-14.31	*UQW818	289438	7796022
94700858	94	70	858	321.70	978553.252	978631.145	0.00	-14.57	*UQW818	288969	7796629
94700859	94	70	859	328.70	978551.730	978630.571	0.00	-14.14	*UQW818	289293	7797734
94700860	94	70	860	320.10	978552.992	978631.235	0.00	-15.23	*UQW818	288223	7796447
94700861	94	70	861	317.50	978553.252	978631.464	0.00	-15.71	*UQW818	287261	7795997
94700862	94	70	862	342.50	978547.361	978629.866	0.00	-15.08	*UQW818	293503	7799136
94700863	94	70	863	317.50	978554.316	978632.180	0.00	-15.37	*UQW818	286278	7794614
94700864	94	70	864	314.40	978555.043	978632.623	0.00	-15.69	*UQW818	285806	7793760
94700865	94	70	865	315.00	978556.876	978633.124	0.00	-14.24	*UQW818	285585	7792798
94700866	94	70	866	312.30	978556.582	978633.663	0.00	-15.61	*94RPT	285364	7791764
94700867	94	70	867	312.30	978557.663	978634.121	0.00	-14.98	*UQW818	285679	7790892
94700868	94	70	868	312.90	978558.286	978634.580	0.00	-14.70	*UQW818	286052	7790018
94700869	94	70	869	311.10	978559.791	978635.100	0.00	-14.07	*UQW818	286280	7789028
94700870	94	70	870	310.50	978560.310	978635.551	0.00	-14.12	*UQW818	286970	7788174
94700871	94	70	871	312.90	978559.696	978635.925	0.00	-14.64	*UQW818	287503	7787466
94700872	94	70	872	310.20	978560.258	978635.595	0.00	-14.27	*UQW818	285897	7788077
94700873	94	70	873	310.30	978560.795	978635.926	0.00	-14.05	*UQW818	285028	7787434

STN_CODE	YR	SVY	STATN	ELEV	GOBS	GTHEO	TC	BOUG	FLAG	EASTING	NORTHING
94700874	94	70	874	313.60	978559.359	978635.140	0.00	-14.05	*UQW818	287274	7788964
94700875	94	70	875	311.30	978560.803	978634.552	0.00	-12.47	*UQW818	284894	7790059
94700876	94	70	876	312.40	978561.106	978634.836	0.00	-12.23	*UQW818	284109	7789506
94700877	94	70	877	310.50	978562.533	978635.079	0.00	-11.42	*UQW818	283280	7789031
94700878	94	70	878	307.90	978563.217	978635.367	0.00	-11.54	*UQW818	282505	7788472
94700879	94	70	879	308.10	978564.237	978635.594	0.00	-10.71	*UQW818	281618	7788027
94700880	94	70	880	306.40	978566.365	978635.735	0.00	-9.06	*UQW818	280857	7787748
94700881	94	70	881	316.80	978557.940	978634.238	0.00	-13.94	*UQW818	286710	7790680
94700882	94	70	882	319.80	978557.205	978634.230	0.00	-14.07	*UQW818	287664	7790708
94700883	94	70	883	336.50	978545.571	978627.994	0.00	-16.18	*UQW818	294702	7802742
94700884	94	70	884	318.10	978553.866	978631.035	0.00	-14.55	*UQW818	286880	7796815
94700885	94	70	885	317.70	978553.330	978630.935	0.00	-15.07	*UQW818	286156	7796998
94700886	94	70	886	318.40	978552.110	978630.906	0.00	-16.12	*UQW818	284997	7797039
94700887	94	70	887	319.00	978552.413	978630.715	0.00	-15.51	*94RPT	284456	7797399
94700888	94	70	888	314.70	978550.458	978628.624	0.00	-16.22	*UQW818	280626	7801364
94700889	94	70	889	307.50	978550.726	978628.230	0.00	-16.97	*UQW818	280347	7802116
94700890	94	70	890	318.80	978552.266	978629.334	0.00	-14.31	*UQW818	283496	7800036
94700891	94	70	891	325.30	978551.505	978629.752	0.00	-14.21	*UQW818	284051	7799240
94700892	94	70	892	322.20	978551.444	978630.090	0.00	-15.22	*UQW818	284656	7798600
94700893	94	70	893	318.20	978552.300	978630.626	0.00	-15.69	*UQW818	284529	7797571
94700894	94	70	894	319.90	978552.889	978630.855	0.00	-15.00	*UQW818	283512	7797118
94700895	94	70	895	319.20	978552.932	978630.825	0.00	-15.06	*94RPT	282684	7797166
94700896	94	70	896	321.50	978551.591	978630.223	0.00	-15.35	*UQW818	282454	7798318
94700897	94	70	897	324.50	978550.804	978629.691	0.00	-15.01	*UQW818	282263	7799335
94700898	94	70	898	317.40	978551.660	978629.314	0.00	-15.17	*UQW818	281746	7800053
94700899	94	70	899	326.50	978549.948	978626.519	0.00	-12.30	*UQW818	296658	7805600
94700900	94	70	900	314.10	978552.136	978629.102	0.00	-15.14	*UQW818	280823	7800448
94700901	94	70	901	312.00	978551.410	978628.862	0.00	-16.04	*UQW818	279990	7800899
94700902	94	70	902	315.00	978549.749	978628.781	0.00	-17.03	*UQW818	279172	7801043
94700903	94	70	903	328.60	978545.848	978628.774	0.00	-18.24	*UQW818	278111	7801044
94700904	94	70	904	328.30	978546.168	978628.793	0.00	-18.00	*UQW818	277172	7800996
94700905	94	70	905	319.50	978552.785	978631.018	0.00	-15.34	*UQW818	281781	7796786
94700906	94	70	906	322.80	978552.370	978631.208	0.00	-15.30	*UQW818	280914	7796411
94700907	94	70	907	326.90	978552.153	978631.491	0.00	-14.99	*UQW818	280035	7795857
94700908	94	70	908	326.50	978553.987	978631.500	0.00	-13.24	*UQW818	279021	7795826
94700909	94	70	909	327.40	978554.117	978631.519	0.00	-12.95	*UQW818	278079	7795778
94700910	94	70	910	324.30	978552.621	978631.588	0.00	-15.13	*UQW818	276538	7795626
94700911	94	70	911	320.70	978553.416	978631.801	0.00	-15.26	*UQW818	275829	7795209
94700912	94	70	912	317.30	978554.368	978632.026	0.00	-15.20	*UQW818	274932	7794768
94700913	94	70	913	315.50	978557.006	978632.224	0.00	-13.11	*UQW818	273949	7794375
94700914	94	70	914	311.80	978557.110	978632.397	0.00	-13.91	*UQW818	273132	7794034
94700915	94	70	915	307.70	978558.330	978632.601	0.00	-13.70	*UQW818	272004	7793629
94700916	94	70	916	323.70	978552.283	978631.467	0.00	-15.46	*UQW818	281016	7795915
94700917	94	70	917	320.20	978553.209	978631.410	0.00	-15.17	*UQW818	282025	7796036
94700918	94	70	918	334.00	978547.707	978627.417	0.00	-13.96	*UQW818	295768	7803863

Appendix 3

Carpentaria Zinc Belt Petrophysical Data

including data from previous studies and properties inferred from field data, listed in stratigraphic order

Abbreviations and units used:

sort	Unique ID number linking to U.Tas. Geology Dept. catalogue (Appendix 4)
Dry wt	Weight after oven-drying, in grams
SG sat	Specific gravity (water-saturated), in g/cm^3 (tonnes/m^3)
Susc	Magnetic susceptibility, in SI x 10^3
Velocity	Sonic velocity, in metres per second
Resistivity	Galvanic resistivity, in ohm-metres
IP%	Chargeability
TC1	Gamma ray spectrometer total count channel 1, in counts per minute (cpm)
K	Gamma ray spectrometer K channel count (cpm)
Th	Gamma ray spectrometer Th channel count (cpm)
U	Gamma ray spectrometer U channel count (cpm)
Source	Refers to either a drillhole, sample or literature source; see also 'Notes' column

Abbreviation	**Meaning**
AMcP	sample collected by A. McPherson (see McPherson, 1994)
B.C. Jones	sample collected by B. Jones, Uni. of Tas.
Clark	Clark, 1980
Cooper	sample collected by S. Cooper, Uni. of Tas.
DEL	Leaman 1991a&b, 1996, 1998, pers. comm.
Est	Estimated from field data by the author
F&B	Fallon and Busuttil, 1992
Gibb	Gibb, 1967
GW	sample collected by G. Webber, Lady Loretta
Harrison; PLH	Harrison, 1980
Hilton	Hilton Mine sample
Hone et al	Hone et al., 1987
HYC	HYC (McArthur River Mine) sample
Isa	Mount Isa Mine sample
Mammoth	Mammoth Cu ore sample
Mt. Oxide	Mt. Oxide Cu ore sample
Neumann	Neumann, 1964
P.A.	P.A. Cu mine ore sample
R&C	Rivera and Challis, 1972
S&H	Stewart and Hoyling, 1963
Shirley	Shirley, 1976
Silver King	Silver King mine sample
Young	Young, 1984

ID	Field or Uni. of Tas. Geology Dept. catalogue ID number
Mbr	Stratigraphic member or locality

Abbreviations used	**Meaning**
CFZ	Carlton Fault Zone
CU	'Cyclic unit'
LC	'Lower Carbonate unit'
LS	'Lower Siltstone unit'
MU	'Massive unit'
OH	'Ore horizon'
OS	'Ore sediments'
PU	'Pyritic unit'
UC	'Upper Carbonate unit'

Lithology	Described using standard AGSO abbreviations (see Appendix 7)
E	Sample location easting in UTM Zone 54, Australian Geodetic Datum 1966
N	Sample location northing in UTM Zone 54, Australian Geodetic Datum 1966
Depth	in metres (if drillhole sample)
	'S' = 'surface', 'F' = 'fresh', 'SW' = 'slightly weathered
Notes	'DSO' = 'Direct Shipping Ore'

Appendix 3
Mount Isa Basin Petrophysics

sort	Unit	Dry wt	Porosity	SG sat	Susc	Velocity	Resistivity	IP%	TC1	TC2	K	U	Th	Source	ID	Mbr	Lithology	E	N	Depth	Notes
1	Hooray Sst (K)			2.10										Harrison							
2	Cretaceous sandstone			1.75										Neumann			SDST			S	
3	Carpentaria Basin			2.50	0.00									DEL							
4	Bukalara Sandstone			2.23										Neumann						S	
5	Cambrian Georgina Basin			2.70	0.00									PLH + est			SDY LMST DLST				
6	V Creek Limestone		0.06	2.65			5							Morstone 1	3101		F LMST	239178	7834113	83.5	S&H
7	V Creek Limestone	121.4	0.05	2.67	0.09									Morstone 1	3001		F LMST	239178	7834113	83.5	
8	Currant Bush Limestone		0.08	2.50			200							Morstone 1	3103		SLY LMST	239178	7834113	196.3	S&H
9	Currant Bush Limestone	120.3	0.02	2.59	0.03									Morstone 1	3003		SLY LMST	239178	7834113	196.3	
10	Thorntonia Limestone		0.03	2.71			2000							Morstone 1	3102		C LMST	239178	7834113	286.0	S&H
11	Thorntonia Limestone	92.2	0.01	2.72	0.02									Morstone 1	3002		C LMST	239178	7834113	286.0	
12	Camooweal Dolomite			2.82										Urandangi			CHY DLST				Gibb
13	Tindall Limestone			2.72										Neumann			LMST			S	
14	Georgina Basin Cambrian			2.50	0.00									DEL							
15	Nutwood Downs Basalt			2.98										Neumann			BLT			S	
16	Roper Group?			2.50										Neumann			SDST			S	
17	Roper Group?			2.51										Neumann			SLST			S	
18	Roper Group?			2.56										Neumann			SHLE			S	
19	S Nicholson/Pilpah Sst			2.59	0.20									PLH, DEL, JND							
20	Mullera Formation						80							Morstone 1	3104		MIC CLST	239178	7834113	385.3	S&H
21	Mullera Formation	330.6	0.10	2.50	0.14				941	259	15	10	3	Morstone 1	3004		GR MIC CLST	239178	7834113	385.3	corr 83306
22	Mullera Formation						120							Morstone 1	3105		FER MIC SDST	239178	7834113	385.9	S&H
23	Mullera Formation	950.5	0.10	2.59	0.25				317	71	3	10	5	Morstone 1	3005		FER MIC SDST	239178	7834113	385.9	
24	Mullera Formation						500							Morstone 1	3106		MIC CLST	239178	7834113	471.9	S&H
25	Mullera Formation	408.2	0.10	2.49	0.21				1055	243	33	22	15	Morstone 1	3006		MIC CLST	239178	7834113	471.9	
26	Constance Sandstone		0.10	2.58			600							Morstone 1	3107		F SLY SDST	239178	7834113	539.2	S&H
27	Constance Sandstone	451.1	0.07	2.57	0.35				883	207	39	16	1	Morstone 1	3007		F SLY SDST	239178	7834113	539.2	
28	Constance Sandstone		0.06	2.77			400							Morstone 1	3108		FER MIC SDST	239178	7834113	649.1	S&H
29	Constance Sandstone	276.1	0.05	2.72	0.13									Morstone 1	3008		FER MIC SDST	239178	7834113	649.1	
30	Constance Sandstone		0.14	2.50										Morstone 1	3109		FER SDST	239178	7834113	738.6	S&H
31	Constance Sandstone	673.4	0.06	2.43	0.05				571	1	-11	-6	1	Morstone 1	3009		FER SDST	239178	7834113	738.6	
32	Constance Sandstone	190.5	0.03	2.64	0.20	4550	11600	0.9						Amoco83-3	83313		SLY M SDST	214300	7971600	61.2	highly irregular IP
33	Constance Sandstone	733.6	0.02	2.65	0.16	5020	5805	1.0						Amoco83-3	83312		M SDST	214300	7971600	72.2	
34	Constance Sandstone	341.7	0.01	2.58	0.02	5350								Amoco83-3	83311		VC SDST	214300	7971600	212.7	
35	Constance Sandstone	258.1	0.04	2.61	0.09	4380	525	0.8						Amoco83-3	83310		HM M SDST	214300	7971600	248.8	
36	Constance Sandstone	176.9	0.02	2.67	0.23		2380	0.9						Amoco83-3	83309		SLY F SDST	214300	7971600	258.9	
37	Constance Sandstone	79.1	0.09	2.90	0.39		7181	2.1						Amoco83-3	83308		HM CLST	214300	7971600	259.7	
38	Constance Sandstone	66.9	0.02	2.66	0.18	5200	11479	1.1						Amoco83-3	83307		SLY F SDST	214300	7971600	273.3	
39	Constance Sandstone	84.3	0.03	2.63	0.09		2154	2.5						Amoco83-3	83306		GR CLAY F SDST	214300	7971600	279.8	corr 3004
40	Constance Sandstone	337.4	0.01	2.67	0.32		16552	0.4						Amoco83-3	83305		SDY CAR SHLE	214300	7971600	527.0	

Appendix 3
Mount Isa Basin Petrophysics

sort	Unit	Dry wt	Porosity	SG sat	Susc	Velocity	Resistivity	IP%	TC1	TC2	K	U	Th	Source	ID	Mbr	Lithology	E	N	Depth	Notes
41	Constance Sandstone	113.7	0.01	2.66	0.10	5380	16179	2.2						Amoco83-3	83304		F SDST	214300	7971600	542.2	
42	Constance Sandstone	411.8	0.04	2.58	0.09	5010								Amoco83-3	83303		RE M SDST	214300	7971600	544.6	
43	Constance Sandstone	120.7	0.01	2.65	0.05		3734	0.8						Amoco83-3	83302		PYR SLY F SDST	214300	7971600	562.1	
44	Constance Sandstone	294.9	0.01	2.61	0.02	5390	23859	1.0						Amoco83-3	83301		SLF F SDST	214300	7971600	570.3	
45	L.Prot. dolomite'			2.74										Burketown 1			DLST	351864	7998188	856	Shirley
46	L.Prot. dolomite'			2.78										Burketown 1			DLST	351864	7998188	900	Shirley
47	L.Prot. dolomite'			2.84										Burketown 1			DLST	351864	7998188	950	Shirley
48	L.Prot. dolomite'			2.62										Burketown 1			DLST	351864	7998188	994	Shirley
49	granite			2.63										Mornington Is. 1			GRT	307974	8163832	822	Shirley
50	quartzite			2.66										Mornington Is. 2			QZT	339902	8175161	902	Shirley
51	Lawn Hill Fm?	983.1	0.02	5.20	0.16		138	44.8						Silver King	110946		GN PY CCP SLST			0	dump material
52	Riversleigh Siltstone	627.2	0.01	2.66	0.18	5460								Amoco83-1	83127		CAR SHLE	257200	7913000	96.2	
53	Riversleigh Siltstone	132.0	0.00	2.64	0.07	5720	9477	4.1						Amoco83-1	83126		PYR F SDST	257200	7913000	110.7	
54	Riversleigh Siltstone	368.1	0.00	2.64	0.13	5710								Amoco83-1	83125		PYR F SDST	257200	7913000	138.4	
55	Riversleigh Siltstone	404.1	0.00	2.63	0.12	5570								Amoco83-1	83124		PYR CAR SHLE	257200	7913000	198.6	
56	Riversleigh Siltstone	171.3	0.01	2.67	0.14									Amoco83-1	83123		F SDST	257200	7913000	204.9	
57	Riversleigh Siltstone	572.5	0.01	2.62	0.14	5480								Amoco83-1	83122		PYR CAR SHLE	257200	7913000	222.8	
58	Riversleigh Siltstone	203.2	0.01	2.68	0.17		2439	9.4						Amoco83-1	83121		PYR CAR SHLE	257200	7913000	229.1	
59	Riversleigh Siltstone	338.3	0.02	2.63	0.15	4650								Amoco83-1	83120		SLST	257200	7913000	236.0	
60	Riversleigh Siltstone	277.2	0.00	2.69	0.18		4182	4.9						Amoco83-1	83119		PYR CAR SHLE	257200	7913000	265.3	
61	Riversleigh Siltstone	215.2	0.00	2.65	0.09	5760	765862	8.9						Amoco83-1	83118		SLST	257200	7913000	268.8	
62	Riversleigh Siltstone	145.8	0.01	2.64	0.10									Amoco83-1	83117		SLY F SDST	257200	7913000	295.6	
63	Riversleigh Siltstone	151.2	0.02	2.64	0.13		115	11.6						Amoco83-1	83116		CAR SHLE	257200	7913000	327.1	
64	Riversleigh Siltstone	456.0	0.04	2.65	0.12		113	9.4						Amoco83-1	83115		SDY CAR SHLE	257200	7913000	352.2	
65	Riversleigh Siltstone	136.5	0.04	2.67	0.11		75	7.4						Amoco83-1	83114		SLY C SDST	257200	7913000	406.7	weak cleavage oblique to bedding
66	Riversleigh Siltstone	121.9	0.03	2.74	0.07		53	13.8						Amoco83-1	83113		LAY VN PYR SHLE	257200	7913000	431.7	
67	Riversleigh Siltstone	291.8	0.03	2.84	0.13		118	8.6						Amoco83-1	83112		LAY PYR CAR SHLE	257200	7913000	448.4	cryptalgal
68	Riversleigh Siltstone	500.9	0.02	2.71	0.13		136	13.8						Amoco83-1	83111		SDY PYR CAR SHLE	257200	7913000	453.9	
69	Riversleigh Siltstone	179.0	0.02	2.64	0.11		63	13.7						Amoco83-1	83110		SDY CAR SHLE	257200	7913000	454.1	
70	Riversleigh Siltstone	239.7	0.02	2.67	0.14		76	22.0						Amoco83-1	83109		PYR CAR SHLE	257200	7913000	484.5	
71	Riversleigh Siltstone	511.5	0.03	2.67	0.15		424	1.8						Amoco83-1	83108		SLST	257200	7913000	520.5	
72	Riversleigh Siltstone	157.6	0.01	2.73	0.14		1457	0.7						Amoco83-1	83107		SHLE	257200	7913000	540.0	
73	Riversleigh Siltstone	316.4	0.01	2.69	0.20		3303	6.7						Amoco83-1	83106		SHLE	257200	7913000	561.6	
74	Riversleigh Siltstone	270.6	0.00	2.69	0.17	5810	13674	1.8						Amoco83-1	83105		SHLE	257200	7913000	565.1	
75	Riversleigh Siltstone	496.9	0.01	2.71	0.20		1928	1.6						Amoco83-1	83104		SLY SHLE	257200	7913000	591.6	
76	Riversleigh Siltstone	177.5	0.01	2.69	0.15									Amoco83-1	83103		SLST	257200	7913000	608.1	
77	Riversleigh Siltstone	342.1	0.00	2.68	0.13									Amoco83-1	83102		SLST	257200	7913000	622.4	
78	Riversleigh Siltstone	190.3	0.00	2.65	0.11									Amoco83-1	83101		SDY SLST	257200	7913000	634.8	
79	Riversleigh Siltstone			2.65	0.30									CM45	34538		CAR SHLE	269500	7888000	188.9	Aberfoyle
80	Riversleigh Siltstone			2.69	0.26									CM45	34539		CAR SHLE	269500	7888000	191.1	Aberfoyle

Appendix 3

Mount Isa Basin Petrophysics

sort	Unit	Dry wt	Porosity	SG sat	Susc	Velocity	Resistivity	IP%	TC1	TC2	K	U	Th	Source	ID	Mbr	Lithology	E	N	Depth	Notes
81	Riversleigh Siltstone	627.6	0.02	2.70	0.11	4380	822	2.8	1445	513	73	6	5	CM45	2086		LA SLST	269500	7888000	378	
82	Riversleigh Siltstone	236.2	0.00	2.71	0.14	5490	48295	2.8						CM45	2137		SLST	269500	7888000	380	
83	Riversleigh Siltstone	293.5	0.00	2.70	0.16	5630	21496	7.3	707	255	29	14	9	CM45	2138		SLST	269500	7888000	380	
84	Shady Bore Quartzite	787.6	0.02	2.42	0.03	5100	190400	2.3	205	21	-11	14	7	GW	1078		SDST			0	
85	Shady Bore Quartzite	919.9	0.03	2.35	0.02	4740	24444	2.5	91	-19	1	-4	-7	GW	1079		CLAY CL SDST			0	
86	Shady Bore Quartzite	1167.4	0.02	2.39	0.02	4890	121846	2.3	261	31	-27	4	-3	GW	1080		CLAY CL SDST			0	
87	Shady Bore Quartzite	1601.4	0.03	2.33	0.02	5080	197867	3.2	117	17	-15	8	-5	GW	1088		CLAY CL SDST			0	
89	Lady Loretta Fm			2.75	0.21									LA64	1216440		CAR SHLE			307.2	Aberfoyle
90	Lady Loretta Fm			3.27	0.67									LA64	1216441		CAR SHLE			311.6	Aberfoyle
91	Lady Loretta Fm			3.19	0.68									LA64	1216442		CAR SHLE			314.05	Aberfoyle
92	Lady Loretta Fm			3.07	0.52									LA64	1216443		CAR SHLE			315	Aberfoyle
93	Lady Loretta Fm			2.78	0.39									LA64	1216444		CAR SHLE			316	Aberfoyle
94	Lady Loretta Fm			2.76	0.35									LA64	1216445		CAR SHLE			316.31	Aberfoyle
95	Lady Loretta Fm			2.85	0.49									LA64	1216446		CAR SHLE			317.55	Aberfoyle
96	Lady Loretta Fm			2.87	0.48									LA64	1216447		CAR SHLE			318.7	Aberfoyle
97	Lady Loretta Fm			3.06	0.54									LA64	1216448		CAR SHLE			319.35	Aberfoyle
98	Lady Loretta Fm			2.75	0.30									LA64	1216449		CAR SHLE			320.4	Aberfoyle
99	Lady Loretta Fm			3.12	0.68									LA64	1216450		CAR SHLE			321	Aberfoyle
100	Lady Loretta Fm			2.96	0.59									LA64	1216451		CAR SHLE			321.1	Aberfoyle
101	Lady Loretta Fm			2.98	0.68									LA64	1216452		CAR SHLE			321.5	Aberfoyle
102	Lady Loretta Fm			2.77	0.48									LA64	1216453		CAR SHLE			321.8	Aberfoyle
103	Lady Loretta Fm			3.00	0.70									LA64	1216454		CAR SHLE			322	Aberfoyle
104	Lady Loretta Fm			2.79	0.53									LA64	1216455		CAR SHLE			417.9	Aberfoyle
105	Lady Loretta Fm			2.80	0.44									LA64	1216456		CAR SHLE			418.7	Aberfoyle
106	Lady Loretta Fm			2.77	0.48									LA64	1216457		CAR SHLE			418.9	Aberfoyle
107	Lady Loretta Fm			2.74	0.39									LA64	1216458		CAR SHLE			419.1	Aberfoyle
108	Lady Loretta Fm			3.02	0.58									LA64	1216459		CAR SHLE			419.9	Aberfoyle
109	Lady Loretta Fm			2.75	0.41									LA64	1216460		CAR SHLE			420	Aberfoyle
110	Lady Loretta Fm			2.74	0.45									LA64	1216461		CAR SHLE			420.1	Aberfoyle
111	Lady Loretta Fm			2.89	0.50									LA64	1216462		CAR SHLE			420.5	Aberfoyle
112	Lady Loretta Fm			2.77	0.33									LA64	1216463		CAR SHLE			487	Aberfoyle
113	Lady Loretta Fm			3.46	0.82									LA64	1216464		CAR SHLE			488	Aberfoyle
114	Lady Loretta Fm			2.77	0.31									LA64	1216465		CAR SHLE			489.2	Aberfoyle
115	Lady Loretta Fm			3.13	0.72									LA64	1216466		CAR SHLE			489.25	Aberfoyle
116	Lady Loretta Fm			3.62	1.01									LA64	1216467		CAR SHLE			489.3	Aberfoyle
117	Lady Loretta Fm			3.01	0.49									LA64	1216468		CAR SHLE			489.35	Aberfoyle
118	Lady Loretta Fm			3.40	0.82									LA64	1216469		CAR SHLE			489.4	Aberfoyle
119	Barney Ck Fm	206.3	0.02	3.40	0.12		494	13.9	385	119	33	-2	1	HYC	6013	ore	GN SP PY CCP			250	4 O/B
120	Barney Ck Fm	192.1	-2.07	1.00	0.12									HYC	6014	ore	GN SP PY CCP			250	4 O/B
121	Barney Ck Fm	75.1	-2.38	1.00	0.12		175	10.3						HYC	6015	ore	GN SP PY CCP			250	4 O/B

Appendix 3

Mount Isa Basin Petrophysics

sort	Unit	Dry wt	Porosity	SG sat	Susc	Velocity	Resistivity	IP%	TC1	TC2	K	U	Th	Source	ID	Mbr	Lithology	E	N	Depth	Notes
122	Barney Ck Fm	1262.5	0.02	3.33	0.18		469	14.5	747	221	3	-6	5	HYC	6016	ore	GN SP PY CCP			250	4 O/B
123	Barney Ck Fm	170.5	0.03	3.40	0.14		239	16.9						HYC	6017	ore	GN SP PY CCP			250	4 O/B
124	Barney Ck Fm	57.7	0.00	3.35	0.11		85	18.8						HYC	6018	ore	GN SP PY CCP			250	4 O/B
125	Barney Ck Fm	56.0	0.02	3.30	0.07		590	19.9						HYC	6019	ore	GN SP PY CCP			250	4 O/B
126	Barney Ck Fm	301.6	0.02	3.39	0.11		1845	16.5	261	77	-9	-2	-1	HYC	6008	ore	GN SP PY CCP			300	2 O/B
127	Barney Ck Fm	110.9	0.03	3.24	0.12		1080	15.9						HYC	6009	ore	GN SP PY CCP			300	2 O/B
128	Barney Ck Fm	124.5	0.02	3.48	0.09		780	10.2	365	-11	7	2	9	HYC	6010	ore	GN SP PY CCP			300	2 O/B
129	Barney Ck Fm	46.1	0.03	3.47	0.08		360	15.6						HYC	6011	ore	GN SP PY CCP			300	2 O/B
130	Barney Ck Fm	34.1	0.00	3.52	0.06		368	14.7						HYC	6012	ore	GN SP PY CCP			300	2 O/B
131	Barney Ck Fm	9.6	0.03	2.69	0.06		387	0.4						Dept	101231	HYC	CAR SHLE				
132	Barney Ck Fm	18.0	0.00	2.77	0.09		16240	1.9						Dept	101232	HYC	LA TFC DLST			307.8	WH1A
133	Lady Loretta Fm				2.14		4	52.0						P63A	7011	OH	GN SP PY			468.5	R&C
134	Lady Loretta Fm	782.0	0.00	4.50	1.14		113	20.8	37	-65	1				6007	ore	GN SP			400	
135	Lady Loretta Fm			3.91	1.38									LL ore-12	121212	ore	GN SP PY			400	Aberfoyle
136	Lady Loretta Fm	499.8	0.00	4.59	0.88	4380	252	72.6	31	-35	5	14	3		1005	ore	GN SP PY			400	
137	Lady Loretta Fm	544.5	0.00	4.49	0.70	4520	437	56.7	41	55	-9	8	-1		1007	ore	GN SP PY			400	
138	Lady Loretta Fm	331.4	0.00	4.26	0.59	4450	202	35.7	41	39	-11	4	-3		1008	ore	GN SP PY			400	
139	Lady Loretta Fm				1.76		1	29.0							7001	PU	BED PY			101	R&C
140	Lady Loretta Fm	187.5	0.00	3.76	2.11	6000	99999999							221EH00	110739	PU	FER SHLE			3.0	
141	Lady Loretta Fm	356.8	0.04	3.10	1.26	4340	1299	1.1	281	-859	3	-10	-3	221EH00	110740	PU	FER SLST			7.3	
142	Lady Loretta Fm	221.8	0.05	3.24	1.53	5170	1616	1.5						221EH00	110741	PU	SD SLST			13.3	
143	Lady Loretta Fm	222.1	0.00	3.11	0.80									221ED61	110743	PU	DMT SLST			47.5	
144	Lady Loretta Fm	1041.8	0.00	2.99	0.89				1353	-859	51	18	7	221ED61	110744	PU	PYR SHLE SLST			50.0	
145	Lady Loretta Fm	251.0	0.00	4.53	1.32	6360	19	26.4						221WD80	110745	PU	PY			4.7	
146	Lady Loretta Fm	326.3	0.07	3.06	1.68	4590			39	-859	-7	10	1	221WD80	110746	PU	GTY PYR SLST			7.8	
147	Lady Loretta Fm	419.5	0.04	3.27	1.56	5220								221WD80	110747	PU	FER SLST			11.8	
148	Lady Loretta Fm	376.5	0.03	2.84	0.25		412	2.9	843	-859	35	6	7	221WD44	110748	MU	SHLE			7.0	
149	Lady Loretta Fm	135.6	0.00	3.85	0.78									221WD44	110749	OH	SUL DMT SHLE			18.0	
150	Lady Loretta Fm	324.4	0.01	4.04	0.78	5070			37	-859	-5	-4	1	221WD44	110750	OH	SUL DMT SHLE			19.0	
151	Lady Loretta Fm	409.3	0.01	3.84	0.47	5140	31	12.3	7	-859	-3	0	1	221WD44	110751	OH	SUL DMT SHLE			23.0	
152	Lady Loretta Fm	254.3	0.01	4.71	0.40	4490	48	20.3						221WD44	110752	OH	SP GN PY			42.6	
153	Lady Loretta Fm	351.4	0.01	4.43	1.31	6710	8	13.3	-45	-859	-27	-18	-1	221WD44	110754	PU	PY SP			49.3	
154	Lady Loretta Fm	310.8	0.03	2.81	0.36	3820	948	0.6						221WD20	110755	MU	MDST			0.1	E1
155	Lady Loretta Fm	49.0	0.05	2.83	0.28	3790	324	1.0						221WD20	110756	MU	SLST			2.5	E2i
156	Lady Loretta Fm	244.0	0.02	3.00	0.47	4390	255	2.6						221WD20	110757	MU	PYR SLST			8.5	
157	Lady Loretta Fm	281.8	0.01	3.19	0.49	4210	101	18.8						221WD20	110758	MU	SUL SHLE			21.0	
158	Lady Loretta Fm	446.3	0.01	2.77	0.28	5130								221WD20	110759	MU	DMT SLST			27.0	
159	Lady Loretta Fm	328.7	0.01	3.94	0.59	4880								221WD20	110760	OH	SP GN PY			32.8	
160	Lady Loretta Fm	330.2	0.01	3.46	0.45	5040	13	17.6						221WD20	110761	OH	PY SP GN			44.0	
161	Lady Loretta Fm	567.3	0.02	3.20	1.23	4800	1001	0.7						221W05	110763	MU	FER SDY C SLST			0.5	

Appendix 3

Mount Isa Basin Petrophysics

sort	Unit	Dry wt	Porosity	SG sat	Susc	Velocity	Resistivity	IP%	TC1	TC2	K	U	Th	Source	ID	Mbr	Lithology	E	N	Depth	Notes
162	Lady Loretta Fm	240.9	0.03	2.85	0.35		452	2.0						221Wi05	110764	MU	SHLE			1.8	
163	Lady Loretta Fm	545.3	0.05	2.87	0.68	4010	492	2.6						221Wi05	110765	MU	FER SLST			6.0	
164	Lady Loretta Fm	297.8	0.03	2.95	0.65	4170	287	6.9						221Wi05	110766	MU	SLST			17.4	
165	Lady Loretta Fm	448.8	0.03	2.83	0.34	4350	433	0.5						221Wi05	110767	MU	MDST			19.7	
166	Lady Loretta Fm	413.5	0.02	2.86	0.35	4670	807	1.0						221Wi05	110768	MU	MDST			26.7	
167	Lady Loretta Fm	474.0	0.03	2.78	0.57	4150	1383	1.9						221Wi05	110769	MU	FER MDST			36.7	BAKED 110770 onwards
168	Lady Loretta Fm	163.3	0.06	2.76	0.23		760	4.4						221Wi05	110770	MU	PYR SHLE			41.5	
169	Lady Loretta Fm	218.3	0.01	3.76	0.57	4780	29	16.9						221Wi05	110772	OH	PY SP GN			45.8	between
170	Lady Loretta Fm	270.7	0.01	3.86	0.72									221Wi05	110773	OH	SHLE			49.3	magnetic
171	Lady Loretta Fm	289.2	0.01	3.39	1.36	5790								221Wi05	110776	PU	SD MDST			53.5	susceptibility
172	Lady Loretta Fm	46.6	0.08	2.61	0.11	4070	216	2.9						221Wi05	110777	PU	CAR MDST			57.2	
173	Lady Loretta Fm	143.1	0.02	2.98	1.05		779	3.3						221Wi05	110778	PU	PY (SD?)			58.0	alteration
174	Lady Loretta Fm	452.0	0.02	2.97	0.81	5180	353	3.1						221Wi40	110779	MU	FER SLST			1.0	index??
175	Lady Loretta Fm	199.4	0.11	2.56	0.18	3540	196	5.7						221Wi40	110780	CU	SLST			2.2	
176	Lady Loretta Fm	771.9	-1.93	1.00	0.36	4640								221Wi40	110781	CU	PYR SLST			9.7	
177	Lady Loretta Fm	623.1	0.03	3.09	1.18	4570								221Wi40	110782	CU	FER SLST			23.7	
178	Lady Loretta Fm	746.9			1.23									221Wi40	110784	PU	PYR SLST			60.2	
179	Lady Loretta Fm	264.4	0.07	2.74	0.51		163	11.1						245EI22	110785	CU	SLST			1.0	H1
180	Lady Loretta Fm	262.4	0.05	2.94	0.73		125	3.9						245EI22	110786	CU	LA PYR SLST			4.9	
181	Lady Loretta Fm	637.3	0.04	2.92	0.72		347	1.0						245EI22	110787	CU	MDST			7.0	H3
182	Lady Loretta Fm	171.9	0.13	2.41	0.08		358	0.9						245EI22	110788	CU	F SLY SDST			16.5	H4
183	Lady Loretta Fm	456.4	0.01	3.87	0.10	4080	673	7.7						245EI22	110790	OH	PORS BRT PY SP GN			26.0	
184	Lady Loretta Fm	342.7	0.02	3.04	0.14	4790								245EI22	110792	OH	PY SP BRT			35.8	
185	Lady Loretta Fm	373.8	0.05	2.60	0.04									245EI22	110793	OS	SLST			40.2	
186	Lady Loretta Fm	245.9	0.00	2.66	0.06		126	0.4						245EI22	110794	OS	MDST			42.2	
187	Lady Loretta Fm	612.3	0.04	2.64	0.06		324	0.8						245EI22	110795	OS	BX			46.0	
188	Lady Loretta Fm	1119.9	0.02	2.98	0.11		401	3.9						245EI22	110796	OS	SP GN PY BRT			47.6	
189	Lady Loretta Fm	1009.1	0.00	3.72	0.21									245EI22	110797	OH	SLY LAY PY SP			61.3	
190	Lady Loretta Fm	287.9	0.01	3.93	0.22		235	14.1						245EI22	110798	OH	SP GN			86.1	
191	Lady Loretta Fm	449.2	0.00	3.29	0.16									245EI22	110799	OH	SP GN			90.7	
192	Lady Loretta Fm	162.9	0.08	2.46	0.06		600	6.4						245EI22	110800	OH	SP CHRT			96.6	
193	Lady Loretta Fm	249.0	0.00	2.67	0.04		111724	2.9						245EI22	110801	OH	CHRT			96.9	
194	Lady Loretta Fm	114.4	0.02	2.65	0.04		46271	3.3						245EI22	110802	OH	STRO CHRT			96.7	
195	Lady Loretta Fm	300.1	0.00	2.82	0.06									245EI22	110803	OH	SP PY VN CHRT BX			105.4	
196	Lady Loretta Fm	333.3	0.07	2.58	0.07									245EI22	110806	PU	CAR SHLE			116.3	
197	Lady Loretta Fm				0.42									245EI22	110807	PU	CAR SHLE			117.2	
198	Lady Loretta Fm	114.8	0.13	2.50	0.20		219	1.2						245EI01	110809	CU	SLST			8.5	I1
199	Lady Loretta Fm	26.2	0.17	2.44	0.06		248	2.3						245EI01	110810	CU	SHLE			11.1	I2
200	Lady Loretta Fm	439.2	0.07	2.60	0.32		215	1.1						245EI01	110811	CU	SLY SHLE			12.2	
201	Lady Loretta Fm	94.6	0.09	2.60	0.12		249	0.6						245EI01	110812	MU	DMT SLST			21.0	I4

Appendix 3

Mount Isa Basin Petrophysics

sort	Unit	Dry wt	Porosity	SG sat	Susc	Velocity	Resistivity	IP%	TC1	TC2	K	U	Th	Source	ID	Mbr	Lithology	E	N	Depth	Notes
202	Lady Loretta Fm	261.3	0.00	3.51	- 0.16									245EI01	110814	OH	SP GN			33.4	
203	Lady Loretta Fm	481.8	0.01	3.47	0.15	5040	45	22.0						245EI01	110815	OH	SILI SP GN			59.8	
204	Lady Loretta Fm	122.6	0.00	3.19	0.07	5220	226	14.1						245EI01	110816	OH	CHY SP GN			59.8	
205	Lady Loretta Fm	506.8	0.01	2.99	0.07									245EI01	110817	OH	SP GN			57.8	
206	Lady Loretta Fm	534.9	0.01	4.08	0.20	4670	19	9.0						245EI01	110818	OH	SILI SP GN			62.0	
207	Lady Loretta Fm	459.4	0.00	3.11	0.25									245EI01	110819	OH	SP GN PY			67.0	
208	Lady Loretta Fm	67.7			0.50									245EI01	110821	OH	PY			78.5	CA,PD,P
209	Lady Loretta Fm	472.3	0.02	2.63	0.05		304	6.2						245EI01	110822	PU	FR DLST			85.9	
210	Lady Loretta Fm	219.5	0.12	2.58	0.33		215	1.7						245ED25	110823	CU	MDST			4.6	J1
211	Lady Loretta Fm	231.4	0.07	2.67	0.47		158	2.7						245ED25	110824	CU	FR SLST			11.5	J2
212	Lady Loretta Fm	445.2	0.14	2.52	0.09		266	1.4						245ED25	110825	CU	FR F SLST			18.0	
213	Lady Loretta Fm	271.2	0.15	2.51	0.14		179	2.8						245ED25	110826	CU	FR F SLST			19.7	
214	Lady Loretta Fm	302.2	0.00	3.85	0.10	4540								245ED25	110827	OH	BRT SP PY GN			36.5	
215	Lady Loretta Fm	224.8	0.00	4.12	0.18	4590	47020	11.9						245ED25	110828	OH	BRT SP PY GN			48.4	
216	Lady Loretta Fm	208.0	0.00	3.92	0.29	4760	1780	10.9						245ED25	110829	OH	SP GN			63.3	DSO
217	Lady Loretta Fm				0.74									245ED25	110830	PU	LAY PY			71.0	CA,PD,P
218	Lady Loretta Fm	100.2	0.06	2.56	0.06	4160	302	3.2						245ED25	110831	PU	GY SHLE			72.2	J9
219	Lady Loretta Fm	321.8			0.63									245ED25	110832	PU	LA PY			74.6	CA,PD,P
220	Lady Loretta Fm	447.2	0.03	3.18	1.59	4960								245ED25	110833	PU	BN MDST			78.5	
221	Lady Loretta Fm	258.2	0.06	2.93	0.69	4920	285	0.7						245V90	110834	CU	SLST			3.4	K1
222	Lady Loretta Fm	231.6	0.13	2.61	0.39	3670	490	1.6						245V90	110835	CU	SLST			4.0	
223	Lady Loretta Fm	708.9	0.05	2.81	0.35	4440	176	0.7						245V90	110836	CU	SLY SHLE			4.9	
224	Lady Loretta Fm	1114.8	0.08	2.72	0.74		438	0.8						245V90	110837	CU	SLY SHLE			11.9	
225	Lady Loretta Fm	336.7	0.03	2.87	0.54									245V90	110838	MU	F SLST			17.2	
226	Lady Loretta Fm	250.7	0.04	2.78	0.24		208	1.0						245V90	110839	MU	MDST			20.0	
227	Lady Loretta Fm	305.5	0.04	2.87	0.32		82	9.2						245V90	110840	MU	CAR SHLE			22.5	red mineral
228	Lady Loretta Fm	197.2	0.03	3.44	0.29	4470	118	20.9						245V90	110841	OH	LAY SP GN			27.7	
229	Lady Loretta Fm	218.8	0.02	3.51	0.26									245V90	110842	OH	SP GN PY			28.5	P
230	Lady Loretta Fm	327.8	0.16	2.44	0.26		287	1.2						245V90	110843	OS	GY SLST			33.5	
231	Lady Loretta Fm	179.1	0.12	2.67	0.63	4080	233	1.4						245V90	110844	OS	GY BN SLST			35.0	
232	Lady Loretta Fm	203.2	0.11	2.81	0.76		168	2.2						245V90	110845	OS	BN MDST			41.4	
233	Lady Loretta Fm	102.2	0.16	2.50	0.07		115	0.4						245V90	110846	OS	SLST			42.0	
234	Lady Loretta Fm	157.5	0.00	3.56	0.23		75	10.0						245V90	110847	OH	LAY SP GN			56.5	
235	Lady Loretta Fm	222.4	0.00	3.70	0.28		18	13.0						245V90	110848	OH	PYR SP GN			60.0	P
236	Lady Loretta Fm	268.9	0.00	4.53	0.31	4580	35	23.3						245V90	110849	OH	SP GN			63.0	DSO
237	Lady Loretta Fm	699.2	0.03	2.76	1.06									245V90	110850	PU	LA PY			84.0	
238	Lady Loretta Fm	468.9	0.09	2.47	0.03		284	4.6						245V90	110851	PU	GY CALC MDST			97.0	
239	Lady Loretta Fm	320.4	0.04	2.85	0.67	4560	790	2.3						234ED30	110853	CU	SD SLST			10.8	L2
240	Lady Loretta Fm	310.8	0.07	2.76	0.52		12633	10.1						234ED30	110854	CU	PY			16.7	P
241	Lady Loretta Fm	661.5	0.09	2.61	0.34	3810	227	1.4						234ED30	110855	CU	MDST			30.3	L4

Appendix 3

Mount Isa Basin Petrophysics

sort	Unit	Dry wt	Porosity	SG sat	Susc	Velocity	Resistivity	IP%	TC1	TC2	K	U	Th	Source	ID	Mbr	Lithology	E	N	Depth	Notes
242	Lady Loretta Fm	336.0	0.02	2.92	0.64	5210								234ED30	110856	CU	SD SLST			34.8	L5
243	Lady Loretta Fm	315.1	0.05	2.54	0.06									234ED30	110857	MU	SLST			51.0	
244	Lady Loretta Fm	578.5	0.01	2.66	0.06	5050	1584	1.0						234ED30	110858	MU	MDST			54.4	L7
245	Lady Loretta Fm	861.0	0.00	3.87	0.15	4620	1226	16.1						234ED30	110859	OH	PY SP GN			56.5	
246	Lady Loretta Fm	475.2	0.00	4.22	0.14	4530								234ED30	110860	OH	PY SP GN			59.8	
247	Lady Loretta Fm		3.93	3.93	0.36	4910	443	13.3						234ED30	110863	OH	PY SP GN			68.0	P
248	Lady Loretta Fm				0.13									234ED30	110864	OH	PYR CAR SHLE			71.3	
249	Lady Loretta Fm	556.8	0.06	2.81	0.86	4750	538	1.0						234ED30	110865	PU	PY SLST			104.1	L14
250	Lady Loretta Fm	292.9	0.11	2.57	0.24		193	6.0						234ED30	110866	PU	PYR SHLE			106.0	L15
251	Lady Loretta Fm	390.7	0.00	3.14	0.88		61	6.1						234ED30	110867	PU	LA PY			111.9	decomposed
252	Lady Loretta Fm	591.8	0.02	2.88	0.54		24	7.6						234ED30	110868	PU	PYR CAR SHLE			118.2	
253	Lady Loretta Fm	163.2	0.05	2.61	0.28		281	9.3						234ED30	110869	PU	SLST			124.4	
254	Lady Loretta Fm	368.7	0.03	2.69	0.41		131	6.5						234ED30	110870	PU	PYR CAR SHLE			124.9	
255	Lady Loretta Fm	626.7	0.01	3.07	0.67	5320								234ED30	110871	PU	PYR CAR MDST			133.0	
256	Lady Loretta Fm	107.9	0.01	2.74	0.12	5600	1144	3.1						234ED30	110872	PU	SLST			135.1	L21
257	Lady Loretta Fm	94.5	0.03	2.71	0.53		168	13.1						234ED30	110873	PU	PYR CAR SHLE			140.0	
258	Lady Loretta Fm	713.6	0.07	2.68	0.52									234ED30	110874	PU	PYR SLST			143.6	
259	Lady Loretta Fm	1036.3	0.04	2.81	0.77		175	8.5						234ED30	110875	LS	SLY MDST			155.0	PT
260	Lady Loretta Fm	208.2	0.02	2.73	0.16	5070	449	4.1						234ED30	110876	LS	MDST			173.0	L25
261	Lady Loretta Fm	202.9	0.01	2.71	0.12	5050	356	10.7						234ED30	110877	LS	MDY SLST			177.4	
262	Lady Loretta Fm	364.4	0.00	2.75	0.19	5470	345	15.7						234ED30	110878	LS	SLST			182.0	L27
263	Lady Loretta Fm													234ED30	110879	LS				184.8	
264	Lady Loretta Fm													234ED30	110880	LS				185.5	
265	Lady Loretta Fm	628.9	0.01	2.76	0.21	4930	826	9.7						234ED30	110881	LS	SLST			188.8	
266	Lady Loretta Fm	196.0	0.01	2.71	0.11	4840	1352	7.3						234ED30	110882	LS	MDST			189.1	L31
267	Lady Loretta Fm	262.4	0.05	2.82	0.44	4230	529	2.1						233ED30	110883	CU	SHLE			13.3	M1
268	Lady Loretta Fm	186.5	0.05	2.82	0.39		340	2.6						233ED30	110884	CU	MDY SLST			19.5	
269	Lady Loretta Fm	157.7	0.07	2.79	0.59	4450	329	1.4						233ED30	110885	CU	SD SLST			39.1	
270	Lady Loretta Fm	106.7	0.07	2.77	0.30	3820	204	0.7						233ED30	110886	CU	SLST			46.1	M4
271	Lady Loretta Fm	174.0	0.03	2.98	0.57		135	2.1						233ED30	110887	CU	SLST			48.0	
272	Lady Loretta Fm	536.9	0.05	2.61	0.15		135	1.3						233ED30	110888	CU	SDY SLST			58.8	1-88 osc
273	Lady Loretta Fm	47.2	0.06	2.59	0.03	3510	773	0.4						233ED30	110889	MU	SHLE			61.4	M7
274	Lady Loretta Fm	95.3	0.00	3.97	0.11	4580	627	2.7						233ED30	110890	OH	PY			66.0	CA,PD,P
275	Lady Loretta Fm	262.0	0.00	3.65	0.04	4980	7649	7.2						233ED30	110891	OH	SLY SP GN PY			68.9	
276	Lady Loretta Fm	430.2	0.00	4.03	0.23	4960	512	10.0						233ED30	110892	OS	SILI SP GN PY			75.4	
277	Lady Loretta Fm	287.7	0.02	3.46	0.11	4780								233ED30	110893	OS	SILI SP GN PY BX			76.4	
278	Lady Loretta Fm				0.15									233ED30	110894	OH	PY			85.4	
279	Lady Loretta Fm	260.5	0.07	2.64	0.26	3410	660	4.6						233ED30	110895	PU	SLST			95.4	
280	Lady Loretta Fm	318.0	0.08	2.64	0.19	4170	898	1.0						233ED30	110896	PU	SLST			96.0	M14
281	Lady Loretta Fm	219.1	0.10	2.52	0.11									233ED30	110897	PU	SLST			103.4	

Appendix 3

Mount Isa Basin Petrophysics

sort	Unit	Dry wt	Porosity	SG sat	Susc	Velocity	Resistivity	IP%	TC1	TC2	K	U	Th	Source	ID	Mbr	Lithology	E	N	Depth	Notes
282	Lady Loretta Fm	171.3	0.09	2.51	0.09		86	3.8						233ED30	110898	PU	SLST			108.2	
283	Lady Loretta Fm	498.8	0.04	2.88	0.79		445	0.7						231ED62	110899	CU	FR PYR MDST			6.0	N1
284	Lady Loretta Fm	264.2	0.10	2.67	0.21	3860	262	0.9						231ED62	110900	CU	MDST			16.8	N2
285	Lady Loretta Fm	110.3	0.08	2.44	0.88		103	1.8						231ED62	110901	CU	PY			20.3	CA,PD,P
286	Lady Loretta Fm	320.8	0.01	2.84	0.23	5810	1913	0.9						231ED62	110902	CU	PYR SLST			24.8	N4
287	Lady Loretta Fm	88.9	0.04	2.93	0.39	4960	195	0.5						231ED62	110903	CU	MDY SLST			29.4	N5
288	Lady Loretta Fm	330.2	0.02	3.01	0.76	5500								231ED62	110904	CU	SD SLST			32.1	
289	Lady Loretta Fm	119.3	0.06	2.76	0.28	4980	243	1.4						231ED62	110905	CU	SLST			38.2	N7
290	Lady Loretta Fm	375.0	0.04	2.91	0.44		962	2.4						231ED62	110906	CU	PY			57.0	
291	Lady Loretta Fm	478.2	0.01	2.84	0.27	5260	685	2.0						231ED62	110907	CU	SLST			64.5	
292	Lady Loretta Fm	192.5	0.01	2.84	0.14	5420	1065	1.2						231ED62	110908	CU	SLY SHLE			69.6	N10
293	Lady Loretta Fm	543.5	0.02	2.79	0.32	5550								231ED62	110909	CU	PYR SLST			70.1	
294	Lady Loretta Fm	218.9	0.04	2.73	0.18		289	1.6						231ED62	110910	CU	CU SHLE			71.9	
295	Lady Loretta Fm	386.9	0.01	2.81	0.24	5320	3938	1.3						231ED62	110911	MU	SLST			76.8	
296	Lady Loretta Fm	125.8	0.01	2.80	0.11									231ED62	110912	MU	SHLE			78.4	N14
297	Lady Loretta Fm	240.9	0.01	3.22	0.19	5260	271	13.5						231ED62	110913	OH	SP GN SUL SHLE			90.6	
298	Lady Loretta Fm	133.1	0.00	3.85	0.69	5060	238	15.5						231ED62	110914	OH	SP GN QZ SUL			93.0	
299	Lady Loretta Fm	137.5	0.06	2.78	0.51	4700	263	4.3						231ED62	110915	OH	SP SLST			100.8	
300	Lady Loretta Fm				0.28									231ED62	110916	OH	PYR SHLE			104.5	
301	Lady Loretta Fm	252.1	0.00	3.53	1.62	5410								231ED62	110917	PU	PY SD DLST			111.2	
302	Lady Loretta Fm	280.9	0.03	2.91	0.71	5050	1126	1.9						231ED62	110918	PU	SD SLST			135.1	
303	Lady Loretta Fm				0.34									231ED62	110919	PU	LA PY			137.5	CA,PD,P
304	Lady Loretta Fm	133.9	0.09	2.65	0.28	4460								231ED62	110920	LS	SLST			139.8	N22
305	Lady Loretta Fm	99.5	0.03	2.71	0.13		355	2.8						231ED62	110921	LS	SLY MDST			150.5	N23
306	Lady Loretta Fm	66.9	0.06	2.57	0.31		103	9.3						231ED62	110922	LS	PYR SHLE			154.8	
307	Lady Loretta Fm	107.4	0.08	2.52	0.27		147	8.0						231ED62	110923	LS	PYR CU SLST			155.4	
308	Lady Loretta Fm	195.7	0.07	2.51	0.09		172	9.1						231ED62	110924	LS	SLST			157.7	N26
309	Lady Loretta Fm	731.7	0.01	2.90	0.53	5690	705	1.9						233WD79	110925	CU	PYR SLY SHLE			24.3	
310	Lady Loretta Fm	144.0	0.05	2.79	0.23	4990	1029	3.5						233WD79	110926	CU	SD SLST			29.8	O2
311	Lady Loretta Fm	190.6	0.04	2.80	0.58	4620	1191	2.0						233WD79	110927	CU	SD SLST			37.5	O3
312	Lady Loretta Fm	125.7	0.01	2.78	0.15	5130	1539	0.5						233WD79	110928	CU	GY SHLE			38.5	O4
313	Lady Loretta Fm	384.1	0.14	2.56	0.53		227	1.0						233WD79	110929	CU	SLST			72.3	O5
314	Lady Loretta Fm	238.1	0.14	2.36	0.30	4020	272	1.0						233WD79	110930	CU	F SDST			74.0	
315	Lady Loretta Fm	262.0	0.03	3.14	0.78									233WD79	110931	OH	FR SUL SD BX			87.8	
316	Lady Loretta Fm	176.6	0.00	4.48	1.35		24	20.7						233WD79	110932	PU	LA PY SP			120.5	
317	Lady Loretta Fm				2.06									233WD79	110933	PU	SD DLST			121.4	
318	Lady Loretta Fm	403.0	0.01	3.00	0.29		205	12.8						233WD64	110936	CU	PYR MDY SLST			47.1	
319	Lady Loretta Fm	250.2	0.04	2.81	0.72	4950	1311	1.8						233WD64	110937	MU	SLY SHLE			74.1	P2
320	Lady Loretta Fm	324.3	0.01	3.68	0.37	4870	146	10.6						233WD64	110938	OH	PYR SHLE			78.4	PT
321	Lady Loretta Fm	248.2	0.04	2.89	0.32	4290	293	18.4						233WD64	110939	OS	CU SLY SHLE			79.4	P4

Appendix 3
Mount Isa Basin Petrophysics

sort	Unit	Dry wt	Porosity	SG sat	Susc	Velocity	Resistivity	IP%	TC1	TC2	K	U	Th	Source	ID	Mbr	Lithology	E	N	Depth	Notes
322	Lady Loretta Fm	218.6	0.06	2.96	0.54		27	9.7						233WD64	110940	OS	FR PYR SED BX			80.8	
323	Lady Loretta Fm	263.2	0.03	3.58	0.26	4500	56	21.9						236ED77	111555	OH	SP GN PY			94.8	
324	Lady Loretta Fm	652.7	0.00	3.41	0.06	4930	8787	2.8						242EI28	111556	OH	LA PY BRT CHRT			74.6	
325	Lady Loretta Fm	310.5	0.01	3.32	0.04									236EI10	111557	OH	LA SP BRT PY			68.2	
326	Lady Loretta Fm	385.9	0.00	4.35	0.02	4210	6449	2.9						242EI28	111558	OH	SP BRT PY			70.9	
327	Lady Loretta Fm	129.1	0.10	2.62	0.33	4270	547	3.9						233ED73	111559	OS	DMT SLST			106.5	
328	Lady Loretta Fm	374.6	0.05	2.91	0.36		107	14.0						233WD46	111560	OS	DMT SUL BX			78.7	
329	Lady Loretta Fm	149.6	0.01	4.21	0.54									227ED87	111561	OH	RX PY SP HEM			86.8	
330	Lady Loretta Fm	587.3	0.01	3.66	0.11									245ED49	111562	OH	SH SP BRT CHRT			33.7	
331	Lady Loretta Fm	469.7	0.00	4.13	0.10	4870	25055	6.3						242ED35	111563	OH	SH BA SP BRT			45.0	
332	Lady Loretta Fm	157.4	0.01	2.72	0.05	5450	1160	5.8						239EI31	111564	OH	MAS CHRT VN PY SP			119.7	
333	Lady Loretta Fm	213.2	0.00	4.34	0.07		50391	4.0						242ED13	111565	OH	STRO SP BRT			53.2	
334	Lady Loretta Fm	402.7	0.01	4.12	0.06	3980	184	14.9						242EI28	111566	OH	PY BRT SP			70.7	
335	Lady Loretta Fm	599.1	0.00	4.29	0.03		26977	1.3						242ED13	111567	OH	SH SP BRT			44.4	
336	Lady Loretta Fm	113.6	0.01	4.01	0.07		39565	4.9						239ED07	111568	OH	PY SP BRT			45.2	PS
337	Lady Loretta Fm	111.8	0.01	3.93	0.43	5320	33	14.4						224WD27	111569	OH	MAS BED PY QZ SP APY			44.1	PS
338	Lady Loretta Fm	330.9	0.01	4.24	0.51									222WD42	111570	OH	SP GN PY			43.8	PS
339	Lady Loretta Fm	182.4	0.01	3.76	0.34									224WD27	111571	OH	SP GN PY CCP			35.4	PS
340	Lady Loretta Fm	104.9	0.00	3.99	0.47	4460	78	22.7						228WD66	111572	OH	SP GN PY HEM CARB			91.9	PS
341	Lady Loretta Fm	78.8	0.00	3.57	0.27		11	11.9						221WD44	111573	OH	BA SP GN PY VN QZ HEM CARB			17.1	PS,AS
342	Lady Loretta Fm	132.1	0.02	3.46	0.21		185	32.6						245ED80	111574	OH	SP PY SHLE			30.3	PS
343	Lady Loretta Fm	216.3	0.00	3.49	0.24		16	25.3						234ED81	111575	OH	BA SP GN PY VN QZ HEM CARB			95.1	PS
344	Lady Loretta Fm				0.26									233WD55	111576	OH	SLY SP GN PY CCP SHLE			79.1	PS,AS
345	Lady Loretta Fm	78.0	0.00	4.26	0.08		45205	9.0						236ED12	111577	OH	STRO SP BRT PY			66.9	PS
346	Lady Loretta Fm	326.7	0.00	4.25	0.16		78367	15.3						242ED13	111578	OH	SH BRT CHRT SP PY			31.3	PS
347	Lady Loretta Fm	250.3	0.00	4.08	0.75									222ED75	111579	OH	MA CAR SP CARB QZ			48.6	PS
348	Lady Loretta Fm	131.0	0.00	4.70	0.74	4300	38	19.0						234WD45	111580	OH	MA RX SP GN PY			95.0	PS
349	Lady Loretta Fm	837.3	0.04	2.77	0.56		562	2.6						74P148	111963	UC	MDST			77.5	Q2
350	Lady Loretta Fm	121.6	0.02	2.82	0.31		258	2.2						74P148	111964	UC	SLST			81.5	Q3
351	Lady Loretta Fm	205.8	0.03	2.72	0.21		244	1.6						74P148	111965	UC	MDST			81.6	Q4
352	Lady Loretta Fm	1181.7	0.02	2.87	0.83		203	3.5						74P148	111966	UC	FER SLST			93.6	Q5
353	Lady Loretta Fm	615.9	0.03	2.85	1.33		410	2.0						74P148	111967	UC	SD SLST			97.8	Q6
354	Lady Loretta Fm	212.0	0.00	3.12	0.97		36	8.3						74P148	111968	CU	MA PY			130.2	Q7
355	Lady Loretta Fm	273.0	0.07	2.68	0.29									74P148	111969	CU	MDST			134.4	Q8
356	Lady Loretta Fm	333.1	0.10	2.56	0.17									74P148	111970	CU	SLST			135.5	Q9
357	Lady Loretta Fm	525.5			0.53									74P148	111971	CU	PYR SLST			150.9	Q10
358	Lady Loretta Fm	424.3	0.07	2.59	0.15		148	0.4						74P148	111972	CU	PYR SLST			158.5	Q11
359	Lady Loretta Fm				0.28									74P148	111973	CU	BA PY			162.0	Q12
360	Lady Loretta Fm	586.2	0.04	2.61	0.36		154	0.8						74P148	111974	CU	BA PYR SLST			162.5	OH 177.8
361	Lady Loretta Fm	994.3	0.15	2.45	0.11		84	4.5						74P148	111977	PU	GY MDST			200.0	Q15

Appendix 3

Mount Isa Basin Petrophysics

sort	Unit	Dry wt	Porosity	SG sat	Susc	Velocity	Resistivity	IP%	TC1	TC2	K	U	Th	Source	ID	Mbr	Lithology	E	N	Depth	Notes
362	Lady Loretta Fm	317.3	0.00	2.49	0.25		64	5.2						74P148	111978	PU	PY			207.0	Q17
363	Lady Loretta Fm	721.8	0.00	2.53	0.21		41	5.5						74P148	111979	PU	LA SLST			207.2	Q18
364	Lady Loretta Fm				0.51									74P148	111980	PU	LA MA PY			209.4	Q19
365	Lady Loretta Fm				0.22									74P148	111981	PU	PYR SLST			215.5	Q20
366	Lady Loretta Fm	473.7	0.00	2.45	0.18		82	2.1						74P148	111982	PU	PYR SLST			220.2	Q21
367	Lady Loretta Fm	862.4	0.01	3.04	0.31		147	11.3						74P148	111984	PU	PYR SLST			239.0	Q23
368	Lady Loretta Fm	1015.1	0.00	2.89	0.28		62	20.7						74P148	111985	PU	PYR MDY SLST			240.4	Q24
369	Lady Loretta Fm	1171.7	0.00	2.95	0.59		361	7.5						74P148	111986	LC	PYR MDY SLST			248.5	Q25
370	Lady Loretta Fm	478.1	0.03	2.70	0.19		465	8.2						74P148	111987	LC	F SLST			260.8	Q26
371	Lady Loretta Fm	993.8	0.02	2.74	0.23		254	8.3						74P148	111988	LC	DK SLST			266.2	Q27
372	Lady Loretta Fm													44P2	94200002	PU	PYR SLST			210	
373	Lady Loretta Fm													44P2	94200003	LC	SLST			268	
374	Lady Loretta Fm													44P2	94200004	LC	SLST			352	
375	Lady Loretta Fm													153P68	94200005	CU	SLST			244	
376	Lady Loretta Fm													153P68	94200006	OH	PYR SLST			272	
377	Lady Loretta Fm													153P68	94200007	OH	PYR SLST			276	
378	Lady Loretta Fm													153P68	94200010	PU	PYR SLST			312	
379	Lady Loretta Fm													153P68	94200011	PU	SLST			315	
380	Lady Loretta Fm				0.30									153P68	94200012	LC	SLST			338	
381	Lady Loretta Fm				0.01									153P68	94200013	LC	SLST			387	
382	Lady Loretta Fm	77.3	0.01	2.82	0.18		2720	1.4						150P126	111989	CU	GY DMT SHLE			191.5	R1
383	Lady Loretta Fm	514.8	0.01	2.95	0.39		525	5.1						150P126	111990	CU	PYR SLST			197.8	R2
384	Lady Loretta Fm	249.3	0.00	2.91	0.27		2790	10.0						150P126	111991	CU	DMT SLST			232.1	R3
385	Lady Loretta Fm	462.6	0.00	2.80	0.26		7891	12.8						150P126	111992	CU	MDY DMT SLST			247.6	R4
386	Lady Loretta Fm	118.6	0.00	2.81	0.22		631	22.7						150P126	111993	CU	PYR MDY DMT SLST			262.8	R5
387	Lady Loretta Fm	451.3	0.01	2.83	0.28		1789	3.0						150P126	111994	CU	PYR SLST			270.5	R6
388	Lady Loretta Fm	390.4	0.00	2.78	0.17		1252	1.5						150P126	111996	CU	DMT SLST			312.7	R8
389	Lady Loretta Fm	1199.2	0.00	2.80	0.22		2080	13.8						150P126	111998	CU	DMT SLST			318.5	
390	Lady Loretta Fm	119.4	0.00	2.82	0.29		58489	4.2						150P126	111999	CU	SLST			330.0	
391	Lady Loretta Fm	282.2	0.00	2.82	0.26									150P126	112000	CU	SLST			334.4	
392	Lady Loretta Fm	164.4	0.01	3.06	0.99		2407	5.4						150P126	112001	OH	PYR C RX DLST			335.6	
393	Lady Loretta Fm	140.1	0.00	3.68	1.54		441	61.5						150P126	112002	OH	PYR C RX DLST			341.5	R10
394	Lady Loretta Fm	110.3	0.00	3.90	0.68		295	50.0						150P126	112003	OH	PYR C RX DLST			345.8	R11
395	Lady Loretta Fm	167.6	0.00	3.91	1.65		89	48.4						150P126	112004	OH	PYR C RX DLST			347.5	R12
396	Lady Loretta Fm	114.6	0.01	3.89	1.01		130	53.1						150P126	112005	OH	PYR C RX DLST			355.5	R13
397	Lady Loretta Fm	153.8	0.00	3.78	0.45		82	15.7						150P126	112006	OH	PYR C RX DLST			360.0	R14
398	Lady Loretta Fm	296.4	0.01	3.91	0.93		147	15.2						150P126	112007	PU	CHY PYR ?SLST			391.0	R15
399	Lady Loretta Fm	78.9	0.00	3.07	0.51		144538	7.7						150P126	112008	PU	CHY ?CAR ?SLST			392.3	R16
400	Lady Loretta Fm	108.8	0.00	2.88	0.22		136086	11.0						150P126	112009	PU	SLF PYR DLST			416.8	R17
401	Lady Loretta Fm	159.0	0.00	2.87	0.33		189192	7.2						150P126	112010	PU	SLST			417.0	

Appendix 3

Mount Isa Basin Petrophysics

sort	Unit	Dry wt	Porosity	SG sat	Susc	Velocity	Resistivity	IP%	TC1	TC2	K	U	Th	Source	ID	Mbr	Lithology	E	N	Depth	Notes
402	Lady Loretta Fm	1189.6	0.00	2.83	0.17		1794	8.6						134P151	112011	LC	MDY PYR SLST			444.0	S1
403	Lady Loretta Fm	568.6	0.01	2.76	0.27		2013	1.7						134P151	112012	LC	DMT SLST			431.2	S2
404	Lady Loretta Fm	57.1			0.57									134P151	112013	PU	MA PY			409.6	S3
405	Lady Loretta Fm	182.8	0.01	2.90	0.51		4378	1.5						134P151	112014	PU	RX DMT SLST			391.5	
406	Lady Loretta Fm	41.8	0.00	3.10	0.19		58	5.5						134P151	112015	PU	C MA PY			370.1	S4
407	Lady Loretta Fm	284.7	0.01	3.50	0.70		96	16.3						134P151	112016	PU	LA PYR DMT SLST			428.9	S5
408	Lady Loretta Fm	205.3	0.01	2.98	0.31		269	16.8						134P151	112017	OH	PYR SLST			354.0	S6
409	Lady Loretta Fm	774.3	0.01	2.89	0.30		588	18.5						134P151	112018	OH	PYR DMT SLST			353.5	S7
410	Lady Loretta Fm				0.21									134P151	112019	OH	PYR SLST			353.0	S8
411	Lady Loretta Fm	1080.1	0.01	2.76	0.19		646	0.9						134P151	112021	CU	DMT MDY SLST			294.8	S10
412	Lady Loretta Fm	1370.7	0.00	2.89	0.45		940	3.1						134P151	112022	CU	DMT MDY PYR SLST			260.0	S11
413	Lady Loretta Fm	432.2	0.01	2.81	0.28		1849	4.8						134P151	112023	CU	MDY DMT SLST			276.8	S12
414	Lady Loretta Fm	845.1	0.01	2.81	0.24		702	2.9						134P151	112024	UC	PYR DMT MDST			181.5	S13
415	Lady Loretta Fm	681.7	0.01	2.84	0.36		762	1.6						153P114	112025	CU	PYR DMT SLST			301.8	P114-1
416	Lady Loretta Fm	649.8	0.01	2.94	0.43		289	4.4						153P114	112026	CU	PYR DMT SLST			321.6	P114-2
417	Lady Loretta Fm	813.6	0.01	2.83	0.31		906	25.7						153P114	112027	CU	PYR DMT SLST			340.0	P114-3
418	Lady Loretta Fm	695.4	0.01	2.90	0.36		511	12.3						153P114	112028	CU	PYR DMT SLST			350.0	P114-4
419	Lady Loretta Fm	1086.7	0.01	2.70	0.13		199	12.3						225P155	112029	LS	DMT CAR SHLE			302.7	P155-1
420	Lady Loretta Fm	1899.1	0.01	2.78	0.39		3558	6.0						225P155	112030	LS	LA CAR MDY DMT SLST			338.5	P155-2
421	Lady Loretta Fm	1733.8	0.01	2.77	0.19		1201	4.9						225P155	112031	LS	LA CAR DMT SLST			365.9	P155-3
422	Lady Loretta Fm	616.1	0.00	2.77	0.16		1251	4.5						225P155	112032	LS	DMT SLY MDST			395.3	P155-4
423	Lady Loretta Fm	1112.5	0.01	2.76	0.14		677	17.8						225P155	112033	LS	DMT SLST			528.9	P155-5
424	Lady Loretta Fm	612.7	0.03	2.54	0.45		269	1.9						212P138	112035	OH	PYR SHLE			202.0	T1
425	Lady Loretta Fm	434.9	0.05	2.69	0.50		98	3.7						212P138	112037	OH	FER SLST			210.8	T3
426	Lady Loretta Fm	188.4	0.04	2.70	0.22		241	1.2						212P138	112038	OH	SHLE			220.0	T4
427	Lady Loretta Fm	29.2	0.08	2.62	0.15		540	1.6						212P138	112039	PU	SLST			243.5	T5
428	Lady Loretta Fm	208.4	0.03	3.36	1.32		3960	2.8						212P84	112046	PU	SD			202.0	W3
429	Lady Loretta Fm	337.5	0.04	2.77	0.28		233	11.5						212P84	112047	PU	SLY PYR DLST			211.0	W4
430	Lady Loretta Fm	600.4	0.02	2.89	0.34		170	11.5						212P84	112048	PU	DMT PYR SLST			222.6	W5
431	Lady Loretta Fm	155.4	0.01	2.87	0.22		57	13.5						212P84	112050	PU	DMT MDST			227.5	W7
432	Lady Loretta Fm	215.3	0.02	2.71	0.18		293	3.9						212P84	112051	LS	DMT SLST			232.0	W8
433	Lady Loretta Fm	502.9	0.01	2.77	0.24		417	11.4						212P84	112052	LS	DMT MDST			232.2	W9
434	Lady Loretta Fm	705.2	0.00	2.83	0.27		1681	1.6						212P84	112055	LS	SLY DLST			248.6	W12
435	Lady Loretta Fm	231.1	0.02	2.61	0.38		562	2.6						212P84	112059	LS	MDST			259.7	W16
436	Lady Loretta Fm	394.9	0.01	2.71	0.10		963	6.8						212P84	112062	LS	DMT SLST			273.3	W19
437	Lady Loretta Fm	147.2	0.01	3.91	0.54		14	19.4						212P96	112064	CU	LA PY			238.0	X1
438	Lady Loretta Fm	226.7	0.05	2.65	0.12		289	8.5						212P96	112069	LS	SLST			317.0	X7
439	Lady Loretta Fm	507.7	0.06	2.56	0.22		159	2.9						212P96	112070	LS	SLST			317.2	X8
440	Lady Loretta Fm	372.6	0.02	3.08	0.78		56	6.6						221P87	112072	CU	PYR SD SLST			296.6	Y2
441	Lady Loretta Fm	81.1	0.03	2.79	0.21		198	1.8						221P87	112073	CU	SHLE			297.0	Y3

Appendix 3

Mount Isa Basin Petrophysics

sort	Unit	Dry wt	Porosity	SG sat	Susc	Velocity	Resistivity	IP%	TC1	TC2	K	U	Th	Source	ID	Mbr	Lithology	E	N	Depth	Notes
442	Lady Loretta Fm	190.7	0.11	2.54	0.13		395	1.0						221P87	112074	CU	SHLE			297.3	Y4
443	Lady Loretta Fm	243.3	0.05	2.75	0.57									221P87	112075	CU	SD			301.6	Y5
444	Lady Loretta Fm	242.1	0.00	3.29	0.54		59	16.0						221P87	112076	PU	DMT PY			506.0	Y6
445	Lady Loretta Fm	573.0	0.00	3.25	0.90									221P87	112077	PU	DMT MDY PY			571.5	Y7
446	Lady Loretta Fm	497.0	0.00	3.58	0.81		417	11.0						221P87	112078	PU	DMT MDY PY			574.5	Y8
447	Lady Loretta Fm	167.6	0.00	3.94	0.86		43	13.0						221P87	112080	PU	DMT PY			581.7	Y10
448	Lady Loretta Fm	396.7	0.08	2.58	0.06		295	2.1						248P109	112083	OS	GY SLST			131.2	V1
449	Lady Loretta Fm	303.3	0.02	2.65	0.05		265	4.1						248P109	112091	PU	PYR SHLE			185.0	V9
450	Lady Loretta Fm	90.6	0.16	2.46	0.14		152	0.8						248P109	112096	OS	PYR CAR SHLE			124.0	V14
451	Lady Loretta Fm			2.53										248P123A	8002	OS				358.0	
452	Lady Loretta Fm			4.28										248P123A	8003	OH	SP GN			407.0	
453	Lady Loretta Fm			2.46										248P123A	8004	PU				420.0	
454	Lady Loretta Fm			3.66										248P123A	8005	PU	PY			427.0	
455	Lady Loretta Fm			4.31										232M4/8	8001	OH	SP GN			365.0	
456	Lady Loretta Fm			2.60										237P117B	8006	CU				243.5	
457	Lady Loretta Fm			2.61										237P117B	8007	CU				253.5	
458	Lady Loretta Fm			2.67										237P117B	8008	CU				263.5	
459	Lady Loretta Fm			2.67										237P117B	8009	CU				273.5	
460	Lady Loretta Fm			2.76										237P117B	8010	CU				316.5	
461	Lady Loretta Fm			2.83										237P117B	8011	CU				326.5	
462	Lady Loretta Fm			2.84										237P117B	8012	CU				336.5	
463	Lady Loretta Fm			2.86										237P117B	8013	CU				346.5	
464	Lady Loretta Fm			2.88										237P117B	8014	CU				356.5	
465	Lady Loretta Fm			2.80										237P117B	8015	CU				366.5	
466	Lady Loretta Fm			2.72										237P117B	8016	CU				376.5	
467	Lady Loretta Fm			2.79										237P117B	8017	CU				386.5	
468	Lady Loretta Fm			3.71										237P117B	8018	PU	PY			450.0	
469	Lady Loretta Fm			3.04										237P117B	8019	PU	PY			460.0	
470	Lady Loretta Fm			3.31										237P117B	8020	PU	PY			470.0	
471	Lady Loretta Fm			3.69										237P117B	8021	PU	PY			480.0	
472	Lady Loretta Fm			3.43										237P117B	8022	PU	PY			487.5	
473	Lady Loretta Fm			3.03										237ED75	8023	OH	SP GN				
474	Lady Loretta Fm			4.36										230WD55	8024	OH	SP GN				
475	Lady Loretta Fm	82.4	0.00	2.86	0.21		4916	6.2						242P121	112097	LC	PYR DMT SLST			495.5	P121
476	Lady Loretta Fm?	89.2	0.01	2.72	0.11		286	23.9						242P121	112098	LC	DMT SLST			527.5	P121
477	Lady Loretta Fm?	107.0	0.00	2.92	0.17		3084	7.6						242P121	112099	LC	BR SLY DLST			544.5	P121
478	Lady Loretta Fm?	174.0	0.00	2.88	0.23		2819	9.0						242P121	112100	LC	BR SLY DLST			553.5	P121
479	Lady Loretta Fm?	49.2	0.01	2.88	0.11		6247	14.3						242P121	112101	LC	BR SLY DLST			564.6	P121
480	Lady Loretta Fm?	52.1	0.00	2.86	0.14		99999999							242P121	112102	LC	BR SLY DLST			603.0	P121
481	Lady Loretta Fm?	136.1	0.01	2.84	0.16		3130	6.5						242P121	112103	LC	BR PYR SLY DLST			610.0	P121

Appendix 3
Mount Isa Basin Petrophysics

sort	Unit	Dry wt	Porosity	SG sat	Susc	Velocity	Resistivity	IP%	TC1	TC2	K	U	Th	Source	ID	Mbr	Lithology	E	N	Depth	Notes
482	Lady Loretta Fm	546.6	0.02	2.72	0.18		297	14.4						177P164	112104	LC	DMT SLST			119.0	P164-1
483	Lady Loretta Fm	876.6	0.01	2.76	0.17									177P164	112105	LC	DMT SLST			146.0	P164-2
484	Lady Loretta Fm	722.1	0.01	2.75	0.11		973	20.0						177P164	112106	LC	DMT SLST			177.0	P164-3
485	Lady Loretta Fm	1247.3	0.00	2.78	0.16	5760	6486	3.0	1362	494	45	20	7	189P163	1025	LC	DMT CAR PY SHLE	297184	7811973	148	
486	Lady Loretta Fm	1029.5	0.03	2.72	0.09	4550	1147	1.1	950	240	37	18	-1	172P165	1026	LC	SD SLST	297174	7812249	74.2	
487	Lady Loretta Fm	1145.3	0.07	2.60	0.18	4800	184	3.3	1474	390	55	4	3	189P163	1027	LC	FER DMT CAR SLST	297184	7811973	111	
488	Lady Loretta Fm	994.1	0.01	2.75	0.23	5630	682	9.2	794	282	17	8	1	177P164	1029	LC	DMT CAR PY SLST	297174	7812249	173.6	
489	Lady Loretta Fm	1160.5	0.01	2.78	0.11	6100	5108	8.7	708	206	21	22	-3	177P164	1030	LC	DMT CAR SLST	297181	7812052	88.5	
490	Lady Loretta Fm	431.9	0.09	2.37	0.08	4260	1063	2.2	1078	398	87	10	9	177P164	1031	LC	WEA SLST	297181	7812052	61.5	
491	Lady Loretta Fm	716.8	0.01	2.75	0.09	5430	2469	2.3	1640	524	45	10	3	177P164	1032	LC	CAR SLST	297181	7812052	121	
492	Lady Loretta Fm	1224.4	0.01	2.74	0.13	5620	82	16.0	1015	283	31	16	13	177P164	1048	LC	CAR DMT SLST	297181	7812052	142	
493	Lady Loretta Fm	585.6	0.02	2.67	0.05	5460	9618	2.3	635	171	27	12	-1	CM2	2003		FER DMT SLST	297181	7812052	223	
494	Lady Loretta Fm	556.7	0.10	2.39	0.08	3790	626	1.3	941	307	43	2	9	CM2	2004		FER SLST	298206	7827459	226	
495	Lady Loretta Fm	516.0	0.01	2.76	0.07	6130	88760	2.1	239	27	1	-2	-1	CM2	2005		FER STRO DLST	298206	7827459	231	
496	Lady Loretta Fm	557.9	0.01	2.70	0.06	5880	80415	2.4	381	45	-7	0	1	CM2	2006		FER STRO DLST	298206	7827459	233	
497	Lady Loretta Fm	437.3	0.02	2.70	0.06	5150	35517	1.7	373	141	15	2	-1	CM2	2007		SLY DLST	298206	7827459	234	
498	Lady Loretta Fm	732.1	0.03	2.70	0.08	5720	2923	1.5	683	259	23	-2	3	CM2	2008		FER STRO DLST	298206	7827459	235	
499	Lady Loretta Fm	293.9			0.49									227WD45	134815	OH	FELD CHRT			65.5	
500	Lady Loretta Fm	67.9	0.01	2.76	0.13		7200	1.3						137P150	134816	UC	F SDST			114.6	
501	Lady Loretta Fm	99.7	0.28	2.00	0.09	2590	251	1.0						74P148	134817	UC	ALT DMT PYR SLST			69.4	
502	Lady Loretta Fm	273.0	0.03	2.81	0.35		1200	11.7						228ED78	134818	MU	FELD CHRT PY			89.5	
503	Lady Loretta Fm	30.0	0.04	2.56	0.02		570	2.0						239ED07	134819	OS	GP CHRT			34.3	0-46 osc
504	Lady Loretta Fm	851.1	0.00	4.10	1.23									227WD45	134820	OH	GN SP PY			93.1	
505	Lady Loretta Fm	438.2	0.01	3.72	0.42	5450	45	18.5						233WD70	134821	OH	PY GN SP			94.9	
506	Lady Loretta Fm	394.4	0.00	4.05	2.57		52	24.1						233WD70	134822	OH	BRT PY GP			90.1	
507	Lady Loretta Fm	359.5	0.01	3.76	0.37		25	26.7						236WD05	134823	OH	PY SP GN			42.9	
508	Lady Loretta Fm	441.9	0.00	3.95	0.07									236ED12	134824	OH	BRT CHRT			66.7	
509	Lady Loretta Fm	303.0	0.01	2.98	0.08									239EI14	134825	OH	STRO SP CHRT			97.1	
510	Lady Loretta Fm	209.5	0.00	2.77	0.10		1561	10.5						164P122	134826	CU	GP SLST			210.0	
511	Lady Loretta Fm	52.4	0.01	2.75	0.06		943	0.7						236ED12	134827	OS	GP SLST			43.5	
512	Lady Loretta Fm	85.2	0.07	2.62	0.05									239ED07	134828	OS	CHRT			34.2	
513	Lady Loretta Fm	531.2	0.00	4.25	0.08									242EI28	134829	OH	BRT SP PY			71.0	
514	Lady Loretta Fm	217.5	0.00	4.34	0.08		3669	0.9						242ED13	134830	OH	STRO SP BRT CHRT			53.2	
515	Lady Loretta Fm				0.20									242EI28	134831	OS	GP CHRT			66.7	
516	Lady Loretta Fm	516.7	0.00	4.32	0.10		898	1.9						242ED13	134832	OH	GP SP BRT CHRT			55.0	
517	Lady Loretta Fm	347.6	0.09	2.65	0.30									242ED62	134833	MU	SLY MDST			41.0	
518	Lady Loretta Fm	566.8	0.04	2.92	0.42									242ED88	134834	OH	SD FELD CHRT SP GN PY			43.7	
519	Lady Loretta Fm	112.3	0.01	4.35	0.11		15762	4.3						236EI10	134836	OH	BRT SP			65.2	
520	Lady Loretta Fm	230.5	0.00	4.42	0.05		1916	4.2						236EI10	134837	OH	BRT SP GN			59.5	
521	Lady Loretta Fm	699.7	0.01	2.79	0.13	5960								Amoco83-5	83553		F DLST	269800	7898900	17.0	

Appendix 3

Mount Isa Basin Petrophysics

sort	Unit	Dry wt	Porosity	SG sat	Susc	Velocity	Resistivity	IP%	TC1	TC2	K	U	Th	Source	ID	Mbr	Lithology	E	N	Depth	Notes
522	Lady Loretta Fm	219.4	0.01	2.76	0.13		7876	2.0						Amoco83-5	83515		SLY DLST	269800	7898900	27.0	
523	Lady Loretta Fm	188.8	0.01	2.84	0.15		20039	7.1						Amoco83-5	83552		F DLST	269800	7898900	43.6	
524	Lady Loretta Fm	66.0	0.00	2.80	0.06		62679	2.9						Amoco83-5	83516		SLY DLST	269800	7898900	59.5	
525	Lady Loretta Fm	158.8	0.02	2.74	0.13		1766	2.7						Amoco83-5	83517		SLY DLST	269800	7898900	72.2	
526	Lady Loretta Fm	354.0	0.01	2.97	0.11		60878	1.8						Amoco83-5	83518		FER BR DLST	269800	7898900	88.2	
527	Lady Loretta Fm	1017.4	0.03	2.81	0.12	5520								Amoco83-5	83551		FER BR DLST	269800	7898900	91.6	
528	Lady Loretta Fm	306.5	0.02	2.78	0.15		1289	0.7						Amoco83-5	83519		SLY DLST	269800	7898900	138.1	
529	Lady Loretta Fm	225.7	0.01	2.81	0.12	5930	10149	1.0						Amoco83-5	83547		SDY SD VN DLST	269800	7898900	156.4	
530	Lady Loretta Fm	428.7	0.01	2.79	0.16	5180								Amoco83-5	83594		SD VN RE M DLST	269800	7898900	162.5	
531	Lady Loretta Fm	199.3	0.00	2.83	0.10	6310	53220	2.3						Amoco83-5	83521		SLY DLST	269800	7898900	196.8	
532	Lady Loretta Fm	245.1	0.05	2.75	0.18		635	0.6						Amoco83-5	83544		GR PU DMT SLST	269800	7898900	236.7	
533	Lady Loretta Fm	133.8	0.01	2.81	0.14		5649	2.7						Amoco83-5	83545		SLY DLST	269800	7898900	238.9	
534	Lady Loretta Fm	243.1	0.02	2.81	0.19	5770	19946	1.0						Amoco83-5	83543		SLF DLST	269800	7898900	244.1	
535	Lady Loretta Fm	159.0	0.00	2.81	0.10									Amoco83-5	83522		SLY DLST	269800	7898900	256.9	
536	Lady Loretta Fm	410.1	0.00	2.85	0.11	6810								Amoco83-5	83523		DLST	269800	7898900	266.7	
537	Lady Loretta Fm	511.8	0.00	2.83	0.20	6200								Amoco83-5	83542		DLST	269800	7898900	302.7	
538	Lady Loretta Fm	352.6	0.00	2.82	0.29	5790	6527	1.2						Amoco83-5	83532		SLY F DLST	269800	7898900	328.3	
539	Lady Loretta Fm	314.5	0.00	2.85	0.23		5895	1.1						Amoco83-5	83595		DLST	269800	7898900	331.9	
540	Lady Loretta Fm	283.9	0.00	2.80	0.15	5920	31411	2.4						Amoco83-5	83596		SLY DLST	269800	7898900	342.4	
541	Lady Loretta Fm	398.0	0.01	2.79	0.29		4892	1.7						Amoco83-5	83531		DMT SLST	269800	7898900	344.3	
542	Lady Loretta Fm	649.8	0.01	2.80	0.34		1153	1.0						Amoco83-5	83530		SLY BR DLST	269800	7898900	369.4	
543	Lady Loretta Fm	224.6	0.01	2.76	0.22		899	0.8						Amoco83-5	83597		DMT SLST	269800	7898900	376.6	
544	Lady Loretta Fm	221.1	0.01	2.78	0.12		2182	0.7						Amoco83-5	83529		SLY DLST	269800	7898900	379.9	
545	Lady Loretta Fm	267.7	0.01	2.78	0.20		2822	1.3						Amoco83-5	83528		M DLST	269800	7898900	380.9	
546	Lady Loretta Fm	122.3	0.01	2.72	0.14		5050	2.4						Amoco83-5	83524		DMT SLST	269800	7898900	389.5	
547	Lady Loretta Fm	84.1	0.00	2.85	0.06		99999999							Amoco83-5	83525		DLST	269800	7898900	395.0	
548	Lady Loretta Fm	136.6	0.00	2.85	0.08	6760	99999999							Amoco83-5	83533		DLST	269800	7898900	395.2	
549	Lady Loretta Fm	180.1	0.03	2.69	0.16		636	1.0						Amoco83-5	83534		SLST	269800	7898900	396.4	
550	Lady Loretta Fm	257.4	0.01	2.76	0.22		996	0.6						Amoco83-5	83535		DMT SLST	269800	7898900	401.5	
551	Lady Loretta Fm	636.5	0.01	2.75	0.22		2073	1.0						Amoco83-5	83527		SLY DLST	269800	7898900	401.8	
552	Lady Loretta Fm	155.6	0.00	2.84	0.08	6500	313636	5.7						Amoco83-5	134842		GP DMT SLST CLST	269800	7898900	407.7	
553	Lady Loretta Fm	256.5	0.00	2.83	0.09	6560	99999999							Amoco83-5	134841		GP DMT SLST CLST	269800	7898900	419.2	
554	Lady Loretta Fm	106.6	0.02	2.78	0.19		2300	0.8						Amoco83-5	83538		RE SLY DLST	269800	7898900	420.0	
555	Lady Loretta Fm	159.7	0.01	2.76	0.17		11616	1.5						Amoco83-5	134840		DMT MDY SLST GNL CNGL	269800	7898900	421.6	
556	Lady Loretta Fm	115.1	0.01	2.75	0.17	5110	2686	0.8						Amoco83-5	83598		GR SLY DLST	269800	7898900	423.8	
557	Lady Loretta Fm	246.4	0.01	2.69	0.25		1019	1.1						Amoco83-5	83539		DMT SLST	269800	7898900	424.5	
558	Lady Loretta Fm	64.9	0.01	2.75	0.15		3068	1.7						Amoco83-5	83540		M DMT SLST	269800	7898900	428.8	
559	Lady Loretta Fm	144.8	0.01	2.76	0.23		2559	0.9						Amoco83-5	83599		DMT SHLE	269800	7898900	435.9	
560	Lady Loretta Fm	72.1	0.02	2.75	0.15		1272	0.6						Amoco83-5	83541		SLY DLST	269800	7898900	439.2	
561	Lady Loretta Fm	191.6	0.01	2.75	0.16		16422	1.8						Amoco83-5	134839		DMT SLY MDST	269800	7898900	465.9	

Appendix 3

Mount Isa Basin Petrophysics

sort	Unit	Dry wt	Porosity	SG sat	Susc	Velocity	Resistivity	IP%	TC1	TC2	K	U	Th	Source	ID	Mbr	Lithology	E	N	Depth	Notes
562	Lady Loretta Fm	144.3	0.00	2.81	0.10	6500	13828	1.2						Amoco83-5	134846		BR DLST	269800	7898900	469.0	
563	Lady Loretta Fm	105.0	0.00	2.82	0.08	6360	98356	3.5						Amoco83-5	83501		SLY DLST	269800	7898900	494.2	
564	Lady Loretta Fm	199.2	0.02	2.75	0.21	5230	3560	1.1						Amoco83-5	83514		DMT MDST	269800	7898900	507.8	
565	Lady Loretta Fm	142.5	0.01	2.74	0.29	5040	2716	0.8						Amoco83-5	83513		DMT MDST	269800	7898900	508.7	
566	Lady Loretta Fm	599.2	0.00	2.80	0.09	6030	6770	1.0						Amoco83-5	83512		SLY DLST	269800	7898900	514.5	
567	Lady Loretta Fm	160.1	0.03	2.72	0.29		1369	7.1						Amoco83-5	83511		DMT SLST	269800	7898900	526.7	
568	Lady Loretta Fm	72.5	0.00	2.74	0.11	5880	14187	1.5						Amoco83-5	83549		SLY F DLST	269800	7898900	529.1	
569	Lady Loretta Fm	70.5	0.02	2.69	0.15	4290	15636	1.9						Amoco83-5	83510		DMT SLST	269800	7898900	533.9	
570	Lady Loretta Fm	223.0	0.00	2.76	0.13		34847	1.7						Amoco83-5	134843		DMT SLY MDST	269800	7898900	536.1	
571	Lady Loretta Fm	175.0	0.00	2.81	0.06	6200								Amoco83-5	134844		LA DLST	269800	7898900	538.1	
572	Lady Loretta Fm	319.6	0.01	2.75	0.16		2555	1.3						Amoco83-5	83555		GR DMT SLST	269800	7898900	541.8	
573	Lady Loretta Fm	131.2	0.00	2.82	0.04	6140	21781	3.1						Amoco83-5	83556		DLST	269800	7898900	548.0	
574	Lady Loretta Fm	251.3	0.00	2.74	0.18	6290	17012	1.0						Amoco83-5	134845		EVAP DLST	269800	7898900	558.4	
575	Lady Loretta Fm	595.3	0.01	2.78	0.35	5210	2978	1.6						Amoco83-5	83509		DMT SLST	269800	7898900	563.2	
576	Lady Loretta Fm	331.9	0.00	2.82	0.14	5670	6292	0.8						Amoco83-5	83508		MDY DLST	269800	7898900	581.2	
577	Lady Loretta Fm	154.6	0.07	2.62	0.05		193	2.9						242ED35	134848	OS	DLST			39.2	
579	Lady Loretta Fm			2.73			4540	7.1						P64	7021	Ptx5b	BR CAR DMT SLST			96.0	R&C
580	Lady Loretta Fm			2.71			2380	2.4						P64	7022	Ptx5b	CAR DMT SLST			118.9	R&C
581	Lady Loretta Fm			2.90			659	14.7						P65	7023	Ptx5b	BR CAR DMT SLST			117.3	R&C
582	Lady Loretta Fm	194.9	0.00	2.78	0.04									CM35	2150		DLST	298750	7827000	120.4	CM35 at low angle to dip
583	Lady Loretta Fm	170.7	0.00	2.83	0.08									CM35	2151		DLST	298750	7827000	131.0	
584	Lady Loretta Fm	159.7	0.00	2.84	0.08									CM35	2152		STRO DLST	298750	7827000	141.1	
585	Lady Loretta Fm	66.0	0.01	2.79	0.08		2361	4.8						CM35	2153		SLY DLST	298750	7827000	141.3	
586	Lady Loretta Fm	167.4	0.01	2.86	0.10		326627	5.7						CM35	2154		DLST	298750	7827000	146.8	
587	Lady Loretta Fm	221.4	0.00	2.87	0.09		99999999							CM35	2155		STRO DLST	298750	7827000	158.9	
588	Lady Loretta Fm	190.3	0.00	2.87	0.11									CM35	2156		DLST	298750	7827000	159.0	
589	Lady Loretta Fm	174.7	0.00	2.85	0.10									CM35	2157		PYR DLST	298750	7827000	170.0	
590	Lady Loretta Fm	212.6	0.00	2.82	0.08									CM35	2158		SLY DLST	298750	7827000	181.0	
591	Lady Loretta Fm	196.5	0.00	2.84	0.10									CM35	2159		DLST	298750	7827000	190.3	
592	Lady Loretta Fm	215.6	0.00	2.85	0.08									CM35	2160		BU DLST	298750	7827000	200.0	
593	Lady Loretta Fm	197.4	0.00	2.83	0.10									CM35	2161		SLY DLST	298750	7827000	210.6	
594	Lady Loretta Fm	186.5	0.01	2.83	0.12									CM35	2162		DLST	298750	7827000	220.0	
595	Lady Loretta Fm	138.7	0.02	2.81	0.10									CM35	2163		STRO DLST	298750	7827000	230.0	
596	Lady Loretta Fm	241.3	0.01	2.83	0.10									CM35	2164		SLY DLST	298750	7827000	240.0	
597	Lady Loretta Fm	214.7	0.01	2.85	0.13									CM35	2165		DLST	298750	7827000	250.0	
598	Lady Loretta Fm	51.3	0.01	2.82	0.10		2751	46.7						CM35	2166		QZ DMT SLST	298750	7827000	259.8	
599	Lady Loretta Fm	175.8	0.01	2.83	0.13		34986	13.3						CM35	2167		DLST	298750	7827000	260.8	
600	Lady Loretta Fm	126.7	0.00	2.84	0.09		99999999							CM35	2168		DLST	298750	7827000	266.0	
601	Lady Loretta Fm	130.8	0.00	2.80	0.04		99999999							CM35	2169		SLY DLST	298750	7827000	267.5	
602	Lady Loretta Fm	117.6	0.00	2.88	0.11		99999999							CM35	2170		DLST	298750	7827000	270.0	

Appendix 3

Mount Isa Basin Petrophysics

sort	Unit	Dry wt	Porosity	SG sat	Susc	Velocity	Resistivity	IP%	TC1	TC2	K	U	Th	Source	ID	Mbr	Lithology	E	N	Depth	Notes	
603	Lady Loretta Fm	199.1	0.01	2.82	0.10									CM35	2171		DLST	298750	7827000	280.0		
604	Lady Loretta Fm	75.7	0.00	2.74	0.04		746715	3.7						CM35	2172		QZ DLST	298750	7827000	286.0		
605	Lady Loretta Fm	192.3	0.01	2.82	0.09									CM35	2173		DLST	298750	7827000	289.3		
606	Lady Loretta Fm	131.0	0.02	2.76	0.06									CM35	2174		PI DLST	298750	7827000	311.2		
607	Lady Loretta Fm	186.4	0.01	2.83	0.10									CM35	2175		SLY DLST	298750	7827000	320.2		
608	Lady Loretta/Esp? contact Fm	508.4	0.00	2.72	0.18		530997	5.3						CM35	134838		STRO CHRT	298750	7827000	320.5		
609	Esperanza Formation?	93.8	0.00	2.87	0.09		99999999							CM35	2176		DLST	298750	7827000	330.0		
610	Esperanza Formation?	175.1	0.08	2.64	0.08									CM35	2177		BU SLY DLST	298750	7827000	340.2		
611	Esperanza Formation?	294.3	0.00	2.84	0.20		1445	13.9						242P121	134847	LC	SD DLST			593.0		
612	Esperanza Formation?				0.69		34000	1.2						P69	7007	CFZ	SLF DLST			410.0	R&C	
613	Esperanza Formation	1936.0	0.04	2.42	0.04	4950	11900	1.5	815	165	23	2	5	GW	1085	Plx4	F SDST			0		
614	Esperanza Formation	1187.6	0.19	2.15	0.13	1940	895	2.2	511	97	29	4	1	GW	1045	Plx4	FER F SDST			0		
615	Esperanza Formation	1335.7	0.19	2.17	0.13	1690	856	2.4	531	163	9	14	7	GW	1046	Plx4	FER F SDST			0		
616	Esperanza Formation	1422.1	0.02	2.46	0.01	5390	147236	3.6	271	11	-11	-12	-1	GW	1071	Plx4	STRO CHRT			0		
617	Esperanza Formation	1341.0	0.01	2.47	0.01	5390	55317	2.5	261	-41	-1	4	9	GW	1072	Plx4	STRO CHRT			0		
618	Esperanza Formation			2.61	0.24									CM8	31383		CAR SHLE	293308	7843904	226.29	Aberfoyle	
619	Esperanza Formation			2.61	0.19									CM8	31384		CAR SHLE	293308	7843904	227.1	Aberfoyle	
620	Esperanza Formation			2.64	0.26									CM8	31385		CAR SHLE	293308	7843904	230.65	Aberfoyle	
621	Esperanza Formation			2.69	0.20									CM8	31386		CAR SHLE	293308	7843904	230.78	Aberfoyle	
622	Esperanza Formation	556.1	0.03	2.71	0.10	4860	31	8.7	729	269	27	14	13	CM8	2009		CAR DMT PY SLST	293308	7843904	234		
623	Esperanza Formation	302.4	0.04	2.65	0.07	4790	66	7.9	797	197	13	2	-5	CM8	2010		CAR DMT PY SHLE	293308	7843904	240	py/dol blobs	
624	Esperanza Formation	229.9	0.04	2.61	0.08	4650	76	10.7	583	215	27	4	-3	CM8	2011		CAR DMT PY SHLE	293308	7843904	240	py/dol blobs	
625	Esperanza Formation	297.3	0.01	2.65	0.05									CM8	2012		CAR SHLE	293308	7843904	247		
626	Esperanza Formation	224.7	0.00	2.65	0.09	5450	210532	3.4	481	147	37	14	1	CM8	2013		PY SLST	293308	7843904	252		
627	Esperanza Formation	711.4	0.00	2.63	0.09	5700	685693	24.9	939	295	55	4	9	CM8	2014		LA MIC SLST	293308	7843904	257		711.4
628	Esperanza Formation	423.5	0.00	2.64	0.09	5610	2158980	9.6	611	187	41	12	3	CM8	2015		LA SLST	293308	7843904	264		423.5
629	Esperanza Formation	721.2	0.00	2.71	0.14	5710	133	29.3	871	309	41	-2	13	CM8	2016		DMT SLST	293308	7843904	270		721.2
630	Esperanza Formation	724.5	0.01	2.72	0.14	5710	4356	7.5	767	229	31	-4	5	CM8	2017		LA DMT SLST	293308	7843904	276		724.5
631	Esperanza Formation	653.1	0.01	2.65	0.08	5150	28	14.3	1091	225	45	22	1	CM8	2018		CAR DMT SLST	293308	7843904	282		735.7
632	Esperanza Formation	243.7	0.05	2.64	0.05		427	8.7						CM8	2019		CAR DMT PY SHLE	293308	7843904	291		653.1
633	Esperanza Formation	162.4	0.04	2.64	0.06		139	16.5						CM8	2020		CAR PY SHLE	293308	7843904	291		
634	Esperanza Formation	160.9	0.04	2.64	0.06	4440	89	12.8	813	195	27	10	3	CM8	2021		CAR SHLE	293308	7843904	295		
635	Esperanza Formation	275.2	0.03	2.64	0.06	4320	64	12.2	971	285	31	0	9	CM8	2022		CAR MDST	293308	7843904	295		
636	Esperanza Formation	648.5	0.01	2.69	0.10	5460	3052	1.2	771	187	11	2	3	CM8	2023		DMT SLST	293308	7843904	300		
637	Esperanza Formation	442.4	0.01	2.73	0.10	5920	389684	2.2	237	47	15	10	-1	CM8	2024		STRO SLY DLST	293308	7843904	306		
638	Esperanza Formation	266.9	0.07	2.56	0.06	4690	4799	2.3	297	183	11	4	5	CM8	2025		FER SDY DLST	293308	7843904	311		
639	Esperanza Formation	389.8	0.00	2.75	0.15	5560	11761	2.0	569	251	17	-2	7	CM8	2026		SLY DLST	293308	7843904	319		
640	Esperanza Formation			2.72	0.13									CM2	313206		CAR SHLE	293308	7843904		Aberfoyle	
641	Esperanza Formation			2.58	0.06									CM33	3133311		CAR GPT SHLE	298206	7827459	129	Aberfoyle	
642	Esperanza Formation	199.0	0.00	3.95	0.07		12250	6.1						BB002	133682		PY CCP SP DLST	271000	7917450	184.5		

Appendix 3

Mount Isa Basin Petrophysics

sort	Unit	Dry wt	Porosity	SG sat	Susc	Velocity	Resistivity	IP%	TC1	TC2	K	U	Th	Source	ID	Mbr	Lithology	E	N	Depth	Notes
644	Paradise Ck Fm?	1380.2	0.05	2.41	0.04	5150	9552	3.2	409	19	-1	0	15	GW	1009	Ptx3	SLF DMT SLST	295000	7812000		
645	Paradise Ck Fm?	1011.1	0.07	2.38	0.02	4780	2418	1.8	377	111	25	4	5	GW	1009	Ptx3	SLF DMT SLST	295000	7812000		
646	Paradise Ck Fm?	295.5	0.06	2.44	0.07	4700	1239	1.1	249	113	3	12	13	GW	1009	Ptx3	SLF DMT SLST	295000	7812000		
647	Paradise Ck Fm?	281.3	0.08	2.43	0.09	4820	2170	1.6	173	93	19	14	3	GW	1010	Ptx3	SLF DMT SLST	295000	7812000		
648	Paradise Ck Fm?	116.8	0.11	2.29	0.01	4310	789	3.2						GW	1011	Ptx3	DMT SLST	295000	7812000		
649	Paradise Ck Fm?	822.6	0.16	2.11	0.04	2980	1876	3.6	483	215	27	12	11	GW	1012	Ptx3	F SDST	295000	7812000		
650	Paradise Ck Fm?	653.4	0.15	2.11	0.02	3160	1837	3.2	427	225	41	10	11	GW	1012	Ptx3	F SDST	295000	7812000		
651	Paradise Ck Fm?	905.1	0.16	2.09	0.03	2880	2061	3.3	781	163	33	16	5	GW	1012	Ptx3	F SDST	295000	7812000		
652	Paradise Ck Fm?	968.5	0.16	2.09	0.02	2880	1432	2.1	535	199	43	8	3	GW	1012	Ptx3	F SDST	295000	7812000		
653	Paradise Ck Fm?	1183.1	0.03	2.83	0.42	4940	33494	4.6	2437	649	55	40	3	GW	1064	Ptx3	HM CHRT BX	295000	7812000		
654	Paradise Ck Fm?	1464.9	0.03	2.86	0.52	5050	21600	2.8	2571	613	15	20	7	GW	1065	Ptx3	HM CHRT BX	295000	7812000		
655	Paradise Ck Fm	185.0	0.00	2.77	0.08	6230								BB001	133673		DMT CNGL	271500	7917510	273.6	
656	Paradise Ck Fm	76.4	0.00	2.82	0.07		43994	1.5						BB002	133674		OO DLST	271000	7917450	254.3	
657	Paradise Ck Fm	571.7	0.00	2.87	0.13	6350								BB002	133675		OO DLST	271000	7917450	108.4	
658	Paradise Ck Fm	469.1	0.00	2.88	0.23	6580								BB001	133676		DMT GNST	271500	7917510	101.5	
659	Paradise Ck Fm	207.2	0.05	2.72	0.08									BB001	133677		DMT SLST	271500	7917510	215.0	
660	Paradise Ck Fm	88.4	0.01	2.71	0.06		1851	5.1						BB001	133678		CAR MDST	271500	7917510	262.0	
661	Paradise Ck Fm	710.3	0.02	2.81	0.15		121739	1.6						Cooper	133679		STRO DMT SLST	271650	7917550	0	
662	Paradise Ck Fm	221.5	0.00	2.86	0.08		22257	4.5						BB002	133680		GP EVAP DLST	271000	7917450	132.6	
663	Paradise Ck Fm	401.3	0.00	4.12	0.07									BB002	133683		PY CCP SP DLST	271000	7917450	209.8	
664	Paradise Ck Fm	609.3	0.08	2.60	0.16		253	1.6						Cooper	133684		STRO DMT SLST	271550	7916000	0	
665	Paradise Ck Fm													P7	8051	Plx4a	CHRT BX			90.5	
666	Paradise Ck Fm													P10	8049	Ptx3	CHRT BX			90.5	
667	Paradise Ck Fm													P10	8050	Ptx3	CHRT BX			153	
668	Paradise Ck Fm													P11	8047	Ptx3	WEA SHLE			84	
669	Paradise Ck Fm													P11	8048	Ptx3	CHRT BX			182	
670	Paradise Ck Fm	169.6	0.00	2.80	0.07		541	20.4						P47	4006	Ptx3	BR SLY SUL CAR DLST	295057	7812155	104.4	
671	Paradise Ck Fm													P47	8028	Ptx3	DMT SHLE			107.5	
672	Paradise Ck Fm													P47	8033	Ptx3	DMT SHLE			132.5	
673	Paradise Ck Fm													LA13	8035	Ptx3	DMT SHLE			124	
674	Paradise Ck Fm	152.3	0.01	2.79	0.16		4831	0.5						X58/13	4007	Ptx3?	HM DMT SLST	296070	7812850	240.25	
675	Paradise Ck Fm	787.9	0.16	2.46	0.11	5490	452	0.8	971	177	49	4	1	GW	1055		SLY DLST	295500	7813000	0	14-50 osc.
676	Paradise Ck Fm	1504.7	0.09	2.60	0.13	5460	921	0.5	1201	295	51	8	11	GW	1056		SLY DLST	295500	7813000	0	7-49 osc.
677	Paradise Ck Fm	1726.3	0.06	2.66	0.16	5520	1932	0.4	1081	331	41	6	-1	GW	1057		SLY DLST	295500	7813000	0	longest axis
678	Paradise Ck Fm	1802.1	0.16	2.39	0.20	3810	1441	1.1	1419	211	19	0	3	GW	1053	Ptx2	SLY F SDST	295800	7812400	0	
679	Paradise Ck Fm	1323.4	0.16	2.33	0.23	3360	1349	0.2	967	149	5	8	13	GW	1054	Ptx2	SLY F SDST	295800	7812400	0	along bedding
680	Paradise Ck Fm	1690.5	0.08	2.44	0.22	5080	10778	0.0	517	27	23	12	1	GW	1074	Ptx2	HM CHRT BX	295800	7812400	0	
681	Paradise Ck Fm	1831.7	0.09	2.42	0.18	4960	7402	4.4	533	41	9	16	7	GW	1075	Ptx2	HM CHRT BX	295800	7812400	0	
682	Paradise Ck Fm		0.03	2.78	0.13										5501		DMT SLST	308600	7799200	200	Hone et al
683	Paradise Ck Fm		0.02	2.71	0.00										5502		SLST DLST	308600	7799200	400	Hone et al

Appendix 3
Mount Isa Basin Petrophysics

sort	Unit	Dry wt	Porosity	SG sat	Susc	Velocity	Resistivity	IP%	TC1	TC2	K	U	Th	Source	ID	Mbr	Lithology	E	N	Depth	Notes
684	Paradise Ck Fm		0.01	2.73	0.00										5503		DMT SLST	308600	7799200	600	Hone et al
685	Paradise Ck Fm		0.01	2.72										GSQLH3	5301		DMT SLST	276000	7927500	94	Hone et al
686	Paradise Ck Fm		0.02	2.72	0.13										5504			307000	7767500	221	Hone et al
687	Paradise Ck Fm	85.4	0.03	2.72	0.06		200	13.8						P4?	4005		BR CAR DMT SLST PY CCP	295300	7812200	101.4	
689	Paradise Ck Fm			2.67	0.13									CM10	3131008		CAR SHLE	290052	7882681	173.8	Aberfoyle
690	Paradise Ck Fm			2.63	0.13									CM10	3131009		CAR SHLE	290052	7882681	294	Aberfoyle
691	Paradise Ck Fm			2.59	0.25									CM10	3131010		CAR SHLE	290052	7882681	156.21	Aberfoyle
692	Paradise Ck Fm			2.61	0.29									CM10	3131011		CAR SHLE	290052	7882681	158.22	Aberfoyle
693	Paradise Ck Fm			2.62	0.24									CM10	3131012		CAR SHLE	290052	7882681	160.1	Aberfoyle
694	Paradise Ck Fm			2.64	0.23									CM10	3131013		CAR SHLE	290052	7882681	160.8	Aberfoyle
695	Paradise Ck Fm			2.66	0.26									CM10	3131014		CAR SHLE	290052	7882681	163.5	Aberfoyle
696	Paradise Ck Fm			2.80	0.23									CM10	3131015		CAR SHLE	290052	7882681	164	Aberfoyle
697	Paradise Ck Fm			2.65	0.13									CM10	3131016		CAR SHLE	290052	7882681	166.5	Aberfoyle
698	Paradise Ck Fm			2.67	0.23									CM10	3131017		CAR SHLE	290052	7882681	166.7	Aberfoyle
699	Paradise Ck Fm			2.67	0.21									CM10	3131018		CAR SHLE	290052	7882681	175.4	Aberfoyle
700	Paradise Ck Fm			2.73	0.13									CA4	31401		CAR DMT SHLE	288850	7883900	438	Aberfoyle
701	Paradise Ck Fm			2.72	0.13									CA4	31402		DMT CAR SHLE	288850	7883900	580.1	Aberfoyle
702	Paradise Ck Fm			2.76	0.19									CA4	31403		CAR GPT SHLE	288850	7883900	672.6	Aberfoyle
703	Paradise Ck Fm			2.74	0.19									CA4	31404		CAR SHLE	288850	7883900	718	Aberfoyle
704	Paradise Ck Fm			2.74	0.19									CA4	31405		CAR SHLE	288850	7883900	729	Aberfoyle
705	Paradise Ck Fm			2.71	0.19									CM21	3132110		CAR GPT SHLE	303174	7822280	224	Aberfoyle
706	Paradise Ck Fm	673.1	0.01	2.65	0.09	5330	112	18.0	1077	291	35	-8	-5	CM42	2071		MDY SLST	303950	7821900	105	
707	Paradise Ck Fm	208.9	0.02	2.65	0.08	4560	148	17.0						CM42	2072		CAR SHLE	303950	7821900	110	
708	Paradise Ck Fm	377.4	0.01	2.64	0.08	5030	77	18.0	1049	327	29	20	-3	CM42	2073		CAR SHLE	303950	7821900	110	
709	Paradise Ck Fm	128.7	0.02	2.66	0.08	4000	203	17.5						CM42	2074		CAR SHLE	303950	7821900	111	
710	Paradise Ck Fm	646.0	0.01	2.90	0.09	5350	138	20.0	1153	343	19	18	3	CM42	2075		CAR PY SHLE	303950	7821900	111	
711	Paradise Ck Fm	389.0	0.02	2.66	0.08	4930	90	20.9	1171	377	27	12	7	CM42	2076		CAR SHLE	303950	7821900	116	
712	Paradise Ck Fm	135.3	0.03	2.61	0.10	3850	212	16.1						CM42	2077		CAR SHLE	303950	7821900	123	
713	Paradise Ck Fm	284.3	0.03	2.66	0.12	4440	97	16.7	885	245	15	4	5	CM42	2078		CAR PY SHLE	303950	7821900	123	
714	Paradise Ck Fm	447.8	0.04	2.63	0.10	4340	65	18.3	1567	457	47	4	-1	CM42	2079		CAR SHLE	303950	7821900	127	
715	Paradise Ck Fm	857.4	0.01	2.80	0.12	6360	2761	16.2	507	171	-11	4	-7	CM42	2080		SLY DMT ARNT	303950	7821900	215	
716	Paradise Ck Fm	507.4	0.02	2.79	0.08	6320	2178	10.5	397	7	1	4	-3	CM42	2081		SLY PY DLST	303950	7821900	220	
717	Paradise Ck Fm	634.1	0.01	2.78	0.11	5930	791	9.5	755	71	15	2	3	CM42	2082		SLY DLST	303950	7821900	221	
718	Paradise Ck Fm	874.0	0.02	2.80	0.05	6450	232	13.7	633	117	5	-2	-7	CM42	2083		SLY CAR PY DMT ARNT	303950	7821900	227	
719	Paradise Ck Fm	502.3	0.01	2.68	0.07	5310	63	18.5	1095	253	51	18	3	CM42	2084		CAR SLST	303950	7821900	239	
720	Paradise Ck Fm	292.1	0.02	2.68	0.10	4610	109	16.1	747	185	17	8	-1	CM42	2085		LA SLST	303950	7821900	244	
721	Paradise Ck Fm	196.8	0.02	2.68	0.14	3720	166	17.6						CM42	2002		CAR SHLE	303950	7821900	244	
722	Paradise Ck Fm	538.9	0.02	2.78	0.08	6450	6839	4.3	289	59	25	-12	-1	CM20	2063		PY DLST	302814	7822727	231	
723	Paradise Ck Fm	492.8	0.01	2.82	0.08	6560	9143	9.2	309	33	-1	2	-1	CM20	2064		LMST DLST	302814	7822727	235	
724	Paradise Ck Fm	476.7	0.01	2.82	0.12	6360	2311	6.6	545	103	13	4	1	CM20	2065		LMST DLST	302814	7822727	237	

Appendix 3
Mount Isa Basin Petrophysics

sort	Unit	Dry wt	Porosity	SG sat	Susc	Velocity	Resistivity	IP%	TC1	TC2	K	U	Th	Source	ID	Mbr	Lithology	E	N	Depth	Notes
725	Paradise Ck Fm	759.3	0.01	2.82	0.10	6620	6770	3.4	415	37	21	0	1	CM20	2066		SUL DLST	302814	7822727	240	
726	Paradise Ck Fm	756.1	0.00	2.83	0.09	6710	7531	3.0	297	-45	-7	0	-3	CM20	2067		LMST DLST	302814	7822727	243	
727	Paradise Ck Fm	762.4	0.00	2.83	0.11	6720	35740	5.4	467	93	3	8	-5	CM20	2068		LMST DMT ARNT	302814	7822727	247	
728	Paradise Ck Fm	751.2	0.01	2.79	0.09	6090	4772	6.1	433	51	15	-10	-7	CM20	2069		SLY DMT ARNT	302814	7822727	248	
729	Paradise Ck Fm	748.2	0.01	2.76	0.09	5840	697	18.9	481	43	-5	2	3	CM20	2070		SLY DLST	302814	7822727	252	
730	Paradise Ck Fm	1274.5	0.02	2.47	0.01	5070	50870	1.2	165	67	-9	-4	7	GW	1004	Plx1.5	C SDST	295400	7812700	0	
731	Paradise Ck Fm	1392.0	0.02	2.47	0.01	4860	93971	1.8	137	-27	5	-2	1	GW	1004	Plx1.5	C SDST	295400	7812700	0	
732	Paradise Ck Fm	1416.3	0.09	2.36	0.03	4290	2535	0.5	223	-59	-11	2	-1	GW	1066	Plx1.5	M FEL SDST	295400	7812700	0	
733	Paradise Ck Fm	1553.4	0.08	2.38	0.02	4270	1085	5.0	363	19	-9	0	5	GW	1067	Plx1.5	M FEL SDST	295400	7812700	0	
734	Paradise Ck Fm	1218.0	0.05	2.41	0.01	5430	19712	1.3	197	61	-17	4	7	GW	1062	Plx1	CHRT	295400	7812700	0	
735	Paradise Ck Fm	1603.7	0.04	2.44	0.02	5660	38904	1.4	211	15	-1	-10	-3	GW	1063	Plx1	CHRT	295400	7812700	0	
736	Paradise Ck Fm	1397.7	0.04	2.45	0.02	5080	73362	2.8	141	-13	-7	-4	3	GW	1070	Plx1	STRO CHRT	295400	7812700	0	
737	Paradise Ck Fm	1597.9	0.02	2.50	0.01	5250	180290	2.3	389	-11	-5	-4	3	GW	1076	Plx1	STRO CHRT	295400	7812700	0	
738	Paradise Ck Fm	47.0	0.01	2.78	0.13		1227	3.3						LA67	4001	Plx1	DMT SLST	294978	7812353	215.9	
739	Paradise Ck Fm	91.8	0.05	2.68	0.12		174	13.3						P43	4002	Plx1	DMT CAR PYR SLST	295072	7812245	100.3	
740	Paradise Ck Fm	78.5	0.00	2.80	0.05		38544	9.9						P43	4003	Plx1	SLY PYR DLST	295072	7812245	105.5	
741	Paradise Ck Fm	84.6	0.00	2.80	0.06		525	12.2						P43	4004	Plx1	SLY SUL DLST	295072	7812245	106.8	
742	Paradise Ck Fm				0.10		6	50.0						P44	7008	Plx1	CAR SHLE			130.2	R&C
743	Paradise Ck Fm						1053	16.0						P92L	7012	Plx1	PY BN SLST			79.9	550
744	Paradise Ck Fm						1647	1.0						P92L	7013	Plx1	FER SLST			88.7	860
745	Paradise Ck Fm						2049	1.0						P92L	7014	Plx1	CHY DMT SLST CC PY			121.9	1070
746	Paradise Ck Fm						1	54.0						P92L	7015	Plx1	SLF DLST CC BN			194.8	0.3
747	Paradise Ck Fm						402	9.0						P92L	7016	Plx1	DMT CAR SLST PY			223.4	210
748	Paradise Ck Fm						6703	2.0						P92L	7017	Plx1	CAR SLY SHLE PY CCP			280.4	3500
749	Paradise Ck Fm						121	12.7						LA23	7024	Plx1				117	
750	Paradise Ck Fm						151	6.1						LA23	7025	Plx1				117.1	
751	Paradise Ck Fm													P46	8025	Plx1	WEA CU ORE SHLE			44.5	
752	Paradise Ck Fm													LA20	8026	Plx1	WEA CU ORE SHLE			63	
753	Paradise Ck Fm													LA12	8027	Plx1	WEA CU ORE SHLE			54	
754	Paradise Ck Fm													LA20	8029	Plx1	WEA CU ORE SHLE			49.5	
755	Paradise Ck Fm													LA49	8030	Plx1	WEA CU ORE SHLE			53.5	
756	Paradise Ck Fm													LA12	8031	Plx1	WEA CU ORE SHLE			46.5	
757	Paradise Ck Fm													LA17	8032	Plx1	WEA CU ORE SHLE			37.5	
758	Paradise Ck Fm													LA40	8034	Plx1	WEA CU ORE SHLE			22.5	
759	Paradise Ck Fm													LA40	8036	Plx1	WEA CU ORE SHLE			12.5	
760	Paradise Ck Fm													LA10	8037	Plx1	WEA CU ORE SHLE			11.5	
761	Paradise Ck Fm													LA6	8038	Plx1	WEA CU ORE SHLE			33	
762	Paradise Ck Fm													LA25	8039	Plx1	WEA CU ORE SHLE			36.5	
763	Paradise Ck Fm													LA29	8040	Plx1	WEA CU ORE SHLE			35	
764	Paradise Ck Fm														8041	Plx1	WEA CU ORE SHLE			16	

Appendix 3

Mount Isa Basin Petrophysics

sort	Unit	Dry wt	Porosity	SG sat	Susc	Velocity	Resistivity	IP%	TC1	TC2	K	U	Th	Source	ID	Mbr	Lithology	E	N	Depth	Notes
765	Paradise Ck Fm														8042	Plx1	WEA CU ORE SHLE			36	
766	Paradise Ck Fm														8043	Plx1	WEA CU ORE SHLE			56	
767	Paradise Ck Fm														8044		CC			122	
768	Paradise Ck Fm														8045		CC			153	
769	Paradise Ck Fm														8046		CC			184	
770	Paradise Ck Fm													P41	8052	Plx1	DMT SHLE			93	
771	Paradise Ck Fm													P41	8053	Plx1	DMT SHLE			103	
772	Paradise Ck Fm													P41	8054	Plx1	DMT SHLE			113	
773	Paradise Ck Fm		0.03	2.74	0.00									GSQLH4	5601		DLST	274800	7926300	75	Hone et al
774	Paradise Ck Fm	267.2	0.02	2.70	0.09	5750	23327	3.4	425	191	5	0	7	GSQLH4	5301		SLY DLST	274800	7926300	91.2	
775	Paradise Ck Fm		0.00	2.73										GSQLH4	5602		DLST	274800	7926300	100	Hone et al
776	Paradise Ck Fm	125.5	0.01	2.78	0.04	6550	99999999							GSQLH4	5302		STRO DLST	274800	7926300	120.1	
777	Paradise Ck Fm	239.3	0.00	2.82	0.10	6530	705563	2.0	157	1	1	12	5	GSQLH4	5401		M DLST	274800	7926300	137.3	
778	Paradise Ck Fm	91.5	0.00	2.79	0.06	5900	238428	2.3						GSQLH4	5442		SLY DLST	274800	7926300	145.3	
779	Paradise Ck Fm	54.9	0.00	2.72	0.05	5150	9198	1.2						GSQLH4	5402		DMT PYR SLST	274800	7926300	170.6	
780	Paradise Ck Fm	68.5	0.00	2.81	0.08		605288	5.4						GSQLH4	5440		STRO DLST	274800	7926300	174.0	
781	Paradise Ck Fm	83.2	0.00	2.86	0.11	6580	450457	3.5						GSQLH4	5403		STRO PYR DLST	274800	7926300	175.3	
782	Paradise Ck Fm	41.2	0.00	2.78	0.06	6330	1605005	4.3						GSQLH4	5404		PYR DLST	274800	7926300	176.0	
783	Paradise Ck Fm	82.7	0.00	2.85	0.09	6590	99999999							GSQLH4	5405		C DLST	274800	7926300	177.1	
784	Paradise Ck Fm	181.2	0.01	2.79	0.08	5990								GSQLH4	5439		ALT SLY DLST	274800	7926300	180.1	
785	Paradise Ck Fm	117.2	0.03	2.67	0.07	4710	1063	1.9						GSQLH4	5438		ALT DMT SLST	274800	7926300	185.8	
786	Paradise Ck Fm	114.0	0.00	2.78	0.08	6150	228871	2.1						GSQLH4	5412		RE SLY M DLST	274800	7926300	187.3	
787	Paradise Ck Fm	167.2	0.03	2.77	0.10	6190								GSQLH4	5441		VU DLST	274800	7926300	189.3	
788	Paradise Ck Fm	119.9	0.00	2.84	0.12	6550	99999999							GSQLH4	5413		DLST	274800	7926300	193.2	
789	Paradise Ck Fm	98.5	0.00	2.83	0.09	6580	99999999							GSQLH4	5306		STRO DLST	274800	7926300	198.6	
790	Paradise Ck Fm		0.00	2.87	0.09									GSQLH4	5603		DLST	274800	7926300	200	Hone et al
791	Paradise Ck Fm	92.0	0.00	2.77	0.12	5900	135301	1.9						GSQLH4	5437		ALT STRO SLY DLST	274800	7926300	205.4	
792	Paradise Ck Fm	59.3	0.02	2.81	0.10	4820	99999999							GSQLH4	5414		RE DLST	274800	7926300	207.0	
793	Paradise Ck Fm	58.1	0.00	2.80	0.06	5190								GSQLH4	5416		DLST	274800	7926300	217.6	
794	Paradise Ck Fm	48.8	0.00	2.85	0.08	6180	99999999							GSQLH4	5415		STRO PYR DLST	274800	7926300	219.3	
795	Paradise Ck Fm	196.8	0.00	2.76	0.07	5790								GSQLH4	5417		SLY STRO DLST	274800	7926300	229.5	
796	Paradise Ck Fm	78.5	0.00	2.85	0.05	5820	99999999							GSQLH4	5436		SDY DLST	274800	7926300	232.1	
797	Paradise Ck Fm	67.3	0.00	2.87	0.08	6560	99999999							GSQLH4	5418		STRO PYR DLST	274800	7926300	237.6	
798	Paradise Ck Fm	102.1	0.00	2.81	0.08	6400	676362	2.3						GSQLH4	5419		BR DLST	274800	7926300	239.0	
799	Paradise Ck Fm	60.6	0.00	2.83	0.08	6020	1069123	3.5						GSQLH4	5420		STRO PYR DLST	274800	7926300	241.2	
800	Paradise Ck Fm	89.2	0.00	2.89	0.08	6400	333871	3.5						GSQLH4	5421		M PYR DLST	274800	7926300	267.1	
801	Paradise Ck Fm	158.5	0.00	2.85	0.07	6670	99999999							GSQLH4	5422		M DLST	274800	7926300	270.1	
802	Paradise Ck Fm	81.5	0.00	2.89	0.09	6590	99999999							GSQLH4	5423		DLST	274800	7926300	276.1	
803	Paradise Ck Fm	97.1	0.01	2.79	0.05	5900	99999999							GSQLH4	5303		GP DLST	274800	7926300	276.4	
804	Paradise Ck Fm		0.00	2.86	0.09									GSQLH4	5604		DLST	274800	7926300	300	Hone et al

Appendix 3

Mount Isa Basin Petrophysics

sort	Unit	Dry wt	Porosity	SG sat	Susc	Velocity	Resistivity	IP%	TC1	TC2	K	U	Th	Source	ID	Mbr	Lithology	E	N	Depth	Notes
805	Paradise Ck Fm	220.4	0.00	2.79	0.07	5430	111796	2.0	373	57	7	-4	3	GSQLH4	5424		M SLY DLST	274800	7926300	300.2	
806	Paradise Ck Fm	55.8	0.01	2.91	0.06	6200	72411	18.4						GSQLH4	5425		BR PYR DLST	274800	7926300	301.8	
807	Paradise Ck Fm	109.6	0.01	2.78	0.08	6260	321651	3.1						GSQLH4	5426		RE CHY DLST	274800	7926300	320.5	
808	Paradise Ck Fm	340.5	0.01	2.82	0.07	6300			105	13	-11	-6	7	GSQLH4	5427		RE DLST	274800	7926300	328.0	
809	Paradise Ck Fm	127.9	0.01	2.80	0.05	6240	214578	2.2						GSQLH4	5429		RE DLST	274800	7926300	330.2	
810	Paradise Ck Fm	43.8	0.01	2.73	0.05	4600	12787	1.0						GSQLH4	5430		DMT SLST	274800	7926300	368.8	
811	Paradise Ck Fm	100.2	0.01	2.81	0.06	6250	77350	2.3						GSQLH4	5431		RE DLST	274800	7926300	383.7	
812	Paradise Ck Fm		0.00	2.86	0.00									GSQLH4	5605		DLST	274800	7926300	400	Hone et al
813	Paradise Ck Fm	170.5	0.00	2.82	0.10	6560	99999999							GSQLH4	5432		SLY PYR STRO DLST	274800	7926300	426.2	
814	Paradise Ck Fm	89.3	0.04	3.83	0.08		99	12.3						Dept	101942	ore	CC CUP			0.0	P.A.
815	Paradise Ck Fm	1775.2	0.07	2.58	7.85		4000	2.8	293	17	-15	-8	1	Dept	109971					0	
816	Paradise Ck Fm	678.4	0.06	2.67	0.09		1560	2.4	329	-859	-7	-2	-3	Dept	109972					0	
817	Paradise Ck Fm	854.8	0.02	2.75	0.18		20475	1.4	149	-859	-19	4	1	Dept	109973					0	
818	Paradise Ck Fm	1430.7	0.13	2.48	0.25		1440	2.0	381	-859	-7	0	1	Dept	109974					0	
819	Paradise Ck Fm	336.5	0.01	2.79	0.13		240000	5.0	221	-859	-3	-10	-3	Dept	109975					0	
820	Paradise Ck Fm	562.9	0.02	2.53	0.02		98824	1.4						B. C. Jones	133604		CHRT	273677	7917334	0	
823	Mount Oxide Chert	997.0	0.01	2.58	0.01	4870	150207	1.2	265	85	3	4	-1	GW	1001	Pmo	CHRT	295900	7813300	0	
824	Mount Oxide Chert	1222.1	0.01	2.58	0.01	4880	44754	0.7	149	29	-9	6	-5	GW	1001	Pmo	CHRT	295900	7813300	0	
825	Mount Oxide Chert	171.4	0.01	2.60	0.01	5190	81482	1.2						GW	1002	Pmo	CHRT	295900	7813300	0	
826	Mount Oxide Chert	157.0	0.01	2.61	0.00									GW	1003	Pmo	CHRT	295900	7813300	0	
827	Mount Oxide Chert	1601.7	0.01	2.62	0.01	5630	1957576	2.6	369	63	-3	2	5	GW	1073	Pmo	CHRT	295900	7813300	0	
828	Mount Oxide Chert	1309.0	0.04	2.50	0.03	5420	2152500	3.0	359	27	-3	-4	7	GW	1077	Pmo	CHRT	295900	7813300	0	
829	Gunpowder Ck Fm	657.9	0.09	2.73	0.16		1184	3.2	221	185	-11	4	-3	Dept	101943	ore	AZ			0	MtOxide
830	Gunpowder Ck Fm	812.5	0.11	2.25	0.23		1322	3.0							109979					0	
831	Gunpowder Ck Fm		0.00	2.72	0.13									GSQLH4	5606	c	DMT SLST	274800	7926300	430	Hone et al
832	Gunpowder Ck Fm	262.0	0.00	2.76	0.11	4700	54673	1.5	799	183	5	0	1	GSQLH4	5436	c	DMT SLST	274800	7926300	432.5	
833	Gunpowder Ck Fm	101.0	0.02	2.73	0.08	5310	9935	2.5						GSQLH4	5304	c	DMT SLST	274800	7926300	433.0	
834	Gunpowder Ck Fm	110.9	0.00	2.74	0.09	5590	5437	5.1						GSQLH4	5433	c	DMT SLST	274800	7926300	435.5	
835	Gunpowder Ck Fm	36.5	0.01	2.71	0.07	4830	7467	1.2						GSQLH4	5434	c	RE DMT SLST	274800	7926300	437.9	
836	Gunpowder Ck Fm	239.2	0.00	2.72	0.10	5570			319	61	19	-6	5	GSQLH4	5428	c	DMT SLST	274800	7926300	438.0	
837	Gunpowder Ck Fm	245.2	0.00	2.78	0.11	6150			345	105	11	-8	-1	GSQLH4	5435	c	DMT SLST	274800	7926300	444.2	
838	Gunpowder Ck Fm	119.2	0.00	2.74	0.11	5710	5741	2.3						GSQLH4	5305	c	DMT SLST	274800	7926300	447.4	
839	Gunpowder Ck Fm		0.00	2.75	0.00									GSQLH4	5607	c	DMT SLST	274800	7926300	445	Hone et al
840	Gunpowder Ck Fm?	73.6	0.01	2.70	0.12	4020	647	18.2						CM19	2055		CAR SLST	304278	7823128	295	
841	Gunpowder Ck Fm?	149.0	0.01	2.71	0.12	3500	1014	15.4						CM19	2056		CAR SLST	304278	7823128	295	
842	Gunpowder Ck Fm?	240.5	0.01	2.70	0.14		993	16.9						CM19	2057		CAR SHLE	304278	7823128	298	
843	Gunpowder Ck Fm?	52.1	0.01	2.72	0.21									CM19	2058		CAR SLST	304278	7823128	301	
844	Gunpowder Ck Fm?	103.4	0.01	2.73	0.17	4150	1183	8.2						CM19	2059		CAR SLST	304278	7823128	301	
845	Gunpowder Ck Fm?	126.1	0.01	2.70	0.14	4530	2624	10.2						CM19	2060		MIC SLST	304278	7823128	304	
846	Gunpowder Ck Fm?	42.9	0.02	2.70	0.12									CM19	2061		LA SLST	304278	7823128	308	

Appendix 3

Mount Isa Basin Petrophysics

sort	Unit	Dry wt	Porosity	SG sat	Susc	Velocity	Resistivity	IP%	TC1	TC2	K	U	Th	Source	ID	Mbr	Lithology	E	N	Depth	Notes
847	Gunpowder Ck Fm?	83.6	0.02	2.72	0.13									CM19	2062		LA SLST	304278	7823128	308	
848	Gunpowder Ck Fm?	61.9	0.02	2.71	0.17	3080	1780	16.4						CM17	2034		GR CAR SHLE	302814	7822727	287	
849	Gunpowder Ck Fm?	94.8	0.02	2.73	0.16	3550	1584	8.7						CM17	2035		GR CAR SHLE	302814	7822727	287	
850	Gunpowder Ck Fm?	169.2	0.01	2.72	0.18	3700	2583	7.8						CM17	2036		GR CAR SHLE	302814	7822727	287	
851	Gunpowder Ck Fm?	130.8	0.01	2.72	0.20	3430	2343	9.8						CM17	2037		GR CAR SHLE	302814	7822727	289	
852	Gunpowder Ck Fm?	230.6	0.01	2.72	0.21	4500	1735	12.3	623	229	19	16	7	CM17	2038		GR CAR SHLE	302814	7822727	289	
853	Gunpowder Ck Fm?	186.7	0.01	2.73	0.18		6404	13.5						CM17	2039		GR CAR SHLE	302814	7822727	300	8-36 osc
854	Gunpowder Ck Fm?	121.5	0.01	2.73	0.22		2028	8.9						CM17	2040		GR CAR SHLE	302814	7822727	300	
855	Gunpowder Ck Fm?	251.4	0.01	2.72	0.20	3490	2268	13.3						CM17	2041		GR CAR SHLE	302814	7822727	300	
856	Gunpowder Ck Fm?	148.3	0.01	2.73	0.17									CM17	2042		GR CAR SHLE	302814	7822727	304	
857	Gunpowder Ck Fm?	284.8	0.01	2.74	0.23		1093	11.0						CM17	2043		GR CAR SHLE	302814	7822727	304	
858	Gunpowder Ck Fm?	254.9	0.01	2.74	0.25	2730	929	14.4						CM17	2044		GR CAR SHLE	302814	7822727	304	
859	Gunpowder Ck Fm?	106.9	0.02	2.73	0.16									CM17	2027		GR CAR SHLE	302814	7822727	307	
860	Gunpowder Ck Fm?	107.3	0.02	2.72	0.15		1551	16.1						CM17	2028		GR CAR SHLE	302814	7822727	307	
861	Gunpowder Ck Fm?	98.0	0.02	2.73	0.16		2878	15.9						CM17	2029		GR CAR SHLE	302814	7822727	307	
862	Gunpowder Ck Fm?	126.3	0.02	2.73	0.18									CM17	2030		GR CAR SHLE	302814	7822727	307	
863	Gunpowder Ck Fm?	49.2	0.02	2.73	0.17	1810	1956	11.3						CM17	2031		GR CAR SHLE	302814	7822727	309	
864	Gunpowder Ck Fm?	129.2	0.02	2.73	0.17									CM17	2032		GR CAR SHLE	302814	7822727	309	
865	Gunpowder Ck Fm?	148.9	0.01	2.74	0.17									CM17	2033		GR CAR SHLE	302814	7822727	309	
866	Gunpowder Ck Fm?	248.5	0.00	2.77	0.26	4870	3796	1.3						CM17	2045		RE LA MIC SLY SHLE	302814	7822727	479	
867	Gunpowder Ck Fm?	281.4	0.01	2.77	0.24	5040	2672	1.1	983	229	57	14	5	CM17	2046		RE LA MIC SLY SHLE	302814	7822727	479	
868	Gunpowder Ck Fm?	445.4	0.01	2.75	0.25	5000	2521	1.6	1083	441	55	22	1	CM17	2047		RE LA MIC SLY SHLE	302814	7822727	483	
869	Gunpowder Ck Fm?	88.5	0.01	2.77	0.20	4170	3113	1.0						CM17	2048		RE LA MIC SLY SHLE	302814	7822727	491	
870	Gunpowder Ck Fm?	326.7	0.01	2.77	0.20	5070	1865	1.0	1033	279	21	24	11	CM17	2049		RE LA MIC SLY SHLE	302814	7822727	491	
871	Gunpowder Ck Fm?	115.2	0.01	2.79	0.21	3950	3776	0.8						CM17	2050		RE LA MIC SLY SHLE	302814	7822727	495	
872	Gunpowder Ck Fm?	456.8	0.00	-0.25	0.19	5160	3356	1.4	1307	429	47	10	3	CM17	2051		RE LA MIC SLY SHLE	302814	7822727	495	
873	Gunpowder Ck Fm?	174.8	0.00	2.78	0.22	4340	3330	0.9						CM17	2052		RE LA MIC SLY SHLE	302814	7822727	496	
874	Gunpowder Ck Fm?	253.3	0.00	2.78	0.22	5050	3418	0.9	863	321	43	12	3	CM17	2053		RE LA MIC SLY SHLE	302814	7822727	496	
875	Gunpowder Ck Fm?	297.9	0.00	2.76	0.20	5130	3942	1.2	847	321	39	20	11	CM17	2054		RE LA MIC SLY SHLE	302814	7822727	501	
876	Gunpowder Ck Fm			2.43			23	10.3						P107	7018		PYR CAR SHLE			39.6	12
877	Gunpowder Ck Fm			2.52			8	24.0						P107	7019		PYR CAR SHLE			44.2	4
878	Gunpowder Ck Fm			2.36			4	4.5						P107	7020		PYR CAR SHLE			55.8	2
879	Gunpowder Ck Fm	173.9	0.01	2.73	0.19		1115	10.9						CM31	2110		CAR SLST	300987	7837708	248	
880	Gunpowder Ck Fm	238.5	0.01	2.73	0.17	4720	1422	10.2	789	159	45	14	9	CM31	2111		MIC SLST	300987	7837708	248	
881	Gunpowder Ck Fm	237.8	0.00	2.74	0.33		11987	3.7						CM31	2112		SLST	300987	7837708	252	
882	Gunpowder Ck Fm	157.3	0.01	2.74	0.20		2230	9.6						CM31	2113		CAR SLST	300987	7837708	252	
883	Gunpowder Ck Fm	263.8	0.00	2.73	0.24	5230	6358	2.9	505	135	1	6	-3	CM31	2114		MIC SLST	300987	7837708	252	
884	Gunpowder Ck Fm	573.4	0.00	2.72	0.27	5490	13180	2.2	937	237	35	14	11	CM31	2115		MIC SLST	300987	7837708	265	
885	Gunpowder Ck Fm	456.4	0.00	2.71	0.27	5530	18206	1.2	825	195	25	18	-3	CM31	2116		MIC XB SLST	300987	7837708	270	
886	Gunpowder Ck Fm	700.4	0.00	2.72	0.24	5640	28427	1.9	817	269	23	-2	1	CM31	2117		MIC SLST	300987	7837708	278	

Appendix 3

Mount Isa Basin Petrophysics

sort	Unit	Dry wt	Porosity	SG sat	Susc	Velocity	Resistivity	IP%	TC1	TC2	K	U	Th	Source	ID	Mbr	Lithology	E	N	Depth	Notes
887	Gunpowder Ck Fm	266.0	0.01	2.71	0.23	4850	2883	4.4	679	175	-7	14	-3	CM31	2118		CAR MIC SLST	300987	7837708	283	
888	Gunpowder Ck Fm	247.2	0.01	2.70	0.19		4359	12.1						CM31	2119		CAR SLST	300987	7837708	283	
889	Gunpowder Ck Fm	291.1	0.01	2.70	0.21		8803	2.5						CM31	2120		SDY SLST	300987	7837708	284	
890	Gunpowder Ck Fm	527.3	0.00	2.72	0.21	5460	5351	1.7	953	227	37	18	5	CM31	2121		MIC SLST	300987	7837708	284	
891	Gunpowder Ck Fm	244.6	0.01	2.71	0.17		1568	9.4						CM31	2122		CAR SLST	300987	7837708	289	
892	Gunpowder Ck Fm	600.0	0.00	2.74	0.28	5430	6223	1.8	881	177	21	-2	3	CM31	2123		MIC SLST	300987	7837708	307	
893	Gunpowder Ck Fm	633.7	0.00	2.73	0.25	5240	5295	3.3	1023	211	1	12	7	CM31	2124		MIC SLST	300987	7837708	313	
894	Gunpowder Ck Fm	680.1	0.01	2.73	0.23	5350	3441	2.9	1175	263	37	0	7	CM31	2125		MIC SLST	300987	7837708	310	
895	Gunpowder Ck Fm	281.2	0.01	2.73	0.18	5020	1945	8.9	1017	209	17	-2	1	CM31	2126		MIC CAR SLST	300987	7837708	323	
896	Gunpowder Ck Fm	279.9	0.01	2.73	0.22		2904	6.8						CM31	2127		CAR SLST	300987	7837708	325	
897	Gunpowder Ck Fm	387.2	0.00	2.73	0.20	5350	6130	2.3	787	267	23	2	1	CM31	2128		MIC SLST	300987	7837708	325	44-90 osc
898	Gunpowder Ck Fm	247.3	0.01	2.73	0.19	4980	2062	4.7	921	283	61	2	9	CM31	2129		MIC SLST	300987	7837708	329	
899	Gunpowder Ck Fm	290.0	0.01	2.73	0.21		3426	2.2						CM31	2130		SLST	300987	7837708	332	
900	Gunpowder Ck Fm	187.4	0.01	2.74	0.24		2475	0.8						CM31	2131		SLST	300987	7837708	332	
901	Gunpowder Ck Fm	638.1	0.01	2.74	0.29	5290	5666	1.2	1275	387	21	4	11	CM31	2132		MIC SLST	300987	7837708	337	
902	Gunpowder Ck Fm	462.2	0.00	2.72	0.29	5590	39423	1.7	743	161	35	8	7	CM31	2133		MIC SDY SLST	300987	7837708	339	
903	Gunpowder Ck Fm	386.6	0.01	2.74	0.26	5220	3526	0.5	1185	275	15	18	-1	CM31	2134		SLST	300987	7837708	341	
904	Gunpowder Ck Fm	604.5	0.03	2.67	0.18	4540	962	0.6	1091	283	19	8	11	CM31	2135		VU SDY SLST	300987	7837708	343.9	38-90 osc
905	Gunpowder Ck Fm	203.3	0.01	2.73	0.25		4738	0.9						CM31	2135		SLST	300987	7837708	344.1	
906	Gunpowder Ck Fm	1307.5	0.21	2.10	0.02	2960	1079	2.2	806	254	-3	18	3	GW	1013	Plug3	F SLY SDST	294600	7812500	0	
907	Gunpowder Ck Fm	1173.6	0.19	2.12	0.02	3220	830	1.2	872	168	9	12	1	GW	1013	Plug3	F SLY SDST	294600	7812500	0	
908	Gunpowder Ck Fm	1152.2	0.12	2.23	0.01	4010	3287	0.9	927	201	11	6	3	GW	1034	Plug3	MIC SLY SDST	294600	7812500	0	
909	Gunpowder Ck Fm	451.0	0.09	2.27	0.03	4400	625	2.8	611	181	9	4	-3	GW	1035	Plug3	MIC SLY SDST	294600	7812500	0	
910	Gunpowder Ck Fm	931.5	0.09	2.31	0.02	4090	2176	2.7	935	169	19	-4	7	GW	1036	Plug3	MIC SLY SDST	294600	7812500	0	
911	Gunpowder Ck Fm	271.5	0.17	2.23	0.02	1980	1034	1.4	343	111	7	6	5	GW	1037	Plug3	MIC SLY SDST	294600	7812500	0	
912	Gunpowder Ck Fm	845.8	0.15	2.22	0.02	3460	1479	1.0	701	151	3	8	-5	GW	1038	Plug3	MIC SLY SDST	294600	7812500	0	
913	Gunpowder Ck Fm	311.7	0.10	2.25	0.03	4050	564	0.6	671	123	19	10	-1	GW	1039	Plug3	MIC SLY SDST	294600	7812500	0	
914	Gunpowder Ck Fm	237.9	0.09	2.29	0.02									GW	1040	Plug3	MIC SLY SDST	294600	7812500	0	
915	Gunpowder Ck Fm	1384.9	0.15	2.21	0.02	2960	1987	1.6	681	115	-1	6	11	GW	1058	Plug3	SLY F SDST	294600	7812500	0	
916	Gunpowder Ck Fm	1378.7	0.15	2.24	0.03	2710	2862	0.5	683	155	-9	2	-1	GW	1059	Plug3	SLY F SDST	294600	7812500	0	15-55 osc.
917	Gunpowder Ck Fm	1703.1	0.07	2.64	0.09	4720	1123	0.9	590	132	13	12	-3	GW	1014	Plug2	DMT SLST	296100	7813100	0	66-94 osc.
918	Gunpowder Ck Fm	1702.9	0.08	2.61	0.08	4750	640	0.5	902	262	11	16	1	GW	1015	Plug2	DMT SLST	296100	7813100	0	
919	Gunpowder Ck Fm	150.1	0.09	2.60	0.03	4580	784	1.3						GW	1016	Plug2	DMT SLST	296100	7813100	0	
920	Gunpowder Ck Fm	100.3	0.07	2.63	0.03									GW	1017	Plug2	DMT SLST	296100	7813100	0	
921	Gunpowder Ck Fm	169.8	0.12	2.42	0.10	4450	674	1.4						GW	1019	Plug2	DMT SLST	296100	7813100	0	
922	Gunpowder Ck Fm	1405.2	0.21	2.86	0.64	5020	4042	2.8	2384	638	29	26	7	GW	1022	Plug2	HM CAR MIC SLST	296100	7813100	0	10-80 fluctuation in IP
923	Gunpowder Ck Fm	546.3	0.37	2.13	0.24	1260	161	5.0	880	98	23	18	5	GW	1023	Plug2	HM SLST	296100	7813100	0	
924	Gunpowder Ck Fm	1492.6	0.35	2.19	0.37	1970	276	3.6	1162	396	25	10	5	GW	1024	Plug2	HM MIC SLST	296100	7813100	0	
925	Gunpowder Ck Fm	1588.2	0.13	2.46	0.31	5370	1991	1.5	797	237	19	4	-1	GW	1051	Plug2	SLY F DLST	296100	7813100	0	
926	Gunpowder Ck Fm	1553.0	0.15	2.39	0.31	4820	3096	1.4	783	213	3	6	7	GW	1052	Plug2	SLY F DLST	296100	7813100	0	17-68 osc.

Appendix 3

Mount Isa Basin Petrophysics

sort	Unit	Dry wt	Porosity	SG sat	Susc	Velocity	Resistivity	IP%	TC1	TC2	K	U	Th	Source	ID	Mbr	Lithology	E	N	Depth	Notes
927	Gunpowder Ck Fm	1321.6	0.16	2.25	0.07	3440	528	2.5	1767	491	57	22	17	GW	1043	Plug1	GR SLST	296700	7813500	0	
928	Gunpowder Ck Fm	1555.1	0.15	2.24	0.04	3410	804	0.3	1889	483	47	14	7	GW	1044	Plug1	GR SLST	296700	7813500	0	
929	Gunpowder Ck Fm	1315.0	0.11	2.44	0.14	4750	2205	0.5	1967	501	89	24	1	GW	1049	Plug1	SDY SLST	296700	7813500	0	
930	Gunpowder Ck Fm	1245.8	0.12	2.45	0.15	4050	3873	0.1	1801	421	47	4	9	GW	1050	Plug1	SDY SLST	296700	7813500	0	
931	Gunpowder Ck Fm	1794.1	0.17	2.31	0.11	2860	1271	3.4	2089	573	55	28	23	GW	1060	Plug1	FER SLST	296700	7813500	0	
932	Gunpowder Ck Fm	1826.4	0.18	2.31	0.11	2760	1412	2.2	2017	561	39	14	15	GW	1061	Plug1	FER SLST	296700	7813500	0	
933	Gunpowder Ck Fm		0.02	2.67	0.13										5201	Pmw3	F SLST	308000	7799200	99	Hone et al
934	Gunpowder Ck Fm		0.02	2.74	0.13										5202	Pmw3	F SLST	308000	7799200	250	Hone et al
935	Gunpowder Ck Fm		0.01	2.72	0.13										5203	Pmw2	MIC SLST	308000	7799200	364	Hone et al
936	Gunpowder Ck Fm	314.1	0.00	2.76	0.14	5800	6284	4.9	631	195	27	10	5	GSQLH3	5015	c	DMT CHY PYR F SLST	276000	7927500	100.9	
937	Gunpowder Ck Fm		0.00	2.75	0.13									GSQLH3	5204	Pmwc	SLST	276000	7927500	102	Hone et al
938	Gunpowder Ck Fm	173.9	0.01	2.72	0.11	5160	7320	6.0						GSQLH3	5016	c	DMT PYR F SDST	276000	7927500	103.9	
939	Gunpowder Ck Fm	506.9	0.00	2.76	0.13	6230	107887	2.3	429	151	33	14	21	GSQLH3	5017	c	SDY DLST	276000	7927500	109.8	
940	Gunpowder Ck Fm		0.00	2.67	0.31									GSQLH3	5205	Pmwc	SLST	276000	7927500	126	Hone et al
941	Gunpowder Ck Fm		0.01	2.81	0.25									GSQLH3	5206	Pmwc	DLST	276000	7927500	130	Hone et al
942	Gunpowder Ck Fm	562.8	0.00	2.74	0.11	6020	20349	1.5	347	97	27	-2	-1	GSQLH3	5018	c	C DLST	276000	7927500	131.9	
943	Gunpowder Ck Fm		0.00	2.65	0.10									GSQLH3	5207	Pmwc	DMT SLST	276000	7927500	140	Hone et al
944	Gunpowder Ck Fm	265.6	0.00	2.63	0.09	5420	49	33.5	867	331	35	8	5	GSQLH3	5019	c	CAR PYR SLST	276000	7927500	150	
945	Gunpowder Ck Fm	280.2	0.00	2.74	0.16	6080	1085384	7.5	643	65	39	8	5	GSQLH3	5020	c	CALC PY SDST	276000	7927500	150.8	
946	Gunpowder Ck Fm		0.00	2.61	0.19									GSQLH3	5208	Pmwc	CAR SHLE	276000	7927500	153	Hone et al
947	Gunpowder Ck Fm	314.0	0.00	2.64	0.08	5350	11788	8.6	795	235	41	2	1	GSQLH3	5021	c	SLY CAR SDST	276000	7927500	154.6	
948	Gunpowder Ck Fm	225.6	0.00	2.73	0.10	5700	29585	10.0	491	179	37	4	5	GSQLH3	5022	c	SLY PYR SDST	276000	7927500	157.3	
949	Gunpowder Ck Fm		0.01	2.64	0.13									GSQLH3	5209	Pmwc	CAR SHLE	276000	7927500	160	Hone et al
950	Gunpowder Ck Fm	347.3	0.00	2.81	0.15	6430	58453	2.6	433	57	21	6	-1	GSQLH3	5023	c	SLY CALC SDST	276000	7927500	162.9	
951	Gunpowder Ck Fm	394.1	0.00	2.84	0.13	6850	1107169	4.8	91	99	15	6	9	GSQLH3	5024	c	DLST	276000	7927500	171.5	
952	Gunpowder Ck Fm	209.4	0.00	2.85	0.19	6690	963858	5.6	109	23	-5	2	-3	GSQLH3	5025	c	BED BR PYR DLST	276000	7927500	174.2	
953	Gunpowder Ck Fm		0.01	2.76	0.19									GSQLH3	5210	Pmwc	DLST	276000	7927500	175	Hone et al
954	Gunpowder Ck Fm	252.7	0.01	2.80	0.11	6350	1004019	5.3	125	-3	17	6	-5	GSQLH3	5100	c	GP DLST	276000	7927500	185.3	
955	Gunpowder Ck Fm	458.7	0.00	2.83	0.13	6600	4671	2.0	167	49	7	-6	7	GSQLH3	5026	c	BR DLST	276000	7927500	190.1	
956	Gunpowder Ck Fm	449.8	0.00	2.82	0.10	6570	903833	7.1	195	47	29	-2	1	GSQLH3	5027	c	BR DLST	276000	7927500	197.8	
957	Gunpowder Ck Fm		0.00	2.81	0.05									GSQLH3	5211	Pmwc	DLST	276000	7927500	201	Hone et al
958	Gunpowder Ck Fm	149.7	0.00	2.82	0.17		22582	1.7						GSQLH3	5028	c	SDY DLST	276000	7927500	224.7	
959	Gunpowder Ck Fm	346.1	0.00	2.84	0.24	6580	69936	3.6	259	35	-7	4	9	GSQLH3	5042	c	SDY BR DLST	276000	7927500	225	
960	Gunpowder Ck Fm	309.2	0.00	2.81	0.09	6380	99999999		95	47	-15	8	1	GSQLH3	5101	c	CHY DLST	276000	7927500	263.7	
961	Gunpowder Ck Fm	190.0	0.00	2.87	0.16	6590	88689	2.4						GSQLH3	5029	c	SDY PYR GP DLST	276000	7927500	301	
962	Gunpowder Ck Fm		0.00	2.81	0.10									GSQLH3	5212	Pmwc	DMT SLST	276000	7927500	301	Hone et al
963	Gunpowder Ck Fm	321.4	0.00	2.83	0.15	6620	99999999		89	13	3	8	1	GSQLH3	5030	c	SDY GP DLST	276000	7927500	303.4	
964	Gunpowder Ck Fm	246.8	0.00	2.81	0.13	6280	28979	1.6	241	195	25	2	1	GSQLH3	5102	c	DMT PYR SDST	276000	7927500	338.8	
965	Gunpowder Ck Fm	300.6	0.00	2.83	0.31	6200	99999999		49	-5	7	6	1	GSQLH3	5031	c	DMT PYR SDST	276000	7927500	341.8	
966	Gunpowder Ck Fm		0.00	2.83	0.25									GSQLH3	5213	Pmwc	DMT SLST	276000	7927500	350	Hone et al

Appendix 3

Mount Isa Basin Petrophysics

sort	Unit	Dry wt	Porosity	SG sat	Susc	Velocity	Resistivity	IP%	TC1	TC2	K	U	Th	Source	ID	Mbr	Lithology	E	N	Depth	Notes
967	Gunpowder Ck Fm	63.7	0.00	2.77	0.08	5640	15005	12.8						GSQLH3	5032	c	DMT SLY PYR SDST	276000	7927500	365	
968	Gunpowder Ck Fm	29.5	0.01	2.64	0.05	5370	38100	1.4						GSQLH3	5103	b	VND SDST	276000	7927500	369.2	
969	Gunpowder Ck Fm	125.7	0.00	2.78	0.14	5710	99999999							GSQLH3	5104	b	DMT PYR SDST	276000	7927500	369.9	
970	Gunpowder Ck Fm		0.00	2.83	0.38									GSQLH3	5214	Pmwb	SLST	276000	7927500	370	Hone et al
971	Gunpowder Ck Fm	77.2	0.00	2.85	0.14	6430	99999999							GSQLH3	5033	b	SDY DLST	276000	7927500	373.1	
972	Gunpowder Ck Fm	129.0	0.02	2.83	0.20	6310	99999999		181	75	7	6	-3	GSQLH3	5105	b	SDY DLST	276000	7927500	373.9	
973	Gunpowder Ck Fm		0.00	2.70	0.25									GSQLH3	5215	Pmwb	DMT SLST	276000	7927500	390	Hone et al
974	Gunpowder Ck Fm	55.3	0.00	2.74	0.07		150844	3.5						GSQLH3	5034	b	PYR C SDST	276000	7927500	391.4	
975	Gunpowder Ck Fm		0.01	3.03	16.34									GSQLH3	5216	Pmwb	DLST	276000	7927500	395	Hone et al
976	Gunpowder Ck Fm	140.6	0.01	2.81	0.16	5810	18389	3.3	627	175	51	18	1	GSQLH3	5106	b	DMT PYR SDST	276000	7927500	396.7	
977	Gunpowder Ck Fm	119.7	0.01	3.18	3.25	5490	1836	21.0						GSQLH3	5035	b	PYR DMT SDST	276000	7927500	396.9	
978	Gunpowder Ck Fm		0.01	2.68										GSQLH3	5217	Pmwa	SDST	276000	7927500	407	Hone et al
979	Gunpowder Ck Fm		0.00	2.62	0.31									GSQLH3	5218	Pmwa	SDST	276000	7927500	410	Hone et al
980	Gunpowder Ck Fm	93.6	0.00	2.67	0.08	5620	99999999							GSQLH3	5107	a	CAR PYR SDST	276000	7927500	414.35	
981	Gunpowder Ck Fm	119.0	0.00	2.66	0.05	5670	99999999							GSQLH3	5108	a	PYR M SDST	276000	7927500	419	
982	Gunpowder Ck Fm	30.4	0.01	2.72	0.03		21382	15.6						GSQLH3	5036	a	CAR PYR SHLE	276000	7927500	419.6	
983	Gunpowder Ck Fm	57.9	0.01	2.67	0.06		4562	14.5						GSQLH3	5037	a	CAR PYR SHLE	276000	7927500	422.3	
984	Gunpowder Ck Fm	65.9	0.00	2.64	0.06	5280	7278	30.5						GSQLH3	5038	a	SDY CAR PYR SLST	276000	7927500	425.3	
985	Gunpowder Ck Fm	58.1	0.00	2.65	0.08	5210	1009	6.1						GSQLH3	5039	a	CAR PYR MDST	276000	7927500	429.8	
986	Gunpowder Ck Fm		0.00	2.63	0.19									GSQLH3	5219	Pmwa	CAR PYR SHLE	276000	7927500	430	Hone et al
988	Gunpowder Ck Fm													B. C. Jones							
989	Gunpowder Ck Fm													B. C. Jones							
990	Gunpowder Ck Fm													B. C. Jones							
991	Gunpowder Ck Fm	189.8	0.05	2.40	0.02		3520	2.4						B. C. Jones	133611	6	PYR M SDST	273061	7918000	0	TS
992	Gunpowder Ck Fm	572.3	0.03	2.71	0.09		99999999								133608	5	SDY DLST	273798	7917381	0	TS
993	Gunpowder Ck Fm	79.8	0.00	2.72	0.09	5900	132059	7.9						WC1	133610	5	SLF DMT BX	272902	7917438	>100	TS
994	Gunpowder Ck Fm	175.0	0.01	2.75	0.06	6250								WC1	133606	5	ALT DLST	272902	7917438	146.58	TS
995	Gunpowder Ck Fm	59.1	0.01	2.78	0.09	5800	7179	3.0						WC1	133605	5	SLF DLST	272902	7917438	215.25	TS
996	Gunpowder Ck Fm	56.4	0.01	2.74	0.07	5940	26298	2.8						WC1	133603	5	CHY DLST	272902	7917438	237.14	TS
997	Gunpowder Ck Fm	65.9	0.00	2.82	0.09	6400	45739	2.8						WC1	133607	4	STRO DLST	272902	7917438	344.4	TS
998	Gunpowder Ck Fm	61.4	0.00	2.76	0.06	5480	68868	4.5						WC1	133602	3	MIC PYR C SDST	275463	7918054	383	TS
999	Gunpowder Ck Fm	184.6	0.29	2.09	0.08		214	1.5							133600	2	MIC SLST	275382	7418200	0	TS
1000	Gunpowder Ck Fm	28.6	0.01	2.68	0.07	5290	984	9.9							133599	1	CAR MDST	277808	7917276	>100	TS
1001	Gunpowder Ck Fm			2.77	0.25									CM7	313701		CAR SHLE	295635	7827009	123.9	Aberfoyle
1002	Gunpowder Ck Fm				0.25									CM7	313702		CAR SHLE	295635	7827009	129.64	Aberfoyle
1003	Gunpowder Ck Fm	208.1	0.02	2.77	0.17	5610	160	12.1						CM7	2087		DMT CAR SLST	295635	7827009	135	
1004	Gunpowder Ck Fm	220.4	0.02	2.78	0.14									CM7	2088		DMT CAR SLST	295635	7827009	135	
1005	Gunpowder Ck Fm	725.2	0.02	2.75	0.17	5340	2248	14.0	759	211	11	8	11	CM7	2089		DMT CAR SLST	295635	7827009	136	amt band w angular clasts
1006	Gunpowder Ck Fm	930.7	0.02	2.74	0.11	5440	3394	5.7	1323	327	43	26	9	CM7	2090		DMT SLST	295635	7827009	138	
1007	Gunpowder Ck Fm	195.6	0.03	2.67	0.06		184	21.4						CM7	2091		CAR MDST	295635	7827009	141	

Appendix 3

Mount Isa Basin Petrophysics

sort	Unit	Dry wt	Porosity	SG sat	Susc	Velocity	Resistivity	IP%	TC1	TC2	K	U	Th	Source	ID	Mbr	Lithology	E	N	Depth	Notes
1008	Gunpowder Ck Fm	277.6	0.02	2.74	0.10	5180	5197	9.1	697	123	11	4	5	CM7	2092		DMT CAR SLST	295635	7827009	141	
1009	Gunpowder Ck Fm	754.4	0.01	2.75	0.09	5350	753	18.2	1121	291	35	14	5	CM7	2093		DMT CAR PY SLST	295635	7827009	145	
1010	Gunpowder Ck Fm	244.6	0.00	2.89	0.15	6130	1366	18.7						CM7	2094		DMT QZ CAR SUL BX	295635	7827009	150	
1011	Gunpowder Ck Fm	535.4	0.00	2.88	0.17	6710	592	15.8	157	-25	11	6	1	CM7	2095		DMT QZ CAR SUL BX	295635	7827009	151	
1012	Gunpowder Ck Fm	364.1	0.02	2.74	0.09	5300	94	22.5	819	271	29	2	9	CM7	2096		CAR PY SLST	295635	7827009	152	
1013	Gunpowder Ck Fm	348.6	0.02	2.86	0.17	6460	140	17.2	811	169	19	26	1	CM7	2097		CAR SUL DMT BX	295635	7827009	155	
1014	Gunpowder Ck Fm	479.8	0.02	2.73	0.11	4870	261	15.6	979	219	37	12	7	CM7	2098		CAR PY SHLE	295635	7827009	160	
1015	Gunpowder Ck Fm	624.6	0.01	2.78	0.11	5680	418	12.6	973	273	15	14	5	CM7	2099		CAR DMT PY SLST	295635	7827009	169	
1016	Gunpowder Ck Fm	201.7	0.01	2.78	0.10		4032	25.8						CM7	2100		CAR SLY DLST	295635	7827009	171	
1017	Gunpowder Ck Fm	510.2	0.01	2.76	0.12	5150	279	14.5	831	251	13	6	5	CM7	2101		CAR DMT SLST	295635	7827009	171	
1018	Gunpowder Ck Fm	934.4	0.02	2.71	0.07	5000	146	11.5	1397	371	29	14	13	CM7	2102		CAR SDY SLST	295635	7827009	175	
1019	Gunpowder Ck Fm	739.4	0.01	2.70	0.11	5450	41	13.7	1395	467	45	12	5	CM7	2103		DMT ?SD SLY SDST	295635	7827009	181	core-parallel cleavage
1020	Gunpowder Ck Fm	249.1	0.01	2.73	0.09	5610	291	13.6	679	215	45	12	1	CM7	2104		MIC DMT SLY SDST	295635	7827009	186	
1021	Gunpowder Ck Fm	397.1	0.01	2.72	0.09	5430	119	20.0	1111	247	21	4	-1	CM7	2105		DMT ?SD SLY SLST	295635	7827009	186	
1022	Gunpowder Ck Fm	617.6	0.01	2.74	0.11	5570	45	14.0	997	337	3	2	13	CM7	2106		DMT ?SD SLY SDST	295635	7827009	189	core-parallel cleavage
1023	Gunpowder Ck Fm	609.7	0.01	2.75	0.09	5720	316	14.1	1145	307	43	8	-3	CM7	2107		DMT ?SD SLY PY SDST	295635	7827009	192	core-parallel cleavage
1024	Gunpowder Ck Fm	431.6	0.01	2.76	0.09	5330	174	9.9	891	195	31	14	-3	CM7	2108		DMT ?SD PY SLST	295635	7827009	197	
1025	Gunpowder Ck Fm	573.4	0.01	2.75	0.08	5310	305	12.6	695	307	-15	16	-1	CM7	2109		DMT ?SD PY SLST	295635	7827009	199	
1026	Gunpowder Ck Fm			2.81	0.29									CM9	313907		CAR SHLE	290953	7882880	164.81	Aberfoyle
1027	Gunpowder Ck Fm			2.75	0.18									CM9	313908		CAR SHLE	290953	7882880	165.6	Aberfoyle
1028	Gunpowder Ck Fm			2.75	0.21									CM9	313909		CAR SHLE	290953	7882880	167.4	Aberfoyle
1029	Gunpowder Ck Fm			2.70	0.21									CM31	3133119		CAR SHLE	300987	7837708	170.5	Aberfoyle
1030	Gunpowder Ck Fm			2.70	0.30									CM31	3133120		CAR SHLE	300987	7837708	171	Aberfoyle
1031	Gunpowder Ck Fm			2.67	0.20									CM31	3133121		CAR SHLE	300987	7837708	174.81	Aberfoyle
1032	Gunpowder Ck Fm			2.67	0.30									CM31	3133122		CAR SHLE	300987	7837708	175.3	Aberfoyle
1033	Gunpowder Ck Fm			2.67	2.58									CM40	3134023		CAR SHLE	291100	7887400	164.74	Aberfoyle
1034	Gunpowder Ck Fm			2.67	7.25									CM40	3134024		CAR SHLE	291100	7887400	174.67	Aberfoyle
1035	Gunpowder Ck Fm			2.69	0.29									CM41	3134025		CAR SHLE	304313	7819139	111	Aberfoyle
1036	Gunpowder Ck Fm			2.67	0.28									CM41	3134026		CAR SHLE	304313	7819139	118	Aberfoyle
1037	Gunpowder Ck Fm			2.63	0.16									CM41	3134027		CAR SHLE	304313	7819139	119.3	Aberfoyle
1038	Gunpowder Ck Fm			2.65	0.19									CM41	3134028		CAR SHLE	304313	7819139	123.1	Aberfoyle
1039	Gunpowder Ck Fm			2.57	0.18									CM41	3134029		CAR SHLE	304313	7819139	126.5	Aberfoyle
1040	Gunpowder Ck Fm			2.52	0.19									CM41	3134030		CAR SHLE	304313	7819139	134.87	Aberfoyle
1041	Gunpowder Ck Fm			2.52	0.15									CM41	3134031		CAR SHLE	304313	7819139	135.6	Aberfoyle
1042	Gunpowder Ck Fm			2.52	0.21									CM41	3134032		CAR SHLE	304313	7819139	135.7	Aberfoyle
1043	Gunpowder Ck Fm			2.56	0.18									CM41	3134033		CAR SHLE	304313	7819139	136.4	Aberfoyle
1044	Gunpowder Ck Fm			2.60	0.19									CM41	3134034		CAR SHLE	304313	7819139	138.5	Aberfoyle
1045	Gunpowder Ck Fm			2.65	0.31									CM41	3134035		CAR SHLE	304313	7819139	146.95	Aberfoyle
1046	Gunpowder Ck Fm			2.67	0.35									CM41	3134036		CAR SHLE	304313	7819139	147.1	Aberfoyle
1047	Gunpowder Ck Fm			2.86	0.24									CM41	3134037		CAR SHLE	304313	7819139	148.6	Aberfoyle

Appendix 3
Mount Isa Basin Petrophysics

sort	Unit	Dry wt	Porosity	SG sat	Susc	Velocity	Resistivity	IP%	TC1	TC2	K	U	Th	Source	ID	Mbr	Lithology	E	N	Depth	Notes
1050	Torpedo Ck Qtzite	1813.3	0.00	2.62	0.00	5760	4608000	6.6	245	-1	-5	4	-5	GW	1006		QZT	296600	7813100	0	
1051	Torpedo Ck Qtzite	1285.8	0.00	2.61	0.01	5630	9999999		215	109	7	6	11	GW	1006		QZT	296600	7813100	0	
1052	Torpedo Ck Qtzite	1156.5	0.00	2.62	0.01	5660	5131098	3.5	205	75	-15	-2	7	GW	1006		QZT	296600	7813100	0	
1053	Torpedo Ck Qtzite	1203.2	0.00	2.62	0.00	5690	597838	2.9	179	19	-13	-8	-7	GW	1006		QZT	296600	7813100	0	
1054	Torpedo Ck Qtzite	361.9	0.00	2.60	0.01	5620	99999999		119	-1	-5	2	9	GW	1081	Plug0	QZT	296600	7813100	0	
1055	Torpedo Ck Qtzite	724.2	0.01	2.60	0.01	5290	99999999		111	1	-25	-12	5	GW	1082	Plug0	QZT	296600	7813100	0	
1056	Torpedo Ck Qtzite	1284.2	0.00	2.61	0.00	5480	11647059	2.5	253	-67	1	-6	1	GW	1083	Plug0	QZT	296600	7813100	0	
1057	Torpedo Ck Qtzite	1435.5	0.01	2.60	0.01	5070	6192857	2.2	199	19	-9	2	5	GW	1084	Plug0	QZT	296600	7813100	0	
1058	Torpedo Ck Qtzite	1514.1	0.01	2.59	0.03	5160	373864	1.7	262	24	-30	22	-1	GW	1086	Plug0	QZ CNGL	296600	7813100	0	SCF clasts?
1059	Torpedo Ck Qtzite	1611.9	0.01	2.60	0.01	5130	242278	1.6	386	60	24	2	1	GW	1087	Plug0	QZ CNGL	296600	7813100	0	SCF clasts?
1060	Torpedo Ck Qtzite	56.9	0.00	2.66	0.10	5590	720251	4.2						GSQLH3	5109		FEL M SDST	276000	7927500	437.53	
1061	Torpedo Ck Qtzite	53.7	0.01	2.71	0.08	4810	1574	19.6						GSQLH3	5110		SDY CAR SLST	276000	7927500	439	
1062	Torpedo Ck Qtzite		0.00	2.69	0.31									GSQLH3	5220		ARK SDST	276000	7927500	440	Hone et al
1063	Torpedo Ck Qtzite	88.0	0.00	2.69	0.08	5430	99999999							GSQLH3	5111		SLY PYR SDST	276000	7927500	441.49	
1064	Torpedo Ck Qtzite	78.7	0.00	2.71	0.10	5180	103226	6.0						GSQLH3	5112		PB PYR CNGL	276000	7927500	442.85	
1065	Torpedo Ck Qtzite	111.6	0.00	2.68	0.07	5630	99999999		675		27	12	-1	GSQLH3	5113		VC PYR SDST	276000	7927500	449	
1067	Torpedo Ck Qtzite	633.3	0.05	2.45	0.05		116895	3.9						B. C. Jones	133613	1	QZT	272876	7919386	0	
1068	Torpedo Ck Qtzite	501.4	0.08	2.48	0.10		9706	1.3						B. C. Jones	133615	2	HET CNGL	273048	7916420	0	
1072	Spear/Kennedy Siltst			2.74										DEL							
1073	Spear/Kennedy Siltst			2.75										DEL							
1074	Urquhart Shale			3.48										Isa		ore					F&B
1075	Urquhart Shale			3.67	5.03									Isa		ore					Hone et al
1076	Urquhart Shale			4.15	2.51									Isa		ore					Hone et al
1077	Urquhart Shale			3.69	43.98									Isa		ore					Hone et al
1078	Urquhart Shale			3.56	11.31									Isa		ore					Hone et al
1079	Urquhart Shale			2.71	0.05									Isa Cu		ore					Hone et al
1080	Urquhart Shale			3.08	0.09									Isa Cu		ore					Hone et al
1081	Urquhart Shale			4.21	69.12									Hilton		ore					Hone et al
1082	Urquhart Shale			3.51	2.01									Hilton		ore					Hone et al
1083	Urquhart Shale	388.7	0.01	3.73	6.48	5810	76875	26.3						Hilton	111740		PY PO				PS,h/w py mkr
1084	Urquhart Shale	445.2	0.01	2.86	2.23	5830	26338	10.9						Hilton	111741		PO SLST				PS, 7o/b
1085	Urquhart Shale	433.2	0.01	3.92	1.63	6250	1090	27.0						Hilton	111742		BED PY				PS
1086	Urquhart Shale	844.6	0.00	3.91	2.56	5440	951	14.5						Hilton	111743		BA MAS GN SP				PS
1087	Urquhart Shale	752.0	0.00	3.63	23.00	5310	1060	19.6						Hilton	111744		BA PY PO CARB				PS
1088	Urquhart Shale				20.80									Hilton	111745		SP GN PO BX				
1089	Urquhart Shale	476.3	0.00	2.91	3.20	6260	99999999							Hilton	111746		PO SLST				PS
1090	Urquhart Shale			2.75										DEL							
1091	Urquhart Shale			2.77										DEL							
1092	Native Bee Siltstone			2.75										DEL							
1093	Breakaway Shale			2.69										DEL							

Appendix 3

Mount Isa Basin Petrophysics

sort	Unit	Dry wt	Porosity	SG sat	Susc	Velocity	Resistivity	IP%	TC1	TC2	K	U	Th	Source	ID	Mbr	Lithology	E	N	Depth	Notes
1094	Breakaway Shale			2.70										DEL							
1095	Moondarra Siltstone			2.73										DEL							
1097	Surprise Ck Fm	1357.6	0.01	2.53	0.03	5220	202526	1.6	425	37	-11	14	-3	GW	1068	Pty	M SDST	297100	7813300	0	
1098	Surprise Ck Fm	1294.2	0.02	2.53	0.02	5110	82286	2.0	429	-3	-23	14	7	GW	1069	Pty	M SDST	297100	7813300	0	
1099	Surprise Ck Fm	661.8	-1.24	4.54	0.04	5020	64488	2.4	265	-1	1	0	3	GW	1089	Pty	C SDST	297100	7813300	0	
1100	Surprise Ck Fm	1136.7	0.02	2.56	0.02	5370	155172	2.1	359	-9	-1	10	3	GW	1090	Pty	C SDST	297100	7813300	0	
1101	Surprise Ck Fm	1733.9	0.01	2.58	0.28	5270	2297143	2.9	347	-23	-11	6	-7	GW	1091	Pty	M SDST	297100	7813300	0	longest axis
1102	Surprise Ck Fm	1421.4	0.01	2.57	0.30	5520	160160	1.7	369	51	-3	2	5	GW	1092	Pty	CLAY CL M SDST	297100	7813300	0	longest axis
1103	Surprise Ck Fm	1790.6	0.02	2.55	0.03	5290	114646	2.2	413	59	-11	0	-3	GW	1093	Pty	M SDST	297100	7813300	0	longest axis
1104	Surprise Ck Fm			2.64										Young						0	
1105	Surprise Ck Fm			2.65										Young						0	
1106	Surprise Ck Fm			2.60										DEL							
1107	Surprise Ck Fm			2.68										Young							
1108	Surprise Ck Fm			2.73										Young							
1109	Surprise Ck Fm			2.70										Young							
1110	Surprise Ck Fm			2.72										Young							
1111	Surprise Ck Fm	295.5	0.03	2.59	0.04									AMcP	130063	Pra	QZ ARNT	309900	7866545	0	TS
1112	Surprise Ck Fm	1211.9	0.02	2.59	0.22									AMcP	130064	Pra	SDST RHY BX	308865	7866758	0	
1113	Surprise Ck Fm				0.06		2700	0.4						P72	7006	Pra	QTZT			190	
1114	Surprise Ck Fm			2.62	0.30									Est							
1115	Sybella Granite	602.8	0.01	2.67	16.20		15050	2.5	1171	365	43	12	-1	Dept	19946		GRT			0	bl fabric
1116	Sybella Granite			2.61										Young							
1117	Sybella Granite			2.68										Young							
1118	Sybella Granite			2.65										Young							
1119	Sybella Granite			2.63										Young							
1120	Sybella Granite			2.69										Young							
1121	Fiery Ck Volcanics		0.01	2.53	0.13									Hone et al	5608		RHY IGM	317700	7841600	0	Hone et al
1122	Fiery Ck Volcanics				0.25									Dunster			QF SDST				
1123	Fiery Ck Volcanics				0.65									Dunster			MAF V				
1124	Fiery Ck Volcanics	704.1	0.03	2.80	0.36	4870			923	273	94	4	-3	AMcP	5		BLT			0	
1125	Fiery Ck Volcanics	854.2	0.03	2.50	0.04	4680			309	15	12	-2	9	AMcP	10		FEL F SDST			0	
1126	Fiery Ck Volcanics	1041.3	0.04	2.49	0.05	4030	23328	1.6	437	93	20	8	5	AMcP	10		FEL F SDST			0	
1127	Fiery Ck Volcanics	579.1	0.09	2.71	0.58	4260	2807	1.7	549	287	54	8	3	AMcP	12		BLT			0	
1128	Fiery Ck Volcanics	377.1	0.02	2.75	0.38	5430			521	217	52	10	11	AMcP	17		BLT			0	
1129	Fiery Ck Volcanics	1022.9	0.03	2.76	0.30	5310			1235	353	26	8	5	AMcP	20		RHD CNGL			0	
1130	Fiery Ck Volcanics	334.9	0.04	2.56	0.15	4600	2547	1.1	1801	547	102	26	3	AMcP	24		RHY			0	
1131	Fiery Ck Volcanics	120.2	0.08	2.50	0.14									AMcP	24		RHY			0	
1132	Fiery Ck Volcanics	978.6	0.01	2.63	0.13	5180			1357	401	40	16	7	AMcP	33		F MIC SDST			0	
1133	Fiery Ck Volcanics	341.1	0.04	2.65	0.21	4880			365	87	12	-4	-1	AMcP	37		PTB			0	
1134	Fiery Ck Volcanics	238.4	0.06	2.52	0.19									AMcP	66		RHY			0	

Appendix 3

Mount Isa Basin Petrophysics

sort	Unit	Dry wt	Porosity	SG sat	Susc	Velocity	Resistivity	IP%	TC1	TC2	K	U	Th	Source	ID	Mbr	Lithology	E	N	Depth	Notes
1135	Fiery Ck Volcanics	347.5	0.05	2.51	0.11	4630	3935	0.9	1259	411	36	8	-3	AMcP	71		RHY			0	
1136	Fiery Ck Volcanics	242.1	0.03	2.56	0.14	4600			937	275	52	0	-3	AMcP	88		RHY			0	
1137	Fiery Ck Volcanics	109.0	0.01	2.57	0.08	4190								AMcP	90		RHY			0	
1138	Fiery Ck Volcanics	265.7	0.07	2.45	0.06	4400	2291	1.4	819	279	30	0	13	AMcP	139		RHY			0	
1139	Fiery Ck Volcanics	389.1	0.03	2.55	0.10	4710			1447	499	78	20	9	AMcP	140		RHY			0	
1140	Fiery Ck Volcanics	285.7	0.02	2.63	0.04	5110			145	7	2	6	-1	AMcP	141		RHY			0	
1141	Fiery Ck Volcanics	218.5	0.03	2.55	0.08	5400	5547	3.2						AMcP	170		RHY BX			0	
1142	Fiery Ck Volcanics	113.0	0.04	2.52	0.06									AMcP	170		RHY			0	
1143	Fiery Ck Volcanics	144.2	0.11	2.41	0.12									AMcP	180		QZ VN RHY			0	
1144	Fiery Ck Volcanics	269.4	0.12	2.58	0.29	3360	453	2.8	617	249	40	0	1	AMcP	223		WEA BLT			0	
1145	Fiery Ck Volcanics	266.1	0.05	2.56	0.14	4620	11508	1.3						AMcP	248		RHY BX			0	
1146	Fiery Ck Volcanics	342.2	0.06	2.53	0.16	4380			953	251	36	-4	7	AMcP	249		RHY BX			0	
1147	Fiery Ck Volcanics	180.1	0.03	2.56	0.10	5130	1036	1.4						AMcP	251		RHY			0	
1148	Fiery Ck Volcanics	280.0	0.03	2.56	0.12	5070	5176	0.6	1407	331	50	8	1	AMcP	272		RHY			0	
1149	Fiery Ck Volcanics	278.8	0.02	2.60	0.04	4950	21867	1.6	495	97	36	8	11	AMcP	299		C RHY			0	
1150	Fiery Ck Volcanics	545.1	0.02	2.53	0.03	5120	8400	0.7	1931	499	98	16	11	AMcP	310		ALT RHY			0	
1151	Fiery Ck Volcanics	817.0	0.06	2.58	0.19	4660	47727	3.4	1157	373	100	20	1	AMcP	317		HET CNGL			0	
1152	Fiery Ck Volcanics	51.1	0.01	2.62	0.03	5430								AMcP	324		LTH SDST			0	
1153	Fiery Ck Volcanics	74.7	0.03	2.55	0.02									AMcP	332		RHY			0	
1154	Fiery Ck Volcanics	744.6	0.03	2.54	0.06	5060	208636	3.3	1065		42	4	9	AMcP	333		SLF HET BX			0	
1155	Fiery Ck Volcanics	868.8	0.02	2.49	0.07									AMcP	130055	Pfc	FEL SDST	301388	7867840	0	TS
1156	Fiery Ck Volcanics	292.9	0.03	2.55	0.13									AMcP	130056	Pfc	HET VOL BX	310025	7866370	0	TS
1157	Fiery Ck Volcanics	819.9	0.06	2.40	0.20									AMcP	130057	Pfc	HET VOL BX	310063	7866363	0	TS
1158	Fiery Ck Volcanics	236.1	0.12	2.30	0.13									AMcP	130058	Pfc	HET CNGL	310056	7866405	0	TS
1159	Fiery Ck Volcanics	47.6	0.04	2.53	0.08									AMcP	130059	Pfc	HET CNGL	310056	7866405	0	TS
1160	Fiery Ck Volcanics	423.4	0.04	2.72	0.35									AMcP	130060	Pfc	HET SDY VOL BX	302477	7868880	0	TS
1161	Fiery Ck Volcanics	701.9	0.01	2.58	0.17									AMcP	130061	Pfc	LTH SDST	309711	7866004	0	TS
1162	Fiery Ck Volcanics	284.5	0.17	2.13	0.10									AMcP	130062	Pfc	MIC GNL SDST	309400	7866250	0	TS
1163	Fiery Ck Volcanics	630.9	0.02	2.60	0.23									AMcP	130065	Pfcr	MAS KFS ALT RHY	306965	7866124	0	TS
1164	Fiery Ck Volcanics	616.3	0.02	2.57	0.13									AMcP	130066	Pfcr	RHY	308000	7866925	0	microgranite dyke
1165	Fiery Ck Volcanics	811.6	0.05	2.54	0.28									AMcP	130067	Pfcr	MAS KFS ALT RHY	308994	7868455	0	TS
1166	Fiery Ck Volcanics	592.8	0.03	2.54	0.05									AMcP	130068	Pfcr	KFS ALT RHY	309397	7865490	0	sdst & mafic xenoliths
1167	Fiery Ck Volcanics	15.1	0.08	2.48	0.06									AMcP	130069	Pfcr	SLF BR RHY	309550	7866125	0	TS
1168	Fiery Ck Volcanics	231.8	0.23	2.26	0.09									AMcP	130073	Pfcv	ALT AMY BLT	302590	7867176	0	contact upper basalt & SCF
1169	Fiery Ck Volcanics	1037.5	0.12	2.62	0.46									AMcP	130071	Pfcv	KFS ALT BLT	302060	7875500	0	
1170	Fiery Ck Volcanics	1679.5	0.03	2.85	0.56									AMcP	130072	Pfcv	KFS ALT BLT	302457	7868004	0	TS
1171	Fiery Ck Volcanics	25.8	0.14	2.40	0.06					365				AMcP	130070	Pfcv	ALT BLT	309777	7865960	0	lower basalt
1172	Fiery Ck Volcanics	527.5	0.17	2.61	1.06	3040	574	4.2	762	152	53	6	3	GW	1020		WEA BLT	296100	7814350	0	45-75 osc.
1173	Fiery Ck Volcanics	190.3	0.13	3.06	0.55										1033		WEA BLT	296100	7814350	0	
1174	Fiery Ck Volcanics	1008.4	0.05	3.23	0.48	4590	8766	2.1	397	75	15	0	5		1041		WEA BLT	296100	7814350	0	

Appendix 3

Mount Isa Basin Petrophysics

sort	Unit	Dry wt	Porosity	SG sat	Susc	Velocity	Resistivity	IP%	TC1	TC2	K	U	Th	Source	ID	Mbr	Lithology	E	N	Depth	Notes
1175	Fiery Ck Volcanics	280.5	0.06	3.14	0.40	3450	3675	1.5	243	19	3	0	1		1042		WEA BLT	296100	7814350	0	
1176	Fiery Ck Volcanics	1521.5	0.13	2.54	1.06	4210	1372	2.8	1287	399	77	12	-1		1047		BLT	296100	7814350	0	55-75 osc.
1179		469.0	0.04	2.65	0.16	5230			703	237	26	-4	1	AMcP	8		DMT SLST			0	
1180		1073.4	0.10	2.43	0.11	3670	1455	0.7	1217	215	30	8	9	AMcP	14		LTH MIC SDST			0	
1181		933.2	0.01	2.60	0.11	5070			1495	369	58	8	-1	AMcP	30		F SDST			0	
1182		274.9	0.02	2.60	0.10	5540								AMcP	32		MIC SDST			0	
1183		324.0	0.02	2.61	0.42	4470			283	107	10	0	-1	AMcP	44		M FEL SDST			0	
1184		1246.7	0.12	2.28	0.07	4250			1015	189	12	-2	3	AMcP	86		C ARKS			0	
1185		168.7	0.10	2.35	0.08									AMcP	101		F HM SDST			0	
1186		421.2	0.07	2.65	0.21				973	401	52	0	1	AMcP	136		LTH SDST			0	
1187		327.4	0.01	2.60	0.07	5600	651429	3.1	553	139	20	4	3	AMcP	209		F FEL MIC SDST			0	
1188		279.1	0.01	2.80	0.18	5630	38125	5.0						AMcP	225		LTH CNGL			0	
1189		254.4	0.12	2.35	0.06	3850	537	2.0						AMcP	243		DMT SLST			0	
1190		732.3	0.04	2.53	0.07	4780	11688	4.9	639	181	22	8	3	AMcP	246		SDY SLST			0	
1191		384.0	0.01	2.57	0.04	5480	50118	2.1	167	25	24	-2	-5	AMcP	247		F LTH SDST			0	
1192		1178.0	0.10	2.28	0.04	4450	15484	1.9	205	53	6	4	-3	AMcP	303		FEL MIC SDST			0	
1193		522.5	0.02	2.63	0.11	5110	3016	1.7	867	175	38	8	3	AMcP	501		M LTH SDST			0	
1194		39.2	0.05	2.45	0.02	4360	13488	1.5						AMcP	502		FEL SDST			0	
1195		34.1	0.30	2.90	0.19	2740	487	7.8						AMcP	503		CAR SLST			0	
1197	Bigie Formation			2.62	0.25									Dunster							
1198	Bigie Formation	157.1	0.02	2.63	0.11	5360	18270	4.1						AMcP	269		SDST			0	
1199	Bigie Formation	94.5	0.08	2.46	0.04									AMcP	10334		FEL SDST			0	
1200	Bigie Formation	252.5	0.16	2.37	0.20									AMcP	130053		HM LTH SDST	308500	7865508	0	
1201	Bigie Formation	184.3	0.03	2.56	0.10									AMcP	130054		BX	308254	7865300	0	
1202	Weberra Granite			2.54	0.00									Hone et al	78206098		GRT	332700	7884300	F-SW	Hone et al
1203	Weberra Granite			2.59	0.00									Hone et al	78206100		GRT	328200	7885200	F-SW	Hone et al
1204	Weberra Granite			2.55	0.00									Hone et al	78206101		GRT	328200	7885000	F-SW	Hone et al
1205	Weberra Granite			2.56	0.13									Hone et al	78206102		GRT	328200	7888200	F-SW	Hone et al
1206	Weberra Granite			2.54	0.25									Hone et al	78206103		GRT	323400	7883200	F-SW	Hone et al
1208	Quilalar Formation			2.65	0.30									Est (C&E)							
1209	Quilalar Formation	861.0	0.04	2.49	0.06	3990	12444	3.5	509	145	2	-2	-1	AMcP	334		C SDST			0	
1210	Quilalar Formation	288.2	0.05	2.46	0.06									AMcP	130052	Pqw	QZ ARNT	307956	7867358	0	
1211	Corella Formation			2.73	0.28									Hone et al							Hone et al
1212	Corella Formation			2.84	3.50									Hone et al							Hone et al
1213	Corella Formation			2.68	0.01									Hone et al							Hone et al
1214	Corella Formation			2.70	0.01									Hone et al							Hone et al
1215	Corella Formation			2.69	0.22									Hone et al							Hone et al
1216	Corella Formation			2.98	132.10									Hone et al							Hone et al
1217	Corella Formation			2.82	2.20									Hone et al							Hone et al
1218	Corella Formation			2.72	28.30									Hone et al							Hone et al

Appendix 3

Mount Isa Basin Petrophysics

sort	Unit	Dry wt	Porosity	SG sat	Susc	Velocity	Resistivity	IP%	TC1	TC2	K	U	Th	Source	ID	Mbr	Lithology	E	N	Depth	Notes
1219	Corella Formation			2.76	43.30									Hone et al							Hone et al
1220	Corella Formation			2.80	25.90									Hone et al							Hone et al
1221	Corella Formation			2.90	38.70									Hone et al							Hone et al
1222	Corella Formation			2.63	0.52									Hone et al							Hone et al
1223	Corella Formation			2.86	0.62									Hone et al							Hone et al
1224	Corella Formation			2.66	0.08									Hone et al							Hone et al
1225	Corella Formation			2.61	0.28									Hone et al							Hone et al
1226	Corella Formation			2.71	1.20									Hone et al							Hone et al
1227	Corella Formation			2.85	0.90									Hone et al							Hone et al
1228	Corella Formation			2.64	0.33									Hone et al							Hone et al
1229	Corella Formation			3.01	0.43									Hone et al							Hone et al
1230	Corella Formation			2.89	38.00									Hone et al							Hone et al
1231	Corella Formation			3.01	27.00									Hone et al							Hone et al
1232	Corella Formation			2.68	0.50									Hone et al							Hone et al
1233	Corella Formation			3.06	0.50									Hone et al							Hone et al
1234	Corella Formation			2.88	0.13									Hone et al							Hone et al
1235	Corella Formation			2.84	0.50									Hone et al							Hone et al
1236	Corella Formation			2.61	0.00									Hone et al							Hone et al
1237	Corella Formation			2.79										Hone et al							Hone et al
1238	Corella Formation			2.62										Hone et al							Hone et al
1239	Corella Formation			2.69	0.63									Hone et al							Hone et al
1240	Corella Formation			2.66	1.70									Hone et al							Hone et al
1241	Corella Formation			2.74	35.19									Hone et al							Hone et al
1242	Corella Formation			2.73	2.51									Hone et al							Hone et al
1243	Corella Formation			2.71	6.28									Hone et al							Hone et al
1244	Corella Formation			2.80	0.13									Hone et al							Hone et al
1245	Corella Formation			2.70	9.20									Hone et al							Hone et al
1246	Corella Formation			2.70	0.19									Hone et al							Hone et al
1247	Corella Formation			2.75	0.63									Hone et al							Hone et al
1248	Corella Formation			2.87	0.88									Hone et al							Hone et al
1249	Corella Formation			2.69	15.08									Hone et al							Hone et al
1250	Corella Formation			3.48	7.54									Hone et al							Hone et al
1251	Corella Formation			3.63	1.63									Hone et al							Hone et al
1252	Corella Formation			2.83	0.38									Hone et al							Hone et al
1253	Corella Formation			2.73	0.00									Hone et al							Hone et al
1254	Corella Formation			2.73	0.25									Hone et al							Hone et al
1255	Corella Formation			3.08	1.26									Hone et al							Hone et al
1256	Corella Formation			3.06	1.00									Hone et al							Hone et al
1257	Corella Formation			2.79	7.79									Hone et al							Hone et al
1258	Corella Formation			2.69	0.44									Hone et al							Hone et al

Appendix 3

Mount Isa Basin Petrophysics

sort	Unit	Dry wt	Porosity	SG sat	Susc	Velocity	Resistivity	IP%	TC1	TC2	K	U	Th	Source	ID	Mbr	Lithology	E	N	Depth	Notes
1259	Corella Formation			2.65	0.31									Hone et al							Hone et al
1260	Corella Formation			2.82	0.50									Hone et al							Hone et al
1261	Corella Formation			2.74	1.45									Hone et al							Hone et al
1262	Corella Formation			2.71	0.88									Hone et al							Hone et al
1263	Corella Formation			2.61	0.13									Hone et al							Hone et al
1264	Corella Formation			2.66	0.38									Hone et al							Hone et al
1265	Corella Formation			2.69	0.50									Hone et al							Hone et al
1266	Corella Formation			2.70	0.50									Hone et al							Hone et al
1267	Corella Formation			2.70	1.51									Hone et al							Hone et al
1268	Corella Formation			2.69	0.25									Hone et al							Hone et al
1269	Corella Formation			2.69	0.13									Hone et al							Hone et al
1270	*Corella Formation*			*2.70*	*0.44*									*Hone et al*							Hone et al
1271	Corella Formation			2.73	0.50									Hone et al							Hone et al
1272	Corella Formation			2.71	0.13									Hone et al							Hone et al
1276	Corella Formation													Hone et al							Hone et al
1277	post-Myally dolerite			2.92	12.50									Est							
1278	Lochness Formation	549.5	0.15	2.12	0.09		741	2.4	1395		5	4	9	Dept	109976					0	
1279	Lochness Formation	705.0	0.02	2.65	0.16	5620	6538	1.9	1657	495	94	12	9	AMcP	336		F FER SLST			0	
1280	Lochness Formation	39.2	0.08	2.40	0.05									AMcP	336		FEL SDST				335I
1281	Lochness Formation	505.4	0.04	2.61	0.14	5930	18739	3.5	597	109	18	16	3	AMcP	335		*SLF DLST*			*0*	
1282	Lochness Formation	225.4	0.03	2.67	0.10	4850	157	6.5						AMcP	335		HM DLST			0	
1283	Lochness Formation	77.9	0.10	2.32	0.07			18.0						AMcP	10335		FER FEL SDST				335K
1284	Lochness Formation	1860.5	0.02	2.61	0.06									AMcP	130047		FER FEL SDST	309335	7867550	0	
1285	Lochness Formation	125.5	0.08	2.49	0.10									AMcP	130048		HM DMT SDST	309335	7867550	0	
1286	Lochness Formation	26.4	0.07	2.50	0.17									AMcP	130049		LTH DMT MDST	309335	7867550	0	
1287	Lochness Formation	300.7	0.05	2.58	0.16									AMcP	130050		STRO CHRT	309335	7867550	0	
1288	Lochness Formation	125.2	0.17	2.15	0.04									AMcP	130051		QZ ARNT	309335	7867550	0	
1289	Whitworth Quartzite	454.4	0.06	3.45	0.31		405	14.0						Dept	101945	ore	CC				Mammoth
1290	Whitworth Quartzite	179.1	0.01	2.93	0.03		110	23.7						Dept	101945	ore	CC BX				Mammoth
1291	Myally Subgroup			2.60	0.03									F&B							
1292	Myally Subgroup			2.65	0.05									F&B							
1293	Myally Subgroup			2.49										Young						0	
1294	Myally Subgroup			2.64										Young						0	
1295	Myally Subgroup			2.65										Young						0	
1296	*Myally Subgroup*			*2.68*										*Young*							
1297	Myally Subgroup			2.73										Young							
1298	Myally Subgroup			2.70										Young							
1299	Myally Subgroup			2.72										Young							
1300	Myally Subgroup			2.60	0.05									DEL, JND							
1301	Eastern Ck Volcs		0.02	2.77	2.61									Isa	5609	greenstone	CL AB QZ MET BLT	340400	7707400	900	Hone et al

Appendix 3

Mount Isa Basin Petrophysics

sort	Unit	Dry wt	Porosity	SG sat	Susc	Velocity	Resistivity	IP%	TC1	TC2	K	U	Th	Source	ID	Mbr	Lithology	E	N	Depth	Notes
1344	Eastern Ck Volcs			3.00	63.00									Young							
1345	Eastern Ck Volcs			2.81	65.35									Young							
1346	Eastern Ck Volcs			2.93	38.00									Young							
1347	Eastern Ck Volcs			2.91	50.27									Young							
1348	Eastern Ck Volcs			2.88	75.40									Young							
1349	Eastern Ck Volcs			2.90	44.00									Young							
1350	Eastern Ck Volcs			2.85	47.70									F&B							
1351	Eastern Ck Volcs			2.85	50.27									DEL							
1352	Eastern Ck Volcs			3.00	75.40									DEL							
1355	"Mafics"			2.85	62.83									DEL							
1357	Kamarga Volcanics	651.9	0.00	2.92	28.00	6340	2647059	11.1							6001		BLT	275500	7918500	0	float in ck
1358	Kamarga Volcanics	340.0	0.19	2.24	0.18				729	271	35	6	-3		6002		WEA VE BLT	275000	7918500	0	
1359	*Kamarga Volcanics*	1684.0	0.09	2.58	0.50				1453	499	85	-4	-1		6003		WEA BLT	275000	7918500	0	
1360	Kamarga Volcanics	271.3	0.06	2.58	0.52		19359	4.5							6004		WEA BLT	273630	7919009	0	
1361	Kamarga Volcanics	1860.3	0.07	2.57	0.57	4240	6721	3.2							6005		WEA BLT	278933	7918382	0	
1362	Kamarga Volcanics	677.2	0.03	2.59	0.05		20897	4.1						B. C. Jones	133609		SDST	275000	7918500	0	1-11 osc
1363	Kamarga Volcanics	718.8	0.02	2.79	1.25		121333	9.6						B. C. Jones	133612		BLT	275000	7918500	0	
1364	Leander Quartzite			2.60	0.20									Est							
1365	Mount Guide Quartzite			2.66	0.10									Young							
1366	Mount Guide Quartzite			2.62										Young							
1367	Mount Guide Quartzite			2.64										Young							
1368	Mount Guide Quartzite			2.64										Young							
1369	Mount Guide Quartzite			2.67										Young							
1370	*May Downs Gneiss*			2.64										Young							
1371	May Downs Gneiss			2.63										Young							
1372	May Downs Gneiss			2.66										Young							
1373	Ewen Granite			2.69	4.00									Est (C&E)							
1374	Bottletree Fm		0.02	2.65	50.27									Hone et al	77530370		MET DAC	349200	7675600		Hone et al
1375	Argylla Fm		0.00	2.95	0.50									Hone et al	80530056		AMP	425500	7629900		Hone et al
1376	Argylla Fm		0.02	2.68	21.99									Hone et al	76535067		GNS	375800	7655600		Hone et al
1377	Argylla Fm		0.01	2.68	1.89									Hone et al	77535050		GNS	376900	7658500		Hone et al
1378	Argylla Fm		0.00	2.65	23.93									Hone et al			MET RHY	392000	7707500		Hone et al
1379	Argylla Fm		0.01	2.66	7.54									Hone et al			FLS MET EXV	393600	7704700		Hone et al
1380	Argylla Fm		0.02	2.69	37.70									Hone et al			FLS MET EXV	394000	7709900		Hone et al
1381	*Argylla Fm*		*0.00*	*2.66*	*3644.25*									*Hone et al*			*FLS MET EXV*	*391300*	*7705000*		*Hone et al*
1382	Argylla Fm		0.00	2.69	47.00									Hone et al	7287	Pea3	POR RHY			F	72\87
1383	Argylla Fm		0.00	2.68										Hone et al	7289	Pea4	MX POR RHY			F	72\89
1384	Argylla Fm		0.00	2.62										Hone et al	7290	Pea5	FEL SDST	419946	7683194	SW	72\90
1385	Argylla Fm			2.63										Young				422026	7683204	0	
1386	Tewinga Gp		0.03	2.55	0.00									Hone et al	78531785		GNS	424105	7683213		

Appendix 3

Mount Isa Basin Petrophysics

sort	Unit	Dry wt	Porosity	SG sat	Susc	Velocity	Resistivity	IP%	TC1	TC2	K	U	Th	Source	ID	Mbr	Lithology	E	N	Depth	Notes
1387	Tewinga Gp		0.01	2.75	28.90									Hone et al	79530117		CNGL				
1388	Tewinga Gp		0.03	2.69	0.25									Hone et al	77530301		GNS				
1389	Tewinga Gp		0.02	2.79	66.60									Hone et al	77530196		MET GYWK	351700	7624800		
1390	Tewinga Gp		0.02	2.65	28.90									Hone et al	77530262		MET IGM GNS	356100	7632700		
1391	Tewinga Gp		0.00	2.72	1.13									Hone et al	77530720		MET AGL	351800	7603700		
1392	Tewinga Gp		0.05	2.63	0.31									Hone et al	77530018		GNS	356500	7577300		
1393	Tewinga Gp		0.01	2.64	0.05									Hone et al	77531107		GNS	355500	7576400		
1394	Tewinga Gp		0.02	2.61	1.82									Hone et al	77530242		GNS	354700	7629900		
1395	Tewinga Gp		0.00	2.59	0.50									Hone et al	77530179		GNS	352700	7623000		
1396	Tewinga Gp		0.00	2.67	0.19									Hone et al	77530304		GNS	355200	7619300		
1397	Tewinga Gp		0.01	2.61	0.10									Hone et al	77530306		GNS	354400	7619500		
1399	Yeldham Granite		0.00	2.67	10.05									GSQLH3	5611		GRT	276000	7927500	453	Hone et al
1400	Yeldham Granite	166.8	0.01	2.79	0.24	5060	1497	4.3	801	239	49	2	-3	GSQLH3	5007		PYR AFS	276000	7927500	453.4	
1401	Yeldham Granite	176.9	0.00	2.69	0.17	5490			801	239	49	2	-3	GSQLH3	5006		QAS	276000	7927500	453.6	
1402	Yeldham Granite	128.3	0.00	2.73	0.55	5840	49830	2.1	999	347	39	4	-7	GSQLH3	5005		AFG	276000	7927500	454.4	
1403	Yeldham Granite	125.1	0.00	2.77	13.30	5510	10929	1.3	999	347	39	4	-7	GSQLH3	5004		PYR AFS	276000	7927500	454.9	
1404	Yeldham Granite	153.6	0.00	2.71	0.19	5620	24744	1.1	1033	425	79	6	-3	GSQLH3	5003		PYR AFG	276000	7927500	458	
1405	Yeldham Granite		0.00	2.65	0.19									GSQLH3	5612		GRT	276000	7927500	458	Hone et al
1406	Yeldham Granite	162.4	0.00	2.63	0.15	5710	126820	1.9	1033	425	79	6	-3	GSQLH3	5002		AFG	276000	7927500	458.8	
1407	Yeldham Granite	46.1	0.01	2.69	4.79	5750	246326	3.5						GSQLH3	5001		PYR QAS	276000	7927500	460	
1408	Yeldham Granite	106.3	0.04	2.66	0.16		23151	1.8						B. C. Jones	133598		TOUR GRT	274829	7919146	0	pegmatitic
1409	Yeldham Granite	681.5	0.03	2.57	0.09		11040	2.3						B. C. Jones	133601		GRT	273132	7919377	0	
1411	Basement Metamorphic	107.0	0.16	2.45	0.10	4810	312	2.6						B. C. Jones	133614		MS QZ SCHT	273356	7918914	0	?xenolith
1412	Leichhardt Volcanics		0.01	2.66	6.28									Hone et al	1142930		QF PHY	383300	7720000		K42930
1413	Leichhardt Volcanics		0.00	2.64	1.63									Hone et al			IGM	371400	7851200	F	Hone et al
1414	Leichhardt Volcanics		0.00	2.63	0.38									Hone et al	77530569	Pels	QF PHY	368300	7596400	SW	Hone et al
1415	Leichhardt Volcanics		0.01	2.68	2.01									Hone et al	7953345		PHY	357500	7589000	SW	7953 C45
1416	Leichhardt Volcanics		0.00	2.64	15.83									Hone et al	7953398		MET IGM	369000	7606000	SW	7953 C98
1417	Leichhardt Metamorphics			2.61										Young							
1418	Leichhardt Metamorphics			2.66										Young							
1421	"Felsics"			2.79	37.70									DEL							
1423	Candover Mets			2.79	1.00									Est							
1424	Kalkadoon Granodiorite		0.02	2.70	0.31									Hone et al	78206138		?granite	369200	7666500	F	Hone et al
1425	Kalkadoon Granodiorite		0.02	2.69	0.31									Hone et al	78206138		?granite	368500	7666800	F	Hone et al
1426	Kalkadoon Granodiorite		0.03	2.68	0.19									Hone et al	78206138		?granite	367600	7667800	F	Hone et al
1427	Kalkadoon Granodiorite		0.01	2.74	0.13									Hone et al	78206142		?granite	364900	7669000	F	Hone et al
1428	Kalkadoon Granodiorite		0.00	2.73	0.25									Hone et al	78205133		adamellite	353500	7642800	F	Hone et al
1429	Kalkadoon Granodiorite		0.04	2.62	0.38									Hone et al	77530948		leucogneiss	353400	7585700		Hone et al
1430	Kalkadoon Granodiorite		0.01	2.68	0.63									Hone et al	78206048		?granite	372500	7730600		Hone et al
1431	Kalkadoon Granodiorite		0.02	2.62	0.13									Hone et al	78206084		?granite	367600	7723200		Hone et al

Appendix 3

Mount Isa Basin Petrophysics

sort	Unit	Dry wt	Porosity	SG sat	Susc	Velocity	Resistivity	IP%	TC1	TC2	K	U	Th	Source	ID	Mbr	Lithology	E	N	Depth	Notes
1432	Kalkadoon Granodiorite		0.00	2.74	1.26									Hone et al	78206043		?granite	371900	7723800	F-SW	Hone et al
1433	Kalkadoon Granodiorite		0.01	2.66	0.38									Hone et al	78206064		?granite	372100	7691400	F-SW	Hone et al
1434	Kalkadoon Granodiorite		0.02	2.66	0.13									Hone et al	78206061		?granite	368000	7694800	F-SW	Hone et al
1435	Kalkadoon Granodiorite		0.00	2.66	0.13									Hone et al	78206000		?granite	391000	7815300	F-SW	Hone et al
1436	Kalkadoon Granodiorite		0.00	2.61	0.06									Hone et al	78206003		?granite	389900	7816500	F-SW	Hone et al
1437	Kalkadoon Granodiorite		0.00	2.60	0.06									Hone et al	78206004		?granite	390500	7816100	F-SW	Hone et al
1438	Kalkadoon Granodiorite		0.01	2.62	0.06									Hone et al	78206005		?granite	390600	7815700	F-SW	Hone et al
1439	Kalkadoon Granodiorite		0.00	2.66	0.25									Hone et al	78206006		?granite	390900	7814600	F-SW	Hone et al
1440	Kalkadoon Granodiorite		0.00	2.73	0.50									Hone et al	78206052		?granite	372700	7752100	F-SW	Hone et al
1441	Kalkadoon Granodiorite		0.00	2.75	0.19									Hone et al	78206053		?granite	374700	7751700	F-SW	Hone et al
1442	Kalkadoon Granodiorite		0.02	2.62	0.57									Hone et al	78206055		?granite	373900	7741000	F-SW	Hone et al
1443	Kalkadoon Granodiorite		0.01	2.78	0.38									Hone et al	78206056		?granite	372800	7738700	F-SW	Hone et al
1444	Kalkadoon Granite			2.65										Young							
1448	Big Toby Granite		0.00	2.64	0.10									Hone et al	78206069		?granite	311600	7701700		Hone et al
1449	Big Toby Granite		0.00	2.68	0.25									Hone et al	78206070		?granite	312300	7701500		Hone et al
1450	Big Toby Granite		0.01	2.67	0.25									Hone et al	78206071		?granite	312300	7701400		Hone et al
1451	Big Toby Granite		0.01	2.76	0.38									Hone et al	78206078		?granite	306700	7692700		Hone et al
1452	Big Toby Granite		0.01	2.64	6.54									Hone et al	78206079		?granite	306800	7692600		Hone et al

Appendix 4

University of Tasmania School of Earth Sciences
Rock Store Catalogue extract

showing samples catalogued by the author

Unlabelled field at left (bottom) contains 6-digit unique Rock Catalogue ID numbers assigned to catalogued specimens by the curator.

'Field ID' corresponds to the field titled 'ID' in Appendix 3.

'Sort' contains unique ID numbers linking the Rock Catalogue database with the petrophysical database listed in Appendix 3.

'Rock' and 'Description' contain lithological identifiers and qualifiers coded using standard AGSO abbreviations (Appendix 7).

'AMG E' and 'AMG N' locate all catalogued specimens on AGD66, UTM Zone 54, with the exception of McArthur River area samples which are in UTM Zone 53.

	ID(=Field#	Sort	Rock	Description	AMG E	AMG N	Biostrat	Lithostrat (Unit)	Preps	Comments	Area
137154	6.0	1124	BLT		309000	7866000	Statherian	Fiery Ck Volcanics	R		Riversleigh Fold Zone
137155	10.0	1125	SDST	FEL F	309000	7866000	Statherian	Fiery Ck Volcanics	R		Riversleigh Fold Zone
137156	10.0	1126	SDST	FEL F	309000	7866000	Statherian	Fiery Ck Volcanics	R		Riversleigh Fold Zone
137157	12.2	1127	BLT		309000	7866000	Statherian	Fiery Ck Volcanics	R		Riversleigh Fold Zone
137158	17.0	1128	BLT		309000	7866000	Statherian	Fiery Ck Volcanics	R		Riversleigh Fold Zone
137159	20.0	1129	CNGL	RHD	309000	7866000	Statherian	Fiery Ck Volcanics	R		Riversleigh Fold Zone
137160	24.0	1130	RHY		309000	7866000	Statherian	Fiery Ck Volcanics	R		Riversleigh Fold Zone
137161	24.0	1131	RHY		309000	7866000	Statherian	Fiery Ck Volcanics	R		Riversleigh Fold Zone
137162	33.2	1132	SDST	F MIC	309000	7866000	Statherian	Fiery Ck Volcanics	R		Riversleigh Fold Zone
137163	37.1	1133	PTB		309000	7866000	Statherian	Fiery Ck Volcanics	R		Riversleigh Fold Zone
137164	66.0	1134	RHY		309000	7866000	Statherian	Fiery Ck Volcanics	R		Riversleigh Fold Zone
137165	71.0	1135	RHY		309000	7866000	Statherian	Fiery Ck Volcanics	R		Riversleigh Fold Zone
137166	88.0	1136	RHY		309000	7866000	Statherian	Fiery Ck Volcanics	R		Riversleigh Fold Zone
137167	90.0	1137	RHY		309000	7866000	Statherian	Fiery Ck Volcanics	R		Riversleigh Fold Zone
137168	139.0	1138	RHY		309000	7866000	Statherian	Fiery Ck Volcanics	R		Riversleigh Fold Zone
137169	140.0	1139	RHY		309000	7866000	Statherian	Fiery Ck Volcanics	R		Riversleigh Fold Zone
137170	141.0	1140	RHY		309000	7866000	Statherian	Fiery Ck Volcanics	R		Riversleigh Fold Zone
137171	170.0	1141	BX	RHY	309000	7866000	Statherian	Fiery Ck Volcanics	R		Riversleigh Fold Zone
137172	170.0	1142	RHY		309000	7866000	Statherian	Fiery Ck Volcanics	R		Riversleigh Fold Zone
137173	180.0	1143	RHY	QZ VN	309000	7866000	Statherian	Fiery Ck Volcanics	R		Riversleigh Fold Zone
137174	223.0	1144	BLT	WEA	309000	7866000	Statherian	Fiery Ck Volcanics	R		Riversleigh Fold Zone
137175	248.3	1145	BX	RHY	309000	7866000	Statherian	Fiery Ck Volcanics	R		Riversleigh Fold Zone
137176	248.5	1146	BX	RHY	309000	7866000	Statherian	Fiery Ck Volcanics	R		Riversleigh Fold Zone
137177	251.1	1147	RHY		309000	7866000	Statherian	Fiery Ck Volcanics	R		Riversleigh Fold Zone
137178	269.0	1198	SDST		308400	7865400	Statherian	Bigie Formation	R		Riversleigh Fold Zone
137179	272.0	1148	RHY		309000	7866000	Statherian	Fiery Ck Volcanics	R		Riversleigh Fold Zone
137180	289.0	1149	RHY	C	309000	7866000	Statherian	Fiery Ck Volcanics	R		Riversleigh Fold Zone
137181	310.1	1150	RHY	ALT	309000	7866000	Statherian	Fiery Ck Volcanics	R		Riversleigh Fold Zone
137182	317.0	1151	CNGL	HET	309000	7866000	Statherian	Fiery Ck Volcanics	R		Riversleigh Fold Zone
137183	324.0	1152	SDST	LTH	309000	7866000	Statherian	Fiery Ck Volcanics	R		Riversleigh Fold Zone
137184	332.3	1153	RHY		309000	7866000	Statherian	Fiery Ck Volcanics	R		Riversleigh Fold Zone
137185	333.0	1154	BX	SLF HET	309000	7866000	Statherian	Fiery Ck Volcanics	R		Riversleigh Fold Zone
137186	334.4	1209	SDST	C	308000	7867000	Statherian	Quilalar Formation	R		Riversleigh Fold Zone
137187	335.1	1281	DLST	SLF	309335	7867550	Statherian	Lochness Formation	R		Riversleigh Fold Zone
137188	335.2	1282	DLST	HM	309335	7867550	Statherian	Lochness Formation	R		Riversleigh Fold Zone
137189	335.9	1279	SLST	F FER	309335	7867550	Statherian	Lochness Formation	R		Riversleigh Fold Zone
137190	335.9	1280	SDST	FEL	309335	7867550	Statherian	Lochness Formation	R	335l	Riversleigh Fold Zone
137191	500.0	1339	BLT	MET	322000	7868000	Statherian	Eastern Ck Volcs	R		Riversleigh Fold Zone
137192	1001.1	823	CHRT		295900	7813300	Statherian	Mount Oxide Chert Mb	R		Lady Loretta
137193	1001.2	824	CHRT		295900	7813300	Statherian	Mount Oxide Chert Mb	R		Lady Loretta
137194	1002.0	825	CHRT		295900	7813300	Statherian	Mount Oxide Chert Mb	R		Lady Loretta
137195	1003.0	826	CHRT		295900	7813300	Statherian	Mount Oxide Chert Mb	R		Lady Loretta
137196	1004.1	730	SDST	C	295400	7812700	Statherian	Paradise Ck Fm	R	Pbx1.5	Lady Loretta
137197	1004.2	731	SDST	C	295400	7812700	Statherian	Paradise Ck Fm	R	Pbx1.5	Lady Loretta
137198	1005.0	136	SUL	GN SP PY	297200	7812700	Statherian	Lady Loretta Fm	R	ore	Lady Loretta
137199	1006.1	1050	QZT		296600	7813100	Statherian	Torpedo Ck Qtzite	R		Lady Loretta
137200	1006.2	1051	QZT		296600	7813100	Statherian	Torpedo Ck Qtzite	R		Lady Loretta
137201	1006.3	1052	QZT		296600	7813100	Statherian	Torpedo Ck Qtzite	R		Lady Loretta
137202	1006.4	1053	QZT		296600	7813100	Statherian	Torpedo Ck Qtzite	R		Lady Loretta
137203	1007.0	137	SUL	GN SP PY	297200	7812700	Statherian	Lady Loretta Fm	R	ore	Lady Loretta
137204	1008.0	138	SUL	GN SP PY	297200	7812700	Statherian	Lady Loretta Fm	R	ore	Lady Loretta
137205	1009.1	844	SLST	SLF DMT	295000	7812000	Statherian	Paradise Ck Fm?	R	Pbx3	Lady Loretta
137206	1009.2	845	SLST	SLF DMT	295000	7812000	Statherian	Paradise Ck Fm?	R	Pbx3	Lady Loretta
137207	1009.3	846	SLST	SLF DMT	295000	7812000	Statherian	Paradise Ck Fm?	R	Pbx3	Lady Loretta
137208	1010.0	847	SLST	SLF DMT	295000	7812000	Statherian	Paradise Ck Fm?	R	Pbx3	Lady Loretta
137209	1011.0	848	SLST	DMT	295000	7812000	Statherian	Paradise Ck Fm?	R	Pbx3	Lady Loretta
137210	1012.1	649	SDST	F	295000	7812000	Statherian	Paradise Ck Fm?	R	Pbx3	Lady Loretta
137211	1012.2	650	SDST	F	295000	7812000	Statherian	Paradise Ck Fm?	R	Pbx3	Lady Loretta
137212	1012.3	651	SDST	F	295000	7812000	Statherian	Paradise Ck Fm?	R	Pbx3	Lady Loretta
137213	1012.4	652	SDST	F	295000	7812000	Statherian	Paradise Ck Fm?	R	Pbx3	Lady Loretta
137214	1013.1	906	SDST	F SLY	294600	7812500	Statherian	Gunpowder Ck Fm	R	Plug3	Lady Loretta
137215	1013.2	907	SDST	F SLY	294600	7812500	Statherian	Gunpowder Ck Fm	R	Plug3	Lady Loretta
137216	1014.0	917	SLST	DMT	296100	7813100	Statherian	Gunpowder Ck Fm	R	Plug2	Lady Loretta
137217	1015.0	918	SLST	DMT	296100	7813100	Statherian	Gunpowder Ck Fm	R	Plug2	Lady Loretta
137218	1016.0	919	SLST	DMT	296100	7813100	Statherian	Gunpowder Ck Fm	R	Plug2	Lady Loretta
137219	1017.0	920	SLST	DMT	296100	7813100	Statherian	Gunpowder Ck Fm	R	Plug2	Lady Loretta
137220	1018.0	1303	BLT	MET	295622	7814095	Statherian	Eastern Ck Volcs	R		Lady Loretta
137221	1019.0	921	SLST	DMT	296100	7813100	Statherian	Gunpowder Ck Fm	R	Plug2	Lady Loretta
137222	1020.0	1172	BLT	WEA	296100	7814350	Statherian	Fiery Ck Volcanics	R	45-75 osc.	Lady Loretta
137223	1021.0	1304	BLT	MET	295622	7814095	Statherian	Eastern Ck Volcs	R		Lady Loretta
137224	1022.0	922	SLST	HM CAR MIC	296100	7813100	Statherian	Gunpowder Ck Fm	R	Plug2	Lady Loretta
137225	1023.0	923	SLST	HM	296100	7813100	Statherian	Gunpowder Ck Fm	R	Plug2	Lady Loretta
137226	1024.0	924	SLST	HM MIC	296100	7813100	Statherian	Gunpowder Ck Fm	R	Plug2	Lady Loretta
137227	1025.0	485	SHLE	DMT CAR PY	297184	7811973	Statherian	Lady Loretta Fm	R		Lady Loretta
137228	1026.0	486	SLST	SD	297174	7812249	Statherian	Lady Loretta Fm	R		Lady Loretta
137229	1027.0	487	SLST	FER DMT CAR	297184	7811973	Statherian	Lady Loretta Fm	R		Lady Loretta
137230	1028.0	1305	BLT	MET	295622	7814095	Statherian	Eastern Ck Volcs	R	anisotropy?	Lady Loretta
137231	1029.0	488	SLST	DMT CAR PY	297174	7812249	Statherian	Lady Loretta Fm	R		Lady Loretta
137232	1030.0	489	SLST	DMT CAR	297181	7812052	Statherian	Lady Loretta Fm	R		Lady Loretta
137233	1031.0	490	SLST	WEA	297181	7812052	Statherian	Lady Loretta Fm	R		Lady Loretta
137234	1032.0	491	SLST	CAR	297181	7812052	Statherian	Lady Loretta Fm	R		Lady Loretta
137235	1033.0	1173	BLT	WEA	296100	7814350	Statherian	Fiery Ck Volcanics	R		Lady Loretta
137236	1034.0	908	SDST	MIC SLY	294600	7812500	Statherian	Gunpowder Ck Fm	R	Plug3	Lady Loretta
137237	1035.0	909	SDST	MIC SLY	294600	7812500	Statherian	Gunpowder Ck Fm	R	Plug3	Lady Loretta
137238	1036.0	910	SDST	MIC SLY	294600	7812500	Statherian	Gunpowder Ck Fm	R	Plug3	Lady Loretta
137239	1037.0	911	SDST	MIC SLY	294600	7812500	Statherian	Gunpowder Ck Fm	R	Plug3	Lady Loretta
137240	1038.0	912	SDST	MIC SLY	294600	7812500	Statherian	Gunpowder Ck Fm	R	Plug3	Lady Loretta

137241	1039.0	913	SDST	MIC SLY	294600	7812500	Statherian	Gunpowder Ck Fm	R	Plug3	Lady Loretta
137242	1040.0	914	SDST	MIC SLY	294600	7812500	Statherian	Gunpowder Ck Fm	R	Plug3	Lady Loretta
137243	1041.0	1174	BLT	WEA	296100	7814350	Statherian	Fiery Ck Volcanics	R		Lady Loretta
137244	1042.0	1175	BLT	WEA	296100	7814350	Statherian	Fiery Ck Volcanics	R		Lady Loretta
137245	1043.0	927	SLST	GR	296100	7813100	Statherian	Gunpowder Ck Fm	R	Plug1	Lady Loretta
137246	1044.0	928	SLST	GR	296100	7813100	Statherian	Gunpowder Ck Fm	R	Plug1	Lady Loretta
137247	1045.0	614	SDST	FER F	297500	7813200	Statherian	Esperanza Formation	R	Ptx4	Lady Loretta
137248	1046.0	615	SDST	FER F	297500	7813200	Statherian	Esperanza Formation	R	Ptx4	Lady Loretta
137249	1047.0	1176	BLT		296100	7814350	Statherian	Fiery Ck Volcanics	R	55-75 osc.	Lady Loretta
137250	1048.0	492	SLST	CAR DMT	297181	7812052	Statherian	Lady Loretta Fm	R		Lady Loretta
137251	1049.0	929	SLST	SDY	296100	7813100	Statherian	Gunpowder Ck Fm	R	Plug1	Lady Loretta
137252	1050.0	930	SLST	SDY	296100	7813100	Statherian	Gunpowder Ck Fm	R	Plug1	Lady Loretta
137253	1051.0	925	DLST	SLY F	296100	7813100	Statherian	Gunpowder Ck Fm	R	Plug2	Lady Loretta
137254	1052.0	926	DLST	SLY F	296100	7813100	Statherian	Gunpowder Ck Fm	R	Plug2	Lady Loretta
137255	1053.0	678	SDST	SLY F	295800	7812400	Statherian	Paradise Ck Fm	R	Ptx2	Lady Loretta
137256	1054.0	679	SDST	SLY F	295800	7812400	Statherian	Paradise Ck Fm	R	Ptx2	Lady Loretta
137257	1055.0	675	DLST	SLY	295500	7813000	Statherian	Paradise Ck Fm	R		Lady Loretta
137258	1056.0	676	DLST	SLY	295500	7813000	Statherian	Paradise Ck Fm	R		Lady Loretta
137259	1057.0	677	DLST	SLY	295500	7813000	Statherian	Paradise Ck Fm	R		Lady Loretta
137260	1058.0	915	SDST	SLY F	294600	7812500	Statherian	Gunpowder Ck Fm	R	Plug3	Lady Loretta
137261	1059.0	916	SDST	SLY F	294600	7812500	Statherian	Gunpowder Ck Fm	R	Plug3	Lady Loretta
137262	1060.0	931	SLST	FER	296100	7813100	Statherian	Gunpowder Ck Fm	R	Plug1	Lady Loretta
137263	1061.0	932	SLST	FER	296100	7813100	Statherian	Gunpowder Ck Fm	R	Plug1	Lady Loretta
137264	1062.0	734	CHRT		295400	7812700	Statherian	Paradise Ck Fm	R	Ptx1	Lady Loretta
137265	1063.0	735	CHRT		295400	7812700	Statherian	Paradise Ck Fm	R	Ptx1	Lady Loretta
137266	1064.0	653	BX	HM CHRT	295000	7812000	Statherian	Paradise Ck Fm?	R	Ptx3	Lady Loretta
137267	1065.0	654	BX	HM CHRT	295000	7812000	Statherian	Paradise Ck Fm?	R	Ptx3	Lady Loretta
137268	1066.0	732	SDST	M FEL	295400	7812700	Statherian	Paradise Ck Fm	R	Ptx1.5	Lady Loretta
137269	1067.0	733	SDST	M FEL	295400	7812700	Statherian	Paradise Ck Fm	R	Ptx1.5	Lady Loretta
137270	1068.0	1097	SDST	M	297100	7813300	Statherian	Surprise Ck Fm			Lady Loretta
137271	1069.0	1098	SDST	M	297100	7813300	Statherian	Surprise Ck Fm			Lady Loretta
137272	1070.0	736	CHRT	STRO	295400	7812700	Statherian	Paradise Ck Fm	R	Ptx1	Lady Loretta
137273	1071.0	616	CHRT	STRO	297500	7813200	Statherian	Esperanza Formation	R	Ptx4	Lady Loretta
137274	1072.0	617	CHRT	STRO	297500	7813200	Statherian	Esperanza Formation	R	Ptx4	Lady Loretta
137275	1073.0	827	CHRT		295900	7813300	Statherian	Mount Oxide Chert Mb	R		Lady Loretta
137276	1074.0	680	BX	HM CHRT	295800	7812400	Statherian	Paradise Ck Fm	R	Ptx2	Lady Loretta
137277	1075.0	681	BX	HM CHRT	295800	7812400	Statherian	Paradise Ck Fm	R	Ptx2	Lady Loretta
137278	1076.0	737	CHRT	STRO	295400	7812700	Statherian	Paradise Ck Fm	R	Ptx1	Lady Loretta
137279	1077.0	828	CHRT		295900	7813300	Statherian	Mount Oxide Chert Mb	R		Lady Loretta
137280	1078.0	84	SDST		296700	7812300	Statherian	Shady Bore Quartzite	R		Lady Loretta
137281	1079.0	85	SDST	CLAY CL	296700	7812300	Statherian	Shady Bore Quartzite	R		Lady Loretta
137282	1080.0	86	SDST	CLAY CL	296700	7812300	Statherian	Shady Bore Quartzite	R		Lady Loretta
137283	1081.0	1054	QZT		296600	7813100	Statherian	Torpedo Ck Qtzite			Lady Loretta
137284	1082.0	1055	QZT		296600	7813100	Statherian	Torpedo Ck Qtzite			Lady Loretta
137285	1083.0	1056	QZT		296600	7813100	Statherian	Torpedo Ck Qtzite			Lady Loretta
137286	1084.0	1057	QZT		296600	7813100	Statherian	Torpedo Ck Qtzite			Lady Loretta
137287	1085.0	613	SDST	F	297500	7813200	Statherian	Esperanza Formation	R	Ptx4	Lady Loretta
137288	1086.0	1058	CNGL	QZ	296600	7813100	Statherian	Torpedo Ck Qtzite		SCF clasts?	Lady Loretta
137289	1087.0	1059	CNGL	QZ	296600	7813100	Statherian	Torpedo Ck Qtzite		SCF clasts?	Lady Loretta
137290	1088.0	87	SDST	CLAY CL	296700	7812300	Statherian	Shady Bore Quartzite	R		Lady Loretta
137291	1089.0	1099	SDST	C	297100	7813300	Statherian	Surprise Ck Fm			Lady Loretta
137292	1090.0	1100	SDST	C	297100	7813300	Statherian	Surprise Ck Fm			Lady Loretta
137293	1091.0	1101	SDST	M	297100	7813300	Statherian	Surprise Ck Fm		longest axis	Lady Loretta
137294	1092.0	1102	SDST	CLAY CL M	297100	7813300	Statherian	Surprise Ck Fm		longest axis	Lady Loretta
137295	1093.0	1103	SDST	M	297100	7813300	Statherian	Surprise Ck Fm		longest axis	Lady Loretta
137296	2002.0	721	SHLE	CAR	303950	7821900	Statherian	Paradise Ck Fm	R		Riversleigh Fold Zone
137297	2003.0	493	SLST	FER DMT	297181	7812052	Statherian	Lady Loretta Fm	R		Riversleigh Fold Zone
137298	2004.0	494	SLST	FER	298206	7827459	Statherian	Lady Loretta Fm	R		Riversleigh Fold Zone
137299	2005.0	495	DLST	FER STRO	298206	7827459	Statherian	Lady Loretta Fm	R		Riversleigh Fold Zone
137300	2006.0	496	DLST	FER STRO	298206	7827459	Statherian	Lady Loretta Fm	R		Riversleigh Fold Zone
137301	2007.0	497	DLST	SLY	298206	7827459	Statherian	Lady Loretta Fm	R		Riversleigh Fold Zone
137302	2008.0	498	DLST	FER STRO	298206	7827459	Statherian	Lady Loretta Fm	R		Riversleigh Fold Zone
137303	2009.0	622	SLST	CAR DMT PY	293308	7843904	Statherian	Esperanza Formation	R		Riversleigh Fold Zone
137304	2010.0	623	SHLE	CAR DMT PY	293308	7843904	Statherian	Esperanza Formation	R	py/dol blobs	Riversleigh Fold Zone
137305	2011.0	624	SHLE	CAR DMT PY	293308	7843904	Statherian	Esperanza Formation	R	py/dol blobs	Riversleigh Fold Zone
137306	2012.0	625	SHLE	CAR	293308	7843904	Statherian	Esperanza Formation	R		Riversleigh Fold Zone
137307	2013.0	626	SLST	PY	293308	7843904	Statherian	Esperanza Formation	R		Riversleigh Fold Zone
137308	2014.0	627	SLST	LA MIC	293308	7843904	Statherian	Esperanza Formation	R	711.4	Riversleigh Fold Zone
137309	2015.0	628	SLST	LA	293308	7843904	Statherian	Esperanza Formation	R	423.5	Riversleigh Fold Zone
137310	2016.0	629	SLST	DMT	293308	7843904	Statherian	Esperanza Formation	R	721.2	Riversleigh Fold Zone
137311	2017.0	630	SLST	LA DMT	293308	7843904	Statherian	Esperanza Formation	R	724.5	Riversleigh Fold Zone
137312	2018.0	631	SLST	CAR DMT	293308	7843904	Statherian	Esperanza Formation	R	735.7	Riversleigh Fold Zone
137313	2019.0	632	SHLE	CAR DMT PY	293308	7843904	Statherian	Esperanza Formation	R	653.1	Riversleigh Fold Zone
137314	2020.0	633	SHLE	CAR PY	293308	7843904	Statherian	Esperanza Formation	R		Riversleigh Fold Zone
137315	2021.0	634	SHLE	CAR	293308	7843904	Statherian	Esperanza Formation	R		Riversleigh Fold Zone
137316	2022.0	635	MDST	CAR	293308	7843904	Statherian	Esperanza Formation	R		Riversleigh Fold Zone
137317	2023.0	636	SLST	DMT	293308	7843904	Statherian	Esperanza Formation	R		Riversleigh Fold Zone
137318	2024.0	637	DLST	STRO SLY	293308	7843904	Statherian	Esperanza Formation	R		Riversleigh Fold Zone
137319	2025.0	638	DLST	FER SDY	293308	7843904	Statherian	Esperanza Formation	R		Riversleigh Fold Zone
137320	2026.0	639	DLST	SLY	293308	7843904	Statherian	Esperanza Formation	R		Riversleigh Fold Zone
137321	2027.0	859	SHLE	GR CAR	302814	7822727	Statherian	Gunpowder Ck Fm?	R		Riversleigh Fold Zone
137322	2028.0	860	SHLE	GR CAR	302814	7822727	Statherian	Gunpowder Ck Fm?	R		Riversleigh Fold Zone
137323	2029.0	861	SHLE	GR CAR	302814	7822727	Statherian	Gunpowder Ck Fm?	R		Riversleigh Fold Zone
137324	2030.0	862	SHLE	GR CAR	302814	7822727	Statherian	Gunpowder Ck Fm?	R		Riversleigh Fold Zone
137325	2031.0	863	SHLE	GR CAR	302814	7822727	Statherian	Gunpowder Ck Fm?	R		Riversleigh Fold Zone
137326	2032.0	864	SHLE	GR CAR	302814	7822727	Statherian	Gunpowder Ck Fm?	R		Riversleigh Fold Zone
137327	2033.0	865	SHLE	GR CAR	302814	7822727	Statherian	Gunpowder Ck Fm?	R		Riversleigh Fold Zone
137328	2034.0	848	SHLE	GR CAR	302814	7822727	Statherian	Gunpowder Ck Fm?	R		Riversleigh Fold Zone

137329	2035.0	849	SHLE	GR CAR	302814	7822727	Statherian	Gunpowder Ck Fm?	R		Riversleigh Fold Zone
137330	2036.0	850	SHLE	GR CAR	302814	7822727	Statherian	Gunpowder Ck Fm?	R		Riversleigh Fold Zone
137331	2037.0	851	SHLE	GR CAR	302814	7822727	Statherian	Gunpowder Ck Fm?	R		Riversleigh Fold Zone
137332	2038.0	852	SHLE	GR CAR	302814	7822727	Statherian	Gunpowder Ck Fm?	R		Riversleigh Fold Zone
137333	2039.0	853	SHLE	GR CAR	302814	7822727	Statherian	Gunpowder Ck Fm?	R	8-36 osc	Riversleigh Fold Zone
137334	2040.0	854	SHLE	GR CAR	302814	7822727	Statherian	Gunpowder Ck Fm?	R		Riversleigh Fold Zone
137335	2041.0	855	SHLE	GR CAR	302814	7822727	Statherian	Gunpowder Ck Fm?	R		Riversleigh Fold Zone
137336	2042.0	856	SHLE	GR CAR	302814	7822727	Statherian	Gunpowder Ck Fm?	R		Riversleigh Fold Zone
137337	2043.0	857	SHLE	GR CAR	302814	7822727	Statherian	Gunpowder Ck Fm?	R		Riversleigh Fold Zone
137338	2044.0	858	SHLE	GR CAR	302814	7822727	Statherian	Gunpowder Ck Fm?	R		Riversleigh Fold Zone
137339	2045.0	866	SHLE	RE LA MIC SLY	302814	7822727	Statherian	Gunpowder Ck Fm?	R		Riversleigh Fold Zone
137340	2046.0	867	SHLE	RE LA MIC SLY	302814	7822727	Statherian	Gunpowder Ck Fm?	R		Riversleigh Fold Zone
137341	2047.0	868	SHLE	RE LA MIC SLY	302814	7822727	Statherian	Gunpowder Ck Fm?	R		Riversleigh Fold Zone
137342	2048.0	869	SHLE	RE LA MIC SLY	302814	7822727	Statherian	Gunpowder Ck Fm?	R		Riversleigh Fold Zone
137343	2049.0	870	SHLE	RE LA MIC SLY	302814	7822727	Statherian	Gunpowder Ck Fm?	R		Riversleigh Fold Zone
137344	2050.0	871	SHLE	RE LA MIC SLY	302814	7822727	Statherian	Gunpowder Ck Fm?	R		Riversleigh Fold Zone
137345	2051.0	872	SHLE	RE LA MIC SLY	302814	7822727	Statherian	Gunpowder Ck Fm?	R		Riversleigh Fold Zone
137346	2052.0	873	SHLE	RE LA MIC SLY	302814	7822727	Statherian	Gunpowder Ck Fm?	R		Riversleigh Fold Zone
137347	2053.0	874	SHLE	RE LA MIC SLY	302814	7822727	Statherian	Gunpowder Ck Fm?	R		Riversleigh Fold Zone
137348	2054.0	875	SHLE	RE LA MIC SLY	302814	7822727	Statherian	Gunpowder Ck Fm?	R		Riversleigh Fold Zone
137349	2055.0	840	SLST	CAR	304278	7823128	Statherian	Gunpowder Ck Fm?	R		Riversleigh Fold Zone
137350	2056.0	841	SLST	CAR	304278	7823128	Statherian	Gunpowder Ck Fm?	R		Riversleigh Fold Zone
137351	2057.0	842	SHLE	CAR	304278	7823128	Statherian	Gunpowder Ck Fm?	R		Riversleigh Fold Zone
137352	2058.0	843	SLST	CAR	304278	7823128	Statherian	Gunpowder Ck Fm?	R		Riversleigh Fold Zone
137353	2059.0	844	SLST	CAR	304278	7823128	Statherian	Gunpowder Ck Fm?	R		Riversleigh Fold Zone
137354	2060.0	845	SLST	MIC	304278	7823128	Statherian	Gunpowder Ck Fm?	R		Riversleigh Fold Zone
137355	2061.0	846	SLST	LA	304278	7823128	Statherian	Gunpowder Ck Fm?	R		Riversleigh Fold Zone
137356	2062.0	847	SLST	LA	304278	7823128	Statherian	Gunpowder Ck Fm?	R		Riversleigh Fold Zone
137357	2063.0	722	DLST	PY	302814	7822727	Statherian	Paradise Ck Fm	R		Riversleigh Fold Zone
137358	2064.0	723	DLST	LMST	302814	7822727	Statherian	Paradise Ck Fm	R		Riversleigh Fold Zone
137359	2065.0	724	DLST	LMST	302814	7822727	Statherian	Paradise Ck Fm	R		Riversleigh Fold Zone
137360	2066.0	725	DLST	SUL	302814	7822727	Statherian	Paradise Ck Fm	R		Riversleigh Fold Zone
137361	2067.0	726	DLST	LMST	302814	7822727	Statherian	Paradise Ck Fm	R		Riversleigh Fold Zone
137362	2068.0	727	ARNT	LMST DMT	302814	7822727	Statherian	Paradise Ck Fm	R		Riversleigh Fold Zone
137363	2069.0	728	ARNT	SLY DMT	302814	7822727	Statherian	Paradise Ck Fm	R		Riversleigh Fold Zone
137364	2070.0	729	DLST	SLY	302814	7822727	Statherian	Paradise Ck Fm	R		Riversleigh Fold Zone
137365	2071.0	706	SLST	MDY	303950	7821900	Statherian	Paradise Ck Fm	R		Riversleigh Fold Zone
137366	2072.0	707	SHLE	CAR	303950	7821900	Statherian	Paradise Ck Fm	R		Riversleigh Fold Zone
137367	2073.0	708	SHLE	CAR	303950	7821900	Statherian	Paradise Ck Fm	R		Riversleigh Fold Zone
137368	2074.0	709	SHLE	CAR	303950	7821900	Statherian	Paradise Ck Fm	R		Riversleigh Fold Zone
137369	2075.0	710	SHLE	CAR PY	303950	7821900	Statherian	Paradise Ck Fm	R		Riversleigh Fold Zone
137370	2076.0	711	SHLE	CAR	303950	7821900	Statherian	Paradise Ck Fm	R		Riversleigh Fold Zone
137371	2077.0	712	SHLE	CAR	303950	7821900	Statherian	Paradise Ck Fm	R		Riversleigh Fold Zone
137372	2078.0	713	SHLE	CAR PY	303950	7821900	Statherian	Paradise Ck Fm	R		Riversleigh Fold Zone
137373	2079.0	714	SHLE	CAR	303950	7821900	Statherian	Paradise Ck Fm	R		Riversleigh Fold Zone
137374	2080.0	715	ARNT	SLY DMT	303950	7821900	Statherian	Paradise Ck Fm	R		Riversleigh Fold Zone
137375	2081.0	716	DLST	SLY PY	303950	7821900	Statherian	Paradise Ck Fm	R		Riversleigh Fold Zone
137376	2082.0	717	DLST	SLY	303950	7821900	Statherian	Paradise Ck Fm	R		Riversleigh Fold Zone
137377	2083.0	718	ARNT	SLY CAR PY DMT	303950	7821900	Statherian	Paradise Ck Fm	R		Riversleigh Fold Zone
137378	2084.0	719	SLST	CAR	303950	7821900	Statherian	Paradise Ck Fm	R		Riversleigh Fold Zone
137379	2085.0	720	SLST	LA	303950	7821900	Statherian	Paradise Ck Fm	R		Riversleigh Fold Zone
137380	2086.0	81	SLST	LA	269500	7886000	Statherian	Riversleigh Siltstone	R		Riversleigh Fold Zone
137381	2087.0	1003	SLST	DMT CAR	295635	7827009	Statherian	Gunpowder Ck Fm	R		Riversleigh Fold Zone
137382	2088.0	1004	SLST	DMT CAR	295635	7827009	Statherian	Gunpowder Ck Fm	R		Riversleigh Fold Zone
137383	2089.0	1005	SLST	DMT CAR	295635	7827009	Statherian	Gunpowder Ck Fm	R	amt band w angular clasts	Riversleigh Fold Zone
137384	2090.0	1006	SLST	DMT	295635	7827009	Statherian	Gunpowder Ck Fm	R		Riversleigh Fold Zone
137385	2091.0	1007	MDST	CAR	295635	7827009	Statherian	Gunpowder Ck Fm	R		Riversleigh Fold Zone
137386	2092.0	1008	SLST	DMT CAR	295635	7827009	Statherian	Gunpowder Ck Fm	R		Riversleigh Fold Zone
137387	2093.0	1009	SLST	DMT CAR PY	295635	7827009	Statherian	Gunpowder Ck Fm	R		Riversleigh Fold Zone
137388	2094.0	1010	BX	DMT QZ CAR SUL	295635	7827009	Statherian	Gunpowder Ck Fm	R		Riversleigh Fold Zone
137389	2095.0	1011	BX	DMT QZ CAR SUL	295635	7827009	Statherian	Gunpowder Ck Fm	R		Riversleigh Fold Zone
137390	2096.0	1012	SLST	CAR PY	295635	7827009	Statherian	Gunpowder Ck Fm	R		Riversleigh Fold Zone
137391	2097.0	1013	BX	CAR SUL DMT	295635	7827009	Statherian	Gunpowder Ck Fm	R		Riversleigh Fold Zone
137392	2098.0	1014	SHLE	CAR PY	295635	7827009	Statherian	Gunpowder Ck Fm	R		Riversleigh Fold Zone
137393	2099.0	1015	SLST	CAR DMT PY	295635	7827009	Statherian	Gunpowder Ck Fm	R		Riversleigh Fold Zone
137394	2100.0	1016	DLST	CAR SLY	295635	7827009	Statherian	Gunpowder Ck Fm	R		Riversleigh Fold Zone
137395	2101.0	1017	SLST	CAR DMT	295635	7827009	Statherian	Gunpowder Ck Fm	R		Riversleigh Fold Zone
137396	2102.0	1018	SLST	CAR SDY	295635	7827009	Statherian	Gunpowder Ck Fm	R		Riversleigh Fold Zone
137397	2103.0	1019	SDST	DMT ?SD SLY	295635	7827009	Statherian	Gunpowder Ck Fm	R	core-parallel cleavage	Riversleigh Fold Zone
137398	2104.0	1020	SDST	MIC DMT SLY	295635	7827009	Statherian	Gunpowder Ck Fm	R		Riversleigh Fold Zone
137399	2105.0	1021	SLST	DMT ?SD SLY	295635	7827009	Statherian	Gunpowder Ck Fm	R		Riversleigh Fold Zone
137400	2106.0	1022	SDST	DMT ?SD SLY	295635	7827009	Statherian	Gunpowder Ck Fm	R	core-parallel cleavage	Riversleigh Fold Zone
137401	2107.0	1023	SDST	DMT ?SD SLY PY	295635	7827009	Statherian	Gunpowder Ck Fm	R	core-parallel cleavage	Riversleigh Fold Zone
137402	2108.0	1024	SLST	DMT ?SD PY	295635	7827009	Statherian	Gunpowder Ck Fm	R		Riversleigh Fold Zone
137403	2109.0	1025	SLST	DMT ?SD PY	295635	7827009	Statherian	Gunpowder Ck Fm	R		Riversleigh Fold Zone
137404	2110.0	879	SLST	CAR	300987	7837708	Statherian	Gunpowder Ck Fm	R		Riversleigh Fold Zone
137405	2111.0	880	SLST	MIC	300987	7837708	Statherian	Gunpowder Ck Fm	R		Riversleigh Fold Zone
137406	2112.0	881	SLST		300987	7837708	Statherian	Gunpowder Ck Fm	R		Riversleigh Fold Zone
137407	2113.0	882	SLST	CAR	300987	7837708	Statherian	Gunpowder Ck Fm	R		Riversleigh Fold Zone
137408	2114.0	883	SLST	MIC	300987	7837708	Statherian	Gunpowder Ck Fm	R		Riversleigh Fold Zone
137409	2115.0	884	SLST	MIC	300987	7837708	Statherian	Gunpowder Ck Fm	R		Riversleigh Fold Zone
137410	2116.0	885	SLST	MIC XB	300987	7837708	Statherian	Gunpowder Ck Fm	R		Riversleigh Fold Zone
137411	2117.0	886	SLST	MIC	300987	7837708	Statherian	Gunpowder Ck Fm	R		Riversleigh Fold Zone
137412	2118.0	887	SLST	CAR MIC	300987	7837708	Statherian	Gunpowder Ck Fm	R		Riversleigh Fold Zone
137413	2119.0	888	SLST	CAR	300987	7837708	Statherian	Gunpowder Ck Fm	R		Riversleigh Fold Zone
137414	2120.0	889	SLST	SDY .	300987	7837708	Statherian	Gunpowder Ck Fm	R		Riversleigh Fold Zone
137415	2121.0	890	SLST	MIC	300987	7837708	Statherian	Gunpowder Ck Fm	R		Riversleigh Fold Zone
137416	2122.0	891	SLST	CAR	300987	7837708	Statherian	Gunpowder Ck Fm	R		Riversleigh Fold Zone

137417	2123.0	892	SLST	MIC	300987	7837708	Statherian	Gunpowder Ck Fm	R		Riversleigh Fold Zone
137418	2124.0	893	SLST	MIC	300987	7837708	Statherian	Gunpowder Ck Fm	R		Riversleigh Fold Zone
137419	2125.0	894	SLST	MIC	300987	7837708	Statherian	Gunpowder Ck Fm	R		Riversleigh Fold Zone
137420	2126.0	895	SLST	MIC CAR	300987	7837708	Statherian	Gunpowder Ck Fm	R		Riversleigh Fold Zone
137421	2127.0	896	SLST	CAR	300987	7837708	Statherian	Gunpowder Ck Fm	R		Riversleigh Fold Zone
137422	2128.0	897	SLST	MIC	300987	7837708	Statherian	Gunpowder Ck Fm	R	44-90 osc	Riversleigh Fold Zone
137423	2129.0	898	SLST	MIC	300987	7837708	Statherian	Gunpowder Ck Fm	R		Riversleigh Fold Zone
137424	2130.0	899	SLST		300987	7837708	Statherian	Gunpowder Ck Fm	R		Riversleigh Fold Zone
137425	2131.0	900	SLST		300987	7837708	Statherian	Gunpowder Ck Fm	R		Riversleigh Fold Zone
137426	2132.0	901	SLST	MIC	300987	7837708	Statherian	Gunpowder Ck Fm	R		Riversleigh Fold Zone
137427	2133.0	902	SLST	MIC SDY	300987	7837708	Statherian	Gunpowder Ck Fm	R		Riversleigh Fold Zone
137428	2134.0	903	SLST		300987	7837708	Statherian	Gunpowder Ck Fm	R		Riversleigh Fold Zone
137429	2135.0	904	SLST	VU SDY	300987	7837708	Statherian	Gunpowder Ck Fm	R	38-90 osc	Riversleigh Fold Zone
137430	2136.0	905	SLST		300987	7837708	Statherian	Gunpowder Ck Fm	R		Riversleigh Fold Zone
137431	2137.0	82	SLST		269500	7888000	Statherian	Riversleigh Siltstone	R		Riversleigh Fold Zone
137432	2138.0	83	SLST		269500	7888000	Statherian	Riversleigh Siltstone	R		Riversleigh Fold Zone
137433	2150.0	582	DLST		298750	7827000	Statherian	Lady Loretta Fm	R	CM35 at low angle to dip	Riversleigh Fold Zone
137434	2151.0	583	DLST		298750	7827000	Statherian	Lady Loretta Fm	R		Riversleigh Fold Zone
137435	2152.0	584	DLST	STRO	298750	7827000	Statherian	Lady Loretta Fm	R		Riversleigh Fold Zone
137436	2153.0	585	DLST	SLY	298750	7827000	Statherian	Lady Loretta Fm	R		Riversleigh Fold Zone
137437	2154.0	586	DLST		298750	7827000	Statherian	Lady Loretta Fm	R		Riversleigh Fold Zone
137438	2155.0	587	DLST	STRO	298750	7827000	Statherian	Lady Loretta Fm	R		Riversleigh Fold Zone
137439	2156.0	588	DLST		298750	7827000	Statherian	Lady Loretta Fm	R		Riversleigh Fold Zone
137440	2157.0	589	DLST	PYR	298750	7827000	Statherian	Lady Loretta Fm	R		Riversleigh Fold Zone
137441	2158.0	590	DLST	SLY	298750	7827000	Statherian	Lady Loretta Fm	R		Riversleigh Fold Zone
137442	2159.0	591	DLST		298750	7827000	Statherian	Lady Loretta Fm	R		Riversleigh Fold Zone
137443	2160.0	592	DLST	BU	298750	7827000	Statherian	Lady Loretta Fm	R		Riversleigh Fold Zone
137444	2161.0	593	DLST	SLY	298750	7827000	Statherian	Lady Loretta Fm	R		Riversleigh Fold Zone
137445	2162.0	594	DLST		298750	7827000	Statherian	Lady Loretta Fm	R		Riversleigh Fold Zone
137446	2163.0	595	DLST	STRO	298750	7827000	Statherian	Lady Loretta Fm	R		Riversleigh Fold Zone
137447	2164.0	596	DLST	SLY	298750	7827000	Statherian	Lady Loretta Fm	R		Riversleigh Fold Zone
137448	2165.0	597	DLST		298750	7827000	Statherian	Lady Loretta Fm	R		Riversleigh Fold Zone
137449	2166.0	598	SLST	QZ DMT	298750	7827000	Statherian	Lady Loretta Fm	R		Riversleigh Fold Zone
137450	2167.0	599	DLST		298750	7827000	Statherian	Lady Loretta Fm	R		Riversleigh Fold Zone
137451	2168.0	600	DLST		298750	7827000	Statherian	Lady Loretta Fm	R		Riversleigh Fold Zone
137452	2169.0	601	DLST	SLY	298750	7827000	Statherian	Lady Loretta Fm	R		Riversleigh Fold Zone
137453	2170.0	602	DLST		298750	7827000	Statherian	Lady Loretta Fm	R		Riversleigh Fold Zone
137454	2171.0	603	DLST		298750	7827000	Statherian	Lady Loretta Fm	R		Riversleigh Fold Zone
137455	2172.0	604	DLST	QZ	298750	7827000	Statherian	Lady Loretta Fm	R		Riversleigh Fold Zone
137456	2173.0	605	DLST		298750	7827000	Statherian	Lady Loretta Fm	R		Riversleigh Fold Zone
137457	2174.0	606	DLST	PI	298750	7827000	Statherian	Lady Loretta Fm	R		Riversleigh Fold Zone
137458	2175.0	607	DLST	SLY	298750	7827000	Statherian	Lady Loretta Fm	R		Riversleigh Fold Zone
137459	2176.0	609	DLST		298750	7827000	Statherian	Esperanza Formation?	R		Riversleigh Fold Zone
137460	2177.0	610	DLST	BU SLY	298750	7827000	Statherian	Esperanza Formation?	R		Riversleigh Fold Zone
137461	4001.0	738	SLST	DMT	294978	7812353	Statherian	Paradise Ck Fm	R		Lady Annie
137462	4002.0	739	SLST	DMT CAR PYR	295072	7812245	Statherian	Paradise Ck Fm	R		Lady Annie
137463	4003.0	740	DLST	SLY PYR	295072	7812245	Statherian	Paradise Ck Fm	R		Lady Annie
137464	4004.0	741	DLST	SLY SUL	295072	7812245	Statherian	Paradise Ck Fm	R		Lady Annie
137465	4005.0	687	SLST	BR CAR DMT PY CCP	295300	7812200	Statherian	Paradise Ck Fm	R		Lady Annie
137466	4006.0	670	DLST	BR SLY SUL CAR	295057	7812155	Statherian	Paradise Ck Fm	R		Lady Annie
137467	4007.0	674	SLST	HM DMT	296070	7812850	Statherian	Paradise Ck Fm	R		Lady Annie
137468	6001.0	1357	BLT		275500	7918500	Statherian	Kamarga Volcanics	R	float in ck	Kamarga Dome
137469	6002.0	1358	BLT	WEA VE	275000	7918500	Statherian	Kamarga Volcanics	R		Kamarga Dome
137470	6003.0	1359	BLT	WEA	275000	7918500	Statherian	Kamarga Volcanics	R		Kamarga Dome
137471	6004.0	1360	BLT	WEA	273630	7919009	Statherian	Kamarga Volcanics	R		Kamarga Dome
137472	6005.0	1361	BLT	WEA	278933	7918382	Statherian	Kamarga Volcanics	R		Kamarga Dome
137473	6007.0	134	SUL	GN SP	297200	7812700	Statherian	Lady Loretta Fm	R	ore	Lady Loretta
137474	6008.0	126	SUL	GN SP PY CCP	617400	8182600	Statherian	Barney Ck Fm	R	2 O/B	McArthur River
137475	6009.0	127	SUL	GN SP PY CCP	617400	8182600	Statherian	Barney Ck Fm	R	2 O/B	McArthur River
137476	6010.0	128	SUL	GN SP PY CCP	617400	8182600	Statherian	Barney Ck Fm	R	2 O/B	McArthur River
137477	6011.0	129	SUL	GN SP PY CCP	617400	8182600	Statherian	Barney Ck Fm	R	2 O/B	McArthur River
137478	6012.0	130	SUL	GN SP PY CCP	617400	8182600	Statherian	Barney Ck Fm	R	2 O/B	McArthur River
137479	6013.0	119	SUL	GN SP PY CCP	617400	8182600	Statherian	Barney Ck Fm	R	4 O/B	McArthur River
137480	6014.0	120	SUL	GN SP PY CCP	617400	8182600	Statherian	Barney Ck Fm	R	4 O/B	McArthur River
137481	6015.0	121	SUL	GN SP PY CCP	617400	8182600	Statherian	Barney Ck Fm	R	4 O/B	McArthur River
137482	6016.0	122	SUL	GN SP PY CCP	617400	8182600	Statherian	Barney Ck Fm	R	4 O/B	McArthur River
137483	6017.0	123	SUL	GN SP PY CCP	617400	8182600	Statherian	Barney Ck Fm	R	4 O/B	McArthur River
137484	6018.0	124	SUL	GN SP PY CCP	617400	8182600	Statherian	Barney Ck Fm	R	4 O/B	McArthur River
137485	6019.0	125	SUL	GN SP PY CCP	617400	8182600	Statherian	Barney Ck Fm	R	4 O/B	McArthur River
137486	10334.0	1199	SDST	FEL	308400	7865400	Statherian	Bigie Formation	R		Riversleigh Fold Zone
137487	10335.0	1283	SDST	FER FEL	309335	7867550	Statherian	Lochness Formation	R	335K	Riversleigh Fold Zone

Appendix 7

GIS Authority Tables and Key Databases

This appendix lists the key GIS attribute tables (stratigraphy STRAT.DAT, lithology LITH.DAT and mineral occurrences MINOCC.PAT). These may be related to the accompanying authority tables which define the codes used. Most authority tables have been adopted from those of the Australian Geological Survey Organisation; other, minor tables were developed by the author. The lithological name and qualifier abbreviations encoded in these authority tables have also been used throughout the main text and figures, and in Appendices 3 and 4.

CODE	SYMBOL	UNIT	TEXTSYM	REGION	LOCAL	SPGRP	GRP	SBGRP	FRM	MBR	ERA	PERIOD	EPOCH	DIV	MINAGE	MAXAGE	STRMIN	STRMAX	STRMED	ZMIN	ZMAX	ZMED	ZMEAN	UNDER	OVER
1	52			1			0	0	0	0					0	0	0	0	0	0	0	0	0	0	0
100	20	Quaternary alluvium	Qa	0		PH	0	0	0	0	CZ	QU			0	2	0	0	0	0	0	0	0	0	0
110	26	Undifferentiated cover	Cz	0		PH	0	0	0	0	CZ	TQ			0	65	0	0	0	0	0	0	0	0	0
120	4	Black soil	Czb	0		PH	0	0	0	0	CZ	TQ			0	65	0	0	0	0	0	0	0	0	0
130	14	Ferricrete	Czl	0		PH	0	0	0	0	CZ	TQ			0	65	0	0	0	0	0	0	0	0	0
200	11	Golliger beds	Tg	0		PH	0	0	7522	0	CZ	TT			2	65	0	0	0	0	0	0	0	0	0
300	19		Kl	20		PH	0	0	13380	0	MZ	KR	LO		95	135	0	20	10	0	0	0	0	0	0
301	19	Cretaceous clastics	Kl	95		PH	0	0	13380	0	MZ	KR	LO		95	135	0	100	50	0	0	0	0	0	0
400	25	Top Springs Limestone	C-mt	38		PH	0	0	18426	0	PZ	CM	MI	EA	523	530	0	92	46	0	0	0	0	0	0
450	121		C-m	38		PH	0	0	0	0	PZ	CM	MI		510	530	0	500	250	0	0	0	0	0	0
500	24		C-lb	38		PH	0	0	2840	0	PZ	CM	EA		523	570	30	100	65	0	0	0	0	0	0
501	24	Bukalara Sandstone	C-lb	38	AR	PH	0	0	2840	0	PZ	CM	EA		523	570	30	300	165	0	0	0	0	0	0
510	128		C-la	38		PH	0	0	488	0	PZ	CM	EA		523	570	0	37	19	0	0	0	0	0	0
511	128		C-la	24		PH	0	0	488	0	PZ	CM	EA		523	570	0	122	61	0	0	0	0	0	0
800	1		P-P_z	52			0	0	0	0					250	1398	0	0	0	0	0	0	0	0	0
900	41		P_dl	52	BS		0	0	0	0	MP	ET			1280	1300	0	0	0	0	0	0	0	0	0
1000	81	Roper Group	P_r	52		PC	16319	0	0	0	MP	EC			1398	1600	1080	3160	2120	0	-3160	-2120	-1760	2000	0
1200	96	Roper Group - Maiwok Subgroup	P_r	52		PC	16319	25195	0	0	MP	EC			1398	1600	0	800	800	0	-800	-800	-533	0	0
1210	0		P_rm	52		PC	16319	25195	11570	0	MP	EC			1398	1600	0	350	350	0	-350	-350	-233	1220	0
1212	15	Kyalla Member	P_rmy	52		PC	16319	25195	11570	26679	MP	EC			1398	1600	0	200	200	0	-200	-200	-133	1213	0
1213	98	Sherwin Ironstone Member	P_rz	52	BS	PC	16319	25195	11570	16833	MP	EC			1398	1600	0	20	10	0	-220	-210	-143	1214	1212
1214	79	Moroak Sandstone Member	P_rmk	52		PC	16319	25195	11570	29293	MP	EC			1398	1600	0	150	150	0	-350	-350	-233	1220	1213
1220	80	Velkerri Formation	P_rv	52		PC	16319	25195	19074	0	MP	EC			1398	1600	0	450	450	-350	-800	-800	-650	1410	1214
1400	81	lower Roper Group	P_r	52		PC	16319	0	0	0	MP	EC			1398	1600	730	2360	1545	-800	-3160	-2345	-2102	2000	1200
1410	18	Bessie Creek Sandstone	P_re	52		PC	16319	0	24715	0	MP	EC			1398	1600	40	370	205	-800	-1170	-1005	-992	1420	1220
1411	18	Bessie Creek Sandstone	P_re	52	AR	PC	16319	0	24715	0	MP	EC			1398	1600	120	180	150	-800	-980	-950	-910	1421	1220
1420	97		P_ro	52		PC	16319	0	27379	0	MP	EC			1398	1600	130	500	315	-840	-1670	-1320	-1277	1432	1410
1421	97	Corcoran Formation	P_ro	52	AR	PC	16319	0	27379	0	MP	EC			1398	1600	130	180	155	-920	-1160	-1105	-1062	1432	1411
1430	82	Abner Sandstone	P_ra	52		PC	16319	0	55	0	MP	EC			1398	1600	70	590	330	-970	-2260	-1650	-1627	1440	1420
1432	13	Hodgson Sandstone Mbr	P_rah	52		PC	16319	0	55	27800	MP	EC			1398	1600	40	270	155	-970	-1940	-1260	-1390	1434	1420
1433	13	Hodgson Sandstone Mbr	P_rah	52	EB	PC	16319	0	55	27800	MP	EC			1398	1600	0	40	40	-970	-1710	-1145	-1275	1434	1420
1434	12	Jalboi Member	P_raj	52		PC	16319	0	55	8842	MP	EC			1398	1600	10	30	20	-1010	-1970	-1280	-1420	1436	1432
1436	17	Arnold Sandstone Member	P_rax	52	WB	PC	16319	0	55	28334	MP	EC			1398	1600	240	290	265	-1020	-2260	-1545	-1608	1440	1434
1437	17	Arnold Sandstone Member	P_rax	52	EB	PC	16319	0	55	28334	MP	EC			1398	1600	30	50	40	-1010	-1790	-1185	-1328	1440	1434
1440	6	Crawford Formation	P_rr	52		PC	16319	0	27754	0	MP	EC			1398	1600	110	140	125	-1460	-2400	-1775	-1878	1450	1436
1450	87	Mainoru Formation	P_ru	52		PC	16319	0	11034	0	MP	EC			1398	1600	250	300	275	-1600	-2700	-2050	-2117	1460	1440
1451	87	Mainoru Formation	P_ru	52	AR	PC	16319	0	11034	0	MP	EC			1398	1600	0	600	600	-1600	-3000	-2250	-2283	1460	1440
1460	98		P_ri	52		PC	16319	0	10424	0	MP	EC			1398	1600	80	120	100	-1850	-2820	-2150	-2273	1465	1450
1461	98	Limmen Sandstone	P_ri	52	EB	PC	16319	0	10424	0	MP	EC			1398	1600	10	20	15	-1850	-2720	-2065	-2212	1465	1451
1465	5	Mantungula Formation	P_rn	52		PC	16319	0	23782	0	MP	EC			1398	1600	30	40	35	-1930	-2860	-2100	-2297	0	1460
1600	85	South Nicholson Group	P_q	75		PC	17123	0	0	0	MP	EC			1398	1600	1000	1800	1400	0	-1800	-1400	-1067	0	0
2000	60	Nathan Group	P_n	52		PC	26072	0	0	0	MP	CL			1400	1600	0	1600	1600	-1080	-4760	-3720	-3187	3000	1400
2100	59	Kams Dolomite	P_k	52		PC	0	0	9292	0	MP	CL			1400	1600	100	250	175	-1080	-3410	-2295	-2262	0	0
2110	50	Dungaminnie Formation	P_ng	52		PC	26072	0	5843	0	MP	CL			1400	1600	0	240	240	-1080	-3400	-2360	-2280	2120	1465
2120	55	Balbirini Dolomite	P_nz	52		PC	26072	0	923	0	MP	CL			1400	1600	890	1500	1240	-1320	-4900	-3600	-3273	2130	2110
2130	57	Smythe Sandstone	P_ny	52		PC	26072	0	17019	0	MP	CL			1400	1600	15	250	133	-2210	-5150	-3733	-3698	3310	2120
3000	35	undivided McArthur Group	P_m	52		PC	11512	0	0	0	PP	ST			1600	1719	2150	4500	3325	-2225	-9260	-7045	-6177	4000	2000

CODE	SYMBOL	UNIT	TEXTSYM	REGION	LOCAL	SPGRP	GRP	SBGRP	FRM	MBR	ERA	PERIOD	EPOCH	DIV	MINAGE	MAXAGE	STRMIN	STRMAX	STRMED	ZMIN	ZMAX	ZMED	ZMEAN	UNDER	OVER
3100	92	upper McNamara Group	P_mu	54	RF	PC	11575	0	0	0	PM	CS			1589	1660	2570	6500	4535	-1000	-8300	-5935	-5078	3200	1600
3200	95	lower McNamara Group	P_ml	54	RF	PC	11575	0	0	0	PP	ST			1600	1679	2940	4240	3590	-3570	-12540	-9525	-8545	3800	3100
3300	36	undivided Batten Subgroup	P_m	52		PC	11512	1257	0	0	PP	ST			1600	1647	150	1000	575	-2225	-5760	-4295	-4093	3810	2130
3310	42	Amos Formation	P_mm	52		PC	11512	1257	25781	0	PP	ST			1600	1647	0	90	90	-2225	-4850	-3810	-3628	3320	2130
3315	44	Looking Glass Formation	P_mo	52		PC	11512	1257	10647	0	PP	ST			1600	1647	30	70	50	-2315	-4920	-3860	-3698	3320	2130
3320	82	Stretton Sandstone	P_mr	52		PC	11512	1257	17426	0	PP	ST			1600	1647	5	270	138	-2345	-5190	-3998	-3844	3330	3310
3330	45	Yalco Formation	P_mj	52		PC	11512	1257	20758	0	PP	ST			1600	1647	50	250	150	-2350	-5440	-4148	-3979	3342	3320
3340	0		P_mn	52		PC	11512	1257	10891	0	PP	ST			1600	1647	50	600	325	-2400	-6040	-4473	-4304	3610	3330
3342	120	Donnegan Member	P_mnd	52		PC	11512	1257	10891	5608	PP	ST			1600	1647	0	134	67	-2400	-5574	-4215	-4063	3344	3330
3344	124	Hot Spring Member	P_mnh	52		PC	11512	1257	10891	23654	PP	ST			1600	1647	50	350	200	-2400	-5924	-4415	-4246	3346	3342
3346	129	Caranbirini Member	P_mnc	52		PC	11512	1257	10891	23467	PP	ST			1600	1647	0	300	150	-2450	-6224	-4565	-4413	3610	3344
3500	46	Fickling Group	P_j	54	RF	PC	6631	0	0	0	PP	ST			1600	1719	950	1140	1045	-1000	-2940	-2445	-2128	0	1600
3510	10	Fish River Formation	P_jf	54	RF	PC	6631	0	6682	0	PP	ST			1600	1719	10	250	130	-1950	-3190	-2575	-2572	0	1600
3600	51	undivided Umbolooga Subgroup	P_m	52		PC	11512	18813	0	0	PP	ST			1600	1719	2000	3300	2650	-2375	-8960	-6383	-5906	4010	3346
3610	43	Reward Dolomite	P_mx	52		PC	11512	18813	16057	0	PP	ST			1600	1647	30	350	190	-2375	-6110	-4485	-4323	3620	3346
3620	100	Barney Creek Formation	P_mq	52		PC	11512	18813	1130	0	PP	ST			1633	1647	10	900	455	-2405	-7010	-4940	-4785	3632	3810
3630	53	Teena Dolomite	P_mp	52		PC	11512	18813	26166	0	PP	ST			1633	1719	15	130	73	-2415	-7140	-5013	-4858	3640	3632
3632	39	Coxco Dolomite Member	P_mpc	52		PC	11512	18813	26166	27753	PP	ST			1633	1719	15	70	43	-2415	-7080	-4983	-4826	3630	3620
3640	0		P_me	52		PC	11512	18813	27398	0	PP	ST			1633	1719	0	620	620	-2430	-7760	-5633	-5274	3650	3630
3642	49	Mitchell Yard Dolomite Member	P_mei	52		PC	11512	18813	27398	27836	PP	ST			1633	1719	0	300	150	-2430	-7760	-5633	-5274	3644	3630
3644	48	Mara Dolomite Member	P_mea	52		PC	11512	18813	27398	11224	PP	ST			1633	1719	0	320	160	-2430	-7760	-5633	-5274	3650	3642
3650	113	Myrtle Shale	P_mf	52		PC	11512	18813	13660	0	PP	ST			1633	1719	40	60	50	-3050	-7820	-5683	-5518	3660	3644
3660	92	Leila Sandstone	P_mi	52		PC	11512	18813	25162	0	PP	ST			1633	1719	0	30	15	-3090	-7850	-5698	-5546	3670	3650
3670	52	Tooganinie Formation	P_mt	52		PC	11512	18813	18349	0	PP	ST			1633	1719	0	200	200	-3090	-8050	-5898	-5679	3680	3660
3680	83	Tatoola Sandstone	P_md	52		PC	11512	18813	17896	0	PP	ST			1633	1719	80	350	215	-3290	-8400	-6113	-5934	3690	3670
3681	83	Tatoola Sandstone	P_md	52	TP	PC	11512	18813	17896	0	PP	ST			1633	1719	80	150	115	-3290	-8200	-6013	-5834	3690	3670
3690	21	Amelia Dolomite	P_ma	52		PC	11512	18813	25760	0	PP	ST			1633	1719	50	150	100	-3370	-8550	-6213	-6044	3710	3680
3691	21	Amelia Dolomite	P_ma	52	SB	PC	11512	18813	25760	0	PP	ST			1633	1719	150	180	165	-3370	-8580	-6278	-6076	3710	3680
3710	89	Mallapunyah Formation	P_ml	52		PC	11512	18813	11103	0	PP	ST			1633	1719	100	450	275	-3420	-9000	-6488	-6303	3720	3690
3711	89		P_ml	52	MD	PC	11512	18813	11103	0	PP	ST			1633	1719	200	220	210	-3520	-8770	-6488	-6259	3720	3690
3712	89	Mallapunyah Formation	P_ml	52	TR	PC	11512	18813	11103	0	PP	ST			1633	1719	200	220	210	-3420	-8770	-6423	-6204	3720	3690
3713	89		P_ml	52	MH	PC	11512	18813	11103	0	PP	ST			1633	1719	100	110	105	-3420	-8660	-6318	-6133	3720	3690
3714	89		P_ml	52	FI	PC	11512	18813	11103	0	PP	ST			1633	1719	250	300	275	-3520	-8850	-6553	-6308	3720	3690
3715	89	Mallapunyah Formation	P_ml	52	WB	PC	11512	18813	11103	0	PP	ST			1633	1719	300	450	375	-3520	-9000	-6588	-6369	3720	3690
3720	86	Masterton Sandstone	P_ms	52		PC	11512	18813	25730	0	PP	ST			1633	1719	40	650	345	-3520	-9650	-6833	-6668	4010	3710
3721	86		P_ms	52	MD	PC	11512	18813	25730	0	PP	ST			1633	1719	50	150	100	-3720	-8920	-6588	-6409	4010	3711
3722	86		P_ms	52	MH	PC	11512	18813	25730	0	PP	ST			1633	1719	40	40	40	-3520	-8700	-6358	-6193	4010	3713
3723	86		P_ms	52	BR	PC	11512	18813	25730	0	PP	ST			1633	1719	250	650	450	-3820	-9650	-7038	-6836	4010	3710
3724	86		P_ms	52	ST	PC	11512	18813	25730	0	PP	ST			1633	1719	650	650	650	-3620	-9420	-7073	-6704	4010	3710
3725	86		P_ms	52	SR	PC	11512	18813	25730	0	PP	ST			1633	1719	150	200	175	-3620	-8970	-6598	-6396	4010	3710
3726	86	Masterton Sandstone	P_ms	52	TR	PC	11512	18813	25730	0	PP	ST			1633	1719	150	200	175	-3620	-8970	-6598	-6396	4010	3712
3800	101	Surprise Creek Formation	P_r	54	RF	C3	0	0	17551	0	PP	ST			1646	1679	0	2000	2000	-6510	-14540	-11525	-10858	0	3200
4000	99	Tawallah Group	P_t	52		PC	17902	0	0	0	PP	ST			1707	1800	0	5000	5000	-4375	-13960	-12045	-10227	5000	3600
4010	106	Tanumbirini Rhyolite	P_tt	52		PC	17902	0	17800	0	PP	ST			1707	1719	0	100	100	-4375	-9360	-6933	-6889	4020	3720
4020	91	Warramana Sandstone	P_tm	52		PC	17902	0	24563	0	PP	ST			1707	1800	0	120	120	-4475	-9480	-7053	-7003	4030	4010
4025	111	Packsaddle Microgranite	P_gp	52	WS	PC	17902	0	14735	0	PP	ST			1707	1800	0	0	0	-4595	-9660	-7233	-7163	4030	4000
4030	69	Gold Creek Volcanics	P_tg	52		PC	17902	0	7486	0	PP	ST			1707	1800	0	180	180	-4595	-9660	-7233	-7163	4040	4020

CODE	SYMBOL	UNIT	TEXTSYM	REGION	LOCAL	SPGRP	GRP	SBGRP	FRM	MBR	ERA	PERIOD	EPOCH	DIV	MINAGE	MAXAGE	STRMIN	STRMAX	STRMED	ZMIN	ZMAX	ZMED	ZMEAN	UNDER	OVER
4040	93	Wollogorang Formation	P_to	52		PC	17902	0	20358	0	PP	ST			1707	1800	100	150	125	-4775	-9810	-7358	-7314	4050	4030
4050	108	Settlement Creek Volcanics	P_te	52		PC	17902	0	16775	0	PP	ST			1707	1800	0	100	100	-4875	-9910	-7458	-7414	4060	4040
4055	73	Peters Creek Volcanics	P_u	54	RF	PC	0	0	15114	0	PP	ST			1707	1800	1500	2000	1750	-1960	-5190	-4325	-3825	5100	4000
4060	88	Wununmantyala Sandstone	P_tn	52		PC	17902	0	27950	0	PP	ST			1707	1800	200	520	360	-4975	-10430	-7818	-7741	4070	4050
4061	88		P_tn	52	TR	PC	17902	0	27950	0	PP	ST			1707	1800	200	400	300	-4975	-10310	-7758	-7681	4070	4050
4062	88	Wununmantyala Sandstone	P_tn	52	SR	PC	17902	0	27950	0	PP	ST			1707	1800	0	200	200	-4975	-10110	-7658	-7581	4070	4050
4070	85	Aquarium Formation	P_tq	52		PC	17902	0	513	0	PP	ST			1707	1800	150	200	175	-5175	-10630	-7993	-7933	4082	4060
4080	94	Sly Creek Sandstone	P_tl	52		PC	17902	0	26142	0	PP	ST			1707	1800	530	930	730	-5325	-11560	-8723	-8536	4090	4070
4082	95	Rosie Creek Sandstone Mbr	P_tlr	52		PC	17902	0	26142	16356	PP	ST			1707	1800	130	160	145	-5855	-10790	-8138	-8261	4080	4070
4090	70	Seigal Volcanics	P_ts	52		PC	17902	0	16726	0	PP	ST			1707	1800	300	400	350	-6155	-11960	-9073	-9063	4110	4080
4095	43	dolerite	P_dl	52		PC	0	0	0	0	PP	ST			1707	1800	0	0	0	-6155	-11960	-9073	-9063	0	4080
4110	90	Yiyintyi Sandstone	P_ty	52		PC	17902	0	21009	0	PP	ST			1707	1800	3000	3000	3000	-8455	-14960	-12073	-11163	5000	4090
4120	90		P_tw	52		PC	0	0	0	0	PP	ST			1707	1800	20	1900	960	-6455	-16860	-13033	-12116	0	0
4150	116	Benmara beds	P_tb	56		PC	0	0	1488	0	PP	ST			1600	1800	0	0	518	-4375	-9478	-6901	-6918	0	0
4190	109	Fiery Creek Volcanics	P_fv	54	RF	C3	0	0	6639	0	PP	ST			1677	1679	100	250	175	-8510	-14790	-11700	-11667	4200	3800
4200	107	Bigie Formation	P_f	54	RF	C3	0	0	1621	0	PP	ST			1677	1679	60	600	330	-8610	-15390	-12030	-12010	4300	4190
4250	77	Carrara Range Group	P_c	54	RF	C3	3879	0	0	0	PP	ST			1646	1800	1420	2610	2015	-6510	-15150	-11540	-11067	0	0
4300	58	Qullalar Formation	P_q	54	RF	C2	0	0	15764	0	PP	ST			1677	1800	300	1500	900	-8670	-16890	-12930	-12830	0	4200
4700	74	Kamarga Volcanics	P_lv	54	KM	C2	0	0	9158	0	PP	ST			1677	1800	1400	0	1400	-8970	-18290	-14330	-13863	0	0
4800	112	Yeldham Granite	P_gy	54	KM	TD	0	0	20928	0	PP	OR			1800	1820	0	0	0	-10370	-18290	-13683	-13683	0	0
4900	119	Nicholson Granite Complex	P_gn	56		TD	30724	14123	0	0	PP	SO			1705	1860	0	0	0	-9375	-13960	-9375	-10227	5100	4000
5000	84	Scrutton Volcanics	P_ls	52		TD	0	0	16698	0	PP	OR			1844	1858	0	0	0	-9375	-17980	-16045	-14560	6000	4110
5100	105	Cliffdale Volcanics	P_c	56		TD	30724	0	4151	0	PP	SO			1750	1860	4000	0	4000	-3460	-17980	-16045	-12588	6000	4000
6000	62	Murphy Metamorphics	P_lm	56		OD	0	0	13528	0	PP	OR			1860	2000	0	0	0	-7460	0	-20045	-20045	0	5100

CODE	LITH_ID	CLASS	TYPE	COMP	GEN	ENV	LITH	PROP	QUAL	MIN	WEATH
1	1	W						0			
100	2	U	EPC		L	F	GVL	0			
100	3	U	EPC		L	F	SND	0			
100	4	U	EPC		L	F	SLT	0			
110	5	U	EPC		L	EU		0			
120	6	U	EPC		L	EE	CLY	0			
130	7	U	CHEM		L	EE	FRCT	0			
200	8	S	CHEM	CARB	M	S	LMST	0	MAS		
300	9	S	EPC		M	S	SLST	0	FER SDY		
300	10	S	EPC		M	S	MDST	0	FER FI		
300	11	S	EPC	HET	L	F	SDST	0	C P FP		
300	12	S	EPC	LTH	L	F	CNGL	0			
301	13	S	EPC	LTH	L	F	SDST	0	C P FP CLAY		
301	14	S	EPC	LTH	L	F	CNGL	0			
400	15	S	CHEM	CARB	M	S	LMST	0	GY VU OO FI		
400	16	S	CHEM	CARB	M	S	LMST	1	STRO		
450	17	S	EPC		M	U		0			
500	18	S	EPC	QF	C	UD	SDST	0	F C FRI BED XB		
501	19	S	EPC	QF	C	UD	SDST	0	F C FRI BED XB		
510	20	I	EXV	MAF	I	SA	BLT	0	THL		
511	21	I	EXV	MAF	I	SA	BLT	0	THL		
800	22	M	CX		L	EU		0			
900	23	I	ITV	MAF	I	SI	DLT	0			
1000	24	S	EPC	QZ	M		ARNT	80	QZ CYC		
1000	25	S	EPC	QZ	M		MDST	10	CYC		
1000	26	S	EPC	QZ	M		SLST	10	CYC		
1200	27	S	EPC	QZ	M		SDST	50	F FLAG MIC		
1200	28	S	EPC	QZ	M		SHLE	30			
1200	29	S	EPC	QZ	M		SLST	20			
1210	30	S	EPC	QZ	M	S	ARNT	50	F C		
1210	31	S	EPC	QZ	M	S	SLST	50			
1212	32	S	EPC	QZ	M	S	SLST	50	MIC		RC
1212	33	S	EPC	QZ	M	S	CLST	25			RC
1212	34	S	EPC	QZ	M	S	MDST	20			RC
1212	35	S	EPC	QZ	M	S	SDST	5	TN		RC
1213	36	S	CHEM		M	S	IRST	0	OO		
1213	37	S	EPC		M	S	SDST	0		SD	
1213	38	S	EPC		M	S	SDST	0	CLT		
1213	39	S	EPC		M	S	SHLE	0	PYR CAR		
1214	40	S	EPC	QZ	C	VS	ARNT	0	M TN TK XB MC		PK
1220	41	S	EPC		M	CSH	SHLE	50	RE PU ORG		RC
1220	42	S	EPC		M	CSH	MDST	30	SLY ORG		RC
1220	43	S	EPC		M	CSH	SLST	20	FER MIC ORG		RC
1400	44	S	EPC	QZ	M		ARNT	50			RS
1400	45	S	EPC	QZ	M		MDST	30			RC
1400	46	S	EPC	QZ	M		SLST	20			RC
1410	47	S	EPC	QF	C	SF	ARNT	0	C FER FRI XB RM		RS
1411	48	S	EPC	QF	C	SF	ARNT	0	C FER FRI XB RM		RS
1420	49	S	EPC	QZ	M	S	MDST	50	PLE PU GR RUC	GLT	RC
1420	50	S	EPC	QZ	M	S	SLST	30	MIC	GLT	RC
1420	51	S	EPC	QZ	M	S	SDST	20	F	GLT	RC
1421	52	S	EPC	QZ	M	S	MDST	50	PLE PU GR RUC	GLT	RC
1421	53	S	EPC	QZ	M	S	SLST	30	MIC	GLT	RC
1421	54	S	EPC	QZ	M	S	ARNT	20	F	GLT	RC
1430	55	S	EPC	QZ	C	VS	ARNT	95	M C		RS
1430	56	S	EPC	QZ	C	VS	SLST	5	FER MIC		RC
1432	57	S	EPC	QZ	C	VS	ARNT	0	M W LPX LTX	GLT	PK
1433	58	S	EPC	QZ	C	VS	ARNT	0	M W LPX LTX	GLT	PK
1434	59	S	EPC	QZ	C	SF	MDST	20	RE		RC
1434	60	S	EPC	QZ	C	SF	SDST	20	FER		RC
1434	61	S	EPC	QZ	C	SF	CNGL	20	QZ GNL		RC

CODE	LITH_ID	CLASS	TYPE	COMP	GEN	ENV	LITH	PROP	QUAL	MIN	WEATH
1434	62	S	EPC	QZ	C	SF	ARNT	20	M		RC
1434	63	S	EPC	QZ	C	SF	ARNT	20	VF MIC MC HX		RC
1436	64	S	EPC	QZ	C	VS	ARNT	0	M W LPX	GLT	PK
1437	65	S	EPC	QZ	C	VS	ARNT	0	M W LPX	GLT	PK
1440	66	S	EPC	QF	C	SF	SDST	50	FER F MIC LPX LTX HX SOM	GLT	RS
1440	67	S	EPC	QF	C	SF	SLST	40	F MIC RUC MC CV		RS
1440	68	S	EPC	QF	C	SF	MDST	5			RS
1440	69	S	EPC	FEL	C	SF	SDST	5		GLT	RS
1450	70	S	EPC		C	P	SLST	50	RE BN MIC		RC
1450	71	S	EPC		C	P	SDST	40	VF RE BN MIC		RC
1450	72	S	EPC		C	P	SLST	2	DMT		RC
1450	73	S	EPC		C	P	MDST	2	PLE PU		RC
1450	74	S	EPC		M	S	SLST	2	LMN MIC MDY GR PU		RC
1450	75	S	EPC		M	S	SDST	2	F	GLT	RC
1450	76	S	EPC		M	S	SLST	2		GLT	RC
1451	77	S	EPC		C	P	SLST	50	RE BN MIC		RC
1451	78	S	EPC		C	P	SDST	30	VF RE BN MIC		RC
1451	79	S	EPC		C	P	SLST	2	DMT		RC
1451	80	S	EPC		C	P	MDST	2	PLE PU		RC
1451	81	S	EPC		M	S	SLST	2	LMN MIC MDY GR PU		RC
1451	82	S	EPC		M	S	SDST	2	F	GLT	RC
1451	83	S	EPC		M	S	SLST	2		GLT	RC
1451	84	S	EPC	FEL	C	S	SDST	10	F M		RC
1460	85	S	EPC	QZ	L	F	SDST	70	F PI LPX LTX FS LC SOM		RS
1460	86	S	EPC		L	F	SLST	10	GY MIC		RS
1460	87	S	EPC	QZ	L	F	SDST	10	VF		RS
1460	88	S	EPC	QZ	L	F	SDST	10	FER P PBY		RS
1461	89	S	EPC	QZ	L	F	SDST	60	F PI LPX LTX FS LC SOM		RS
1461	90	S	EPC		L	F	SLST	10	GY MIC		RS
1461	91	S	EPC	QZ	L	F	SDST	10	VF		RS
1461	92	S	EPC	QZ	L	F	SDST	20	FER P PBY		RS
1465	93	S	EPC		C	F S	BX	20	CGC		RC
1465	94	S	EPC		C	F S	MDST	40	RE BN MIC LA ORG		RC
1465	95	S	EPC		C	F S	SLST	20	RE BN MIC LA		RC
1465	96	S	EPC		C	F S	SDST	20		GLT	RC
1600	97	S	EPC	QZ	C		SDST	40			
1600	98	S	EPC	QZ	C		CNGL	20			
1600	99	S	EPC	QZ	M	S	SLST	20			
1600	100	S	EPC	QZ	M	S	SHLE	15			
1600	101	S	EPC	QZ	M	S	IRST	5			
2000	102	S	CHEM	CARB	C	P	DLST	80	SDY SLY CHY STRO		
2100	103	S	EPC	QZ	C	P	ARNT	40	PBY CHY XB RM		RC
2100	104	S	CHEM	CARB	C	P	DLST	40	CHY XB RM	GP HL	RC
2100	105	S	CHEM	CARB	C	P	DLST	20	STRO		RC
2110	106	S	CHEM	CARB	C	P	DLST	40	LA SDY STRO SSD OO RM		
2110	107	S	EPC		C	P	DLST	25	F STRO SSD OO RM		
2110	108	S	EPC		C	P	SDST	20	F TN CGC		
2110	109	S	EPC		C	P	SLST	15	TN		
2120	110	S	CHEM	CARB	C	PA	DLST	20	F		RC
2120	111	S	CHEM	CARB	C	PA	DLST	20	F STRO		RC
2120	112	S	CHEM	CARB	C	PA	DLST	10	RXL		RC
2120	113	S	EPC		C	PA	SLST	15	DMT		RC
2120	114	S	EPC		C	PA	SHLE	15	DMT		RC
2120	115	S	CHEM	CARB	C	PA	DLST	10	SLY EVAP PS STRO CHY		RC
2120	116	S	CHEM	CARB	C	PA	DLST	5	SLF OO		RC
2120	117	I	VCC	ITM	I	PA	TUF	1	PI		RC
2120	118	S	EPC		L	PA	SDST	1	TN		RC
2130	119	S	EPC	PLY	L	F	CNGL	40	MAS C		RS
2130	120	S	EPC	LTH	L	F	SDST	30	PBY CHY P XB		RS
2130	121	S	EPC	HET	L	FB	SDST	25			RS
2130	122	S	CHEM	CARB	L	L	DLST	5	SDY		RS

CODE	LITH_ID	CLASS	TYPE	COMP	GEN	ENV	LITH	PROP	QUAL	MIN	WEATH
3000	123	S	CHEM	CARB	C		DLST	50	SLY		
3000	124	S	EPC		M	S	SLST	40	DMT		
3000	125	S	EPC		C		ARNT	10			
3100	126	S	EPC		M		SHLE	25			
3100	127	S	EPC		M		SHLE	25	CAR		
3100	128	S	EPC		M		SLST	10			
3100	129	S	EPC		M		SLST	15	CAR		
3100	130	S	EPC		M		SDST	20			
3200	131	S	CHEM	CARB	C		DLST	30	SLY STRO		
3200	132	S	CHEM		C		CHRT	20	STRO		
3200	133	S	EPC		M	S	SLST	25	DMT		
3200	134	S	EPC		M	S	SLST	15	DMT CAR		
3200	135	S	EPC		C		SDST	10	F		
3200	136	I	VCC		I		TUF	0			
3300	137	S	CHEM	CARB	C		DLST	50	SLY SDY STRO		
3300	138	S	EPC		C		SLST	30	DMT		
3300	139	S	EPC		C		SDST	20	DMT		
3300	140	S	EPC		C		SLST	1	DMT CAR PYR		
3310	141	S	CHEM	CARB	C	P	DLST	40	MAS PBX ST RX PIS		KS
3310	142	S	EPC		L	L	SLST	30	RE		KS
3310	143	S	EPC		L	L	SDST	20	F		KS
3310	144	S	CHEM	CARB	C	P	DLST	10	SDY		KS
3315	145	S	CHEM	CARB	M	S	DLST	70	SLF STRO		RC
3315	146	S	CHEM	CARB	M	S	DLST	15			RC
3315	147	S	CHEM	CARB	M	S	DLST	15	SDY		RC
3320	148	S	EPC	QZ	M	S	ARNT	0	F M TN SLF WB RM SOM CV	GLT	RS
3330	149	S	CHEM	CARB	L	PA	DLST	40	F TN STRO SLF MC PS	GP	RS
3330	150	S	CHEM	CARB	L	PA	DLST	30	F SLY SLF STRO MC PS	GP	RS
3330	151	S	CHEM	CARB	L	PA	DLST	25	SLF STRO MC PS	GP	RS
3330	152	S	EPC	LTH	L	PA	SDST	5	F CHY LA SLF MC		RS
3340	153	S	EPC		C	P	SLST	30	DMT		
3340	154	S	CHEM	CARB	C	P	DLST	30			
3340	155	S	CHEM	CARB	C	P	DLST	30	STRO CHY		
3340	156	S	EPC		C	P	SDST	10	DMT		
3342	157	S	EPC		C	SB	SLST	40	DMT CHY TN RM XB		RC
3342	158	S	EPC		C	SB	SDST	30	F C DMT CHY TN RM XB		RC
3342	159	S	CHEM	CARB	C	SB	DLST	30	CHY		RC
3344	160	S	EPC		C	IS	SLST	25	TN DMT EVAP PS CHY MC	HL	RS
3344	161	S	CHEM	CARB	C	IS	DLST	20	F TN SLY EVAP PS CHY MC	HL	RS
3344	162	S	EPC	QZ	C	IS	SDST	10	F RM XB	HL	RS
3344	163	S	CHEM	CARB	C	IS	DLST	15	CHY STRO MC EVAP PS	HL	RS
3344	164	S	CHEM	CARB	C	IS	DLST	10	MC EVAP PS	HL	RS
3344	165	S	CHEM	CARB	C	IS	DLST	10	SDY MC EVAP PS	HL	RS
3344	166	S	EPC		C	IS	SDST	10	DMT RM XB	HL	RS
3346	167	S	EPC		C	LA IS	SLST	10	TN DMT		RC
3346	168	S	EPC		C	LA IS	SHLE	10	TN DMT		RC
3346	169	S	EPC		C	LA IS	SLST	30	TN DMT CAR PYR		RC
3346	170	S	EPC		C	LA IS	SHLE	15	TN DMT CAR PYR		RC
3346	171	S	CHEM	CARB	C	LA IS	DLST	15	F SLY		RC
3346	172	S	CHEM	CARB	C	LA IS	DLST	5	F EVAP PS		RC
3346	173	S	CHEM	CARB	C	LA IS	DLST	10			RC
3346	174	S	EPC	CARB	C	LA IS	BX	5	LEN		RC
3500	175	S	CHEM	CARB	C		DLST	30	SLY STRO		
3500	176	S	EPC		C		SLST	25	DMT		
3500	177	S	EPC		C		SHLE	20	DMT		
3500	178	S	CHEM	CARB	C		CHRT	15	STRO		
3500	179	S	EPC		C		SDST	10			
3510	180	S	EPC		C	IS	SDST	40			
3510	181	S	EPC		C	IS	SLST	30			
3510	182	S	EPC		C	IS	SHLE	15			
3510	183	S	EPC		C	IS	CNGL	5			

CODE	LITH_ID	CLASS	TYPE	COMP	GEN	ENV	LITH	PROP	QUAL	MIN	WEATH
3600	184	S	CHEM	CARB	C		DLST	40	F SLY CYC		
3600	185	S	EPC		C		SLST	30	DMT CYC EVAP		
3600	186	S	EPC		C		SDST	25			
3600	187	S	EPC		C		SHLE	5	PYR		
3610	188	S	CHEM	CARB	L	L	DLST	30	F CHY EVAP PS	PY	RS
3610	189	S	CHEM	CARB	L	L	DLST	20	F STRO CHY EVAP PS	PY	RS
3610	190	S	CHEM	CARB	L	L	DLST	20	F SLY CHY EVAP PS	PY	RC
3610	191	S	CHEM	CARB	L	L	DLST	15		PY	RS
3610	192	S	CHEM	CARB	L	L	DLST	5	SDY TN LEN RM XB SSD EVAP PS	PY	RS
3610	193	S	CHEM	CARB	L	L	DLST	5	C TN LEN RM XB SSD EVAP PS	PY	RS
3610	194	S	EPC		L	L	SDST	5	DMT TN LEN RM XB SSD EVAP PS	PY	RS
3620	195	S	EPC		C	LA	SHLE	35	DMT CAR PYR TN LA	GP	RC
3620	196	S	EPC		C	LA	SLST	30	DMT CAR PYR TN LA	GP	RC
3620	197	S	CHEM	CARB	C	LA	DLST	30	F	GP	RC
3620	198	S	EPC	PLY	C	FD	BX	1	DMT		RC
3620	199	S	EPC		C	LA	SDST	1			RC
3620	200	I	VCC	FLS	I		TUF	1			RC
3630	201	S	CHEM	CARB	C	LA	DLST	30	F TN LA		RC
3630	202	S	CHEM	CARB	C	LA	DLST	30	F SLF TN LA		RC
3630	203	S	EPC		C	LA	SHLE	15	DMT		RC
3630	204	S	EPC		C	LA	SDST	10	DMT		RC
3630	205	S	EPC	PLY	C	LA	BX	5	RUC		RC
3630	206	S	EPC	PLY	C	LA	CNGL	5			RC
3630	207	S	CHEM	CARB	C	LA	DLST	5			RC
3632	208	S	CHEM	CARB	C	LA	DLST	90	F GY XL TFC EVAP PS	GP	RC
3632	209	S	CHEM	CARB	C	LA	DLST	1	F GY XL STRO TFC EVAP PS	GP	RC
3632	210	S	EPC		C	LA	SHLE	5	DMT		RC
3632	211	S	EPC		C	LA	SLST	5	DMT		RC
3640	212	S	CHEM	CARB	C	LA	DLST	90	STRO BR		KS
3640	213	S	EPC		C	LA	SLST	5			RC
3640	214	S	EPC		C	LA	SDST	5			RS
3640	215	S	EPC		C	LA	MDST	1	TFC		RC
3642	216	S	CHEM	CARB	C	LA	DLST	0	F MAS DK GY		KS
3644	217	S	CHEM	CARB	C	LA	DLST	30	F EVAP PS	HL	RS
3644	218	S	CHEM	CARB	C	LA	DLST	25	F STRO EVAP PS	HL	RS
3644	219	S	EPC		C	LA	SLST	20	DMT EVAP PS	HL	RS
3644	220	S	CHEM	CARB	C	LA	DLST	15	EVAP PS SLF	HL	RS
3644	221	S	EPC	LTH	C	LA	BX	10	DMT		RS
3650	222	S	EPC		L	FL	SLST	30	DMT TN LA PS RE	HL	RC
3650	223	S	EPC		L	FL	SHLE	25	DMT TN LA PS RE	HL	RC
3650	224	S	EPC		L	FL	SDST	20	F DMT TN PS	HL	RC
3650	225	S	CHEM	CARB	L	FL	DLST	15	F		RC
3650	226	S	CHEM	CARB	L	FL	DLST	10	F STRO		RC
3660	227	S	EPC		M	S	SDST	90	DMT F C P XB RM GY	GLT	RC RS
3660	228	S	CHEM	CARB	M	S	DLST	10	SDY TN STRO		RC RS
3670	229	S	CHEM	CARB	C	IS	DLST	25	F MC PS BU PI	GP HL	RC
3670	230	S	CHEM	CARB	C	IS	DLST	20	F STRO MC PS BU PI	GP HL	RC
3670	231	S	EPC		C	IS	SHLE	15	DMT MC PS	GP HL	RC
3670	232	S	EPC		C	IS	SLST	15	DMT MC PS	GP HL	RC
3670	233	S	CHEM	CARB	C	IS	DLST	10	OO RM XB MC PS BU PI	GP HL	RC
3670	234	S	EPC	QZ	C	IS	SDST	10	RM XB MC PS	GP HL	RC
3670	235	S	CHEM	CARB	C	IS	DLST	5	CHY BR OO STRO BU PI	GP HL	RC
3680	236	S	EPC	LTH	C	P SF	SDST	50	M TN ME RM RUC EVAP PS		RS
3680	237	S	EPC	QZ	C	P SF	SDST	25	F TN WH XB SOM RM HX		RS
3680	238	S	EPC		C	P SF	SHLE	5	TN		RS
3680	239	S	EPC		C	P SF	SHLE	2	DMT TN GY GR RE		RS
3680	240	S	EPC		C	P SF	SLST	5	TN SOM		RS
3680	241	S	EPC		C	P SF	SLST	5	DMT TN SOM		RS
3680	242	S	EPC		C	P SF	SDST	2	VF XB SOM RM HX	GLT	RS
3680	243	S	CHEM	CARB	C	P SF	DLST	2	F		RC
3680	244	S	CHEM	CARB	C	P SF	DLST	2	F STRO		RC

CODE	LITH_ID	CLASS	TYPE	COMP	GEN	ENV	LITH	PROP	QUAL	MIN	WEATH
3680	245	S	CHEM	CARB	C	P SF	DLST	2			RC
3681	246	S	EPC	QZ	C	P SF	SDST	50	F TN WH XB SOM RM HX		RS
3681	247	S	EPC		C	P SF	SHLE	10	TN		RS
3681	248	S	EPC		C	P SF	SHLE	4	DMT TN GY GR RE LA		RS
3681	249	S	EPC		C	P SF	SLST	10	TN SOM		RS
3681	250	S	EPC		C	P SF	SLST	10	DMT TN SOM		RS
3681	251	S	EPC		C	P SF	SDST	4	VF XB SOM RM HX	GLT	RS
3681	252	S	CHEM	CARB	C	P SF	DLST	4	F		RC
3681	253	S	CHEM	CARB	C	P SF	DLST	4	F STRO		RC
3681	254	S	CHEM	CARB	C	P SF	DLST	4			RC
3690	255	S	CHEM	CARB	C	SB	DLST	60	F STRO		RC
3690	256	S	CHEM	CARB	C	SB	DLST	20	F SLY OO BR CGC		RC
3690	257	S	CHEM	CARB	C	SB	DLST	10	OO BR CGC		RC
3690	258	S	CHEM	CARB	C	SB	DLST	5	F EVAP PS	SD	RC
3690	259	S	EPC		C	SB	SHLE	2			RC
3690	260	S	EPC		C	SB	SDST	1	F		RC
3691	261	S	CHEM	CARB	C	SB	DLST	60	F STRO		RC
3691	262	S	CHEM	CARB	C	SB	DLST	20	F SLY OO BR CGC		RC
3691	263	S	CHEM	CARB	C	SB	DLST	10	OO BR CGC		RC
3691	264	S	CHEM	CARB	C	SB	DLST	5	F EVAP PS	SD	RC
3691	265	S	EPC		C	SB	SHLE	2			RC
3691	266	S	EPC		C	SB	SDST	1	F		RC
3710	267	S	EPC		C	SB	SHLE	35	RE PU DMT CHY MC PS	GP HL	RC
3710	268	S	EPC		C	SB	SLST	30	RE PU DMT CHY MC PS	GP HL	RC
3710	269	S	EPC		C	SB	SDST	15	CHY XB RM	GP HL	RS
3710	270	S	CHEM	CARB	C	SB	DLST	20	STRO PS	GP HL	RC
3711	271	S	EPC		C	SB	SHLE	25	RE PU DMT MC PS	GP HL	RC
3711	272	S	EPC		C	SB	SLST	25	RE PU DMT MC PS	GP HL	RC
3711	273	S	EPC		C	SB	SDST	10	F SLY XB RM	GP HL	RS
3711	274	S	CHEM	CARB	C	SB	DLST	25	F STRO EVAP PS	GP HL	RC
3711	275	S	EPC		C	SB	SDST	15	DMT CHY XB RM	GP HL	RS
3712	276	S	EPC		C	SB	SHLE	25	RE PU DMT MC PS	GP HL	RC
3712	277	S	EPC		C	SB	SLST	30	RE PU DMT MC PS	GP HL	RC
3712	278	S	EPC		C	SB	SDST	15	DMT XB RM		RS
3712	279	S	CHEM	CARB	C	SB	DLST	20	STRO PS	GP HL	RC
3712	280	S	EPC		C	SB	SHLE	10	GY ORG DMT		RC
3713	281	S	EPC		C	SB	SHLE	20	RE PU DMT MC PS	GP HL	RC
3713	282	S	EPC		C	SB	SLST	50	RE PU DMT MC PS	GP HL	RC
3713	283	S	EPC		C	SB	SDST	15	XB RM	GP HL	RS
3713	284	S	CHEM	CARB	C	SB	DLST	14	STRO PS	GP HL	RC
3713	285	S	CHEM	CARB	C	SB	DLST	1	MAS	GP SD	RC
3714	286	S	EPC		C	SB	SHLE	45	RE PU DMT CHY MC PS	GP HL	RC
3714	287	S	EPC		C	SB	SLST	25	RE PU DMT CHY MC PS	GP HL	RC
3714	288	S	EPC		C	SB	SDST	5	XB RM	GP HL	RS
3714	289	S	CHEM	CARB	C	SB	DLST	20	STRO PS	GP HL	RC
3714	290	S	CHEM	CARB	C	SB	DLST	5	F PS	GP HL	RC
3715	291	S	EPC		C	SB	SHLE	25	RE PU DMT CHY MC PS	GP HL	RC
3715	292	S	EPC		C	SB	SLST	20	RE PU DMT CHY MC PS	GP HL	RC
3715	293	S	EPC		C	SB	SDST	30	CHY XB RM	GP HL	RS
3715	294	S	CHEM	CARB	C	SB	DLST	25	STRO CHY PS	GP HL	RC
3720	295	S	EPC	QZ	L	F	ARNT	40	PI BN BU F M LPX LTX RM		RS
3720	296	S	EPC		M	IS	SDST	5	VF		RC
3720	297	S	EPC		M	IS	SLST	5			RC
3720	298	S	EPC		M	IS	SDST	25	M C FER PS	HL GP	RS
3720	299	S	EPC	LTH	L	F	SDST	15	C VC P FER		RS
3720	300	S	EPC	LTH	L	F	CNGL	10	SDY		RS
3721	301	S	EPC	QZ	L	F	ARNT	50	PI BN BU F M LPX LTX RM		RS
3721	302	S	EPC		M	IS	SDST	5	VF		RC
3721	303	S	EPC		M	IS	SLST	5			RC
3721	304	S	EPC		M	IS	SDST	35	M C FER PS	HL GP	RS
3721	305	S	EPC	LTH	L	F	SDST	2	C VC P FER		RS

CODE	LITH_ID	CLASS	TYPE	COMP	GEN	ENV	LITH	PROP	QUAL	MIN	WEATH
3721	306	S	EPC	LTH	L	F	CNGL	1	SDY		RS
3722	307	S	EPC	QZ	L	F	ARNT	55	PI BN BU F M LPX LTX RM		RS
3722	308	S	EPC		M	IS	SDST	5	VF		RC
3722	309	S	EPC		M	IS	SLST	5			RC
3722	310	S	EPC		M	IS	SDST	35	M C FER PS	HL GP	RS
3723	311	S	EPC	QZ	L	F	ARNT	40	PI BN BU F M LPX LTX RM		RS
3723	312	S	EPC		M	IS	SDST	5	VF		RC
3723	313	S	EPC		M	IS	SLST	5			RC
3723	314	S	EPC		M	IS	SDST	25	M C FER PS	HL GP	RS
3723	315	S	EPC	LTH	L	F	SDST	15	C VC P FER		RS
3723	316	S	EPC	LTH	L	F	CNGL	10	SDY		RS
3724	317	S	EPC	QZ	L	F	ARNT	10	PI BN BU F M LPX LTX RM		RS
3724	318	S	EPC		M	IS	SDST	5	VF		RC
3724	319	S	EPC		M	IS	SLST	5			RC
3724	320	S	EPC		M	IS	SDST	5	M C FER PS	HL GP	RS
3724	321	S	EPC	LTH	L	F	SDST	40	C VC P FER		RS
3724	322	S	EPC	HET	L	F	CNGL	35	SDY		RS
3725	323	S	EPC	QZ	L	F	ARNT	50	PI BN BU F M LPX LTX RM		RS
3725	324	S	EPC		M	IS	SDST	5	VF		RC
3725	325	S	EPC		M	IS	SLST	5			RC
3725	326	S	EPC		M	IS	SDST	35	M C FER PS	HL GP	RS
3725	327	S	EPC	LTH	L	F	SDST	1	C VC P FER		RS
3725	328	S	EPC	LTH	L	F	CNGL	1	SDY		RS
3726	329	S	EPC	QZ	L	F	ARNT	30	PI BN BU F M LPX LTX RM		RS
3726	330	S	EPC		M	IS	SDST	5	VF		RC
3726	331	S	EPC		M	IS	SLST	5			RC
3726	332	S	EPC		M	IS	SDST	15	M C FER PS	HL GP	RS
3726	333	S	EPC	LTH	L	F	SDST	25	C VC P FER		RS
3726	334	S	EPC	LTH	L	F	CNGL	20	SDY		RS
3800	335	S	EPC		C	FB	SDST	30			RS
3800	336	S	EPC		M	S	SLST	30			RS
3800	337	S	EPC		M	S	SHLE	30			RC
3800	338	S	EPC	HET	L	FB AF	CNGL	5			RS
3800	339	S	CHEM	CARB	M	S	DLST	5			RS
4000	340	S	EPC		L C M		SDST	50			RS
4000	341	S	EPC		L		CNGL	10			RS
4000	342	I	EXV	MAF	I	SA	BLT	10			RC
4000	343	I	EXV	FLS	I	SA	RHY	5			
4000	344	I	ITV	FLS	I	SI	RHY	5			
4000	345	S	EPC		M		SLST	10			RC
4000	346	S	CHEM	CARB	L C M		DLST	10			RC
4010	347	I	EXV	FLS	I	SA	RHY	0	POR		RC
4020	348	S	EPC	FEL	L	F	SDST	40	M C XB RM		RS
4020	349	S	EPC	LTH	L	F	SDST	40	M C XB RM		RS
4020	350	S	EPC	HET	L	F	SDST	15	CGC		RS
4020	351	S	EPC		L	F	SHLE	5			RS
4025	352	I	ITV	FLS	I	PLH	GRT	0	F POR	HEM	RS
4030	353	I	EXV	MAF	I	SA	BLT	50	AMY VE		RC
4030	354	I	ITV	MAF	I	SI DY	DLT	5			RC
4030	355	S	EPC	FEL	L	L	SDST	15	VF M P XB MIC		RC
4030	356	I	ITV	MAF	I	L	BX	10	BLTC SDY MDY		RC
4040	357	S	CHEM	CARB	L	FL	DLST	20	F TN SUL BTM	PY	RC
4040	358	S	CHEM	CARB	L	FL	DLST	5	F STRO SUL BTM	PY	RC
4040	359	S	EPC	CARB	L	FL	BX	1	C DMT		RC
4040	360	S	EPC		L	FL	SHLE	15	EVAP PS		RC
4040	361	S	EPC		L	L	SHLE	15	ORG SUL DMT	PY	RC
4040	362	S	EPC		M	S	SDST	15	FER DMT XB		RC
4040	363	S	EPC	QZ	M	S	ARNT	20	WH		RC
4040	364	S	EPC		M	S	CNGL	5	PB		RC
4040	365	S	CHEM	CARB	C	LA	DLST	5	XL		RC
4050	366	I	EXV	MAF	I	SA	BLT	30	RE BN GY F M		RC

CODE	LITH_ID	CLASS	TYPE	COMP	GEN	ENV	LITH	PROP	QUAL	MIN	WEATH
4050	367	I	EXV	FLS	I	SA	RHY	10	BA	AB	RC
4050	368	S	EPC		L	L	SHLE	15	HFL		RC
4050	369	S	CHEM	CARB	L	L	DLST	10	F SLY HFL		RC
4050	370	S	EPC		L	L	SDST	5	FER		RC
4050	371	S	EPC	CARB	L	L	BX	5	DMT		RC
4050	372	I	ITV	MAF	I	SI	DLT	25	HK MTS		RC
4055	373	I	EXV	MAF	I	SA	BLT	30	POT		
4055	374	I	EXV	FLS	I	SA	RHY	25	POT		
4055	375	I	EXV	ITM	I	SA	TRC	15	POT		
4055	376	S	EPC		L	F	SDST	5			
4055	377	S	EPC		L	F	SLST	5			
4055	378	I	VCC		I		TUF	5			
4055	379	S	CHEM	CARB	C	LA	DLST	5			
4055	380	S	EPC		L	F	CNGL	5			
4055	381	S	EPC		L	FL	MDST	5			
4060	382	S	EPC	QF	C	SF P	SDST	60	M RE GY FER W TN ME LA LPX RM		RS
4060	383	S	EPC		C	SF P	SHLE	30	FER RE TN		RC
4060	384	S	EPC	LTH	C	SF P	CNGL	2	SDY		RS
4060	385	S	EPC	QZ	C	SF P	SDST	5	C P PBY		RS
4061	386	S	EPC	QF	C	SF P	SDST	60	M RE GY FER W TN ME LA LPX RM		RS
4061	387	S	EPC		C	SF P	SHLE	30	FER RE TN		RC
4061	388	S	EPC	LTH	C	SF P	CNGL	1	SDY		RS
4061	389	S	EPC	QZ	C	SF P	SDST	7	C P PBY		RS
4062	390	S	EPC	QF	C	SF P	SDST	60	M RE GY FER W TN ME LA LPX RM		RS
4062	391	S	EPC		C	SF P	SHLE	30	FER RE TN		RC
4062	392	S	EPC	QZ	C	SF P	ARNT	3	C P		RS
4062	393	S	EPC	QZ	C	SF P	SDST	5	C P PBY		RS
4070	394	S	CHEM	CARB	M	CSH	DLST	10	RE PU GY		RC
4070	395	S	CHEM	CARB	M	CSH	DLST	10	RE PU GY RX		RC
4070	396	S	CHEM	CARB	M	CSH	DLST	10	F TN		RC
4070	397	S	CHEM	CARB	M	CSH	DLST	10	F SLY		RC
4070	398	S	CHEM	CARB	M	CSH	DLST	10	F M		RC
4070	399	S	CHEM	CARB	M	CSH	DLST	10	F M WB XB		RC
4070	400	S	EPC		M	CSH	SHLE	20	TN ME RE GR MIC		RC
4070	401	S	EPC	QZ	M	CSH	SDST	10	F TN ME RM XB HX RUC		RC
4070	402	S	EPC	QZ	M	CSH	SDST	5	F TN ME RM XB HX RUC	GLT	RC
4070	403	S	EPC	QZ	M	CSH	SDST	5	F TN ME RM XB HX RUC MIC		RC
4080	404	S	EPC	QZ	C	SF IS	ARNT	10	F M ME PBY		RS
4080	405	S	EPC	QZ	C	SF IS	ARNT	70	F M ME LPX LTX RM		RS
4080	406	S	EPC	QZ	C	SF IS	ARNT	5	F M ME LPX LTX RM GR		RS
4080	407	S	EPC	QZ	C	SF IS	ARNT	1	F M ME MC		RS
4080	408	S	EPC		C	SF IS	SLST	5	TN MIC		RS
4080	409	S	EPC		C	SF IS	SHLE	5	TN MIC		RS
4082	410	S	EPC		M	S	SDST	20	VF VC CGC SOM RM LPX LTX		RS
4082	411	S	EPC	FEL	M	S	SDST	20	VF VC CGC SOM RM LPX LTX		RS
4082	412	S	EPC	QF	M	S	ARKS	20	VF VC CGC FER SOM RM LPX LTX		RS
4082	413	S	EPC		M	S	SDST	20	VF VC CGC SOM RM LPX LTX	GLT	RS
4082	414	S	EPC		M	S	SLST	10	FER LA		RS
4082	415	S	EPC		M	S	SHLE	10	FER LA		RS
4090	416	I	EXV	MAF	I	SA	BLT	0	AMY		RC
4095	417	I	ITV	MAF	I	SI	DLT	0			RC
4110	418	S	EPC	QZ	L M	F S	SDST	40	ME M P LPX LTX RM		RS
4110	419	S	EPC	FEL	L M	F S	SDST	20	ME M P LPX LTX RM		RS
4110	420	S	EPC	QZ	L M	F S	SDST	30	ME C P PBY		RS
4110	421	S	EPC	FEL	L M	F S	SDST	10	ME C P PBY		RS
4120	422	S	EPC		L	FB	SDST	40	CGC TK VTK LTX		RS
4120	423	S	EPC	QZ	L	FB	SDST	30	TK VTK LTX		RS
4120	424	S	EPC		L	FB AF	CNGL	30	TK VTK LTX		RS
4150	425	S	EPC	FEL			SDST	0			
4150	426	S	EPC	QZ			SDST	0			
4150	427	I	EXV	FLS	I		TRC	0			

CODE	LITH_ID	CLASS	TYPE	COMP	GEN	ENV	LITH	PROP	QUAL	MIN	WEATH
4150	428	I	EXV	FLS	I		RHY	0			
4150	429	S	EPC				SLST	0			
4150	430	S	EPC				ARKS	0			
4150	431	S	EPC				CNGL	0	PBY		
4150	432	I	VCC		I		IGM	0			
4150	433	S	EPC				AGL	0			
4190	434	I	EXV	FLS	I	SA	RHY	50	POT FER	HEM	RC
4190	435	I	EXV	MAF	I	SA	TYB	25	POT FER	HEM	RC
4190	436	S	EPC		L	F	SDST	15	FER	HEM	RS
4190	437	S	EPC		L	F	CNGL	10	FER	HEM	RS
4200	438	S	EPC	LTH	L	F	SDST	25	FER	HEM	RS
4200	439	S	EPC	FEL	L	F	SDST	25	FER	HEM	RS
4200	440	S	EPC		L	F	SDST	20	PBY FER	HEM	RS
4200	441	S	EPC		L	F	CNGL	10	FER	HEM	RS
4200	442	S	EPC		L	F	SLST	5	FER	HEM	RS
4200	443	S	EPC		L	F	SHLE	5	FER	HEM	RS
4200	444	S	CHEM	CARB	L	F	DLST	5	SLY FER	HEM	RS
4200	445	S	CHEM	CARB	L	F	LMST	5	FER	HEM	RS
4250	446	I	EXV	MAF	I	SA	BLT	0	POT		
4250	447	I	EXV	ITM	I	SA	TRC	0	POT		
4250	448	I	EXV	FLS	I	SA	RHY	0	POR POT		
4250	449	S	EPC	QZ	L	F	SDST	0			
4250	450	S	EPC	LTH	L	F	CNGL	5	PB BO CB		
4300	451	S	EPC		C		SLST	10	DMT		
4300	452	S	EPC		C		SDST	10	DMT		
4300	453	S	CHEM	CARB	C		DLST	10	STRO		
4300	454	S	EPC		C		SHLE	10			
4300	455	S	EPC	FEL	C		SDST	15			
4300	456	S	EPC		C		SLST	5	CALC		
4300	457	I	EXV	FLS	I		TUF	1			
4300	458	S	EPC		C		SDST	5	MIC		
4300	459	S	EPC		C		SLST	5	MIC		
4300	460	S	EPC	CARB	C		BX	5	DMT		
4300	461	S	EPC	QZ	C		SDST	10			
4300	462	S	EPC		C		SDST	5	MDY		
4300	463	S	EPC		C		SLST	4			
4300	464	S	EPC		C		CNGL	2			
4300	465	I	EXV	MAF	I	SA	BLT	1			
4700	466	I	EXV	MAF	I	SA	BLT	65	AMY MAS		
4700	467	S	EPC	FEL	L M	F S	SDST	15	FER		
4700	468	S	EPC		L M	F S	ARKS	10	FER		
4700	469	S	EPC		L M	F S	SDST	10	CGC FER		
4800	470	I	ITV	FLS	I	PL	GRT	85	PI GY EQ M	MS	
4800	471	I	ITV	FLS	I	PL	GRT	5		HBL	
4800	472	I	ITV	FLS	I	PL	PEG	5			
4800	473	I	ITV	FLS	I	PL	GRT	5	GRSN		
4900	474	I	ITV	FLS	I	PL	GRT	40	POR XE	BT	
4900	475	I	ITV	FLS	I	PL	GRT	35	POR XE	HBL BT	
4900	476	I	ITV	FLS	I	PL	GRT	5	LCC		
4900	477	I	ITV	FLS	I	PL	GRT	5	GRSN		
4900	478	I	ITV	FLS	I	PL	GRT	5	MX		
4900	479	I	ITV	FLS	I	PL	GRT	5		MS	
4900	480	I	ITV	FLS	I	PL	GRD	5		HBL	
5000	481	I	EXV	FLS	I	SA	DAC	35	PYC		RC
5000	482	I	EXV	FLS	I	SA	IGM	30	RHD PYC		RC
5000	483	I	EXV	FLS	I	SA	TUF	20	PYC		RC
5000	484	I	ITV	MAF	I	DY SI	DLT	1			RC
5000	485	I	EXV	MAF	I	SA	BLT	1			RC
5000	486	S	VCC	FEL	L M	F S	SDST	10	TFC F M P TN XL RM		RS
5100	487	I	EXV	FLS	I	SA	IGM	30	RHD PYC		
5100	488	I	EXV	FLS	I	SA	RHY	30			

Appendix 7, lith_dat

CODE	LITH_ID	CLASS	TYPE	COMP	GEN	ENV	LITH	PROP	QUAL	MIN	WEATH
5100	489	I	EXV	FLS	I	SA	DAC	30			
5100	490	I	EXV	FLS	I	SA	TUF	5	PYC		
5100	491	S	VCC	FEL	L	F	CNGL	5			
6000	492	M	REG	QF			SCHT	25	MIC		
6000	493	M	REG	QF			GNS	25	MIC		
6000	494	M	REG				PHYL	20			
6000	495	M	REG	QZ			QZT	10			
6000	496	M	REG				SLST	10	MET		
6000	497	M	REG				IRST	5	CHY		
6000	498	M	REG				SCHT	5	PYR CAR		
350	499	I	ITV	MAF	I	PLH	KBL	0			
350	500	I	ITV	MAF	I	PLH	PER	0			
4030	501	I	EXV	ITM	I	SA	TRC	15			RS
4030	502	I	EXV	FLS	I	SA	RHY	5			RC
3100	503	S	EPC		M		SLST	5	TFC		

MINOCC_ID	NAME	MAJCOM	MINCOM	OPS	SHAPE	HOST	HOSTLITH	SUBHOSTLITH	WALLROCK	SUBWALLROCK	OREMIN	SUBOREMIN	SECMIN	SUBSECMIN	GRAINSIZE	STYLE	DIST1STFLT	DISTFAULTS	DISTFOLDS	DISTREFAULT	EASTING	NORTHING
1	Mariner North	Pb		O	SB	3670	235	230	0	0	GN		CER		F	BR	2042	172	6453	428	559900	8227100
2		Fe		O	IR	3715	292	0	0	0	HEM						2208	353	6304	572	568300	8229300
3		Fe		O	IR	3715	292	0	0	0	HEM						2550	1252	2118	1626	572500	8229500
4		Fe		O	IR	3715	292	0	0	0	HEM						1044	341	626	276	574300	8228500
5	Tawallah Pocket	Cu		P	VN	3690	257	259	0	0	CCP		MAL		F	DI	2384	67	5535	73	570200	8225800
6		Ba		O	VN	4070	396	394	0	0	BRT				VC		1847	302	8711	844	561400	8224200
7	Mariner	Pb	Zn	P	SB	3670	235	230	234	0	GN	SP	CER		M	BR MV	351	52	7111	325	559800	8223500
8	M1	Pb		O	SB	3670	235	0	230	0	GN	PY CCP	CER	MAL	M C	DI	9702	169	5464	482	549800	8219200
9		Cu		O	SB	4050	371	368	369	372	CCP		MAL	CC	F		2902	1036	9018	1450	566000	8216800
10	Great Scott	Pb	Zn Cu	P	SB	3670	230	0	229	231	GN	CCP PY	MAL	CER	C	DI MV	1726	1726	12304	1722	565000	8210500
11		Ba		O	VN	4050	367	0	0	0	BRT	PY CCP			VC		869	102	14984	442	563300	8208300
12		Cu		O	SB	4040	357	0	358	0	CCP	PY	MAL	AZ CC	C	DI	1227	105	15343	793	563000	8206100
13		Pb	Cu	O	SB	3715	294	0	0	0	CCP	GN	MAL	CER	M C	DI	4128	4	19959	567	560700	8203500
14	Johnstons	Cu Pb		AM	VN	3670	231	229	231	232	CCP	GN PY APY	MAL	CER ANG CCL PYM	F	SZ	3311	1000	16191	3145	568400	8201900
15	M2	Ba		O	VN	3690	255	0	258	0	BRT				VC	MA	3051	426	15061	3078	572900	8201400
16	Carantsinni	Zn	Pb Ag	P	SB	3620	196	195	197	0	SP	GN CCP			M F	BR MV	374	374	1396	579	614600	8198300
17		Mn		O	IR	2120	112	0	0	0	PSI	PYL RDS					1589	1242	3092	1547	588100	8194300
18	Berjaya	Zn	Pb Cu	P	SF	3346	170	169	171	0	SP	PY CCP GN			M F	DI LA	12947	624	6079	9157	600100	8183200
19	Bindawodgie	Cu Pb		AM	SB	3610	191	188	0	0	GN		MAL			BR	15161	2962	3380	8649	603500	8183800
20	Reward	Pb Zn		AM	SB	3610	191	0	0	0			CER ANG	PYM ACN		BR	15025	3266	3145	9010	603800	8183500
21	Teena	Pb Zn		O	SF	3620	198	0	0	0			CER ANG				13012	2589	2214	11002	606100	8182200
22	Bald Hills (Bulburra)	Pb Zn	Ag Cu	AM	SB	3610	191	189	188	0	GN	SP CCP	CER	MAL HDZ	C	DI MV BR	8638	58	2148	8789	610500	8182900
23		Pb	Cu	O	SB	3620	195	0	195	200	GN	CCP	MAL	CER	F	LA MV	8609	206	2544	8818	610600	8182500
24	W-Fold (Wickans Hill)	Pb Zn		P	SF	3620	195	195	200	195	SP	GN PY	CER	HMM ANG	VF	LA BE	7966	176	2654	8156	611200	8182600
25	Blondi	Pb		P	SB	3610	188	0	0	0	GN						4863	2840	2551	4808	614000	8184900
26	Emu Plains	Pb Zn	Ag	P	SF	3620	195	198	195	0	SP	PY CCP GN			VF	LA	2406	1536	3036	2502	616500	8184800
27	Barney Creek	Pb	Ag	O	SB	3644	216	0	216	0	GN		CER		C	MV	2445	393	3673	2688	616700	8183400
28	Barneys	Pb	Ag	O	SB	3630	202	207	201	203	GN		CER		C	DI MV	3431	184	4137	3729	615900	8182400
29	HYC	Zn Pb Ag	Cu	DM	SF	3629	195	198	0	0	SP GN	PY CCP	HMM		VF	LA BE	1923	1184	2864	2216	617400	8182600
30	Cooley II	Cu	Pb Zn	D	SB	3640	212	0	0	0	CCP	BN GN SP PY			C	BR	15	15	868	292	619400	8182400
31	Cooley I	Zn Pb	Cu	D	SB	3640	212	0	0	0	GN	SP	CER		C	BR MV	21	21	886	322	619450	8182150
32	Cooley III	Pb Zn	Cu	D	SB	3640	212	0	0	0	GN SP				C	BR	297	297	1176	592	619200	8182000
33	Ridge I	Pb Zn	Cu	D	SB	3620	198	195	0	0	GN SP	PY TTH			C	BR	1010	1010	1873	1279	618400	8182300
34	Ridge II	Pb Zn	Cu	D	SB	3620	198	0	0	0	GN	SP PY TTH			C	BR	884	884	1737	1176	618600	8182000
35	Buffalo Lagoon	Pb		O	SB	3642	216	0	216	0	GN	PY	CER		C	DI	15458	1883	6679	12960	602400	8179300
36		Ba		O	VN	4050	366	0	0	0	BRT				VC		1642	3	3931	1731	577400	8177300
37	Mitchell Yard	Zn Pb		P	SF	3620	195	0	200	0	SP	GN PY			F	DI	6085	1877	5596	5991	612000	8176700
38	Myrtle Basin	Pb Zn	Ag Cu	P	SF	3620	195	195	195	200	SP	GN			M F	MV	9516	562	2351	3588	610300	8166800
39	Cooks	Zn Pb		D	SB	3610	191	0	0	0	GN SP	PY MCS CCP	CER		C	BR MV NO	383	72	989	151	622400	8172700
40	Cox	Zn Pb		D	SB	3610	191	0	0	0	SP GN	PY MCS CCP	CER		C	BR MV NO	377	367	333	181	622500	8171900
41	Turnbull	Pb		AM	SB	3644	221	0	0	0	GN				C	BR	1298	180	561	498	623500	8171200
42	Squib	Cu	Pb	AM	SB	3644	221	0	0	0	CCP		MAL	AZ CC	C	BR	1332	36	504	687	623600	8170500
43		Cu	Pb Zn	AM	SB	3644	221	0	0	0	CCP SP	PY	MAL CC	AZ	C	BR	1351	134	522	851	623700	8169700
44		Cu	Pb	O	VN	3644	218	0	0	0	CCP	GN					7876	20	596	7875	595800	8170300
45		Cu	Ba	O	SB	3660	228	0	227	0	CCP	PY	MAL		M F	DI	10717	2806	4330	3395	563200	8167100
46	Barney Creek Basin	Pb Zn	Ag Cu	O	SF	3620	195	0	195	0	SP	GN PY			F	DI MV	14440	1180	7486	12870	603800	8174600
47		Cu		O	SB	3644	220	0	218	220	CCP	PY	MAL		F	DI MV	3122	3122	2444	2300	570500	8159600
48	Larra Keyah	Pb	Cu	O	UN	3342	157	0	0	0							1457	327	2332	919	625000	8163500
49	Amelia	Pb	Cu	O	SB	3610	191	0	0	0	GN		MAL		C	BR	931	130	2725	596	625300	8160000
50	Margoo	Cu		P	SB	3644	217	218	220	218	CCP		MAL	CC	M F	MV	5527	731	2129	1297	549700	8147300
51	Mystery Mine	Cu		AM	UN	3330	151	0	152	149			MAL				580	580	2205	384	580400	8144300
52		Ba		O	VN	3644	217	0	217	0	BRT				C		130	130	762	63	570100	8139400
53		Cu		O	VN	3691	262	0	261	0	CCP	PY	MAL		F	DI MV	607	24	6106	396	575200	8135000

LITH	LITHNAME	ALTNAME	PARENT	Q		LITH	LITHNAME	ALTNAME	PARENT	Q
ADK	adakite			I		MPD	melilite-bearing peridotite		MLT	I
AFG	alkali feldspar granite		GRT	I		MPT	melilite-bearing pyroxenite		MLT	I
AFS	alkali feldspar syenite		SYN	I		MSK	miaskite		MZD	I
AGB	analcime gabbro	teschenite		I		MSS	missourite		FDL	I
AGL	agglomerate			I		MTS	metasomatite			M
AGLT	argillite			S		MTX	matrix			H
ALB	albitite			I		MUD	mud			R
ALO	alnoite		LPY	I		MUG	mugearite		ANT	I
AMP	amphibolite			M		MUV	melilite-bearing ultramafic volcanic		MLT	I
ANA	analcimite		FDT	I		MYL	mylonite			M
ANS	anorthosite			I		MZB	monzogabbro			I
ANT	andesite			I		MZD	monzodiorite		MZD	I
APL	aplite			I		MZG	monzogranite		GRT	I
ARKS	arkose			S		MZT	monzonite			I
ARNT	arenite			S		NGB	nepheline gabbro	theralite	GAB	I
ASH	ash			I		NLL	nephelinolite		FDL	I
BAD	basaltic andesite			I		NMD	nepheline monzodiorite	essexite	MZD	I
BDST	boundstone			S		NMG	nepheline monzogabbro	essexite	MZB	I
BHRK	beachrock			S		NPH	nephelinite		FDT	I
BIOC	biocarbonate			S		NRT	norite		GAB	I
BIOM	biomicrite			S		NSY	nepheline syenite		SYN	I
BIOS	biosparite			S		NVLT	novaculite			S
BLD	boulder			S		OBS	obsidian			I
BLT	basalt			I		OCP	olivine clinopyroxenite		PRX	I
BMT	benmoreite		ANT	I		ODT	opx diorite	norite	CHR	I
BNBD	bone bed			S		OFG	opx alkali feldspar granite		CHR	I
BON	boninite			I		OFS	opx alkali feldspar syenite		CHR	I
BSN	basanite			I		OGD	opx granodiorite	opdalite	CHR	I
BTH	bomb	block tephra	TPH	I		OGT	opx granite	charnockite	CHR	I
BX	breccia			H		OHP	olivine hornblende pyroxenite		PRX	I
CBT	carbonatite			I		OHT	olivine hornblendite		HBT	I
CCT	calciocarbonatite		CBT	I		OMD	opx monzodiorite	jotunite	CHR	I
CHAR	charnockite			I		OML	olivine melilitolite		MLL	I
CHLK	chalk			S		OMT	olivine melilitite		MLT	I
CHRT	chert			S		OMZ	opx monzonite	mangerite	CHR	I
CHT	chromitite			I		OOP	olivine orthopyroxenite		PRX	I
CLAS	clast			H		OOZ	ooze			S
CLCR	calcrete			R		OPHL	ophiolite			I
CLST	claystone			S		OPN	orthopyroxene norite		GAB	I
CLY	clay			R		OPT	orthopyroxenite		PRX	I
CMP	camptonite		LPY	I		ORE	ore			H
CNGL	conglomerate			S		OST	opx syenite		CHR	I
COAL	coal			S		OTT	opx tonalite	enderbite	CHR	I
COM	comendite		RHY	I		OWT	olivine websterite		PRX	I
CPT	clinopyroxenite		PRX	I		PBS	phonolitic basanite		BSN	I
CQNA	coquina			S		PBT	picrobasalt		BLT	I
CRNL	carnieule			S		PCLN	porcellanite			S
DAC	dacite			I		PCT	picrite			I
DLST	dolostone			S		PEAT	peat			S
DLT	dolerite		GAB	I		PEG	pegmatite			I
DMCT	diamictite			S		PELT	pelite			S
DRT	diorite			I		PER	peridotite			I
DST	dust			R		PFD	phonolitic foidite		FDT	I
DTMT	diatomite			S		PHD	plagioclase-bearing hornblendite		HBT	I
DUN	dunite		PER	I		PHP	pyroxene hornblende peridotite		PER	I
EGL	eclogite			M		PHSP	phosphorite			S
EVPT	evaporite			S		PHT	pyroxene hornblendite		HBT	I
FAN	foid-bearing anorthosite		ANS	I		PHY	porphyry			I
FAT	foid-bearing alkali feldspar trachyte		TRC	I		PHYL	phyllite			M
FBG	foid-bearing gabbro		GAB	I		PKR	peralkaline rhyolite		RHY	I
FBM	foid-bearing monzonite		MZT	I		PLZ	polzenite		LPY	I
FCT	ferrocarbonatite		CBT	I		PML	pyroxene melilitolite		MLL	I
FDI	foid-diorite		DRT	I		PNT	phonolite			I
FDL	foidolite			I		POM	pyroxene olivine melilitolite		MLL	I
FDR	foid-bearing diorite		DRT	I		PPD	pyroxene peridotite		PER	I
FDT	foidite			I		PPX	plagioclase-bearing pyroxenite		PRX	I
FFS	foid-bearing alkali feldspar syenite		SYN	I		PRX	pyroxenite			I
FGLT	fanglomerate			S		PSMT	psammite			S
FGS	fergusite		FDT	I		PTB	potassic trachybasalt		BLT	I
FLNT	flint			S		PTR	phonolitic tephrite		TPT	I
FLT	foid-bearing latite		LTT	I		PTT	pantellerite		RHY	I
FMD	foid-bearing monzodiorite		MZD	I		QAS	quartz alkali feldspar syenite		SYN	I
FMG	foid-bearing monzogabbro		MZB	I		QGB	quartz gabbro		GAB	I
FNT	fenite			I		QMD	quartz monzodiorite		MZD	I
FRCT	ferricrete			R		QMG	quartz monzogabbro		MZB	I
FSY	foid-bearing syenite		SYN	I		QTE	quartzolite		QZG	I
FTR	foid-bearing trachyte		TRC	I		QTY	quartz trachyte		TRC	I
GAB	gabbro			I		QZA	quartz anorthosite		ANS	I
GBN	gabbronorite		GAB	I		QZD	quartz diorite		DRT	I
GFL	granofels			M		QZG	quartz-rich granitoid			I
GNS	gneiss			M		QZL	quartz latite		LTT	I

GNST	grainstone			S		QZM	quartz monzonite		MZT	I
GOUG	gouge			H		QZS	quartz syenite		SYN	I
GPST	grapestone			S		QZT	quartzite			M
GRD	granodiorite			I		RCL	residual clay			R
GRN	granulite			M		RDLT	radiolarite			S
GRP	granophyre			I		RHD	rhyodacite		DAC	I
GRSN	greisen			M		RHY	rhyolite			I
GRT	granite			I		ROCK	rock			H
GRU	grus			R		SAN	sannaite		LPY	I
GSN	gossan			R		SCHT	schist			M
GST	greenstone			M		SDST	sandstone			S
GUN	guano			S		SDT	sodalitite		FDT	I
GVL	gravel			R		SED	sediment			H
GYST	geyserite			S		SHK	shonkinite		SYN	I
GYT	gyttja			S		SHLE	shale			S
GYWK	greywacke			S		SHT	shoshonite		ANT	I
HBT	hornblendite			I		SKN	skarn			M
HDG	hornblende gabbro		GAB	I		SLA	slate			M
HFL	hornfels			M		SLCT	silcrete			R
HWT	hawaiite		BLT	I		SLST	siltstone			S
HYA	hyaloclastite			I		SLT	silt			R
HZB	harzburgite		PER	I		SMD	sodalite monzodiorite		MZD	I
IGM	ignimbrite		TUF	I		SND	sand			R
IJL	ijolite		FDL	I		SPGT	sparagmite			S
IRFM	iron formation			S		SPIL	spilite			I
IRST	ironstone			S		SPT	spessartite		LPY	I
KBL	kimberlite			I		SRLT	saprolite			R
KTT	komatiite			I		SRP	serpentinite			M
KZT	kerzantite		LPY	I		SSY	sodalite syenite		SYN	I
LAG	lag			R		SYG	syenogranite		GRT	I
LATT	laterite			R		SYN	syenite			I
LAVA	lava			I		TBDT	turbidite			S
LBG	limburgite		BSN	I		TDJ	trondhjemite		TNL	I
LCTT	leucitite		FDT	I		TFD	tephritic	foidite	FDT	I
LHZ	lherzolite		PER	I		TFT	tuffite			I
LMST	limestone			S		TLL	till			S
LOM	loam			R		TLLD	tilloid			S
LOS	loess			R		TLLT	tillite			S
LPR	lamprolite			I		TNL	tonalite			I
LPY	lamprophyre			I		TPH	tephra			I
LTT	latite			I		TPL	tephritic phonolite		PNT	I
MARL	marl			S		TPT	tephrite			I
MBL	marble			M		TRC	trachyte			I
MCH	melmechite			I		TRVN	travertine			S
MCQ	monchiquite		LPY	I		TTL	troctolite		GAB	I
MCRT	micrite			S		TUF	tuff			I
MCT	magnesiocarbonatite		CBT	I		TYA	trachyandesite		ANT	I
MDST	mudstone			S		TYB	trachybasalt		BLT	I
METB	metabasite			M		TYD	trachydacite		DAC	I
MIG	migmatite			M		URT	urtite		FDL	I
MLG	melteigite		FDT	I		VGT	vogesite		LPY	I
MLL	melilitolite			I		VEIN	vein			H
MLT	melilitite			I		WEB	websterite		PRX	I
MNTT	minette		LPY	I		WHL	wehrlite		PER	I

class.aut			env.aut			comp.aut	
CLASS	CLASSNAME		ENV	NAME		COMP	COMPOSITION
W	Water		A	abyssal		CARB	carbonate
U	Unconsolidated		AE	aeolian		HET	heterolithic
S	Sedimentary		AF	alluvial fan		LTH	lithic
I	Igneous		BA	bathyal to abyssal (>200m)		QF	quartzo-feldspathic
M	Metamorphic		CSH	continental shelf		MAF	mafic
			D	deltaic		QZ	quartz
			DF	delta front		FEL	feldspathic
div.aut			DL	lower delta plain		ITM	intermediate
DIV	DIVNAME		DP	pro delta		PLY	polymict
EA	Early		DU	upper delta plain		FLS	felsic
			DY	dyke			
			E	estuarine			
epoch.aut			EE	erosional		era.aut	
EPOCH	EPOCHNAME		EU	unclassified		ERA	ERANAME
LO	Lower		F	fluvial		CZ	Cainozoic
MI	Middle		FB	fluvial-braided		MZ	Mesozoic
EA	Early		FD	debris flow		PZ	Palaeozoic
			FL	fluvial-lacustrine		MP	Mesoproterozoic
			FM	fluvial-meandering		PM	Mesoproterozoic-Palaeoproterozoic
frm.aut			G	glacial		PP	Palaeoproterozoic
FRM	STRATNAME		IGN	igneous body			
7522	Golliger Beds		IS	intertidal/supratidal			
13380	Mullaman beds		L	lacustrine		gen.aut	
18426	Top Springs Limestone		LA	lagoon		GEN	GENESIS
2840	Bukalara Sandstone		NKN	unknown/no data		C	coastal
488	Antrim Plateau Volcanics		P	paralic		I	igneous
11570	McMinn Formation		PA	playa		L	land
19074	Velkerri Formation		PL	pluton		M	marine
26387	Bessie Creek Formation		PLH	high-level pluton			
27379	Corcoran Formation		PLU	low-level pluton			
55	Abner Sandstone		S	shallow (0-200m)		local.aut	
27754	Crawford Formation		SA	subaerial		LOCAL	AREA
11034	Mainoru Formation		SB	sabhka		AR	Abner Range
10424	Limmen Sandstone		SF	shoreface		BS	Bauhinia Shelf
23762	Mantungula Formation		SFL	lower shoreface		EB	eastern Bauhinia Downs
9292	Karns Dolomite		SFM	middle shoreface		WB	western Bauhinia Downs
5843	Dungaminnie Formation		SFU	upper shoreface		SB	southern Bauhinia Downs
923	Balbirini Dolomite		SI	sill		RF	Riversleigh Fold Belt
17019	Smythe Sandstone		SM	submarine		TP	Tawallah Pocket
25761	Amos Formation		SS	starved shelf		MD	Mallapunyah Dome
10647	Looking Glass Formation		U	unclassified		TR	Tawallah Range
17426	Stretton Sandstone		UD	unclassified depositional		MH	Masterton Horst
20758	Yalco Formation		VS	very shallow (0-20m)		FI	Foelsche Inlier
10891	Lynott Formation					BR	Batten Range
6682	Fish River Formation					ST	Sawtooth Range
1488	Benmara beds		qual.aut			SR	Scrutton Range
16057	Reward Dolomite		QUAL	QUALIFIER		WS	Wearyan Shelf
1130	Barney Creek Formation		ADC	adcumulate		KM	Kamarga Dome
26166	Teena Dolomite		AGAL	agal			
27398	Emmerugga Dolomite		ALK	alkali			
13660	Myrtle Shale		ALT	altered		min.aut	
25162	Leila Sandstone		AMY	amygdaloidal		MIN	MINERAL
18349	Tooganinie Formation		APH	aphanitic		AB	albite
17896	Tatoola Sandstone		ARE	arenaceous		ACN	acanthite
25760	Amelia Dolomite		ARG	argillic		ACT	actinolite
11103	Mallapunyah Formation		ARK	arkosic		ADS	andesine
25730	Masterton Sandstone		BA	banded		ADU	adutaria
17551	Surprise Creek Formation		BAS	basic		AEG	aegirine
17800	Tanumbirini Rhyolite		BED	bedded		ALM	almandine
24563	Warramana Sandstone		BLTC	basaltic		ALN	allanite
14735	Packsaddle Microgranite		BN	brown		AMPH	amphibole
7486	Gold Creek Volcanics		BO	bouldery		AN	anorthite
20358	Wollogorang Formation		BR	brecciated		AND	andalusite
16775	Settlement Creek Volcanics		BTM	bituminous		ANG	anglesite
15114	Peters Creek Volcanics		BU	buff		ANH	anhydrite
27950	Wununmantyala Sandstone		C	coarse		ANK	ankerite
513	Aquarium Formation		CALC	calcareous		ANL	analcime
26142	Sly Creek Sandstone		CAR	carbonaceous		ANR	anorthoclase
16726	Seigal Volcanics		CB	cobble		AP	apatite
21009	Yiyintyi Sandstone		CGC	conglomeratic		APY	arsenopyrite
6639	Fiery Creek Volcanics		CHY	cherty		ARF	arfvedsonite
1621	Bigie Formation		CL	clast		ARG	aragonite
15764	Quilalar Formation		CLAC	clastic		ATH	anthophyllite
9156	Kamarga Volcanics		CLAY	clay mineral		ATN	autunite
20928	Yeldham Granite		CLC	calcic		AU	gold
14123	Nicholson Granite Complex		CLD	chloritoid		AUG	augite
16698	Scrutton Volcanics		CLT	chloritic		AZ	azurite
4151	Cliffdale Volcanics		CM	cement		BN	bornite
13528	Murphy Metamorphics		CS	calc-silicate		BRA	brannerite
			CUMU	cumulate		BRL	beryl
			CV	convolute		BRT	barite
period.aut			CX	cryptoexplosive		BT	biotite
PERIOD	PERIODNAME		CYC	cyclic		BTW	bytownite
QU	Quaternary		DIA	diapiric		CAL	calcite
TQ	Tertiary-Quaternary		DK	dark		CAMP	clino-amphibole
TT	Tertiary		DMT	dolomitic		CARB	carbonate
KR	Cretaceous		DY	dyke		CC	chalcocite
CM	Cambrian		EQ	equigranular		CCL	chrysocolla
ET	Ectasian		EU	eutaxitic		CCP	chalcopyrite

EC	Eclasian-Calymmian
CL	Calymmian
CS	Calymmian-Statherian
ST	Statherian
SO	Statherian-Orosirian
OR	Orosirian
region.aut	
REGION	PROVINCE
1	Gulf of Carpentaria
20	Carpentaria Basin
24	Daly River Basin
38	Georgina Basin
52	McArthur Basin
54	Mount Isa Inlier
56	Murphy Inlier
75	South Nicholson Basin
95	Dunmarra Basin
sbgrp.aut	
SBGRP	STRATNAME
25195	Maiwok Subgroup
1257	Batten Subgroup
18813	Umbolooga Subgroup
spgrp.aut	
SPGRP	NAME
PH	Phanerozoic cover
PC	North Australian platform cover
C3	Cover sequence 3
C2	Cover sequence 2
TD	Transitional domain volcanics and plutons
OD	Basement orogenic domain
style.aut	
STYLE	GEOMETRY
BE	bed
BR	breccia
DI	disseminated
LA	laminated
MA	massive
MV	multiple vein
NO	nodular
PI	pisolitic
RE	residual
RPL	replacement
SV	single vein
SZ	shear zone
type.aut	
TYPE	TYPENAME
EPC	epiclastic
CHEM	chemical
EXV	extrusive
CX	cryptoexplosive
VCC	volcaniclastic
ITV	intrusive
REG	regional
CON	contact
weath.aut	
WEATH	WEATHERING
RC	recessive
PK	pseudo-karstic
RS	resistive
KS	karstic
ops.aut	
OPS	OPSTATUS
AM	abandoned mine
D	deposit
O	occurrence
OM	operating mine
P	prospect
UN	unknown
mbr.aut	
MBR	STRATNAME
26679	Kyalla Member
16833	Sherwin Ironstone Member
29293	Moroak Sandstone Member
27800	Hodgson Sandstone Member
8842	Jalboi Member

EVAP	evaporitic
F	fine
FA	fault
FER	ferruginous
FI	fossil invertebrates
FIA	fiamme
FLAG	flaggy
FO	foliated
FOI	feldspathoidal
FOID	foid
FP	fossil plants
FR	fractured
FRI	friable
FS	flame structures
GL	glassy
GNL	granule
GPT	graphitic
GR	green
GRAN	granitic
GRSN	greisen
GTY	gritty
GY	grey
HFL	hornfels
HGR	high-grade
HK	high-K
HM	hematitic
HMG	high-Mg
HX	hummocky cross bed
KAO	kaolinised
LA	laminated
LAY	layered
LC	load casts
LCC	leucocratic
LEN	lenticular bedding
LGR	low-grade
LK	low-K
LMN	laminated
LPL	lapilli
LPX	low-angle planar cross bedding
LTX	low-angle trough cross bedding
M	medium-grained
MAS	massive
MC	mud cracks
MCC	melanocratic
MCL	mesocumulate
MDY	muddy
ME	medium-bedded
MEG	megacrystic
MET	meta
MGSN	magnesian
MIC	micaceous
MICA	mica
MK	medium-K
MT	matrix
MTS	metasomatic
MX	microcrystalline
MY	mylonitic
OCL	orthocumulate
OO	oolitic
ORG	organic
ORT	ortho
P	poorly sorted
PAR	para
PB	pebble
PBX	pseudobrecciated
PBY	pebbly
PCR	picro
PEL	pelitic
PERA	peralkaline
PHC	phosphatic
PIS	pisolitic
PI	pink
PL	pluton
PLE	pale
PLH	high-level pluton
PLL	low-level pluton
POIK	poikilitic
POR	porphyritic
PORS	porous
POT	potassic
PS	pseudomorphs
PSC	psammitic
PU	purple
PYC	pyroclastic
PYR	pyritic
QZ	quartz
RDL	radiolarian
RE	red
RHD	rhyodacitic
RICH	rich
RL	rhythmic-layered

CER	cerussite
CHR	chromite
CIN	cinnabar
CL	chlorite
CLAY	clay mineral
CLD	chloritoid
CNT	carnotite
COAL	coal
COF	coffinite
COR	corundum
CPX	clinopyroxene
CRD	cordierite
CRS	cristobalite
CST	cassiterite
CU	copper
CUM	cummingtonite
CUP	cuprite
CV	covellite
CZO	clinozoisite
DI	diopside
DMD	diamond
DOL	dolomite
EN	enstatite
EP	epidote
FELD	feldspar
FL	fluorite
FSPD	feldspathoid
FY	fayalite
GLN	glaucophane
GLT	glauconite
GN	galena
GNL	greenalite
GNT	garnet
GP	gypsum
GR	graphite
GRS	grossular
GT	goethite
HBL	hornblende
HDZ	hydrozincite
HEM	hematite
HL	halite
HMM	hemimorphite
ILL	illite
ILM	ilmenite
JD	jadeite
JRD	jordanite
KFS	k-feldspar
KLN	kaolinite
KY	kyanite
LAB	labradorite
LCT	leucite
LMT	laumontite
LWS	lawsonite
MAL	malachite
MC	microcline
MCS	marcasite
MGS	magnesite
MGT	magnetite
MICA	mica
MNT	montmorillonite
MNZ	monazite
MOL	molybdenite
MS	muscovite
NE	nepheline
OAMP	orthoamphibole
OGC	oligoclase
OL	olivine
OPL	opal
OPQ	opaque mineral
OPX	orthopyroxene
OR	orthoclase
PGT	pigeonite
PHL	phlogopite
PHOS	phosphate
PL	plagioclase
PMP	pumpellyite
PO	pyrrhotite
PPU	phosphuranylite
PRH	prehnite
PRL	pyrophyllite
PRP	pyrope
PRS	proustite
PSI	psilomelane
PY	pyrite
PYL	pyrolusite
PYM	pyromorphite
PYRX	pyroxene
QZ	quartz
RBK	riebeckite
RDN	rhodonite
RDS	rhodochrosite

28334	Arnold Sandstone Member		RM	ripple marks		RT	rutile
5608	Donnegan Member		RUC	rip-up-clasts		SA	sanidine
23654	Hot Spring Member		RX	recrystallised		SCH	scheelite
23467	Caranbirini Member		RXL	ripple cross laminae		SCP	scapolite
27753	Coxco Dolomite Member		SA	subaerial		SD	siderite
27836	Mitchell Yard Dolomite Member		SDC	sodic		SERC	sericite
11224	Mara Dolomite Member		SDY	sandy		SERP	serpentine
16356	Rosie Creek Sandstone Member		SER	sericitic		SIL	sillimanite
			SH	sheared		SKD	sklowdowskite
			SI	sill		SLE	saleeite
minclass.aut			SILI	siliceous		SP	sphalerite
CLASS	MINCLASS		SLF	silicified		SPL	spinel
UN	unknown		SLY	silty		SPS	spessartine
SF	stratiform		SM	submarine		SRL	schorl
SB	stratabound		SOM	sole markings		ST	staurolite
VN	vein		SSD	soft sediment deformation		STB	stibnite
IR	irregular		ST	stylolitic		STP	stilpnometane
PL	pipe-like		STRO	stromatolitic		SUL	sulphur
			SUL	sulphidic		TBR	torbernite
			TCY	trachy		TLC	talc
com.aut			TFC	tuffaceous		TNT	tennantite
COM	COMMODITY		THL	tholeiitic		TOUR	tourmaline
Ag	silver		TK	thick-bedded		TOZ	topaz
Au	gold		TN	thin-bedded		TR	tremolite
Ba	barium		TPI	tephri		TRD	tridymite
Cu	copper		UB	ultrabasic		TTH	tetrahedrite
Fe	iron		UM	ultramafic		TTN	titanite
Mn	manganese		UNW	unwelded		USP	ulvospinel
Pb	lead		VC	very coarse		URN	uraninite
U	uranium		VE	vesicular		URP	uranophane
Zn	zinc		VF	very fine		VES	vesuvianite
			VI	vitric		VRM	vermiculite
			VN	vein		WFM	wolframite
grp.aut			VND	veined		WO	wollastonite
GRP	STRATNAME		VOL	volcanic		WRD	wardite
16319	Roper Group		VTK	very thickly-bedded		ZEOL	zeolite
17123	South Nicholson Group		VU	vuggy		ZRN	zircon
26072	Nathan Group		W	well-sorted			
11512	McArthur Group		WB	wavy bedding			
11575	McNamara Group		WEA	weathered			
6631	Fickling Group		WEL	welded			
17902	Tawallah Group		WH	white			
3679	Carrara Range Group		XB	cross-bedded			
			XE	xenolith			
			XL	crystalline			
			XLA	cross-laminated			

CODE	SIO2MEAN	SIO2MED	SIO2MIN	SIO2MAX	TIO2MEAN	TIO2MED	TIO2MIN	TIO2MAX	AL2O3MEAN	AL2O3MED	AL2O3MIN	AL2O3MAX	FE203TOTMEAN	FE203TOTMEAN	FE203TOTMIN	FE203TOTMAX	FE2O3MEAN	FE2O3MED	FE2O3MIN	FE2O3MAX	FEOMEAN	FEOMED	FEOMIN	FEOMAX
2120	3.04	3.04	1.92	4.16	0.02	0.02	0.02	0.02	0.25	0.25	0.25	0.25					2.13	2.13	0.80	3.45				
2130	62.11	65.35	26.30	79.00	0.25	0.20	0.11	0.51	10.41	12.15	2.20	19.00	1.62	1.00	0.75	5.60	0.71	0.57	0.37	1.74	0.52	0.46	0.21	1.01
3310	72.33	72.33	66.98	77.67	0.21	0.21	0.12	0.30	13.64	13.64	10.95	16.33					0.45	0.45	0.30	0.60				
3315	58.80	59.05	27.60	83.30	0.10	0.11	-0.01	0.22	2.48	2.12	0.54	6.40	0.99	0.87	0.18	1.87	0.37	0.40	-0.45	0.78	0.57	0.56	0.18	0.98
3320	76.07	80.00	43.00	91.00	0.27	0.26	0.17	0.44	7.96	7.95	3.58	11.80	2.03	1.86	0.29	4.08	0.89	0.90	0.15	2.05	1.03	0.82	0.13	2.69
3330	48.97	48.85	6.95	86.40	0.14	0.12	-0.01	0.59	3.97	2.65	0.36	15.20	1.12	1.00	0.39	2.34	0.50	0.22	-0.03	10.87	0.67	0.64	0.27	1.59
3340	63.17	61.65	50.70	79.90	0.27	0.23	0.14	0.60	8.29	8.65	2.88	13.50	1.34	1.40	0.50	2.02	0.91	1.00	0.09	1.53	0.39	0.40	0.13	0.70
3342	52.57	52.70	17.70	78.50	0.23	0.18	-0.01	0.51	7.26	6.65	0.44	15.80	1.68	1.55	0.51	4.53	0.42	0.35	-0.43	1.24	0.94	0.91	0.57	1.58
3344	52.95	53.60	10.80	93.10	0.17	0.17	-0.01	0.44	5.72	5.60	0.17	13.40	1.60	1.51	0.25	4.56	0.48	0.43	-0.05	3.30	0.98	0.92	0.20	3.43
3346	58.66	58.40	18.00	80.70	0.24	0.24	0.06	0.47	7.17	7.10	2.02	14.70	4.42	2.64	0.58	22.80	2.99	1.23	-0.08	19.53	1.18	1.06	0.31	4.63
3610	29.99	30.19	0.66	84.33	0.15	0.13	-0.01	0.59	3.49	2.84	0.10	13.91	1.40	1.30	0.45	3.70	0.76	0.56	0.00	3.65	0.88	0.75	0.00	3.99
3620	43.26	43.16	2.05	83.04	0.27	0.24	0.00	3.79	7.58	7.67	0.04	19.50	2.16	1.72	0.30	10.90	2.58	1.35	0.02	38.71	5.77	3.78	0.00	38.60
3630	27.98	21.37	1.82	73.40	0.21	0.22	0.00	0.54	4.65	1.82	0.40	17.67	1.62	1.00	0.45	5.79	0.67	0.30	0.00	3.29	2.59	0.86	0.00	11.60
3632	14.54	8.37	3.66	70.95	0.24	0.24	0.00	1.00	3.00	1.39	0.64	15.30	1.47	0.83	0.25	6.21	0.45	0.12	-0.01	4.82	1.13	0.61	0.23	5.25
3642	6.48	1.85	0.25	65.50	0.17	0.21	0.00	0.47	0.84	0.31		10.10	1.85	0.87	0.37	6.70	0.16	0.10	0.00	0.74	1.48	0.65	0.27	5.89
3644	18.68	8.91	0.15	95.83	0.14	0.19	0.00	0.56	0.96	0.40		11.40	1.04	0.75	0.33	4.74	0.34	0.12	-0.01	3.08	0.67	0.55	0.00	3.94
3650	41.14	45.12	10.85	53.13	0.28	0.33	0.05	0.43	6.39	7.35	0.14	11.18	3.63	2.81	1.90	8.08	2.21	1.78	0.06	8.42	1.30	1.38	0.73	1.71
3660	26.06	26.82	14.58	36.50	0.24	0.25	0.19	0.29	2.42	1.57	0.89	6.58	2.14	1.93	1.52	3.22	0.89	0.84	0.35	1.61	1.13	1.20	0.66	1.45
3670	28.36	21.81	4.33	87.75	0.10	0.03	0.00	0.42	2.57	0.98	0.22	12.43	2.12	2.05	0.89	4.79	1.15	0.72	0.10	5.89	1.39	1.50	0.00	1.95
3680	68.93	80.20	9.54	98.08	0.20	0.19	0.04	0.43	6.43	4.86	0.60	14.87					2.57	1.91	0.35	10.77				
3681	68.93	80.20	9.54	98.08	0.20	0.19	0.04	0.43	6.43	4.86	0.60	14.87					2.57	1.91	0.35	10.77				
3690	26.96	21.02	1.45	65.57	0.12	0.06	0.02	0.58	2.81	1.26	0.21	15.57					2.67	1.40	0.50	9.97				
3691	26.96	21.02	1.45	65.57	0.12	0.06	0.02	0.58	2.81	1.26	0.21	15.57					2.67	1.40	0.50	9.97				
3710	59.11	60.47	27.76	88.65	0.19	0.19	0.02	0.40	4.70	5.19	0.20	9.54					2.56	1.56	0.30	18.47				
3711	59.11	60.47	27.76	88.65	0.19	0.19	0.02	0.40	4.70	5.19	0.20	9.54					2.56	1.56	0.30	18.47				
3712	59.11	60.47	27.76	88.65	0.19	0.19	0.02	0.40	4.70	5.19	0.20	9.54					2.56	1.56	0.30	18.47				
3713	59.11	60.47	27.76	88.65	0.19	0.19	0.02	0.40	4.70	5.19	0.20	9.54					2.56	1.56	0.30	18.47				
3714	59.11	60.47	27.76	88.65	0.19	0.19	0.02	0.40	4.70	5.19	0.20	9.54					2.56	1.56	0.30	18.47				
3715	59.11	60.47	27.76	88.65	0.19	0.19	0.02	0.40	4.70	5.19	0.20	9.54					2.56	1.56	0.30	18.47				
3720	90.76	90.76	90.76	90.76	0.26	0.26	0.26	0.26	4.79	4.79	4.79	4.79	1.15	1.15	1.15	1.15	1.05	1.05	1.05	1.05	0.09	0.09	0.09	0.09
3721	90.76	90.76	90.76	90.76	0.26	0.26	0.26	0.26	4.79	4.79	4.79	4.79	1.15	1.15	1.15	1.15	1.05	1.05	1.05	1.05	0.09	0.09	0.09	0.09
3722	90.76	90.76	90.76	90.76	0.26	0.26	0.26	0.26	4.79	4.79	4.79	4.79	1.15	1.15	1.15	1.15	1.05	1.05	1.05	1.05	0.09	0.09	0.09	0.09
3723	90.76	90.76	90.76	90.76	0.26	0.26	0.26	0.26	4.79	4.79	4.79	4.79	1.15	1.15	1.15	1.15	1.05	1.05	1.05	1.05	0.09	0.09	0.09	0.09
3724	90.76	90.76	90.76	90.76	0.26	0.26	0.26	0.26	4.79	4.79	4.79	4.79	1.15	1.15	1.15	1.15	1.05	1.05	1.05	1.05	0.09	0.09	0.09	0.09
3725	90.76	90.76	90.76	90.76	0.26	0.26	0.26	0.26	4.79	4.79	4.79	4.79	1.15	1.15	1.15	1.15	1.05	1.05	1.05	1.05	0.09	0.09	0.09	0.09
3726	90.76	90.76	90.76	90.76	0.26	0.26	0.26	0.26	4.79	4.79	4.79	4.79	1.15	1.15	1.15	1.15	1.05	1.05	1.05	1.05	0.09	0.09	0.09	0.09
4010	76.05	76.37	73.95	77.50	0.37	0.37	0.34	0.39	14.45	13.98	13.57	15.90	3.63	3.59	3.32	3.88	3.38	3.38	3.38	3.38	0.12	0.12	0.12	0.12
4025	49.75	57.72	4.06	72.57	0.31	0.31	0.06	0.55	8.36	10.76	1.27	12.28					5.38	5.40	2.73	7.91	2.00	2.00	2.00	2.00
4030	50.92	47.57	38.81	79.65	2.33	2.43	0.37	3.06	14.63	14.70	6.79	19.00	12.20	13.07	2.18	16.24	9.55	11.21	0.86	15.87	2.69	1.90	0.09	9.80
4040	52.10	52.10	52.10	52.10	0.53	0.53	0.53	0.53	13.86	13.86	13.86	13.86	20.57	20.57	20.57	20.57	20.57	20.57	20.57	20.57				
4050	49.71	49.01	40.72	62.58	2.40	2.39	1.95	2.81	14.03	13.96	11.85	17.00	11.20	12.23	2.61	17.64	6.92	3.63	1.94	19.60	5.64	4.82	0.10	12.60
4090	49.83	49.95	47.67	51.90	1.37	1.22	1.07	2.17	13.66	13.95	11.21	15.39	11.42	11.20	10.26	14.92	4.64	3.80	1.70	8.27	6.98	7.27	3.63	11.50
4095	51.98	52.13	51.30	52.52	1.67	1.77	1.46	1.78	14.05	13.82	13.59	14.74					2.88	2.64	1.77	4.22	9.45	9.55	8.45	10.35
4900	70.19	71.90	56.82	85.69	0.36	0.34	0.07	0.76	13.64	13.75	6.74	16.05					0.94	0.93	0.31	1.96	2.39	1.75	0.30	6.41
5000	63.92	65.27	47.62	65.95	0.86	0.69	0.67	2.63	14.25	14.45	12.58	14.66	6.20	5.35	4.79	15.87	4.06	2.54	2.15	7.49	4.19	2.64	2.38	7.54
5100	69.50	70.54	55.48	79.05	0.34	0.24	0.03	0.85	14.07	13.99	10.28	17.01					1.42	1.32	0.25	4.07	1.80	1.40	0.15	5.45

CODE	MNOMEAN	MNOMED	MNOMIN	MNOMAX	MGOMEAN	MGOMED	MGOMIN	MGOMAX	CAOMEAN	CAOMED	CAOMIN	CAOMAX	NA2OMEAN	NA2OMED	NA2OMIN	NA2OMAX	K2OMEAN	K2OMED	K2OMIN	K2OMAX	P2O5MEAN	P2O5MED	P2O5MIN	P2O5MAX	H2O_MEAN	H2O_MED
2120	0.36	0.36	0.26	0.45	19.94	19.94	19.93	19.94	28.84	28.84	28.75	28.92	0.31	0.31	0.30	0.31	0.08	0.08	0.06	0.09	0.05	0.05	0.04	0.05		
2130	0.08	0.06	-0.01	0.26	4.07	3.50	0.75	14.20	4.79	3.66	0.09	20.80	0.03	0.03	-0.01	0.06	7.33	7.60	1.32	14.70	0.09	0.10	0.03	0.15		
3310	0.02	0.02	0.01	0.02	0.04	0.04	0.04	0.04	0.04	0.04	0.03	0.05	0.01	0.01	0.01	0.01	11.99	11.99	9.49	14.48	0.03	0.03	0.02	0.03		
3315	0.11	0.11	0.02	0.21	7.57	7.78	1.31	13.90	10.97	10.75	1.45	20.90	0.01	0.02	-0.01	0.06	1.54	1.24	0.14	4.26	0.14	0.11	0.03	0.37		
3320	0.04	-0.01	-0.01	0.27	2.02	1.01	0.26	7.95	1.76	0.17	0.09	9.80	0.02	0.02	-0.01	0.05	5.33	4.83	2.70	7.85	0.08	0.08	0.02	0.16		
3330	0.16	0.16	-0.01	0.45	9.38	9.90	0.22	18.80	12.81	13.50	0.06	27.80	0.35	0.02	-0.01	10.30	2.30	1.38	0.05	9.40	0.09	0.06	-0.01	0.51		
3340	0.06	0.07	-0.01	0.13	4.31	4.10	0.68	8.35	6.42	6.38	0.30	12.20	0.03	0.03	-0.01	0.05	6.63	7.08	2.24	11.30	0.29	0.13	0.07	1.67		
3342	0.12	0.12	-0.01	0.31	8.43	8.70	0.03	16.30	9.06	8.40	0.16	23.90	2.52	0.01	-0.01	14.40	2.59	2.14	0.06	7.75	0.10	0.09	-0.01	0.32		
3344	0.15	0.14	-0.01	0.66	8.50	8.45	0.10	17.80	10.27	10.10	0.11	26.90	0.12	0.04	-0.01	0.79	3.26	3.12	-0.05	10.50	0.08	0.08	-0.01	0.41		
3346	0.26	0.13	0.02	2.76	4.89	4.42	0.64	14.60	6.75	6.20	0.15	22.80	0.47	0.08	-0.01	4.54	3.91	3.60	1.13	12.10	0.23	0.11	0.02	6.55		
3610	0.12	0.11	0.02	0.36	12.54	12.50	0.22	20.68	19.35	20.31	0.11	30.11	0.20	0.13	-0.01	1.26	2.54	2.07	0.02	12.25	0.10	0.06	0.00	1.00	0.27	0.15
3620	0.25	0.12	0.00	4.83	7.05	6.21	0.01	20.70	10.97	9.33	0.06	34.80	0.34	0.11	-0.01	7.25	4.73	4.47	0.07	15.66	0.17	0.12	0.01	1.81	1.09	0.75
3630	0.22	0.10	0.01	1.06	13.01	15.62	0.03	20.70	18.39	21.95	0.20	29.18	0.28	0.15	0.01	1.55	3.68	1.23	0.24	15.87	0.06	0.03	0.01	0.28	0.57	0.28
3632	0.20	0.13	0.01	0.76	16.31	18.33	0.17	20.33	23.96	26.29	0.49	28.62	0.30	0.29	0.00	0.75	2.19	1.06	0.12	13.26	0.09	0.05	0.01	0.44	0.20	0.16
3642	0.20	0.12	0.01	0.60	18.89	19.41	2.97	25.77	27.68	29.28	5.06	31.20	0.36	0.29	0.03	0.78	0.61	0.08	0.00	8.21	0.04	0.02	0.00	0.46	0.19	0.16
3644	0.10	0.09	0.00	0.45	16.58	18.88	0.30	31.83	23.95	27.76	0.35	30.80	0.28	0.25	0.03	0.70	0.59	0.17	0.01	9.65	0.02	0.01	0.00	0.17	0.14	0.11
3650	0.08	0.07	0.03	0.19	9.86	8.99	6.06	18.24	13.10	11.94	8.10	25.91	0.21	0.14	0.11	0.55	3.59	4.66	0.13	8.31	0.07	0.07	0.01	0.12	0.88	0.76
3660	0.15	0.16	0.07	0.19	13.96	13.71	10.46	16.80	20.52	20.30	15.33	24.44	0.29	0.27	0.13	0.52	1.33	1.06	0.32	3.68	0.06	0.05	0.03	0.10	0.32	0.22
3670	0.09	0.08	0.02	0.35	13.40	15.06	1.53	19.70	20.03	23.10	2.84	29.32	0.18	0.15	0.01	0.44	1.45	0.53	0.04	6.04	0.04	0.04	0.00	0.13	0.34	0.13
3680	0.09	0.05	0.01	0.34	3.40	0.61	0.04	15.74	5.19	0.14	0.02	24.68	0.21	0.19	0.10	0.31	4.31	3.53	0.14	10.30	0.09	0.07	0.04	0.26		
3681	0.09	0.05	0.01	0.34	3.40	0.61	0.04	15.74	5.19	0.14	0.02	24.68	0.21	0.19	0.10	0.31	4.31	3.53	0.14	10.30	0.09	0.07	0.04	0.26		
3690	0.14	0.12	0.01	0.42	14.43	14.55	0.60	32.91	18.83	19.00	0.09	31.87	0.23	0.24	0.01	0.46	1.78	0.80	0.09	11.52	0.07	0.06	0.01	0.21		
3691	0.14	0.12	0.01	0.42	14.43	14.55	0.60	32.91	18.83	19.00	0.09	31.87	0.23	0.24	0.01	0.46	1.78	0.80	0.09	11.52	0.07	0.06	0.01	0.21		
3710	0.13	0.10	0.03	0.39	6.48	6.76	0.06	13.63	8.34	8.01	0.07	19.37	0.25	0.25	0.15	0.47	2.88	3.18	0.05	5.69	0.10	0.10	0.04	0.17		
3711	0.13	0.10	0.03	0.39	6.48	6.76	0.06	13.63	8.34	8.01	0.07	19.37	0.25	0.25	0.15	0.47	2.88	3.18	0.05	5.69	0.10	0.10	0.04	0.17		
3712	0.13	0.10	0.03	0.39	6.48	6.76	0.06	13.63	8.34	8.01	0.07	19.37	0.25	0.25	0.15	0.47	2.88	3.18	0.05	5.69	0.10	0.10	0.04	0.17		
3713	0.13	0.10	0.03	0.39	6.48	6.76	0.06	13.63	8.34	8.01	0.07	19.37	0.25	0.25	0.15	0.47	2.88	3.18	0.05	5.69	0.10	0.10	0.04	0.17		
3714	0.13	0.10	0.03	0.39	6.48	6.76	0.06	13.63	8.34	8.01	0.07	19.37	0.25	0.25	0.15	0.47	2.88	3.18	0.05	5.69	0.10	0.10	0.04	0.17		
3715	0.13	0.10	0.03	0.39	6.48	6.76	0.06	13.63	8.34	8.01	0.07	19.37	0.25	0.25	0.15	0.47	2.88	3.18	0.05	5.69	0.10	0.10	0.04	0.17		
3720	0.01	0.01	0.01	0.01	0.04	0.04	0.04	0.04	0.06	0.06	0.06	0.06	0.06	0.06	0.06	0.06	0.07	0.07	0.07	0.07	0.11	0.11	0.11	0.11		
3721	0.01	0.01	0.01	0.01	0.04	0.04	0.04	0.04	0.06	0.06	0.06	0.06	0.06	0.06	0.06	0.06	0.07	0.07	0.07	0.07	0.11	0.11	0.11	0.11		
3722	0.01	0.01	0.01	0.01	0.04	0.04	0.04	0.04	0.06	0.06	0.06	0.06	0.06	0.06	0.06	0.06	0.07	0.07	0.07	0.07	0.11	0.11	0.11	0.11		
3723	0.01	0.01	0.01	0.01	0.04	0.04	0.04	0.04	0.06	0.06	0.06	0.06	0.06	0.06	0.06	0.06	0.07	0.07	0.07	0.07	0.11	0.11	0.11	0.11		
3724	0.01	0.01	0.01	0.01	0.04	0.04	0.04	0.04	0.06	0.06	0.06	0.06	0.06	0.06	0.06	0.06	0.07	0.07	0.07	0.07	0.11	0.11	0.11	0.11		
3725	0.01	0.01	0.01	0.01	0.04	0.04	0.04	0.04	0.06	0.06	0.06	0.06	0.06	0.06	0.06	0.06	0.07	0.07	0.07	0.07	0.11	0.11	0.11	0.11		
3726	0.01	0.01	0.01	0.01	0.04	0.04	0.04	0.04	0.06	0.06	0.06	0.06	0.06	0.06	0.06	0.06	0.07	0.07	0.07	0.07	0.11	0.11	0.11	0.11		
4010	0.01	0.01	0.00	0.01	0.05	0.05	0.04	0.06	0.00	0.00	-0.01		0.12	0.10	0.03	0.32	0.22	0.20	0.18	0.29	0.05	0.05	0.04	0.07		
4025	0.38	0.20	0.02	1.13	6.57	4.80	0.14	17.92	8.82	4.28	0.04	26.04	0.12	0.10	0.03	0.29	5.68	6.60	0.83	9.13	0.24	0.07	0.01	1.18	0.99	0.99
4030	0.09	0.07	0.01	0.20	4.80	4.87	0.12	9.85	2.37	1.78	0.02	8.48	1.62	0.28	0.02	5.10	6.19	5.86	0.43	13.61	0.39	0.42	0.08	0.66	1.59	0.00
4040	0.57	0.57	0.57	0.57	0.62	0.62	0.62	0.62	0.02	0.02	0.02	0.02	0.28	0.28	0.28	0.28	9.27	9.27	9.27	9.27	0.17	0.17	0.17	0.17		
4050	0.20	0.19	0.02	0.45	5.44	5.32	0.13	13.59	3.81	4.23	0.01	8.31	1.56	1.88	0.01	4.67	5.49	3.65	1.58	14.20	0.45	0.44	0.03	0.84	1.96	1.72
4090	0.13	0.15	0.00	0.21	8.17	8.17	5.30	12.00	6.01	6.20	1.50	10.19	1.17	1.22	0.05	2.57	3.36	2.63	0.48	7.05	0.15	0.14	0.10	0.25		
4095	0.19	0.18	0.17	0.22	4.04	3.71	3.55	4.87	6.74	6.63	6.50	6.90	2.15	2.16	2.08	2.22	3.04	3.07	2.97	3.08	0.31	0.24	0.23	0.45	2.47	2.43
4900	0.06	0.05	0.03	0.12	1.28	0.57	0.04	6.70	1.82	1.29	0.21	5.03	2.37	2.70	0.02	3.57	5.32	5.38	2.87	8.78	0.10	0.09	-0.04	0.27	1.01	0.97
5000	0.08	0.06	0.05	0.23	2.13	1.82	1.71	5.28	1.86	1.59	0.69	5.57	2.50	2.55	2.15	2.67	5.26	5.55	2.39	5.78	0.22	0.16	0.15	0.92		
5100	0.05	0.04	0.01	0.12	1.19	0.47	0.18	6.07	1.86	1.11	0.03	5.25	2.54	2.62	0.18	4.68	5.31	5.21	3.11	9.63	0.05	-0.04	-0.04	0.32	1.14	0.98

CODE	H2O_MIN	H2O_MAX	CO2MEAN	CO2MED	CO2MIN	CO2MAX	SMEAN	SMED	SMIN	SMAX	ORGCMEAN	ORGCMED	ORGCMMIN	ORGCMAX	LOIMEAN	LOIMED	LOIMIN	LOIMAX	RESTMEAN	RESTMED	RESTMIN	RESTMAX	TOTALMEAN	TOTALMED	TOTALMIN	TOTALMAX	N
2120																											2
2130															8.80	6.98	1.89	32.61	0.10	0.09	0.04	0.27	99.51	99.75	97.99	100.67	12
3310																											2
3315															16.89	16.88	2.92	32.01	0.13	0.13	0.07	0.24	99.63	99.87	98.40	100.58	10
3320															3.89	1.78	0.52	16.40	0.10	0.06	0.05	0.30	99.35	99.40	98.01	100.25	6
3330															20.55	21.08	0.47	43.10	0.20	0.19	0.05	0.40	100.24	100.37	98.33	102.11	86
3340															9.17	8.64	1.42	18.77	0.14	0.13	0.09	0.25	99.92	100.11	98.76	100.86	12
3342															15.06	14.80	0.65	37.34	0.18	0.18	0.08	0.35	99.86	100.56	83.86	101.98	33
3344															18.75	16.22	0.91	40.43	0.23	0.21	0.05	0.63	99.45	99.66	70.16	101.02	197
3346															11.70	10.71	3.36	35.17	0.34	0.26	0.09	2.41	98.58	98.93	94.66	101.04	129
3610	0.00	1.20	29.47	31.05	0.26	46.40	0.83	0.70	0.01	3.13	0.79	0.73	0.10	2.17	8.09	0.50	-0.89	44.08	0.22	0.19	0.14	0.33	99.02	99.17	96.87	101.51	80
3620	0.04	7.04	17.48	16.20	0.01	44.70	4.60	1.50	0.01	34.50	0.73	0.43	0.01	4.88	11.22	8.00	-2.37	44.19	0.22	0.20	0.12	0.31	99.49	99.58	95.61	100.73	387
3630	0.06	2.03	29.79	32.30	0.19	45.30	1.15	0.10	0.01	9.09	0.16	0.07	0.01	0.72	0.37	-0.03	-1.21	8.18									34
3632	0.02	0.74	37.92	41.75	1.20	44.60	2.18	2.18	2.18	2.18					3.41	0.00	-0.66	41.70					99.26	99.29	98.87	99.61	39
3642	0.01	0.64	43.20	45.70	7.70	47.30	0.48	0.48	0.32	0.59	0.14	0.12	0.06	0.24	0.08	0.11	-0.77	0.68									35
3644	0.00	0.78	37.53	43.50	0.72	47.30	0.02	0.02	0.02	0.02	0.01	0.01	0.01	0.01	-0.05	0.01	-4.16	1.03									123
3650	0.05	1.82	19.81	17.90	9.07	39.80									0.49	0.52	-1.06	2.24									10
3660	0.04	0.88	31.70	31.20	23.60	37.40									0.03	0.05	-0.09	0.12									5
3670	0.02	1.79	29.44	33.90	4.93	44.50									-0.09	-0.13	-0.77	0.83									53
3680																											9
3681																											9
3690																											47
3691																											47
3710																											25
3711																											25
3712																											25
3713																											25
3714																											25
3715																											25
3720															2.61	2.61	2.61	2.61	0.14	0.14	0.14	0.14	100.05	100.05	100.05	100.05	1
3721															2.61	2.61	2.61	2.61	0.14	0.14	0.14	0.14	100.05	100.05	100.05	100.05	1
3722															2.61	2.61	2.61	2.61	0.14	0.14	0.14	0.14	100.05	100.05	100.05	100.05	1
3723															2.61	2.61	2.61	2.61	0.14	0.14	0.14	0.14	100.05	100.05	100.05	100.05	1
3724															2.61	2.61	2.61	2.61	0.14	0.14	0.14	0.14	100.05	100.05	100.05	100.05	1
3725															2.61	2.61	2.61	2.61	0.14	0.14	0.14	0.14	100.05	100.05	100.05	100.05	1
3726															2.61	2.61	2.61	2.61	0.14	0.14	0.14	0.14	100.05	100.05	100.05	100.05	1
4010															5.16	5.11	4.89	5.47	0.17	0.17	0.17	0.17	100.12	99.96	99.49	100.89	6
4025	0.75	1.23	20.80	19.57	1.92	42.13																	100.12	99.83	99.29	102.24	6
4030	0.00	7.91	0.47	0.00	0.00	6.00									4.07	3.60	0.83	7.70	0.27	0.25	0.19	0.38	99.48	100.08	84.17	100.76	35
4040															2.42	2.42	2.42	2.42	0.37	0.37	0.37	0.37	100.78	100.78	100.78	100.78	1
4050	0.00	6.98	0.60	0.00	0.00	4.80									5.85	5.75	1.40	11.34	0.35	0.33	0.19	0.59	99.98	99.89	99.31	100.57	43
4090															3.87	3.76	2.89	5.07	0.34	0.34	0.34	0.34	100.16	100.14	100.00	100.35	12
4095	2.42	2.55																					99.13	99.06	99.05	99.27	3
4900	0.40	1.88																					99.54	99.48	98.85	100.15	29
5000															2.68	2.48	2.05	4.69	0.27	0.27	0.25	0.29	99.94	99.89	99.31	100.58	13
5100	0.40	2.77																					99.34	99.33	98.31	99.96	42

CODE	AGMEAN	AGMED	AGMIN	AGMAX	ASMEAN	ASMED	ASMIN	ASMAX	BMEAN	BMED	BMIN	BMAX	BAMEAN	BAMED	BAMIN	BAMAX	BEMEAN	BEMED	BEMIN	BEMAX	BIMEAN	BIMED	BIMIN	BIMAX	BRMEAN	BRMED	BRMIN	BRMAX	CAMEAN	CAMED
2120													23	23	21	25														
2130					4.0	3.0	1.0	19.0					207	214	98	331					-2	-2	-2	-2						
3310													357	357	354	359														
3315																														
3330					6.0	2.0	-0.5	97.0					165	136	20	608	1	1	0	4	-2	-2	-2	2						
3342					3.0	2.0	1.0	12.0					199	201	59	355	1	1	0	2	-2	-2	-2	-2						
3344					6.0	4.0	-1.0	61.0					327	274	28	2007	1	1	0	3	-2	-2	-2	-2						
3346																														
3610	2	2	1	3	16.0	5.0	0	123.0	1	0	0	40	168	148	10	594	0	-1	-1	4	-2	-2	-2	9	0.3	0	0	3.1		
3620	5	2	-1	136	177.0	30.0	0	2300.0	43	15	0	400	302	250	26	2928	0	-1	-1	4	-1	-2	-2	3	1.5	1.3		8.5		
3630	1	1	-1	3	17.0	4.0	0	226.0	10	0	0	150	365	63	18	3728	0	-1	-1	2	-2	-2	-2	4						
3632	2	2	-1	3	2.0	1.0	0	15.0					152	75	14	934	0	-1	-1	5	-2	-2	-2	5						
3642	1	1	-1	3	4.0	1.0	0	33.0					20	14	-4	68	-1	-1	-1	-1	-2	-2	-2	2						
3644	1	1	-1	3	3.0	1.0	0	24.0	-1	0	-100	20	368	35	5	9387	-1	-1	-1	3	-2	-2	-2	4						
3650	1	1	-1	2	6.0	3.0	1.0	27.0					2357	1067	302	8678	-1	-1	-1	3	-2	-2	-2	-2						
3660	1	1	-1	2	10.0	10.0	3.0	20.0					4161	4535	753	7079	2	1	-1	7	-2	-2	-2	-2						
3670	0	-1	-1	1	8.0	5.0	0	39.0					1194	236	13	15281	-1	-1	-1	4	-2	-2	-2	5						
3680													275	277	51	416														
3681													275	277	51	416														
3690													762	223	1	9184														
3691													762	223	1	9184														
3710													1018	272	1	7791														
3711													1018	272	1	7791														
3712													1018	272	1	7791														
3713													1018	272	1	7791														
3714													1018	272	1	7791														
3715													1018	272	1	7791														
3720					12.0	12.0	12.0	12.0					356	356	356	356					-2	-2	-2	-2						
3721					12.0	12.0	12.0	12.0					356	356	356	356					-2	-2	-2	-2						
3722					12.0	12.0	12.0	12.0					356	356	356	356					-2	-2	-2	-2						
3723					12.0	12.0	12.0	12.0					356	356	356	356					-2	-2	-2	-2						
3724					12.0	12.0	12.0	12.0					356	356	356	356					-2	-2	-2	-2						
3725					12.0	12.0	12.0	12.0					356	356	356	356					-2	-2	-2	-2						
3726					12.0	12.0	12.0	12.0					356	356	356	356					-2	-2	-2	-2						
4010													60	60	52	68														
4025													2742	1024	295	12600														
4030					8.0	4.0	1.0	40.0					751	774	80	1400	1	1	1	2	1	-2	-2	12					67	46
4040					13.0	13.0	13.0	13.0					1727	1727	1727	1727	2	2	2	2	5	5	5	5						
4050					12.0	7.0	1.0	59.0					1848	1225	83	14100	1	1	1	2	3	-2	-2	16					39	38
4090					6.0	5.0	2.0	14.0					456	304	220	1260	2	2	2	2	5	6	-2	8					156	183
4095					4.0	5.0	3.0	5.0					703	559	537	1014	2	2	1	2	0	0	-2	2						
4900					4.0	2.0	-1.0	70.0					790	804	7	1690	4	3	1	9	-1	-2	-2	4						
5000					4.0	5.0	4.0	5.0					957	962	639	1087	3	3	2	3	-2	-2	-2	-2						
5100					3.0	2.0	-1.0	23.0					1118	1073	115	2414	3	3	1	5	0	1	-2	2						

CODE	CAMIN	CAMAX	CDMEAN	CDMED	CDMIN	CDMAX	CEMEAN	CEMED	CEMIN	CEMAX	CLMEAN	CLMED	CLMIN	CLMAX	COMEAN	COMED	COMIN	COMAX	CRMEAN	CRMED	CRMIN	CRMAX	CSMEAN	CSMED	CSMIN	CSMAX	CUMEAN	CUMED	CUMIN
2120							16	16	7	24					7	7	3	11	10	10	9	11					16	16	7
2130																			14	9	1	47							
3310							59	59	47	70					1	1	1	1	5	5	2	7					1	1	1
3315																													
3330							21	21	21	21					0	0	0	18	14	10	1	46					71	71	71
3342																			18	16	6	39							
3344																			16	16	1	45							
3346																													
3610							27	20	-5	166					3	-2	-2	41	37	31	1	129	1	0	-3	11	7	5	-1
3620			118	10	6	600	67	53	12	296					18	12	-2	140	61	38		710	1	0	-3	16	161	14	-1
3630							46	10	-5	454					2	-2	-2	20	54	27	1	340	0	-3	-3	5	19	4	-1
3632							24	12	5	140					-1	-2	-2	9	27	18	8	212	0	-3	-3	6	4	0	-1
3642							1	-5	-5	18					0	-2	-2	20	23	7	1	167	2	4	-3	7	3	-1	-1
3644							7	6	-5	84					0	-2	-2	9	50	13	-1	551	1	3	-3	8	7	1	-1
3650							47	51	-5	111					0	-2	-2	6	43	42	1	69	5	6	-3	9	12	3	-1
3660							32	27	8	70					1	-2	-2	13	55	47	26	95	2	4	-3	6	17	14	3
3670							25	20	-5	77					3	3	-2	16	45	23	1	401	1	3	-3	9	34	8	-1
3680							51	37	19	101					7	2	1	29	19	19	2	46					4	1	1
3681							51	37	19	101					7	2	1	29	19	19	2	46					4	1	1
3690							28	25	1	74					7	3	1	75	14	7	1	96					74	32	1
3691							28	25	1	74					7	3	1	75	14	7	1	96					74	32	1
3710							46	51	1	141					5	4	1	18	40	22	1	519					209	26	1
3711							46	51	1	141					5	4	1	18	40	22	1	519					209	26	1
3712							46	51	1	141					5	4	1	18	40	22	1	519					209	26	1
3713							46	51	1	141					5	4	1	18	40	22	1	519					209	26	1
3714							46	51	1	141					5	4	1	18	40	22	1	519					209	26	1
3715							46	51	1	141					5	4	1	18	40	22	1	519					209	26	1
3720															-2	-2	-2	-2	8	8	8	8							
3721															-2	-2	-2	-2	8	8	8	8							
3722															-2	-2	-2	-2	8	8	8	8							
3723															-2	-2	-2	-2	8	8	8	8							
3724															-2	-2	-2	-2	8	8	8	8							
3725															-2	-2	-2	-2	8	8	8	8							
3726															-2	-2	-2	-2	8	8	8	8							
4010							156	156	146	166									2	2	2	2					3	2	2
4025																													
4030	23	132					66	68	34	90					132	29	4	1240	101	38	9	355					13	10	6
4040															42	42	42	42	85	85	85	85							
4050	27	51					58	63	20	86					24	24	-2	42	39	41	2	70					102	40	10
4090	64	220					41	40	30	60					42	46	20	62	237	200	26	897					76	65	21
4095											152	163	104	189	45	45	45	45	51	51	5	97							
4900											145	127	41	367	12	9	-2	43	18	18	9	26							
5000							109	110	81	136					21	12	11	39	40	34	31	103					13	14	6
5100											113	81	26	372	15	14	2	37	37	6	2	409							

CODE	CUMAX	DYMEAN	DYMED	DYMIN	DYMAX	ERMEAN	ERMED	ERMIN	ERMAX	EUMEAN	EUMED	EUMIN	EUMAX	FMEAN	FMED	FMIN	FMAX	GAMEAN	GAMED	GAMIN	GAMAX	GDMEAN	GDMED	GDMIN	GDMAX	GEMEAN	GEMED	GEMIN	GEMAX	HFMEAN
2120	24																													
2130																		10	10	3	20					3.0	3.0	1.0	5.0	5
3310	1																													
3315																														
3330	71																	6	5	1	17					1.0	1.0	-1.0	6.0	0
3342																		7	6	2	13					2.0	2.0	-1.0	4.0	1
3344																		7	7	1	18					2.0	2.0	-1.0	5.0	1
3346																														
3610	81																	3	2	0	11					1.0	1.0	0	3.0	2
3620	5800																	7	6	0	16					3.0	1.0	0	60.0	4
3630	251																	3	2	0	15					0	0	0	1.0	1
3632	64																	2	1	0	11					0	0	0	1.0	0
3642	41																	1	0	0	8					0	0	0	1.0	-1
3644	378																	1	0	0	8					0	0	0	3.0	-1
3650	51																	7	9	0	13					1.0	2.0	0	2.0	2
3660	39																	2	0	0	6					0	0	0	1.0	1
3670	312																	2	0	0	14					1.0	1.0	0	2.0	0
3680	21																													
3681	21																													
3690	373																													
3691	373																													
3710	3038																													
3711	3038																													
3712	3038																													
3713	3038																													
3714	3038																													
3715	3038																													
3720																										2.0	2.0	2.0	2.0	5
3721																										2.0	2.0	2.0	2.0	5
3722																										2.0	2.0	2.0	2.0	5
3723																										2.0	2.0	2.0	2.0	5
3724																										2.0	2.0	2.0	2.0	5
3725																										2.0	2.0	2.0	2.0	5
3726																										2.0	2.0	2.0	2.0	5
4010	5	5.30	5.30	4.61	5.98	4.04	4.04	3.62	4.47	1.34	1.34	1.29	1.39									3.61	3.61	3.18	4.03					
4025																														
4030	24	7.13	7.83	5.50	8.05	3.84	4.28	2.82	4.41	2.47	2.63	2.03	2.76					20	22	5	30	8.29	8.99	6.52	9.37	2.0	1.0	-1.0	4.0	7
4040																		20	20	20	20					1.0	1.0	1.0	1.0	4
4050	930	6.60	6.53	6.34	6.92	3.96	3.92	3.80	4.16	2.02	2.01	1.87	2.17					19	21	5	26	7.06	7.05	6.70	7.44	2.0	2.0	1.0	6.0	7
4090	135	4.56	4.53	4.46	4.70	2.80	2.78	2.77	2.86	1.13	1.12	1.08	1.18					21	20	14	26	4.48	4.49	4.40	4.54	3.0	4.0	1.0	4.0	4
4095														550	550	400	700	24	24	23	25					2.0	2.0	2.0	2.0	5
4900														1250	950	700	2400	19	19	14	26					1.0	1.0	1.0	2.0	6
5000	17	6.18	6.21	4.61	7.73	3.97	4.08	2.79	5.04	1.48	1.49	1.15	1.79					21	20	18	24	6.51	6.50	4.95	8.07	1.0	1.0	1.0	2.0	8
5100														401	400	-200	1200	19	19	5	26					1.0	2.0	-1.0	2.0	6

CODE	HFMED	HFMIN	HFMAX	HOMEAN	HOMED	HOMIN	HOMAX	LAMEAN	LAMED	LAMIN	LAMAX	LIMEAN	LIMED	LIMIN	LIMAX	MNMEAN	MNMED	MNMIN	MNMAX	MOMEAN	MOMED	MOMIN	MOMAX	NBMEAN	NBMED	NBMIN	NBMAX	NDMEAN	NDMED	NDMIN
2120								1	1	1	1					3235	3235	2379	4090					4	4	3	4			
2130	5	-2	11																	0	-2	-2	3	11	13	2	23			
3310								39	39	33	45					38	38	1	74					19	19	19	19			
3315																														
3330	-2	-2	6					1	1	1	1	17	8	0	109	3945	3945	3945	3945	0	-2	-2	4	3	3	-2	15			
3342	2	-2	5									97	73	11	242					1	2	-2	9	5	4	-2	10			
3344	2	-2	9									63	54	0	257					0	-2	-2	6	5	6	-2	17			
3346																														
3610	2	-2	13					14	9	2	91	6	4	2	40	1095	910	133	3998	7	6	4	17	3	3	-2	18	9	8	-2
3620	4	-2	9					33	25	1	160	31	23	1	230	1953	1146	34	36886	9	7	1	40	11	11	-2	51	25	20	3
3630	0	-2	10					28	5	-2	311	29	4	-1	450	1191	683	48	6162	7	7	5	10	4	2	-2	21	7	4	-2
3632	-2	-2	11					13	6	-2	87	6	3	1	37	1889	977	56	8184	6	6	0	8	2	2	-2	22	7	5	-2
3642	-2	-2	4					2	3	-2	7	4	2	-1	18	1969	1053	30	6426	7	6	5	18	-2	-2	-2	2	0	-2	-2
3644	-2	-2	6					4	3	-2	42	6	3	-1	38	874	743	52	4337	6	6	3	18		-2	-2	17	2	2	-2
3650	3	-2	5					25	28	2	53	41	38	3	73	690	647	264	1401	7	7	6	11	8	10	-2	15	21	21	5
3660	3	-2	3					16	13	6	33	12	6	3	43	1256	1162	858	1832	8	8	5	10	2	2	-2	7	14	12	5
3670	-2	-2	6					10	5	-2	38	15	6	2	71	816	714	137	3115	7	7	5	11	3	3	-2	17	10	8	-2
3680								21	17	1	50					787	331	2	3073					10	8	1	25			
3681								21	17	1	50					787	331	2	3073					10	8	1	25			
3690								8	1	1	47					1147	954	36	3740					6	5	1	32			
3691								8	1	1	47					1147	954	36	3740					6	5	1	32			
3710								20	21	1	74					1045	810	174	3329					9	9	1	17			
3711								20	21	1	74					1045	810	174	3329					9	9	1	17			
3712								20	21	1	74					1045	810	174	3329					9	9	1	17			
3713								20	21	1	74					1045	810	174	3329					9	9	1	17			
3714								20	21	1	74					1045	810	174	3329					9	9	1	17			
3715								20	21	1	74					1045	810	174	3329					9	9	1	17			
3720	5	5	5									14	14	14	14					-2	-2	-2	-2	10	10	10	10			
3721	5	5	5									14	14	14	14					-2	-2	-2	-2	10	10	10	10			
3722	5	5	5									14	14	14	14					-2	-2	-2	-2	10	10	10	10			
3723	5	5	5									14	14	14	14					-2	-2	-2	-2	10	10	10	10			
3724	5	5	5									14	14	14	14					-2	-2	-2	-2	10	10	10	10			
3725	5	5	5									14	14	14	14					-2	-2	-2	-2	10	10	10	10			
3726	5	5	5									14	14	14	14					-2	-2	-2	-2	10	10	10	10			
4010								86	86	77	94													24	24	22	26	45	45	40
4025																								22	21	21	23			
4030	6	2	17	1.49	1.65	1.06	1.77	28	26	20	40	23	18	5	57					-1	-2	-2	2	15	15	-20	27	39	43	30
4040	4	4	4									9	9	9	9					6	6	6	6	11	11	11	11			
4050	7	3	13					38	31	19	82	22	14	4	55					0	2	-2	3	10	11	-4	26	33	32	32
4090	4	4	4	0.95	0.97	0.88	1.00	24	30	14	30	31	28	20	54					1	2	-2	2	8	9	4	11	17	17	16
4095	5	4	5									40	34	31	55					6	6	5	7	11	11	8	13			
4900	6	4	7									63	33	5	712					2	3	-3	9	15	13	3	70			
5000	8	7	9					53	55	39	65	14	12	11	19					-2	-2	-2	-2	13	13	12	18	44	44	33
5100	6	3	13									20	18	2	55					3	3	-3	5	12	11	4	29			

CODE	NDMAX	NIMEAN	NIMED	NIMIN	NIMAX	PBMEAN	PBMED	PBMIN	PBMAX	PRMEAN	PRMED	PRMIN	PRMAX	RBMEAN	RBMED	RBMIN	RBMAX	SMEAN	SMED	SMIN	SMAX	SBMEAN	SBMED	SBMIN	SBMAX	SCMEAN	SCMED	SCMIN	SCMAX	SEMEAN
2120		26	26	18	33	21	21	1	40					1	1	1	1									1	1	1	1	
2130		7	6	4	15	4	4	-5	19																	9	9	2	17	
3310		12	12	10	13	2	2	1	3					95	95	67	122									1	1	1	1	
3315						5	5	5	5																					
3330		6	5	1	21	9	5	-5	70					1	1	1	1									13	13	1	24	
3342		8	8	3	13	6	6	-5	33					117	115	10	221									13	14	4	19	
3344		7	7	2	18	27	13	-5	936																	12	13	3	19	
3346						52	40	-5	140																					
3610	46	9	4	1	150	15	8	-2	200	1.00	-2.00	-2.00	13.00	40	31	-1	129	1616	130	40	31340					12	12	1	18	-1
3620	101	25	17	1	400	3304	25	-2	130000	4.00	3.00	-2.00	29.00	98	94	1	295	3728	160	60	49020	22	0	0	410	10	10		25	
3630	63	11	6	-1	44	22	7	-2	214	1.00	-2.00	-2.00	20.00	33	10	2	143	190	130	70	880					10	11	1	15	-1
3632	46	4	2	-1	30	4	2	-2	19	0.00	-2.00	-2.00	11.00	25	11	2	194	158	135	50	590					11	12	2	15	-1
3642	7	1	1	-1	10	7	3	-2	36	-2.00	-2.00	-2.00	4.00	1	-1	-1	13	167	150	40	410					10	10	8	13	-1
3644	27	3	2	-1	25	5	3	-2	43	-1.00	-2.00	-2.00	7.00	9	2	-1	116	197	130	-3	1990					9	10	-1	15	-1
3650	39	15	16	4	26	8	6	1	28	6.00	6.00	-2.00	10.00	97	103	1	210	465	240	60	2130					10	11	4	13	-1
3660	26	7	6	4	11	13	15	4	19	2.00	3.00	-2.00	6.00	45	23	6	98	1256	1630	180	1740					10	11	8	13	-1
3670	27	12	11	-1	36	11	6	-2	67	2.00	3.00	-2.00	8.00	37	10	-1	237	439	180	50	3650					8	10	1	16	-1
3680		21	19	12	35	16	11	1	76					94	84	2	205									3	2	1	7	
3681		21	19	12	35	16	11	1	76					94	84	2	205									3	2	1	7	
3690		21	18	11	66	6	1	1	30					35	9	1	245									4	2	1	22	
3691		21	18	11	66	6	1	1	30					35	9	1	245									4	2	1	22	
3710		37	22	11	387	5	3	1	32					74	89	1	163									5	5	1	14	
3711		37	22	11	387	5	3	1	32					74	89	1	163									5	5	1	14	
3712		37	22	11	387	5	3	1	32					74	89	1	163									5	5	1	14	
3713		37	22	11	387	5	3	1	32					74	89	1	163									5	5	1	14	
3714		37	22	11	387	5	3	1	32					74	89	1	163									5	5	1	14	
3715		37	22	11	387	5	3	1	32					74	89	1	163									5	5	1	14	
3720		2	2	2	2	9	9	9	9																	5	5	5	5	
3721		2	2	2	2	9	9	9	9																	5	5	5	5	
3722		2	2	2	2	9	9	9	9																	5	5	5	5	
3723		2	2	2	2	9	9	9	9																	5	5	5	5	
3724		2	2	2	2	9	9	9	9																	5	5	5	5	
3725		2	2	2	2	9	9	9	9																	5	5	5	5	
3726		2	2	2	2	9	9	9	9																	5	5	5	5	
4010	50	2	2	1	3	26	27	14	32	15.00	15.00	14.00	17.00	4	3	3	5									7	7	7	7	
4025						6	6	5	7																					
4030	45	78	55	3	252	20	10	2	120	9.00	10.00	7.00	11.00	90	64	13	285									26	25	4	39	
4040		31	31	31	31	54	54	54	54																	10	10	10	10	
4050	33	23	24	1	38	38	16	2	157	8.00	8.00	8.00	8.00	122	103	15	250									30	32	7	50	
4090	17	140	139	27	239	56	7	2	495	4.00	4.00	4.00	4.00	89	80	29	160									25	20	15	40	
4095		39	39	30	48	16	15	13	21									534	433	321	849					34	32	30	39	
4900		12	3	-2	85	32	34	3	58									43	32	6	232					11	8	-2	28	
5000	55	18	14	10	64	14	13	4	30	12.00	12.00	9.00	15.00	234	238	204	250									15	15	13	27	
5100		10	2	-2	121	23	24	7	50									78	29	9	1030					11	9	2	26	

CODE	SEMED	SEMIN	SEMAX	SMMEAN	SMMED	SMMMIN	SMMAX	SNMEAN	SNMED	SNMIN	SNMAX	SRMEAN	SRMED	SRMIN	SRMAX	TAMEAN	TAMED	TAMIN	TAMAX	TBMEAN	TBMED	TBMIN	TBMAX	THMEAN	THMED	THMIN	THMAX	TLMEAN	TLMED
2120												30	30	15	44									1.0	1.0	1.0	1.0		
2130								3	4	-2	9	25	30	-20	43	0	-2	-2	5					15.0	18.0	3.0	36.0		
3310												9	9	6	12									18.0	18.0	17.0	19.0		
3315												-20	-20	-20	-20														
3330								0	-2	-2	5	48	41	-20	167	-1	-2	-2	6					4.0	4.0	-2.0	23.0		
3342								1	2	-2	4	32	28	-20	82	-1	-2	-2	3					8.0	9.0	-2.0	20.0		
3344								2	3	-2	11	29	33	-20	70	-1	-2	-2	5					7.0	7.0	-2.0	20.0		
3346												39	40	20	80														
3610	-1	-1	2					1	2	-2	5	39	31	5	220	-2	-2	-2	3					4.0	3.0	-2.0	25.0		
3620	-1	-1	15					2	2	-2	5	29	26	1	161	-1	-2	-2	10					11.0	10.0	-2.0	44.0	27	1
3630	-1	-1	-1					0	-2	-2	5	31	28	4	90	-1	-2	-2	3					4.0	-2.0	-2.0	34.0	100	100
3632	-1	-1	1					1	2	-2	5	31	26	11	75	-2	-2	-2	3					2.0	-2.0	-2.0	28.0		
3642	-1	-1	-1					1	-2	-2	5	27	21	7	157	-1	-2	-2	5					-2.0	-2.0	-2.0	2.0		
3644	-1	-1	-1					0	-2	-2	4	38	30	3	275	-2	-2	-2	15					-1.0	-2.0	-2.0	11.0		
3650	-1	-1	-1					2	4	-2	5	49	44	26	89	-1	-2	-2	3					7.0	8.0	-2.0	15.0		
3660	-1	-1	-1					-1	-2	-2	4	64	48	27	124	-1	-2	-2	4					3.0	3.0	-2.0	7.0		
3670	-1	-1	-1					0	-2	-2	5	38	31	5	158	-1	-2	-2	3					2.0	1.0	-2.0	17.0		
3680												18	20	2	29									5.0	1.0	1.0	15.0		
3681												18	20	2	29									5.0	1.0	1.0	15.0		
3690												62	37	9	634									3.0	1.0	1.0	26.0		
3691												62	37	9	634									3.0	1.0	1.0	26.0		
3710												85	44	11	698									3.0	1.0	1.0	15.0		
3711												85	44	11	698									3.0	1.0	1.0	15.0		
3712												85	44	11	698									3.0	1.0	1.0	15.0		
3713												85	44	11	698									3.0	1.0	1.0	15.0		
3714												85	44	11	698									3.0	1.0	1.0	15.0		
3715												85	44	11	698									3.0	1.0	1.0	15.0		
3720								2	2	2	2	159	159	159	159	-2	-2	-2	-2					14.0	14.0	14.0	14.0		
3721								2	2	2	2	159	159	159	159	-2	-2	-2	-2					14.0	14.0	14.0	14.0		
3722								2	2	2	2	159	159	159	159	-2	-2	-2	-2					14.0	14.0	14.0	14.0		
3723								2	2	2	2	159	159	159	159	-2	-2	-2	-2					14.0	14.0	14.0	14.0		
3724								2	2	2	2	159	159	159	159	-2	-2	-2	-2					14.0	14.0	14.0	14.0		
3725								2	2	2	2	159	159	159	159	-2	-2	-2	-2					14.0	14.0	14.0	14.0		
3726								2	2	2	2	159	159	159	159	-2	-2	-2	-2					14.0	14.0	14.0	14.0		
4010				5.75	5.75	5.16	6.35					99	100	74	121									42.0	42.0	40.0	42.0		
4025												43	39	23	81														
4030				8.42	9.12	6.63	9.52	0	-2	-2	4	85	44	5	350	-2	-2	-2	2	1.16	1.29	0.89	1.31	20.0	5.0	-20.0	389.0		
4040								5	5	5	5	75	75	75	75	-2	-2	-2	-2					15.0	15.0	15.0	15.0		
4050				6.60	6.62	6.56	6.63	2	3	-2	8	109	100	11	210	-1	-2	-2	3					9.0	8.0	4.0	48.0		
4090				3.98	4.00	3.83	4.10	3	4	-2	6	147	117	50	350	-2	-2	-2	-2	0.68	0.67	0.64	0.72	5.0	4.0	4.0	8.0		
4095								3	3	2	5	285	271	197	387	0	0	-2	2					10.0	9.0	8.0	14.0		
4900								13	5	2	167	186	131	9	490	-2	-2	-2	-2					25.0	23.0	7.0	58.0		
5000				7.62	7.62	5.76	9.49	2	3	-2	4	186	200	41	276	-1	-2	-2	2					20.0	21.0	8.0	27.0		
5100								5	4	2	31	195	177	27	484	-1	-2	-2	7					26.0	24.0	9.0	52.0		

CODE	TLMIN	TLMAX	UMEAN	UMED	UMIN	UMAX	VMEAN	VMED	VMIN	VMAX	WMEAN	WMED	WMIN	WMAX	YMEAN	YMED	YMIN	YMAX	YBMEAN	YBMED	YBMIN	YBMAX	ZNMEAN	ZNMED	ZNMIN	ZNMAX	ZRMEAN	ZRMED	ZRMIN	ZRMAX	N
2120							13	13	6	19					3	3	1	5					209	209	3	414	2	2	1	3	2
2130			3.0	2.0	1.0	5.0	27	22	15	56	-3	-3	-3	-3	26	22	11	57					17	12	3	39	193	193	54	354	13
3310							7	7	1	12					28	28	15	40					1	1	1	1	142	142	111	172	2
3315																							6	6	6	6					1
3330			1.0	1.0	-1.0	19.0	18	16	-2	57	57	53	-3	215	11	9	1	47					12	8	1	106	77	66	5	226	80
3342			1.0	0	-1.0	5.0	23	22	11	44	51	45	22	103	16	16	5	25					15	12	7	28	114	117	14	233	34
3344			1.0	2.0	-1.0	4.0	18	18	-2	60	110	75	18	556	16	16	2	36					58	19	3	924	103	89	3	369	142
3346																							87	36	6	640					19
3610		5	2.0	1.0	0	7.0	17	14	-2	56	-1	-3	-3	5	10	10	-1	28					24	5	1	360	75	56	4	310	67
3620	0	655	4.0	3.0	0	22.0	48	35	2	250	0	0	-3	40	23	22	1	62					7263	49	1	240000	166	122	8	6890	358
3630	100	100	1.0	1.0	0	5.0	21	15	3	150	-2	-3	-3	5	11	8	2	41					43	4	1	527	88	40	4	527	34
3632			2.0	1.0	0	14.0	13	8	-2	68	-2	-3	-3	6	9	6	3	66					18	12	0	180	42	20		350	39
3642			1.0	1.0	0	4.0	2	-2	-2	40	-2	-3	-3	6	2	2	-1	7					13	4	2	142	13	4	-1	142	35
3644			1.0	0	0	4.0	6	5	-2	37	-2	-3	-3	5	4	2	-1	21					11	6	1	126	15	5	-1	137	123
3650			3.0	3.0	0	4.0	37	33	7	75	1	0	-3	7	15	15	5	27					18	14	1	34	85	92	8	145	10
3660			3.0	2.0	1.0	6.0	22	21	10	33	-3	-3	-3	-3	12	12	6	21					10	10	4	14	63	68	23	89	5
3670			1.0	1.0	0	4.0	15	10	-2	50	-1	-3	-3	6	11	9	1	27					21	5	1	656	40	19	-1	203	53
3680							15	12	5	35					20	15	5	48					7	1	1	43	162	166	14	262	9
3681							15	12	5	35					20	15	5	48					7	1	1	43	162	166	14	262	9
3690							19	10	1	182					10	8	1	79					7	1	1	80	49	23	1	317	47
3691							19	10	1	182					10	8	1	79					7	1	1	80	49	23	1	317	47
3710							27	20	1	176					14	15	3	27					8	7	0	26	102	89	1	350	25
3711							27	20	1	176					14	15	3	27					8	7	0	26	102	89	1	350	25
3712							27	20	1	176					14	15	3	27					8	7	0	26	102	89	1	350	25
3713							27	20	1	176					14	15	3	27					8	7	0	26	102	89	1	350	25
3714							27	20	1	176					14	15	3	27					8	7	0	26	102	89	1	350	25
3715							27	20	1	176					14	15	3	27					8	7	0	26	102	89	1	350	25
3720			3.0	3.0	3.0	3.0	19	19	19	19					27	27	27	27					5	5	5	5	207	207	207	207	1
3721			3.0	3.0	3.0	3.0	19	19	19	19					27	27	27	27					5	5	5	5	207	207	207	207	1
3722			3.0	3.0	3.0	3.0	19	19	19	19					27	27	27	27					5	5	5	5	207	207	207	207	1
3723			3.0	3.0	3.0	3.0	19	19	19	19					27	27	27	27					5	5	5	5	207	207	207	207	1
3724			3.0	3.0	3.0	3.0	19	19	19	19					27	27	27	27					5	5	5	5	207	207	207	207	1
3725			3.0	3.0	3.0	3.0	19	19	19	19					27	27	27	27					5	5	5	5	207	207	207	207	1
3726			3.0	3.0	3.0	3.0	19	19	19	19					27	27	27	27					5	5	5	5	207	207	207	207	1
4010			4.0	5.0	4.0	6.0	14	15	10	17					31	31	23	37	4.45	4.45	4.15	4.75	19	18	11	27	398	402	381	414	5
4025			3.0	3.0	2.0	3.0	67	35	8	160					55	55	51	59					15	14	7	28	314	417	16	550	6
4030			3.0	3.0	1.0	19.0	249	257	41	413					37	36	9	74	3.23	3.57	2.43	3.70	134	101	2	1240	227	219	60	548	35
4040			7.0	7.0	7.0	7.0	247	247	247	247					25	25	25	25					55	55	55	55	130	130	130	130	1
4050			3.0	3.0	1.0	6.0	257	266	15	430					37	37	22	55	3.31	3.26	3.21	3.47	133	131	4	366	206	200	161	414	44
4090			3.0	4.0	1.0	5.0	201	210	39	310					28	22	18	82	2.50	2.51	2.48	2.52	97	87	26	200	136	133	112	180	12
4095			3.0	3.0	3.0	4.0	332	322	281	394	-3	-3	-3	-3	38	44	23	47					126	126	113	138	191	203	162	208	3
4900			7.0	6.0	3.0	24.0	38	27	-2	161	1	-3	-3	20	36	31	16	107					46	37	5	114	168	181	28	280	29
5000			5.0	5.0	3.0	7.0	73	62	60	201					37	36	35	47	3.41	3.43	2.49	4.31	98	74	52	376	271	274	225	284	13
5100			7.0	6.0	2.0	15.0	29	7	-2	126	21	-3	-3	280	35	29	18	129					51	44	11	107	220	225	79	506	42

CODE	AUMEAN	AUMED	AUMIN	AUMAX	HGMEAN	HGMED	HGMIN	HGMAX	PDMEAN	PDMED	PDMIN	PDMAX	PTMEAN	PTMED	PTMIN	PTMAX	N
3620	3.7	2.3	0.1	22.7	320	190	30	1740								0.0	45
4025	3.0	3.0	3.0	3.0					3.0	3.0	3.0	3.0	-5.0	-5.0	-5.0	-5.0	2
4030	20.0	20.0	20.0	20.0					0.1	-0.5	-0.5	3.0	10.1	0.2	-0.5	60.0	6
4050									-0.5	-0.5	-0.5	-0.5	1.0	1.0	1.0	1.0	1

Economic Geology
Vol. 93, 1998, pp. 1295–1306

Gravity, Magnetic and Radiometric Evidence for the Geological Setting of the Lady Loretta Pb-Zn-Ag Deposit—A Qualitative Appraisal

MARK L. DUFFETT[†,*]

Centre for Ore Deposit Research, University of Tasmania, Hobart, Tasmania 7001, Australia

Abstract

Semi-regional gravity, magnetic and radiometric data sets, augmented by a prospect-scale gravity survey, have been used to qualitatively assess the geological setting of the Lady Loretta Pb-Zn-Ag deposit. Regional gravity and magnetic fields are influenced chiefly by the Eastern Creek Volcanics and are sensitive to the thicknesses of overlying clastic and dolomitic sedimentary sequences, including the McNamara Group which hosts the mineralization. These are primarily controlled by Isan orogeny deformation, but a number of earlier structures are discernible. The most important of these postulated syndepositional structures are a west-northwest-oriented bounding fault extending from Lady Loretta to the Mount Gordon fault along the Redie Creek fault, and a possible sub-basin or zone of alteration beneath the Lady Loretta orebody, which manifests as a magnetic low.

Prospect-scale gravity data contain anomalies clearly associated with the mineralized strata at Lady Loretta. Contrasts between McNamara Group formations as well as older units are also apparent, reflecting differences in lithology or weathering characteristics. Higher Bouguer gravity signatures tend to be associated with the more dolomitic units.

The radiometric data set allows for the mapping of surface geochemical signatures that are sensitive to a number of geological parameters. These include sedimentological factors such as provenance, maturity, and proportion of argillaceous material, as well as chemical alteration. This variation occurs within as well as between mapped stratigraphic units, and is itself variable across the region. Potassium-channel signatures are an example of this, implying a general westerly decrease in argillaceous or feldspathic content within some formations. Some radiometrically distinct layers visible within sedimentary units appear to be absent at the equivalent stratigraphic level elsewhere. These observations may have implications for attempts to erect a regional sequence stratigraphic framework based on gamma ray logs from relatively few locations.

Introduction

GEOPHYSICAL METHODS can be applied to exploration for stratiform sediment-hosted base metal deposits at all scales, ranging from the identification of prospective rift/sag basin settings to direct detection of ore. Although genetic models for this type of base metal mineralization are still the subject of much debate (see for example, Table 1 of Eldridge et al., 1993; Perkins, 1995; Large et al., 1996; Hinman, 1996), most authors agree on the importance of understanding structures controlling basin evolution, deformation history, and mineralizing fluid pathways. By providing crucial three-dimensional perspective and regional scope, gravity, magnetic and radiometric methods can contribute significantly to determination of basin geometry, nature of sedimentary fill, and subsequent alteration and deformation (e.g., Leaman, 1991), in addition to detection of ore signatures at the prospect scale. This paper aims to demonstrate qualitative applications of these methods with reference to the geological setting of a particular deposit, Lady Loretta.

Lady Loretta is a stratiform sediment-hosted base metal deposit approximately 135 km north-northwest of Mount Isa. Most recently published reserves are 8.3 million metric tons (Mt) of massive sulfide ore at 8.5 percent Pb, 18.4 percent Zn and 125 g/t Ag (Hancock and Purvis, 1990). Geophysical methods (mainly induced polarization) have been applied to the prospect area since 1964, usually in efforts to discover additional copper resources to the nearby Lady Annie Cu deposit, known since before 1920 (Lewis, 1975). The Pb-Zn-Ag mineralization was discovered in 1969 by drilling on a soil geochemical anomaly (Cox and Curtis, 1977), although unpublished internal company reports, stored on-site, suggest induced polarization anomalies coincident with the Lady Loretta orebody were defined almost simultaneously. More recently, Anderson et al. (1993) reported results from a new airborne electromagnetic (EM) system flown over the deposit and surrounding areas, which appeared to map conductive strata effectively, although no signature unique to the location of known ore was apparent. A mining feasibility study is being conducted by the current owners of the prospect, Buka Minerals NL.

This paper describes preliminary results from studies of gravity, magnetic and radiometric data from the immediate area and broader setting of Lady Loretta, which were undertaken with the goal of better defining the evolution and deformation history of the host basin. Qualitative interpretations of regional data sets are presented, along with an assessment of additional gravity data acquired at closer spacing around the deposit.

Regional Geology

The Lady Loretta mineralization lies near the western edge of the exposed Mount Isa inlier (reinterpreted in terms of a basin by McConachie et al., 1993), within a structural domain defined by McConachie et al. (1993) as the Riversleigh fold zone (Fig. 1). The Riversleigh fold zone largely corresponds to the area widely known (e.g., Blake and Stewart, 1992) as

† Email: duffettm@gis.ntu.edu.au
* Present address: Faculty of Science, Northern Territory University, Darwin, NT 0909, Australia.

0361-0128/98/2028/1295-12$6.00

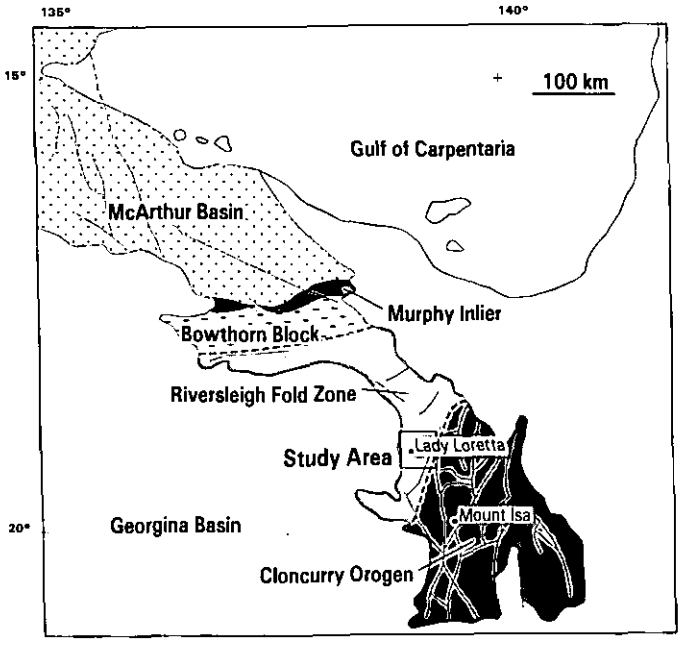

FIG. 1. Major subdivisions of the outcropping Mount Isa basin, after McConachie et al. (1993).

the Lawn Hill platform, while the "Cloncurry Orogen" depicted on Figure 1, also after McConachie et al. (1993), is a more highly deformed region encompassing all other tectonic sub-units of the Mount Isa inlier east of the Mount Gordon fault.

The oldest rocks exposed in the study area (Figs. 1, 2, Table 1) are those of the Haslingden Group, comprising thick basal quartzite (Leander Quartzite), voluminous mafic volcanics (Eastern Creek Volcanics), and predominantly siliciclastic sediments (Myally Subgroup). The Eastern Creek Volcanics, the maximum measured thickness of which exceeds 7 km (Blake and Stewart, 1992), have been subdivided into three members: the Cromwell metabasalt and Pickwick metabasalt, separated by hundreds of meters of siliciclastic sediments (Lena Quartzite Member). Both volcanic members have compositions similar to those of continental tholeiites (Wilson et al., 1985). A number of sandstone beds are also intercalated within the volcanic members, particularly towards the top of the Pickwick metabasalt, but these are not volumetrically significant. There is some persistence of mafic volcanic rocks into the overlying siliciclastic Myally Subgroup.

The base of the Haslingden Group is thought to mark the onset of an episode of east-west extensional rifting, with a renewed phase of rifting resulting from north-south extension

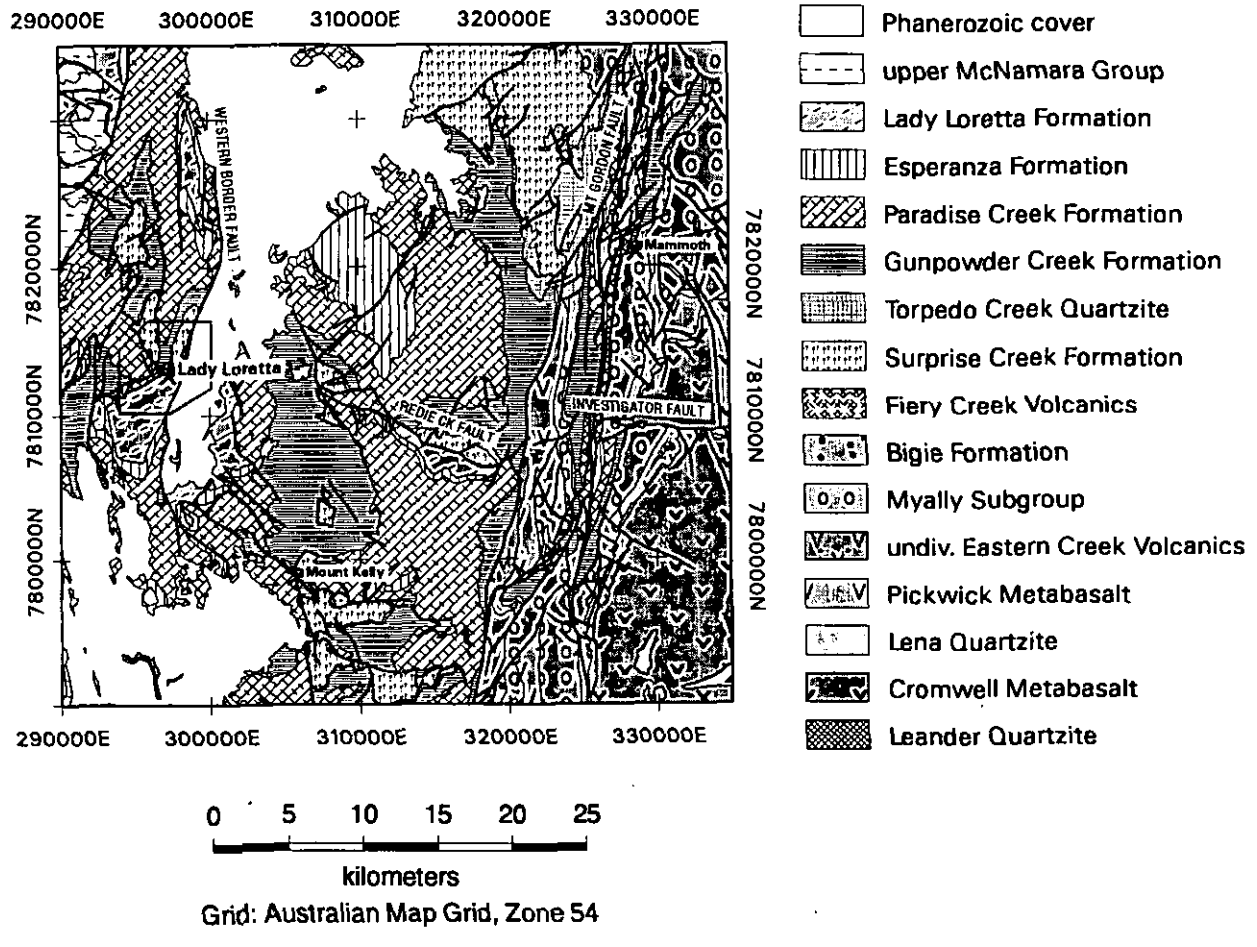

FIG. 2. Geology of the Lady Loretta region, modified after Hutton et al. (1985). See text for more detailed description of units. Boxed area is that depicted in Figures 4a and b.

TABLE 1. Unit Descriptions

Phanerozoic (Cenozoic, Mesozoic, Cambrian)	Siltstone, conglomerate, sandstone, limestone, phosphorite, colluvium, black soil, duricrust
McNamara Group	
Riversleigh Siltstone	Fine siltstone, shale; thin coarse siltstone interbeds
Shady Bore Quartzite	Orthoquartzite; fine sandstone and siltstone interbeds
Lady Loretta Formation	Dolomite, dolomitic siltstone, limestone, carbonaceous and sulfidic shale
Esperanza Formation	Chert, dolomite, siliceous and dolomitic siltstone
Paradise Creek Formation	Dolomite, dolomitic siltstone, minor tuff
Gunpowder Creek Formation	Siltstone, dolomitic and carbonaceous siltstone, fine sandstone, feldspathic and pyritic quartzite
Torpedo Creek Quartzite	Medium orthoquartzite, conglomerate
Surprise Creek Formation	Siltstone, feldspathic sandstone, quartzite
Fiery Creek Volcanics	Rhyolite, agglomerate, basalt and trachybasalt
Bigie Formation	Feldspathic and lithic sandstone, pebbly sandstone
Haslingden Group	
Myally Subgroup	Feldspathic quartzite and sandstone, dolomitic siltstone
Eastern Creek Volcanics (Pickwick metabasalt, Lena Quartzite, Cromwell metabasalt)	Metabasalt, feldspathic quartzite, orthoquartzite
Leander Quartzite	Orthoquartzite, feldspathic quartzite

commencing with the Pickwick metabasalt and extending through to near the top of the Myally Subgroup (O'Dea et al. 1997). The Haslingden Group was deposited between 1790 ± 10/8 Ma and 1737 ± 15 Ma (Page, 1983). All Haslingden Group units are intruded by dolerite dikes and sills of undetermined age. A subsequent sag phase unit, the dolomitic-arenaceous Quilalar Formation, was apparently either completely eroded or never deposited in the Lady Loretta region.

Onset of another rift-sag cycle is recorded by deposition of the Bigie Formation, a redbed conglomerate and sandstone sequence. It is overlain conformably by the bimodal, intensely altered Fiery Creek Volcanics, which have been dated by R. Page at 1709 ± 3 Ma (written commun. quoted in Betts et al., 1996). Post-rift sedimentation resulted in deposition of the fining-upward siliciclastic Surprise Creek Formation over the Fiery Creek Volcanics disconformably or with slight angular unconformity (Derrick et al., 1980). Betts et al. (1996) judged this contact to be conformable at the Fiery Creek Dome, north of Lady Loretta, but this is inconsistent with pre-Surprise Creek Formation weathering of Fiery Creek Volcanics observed in the same area by McPherson (1994). Another unconformity separates the Surprise Creek Formation from the basal formation of the McNamara Group: the Torpedo Creek Quartzite (Hutton et al., 1981); however, this is claimed to be a conformable contact by Betts et al. (1996), who consider the Torpedo Creek Quartzite an upper member of the Surprise Creek Formation.

The sag phase of the rift-sag cycle continued with deposition of the McNamara Group, a sedimentary sequence dominated by varying proportions of carbonate and fine-grained clastic rocks. Broadly speaking, dolomite increases with stratigraphic level at the expense of the siliciclastic component, with siltstone and sandstone dominant overall in the Torpedo Creek Quartzite and Gunpowder Creek Formation giving way to dolomites and dolomitic shales in the overlying Paradise Creek, Esperanza, and Lady Loretta Formations. The Lady Loretta Formation is host to the Lady Loretta Pb-Zn-Ag mineralization. Renewed clastic sedimentation is recorded by subsequent McNamara Group formations outcropping in the area; the Shady Bore Quartzite and the Riversleigh Siltstone. The depositional age of the McNamara Group is constrained by a Paradise Creek Formation zircon-bearing tuff dated at 1653 Ma by Page et al. (1994a), and a similar tuff in the Lawn Hill Formation (Upper McNamara Group; host to the Century Zn-Pb deposit) with an age of 1595 ± 6 Ma (Page et al., 1994b).

At least three post-McNamara Group regional deformation events have been recognized by previous workers in the Mount Isa Basin. D_1 has been interpreted as extensive north-to-south-directed thrusting (Bell, 1983). D_2 accompanied peak regional metamorphism (lower to sub-greenschist facies in this region), and caused major tight to open, upright, gently north- or south-plunging folds. The D_3 event is predominantly strike-slip faulting as a result of brittle style sub-east-west compression (Richard Keele, written commun., 1995). The Mount Gordon fault (separating the Riversleigh fold zone from the Cloncurry orogen to the east) is a typical D_3 fault; whilst its total magnitude of displacement is unknown, similar faults in the Mount Isa basin record strike-slip displacements of many kilometers.

Prospect Geology

A local stratigraphic subdivision within the Lady Loretta Formation has been established and refined by previous workers on the deposit (Hancock and Purvis, 1990, and associated references). Siderite, massive pyrite, and carbonaceous shale-bearing units, as well as the ore sequence itself, are of particular geophysical interest due to high density and or electrical conductivity. Sulfides constitute over 75 percent of the ore beds, comprising finely banded sphalerite, galena, and pyrite, and up to 90 percent of the pyritic unit immediately stratigraphically below the ore (Fig. 5; Hancock and Purvis, 1990). Carr (1984) also recorded significant proportions of pyrite (up to over 50%) extending farther into both the footwall and hanging-wall calcareous fine-grained siliciclastic sequences. The ore sequence contains a barite-chert Zn-rich, Pb-poor facies, mainly confined to the northeastern edge of the orebody. Further details may be found in Hancock and Purvis (1990) and Carr (1981).

Economic mineralization at Lady Loretta is confined to the limbs and keel of a syncline, locally known as the "Small syncline" (Fig. 4a). Plunge is gently to the southwest in the northern part of the syncline, but to the northeast in the southern part, imparting an overall rough canoe-shape to the orebody such that depth of the ore sequence nowhere exceeds 500 m. The stratigraphic equivalent of the ore sequence can be traced within another, north-plunging syncline immediately to the southwest ("Big syncline"), but the original geometric relationship between the two synclines, now

separated by the north-south-trending Syncline Dividing fault, is not clear. The Big syncline equivalent of the ore sequence is dominantly pyritic, with only minor base metal mineralization present (Hancock and Purvis, 1990).

The Lady Loretta deposit lies near the convergence of a number of significant structures, at least some of which appear from geological survey (Fig. 2; Hutton et al., 1985) and local prospect mapping (Hancock and Purvis, 1990) to have been reactivated a number of times during the structural history (Richard Keele, written commun., 1995). The ore sequence is truncated to the northwest by the northeast-trending Carlton fault zone (Fig. 4a), which juxtaposes older basin units to the north against the Lady Loretta Formation to the south (Figs. 2, 4a). The Carlton fault swings into convergence with the north-northeast-trending Western Border fault, which truncates Phanerozoic (Cambrian and Mesozoic) cover rocks 1.5 km east of the deposit (Figs. 2, 4a). A few hundred meters north of the deposit, the arcuate Leopard fault defines the southern boundary of two blocks of Surprise Creek Formation, implying over a kilometer of apparent vertical displacement. The Leopard fault has been identified as a growth fault during deposition of the upper Surprise Creek Formation and Lower McNamara Group (Richard Keele, writ. commun., 1995), but no sedimentological evidence for growth faulting during deposition of the Lady Loretta ore sequence has been found. Carr (1981) proposed the Carlton fault as the source conduit for Pb-Zn mineralizing fluids, but this has not been borne out by later work (Aheimer, 1994).

Data Sources

Gravity data have been acquired at two scales, the first at 1-km spacing on vehicular tracks within 30 km of Lady Loretta (Fig. 3), and the second at approximately 250 m spacing in a 6×5 km area including the deposit (Fig. 4b). Height control for the latter survey was mainly from spot heights on detailed topographic maps derived from controlled photogrammetry, as well as surveyed trigonometric points and drill collars, with independent control from a pair of microbarometers. Accuracy of heights for the prospect-scale survey is hence estimated at 1.5 m, while many stations will be of substantially better accuracy than this. Overall accuracy for the local survey is estimated at 0.25 mgal.

Elevation determinations for the semi-regional survey were chiefly derived from loop traverses with three microbarometers, utilizing the methods of Leaman (1984) and absolute height controls from state permanent marks, bench marks, and spot heights wherever practicable. Horizontal positions were determined with the aid of a hand-held Global Positioning System (GPS) unit. The resulting uncertainty in absolute Bouguer gravity values for this survey is estimated not to exceed 0.5 mgal. All prospect-scale gravity data were fully terrain-corrected out to a radius of 21 km, as well as the semi-regional traverse data wherever the terrain effect was judged likely to exceed 0.05 mgals. These data have been merged with regional Geological Survey of Queensland 1-km-spaced traverse and Australian Geological Survey Organisation

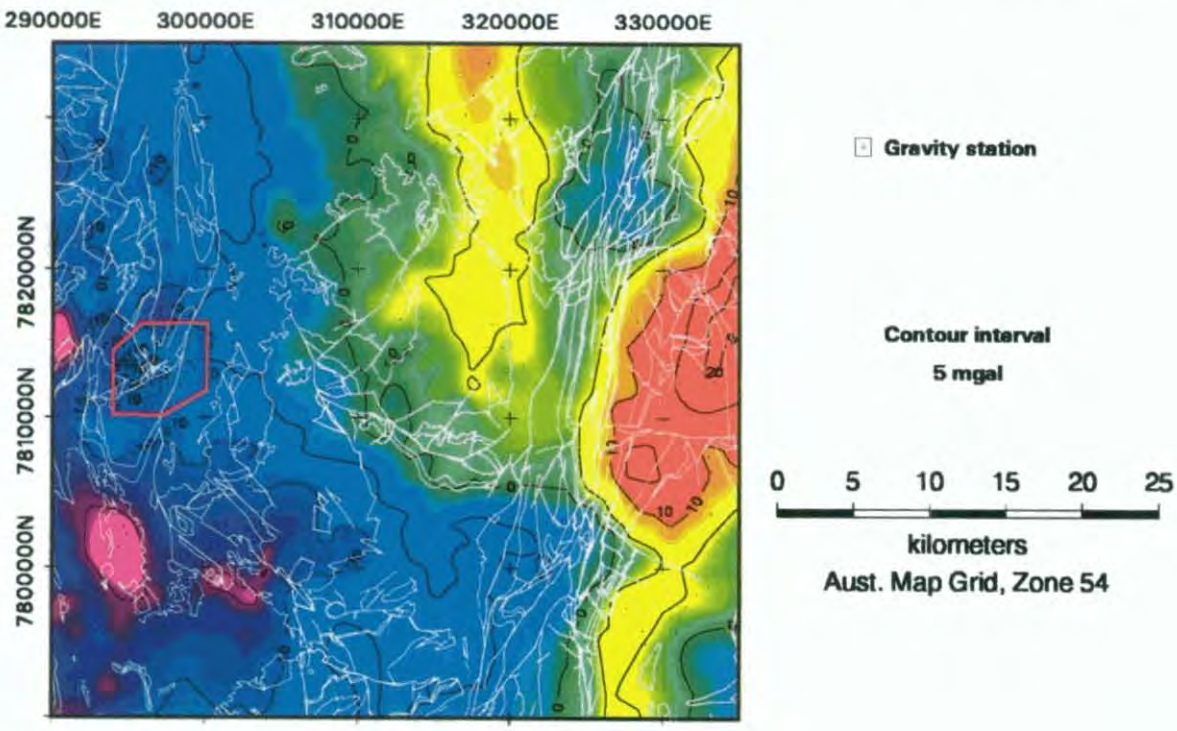

FIG. 3. Regional Bouguer gravity pseudocolor image; red = high, purple = low, contour lines in black. Bouguer reduction and terrain-correction density 2.67 t/m^3. Simplified geological outlines and faults in white. Boxed area is that depicted in Figure 4a and b.

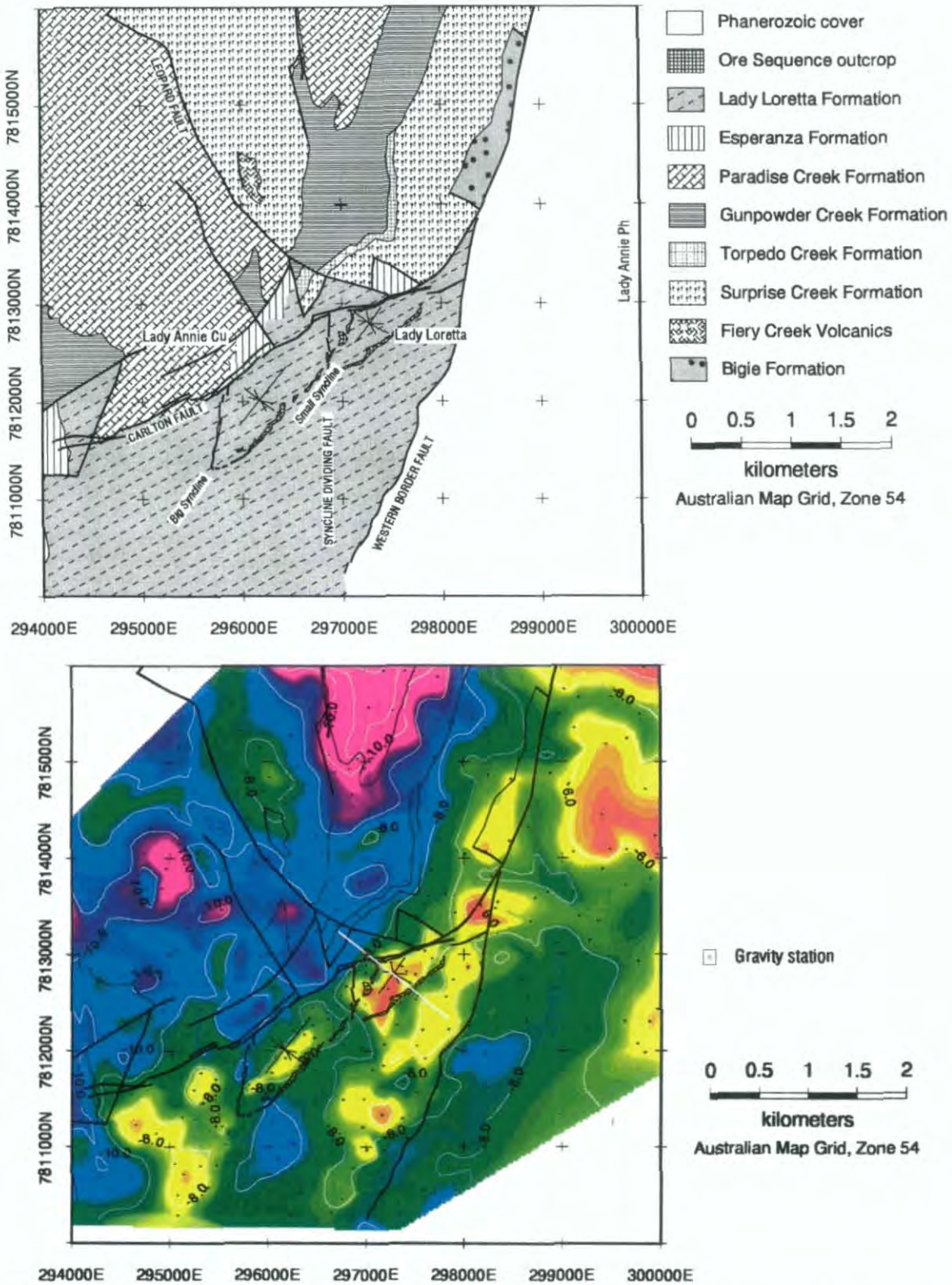

FIG. 4. a. Prospect-scale geology, modified after Hutton et al. (1985) and unpublished company mapping. "Ore Sequence outcrop" denotes surface exposures of the Lady Loretta stratiform ore and equivalents. b. Prospect-scale Bouguer gravity. Bouguer reduction and terrain-correction density 2.67 t/m^3. Image is a residual after subtraction of a fifth-order polynomial surface. Contours (white) 1 mgal apart are of the raw data. Geological linework overlay in black; thick lines are faults, thin lines stratigraphic contacts. Thicker white line indicates position of cross section (approximately mine section 2300 N) depicted in Figure 5.

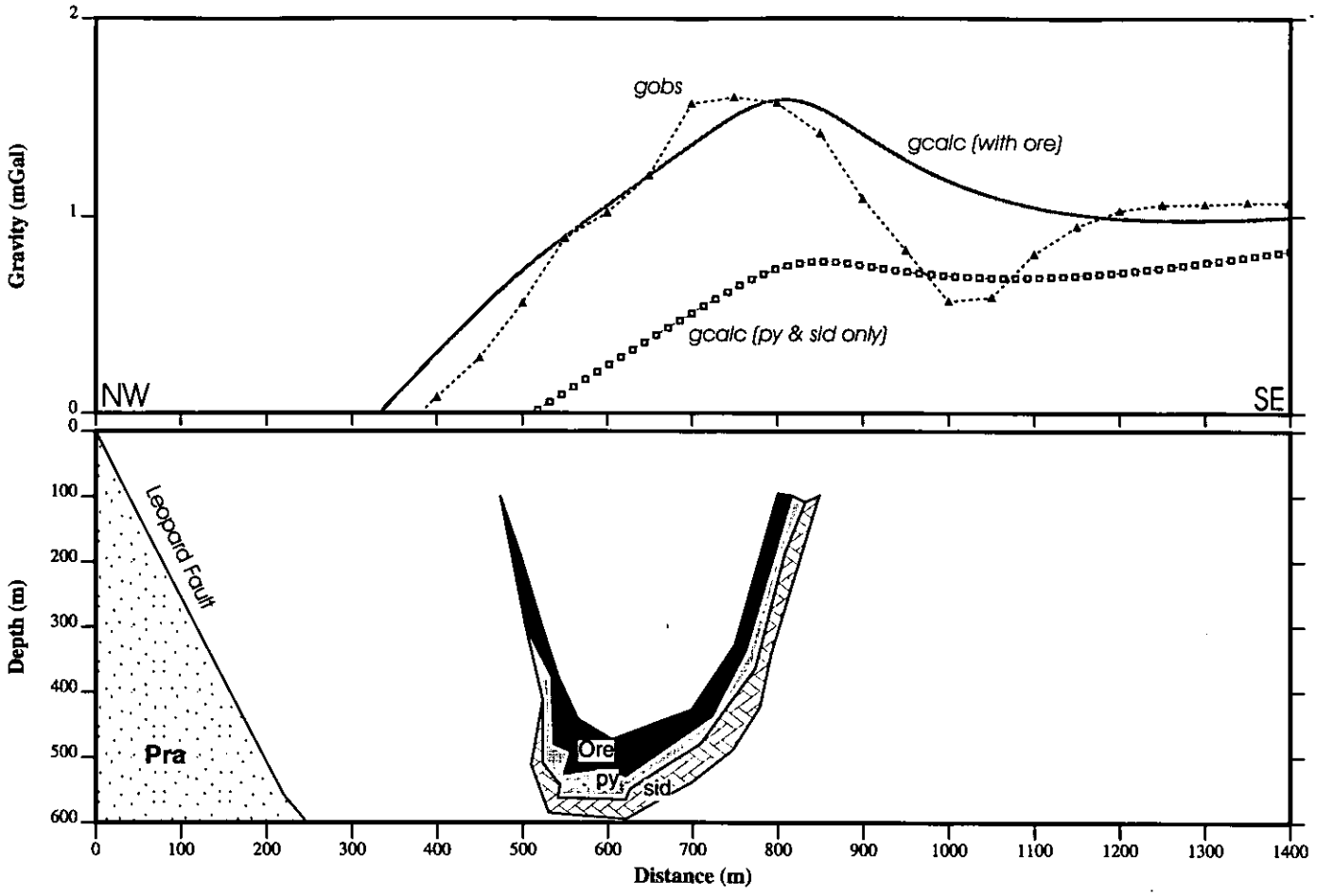

FIG. 5. Forward two-dimensional gravity model cross section, Lady Loretta Small syncline, looking northeast. Ore = galena-sphalerite ore (density 4.0 t/m³), py = pyritic unit (density 3.5 t/m³), sid = sideritic unit (density 3.45 t/m³). Background density 2.75 t/m³. Smooth line (gcalc with ore) is calculated Bouguer anomaly arising from all elements of the mineralized system; boxed line (gcalc, py and sid only) is the calculated signature in the absence of Pb-Zn ore; "gobs" (triangles and dashes) is observed Bouguer anomaly. "Pra" denotes low-density (2.63 t/m³) sandstones of the Surprise Creek Formation. Geology from mine section 2300 N, after fig. 3 of Hancock and Purvis (1990).

reconnaissance data, as well as a limited number of stations acquired by mineral exploration companies. The principal source for airborne magnetic (Fig. 6) and four-channel (potassium-uranium-thorium + total-count) radiometric data (Fig. 7) displayed in this paper is a survey flown by Geoterrex for Ashton Mining in 1987 (Queensland Dept. of Mines and Energy open file report CR18153B; Keith Jones, writ. commun., 1995). Flight lines were oriented north-south, with a nominal spacing of 250 m and terrain clearance 80 m. The data presented in the images (Figs. 6, 7) have been resampled to a 50 m by 50 m grid cell size by Ashton Mining.

Rock Properties

Published petrophysical data from rocks of the Lady Loretta region are scarce; however, large data sets (Young, 1984; Fallon and Busuttil, 1992) are available from correlative units in the vicinity of the Mount Isa Cu-Pb-Zn mine some 130 km to the south-southeast. These, together with data from a province-wide study by Hone et al. (1987), new Lady Loretta region data from the author's unpublished data, and bulk properties inferred by Leaman (1991) are summarized in Table 2. Density values given are broad, probable bulk wet specific gravity ranges for unweathered, typical samples of the formations listed; full statistical analysis of the most recent work being not yet completed. For all units except the Cambrian sediments and the Myally Subgroup to Surprise Creek Formation inclusive, the values given in Table 2 are based on at least 10 (usually many more) measurements of drill core samples. In the case where units have not been adequately characterized by previous interpretations (Leaman, 1991) or directly measured data on fresh samples, and for all radiometric signatures, the qualitative interpretation has assumed likely properties inferred from lithological and petrological descriptions.

Gravity

On regional compilations of the Bouguer gravity anomaly (e.g., Wellman, 1992), the Mount Isa inlier can be discerned as a series of sublongitudinal, gently arcuate belts of alternating highs and lows, superimposed on a general regional high. The arcuate belts roughly correspond to major geological divisions defined from surface mapping. The Lady Loretta

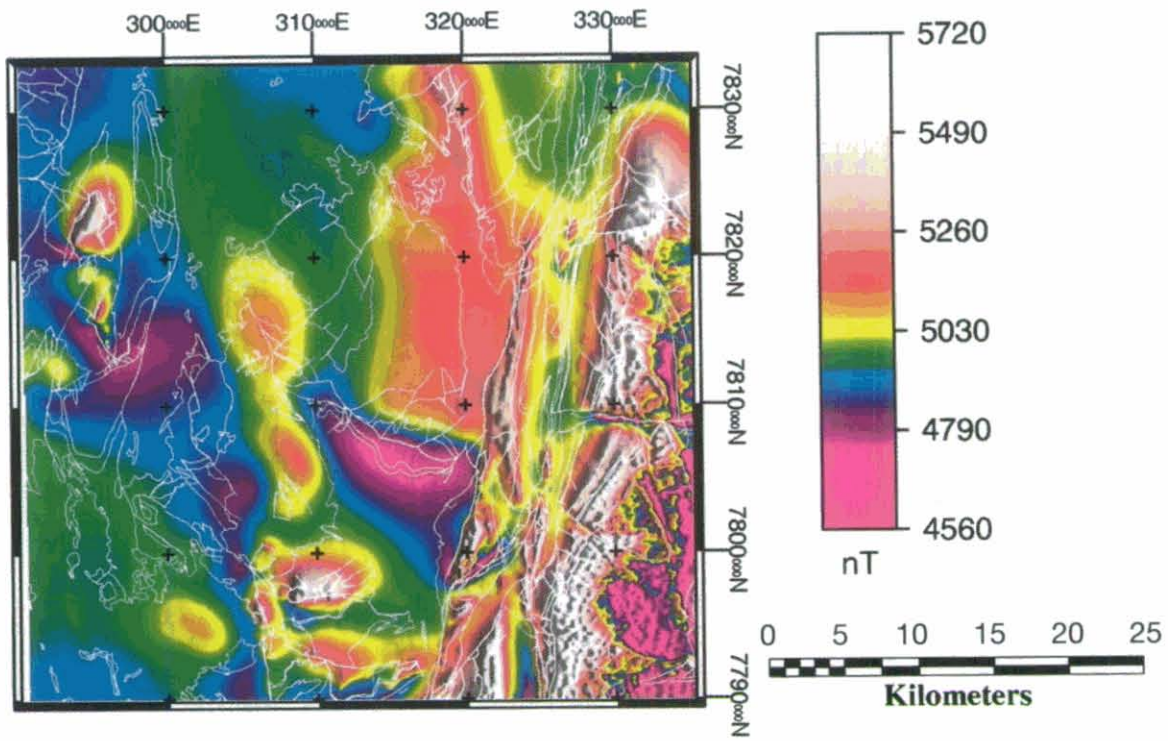

FIG. 6. Total magnetic intensity pseudocolor image. Intensity overlay simulates illumination from the east. Geological linework in white.

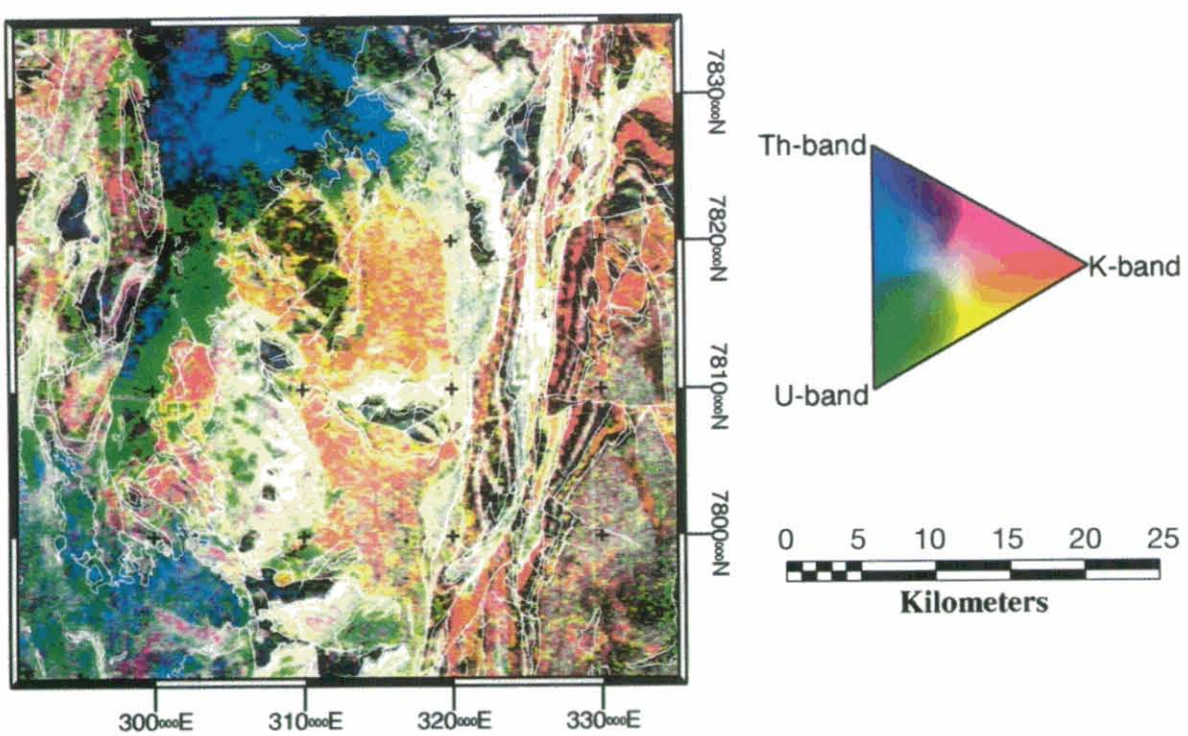

FIG. 7. Radiometric image. Geological linework in white.

TABLE 2. Physical Properties, Lady Loretta Region

Unit	Density t/m³	Susceptibility SI × 10³
Cambrian sediments	2.52–2.66	0.05
Lady Loretta Formation	2.75–2.78	0.45
Esperanza Formation	2.65–2.69	0.10
Paradise Creek Formation	2.70–2.76	0.10
Gunpowder Creek Formation	2.67–2.74	0.30
Torpedo Creek Quartzite	2.64–2.66	0.05
Surprise Creek Formation	2.60–2.65	0.10
Fiery Creek Volcanics	2.62–2.72	0.50
Bigie Formation	2.57–2.62	0.12
Myally Subgroup	2.61–2.65	0.10
Eastern Creek Volcanics	2.85–2.91	50–80

region lies astride the edge of the westernmost of these belts; the gravity field here (Fig. 3) decreases gently westward toward the edge of the inlier. Superimposed on this regional gradient is a gravity high east of the Mount Gordon fault zone associated with exposure of the Eastern Creek Volcanics, and a low west of Lady Loretta caused by Paleozoic and, probably, Neoproterozoic sediments of the Georgina basin. The highest Bouguer gravity values are observed north of the east-west-trending Investigator fault, implying an apparent thicker accumulation of Eastern Creek Volcanics here compared to the rest of the area east of the Mount Gordon fault zone ("Leichhardt Rift" of O'Dea et al., 1997). Much Bouguer anomaly character in areas of McNamara Group outcrop is interpretable in terms of an inverse relationship with preserved thickness of McNamara Group, Surprise Creek Formation and Myally subgroup metasediments overlying the dense Eastern Creek Volcanics. This is, in turn, primarily controlled by north-south-trending D_2 fold structures formed during the Isan orogeny; thus the linear gravity high splaying north away from the Mount Gordon fault zone is interpreted as an anticline bringing the Eastern Creek Volcanics near to the surface.

However, more subtle effects can also be interpreted from sequences within the McNamara Group on close inspection. A gross fining-upward trend, in conjunction with an increasing proportion of dolomitic sediments, leads to implied increased density values in the McNamara Group from the Torpedo Creek Quartzite to the Lady Loretta Formation, partly offsetting the effect of increasing vertical distance from the Eastern Creek Volcanics.

There are suggestions of east-west to west-northwest and sub-northeast trends offsetting the major north-south structures. The west-northwest-trending low passing through the Lady Loretta and Lady Annie deposits and continuing south of the west-northwest-trending Redie Creek fault (GR 315000E 7808000N) may be a manifestation of thicker McNamara Group sediments filling the "Paradise Graben" of Dunnet (1976). This trend has also been noted as a regional axis defining a change in fold plunge direction by R. Keele (writ. commun., 1995). Alternatively, the thicker development of McNamara Group may simply be an artifact of basin inversion geometry, in which case the (half) graben would have been located north of the Redie Creek fault.

Prospect Gravity

In the Lady Loretta area (Fig. 4b), variations within McNamara Group sequences are more apparent. The most prominent structure is coincident with the western end of the mapped Carlton fault, but diverges along or, more precisely, beneath the Gunpowder Creek Formation/Surprise Creek Formation unconformity north of the deposit. Another structure mapped as a major fault, the Western Border fault, has a more subdued expression. This makes significant vertical displacement on the fault appear unlikely, though large strike-slip displacement is not precluded (cf. Van Dijk, 1991). Lowest Bouguer values are associated with the Paradise Creek Formation, while the highest are associated with outcrops of Lady Loretta Formation both south of the Carlton fault, and inferred beneath Cambrian cover east of the Western Border fault. The more siliciclastic and hence less dense units—Torpedo Creek Quartzite, Surprise Creek Formation, and Bigie Formation, paradoxically are also associated with relatively high Bouguer values, reflecting the lower structural level exposed. This is especially apparent across the arcuate west-northwest- to north-northwest-trending Leopard fault, which juxtaposes a block of Surprise Creek Formation (Bouguer high) against Paradise Creek Formation (irregular but generally lower Bouguer values) northwest of Lady Loretta.

Subtle character within formations may be partially due to differential weathering of various lithologies. An example of this is a shallow (amplitude approximately 1 mgal) gravity low at GR 294800 7812800, immediately west of the Lady Annie Cu deposit, which is the position of the "Mount Lorrie Deep Weathering Trough," defined by drilling as a zone of deep oxidation extending below 320 m depth (Lewis, 1975). Exploration drilling (unpub. company data held on-site) demonstrates that depth of weathering, though variable, frequently exceeds 100 m in this region; deepest oxidation usually being associated with faults.

The Lady Loretta mineralization is evident as a high of about 1 mgal amplitude, spatially associated with the keel of the Small syncline (Fig. 4b). Pb-Zn ore, with a bulk density (dry) of 4.0 ± 0.5 t/m³ (average based on an unspecified number—probably hundreds—of samples, R.A. Rivera and A. Challis, 1972; Placer Prospecting Ltd. unpub. data) is at least partially responsible for the anomaly, though massive pyrite above and below the ore sequence, barite within the ore sequence, especially near the surface, and the sideritic halo are all likely to be significant additional contributors (Fig. 5). A weaker gravity high over the axis of the Big syncline (GR 296200 7812000), deeper than the keel of the Small syncline, is also interpreted as being due to pyrite and siderite in and surrounding the correlative ore sequence. As the Big and Small synclines have similar geometries, and the sulfidic ore sequence is known to be present in the Big syncline, it is reasonable to propose that the increased intensity of the anomaly (implying greater excess mass) in the Small syncline is due wholly to the presence of galena-rich ore. A gravity forward model based on a published cross section of the ore deposit (Fig. 5) supports this contention, as the anomaly calculated for the mineralized system is up to a factor of two greater in amplitude (and matches the observed data better)

with Pb-Zn ore present than for the associated pyrite and siderite alone. The slight discrepancy between observed data and the calculated signature of the preferred model in the footwall on the southeastern limb of the syncline may be due to anomalously intense and deep weathering of sulfide minerals in this area.

An irregularly developed north-northeast-trending linear feature between the orebody and the Western Border fault occurs over outcropping Lady Loretta Formation hundreds of meters stratigraphically below the ore sequence. Evidently untested by drilling, it may denote another horizon of anomalous mineralization (sulfide and or siderite), but is more likely to arise from a more dolomite-rich or weathering-resistant facies of the Lady Loretta Formation, based on considerations of surface dips, anomaly amplitude, and anomaly wavelength. The latter option is preferred because any stratiform sulfide body of sufficient grade and dimensions to give rise to the observed anomaly should possess some surface indications, whether geological or geochemical, given the steep (>60°) dips and consistent northeast to north-northeast strikes observed from outcrops in the corresponding area.

Magnetics

The aeromagnetic data (Fig. 6) are very effective in mapping the Eastern Creek Volcanics both in outcrop and subcrop as well as beneath the Mount Isa basin sediments. Within the Eastern Creek Volcanics, the Pickwick metabasalt appears less magnetic than the thicker mafic member beneath it (Cromwell metabasalt). Caution must be exercised, however, in interpreting these units as coherent magnetic entities, as magnetite abundance in the Eastern Creek Volcanics appears largely controlled by alteration systems (Wyborn, 1987). Clear alteration effects can be observed along many faults cutting the Eastern Creek Volcanics, both as magnetic highs (magnetite productive) and lows (magnetite destructive).

Remanent magnetization is dominant over induced magnetization by a factor (Koenigsberger ratio) of around 20 in this region, but the highly variable directions of the remanent magnetization on scales from tens to a hundred meters tend to cancel out at aeromagnetic survey altitudes (Clark, 1980). The high frequency variations in remanent magnetization direction possibly arise from a combination of lightning strikes, exposure effects during the Tertiary, and remanent magnetization directions acquired at different times, implying considerable heterogeneity in magnetic mineralogy within the Eastern Creek Volcanics (Clark, 1980). Some residual variability from this source may be responsible for the high frequency magnetic character observed over outcropping Eastern Creek Volcanics. No magnetic response is discernible either from the sediments (compare with Anderson et al., 1993) or the Fiery Creek Volcanics, though further processing and filtering may enable recognition of a magnetic signature from basalts contained in the latter (Betts et al., 1994), which field and hand specimen measurements show to have a susceptibility of around 1×10^{-3} SI.

As with the gravity, broad linear anomalies associated with north-south-trending uplifts correspond to anticlines mapped at the surface. These uplifts or domes may have been emplaced during D_1 north-south-directed thrusting (Van Dijk, 1991), or may be a simple consequence of D_2 east-west shortening. More intense, localized anomalies denote uplifts of possibly earlier origin in the vicinity of Redie Creek, Mount Kelly, and beneath outcrops of Surprise Creek Formation north of Lady Loretta. The largest magnetic anomaly in the Mount Kelly area (GR 310000E, 7798000N) surprisingly coincides with outcrops of Paradise Creek and Esperanza Formations. If this magnetic anomaly is wholly due to Eastern Creek Volcanics metabasalts, as has been assumed throughout this region, this implies that a great deal of the intervening sedimentary section (from Myally Subgroup to Gunpowder Creek Formation) is missing, having been removed structurally (by a fault dipping shallowly to the north), erosionally, or never deposited. The latter two possibilities would suggest that this area may have been on the uplifted footwall or flexural margin of a west-northwest-trending rift graben during deposition of the lower McNamara Group. This interpretation is supported by a radiometric signature distinctly lacking in potassium relative to Paradise Creek Formation outcrops elsewhere (see below), explicable as a near-absence of clastic sedimentation in this area.

A northeast-trending break in the magnetic field extending parallel with the Carlton fault from GR 290000E 7815000N toward the Mount Oxide Cu deposit 25 km north of Mammoth, with implied north-side-up displacement, corresponds to an extended version of a dextral "megashear/kink band" identified by Keele (writ. commun., 1995). A linear magnetic low superimposed on (or overprinted by) other structures links Lady Loretta with the Redie Creek and Investigator faults, corresponding to the gravity signature of the "Paradise Graben." An alternative or additional explanation for the magnetic low beneath and to the east of the Lady Loretta deposit is magnetite-destructive alteration of Eastern Creek Volcanics by hydrothermal fluids, as mapped on a wider scale in the footwall of the Mount Isa mine by Leaman (1991). This interpretation is supported by relatively very low magnetic susceptibilities (0.25×10^{-3} SI) measured on greenstones drilled from over 500 m depth, 1.5 km north of Lady Annie. It is interesting to note that the areal extents of the magnetic low at Lady Loretta and the magnetite-destructive alteration mapped by Leaman at Mount Isa (2–3 km^2 vs. 18–20 km^2) are in similar proportion to that of total amounts of Pb-Zn mineralization present at each deposit (~2.2 Mt combined Pb-Zn metal at Lady Loretta versus ~20 Mt estimated pre-mining combined Pb-Zn metal at Mount Isa, calculated from figures contained in Hancock and Purvis, 1990, and Forrestal, 1990). There is no direct ore response in the aeromagnetic data over Lady Loretta, which is consistent with the virtual absence of magnetite or pyrrhotite from the ore sequence and associated sulfides.

As at Mount Kelly, the presence of high-frequency, high-amplitude anomalies coincident with outcrops of the Surprise Creek Formation and Fiery Creek Volcanics north of Lady Loretta implies the presence of magnetic Eastern Creek Volcanics at relatively shallow depths (of the order of hundreds of meters) in these areas. The sedimentary section between the Myally Subgroup and Surprise Creek Formation, inclusively, is therefore interpreted to be greatly thinned in this region also, consistent with the area having been relatively high during the corresponding period of basin evolution.

Radiometrics

Radiometric data (Fig. 7) reveal many stratigraphic details not present in published geological mapping, as well as mapping intraformational variations in K, U, and Th abundance. K-enrichment of the Pickwick metabasalt is discernible near the Mammoth Cu mine, an alteration effect related by Wilson et al. (1985) to Cu removal from the Eastern Creek Volcanics, supporting the conclusion of Scott and Taylor (1982) that the Eastern Creek Volcanics were the source for the Mammoth Cu. K-enrichment of Eastern Creek Volcanics has also been linked to the passage of Pb-Zn mineralizing fluids (Wyborn, 1987). The Pickwick metabasalt also appears generally depleted in U and Th in comparison to the Cromwell metabasalt. Higher in the Haslingden Group, feldspathic sandstones are picked out by high K-channel counts, while micaceous and argillaceous strata are high in all three channels.

The Bigie Formation and—surprisingly, given the level of potassic alteration mapped elsewhere (Hutton and Wilson, 1984)—the Fiery Creek Volcanics appear to be generally low in all channels. Only one outcrop of Fiery Creek Volcanics is of sufficient extent in this area to have its radiometric signature mapped reliably, given the 50 × 50-m grid cell size, and here all channels are low, with the exception of a locally K- and U-enriched patch on the eastern side (GR 324000E 7835000N).

There is a striking contrast between the lower and upper members of the Surprise Creek Formation. Through most of the region, only the lower, arenaceous unit has been preserved/deposited, and outcrops of it display very little radiometric response. An exception is a small area at the eastern end of the Redie Creek fault, possibly reflecting an increased feldspathic, micaceous or heavy mineral detrital component sourced from the east (see below). The upper unit is strikingly high in all channels, consequent from its much more argillaceous composition. The radiometric signal tends to diminish in outcrops to the west due to increasing masking effects from Phanerozoic weathering and cover, or dilution by a mature, quartzose sedimentary source.

The Torpedo Creek Quartzite at the base of the McNamara Group is often too thin (<100 m) to be delineated by airborne radiometrics, especially where it directly overlies the compositionally similar arenaceous unit of the Surprise Creek Formation. Only where the argillaceous Surprise Creek Formation has been preserved beneath relatively flat-lying Torpedo Creek Quartzite can the Torpedo Creek Quartzite be clearly distinguished as a low-count, arenaceous unit.

The Gunpowder Creek Formation is one of the most radioactive of all outcropping units in this region, equaled only by the upper argillaceous/micaceous member of the Surprise Creek Formation. At least four members of the Gunpowder Creek Formation are discernible from the radiometric image. A thin, patchy basal member of low readings in all channels, albeit relatively Th-rich, soon gives way to high-count micaceous siltstones, sandstones, and carbonaceous shales. These diminish slightly near the middle of the formation, possibly resulting from an increase in proportion of carbonates, before increasing again at the top of the formation, interpreted to correspond to carbonaceous shales known to occur in this stratigraphic position (Hutton and Wilson, 1985).

Potassium dominates the radiometric signature of much of the Paradise Creek Formation in a relative sense, though this influence diminishes to the south and west. A number of factors could be responsible for the reduction in K relative to other radioelements, including variations in the proportion of tuffaceous input to sedimentation (Page, 1981), and reductions in total siliciclastic input, with a corresponding increase in dolomite content. Heterogeneity of radiometric signature is most clearly demonstrated north and south of the Redie Creek fault, an example being a low-K bed at the top of the formation (GR 313000E 7815000N) which has no counterpart below the Esperanza Formation south of the fault (GR 317000E 7804000N).

A potassium-rich horizon clearly marks the base of the Esperanza Formation, probably corresponding to the maximum flooding surface identified from gamma ray logging by Southgate et al. (1996). This signature is obscured, however, in areas where bedding is steeply inclined, thus restricting outcrop area. The remainder of the Esperanza Formation, on the other hand, is generally low in all channels. Thin, silty bands of high-K only become apparent where shallow dips enable apparent bed thicknesses to exceed sample spacing. A prominent exception to this generally low radioelement signature is the band of Esperanza Formation immediately south of the Redie Creek fault, where the basal K-rich horizon may be thicker.

The Lady Loretta Formation marks a return to the generally higher-count, more potassic signatures of the Paradise Creek Formation, though the Lady Loretta Formation is the most heterogeneous of all McNamara Group units. A distinct absence of potassium at the base possibly denotes the onset of a new depositional cycle. Resumption of shale- and siltstone-dominant deposition can be seen regionally in the red bands overlying the basal unit, but this facies is either obscured or absent in the Dayview or Debut syncline north of Lady Loretta (GR 299000E 7826000N). No distinct signature related to the Lady Loretta mineralization is manifest except for low counts in all channels in the vicinity of the Small and Big synclines, probably influenced by topography as well as geology, and a possible slight increase in counts through all three channels relative to other Lady Loretta Formation outcrops in the core of the greater Lady Loretta syncline (a megascopic manifestation of the Big syncline, located at GR 295600E 7810700N). A similar signature to the latter, though slightly more K-dominated, may be replicated in the Lady Loretta Formation abutting the Redie Creek fault.

Patches of high U-channel count within Phanerozoic cover west of Lady Loretta relate to uranium associated with major Cambrian accumulations of phosphate. Some extraction of these deposits has taken place intermittently over the last few decades at the Lady Annie Phosphate mine (labeled as "Lady Annie Ph" on Fig. 4a; not to be confused with the nearby Lady Annie Cu deposit).

All McNamara Group formations with the possible exception of the Gunpowder Creek Formation exhibit a distinct increase in K and Th from west to east, approaching the Mount Gordon fault, possibly reflecting increasing immaturity, tuffaceous input to sedimentation or proximity to a mixed felsic/mafic sediment source. These and other regional intraformational radiometric variabilities detailed above appear likely to

arise from sources other than eustatic sea-level changes. Possible pitfalls in attempts to construct a regional sequence stratigraphic framework based on gamma logs from a small number of locations (e.g., Southgate et al., 1996) may be indicated, in that gamma ray peaks and cycles present in some areas appear likely from the remotely sensed data to be subdued or completely absent in others. This problem, however, may represent an opportunity, in that remotely sensed radiometric data might be used to track at least the low frequency variations in gamma-ray signature across the entire outcrop area of the basin. Such data would assist in the correlation between detailed logging sites and, possibly, in defining areas of anomalous sub-basin development.

Conclusions

The gravity field in the region of Lady Loretta is primarily controlled by variations in both composition and geometry of the basement to the McNamara Group, with relative gravity lows generally corresponding to increases in preserved thickness of the McNamara Group. Variations on this general theme can be interpreted in terms of primary basin structures on a regional scale. An example of this is a possible west-northwest-trending paleo-graben bounded by the Redie Creek and Leopard faults, and adjacent to the Lady Loretta mineralization. Such putative basin development structures and later Isan orogeny overprints are difficult, however, to separate by qualitative inspection. Similar principles and limitations apply to the magnetic field, although its interpretation is better constrained by the assumption that the Eastern Creek Volcanics are the dominant magnetic unit, and constitute "magnetic basement" in this region. An uplifted footwall or flexural margin bounding a half-graben, which developed to the north during lower McNamara Group time, is implied by a magnetic high directly underlying Paradise Creek and Esperanza Formation in the Mount Kelly area.

Semidetailed gravity data centered on Lady Loretta clearly demonstrate a paradoxical positive Bouguer anomaly contrast between the Lady Loretta and Paradise Creek Formations, an effect opposite to that expected from the implied increased vertical depth to "basement" (Eastern Creek Volcanics). This may reflect a gross up-sequence change in McNamara Group lithology, with predominantly siliciclastic sedimentation giving way to denser dolomitic and shaly lithologies; structurally controlled variation in the lower siliciclastic units; or simply differential weathering. Prospect-scale gravity data demonstrate the possibility of detecting sediment-hosted Pb-Zn mineralization (Small syncline) within a dolomite/shale host, standing out above anomalies arising from other sulfidic/sideritic accumulations (Big syncline) and differential weathering.

Alteration types in the Eastern Creek Volcanics, possibly related to Pb-Zn and Cu mineralizing events, can be distinguished and mapped using a combination of aeromagnetic and radiometric data sets. Such a base metal-mobilizing alteration event signature may be present as a component of the magnetic low centered near the Lady Loretta mineralization. Variations in the broader magnetic signature of the Eastern Creek Volcanics may be ascribed to gross structural controls, namely dip and preserved thickness.

Radiometric data are clearly useful in this environment as a means of defining lithological changes within formations, as well as being an aid to general geological mapping. They are capable of discriminating quite subtle lithogeochemical differences, providing insights into the regional variations of sediment maturity, provenance, and carbonaceous content. As such, the broad spatial coverage of airborne radiometrics should be used wherever possible to complement attempts to erect a sequence stratigraphic framework using detailed gamma ray logging at few, widely spaced locations.

Acknowledgments

Stuart Bull, John Dunster, Richard Keele, and Lesley Wyborn are thanked for fruitful discussions and reviews, as is Peter McGoldrick, who suggested this paper. Provision of geophysical data by Bernie Stockill of the Geological Survey of Queensland, Keith Jones of Ashton Mining and CRA Exploration personnel is appreciated. Supply of digital geological data by the Australian Geological Survey Organisation is gratefully acknowledged. Michael Roach assisted with image processing. The paper was substantially improved by comments from Nick Sheard, Gary Fallon, and Pat Williams. This work is supported by an Australian Geological Survey Organisation Postgraduate Award, and received invaluable assistance from the former Pancontinental Mining Ltd. The Centre for Ore Deposit Research generously sponsored the color plates presented here. This research was supported by the Australian Research Council's Research Centres Program.

REFERENCES

Aheimer, M.A., 1994, Geology and geochemistry of the Lady Loretta SSH base metal deposit, northwest Queensland: Unpublished B.Sc. honors thesis, Hobart, University of Tasmania, Centre for Ore Deposit and Exploration Studies, 130 p.

Anderson, H.F., Duncan, A.C., and Lynch, S.M., 1993, Geological mapping capabilities of the QUESTEM airborne electromagnetic system for mineral exploration—Mt. Isa Inlier, Queensland: Exploration Geophysics, v. 24, p. 333–340.

Bell, T.H., 1983, Thrusting and duplex formation at Mount Isa, Queensland, Australia: Nature, v. 304, p. 493–497.

Betts, P.G., Jones, M., and Valenta, R.K., 1994, Utilisation of aeromagnetic data for structural analysis—the Fiery Creek Dome Region, Mt. Isa Inlier: 7th Australasian Remote Sensing Conference, Melbourne, March 1994, Proceedings, p. 33–38.

Betts, P., Pound, K., and Lister, G., 1996, Episodic rift-sag sequence in cover sequence three, northwestern Mount Isa Inlier [abs.]: Geological Society of Australia Abstracts, v. 41, p. 32.

Blake, D.H., and Stewart, A.J., 1992, Stratigraphic and tectonic framework, Mount Isa Inlier; in Stewart, A.J., and Blake, D.H., eds., Detailed studies of the Mount Isa Inlier: Australian Geological Survey Organisation Bulletin 243, p. 1–11.

Carr, G.R., 1981, The mineralogy, petrology and geochemistry of the zinc-lead-silver ores and their host sedimentary rocks at Lady Loretta, northwest Queensland: Unpublished Ph.D. thesis, University of Wollongong.

——1984, Primary geochemical and mineralogical dispersion in the vicinity of the Lady Loretta Zn-Pb-Ag deposit, NW Queensland: Journal of Geochemical Exploration, v. 22, p. 217–238.

Clark, D.A., 1980, Magnetic properties of rocks from the Mount Isa area: North Ryde, Australian Commonwealth Scientific and Industrial Research Organization (CSIRO) Division of Mineral Physics, Restricted Investigation Report 1149R, 20 p.

Cox, R., and Curtis, R., 1977, The discovery of the Lady Loretta zinc-lead-silver deposit, North-west Queensland; A geochemical exploration case history: Journal of Geochemical Exploration, v. 8, p. 189–202.

Derrick, G.M., Wilson, I.H., and Sweet, I.P., 1980, The Quilalar and Surprise Creek Formations—new Proterozoic units from the Mount Isa Inlier:

Their regional sedimentology and application to regional correlation: Bureau of Mineral Resources (BMR) Journal of Australian Geology and Geophysics, v. 5, p. 215–223.

Dunnet, D., 1976, Some aspects of the Panantarctic cratonic margin in Australia: Philosophical Transactions of the Royal Society of London, v. A280, p. 641–654.

Eldridge, C.S., Williams, N., and Walshe, J.L., 1993, Sulfur isotope variability in sediment-hosted massive sulfide deposits as determined using the ion microprobe SHRIMP: II. A study of the H.Y.C. deposit at McArthur River, Northern Territory, Australia: Economic Geology, v. 88, p. 1–26.

Fallon, G.N., and Busuttil, S., 1992, An appraisal of the geophysical effects of the Mount Isa ore bodies: Exploration Geophysics, v. 23, p. 133–140.

Forrestal, P.J., 1990, Mount Isa and Hilton silver-lead-zinc deposits: Australasian Institute of Mining and Metallurgy Monograph 14, p. 927–934.

Gulson, B.L., Perkins, W.G., and Mizon, K.J., 1983, Lead isotope studies bearing on the genesis of copper ore bodies at Mount Isa, Queensland: Economic Geology, v. 78, p. 1466–1504.

Hancock, M.C. and Purvis, A.H., 1990, Lady Loretta silver-lead-zinc deposit: Australasian Institute of Mining and Metallurgy Monograph 14, p. 943–948.

Hinman, M., 1996, Constraints, timing and processes of stratiform base metal mineralization at the HYC Ag-Pb-Zn deposit, McArthur River: James Cook University of North Queensland Economic Geology Research Unit Contribution 55, p. 56–59.

Hone, I.G., Carberry, V.P., and Reith, H.G., 1987, Physical property measurements on rock samples from the Mount Isa Inlier, northwest Queensland: Australia Bureau of Mineral Resources, Report 265, 30 p.

Hutton, L.J., and Wilson, I.H., 1984, Mount Oxide Region, Queensland—1:100,000 geological map commentary: Bureau of Mineral Resources, 27 p.

——1985, Mammoth Mines Region, Queensland—1:100,000 geological map commentary: Bureau of Mineral Resources, Australia.

Hutton, L.J., Cavaney, R.J., and Sweet, I.P., 1981, New and revised stratigraphic units, Lawn Hill platform, northwest Queensland: Queensland Government Mining Journal, v. 82, p. 423–434.

Hutton, L.J., Derrick, G.M., and Gallagher, J., 1985, Geology of the Mammoth Mines region: Geological map, Bureau of Mineral Resources, Australia, scale, 1:100,000.

Large, R., Bull, S., Cooke, D., and McGoldrick, P., 1996, Review of genetic models at HYC: constraints from new sedimentology, alteration halo studies and fluid chemical modelling: James Cook University of North Queensland Economic Geology Research Unit, Contribution 55, p. 72–74.

Leaman, D.E., 1984, Notes on microbarometer elevation determinations: Exploration Geophysics, v. 15, p. 53–59.

——1991, Geophysical constraints and alteration of the Eastern Creek Volcanics, Mt Isa, Queensland: Australian Journal of Earth Sciences, v. 38, p. 457–472.

Lewis, R.W., 1975, Lady Annie secondary copper deposit, in Knight, C.L., ed., Economic geology of Australia and Papua New Guinea; 1, Metals: Australasian Institute of Mining and Metallurgy, Monograph 5, p. 1023–1033.

McConachie, B.A., Barlow, M.G., Dunster, J.N., Meaney, R.A., and Schaap, A.D., 1993, The Mount Isa Basin—definition, structure and petroleum geology: Australian Petroleum Exploration Association (APEA) Journal, v. 33, p. 237–257.

McPherson, A.L., 1994, Volcanology and sedimentology of the Palaeoproterozoic Fiery Creek Volcanics and adjacent units, northwest Queensland: Unpublished B.Sc. honors thesis, University of Tasmania, 123 p.

O'Dea, M.G., Lister, G.S., MacCready, T., Betts, P.G., Oliver, N.H.S., Pound, K.S., Huang, W., and Valenta, R.K., 1997, Geodynamic evolution of the Proterozoic Mount Isa terrain, *in* Burg, J.P., and Ford, M., eds., Orogeny through time: Geological Society Special Publication 121, p. 99–122.

Page, R.W., 1981, Depositional ages of the stratiform base metal deposits at Mount Isa and McArthur River, Australia, based on U-Pb zircon dating of concordant tuff horizons: Economic Geology, v. 76, p. 648–658.

——1983, Timing of superposed volcanism in the Proterozoic Mount Isa Inlier, Australia: Precambrian Research, v. 21, p. 223–245.

Page, R.W., Sun, S., and Carr, G., 1994a, Proterozoic sediment-hosted lead-zinc-silver deposits in northern Australia—U-Pb zircon and Pb isotope studies [abs]: Geological Society of Australia Abstracts, v. 37, p. 334–335.

——1994b, U-Pb zircon and Pb isotope studies in relation to Proterozoic sediment-hosted lead-zinc-silver deposits in northern Australia [abs]: *in* Lanphere, M.A., Dalrymple G.B., and Turrin, B.D., eds., Abstracts of the Eighth International Conference on Geochronology, Cosmochronology and Isotope Geology: U.S. Geological Survey Circular 1107, p. 240.

Perkins, W.G., 1995, Features of the Mount Isa Cu-Pb-Zn deposit and comparison with Hilton, McArthur River and Mount Novit: Evidence for a late syndeformational replacement origin?: Metallogeny of Proterozoic Basins: University of British Columbia, Vancouver Mineral Deposit Research Unit, May, 1995, Short Course Notes, v. 19.

Scott, K.M., and Taylor, G.F., 1982, Eastern Creek Volcanics as the source of copper at the Mammoth mine, northwest Queensland: Bureau of Mineral Resources (BMR) Journal of Australian Geology and Geophysics, v. 7, p. 93–98.

Southgate, P.N., Bradshaw, B.E., Jackson, M.J., Krassay, A.A., McConachie, B.A., Scott, D.L., and Wells, A.T., 1996, Integrated Proterozoic basin analysis: constructing a regional structural and sequence stratigraphic framework for northern Australia: James Cook University of North Queensland Economic Geology Research Unit Contribution, 55, p. 132–136.

Van Dijk, P.M., 1991, Regional syndeformational copper mineralization in the western Mount Isa Block, Australia: Economic Geology, v. 86, p. 278–301.

Wellman, P., 1992, Structure of the Mount Isa region inferred from gravity and magnetic anomalies: Exploration Geophysics, v. 23, p. 417–422.

Wilson, I.H., Derrick, G.M., and Perkin, D.J., 1985, Eastern Creek Volcanics; their geochemistry and possible role in copper mineralization at Mount Isa, Queensland: Bureau of Mineral Resources (BMR) Journal of Australian Geology and Geophysics, v. 9, p. 319–328.

Wyborn, L.A.I., 1987, The petrology and geochemistry of alteration assemblages in the Eastern Creek Volcanics as a guide to copper and uranium mobility associated with regional metamorphism and deformation, Mount Isa, Queensland, *in* Pharaoh, T.C., Beckinsale, R.D., and Rickard, D.T., eds., Geochemistry and mineralization of Proterozoic volcanic suites: Geological Society Special Publication 33, p. 425–434.

Young, M.E., 1984, Gravity and magnetic results from Mount Isa district, Australia: Transactions of the Institute of Mining and Metallurgy, v. B93, p. 78–86.

Exploration Geophysics (1997) 28, 39-42

McArthur Basin Architecture — a New Perspective from Geophysics and GIS

Mark L. Duffett
Centre for Ore Deposit and Exploration Studies,
University of Tasmania,
GPO Box 252-79C,
Hobart, Tas 7001.
Phone (03) 6220 2391
Facsimile (03) 6220 2547
e-mail (preferred): M.Duffett@geol.utas.edu.au

David E. Leaman
Leaman Geophysics,
GPO Box 320D,
Hobart, Tas 7001.
(also Centre for Ore Deposit and Exploration Studies)

ABSTRACT

Interpretations of the gross geometry of the McArthur Basin from regional potential field data are presented as a 2.5-D component of a metallogenic geographic information system (GIS) developed for the region. The McArthur Group, host to the major HYC Pb–Zn deposit, is seen to extend well beyond its eastern limit of outcrop as defined by the Emu Fault. Units identified as prospective using lithological criteria encoded in the GIS contain all known stratiform base metal mineralisation. Such deposits are preferentially located on the periphery of the thickest accumulations of McArthur Group sedimentary rocks.

Volcanism in the upper and lower Tawallah Group is much more voluminous than its comparatively small stratigraphic thickness measured in outcrop would suggest. Over 15 km of basin fill (including volcanic rocks) is implied in some areas, but this may vary rapidly, implying considerable pre-McArthur Group structural development. A number of lineaments visible in the isochore images converge at the position of HYC, indicating bounding fault and strike-slip fault activity at this location during a large portion of basin evolution. These structures do not necessarily correspond to major regional faults interpreted from surface mapping.

Keywords: McArthur Basin, basin architecture, gravity, magnetics, GIS, metallogeny, structure, Proterozoic

INTRODUCTION

The McArthur Basin contains a world-class, stratiform sediment-hosted base metal (SSHBM) deposit (HYC) which, because of its relatively undeformed and unmetamorphosed state, has been widely used as a basis for models of SSHBM mineralisation. Many of these models postulate ore deposition as a result of fluid flow within a rift-sag tectonic environment, although basin morphology is not well constrained by surface mapping due to very limited exposure of many of the deeper basin units. It is necessary to constrain such models in the third dimension by defining the geometry of basins and the bounding faults which may control fluid migration. This has been attempted by integrating geophysical interpretation results as a 3-D component in a metallogenic geographical information system (GIS).

GEOPHYSICAL ANALYSIS

Rigorous quantitative analysis of Australian Geological Survey Organisation (AGSO) regional Bouguer gravity and magnetic data has been employed to investigate the geometry of the McArthur and Tawallah Groups, as well as that of the underlying 'basement' units. Complementary interpretation of an interlocking array of 2-D gravity and magnetic profiles was undertaken by forward modelling constrained by application of the criteria of Leaman (1994). The results were used to generate isochore and structure contour maps of all major basin components. These maps reveal the gross morphology of the basin fill, its basement, and units which, while correlated with exposed rocks, are much more voluminous than hitherto suspected from their exposure. Further details of some of the issues faced during interpretation may be found in Leaman (1996).

MCARTHUR BASIN GIS

Structure and isochore contours were digitised using the Arc/Info® GIS software. The process of contouring and gridding, while inevitably leading to some smoothing of discontinuities, enabled redisplay and analysis of the geophysically derived structural information with respect to other geoscientific data in the GIS. These data included AGSO and Northern Territory Geological Survey 1:250 000, 1:500 000 and 1:1 000 000 scale geological mapping (Pietsch et al., 1991; Blake, 1987; and Plumb, 1988, respectively), lithogeochemistry from a number of sources, and a mineral deposit database modified from that of the Northern Territory Geological Survey (B. Roberts, pers. comm., 1995). The gross basin units are presented in the poster accompanying this paper as a series of 3-D rendered (isometric) views displayed in relation to their outcropping equivalents, regional first-order fault structures and various mineral occurrence types.

(Upper) McArthur Group

The upper McArthur Group (incorporating the upper Umbolooga and Batten Subgroups, Figure 1) is generally more dolomitic and hence denser than the coarser, more siliciclastic sequences above and below it. The Group is largely truncated by the Tawallah Fault to the west, but extends beyond the Emu Fault to the east, though there are some indications of rapid thickness variation associated with the Emu Fault. The thick accumulation of McArthur Group sedimentary section south of HYC supports interpretations of transpressional or transtensional sub-basin development associated with the Emu Fault.

'Prospective units' depicted in Figure 1 are defined as all McArthur Group formations with a significant component of reducing lithologies. These were extracted from the GIS by selecting all McArthur Group units with a proportion of carbonaceous or sulphidic lithologies exceeding 5% of the total volume of the unit. Only the Carrapbirini Member

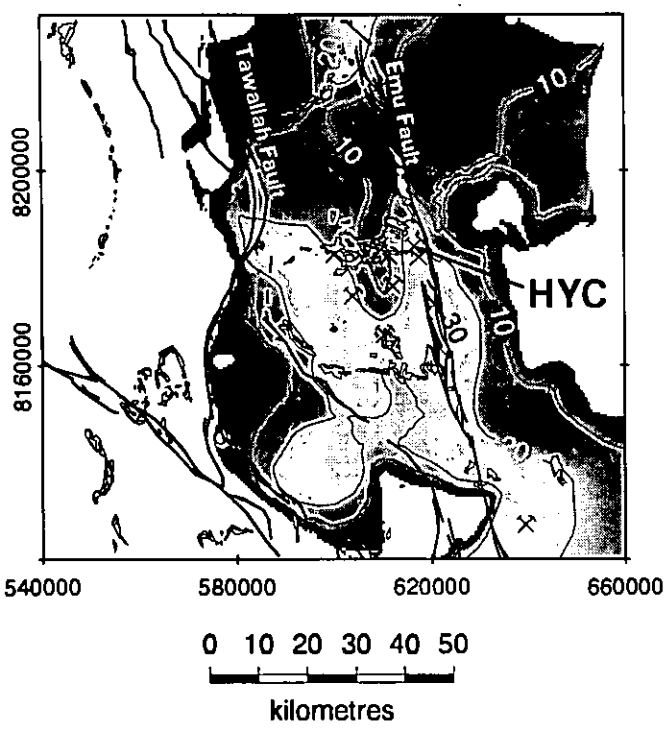

Figure 1. Preserved McArthur Group thickness (greyscale image), with contours marked in hundreds of metres. Outcrops of prospective units (Caranbirini Member, Reward Dolomite, Barney Creek Formation) overlaid in black-outlined white polygons, along with major regional fault systems (thicker black lines). Crossed picks are locations of stratiform Pb–Zn mineralisation, and the HYC deposit is labelled. Grid from Zone 53 of Australian Map Grip (AMG).

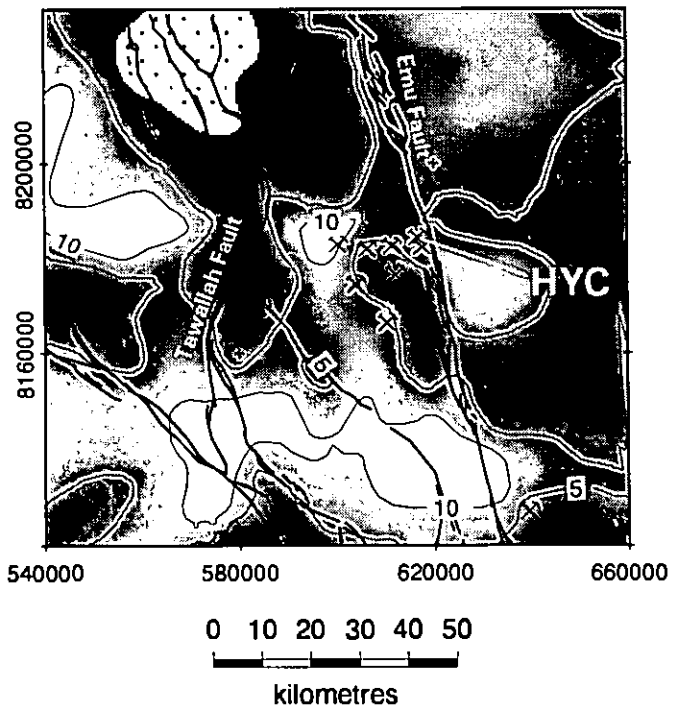

Figure 2. Preserved thickness of upper Tawallah Group volcanic rocks (Settlement Creek Volcanics and Gold Creek Volcanics) rendered as greyscale image, with contours marked in hundreds of metres. Outcrops of Settlement Creek Volcanics and Gold Creek Volcanics overlaid and major faults indicated as in Figure 1. Crossed picks denote locations of stratiform Pb-Zn mineralisation. The stippled area indicates absence of upper Tawallah Group volcanic rocks.

Reward Dolomite and Barney Creek Formation fulfil these criteria, and all known stratiform lead–zinc mineralisation is confined within these units. Most stratiform Pb–Zn deposits occur not in the centre of the thickest accumulations of McArthur Group, but rather on their periphery. This observation is consistent with genetic models which postulate bounding faults on grabens and half-grabens as favourable paths for migration of mineralising fluids.

(Mid-upper) Tawallah Group

Upper Tawallah Group igneous rocks vary in thickness up to more than 1200 m (Figure 2), though this thicker development of units correlated with the Settlement Creek and Gold Creek Volcanics is invariably confined to depths greater than 2 km. Conversely, outcrops of the upper Tawallah Group mafic units are clearly restricted to areas where their preserved thickness is relatively low, implying that these structurally elevated areas also experienced considerable uplift and erosion during basin development. Generally these predominantly mafic units underlie the McArthur Group at an average depth of around 2700 m. Most thickening appears to be associated with sub-east–west trends. Many copper prospects occur in areas of greatest discontinuity separating thicker and thinner volumes of igneous accumulation. Similarly, many base metal deposits appear peripheral to more substantial developments of the upper Tawallah igneous units, again implying an association with long-lived basin bounding faults.

Flood volcanic rocks

An enormous volume of highly magnetic basalts underlies the entire greater McArthur/Mount Isa Basin region extending from the Urapunga Fault Zone past Century in the southeast (Figure 3). The only exceptions are apparent onlaps onto the Murphy Inlier and a number of roughly east–west and approximately northwest-trending patches in the McArthur River region. The base of this basalt pile extends below 15 km depth, but averages around 6 km. There are few indications of a proto-Batten Trough, though a possible major north–south-trending strike-slip fault is visible in the position of the present Emu Fault. This geometry can be interpreted as indicating north–south extension at this time. As with the upper Tawallah Group igneous units, these mafic volcanic rocks are much thinner where they outcrop as the Seigal Volcanics. This assemblage is also correlated with the Eastern Creek Volcanics of the Mount Isa Basin.

Lower volcanic rocks

A separate magnetic source (though less magnetic than the mafic volcanic units) has been delineated below the flood volcanic rocks, and is tentatively correlated with the Scrutton Volcanics and other felsic igneous units of the Barramundi Orogeny (Etheridge et al., 1987). It averages 2.5 km in thickness, rising from a base depth of over 20 km in the west towards its exposed localities on the Murphy Inlier and northwest of HYC in the Tawallah Range, near the eastern end of an elongated east–west uplift structure. Its base has a mean depth exceeding 8.5 km.

Granitoids

Granitoids of varying composition comprise much of the basement throughout the greater McArthur Basin region. Apart from their rise to exposure in the Murphy Inlier, the granitoids are generally deeper than 6 km, but their general relief exceeds 10 km. A number of younger plutons in the Batten Trough and south of the Murphy Inlier, including the

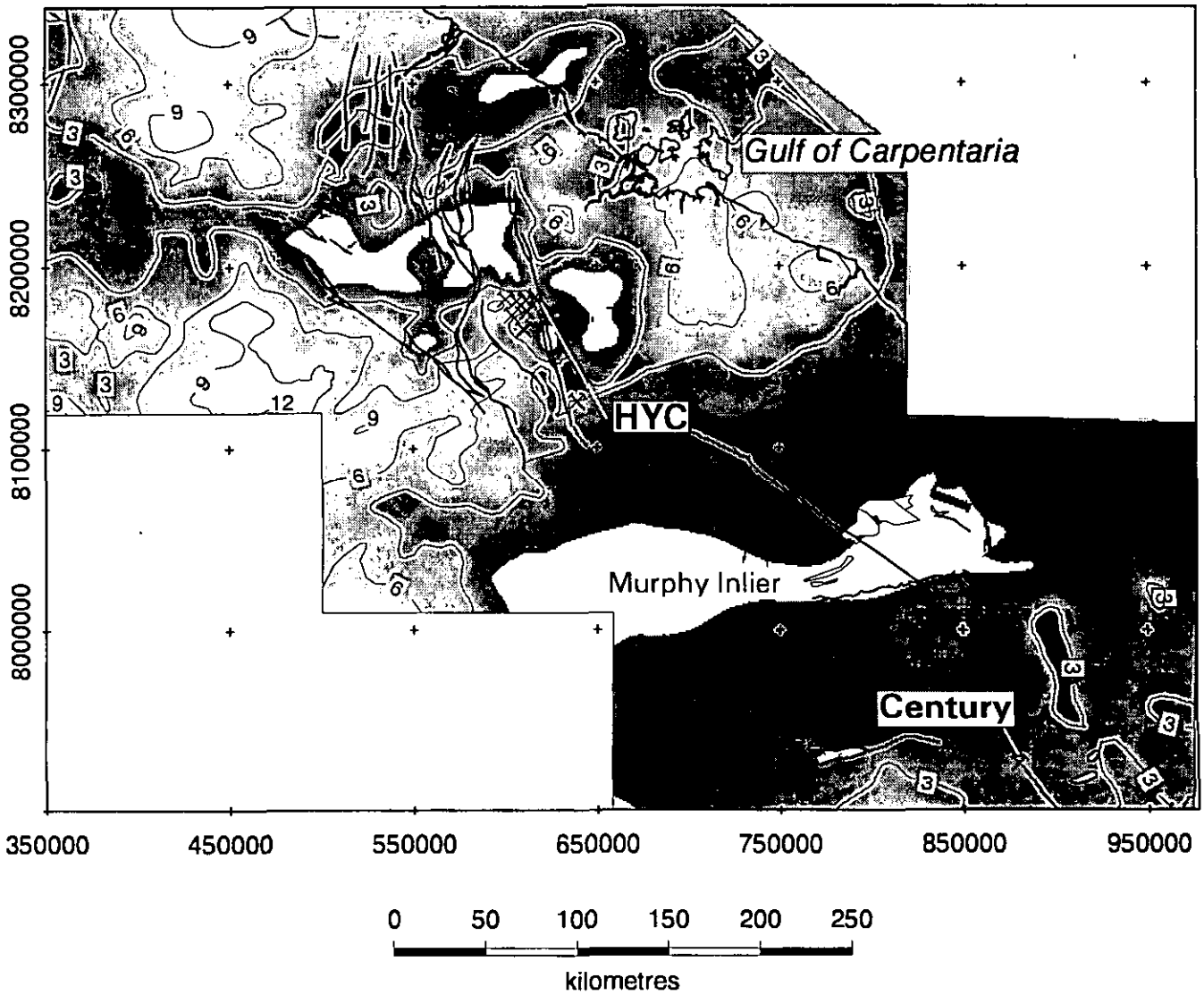

Figure 3. Preserved thickness of inferred continental flood basalts, with isochores (preserved thickness contours; thin black lines) at 3 km intervals. Outcropping probable or possible correlative units overlaid in white (Seigal Volcanics, lower Peters Creek Volcanics, Kamarga Volcanics, Carrara Range Group), along with major regional faults and coastline (heavier black lines). Stratiform Pb–Zn mineralisation located by crossed picks, with major deposits labelled. Note change in scale from Figures 1 and 2. Grid from Zone 53, AMG.

Yeldham Granite in the core of the Kamarga Dome, may penetrate basin units. The Murphy Inlier occurs near a major change in granitoid character.

CONCLUDING REMARKS

Combination of rigorous geophysical analysis and GIS-supported display and integration with other datasets permits a new view of the McArthur Basin and its mineralisation. Though other authors have pointed out the need to incorporate gravity and magnetic datasets into metallogenic GIS (see, for example, Knox-Robinson et al., 1992; Wyborn et al., 1994), the three-dimensional utility of such data is not fully realised without the capacity to include quantitative interpretations based on these data in the GIS. Isometric views of structure contours and isochores enable easier visualisation of relationships between basin geometry, faults and mineral occurrences. Syngenetic/diagenetic mineralisation is not only spatially associated with faults mapped at the surface, but also with discontinuities in gross basin components interpreted as basin-bounding structures active during deposition.

Many units which comprise a small proportion of outcropping McArthur Basin and basement rocks are seen to be more volumetrically significant. Total preserved thickness of the basin is over 15 km, and may exceed 20 km, when volcanic components of the basin fill are considered. Geologically interpreted major structures mapped at the surface may not necessarily have been significant, or possessed their present geometry, throughout the basin's evolution. Such information must be considered in developing metallogenic models incorporating tectonic setting and regional fluid flow.

ACKNOWLEDGMENTS

This work was undertaken as part of AMIRA project P384, which ran from 1992 to mid-1995. The support of sponsoring companies through AMIRA is gratefully acknowledged.

REFERENCES

Blake, D.H., 1987, Geology of the Mount Isa Inlier and environs, Queensland and the Northern Territory: Bureau of Mineral Resources, Bulletin **225**, 83pp.

Etheridge, M.A., Rutland, R.W.R. and Wyborn, L.A.I., 1987, Orogenesis and tectonic process in the early to middle Proterozoic of northern Australia. In Kroner, A., ed., Proterozoic lithospheric evolution: Geodynamics Series **17**, 131-147. (American Geophysical Union and Geological Society of America, Washington D.C.)

Knox-Robinson, C.M., Robinson, D.C. and Groves, D.I., 1992, The use of geographical information systems as a gold prospectivity mapping tool, with reference to the Yilgarn Block, Western Australia: requirements and limitations: In Geological applications of geographic information systems (GIS): Australian Institute of Geoscientists, Bulletin **12**, 71-82.

Leaman, D.E., 1994, Criteria for evaluation of potential field interpretations: First Break **12**, 181-191.

Leaman, D.E., 1996, Are thick volcanic piles concealed in north Australian Proterozoic basins?: Exploration Geophysics **27**, 13-20.

Pietsch, B.A., Rawlings, D.J., Creaser, P.M., Kruse, P.D., Ahmad, M., Ferenczi, P.A. and Findhammer, T.L.R., 1991, Bauhinia Downs SE53-3. 1:250,000 geological map series. Northern Territory Geological Survey.

Plumb, K.A., 1988, Geology of the McArthur Basin (1:1,000,000 scale map). Bureau of Mineral Resources, Canberra.

Wyborn, L.A.I., Gallagher, R., Jaques, A.L., Jagodzinski, E.A., Thost, D. and Ahmad, M., 1994, Developing metallogenic geographic information systems: examples from Mount Isa, Kakadu and Pine Creek: AusIMM Darwin Annual Conference Proceedings, pp. 129-133.